

ORGANIC LIGANDS IN MARINE TRACE METAL BIOGEOCHEMISTRY

EDITED BY: Kristen N. Buck, Maeve C. Lohan, Sylvia G. Sander,
Christel Hassler and Ivanka Pižeta

PUBLISHED IN: Frontiers in Marine Science





frontiers

Frontiers Copyright Statement

© Copyright 2007-2017 Frontiers Media SA. All rights reserved.

All content included on this site, such as text, graphics, logos, button icons, images, video/audio clips, downloads, data compilations and software, is the property of or is licensed to Frontiers Media SA ("Frontiers") or its licensees and/or subcontractors. The copyright in the text of individual articles is the property of their respective authors, subject to a license granted to Frontiers.

The compilation of articles constituting this e-book, wherever published, as well as the compilation of all other content on this site, is the exclusive property of Frontiers. For the conditions for downloading and copying of e-books from Frontiers' website, please see the Terms for Website Use. If purchasing Frontiers e-books from other websites or sources, the conditions of the website concerned apply.

Images and graphics not forming part of user-contributed materials may not be downloaded or copied without permission.

Individual articles may be downloaded and reproduced in accordance with the principles of the CC-BY licence subject to any copyright or other notices. They may not be re-sold as an e-book.

As author or other contributor you grant a CC-BY licence to others to reproduce your articles, including any graphics and third-party materials supplied by you, in accordance with the Conditions for Website Use and subject to any copyright notices which you include in connection with your articles and materials.

All copyright, and all rights therein, are protected by national and international copyright laws.

The above represents a summary only. For the full conditions see the Conditions for Authors and the Conditions for Website Use.

ISSN 1664-8714

ISBN 978-2-88945-376-4

DOI 10.3389/978-2-88945-376-4

About Frontiers

Frontiers is more than just an open-access publisher of scholarly articles: it is a pioneering approach to the world of academia, radically improving the way scholarly research is managed. The grand vision of Frontiers is a world where all people have an equal opportunity to seek, share and generate knowledge. Frontiers provides immediate and permanent online open access to all its publications, but this alone is not enough to realize our grand goals.

Frontiers Journal Series

The Frontiers Journal Series is a multi-tier and interdisciplinary set of open-access, online journals, promising a paradigm shift from the current review, selection and dissemination processes in academic publishing. All Frontiers journals are driven by researchers for researchers; therefore, they constitute a service to the scholarly community. At the same time, the Frontiers Journal Series operates on a revolutionary invention, the tiered publishing system, initially addressing specific communities of scholars, and gradually climbing up to broader public understanding, thus serving the interests of the lay society, too.

Dedication to quality

Each Frontiers article is a landmark of the highest quality, thanks to genuinely collaborative interactions between authors and review editors, who include some of the world's best academicians. Research must be certified by peers before entering a stream of knowledge that may eventually reach the public - and shape society; therefore, Frontiers only applies the most rigorous and unbiased reviews.

Frontiers revolutionizes research publishing by freely delivering the most outstanding research, evaluated with no bias from both the academic and social point of view.

By applying the most advanced information technologies, Frontiers is catapulting scholarly publishing into a new generation.

What are Frontiers Research Topics?

Frontiers Research Topics are very popular trademarks of the Frontiers Journals Series: they are collections of at least ten articles, all centered on a particular subject. With their unique mix of varied contributions from Original Research to Review Articles, Frontiers Research Topics unify the most influential researchers, the latest key findings and historical advances in a hot research area! Find out more on how to host your own Frontiers Research Topic or contribute to one as an author by contacting the Frontiers Editorial Office: researchtopics@frontiersin.org

ORGANIC LIGANDS IN MARINE TRACE METAL BIOGEOCHEMISTRY

Topic Editors:

Kristen N. Buck, University of South Florida, United States

Maeve C. Lohan, University of Southampton, United Kingdom

Sylvia G. Sander, University of Otago, New Zealand

Christel Hassler, University of Geneva, Switzerland

Ivanka Pižeta, Ruđer Bošković Institute, Croatia



Krka River National Park, Croatia

Photo credit: Kristen Buck.

This research topic highlights the most recent accomplishments of a Scientific Committee on Oceanic Research (SCOR) Working Group, SCOR WG 139: Organic Ligands - A Key Control on Trace Metal Biogeochemistry in the Ocean.

Citation: Buck, K. N., Lohan, M. C., Sander, S. G., Hassler, C., Pižeta, I., eds. (2017). Organic Ligands in Marine Trace Metal Biogeochemistry. Lausanne: Frontiers Media. doi: 10.3389/978-2-88945-376-4

Table of Contents

1. Introduction

06 Editorial: Organic Ligands—A Key Control on Trace Metal Biogeochemistry in the Ocean

Kristen N. Buck, Maeve C. Lohan, Sylvia G. Sander, Christel Hassler and Ivanka Pižeta

2. Methodological Advances

08 An Intercomparison of Dissolved Iron Speciation at the Bermuda Atlantic Time-series Study (BATS) Site: Results from GEOTRACES Crossover Station A

Kristen N. Buck, Loes J. A. Gerringa and Micha J. A. Rijkenberg

22 Determination of the Side-Reaction Coefficient of Desferrioxamine B in Trace-Metal-Free Seawater

Johan Schijf and Shannon M. Burns

37 Fe- and Cu-Complex Formation with Artificial Ligands Investigated by Ultra-High Resolution Fourier-Transform Ion Cyclotron Resonance Mass Spectrometry (FT-ICR-MS): Implications for Natural Metal-Organic Complex Studies

Hannelore Waska, Andrea Koschinsky and Thorsten Dittmar

56 Identification of Metallophores and Organic Ligands in the Chemosphere of the Marine Macroalga *Ulva* (Chlorophyta) and at Land-Sea Interfaces

Thomas Wichard

66 Evaluation of Immobilized Metal-Ion Affinity Chromatography and Electrospray Ionization Tandem Mass Spectrometry for Recovery and Identification of Copper(II)-Binding Ligands in Seawater Using the Model Ligand 8-Hydroxyquinoline

Richard L. Nixon and Andrew R. S. Ross

3. Iron-binding ligands

3.1. Sources

76 Ferrioxamine Siderophores Detected amongst Iron Binding Ligands Produced during the Remineralization of Marine Particles

Imelda B. Velasquez, Enitan Ibisani, Elizabeth W. Maas, Philip W. Boyd Scott Nodder and Sylvia G. Sander

90 Iron-Binding Ligands in the Southern California Current System: Mechanistic Studies

Randelle M. Bundy, Mingshun Jiang, Melissa Carter and Katherine A. Barbeau

- 107** *First Evaluation of the Role of Salp Fecal Pellets on Iron Biogeochemistry*
Damien J. E. Cabanes, Louiza Norman, Juan Santos-Echeandía, Morten H. Iversen, Scarlett Trimborn, Luis M. Laglera and Christel S. Hassler
- 3.2. New links between iron, viruses and ligands**
- 117** *Phytoplankton Virus Production Negatively Affected by Iron Limitation*
Hans A. Slagter, Loes J. A. Gerringa and Corina P. D. Brussaard
- 128** *The Ferrojan Horse Hypothesis: Iron-Virus Interactions in the Ocean*
Chelsea Bonnain, Mya Breitbart and Kristen N. Buck
- 3.3. Emerging paradigms**
- 139** *Toward a Regional Classification to Provide a More Inclusive Examination of the Ocean Biogeochemistry of Iron-Binding Ligands*
Christel S. Hassler, Constant M. G. van den Berg and Philip W. Boyd
- 158** *A Compilation of Iron Speciation Data for Open Oceanic Waters*
Salvatore Caprara, Kristen N. Buck, Loes J. A. Gerringa, Micha J. A. Rijkenberg and Damiano Monticelli
- 4. Copper speciation and cycling**
- 165** *Structural Characterization of Natural Nickel and Copper Binding Ligands along the US GEOTRACES Eastern Pacific Zonal Transect*
Rene M. Boiteau, Claire P. Till, Angel Ruacho, Randelle M. Bundy, Nicholas J. Hawco, Amy M. McKenna, Katherine A. Barbeau, Kenneth W. Bruland, Mak A. Saito and Daniel J. Repeta
- 181** *Using ⁶⁷Cu to Study the Biogeochemical Cycling of Copper in the Northeast Subarctic Pacific Ocean*
David M. Semeniuk, Randelle M. Bundy, Anna M. Posacka, Marie Robert, Katherine A. Barbeau and Maria T. Maldonado
- 200** *Chemical Speciation of Copper in a Salt Marsh Estuary and Bioavailability to Thaumarchaeota*
Hannah Whitby, James T. Hollibaugh and Constant M. G. van den Berg
- 5. Distribution studies of metal-binding organic ligands**
- 215** *Distribution and Speciation of Dissolved Iron in Jiaozhou Bay (Yellow Sea, China)*
Han Su, Rujun Yang, Ivanka Pižeta, Dario Omanović, Shirong Wang and Yan Li
- 232** *Fe-Binding Dissolved Organic Ligands in the Oxidic and Suboxic Waters of the Black Sea*
Loes J. A. Gerringa, Micha J. A. Rijkenberg, Johann Bown, Andrew R. Margolin, Patrick Laan and Hein J. W. de Baar
- 248** *Voltammetric Investigation of Hydrothermal Iron Speciation*
Charlotte Kleint, Jeffrey A. Hawkes, Sylvia G. Sander and Andrea Koschinsky
- 259** *Dissolved Zn and its speciation in the northeastern Indian Ocean and the Andaman Sea*
Taejin Kim, Hajime Obata and Toshitaka Gamo

6. Trace metal speciation in a changing ocean

273 *Influence of Ocean Acidification on the Organic Complexation of Iron and Copper in Northwest European Shelf Seas; a Combined Observational and Model Study*

Lizeth Avendaño, Martha Gledhill, Eric P. Achterberg, Victoire M. C. Rérolle and Christian Schlosser

292 *Toward a Quality-Controlled and Accessible Pitzer Model for Seawater and Related Systems*

David R. Turner, Eric P. Achterberg, Chen-Tung A. Chen, Simon L. Clegg, Vanessa Hatje, Maria T. Maldonado, Sylvia G. Sander, Constant M. G. van den Berg and Mona Wells



Editorial: Organic Ligands—A Key Control on Trace Metal Biogeochemistry in the Ocean

Kristen N. Buck^{1*}, Maeve C. Lohan², Sylvia G. Sander³, Christel Hassler⁴ and Ivanka Pižeta⁵

¹ Trace Metal Biogeochemistry, College of Marine Science, University of South Florida, Tampa, FL, United States,

² Department of Earth and Ocean Science, National Oceanography Centre, University of Southampton, Southampton,

United Kingdom, ³ Department of Chemistry, University of Otago, Dunedin, New Zealand, ⁴ Department F.-A. Forel for Environmental and Aquatic Sciences, Université de Genève, Geneva, Switzerland, ⁵ Division for Marine and Environmental Research, Ruđer Bošković Institute, Zagreb, Croatia

Keywords: trace metals, organic ligands, metal speciation, ocean biogeochemistry, marine science

Editorial on the Research Topic

Organic Ligands—A Key Control on Trace Metal Biogeochemistry in the Ocean

This Research Topic results from the activities of Scientific Committee on Oceanic Research Working Group (SCOR WG) 139: Organic Ligands—A Key Control on Trace Metal Biogeochemistry in the Ocean. Organic ligands govern the bioavailability of trace metals that are essential micronutrients to marine phytoplankton and exert a major influence on the global carbon cycle. The aim of SCOR WG 139 has been to improve understanding of metal-binding ligands in the oceans, and their pivotal biogeochemical functions in the oceans, through an interdisciplinary collaboration of trace metal biogeochemists, organic geochemists and biogeochemical modelers.

Three central goals of this WG were to:

1. Promote improvements in quality, accessibility, and development of analytical methodologies for characterizing metal-binding ligands in seawater.
2. Characterize which components of the dissolved organic matter pool make a significant contribution to the biogeochemistry of trace metals in the oceans.
3. Identify the role of ligands in microbial ecology and marine biogeochemical cycles.

Several papers in this Research Topic emphasize improvements in methodology for characterizing metal-binding organic ligands in seawater. Best practices for comparing competitive ligand exchange-adsorptive cathodic stripping voltammetry (CLE-AdCSV) results are provided in a GEOTRACES field data intercomparison (Buck et al.). The assessment of side reaction coefficients of a model siderophore by voltammetry (Schijf and Burns) and of the complexes formed between model ligands and iron and copper using voltammetry and Fourier transform-ion cyclotron resonance-mass spectrometry (FT-ICR-MS) (Waska et al.) illustrate the heterogeneity of metal-ligand complexes. Waska et al. also underscore the strength of combining CLE-AdCSV and mass spectrometry tools to characterize metal-binding ligands. In a Perspective, Wichard details the applicability of metal isotope coded profiling in ultra high performance liquid chromatography-electrospray ionization-mass spectrometry (UHPLC-ESI-MS) to identify metal-binding organic ligands and decipher their ecosystem function. A crucial step in mass spectrometry ligand identification is the separation of metal-binding ligands from the seawater matrix. In their paper, Nixon and Ross document an 81% average recovery of a model copper ligand on an immobilized metal-ion affinity chromatography (IMAC) column.

OPEN ACCESS

Edited and reviewed by:

Eric Pieter Achterberg,
GEOMAR Helmholtz Centre for Ocean
Research Kiel (HZ), Germany

*Correspondence:

Kristen N. Buck
kristenbuck@usf.edu

Specialty section:

This article was submitted to
Marine Biogeochemistry,
a section of the journal
Frontiers in Marine Science

Received: 12 July 2017

Accepted: 15 September 2017

Published: 26 September 2017

Citation:

Buck KN, Lohan MC, Sander SG,
Hassler C and Pižeta I (2017) Editorial:
Organic Ligands—A Key Control on
Trace Metal Biogeochemistry in the
Ocean. *Front. Mar. Sci.* 4:313.
doi: 10.3389/fmars.2017.00313

Rapidly advancing mass spectrometry tools coupled with CLE-AdCSV has led to new insights into metal and ligand cycling in the ocean. Using a combination of CLE-AdCSV, LC-ESI-MS and chemical assays, Velasquez et al. show siderophore production during particle remineralization, representing a novel source of strong iron-binding ligands to subsurface waters. Bundy et al. also report iron-binding ligand sources in particle remineralization experiments, and variable photochemical losses. The production of strong iron-binding ligands during remineralization (Bundy et al.; Velasquez et al.) has important implications for iron resupply to the surface ocean, providing a mechanism for stabilizing subsurface iron. Fecal pellets from salps were found to be a source of iron-binding humic-like substances and a vector for iron transport to the deep Southern Ocean, suggesting a tendency for iron export over recycling where salps are abundant (Cabanes et al.).

Two papers in this Research Topic highlight exciting new links between viruses, iron and ligands in the ocean. Iron limitation was found by Slagter et al. to reduce viral infection of marine phytoplankton and the extent of iron cycling through the viral shunt. Bonnain et al. build on established literature in non-marine model systems to propose that viruses themselves are iron-binding organic ligands in the oceans and that iron in virus tails may serve as a Trojan horse for viral infection of bacteria.

An emerging paradigm regarding iron-binding ligands in seawater is the combined contribution of siderophores, humic-like substances and exopolysaccharides to the ligand pool. Hassler et al. use these ligand groups to propose regional distinctions in iron speciation and identify knowledge gaps. In a data report, Caprara et al. note that nearly 70% of the existing open ocean iron speciation data originate from the Atlantic, creating an inherent bias in evaluating global distribution patterns.

Compared to iron, the organic complexation of other bioactive metals is less understood. The application of LC-ESI-MS to South Pacific surface waters identified a diverse suite of copper- and nickel-binding organic ligands (Boiteau et al.). A copper radiotracer method introduced by Semeniuk et al. and applied with CLE-AdCSV showed rapid cycling of copper by natural phytoplankton communities in the North Pacific. Voltammetric measurements of copper-binding ligands, humic substances and thiols in a salt marsh estuary suggest that ammonia-oxidizing archaea also grow on organically complexed copper (Whitby et al.).

CLE-AdCSV studies of metal-binding organic ligand distributions continue to inform understanding of the role these ligands play in ocean biogeochemistry. In this Research Topic, stabilization of dissolved iron inputs was attributed to strong iron-binding organic ligands in the Yellow Sea (Su et al.), in a buoyant hydrothermal plume from a shallow island arc system (Kleint et al.) and across the redox boundary of the Black Sea (Gerringa et al.). In the first CLE-AdCSV study of zinc speciation

in the Indian Ocean, Kim et al. report a predominant river influence in this region.

Changing ocean chemistry is expected to influence the speciation, bioavailability, and biogeochemical cycling of trace metals in seawater. Avendaño et al. use a combination of CLE-AdCSV and speciation modeling to evaluate how declining seawater pH levels alters the complexation of iron and copper by natural organic ligands in shelf seas. This Research Topic also introduces a new SCOR working group, SCOR WG 145, aimed at developing a quality controlled and widely accessible model of trace metal speciation across ocean chemistry conditions (Turner et al.).

This Research Topic emphasizes vast methodological improvements made in quantifying and identifying metal-binding ligands in seawater, and advancements in our understanding of how organic ligands govern trace metal speciation and how they are cycled through marine biological processes. Altogether, these studies point to the diverse range of metal-binding organic ligands present in the ocean and highlight the crucial role they play in supporting primary productivity by maintaining essential bioactive trace metals in the upper water column.

AUTHOR CONTRIBUTIONS

All authors listed have made a substantial, direct and intellectual contribution to the work, and approved it for publication.

FUNDING

The activities of WG 139 were supported by the Scientific Committee on Oceanic Research (SCOR), U.S. National Science Foundation grant OCE-1243377 and by national SCOR committees. We acknowledge funding agencies from the many nations that supported the science presented here.

ACKNOWLEDGMENTS

We sincerely thank the authors in this SCOR WG 139 Research Topic and hope readers enjoy them as much as we have. We especially thank SCOR Executive Director Ed Urban for his support and guidance of SCOR WG 139.

Conflict of Interest Statement: The authors declare that the research was conducted in the absence of any commercial or financial relationships that could be construed as a potential conflict of interest.

Copyright © 2017 Buck, Lohan, Sander, Hassler and Pižeta. This is an open-access article distributed under the terms of the Creative Commons Attribution License (CC BY). The use, distribution or reproduction in other forums is permitted, provided the original author(s) or licensor are credited and that the original publication in this journal is cited, in accordance with accepted academic practice. No use, distribution or reproduction is permitted which does not comply with these terms.



An Intercomparison of Dissolved Iron Speciation at the Bermuda Atlantic Time-series Study (BATS) Site: Results from GEOTRACES Crossover Station A

Kristen N. Buck^{1*}, Loes J. A. Gerringa² and Micha J. A. Rijkenberg²

¹ College of Marine Science, University of South Florida, St. Petersburg, FL, USA, ² Department of Ocean Systems, NIOZ Royal Netherlands Institute for Sea Research, Utrecht University, Texel, Netherlands

OPEN ACCESS

Edited by:

Sunil Kumar Singh,
Physical Research Laboratory, India

Reviewed by:

Mariko Hatta,
University of Hawaii, USA
Peter L. Morton,
Florida State University/National High
Magnetic Field Lab, USA
Hajime Obata,
University of Tokyo, Japan

*Correspondence:

Kristen N. Buck
kristenbuck@usf.edu

Specialty section:

This article was submitted to
Marine Biogeochemistry,
a section of the journal
Frontiers in Marine Science

Received: 30 July 2016

Accepted: 28 November 2016

Published: 15 December 2016

Citation:

Buck KN, Gerringa LJA and
Rijkenberg MJA (2016) An
Intercomparison of Dissolved Iron
Speciation at the Bermuda Atlantic
Time-series Study (BATS) Site:
Results from GEOTRACES Crossover
Station A. *Front. Mar. Sci.* 3:262.
doi: 10.3389/fmars.2016.00262

The organic complexation of dissolved iron (Fe) was determined in depth profile samples collected from GEOTRACES Crossover Station A, the Bermuda Atlantic Time-series Study (BATS) site, as part of the Dutch and U.S. GEOTRACES North Atlantic programs in June 2010 and November 2011, respectively. The two groups employed distinct competitive ligand exchange-adsorptive cathodic stripping voltammetry (CLE-AdCSV) methods, and resulting ligand concentrations and conditional stability constants from each profile were compared. Excellent agreement was found between the total ligand concentrations determined in June 2010 and the strongest, L₁-type, ligand concentrations determined in November 2011. Yet a primary distinction between the datasets was the number of ligand classes observed: A single ligand class was characterized in the June 2010 profile while two ligand classes were observed in the November 2011 profile. To assess the role of differing interpretation approaches in determining final results, analysts exchanged titration data, and accompanying parameters from the profiles for reinterpretation. The reinterpretation exercises highlighted the considerable influence of the sensitivity (S) parameter applied on interpretation results, consistent with recent intercalibration work on interpretation of copper speciation titrations. The potential role of titration data structure, humic-type substances, differing dissolved Fe concentrations, and seasonality are also discussed as possible drivers of the one vs. two ligand class determinations between the two profiles, leading to recommendations for future studies of Fe-binding ligand cycling in the oceans.

Keywords: Iron-binding ligands, method intercomparison, voltammetry, chemical speciation, seawater

INTRODUCTION

Iron (Fe) is an essential micronutrient, limiting phytoplankton growth in large regions of the surface ocean (de Baar et al., 2005; Boyd et al., 2007). The bioavailability of Fe to phytoplankton in the ocean is complicated by the limited supply of Fe from remote crustal sources (Tagliabue et al., 2014) and the overwhelming complexation of dissolved Fe (DFe) by organic ligands in seawater (Gledhill and Buck, 2012). Organic complexation allows Fe to overcome its low inorganic solubility

in oxygenated seawater (Kuma et al., 1996; Liu and Millero, 2002), though the resulting Fe-organic ligand complexes require specialized uptake mechanisms for Fe acquisition (Maldonado et al., 2005; Hopkinson and Morel, 2009; Shaked and Lis, 2012). Most recently, the organic complexation of DFe in the Atlantic ocean was characterized in consecutive basin-scale studies of DFe speciation that overlapped at Crossover Station A at the Bermuda Atlantic Time-series Study site as part of the international GEOTRACES program (Buck et al., 2015; Gerringa et al., 2015).

Fe-binding ligand concentrations and their conditional stability constants in seawater are typically determined using competitive ligand exchange-adsorptive cathodic stripping voltammetry (CLE-AdCSV) techniques (Gledhill and van den Berg, 1994; Rue and Bruland, 1995; Croot and Johansson, 2000). These techniques involve equilibrating filtered and buffered seawater samples with a range of inorganic DFe additions and a single concentration addition of a well-characterized competing (or “added”) ligand before analysis of each titration point by AdCSV on a hanging mercury drop electrode. The sequence and equilibration times of added DFe and competing ligand vary across techniques (e.g., Buck et al., 2012; Gledhill and Buck, 2012). Titration data from AdCSV analyses are subsequently interpreted using a combination of linear and/or non-linear interpretation approaches to determine ambient Fe-binding ligand concentrations and conditional stability constants from each sample titration.

These ligands are commonly described by ligand classes, denoted L_1, L_2, \dots, L_i , where L_1 is the strongest ligand class detected, L_2 weaker, etc. These ligand classes are operationally defined by their associated conditional stability constants ($K_{FeL_i, Fe'}^{cond}$). In cases where only a single ligand class is detected, this notation is often simplified to L or L_T for ligand concentrations and for $K_{FeL, Fe'}^{cond}$, the associated conditional stability constant. In published datasets of DFe speciation, the reported values of $\log K_{FeL, Fe'}^{cond}$, $K_{FeL_1, Fe'}^{cond}$, and $\log K_{FeL_2, Fe'}^{cond}$ show considerable overlap, and it has been proposed that these ligand classes be defined by specific ranges in $\log K_{FeL_i, Fe'}^{cond}$ values (Gledhill and Buck, 2012). The complexation capacity or competition strength of these ligands is described by α_{FeL} , which is a function of the free (not bound to Fe, “excess”) ligand concentration ($[L'_i] = [L_i] - [DFe]$) and associated stability constant ($\log K_{FeL_i, Fe'}^{cond}$) of all ligand classes present: $\alpha_{FeL} = \sum [L'_i] * K_{FeL_i, Fe'}^{cond}$.

Of these different ligand classes, stronger L_1 -type ligands ($\log K_{FeL_1, Fe'}^{cond} > 12$) and siderophores in particular have been shown to play a distinct role in Fe solubility (Cheah et al., 2003; Buck et al., 2007; Rijkenberg et al., 2008; Wagener et al., 2008; Aguilar-Islas et al., 2010; Mendez et al., 2010; Bundy et al., 2014; Fishwick et al., 2014), though characterizing more than one ligand class during the interpretation of CLE-AdCSV titration datasets is challenging (Hudson et al., 2003; Wu and Jin, 2009; Laglera et al., 2013). In addition to requiring sufficient titration points to quantify more than one ligand class with suitable error estimates, resolving multiple ligand classes also requires that the alpha coefficients of the proposed ligand classes are suitably different (Hudson

et al., 2003; Wu and Jin, 2009) and larger than the center of the analytical window (α_{FeL} of the added competing ligand) employed (Laglera et al., 2013).

There are several CLE-AdCSV techniques for DFe speciation in seawater, which are typically defined by the choice of added competitive ligand employed for the titrations, though titration conditions (pH, temperature, concentration of added ligand, order and range of Fe and ligand additions, equilibration times) may also vary (Gledhill and Buck, 2012). The interpretation techniques used to obtain ligand concentrations and conditional stability constants from the titration data generated by CLE-AdCSV are diverse as well, and several new techniques have emerged recently (Sander et al., 2011; Laglera et al., 2013; Gerringa et al., 2014; Omanović et al., 2015). At this time, there are no established reference samples for DFe speciation, and intercomparison activities are a useful alternative for assessing how these different CLE-AdCSV approaches compare.

A field intercomparison study was previously conducted for DFe speciation at three depths in the central North Pacific as part of GEOTRACES intercalibration activities (Buck et al., 2012). In that study, each analyst applied their chosen CLE-AdCSV technique shipboard to samples collected from the same GO-Flo bottle for each of three depths, and final results were compared across the different analysts. Results of this initial intercalibration effort indicated the best agreement between analysts employing the same CLE-AdCSV and interpretation techniques. Distinctions between interpretation techniques were highlighted in part to explain poorer agreement between analysts using different approaches, though analysts did not exchange titration data or directly compare interpretation techniques (Buck et al., 2012). More recently, intercomparison exercises focused on interpretation techniques applied to estuarine (Laglera et al., 2013) and simulated (Pižeta et al., 2015) copper speciation data have found that the interpretation technique employed can have a dramatic impact on results reported from the same original titration data when the ligand characteristics for multiple ligand classes are analyzed.

Here we present a comparison of DFe speciation datasets generated from the GEOTRACES Crossover Station A at the Bermuda Atlantic Time-series Study (BATS) site as part of the Dutch and U.S. GEOTRACES expeditions in the North Atlantic in June, 2010 (Gerringa et al., 2015) and November, 2011 (Buck et al., 2015), respectively. In addition to comparing full water column datasets from BATS between the two occupations, we also report results of reinterpretation exercises conducted with the original titration data from both BATS profiles. The impact of the chosen sensitivity parameter on the final results from each interpretation approach was also compared between analysts in this exercise.

MATERIALS AND METHODS

Sample Collection

Dissolved Fe (DFe) and DFe speciation samples were collected following stringent trace metal clean protocols, which are outlined in the GEOTRACES Cruise and Methods Manual

(Cutter et al., 2010). At the GEOTRACES Crossover Station A, Bermuda Atlantic Time-series Study (BATS) site, full water column depth profile samples were collected first by the Dutch GEOTRACES program in June 2010 and subsequently by the U.S. GEOTRACES program in November 2011 (Figure 1). Specifics of sample collection and analyses between the two groups participating in this intercalibration are provided under the methods descriptions below.

Dissolved Iron (DFe) Analyses

Total DFe concentrations are required for the interpretation of titrations for DFe speciation. The complete details of DFe analyses were published with the original basin-scale datasets (Rijkenberg et al., 2014; Sedwick et al., 2015). Briefly, in both cases, samples for DFe were collected separately from speciation samples in acid-cleaned low density polyethylene (LDPE) bottles. These samples were filtered through the same filters (<0.2 μm , see details below) used for the collection of speciation samples. DFe samples were acidified to 0.024 M hydrochloric acid (HCl) with high purity HCl (Johnson et al., 2007) and DFe concentrations were determined by flow injection analysis (FIA: Rijkenberg et al., 2014; Sedwick et al., 2015). Applying these analyses to reference standards from the SAFE (Johnson et al., 2007) and GEOTRACES programs resulted in DFe concentrations within the range of consensus values reported for each reference sample (Rijkenberg et al., 2014; Sedwick et al., 2015). Both of the DFe datasets used for DFe speciation calculations in this intercomparison were also included in the 2014 GEOTRACES Intermediate Data Product (Mawji et al., 2015).

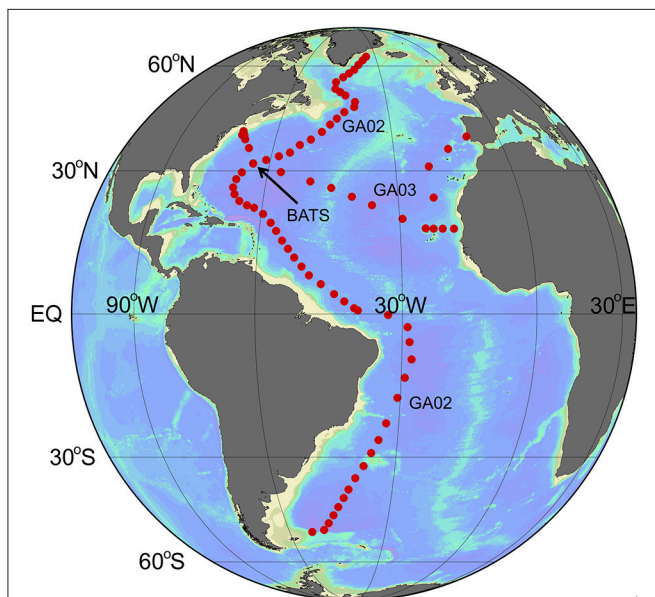


FIGURE 1 | Map of stations sampled as part of GEOTRACES cruises GA02 and GA03. The Bermuda Atlantic Time-series Study (BATS) site, which serves as GEOTRACES Crossover Station A, is highlighted as the focus of this intercomparison study.

2-(2-Thiazolylazo)-P-Cresol (TAC) Method

Filtered seawater (0.2 μm , Sartobran 300 cartridges) samples of 13 depths per station, representing the entire water column, were sampled on June 13, 2010 as part of the Dutch GEOTRACES program from an ultra-clean titanium depth sampler (de Baar et al., 2008). Samples from BATS were kept in a refrigerator (4°C) until analyzed shipboard between June 15 and June 17, 2010, within 4 days of sample collection.

TAC (2-(2-Thiazolylazo)-p-cresol) was used as a competing ligand to titrate the natural DFe-binding ligands by adding increasing concentrations of DFe to sub-samples. The bulk sample was buffered to a pH of 8.05 with 5 mM mixed ammonium-borate buffer cleaned of Fe using a TAC addition that was subsequently removed over a SEP-PAK column (Gerringa et al., 2015). The titrations consisted of 14 sub-samples with DFe additions of 0, 0.2, 0.4, 0.6, 0.8, 1, 1.2, 1.5, 2, 2.5, 3, 4, 6, and 8 nM Fe. The competing ligand “TAC” was used with a final concentration of 10 μM , resulting in $\alpha_{\text{Fe}(\text{TAC})_2}$ of 251 as the center of the analytical window. The $\text{Fe}(\text{TAC})_2$ complex was measured after equilibration (> 6 h) by adsorptive cathodic stripping voltammetry (AdCSV) (Croot and Johansson, 2000). Each of the 14 sub-samples was measured twice, resulting in a total of 28 titration data points.

The voltammetric equipment consisted of a $\mu\text{Autolab}$ potentiostat (Type II and III, Ecochemie, The Netherlands), and a mercury drop electrode (model VA 663 from Metrohm) connected to a Metrohm-Applikon (778) sample changer. To prevent interference to analyses from motions of the ship, the electrode stand with the mercury drop electrode was stabilized on a wooden board hung with elastic bands inside an aluminum frame constructed at the Netherlands Institute for Sea Research (NIOZ). As a result, movements of the ship did not disturb measurements even during bad weather. All equipment was protected against electrical noise by a current filter (Fortress 750, Best Power).

During the course of the cruise, the TAC reagent used for analyses was found to contain relatively high Fe, resulting in an inadvertent addition of 0.5 nM Fe to the Crossover Station A/BATS profile samples (Gerringa et al., 2015). Thus, it is important to measure the Fe content in new batches of added competing ligands such as TAC since the quality with respect to Fe content was found to be variable between batches. The affected profile data from Crossover Station A/BATS was corrected by including this additional 0.5 nM Fe in the ambient DFe value used for titration data interpretation.

For the titration data interpretation a method was used in which the sensitivity (S), the conditional stability constant ($K_{\text{FeL}_i, \text{Fe}'}^{\text{cond}}$), and the ligand concentration ($[\text{L}_i]$), are estimated using non-linear regression (Gerringa et al., 2014). By including S as an unknown parameter in the non-linear regression, S is corrected for the possibility that the visually linear part of the titration curve is still affected by unsaturated natural ligands. The non-linear regression method is simple to calculate, requiring easily available software (e.g., **R**) capable of least-squares regression or simplex regression, and calculates the

standard errors (SE) of the fitted parameters. It is well-suited for the estimation of three or, if two ligand classes are assumed, five parameters out of a relatively small number of observations (Gerringa et al., 2014). At least four titration points per distinguished ligand group, together with a minimum of four titration points where the ligands are saturated, are necessary to obtain statistically reliable estimates of S , $K_{FeL_i,Fe'}^{cond}$, and $[L_i]$.

Salicylaldoxime (SA) Method

Depth profile samples collected as part of the U.S. GEOTRACES program were obtained using a trace metal clean sampling rosette deployed on a Kevlar line (Cutter and Bruland, 2012). For speciation samples, seawater was filtered through 0.2 μm Acropak (Pall Acropak 500) filters into acid-cleaned and Milli-Q ($>18.2\text{ M}\Omega\text{ cm}$)-filled narrow mouth fluorinated polyethylene bottles (FPE, Nalgene) that had been rinsed three times with sample prior to filling (Cutter et al., 2010; Buck et al., 2012). The speciation samples from Crossover Station A/BATS were collected on November 19, 2011, frozen at -20°C and returned to the laboratory for analysis in June 2012. A total of 37 depths were sampled from this profile for DFe and DFe speciation.

Sample analyses for Fe-binding ligands using the SA method were conducted as described in Buck et al. (2015) on a BioAnalytical Systems (BASi) controlled growth mercury electrode (static drop setting, drop size 14) coupled to a BASi Epsilon $\epsilon 2$ voltammetric analyzer. Frozen speciation samples were thawed at room temperature, shaken, and distributed in 10-mL aliquots into lidded Teflon vials (Savillex) that had been previously conditioned with the expected Fe and SA additions in buffered Milli-Q. Each 10-mL sample aliquot was buffered to $\text{pH}_{\text{NBS}} 8.2$ with a chelexed-cleaned ammonium-borate buffer (Ellwood and van den Berg, 2001; Buck et al., 2007). Titrations consisted of 13 points: Two ambient (+0 nM Fe) measurements followed by ten dissolved Fe additions of +0.25, 0.5, 0.75, 1, 1.5, 2, 2.5, 3.5, 5, and 7.5 nM Fe. DFe additions were allowed to equilibrate with natural ligands in the samples for at least 2 h, or overnight at 4°C in the refrigerator (Buck et al., 2007). An addition of 25 μM SA (analytical window, $\alpha_{FeSA} = 79$; Buck et al., 2007) to each titration vial was then made and allowed to equilibrate for at least 15 min prior to commencing AdCSV analyses (Rue and Bruland, 1995; Buck et al., 2007, 2015). Each titration point was analyzed once, generating a total of 12 points in each sample titration.

Titration data generated by CLE-AdCSV with SA was interpreted using a combination of van den Berg/Ružić and Scatchard linearization techniques (Scatchard, 1949; Ružić, 1982; van den Berg, 1982) as described previously (Rue and Bruland, 1995, 1997; Buck et al., 2007, 2012, 2015). In this approach, the sensitivity S for each sample titration was determined from the slope of the last few titration points. Results from the output of the two linearizations were then combined from each titration to determine averages for ligand concentrations and conditional stability constants (Buck et al., 2015). An inorganic side reaction coefficient for Fe of 10^{10} was employed when converting between $\log K_{FeL_i,Fe'}^{cond}$ and $\log K_{FeL_i,Fe^{3+}}^{cond}$ notations of the conditional stability constant.

Intercomparison Activities

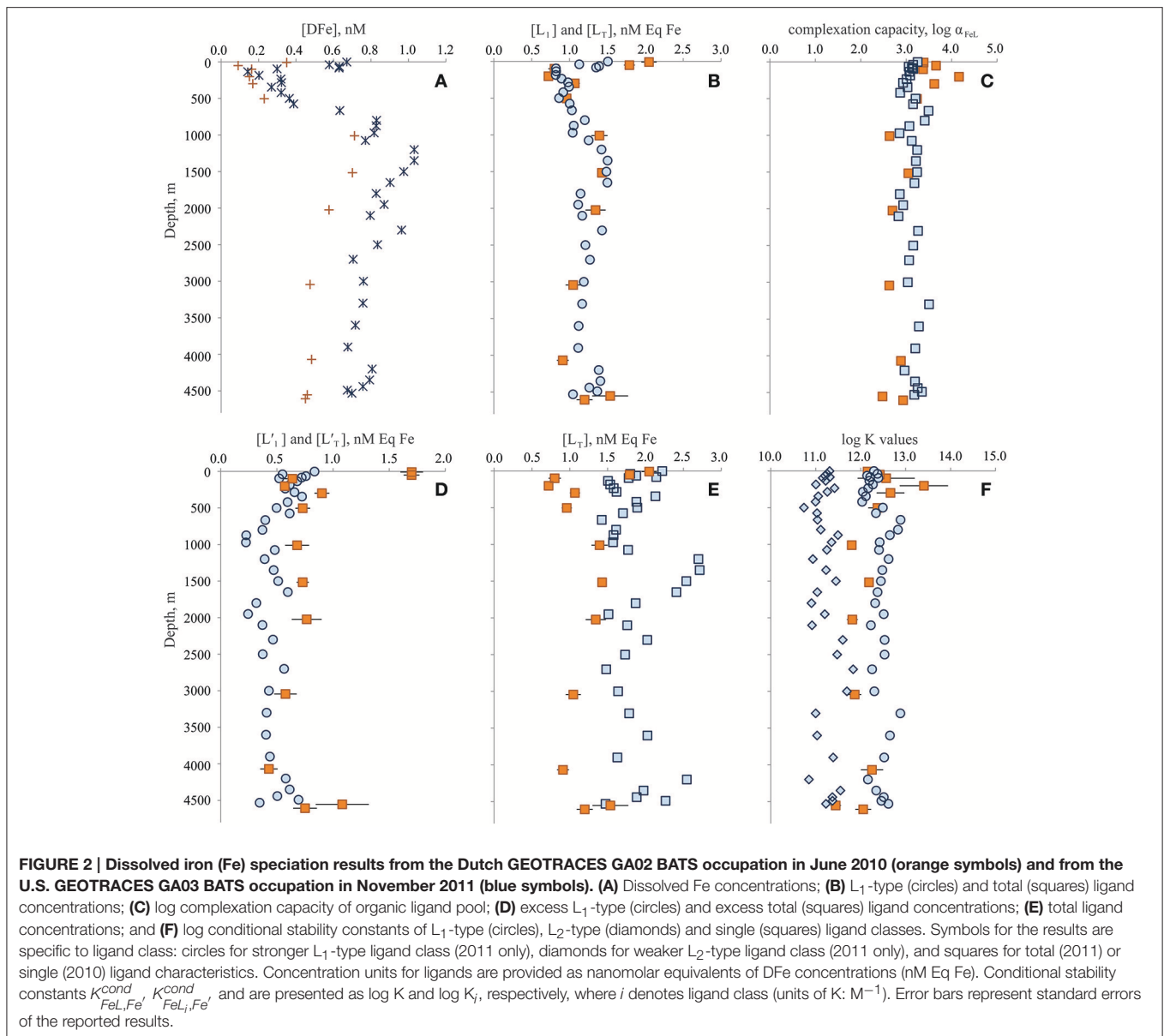
Dissolved Fe speciation results from separate occupations of Crossover Station A/BATS by independent analytical groups were compared in terms of dissolved Fe-binding ligand concentrations ($[L_i]$), their associated conditional stability constants ($K_{FeL_i,Fe'}^{cond}$), and resulting organic complexation capacity (α_{FeL} , where $\alpha_{FeL} = \sum [L'_i] * K_{FeL_i,Fe'}^{cond}$, and $[L'_i] = [L_i] - [DFe]$; see Gledhill and Buck, 2012 and references therein for additional information). These terms were determined by each group from a combination of analyzing samples by CLE-AdCSV to generate titration data and then mathematically deriving the Fe speciation terms from their titration data. The theory behind these interpretation techniques and visualizations of their application to natural samples can be found in the original literature for each method (Gerringa et al., 1995, 2014; Rue and Bruland, 1995) and in a recent interpretation intercalibration of idealized copper speciation data (Pižeta et al., 2015). In this intercomparison exercise, samples were not available for each group to conduct CLE-AdCSV analyses on the same samples. Instead, in addition to comparing final speciation results, the two groups exchanged CLE-AdCSV titration data from the BATS water column and then determined the organic complexation terms for the exchanged data using their own interpretation approach, which allowed a comparison of how interpretation technique influence profile speciation results. As part of this comparison of applying different interpretation techniques to exchanged titration data, the relative contribution of the sensitivity parameter chosen between interpretations was specifically addressed by either including a sensitivity value in the data exchange (“S given”) or not (“S determined”).

Altogether, there are three intercomparison activities reported here: (1) a comparison of reported Fe speciation results from GEOTRACES Crossover Station A/BATS; (2) a comparison of results derived from exchanging CLE-AdCSV titration data from the BATS water column for complete reinterpretation; and (3) a comparison of results after exchanging BATS titration data for the reinterpretation but given the sensitivity value determined by the original analyst for each dataset.

RESULTS

As part of the Dutch and U.S. GEOTRACES programs, the organic complexation of dissolved Fe was determined through the entire water column of the Bermuda Atlantic Time-series Study (BATS) site twice, first in June 2010 (Gerringa et al., 2015) and again in November 2011 (Buck et al., 2015). Dissolved Fe concentrations differed through the water column between the two occupations (**Figure 2A**; Rijkenberg et al., 2014; Sedwick et al., 2015). In both cases, however, organic Fe-binding ligands were reported in excess of DFe concentrations throughout the water column, and thermodynamically stable (“strong”) organic DFe complexes were the dominant chemical form of DFe at all depths (**Figures 2A–F**; Buck et al., 2015; Gerringa et al., 2015).

In June 2010, Gerringa et al. (2015) reported a single ligand class of total concentration range $[L_T] = 0.72\text{--}2.05\text{ nM Eq Fe}$ (average: $1.25 \pm 0.39\text{ nM Eq Fe}$, $n = 13$) over the entire water



column with an average $\log K_{FeL_1,Fe'}^{cond}$ of 12.23 ± 0.49 ($n = 13$). In November 2011, Buck et al. (2015) reported two ligand classes at BATS. The stronger L₁-type ligand class was measured with very similar concentrations ($[L_1] = 0.82\text{--}1.51$ nM Eq Fe, average: 1.16 ± 0.21 nM Eq Fe, $n = 37$) and conditional stability constants (average $\log K_{FeL_1,Fe'}^{cond} = 12.42 \pm 0.23$, $n = 37$) to the single ligand class reported by Gerringa et al. (2015) for this station in June 2010 (Figure 2B). An additional weaker L₂-type ligand class (average $\log K_{FeL_2,Fe'}^{cond} = 11.28 \pm 0.24$) was also detected in these samples (Buck et al., 2015), leading to higher total ligand ($[L_T] = [L_1] + [L_2]$) concentrations ($1.47\text{--}2.41$ nM Eq Fe, average: 1.82 ± 0.24 nM Eq Fe, $n = 37$) in the November 2011 water column than reported by Gerringa et al. (2015; Figure 2E).

Excess ligand concentrations ($[L'_T] = [L_T] - [DFe]$) were highest in the shallowest samples of the June 2010

profile (1.70 nM Eq Fe, $n = 2$) and averaged 0.71 ± 0.17 nM Eq Fe ($n = 11$) through the rest of the water column (Figure 2D). In the November 2011 profile, two ligand classes were determined. Excess L₁-type ligand concentrations ($[L'_1] = [L_1] - [DFe]$) were also higher near the surface (0.72 ± 0.12 nM Eq Fe in upper 85 m, $n = 4$), in November 2011 and averaged 0.48 ± 0.13 nM Eq Fe through the rest of the water column (Figure 2D). Excess total ligand concentrations ($[L'_T] = [L_T] - [DFe] = [L_1] + [L_2] - [DFe]$) in November 2011 averaged 1.15 ± 0.26 nM Eq Fe through the water column. The elevated concentration of an especially strong ligand detected in the upper water column of the June 2010 profile contributed to higher organic complexation capacity ($\log \alpha_{FeL} = 3.57 \pm 0.33$, $n = 6$) in the upper 500 m compared to deeper waters ($\log \alpha_{FeL} = 2.76 \pm 0.20$, $n = 7$; Figure 2).

Below 500 m, however, the measured complexation capacity was similar between the two occupations, if not slightly higher in the November 2011 profile ($\log \alpha_{FeL} = 3.16 \pm 0.18$, $n = 25$; **Figure 2C**).

Reinterpretation Exercise

For the reinterpretation exercise, analysts exchanged CLE-AdCSV titration data and applied the interpretation technique used on their own data to the titration data received from the other group. Applying the combined van den Berg/Ružić and Scatchard linearization approaches (Rue and Bruland, 1995; Buck et al., 2012) to the June 2010 dataset resulted in similar $[L_T]$ and $\log K_{FeL_i, Fe'}^{cond}$ as reported from the original Gerringa et al. (2014)-based interpretation of the same data (**Figures 3A,B**). This agreement was even better when the sensitivity parameter given by Gerringa et al. (2015) was used in the reinterpretation (**Figures 3C,D**). Thus, in the case of the June 2010 dataset, both the original analyst and the reinterpretation results agreed that one ligand class was the best fit for these BATS titrations.

This was not the case for the November 2011 dataset. The Gerringa et al. (2014) non-linear interpretation approach reported predominantly a single ligand class as the best fit to the November 2011 titration data (data not shown). Allowing the determination of two ligand classes from these titration data using this approach resulted in large standard deviations for the results (**Figures 4A,B**). However, as seen in the one ligand class reinterpretation, agreement between the average $[L_i]$ and $\log K_{FeL_i, Fe'}^{cond}$ reported by the two interpretation techniques for this dataset was improved considerably by including the sensitivity

value used in the original interpretation for the data exchange reinterpretation (**Figures 4C,D**). In the November 2011 titration data, curvature evident in the Scatchard plots was consistent with the presence of more than one ligand class (Rue and Bruland, 1995; Buck et al., 2012). The difficulty in quantifying a second ligand class in the Gerringa et al. (2014) non-linear interpretation of the 2011 data may in part reflect insufficient titration points in the interpretation limiting the degrees of freedom available to calculate the additional parameters required of two ligand classes with statistical certainty, regardless of whether the additional ligand class is present (Hudson et al., 2003; Wu and Jin, 2009; Gerringa et al., 2014).

DISCUSSION

Influence of Interpretation Approach on Fe Speciation Results

By swapping CLE-AdCSV titration datasets, analysts in this BATS intercomparison study were able to evaluate how the applied data interpretation approach influenced the speciation results. When determining a single ligand class from BATS titration data, the two interpretation approaches calculated similar ligand concentrations and conditional stability constants for that ligand class (**Figure 4**). Determining two ligand classes, as seen in the November 2011 titration dataset, was more challenging and resulted in poorer agreement between the interpretation approaches, especially for the second (weaker) ligand class (**Figure 5**). In particular, while the average ligand concentrations and conditional stability constants resulting from the two interpretation techniques approached each other, the

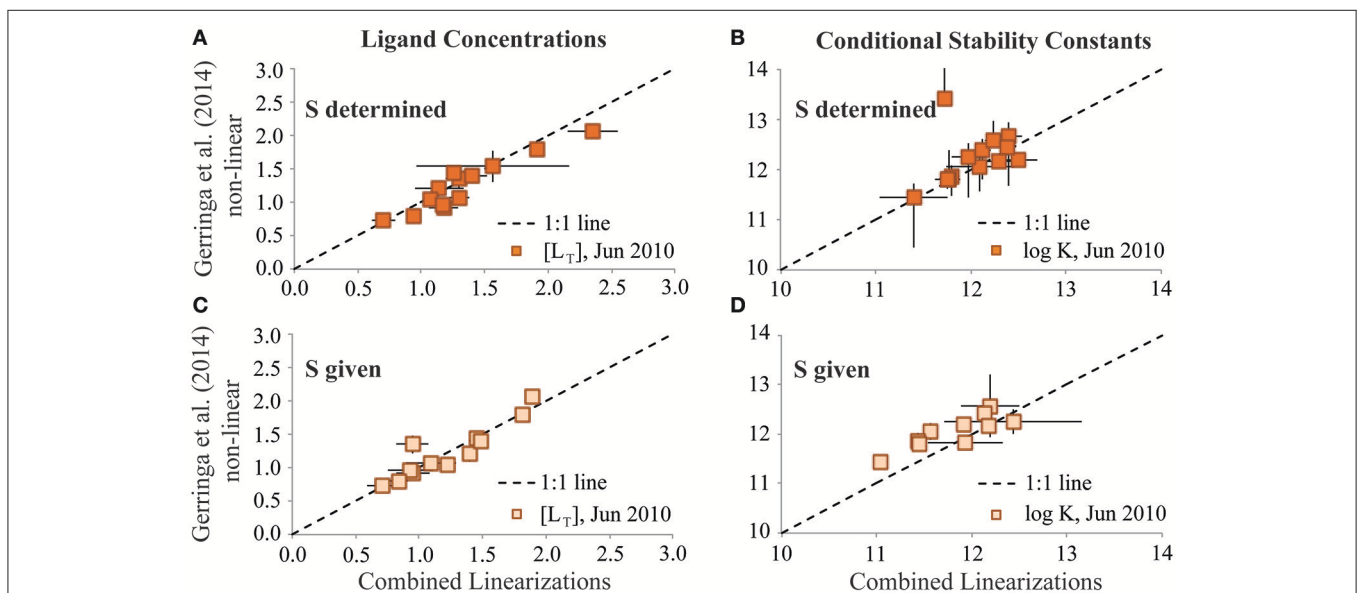
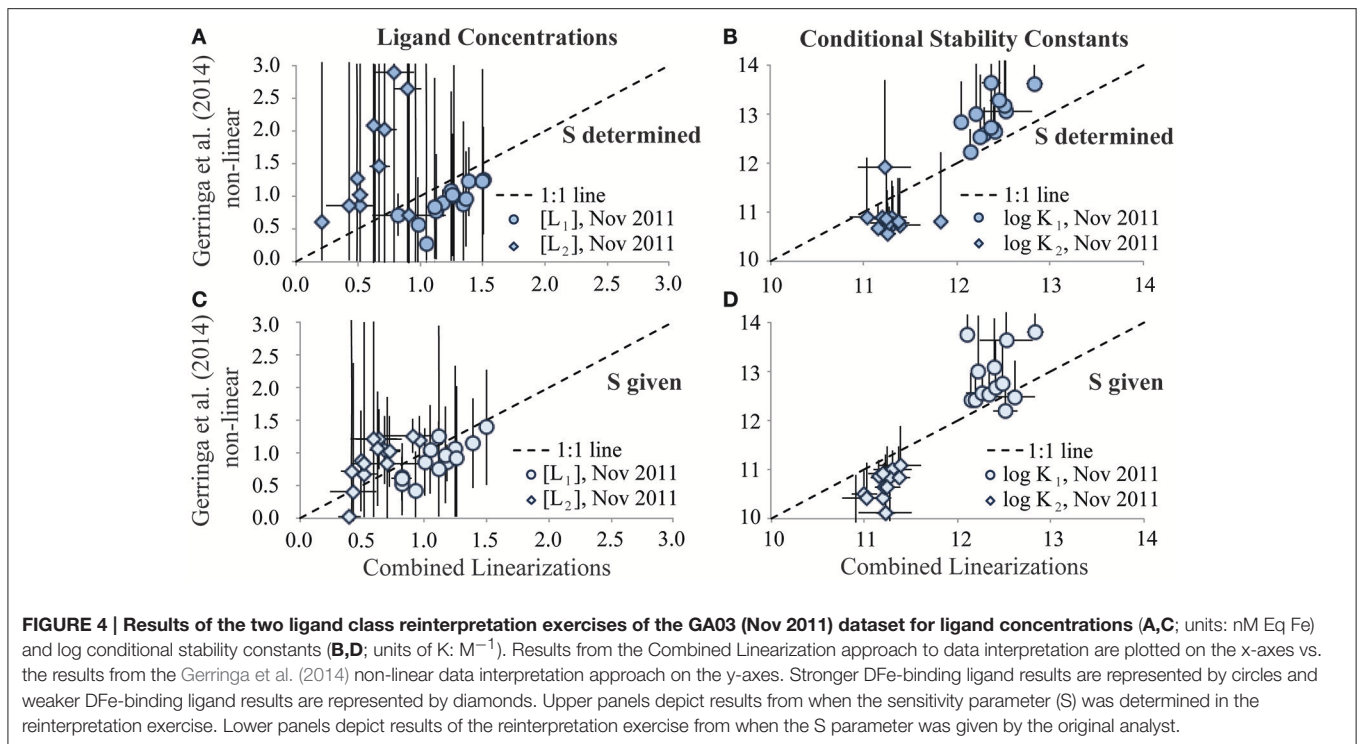


FIGURE 3 | Results of the single ligand class reinterpretation exercises of the GA02 (June 2010) dataset for ligand concentrations (A,C; units: nM Eq Fe) and log conditional stability constants (B,D; units of $K: M^{-1}$). Results from the Combined Linearization approach to data interpretation are plotted on the x-axes vs. the results from the Gerringa et al. (2014) non-linear data interpretation approach on the y-axes. Upper panels depict results from when the sensitivity parameter (S) was determined in the reinterpretation exercise. Lower panels depict results of the reinterpretation exercise from when the S parameter was given by the original analyst.



standard deviations determined for these parameters by the Gerringa et al. (2014) technique were very large (Figure 5). This suggests that despite the curvature in the transformed Scatchard plot, the Gerringa et al. (2014) approach would determine a second ligand class from only 36% of the November 2011 samples.

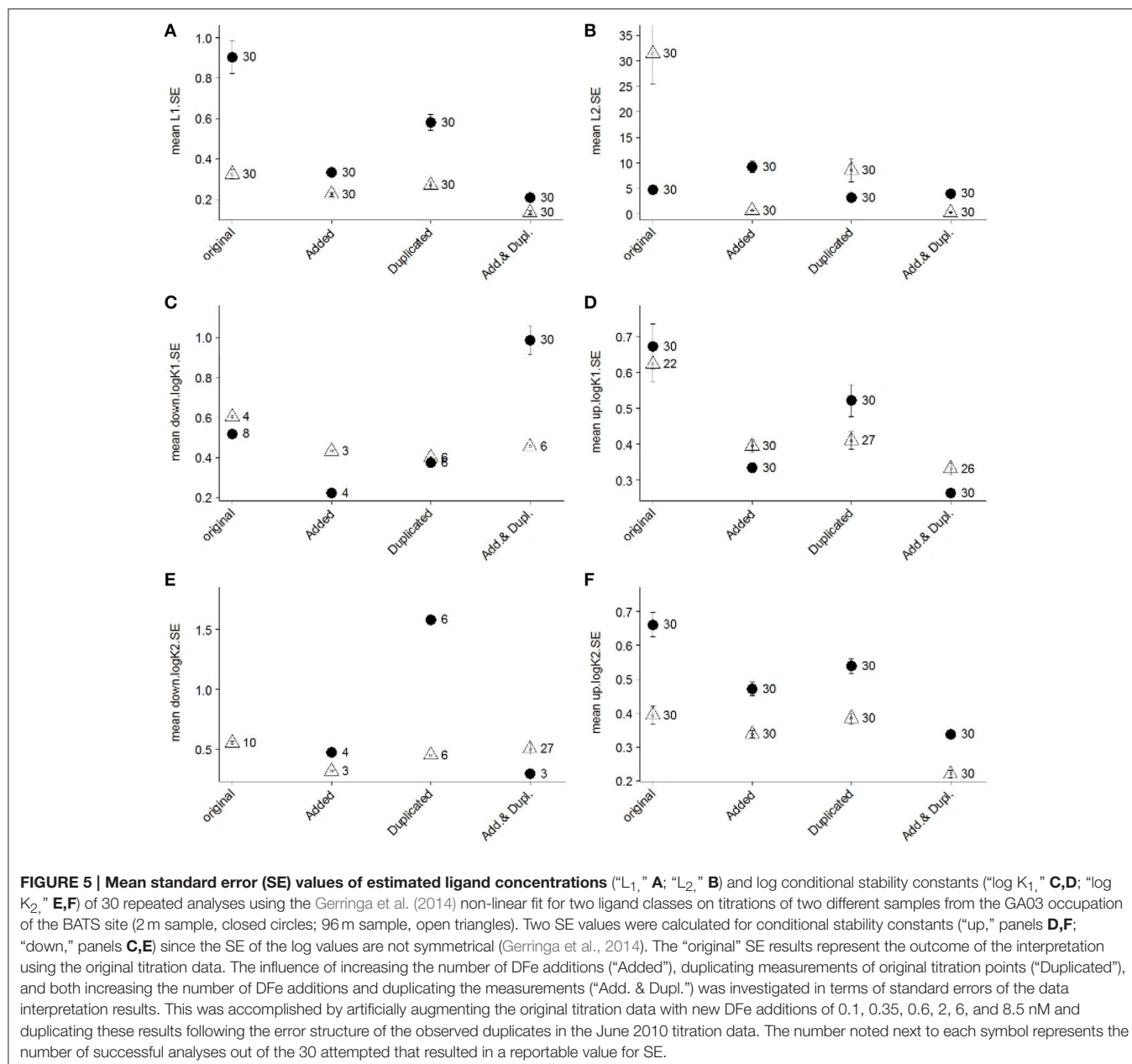
The Gerringa et al. (2014) approach is mathematically robust, requiring at least twelve titration points to determine two ligand classes with confidence—four for each ligand class and four for the linear section of the titration curve to determine sensitivity (Gerringa et al., 2014). The combined linearization approach applied to the November 2011 dataset was not limited by this data structure, as this more traditional technique does not incorporate error calculations in the determination of speciation parameters. Instead, the average and standard deviation of the output from the two linearization techniques (van den Berg/Ružić, Scatchard) has previously been reported from studies using this data interpretation approach (e.g., Buck et al., 2012). However, since the two linearizations are not independent for a given titration dataset and the data fitting errors cannot be taken into account, the standard deviations of their averaged results underestimates the error in the interpretation. Most recently, the average parameter values from the combined linearizations were reported, and standard deviations were reserved to reflect the reproducibility of results derived from multiple independent titrations rather than quality of the titration data fitting (Buck et al., 2015).

In the Gerringa et al. (2014) paper, the authors evaluated the influence of numbers of titration points on derived standard deviations for the speciation parameters (see Figure 5 in

Gerringa et al., 2014). In that case, the focus was on determining a single ligand class. It seems clear in the intercomparison here that there were insufficient titration points in the November 2011 dataset to allow for a robust determination of two ligand classes from the data. These titrations consisted of twelve DFe additions, the minimum number recommended for two ligand class determinations in the non-linear transformations (Wu and Jin, 2009; Gerringa et al., 2014). Yet titrating the excess strong DFe-binding ligands that were present in most of the November BATS samples with the first few DFe additions in the analyses left no measurable Fe bound to the added ligand (i.e., FeSA) at the beginning of the titrations, reducing the number of data points available for the interpretation to fewer than twelve.

Moving forward, the Gerringa et al. (2014) and similarly robust data interpretation techniques (Sander et al., 2011; Omanović et al., 2015) are preferred approaches to deriving metal speciation parameters from titration data (Pižeta et al., 2015). Accompanying this shift in interpretation approaches, titration datasets will require more individual data points to allow for the determination of more than one ligand class. This can be accomplished by increasing the number of DFe additions used in the titrations, by analyzing the different DFe additions more than once, or by doing both. Using representative titrations from the November 2011 BATS dataset, we investigated each of these potential modes of increasing titrations points on the standard deviations of results for two ligand classes derived from the Gerringa et al. (2014) approach for data interpretation.

Results of this assessment indicated that the combination of both increasing number of DFe additions and duplicating each titration point measurement resulted in the lowest standard



errors for ligand concentrations and conditional stability constants (Figure 5). Increasing the number of unique DFe additions considerably reduced the standard errors of the results (Figure 5). In practice, however, it can be challenging to anticipate where in the titrations to incorporate these additions as well as to implement sufficient resolution of DFe additions in the curved section of the titrations when excess ligand concentrations are low. Correspondingly, duplicating the measurement of existing DFe additions may be a more practical approach to increasing titration data points, though this approach was not as consistent in improving the precision of results (Figure 5). It might also be necessary in some cases to be satisfied with unknown or relatively large SE values of estimated parameters

or with acknowledging that an additional ligand class probably exists (e.g., when curvature in Scatchard plots is evident) without having sufficient data resolution to resolve the $[L_i]$ or $K_{FeL_i,Fe'}^{cond}$ values.

Overall, the observation of one or two ligand classes in the GEOTRACES BATS datasets for DFe speciation did not result solely from the different interpretation approaches applied. This is evident from the reinterpretation of the June 2010 titration data- applying the combined linearization approach did not elucidate a second ligand class in that data. Instead, the one or two ligand class characteristics of the BATS samples originates from the CLE-AdCSV titrations, with curvature in the November 2011 25 μ M SA Scatchard plots supporting the presence of a second

ligand class in those samples. Where interpretation approach clearly did play a role in the determination of one or two ligand classes was in the reinterpretation of the November 2011 datasets. Regardless of whether two ligand classes were indeed present, the number of data points in those titrations was insufficient to allow the robust determination of two ligand classes using the Gerringa et al. (2014) approach, evident in the large standard deviations of calculated results (Figures 4A–D).

The Particular Importance of the Sensitivity Parameter in Data Interpretation

In the BATS reinterpretation exercises, agreement of results from the different interpretation techniques applied to a given titration dataset was improved considerably by incorporating the sensitivity parameter value from the original interpretation for use in the reinterpretation (Figures 3, 4). These observations highlight the relatively large influence of the sensitivity parameter in titration data interpretation, which is consistent with the results of a previous intercomparison of interpretation approaches for dissolved copper speciation datasets (Pižeta et al., 2015). Surprisingly, when comparing the sensitivity parameter values derived from the two interpretation approaches in the BATS reinterpretation exercises, there were usually not large differences between the sensitivity values (Figures 6A,B). This suggests that even small changes in the sensitivity parameter determined can exert a disproportionate influence on results from the data interpretation. As with all parameters derived from the interpretation of titration data, higher resolution within titration datasets is likely the best way to constrain the determination of this important parameter.

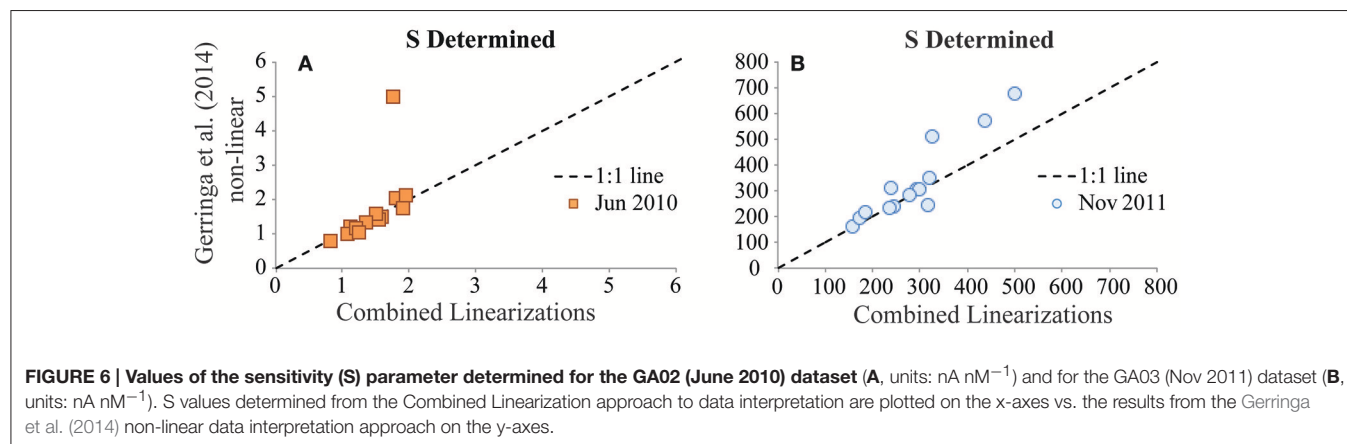
SA, TAC, Suwannee River Fulvic Acid-Type DFe-Binding Ligands, and Analytical Windows

The identification of an additional, weaker ligand class in the 25 μM SA results of the BATS intercomparison exercise appears consistent with the results of a previous intercomparison of DFe speciation techniques conducted as part of the GEOTRACES intercalibration efforts in the central North Pacific (SAFe station) (Buck et al., 2012). In that effort, analysts conducted shipboard

DFe speciation measurements on samples collected from three depths: 125 m (deep chlorophyll max), 1000 and 3000 m. The analysts employing CLE-AdCSV techniques with 10 μM TAC ($\alpha_{\text{Fe}(TAC)_2} = 250$) and 25 μM SA ($\alpha_{\text{FeSA}} = 79$), the same analytical windows employed for the BATS intercomparison here, showed the best agreement in determined ligand concentrations in the 125 m sample. In the 1000 and 3000 m samples, on the other hand, the 10 μM TAC measurements determined roughly half the ligand concentrations measured by the 25 μM SA methods (Buck et al., 2012). Only a single ligand class was reported by all participants in the North Pacific intercomparison, but the curvature of the titration data and the higher ligand concentrations and lower conditional stability constants determined by the 25 μM SA groups were consistent with the 25 μM SA method measuring weaker ligands not determined in the 10 μM TAC analyses.

The influence of freezing DFe speciation samples was also investigated in the previous North Pacific intercomparison exercise (Buck et al., 2012). No significant difference was found in that study between the DFe speciation results from samples analyzed before freezing and after freezing at -20°C , and only one ligand class was identified in all cases (Buck et al., 2012). In the BATS intercomparison, samples collected in November 2011 were stored frozen at -20°C prior to laboratory-based analyses while the samples collected in June 2010 were analyzed shipboard. Given the results of the North Pacific intercomparison (Buck et al., 2012) and the similar observations from an assessment of freezing DFe speciation samples conducted as part of the U.S. GEOTRACES program in the Atlantic (Buck unpublished), the differences in sample storage does not appear to be the best explanation for the presence of an additional weaker DFe-binding ligand class in the November 2011 BATS profile.

In the North Pacific intercomparison, the discrepancy in ligand concentrations and conditional stability constants between the 25 μM SA and the 10 μM TAC results was attributed in part to the presence of humic-type DFe-binding substances (Buck et al., 2012), which were measured at depth at the same central North Pacific station (Laglera and van den Berg, 2009). Humic-type substances, as represented by a Suwannee River Fulvic Acid (SRFA) standard (Arakawa and Aluwihare, 2015)



in AdCSV studies (Laglera et al., 2007), have been shown to serve as an L_2 -type DFe-binding ligand in the coastal Atlantic and the deep Pacific (Laglera and van den Berg, 2009). Of particular relevance to these intercomparison activities, the SRFA standard used to represent these DFe-binding humic substances is masked in CLE-AdCSV measurements made using TAC as the added ligand (Laglera et al., 2011). That is not to say that TAC analyses miss all DFe-binding humic substances, as elevated L_2 -type ligand ($\log K = 11$ – 12) concentrations measured in Arctic outflow waters by TAC were attributed to likely humic-binding substances (Gerringa et al., 2015). However, if DFe-binding ligands analogous to SRFA humic-type substances are present in the BATS samples, they may have been missed by the TAC analyses in June 2010. Indeed, the weaker DFe-binding ligand class determined in the November 2011 dataset had an average conditional stability constant of 11.28 ± 0.24 ($n = 37$), similar to the conditional stability constant determined for SRFA in seawater (11.0, Laglera and van den Berg, 2009).

Finally, the different analytical windows applied by the two groups likely also contributed to the detection of a weaker ligand class of Fe-binding ligands in the $25 \mu\text{M}$ SA ($\alpha_{\text{FeSA}} = 79$) analyses that was not detectable in the $10 \mu\text{M}$ TAC ($\alpha_{\text{Fe(TAC)}_2} = 250$) analyses. The influence of analytical window on speciation results has long been established for copper speciation analyses (Bruland et al., 2000; Buck and Bruland, 2005), where higher analytical windows measure lower concentrations of stronger (i.e., higher conditional stability constant) ligands than lower analytical windows (Bruland et al., 2000). In the Fe speciation measurements at BATS, however, comparable concentrations of the strongest ligand class were determined by both analytical windows while an additional weaker ligand class was determined in the lower analytical window. This apparent discrepancy between the Fe and Cu speciation intercalibrations across analytical windows may simply reflect the different ranges in analytical windows employed- the range is much smaller for Fe ($\alpha_{\text{FeAL}} = 79$ – $250 = 10^{1.9}$ – $10^{2.4}$, this study) than for Cu ($\alpha_{\text{CuAL}} = 10^{2.5}$ – $10^{6.5}$, Bruland et al., 2000). Recent applications of multiple analytical windows for Fe speciation analyses using SA actually depict similar trends as seen in the BATS intercalibration, with lower analytical windows ($\alpha_{\text{FeSA}} = 30, 60$) identifying weaker Fe-binding ligand classes than higher ($\alpha_{\text{FeSA}} = 100, 250$) analytical windows (Bundy et al., 2014, 2015). The application of a lower TAC analytical window has also been shown to result in detection of weaker Fe-binding ligands (Gerringa et al., 2007).

The Speciation of DFe at BATS

Discrepancies in organic complexation results between individual datasets may reflect real seasonal changes at the BATS sampling site, particularly in the upper water column, as has been observed for DFe concentrations (Sedwick et al., 2005). Indeed, the DFe concentrations were quite different between the two GEOTRACES occupations of BATS/GEOTRACES Crossover Station A (Figure 2A; Rijkenberg et al., 2014; Buck et al., 2015; Gerringa et al., 2015; Sedwick et al., 2015). The analytical methods used for the DFe analyses were very similar (Rijkenberg et al., 2014; Buck et al., 2015; Sedwick et al., 2015) and the DFe concentrations results from the

two occupations were successfully intercalibrated and were included in the GEOTRACES Intermediate Data Product (Mawji et al., 2015). Thus, the higher DFe in November 2011 compared to June 2010 in the upper water column may reflect the deposition of North American aerosols with higher fractional solubility of Fe at BATS in the late fall/early winter compared to the predominant deposition of relatively insoluble Saharan dust in the summer months (Sedwick et al., 2007). Previous studies indicate that particles, whether atmospheric, authigenic, biological or resuspended, can greatly influence DFe concentrations and size fractionation in the surface ocean (Sedwick et al., 2005; Buck et al., 2010a,b; Fitzsimmons et al., 2015), and that these influences are largely mediated by the concentrations and conditional stability constants of Fe-binding organic ligands in the water column (Rijkenberg et al., 2008; Wagener et al., 2008; Aguilar-Islas et al., 2010; Boyd et al., 2010; Bundy et al., 2014; Fishwick et al., 2014). The trend of higher DFe in the November 2011 water column was not restricted to the surface ocean though (Figure 2A) and we cannot explain these differences in deeper water masses from seasonality.

The higher DFe in the November 2011 profile at BATS would be expected to influence Fe speciation characteristics depending on the speciation of the DFe increase. The addition of DFe bound to a strong organic ligand (i.e., FeL_1) would increase the concentrations of DFe, L_1 and L_T , while excess ligand (L'_1 and L'_T) concentrations would remain unchanged. On the other hand, the addition of free (inorganic) DFe would titrate ambient stronger ligands (Rijkenberg et al., 2008), decreasing excess ligand concentrations while total ligand concentrations stayed the same. This last case is more consistent with the BATS results, where the total concentrations of stronger L_1 -type ligands were most similar between the two occupations, and average excess stronger ligand concentrations were generally lower in the November 2011 profile with higher DFe. Thus, the difference in DFe between these profiles may represent an addition of inorganic Fe or weakly organically complexed Fe (i.e., FeL_2) to the November 2011 profile, analogous to the dissolution of particulate Fe by ambient strong Fe-binding ligands in the water column or samplers. If the difference in DFe concentrations between the two profiles is simply the result of an analytical offset, however, total ligand concentrations would be affected more than excess ligand concentrations since the change in DFe would not be “seen” by the added ligand (Thuróczy et al., 2010; Gledhill and Buck, 2012). Overall, because DFe is used in the calculation of ligand characteristics and samples were not exchanged for speciation analysis at the different analytical windows applied, it is challenging to delineate between the influences of analytical approach and DFe on the speciation results.

The contamination of TAC with DFe in the June 2010 analyses also complicated the speciation analyses, and in particular the distinction of two ligands. The inadvertently higher first DFe addition from the contamination of TAC may have masked any curvature in the titrations and resulted in loss of information right at the start of these titrations, where the strongest ligand class is typically characterized. However, this bias is not evident in

the intercomparison results. The two profiles agreed best on the concentrations of the strongest DFe-binding ligands (**Figure 2B**), indicating that this strongest ligand class was well-characterized by the two occupations despite the different DFe concentrations between them and the DFe contamination in TAC. Instead, where the two datasets primarily differed was in the total concentrations of ligands measured, with the November 2011 dataset reporting an additional weaker ligand class in excess of DFe, which was not determined in the June 2010 profile. As noted above, the identification of a weaker ligand class in the November 2011 BATS profile likely derives from the different analytical windows applied and from the ability of the salicylaldoxime technique to measure Suwannee River Fulvic Acid (SRFA)-type ligands, which in turn may provide insight into DFe-binding ligand identity in these waters (Laglera and van den Berg, 2009; Laglera et al., 2011).

Beyond the differences in total ligand concentrations resulting from the presence of a weaker ligand class in one of the two BATS profiles, some seasonality may be evinced by differences in the strongest DFe-binding ligands, which otherwise compared well between occupations (**Figure 2B**). For example, in the upper water column, and in particular near the surface of the profiles, the stronger DFe-binding organic ligand concentrations were higher, with higher conditional stability constants, in the June 2010 profile compared to November 2011 (**Figures 2B,F**). These higher strong ligand concentrations resulted in a nearly order of magnitude higher DFe complexation capacity (α_{FeL}) in the upper 500 m of the water column in June 2010 (**Figure 2C**). Below 500 m and through the rest of the water column, $\log \alpha_{FeL}$ was higher in the November 2011 profile (**Figure 2C**), reflecting the additional complexation capacity gained from the weaker ligand class determined in those samples. This weaker ligand class was also present in the upper water column samples of the November 2011 profile, though clearly the strongest DFe-binding ligands dominated organic complexation capacity of DFe in these waters.

CONCLUSIONS

The two occupations of the GEOTRACES Crossover Station A at the Bermuda Atlantic Time-series Study (BATS) site highlight the ubiquitous presence of organic DFe-binding ligands in the North Atlantic water column. The two analytical approaches showed excellent agreement in characterizing the strongest DFe-binding organic ligands throughout the profiles, independent of the considerable differences in DFe concentrations or the different CLE-AdCSV and data interpretation approaches between the two occupations. Given the importance of the strongest DFe-binding organic ligands in complexing ambient DFe and governing DFe cycling processes, these results are encouraging for continued integration of organic complexation datasets. A primary distinction in speciation results between the two datasets is the presence of a second weaker DFe-binding ligand class identified in the November 2011 profile that was not characterized in the June 2010 profile. Independent studies of humic-type substances suggest that this discrepancy may reflect

a difference in the abilities of the added ligands employed in the CLE-AdCSV measurements to detect Suwannee River Fulvic Acid-type DFe-binding ligands in seawater. If this is indeed the case, it suggests that these SRFA-type ligands are a component of the weaker DFe-binding ligand pool at BATS, though it is also clear that the strongest DFe-binding organic ligands dominate the organic complexation capacity in these profiles. The lower analytical window applied to the November 2011 speciation analyses may also have contributed to the detection of a weaker ligand class in that profile.

In swapping CLE-AdCSV titration data and conducting reinterpretation exercises between the two groups, it became apparent that the number of number of titration points and the sensitivity parameter values employed in the interpretation substantially influenced the DFe speciation results calculated from a given titration. As was already concluded by Gerringa et al. (2014), without a suitable number of titration data points, interpretation techniques that take into account data fitting errors either will not allow characterization of more than one ligand class and/or will return high standard errors of the results, both resulting from inadequate data structure (degrees of freedom) provided by the titration data. Correspondingly, increasing the number of DFe additions in CLE-AdCSV analyses to generate at least 12 non-zero titration data points whenever possible and even duplicating titration data analyses can substantially increase precision in calculated results. The emergence of new and increasingly robust data interpretation techniques for speciation measurements allows for increasingly precise characterizations of the DFe-binding ligand pool in the oceans, and facilitating the availability of CLE-AdCSV titration datasets for use in reinterpretation exercises is encouraged to continue development in this area. Including the sensitivity (*S*) parameter value used in original interpretations was found to be especially useful for evaluating the results from reinterpretation exercises. This parameter in particular exerted a disproportionate influence on results, with small discrepancies in *S* leading to larger deviations in ligand concentrations and conditional stability constants. These results emphasize the importance of consistent determination of *S* in CLE-AdCSV analyses.

There was excellent agreement in characterizations of the strongest DFe-binding organic ligands in the BATS profiles between the two occupations. Differences in the concentrations and conditional stability constants of these stronger Fe-binding ligands in the upper 500 m of the water column, and the resulting differences in the organic complexation capacity for DFe, point to seasonality of DFe speciation at BATS. In June 2010, higher concentrations of stronger DFe-binding ligands in the upper water column resulted in a nearly order of magnitude of increase in DFe complexation capacity compared to the November 2011 profile in these waters. This may reflect strong DFe-binding ligand production in response to Saharan dust deposition, as has been observed in previous studies in the Eastern Atlantic and Mediterranean, though in general the interactions between Fe speciation, organic ligands and natural particles are poorly understood. Moving forward, the combination of targeted process studies and basin-scale surveys of DFe-binding ligand distributions, as exemplified by the ongoing GEOTRACES

program, is critical for deciphering the complex biogeochemistry of Fe in the oceans as well as the biogeochemistry of the organic ligands that play such an important role in Fe cycling.

Recommendations from This Fe Speciation Intercomparison Exercise:

1. Expand titrations to include at least 12 non-zero titration points. Given the seeming ubiquitous presence of excess Fe-binding organic ligands in seawater, this may require more than 12 DFe additions in each titration.
2. Apply non-linear data interpretation approaches (Sander et al., 2011; Gerringa et al., 2014; Omanović et al., 2015; Pižeta et al., 2015) in order to quantify errors in data fitting whenever titration data structure allows.
3. Share raw titration data for reinterpretation across groups and include value of sensitivity parameter determined in the interpretation.
4. Depending on water budgets, the application of multiple analytical windows and/or shared water samples allow for direct comparison across CLE-AdCSV techniques. Alternatively, analysts may prefer to choose a common analytical window to apply.

REFERENCES

- Aguilar-Islas, A. M., Wu, J., Rember, R., Johansen, A. M., and Shank, L. M. (2010). Dissolution of aerosol-derived iron in seawater: leach solution chemistry, aerosol type, and colloidal iron fraction. *Mar. Chem.* 120, 25–33. doi: 10.1016/j.marchem.2009.01.011
- Arakawa, N., and Aluwihare, L. (2015). Direct identification of diverse alicyclic terpenoids in Suwannee River Fulvic Acid. *Environ. Sci. Technol.* 49, 4097–4105. doi: 10.1021/es5055176
- Boyd, P. W., Ibanami, E., Sander, S. G., Hunter, K. A., and Jackson, G. A. (2010). Remineralization of upper ocean particles: implications for iron biogeochemistry. *Limnol. Oceanogr.* 55, 1271–1288. doi: 10.4319/lo.2010.55.3.1271
- Boyd, P. W., Jickells, T., Law, C. S., Blain, S., Boyle, E. A., Buesseler, K. O., et al. (2007). Mesoscale iron enrichment experiments 1993–2005: synthesis and future directions. *Science* 315, 612–617. doi: 10.1126/science.1131669
- Bruland, K. W., Rue, E. L., Donat, J. R., Skrabal, S. A., and Moffett, J. W. (2000). Intercomparison of voltammetric techniques to determine the chemical speciation of dissolved copper in a coastal sample. *Anal. Chim. Acta* 405, 99–113. doi: 10.1016/S0003-2670(99)00675-3
- Buck, C. S., Landing, W. M., and Resing, J. A. (2010a). Particle size and aerosol iron solubility: a high-resolution analysis of Atlantic aerosols. *Mar. Chem.* 120, 14–24. doi: 10.1016/j.marchem.2008.11.002
- Buck, C. S., Landing, W. M., Resing, J. A., and Measures, C. I. (2010b). The solubility and deposition of aerosol Fe and other trace elements in the North Atlantic Ocean: Observations from the A16N CLIVAR/CO2 repeat hydrography section. *Mar. Chem.* 120, 57–70. doi: 10.1016/j.marchem.2008.08.003
- Buck, K. N., and Bruland, K. W. (2005). Copper speciation in San Francisco Bay: a novel approach using multiple analytical windows. *Mar. Chem.* 96, 185–198. doi: 10.1016/j.marchem.2005.01.001
- Buck, K. N., Lohan, M. C., Berger, C. J. M., and Bruland, K. W. (2007). Dissolved iron speciation in two distinct river plumes and an estuary: implications for riverine iron supply. *Limnol. Oceanogr.* 52, 843–855. doi: 10.4319/lo.2007.52.2.0843

AUTHOR CONTRIBUTIONS

KB generated the November 2011 dissolved Fe speciation dataset from BATS as part of the U.S. GEOTRACES program in the North Atlantic. LG and MR generated the June 2010 dissolved Fe speciation dataset from BATS as part of the Dutch GEOTRACES program in the West Atlantic. KB and MR each created figures for the manuscript, and MR completed the statistical analyses of the titration data structure. KB was the lead writer of the manuscript, supported by equal writing contributions from MR and LG.

ACKNOWLEDGMENTS

The authors thank the Captains and crews of the R/V Knorr (KN204; Captain Kent Sheasley) and the R/V Pelagia (64PE321; Captain Bert Puijman) for their support and hospitality during these field studies. We further thank Hein de Baar and our collaborators in the GEOTRACES program, as well as our collaborators in our respective institutions, for making this work possible. This work was funded to KB by grants from the U.S. National Science Foundation, OCE-0927453 and OCE-1441969, and to LG and MR by grants from the Dutch funding agency ZKO, project number 839.08.410.

- Buck, K. N., Moffett, J. W., Barbeau, K. A., Bundy, R. M., Kondo, Y., and Wu, J. (2012). The organic complexation of iron and copper: an intercomparison of competitive ligand exchange-adsorptive cathodic stripping voltammetry (CLE-ACSV) techniques. *Limnol. Oceanogr. Methods* 10, 496–515. doi: 10.4319/lom.2012.10.496
- Buck, K. N., Sohst, B., and Sedwick, P. N. (2015). The organic complexation of dissolved iron along the U.S. GEOTRACES (GA03) North Atlantic Section. *Deep Sea Res. II* 116, 152–165. doi: 10.1016/j.dsr2.2014.11.016
- Bundy, R. M., Abdulla, H. A. N., Hatcher, P. G., Biller, D. V., Buck, K. N., and Barbeau, K. A. (2015). Iron-binding ligands and humic substances in the San Francisco Bay estuary and estuarine-influenced shelf regions of coastal California. *Mar. Chem.* 173, 183–194. doi: 10.1016/j.marchem.2014.11.005
- Bundy, R. M., Biller, D. V., Buck, K. N., Bruland, K. W., and Barbeau, K. A. (2014). Distinct pools of dissolved iron-binding ligands in the surface and benthic boundary layer of the California Current. *Limnol. Oceanogr.* 59, 769–787. doi: 10.4319/lo.2014.59.3.0769
- Cheah, S.-F., Kraemer, S. M., Cervini-Silva, J., and Sposito, G. (2003). Steady-state dissolution kinetics of goethite in the presence of desferrioxamine B and oxalate ligands: implications for the microbial acquisition of iron. *Chem. Geol.* 198, 63–75. doi: 10.1016/S0009-2541(02)00421-7
- Croot, P. L., and Johansson, M. (2000). Determination of iron speciation by cathodic stripping voltammetry in seawater using the competing ligand 2-(2-thiazolylazo)-*p*-cresol (TAC). *Electroanalysis* 12, 565–576. doi: 10.1002/(SICI)1521-4109(200005)12:8<565::AID-ELAN565>3.0.CO;2-L
- Cutter, G. A., and Bruland, K. W. (2012). Rapid and noncontaminating sampling system for trace elements in global ocean surveys. *Limnol. Oceanogr. Methods* 10, 425–436. doi: 10.4319/lom.2012.10.425
- Cutter, G., Andersson, P., Codispoti, L., Croot, P., Francois, R., Lohan, M., et al. (eds.). (2010). *Sampling and Sample-Handling Protocols for GEOTRACES Cruises Version 1.0 Edn.* GEOTRACES.
- de Baar, H. J. W., Boyd, P. W., Coale, K. H., Landry, M. R., Tsuda, A., Assmy, P., et al. (2005). Synthesis of iron fertilization experiments: From the iron age in the age of enlightenment. *J. Geophys. Res. Oceans* 110:C09S16. doi: 10.1029/2004JC002601
- de Baar, H. J. W., Timmermans, K. R., Laan, P., De Porto, H. H., Ober, S., Blom, J. J., et al. (2008). Titan: a new facility for ultraclean sampling of trace elements

- and isotopes in the deep oceans in the international Geotraces program. *Mar. Chem.* 111, 4–21. doi: 10.1016/j.marchem.2007.07.009
- Ellwood, M. J., and van den Berg, C. M. G. (2001). Determination of organic complexation of cobalt in seawater by cathodic stripping voltammetry. *Mar. Chem.* 75, 33–47. doi: 10.1016/S0304-4203(01)00024-X
- Fishwick, M. P., Sedwick, P. N., Lohan, M. C., Worsfold, P. J., Buck, K. N., Church, T. M., et al. (2014). The impact of changing surface ocean conditions on the dissolution of aerosol iron. *Global Biogeochem. Cycles* 28, 1235–1250. doi: 10.1002/2014GB004921
- Fitzsimmons, J. N., Bundy, R. M., Al-Subia, S. N., Barbeau, K. A., and Boyle, E. A. (2015). The composition of dissolved iron in the dusty surface ocean: an exploration using size-fractionated iron-binding ligands. *Mar. Chem.* 174, 125–135. doi: 10.1016/j.marchem.2014.09.002
- Gerringa, L. J. A., Herman, P. M. J., and Poortvliet, T. C. W. (1995). Comparison of the linear van den Berg/Ruzić transformation and a non-linear fit of the Langmuir isotherm applied to Cu speciation data in the estuarine environment. *Mar. Chem.* 48, 131–142. doi: 10.1016/0304-4203(94)00041-B
- Gerringa, L. J. A., Rijkenberg, M. J. A., Schoemann, V., Laan, P., and de Baar, H. J. W. (2015). Organic complexation of iron in the West Atlantic Ocean. *Mar. Chem.* 177, 434–446. doi: 10.1016/j.marchem.2015.04.007
- Gerringa, L. J. A., Rijkenberg, M. J. A., Thuróczy, C.-E., and Maas, L. R. M. (2014). A critical look at the calculation of the binding characteristics and concentration of iron complexing ligands in seawater with suggested improvements. *Environ. Chem.* 11, 114–136. doi: 10.1071/EN13072
- Gerringa, L. J. A., Rijkenberg, M. J. A., Wolterbeek, H. T., Verburg, T. G., Boye, M., and de Baar, H. J. W. (2007). Kinetic study reveals weak Fe-binding ligand, which affects the solubility of Fe in the Scheldt estuary. *Mar. Chem.* 103, 30–45. doi: 10.1016/j.marchem.2006.06.002
- Gledhill, M., and Buck, K. N. (2012). The organic complexation of iron in the marine environment: a review. *Front. Microbiol.* 3:69. doi: 10.3389/fmicb.2012.00069
- Gledhill, M., and van den Berg, C. M. G. (1994). Determination of complexation of iron (III) with natural organic complexing ligands in seawater using cathodic stripping voltammetry. *Mar. Chem.* 47, 41–54. doi: 10.1016/0304-4203(94)90012-4
- Hopkinson, B. M., and Morel, F. M. M. (2009). The role of siderophores in iron acquisition by photosynthetic marine microorganisms. *Biometals* 22, 659–669. doi: 10.1007/s10534-009-9235-2
- Hudson, R. J. M., Rue, E. L., and Bruland, K. W. (2003). Modeling complexometric titrations of natural water samples. *Environ. Sci. Technol.* 37, 1553–1562. doi: 10.1021/es025751a
- Johnson, K. S., Boyle, E., Bruland, K. W., Coale, K. H., Measures, C., Moffett, J. W., et al. (2007). The SAFe iron intercomparison cruise: an international collaboration to develop dissolved iron in seawater standards. *EOS* 88, 131–132. doi: 10.1029/2007EO110003
- Kuma, K., Nishioka, J., and Matsunaga, K. (1996). Controls on iron(III) hydroxide solubility in seawater: the influence of pH and natural organic chelators. *Limnol. Oceanogr.* 41, 396–407. doi: 10.4319/lo.1996.41.3.0396
- Laglera, L. M., Battaglia, G., and van den Berg, C. M. G. (2007). Determinations of humic substances in natural waters by cathodic stripping voltammetry of their complexes with iron. *Anal. Chim. Acta* 599, 58–66. doi: 10.1016/j.aca.2007.07.059
- Laglera, L. M., Battaglia, G., and van den Berg, C. M. G. (2011). Effect of humic substances on the iron speciation in natural waters by CLE/CSV. *Mar. Chem.* 127, 134–143. doi: 10.1016/j.marchem.2011.09.003
- Laglera, L. M., Downes, J., and Santos-Echeandía, J. (2013). Comparison and combined use of linear and non-linear fitting for the estimation of complexing parameters from metal titrations of estuarine samples by CLE/AdCSV. *Mar. Chem.* 155, 102–112. doi: 10.1016/j.marchem.2013.06.005
- Laglera, L. M., and van den Berg, C. M. G. (2009). Evidence for geochemical control of iron by humic substances in seawater. *Limnol. Oceanogr.* 54, 610–619. doi: 10.4319/lo.2009.54.2.0610
- Liu, X., and Millero, F. J. (2002). The solubility of iron in seawater. *Mar. Chem.* 77, 43–54. doi: 10.1016/S0304-4203(01)00074-3
- Maldonado, M. T., Strzepek, R. F., Sander, S., and Boyd, P. W. (2005). Acquisition of iron bound to strong organic complexes, with different Fe binding groups and photochemical reactivities, by plankton communities in Fe-limited subantarctic waters. *Global Biogeochem. Cycles* 19:GB4S23. doi: 10.1029/2005GB002481
- Mawji, E., Schlitzer, R., Dodas, E. M., Abadie, C., Abouchami, W., Anderson, R. F., et al. (2015). The GEOTRACES intermediate data product 2014. *Mar. Chem.* 177(Pt 1), 1–8. doi: 10.1016/j.marchem.2015.04.005
- Mendez, J., Guieu, C., and Adkins, J. (2010). Atmospheric input of manganese and iron to the ocean: seawater dissolution experiments with Saharan and North American dusts. *Mar. Chem.* 120, 34–43. doi: 10.1016/j.marchem.2008.08.006
- Omanović, D., Garnier, C., and Pižeta, I. (2015). ProMCC: an all-in-one tool for trace metal complexation studies. *Mar. Chem.* 173, 25–39. doi: 10.1016/j.marchem.2014.10.011
- Pižeta, I., Sander, S. G., Hudson, R. J. M., Omanovic, D., Baars, O., Barbeau, K. A., et al. (2015). Interpretation of complexometric titration data: an intercomparison of methods for estimating models of trace metal complexation by natural organic ligands. *Mar. Chem.* 173, 3–24. doi: 10.1016/j.marchem.2015.03.006
- Rijkenberg, M. J., Middag, R., Laan, P., Gerringa, L. J., van Aken, H. M., Schoemann, V., et al. (2014). The distribution of dissolved iron in the West Atlantic Ocean. *PLoS ONE* 9:e101323. doi: 10.1371/journal.pone.0101323
- Rijkenberg, M. J. A., Powell, C. F., Dall'Osto, M., Nielsdottir, M. C., Patey, M. D., Hill, P. G., et al. (2008). Changes in iron speciation following a Saharan dust event in the tropical North Atlantic Ocean. *Mar. Chem.* 110, 56–67. doi: 10.1016/j.marchem.2008.02.006
- Rue, E. L., and Bruland, K. W. (1995). Complexation of iron(III) by natural organic ligands in the Central North Pacific as determined by a new competitive ligand equilibration adsorptive cathodic stripping voltammetric method. *Mar. Chem.* 50, 117–138. doi: 10.1016/0304-4203(95)00031-L
- Rue, E. L., and Bruland, K. W. (1997). The role of organic complexation on ambient iron chemistry in the equatorial Pacific Ocean and the response of a mesoscale iron addition experiment. *Limnol. Oceanogr.* 42, 901–910. doi: 10.4319/lo.1997.42.5.0901
- Ruzić, I. (1982). Theoretical aspects of the direct titration of natural waters and its information yield for trace metal speciation. *Anal. Chim. Acta* 140, 99–113. doi: 10.1016/S0003-2670(01)95456-X
- Sander, S. G., Hunter, K. A., Harms, H., and Wells, M. (2011). Numerical approach to speciation and estimation of parameters used in modeling trace metal bioavailability. *Environ. Sci. Technol.* 45, 6388–6395. doi: 10.1021/es200113v
- Scatchard, G. (1949). The attractions of proteins for small molecules and ions. *Ann. N. Y. Acad. Sci.* 51, 660–672. doi: 10.1111/j.1749-6632.1949.tb27297.x
- Sedwick, P. N., Church, T. M., Bowie, A. R., Marsay, C. M., Ussher, S. J., Achilles, K. M., et al. (2005). Iron in the Sargasso Sea (Bermuda Atlantic Time-series Study region) during summer: eolian imprint, spatiotemporal variability, and ecological implications. *Global Biogeochem. Cycles* 19:GB4006. doi: 10.1029/2004GB002445
- Sedwick, P. N., Sholkovitz, E. R., and Church, T. M. (2007). Impact of anthropogenic combustion emissions on the fractional solubility of aerosol iron: evidence from the Sargasso Sea. *Geochem. Geophys. Geosyst.* 8:Q10QQ06. doi: 10.1029/2007GC001586
- Sedwick, P. N., Sohst, B. M., Ussher, S. J., and Bowie, A. R. (2015). A zonal picture of the water column distribution of dissolved iron(II) during the U.S. GEOTRACES North Atlantic transect cruise (GEOTRACES GA03). *Deep Sea Res. II* 116, 166–175. doi: 10.1016/j.dsr2.2014.11.004
- Shaked, Y., and Lis, H. (2012). Disassembling iron availability to phytoplankton. *Front. Microbiol.* 3:123. doi: 10.3389/fmicb.2012.00123
- Tagliabue, A., Aumont, O., and Bopp, L. (2014). The impact of different external sources of iron on the global carbon cycle. *Geophys. Res. Lett.* 41, 920–926. doi: 10.1002/2013GL059059
- Thuróczy, C.-E., Gerringa, L. J. A., Klunder, M. B., Middag, R., Laan, P., Timmermans, K. R., et al. (2010). Speciation of Fe in the Eastern North Atlantic Ocean. *Deep Sea Res. I* 57, 1444–1453. doi: 10.1016/j.dsr.2010.08.004

- van den Berg, C. M. G. (1982). Determination of copper complexation with natural organic ligands in sea water by equilibrium with MnO_2 : I. theory. *Mar. Chem.* 11, 307–322. doi: 10.1016/0304-4203(82)90028-7
- Wagener, T., Pulido-Villena, E., and Guieu, C. (2008). Dust iron dissolution in seawater: results from a one-year time-series in the Mediterranean Sea. *Geophys. Res. Lett.* 35:L16601. doi: 10.1029/2008GL034581
- Wu, J., and Jin, M. (2009). Competitive ligand exchange voltammetric determination of iron organic complexation in seawater in two-ligand case: examination of accuracy using computer simulation and elimination of artifacts using iterative non-linear multiple regression. *Mar. Chem.* 114, 1–10. doi: 10.1016/j.marchem.2009.03.001

Conflict of Interest Statement: The authors declare that the research was conducted in the absence of any commercial or financial relationships that could be construed as a potential conflict of interest.

Copyright © 2016 Buck, Gerringa and Rijkenberg. This is an open-access article distributed under the terms of the Creative Commons Attribution License (CC BY). The use, distribution or reproduction in other forums is permitted, provided the original author(s) or licensor are credited and that the original publication in this journal is cited, in accordance with accepted academic practice. No use, distribution or reproduction is permitted which does not comply with these terms.



Determination of the Side-Reaction Coefficient of Desferrioxamine B in Trace-Metal-Free Seawater

Johan Schijf^{1*} and Shannon M. Burns^{2,3}

¹ Chesapeake Biological Laboratory, University of Maryland Center for Environmental Science, Solomons, MD, USA,

² Department of Marine Sciences, University of Georgia, Athens, GA, USA, ³ College of Marine Science, University of South Florida, St. Petersburg, FL, USA

OPEN ACCESS

Edited by:

Sylvia Gertrud Sander,
University of Otago, New Zealand

Reviewed by:

Robert J. M. Hudson,
University of Illinois at
Urbana-Champaign, USA
David Turner,
University of Gothenburg, Sweden

*Correspondence:

Johan Schijf
schijf@cbl.umces.edu

Specialty section:

This article was submitted to
Marine Biogeochemistry,
a section of the journal
Frontiers in Marine Science

Received: 31 March 2016

Accepted: 20 June 2016

Published: 13 July 2016

Citation:

Schijf J and Burns SM (2016)
Determination of the Side-Reaction
Coefficient of Desferrioxamine B in
Trace-Metal-Free Seawater.
Front. Mar. Sci. 3:117.
doi: 10.3389/fmars.2016.00117

Electrochemical techniques like adsorptive cathodic stripping voltammetry with competitive ligand equilibration (ACSV-CLE) can determine total concentrations of marine organic ligands and their conditional binding constants for specific metals, but cannot identify them. Individual organic ligands, isolated from microbial cultures or biosynthesized through genomics, can be structurally characterized via NMR and tandem MS analysis, but this is tedious and time-consuming. A complementary approach is to compare known properties of natural ligands, particularly their conditional binding constants, with those of model organic ligands, measured under suitable conditions. Such comparisons cannot be meaningfully interpreted unless the side-reaction coefficient (SRC) of the model ligand in seawater is thoroughly evaluated. We conducted series of potentiometric titrations, in non-coordinating medium at seawater ionic strength (0.7 M NaClO₄) over a range of metal:ligand molar ratios, to study complexation of the siderophore desferrioxamine B (DFOB) with Mg and Ca, for which it has the highest affinity among the major seasalt cations. From similar titrations of acetohydroxamic acid in the absence and presence of methanesulfonate (mesylate), it was determined that Mg and Ca binding to this common DFOB counter-ion is not strong enough to interfere with the DFOB titrations. Stability constants were measured for all DFOB complexes with Mg and Ca including, for the first time, the bidentate complexes. No evidence was found for Mg and Ca coordination with the DFOB terminal amine. From the improved DFOB speciation, we calculated five SRCs for each of the five (de)protonated forms of DFOB in trace-metal-free seawater, yet we also present a more convenient definition of a single SRC that allows adjustment of all DFOB stability constants to seawater conditions, no matter which of these forms is selected as the “component” (reference species). An example of Cd speciation in seawater containing DFOB illustrates the non-trivial use of different SRCs for polyprotic, polydentate organic ligands.

Keywords: desferrioxamine B, siderophore, potentiometric titration, stability constant, side-reaction coefficient, seawater, magnesium, calcium

INTRODUCTION

Organic ligands dominate the solution speciation in seawater of many trace metals, notably Fe (Rue and Bruland, 1995), Co (Baars and Croot, 2015), Ni (van den Berg and Nimmo, 1987), Cu (Jacquot et al., 2013), Zn (Jakuba et al., 2012), Cd (Baars et al., 2014), and Pb (Capodaglio et al., 1998). Ligand concentrations and conditional stability constants can be measured for specific metals using electrochemical techniques (Pizeta et al., 2015), but the identity of these molecules remains largely unknown. Whereas for several metals a division has traditionally been made into a class of strong ligands (L1) and a more abundant class of weaker ligands (L2), based on the observed stability constants (Coale and Bruland, 1988), it has been argued that such divisions are an instrumental artifact and actually reflect a continuum of compounds spanning a broad window of metal affinities (Town and Filella, 2000). Evidence exists, particularly in coastal waters, for a prominent role in organic Fe and Cu complexation played by humic acids (Bundy et al., 2015; Whitby and van den Berg, 2015), an ill-defined assemblage of large, non-specific ligands that are refractory breakdown products of marine, or possibly terrestrial, organic matter.

Nonetheless, marine microbes doubtlessly make unique ligands to regulate the bioavailability or, in some cases, the toxicity of various metals. A plain colorimetric assay revealed widespread bacterial utilization of compounds with hydroxamate functionality (Trick, 1989). By analogy with terrestrial bacteria, fungi, and plants (Neilands, 1981; Neilands and Leong, 1986), these were provisionally categorized as siderophores, which facilitate Fe(III) acquisition although they have also been implicated in Cu(II) binding (McKnight and Morel, 1980; Springer and Butler, 2016). Advanced organic mass spectrometry (ESI-MS) techniques (McCormack et al., 2003) have shown that desferrioxamines, a family of trihydroxamate siderophores, occur at low-pM concentrations in surface waters throughout much of the Atlantic Ocean (Mawji et al., 2008). However, most marine siderophores are structurally very different from terrestrial analogs, even if they contain the same functional groups (Vraspir and Butler, 2009), driving a search for novel amphiphilic ligands, several of which have now been isolated from Fe-limited cultures (Martinez et al., 2000; Kem et al., 2014), or biosynthesized through genomics (Zane et al., 2014). More sophisticated procedures are being developed for detecting organic ligands in seawater, either linking conventional ESI-MS with metal-specific extractions, such as immobilized metal affinity chromatography (Ross et al., 2003) and HPLC-ICP-MS (Boiteau et al., 2013), or relying on the power of ultrahigh-resolution FT-ICR-MS (Waska et al., 2015) for a less targeted approach. Both methods are able to ascertain the presence of known compounds, but cannot readily identify unknowns. Full elucidation of molecular structures still requires painstaking NMR and/or tandem MS analysis (Martin et al., 2006), assuming a sufficient quantity can be separated and purified.

A complementary strategy for characterizing marine organic ligands is to perform in-depth investigations of metal complexes

with commercially available model compounds at seawater ionic strength ($I = 0.7$), in order to construct realistic speciation diagrams for comparison with electrochemical data. While this may not lead to the identification of new ligands, it could help eliminate certain ligand classes from further consideration. Siderophores like desferrioxamine B (DFOB), albeit highly specific for Fe(III), can bind many metals with great affinity (Kruft et al., 2013). Schijf et al. (2015) recently measured stability constants of metal–DFOB complexes in 0.7 M NaClO₄ and found them to be similar to published conditional stability constants of complexes with marine organic ligands for Cu, Zn, and Pb, yet orders of magnitude smaller for Ni and Cd. It has indeed been suggested that natural Cd-specific ligands contain sulfur-bearing groups (Bruland, 1992; Baars et al., 2014) and do not resemble siderophores. Such comparisons are only meaningful if stability constants measured in non-coordinating media can be adjusted to seawater conditions by correction with a suitable side-reaction coefficient (SRC). Wuttig et al. (2013) calculated the SRC of DFOB in seawater as $\log \alpha_{\text{DFOB}} = 6.25$, yielding a “free DFOB” fraction of the order 10^{-6} , which would effectively make it a very weak ligand. While the authors provide no details of the calculation, their SRC is ostensibly expressed in terms of fully deprotonated DFOB, a species that is virtually non-existent in seawater and does not form any complex with most metals. They moreover used data of Farkas et al. (1999), whose regression model does incorporate a spurious complex with the fully deprotonated ligand, probably accounting for the fact that no stability constants were reported for the bidentate Mg–DFOB and Ca–DFOB complex (see the discussion in Schijf et al., 2015).

We present a comprehensive study of pH-dependent DFOB complexation with Mg and Ca, the two major cations that dominate its speciation in trace-metal-free seawater. Our results are derived from series of potentiometric titrations over a range of metal:ligand (M:L) molar ratios in non-coordinating medium at seawater ionic strength (0.7 M NaClO₄) and include, for the first time, stability constants of the bidentate Mg–DFOB and Ca–DFOB complex. We also examined Mg and Ca binding to methanesulfonate (MSA[−]), ordinarily called mesylate, the counter-ion in pharmaceutical DFOB preparations, which was deemed potentially strong enough to compete with DFOB complexation in our experimental solutions. Since the extremely low pK_a of HMSA precludes measurement of the stability of mesylate complexes by potentiometric titration, it was determined instead by comparing the stability of Mg and Ca complexes with the DFOB-like ligand acetohydroxamic acid (HAH) in the absence and presence of NaMSA. The new data are applied to the calculation of a more convenient definition of the SRC in trace-metal-free seawater that allows a direct conversion from free-ion-based to conditional DFOB stability constants, regardless of how they are expressed. A discussion of Cd complexation in seawater, chosen as an example because of its simple, chloride-dominated inorganic speciation, and its comparatively low affinity for DFOB, demonstrates the non-trivial use and (dis)advantages of different SRCs for polyprotic, polydentate organic ligands.

MATERIALS AND METHODS

Preparation of Reagents and Standards

High-purity magnesium oxide (MgO, 99.995%) and calcium oxide (CaO, 99.995%), as well as desferrioxamine B mesylate ($\geq 92.5\%$), acetohydroxamic acid (CH₃CONHOH, 98%), sodium methanesulfonate (CH₃SO₂ONa, 98%), sodium perchlorate hydrate (NaClO₄·xH₂O, 99.99%), sodium chloride (NaCl, 99.999%), and hydrochloric acid (HCl, 0.9952 M) were purchased from Sigma-Aldrich. Concentrated TraceMetal Grade perchloric acid (HClO₄) and nitric acid (HNO₃) were acquired from Thermo Fisher, and certified, carbonate-free NaOH titrants from Brinkmann. All chemicals were used as received and all stock standards and experimental solutions were made up with Milli-Q water (18.2 MΩ cm) from a Millipore Direct-Q 3UV purification system inside a class-100 laminar flow bench.

A pH standard in 0.7 M NaCl was prepared by dissolving 40.9 g of the salt in 1 L of Milli-Q water and setting the pH to 3.000 ± 0.004 with certified HCl. Sodium perchlorate background electrolyte solution of 0.700 ± 0.001 M was produced by dissolving ~ 100 g of the salt in Milli-Q water in an acid-cleaned PMP volumetric flask and adjusting the density according to the empirical equation of Janz et al. (1970). The final solution was acidified to $\text{pH } 3.0 \pm 0.1$ with concentrated HClO₄, which was determined to have a concentration of 11.40 ± 0.02 M by manual titration with 1.005 M NaOH to the phenol red endpoint ($n = 7$). Sodium methanesulfonate was dissolved in Milli-Q water to make a 0.7 M NaMSA solution that was acidified to $\text{pH } 3.0 \pm 0.1$ with concentrated HClO₄. Acetohydroxamic acid was dissolved in unacidified 0.7 M NaClO₄ to make a 100 mM HAH solution. Magnesium oxide and CaO were dissolved separately in acidified 0.7 M NaClO₄ to which concentrated HClO₄ was then slowly added over a period of several days until completely clear standard solutions of about 100 mM were obtained.

Exact pH values of all metal and ligand solutions were determined with the glass electrode of the autotitrator against the pH 3.000 standard. The pH of the unacidified 100 mM HAH solution was found to be 5.26. Due to the slow dissolution of MgO and CaO, the pH of different batches of the 100 mM Mg and Ca standards ranged from 1.25 to 1.62. Exact concentrations of the Mg and Ca standards were determined with an Agilent 7500cx ICP-MS. The primary standards were diluted with 1% HNO₃ and mixed calibration standards containing 0, 1, 2, 5, and 10 ppm Mg, and 0, 5, 10, 25, and 50 ppm Ca were prepared from a custom multi-element solution (100 ppm Mg+K, 500 ppm Na+Ca; SPEX CertiPrep). To avoid the need for detector cross-calibration, all isotope signals were acquired on the analog detector. Isotope signals at mass 24, 25, and 26 were averaged to derive the Mg concentration. The primary Ca isotope at mass 40 overlaps with ⁴⁰Ar⁺ from the plasma, hence signals at mass 42, 43, 44, 46, and 48 were measured, but only the first three were averaged to derive the Ca concentration. Mass 46 showed a severe polyatomic interference, presumably (²³Na²³Na)⁺ from the background electrolyte, and mass 48 may have had a similar interference from (²⁴Mg²⁴Mg)⁺ at low dilution. All isotope signals were normalized to 10 ppm ⁴⁵Sc, added as an internal

standard. Comparison of exact Mg and Ca concentrations with the gravimetric values indicates only minor hydration of the oxides (≤ 0.4 H₂O).

Potentiometric Titrations and Non-linear Regressions

Detailed descriptions of potentiometric titration and non-linear regression protocols are given in Christenson and Schijf (2011) and Schijf et al. (2015). The Brinkmann Metrohm 809 Titrando autotitrator is operated by Tiamo v.1.2.1 software. Solution pH was continuously monitored with a glass combination electrode, which was calibrated before each titration run against the pH 3.000 standard and checked for proper Nernstian behavior by incremental addition of 1 M HCl to 0.7 M NaCl (59.01 ± 0.03 mV/pH, $r^2 = 0.999998$, 9 points). Solutions (50 mL) of HAH, HAH with Mg or Ca, and DFOB with Mg or Ca, either in 0.7 M NaClO₄ or in mixtures of 0.7 M NaMSA and 0.7 M NaClO₄, were dynamically titrated from the initial pH (~ 3) to pH 11 using 1.005 M NaOH, or to pH 10 using 0.1001 M NaOH, at $T = 25.0 \pm 0.1^\circ\text{C}$. For each system a series of titrations was conducted over a range of ligand concentrations or M:L ratios. A DFOB stock standard (10 mL), enough for three runs, was freshly prepared in acidified 0.7 M NaClO₄ on days that DFOB titrations were scheduled. During titrations, the solutions were magnetically stirred and gently sparged with ultrahigh-purity N₂ gas to exclude atmospheric CO₂. To limit evaporation, the N₂ was first humidified in a sealed bubbler filled with Milli-Q water. Two blank titrations in 0.7 M NaClO₄ confirmed the absence of bicarbonate and other acid/base contaminants. Final data for each run were exported as a comma-delimited Excel file, containing cumulative dispensed titrant volumes and electrode readings (in mV) for the pH standard and experimental solution. These files were converted to a format suitable for the computer code FITEQL4.0 (Herbelin and Westall, 1999) by means of an Excel worksheet template.

Non-linear regressions of the titration data were executed with FITEQL4.0, selecting the optimal speciation model for each system. Definitions of all equilibrium constants used in these models are given in **Table 1**. Values at $I = 0.7$ for the first hydrolysis constant, $\log \beta_1^*$, of Mg and Ca, included in every model, were taken from Millero and Schreiber (1982) and are listed in **Table 5**. Adjustable parameters in the regressions are the acid dissociation or stability constants of interest, initial proton excess, $[\text{H}^+]_T^0$, and total ligand concentration. The value of $[\text{H}^+]_T^0$ was allowed to go negative, to accommodate proton deficiencies. For some systems, the total ligand concentration was fixed at the gravimetric value. Total metal (Mg or Ca) concentrations were always fixed at the ICP-MS measurements. The comparative merits of different fits and different speciation models were assessed from the quality-of-fit parameter, WSOS/DF, where values between 0.1 and 20 generally indicate a good fit (Herbelin and Westall, 1999). Values > 20 are considered poor fits, whereas values < 0.1 suggest that the model is under-constrained (i.e., too many adjustable parameters). The data were analyzed in sequence. First, titrations of HAH alone were fit to determine its pK_a value. Using this value, metal+HAH titrations were

TABLE 1 | Definitions of equilibrium constants used throughout the text.

Constant	Equilibrium reaction	Constant	Equilibrium reaction
K_W	$H_2O(l) \rightleftharpoons H^+ + OH^-$	β_1^*	$M^{2+} + H_2O(l) \rightleftharpoons MOH^+ + H^+$
K_{a1}	$H_4L^+ \rightleftharpoons H^+ + H_3L$	K_{SO}	$M(OH)_2(s) \rightleftharpoons M^{2+} + 2OH^-$
K_{a2}	$H_3L \rightleftharpoons H^+ + H_2L^-$	$SO_4\beta_1$	$M^{2+} + SO_4^{2-} \rightleftharpoons MSO_4$
K_{a3}	$H_2L^- \rightleftharpoons H^+ + HL^{2-}$	$L\beta_1$	$M^{2+} + H_3L \rightleftharpoons MH_3L^{2+}$
K_{a4}	$HL^{2-} \rightleftharpoons H^+ + L^{3-}$	$L\beta_2$	$M^{2+} + H_2L^- \rightleftharpoons MH_2L^+$
$K_a(\text{HMSA})$	$\text{HMSA} \rightleftharpoons H^+ + \text{MSA}^-$	$L\beta_3$	$M^{2+} + HL^{2-} \rightleftharpoons \text{MHL}$
$K_a(\text{HAH})$	$\text{HAH} \rightleftharpoons H^+ + \text{AH}^-$	$L\beta_4$	$M^{2+} + L^{3-} \rightleftharpoons \text{ML}^-$
$MSA\beta_1$	$M^{2+} + \text{MSA}^- \rightleftharpoons \text{M}(\text{MSA})^+$	$R_1 (= L\beta_1)$	$M^{2+} + H_3L \rightleftharpoons \text{MH}_3L^{2+}$
$AH\beta_1$	$M^{2+} + \text{AH}^- \rightleftharpoons \text{M}(\text{AH})^+$	R_2	$M^{2+} + H_3L \rightleftharpoons \text{MH}_2L^+ + H^+$
$AH\beta_2$	$M^{2+} + 2\text{AH}^- \rightleftharpoons \text{M}(\text{AH})_2$	R_3	$M^{2+} + H_3L \rightleftharpoons \text{MHL} + 2H^+$
$AH\beta_{11}^*$	$M^{2+} + \text{AH}^- + H_2O(l) \rightleftharpoons \text{M}(\text{AH})\text{OH} + H^+$		

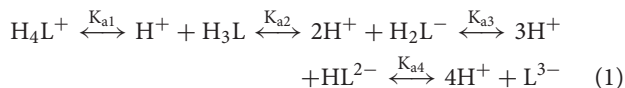
Each constant is shown with its corresponding equilibrium reaction. All reagents and products are aqueous species, unless indicated otherwise. M^{2+} is Mg^{2+} or Ca^{2+} , L^{3-} the fully deprotonated DFOB ligand, MSA^- the mesylate anion ($CH_3SO_3^-$), and AH^- the acetohydroxamate anion (CH_3CONHO^-).

fit to derive the stability constants of Mg–AH and Ca–AH complexes. Titrations in the presence and absence of NaMSA were subsequently compared to estimate the stability constants of Mg–MSA and Ca–MSA complexes, enabling a correction to the metal+DFOB titrations, if necessary. Finally, metal+DFOB titrations were fit, fixing the pK_{ai} of DFOB at values reported by Christenson and Schijf (2011), to determine equilibrium constants of Mg–DFOB and Ca–DFOB complexes, R_j , which are expressed in terms of the species H_3L (where L^{3-} is the fully deprotonated ligand) and incorporate proton exchange (Table 1). These were converted with the pK_{ai} to stability constants of the form $L\beta_j$ (Table 1) that do not incorporate proton exchange (Schijf et al., 2015).

RESULTS

Stability Constants of Mg–MSA and Ca–MSA Complexes

Desferrioxamine B is a linear molecule with three evenly spaced hydroxamic acid groups and an amine group at one end (Figure 1A). The hydroxamic acid groups deprotonate in the pH range 8.5–9.7, while the amine group is predominantly protonated below pH 10.9 (Christenson and Schijf, 2011). The sequential deprotonation of DFOB can be written as



with acid dissociation constants

$$K_{ai} = \frac{[H^+][H_{4-i}L^{(1-i)+}]}{[H_{5-i}L^{(2-i)+}]} \quad (i = 1, 2, 3, 4). \quad (2)$$

At non-alkaline pH, fully protonated DFOB, H_4L^+ , carries a single positive charge. Solid DFOB therefore requires a counterion with a single negative charge to make a neutral compound. A standard pharmaceutical DFOB preparation, marketed under the brand name Desferal[®], uses the methanesulfonate

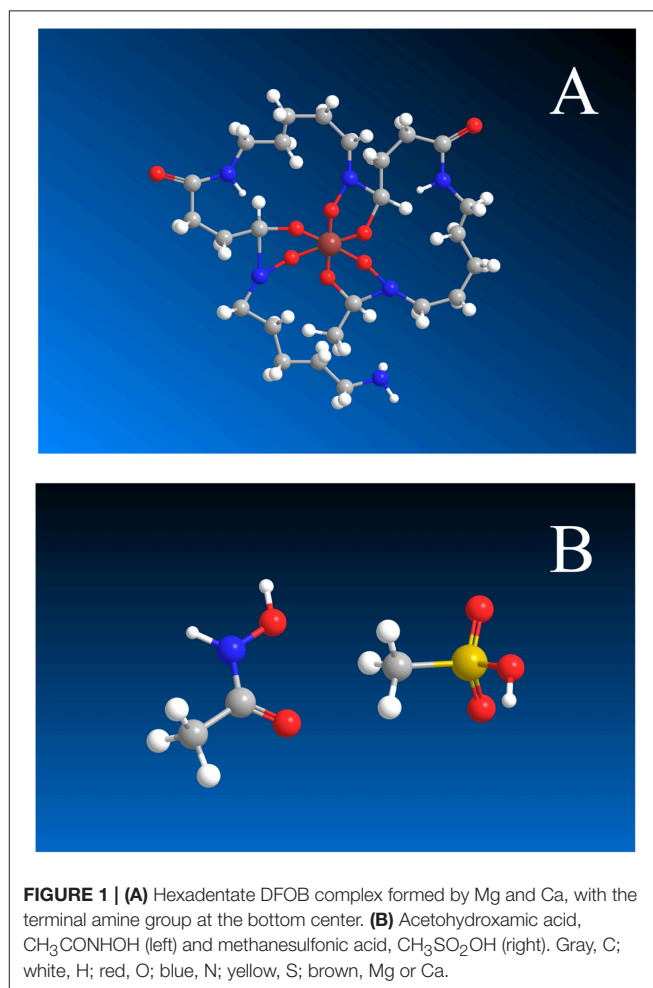


FIGURE 1 | (A) Hexadentate DFOB complex formed by Mg and Ca, with the terminal amine group at the bottom center. **(B)** Acetohydroxamic acid, $CH_3CONHOH$ (left) and methanesulfonic acid, CH_3SO_2OH (right). Gray, C; white, H; red, O; blue, N; yellow, S; brown, Mg or Ca.

anion (MSA^-), often called mesylate. Its protonated form is methanesulfonic acid, or HMSA (Figure 1B).

Hernlem et al. (1996) noted that the inevitable presence in DFOB solutions of an equal amount of MSA^- could lead to a

bias in potentiometric titrations if the latter forms fairly stable complexes with the analyte metal. However, they were unable to determine the pK_a of HMSA, which they believed to be 1.92 from the NIST database (Martell et al., 2004) but found to be certainly <0.9 . Christenson and Schijf (2011) pointed out that the NIST database contains a sign error and that the actual value is -1.92 (Covington and Thompson, 1974), congruent with the observation of Hernlem et al. (1996). Because of this extremely low pK_a value, metal-MSA complexes do not dissociate within our experimental pH window (~ 2 – 11) and their stability constants cannot be directly determined by potentiometric titration. Yet, if stable enough, MSA complexes will effectively increase the concentration of the free metal cation, from which they cannot be distinguished since their formation does not elicit a change in pH, and thereby lower the apparent stability constants of complexes with DFOB or other ligands.

In a study of DFOB complexation with yttrium and the rare earth elements (YREEs), Christenson and Schijf (2011) indirectly estimated the stability of the $\text{Lu}(\text{MSA})^{2+}$ complex by comparing the solubility of $\text{Lu}(\text{OH})_3(\text{s})$ in the absence and presence of MSA^- and found it to be similar to the stability of the structurally related Lu-sulfate complex. They concluded that, with respect to the YREEs, MSA^- is an 8–13 orders of magnitude weaker ligand than DFOB and thus of no consequence. Assuming, for lack of evidence to the contrary, that the stabilities of MSA and sulfate complexes are broadly interchangeable, Schijf et al. (2015) drew the same conclusion in a study of DFOB complexation with Cu, Ni, Zn, Cd, and Pb.

The outcome is different if this rule is applied to Mg and Ca. Stability constants, $\log_{\text{SO}_4}\beta_1$, of the Mg-sulfate and Ca-sulfate complex are 1.01 and 1.03, respectively, at $I = 0.7$ (Millero and Schreiber, 1982), whereas previous estimates of the stability constant, $\log_{\text{L}}\beta_3$ of the hexadentate Mg-DFOB and Ca-DFOB complex are about 3–4 (Farkas et al., 1999). In this case, DFOB may be a no more than three orders of magnitude stronger ligand than MSA^- (Tables 5, 8). The hydroxide salts of Mg and Ca are poorly characterized and fairly soluble (Martell et al., 2004), hence precipitation cannot be used to determine the stability of their MSA complexes, as for Lu (Christenson and Schijf, 2011). However, the aforementioned effect of MSA complexation on potentiometric titrations works to our advantage if we compare the stability constants of Mg and Ca complexes with a suitable ligand in the absence and presence of MSA^- . If the acid dissociation constant of an arbitrary ligand HY and the stability constant of its complex with a divalent metal M are defined as follows (omitting charges for convenience):

$$K_a(\text{Y}) = \frac{[\text{H}][\text{Y}]}{[\text{HY}]} \quad \text{HY} \rightleftharpoons \text{H} + \text{Y} \quad (3a)$$

$$\gamma\beta_1 = \frac{[\text{MY}]}{[\text{M}][\text{Y}]} \quad \text{M} + \text{Y} \rightleftharpoons \text{MY} \quad (3b)$$

then, in the presence of MSA^- , the constant $\gamma\beta_1$ will instead be determined as

$$\gamma\beta'_1 = \frac{[\text{MY}]}{\{[\text{M}] + [\text{M}(\text{MSA})]\}[\text{Y}]} \quad (4)$$

If we define the stability constant of the complex $\text{M}(\text{MSA})^+$ as

$${}_{\text{MSA}}\beta_1 = \frac{[\text{M}(\text{MSA})^+]}{[\text{M}^{2+}][\text{MSA}^-]} \quad \text{M}^{2+} + \text{MSA}^- \rightleftharpoons \text{M}(\text{MSA})^+ \quad (5)$$

(Table 1), it can be shown, by combining Equations (4) and (5), that

$${}_{\text{MSA}}\beta_1 = \frac{(\gamma\beta_1/\gamma\beta'_1) - 1}{[\text{MSA}^-]} \quad (6)$$

The stability constant ${}_{\text{MSA}}\beta_1$ can therefore be calculated from $\gamma\beta_1$ and $\gamma\beta'_1$, measured in the absence and presence of MSA^- , respectively. If ${}_{\text{MSA}}\beta_1$ is small i.e., if $[\text{M}(\text{MSA})^+] \ll [\text{MSA}]_{\text{T}}$, we can assume that $[\text{MSA}^-] = [\text{MSA}]_{\text{T}} - [\text{HMSA}] - [\text{M}(\text{MSA})^+] \approx [\text{MSA}]_{\text{T}}$, since MSA^- does not protonate.

Initially, oxalate, ${}^{-}\text{OOC}-\text{COO}^{-}$, and malonate, ${}^{-}\text{OOC}-\text{CH}_2-\text{COO}^{-}$, were considered for the ligand Y. They form bidentate Mg and Ca complexes with stabilities similar to those of the hexadentate DFOB complexes, so their potentiometric titrations should be affected by MSA^- to a comparable degree. Unfortunately, these diprotic ligands may bind metals with only one of their carboxylate groups (cf. Schijf and Byrne, 2001) and the first dissociation constant of oxalic acid lies just outside the experimental pH window ($pK_{a1} \sim 1$; Kettler et al., 1998), which complicated interpretation of the titration curves. Our choice ultimately fell on acetohydroxamic acid or HAH, $\text{CH}_3-\text{CO}-\text{NHOH}$ (Figure 1B), a monoprotic acid that essentially has the same properties as each of the three hydroxamic acid groups in DFOB.

First, pK_a was determined from 9 titrations of HAH alone in 0.7 M NaClO_4 at concentrations ranging from 5 to 20 mM (Table 2). Two of these titrations were performed in the presence of 70 mM and one in the presence of 140 mM MSA^- , which was added as NaMSA in order to not unduly acidify the experimental solutions. The pK_a values measured in these three titrations were not discernibly different from those measured in the other six, showing as expected that the presence of MSA^- , in itself, had no effect on the pH of the solution. The 9 titrations together yield an average value of $pK_a = 9.257 \pm 0.008$ (Table 5), in beautiful agreement with published measurements of 9.35 in 0.1 M NaNO_3 (Anderegg et al., 1963) and 9.27 ± 0.01 in 0.2 M KCl (Farkas et al., 1999). Unlike the large, linear DFOB molecule (Christenson and Schijf, 2011), equilibrium constants for the small HAH molecule should display Debye-Hückel-like behavior and the value of pK_a does indeed seem to decrease with increasing ionic strength. Values of $[\text{H}^+]_{\text{T}}^0$ are on the order of 100 μM and alternate randomly between proton excess and deficiency. Modeled total HAH concentrations are about 1–4% higher than gravimetric concentrations, with the greatest difference observed at 5 mM HAH (Table 2).

Next, Mg and Ca were titrated in the presence of 5 or 10 mM HAH at nominal M:L ratios of 1:2, 1:1, and 2:1. Six Ca and seven Mg titrations were conducted with HAH alone and six more of each in the presence of 140 mM NaMSA (Tables 3, 4), the highest concentration that was shown not to affect the pK_a measurements. The stability constants of metal-AH complexes and the initial proton excess, $[\text{H}^+]_{\text{T}}^0$, were used

TABLE 2 | Nine titrations (pH 3–11) of acetohydroxamic acid (HAH) in 50 mL of 0.7 M NaClO₄ solution, some in the presence of mesylate (MSA⁻).

[HAH] _T (mM) ^a	[MSA ⁻] (mM)	[HAH] _T (mM) ^b	[H ⁺] _T ⁰ (μM) ^c	pK _a	n ^d	WSOS/DF ^e
5.01	0	5.19	+104	9.262	50	6.90
5.01	0	5.17	+2.91	9.267	50	6.64
5.01	70	5.21	+46.2	9.267	51	6.27
10.0 [‡]	0	10.1	+66.6	9.260	157	3.24
10.0	0	10.2	+99.5	9.249	54	3.47
10.0	0	10.1	-171	9.258	53	3.39
10.0	70	10.1	+28.2	9.251	56	3.36
10.0	140	10.2	-1.20	9.255	55	2.80
20.0	0	20.0	-105	9.242	63	2.50

The final ionic strength was raised by <1% due to addition of the titrant (1.0005 M NaOH). Non-linear regressions were performed with FITEQL4.0, keeping the ionization constant of water fixed at pK_w = 13.740 (Christenson and Schijf, 2011). The acid dissociation constant, pK_a, the initial proton excess, [H⁺]_T⁰, and the total HAH concentration were used as adjustable parameters. All regressions converged in ≤7 iterations.

^aDetermined by weighing.

^bDetermined by non-linear regression.

^cNegative values signify an initial proton deficiency.

^dNumber of titration points.

^eQuality-of-fit parameter (Weighted Sum-Of-Squares divided by the Degrees-of-Freedom); values of 0.1–20 indicate a good fit (Herbelin and Westall, 1999).

[‡]Titrated with 0.1001 M NaOH; final ionic strength lowered by ~10%.

as adjustable parameters in non-linear regressions of the titration curves, whereas the total ligand concentration was fixed at the gravimetric value. For Ca, only the Ca(AH)⁺ complex was needed to produce good fits (WSOS/DF < 1.2). Values of log $\log_{\text{AH}\beta_1}$ were determined to be 2.30 ± 0.03 and 2.25 ± 0.01 in the absence and presence of MSA⁻, respectively (Table 5), comparing favorably with literature values of 2.4 at $I = 0.1$ (Anderegg et al., 1963) and 2.45 ± 0.01 at $I = 0.2$ (Farkas et al., 1999). The value of $\log_{\text{MSA}\beta_1}$, calculated from these averages with Equation (6), is equal to -0.005 (Table 5), but could be as high as 0.2 or as low as -0.4 within the uncertainty of the measurements.

For Mg, inclusion of only the Mg(AH)⁺ complex produced much poorer fits than for Ca (WSOS/DF ≤ 3.5). Addition of the ternary Mg(AH)OH complex, purportedly observed by Farkas et al. (1999), does not significantly improve the fits, while the corresponding stability constant, $\log_{\text{AH}\beta_{11}^*}$, is similar to that of the MgOH⁺ complex and two orders of magnitude lower than the value found by these authors and therefore does not constitute independent prove of its formation. Instead, inclusion of a second-order complex, Mg(AH)₂, does improve the regressions (WSOS/DF < 2.1) and yields stability constants of the expected absolute and relative magnitude: $\log_{\text{AH}\beta_1} = 2.73 \pm 0.01$ and $\log_{\text{AH}\beta_2} = 4.71 \pm 0.05$ (Table 5). The only literature value for $\log_{\text{AH}\beta_1}$ is 2.96 ± 0.03 at $I = 0.2$ (Farkas et al., 1999). The second-order complex had not been previously recognized, yet is known to exist for many other divalent metals (Anderegg et al., 1963). Titrations in the presence of MSA⁻ yield $\log_{\text{AH}\beta_1} = 2.70 \pm 0.02$ and $\log_{\text{AH}\beta_2} = 4.7 \pm 0.1$. Average values of $\log_{\text{AH}\beta_2}$ are statistically equal for the two systems, but $\log_{\text{AH}\beta_1}$ values are consistent with $\log_{\text{MSA}\beta_1} = -0.248$ (Table 5), although it could

TABLE 3 | Thirteen titrations (pH 3–10) of magnesium in 0.7 M NaClO₄ solutions containing 5 or 10 mM acetohydroxamic acid (HAH), some in the presence of 140 mM mesylate (MSA⁻).

[HAH] _T (mM) ^a	[Mg] _T /[HAH] _T	MSA ⁻ present	[H ⁺] _T ⁰ (μM) ^b	log $\log_{\text{AH}\beta_1}$	log $\log_{\text{AH}\beta_2}$	n ^c	WSOS/DF ^d
10.0	0.53	–	-785	2.736	4.705	141	0.0811
10.0	0.53	–	-187	2.747	4.727	147	0.0808
5.01	1.05	–	-832	2.743	4.616	97	0.190
5.01	1.05	–	-191	2.734	4.699	103	0.443
5.01	2.10	–	-815	2.714	4.752	121	1.16
5.01	2.10	–	-318	2.729	4.714	126	0.592
5.00	2.06	–	-148	2.731	4.771	105	0.196
10.0	0.53	+	-226	2.720	4.605	146	0.234
10.0	0.52	+	-136	2.703	4.680	137	0.0851
5.01	1.05	+	-189	2.719	4.572	103	0.632
5.00	1.03	+	-85.4	2.695	4.705	94	0.463
5.00	2.10	+	-349	2.676	4.836	126	2.10
5.00	2.06	+	-153	2.689	4.808	105	0.763

The final ionic strength was lowered by <10% due to addition of the titrant (0.1001 M NaOH). Non-linear regressions were performed with FITEQL4.0, keeping the ionization constant of water fixed at pK_w = 13.740 (Christenson and Schijf, 2011) and the acid dissociation constant of HAH at pK_a = 9.257 (Table 5). Total ligand and metal concentrations were fixed at values determined gravimetrically and by ICP-MS, respectively. Two stability constants, $\log_{\text{AH}\beta_1}$ and $\log_{\text{AH}\beta_2}$, and the initial proton excess, [H⁺]_T⁰, were used as adjustable parameters. All regressions converged in ≤5 iterations.

^aDetermined by weighing.

^bNegative values signify an initial proton deficiency.

^cNumber of titration points.

^dQuality-of-fit parameter (Weighted Sum-Of-Squares divided by the Degrees-of-Freedom); values of 0.1–20 indicate a good fit (Herbelin and Westall, 1999).

be as high as 0.03 or as low as -1.1 within the uncertainty of the measurements. The value of [H⁺]_T⁰ ranges from about -200 to -500 μM for all Mg and Ca titrations, indicating a proton deficiency likely caused by lower accuracy of the glass electrode at the very low pH of the metal standards (Section Preparation of Reagents and Standards).

It is clear from the upper-bound values of $\log_{\text{MSA}\beta_1}$ that complexation of Mg and Ca with MSA⁻ is exceedingly weak, specifically quite a lot weaker than their complexation with sulfate, contrary to what was found for Lu (Christenson and Schijf, 2011). It is noteworthy that, like the corresponding sulfate complexes, the Ca(MSA)⁺ complex appears to be more stable than the Mg(MSA)⁺ complex, which is not seen for complexes with AH⁻ and DFOB (Section Stability Constants of Mg–DFOB and Ca–DFOB Complexes) and not what one would expect based on the smaller ionic radius of Mg²⁺. Whereas the MSA complexes were included in the regression models for the DFOB titrations (Section Stability Constants of Mg–DFOB and Ca–DFOB Complexes), compositions of the experimental solutions, calculated with FITEQL4.0, suggest that their contributions to the total Mg and Ca concentrations are <<1%.

Stability Constants of Mg–DFOB and Ca–DFOB Complexes

Following assessment of the stability of their MSA complexes, titrations of Mg and Ca in the presence of DFOB could be

TABLE 4 | Twelve titrations (pH 3–10) of calcium in 0.7 M NaClO₄ solutions containing 5 or 10 mM acetoxyhydroxamic acid (HAH), some in the presence of 140 mM mesylate (MSA⁻).

[HAH] _T (mM) ^a	[Ca] _T /[HAH] _T	MSA ⁻ present	[H ⁺] _T ⁰ (μM) ^b	log _{AH} β ₁	n ^c	WSOS/DF ^d
10.0	0.47	–	–159	2.314	138	0.0586
5.01	0.97	–	–149	2.330	93	1.08
5.01	0.97	–	–155	2.332	93	1.07
5.00	0.94	–	–166	2.293	95	0.111
5.01	1.94	–	–213	2.287	107	1.19
5.00	1.89	–	–222	2.266	112	0.353
10.0	0.49	+	–328	2.238	136	0.141
10.0	0.47	+	–94.9	2.253	138	0.124
5.00	0.94	+	–77.5	2.251	96	0.340
5.00	0.97	+	–416	2.253	92	0.0849
5.00	1.89	+	–154	2.244	112	0.729
5.00	1.94	+	–633	2.243	107	0.555

The final ionic strength was lowered by <10% due to addition of the titrant (0.1001 M NaOH). Non-linear regressions were performed with FITEQL4.0, keeping the ionization constant of water fixed at pK_W = 13.740 (Christenson and Schijf, 2011) and the acid dissociation constant of HAH at pK_a = 9.257 (Table 5). Total ligand and metal concentrations were fixed at values determined gravimetrically and by ICP-MS, respectively. One stability constant, log_{AH}β₁, and the initial proton excess, [H⁺]_T⁰, were used as adjustable parameters. All regressions converged in 3 iterations.

^aDetermined by weighing.

^bNegative values signify an initial proton deficiency.

^cNumber of titration points.

^dQuality-of-fit parameter (Weighted Sum-Of-Squares divided by the Degrees-of-Freedom); values of 0.1–20 indicate a good fit (Herbelin and Westall, 1999).

evaluated. Since MSA⁻ is the DFOB counter-ion, these titrations always contained equal concentrations of DFOB and MSA⁻ i.e., substantially less MSA⁻ than was added in the HAH titrations. Since Mg and Ca complexes with DFOB were expected to be at most as stable, and probably less stable, than their complexes with AH⁻ (Tables 5, 8), the potentiometric signal, reflecting the contribution of Mg and Ca complexes to the total DFOB concentration, was maximized by increasing the M:L ratio as much as possible, whereby the upper limit is set by the solubility of hydroxide salts at high pH. However, unlike the divalent transition metals where M:L ratios had to be kept below 0.7:1 (Schijf et al., 2015), Mg(OH)₂(s) is fairly soluble and precipitation of Ca(OH)₂(s) is of no concern. Consequently, 9 titrations were performed for Mg with 2 mM DFOB and nominal M:L ratios of 1:1, 3:2, and 2:1 (Table 6), and 9 for Ca with 1 or 2 mM DFOB and nominal M:L ratios of 1:1, 3:2, 2:1, 3:1, and 4:1 (Table 7), requiring maximum Mg or Ca concentrations of ~4 mM. For comparison, the concentrations of Mg and Ca in standard seawater (S = 35) are 54 and 10.5 mM. Compositions of the experimental solutions, calculated with FITEQL4.0, suggest that Mg reached at most 22% of saturation in the DFOB titrations and at most 72% in the HAH titrations, with respect to the “active” form of Mg(OH)₂(s) that precipitates before aging to crystalline brucite (Gjaldbaek, 1925; Einaga, 1981).

In non-linear regressions of the Mg and Ca titrations with DFOB, stability constants, log R_j (Table 1), the initial proton excess, [H⁺]_T⁰, and the total DFOB concentration were used as

TABLE 5 | Stability constants for AH and MSA complexes of Mg and Ca, derived from potentiometric titrations.

Constant	H	Mg	Ca	References
pK _W	13.740			Christenson and Schijf, 2011
log β ₁ [*]		–12.04	–13.00	Millero and Schreiber, 1982
log K _{SO}		–9.38		Einaga, 1981
pK _a (HAH)	9.257 ± 0.008			This work (n = 9)
	9.35 ^a			Anderegg et al., 1963
	9.27 ± 0.01 ^b			Farkas et al., 1999
log _{AH} β ₁		2.73 ± 0.01	2.30 ± 0.03	This work (Mg, n = 7; Ca, n = 6)
		–	2.4 ^a	Anderegg et al., 1963
		2.96 ± 0.03 ^b	2.45 ± 0.01 ^b	Farkas et al., 1999
log _{AH} β ₁₁ [*]		–7.22 ± 0.09 ^b	–	Farkas et al., 1999
log _{AH} β ₂		4.71 ± 0.05	–	This work (n = 7)
pK _a (HMSA)	–1.92 ^c			Covington and Thompson, 1974
log _{SO4} β ₁		1.01	1.03	Millero and Schreiber, 1982
log _{MSA} β ₁		–0.248	–0.005	This work (n = 6)

Uncertainties are based on n replicate titrations, as indicated. Constants taken from the literature are shown for comparison. Other equilibrium constants relevant to the FITEQL4.0 regressions are also listed.

^a0.1 M NaNO₃, 20°C.

^b0.2 M KCl, 25°C.

^cEntry in the NIST database (Martell et al., 2004) has a sign error.

adjustable parameters. The Mg titrations yield average values of log_Lβ₁ = 2.19 ± 0.02, log_Lβ₂ = 3.41 ± 0.04, and log_Lβ₃ = 4.17 ± 0.04 (Table 8). This confirms that Mg forms a bidentate complex with DFOB, which could not be resolved by Farkas et al. (1999), but lends no support to Mg coordination with the terminal amine (Figure 1A). Fits are of good quality (WSOS/DF ~ 0.3–1.0) and modeled total DFOB concentrations exceed gravimetric concentrations by no more than ~2%. Values of [H⁺]_T⁰ are always negative, ranging up to a proton deficiency of about 200 μM, in agreement with the HAH titrations.

For Ca, DFOB complexation is so weak (Figure 2) that the 3-site model used for Mg was under-constrained and the three stability constants could not be determined simultaneously. The fits were therefore executed in several steps. In the first step, a 2-site model was used (Schijf et al., 2015), including only log_Lβ₁ and log_Lβ₂, for which all regressions converged. In the second step, log_Lβ₁ was fixed to the average value, 0.73 ± 0.17, obtained

TABLE 6 | Nine titrations (pH 3–10) of magnesium in 0.7 M NaClO₄ solutions containing equal amounts of DFOB and MSA⁻.

[L] _T (mM) ^a	[Mg] _T /[L] _T	[L] _T (mM) ^b	[H ⁺] _T ⁰ (μM) ^c	log _L β ₁	log _L β ₂	log _L β ₃	n ^d	WSOS/DF ^e
2.02	0.93	2.07	-15.4	2.227	3.374	4.141	106	0.535
2.02	0.94	2.08	-55.1	2.206	3.433	4.201	106	0.444
2.01	1.05	2.04	-27.4	2.169	3.369	4.124	104	0.430
2.02	1.40	2.07	-90.2	2.183	3.473	4.236	111	0.363
2.02	1.40	2.05	-151	2.173	3.430	4.175	110	0.310
2.01	1.57	2.05	-59.9	2.169	3.376	4.143	109	0.687
2.02	1.87	2.07	-148	2.214	3.449	4.223	116	0.552
2.02	1.87	2.05	-209	2.197	3.395	4.169	115	0.651
2.01	2.09	2.06	-88.1	2.160	3.381	4.152	114	1.00

The final ionic strength was lowered by ~7% due to addition of the titrant (0.1001 M NaOH). Non-linear regressions were performed with FITEQL4.0, keeping the ionization constant of water fixed at $pK_W = 13.740$ (Christenson and Schijf, 2011), the stability constant of the Mg–MSA complex at $\log_{MSA}\beta_1 = -0.248$ (Table 5), and the acid dissociation constants of DFOB, pK_{ai} , at values listed in Table 8. Total metal concentrations were fixed at values determined by ICP-MS. The stability constants, $\log_{L}\beta_i$, the initial proton excess, $[H^+]_T^0$, and the total DFOB concentration, $[L]_T$, were used as adjustable parameters. All regressions converged in ≤ 6 iterations.

^aDetermined by weighing.

^bDetermined by non-linear regression.

^cNegative values signify an initial proton deficiency.

^dNumber of titration points.

^eQuality-of-fit parameter (Weighted Sum-Of-Squares divided by the Degrees-of-Freedom); values of 0.1–20 indicate a good fit (Herbelin and Westall, 1999).

TABLE 7 | Nine titrations (pH 3–10) of calcium in 0.7 M NaClO₄ solutions containing equal amounts of DFOB and MSA⁻.

[L] _T (mM) ^a	[Ca] _T /[L] _T	[L] _T (mM) ^b	[H ⁺] _T ⁰ (μM) ^c	log _L β ₁	log _L β ₂	log _L β ₃	n ^d	WSOS/DF ^e
2.02	0.94	2.04	-93.5	0.730	1.617 [‡]	–	96	0.844
		2.01	-120	0.663 [‡]	1.417	1.999		0.695
2.02	1.32	2.12	-61.6	0.669	1.617 [‡]	–	108	0.401
		2.08	-101	0.663 [‡]	1.689	1.971		0.317
2.02	1.32	2.13	-42.4	0.396	1.617 [‡]	–	108	0.669
		2.09	-79.4	0.663 [‡]	1.561	1.972		0.524
2.02	1.76	2.14	-80.9	0.517	1.617 [‡]	–	113	0.709
		2.09	-124	0.663 [‡]	1.614	1.911		0.568
2.02	1.92	2.12	+63.9	0.432	1.617 [‡]	–	103	0.841
		2.07	+19.1	0.663 [‡]	1.609	1.896		0.660
2.02	1.87	2.09	-63.0	0.846	1.617 [‡]	–	103	1.57
		2.05	-102	0.663 [‡]	1.583	1.834		1.45
2.02	2.80	2.16	+11.9	0.548	1.617 [‡]	–	111	1.17
		2.10	-46.9	0.663 [‡]	1.654	1.846		0.992
2.02	2.81	2.14	-55.1	0.875	1.617 [‡]	–	110	0.959
		2.07	-115	0.663 [‡]	1.732	1.821		0.836
1.01	3.52	1.03	-186	0.951	1.617 [‡]	–	86	0.840
		1.01	-208	0.663 [‡]	1.678	1.881		–

The final ionic strength was lowered by <7% due to addition of the titrant (0.1001 M NaOH). The stability constant of the Ca–MSA complex was fixed at $\log_{MSA}\beta_1 = -0.005$ (Table 5); other constraints are the same as in Table 6. For each titration, the two lines represent the final two steps of a 4-step iterative process. Non-linear regressions were alternately performed with a 2-site and a 3-site model (Schijf et al., 2015), wherein $\log_{L}\beta_2$ and $\log_{L}\beta_1$, respectively, were fixed at the average value determined in the preceding step (see text for details). All regressions converged in ≤ 4 iterations.

^aDetermined by weighing.

^bDetermined by non-linear regression.

^cNegative values signify an initial proton deficiency.

^dNumber of titration points.

^eQuality-of-fit parameter (Weighted Sum-Of-Squares divided by the Degrees-of-Freedom); values of 0.1–20 indicate a good fit (Herbelin and Westall, 1999).

[‡]Fixed value determined in the preceding step.

in the first step and used with the full 3-site model to obtain values for $\log_{L}\beta_2$ and $\log_{L}\beta_3$. These two steps were repeated, fixing $\log_{L}\beta_2$ obtained from the second step in the third step, and then

$\log_{L}\beta_1$ obtained from the third step in the fourth and final step. The regressions from step 3 and 4 are shown in Table 7. Average values of $\log_{L}\beta_1 = 0.66 \pm 0.20$ (from step 3) and of $\log_{L}\beta_2 =$

TABLE 8 | Stability constants for DFOB complexes of Mg and Ca, derived from potentiometric titrations.

	This work 0.7 M NaClO ₄ , 25°C	Farkas et al., 1999 0.2 M KCl, 25°C	Anderegg et al., 1963 0.1 M NaNO ₃ , 20°C
DFOB			
pK _{a1}	8.54 ± 0.01 ^a	8.30 ± 0.01	8.39 ^b
pK _{a2}	9.06 ± 0.01 ^a	9.00 ± 0.01	9.03 ^b
pK _{a3}	9.70 ± 0.02 ^a	9.46 ± 0.01	9.70 ^b
pK _{a4}	10.89 ± 0.06 ^a	10.84 ± 0.03	> 11 ^b
Mg (n = 9)			
log _L β ₁	2.19 ± 0.02	—	—
log _L β ₂	3.41 ± 0.04	3.55	—
log _L β ₃	4.17 ± 0.04	3.82	4.30
log _L β ₄	—	2.80	—
Ca (n = 9)			
log _L β ₁	0.66 ± 0.20	—	—
log _L β ₂	1.62 ± 0.09	2.11	—
log _L β ₃	1.90 ± 0.06	2.41	2.64
log _L β ₄	—	3.03	—

Uncertainties are based on *n* replicate titrations, as indicated. Constants taken from the literature are shown for comparison.

^aChristenson and Schijf, 2011.

^b0.1 M NaClO₄ (Schwarzenbach and Schwarzenbach, 1963).

1.62 ± 0.09 and log_Lβ₃ = 1.90 ± 0.06 (from step 4) are listed in **Table 8**.

Subsequent regressions of the titration curves with the unconstrained 3-site model and using 0.66 as the starting value for log_Lβ₁ did not yield meaningful results, which shows that the lack of convergence is not caused by a poor initial guess for this parameter. Speciation calculations for the experimental solutions, based on the results in **Table 8**, reveal that insensitivity to the value of log_Lβ₁ reflects the minute contribution of the corresponding CaH₃L²⁺ complex to the total DFOB concentration. Its absolute contribution was increased by raising the M:L ratio (**Table 7**), which is however bound by other concerns like hydrolysis. Even at our highest M:L ratio of 4:1, the maximum relative contribution of the bidentate complex is only about 0.7% (at pH 8.7) of the total DFOB concentration. A sensitivity analysis was performed by repeating the final regression step for all 9 titrations with log_Lβ₁ fixed at values ranging from 2σ below to 2σ above the mean in increments of 0.1 and recording the resulting values of log_Lβ₂ and log_Lβ₃. The standard deviations of the values thus obtained are no larger than the errors derived from the 9 independent titrations (**Table 8**), indicating that the latter are a good estimate of the uncertainty inherent in this iterative regression process. A better estimate of the true errors might be obtained from a simultaneous fit of all titration curves, were it not that such a large dataset with multiple total metal and ligand concentrations surpasses the capability of FITEQL4.0.

The final fits (**Table 7**) are of good quality (WSOS/DF ~ 0.3–1.5) and modeled total DFOB concentrations exceed gravimetric concentrations by no more than 3–4%. Values of [H⁺]_T⁰ range

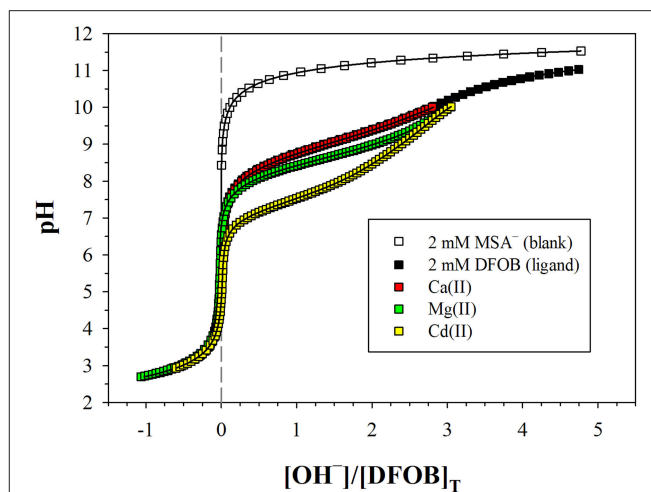


FIGURE 2 | Potentiometric titrations of a DFOB solution and metal+DFOB mixtures in 0.7 M NaClO₄, where pH is plotted against moles of base (OH⁻) added per mole of DFOB. The blank contains 2 mM mesylate (MSA⁻), which is fully deprotonated over the entire pH range. All other solutions contain 2 mM DFOB mesylate. Symbols are measurements. Solid lines are non-linear regressions performed with FITEQL4.0. The more a metal+DFOB titration deviates from that of DFOB alone, the higher the stability of the metal–DFOB complexes formed. Note that the DFOB and Ca+DFOB titrations are almost indistinguishable. Cadmium (Cd), which forms the weakest hexadentate complex among the divalent transition metals (Schijf et al., 2015), is shown for comparison. The M:L ratio is about 1:1 for Mg and Ca, and about 0.7:1 for Cd.

from a proton deficiency of about 200 μM to an excess of 20 μM, probably reflecting the slightly higher pH of the Ca standards. There is no evidence for Ca coordination with the terminal amine (**Figure 1A**) and the bidentate Ca–DFOB complex, which again could not be resolved by Farkas et al. (1999), is even less stable than the bidentate Mg–DFOB complex (**Table 8**). Both our Mg and Ca data yield positive step-wise stability constants for each consecutive hydroxamate bond (Section Calculation of the Side-Reaction Coefficient and Comparison with Published Data).

DISCUSSION

Calculation of the Side-Reaction Coefficient and Comparison with Published Data

Our new DFOB speciations in the presence of Mg and Ca, presented in **Table 8**, are rather different than those reported by Farkas et al. (1999). Although their potentiometric data appears to be of excellent quality, these authors routinely include in their regression models a stability constant for metal complexes with fully deprotonated DFOB, implying coordination of the metal cation with the DFOB terminal amine. However, while such a complex may exist for some tetravalent cations like Sn⁴⁺ (Hernlem et al., 1996) and Hf⁴⁺ (Yoshida et al., 2004), it has not been found for other highly charged cations like Th⁴⁺ (Whisenhunt et al., 1996) or the trivalent lanthanides

(Christenson and Schijf, 2011) and is very unlikely to form with Mg^{2+} and Ca^{2+} . Schijf et al. (2015) emphasized that adding this extra degree of freedom to the regression model can lead to under-constrained fits and probably explains why Farkas et al. (1999) were unable to resolve values for $\log {}_L\beta_1$, whereas the bidentate DFOB complex, analogous to the bidentate AH complex (Table 5), is certainly expected to form as the first of three equivalent steps leading to the stable hexadentate DFOB complex. It also accounts for the fact that values of $\log {}_L\beta_2$, $\log {}_L\beta_3$, and $\log {}_L\beta_4$, reported by Farkas et al. (1999) and shown in Table 8, are either nearly identical or actually become smaller, resulting in thermodynamically anomalous behavior of the step-wise stability constants, $\log K_{j+1} = \log {}_L\beta_{j+1} - \log {}_L\beta_j$ (Schijf et al., 2015). Calculated from our data, these step-wise stability constants are $\log K_2 = 3.41 - 2.19 = 1.22$ and $\log K_3 = 4.17 - 3.41 = 0.76$ for Mg; and $\log K_2 = 1.62 - 0.66 = 0.96$ and $\log K_3 = 1.90 - 1.62 = 0.28$ for Ca (Table 8). We find as expected that (i) they are all of similar magnitude since in each step a bond is formed with a single hydroxamate group; (ii) $\log K_3 < \log K_2$ since the charge of the central cation in each step is shielded by the bond formed in the preceding step; and (iii) the values are lower for Ca^{2+} being the larger of the two ions. In contrast, Farkas et al. (1999) found $\log K_3$ and $\log K_4$ equal to 0.27 and -1.02 for Mg, and 0.30 and 0.62 for Ca, respectively. Their step-wise constants show no systematic pattern and furthermore suggest weak binding to the third hydroxamate group, inconsistent with the high values of $\log {}_L\beta_2$ (Table 8). Again, this is ostensibly due to regression of the data with an incorrect speciation model, not to poor quality of the data itself.

Wuttig et al. (2013) used the speciations of Farkas et al. (1999), appropriate for 0.2 M KCl, to calculate the SRC of DFOB in seawater, obtaining $\log \alpha_{\text{DFOB}} = 6.25$. While the authors presented the data on which the calculation is based (Farkas et al., 1999), they provided no additional information, yet α_{DFOB} appears to be the ratio of the total ligand and the fully deprotonated free-ligand concentrations, $L_T/[L^{3-}]$. This choice was evidently inspired by the equilibrium constants of Farkas et al. (1999), which are all expressed in terms of L^{3-} . The calculation of Wuttig et al. (2013) is reproduced in detail in the third column of Table 9. Each line represents a DFOB solution species, X, which include L^{3-} and the four protonated forms, as well as the complexes with Mg considered by Farkas et al. (1999), $\text{MgH}_3\text{L}^{2+}$, MgHL , and MgL^- , and similarly for Ca. Each number in the third column represents the ratio $[X]/[L^{3-}]$, where the entry corresponding to $X = L^{3-}$ is of course $[L^{3-}]/[L^{3-}] = 1$, per definition. The sum of all species equals the total concentration, hence the sum of these ratios equals $L_T/[L^{3-}] = \alpha_{\text{DFOB}}$ (referred to in Table 9 as $\sum \alpha_L$). Column 4 contains our own calculation of this SRC, using data from Christenson and Schijf (2011) and the present work, appropriate to seawater ionic strength. Column 2 specifies how each ratio $[X]/[L^{3-}]$ is derived from the proton concentration and equilibrium constants listed in Table 8.

The outstanding agreement between our SRC and that of Wuttig et al. (2013) should not be surprising, despite the distinct disagreement between our measured Mg–DFOB and Ca–DFOB stability constants and those of Farkas et al. (1999). Remember that this disagreement is not the result of bad titration data, but

of an incorrect speciation model used to interpret these data. Our acid dissociation constants and those of Farkas et al. (1999) are very close (Table 8) and while the distributions of Mg–DFOB and Ca–DFOB complexes are different, the total still adds up to L_T in each case. Specifically, the sum of the Mg complexes in column 3 and 4 differs by $<1\%$ and while the sum of the Ca complexes differs by more than a factor 2, the latter are only a minor fraction of the total DFOB concentration. Nevertheless, the agreement is somewhat fortuitous for several reasons. First, it seems that Wuttig et al. (2013) used total rather than free concentrations of Mg and Ca, which are about 89% of total concentrations in seawater (Byrne, 2002), primarily as a result of sulfate complexation. Second, Wuttig et al. (2013) expressed pH on the total scale ($\text{pH}_T = -\log\{[\text{H}^+] + [\text{HSO}_4^-]\}$), commonly used for seawater, instead of the free scale ($\text{pH}_f = -\log [\text{H}^+]$), where $\text{pH}_T = \text{pH}_f + 0.13$ at $S = 35$ and $T = 25^\circ\text{C}$ (Byrne, 2002). Finally, Wuttig et al. (2013) attempted to extrapolate the stability constants of Farkas et al. (1999) to seawater ionic strength, which is erroneous because chelates do not conform to Debye–Hückel-type behavior (Anderegg et al., 1963) and equilibrium constants for DFOB have been shown to display little or no ionic strength dependence (Christenson and Schijf, 2011). These corrections seem to have canceled each other out to some extent.

A more relevant issue is the interpretation of the constant $\sum \alpha_L (= \alpha_{\text{DFOB}})$. It says that the ratio $[L^{3-}]/L_T \approx 10^{-6.25} = 5.6 \times 10^{-7}$, implying that only a vanishingly small fraction of the total DFOB concentration is available to form complexes, even in the absence of competing trace metals (like Fe^{3+}). Yet it should be kept in mind that there are four other, protonated forms of the ligand and that the choice of L^{3-} to calculate the SRC, albeit a natural one for many polyprotic ligands, is awkward for DFOB. The reason is that, due to a pK_{a4} of 10.89 (Table 8), L^{3-} is an entirely negligible species in seawater. The top diagrams in Figure 3 show DFOB speciations calculated for trace-metal-free seawater, excluding or including the effect of Mg and Ca. When complexes with Mg and Ca are ignored, $>99\%$ of DFOB is made up of the three most protonated species and the species L^{3-} contributes a mere 0.00077%. Moreover, trace metals form the strongest and most abundant complexes with the protonated species, HL^{2-} and H_2L^- , and less abundant ones with H_3L (Schijf et al., 2015). Complexes with L^{3-} , which would involve full coordination of the metal center with the DFOB terminal amine (Figure 1B), have not been definitively proven to exist, except for one or two tetravalent metal cations. In reality, as shown in the right-hand diagram, $\sim 92\%$ of DFOB is complexed with Mg (and $<1\%$ with Ca). Within the $\sim 7\%$ of the total DFOB concentration not complexed with Mg and Ca, the distribution of species is identical to that in the left-hand diagram. In other words, DFOB complexation with Mg and Ca further reduces the contribution of the species L^{3-} by a factor $100/7 \approx 14$. Hudson et al. (1992) used the kinetics of Fe–DFOB complexation to estimate the rate of water loss from the first hydration sphere of Fe(III), but calculated that only about 28% of DFOB in seawater is bound to Mg. The much larger fraction of Mg-bound DFOB established here intimates higher rates of water loss, which has repercussions for the kinetics of Fe complexation with other strong organic ligands in seawater,

TABLE 9 | Calculation of the side-reaction coefficient of DFOB in seawater, using the data from Table 8.

Species [X]	Equation	Wuttig et al., 2013	$\alpha_L = [X]/[L^{3-}]$	$\alpha_{HL} = [X]/[HL^{2-}]^a$	$\alpha_{H2L} = [X]/[H_2L^-]^b$	$\alpha_{H3L} = [X]/[H_3L]^c$	$\alpha_{H4L} = [X]/[H_4L^+]^d$
[H ₄ L ⁺]	$[H^+]^4/(K_{a1} \times K_{a2} \times K_{a3} \times K_{a4})$	63,096	74,405	205	8.7	1.6	1
[H ₃ L]	$[H^+]^3/(K_{a2} \times K_{a3} \times K_{a4})$	50,119	46,276	128	5.4	1	0.62
[H ₂ L ⁻]	$[H^+]^2/(K_{a3} \times K_{a4})$	7943	8535	24	1	0.18	0.11
[HL ²⁻]	$[H^+]/K_{a4}$	437	362	1	0.042	0.0078	0.0049
[L ³⁻]	per definition	1	1	0.0028	0.00012	0.000022	0.000013
[MgH ₃ L ²⁺]	$(\beta_1 \times [Mg^{2+}] \times [H^+]^3)/(K_{a2} \times K_{a3} \times K_{a4})$	—	344,849	952	40	7.5	4.6
[MgH ₂ L ⁺]	$(\beta_2 \times [Mg^{2+}] \times [H^+]^2)/(K_{a3} \times K_{a4})$	1,493,743	1,055,511	2,913	124	23	14
[MgHL]	$(\beta_3 \times [Mg^{2+}] \times [H^+])/K_{a4}$	152,854	257,876	712	30	5.6	3.5
[MgL ⁻]	$\beta_4 \times [Mg^{2+}]$	33	—	—	—	—	—
[CaH ₃ L ²⁺]	$(\beta_1 \times [Ca^{2+}] \times [H^+]^3)/(K_{a2} \times K_{a3} \times K_{a4})$	—	1966	5.4	0.23	0.042	0.026
[CaH ₂ L ⁺]	$(\beta_2 \times [Ca^{2+}] \times [H^+]^2)/(K_{a3} \times K_{a4})$	10,233	3306	9.1	0.39	0.071	0.044
[CaHL]	$(\beta_3 \times [Ca^{2+}] \times [H^+])/K_{a4}$	1122	267	0.74	0.031	0.0058	0.0036
[CaL ⁻]	$\beta_4 \times [Ca^{2+}]$	11	—	—	—	—	—
	$\sum \alpha_{(H)_iL}$	1,779,591	1,793,355	4,949	210	39	24
	$\log \sum \alpha_{(H)_iL}$	6.25	6.25	3.69	2.32	1.59	1.38
	$\alpha_f = L_T / \sum [H_iL^{i-3}]$	14.6	13.8	13.8	13.8	13.8	13.8
	$\log \alpha_f$	1.17	1.14	1.14	1.14	1.14	1.14

See text for details.

$$^a \alpha_{HL} = \alpha_L \times K_{a4} / [H^+].$$

$$^b \alpha_{H2L} = \alpha_{HL} \times K_{a3} / [H^+].$$

$$^c \alpha_{H3L} = \alpha_{H2L} \times K_{a2} / [H^+].$$

$$^d \alpha_{H4L} = \alpha_{H3L} \times K_{a1} / [H^+].$$

yet a detailed discussion of this issue is outside the scope of our paper.

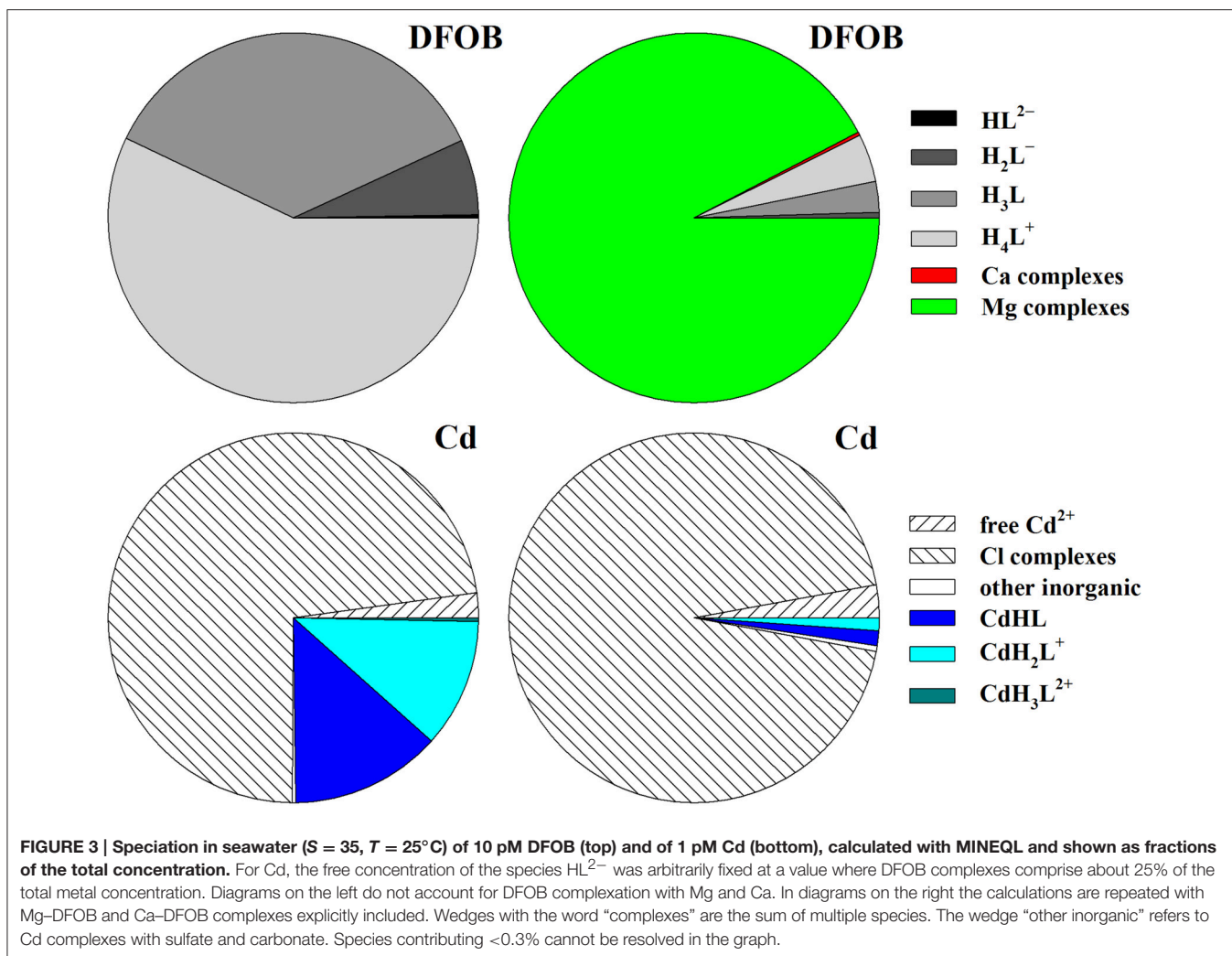
The remaining columns of **Table 9** contain calculations of SRCs corresponding to each of the four protonated DFOB species. It should be noted that the logarithmic values of these constants decrease rapidly with increasing protonation from 6.25 to 1.38, reflecting the contribution of each species to the total DFOB concentration in seawater (**Figure 3**). In the next section we more thoroughly discuss the (dis)advantages of different SRCs for calculating metal speciation in the presence of DFOB and other strong organic ligands, and present a more convenient definition of the SRC of DFOB in trace-metal-free seawater.

Implications for Model Calculations of Metal and DFOB Speciation in Seawater

The concept of SRCs was formalized and their proper use demonstrated by Ringbom and Still (1972). In general, they are a means of correcting free ligand (or metal) concentrations for complexation with cations in the background electrolyte and with competing metals (or ligands), without having to explicitly account for each complex in a speciation model. Their main benefit lies in the calculation of “conditional” stability constants and most of us are familiar with that approach in systems where a metal forms single 1:1 or higher-order complexes with one or more ligands, and *vice versa*. The situation becomes more complicated for large polyprotic, polydentate ligands, which can form more than one type of 1:1 complex with a single metal.

The SRC $\sum \alpha_L (= \alpha_{DFB})$ calculated by Wuttig et al. (2013), can be used to correct metal speciations in seawater in the presence of DFOB for DFOB complexation with Mg and Ca. With a speciation code like MINEQL (Westall et al., 1986), the easiest way is to fix the free concentration of L³⁻ at the value $\sum \alpha_L \times L_T$ and to calculate the metal speciation with elimination of all other DFOB complexes (except for protonation steps), provided all stability constants are expressed in terms of L³⁻ and appropriate to seawater ionic strength. Alternatively, if stability constants are expressed in terms of HL²⁻, its free concentration has to be fixed at the value $\sum \alpha_{HL} \times L_T$ (**Table 9**), and so forth for any of the protonated DFOB species. However, these SRCs cannot be used in the sense intended by Ringbom and Still (1972). It is possible to create “conditional” metal–DFOB stability constants by subtracting $\log \sum \alpha_{(H)_iL}$ from thermodynamic stability constants expressed in terms of H_iL, but these can only be employed in MINEQL either if $\log \sum \alpha_{(H)_iL}$ is also subtracted from the acid dissociation constants, or if the protonation steps are eliminated altogether and the free concentration of H_iL is fixed at the total concentration, L_T. Both yield the correct metal speciation, but the distribution of uncomplexed DFOB among its protonated species will be greatly skewed.

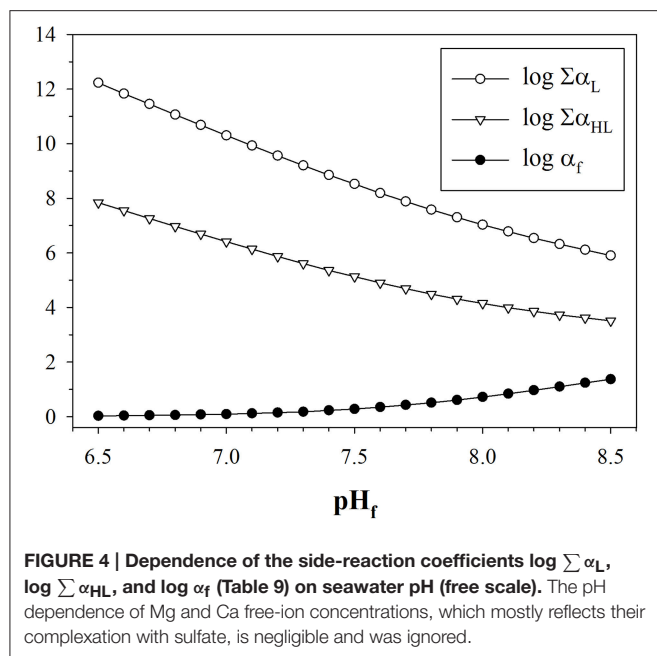
Our primary purpose is to determine an SRC allowing calculation of metal–DFOB stability constants that can be meaningfully compared with the results of ACSV-CLE analyses, which produce conditional stability constants of metal complexes with unknown organic ligands in seawater (Pizeta et al., 2015).



In the typical representation of metal–DFOB stability (Table 8), each constant ${}_L\beta_j$ is expressed in terms of the protonated DFOB species that forms the corresponding complex (Anderegg et al., 1963; Hernlem et al., 1996; Schijf et al., 2015) and would therefore have to be corrected by subtracting a different SRC. However, it is possible to define one single SRC that can correct all metal–DFOB stability constants, regardless of how they are expressed. This is the constant $\alpha_f = L_T / \sum [\text{H}_i\text{L}]$, where the denominator is the sum concentration of all DFOB species that are not complexed with Mg or Ca. The underlying principle is that speciation models do not include trace metal complexation by displacement of Mg or Ca from DFOB complexes. In other words, the constant α_f represents the fraction of DFOB that is available for metal complexation in seawater. This correction is valid as long as the speciation of DFOB is not significantly altered by the presence of the metal. The value of $\log \alpha_f$, shown in Table 9, is the same for each manner of expressing the stability constants. This means that any $\log {}_L\beta_j$ can be converted to a conditional constant for seawater by subtracting 1.14. The value of $\log \alpha_f$ calculated for the speciation of Farkas et al. (1999) is

slightly higher, primarily due to a somewhat greater contribution from the Ca–DFOB complexes. It should be mentioned here that the constant α_f , like the constants $\sum \alpha_{(\text{H})i\text{L}}$, is not only dependent on the composition of seawater, which does not vary much throughout the ocean, but also on pH. Values of $\log \sum \alpha_{\text{H}}$, $\log \sum \alpha_{\text{HL}}$, and $\log \alpha_f$, calculated as in Table 9 over a range of pH relevant to seawater, are shown in Figure 4. Note that the pH dependence of the SRC defined by Wuttig et al. (2013) is opposite to and much larger than that of $\log \alpha_f$.

A typical example of a speciation calculation is shown in the bottom diagrams of Figure 3. On the left is the speciation of dissolved Cd (1 μM), which has the lowest affinity for DFOB among the divalent transition metals (Schijf et al., 2015), where DFOB complexation with Mg and Ca is deliberately excluded. The total DFOB concentration (1.33×10^{-4} M) was arbitrarily chosen so that the contribution of DFOB complexes to the total Cd concentration is almost exactly 25%, the remaining 75% being dominated by Cl complexes, with only $\sim 2\%$ free Cd^{2+} . This concentration is clearly not realistic and only used here to illustrate the effect of DFOB complexation with the major



seawater cations. The speciation was calculated with MINEQL, expressing all DFOB stability constants in terms of HL^{2-} . On the right is the speciation calculated for the same total Cd and DFOB concentrations, but with Mg–DFOB and Ca–DFOB complexes explicitly accounted for. It can be seen that the fraction of the total Cd concentration complexed with DFOB is lowered by a factor $10^{1.14} = 13.8$ (cf. Section Calculation of the Side-Reaction Coefficient and Comparison with Published Data). The contributions of all chloride complexes and free Cd^{2+} are proportionally increased. The presence of Mg and Ca thus effectively lowers the amount of DFOB available for complexation by about an order of magnitude. The same result is obtained if all Mg–DFOB and Ca–DFOB complexes are removed from the calculation and $\log \alpha_f = 1.14$ is subtracted from the Cd–DFOB stability constants (but not the acid dissociation constants) and this is true regardless of what DFOB species is chosen as the “component” in the MINEQL model (Morel and Morgan, 1972).

Schijf et al. (2015) measured stability constants for DFOB complexes with Ni, Cu, Zn, Cd, and Pb at seawater ionic strength and compared these with conditional constants for complexes with unknown organic ligands in seawater, acquired by voltammetric techniques. Based on the speciation of Farkas et al. (1999), the authors estimated that a proper comparison would require $\log \alpha_f = 1.1$ to be subtracted from the measured stability constants, $\log L\beta_j$, which did not alter their conclusion that natural ligands could be siderophore-like for Cu, Zn, and Pb, but not for Ni and Cd. Our new DFOB speciation shows that their estimate of $\log \alpha_f$ was satisfactory.

This discussion highlights some of the theoretical challenges that attend the interpretation of voltammetric data and the calculation of SRCs for unknown ligands. Although measurements indicate that a metal may interact with more than one class of ligand (L1, L2), it is normally assumed

that only single 1:1 complexes occur, presumably involving the fully deprotonated forms (e.g., Coale and Bruland, 1988). However, all natural organic ligands described so far, including those specific to metals other than Fe (Springer and Butler, 2016), are large polyprotic, polydentate molecules that are likely capable of forming more than one 1:1 complex with the metal, depending on conditions. Our investigations of DFOB complexation have revealed that some metals form the most stable complex with the single-protonated species, some with the double-protonated species, yet none with the fully deprotonated species. In addition, at seawater pH, some metals, like Cd (Figure 3) and Zn, may form multiple DFOB complexes in approximately equal amounts. The relative contributions of multiple complexes formed with a single ligand, which ACSV-CLE theory gathers into one cumulative conditional stability constant, are moreover pH dependent (Figure 4). These caveats are particularly salient because voltammetric analyses are rarely executed at ambient pH (Moffett and Dupont, 2007). Until the identities of natural organic ligands and their individual properties are more completely understood, the interpretation of measured conditional stability constants for their complexes with bio-essential metals and the correct definition of their (pH-dependent) SRCs in seawater remains fraught with ambiguity and must be undertaken with sensible caution.

AUTHOR CONTRIBUTIONS

JS designed the experiments, performed most of the titrations, conducted all non-linear regressions and speciation calculations, and wrote the manuscript. SMB performed some of the titrations and calculated the side-reaction coefficients.

FUNDING

The REU project of SMB was funded by NSF (OCE-1262374) and administered by the Maryland Sea Grant Program. Financial support for publication in open-access journals is provided by the University of Maryland.

ACKNOWLEDGMENTS

Alison Zoll rendered the molecular structure in Figure 1A with ChemDraw v.12.0. Our manuscript was significantly improved by the kind comments of reviewers David Turner and Robert Hudson. CBL statistician Dr. Slava Lyubchich gave expert advice on the error analysis of iterative non-linear regressions. We are grateful to the editors of this special volume of *Frontiers in Marine Science* for allowing us to present our work. This is UMCES contribution #5187.

SUPPLEMENTARY MATERIAL

The Supplementary Material for this article can be found online at: <http://journal.frontiersin.org/article/10.3389/fmars.2016.00117>

REFERENCES

- Anderegg, G., l'Eplattenier, F., and Schwarzenbach, G. (1963). Hydroxamatkomplexe II. Die anwendung der pH-methode. *Helv. Chim. Acta* 46, 1400–1408. doi: 10.1002/hlca.19630460435
- Baars, O., Abouchami, W., Galer, S. J. G., Boye, M., and Croot, P. L. (2014). Dissolved cadmium in the Southern Ocean: distribution, speciation, and relation to phosphate. *Limnol. Oceanogr.* 59, 385–399. doi: 10.4319/lo.2014.59.2.0385
- Baars, O., and Croot, P. L. (2015). Dissolved cobalt speciation and reactivity in the eastern tropical North Atlantic. *Mar. Chem.* 173, 310–319. doi: 10.1016/j.marchem.2014.10.006
- Boiteau, R. M., Fitzsimmons, J. N., Repeta, D. J., and Boyle, E. A. (2013). Detection of iron ligands in seawater and marine cyanobacteria cultures by high-performance liquid chromatography-inductively coupled plasma-mass spectrometry. *Anal. Chem.* 85, 4357–4362. doi: 10.1021/ac3034568
- Bruland, K. W. (1992). Complexation of cadmium by natural organic ligands in the central North Pacific. *Limnol. Oceanogr.* 37, 1008–1017.
- Bundy, R. M., Abdulla, H. A. N., Hatcher, P. G., Biller, D. V., Buck, K. N., and Barbeau, K. A. (2015). Iron-binding ligand and humic substances in the San Francisco Bay estuary and estuarine-influenced shelf regions of coastal California. *Mar. Chem.* 173, 183–194. doi: 10.1016/j.marchem.2014.11.005
- Byrne, R. H. (2002). "Speciation in seawater," in *Chemical Speciation in the Environment*, eds A. M. Ure and C. M. Davidson (Oxford, UK: Blackwell Science), 322–357.
- Capodaglio, G., Turetta, C., Toscano, G., Gambarom, A., Scarponi, G., and Cescon, P. (1998). Cadmium, lead and copper complexation in Antarctic coastal seawater. Evolution during the austral summer. *Intern. J. Environ. Anal. Chem.* 71, 195–226.
- Christenson, E. A., and Schijf, J. (2011). Stability of YREE complexes with the trihydroxamate siderophore desferrioxamine B at seawater ionic strength. *Geochim. Cosmochim. Acta* 75, 7047–7062. doi: 10.1016/j.gca.2011.09.022
- Coale, K. H., and Bruland, K. W. (1988). Copper complexation in the Northeast Pacific. *Limnol. Oceanogr.* 33, 1084–1101.
- Covington, A. K., and Thompson, R. (1974). Ionization of moderately strong acids in aqueous solution. Part III. Methane-, ethane-, and propanesulfonic acids at 25°C. *J. Solution Chem.* 3, 603–617.
- Einaga, H. (1981). The hydrolytic precipitation reaction of Mg(II) from aqueous NaNO₃ solution. *J. Inorg. Nucl. Chem.* 43, 229–233.
- Farkas, E., Enyedy, É., and Csóka, H. (1999). A comparison between the chelating properties of some dihydroxamic acids, desferrioxamine B and acetohydroxamic acid. *Polyhedron* 18, 2391–2398.
- Gjaldbaek, J. K. (1925). Untersuchungen über die löslichkeit des magnesiumhydroxyds. I. Von der Existenz verschiedener modifikationen von magnesiumhydroxyd. *Zeitschr. Anorg. Allgem. Chem.* 144, 145–168.
- Herbelin, A. L., and Westall, J. C. (1999). *FITEQL. A Computer Program for Determination of Chemical Equilibrium Constants from Experimental Data. Version 4.0.* Report 99-01, Department of Chemistry, Oregon State University, Corvallis, OR.
- Hernlem, B. J., Vane, L. M., and Sayles, G. D. (1996). Stability constants for complexes of the siderophore desferrioxamine B with selected heavy metal cations. *Inorg. Chim. Acta* 244, 179–184.
- Hudson, R. J. M., Covault, D. T., and Morel, F. M. M. (1992). Investigations of iron coordination and redox reactions in seawater using ⁵⁹Fe radiometry and ion-pair solvent extraction of amphiphilic iron complexes. *Mar. Chem.* 38, 209–235.
- Jacquot, J. E., Kondo, Y., Knapp, A. N., and Moffett, J. W. (2013). The speciation of copper across active gradients in nitrogen-cycle processes in the eastern tropical South Pacific. *Limnol. Oceanogr.* 58, 1387–1394. doi: 10.4319/lo.2013.58.4.1387
- Jakuba, R. W., Saito, M. A., Moffett, J. W., and Xu, Y. (2012). Dissolved zinc in the subarctic North Pacific and Bering Sea: its distribution, speciation, and importance to primary producers. *Global Biogeochem. Cycle* 26:GB2015. doi: 10.1029/2010gb004004
- Janz, G. J., Oliver, B. G., Lakshminarayanan, G. R., and Mayer, G. E. (1970). Electrical conductance, diffusion, viscosity, and density of sodium nitrate, sodium perchlorate, and sodium thiocyanate in concentrated aqueous solutions. *J. Phys. Chem.* 74, 1285–1289.
- Kem, M. P., Zane, H. K., Springer, S. D., Gauglitz, J. M., and Butler, A. (2014). Amphiphilic siderophore production by oil-associating microbes. *Metallomics* 6, 1150–1155. doi: 10.1039/c4mt00047a
- Kettler, R. M., Wesolowski, D. J., and Palmer, D. A. (1998). Dissociation constants of oxalic acid in aqueous sodium chloride and sodium trifluoromethanesulfonate media to 175°C. *J. Chem. Eng. Data* 43, 337–350.
- Kruff, B. I., Harrington, J. M., Duckworth, O. W., and Jarzęcki, A. A. (2013). Quantum mechanical investigation of aqueous desferrioxamine B metal complexes: Trends in structure, binding, and infrared spectroscopy. *J. Inorg. Biochem.* 129, 150–161. doi: 10.1016/j.jinorgbio.2013.08.008
- Martell, A. E., Smith, R. M., and Motekaitis, R. J. (2004). *NIST Critically Selected Stability Constants of Metal Complexes.* NIST Standard Reference Database 46 Version 8.0. Texas A&M University.
- Martin, J. D., Ito, Y., Homann, V. V., Haygood, M. G., and Butler, A. (2006). Structure and membrane affinity of new amphiphilic siderophores produced by *Ochrobactrum* sp. SP18. *J. Biol. Inorg. Chem.* 11, 633–641. doi: 10.1007/s00775-006-0112-y
- Martinez, J. S., Zhang, G. P., Holt, P. D., Jung, H.-T., Carrano, C. J., Haygood, M. G., et al. (2000). Self-assembling amphiphilic siderophores from marine bacteria. *Science* 287, 1245–1247. doi: 10.1126/science.287.545.6.1245
- Mawji, E., Gledhill, M., Milton, J. A., Tarran, G. A., Usher, S., Thompson, A., et al. (2008). Hydroxamate siderophores: occurrence and importance in the Atlantic Ocean. *Environ. Sci. Technol.* 42, 8675–8680. doi: 10.1021/es801884r
- McCormack, P., Worsfold, P. J., and Gledhill, M. (2003). Separation and detection of siderophores produced by marine bacterioplankton using high-performance liquid chromatography with electrospray ionization mass spectrometry. *Anal. Chem.* 75, 2647–2652. doi: 10.1021/ac0340105
- McKnight, D. M., and Morel, F. M. M. (1980). Copper complexation by siderophores from filamentous blue-green algae. *Limnol. Oceanogr.* 25, 62–71.
- Millero, F. J., and Schreiber, D. R. (1982). Use of the ion pairing model to estimate activity coefficients of the ionic components of natural waters. *Am. J. Sci.* 282, 1508–1540.
- Moffett, J. W., and Dupont, C. (2007). Cu complexation by organic ligands in the sub-arctic NW Pacific and Bering Sea. *Deep-Sea Res. I* 54, 586–595. doi: 10.1016/j.dsr.2006.12.013
- Morel, F., and Morgan, J. (1972). A numerical method for computing equilibria in aqueous chemical systems. *Environ. Sci. Technol.* 6, 58–67.
- Neilands, J. B. (1981). Microbial iron compounds. *Ann. Rev. Biochem.* 50, 715–731.
- Neilands, J. B., and Leong, S. A. (1986). Siderophores in relation to plant growth and disease. *Ann. Rev. Plant Physiol.* 37, 187–208.
- Pižeta, I., Sander, S. G., Hudson, R. J. M., Omanović, D., Baars, O., Barbeau, K. A., et al. (2015). Interpretation of complexometric titration data: An intercomparison of methods for estimating models of trace metal complexation by natural organic ligands. *Mar. Chem.* 173, 3–24. doi: 10.1016/j.marchem.2015.03.006
- Ringbom, A., and Still, E. (1972). The calculation and use of a coefficients. *Anal. Chim. Acta* 59, 143–146.
- Ross, A. R. S., Ikonoumou, M. G., and Orians, K. J. (2003). Characterization of copper-complexing ligands in seawater using immobilized copper(II)-ion affinity chromatography and electrospray ionization mass spectrometry. *Mar. Chem.* 83, 47–58. doi: 10.1016/S0304-4203(03)00095-1
- Rue, E. L., and Bruland, K. W. (1995). Complexation of iron(III) by natural organic ligands in the Central North Pacific as determined by a new competitive ligand equilibration/adsorptive cathodic stripping voltammetric method. *Mar. Chem.* 50, 117–138.
- Schijf, J., and Byrne, R. H. (2001). Stability constants for mono- and dioxalato-complexes of Y and the REE, potentially important species in groundwaters and surface freshwaters. *Geochim. Cosmochim. Acta* 65, 1037–1046. doi: 10.1016/S0016-7037(00)00591-3
- Schijf, J., Christenson, E. A., and Potter, K. J. (2015). Different binding modes of Cu and Pb vs. Cd, Ni, and Zn with the trihydroxamate siderophore desferrioxamine B at seawater ionic strength. *Mar. Chem.* 173, 40–51. doi: 10.1016/j.marchem.2015.02.014
- Schwarzenbach, G., and Schwarzenbach, K. (1963). Hydroxamatkomplexe I. die stabilität der eisen(III)-komplexe einfacher hydroxamsäuren und des ferrioxamins B. *Helv. Chim. Acta* 46, 1390–1400.

- Springer, S. D., and Butler, A. (2016). Microbial ligand coordination: consideration of biological significance. *Coord. Chem. Rev.* 306, 628–635. doi: 10.1016/j.ccr.2015.03.013
- Town, R. M., and Filella, M. (2000). Dispelling the myths: is the existence of L1 and L2 ligands necessary to explain metal ion speciation in natural waters? *Limnol. Oceanogr.* 45, 1341–1357. doi: 10.4319/lo.2000.45.6.1341
- Trick, C. G. (1989). Hydroxamate-siderophore production and utilization by marine eubacteria. *Curr. Microbiol.* 18, 375–378.
- van den Berg, C. M. G., and Nimmo, M. (1987). Determination of interactions of nickel with dissolved organic material in seawater using cathodic stripping voltammetry. *Sci. Total Environ.* 60, 185–195.
- Vraspir, J. M., and Butler, A. (2009). Chemistry of marine ligands and siderophores. *Ann. Rev. Mar. Sci.* 1, 43–63. doi: 10.1146/annurev.marine.010908.163712
- Waska, H., Koschinsky, A., Ruiz Chanco, M. J., and Dittmar, T. (2015). Investigating the potential of solid-phase extraction and Fourier-transform ion cyclotron resonance mass spectrometry (FT-ICR-MS) for the isolation and identification of dissolved metal-organic complexes from natural waters. *Mar. Chem.* 173, 78–92. doi: 10.1016/j.marchem.2014.10.001
- Westall, J. C., Zachary, J. L., and Morel, F. M. M. (1986). MINEQL. A Computer Program for the Calculation of the Chemical Equilibrium Composition of Aqueous Systems. Version 1. Report 86-01. Department of Chemistry, Oregon State University, Corvallis, OR.
- Whisenhunt, D. W. Jr., Neu, M. P., Hou, Z., Xu, J., Hoffman, D. C., and Raymond, K. N. (1996). Specific sequestering agents for the actinides. 29. Stability of the thorium(IV) complexes of desferrioxamine B (DFO) and three octadentate catecholate or hydroxypyridinonate DFO derivatives: DFOMTA, DFOCAMC, and DFO-1,2-HOPO. Comparative stability of the plutonium(IV) DFOMTA complex. *Inorg. Chem.* 35, 4128–4136.
- Whitby, H., and van den Berg, C. M. G. (2015). Evidence for copper-binding humic substances in seawater. *Mar. Chem.* 173, 282–290. doi: 10.1016/j.marchem.2014.09.011
- Wuttig, K., Heller, M. I., and Croot, P. L. (2013). Reactivity of inorganic Mn and Mn desferrioxamine B with O₂, O₂⁻, and H₂O₂ in seawater. *Environ. Sci. Technol.* 47, 10257–10265. doi: 10.1021/es4016603
- Yoshida, T., Ozaki, T., Ohnuki, T., and Francis, A. J. (2004). Interactions of trivalent and tetravalent heavy metal-siderophore complexes with *Pseudomonas fluorescens*. *Radiochim. Acta* 92, 749–753. doi: 10.1524/ract.92.9.749.55003
- Zane, H. K., Naka, H., Rosconi, F., Sandy, M., Haygood, M. G., and Butler, A. (2014). Biosynthesis of amphi-enterobactin siderophores by *Vibrio harveyi* BAA-1116: Identification of a bifunctional nonribosomal peptide synthetase condensation domain. *J. Am. Chem. Soc.* 136, 5615–5618. doi: 10.1021/ja5019942

Conflict of Interest Statement: The authors declare that the research was conducted in the absence of any commercial or financial relationships that could be construed as a potential conflict of interest.

Copyright © 2016 Schijf and Burns. This is an open-access article distributed under the terms of the Creative Commons Attribution License (CC BY). The use, distribution or reproduction in other forums is permitted, provided the original author(s) or licensor are credited and that the original publication in this journal is cited, in accordance with accepted academic practice. No use, distribution or reproduction is permitted which does not comply with these terms.



Fe- and Cu-Complex Formation with Artificial Ligands Investigated by Ultra-High Resolution Fourier-Transform ion Cyclotron Resonance Mass Spectrometry (FT-ICR-MS): Implications for Natural Metal-Organic Complex Studies

Hannelore Waska^{1*}, Andrea Koschinsky² and Thorsten Dittmar¹

¹ Research Group for Marine Geochemistry (ICBM-MPI Bridging Group), Institute for Chemistry and Biology of the Marine Environment (ICBM), Carl von Ossietzky University Oldenburg, Oldenburg, Germany, ² Department of Physics and Earth Sciences, Jacobs University Bremen, Bremen, Germany

OPEN ACCESS

Edited by:

Kristen Nicolle Buck,
University of South Florida, USA

Reviewed by:

Martha Gledhill,
GEOMAR Helmholtz Centre for Ocean
Research Kiel, Germany
Rene Boiteau,
Woods Hole Oceanographic
Institution, USA

*Correspondence:

Hannelore Waska
hannelore.waska@uni-oldenburg.de

Specialty section:

This article was submitted to
Marine Biogeochemistry,
a section of the journal
Frontiers in Marine Science

Received: 31 March 2016

Accepted: 22 June 2016

Published: 12 July 2016

Citation:

Waska H, Koschinsky A and Dittmar T
(2016) Fe- and Cu-Complex
Formation with Artificial Ligands
Investigated by Ultra-High Resolution
Fourier-Transform ion Cyclotron
Resonance Mass Spectrometry
(FT-ICR-MS): Implications for Natural
Metal-Organic Complex Studies.
Front. Mar. Sci. 3:119.
doi: 10.3389/fmars.2016.00119

In recent years, electrospray-ionization mass spectrometry (ESI-MS) has been increasingly used to complement the bulk determination of metal-ligand equilibria, for example via competitive ligand exchange-adsorptive cathodic stripping voltammetry (CLE-ACSV). However, ESI-MS speciation analyses may be impacted by instrumental artifacts such as reduction reactions, fragmentation, and adduct formation at the ESI source, changes in the ionization efficiencies of the detected species in relation to sample matrix, and peak overlaps in response to increasing sample complexity. In our study, equilibria of the known artificial ligands citrate, ethylenediaminetetraacetic acid (EDTA), 1-nitroso-2-naphthol (NN), and salicylaldoxime (SA) with iron (Fe) and copper (Cu) were investigated by ultra-high resolution ESI-MS, Fourier-transform ion cyclotron resonance mass spectrometry (FT-ICR-MS), under a variety of sample matrix and ionization settings. The acquired mass spectra were compared with metal-ligand equilibrium data from the literature as well as an adapted speciation model. Overall, the mass spectra produced representative species mentioned in previous reports and predicted by the speciation calculations, such as Fe(Cit), Cu(Cit)₂, Fe(EDTA), Cu(EDTA), Fe(NN)₃, and Cu(SA)₂. The analyses furthermore revealed new species which had been hypothesized but not measured directly using other methods, for example ternary complexes of citrate with Fe and Cu, Cu(SA) monomers, and the dimer Fe(SA)₂. Finally, parallel measurements of a Cu+SA calibration series and a Cu+SA+EDTA competition series indicated that FT-ICR-MS can produce linear responses and low detection limits analogous to those of ACSV. We propose that ultra-high resolution FT-ICR-MS can be used as a representative tool to study interactions of trace metals with artificial as well as natural, unknown ligands at the molecular level.

Keywords: ligands, FT-ICR-MS, iron, copper, EDTA, citrate, salicylaldoxime, 1-nitroso-2-naphthol

INTRODUCTION

Electrospray-ionization mass spectrometry (ESI-MS) has become a promising new technique for the description of metal-ligand equilibria using known ligands. The advantage of ESI-MS resides in its easy application—samples in solution can be swiftly processed under a wide array of conditions—and its soft ionization procedure which allows for the detection of whole metal-organic compounds (Di Marco and Bombi, 2006). The ESI-MS measurements of known metal-ligand mixtures can be compared with speciation data acquired from other methods such as computational speciation modeling, crystallography, or complex affinity titrations. For example, the complexing behavior of citrate, an important natural metal chelator which forms highly diverse species with iron under different pH and stoichiometry conditions, has been studied by ESI-MS in comparison with complementary techniques, such as spectrophotometric titrations and chemical modeling (Gautier-Luneau et al., 2005; Nischwitz and Michalke, 2009; Silva et al., 2009; Bertoli et al., 2015). In parallel to these studies on artificial metal-organic compounds under well-constrained conditions, ESI-MS has recently been applied to identify unknown metal-binding ligands isolated from natural waters, which ubiquitously occur as a component of natural dissolved organic matter (DOM), and which govern the mobility and availability of bioactive trace metals such as iron (Fe) and copper (Cu) (McCormack et al., 2003; Ross et al., 2003; Mawji et al., 2008, 2011; Stenson, 2009; Velasquez et al., 2011). Although the number of studies in the field is scarce, they have shown that ESI-MS is currently the only technique with the potential to study a large number of metal-organic complexes simultaneously at the molecular level: ESI-MS and in particular ESI-FT-ICR-MS (Electrospray-ionization Fourier-transform ion cyclotron resonance mass spectrometry) are capable of resolving the high complexity of DOM, where thousands of unique compounds occur at pico- to nanomolar concentrations (Repeta, 2015). As such, they complement one of the most wide-spread methods currently applied to characterize the bulk metal-binding capacity of natural DOM, competitive ligand exchange-adsorptive cathodic stripping voltammetry (CLE-ACSV, Buck and Bruland, 2005; Buck et al., 2007). CLE-ACSV is highly sensitive (detection limits are usually at pico- to nanomolar levels), quantitative, and metal-ligand speciation can be investigated at near-natural conditions with regards to pH and sample matrix (including ionic strength). However, the high complexity of DOM is not sufficiently represented in CLE-ACSV measurements, even though metal-binding ligands within DOM are treated as a composite of multiple sub-classes defined by the analytical window (i.e., the amount of added artificial ligand for competition with the natural ligands). Furthermore, the natural ligands are investigated based on the response of the added competing artificial ligand, rather than by direct observation of their behavior. ESI-MS, and in particular high-resolution ESI-FT-ICR-MS, thus holds great potential to extend this field of research (Waska et al., 2015).

To complement CLE-ACSV by ESI-MS and ESI-FT-ICR-MS, potential instrument-specific artifacts of the ESI-MS technique have to be taken into account (Di Marco and Bombi, 2006;

Keith-Roach, 2010; Waska et al., 2015). Examples for such effects are:

- (1) **Speciation** changes of the sample, for example through reduction, adduct formation, and fragmentation at the ESI source or in the gas phase can impact metal-ligand equilibria and prevent the detection of target molecules.
- (2) **Signal intensities** of the different species are affected by their net charge in aqueous solutions, but also by **compound specific response factors** influenced by ionization mode and sample matrix (for example, the presence of other ions causing signal enhancement or suppression).
- (3) Sample requirements for the optimum performance of the instrument, such as low ionic strengths, and the addition of organic solvents for ionization enhancement, may prevent **quantitative and qualitative comparisons** of *in vitro* metal-ligand equilibria with those taking place in natural aqueous environments.

All of the above mentioned issues have been known for a while (Di Marco and Bombi, 2006), but only in recent years, systematic, and compound-specific investigations have been increasingly used to evaluate ESI-MS as a quantitative tool in metal-ligand equilibrium studies (Gledhill, 2001; Rellán-Álvarez et al., 2008; Keith-Roach, 2010; Reinoso-Maset et al., 2012). In this study, we aim to address the above mentioned analytical challenges, and report the applicability of ultra-high resolution ESI-FT-ICR-MS for the qualitative and quantitative investigation of metal-ligand equilibria. ESI-FT-ICR-MS is traditionally used to resolve complex mixtures of organic compounds such as natural DOM (Koch et al., 2005). Organic compounds show linear responses in FT-ICR-MS based on their relative abundance in a complex matrix (Seidel et al., 2015), but this approach is rarely used for quantitative studies of known target compounds in natural DOM. Compared to ESI-MS systems with lesser resolving power, the employment of ESI-FT-ICR-MS provides a higher degree of certainty in the detection of monoisotopic mass differences of metal-containing complexes (Waska et al., 2015), and furthermore enables the automatized assignment of molecular formulae based on the Kendrick mass defect (Koch et al., 2007). Both these advantages result in a swifter and more accurate detection of target compounds in known metal-ligand equilibria, and provide the additional opportunity to identify unknown molecules in complex natural mixtures such as DOM.

For our study, we chose two experimental approaches:

- (1) A baseline study of well-known metal-organic complexes in a fixed metal-ligand stoichiometry at fixed pH under different sample matrix and ionization conditions. The resulting qualitative speciation patterns and response factors were compared with speciation data from the literature.
- (2) A quantitative study where a known artificial ligand was titrated with increasing metal concentrations, once in the absence and once in the presence of another known competing ligand analogous to a CLE-ACSV calibration series. The resulting calibration curves were compared to

the results of simultaneous CLE-ACSV measurements of the same sample setup.

The experimental approaches were backed up by metal-ligand speciation calculations using the modeling program PHREEQC (PHREEQC for Windows, version 2.18.00, http://wwwbrr.cr.usgs.gov/projects/GWC_coupled/phreeqc/) with a default minteqv4 database designed to predict metal-ligand speciation in aqueous solutions. This database already included several known ligands, and was extended in the scope of this study to accommodate all investigated artificial ligands, by using conditional stability constants from the literature (e.g., Gledhill and van den Berg, 1994; Abualhaija et al., 2015).

The focus of our study lays on Fe - and Cu- complexes due to their bioactive nature and high affinity for organic ligands (Van den Berg, 1984; Rue and Bruland, 1995; Buck and Bruland, 2005; Buck et al., 2007). For the qualitative study, we chose a representative range of previously described ligands with different functional groups, binding stoichiometries, and binding strengths (**Table 1**): *Citrate* is a naturally occurring, physiologically important metal chelator which has been studied in-depth by ESI-MS and other speciation methods (Gautier-Luneau et al., 2005; Nischwitz and Michalke, 2009; Silva et al., 2009; Bertoli et al., 2015). Because it is a tricarboxylate chelator with an additional binding hydroxyl group, it could be seen as a representative of natural DOM which is largely composed of $C_xH_yO_z$ compounds and also contains a high density of carboxyl and hydroxyl functional groups as revealed by NMR analyses (Hertkorn et al., 2006; Repeta, 2015). *EDTA*, an artificial ligand produced for industrial and pharmaceutical applications, has gained recent interest due to its accumulation in the aquatic environment, where it impacts trace metal mobility (Nowack, 2002). It is a hexadentate ligand with two amine and four carboxylate functional groups and forms strong 1:1 or 1:2 complexes with transition metals and other cations (Chen et al., 2008; Reinoso-Maset et al., 2012). *1-nitroso-2-naphthol* (hereafter referred to as NN) is a hydrophobic metal chelator with a nitroso- and a hydroxyl group. Due to its ability to form strong, electroactive 1:3 complexes with Fe it is used for the determination of free (Van den Berg et al., 1991) and organically bound (Wu and Luther, 1995; Hawkes et al., 2013) Fe in natural water samples via adsorptive cathodic stripping voltammetry (ACSV) and CLE-ACSV, respectively. *Salicylaldehyde oxime* (SA), a salicylaldehyde oxime, is a chelator with an oxime and a hydroxyl functional group which forms 1:1 and 1:2 complexes with Cu and Fe, and is routinely used in the determination of Fe- and Cu-complexing capacities of DOM in natural water samples via CLE-ACSV (Campos and van den Berg, 1994; Rue and Bruland, 1995). For the quantitative study, we chose an SA-EDTA ligand system competing for Cu. This system has been extensively studied by CLE-ACSV under variations of matrix conditions such as pH and ionic strength (Campos and van den Berg, 1994; Buck and Bruland, 2005).

To the best of our knowledge, NN and SA have not been studied in detail by ESI-MS, and none of the abovementioned ligands have been investigated by ultra-high resolution ESI-FT-ICR-MS (Di Marco and Bombi, 2006; Keith-Roach, 2010). Our

study thus lays the foundation to describing the natural metal-DOM pool with two contrasting and complementary techniques (CLE-ACSV and ESI-FT-ICR-MS) in the future.

MATERIALS AND METHODS

Sample Preparation

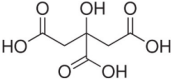
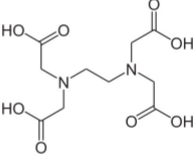
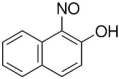
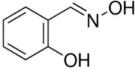
Baseline Setup

We produced a series of metal-ligand complex solutions by adding NIST traceable Fe and Cu standards (Alfa Aesar plasma standard solutions, original stock solutions in 5% HNO_3 , diluted in 0.01 M HCl suprapur for this study) to solutions of citrate (mono-sodium citrate, AppliChem), EDTA (EDTA tripotassium salt dihydrate, AppliChem), NN (1-nitroso-2-naphthol, 99%, Alfa Aesar), and SA (salicylaldehyde oxime $\geq 98\%$, Sigma Aldrich; **Table 1**). With the exception of NN, which was prepared using Optima LC-MS grade methanol (Fisher Chemicals), all ligand solutions were prepared with ultrapure water. The final metal-ligand solutions amounted to 20 μM metal (10 μM Fe and 10 μM Cu) and 100 μM ligand, producing a theoretical metal:ligand stoichiometry of 1:5 each. We chose this stoichiometry to provide sufficient ligands for both trace metals, thus preventing competition for binding sites and enabling simultaneous detection of free ligands as well as Fe- and Cu-complexes. The pH of the solutions was adjusted to $pH = 7.1 \pm 0.2$ in two setups using either sodium hydroxide or aqueous ammonia (both suprapur, Merck) and they were equilibrated overnight (>12 h) at room temperature. Thereafter, methanol (Optima LC-MS grade, Fisher Chemicals) was added to one set of solutions to produce a 1:1 methanol-water matrix, whereas the second set was kept in a water matrix. Both setups amounted to the same final ligand and trace metals concentrations. All solutions were filtered through 0.2 μm PTFE syringe filters prior to measurement.

Quantitative Setup

First, a calibration series was made by titrating increasing amounts of Cu (0–20 μM) to a constant amount of SA (200 μM) in 15 mL polytetrafluorethylene (PTFE) vials (VWR). The pH of the calibration solutions was adjusted to $pH = 7.5 \pm 0.2$ using sodium hydroxide. Subsamples were filtered through 0.2 μm PTFE syringe filters into acid-washed 2 mL Eppendorf safe-lock tubes, and Optima-grade methanol was added to each vial to produce a 1:1 (v:v) sample solution for FT-ICR-MS analysis. In a second treatment, we added 2 μM EDTA to each vessel of the same SA-Cu titration setup (0–20 μM Cu, 200 μM SA), and the samples were allowed to equilibrate overnight. Again, subsamples of the solutions were filtered into pre-cleaned safe-lock tubes and methanol was added prior to FT-ICR-MS measurements to produce a 1:1 (v:v) solution. The dilution with methanol resulted in final concentrations of 100 μM SA, 1 μM EDTA, and 0–10 μM Cu. Both setups (Cu + SA or Cu + EDTA + SA) were reproduced three times with the used reagent solutions being discarded after overnight equilibration, to condition all reaction vessels (PTFE and Eppendorf vials) before final sample preparations for the FT-ICR-MS measurement.

TABLE 1 | Properties of investigated ligands.

Ligand	Structure	logKCu(II)	logKFe(III)	Functional groups	Complex stoichiometry (for Fe and Cu)	References
Citric acid		6.1	11.85	3 carboxylate, 1 hydroxyl	1:2, 1:3 (Fe) 1:2, 1:3 (Cu)	Furia, 1972
EDTA		18.8	25.7	4 carboxylate, 2 amine	1:1 (Fe) 1:1 (Cu)	Furia, 1972
1-nitroso-2-naphthol		8.61	35.32*	1 nitroso, 1 hydroxyl	1:3 (Fe) 1:1 (Cu)	Sathe and Shetty, 1970 *Gledhill and van den Berg, 1994
Salicylaldoxime		11.97 Cu(SA)** 18.43 Cu(SA) ₂ **	6.66 Fe(SA)** 19.90 Fe(SA) ₂ **	1 oxime, 1 hydroxyl	1:1, 1:2 (Fe) 1:1, 1:2 (Cu)	**Abualhajja et al., 2015

All constants are for aqueous solutions with low salinity. *, ** had to be corrected for low salinity (calculated for the samples from this study to a salinity = 1×10^{-5}) based on the equations reported by the cited references.

FT-ICR-MS Analyses

The artificial metal-ligand solutions were analyzed in duplicates (qualitative setup) and triplicates (quantitative setup) on an ultra-high resolution 15 Tesla ESI-FT-ICR-MS (Solarix, Bruker Daltonics). All sample measurements were conducted in positive and negative ionization mode to compare speciation and ionization efficiencies of the complexes under the experimental pH and solvent settings. The measurement parameters were adapted from in-house tuning procedures commonly used for DOM analyses, in broadband scan mode with a syringe flow rate of $120 \mu\text{L h}^{-1}$ and an ion accumulation time of 0.20 s for negative and 0.25 s for positive ionization mode. For each sample, 100 mass scans were accumulated. Calibration was conducted internally using the Bruker DataAnalysis software with an error of <0.1 ppm, based on a specifically created mass list containing the calculated monoisotopic masses of the most dominant free ligands and complexes (Compass IsotopePattern, Bruker Daltonics), as well as known contaminations commonly found in ESI-MS spectra, such as fatty acids (Keller et al., 2008). The calibrated mass spectra were assembled to a common data table using a mass matching in-house Matlab script. To ensure reproducibility of the detected compounds and remove any noise, any detected mass had to occur in all replicate measurements of each setup to be considered for further data processing. Additionally, the acquired mass lists were processed with a Matlab search routine detecting $^{54/56}\text{Fe}$, $^{63/65}\text{Cu}$, $^{35/37}\text{Cl}$, $^{12/13}\text{C}$, and $^{39/41}\text{K}$ monoisotopic patterns based on the mass and abundance differences of the naturally occurring isotopes (Waska et al., 2015). This search routine was modified to detect peaks for up to three elements per molecule ($^{54/56}\text{Fe}$, $^{63/65}\text{Cu}$, $^{35/37}\text{Cl}$), and multiple ionization patterns ($^{12/13}\text{C}$). Thereafter, molecular formulae were assigned with the DataAnalysis software. A maximum mass error of 0.5 ppm was allowed, and the

elements $\text{C}_{1-50}\text{H}_{1-200}\text{O}_{1-100}\text{N}_{0-6}\text{Fe}_{0-3}\text{Cu}_{0-3}\text{Na}_{0-5}\text{Cl}_{0-5}$ were considered, allowing even and odd electron configurations where applicable (radicals with free electrons were not considered). Since EDTA had been added as potassium salt, K_{0-5} was included for the assignment of molecular formulae in the EDTA samples to account for potassium adducts. Only molecular formulae containing the molecular building blocks of the measured ligand (for example, C_6 and O_7 and their multiples for citrate) with a matching isotope pattern ($^{12/13}\text{C}$ plus the corresponding heteroatoms of the calculated molecular formulae) were taken into account. Thus, fragmented complexes or compounds with adducts other than NH_3^+ , Na^+ , K^+ , and Cl^- were not included.

CLE-ACSV Analyses

The Cu + SA ± EDTA titration setups were diluted 1:50 (Cu + SA only) and 1:25 (Cu + SA + EDTA) with ultrapure water and measured by ACSV (Campos and van den Berg, 1994; Waska et al., 2015). Immediately before the measurements, 100 μL of 3M KCl suprapur and 100 μL chelexed HEPES buffer (pH = 7.8) were added. The final solutions had a volume of 10 mL. Addition of KCl and HEPES buffer were included to (i) ensure enough ionic strength for the voltammetric cell, and (ii) achieve a stable pH for a reproducible location (and thus sensitivity) of the Cu-SA peak in the potential-current diagram. The instrument used was a Metrohm 757VA Computrace equipped with a hanging drop mercury electrode (HDME), a 3M KCl-filled reference electrode and a glassy carbon counter electrode. Samples were initially purged for 300 s with high purity Ar gas, then the salicylaldoxime-copper complex was deposited for 60 s at a potential of -50 mV. After an equilibration time of 5 s, the samples were scanned from -50 to -600 mV at a sweep rate of 20 mV s⁻¹. The measurement of each sample was repeated three times.

Speciation Calculations using PHREEQC

To predict ligand and metals speciation, thermodynamic equilibrium calculations were performed using the aqueous geochemical modeling program PHREEQC (Parkhurst and Appelo, 1999) with a minteqv4 database already containing conditional stability constants of EDTA and citrate with a variety of cations including Fe and Cu. Conditional stability constants were implemented into the minteqv4 database as follows: The conditional stability constant ($\log K$) for $\text{Cu}(\text{NN})_2$ was used directly from Sathe and Shetty (1970), whereas for $\text{Fe}(\text{NN})_3$, $\text{Cu}(\text{SA})$, $\text{Cu}(\text{SA})_2$, $\text{Fe}(\text{SA})$, and $\text{Fe}(\text{SA})_2$, $\log K'$ values were adjusted for an approximation of salinity ~ 0 (salinity = 1×10^{-5}) using the respective equations reported by Gledhill and van den Berg (1994) and Abualhaja et al. (2015) (Table 1). To calculate activity coefficients, by default a Davies equation was used by the program. The modified database is provided as Supplementary Information. Sample solutions for the calculations contained the adjusted pH and known added concentrations of Fe, Cu, and ligands. Only Fe(III) and Cu(II) were considered in the calculations, which were the main expected oxidation states of the NIST traceable standard solutions originally provided from Alfa Aesar in 5% HNO_3 . For oxygen and inorganic carbon contents, default concentrations of 64.5 and 0.49 μM , respectively, were incorporated from the PHREEQC examples database. Concentrations of K and Na corresponded to the added amounts of EDTA and citrate salts, respectively. In addition, concentrations of Cl, Na, and N(-3) corresponded to the added amounts of HCl (via the Fe and Cu spikes), NaOH, and aqueous ammonia (during pH adjustments). Because minteqv4 was created for aqueous solutions, the methanol content was not taken into account for the speciation calculations. This and other limitations of the speciation model (for instance, lack of data for complexes with yet unknown stoichiometries, metal valences, or cations such as Na^+ and K^+) may have impacted the outcome and should thus be kept in mind when considering the subsequent interpretations.

RESULTS

Speciation Patterns of the Target Compounds

In both ionization modes, the mass spectra of the investigated metal-ligand solutions were comprised mostly (86–90%) of singly ionized target compounds as revealed by the single charge $^{12/13}\text{C}$ isotope patterns opposed to those with double (9–14%) or triple (1–2%) charge. Moreover, all of the detected metal-ligand complexes were singly charged as well (Tables 2–5). The high mass resolution allowed the confirmation of the majority of the target compounds based on their unique isotopic patterns. For example, in negative ionization mode, the isotope mass differences of the detected complexes were (average of >10 measurements \pm standard deviation): $^{54/56}\text{Fe}$ (1.995329 \pm 0.00003 Da, natural difference: 1.995327 Da), $^{63/65}\text{Cu}$ (1.998198 \pm 0.000006 Da, natural difference: 1.99819 Da), $^{35/37}\text{Cl}$ (1.99705 \pm 0.00003 Da, natural difference: 1.99705 Da), $^{12/13}\text{C}$ (1.00337 \pm

0.00002 Da, natural difference: 1.00336 Da), and $^{39/41}\text{K}$ (1.99824 \pm 0.0002 Da, natural difference: 1.99812 Da). It should be noted that in complexes with a co-occurrence of K and Cu (found only in the solutions with EDTA), the isotope patterns of the two elements could not be resolved from each other due to their similar mass spacing: The overlap of the ^{65}Cu and ^{41}K signals changed the signal intensities of the apparent isotopologues, and prevented detection by the automated Matlab script.

For all investigated ligands and both ionization modes, adduct formation was observed: The dominant adduct was Na^+ , followed by K^+ (only for EDTA measurement setups) and Cl^- . Despite addition of aq. ammonia for pH adjustment in half of the experimental setups, NH_3^+ adducts were rarely found (Tables 2–5). In contrast to the numerous adduct-containing compounds detected via FT-ICR-MS, PHREEQC results had predicted that > 99% of Na^+ , K^+ , and Cl^- occurred as free ions in aqueous solution, while unbound ligand species differed only in their degree of protonation by free H^+ ions. Only sodium citrate species were calculated to occur in non-negligible amounts (732 nM), and only for the sample setup with NaOH as added base.

In the mass spectra, citrate compounds were mostly detected as mono-, di-, and trimers (Table 2), while mono- and dimers prevailed in the PHREEQC calculations. Three out of the four complexes predicted by the speciation calculations also occurred in the FT-ICR-MS spectra: a $\text{Fe}(\text{Cit})$ monomer, a $\text{Cu}(\text{Cit})_2$ dimer, and a $\text{Cu}_2(\text{Cit})_2$ dimer. A $\text{Cu}(\text{Cit})$ monomer predicted by PHREEQC was not detected in the mass spectra; instead, a 2:2 (metal:ligand) complex of Fe with citrate, and a ternary 2:2 complex of Fe and Cu with citrate, were found (Table 2). FT-ICR-MS and PHREEQC speciation results also overall agreed for the EDTA setups: Mostly monomers occurred, and Fe and Cu were exclusively complexed in 1:1 stoichiometries as well (Figure 1, Table 3). Although most detected metal-EDTA complexes in the mass spectra were with Fe(III) and Cu(II), three reduced Fe(II) complexes [$(\text{HEDTA})\text{Fe}(\text{II})^-$ ($m/z = 345.0026$), [$(\text{EDTA})\text{KFe}(\text{II})^-$ ($m/z = 382.9585$), and [$(\text{H}_2\text{EDTA})(\text{NH}_3)\text{Fe}(\text{II})^+$ ($m/z = 363.0361$)] occurred with small intensities (Table 3). NN generally occurred as mono- to trimers in negative, and mono- to pentamers in positive ionization mode. The Cu-NN ratio in the detected complexes was 1:2, while Fe was complexed by NN in 1:3, 1:4, and 1:5 stoichiometries. In negative ionization mode, these metal-NN complexes exclusively contained reduced Fe(II) and Cu(I), while in positive mode, Fe(III)(NN)₃ and Cu(II)(NN)₂ complexes were also detected (Table 4). In comparison, the speciation models predicted the occurrence of free NN exclusively as monomers, while for Fe and Cu, only the 1:3 and 1:2 stoichiometries, respectively, were calculated. Finally, all Cu and Fe were calculated in PHREEQC to be bound to SA in both 1:1 and 1:2 stoichiometries, and free SA was predicted to occur as monomer. Analogous to citrate, free SA also occurred in trimers in addition to the predicted mono-, and dimers in the mass spectra. It was bound to Fe in 1:1 and 1:2, and to Cu in 1:1, 1:2, and 1:3 stoichiometries. Both Cu(I) and Cu(II) were involved in the 1:1 complex formation with SA, while Fe was bound as Fe(III) (Table 5).

TABLE 2 | Detected citrate and citrate ± Fe ± Cu species (bold) in the four analytical setups at the FT-ICR-MS.

Ionization	Species	m/z	MeOH + H ₂ O + NH ₄	H ₂ O + NH ₄	MeOH + H ₂ O + Na	H ₂ O + Na
Negative	[(H ₃ Cit)] ⁻	191.0197	100	100	12.4	70.7
	[(H ₂ Cit)Na] ⁻	213.0017	2.3	1.7	6.8	14.2
	[(HCit)Na ₂] ⁻	234.9836	1.3	0.7	100	100
	[(Cit)Na ₃] ⁻	256.9655			22.2	10.1
	[(H ₂ Cit)Na ₂ Cl] ⁻	270.9603	3.1	1.8	1.2	9.5
	[(HCit)ClFe(III)]⁻	279.9078	1.7			
	[(HCit)Na ₃ Cl] ⁻	292.9423	0.4		21.8	22.3
	[(HCit)Na ₄ Cl ₂] ⁻	350.9008	0.2		10.3	13.7
	[(H ₄ Cit)(H ₃ Cit)] ⁻	383.0467	0.9	2.5		
	[(H ₃ Cit) ₂ Na] ⁻	405.0287	21.5	51.8	0.8	7.7
	[(H ₃ Cit)(H ₂ Cit)Na ₂] ⁻	427.0106	27.9	45.0	1.6	13.2
	[(H ₂ Cit) ₂ Na ₃] ⁻	448.9926	16.1	16.9	2.5	16.2
	[(H₂Cit)₂NaCu(II)]⁻	465.9427	1.5			
	[(H₂Cit)(HCit)Na₂Cu(II)]⁻	487.9246	0.5			
	[(HCit) ₂ Na ₅] ⁻	492.9565	0.1		57.9	39.7
	[(HCit)₂Cu(II)Fe(III)]⁻	496.8723	1.5			
	[(H₂Cit)(HCit)Cu(II)]₂⁻	504.8745	1.1			
	[(Cit)₂NaFe(III)]₂⁻	510.8517	0.9			
	[(HCit)(Cit)NaCu(II)Fe(III)]⁻	518.8542	1.8			
	[(HCit)₂NaCu(II)]₂⁻	526.8567	1.5			
[(H ₃ Cit) ₃ Na ₂] ⁻	619.0378	3.2	10.0			
[(H ₃ Cit) ₂ (H ₂ Cit)Na ₃] ⁻	641.0198	4.2	9.0			
[(H ₃ Cit)(H ₂ Cit) ₂ Na ₄] ⁻	663.0015	3.5	3.6		2.9	
Positive	[(H ₅ Cit)] ⁺	193.0343	10.0	11.5		
	[(H ₅ Cit)(NH ₃)] ⁺	210.0608	76.9	100		
	[(H ₄ Cit)Na] ⁺	215.0162	100	78.3		
	[(H ₃ Cit)Na ₂] ⁺	236.9982	15.1	10.4		
	[(H ₂ Cit)Na ₃] ⁺	258.9801	2.8	2.4		
	[HCitNa ₄] ⁺	280.9620			100	100
	[HCitNa ₅ Cl] ⁺	338.9210			25.5	22.3
	[(H ₄ Cit) ₂ Na] ⁺	407.0432	66.4	78.9		
	[(H ₄ Cit)(H ₃ Cit)Na ₂] ⁺	429.0252	13.1	13.7		
	[(H ₃ Cit) ₂ Na ₃] ⁺	451.0071	11.5	11.5		
	[(H ₃ Cit)(H ₂ Cit)Na ₄] ⁺	472.9891	8.3	8.2		
	[(H₂Cit)₂Cu(II)Fe(III)]⁺	498.8868	2.0			
	[(H₂Cit)(HCit)NaCu(II)Fe(III)]⁺	520.8687	0.9			
	[(H₃Cit)(H₂Cit)Cu(II)]₂(NH₃)]⁺	523.9160	0.4			
	[(H₂Cit)₂NaCu(II)]₂⁺	528.8712	0.9			
	[(HCit)₂Na₂Cu(II)Fe(III)]⁺	542.8506	0.7			
	[(HCit)₂(NH₃)Na₂Cu(II)Fe(III)]⁺	559.8772	0.6			
	[(H ₄ Cit) ₂ (H ₃ Cit)Na ₂] ⁺	621.0523	0.9	1.2		
	[(H ₄ Cit)(H ₃ Cit) ₂ Na ₃] ⁺	643.0342	3.2	3.8		
	[(H ₃ Cit) ₃ Na ₄] ⁺	665.0162	3.9	5.1		
[(H ₃ Cit) ₂ (H ₂ Cit)Na ₅] ⁺	686.9981	2.2	3.0			
[(H ₃ Cit) ₄ Na ₅] ⁺	879.0252	0.8	1.8			

(C₆H₄O₇)⁴⁻ = molecular building block "Cit." m/z = mass-over-charge ratio of the detected compound in FT-ICR-MS. For each sample spectrum, the citrate (or citrate-metal) molecule with the highest relative FT-ICR-MS intensity was set to = 100%, and all other detected compounds are shown in relative intensity to this compound.

TABLE 3 | Detected EDTA and EDTA ± Fe ± Cu species (bold) in the four analytical setups at the FT-ICR-MS.

Ionization	Species	m/z	MeOH + H ₂ O + NH ₄	H ₂ O + NH ₄	MeOH + H ₂ O + Na	H ₂ O + Na
Negative	[(H ₃ EDTA)] ⁻	291.0834* [#]	100	100	12.6	35.6
	[(H ₂ EDTA)Na] ⁻	313.0653	0.8	0.7	13.3	40.2
	[(H ₂ EDTA)K] ⁻	329.0392	44.4	41.8	2.6	5.1
	[HEDTANa ₂] ⁻	335.0472			99.5	81.1
	[EDTAFe(III)]⁻	343.9948*	44.5	44.9	43.1	100
	[(HEDTA)Fe(II)]⁻	345.0026	0.7	0.8	0.1	1.3
	[(HEDTA)NaK] ⁻	351.0212	0.5	0.4	33.4	22.6
	[HEDTACu(II)]⁻	351.9973*	1.8	1.7	1.6	1.8
	[EDTANa ₃] ⁻	357.0292			100	69.5
	[(HEDTA)K ₂] ⁻	366.9951	7.8	6.9	1.2	1.1
	[(EDTA)Na ₂ K] ⁻	373.0033			39.5	24.5
	[(EDTA)NaCu(II)]⁻	373.9793	0.03		1.9	2.7
	[(EDTA)KFe(II)]⁻	382.9585	0.5	0.5	0.1	
	[(EDTA)NaK ₂] ⁻	388.9771			4.6	2.7
	[(EDTA)KCu(II)]⁻	389.9532	2.9	2.8	0.8	0.8
	[(EDTA)K ₃] ⁻	404.9511	1.3	1.0	0.1	
	[EDTANa ₄ Cl] ⁻	414.9878			10.8	8.2
	[EDTANa ₅ Cl ₂] ⁻	472.9464			3.3	2.3
	[(EDTA)Na ₄ KCl ₂] ⁻	488.9204			2.1	1.3
[(EDTA)Na ₅ KCl ₃] ⁻	546.8791			0.6		
[(H ₃ EDTA)(H ₂ EDTA)K ₂] ⁻	659.0861	4.3	3.8			
[(H ₂ EDTA)(HEDTA)Na ₄] ⁻	671.1019			0.4	1.4	
Positive	[H ₅ EDTA] ⁺	293.0979	20.5	18.1		
	[H ₄ EDTANa] ⁺	315.0798 [#]	2.1	2.7		
	[(H ₄ EDTA)K] ⁺	331.0538	100	100		
	[H₂EDTAFe(III)]⁺	346.0094	1.2	1.2		
	[(H ₃ EDTA)Cu] ⁺	354.0119	0.7	0.7		
	[(H ₂ EDTA)Na ₃] ⁺	359.0437 [#]			2.5	26.5
	[(H₂EDTA)(NH₃)Fe(II)]⁺	363.0361	0.4	0.5		
	[(H ₃ EDTA)K ₂] ⁺	369.0097	2.2	2.3		
	[(H ₂ EDTA)KNa ₂] ⁺	375.0177			1.6	11.6
	[(HEDTA)Na ₄] ⁺	381.0258 [#]			100	100
	[(EDTA)Na₂Fe(III)]⁺	389.9732			12.5	97.9
	[(H₂EDTA)KCu(II)]⁺	391.9678	1.0	1.1		
	[(HEDTA)Na ₃ K] ⁺	396.9997			41.1	35.9
	[(EDTA)Na ₅] ⁺	403.0076			12.8	15.9
	[(EDTA)KNaFe(III)]⁺	405.9472	0.02	0.02	4.7	3.8
	[(H ₂ EDTA)K ₃] ⁺	406.9656	0.7	0.7		
	[(HEDTA)Na ₂ K ₂] ⁺	412.9736			6.4	4.9
	[(EDTA)Na ₄ K] ⁺	418.9816			5.4	4.2
	[(EDTA)Na₃Cu(II)]⁺	419.9577			18.3	22.9
[(HEDTA)K₂Cu(II)]⁺	429.9237	0.7	0.8			
[(EDTA)Na₂KCu(II)]⁺	435.9317			9.9	10.3	
[(HEDTA)Na ₅ Cl] ⁺	438.9843			11.2	10.8	

(C₁₀H₁₂N₂O₈)⁴⁻ = molecular building block "EDTA." m/z = mass-over-charge ratio of the detected compound. For each sample spectrum, the EDTA (or EDTA-metal) molecule with the highest relative intensity was set to = 100%, and all other detected compounds are shown in relative intensity to this compound. *Described by Chen et al. (2008) and [#]described by Reinoso-Maset et al. (2012).

TABLE 4 | Detected NN and NN ± Fe ± Cu species (bold) in the four analytical setups at the FT-ICR-MS.

Ionization	Species	m/z	MeOH + H ₂ O + NH ₄	H ₂ O + NH ₄	MeOH + H ₂ O + Na	H ₂ O + Na
Negative	[(NN)] ⁻	172.0404	6.2	18.7	27.3	61.9
	[(NN)NaCl] ⁻	229.9990	0.03		5.0	0.4
	[(NN)Na ₂ Cl ₂] ⁻	287.9577			0.4	0.03
	[(NN) ₂ Na] ⁻	367.0700			2.3	4.7
	[(NN)₂Cu(I)]⁻	407.0099	1.4	0.9	14.8	
	[(NN) ₂ Na ₂ Cl] ⁻	425.0287			0.3	
	[(NN)₃Fe(II)]⁻	572.0551	100	100	100	100
[(NN)₃NaClFe(II)]⁻	630.0140	0.1		0.9	1.0	
Positive	[(H ₂ NN)] ⁺	174.0550	8.1	45.4		
	[(HNN)Na] ⁺	196.0369	0.7	3.3	39.2	60.3
	[N ₂ Na ₂] ⁺	218.0188			3.3	5.8
	[(HNN)Na ₂ Cl] ⁺	253.9955			0.4	0.3
	[(NN)Na ₃ Cl] ⁺	275.9775			0.3	0.6
	[(H ₂ NN)(HNN)] ⁺	347.1026	34.0	100		
	[(HNN) ₂ Na] ⁺	369.0846	1.1	5.8	100	100
	[(HNN)(NN)Na ₂] ⁺	391.0665			16.6	12.8
	[(HNN)(NN)Cu(II)]⁺	408.0166	48.7	36.6	0.8	
	[(NN) ₂ Na ₃] ⁺	413.0485			1.0	2.0
	[(HNN) ₂ Na ₂ Cl] ⁺	427.0433	0.02		0.8	0.4
	[(NN)₂Cu(I)Na]⁺	429.9985	0.3		27.0	
	[(H ₂ NN)(HNN) ₂ (NH ₃)] ⁺	537.1770	0.9	3.0		
	[(HNN) ₃ Na] ⁺	542.1323	0.02		1.0	0.8
	[(HNN) ₂ (NN)Na ₂] ⁺	564.1144			6.1	4.6
	[(HNN)(NN)₂Fe(III)]⁺	573.0619	14.9	19.6		
	[(HNN)₂(NN)Fe(II)]⁺	574.0698	100	95.1		
	[(HNN)(NN)₂NaFe(II)]⁺	596.0514	0.8	1.0	0.03	0.04
	[(NN)₃Fe(II)Na₂]⁺	618.0335			18.5	13.1
	[(NN)₃Cu(II)₂]⁺	641.9782	2.4			
	[(HNN) ₃ (NN)Na ₂] ⁺	737.1622			0.6	0.3
	[(HNN) ₂ (NN) ₂ Na ₃] ⁺	759.1442			0.8	0.9
[(HNN)₂(NN)₂NaFe(II)]⁺	769.0993	0.5		0.2	0.03	
[(HNN)(NN)₃Na₂Fe(II)]⁺	791.0813			29.5	13.0	
[(HNN)₂(NN)₃Na₂Fe(II)]⁺	964.1292			16.1	5.0	

(C₁₀H₆NO₂)⁻ = molecular building block "NN." m/z = mass-over-charge ratio of the detected compound. For each sample spectrum, the NN (or NN-metal) molecule with the highest relative signal intensity was set to = 100%, and all other detected compounds are shown in relative intensity to this compound.

Relative Abundances of the Target Compounds

The relative FT-ICR-MS signal intensities of the target species were generally highest when methanol was present in the samples (Figure 1). In sum, citrate and EDTA compounds had their highest intensities in positive ionization mode when aq. ammonia was the added base. Contrastingly, the NN compounds had highest (total) signal intensities in positive ionization mode after sodium hydroxide additions, and SA compounds had highest signal intensities with sodium hydroxide addition and measurement in negative ionization mode. The citrate speciation patterns were dominated by free uncomplexed ligands, both in relative intensity and number of detected species, particularly in positive ionization mode (Figure 1). In comparison, all detected metal-citrate complexes had much lower intensities

and were only found in the samples with methanol + water and aq. ammonia, albeit in both ionization modes (Table 2). The abundance patterns found in the mass spectra are in line with the PHREEQC-based speciation patterns for citrate, with uncomplexed citrate accounting for the highest concentrations (88 μM), Cu-citrate species contributing the second largest amount (10 μM), and Fe citrate species contributing the least (1.3 μM). Similar to citrate, the EDTA compounds detected in the mass spectra had the highest signal intensities in the samples with methanol + water and aq. ammonia compared to those samples with sodium hydroxide. Overall highest intensities were found for the free uncomplexed EDTA, particularly in positive ionization mode, again as predicted by the PHREEQC calculations (80 μM uncomplexed EDTA; Table 3). However, Fe was calculated to be complexed with EDTA at slightly lower

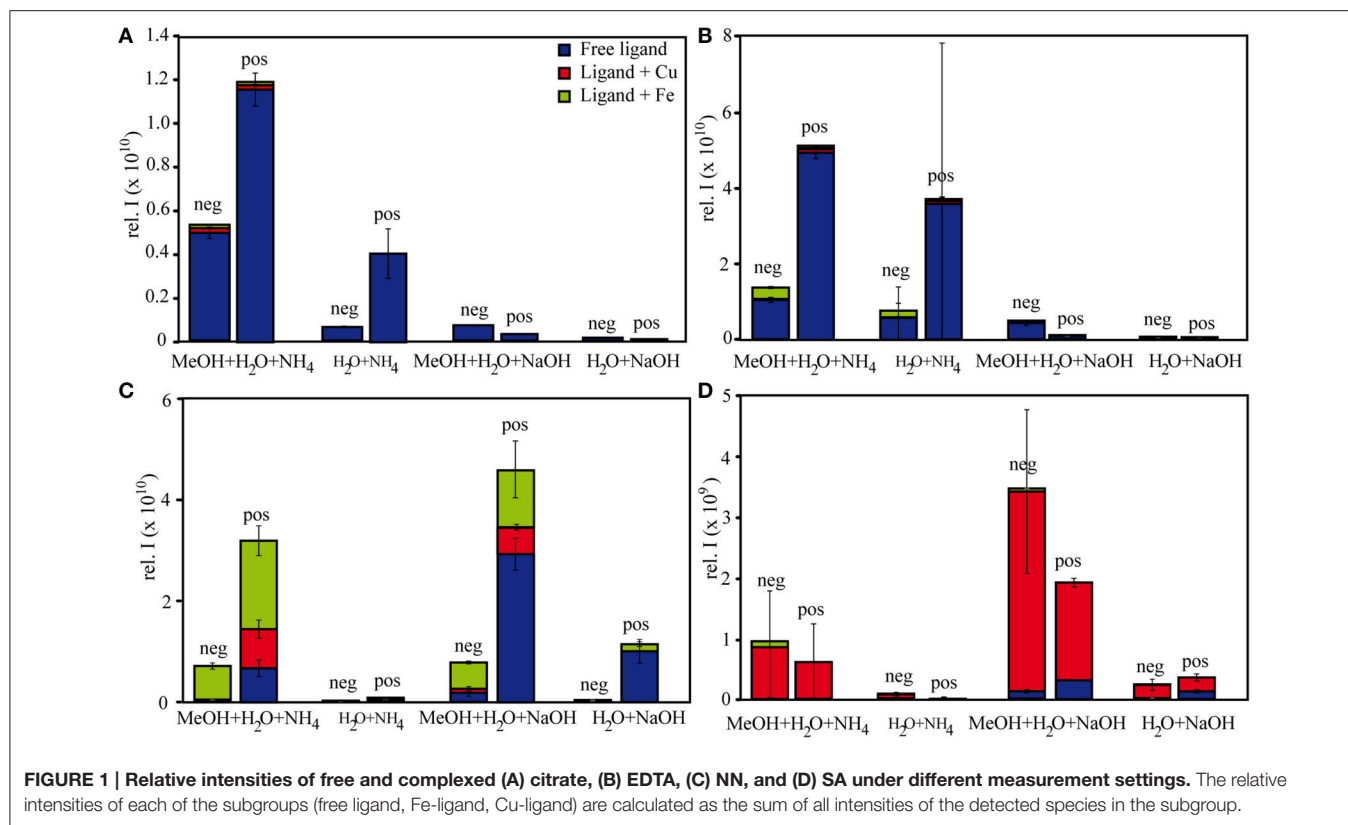
TABLE 5 | Detected SA and SA ± Fe ± Cu species (bold) in the four analytical setups in FT-ICR-MS.

Ionization	Species	m/z	MeOH + H ₂ O + NH ₄	H ₂ O + NH ₄	MeOH + H ₂ O + Na	H ₂ O + Na	
Negative	[(HSA)Na] ⁻	158.0224			1.4	2.5	
	[(H ₂ SA)NaCl] ⁻	193.9990			1.0	1.6	
	[(SA)Cu(II)]⁻	196.9544	9.4	12.1	2.6	3.4	
	[(HSA)Cu(I)]⁻	197.9622	32.2	37.1	9.4	12.5	
	[(HSA)Na ₂ Cl] ⁻	215.9810			1.2	2.2	
	[(HSA)Cl₂Fe(III)]⁻	260.9052	4.7	5.0			
	[(H ₂ SA) ₂ Na] ⁻	295.0700			0.8	1.4	
	[(HSA)₂Fe(III)]⁻	325.9996	11.8	18.5	1.8	3.6	
	[(H₂SA)(HSA)Cu(II)]⁻	334.0021	100	100	100	100	
	[(HSA)₂NaCu(II)]⁻	355.9840			7.0	6.9	
	[(H₂SA)₂(HSA)NaCu(II)]⁻	493.0318			2.0	1.6	
	Positive	[(H ₃ SA)Na] ⁺	160.0369			5.5	18.1
		[(H ₂ SA)Na ₂] ⁺	182.0188			6.0	24.9
[(HSA)Na ₃] ⁺		204.0008			2.3		
[(H ₂ SA)Na ₃ Cl] ⁺		239.9775			3.2	9.1	
[(HSA)Na ₄ Cl] ⁺		261.9594			1.3	4.9	
[(H ₃ SA) ₂ Na] ⁺		297.0846			2.4	9.1	
[(H ₃ SA)(H ₂ SA)Na ₂] ⁺		319.0665			0.9	2.1	
[(H₃SA)(H₂SA)Cu(II)]⁺		336.0166	100	100	0.3		
[(H ₂ SA) ₂ Na ₃] ⁺		341.0485			5.2	25.0	
[(H₂SA)₂NaCu(II)]⁺		357.9985			100	100	
[(H ₂ SA)(HSA)Na ₄] ⁺		363.0304			1.0	7.2	
[(H₂SA)(HSA)Na₂Cu(II)]⁺		379.9805			42.9	85.7	

(C₇H₄NO₂)³⁻ = molecular building block "SA." m/z = mass-over-charge ratio of the detected compound. For each sample spectrum, the SA (or SA-metal) molecule with the highest relative intensity was set to = 100%, and all other detected compounds are shown in relative intensity to this compound.

concentrations than Cu (8 and 10 μM, respectively), while the relative intensities of the detected species in the mass spectra decreased in the order EDTA > Fe(EDTA) > Cu(EDTA). This trend was consistent for all measurement settings, although a tendency of a relative Fe-EDTA decrease with relative Cu-EDTA increase was observed from negative to positive mode (Figure 1). Like EDTA and citrate, the NN and metal-NN compounds detected in the mass spectra had generally higher signal intensities in positive compared to negative ionization mode. In contrast to citrate and EDTA, only the relative intensities of the Fe-NN compounds were enhanced in the samples with methanol + water and aq. ammonia compared to those with sodium hydroxide. The uncomplexed ligands, as well as Cu-NN, always had their highest intensities in the samples with methanol + water measured in positive ionization mode, regardless of the added base (Figure 1). NN was the first ligand in the series for which the mass balances of the speciation calculations started to deviate substantially from the signal intensities of the corresponding compounds in the mass spectra: Calculations predicted free NN to be the major species (70 μM), while uncomplexed NN was only dominant in the FT-ICR-MS measurement settings where its signal intensities were enhanced due to Na adduct formation (Figure 1, Table 4). Furthermore, Cu was predicted to be bound only in low nanomolar concentrations (5 nM), but reached relatively higher signal intensities in the mass spectra, particularly under

conditions favoring ionization of free NN as well: There, the Cu(NN)₂ complex made up almost a third of the most abundant NN species (Table 4). Fe was calculated to occur exclusively as Fe(NN)₃ complex (10 μM) for both types of base addition, and was the dominant complex throughout the mass spectra. In the case of SA, differences between calculated concentrations and detected abundances were even more pronounced: The PHREEQC model predicted SA to occur primarily in its uncomplexed form (82 μM), but the uncomplexed ligand was almost undetectable in the mass spectra (Figure 1, Table 5). In the speciation calculations, Cu was fully complexed (2.7 μM for Cu(SA) and 7.3 μM for Cu(SA)₂), whereas Fe was mostly complexed as Fe(SA)₂ (118 nM), with very small amounts of Fe(SA) (8.2 fM). In line with these calculations, the Cu(SA)₂ peak was most prominent in the mass spectra, with more than 2-fold higher signal intensities than Cu(SA), and up to 50-fold higher signal intensities than the Fe(SA)₂ complex (Table 5). In general, the SA mass spectra also differed from those of the other ligand-metals solutions: The detected SA-compounds had overall lower intensities compared to those of the other metal-ligand solutions (up to one order of magnitude compared to NN, Figure 1), and the intensities of the detected compounds in the mass spectra were highest in samples with methanol+water matrix and sodium hydroxide as added base. Finally, the free, uncomplexed ligands were only detectable with sodium adducts in samples with added sodium hydroxide (Table 5), while Cu-SA



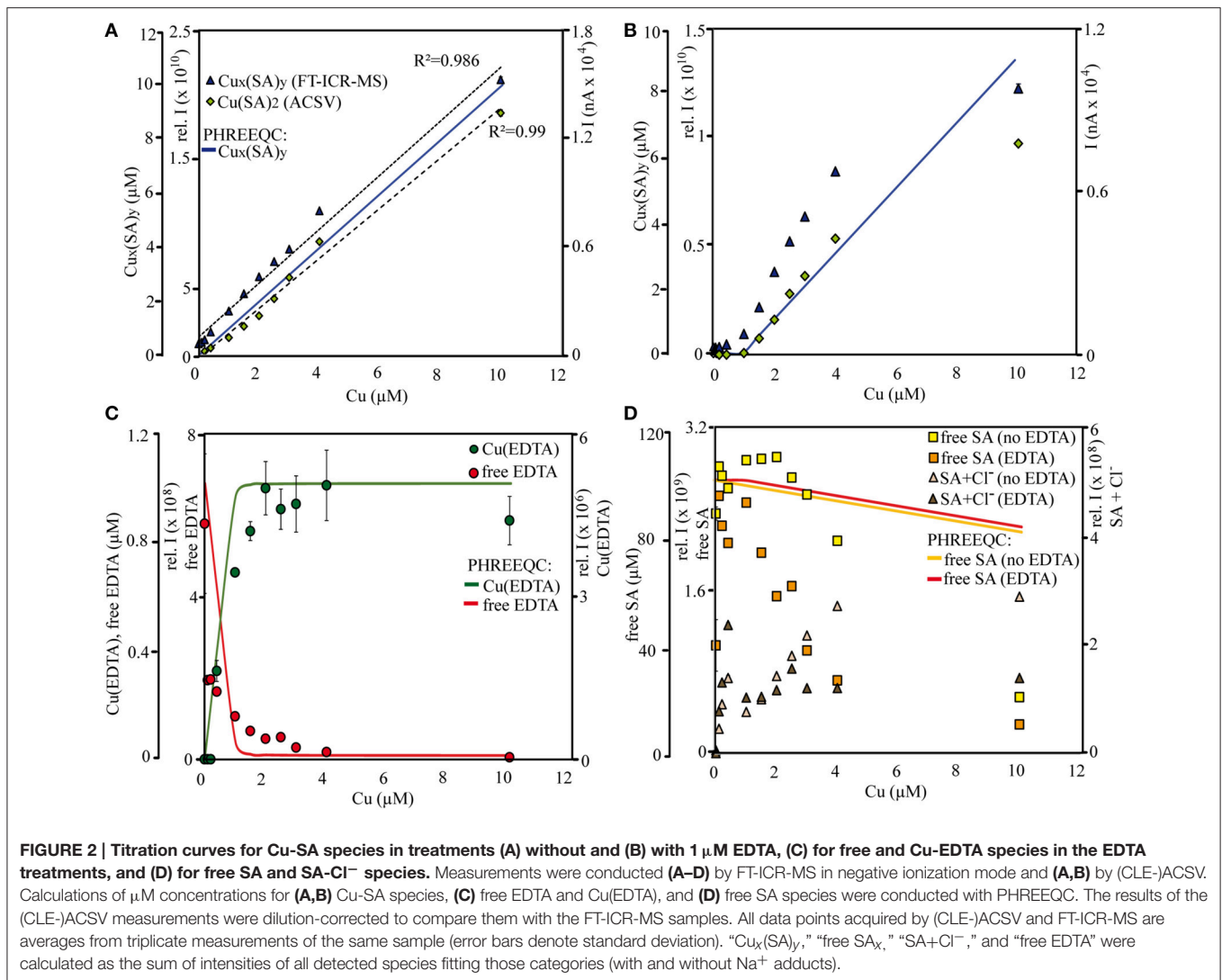
species had the highest signal intensities at all settings (Figure 1, Table 5).

Speciation and Abundances of the SA-Cu-titration Series

Overall, the distribution of the Cu-SA species in the calibration series resembled those of the qualitative SA sample solutions with the methanol + water matrix and sodium hydroxide as added base: Cu-SA mono-, di-, and trimers occurred, and the Cu(II)(SA)₂ complex had the highest signal intensities throughout the calibration series. Based on the results of the initial speciation and abundance experiments including all ligands, only the results from the ESI negative measurements were investigated in detail due to the higher signal intensities of the Cu-SA complexes with this ionization mode compared to ESI positive. In ESI negative mode, two new Cu₂(SA)₄ complexes occurred as well, most notably a [(H₂SA)₂(HSA)₂NaCu(II)₂]⁻ complex at *m/z* = 690.9938, which was detected at about ~ 10% of the signal intensity of the main Cu(II)(SA)₂ compound. The detected Cu-SA species all showed a linear increase in signal intensities when plotted against Cu concentrations, although the fit of the curve appeared to become worse at the highest amount of added Cu. In agreement with the FT-ICR-MS data, parallel measurements of dilutions of the SA-Cu-titration series via ACSV also resulted in linear response curves, although again the calibration curve seemed to decrease slightly at the highest added Cu concentration. Meanwhile, the combined Cu(SA) and Cu(SA)₂ complex concentrations calculated by

PHREEQC showed a linear increase throughout (Figures 2A,B after Cu concentrations >1 μM). In addition, the calculated relative contribution of the Cu(SA) monomer to the Cu_x(SA)_y pool was predicted to be in a similar magnitude (13–16% of the Cu(SA)₂ dimer) than what was derived from the relative signal intensities in the mass spectra (15–20%). The monomer was calculated to increase with increasing Cu concentrations by 2.7%, while FT-ICR-MS measurements revealed a slight decrease of Cu(SA) compared to Cu(SA)₂ species by 2.8%. Thus, the dominance of the Cu(SA)₂ dimer was more important than the relative contributions of the Cu(SA) monomer in instrumental setups and speciation calculations, despite the changes in the SA:Cu stoichiometries over the course of the titrations. As in the qualitative setup, PHREEQC and FT-ICR-MS results differed with regards to the abundance of the free ligand, which had overall lower signal intensities than expected from its concentration in solution, and for which the SA_x and SA_xNa_y⁺ intensities in the mass spectra initially increased upon addition of the first aliquot of the Cu calibration solution, but then decreased continuously over the rest of the titration series, and at much faster rates than the PHREEQC predictions for free SA concentrations (Figure 2D). Meanwhile, the signal intensities of SA species containing Cl⁻ adducts (SA_xNa_y⁺Cl_z⁻) in the mass spectra increased with increasing Cu solution additions (Figure 2D), but these species were likely adduct artifacts and not considered in the PHREEQC calculations.

The same Cu_x(SA)_y species occurred for the EDTA+SA+Cu equilibration titration as for that with SA and Cu alone; again,



Cu(SA)₂ was the species with the highest signal intensities, and free SA as well as SA_xNa_y⁺Cl_z⁻ compounds could be detected. In line with the Cu-SA-calibration series, we only report the ESI negative results here. In addition, several forms of uncomplexed EDTA, as well as one Cu(EDTA) complex ($[(\text{EDTA})\text{NaCu}(\text{II})]^-$, $m/z = 373.9793$) could be identified (Figure 2C). Compared to the calibration series without EDTA, the signal intensities for FT-ICR-MS and current peaks for CLE-ACSV of the Cu_x(SA)_y complexes were overall lower in this titration setup. They increased only from added Cu concentrations > 1 μM and leveled off again at Cu concentrations > 4 μM (Figure 2B). Again, the PHREEQC calculations predicted a similar amount of Cu(SA) compared to Cu(SA)₂ (13%, increasing to 15% at the highest Cu addition) as observed in the mass spectra (20.8%, decreasing to 14.8%). The PHREEQC-derived Cu_x(SA)_y curve did not show the decrease observed at Cu concentrations of 10 μM for the other two methods, and the free SA concentrations did not decrease as steeply in the speciation models as in the mass spectra (Figure 2D). Meanwhile, PHREEQC-calculated

patterns of steeply increasing Cu(EDTA) and sharply decreasing free EDTA concentrations mirrored signal intensity distribution changes recorded from the FT-ICR-MS, albeit with slightly differing curve slopes (Figure 2C). Finally, in the FT-ICR-MS spectra, free, uncomplexed SA, as well as SA_xNa_y⁺Cl_z⁻ again displayed similar increases and decreases, respectively, as in the setup with SA and Cu only (Figure 2D).

DISCUSSION

Metal-Ligand Speciation Patterns: Integrity and Reproducibility

Overall, our findings agreed well with those from other studies and the predictions from the speciation models: Most EDTA-compounds described by previous reports including uncomplexed EDTA and metal-EDTA were detected in this study as well as predicted by the PHREEQC calculations (Table 3, Chen et al., 2008; Reinoso-Maset et al., 2012). In addition, mostly

monomers, and only two dimers were detected, indicating that metal-EDTA equilibrium studies are likely to be comparable amongst different experimental and instrumental setups. Also, $\text{Fe}(\text{NN})_3$ was found to be the dominant metal-NN species in our mass spectra (**Table 4**) in line with our speciation data as well as reports from CLE-ACSV where it is used to study the Fe-complexing capacities of natural seawater samples (Gledhill and van den Berg, 1994; Wu and Luther, 1995; Hawkes et al., 2013). Furthermore, all $\text{Cu}_x(\text{SA})_y$ and $\text{Fe}_x(\text{SA})_y$ species predicted by the PHREEQC calculations and previous studies were found in our mass spectra under the tested conditions (Campos and van den Berg, 1994; Buck and Bruland, 2005; Abualhaija and van den Berg, 2014). One remarkable difference between the PHREEQC calculations and the mass spectra was the higher abundance of molecular assemblages such as tri-, tetra-, and even pentamers in the latter compared to the former (**Tables 2–5**). Analogous to (single ion) adduct formation, the formation of molecular assemblages is not uncommon in ESI. However, because data on the formation of the investigated complexes in aqueous solutions is not available, we also cannot exclude the possibility that such species also exist in aqueous solutions, but cannot be predicted because the thermodynamic equilibrium constants are not known.

Adduct formation in ESI may obscure compound identification (**Tables 2–5**): Na^+ - and K^+ -containing adducts were ubiquitous in positive ionization mode in those samples that contained Na^+ and K^+ in solution or potassium, even though PHREEQC speciation models did not predict significant concentrations of sodiated species in solution. Adduct formation in ESI was particularly pronounced for the metal-citrate solutions, where none of the metal-citrate species previously reported by others (Gautier-Luneau et al., 2005; Nischwitz and Michalke, 2009; Silva et al., 2009; Bertoli et al., 2015) could be found, although their pH and stoichiometry settings were in a comparable range to those in this study. These discrepancies can primarily be explained by a re-distribution of Na^+ , Cl^- , and H^+ (which occurred in the aqueous phase as free ions according to the PHREEQC calculations) during ionization and gas phase transfer. For example, a $\text{Fe}(\text{Cit})$ monomer ($m/z = 279.9078$) and two $\text{Cu}(\text{Cit})_2$ dimers ($m/z = 465.9427$ and 487.9246) had also been described by Bertoli et al. (2015), albeit without a Cl^- adduct for the former and without Na^+ adducts for the latter. Nischwitz and Michalke (2009) also observed a $\text{Cu}(\text{Cit})_2$ complex, but with a NH_3^+ instead of Na^+ adduct. In line with the results from the literature and our FT-ICR-MS data, the PHREEQC calculations predicted the occurrence of a $\text{Fe}(\text{Cit})$ monomer and a $\text{Cu}(\text{Cit})_2$ dimer in aqueous solution. Furthermore, in the case of both PHREEQC calculations and FT-ICR-MS measurements, $\text{Cu}_2(\text{Cit})_2$ complexes were reported to occur (**Table 2**). Finally, the $\text{Fe}_2(\text{Cit})_2$ complex ($m/z = 510.8517$) detected in our study was also listed by Gautier-Luneau et al. (2005) and Silva et al. (2009), there again containing H^+ instead of Na^+ adducts. Together with the FT-ICR-MS data and the PHREEQC speciation results, we conclude that the rearrangement of ions normally expected to freely occur in aqueous solutions, such as Na^+ , Cl^- , and H^+ , produces a wide variety of adducts during ionization. Adduct

formation in ESI is to be expected because ESI functions on this principle. In addition, e^- transfer for metal ions such as Fe and Cu, also takes place during negative ionization mode, as demonstrated especially for the complexes formed with NN (**Table 4**). Any adduct formation would be valid as long as the complex stoichiometry and net charge are preserved. The only compounds for which no literature or PHREEQC speciation data could be found were the $\text{FeCu}(\text{Cit})_2$ complexes (again, with varying amounts of Na^+ and Cl^- adducts, **Table 2**). PHREEQC predicted that <2% of the added Fe would form complexes with citrate, while $7.7 \mu\text{M}$ still occurred as $\text{Fe}(\text{OH})^{2+}$ ions. In principle, it is feasible that the remaining dissolved Fe became attached to $\text{Cu}(\text{Cit})_2$ complexes during ionization. On the other hand, to the best of our knowledge, this is the first ESI-MS study to be conducted with both metals and citrate in the same solution, and while the PHREEQC database does not contain stability constants for such a complex, the stoichiometry is theoretically possible in the aqueous environment considering the often described existence of $\text{Cu}_2(\text{Cit})_2$ and $\text{Fe}_2(\text{Cit})_2$ complexes.

As mentioned above, reduction at the ESI source produced reduced metal-ligand complexes for Fe-NN and Cu-NN, Fe-EDTA, and Cu-SA (Di Marco and Bombi, 2006; Rellán-Álvarez et al., 2008). Oddly, a reduced Fe-NN complex was also detected in positive ionization mode (**Table 4**). It is possible that partial reduction of $\text{Fe}(\text{III})(\text{NN})_3$ happened during equilibration of the aqueous samples, or that $\text{Fe}(\text{II})(\text{NN})_3$ was formed with traces of Fe(II) present in the NIST standard solution, and that this complex has a much higher response factor than $\text{Fe}(\text{III})(\text{NN})_3$, analogous to $\text{Fe}(\text{II})$ nicotianamide opposed to $\text{Fe}(\text{III})$ nicotianamide (Rellán-Álvarez et al., 2008). Changes in the oxidation state may influence the binding strength. For example, it has been suggested that reduction of Fe(III) to Fe(II) during photolysis of siderophores may increase its bioavailability (Barbeau et al., 2001). Nevertheless, the integrity of the $\text{Fe}(\text{II})(\text{NN})_3$ complex indicated that under the soft ionization conditions, the complex was still stable even if binding strengths had decreased. Incidentally, the methanol additions used for the increased ionization efficiencies could also decrease the metal-ligand binding strength, as has been demonstrated for EDTA (Xue and Traina, 1996). Within the parameters of our study, the relative intensity distributions of the samples with and without methanol do not indicate a decrease in complexing capacity with an increase of organic solvent (**Tables 2–5**), and subtle changes may have been masked by matrix-induced changes in response factors.

Metal-ligand equilibria, in particular those involving citrate, are sensitive to changes in pH (Gautier-Luneau et al., 2005; Silva et al., 2009). pH also influences ESI (Di Marco and Bombi, 2006; Van Berkel and Kertesz, 2007). During positive ionization of metal-bipyridyl complexes the pH of the ESI triplets can decrease by 4–5 units (Gatlin and Tureček, 1994) and can increase by 1–2 units during negative ionization of metal-NA complexes (Rellán-Álvarez et al., 2008). At higher pH mononuclear prevail over di- and trinuclear iron citrate complexes (Gautier-Luneau et al., 2005; Silva et al., 2009). Consistently, we found that mononuclear Fe- and Cu-citrate complexes were present in negative ionization

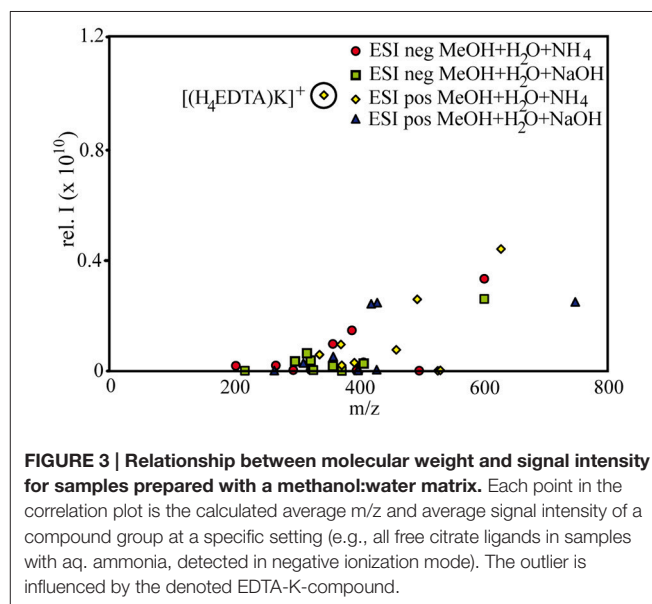
mode, while the samples measured in positive mode exclusively contained dinuclear metal-citrate species (Table 2). This may indicate a relative increase of the pH from positive to negative ionization settings. On the other hand, the relative intensities of the Cu(SA) species compared to those with a Cu(SA)₂ stoichiometry decreased from negative to positive mode in our study, although PHREEQC calculations over a pH range from 2 to 9 resulted in an opposite trend. It is not possible to judge whether any pH changes within the scope of our experiments may have been as dramatic as those reported by others (Gatlin and Tureček, 1994; Rellán-Álvarez et al., 2008). This is, because firstly, only near-neutral settings (7.1 ± 0.2 and 7.5 ± 0.2) were investigated, thus preventing the evaluation of artifacts based on changing ionization efficiencies with changing pH. Secondly, most tested ligands are known to form strong complexes with Fe and Cu above a pH threshold of ~ 5 , and thirdly, excess ligands were always present in solution, providing a certain buffering capacity (Rellán-Álvarez et al., 2008). It should be noted that the curves of the EDTA \pm SA⁺ titration series acquired by FT-ICR-MS matched those produced by (CLE-)ACSV, although the latter had a higher ionic strength and higher (HEPES buffered) pH (7.8) compared to the former, indicating a resilience of the tested metal-ligand equilibria toward the induced changes of the sample matrix. For studies of kinetically more labile metal-organic complexes, additional measures such as higher sample flow rates, generally low ionic strength, and/or the use of a buffer, may further prevent electrochemical interferences of the equilibria at the ESI source (Wang and Agnes, 1999; Van Berkel and Kertesz, 2007).

Relative Abundances of Detected Species: Impact of Response Factors

To a large extent, the observed abundance patterns in signal intensities depicted in Figure 1 can be explained by the relative abundances of the compounds: For example, citrate and EDTA formed 1:2 and 1:1 complexes with Fe and Cu, and thus a comparatively large proportion of free ligands still remained in solution. The high relative intensities of the free ligands corresponded to the results of the PHREEQC calculations as well (88 and 80 μM for unbound citrate and EDTA, respectively). SA formed complexes up to 1:3 stoichiometries, and NN even formed pentamer complexes with Fe, and this relative decrease in free ligands opposed to the relative increase of metal-ligand complexes is also reflected in the intensity distributions in Figure 1. However, the intensity distributions were also influenced by the different response factors (or ionization efficiencies) of the different species in the solution. For example, based on the metal-ligand stoichiometries of the detected complexes and the PHREEQC speciation calculations, SA still should have had a slightly higher amount of free ligands in solution (82 μM) compared to NN (70 μM), but the signal intensities of the free ligands were much smaller for the former compared to the latter (Figure 1). It has been previously proposed that the ionization efficiency of organic compounds increases with increasing pKa and molecular size (Oss et al., 2010). Although the pKa (which increases in the order

of citrate < EDTA < NN < SA) did not seem to have an influence on the relative ionization of the studied compounds, a slight trend of increasing signal intensities with increasing molecular weight was apparent over a wide range of compound types and measurement settings (Figure 3).

Most importantly, large differences in FT-ICR-MS signal intensities (absolute and relative) were found for all tested reagents between negative and positive ionization mode (Figures 1, 4). From Figure 4, it is evident that the signal intensities of all free ligands (citrate, EDTA, NN, and SA) increased through Na⁺ or K⁺ adduct formation in positive mode. This led to the effect that citrate and EDTA, which have net negative charges in aqueous solutions, displayed overall higher signal intensities for all compounds in positive rather than negative ionization mode (Figure 1). Citrate and EDTA solutions were prepared from sodium and potassium salts respectively, and an initial concentration of 100 μM Na⁺ was present in all sample setups for citrate, while all EDTA setups contained 300 μM K⁺. Consequently, adduct formation already occurred in the samples without added sodium hydroxide. In contrast, SA and NN had been prepared from pure ligand stock solutions, and Na adduct formation occurred mainly upon addition of sodium hydroxide, leading to overall higher response factors of the uncomplexed ligands (Figure 4). The additional input of sodium to the citrate and EDTA setups for pH adjustment did not enhance the ionization of sodiated species further, but had an opposite effect, with speciation changing drastically (Tables 2, 3, Figure 4) together with an overall sharp decrease in relative signal intensities of all (free and complexed) target compounds (Figure 1). Reinoso-Maset et al. (2012) demonstrated in their ESI-MS study on Mn-EDTA and Th-EDTA complexes, that ion suppression of EDTA occurred in negative mode as soon as metals salts were added, both through the salt additives Cl⁻ or NO₃⁻, as well as the metal ions themselves, and that signal intensities of target metal-ligand complexes could decrease up



to 72%. Based on our study, we suggest that small additions of cations can in fact increase the response factors in positive ionization mode, but ionization may be severely decreasing once a (sample-specific) threshold of ion concentrations has been crossed. In this respect, it is noteworthy that the added amounts of sodium hydroxide (~1 mM) in this study corresponded to the concentration ranges of the metal salts used in Reinoso-Maset et al. (2012).

In both Cu-SA-calibration series, the signal intensities of the free SA species increased after adding the first Cu aliquot, counterintuitive to the expectations that free ligand abundances should decrease with increasing Cu-SA species formation (Figure 2D). In line with our findings on EDTA and citrate, as well as the qualitative observations of free and Cu-SA ionization patterns upon addition of sodium hydroxide, this also indicates that the addition of (Na^+ , Cl^- , and Cu^{2+}) ions during the first titration had a beneficial effect on the ionization of these selected species (Figures 1, 2D). Nevertheless, the signal intensities of the free SA compounds decreased further on with increasing Cu concentrations, presumably due to scavenging by the added Cu. Overall, all acquired mass spectra had increasing signal intensities over the course of the titrations (as indicated by an increase in the sum of all signal intensities for each sample), because they were governed by the quantitative increase of the newly formed metal-ligand complexes. In fact, linear increases of signal intensities were also found for unknown compounds, for which SA-specific sum formulae could not be assigned a priori using our set criteria. The majority of these compounds were the ^{13}C or ^{65}Cu -containing masses corresponding to the detected species listed in Table 5. However, some new molecules could also be identified based on their linear increase. For example, for a compound with the $m/z = 168.9595$, which occurred in all 11 titration samples, was significantly positively correlated with Cu concentrations (Pearson's $\rho = 0.97$), and contained $^{12/13}\text{C}$ and $^{63/65}\text{Cu}$ isotopologues, we could assign the molecular formula $\text{C}_6\text{H}_4\text{CuNO}$, likely the complex of a by-product from the original SA solution with the added Cu. Thus, the titration series was a useful means to distinguish between non-related singular changes in ionization efficiencies, and actual quantitative responses of newly formed Cu-ligand complexes.

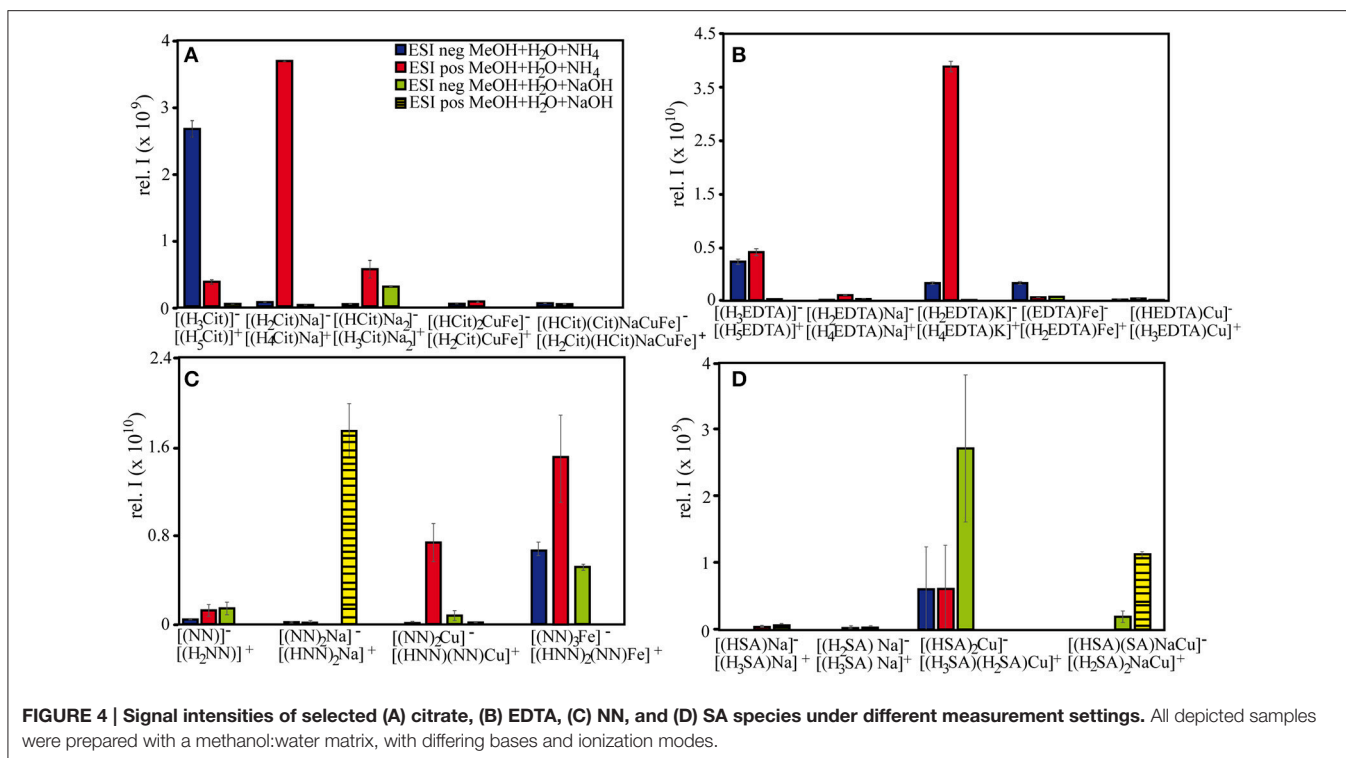
While ionization of free ligands was enhanced due to sodium or potassium adduct formation, signal intensities of metal-ligand complexes did not appear to be influenced by this process. Nevertheless, the relative abundances of the metal-ligand compounds in the mass spectra were not always representative of their thermodynamic equilibrium concentrations in aqueous solutions: For example, in the case of EDTA, the $\text{Fe}(\text{EDTA})$ signal intensities were up to 3-fold higher than expected, while $\text{Cu}(\text{EDTA})$ abundances were 3-fold lower (Figure 1, Table 3). Even more extreme were the discrepancies between free NN and free SA and their metal-ligand complexes, where the latter were up to three orders of magnitude higher than the former, despite the high thermodynamic equilibrium concentrations for the uncomplexed ligands. These patterns can partly be attributed to the relatively poor ionization efficiencies of the unbound ligands, even when their response factors were increased upon adduct formation (Figure 4). Furthermore, Cu in the speciation models was predicted to be fully >99% complexed with three

out of the four added ligands (citrate, EDTA, SA), whereas in solutions with NN, $7\ \mu\text{M}$ free Cu^{2+} were calculated to occur which may have formed adducts to the free ligand at the ESI source, thus increasing the $\text{Cu}(\text{NN})_2$ signature. For Fe, the dominant inorganic forms in aqueous solutions containing citrate and SA were $\text{Fe}(\text{III})\text{oxihydroxides}$, and $\text{Fe}_x(\text{Cit})_y$ and $\text{Fe}_x(\text{SA})_y$ complexes did occur mainly at ESI negative mode where reduction at the ESI source could cause Fe adduct formation as well. As mentioned before, the NN and SA data for the PHREEQC speciation models may not have been sufficient to explain all of the observed patterns; for example, the calculated $\text{Fe}(\text{SA})$ concentrations are very low considering that SA is used as a competitive ligand in CLE-ACSV to study the Fe-complexing capacity of natural DOM (Abualhaija and van den Berg, 2014). Probably, a combination of instrumental effects (different response factors, metal adduct, and molecular assembly formations), and lack of data for “unpredictable” compounds caused the discrepancies between the models and the measured abundance patterns.

Overall, citrate complexes with Fe and/or Cu had similar signal intensities in negative and positive ionization mode, whereas complexes of EDTA, NN, and SA with Fe appeared to ionize better in negative mode and those with Cu were relatively higher in positive mode. In line with our findings, Waska et al. (2015) showed that the desferrioxamine B (DFoB) complex with iron could be detected at concentrations as low as 1 nM via FT-ICR-MS, while DFoB-Cu was detected at the high end of the calibration series (150–300 nM), and only in positive ionization mode. In contrast, Chen et al. (2008) showed higher intensities of Cu-EDTA over Fe-EDTA at negative ionization in their study of a multi-metal-EDTA complex mixture. Finally, Rellán-Álvarez et al. (2008) found that in negative mode, the ionization efficiencies of Cu- complexes of the aminocarboxylate ligand nicotinic acid (NA) were more sensitive to changes in the capillary cone voltages of their ESI-MS(TOF) system, and more likely to decrease sharply with increasing voltages compared to those with Fe. However, all abovementioned trends in response factors of Fe-complexes and Cu-complexes during different ionization modes are empirically derived, and future studies will be necessary to explain the responsible mechanisms.

Qualitative and Quantitative Comparison of FT-ICR-MS with (CLE)-ACSV

The calibration curves of both the FT-ICR-MS and the ACSV measurements remained linear over the course of the titration series, although the curve leveled slightly off at the highest added Cu concentrations (Figure 2A). For ACSV, the limit of detection (LOD) was calculated as $\text{LOD} = 3s + a$ (a = average peak height, s = standard deviation) of the blank signal of the first sample in the titration series, where no Cu had been added. The resulting value corresponded to a Cu concentration of 1.45 nM, which is relatively high for this method (Campos and van den Berg, 1994). This is partly owed to a high Cu blank, and partly to the concentration of SA ($2\ \mu\text{M}$) in the diluted sample which decreases the sensitivity of the method by ~50% compared to the concentrations normally used for the determination of dissolved Cu (20–25 μM SA, Campos and van den Berg). In comparison, the signal intensity of the method detection limit



(MDL, Riedel and Dittmar, 2014) of the ESI-FT-ICR-MS was on average 1.01×10^6 , and corresponded to a LOD of 0.71 nM for the $\text{Cu}(\text{SA})_2$ complex with $m/z = 334.0021$. Thus, this complex is measured with a sensitivity comparable to that acquired by the ACSV method, as well as to iron-siderophore complexes, which had been reported to be detectable in the low nanomolar range for ESI-(FT-ICR)MS (Gledhill, 2001; Waska et al., 2015). If all identified $\text{Cu}_x(\text{SA})_y$ species are taken into account, the resulting calibration curve corresponds to an even lower LOD of 0.41 nM. Even though ACSV only captures the $\text{Cu}(\text{SA})_2$ complex and ESI-FT-ICR-MS revealed a multitude of $\text{Cu}_x(\text{SA})_y$ complexes, LODs in comparable orders of magnitude for the two methods were achieved in our study, and the acquired calibration curves were remarkably similar. We attribute this to the dominance of the $\text{Cu}(\text{SA})_2$ complexes (i.e., the sum of all detected $\text{Cu}(\text{SA})_2$ complexes, including Na^+ adducts) in the mass spectra, which constantly contributed the majority of the $\text{Cu}_x(\text{SA})_y$ signal intensities. The occurrence of several dimer compounds is an artifact of the FT-ICR-MS (due to adduct formation), and all dimers combined contribute to the ACSV signal as one $\text{Cu}_x(\text{SA})_y$ compound.

Analogous to the SA-Cu-calibration series, the detected Cu-complexes in the SA + EDTA + Cu competition series behaved similarly in both FT-ICR-MS and ACSV measurements (Figure 2B), and the $\text{Cu}_x(\text{SA})_y$ dimers dominated the mass spectra throughout (81.7–81.1% contribution to the total signal intensities). Furthermore, the decreasing signal intensities of the free SA and EDTA ligands with increasing Cu concentrations in the FT-ICR-MS mass spectra were similar to those of free SA in the titration series with SA and Cu alone, and indicative of ligand

scavenging of the added Cu (Figure 2D). Due to competition between EDTA and SA for free Cu, a slower increase of the SA-Cu complex signal intensities was found, especially in the low Cu concentration range (0–2 μM). Surprisingly, however, the Cu-SA complex signal intensities only increased linearly between Cu concentrations of 1.5–4 μM and then leveled off in both measurement modes, in contrast to the expectation that more, free SA and Cu should result in higher rates of Cu-SA complex formation (Figure 2B). Meanwhile, the PHREEQC calculations with the known $\text{Cu}_x(\text{SA})_y$ complex stoichiometries did not indicate a substantial equilibrium shift between the mono- and dimer, or a decrease in linearity of all accounted $\text{Cu}_x(\text{SA})_y$ complexes. In the SA + EDTA + Cu measurements *via* FT-ICR-MS, we also did not detect any new compounds in addition to the already described $\text{Cu}_x(\text{SA})_y$, $\text{Cu}(\text{EDTA})$, and free ligand types. Explanations for the decrease of the $\text{Cu}_x(\text{SA})_y$ complex intensities in both FT-ICR-MS and CLE-ACSV at the highest Cu concentration could be 2-fold: (1) through formation of yet unknown $\text{Cu} \pm \text{SA} \pm \text{EDTA}$ compounds which were undetectable in the mass spectra and/or removed from the sample solutions, for example through adsorption to the reaction vessel walls or the PTFE syringe filters before subsequent analyses; (2) due to matrix-dependent “constituent overload” of both ACSV and FT-ICR-MS: In the case of ACSV, through adsorption processes which exceed the surface capacity of the mercury drop of the working electrode (Campos and van den Berg), and in the case of FT-ICR-MS, through ion suppression (Rellán-Álvarez et al., 2008; Reinoso-Maset et al., 2012).

We calculated the concentrations and conditional stability constants of EDTA (**Figure 2B**) based on the two titration curves (the last titration point was omitted), by using the ProMCC software created for voltammetric titrations by Omanović et al. (2015). For the titration curves acquired by CLE-ACSV and FT-ICR-MS, the EDTA concentrations amounted to 1.11 ± 0.02 and $1.00 \pm 0.03 \mu\text{M}$, respectively, while the $\log K_{\text{CuEDTA}}^{\text{CuEDTA}}$ was calculated to be 17.33 ± 0.03 and 15.49 ± 0.04 , respectively. While the calculated concentrations of both methods agreed well with the added amounts of EDTA, the conditional stability constants deviated substantially from each other and from those obtained from the literature. Generally, EDTA binding constants (overall, as well as compared to SA) tend to increase with decreasing ionic strength (Campos and van den Berg, 1994), and thus one would expect a higher $\log K_{\text{CuEDTA}}^{\text{CuEDTA}}$ for the samples measured by FT-ICR-MS compared to those by CLE-ACSV, since the latter contained 0.06M KCl as additional electrolyte. K^+ and Na^+ were present in low amounts, however, and they do not provoke as strong side reactions for EDTA and SA as other salt ions usually found in seawater samples, such as Mg^{2+} or Ca^{2+} . In fact, we observed the opposite trend of a decreasing $\log K_{\text{CuEDTA}}^{\text{CuEDTA}}$ with decreasing ionic strengths of the samples, although it should be noted that they were in line with previous reports: The CLE-ACSV results are in the range of those found by Xue and Traina (1996) based on potentiometric titrations of Cu-EDTA in 50–60% methanol-water mixtures (17.35–17.87), while the FT-ICR-MS results are more similar to those calculated by Boija et al. (2014) for Cu-EDTA (15.0 ± 0.1), who used Ni as a competing metal ion and conducted measurements by ESI-MS. Thus, the acquired conditional stability constants may be subject to method-dependent artifacts (potentiometric vs. ESI-MS). Because PHREEQC calculations are always based on empirically derived parameters, the speciation models can be impacted as well, and this has to be taken into account when comparing models with instrument-derived speciation results.

Implications for Natural Metal-DOM Studies

As demonstrated by our study, FT-ICR-MS is able to capture the speciation of metal-organic complexes with a wide range of structures, binding stoichiometries, and binding strengths, and the detected species agree well with predictions from other analytical methods, earlier ESI-MS reports from the literature, and speciation calculations (**Tables 1–5**). Nevertheless, even simple artificial metal-ligand solutions can produce mass spectra of high complexity due to adduct formation or dimerization during ionization, and care must be taken in the interpretation of the results when true metal-ligand complexes present in aqueous solution are sought to be identified. Based on the signal intensities of the detected compounds (**Figures 1, 2**), we can identify several common trends for all tested ligand types: Overall, highest FT-ICR-MS signal responses were found for methanol-water mixtures, and selective ionization of metal-organic complexes in pure water solutions did not play an important role. In contrast to Stenson (2009), and in line with Silva et al. (2009), we suggest that for metal-ligand measurements, the enhanced

ionization efficiency due to the methanol matrix outweighs any potential advantage of a selective ionization of metal-containing compounds predicted for samples made up with pure water only. Furthermore, it appears that Fe-ligand complexes benefitted most from the addition of aq. ammonia rather than sodium hydroxide, and had highest signal intensities in negative ionization mode. Cu-ligands and free ligand species were overall preferentially ionized in positive mode, and the addition of a base enhanced the free ligand response factors through adduct formation, also particularly in positive ionization mode.

Although only a few specific compounds were investigated, the abovementioned observations may also be applicable to unknown natural ligands found in DOM. Traditionally, DOM is desalinated and pre-concentrated by solid-phase extraction (SPE-DOM), and FT-ICR-MS analyses of the extracts are routinely used for DOM fingerprinting of water masses as well as exometabolome studies (Dittmar et al., 2008). It has been shown that metal-organic complexes, as well as free Fe- and Cu-binding ligands, can be solid-phase extracted together with DOM (Macrellis et al., 2001; McCormack et al., 2003; Mawji et al., 2008, 2011; Velasquez et al., 2011; Waska et al., 2015). For example, in the scope of this study, we tested artificial ligands with a variety of metal-binding functional groups, including carboxylate and hydroxyl groups, as well as N-containing groups such as oximes and amines (**Table 1**). NMR analyses of marine SPE-DOM indicate that it predominantly contains carboxylic groups (Hertkorn et al., 2006; Repeta, 2015), demonstrating that functional groups such as those tested here may also occur in natural ligands. Furthermore, catecholate and hydroxamate groups typical for siderophores have been found in marine SPE-DOM using spectrophotometric methods (Macrellis et al., 2001). CLE-ACSV of natural seawater samples as well as SPE extracts also revealed that uncomplexed SPE-ligands (1) have binding strengths in the range of those found for natural seawater ($\log K_{\text{FeL}}^{\text{FeL}} \sim 12$, Macrellis et al., 2001, $\log K_{\text{CuL}}^{\text{CuL}} \sim 13\text{--}14$, Waska et al., 2015) and (2) are extracted at efficiencies similar to total DOM and higher than those of intact metal-organic complexes (Waska et al., 2015). Therefore, SPE-ligands may represent a near-natural ligand population, and based on the range of the binding strengths tested in this study, we would expect the majority of metal-organic complexes with natural ligands to stay intact during ESI-MS analyses. It should be noted that the conditional stability constants from Waska et al. (2015) were derived from CLE-ACSV titrations of SPE-DOM re-dissolved in artificial seawater to correct for side reactions of SA with salt ions. For FT-ICR-MS analyses, SPE-ligands in the original desalinated extracts have to be used, and as seen from our SA-EDTA-Cu competitive titration, binding strengths may differ substantially depending on matrix and used methodology, especially when side reactions affect some ligand types in DOM to a greater extent than others (Campos and van den Berg, 1994). Thus, conditional stability constants derived from FT-ICR-MS measurements likely do not capture the complexation properties of the original water sample, although they can be used in several other ways, for example to determine ligand concentrations, intercalibrate FT-ICR-MS and CLE-ACSV, or link metal binding of SPE-ligands to other SPE-DOM characteristics such as elemental composition of

detected molecules. SPE-ligands can also be spiked with excess trace metals concentrations, and in past studies, compounds, which newly occurred in DOM mass spectra after metal salt additions, have been identified as metal-organic complexes, and confirmed by isotopic pattern recognition and/or molecular formulae assignment (“presence-absence check,” (McCormack et al., 2003; Mawji et al., 2008; Stenson, 2009; Velasquez et al., 2011)). However, the study presented here confirms previous reports (e.g., Reinoso-Maset et al., 2012) that the response factors of metal-organic compounds, as well as uncomplexed ligands, can be selectively sensitive toward changes in the sample matrix, for example through additives in trace metals solutions (for example NO_3^- , Na^+ , or Cl^-), the trace metals themselves, and enhancement/suppression effects of bases such as aq. ammonia and sodium hydroxide. Thus, simple presence-absence patterns of newly detected compounds have to be treated with caution, particularly when considering that even state-of-the-art ultra-high resolution mass spectrometry still contains uncertainties hampering isotope pattern recognition and molecular formulae assignments, for example due to peak overlaps (Waska et al., 2015). Based on the results from our study, we propose that presence-absence studies could be conducted as titrations within the range of the natural ligand pool instead of excess equilibrations, to track linear increases in signal intensities. This approach still includes uncertainties due to metal adduct formation as opposed to the production of “real” aqueous metal-ligand complexes, and for it to be a valid knock-out criterion, we suggest a co-evaluation of the sample complexing capacity using CLE-ACSV, and/or the employment of a competing ligand such as SA or NN to scavenge excess metals. In addition, molecular formulae assignments and isotope pattern recognition in sample scans at high resolution (for example, through mass window isolation) may aid in the unambiguous identification of metal-organic target compounds in SPE-DOM.

CONCLUSION

In this study, we applied a soft ionization mass spectrometric technique with ultra-high resolution (FT-ICR-MS) to characterize equilibria of the model ligands citrate, EDTA, 1-nitroso-2-naphthol, and salicylaldehyde with iron (Fe) and copper (Cu). In general, methanol-containing samples had much higher sensitivities compared to those only containing water. We also suggest that easily ionized ligands, such as citrate and EDTA (and possibly, carboxylic-rich DOM), produce better results with aqueous ammonia as added base, while less polar ligands such as NN and SA may profit from an ionization-enhancing base like sodium hydroxide. In comparison with a PHREEQC speciation model, the predicted metal-ligand complex stoichiometries all were found in the tested sample solutions, although the patterns were sometimes obscured by

REFERENCES

Abualhaija, M. M., and van den Berg, C. M. G. (2014). Chemical speciation of iron in seawater using catalytic cathodic stripping voltammetry with

instrument-based dimerization or adduct formation. The signal intensities of some compounds (for example, unbound NN and SA, or $\text{Cu}(\text{NN})_2$ and $\text{Fe}(\text{SA})$ complexes) differed from predicted concentrations, indicating that ionization efficiencies may impact the abundance distribution patterns of some metal-ligand equilibria. An intercomparison between CLE-ACSV and FT-ICR-MS revealed that FT-ICR-MS-derived complex formation is a quantitative process which can be used to (1) identify unknown compounds based on their linear increase with increasing added metal concentrations, and (2) calculate the concentration of a titrated free ligand (in the case of this study, EDTA). Although no conclusive evidence was found for an impact of pH or organic solvent (methanol) on the overall integrity of the compounds or their linear increase with increasing concentrations, FT-ICR-MS- and CLE-ACSV-calculated conditional stability constants differed. Thus, we conclude that FT-ICR-MS-derived conditional stability constants can only be compared between similarly processed sample types such as SPE-DOM measured by MS. We finally suggest that CLE-ACSV should be used for an a priori characterization of the natural sample and corresponding SPE-DOM ligand pool, with FT-ICR-MS being applied for subsequent molecular characterizations, for example, based on the methods described in this paper. This approach will provide novel insights into the large, yet unknown pool of small organic ligands still hidden in DOM.

AUTHOR CONTRIBUTIONS

HW planned and conducted this study and wrote the manuscript. TD, AK contributed to data interpretation and writing of the manuscript.

FUNDING

This work was funded by a DFG “Eigene Stelle” fellowship to HW (WA3067/2-1).

ACKNOWLEDGMENTS

We would like to thank Katrin Klaproth, Heike Simon, Andrea Mentges, and Jeff Hawkes for technical assistance and insightful comments on the study. Furthermore, we are indebted to David Turner and Janek Greskowiak for their valuable advice on PHREEQC speciation modeling.

SUPPLEMENTARY MATERIAL

The Supplementary Material for this article can be found online at: <http://journal.frontiersin.org/article/10.3389/fmars.2016.00119>

ligand competition against salicylaldehyde. *Mar. Chem.* 164, 60–74. doi: 10.1016/j.marchem.2014.06.005

Abualhaija, M. M., Whitby, H., and van den Berg, C. M. G. (2015). Competition between copper and iron for humic ligands in estuarine

- waters. *Mar. Chem.* 172, 46–56. doi: 10.1016/j.marchem.2015.03.010
- Barbeau, K., Rue, E. L., Bruland, K. W., and Butler, A. (2001). Photochemical cycling of iron in the surface ocean mediated by microbial iron(III) binding ligands. *Nature* 413, 409–413. doi: 10.1038/35096545
- Bertoli, A. C., Carvalho, R., Freitas, M. P., Ramalho, T. C., Mancini, D. T., Oliveira, M. C., et al. (2015). Structural determination of Cu and Fe-citrate complexes: theoretical investigation and analysis by ESI-MS. *J. Inorg. Biochem.* 144, 31–37. doi: 10.1016/j.jinorgbio.2014.12.008
- Bojja, S., Almesäker, A., Hedenström, E., Bylund, D., Edlund, H., and Norgren, M. (2014). Determination of conditional stability constants for some divalent transition metal ion-EDTA complexes by electrospray ionization mass spectrometry. *J. Mass Spectrom.* 49, 550–556. doi: 10.1002/jms.3372
- Buck, K. N., and Bruland, K. W. (2005). Copper speciation in San Francisco Bay: a novel approach using multiple analytical windows. *Mar. Chem.* 96, 185–198. doi: 10.1016/j.marchem.2005.01.001
- Buck, K. N., Lohan, M. C., Berger, C. J. M., and Bruland, K. W. (2007). Dissolved iron speciation in two distinct river plumes and an estuary: implications for riverine iron supply. *Limnol. Oceanogr.* 52, 843–855. doi: 10.4319/lo.2007.52.2.0843
- Campos, M. L. A. M., and van den Berg, C. M. G. (1994). Determination of copper complexation in sea water by cathodic stripping voltammetry and ligand competition with salicylaldehyde. *Anal. Chim. Acta* 284, 481–496. doi: 10.1016/0003-2670(94)85055-0
- Chen, Z., Sun, Q., Xi, Y., and Owens, G. (2008). Speciation of metal-EDTA complexes by flow injection analysis with electrospray ionization mass spectrometry and ion chromatography with inductively coupled plasma mass spectrometry. *J. Sep. Sci.* 31, 3796–3802. doi: 10.1002/jssc.200800292
- Di Marco, V. B., and Bombi, G. G. (2006). Electrospray mass spectrometry (ESI-MS) in the study of metal-ligand solution equilibria. *Mass Spectrom. Rev.* 25, 347–379. doi: 10.1002/mas.20070
- Dittmar, T., Koch, B., Hertkorn, N., and Kattner, G. (2008). A simple and efficient method for the solid-phase extraction of dissolved organic matter (SPE-DOM) from seawater. *Limnol. Oceanogr. Methods* 6, 230–235. doi: 10.4319/lo.2008.6.230
- Furia, T. E. (1972). “Sequestrants in food,” in *CRC Handbook of Food Additives*, ed T. E. Furia (Boca Raton, FL: CRC Press), 271–294.
- Gatlin, C. L., and Tureček, F. (1994). Acidity determination in droplets formed by electrospraying methanol-water solutions. *Anal. Chem.* 66, 712–718. doi: 10.1021/ac00077a021
- Gautier-Luneau, I., Merle, C., Phanon, D., Lebrun, C., Biaso, F., Serratrice, G., et al. (2005). New trends in the chemistry of iron(III) citrate complexes: correlations between X-ray structures and solution species probed by electrospray mass spectrometry and kinetics of iron uptake from citrate by iron chelators. *Chem. Eur. J.* 11, 2207–2219. doi: 10.1002/chem.200401087
- Gledhill, M. (2001). Electrospray ionization-mass spectrometry of hydroxamate siderophores. *Analyst* 126, 1359–1362. doi: 10.1039/b101268l
- Gledhill, M., and van den Berg, C. M. G. (1994). Determination of complexation of iron(III) with natural organic complexing ligands in seawater using cathodic stripping voltammetry. *Mar. Chem.* 47, 41–54. doi: 10.1016/0304-4203(94)90012-4
- Hawkes, J. A., Gledhill, M., Connelly, D. P., and Achterberg, E. P. (2013). Characterisation of iron-binding ligands in seawater by reverse titration. *Anal. Chim. Acta* 766, 53–60. doi: 10.1016/j.aca.2012.12.048
- Hertkorn, N., Benner, R., Frommberger, M., Schmitt-Kopplin, P., Witt, M., Kaiser, K., et al. (2006). Characterization of a major refractory component of marine dissolved organic matter. *Geochim. Cosmochim. Acta* 70, 2990–3010. doi: 10.1016/j.gca.2006.03.021
- Keith-Roach, M. J. (2010). A review of recent trends in electrospray ionization-mass spectrometry for the analysis of metal-organic ligand complexes. *Anal. Chim. Acta* 678, 140–148. doi: 10.1016/j.aca.2010.08.023
- Keller, B. O., Sui, J., Young, A. B., and Whittall, R. M. (2008). Interferences and contaminants encountered in modern mass spectrometry. *Anal. Chim. Acta* 627, 71–81. doi: 10.1016/j.aca.2008.04.043
- Koch, B. P., Dittmar, T., Witt, M., and Kattner, G. (2007). Fundamentals of molecular formula assignment to ultrahigh resolution mass data of natural organic matter. *Anal. Chem.* 79, 1758–1763. doi: 10.1021/ac061949s
- Koch, B. P., Witt, M., Engbrodt, R., Dittmar, T., and Kattner, G. (2005). Molecular formulae of marine and terrigenous dissolved organic matter detected by electrospray ionization Fourier transform ion cyclotron resonance mass spectrometry. *Geochim. Cosmochim. Acta* 69, 3299–3308. doi: 10.1016/j.gca.2005.02.027
- Macrellis, H. M., Trick, C. G., Rue, E. L., Smith, G., and Bruland, K. W. (2001). Collection and detection of natural iron-binding ligands from seawater. *Mar. Chem.* 76, 175–187. doi: 10.1016/S0304-4203(01)00061-5
- Mawji, E., Gledhill, M., Milton, J. A., Tarran, G. A., Ussher, S., Thompson, A., et al. (2008). Hydroxamate siderophores: occurrence and importance in the Atlantic Ocean. *Environ. Sci. Technol.* 42, 8675–8680. doi: 10.1021/es801884r
- Mawji, E., Gledhill, M., Milton, J. A., Zubkov, M. V., Thompson, A., Wolff, G. A., et al. (2011). Production of siderophore type chelates in Atlantic Ocean waters enriched with different carbon and nitrogen sources. *Mar. Chem.* 124, 90–99. doi: 10.1016/j.marchem.2010.12.005
- McCormack, P., Worsfold, P. J., and Gledhill, M. (2003). Separation and detection of siderophores produced by marine bacterioplankton using high-performance liquid chromatography with electrospray ionization mass spectrometry. *Anal. Chem.* 75, 2647–2652. doi: 10.1021/ac0340105
- Nischwitz, V., and Michalke, B. (2009). Electrospray ionization with selected reaction monitoring for the determination of Mn-citrate, Fe-citrate, Cu-citrate, and Zn-citrate. *Rapid Comm. Mass Spectrom.* 23, 2338–2346. doi: 10.1002/rcm.4156
- Nowack, B. (2002). Environmental chemistry of aminocarboxylate chelating agents. *Environ. Sci. Technol.* 36, 4009–4016. doi: 10.1021/es025683s
- Omanović, D., Garnier, C., and Pižeta, I. (2015). ProMCC: an all-in-one tool for trace metal complexation studies. *Mar. Chem.* 173, 25–39. doi: 10.1016/j.marchem.2014.10.011
- Oss, M., Krueve, A., Herodes, K., and Leito, I. (2010). Electrospray ionization efficiency scale of organic compounds. *Anal. Chem.* 82, 2865–2872. doi: 10.1021/ac902856t
- Parkhurst, D. L., and Appelo, C. A. J. (1999). *User's Guide to PHREEQC (Version 2) – A Computer Program for Speciation, Batch-Reaction, One-Dimensional Transport, and Inverse Geochemical Calculations*. U. S. Geological Survey Water-Resources Investigations Report, 99-4259.
- Reinoso-Maset, E., Worsfold, P. J., and Keith-Roach, M. J. (2012). Evaluation of electrospray ionization mass spectrometry as a technique for the investigation of competitive interactions: a case study of the ternary Th-Mn-EDTA system. *Rapid. Comm. Mass Spectrom.* 26, 2755–2762. doi: 10.1002/rcm.6404
- Rellán-Álvarez, R., Abadía, J., and Álvarez-Fernández, A. (2008). Formation of metal-nicotianamine complexes as affected by pH, ligand exchange with citrate and metal exchange. A study by electrospray ionization time-of-flight mass spectrometry. *Rapid. Comm. Mass Spectrom.* 22, 1553–1562. doi: 10.1002/rcm.3523
- Repeta, D. (2015). “Chemical characterization and cycling of dissolved organic matter,” in *Biogeochemistry of Dissolved Organic Matter*, eds D. A. Hansell and C. A. Carlson (Boston, MA: Academic Press), 21–63.
- Riedel, T., and Dittmar, T. (2014). A method detection limit for the analysis of natural organic matter via Fourier transform ion cyclotron resonance mass spectrometry. *Anal. Chem.* 86, 8376–8382. doi: 10.1021/ac501946m
- Ross, A. R. S., Ikononou, M. G., and Orians, K. J. (2003). Characterization of copper-complexing ligands in seawater using immobilized copper(II)-ion affinity chromatography and electrospray ionization mass spectrometry. *Mar. Chem.* 83, 47–58. doi: 10.1016/S0304-4203(03)00095-1
- Rue, E. L., and Bruland, K. W. (1995). Complexation of iron(III) by natural organic ligands in the Central North Pacific as determined by a new competitive ligand equilibration/adsorptive cathodic stripping voltammetric method. *Mar. Chem.* 50, 117–138. doi: 10.1016/0304-4203(95)00031-L
- Sathe, R. M., and Shetty, S. Y. (1970). Potentiometric studies of the complexes of Be²⁺ and Cu²⁺ with some naphthalene derivatives. *J. Inorg. Nucl. Chem.* 32, 1383–1386. doi: 10.1016/0022-1902(70)80140-3
- Seidel, M., Yager, P. L., Ward, N. D., Carpenter, E. J., Gomes, H. R., Krusche, A. V., et al. (2015). Molecular-level changes of dissolved organic matter along the Amazon River-to-ocean continuum. *Mar. Chem.* 177, 218–231. doi: 10.1016/j.marchem.2015.06.019
- Silva, A. M., Kong, X.-L., Parkin, M. C., Cammack, R., and Hider, R. C. (2009). Iron(III) citrate speciation in aqueous solution. *Dalton Trans.* 40, 8616–8625. doi: 10.1039/b910970f

- Stenson, A. C. (2009). Fourier transform ion cyclotron resonance mass spectral characterization of metal-humic binding. *Rapid. Comm. Mass Spectrom.* 23, 465–476. doi: 10.1002/rcm.3889
- Van Berkel, G. J., and Kertesz, V. (2007). Using the electrochemistry of the electrospray ion source. *Anal. Chem.* 79, 5510–5520. doi: 10.1021/ac071944a
- Van den Berg, C. M. G. (1984). Determination of the complexing capacity and conditional stability constants of complexes of copper(II) with natural organic ligands in seawater by cathodic stripping voltammetry of copper-catechol complex ions. *Mar. Chem.* 15, 1–18. doi: 10.1016/0304-4203(84)90035-5
- Van den Berg, C. M. G., Nimmo, M., Abollino, O., and Mentasi, E. (1991). The determination of trace levels of iron in seawater using adsorptive cathodic stripping voltammetry. *Electroanalysis* 3, 477–484. doi: 10.1002/elan.1140030606
- Velasquez, I., Nunn, B. L., Ibisamni, E., Goodlett, D. R., Hunter, K. A., and Sander, S. G. (2011). Detection of hydroxamate siderophores in coastal and Sub-Antarctic waters off the South Eastern Coast of New Zealand. *Mar. Chem.* 126, 97–107. doi: 10.1016/j.marchem.2011.04.003
- Wang, H., and Agnes, G. R. (1999). Kinetically labile equilibrium shifts induced by the electrospray process. *Anal. Chem.* 71, 4166–4172. doi: 10.1021/ac981375u
- Waska, H., Koschinsky, A., Ruiz Chanchos, M. J., and Dittmar, T. (2015). Investigating the potential of solid-phase extraction and Fourier-transform ion cyclotron resonance mass spectrometry (FT-ICR-MS) for the isolation and identification of dissolved metal-organic complexes from seawater. *Mar. Chem.* 173, 78–92. doi: 10.1016/j.marchem.2014.10.001
- Wu, J., and Luther, G. W. (1995). Complexation of Fe(III) by natural organic ligands in the Northwest Atlantic Ocean by a competitive ligand equilibration method and a kinetic approach. *Mar. Chem.* 50, 159–177. doi: 10.1016/0304-4203(95)00033-N
- Xue, Y., and Traina, S. J. (1996). Stability of metal-organic complexes in acetone- and methanol-water mixtures. *Environ. Sci. Technol.* 30, 3177–3183. doi: 10.1021/es950740l

Conflict of Interest Statement: The authors declare that the research was conducted in the absence of any commercial or financial relationships that could be construed as a potential conflict of interest.

Copyright © 2016 Waska, Koschinsky and Dittmar. This is an open-access article distributed under the terms of the Creative Commons Attribution License (CC BY). The use, distribution or reproduction in other forums is permitted, provided the original author(s) or licensor are credited and that the original publication in this journal is cited, in accordance with accepted academic practice. No use, distribution or reproduction is permitted which does not comply with these terms.



Identification of Metallophores and Organic Ligands in the Chemosphere of the Marine Macroalga *Ulva* (Chlorophyta) and at Land-Sea Interfaces

Thomas Wichard*

Jena School for Microbial Communication, Institute for Inorganic and Analytical Chemistry, Friedrich Schiller University Jena, Jena, Germany

OPEN ACCESS

Edited by:

Sylvia Gertrud Sander,
University of Otago, New Zealand

Reviewed by:

Antonio Cobelo-Garcia,
Spanish National Research Council,
Spain

Oliver Baars,
Princeton University, USA

*Correspondence:

Thomas Wichard
thomas.wichard@uni-jena.de

Specialty section:

This article was submitted to
Marine Biogeochemistry,
a section of the journal
Frontiers in Marine Science

Received: 26 March 2016

Accepted: 11 July 2016

Published: 29 July 2016

Citation:

Wichard T (2016) Identification of Metallophores and Organic Ligands in the Chemosphere of the Marine Macroalga *Ulva* (Chlorophyta) and at Land-Sea Interfaces. *Front. Mar. Sci.* 3:131. doi: 10.3389/fmars.2016.00131

The roles of organic matter in seawater have often been discussed from the aspect of metal toxicity and bioavailability in seawater. In fact, organic ligands, as part of the organic matter, can work as a trace metal ion buffer system. At the same time, however, the release of well-defined metal chelators as exudates by, for example, marine bacteria is necessary to compete with natural metal complexes and sustain the metal acquisition required for several processes including nitrogen fixation. The identification, isolation, and structure elucidation of chelators is, thus, essential to our understanding of metal stress management in the natural habitat and role of these chelators on cellular process. The isolation of an organic ligand from its chemosphere is a challenging task. The purpose of this paper is, therefore, to give an additional perspective on how the effective application of stable isotope pairs of a metal of interest (both cations and oxoanions) combined with mass spectrometric analyses can pave the way to discovering new organic ligands (i.e., metallophores) and the chelating characteristics of dissolved organic matter (DOM): Pairs of isotopes, such as ^{54}Fe and ^{58}Fe (or any other pair of available isotopes of a given metal), can be used to create easily detectable unique isotopic signatures in mass spectra when they are bound by chelators. The identification of organic ligands is outlined for a proposed model system of mutualistic interactions between the green macroalga *Ulva* (Chlorophyta) and associated bacteria, as well as discussed briefly for DOM along land-sea gradients. Overall, the characterization of a broader spectrum of chelators in aquatic systems will open a new window to decipher the eco-physiological functions of organic ligands as a metal ion buffer and metallophores in metal cycling in marine ecosystems.

Keywords: dissolved organic matter, green algae, macroalgae, metal chelation, metal homeostasis, metal uptake, isotopic labeling, siderophores

A SHORT INTRODUCTION: METAL ACQUISITION IN (MACRO)ALGAE AND ASSOCIATED BACTERIA

Maintaining a sufficient internal concentration of essential macro- and micronutrients, despite extracellular environmental stress, is an essential function for any organisms (i.e., nutrient homeostasis). If a given nutrient is insufficiently available and its concentration drops below a critical threshold, growth becomes limited, as demonstrated for several algal species. Conversely, when the external concentration of nutrients increases higher than an acceptable value, growth is impaired because the nutrient becomes toxic. Overall, algal metal homeostasis has to balance between two extremes, enabling the adequate amounts of micronutrients to maintain metal-requiring processes in macroalgae, but not becoming toxic. Heavy metals are, thus, a good example of the necessity of a well-controlled micronutrient uptake and storage in marine algae (Sunda et al., 2005; Hopkinson and Morel, 2009).

The achievement of metal homeostasis requires a well-controlled acquisition of trace metals that both allows improving metal availability (e.g., Fe, Zn, and Mo) under metal limiting conditions and even controls metal entry under metal toxic conditions (e.g., Cu, Cd). The acquisition of metal is, hence, a complex multiple step process, whereby chelators are potentially involved in various steps. Originally known as iron carriers (i.e., siderophores), many chelating agents have an adaptable coordination chemistry not only for cations like Fe, but also for oxoanions, which might be particularly relevant in understanding metal-ligand speciation in ocean waters that are abundant in V(V) and Mo(VI) (Butler, 1998; Soe et al., 2015).

In the terrestrial world, besides important studies on metal acquisition of bacteria (Andrews et al., 2003; Ma et al., 2009), major contributions were made to the understanding of metal homeostasis of plant-microbe interactions and nitrogen-fixing bacteria (Clemens et al., 2002; González-Guerrero et al., 2014). In this context, several model studies were carried out with the nitrogen-fixing soil bacterium *Azotobacter vinelandii* releasing the tris-chatecholate siderophore protochelin (Cornish and Page, 1995; Kraepiel et al., 2009; Harrington et al., 2012). Protochelin is utilized for Fe(III)-, Mo(VI)-, and V(V)-uptake and detoxifies W(VI) (Bellenger et al., 2008; Wichard et al., 2008), demonstrating the multiple functions of one and the same ligand (=metallophore). Overall, the metallophores are exuded by the organism and mobilize the target metal from either a mineral or organic nutrient source by ligand exchange. The target metal-metallophore complex formed is subsequently taken up by the organism through a specific uptake system (Kraepiel et al., 2009; Kraemer et al., 2015).

In marine systems, the trace metal acquisition strategies of the multicellular macroalgae remain largely unknown, although these organisms represent important ecological niches in the coastal marine environment (Miller et al., 2014). This perspective paper, thus, highlights the identification of both algal/bacterial metallophores and organic ligands as part of the dissolved organic matter (DOM) (Figure 1), with a specific focus on the

chemosphere of the marine macroalga *Ulva* and its associated bacteria (Figure 2). Both alga and bacteria contribute to the “soup of organic ligands” which finally increase the bioavailability of metals due to various ligand exchanges with DOM, in the first place, or between each other in a sequestered recruitment process (Figure 2A) when the complex has a sufficiently low enough thermodynamic stability to undergo ligand-exchange reactions (Kraemer et al., 2006). Weak organic ligands can even increase the bioavailability of various metals in the presence of strong organic ligands as shown for Cu, Zn, and Cd (Aristilde et al., 2012; Walsh et al., 2015). Finally, the metallophores transport the scavenged trace metal into the cell mediated by e.g., sideroreceptors (Morrissey and Bowler, 2012). The identification of metal organic ligands in natural samples will pave the way for understanding the organic ligand-mediated metal acquisition (Strategy II) shuttled from DOM to alga (via bacterial metallophores). Hereby, chelator-mediated uptake of iron can also occur indirectly by *in situ* photolysis of the ligand delivering the essential nutrients to the algae, which was proven for dinoflagellates (Amin et al., 2009a).

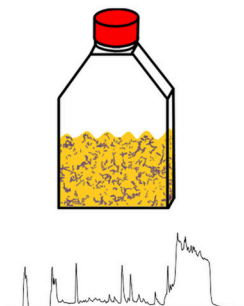
TOWARD THE IDENTIFICATION OF ORGANIC LIGANDS IN MARINE DISSOLVED ORGANIC MATTER

Marine DOM contains metal-binding functional groups (such as carboxylates, phenols, amines, and thiols) with metal-binding affinities and ligand densities spanning many orders of magnitude (Aiken et al., 2011). DOM comprises thus organic ligands that can work as “metal ion buffers” or metallophores. However, their prevalence among marine DOM is poorly established due to the few attempts to determine metal complexes using mass spectrometric approaches. Consequently, the picture of the recruitment processes, starting with the identification of the respective metal speciation till the acquisition and uptake, is pretty incomplete and important pieces of the mosaic are missing for the understanding of the complete metal biogeochemical cycles.

Many of the first-row transition metal ions in seawater are (partially) complexed by undefined organic ligands. Complexing characteristics have been studied widely by, for example, electrochemical (Van Den Berg, 1984; Kramer, 1986; Hering et al., 1987; Buffle, 1988; Gledhill and van den Berg, 1994), chromatographic (Mills et al., 1987; Baffi et al., 1992) and chemiluminescent (Sunda and Huntsman, 1991) techniques for decades and, more recently, on the scale of explorative field surveys (e.g., during GEOTRACES mission). The presence of carboxylate and phenolate groups gives, for example, the humic acids, as part of DOM, the ability to form complexes not only with cations such as Fe(II) and Fe(III), but also with oxoanions such as molybdate and vanadate (Ross et al., 2000; Deicke et al., 2014) measured by mass spectrometry. Despite all these advances in methodology, “*much work is still be done in coupling voltammetry, mass spectrometry techniques, and process studies to better characterize the nature and cycling of Fe-binding ligands*”

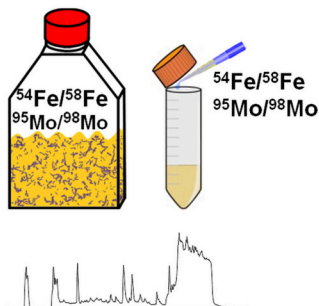
Workflow for the identification of organic ligands: Isotopic labeling and UHPLC-MS measurements

Identification of the natural isotopic signature of metal complexes

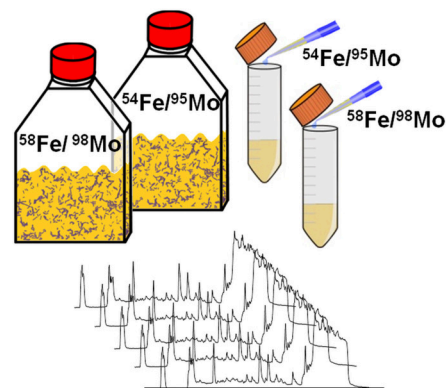


Software-based identification of metallophores by the natural isotopic signature

Metal isotope coded profiling of organic ligands



Software-based identification of metallophores by specific mass differences in isotopic signatures



Metallophore identification by discriminant function analysis

Method development with iron and molybdenum complexes of the metallophore protochelin

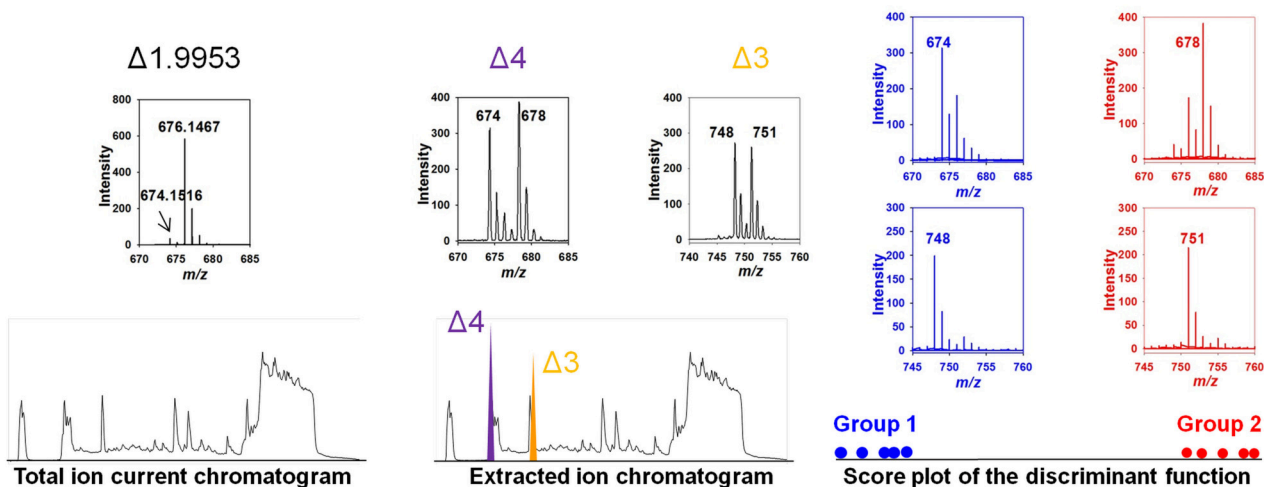
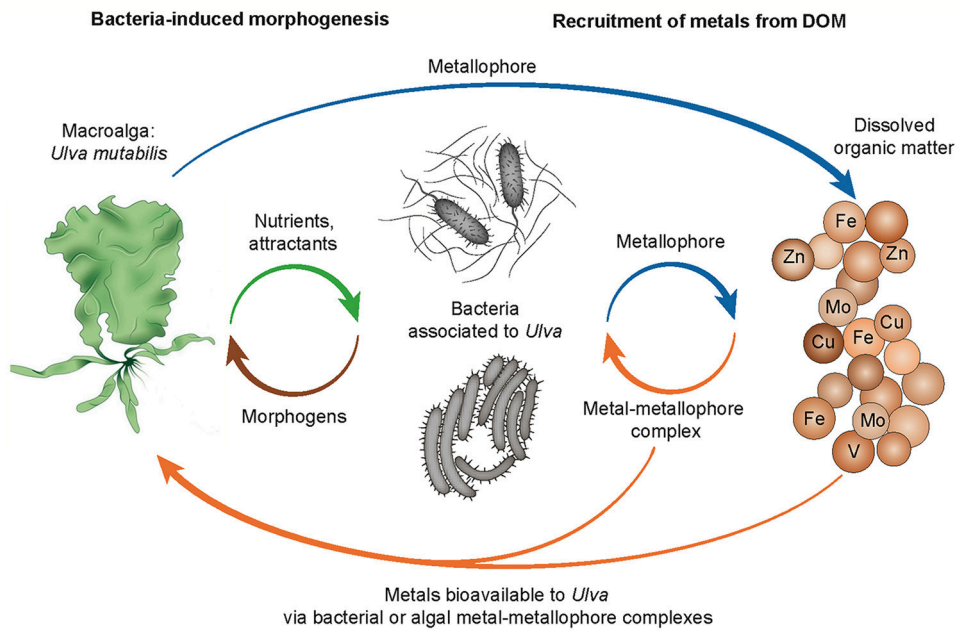
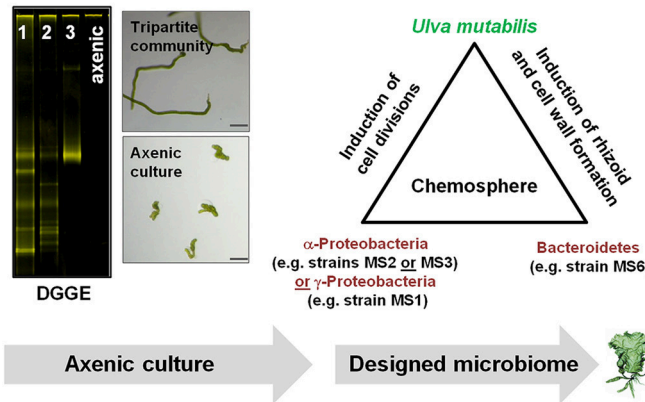


FIGURE 1 | Conceptual workflow for the identification of organic ligands. Three approaches are shown using the isotopic signature of metal complexes for the identification of organic ligands and metallophores (exemplarily demonstrated for the metallophore protochelin). Using high resolution mass spectrometry allows one to identify the natural iron isotopic pattern. Unique isotopic signatures of potential candidates in mass spectra can be identified upon labeling potential chelators with isotopically pure pairs of, for example, ^{54}Fe and ^{58}Fe or ^{95}Mo and ^{98}Mo in natural samples or extracts with an improved signal-to-noise ratio (Deicke et al., 2014). The inserts show mass spectra (of the respective treatments above) recorded in negative ion mode either by Q-Exactive Orbitrap (Thermo Scientific, Germany) or by Q-ToF (Waters, UK) mass spectrometers coupled to an ultra-performance liquid chromatography (UHPLC). Most importantly, the chelating properties of potential chelators must be preserved during the whole analytical process (Deicke et al., 2013). Data processing can be achieved by identification of specific mass differences in the isotopic signatures or discriminant function analysis as outlined by Deicke et al. (2014). Plots are reproduced from Deicke et al. (2014) with permission from the Royal Society of Chemistry.

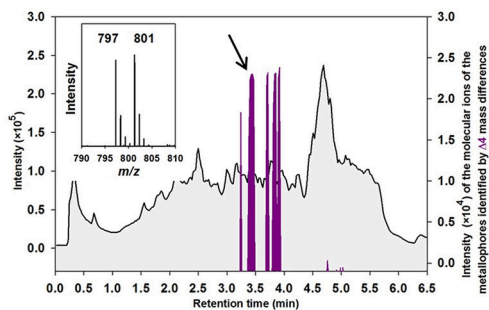
A Mutualistic interactions between *Ulva* and bacteria



B Experimental set-up to control *Ulva*'s microbiome



C Fe-metallophore mapping in *Ulva*'s microbiome



D Fe-chelating ability of tannic acids in DOM

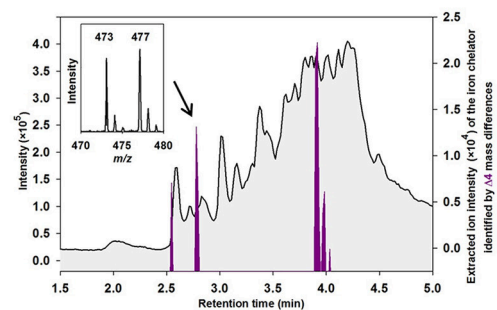


FIGURE 2 | Studying metal acquisitions in *Ulva*'s chemosphere. (A) Mutualistic interactions are vital for *Ulva* and bacteria by releasing morphogens, nutrients, and attractants, and by controlling the metal acquisition by ligand exchange processes (strategy II) from particulate or dissolved metal-organic matter complexes within the chemosphere. **(B)** Axenic cultures of *Ulva* have to be established to achieve reproducible and repeatable conditions for laboratory studies. These conditions (Continued)

FIGURE 2 | Continued

need to be proven rigorously by, for example, PCR-based techniques such as denaturing gradient gel electrophoresis (DGGE) of the supernatant of axenic cultures. The successful purification process can be monitored by progressive purification stages from lane 1 to 3 until axenic cultures are achieved (DGGE-gel) (see also Wichard, 2015). Afterwards, the impact of a designed microbiome can be reliably tested using tri- or multiple-partite systems of *U. mutabilis* and algal morphogenesis-inducing bacteria. Microscopic pictures show an axenic callus-like culture (bottom panel) in comparison to the normal development of 2- to 3-week-old germlings under conditions of *Ulva*'s tripartite community (top panel) (magnification bars = 100 μ m). **(C,D)** Upon labeling with ^{54}Fe and ^{58}Fe , the extracted chromatograms (purple line), identified by the specific $\Delta 4$ mass differences of the molecular ions of the iron complexing ligands, are shown on top of the total ion current chromatogram (TIC): **(C)** Identification of Fe-metallophores produced by bacteria associated to *Ulva* within the tripartite community. **(D)** Mapping of tannic acids bound to iron as a part of dissolved organic matter (DOM) (Deicke et al., 2014).

in the marine environment" as Gledhill and Buck (2012) have recently concluded in their review.

In marine waters of the photic zone it was demonstrated that most ferric ion is almost quantitatively complexed under iron-limited conditions by organic ligands (Donat and Bruland, 1995). These iron complexes (FeL) have pretty high conditional stability constants in seawater, ranging from $\text{Log } K_{\text{Fe}^{3+}\text{L}} = 19$ to $\text{Log } K_{\text{Fe}^{3+}\text{L}} = 23$, which is similar to the stability of bacterial siderophore complexes (Rue and Bruland, 1995). Whether, these strong ligands are indeed siderophores is difficult to establish due to their low concentrations, making the purification and further eco-physiological uptake experiments with the target organism difficult. Nevertheless, other than the stability constant of metal-ligand complexes, several groups succeeded in elucidating the structure of several ligands released by marine bacteria in culture (Reid et al., 1993; Butler and Martin, 2005; Amin et al., 2009b; Sandy and Butler, 2009).

There have only been few reports about the direct identification of metallophores and other organic ligands in the DOM of natural marine samples. Sequestration and decomposition processes of DOM are very dynamic, particularly in the presence of bacteria and sunlight. Thus, the determination of (low concentrated) organic ligands becomes challenging which is essential to understand ligand exchange processes with bacterial or algal metallophores. Up to now strong hydroxamate siderophore such as the ferrioxamines were identified in pre-concentrated water samples collected in the Atlantic Ocean using high performance liquid chromatography coupled to electrospray ionization mass spectrometry (HPLC-ESI-MS) (Gledhill et al., 2004; Mawji et al., 2008). Exploring siderophores in complex matrices can be also achieved upon HPLC-separation by ionizing the samples with inductively coupled plasma-mass spectrometry (ICP-MS). Eluted compounds need to be subsequently analyzed by HPLC-ESI-MS to identify the organic ligand complexing with iron (Mawji et al., 2011; Boiteau et al., 2013). Whereas, the ICP-MS combined with LC allows the easy quantification of metals (and metal-complexes) at very low concentration, ESI-MS measurements provide additional valuable information for structure elucidation, particularly if MS/MS experiments are applied. Using high-resolution-ESI-MS (HR-ESI-MS), hydroxamate-type ligands have been directly identified in seawater samples (Velasquez et al., 2011) or e.g., in fungi (Lehner et al., 2013; Pourhassan et al., 2014) *via* their natural iron-isotope signature. This approach was improved by the application of a newly developed MatLab based program for the identification of natural isotope patterns of metal complexes

(Baars et al., 2014). Using this algorithm, Baars and co-workers could also determine novel metallophores in the culture medium of *A. vinelandii* (Baars et al., 2016). In addition, ESI-MS/MS experiments were suggested to identify metal-ligand complexes through the release of metal species from its respective complex (Tsednee et al., 2016).

With this perspective paper, I like to suggest a *targeted analysis* of low-molecular-weight organic ligands based on fast UHPLC-ESI-MS measurements (**Figure 1**). Metal isotope coded profiling (MICP) of metallophores can reveal organic metal-binding ligands in complex matrices through the identification of specific isotopic signatures. Replacement of, for example, natural iron or molybdenum with isotopically pure $^{54}\text{Fe}/^{58}\text{Fe}$ (ratio 1:1) or $^{95}\text{Mo}/^{98}\text{Mo}$ (ratio 1:1) causes easily detectable unique isotopic signatures in the mass spectra of potential metal-complexing ligands (Deicke et al., 2013, 2014) (**Figure 1**). This can be achieved under laboratory conditions not only in growth media, but also by spiking directly seawater or solid-phase extracts. Importantly, as the relative affinity of the metallophores for e.g., Mo or Fe is dependent on the pH, all experiments needs to be conducted under pH-controlled conditions. The sensitivity of the measurements often increases due to the additional complexation of available ligands. Moreover, the improved ionization efficiency of some metal complexes helps to enhance the signal-to-noise ratio compared to the free ligand at the same chromatographic conditions (Deicke et al., 2013). The methodology does not necessarily depend on HR-ESI-MS measurements and can be applied to any mass spectrometer. However, more sensitive measurements, for example by UHPLC-HR-Q-Exactive Orbitrap mass spectrometry (Thermo-Fisher), might detect even low concentrated metal complexes without solid-phase extraction and further perturbation of the sample. Besides the fact that the methodology cannot be applied to monoisotopic elements, experimenters have to be always conscious about several parameters such as, for example, the selectivity of solid-phase extractions, the ionization efficiency of ESI as well as pH changes and ligand exchanges during the analytical process (see also Di Marco and Bombi, 2006; Keith-Roach, 2010).

The chemical exploration of both low-molecular-weight organic ligands and the metallophore production is a crucial prerequisite to study metal acquisition and homeostasis of an organism. With MICP it was shown that, besides the metallophore protochelin, tannic acids bind molybdate and iron and, thus, contribute to the metal bioavailability (Deicke et al., 2014; Jouogo et al., 2016). *A. vinelandii* produced a

higher amount of metallophores in the presence of tannic acids, which coincides with an active, regulated, and concomitant acquisition of molybdenum and vanadium (Jouogo et al., 2016). The data suggest that tannic acid contribute to the metal bioavailability by both preventing iron precipitation and by decreasing the amount of easily available molybdate. In this way with MICP, two *birds can be killed with one stone*: (i) the identification of metallophores for metal uptake and (ii) organic ligands which solely work as metal buffer in DOM. Upon partly purification, the stable isotope-labeled samples can be then directly applied to short-term-uptake experiments monitored by ICP-MS to test if an essential metal can be recruited from a newly identified metallophore and accumulated by the organism.

PERSPECTIVE APPLICATIONS

As speciation and uptake of trace metals seems to be controlled by organic ligands, our laboratory suggests two strategies to unveil the eco-physiological functions of ligands: (i) controlled mechanistic studies of metal management of the biota, and (ii) explorative targeting surveys of any organic ligand for a given metal. I propose two research lines for laboratory and field-based studies below.

Model System: *Ulva* and Its Associated Bacteria

The marine macroalga *Ulva* is a cosmopolitan seaweed that causes green tides, for example, in shallow coastal environments. This phenomenon is particularly studied in the Yellow Sea (China), using field samples to unveil, for example, growth and development under eutrophic coastal conditions. In our laboratory, we have established a model system where *Ulva* grows under strictly controlled conditions starting with an axenic feedstock of gametes inoculated with specific bacteria inducing the algal morphogenesis in artificial seawater medium (Wichard and Oertel, 2010; Spoerner et al., 2012) (Figure 2B). Hereby, bacteria are essential, as *Ulva* develops into a callus-like morphotypes under axenic conditions (Wichard, 2015). The combination of two specific bacteria from the Rhodobacteraceae (or Halomonadaceae) and Flavobacteriaceae can completely recover the growth and morphogenesis of axenic *Ulva mutabilis* cultures forming a symbiotic tripartite community by releasing morphogenetic compounds (Spoerner et al., 2012), which can also be determined in natural lagoon waters (Grüneberg et al., 2016). The acquisition of trace metals can, thus, be easily simulated in the tripartite community under standardized conditions, along with explorative chemical studies and characterization of new organic ligands used as metallophores for metal recruitment or “metal buffers” in the habitat as a result of, for example, environmental changes. Indeed, the fast growing *Ulva* might face risk of nitrogen and iron limitations in eutrophic waters, which may also affect its microbiome directly, which is, vice versa, essential for *Ulva*'s proper growth, development and morphogenesis. It was

shown recently that macroalgae blooms favor heterotrophic diazotrophic bacteria even in nitrogen-rich coastal surface waters, due potentially to the fast uptake of nitrogen by *Ulva* (Zhang et al., 2015). Given the role of trace metals in the production of Mo-, V-, and/or Fe-dependent nitrogenases, green tides may, thus, trigger metallophore production to increase the bioavailability of trace elements. All these natural conditions can be simplified under controlled laboratory conditions with a designed microbiome starting with axenic cultures of *Ulva* (Figure 2B).

Laboratory experiments are necessary to understand the dynamics of metal bioavailability and recruitment in macroalgae. Model experiments will help to integrate the chemist's and biologist's perspective of “the impact of microbial metabolism on marine dissolved organic matter” (Kujawinski, 2011). To follow up the intriguing ideas expressed in Kujawinski's review, our perspective research line aims, in particular, at investigating the metallome (=all biologically active compounds that contain a metal atom) and the dynamics of metal acquisition within a well-defined community of the green macroalga *U. mutabilis* and an experimentally designed microbiome. Pilot studies have recently revealed that bacteria tightly associated to *U. mutabilis* release unknown organic ligands which complex iron (Figure 2B). Released microbial bacterial siderophores become, therefore, part of the organic matter in the chemosphere and contribute to the recruitment of, for example, iron bound to organic matter and other sources that can now be studied exemplarily within the tripartite community in *U. mutabilis* (Figure 2C). In fact, it has already been demonstrated that nitrate accumulation in *Ulva* thalli in nitrate-rich lagoon waters (Sacca di Goro, Italy) was inversely related to Fe uptake, indicating an influence of Fe limitation on N acquisition (Viaroli et al., 2005). Fast growing *Ulva* might, thus, experience limiting conditions due to the low concentration or poor availability of iron. I hereby hypothesize that *Ulva* benefits from its associated microbiome governing the Fe recruitment. Bacterial siderophores would be shared as public goods (Dumas and Kueemmerli, 2012) within a bacterial-algal mutualism, where heterotrophic bacteria are fed by the algae through the release of carbon sources. Carbohydrates released by *Ulva* might also enhance the iron bioavailability as shown for saccharides in phytoplankton (Hassler et al., 2011). In addition, algal and bacterial exopolymeric substances (EPS) in biofilms can be a source of weaker and stronger ligands in the range from $\log K_{Fe'L} = 10.4$ to $\log K_{Fe'L} = 12.0$ (Hassler et al., 2015). The protocol of MICP has to be further developed for the upcoming research field of metals associated with macromolecules.

Ulva's growth medium can also be modulated by the addition of humic or fulvic acids or any other potential ligands which affect the bioavailability of metals directly and mimic natural conditions, where metals speciation is controlled by organic matter. Laboratory experiments will allow us to measure (i) quantitative and (ii) qualitative changes of the metallophore profile due to environmentally relevant changes in the growth conditions of the bacterial-macroalgal community (Wichard et al., 2009; Jouogo et al., 2016).

The Role of Land-Sea Processes in Modulating the Abundance and Prevalence of Chelators: Finding the Needle in the Haystack

It was suggested that only small amounts of bioavailable iron exist for macroalgae in coastal seawater not affected by inflow from land and that a significant quantity of dissolved iron is complexed to organic ligands, which was demonstrated by ^{59}Fe -labeled iron uptake experiments (Suzuki et al., 1995). With an increasing amount of organic ligands, algae growth declined markedly due to the reduced bioavailable iron concentrations because of complexation (Laglera and van den Berg, 2009; Lee et al., 2009). Combined approaches are, thus, necessary to obtain a complete picture of global element cycles comprising both terrestrial and oceanic components (Butler, 1998). While a lot of investigations dealt originally with the vertical distribution of DOM (Hirose and Tanoue, 1998), there are an increasing number of studies which explore the prevalence and changes of the DOM pool along the estuarine gradient (Sleighter and Hatcher, 2008; Dubinenkov et al., 2015; Medeiros et al., 2015). Hereby, it will be still be challenging to focus on the perspective organic ligands due to the heterogeneous DOM composition (Kujawinski, 2011). However, a comparison of various solid phases has already revealed reliable extraction protocols of DOM (Dittmar et al., 2008; Waska et al., 2015) that can be combined with the isotopic coded profiling proposed (Figures 1, 2D). As DOM contains strong organic ligands also as a signal of biological fresh matter (Hirose, 2000), the identification of organic ligands might be particularly successful in areas where fresh biological material is available. Proxies for terrestrial DOM, for instance, have revealed that terrestrial DOM fluxes, which are often derived from the decomposition of vascular land plants and mobilized nearby river systems, contribute significantly to the total DOM in estuaries and coastal waters (Osburn et al., 2015).

Recent studies continue to focus on the determination and pattern of dissolved matter facilitated by either chromatographic methods (Sandron et al., 2015) or by directly injected solid-phase-extracted compounds using Fourier transform ion cyclotron resonance mass spectrometry (FT-ICR-MS) without additional pre-procedural steps (Hertkorn et al., 2006; Dittmar et al., 2008; Herzsprung et al., 2015). Indeed, the chemical identity of DOM will be the key to the most urgent questions regarding the cycling of DOM in the ocean (Koch et al., 2005) and the subsequent identification of its chelating ability. Overall, hydroxyl functional groups, which can be found predominantly in humic acids (Thurman, 1985), hydroxamic acids, α -hydroxy carboxylic acids, carboxylic acids, oxazolone, and thiazolidine groups are of special interest depending on the metal and its oxidation states from the perspective of coordination chemistry (Springer and Butler, 2016). Some studies have already assigned the specific molecular identity of DOM in seawater samples to carboxyl-rich alicyclic molecules, which are expected to be candidates for metal binding and multiple coordination across cations that also supports aggregation processes (Hertkorn et al., 2006), others identified carbohydrates, lipids, amino acids, amino sugars, and tannins (Sleighter and Hatcher, 2008). In any case,

as the DOM pool is changing continuously and mixing can only partly account for changes along the estuarine gradient (Asmala et al., 2016), the various transformation processes at the land-sea interface will be not predictable. The search for potential ligands or metal complexes along the estuarine gradient becomes, therefore, like “*finding the needle in the haystack*.”

Land-sea processes are particular intriguing as the abundance and fingerprint of organic ligands might vary adjacent to the original source from, for example, terrestrial, permafrost soil, riverine, or marine waters. The source-specific patterns of chelators can change distinctly differently from land to open sea. The FT-ICR-MS studies on Arctic DOM have already demonstrated latitude, pH and water-dependent compositions (Roth et al., 2013; Dubinenkov et al., 2015).

Whereas DOM has often been used as a proxy for bio-productivity in terms of a carbon source, its specific impact as a “*metal buffer*” for biological processes should be investigated as well. Upon the administration of individual isotopes or isotopic pairs, for example, $^{54}\text{Fe}/^{58}\text{Fe}$, $^{63}\text{Cu}/^{65}\text{Cu}$, $^{66}\text{Zn}/^{68}\text{Zn}$, or $^{95}\text{Mo}/^{98}\text{Mo}$ and subsequent measurements by UHPLC-MS or even by direct-inlet FT-ICR-MS organic ligands might be identified that contribute potentially to the regulation of bioavailability and toxicity of metals in the water column.

CONCLUSION

Both controlled laboratory and explorative field studies are necessary to obtain a complete picture of the element cycles in the chemosphere of the suggested model community of *Ulva* and its bacteria. Certainly genome and transcriptome data as well as the establishment of stable transformants in metal homeostasis dysfunctions will help to close the gap of our understanding of *Ulva*'s metal homeostasis. An orchestrated approach is, thus, needed to combine explorative molecular studies (targeted and “omics” analysis, i.e., metabolomics and transcriptomics) with the essential biological and oceanographic metadata and upcoming genomic analysis of *Ulva* (Wichard et al., 2015). Perspective integrated studies that include DOM analysis and the determination of chelators/metallophores will contribute to an improved understanding of DOM-microbe-algal interactions that serve as the base of the metal biogeochemical cycle and affect their own bio-productivity.

AUTHOR CONTRIBUTIONS

TW conceived, designed, and wrote the paper.

ACKNOWLEDGMENTS

I apologize to those colleagues whose work could not be cited owing to space constraints. I want to thank the Deutsche Forschungsgemeinschaft (CRC 1127, ChemBioSys), which supported the sub-project “Metallophores as mediators for metal cycling: development of libraries for metal ion buffering

and as redox carriers as well as profiling of metallophores.” The project presented in the paper has also received funding from the European Union’s Horizon 2020 research and innovation programme under the Marie Skłodowska-Curie grant agreement

No. 642575. I thank Prof. Dr. Georg Pohnert (University Jena) for his great support. I appreciate the efforts of the reviewers and their useful comments and suggestions for improving the manuscript.

REFERENCES

- Aiken, G. R., Hsu-Kim, H., and Ryan, J. N. (2011). Influence of dissolved organic matter on the environmental fate of metals, nanoparticles, and colloids. *Environ. Sci. Technol.* 45, 3196–3201. doi: 10.1021/es103992s
- Amin, S. A., Green, D. H., Hart, M. C., Kuepper, F. C., Sunda, W. G., and Carrano, C. J. (2009a). Photolysis of iron-siderophore chelates promotes bacterial-algal mutualism. *Proc. Natl. Acad. Sci. U.S.A.* 106, 17071–17076. doi: 10.1073/pnas.0905512106
- Amin, S. A., Green, D. H., Küpper, F. C., and Carrano, C. J. (2009b). Vibrioferin, an unusual marine siderophore: iron binding, photochemistry, and biological implications. *Inorg. Chem.* 48, 11451–11458. doi: 10.1021/ic9016883
- Andrews, S. C., Robinson, A. K., and Rodriguez-Quinones, F. (2003). Bacterial iron homeostasis. *FEMS Microbiol. Rev.* 27, 215–237. doi: 10.1016/S0168-6445(03)00055-X
- Aristilde, L., Xu, Y., and Morel, F. M. M. (2012). Weak organic ligands enhance zinc uptake in marine phytoplankton. *Environ. Sci. Technol.* 46, 5438–5445. doi: 10.1021/es300335u
- Asmala, E., Kaartokallio, H., Carstensen, J., and Thomas, D. N. (2016). Variation in riverine inputs affect dissolved organic matter characteristics throughout the estuarine gradient. *Front. Mar. Sci.* 2:125. doi: 10.3389/fmars.2015.00125
- Baars, O., Morel, F. M. M., and Perlman, D. H. (2014). ChelomEx: isotope-assisted discovery of metal chelates in complex media using high-resolution LC-MS. *Anal. Chem.* 86, 11298–11305. doi: 10.1021/ac503000e
- Baars, O., Zhang, X., Morel, F. M. M., and Seyedsayamdost, M. R. (2016). The siderophore metabolome of *Azotobacter vinelandii*. *Appl. Environ. Microbiol.* 82, 27–39. doi: 10.1128/aem.03160-15
- Baffi, F., Ianni, M. C., Cardinale, A. M., Magi, E., Frache, R., and Ravera, M. (1992). Study of reversed-phase C18-silica in liquid-chromatography for the determination of free dissolved amino-acids and copper(II) amino-acid complexes at the picomole level in marine matrices. *Anal. Chim. Acta* 260, 99–106. doi: 10.1016/0003-2670(92)80132-q
- Bellenger, J. P., Wichard, T., Kustka, A. B., and Kraepiel, A. M. L. (2008). Uptake of molybdenum and vanadium by a nitrogen-fixing soil bacterium using siderophores. *Nat. Geosci.* 1, 243–246. doi: 10.1038/ngeo161
- Boiteau, R. M., Fitzsimmons, J. N., Repeta, D. J., and Boyle, E. A. (2013). Detection of iron ligands in seawater and marine cyanobacteria cultures by high-performance liquid chromatography-inductively coupled plasma-mass spectrometry. *Anal. Chem.* 85, 4357–4362. doi: 10.1021/ac3034568
- Buffle, J. (1988). *Complexation Reactions in Aquatic Systems; An Analytical Approach*. Chichester: Ellis Horwood Publisher.
- Butler, A. (1998). Acquisition and utilization of transition metal ions by marine organisms. *Science* 281, 207–210. doi: 10.1126/science.281.5374.207
- Butler, A., and Martin, J. D. (2005). The marine biogeochemistry of iron. *Met. Ions Biol. Syst.* 44, 21–46.
- Clemens, S., Palmgren, M. G., and Krämer, U. (2002). A long way ahead: understanding and engineering plant metal accumulation. *Trends Plant Sci.* 7, 309–315. doi: 10.1016/S1360-1385(02)02295-1
- Cornish, A. S., and Page, W. J. (1995). Production of the triacetatecholate siderophore protochelin by *Azotobacter vinelandii*. *Biometals* 8, 332–338.
- Deicke, M., Bellenger, J.-P., and Wichard, T. (2013). Direct quantification of bacterial molybdenum and iron metallophores with ultra-high-performance liquid chromatography coupled to time-of-flight mass spectrometry. *J. Chromatogr. A* 1298, 50–60. doi: 10.1016/j.chroma.2013.05.008
- Deicke, M., Mohr, J. F., Bellenger, J.-P., and Wichard, T. (2014). Metallophore mapping in complex matrices by metal isotope coded profiling of organic ligands. *Analyst* 139, 6096–6099. doi: 10.1039/c4an01461h
- Di Marco, V. B., and Bombi, G. G. (2006). Electrospray mass spectrometry (ESI-MS) in the study of metal-ligand solution equilibria. *Mass Spectrom. Rev.* 25, 347–379. doi: 10.1002/mas.20070
- Dittmar, T., Koch, B., Hertkorn, N., and Kattner, G. (2008). A simple and efficient method for the solid-phase extraction of dissolved organic matter (SPE-DOM) from seawater. *Limnol. Oceanogr. Methods* 6, 230–235. doi: 10.4319/lom.2008.6.230
- Donat, J. R., and Bruland, K. W. (1995). “Trace elements in the oceans,” in *Trace Elements in Natural Waters*, eds B. Salbu and E. Steinnes (Boca Raton, FL: CRC Press), 247–281.
- Dubinenkov, I., Flerus, R., Schmitt-Kopplin, P., Kattner, G., and Koch, B. P. (2015). Origin-specific molecular signatures of dissolved organic matter in the Lena Delta. *Biogeochemistry* 123, 1–14. doi: 10.1007/s10533-014-0049-0
- Dumas, Z., and Kuemmerli, R. (2012). Cost of cooperation rules selection for cheats in bacterial metapopulations. *J. Evol. Biol.* 25, 473–484. doi: 10.1111/j.1420-9101.2011.02437.x
- Gledhill, M., and Buck, K. N. (2012). The organic complexation of iron in the marine environment: a review. *Front. Microbiol.* 3:69. doi: 10.3389/fmicb.2012.00069
- Gledhill, M., McCormack, P., Ussher, S., Achterberg, E. P., Mantoura, R. F. C., and Worsfold, P. J. (2004). Production of siderophore type chelates by mixed bacterioplankton populations in nutrient enriched seawater incubations. *Mar. Chem.* 88, 75–83. doi: 10.1016/j.marchem.2004.03.003
- Gledhill, M., and van den Berg, C. M. G. (1994). Determination of complexation of iron(III) with natural organic complexing ligands in seawater using cathodic stripping voltammetry. *Mar. Chem.* 47, 41–54. doi: 10.1016/0304-4203(94)90012-4
- González-Guerrero, M., Matthiadis, A., Saez, Á., and Long, T. A. (2014). Fixating on metals: new insights into the role of metals in nodulation and symbiotic nitrogen fixation. *Front. Plant Sci.* 5:45. doi: 10.3389/fpls.2014.00045
- Grueneberg, J., Engelen, A. H., Costa, R., and Wichard, T. (2016). Macroalgal morphogenesis induced by waterborne compounds and bacteria in coastal seawater. *PLoS ONE* 11:e0146307. doi: 10.1371/journal.pone.0146307
- Harrington, J. M., Bargar, J. R., Jarzecki, A. A., Roberts, J. G., Sombers, L. A., and Duckworth, O. W. (2012). Trace metal complexation by the triscatecholate siderophore protochelin: structure and stability. *Biometals* 25, 393–412. doi: 10.1007/s10534-011-9513-7
- Hassler, C. S., Norman, L., Mancuso Nichols, C. A., Clementson, L. A., Robinson, C., Schoemann, V., et al. (2015). Iron associated with exopolymeric substances is highly bioavailable to oceanic phytoplankton. *Mar. Chem.* 173, 136–147. doi: 10.1016/j.marchem.2014.10.002
- Hassler, C. S., Schoemann, V., Nichols, C. M., Butler, E. C. V., and Boyd, P. W. (2011). Saccharides enhance iron bioavailability to Southern Ocean phytoplankton. *Proc. Natl. Acad. Sci. U.S.A.* 108, 1076–1081. doi: 10.1073/pnas.1010963108
- Hering, J. G., Sunda, W. G., Ferguson, R. L., and Morel, F. M. M. (1987). A field comparison of 2 methods for the determination of copper complexation - bacterial bioassay and fixed-potential amperometry. *Mar. Chem.* 20, 299–312. doi: 10.1016/0304-4203(87)90064-8
- Hertkorn, N., Benner, R., Frommberger, M., Schmitt-Kopplin, P., Witt, M., Kaiser, K., et al. (2006). Characterization of a major refractory component of marine dissolved organic matter. *Geochim. Cosmochim. Acta* 70, 2990–3010. doi: 10.1016/j.gca.2006.03.021
- Herzprung, P., Tümping, W. V., Hertkorn, N., Harir, M., Friese, K., and Schmitt-Kopplin, P. (2015). High-field FTICR-MS data evaluation of natural organic matter: are chon5s2 molecular class formulas assigned to ¹³C isotopic m/z and in reality CHO components? *Anal. Chem.* 87, 9563–9566. doi: 10.1021/acs.analchem.5b02549
- Hirose, K. (2000). “Strong organic ligands in seawater: peculiar functional groups in oceanic organic matter-synthesis,” in *Dynamics and Characterization of Marine Organic Matter*, eds N. Handa, E. Tanoue, and T. Hama (Tokyo: Springer), 339–382.

- Hirose, K., and Tanoue, E. (1998). The vertical distribution of the strong ligand in particulate organic matter in the North Pacific. *Mar. Chem.* 59, 235–252. doi: 10.1016/s0304-4203(97)00095-9
- Hopkinson, B. M., and Morel, F. M. M. (2009). The role of siderophores in iron acquisition by photosynthetic marine microorganisms. *Biometals* 22, 659–669. doi: 10.1007/s10534-009-9235-2
- Jougo, N. C., Pourhassan, N., Darnajoux, R., Deicke, M., Wichard, T., Burrus, V., et al. (2016). Effect of organic matter on nitrogenase metal cofactors homeostasis in *Azotobacter vinelandii* under diazotrophic conditions. *Environ. Microbiol. Rep.* 8, 76–84. doi: 10.1111/1758-2229.12353
- Keith-Roach, M. J. (2010). A review of recent trends in electrospray ionisation-mass spectrometry for the analysis of metal-organic ligand complexes. *Anal. Chim. Acta* 678, 140–148. doi: 10.1016/j.aca.2010.08.023
- Koch, B. P., Witt, M., Engbrodt, R., Dittmar, T., and Kattner, G. (2005). Molecular formulae of marine and terrigenous dissolved organic matter detected by electrospray ionization Fourier transform ion cyclotron resonance mass spectrometry. *Geochim. Cosmochim. Acta* 69, 3299–3308. doi: 10.1016/j.gca.2005.02.027
- Kraemer, S. M., Crowley, D. E., and Kretzschmar, R. (2006). Geochemical aspects of phytosiderophores-promoted iron acquisition by plants. *Adv. Agron.* 91, 1–46. doi: 10.1016/S0065-2113(06)91001-3
- Kraemer, S. M., Duckworth, O. W., Harrington, J. M., and Schenkeveld, W. D. C. (2015). Metallophores and Trace Metal Biogeochemistry. *Aquat. Geochem.* 21, 159–195. doi: 10.1007/s10498-014-9246-7
- Kraepiel, A. M. L., Bellenger, J. P., Wichard, T., and Morel, F. M. M. (2009). Multiple roles of siderophores in free-living nitrogen-fixing bacteria. *Biometals* 22, 573–581. doi: 10.1007/s10534-009-9222-7
- Kramer, C. J. M. (1986). Apparent copper complexation capacity and conditional stability constants in North-Atlantic waters. *Mar. Chem.* 18, 335–349. doi: 10.1016/0304-4203(86)90016-2
- Kujawinski, E. B. (2011). “The impact of microbial metabolism on marine dissolved organic matter,” in *Annual Review of Marine Science*, Vol. 3, eds C. A. Carlson and S. J. Giovannoni (Palo Alto, CA: Annual Reviews), 567–599.
- Laglera, L. M., and van den Berg, C. M. G. (2009). Evidence for geochemical control of iron by humic substances in seawater. *Limnol. Oceanogr.* 54, 610–619. doi: 10.4319/lo.2009.54.2.0610
- Lee, J., Park, J. H., Shin, Y. S., Lee, B. C., Chang, N. I., Cho, J., et al. (2009). Effect of dissolved organic matter on the growth of algae, *Pseudokirchneriella subcapitata*, in Korean lakes: the importance of complexation reactions. *Ecotoxicol. Environ. Saf.* 72, 335–343. doi: 10.1016/j.ecoenv.2008.01.013
- Lehner, S. M., Atanasova, L., Neumann, N. K. N., Krska, R., Lemmens, M., Druzhinina, I. S., et al. (2013). Isotope-assisted screening for iron-containing metabolites reveals a high degree of diversity among known and unknown siderophores produced by *Trichoderma* spp. *Appl. Environ. Microbiol.* 79, 18–31. doi: 10.1128/Aem.02339-12
- Ma, Z., Jacobsen, F. E., and Giedroc, D. P. (2009). Coordination chemistry of bacterial metal transport and sensing. *Chem. Rev.* 109, 4644–4681. doi: 10.1021/cr900077w
- Mawji, E., Gledhill, M., Milton, J. A., Tarran, G. A., Ussher, S., Thompson, A., et al. (2008). Hydroxamate siderophores: occurrence and importance in the Atlantic Ocean. *Environ. Sci. Technol.* 42, 8675–8680. doi: 10.1021/es801884r
- Mawji, E., Gledhill, M., Milton, J. A., Zubkov, M. V., Thompson, A., Wolff, G. A., et al. (2011). Production of siderophore type chelates in Atlantic Ocean waters enriched with different carbon and nitrogen sources. *Mar. Chem.* 124, 90–99. doi: 10.1016/j.marchem.2010.12.005
- Medeiros, P. M., Seidel, M., Ward, N. D., Carpenter, E. J., Gomes, H. R., Niggemann, J., et al. (2015). Fate of the Amazon River dissolved organic matter in the tropical Atlantic Ocean. *Global Biogeochem. Cycles* 29, 677–690. doi: 10.1002/2015gb005115
- Miller, E. P., Boettger, L. H., Weerasinghe, A. J., Crumbliss, A. L., Matzanke, B. F., Meyer-Klaucke, W., et al. (2014). Surface-bound iron: a metal ion buffer in the marine brown alga *Ectocarpus siliculosus*? *J. Exp. Bot.* 65, 585–594. doi: 10.1093/jxb/ert406
- Mills, G. L., McFadden, E., and Quinn, J. G. (1987). Chromatographic studies of dissolved organic-matter and copper organic-complexes isolated from estuarine waters. *Mar. Chem.* 20, 313–325. doi: 10.1016/0304-4203(87)90065-x
- Morrissey, J., and Bowler, C. (2012). Iron utilization in marine cyanobacteria and eukaryotic algae. *Front. Microbiol.* 3:43. doi: 10.3389/fmicb.2012.00043
- Osburn, C. L., Boyd, T. J., Montgomery, M. T., Coffin, R. B., Bianchi, T. S., and Paerl, H. W. (2015). Optical proxies for terrestrial dissolved organic matter in estuaries and coastal waters. *Front. Mar. Sci.* 2:127. doi: 10.3389/fmars.2015.00127
- Pourhassan, N., Gagnon, R., Wichard, T., and Bellenger, J.-P. (2014). Identification of the hydroxamate siderophore ferricrocin in *Cladosporium cladosporioides*. *Nat. Prod. Commun.* 9, 539–540.
- Reid, R. T., Live, D. H., Faulkner, D. J., and Butler, A. (1993). A siderophore from a marine bacterium with an exceptional ferric ion affinity constant. *Nature* 366, 455–458. doi: 10.1038/366455a0
- Ross, A. R. S., Ikonou, M. G., and Orians, K. J. (2000). Characterization of dissolved tannins and their metal-ion complexes by electrospray ionization mass spectrometry. *Anal. Chim. Acta* 411, 91–102. doi: 10.1016/s0003-2670(00)00746-7
- Roth, V.-N., Dittmar, T., Gaupp, R., and Gleixner, G. (2013). Latitude and pH driven trends in the molecular composition of DOM across a north south transect along the Yenisei River. *Geochim. Cosmochim. Acta* 123, 93–105. doi: 10.1016/j.gca.2013.09.002
- Rue, E. L., and Bruland, K. W. (1995). Complexation of iron(III) by natural organic-ligands in the central north pacific as determined by a new competitive ligand equilibration adsorptive cathodic stripping voltammetric method. *Mar. Chem.* 50, 117–138. doi: 10.1016/0304-4203(95)00031-1
- Sandron, S., Rojas, A., Wilson, R., Davies, N. W., Haddad, P. R., Shellie, R. A., et al. (2015). Chromatographic methods for the isolation, separation and characterisation of dissolved organic matter. *Environ. Sci.* 17, 1531–1567. doi: 10.1039/C5EM00223K
- Sandy, M., and Butler, A. (2009). Microbial iron acquisition: marine and terrestrial siderophores. *Chem. Rev.* 109, 4580–4595. doi: 10.1021/cr9002787
- Sleighter, R. L., and Hatcher, P. G. (2008). Molecular characterization of dissolved organic matter (DOM) along a river to ocean transect of the lower Chesapeake Bay by ultrahigh resolution electrospray ionization Fourier transform ion cyclotron resonance mass spectrometry. *Mar. Chem.* 110, 140–152. doi: 10.1016/j.marchem.2008.04.008
- Soe, C. Z., Telfer, T. J., Levina, A., Lay, P. A., and Codd, R. (2015). Simultaneous biosynthesis of putrebactin, avaroferrin and bisucaberin by *Shewanella putrefaciens* and characterisation of complexes with iron(III), molybdenum(VI) or chromium(V). *J. Inorg. Biochem.* doi: 10.1016/j.jinorgbio.2015.12.008. [Epub ahead of print].
- Spoerner, M., Wichard, T., Bachhuber, T., Stratmann, J., and Oertel, W. (2012). Growth and thallus morphogenesis of *Ulva mutabilis* (Chlorophyta) depends on a combination of two bacterial species excreting regulatory factors. *J. Phycol.* 48, 1433–1447. doi: 10.1111/j.1529-8817.2012.01231.x
- Springer, S. D., and Butler, A. (2016). Microbial ligand coordination: consideration of biological significance. *Coord. Chem. Rev.* 306(Pt 2), 628–635. doi: 10.1016/j.ccr.2015.03.013
- Sunda, W. G., and Huntsman, S. A. (1991). The use of chemiluminescence and ligand competition with edta to measure copper concentration and speciation in seawater. *Mar. Chem.* 36, 137–163.
- Sunda, W. G., Price, N. M., and Morel, F. M. M. (2005). “Trace metal ion buffers and their use in culture studies,” in *Algal Culturing Techniques*, ed R. A. Andersen (Amsterdam: Elsevier), 35–63.
- Suzuki, Y., Kuma, K., and Matsunaga, K. (1995). Bioavailable iron species in seawater measured by macroalga (*Laminaria japonica*) uptake. *Mar. Biol.* 123, 173–178. doi: 10.1007/bf00350337
- Thurman, E. M. (1985). *Organic Geochemistry of Natural Waters*. Dordrecht: Kluwer.
- Tsednee, M., Huang, Y.-C., Chen, Y.-R., and Yeh, K.-C. (2016). Identification of metal species by ESI-MS/MS through release of free metals from the corresponding metal-ligand complexes. *Sci. Rep.* 6:26785. doi: 10.1038/srep26785
- Van Den Berg, C. M. G. (1984). Direct determination of sub-nanomolar levels of zinc in sea-water by cathodic stripping voltammetry. *Talanta* 31, 1069–1073. doi: 10.1016/0039-9140(84)80252-0
- Velasquez, I., Nunn, B. L., Ibisanni, E., Goodlett, D. R., Hunter, K. A., and Sander, S. G. (2011). Detection of hydroxamate siderophores in coastal and Sub-Antarctic waters off the South Eastern Coast of New Zealand. *Mar. Chem.* 126, 97–107. doi: 10.1016/j.marchem.2011.04.003

- Viaroli, P., Bartoli, M., Azzoni, R., Giordani, G., Mucchino, C., Naldi, M., et al. (2005). Nutrient and iron limitation to *Ulva* blooms in a eutrophic coastal lagoon (Sacca di Goro, Italy). *Hydrobiologia* 550, 57–71. doi: 10.1007/s10750-005-4363-3
- Walsh, M. J., Goodnow, S. D., Vezeau, G. E., Richter, L. V., and Ahner, B. A. (2015). Cysteine enhances bioavailability of copper to marine phytoplankton. *Environ. Sci. Technol.* 49, 12145–12152. doi: 10.1021/acs.est.5b02112
- Waska, H., Koschinsky, A., Chancho, M. J. R., and Dittmar, T. (2015). Investigating the potential of solid-phase extraction and Fourier-transform ion cyclotron resonance mass spectrometry (FT-ICR-MS) for the isolation and identification of dissolved metal-organic complexes from natural waters. *Mar. Chem.* 173, 78–92. doi: 10.1016/j.marchem.2014.10.001
- Wichard, T. (2015). Exploring bacteria-induced growth and morphogenesis in the green macroalga order Ulvales (Chlorophyta). *Front. Plant Sci.* 6:86. doi: 10.3389/fpls.2015.00086
- Wichard, T., and Oertel, W. (2010). Gametogenesis and gamete release of *Ulva mutabilis* and *Ulva lactuca* (Chlorophyta): regulatory effects and chemical characterization of the “swarming inhibitor.” *J. Phycol.* 46, 248–259. doi: 10.1111/j.1529-8817.2010.00816.x
- Wichard, T., Bellenger, J. P., Loison, A., and Kraepiel, A. M. L. (2008). Catechol siderophores control tungsten uptake and toxicity in the nitrogen-fixing bacterium *Azotobacter vinelandii*. *Environ. Sci. Technol.* 42, 2408–2413. doi: 10.1021/es702651f
- Wichard, T., Charrier, B., Mineur, F., Bothwell, J. H., De Clerck, O., and Coates, J. C. (2015). The green seaweed *Ulva*: a model system to study morphogenesis. *Front. Plant Sci.* 6:72. doi: 10.3389/fpls.2015.00072
- Wichard, T., Mishra, B., Myneni, S. C. B., Bellenger, J. P., and Kraepiel, A. M. L. (2009). Storage and bioavailability of molybdenum in soils increased by organic matter complexation. *Nat. Geosci.* 2, 625–629. doi: 10.1038/ngeo589
- Zhang, X., Song, Y., Liu, D., Keesing, J. K., and Gong, J. (2015). Macroalgal blooms favor heterotrophic diazotrophic bacteria in nitrogen-rich and phosphorus-limited coastal surface waters in the Yellow Sea. *Estuar. Coast. Shelf Sci.* 163(Pt A), 75–81. doi: 10.1016/j.ecss.2014.12.015

Conflict of Interest Statement: The author declares that the research was conducted in the absence of any commercial or financial relationships that could be construed as a potential conflict of interest.

Copyright © 2016 Wichard. This is an open-access article distributed under the terms of the Creative Commons Attribution License (CC BY). The use, distribution or reproduction in other forums is permitted, provided the original author(s) or licensor are credited and that the original publication in this journal is cited, in accordance with accepted academic practice. No use, distribution or reproduction is permitted which does not comply with these terms.



Evaluation of Immobilized Metal-Ion Affinity Chromatography and Electrospray Ionization Tandem Mass Spectrometry for Recovery and Identification of Copper(II)-Binding Ligands in Seawater Using the Model Ligand 8-Hydroxyquinoline

Richard L. Nixon¹ and Andrew R. S. Ross^{2*}

OPEN ACCESS

Edited by:

Kristen Nicolle Buck,
University of South Florida, USA

Reviewed by:

Peter Croot,
National University of Ireland, Galway,
Ireland

Daniel James Repeta,
Woods Hole Oceanographic
Institution, USA

*Correspondence:

Andrew R. S. Ross
andrew.ross@dfo-mpo.gc.ca

Specialty section:

This article was submitted to
Marine Biogeochemistry,
a section of the journal
Frontiers in Marine Science

Received: 31 May 2016

Accepted: 11 November 2016

Published: 25 November 2016

Citation:

Nixon RL and Ross ARS (2016)
Evaluation of Immobilized Metal-Ion
Affinity Chromatography and
Electrospray Ionization Tandem Mass
Spectrometry for Recovery and
Identification of Copper(II)-Binding
Ligands in Seawater Using the Model
Ligand 8-Hydroxyquinoline.
Front. Mar. Sci. 3:246.
doi: 10.3389/fmars.2016.00246

¹ Department of Biochemistry and Microbiology, University of Victoria, Victoria, BC, Canada, ² Ocean Sciences Division, Institute of Ocean Sciences, Fisheries and Oceans Canada, Sidney, BC, Canada

Complexation by organic ligands dominates the speciation of iron (Fe), copper (Cu), and other bioactive trace metals in seawater, controlling their bioavailability and distribution in the marine environment. Several classes of high-affinity Fe-binding ligands (siderophores) have been identified in seawater but the chemical structures of marine Cu-complexing ligands remain unknown. Immobilized metal-ion affinity chromatography (IMAC) allows Cu ligands to be isolated from bulk dissolved organic matter (DOM) in seawater and separated into fractions, which can be characterized independently using electrochemical and spectroscopic techniques. Attempts have been made to combine IMAC with electrospray ionization mass spectrometry (ESI-MS) to characterize marine Cu ligands, but results have proven inconclusive due to the lack of tandem mass spectrometry (MS/MS) data to confirm ligand recovery. We used 8-hydroxyquinoline (8-HQ), a well-characterized model ligand that forms strong 1:2 metal:ligand complexes with Cu²⁺ at pH 8 (log $\beta_2 = 18.3$), to evaluate Cu(II)-IMAC and ESI-MS/MS for recovery and identification of copper(II)-complexing ligands in seawater. One-liter samples of 0.45 μm -filtered surface seawater were spiked with 8-HQ at low concentrations (up to 100 nM) and fractionated by IMAC. Fractions eluted with acidified artificial seawater were desalted and re-suspended in methanol via solid-phase extraction (SPE) to obtain extracts suitable for ESI-MS analysis. Recovery of 8-HQ by Cu(II)-IMAC was confirmed unambiguously by MS/MS and found to average 81% based upon accurate quantitation via multiple reaction monitoring (MRM). Cu(II)-IMAC fractionation of unspiked seawater using multiple UV detection wavelengths suggests an optimal fraction size of 2 mL for isolating and analyzing Cu ligands with similar properties.

Keywords: marine copper ligands, organic complexes, immobilized metal-ion affinity chromatography, electrospray ionization tandem mass spectrometry, solid-phase extraction

INTRODUCTION

Organic complexation of dissolved trace metals like iron (Fe) and copper (Cu) exerts a major influence on their mobility, toxicity, and bioavailability in the marine environment (Florence, 1982; Sunda, 1991; Donat and Bruland, 1995; Kraemer, 2004). Several classes of biogenic high-affinity Fe-binding ligands (siderophores) have been identified in seawater and are thought to facilitate iron uptake in marine bacterioplankton (Wilhelm, 1995; Hutchins et al., 1999; McCormack et al., 2003). Copper-carrying analogs (chalkophores) such as methanobactin (log $K_{CuL} \sim 20$; El Ghazouani et al., 2011) are known to be produced by certain methanotrophic bacteria (Kim et al., 2004; Bandow et al., 2012). Culturing experiments have shown that marine phytoplankton are also capable of producing strong, extracellular Cu-binding ligands (McKnight and Morel, 1979, 1980; Moffett et al., 1990; Moffett and Brand, 1996; Leal et al., 1999; Croot et al., 2000; Dupont et al., 2004; Dupont and Ahner, 2005; Wiramanaden et al., 2008). Some of these exudates are thought to act like chalkophores (Semeniuk et al., 2015), promoting biological uptake and utilization of Cu for e.g., photosynthesis, radical detoxification, and iron acquisition (Maldonado et al., 2006). Others may be released to moderate concentrations of free, bioavailable Cu^{2+} ions (Dryden et al., 2004; Leão et al., 2007) that would otherwise be toxic to marine phytoplankton (Sunda, 1991). Although numerous studies have shown that Cu in seawater exists primarily in the form of organic complexes (see Donat and Bruland, 1995) no marine copper ligands have been positively identified.

Originally developed for protein isolation by Porath et al. (1975), immobilized metal-ion affinity chromatography (IMAC) was first applied to the study of marine Cu-complexing ligands by Gordon (1992). The principal advantage of Cu(II)-IMAC is that it enables compounds with an affinity for copper to be isolated from other organic compounds that could interfere with their analysis. IMAC is also capable of resolving compounds into fractions with differing affinities for copper, allowing electrochemical or spectroscopic analysis to be applied specifically to each fraction. Gordon (1992) successfully demonstrated concentration and partial purification of Cu-complexing organic compounds from the Sargasso Sea using IMAC with UV detection, resolving these compounds into two chromatographic peaks or fractions based on their relative affinities for copper. Vertical profiles showed that the lower-affinity (earlier-eluting) peak was invariant with depth whereas the higher-affinity (later-eluting) peak reached a maximum at 60 m. Subsequent applications of Cu(II)-IMAC to natural waters (Gordon et al., 1996, 2000; Midorikawa and Tanoue, 1996, 1998; Donat et al., 1997; Wu and Tanoue, 2001a,b; Paunovic et al., 2005, 2008) employed UV absorbance, fluorescence, chemical analysis, and electrochemical methods such as differential pulse anodic stripping voltammetry (DPASV) to characterize the recovered ligands. Two classes of marine Cu-complexing ligands have been distinguished: a stronger (L_1) class (log $K' = 12$ to 14) present at relative low concentrations (below 10 nM) and found primarily in surface waters, and a weaker (L_2) class (log $K' = 9$ to 12) found at higher concentrations (above 100 nM) and more broadly distributed in the water column

(Vraspir and Butler, 2009). Donat et al. (1997) demonstrated removal of L_1 and L_2 from seawater by Cu(II)-IMAC and detection of L_1 in pooled IMAC eluents. More recently, Cu(II)-IMAC has been used in combination with electrospray ionization mass spectrometry (ESI-MS) to isolate and identify intracellular copper-binding proteins from marine algal cells (Smith et al., 2014), some of which (e.g., chaperones) are thought to bind Cu^+ *in vivo*.

Early attempts to characterize marine Cu-binding ligands using Cu(II)-IMAC and ESI-MS were successful in obtaining molecular weight information from seawater extracts (Ross et al., 2003; Vachet and Callaway, 2003), paving the way for structural analysis using tandem mass spectrometry (MS/MS) (Ross et al., 2000; Wiramanaden et al., 2008). However, results obtained using ESI-MS alone were insufficient to positively identify or optimize the recovery of marine Cu ligands. The latter is important given the typically low concentrations at which organic ligands are present in seawater, and the need for intermediate steps such as solid-phase extraction (SPE) to desalt and concentrate samples prior to MS analysis (Waska et al., 2015). We describe a method for recovery and structural characterization of Cu(II)-complexing ligands in seawater using IMAC, SPE, and ESI-MS/MS. We validate our approach by demonstrating recovery and unambiguous identification of a model organic Cu-binding ligand from seawater at low concentrations (below 100 nM). The compound chosen was 8-hydroxyquinoline (8-HQ), a well-characterized model ligand that is amenable to ESI-MS and forms strong 1:2 metal:ligand complexes with Cu^{2+} at pH 8 (log $\beta_2 = 18.3$; Perrin, 1979; Ross et al., 1998). The ability of 8-HQ to form uncharged, lipophilic complexes makes it a viable model for biological metal-ion carriers (Gårban et al., 2014) as well as for marine Cu-complexing ligands. We also present Cu(II)-IMAC data for oceanic and coastal surface waters using multiple detection wavelengths, which enable fractionation of marine Cu ligands based on UV absorbance and IMAC retention times.

MATERIALS AND METHODS

Reagents

All reagents and solvents were analytical and high-performance liquid chromatography (HPLC) grade, respectively, unless otherwise noted. Hydrochloric acid (12N) was obtained from Anachemia (Vancouver, BC), acetonitrile and methanol from VWR (Mississauga, ON), and ethylenediamine tetraacetic acid (EDTA) and ammonium acetate from Fisher (Pittsburgh, PA). Copper (II) sulfate (99.995% trace metal free), 8-hydroxyquinoline, glutathione, histidine, and tryptophan were obtained from Sigma-Aldrich (St. Louis, MO). Ultrapure deionized water (16–18 M Ω -cm) was prepared using an EMD Super-Q system from Millipore (Billerica, MA). Artificial seawater (ASW) was prepared by dissolving 32 g of Instant Ocean (Blacksburg, VA) in 1 L of ultrapure water, and acidified (aASW) by adding HCl to a concentration of 10 mM (pH 2.1).

Collection of Seawater Samples

Natural seawater was collected from inshore coastal and open ocean surface waters of the northeast Pacific. Oceanic surface

seawater (OSW) was collected at a depth of 5 m near station P22 (49° 41.92' N, 140° 39.98' W) during the June 2015 Line-P cruise aboard the CCGS John P. Tully and transferred directly to a 50-gallon plastic drum using a high-volume Teflon[®] pump (model PFD1 210, Saint-Gobain ASTI, Nanterre, France). Coastal surface seawater (CSW) was collected in plastic tubs lowered by hand from the dock at the Institute of Ocean Sciences (IOS), Sidney, British Columbia during the spring and summer of 2015. Samples from both sources were stored unfiltered in the dark at room temperature, and were pumped through a 0.45- μ m filter (GWV high-capacity groundwater sampling capsule, Pall Corporation, Port Washington, NY) prior to any treatment or analysis.

Immobilized Copper(II)-Ion Affinity Chromatography

Cu(II)-IMAC involves passing filtered aqueous samples through a chelating column charged with Cu²⁺ ions, which are immobilized by tethered functional groups such as iminodiacetate (IDA) or nitrilotriacetate (NTA). Compounds with an affinity for divalent copper are selectively retained on the column, then eluted and recovered using an acidic or competing ligand solution. We performed Cu(II)-IMAC fractionations using two systems. The first was a manually operated dual-column system built in-house during previous studies (Ross et al., 2003) utilizing a single wavelength UV detector (LKB Bromma Uvicord S, Pharmacia Biotech, Uppsala, Sweden), henceforth referred to as the LKB system. The second system was an automated single-column commercial unit developed primarily for protein purification (AKTA PrimePlus, GE Healthcare, Mississauga, ON), which we refer to as the AKTA system. This system was supplied with multiple UV filters and software (PrimeView v5.31) for chromatographic analysis. Both systems were fitted with 5-mL Hi-Trap Chelating Sepharose HP columns (part no. 17-0409-03, GE Healthcare).

The same experimental protocol was applied to each system, all reagents and samples being delivered at a flow rate of 0.9 mL/min (LKB) or 1.0 mL/min (AKTA). Seawater samples and the solutions used to condition, charge, elute and regenerate the IMAC columns were prepared in 1-L acid-washed high-density polyethylene (Nalgene[®]) bottles. After rinsing with 30 mL of deionized water the Hi-Trap columns were charged with 50 μ moles of Cu²⁺ ions by passing 5 mL of a 10 mM copper(II) sulfate solution through each column. The columns were rinsed with 5 mL of ultrapure water and equilibrated with 20–30 mL of acidified artificial seawater (aASW). One-liter samples of natural or artificial seawater, with or without added model ligands, were then passed through each column. When the sample containers were nearly empty, desorption of retained compounds was achieved by eluting the columns with aASW for 20–30 min, during which the UV absorbance of the eluent was monitored at 254 nm (both systems), 214 or 280 nm (AKTA only). Eluent fractions corresponding to major chromatographic peaks were collected in glass scintillation vials (Wheaton, Millville, NJ) and stored at 5°C. The absorbance spectra of selected IMAC fractions were obtained using a UV-Vis spectrophotometer (model 8453, HP Agilent, Mississauga, ON) to confirm the extraction of model

ligands. Following elution the IMAC columns were regenerated by passing 50 mM EDTA in ultrapure water through each column for 15 min to remove the Cu²⁺ ions before repeating the procedure, at all times taking care to avoid entraining air into the system.

Solid-Phase Extraction

We used SPE for off-line desalting of IMAC fractions as this method has the potential to recover unknown organic compounds of varying chemical composition. SPE was performed using a RapidTrace Workstation (Caliper Life Science, Hopkinton, MA) and Oasis 3 cc HLB (hydrophilic-lipophilic) cartridges (Waters Limited, Mississauga, ON). The cartridges contained a polymeric reversed-phase sorbent designed to extract a wide range of acidic, basic, and neutral compounds. HLB cartridges were conditioned with one volume (3 mL) of methanol and rinsed with 3 mL ultrapure water and 3 mL aASW (the IMAC eluent) before loading 2–4 mL of IMAC fraction. Loaded cartridges were rinsed with 3 mL aASW and 3 mL of 5% (v/v) methanol in ultrapure water before eluting with 2 mL methanol, which provided the highest concentration of recovered ligand. The cartridges were then regenerated with 3 mL of methanol and 5 mL ultrapure water, followed by a blank extraction using unspiked aASW to minimize carryover between IMAC fractions (see Section Characterization of Natural Ligands below). Extracts were collected in polypropylene culture tubes (VWR) and stored at 5°C prior to ESI-MS analysis. Selected extracts were also analyzed by ESI-MS to confirm and measure the recovery of model ligands using standards prepared in methanol.

Mass Spectrometry

Model ligand standard solutions and SPE extracts were analyzed by flow-injection (FI) ESI-MS using a tandem quadrupole mass spectrometer (model API 5000, AB Sciex) fitted with an electrospray ion source (Turbo Ionspray; AB Sciex) connected to a high-performance liquid chromatography (HPLC) pump and autosampler (model P680 and ASI-100, Dionex). ESI-MS parameters were optimized using the Taguchi method (Taguchi and Yokoyama, 1994) while infusing a 0.68 μ M solution of 8-HQ in the FI carrier solvent at 100 μ L/min using a syringe pump (Harvard Instruments). The carrier solvent consisted of 1 mM ammonium acetate in 70% (v/v) aqueous acetonitrile (pH 7.6; Ross et al., 2003). Optimal ESI-MS conditions were: DP 120, EP 10, CAD 5, CUR 30, GS1 60, GS2 30, and IS 5500. Fragmentation of the 8-HQ molecular or precursor ion of mass-to-charge ratio (m/z) 146.2 to produce diagnostic fragment or product ions via collision induced dissociation (CID) tandem mass spectrometry (MS/MS) was optimized using the same solution. Two precursor-to-product ion transitions corresponding to loss of water (m/z 146.2 > 128.2) and formation of the tropylium ion (m/z 146.2 > 91.2) from 8-HQ were selected for quantification and confirmation, respectively, via multiple reaction monitoring (MRM) using the instrument software (Analyst v1.6.2). MRM provides specific, sensitive, and accurate quantification of target compounds during FI (or on-line HPLC) analysis. Optimal MRM conditions were CE 40, CXP 19 (146.2 > 91.2), and CE 35,

CXP 24 (146.2 > 128.2). Standard solutions containing 0.5–50 μM 8-HQ were prepared by serial dilution of a stock solution containing 100 μM 8-HQ in methanol (the SPE eluent). The system was calibrated for FI-ESI-MS/MS analysis of SPE extracts using the HPLC pump and autosampler to deliver 10 μL of each 8-HQ standard to the ESI source at flow rate of 100 $\mu\text{L}/\text{min}$ using the FI carrier solvent. Refrigerated SPE extracts were allowed to equilibrate at room temperature, filtered through a 0.22- μm syringe filter (part no. 179718, Canadian Life Science, Peterborough ON), transferred to 2-mL glass vials (Sigma), loaded into the autosampler, and analyzed by MRM under the same conditions as the calibration standards.

Treatment of Seawater Samples

The properties of natural copper-binding compounds were investigated using data from replicate Cu(II)-IMAC experiments. Retention times and peak areas for coastal and oceanic surface seawater samples were compared using different UV detection wavelengths (214, 254, and 280 nm) before and after different treatments. The photochemical and thermal stabilities of natural ligands were examined by placing oceanic seawater samples in water-cooled 1-L PTFE containers within an artificial sun chamber ($\sim 700 \text{ W}/\text{m}^2$; Suntest CPS, Atlas, Mount Prospect, IL) designed to reproduce the spectrum of natural sunlight, with minimal transmission below 280 nm, or immersing and heating them in a water bath ($\sim 60^\circ\text{C}$; Isotemp 3016D, Fisher Scientific) for up to 24 h prior to IMAC. The effects of ionic strength and prior complexation on the recovery of natural ligands were also examined by decreasing salinity with ultrapure deionized water, increasing it to approximately 38‰ with artificial sea salt (Instant Ocean), or spiking the seawater sample with copper(II) sulfate to a concentration of 100 nM and allowing it to equilibrate for several hours before IMAC fractionation.

RESULTS

Immobilized Copper(II)-Ion Affinity Chromatography

UV spectrophotometric analysis of 8-HQ standards and OSW samples spiked with 8-HQ showed that the model ligand absorbs strongly at 254 nm, as noted previously (Zhang et al., 1996), and that the absorbance at this wavelength is proportional to ligand concentration. Using this wavelength to monitor the elution of Cu(II)-IMAC extracts from OSW samples spiked with up to 100 nM 8-HQ produced chromatograms with two significant peaks (Figure 1). The earlier-eluting peak remained essentially unchanged whereas the later-eluting peak increased in area with increasing 8-HQ concentration ($r^2 = 0.9927$). Chromatograms obtained during Cu(II)-IMAC of ASW spiked with 8-HQ contained only the later-eluting peak, while UV absorbance spectra of collected fractions corresponding to this peak matched those of standards contained 8-HQ in aASW (the IMAC eluent).

Our decision to elute the IMAC column with acidified seawater (Midorikawa and Tanoue, 1996) was based on the need to avoid introducing large concentrations of a competing ligand such as glycine, which would interfere with subsequent ESI-MS

analysis, while ensuring that our results could be used to validate those of earlier experiments performed using the same eluent (Ross et al., 2003). Previous studies (Lohan et al., 2005; Milne et al., 2010) suggest that eluting Cu(II)-IMAC columns with acidic solution may displace copper from the column, making it available to form complexes with ligands recovered in the eluent. Because this may affect the quantification of 8-HQ in IMAC fractions using UV absorbance spectrophotometry we relied upon specific, accurate quantification by MRM (see Section Electrospray-Ionization Mass Spectrometry below) to estimate the recovery of model ligands during IMAC.

Solid-Phase Extraction

Since marine Cu ligands have not yet been identified we chose to evaluate a type of SPE cartridge (Waters Oasis HLB) designed to recover as broad a range of organic compounds as possible. SPE conditions were optimized using FI-ESI-MS/MS with MRM to quantify 8-HQ in methanol extracts collected following SPE of 10 μM 8-HQ standards prepared in 2 mL of aASW (the IMAC eluent). The dependence of SPE recovery on elution volume was investigated by using different amounts of methanol (0.5–3.0 mL) to elute the HLB cartridge, and MRM to quantify the amount of 8-HQ in the resulting extracts. Recoveries ranged from less than 10% using 0.5 mL to 90% using 3 mL of methanol. However, the highest concentration of 8-HQ in the SPE extract was obtained using the recommended elution volume of 2 mL (Waters Corporation, 2014), which gave an average recovery ($n = 4$) of $74.4 \pm 2.3 \%$. Rinsing the eluted HLB cartridge with methanol did not appear to retrieve any residual 8-HQ. During preliminary experiments, however, recoveries obtained after extracting several samples using the same cartridge were found to be greater than those obtained using a new cartridge. Carryover was henceforth minimized by performing blank extractions with 2 mL of unspiked aASW between samples. Cu(II)-IMAC fractions were desalted and concentrated for FI-ESI-MS/MS analysis using the optimized SPE protocol, applying a value of 74.4% to correct for recovery during SPE (Table 1).

Electrospray-Ionization Mass Spectrometry

ESI-MS analysis of 8-HQ in methanol detected the protonated molecular ion at m/z 146.2. This was fragmented inside the collision cell of the mass spectrometer to generate a characteristic product-ion MS/MS spectrum for the model ligand (Figure 2). Two discrete and relatively abundant fragments (m/z 128.2 and 91.2) were selected for MRM. The instrument was first calibrated using standards containing 0.5–50 μM 8-HQ in methanol (the SPE eluent). These were analyzed in quadruplicate and the results averaged to generate a linear plot ($r^2 = 0.9794$) of MRM peak area vs. 8-HQ concentration. The lower limit of quantification (LLOQ) was determined by performing replicate analyses ($n = 4$) of the solvent blank, calculating the standard deviation of these measurements, multiplying by 10, and adding this value to the average blank response. The result was substituted into the linear calibration equation to determine a LLOQ of 0.54 μM .

The calibrated FI-ESI-MS/MS system was used to analyze Cu(II)-IMAC fractions obtained from 1-L seawater samples

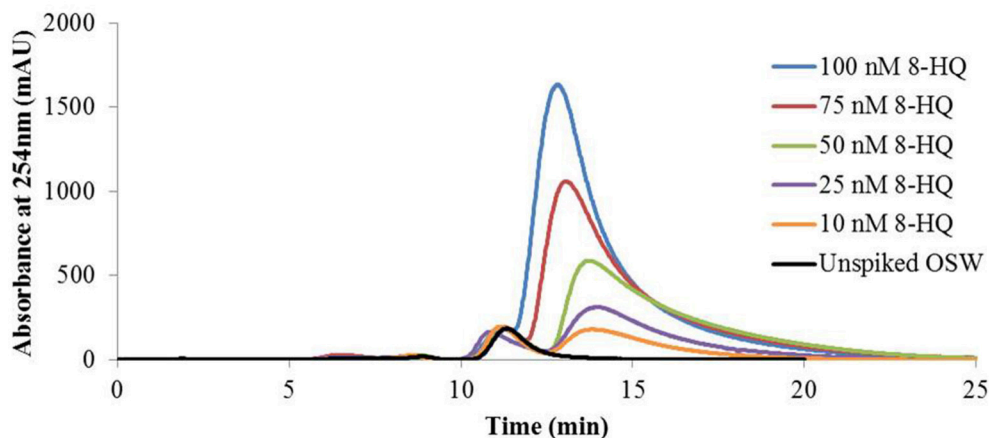


FIGURE 1 | Immobilized copper(II)-ion affinity chromatography (Cu(II)-IMAC) of oceanic surface seawater (OSW) spiked with the model ligand 8-hydroxyquinoline (8-HQ). One-liter OSW samples containing up to 100 nmoles of added 8-HQ were fractionated by Cu(II)-IMAC while monitoring UV absorbance of the eluent at 254 nm using the LKB system (see text). All samples gave rise to a peak at 11 min, attributed to natural copper ligands present in OSW, whereas samples spiked with 8-HQ gave rise to a second elution peak at 12–14 min with area proportional to the amount of ligand added to the OSW sample ($r^2 = 0.9927$).

TABLE 1 | Recovery of the model ligand 8-hydroxyquinoline (8-HQ) from seawater by immobilized copper(II)-ion affinity chromatography (IMAC) and solid-phase extraction (SPE).

8-HQ added to SW sample (nmoles)	8-HQ measured in SPE extract (nmoles)	8-HQ corrected for SPE recovery (nmoles)	% of IMAC fraction used for SPE	8-HQ in IMAC fraction (nmoles)	% added 8-HQ in IMAC fraction	% total IMAC peak in IMAC fraction	% added 8-HQ recovered in IMAC Peak
25	8.0	10.8	46	23.5	94.0	95	98.0
25	8.0	10.8	53	20.4	81.8	97	84.3
50	12.5	16.8	46	36.5	73.0	99	73.8
100	56.2	75.5	100	75.5	75.5	90	83.9
				Mean	81.1		85.2

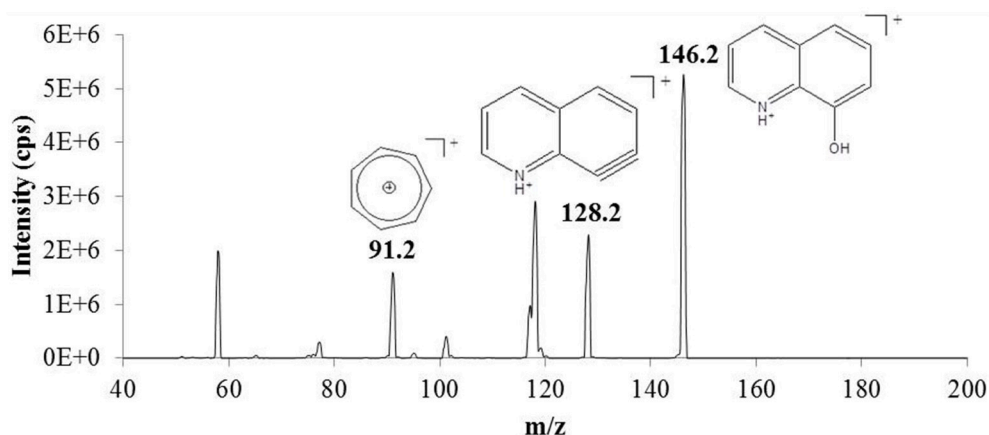


FIGURE 2 | Product-ion mass spectrum of the protonated molecular/precursor ion (m/z 146.2) of 8-hydroxyquinoline (8-HQ) obtained by electrospray ionization-tandem mass spectrometry (ESI-MS/MS). Precursor-to-product ion transitions corresponding to loss of water (m/z 146.2 > 128.2) and formation of the stable tropylium ion (m/z 146.2 > 91.2) were selected for multiple reaction monitoring (MRM) to provide accurate quantification and unambiguous identification of 8-HQ in methanol extracts obtained by solid phase extraction (SPE) (see text).

spiked with up to 100 nmoles 8-HQ (Figure 3). Broadening of the IMAC peak at higher concentrations (Figure 1) meant that the volume of the collected fraction varied from 1 to 10 mL, with a maximum of 4 mL being used for SPE. Variable volumes were accounted for by applying the appropriate corrections during calculation of the 8-HQ concentration in each IMAC fraction. For example, if a 1-L seawater sample spiked with 100 nmoles 8-HQ gave rise to a collected peak fraction of 8 mL, and 4 mL of that fraction were subjected to SPE, the measurement of 25 nmoles 8-HQ in the resulting SPE extract by MRM would indicate that 25% of the spiked ligand had been recovered in the SPE extract and 67% in the original IMAC fraction, following correction for 74.4% recovery during SPE (see Solid-Phase Extraction above). IMAC fractions collected from OSW spiked with 25–100 nmoles 8-HQ were subsequently found to contain an average of $81 \pm 8\%$ of the initial spike (Table 1). By applying a further correction based on the total area of the observed IMAC peak and the area corresponding to the fraction actually collected, it was possible to estimate a total recovery of $85 \pm 9\%$ for the initial Cu(II)-IMAC step (Table 1).

Characterization of Natural Ligands

Cu(II)-IMAC was used to investigate the properties of natural copper ligands from coastal (CSW) and OSW by fractionating unspiked seawater samples and monitoring the IMAC eluent at different wavelengths (214, 254, or 280 nm) using the AKTA system. A representative IMAC chromatogram for CSW (Figure 4A) shows that the natural ligands absorbing most strongly at each wavelength had different retention times, and that peak area was greater for ligands absorbing primarily at 214 nm than for those absorbing at 254 or 280 nm (although differences in molar absorptivity for individual chromophores preclude any inference as to relative ligand concentrations). Similar results were obtained for OSW samples; however, peak area was greater for CSW than for OSW samples (Figure 4B).

Retention times for extracted ligands that absorbed most strongly at a particular wavelength were consistent between samples, but those absorbing primarily at 280 nm had longer retention times (Figure 4C). To investigate the thermal and photochemical stabilities of natural ligands, OSW samples were exposed to heat or artificial sunlight prior to Cu(II)-IMAC. Irradiation of the samples for 24 h decreased the area of the predominant IMAC peak by 40% whereas incubation at 60°C for 24 h without irradiation reduced peak area by 15%. In contrast, changing the salinity of seawater samples or spiking them with Cu²⁺ ions to a concentration of 100 nM had no significant effect on peak area.

DISCUSSION

Cu(II)-IMAC fractionation of surface seawater samples spiked with 8-HQ gave rise to a UV chromatographic peak with a retention time greater than that observed for natural Cu ligands (Figure 1). The area of this peak was proportional to the mass of 8-HQ originally added to the seawater sample. Analysis of collected IMAC fractions by SPE and FI-ESI-MS/MS confirmed that IMAC fractions corresponding to the model ligand peak contained 8-HQ at a concentration proportional to that in the original sample, with an average recovery of 81%. To our knowledge this is the first time that a model Cu-binding ligand has been recovered, positively identified, and accurately quantified in seawater by MS/MS. Our results validate the previous assignment of measured molecular weights to marine Cu-complexing ligands using an earlier version of the same method (Ross et al., 2003). The product-ion spectrum for 8-HQ (Figure 2) also serves to illustrate the kind of structural information that MS/MS can provide for ligands isolated using this method. The order in which model and natural ligands elute from the Cu(II)-IMAC column is consistent with a higher stability constant for the Cu(II) complex of 8-HQ (see Section Introduction). Indeed, the greater binding strength of 8-HQ

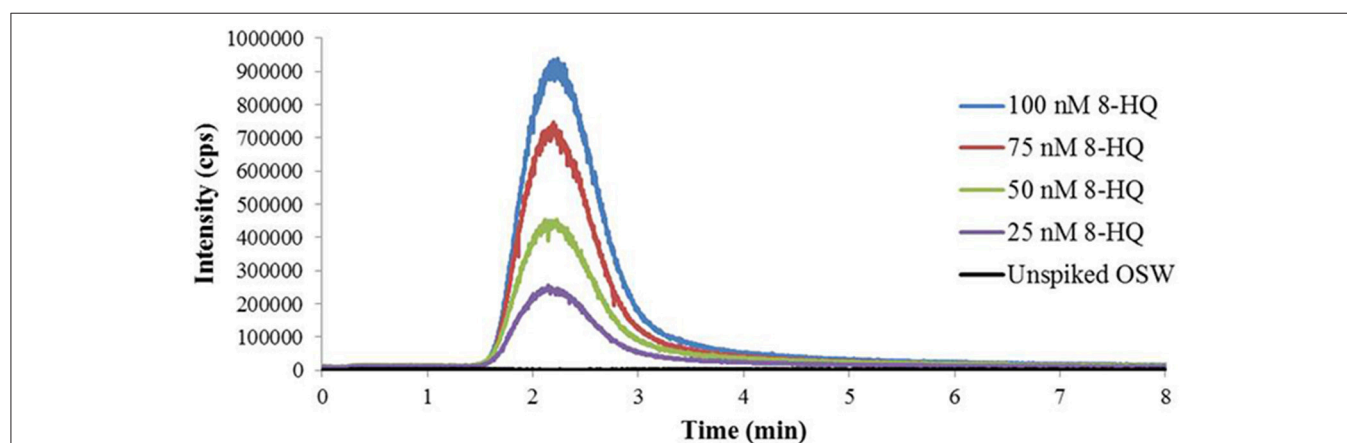


FIGURE 3 | Multiple reaction monitoring (MRM) chromatograms for the m/z 146.2 > 91.2 transition used to quantify the model ligand 8-hydroxyquinoline (8-HQ) in Cu(II)-IMAC fractions desalted by solid-phase extraction (SPE). The fractions correspond to the model ligand peaks observed in the Cu(II)-IMAC chromatogram obtained by fractionating 1-L surface seawater samples spiked with 0–100 nmoles 8-HQ. Ten microliter of each SPE extract were analyzed by flow-injection electrospray ionization tandem mass spectrometry (FI-ESI-MS/MS) using 1 mM ammonium acetate in 70% acetonitrile at 100 μ L/min as the carrier solvent.

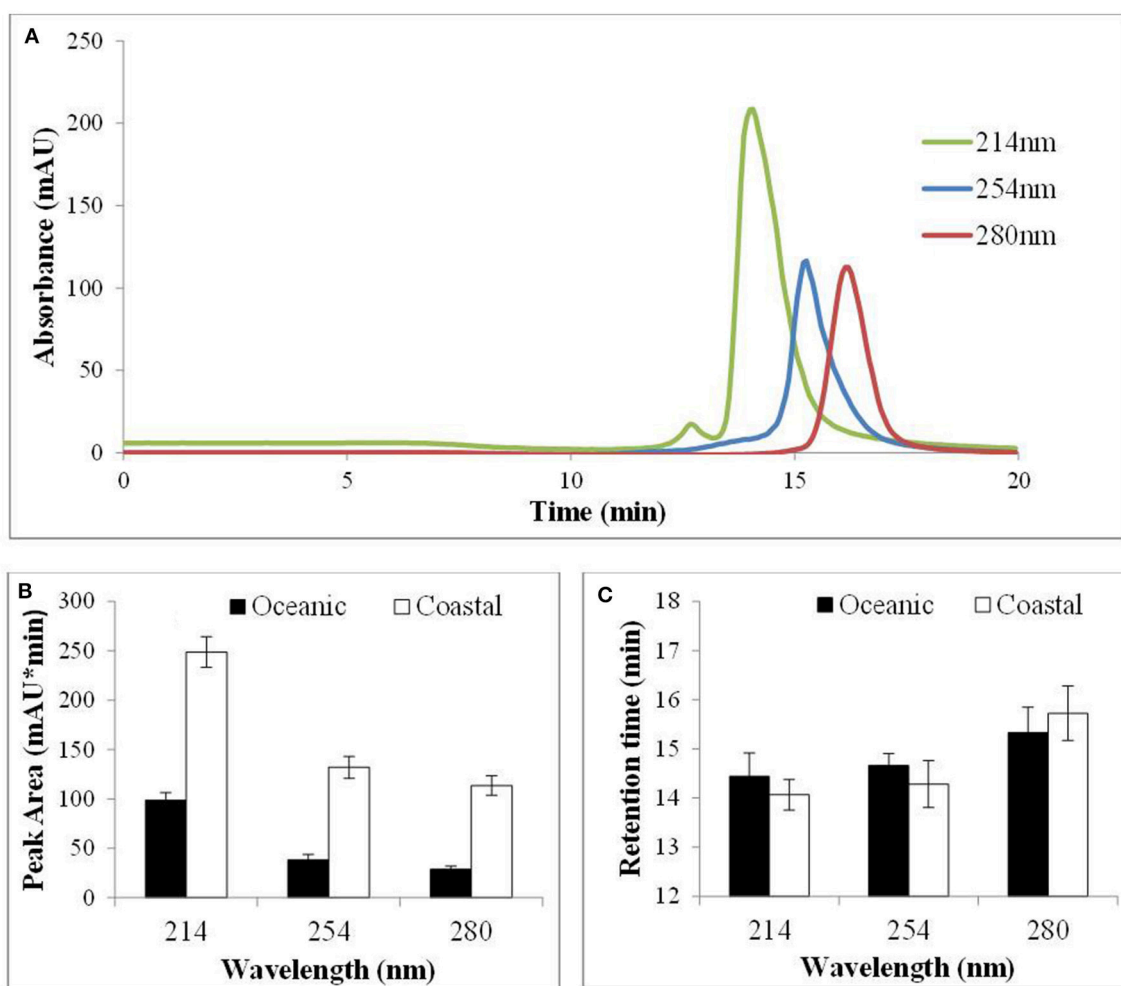


FIGURE 4 | Immobilized copper(II)-ion affinity chromatography of coastal (CSW) and oceanic surface seawater (OSW) samples using the AKTA system (see text) to monitor the elution of replicate samples at 214, 254, and 280 nm. (A) Extracted compounds that absorb most strongly at each wavelength were found to elute at different times. **(B)** Peak areas were reproducible ($n = 10$; error bars represent 1 SD) and were consistently greater for coastal than for oceanic surface seawater. **(C)** Retention times were significantly greater for compounds that absorbed most strongly at 280 nm but were no different for CSW than for OSW samples.

forms the basis for its use in determining total Cu concentrations in seawater by cathodic stripping voltammetry (CSV) and other techniques (Watanabe et al., 1981; Van Den Berg, 1986; Coale et al., 1992). Results obtained using 8-HQ suggest that natural Cu ligands of similar binding strength ($\log K' \sim 18$) may be recovered from seawater using Cu(II)-IMAC, assuming that they are able to form stable ternary complexes with IDA-Cu^{2+} (Paunovic et al., 2005)

The LLOQ of $0.54 \mu\text{M}$ achieved using MRM is equivalent to 1.08 nmoles of 8-HQ in a 2-mL SPE extract. Assuming that 100% of the collected IMAC fraction is used for SPE this corresponds to an original concentration of about 1.8 nM in a 1-L seawater sample, based upon 74.4 % recovery during SPE and 81.1 % during IMAC. Although this is on the order of concentrations measured voltammetrically for the stronger L_1 class of marine Cu ligands, detection and analysis of a specific ligand by ESI-MS/MS will depend on its individual concentration in seawater. Should

greater sensitivity be required the concentration of methanol extracts obtained by SPE can be increased by partial evaporation of the solvent prior to analysis. Pooling Cu(II)-IMAC fractions from replicate seawater samples could also be used to increase the quantity of isolated ligands.

Adding 100 nM copper(II) sulfate to spiked and unspiked OSW did not affect the area of the model or natural ligand peaks observed during IMAC, suggesting that prior complexation with Cu in seawater has no significant effect on ligand recovery (see also Paunovic et al., 2005). Similarly, reducing the sample flow to 0.5 mL/min produced only a slight increase in the areas of model and natural ligand peaks. This suggests that the rates of exchange within the IMAC column are sufficient to achieve good recovery of Cu ligands at 1.0 mL/min despite the relatively short contact time with the sample (~ 5 min), as indicated by results for 8-HQ (Table 1). Repeated fractionation of seawater samples has been shown to provide incremental increases in the recovery

of natural ligands (Donat et al., 1997). However, we found that running seawater samples through the column a second time produced a peak no more than 0.15 times as large as that obtained during the initial extraction, which nevertheless accounts for the incomplete recovery of 8-HQ observed during IMAC (Table 1).

Having evaluated Cu(II)-IMAC for recovery of Cu ligands we proceeded to investigate the fractionation of natural Cu ligands in unspiked CSW and OSW, using the AKTA system to monitor different UV wavelengths. The peak area at a given wavelength and retention time was always greater for coastal than for oceanic samples (Figure 4B). Results obtained previously for northeast Pacific coastal waters, using the more sensitive LKB system (Ross et al., 2003), showed that the IMAC peak corresponding to stronger Cu ligands reduced in size with increasing depth and distance from the mouth of the Fraser River. This is consistent with the production of strong biogenic Cu ligands in surface waters and with riverine input of organic ligands from terrestrial sources, both of which suggest that ligand concentrations are likely to be higher in CSW than in OSW samples. Chromatograms observed for CSW and OSW were consistent for a given wavelength and location, each chromatogram containing a single predominant peak. If this peak represented a single compound, or class of compounds, we would expect peak area to change according to the UV absorbance characteristics of the ligand(s) but the retention time to remain unaltered. This is exactly what we observed for the model ligand 8-HQ in spiked seawater (data not shown). For unspiked surface seawater, however, the retention time for the most abundant ligand peak changed with the detection wavelength (Figures 4A,C).

Gordon et al. (1996) found that the main difference between the two major peaks observed during Cu(II)-IMAC of estuarine samples was that the later-eluting peak absorbed strongly at 280 nm, which they attributed to the presence of proteins or peptides containing aromatic amino acids. They also found that the size of the earlier-eluting peak was reduced by prior treatment with the hydrophobic resin XAD-16. This was attributed to the presence of humic substances, which are known to absorb strongly at 254 nm (Rodrigues et al., 2009). The relative retention times of the peaks detected at 254 and 280 nm in our CSW and OSW samples appear to be consistent with these findings. However, we also observed an earlier-eluting peak using a detection wavelength of 214 nm (Figure 4A), which is characteristic of the peptide bonds found in all proteins. Furthermore, of the two retained fractions observed by Paunovic et al. (2005) in terrestrial organic matter, the earliest-eluting fraction was attributed to peptides and proteins and the later-eluting fraction to aromatic substances, based on comparisons with model ligands. Recovery and analysis of these fractions using a specific detection method like ESI-MS/MS would help to resolve any uncertainties as to the nature of the ligands present. Our results for OSW and CSW suggest that using multiple detection wavelengths can assist in identifying such fractions, and that 2 mL is an appropriate fraction size for capturing ligands with similar UV absorption and Cu-binding characteristics (Figures 4A,C).

Paunovic et al. (2005) suggest that IMAC is an effective tool for fractionating Cu ligands capable of forming ternary complexes with Cu^{2+} and IDA. Although our results for the bi-dentate ligand 8-HQ support this conclusion, we also performed Cu(II)-IMAC on OSW before and after spiking with the hexa-dentate model ligand EDTA, which absorbs at 214 nm in the IMAC eluant. The resulting (214 nm) UV chromatograms were identical, suggested that EDTA was unable to form stable ternary complex with IDA-Cu^{2+} . Previous studies have shown that both stronger (L_1) and weaker (L_2) natural ligands are recovered from seawater by IDA-Cu^{2+} (Donat et al., 1997). However, results for EDTA suggest that recovery of natural multi-dentate ligands including, potentially, chalkophores like methanobactin (Kim et al., 2004) may be limited by steric factors. Nevertheless, model natural ligands tryptophan, histidine, and glutathione were recovered from seawater by Cu(II)-IMAC during preliminary experiments, as indicated by the appearance of additional chromatographic peaks which increased in area with increasing ligand concentration (not shown). The recovery and analysis of natural ligands by SPE and FI-ESI-MS/MS is currently being investigated, along with the use of phytoplankton cultures to produce Cu ligands for further method development and analysis.

CONCLUSION

A method for isolating, identifying, and quantifying Cu(II)-complexing ligands in seawater has been developed. The method, which employs Cu(II)-IMAC fractionation, SPE recovery, and FI-ESI-MS/MS analysis, was evaluated using the strong model ligands 8-HQ and EDTA. An average recovery of 81% was obtained for the bi-dentate ligand 8-HQ, which was positively identified and quantified in seawater by MRM. The hexa-dentate ligand EDTA was not recovered by Cu(II)-IMAC, suggesting that natural multi-dentate ligands may be under-represented by this method. Cu(II)-IMAC of surface seawater samples using multiple detection wavelengths showed that natural Cu ligands can be resolved into fractions suitable for SPE based on UV absorption and retention time. Identification of these natural ligands by FI-ESI-MS/MS is currently being investigated.

AUTHOR CONTRIBUTIONS

The Corresponding Author secured funding for the work and is primarily responsible for its design and conception. The First Author is responsible for acquiring and analyzing the data. Both authors interpreted the data, revised the work for intellectual content, approved the final version, and agree to be accountable for all aspects of the work, including its accuracy and integrity.

FUNDING

Student funding was provided by the NSERC Climate Change and Adaptation Research (CCAR) program in the form of a grant for the Canadian Arctic GEOTRACES program (Application No.

433848-2012) and by the University of Victoria Department of Biochemistry and Microbiology. Additional operational funding was provided by Fisheries and Oceans Canada.

ACKNOWLEDGMENTS

The key contributions to this research of two University of Victoria undergraduate co-op students, Crystal Sommer and

Jose Mendez Campos, are gratefully acknowledged. The authors also wish to thank Alex Hodge for the design and construction of a computer interface for the LKB system, Kyle Simpson for his technical expertise and advice, and Prof. Jay Cullen at the University of Victoria for his invaluable assistance with equilibrium modeling. Finally the authors wish to thank the two reviewers, whose detailed and insightful comments resulted in major improvements to the original manuscript.

REFERENCES

- Bandow, N., Gilles, V. S., Freesmeier, B., Semrau, J. D., Krentz, B., Gallagher, W., et al. (2012). Spectral and copper binding properties of methanobactin from the facultative methanotroph *Methylocystis* strain SB2. *J. Inorg. Biochem.* 110, 72–82. doi: 10.1016/j.jinorgbio.2012.02.002
- Coale, K. H., Johnson, K. S., Stout, P. M., and Sakamoto, C. M. (1992). Determination of copper in sea water using a flow-injection method with chemiluminescence detection. *Anal. Chim. Acta* 266, 345–351. doi: 10.1016/0003-2670(92)85062-B
- Croot, P. L., Moffett, J. W., and Brand, L. E. (2000). Production of extracellular Cu complexing ligands by eucaryotic phytoplankton in response to Cu stress. *Limnol. Oceanogr.* 45, 619–627. doi: 10.4319/lo.2000.45.3.0619
- Donat, J. R., and Bruland, K. W. (1995). *Trace Elements in the Oceans, in Trace Elements in Natural Waters*, 247–280. Boca Raton, FL: CRC Press.
- Donat, J. R., Kango, R. A., and Gordon, A. S. (1997). Evaluation of immobilized metal affinity chromatography for isolation and recovery of strong copper-complexing ligands from marine waters. *Mar. Chem.* 5, 1–10. doi: 10.1016/S0304-4203(97)00008-X
- Dryden, C. L., Gordon, A. S., and Donat, J. R. (2004). Interactive regulation of dissolved copper toxicity by an estuarine microbial community. *Limnol. Oceanogr.* 49, 1115–1122. doi: 10.4319/lo.2004.49.4.1115
- Dupont, C. L., and Ahner, B. A. (2005). Effects of copper, cadmium, and zinc on the production and exudation of thiols by *Emiliania huxleyi*. *Limnol. Oceanogr.* 50, 508–515. doi: 10.4319/lo.2005.50.2.0508
- Dupont, C. L., Nelson, R. K., Bashir, S., Moffett, J. W., and Ahner, B. A. (2004). Novel copper-binding and nitrogen-rich thiols produced and exuded by *Emiliania huxleyi*. *Limnol. Oceanogr.* 49, 1754–1762. doi: 10.4319/lo.2004.49.5.1754
- El Ghazouani, A. I., Basle, A., Firbank, S. J., Knapp, C. W., Gray, J., Graham, D. W., et al. (2011). Copper-binding properties and structures of methanobactins from *Methylophilum trichosporium* OB3b. *Inorg. Chem.* 50, 1378–1391. doi: 10.1021/ic101965j
- Florence, T. M. (1982). The speciation of trace elements in water. *Talanta* 29, 345–364. doi: 10.1016/0039-9140(82)80169-0
- Gârban, Z., Silaghi-Dumitrescu, R., Gârban, G., Avacovici, A., Hadaruga, N., Balta, C., et al. (2014). Metallomics related to gallium compounds: biochemical and xenobiochemical aspects. *Macedonian J. Chem. Chem. Eng.* 1, 39–52. doi: 10.20450/mjcc.2014.131
- Gordon, A. S. (1992). Isolation of compounds with affinity for copper from seawater using immobilized copper ion affinity chromatography. *Mar. Chem.* 38, 1–12. doi: 10.1016/0304-4203(92)90063-G
- Gordon, A. S., Donat, J. R., Kango, R. A., Dyer, B. J., and Stuart, L. M. (2000). Dissolved copper-complexing ligands in cultures of marine bacteria and estuarine water. *Mar. Chem.* 70, 149–160. doi: 10.1016/S0304-4203(00)00019-0
- Gordon, A. S., Dyer, B. J., Kango, R. A., and Donat, J. R. (1996). Copper ligands isolated from estuarine water by immobilized metal affinity chromatography: temporal variability and partial characterization. *Mar. Chem.* 53, 163–172. doi: 10.1016/0304-4203(96)00022-9
- Hutchins, D. A., Witter, A. E., Butler, A., and Luther, G. W. III. (1999). Competition among marine phytoplankton for different chelated iron species. *Nature* 400, 858–861. doi: 10.1038/23680
- Kim, H. J., Graham, D. W., DiSpirito, A. A., Alterman, M. A., Galeva, N., Larive, C. K., et al. (2004). Methanobactin, a copper-acquisition compound from methane-oxidizing bacteria. *Science* 305, 1612–1615. doi: 10.1126/science.1098322
- Kraemer, S. M. (2004). Iron oxide dissolution and solubility in the presence of siderophores. *Aquat. Sci.* 66, 3–18. doi: 10.1007/s00027-003-0690-5
- Leal, M. F. C., Vasconcelos, M. T. S. D., and van den Berg, C. M. G. (1999). Copper-induced release of complexing ligands similar to thiols by *Emiliania huxleyi* in seawater cultures. *Limnol. Oceanogr.* 44, 1750–1762. doi: 10.4319/lo.1999.44.7.1750
- Leão, P. N., Vasconcelos, M. T., and Vasconcelos, V. M. (2007). Role of marine cyanobacteria in trace metal bioavailability in seawater. *Microb. Ecol.* 53, 104–109. doi: 10.1007/s00248-006-9153-6
- Lohan, M. C., Aguilar-Islas, A. M., Franks, R. P., and Bruland, K. W. (2005). Determination of iron and copper in seawater at pH 1.7 with a new commercially available chelating resin, NTA Superflow. *Anal. Chim. Acta* 530, 121–129. doi: 10.1016/j.aca.2004.09.005
- Maldonado, M. T., Allen, A. E., Chong, J. S., Lin, K., Leus, D., Karpenko, N., et al. (2006). Copper-dependent iron transport in coastal and oceanic diatoms. *Limnol. Oceanogr.* 51, 1729–1743. doi: 10.4319/lo.2006.51.4.1729
- McCormack, P., Worsfold, P. J., and Gledhill, M. (2003). Separation and detection of siderophores produced by marine bacterioplankton using high-performance liquid chromatography with electrospray ionization mass spectrometry. *Anal. Chim. Acta* 75, 2647–2652. doi: 10.1021/ac0340105
- McKnight, D. M., and Morel, F. M. M. (1979). Release of weak and strong copper-complexing agents by algae. *Limnol. Oceanogr.* 24, 823–837. doi: 10.4319/lo.1979.24.5.0823
- McKnight, D. M., and Morel, F. M. M. (1980). Copper complexation by siderophores from filamentous blue-green algae. *Limnol. Oceanogr.* 25, 62–71. doi: 10.4319/lo.1980.25.1.0062
- Midorikawa, T., and Tanoue, E. (1996). Extraction and characterization of organic ligands from oceanic water columns by immobilized metal ion affinity chromatography. *Mar. Chem.* 52, 157–171. doi: 10.1016/0304-4203(95)00075-5
- Midorikawa, T., and Tanoue, E. (1998). Molecular masses and chromophoric properties of dissolved organic ligands for copper(II) in oceanic water. *Mar. Chem.* 62, 219–239. doi: 10.1016/S0304-4203(98)00040-1
- Milne, A., Landing, W., Bizimis, M., and Morton, P. (2010). Determination of Mn, Fe, Co, Ni, Cu, Zn, Cd and Pb in seawater using high resolution magnetic sector inductively coupled mass spectrometry (HR-ICP-MS). *Anal. Chim. Acta* 665, 200–207. doi: 10.1016/j.aca.2010.03.027
- Moffett, J. W., and Brand, L. E. (1996). Production of strong, extracellular Cu chelators by marine cyanobacteria in response to Cu stress. *Limnol. Oceanogr.* 41, 388–395. doi: 10.4319/lo.1996.41.3.0388
- Moffett, J. W., Zika, R. G., and Brand, L. E. (1990). Distribution and potential sources and sinks of copper chelators in the Sargasso Sea. *Deep Sea Res.* 37, 27–36. doi: 10.1016/0198-0149(90)90027-S
- Paunovic, I., Schulin, R., and Nowack, B. (2005). Evaluation of immobilized metal-ion affinity chromatography for the fractionation of natural Cu complexing ligands. *J. Chromatogr. A* 1100, 176–184. doi: 10.1016/j.chroma.2005.09.055
- Paunovic, I., Schulin, R., and Nowack, B. (2008). Fractionation of dissolved carbon from soil solution with immobilized metal ion affinity chromatography. *Eur. J. Soil Sci.* 59, 198–207. doi: 10.1111/j.1365-2389.2007.00975.x
- Perrin, D. D. (1979). *Stability Constants of Metal-Ion Complexes. Part B, Organic Ligands*. Oxford: Pergamon Press.

- Porath, J., Carlsson, J., Olsson, I., and Belfrage, G. (1975). Metal chelate affinity chromatography, a new approach to protein fractionation. *Nature* 258, 598–599. doi: 10.1038/258598a0
- Rodrigues, A., Brito, A., Janknecht, P., Proença, M. F., and Nogueira, R. (2009). Quantification of humic acids in surface waters: effects of divalent cations, pH and filtration. *J. Environ. Monit.* 11, 377–382. doi: 10.1039/B811942B
- Ross, A. R. S., Ikonoumou, M. G., and Orians, K. J. (2000). Characterization of dissolved tannins and their metal-ion complexes by electrospray ionization mass spectrometry. *Anal. Chim. Acta* 411, 91–102. doi: 10.1016/S0003-2670(00)00746-7
- Ross, A. R. S., Ikonoumou, M. G., and Orians, K. J. (2003). Characterization of copper-complexing ligands in seawater using immobilized copper(II)-ion affinity chromatography and electrospray ionization mass spectrometry. *Mar. Chem.* 83, 47–58. doi: 10.1016/S0304-4203(03)00095-1
- Ross, A. R. S., Ikonoumou, M. G., Thompson, J. A. J., and Orians, K. J. (1998). Determination of dissolved metal species by electrospray ionization mass spectrometry. *Anal. Chem.* 70, 2225–2235. doi: 10.1021/ac9711908
- Semeniuk, D. M., Bundy, R. M., Payne, C. D., Barbeau, K. A., and Maldonado, M. T. (2015). Acquisition of organically complexed copper by marine phytoplankton and bacteria in the Northeast subarctic Pacific Ocean. *Mar. Chem.* 173, 222–233. doi: 10.1016/j.marchem.2015.01.005
- Smith, C. L., Stauber, J. L., Wilson, M. R., and Jolley, D. F. (2014). The use of immobilised metal affinity chromatography (IMAC) to compare expression of copper-binding proteins in control and copper-exposed marine microalgae. *Anal. Bioanal. Chem.* 406, 305–315. doi: 10.1007/s00216-013-7452-6
- Sunda, W. G. (1991). Trace metal interactions with marine phytoplankton. *Biol. Oceanogr.* 6, 411–442.
- Taguchi, G., and Yokoyama, Y. (1994). *Taguchi Methods: Design of Experiments*. Dearborn, MI: American Supplier Institute.
- Vachet, R. W., and Callaway, M. B. (2003). Characterization of Cu(II)-binding ligands from the Chesapeake Bay using high-performance size-exclusion chromatography and mass spectrometry. *Mar. Chem.* 82, 31–45. doi: 10.1016/S0304-4203(03)00047-1
- Van Den Berg, C. M. G. (1986). Determination of copper, cadmium and lead in seawater by cathodic stripping voltammetry of complexes with 8-hydroxyquinoline. *J. Electroanal. Chem.* 215, 111–121. doi: 10.1016/0022-0728(86)87009-7
- Vraspir, J. M., and Butler, A. (2009). Chemistry of marine ligands and siderophores. *Ann. Rev. Mar. Sci.* 1, 43–58. doi: 10.1146/annurev.marine.010908.163712
- Waska, H., Koschinsky, A., Chanco, M. J. R., and Dittmar, T. (2015). Investigating the potential of solid-phase extraction and Fourier transform-ion cyclotron resonance mass spectrometry (FT-ICR-MS) for the isolation and identification of metal-organic complexes from natural waters. *Mar. Chem.* 173, 78–92. doi: 10.1016/j.marchem.2014.10.001
- Watanabe, H., Goto, K., Taguchi, S., McLaren, J. W., Berman, S. S., and Russell, D. S. (1981). Preconcentration of trace elements in sea water by complexation with 8-hydroxyquinoline and adsorption on C18 bonded silica gel. *Anal. Chem.* 53, 738–739. doi: 10.1021/ac00227a043
- Waters Corporation (2014). *Care and Use Manual for Oasis HLB Cartridges and 96-well Plates*. Available online at: <https://www.waters.com/webassets/cms/support/docs/715000109.pdf>
- Wilhelm, S. W. (1995). Ecology of iron-limited cyanobacteria: a review of physiological responses and implications for aquatic systems. *Aquat. Microb. Ecol.* 9, 295–303. doi: 10.3354/ame009295
- Wiramanaden, C. I. E., Cullen, J. T., Ross, A. R. S., and Orians, K. J. (2008). Cyanobacterial copper-binding ligands isolated from artificial seawater cultures. *Mar. Chem.* 110, 28–41. doi: 10.1016/j.marchem.2008.02.003
- Wu, F., and Tanoue, E. (2001a). Isolation and partial characterization of dissolved copper-complexing ligands in streamwaters. *Environ. Sci. Technol.* 35, 3646–3652. doi: 10.1021/es0019023
- Wu, F., and Tanoue, E. (2001b). Geochemical characterization of organic ligands for copper(II) in different molecular size fractions in Lake Biwa, Japan. *Org. Geochem.* 32, 1311–1318. doi: 10.1016/S0146-6380(01)00094-8
- Zhang, L. G., Ren, X. G., Jiang, D. P., Lu, A. D., and Yuan, J. S. (1996). Effect of metal cation on absorption and fluorescence spectra of metal complexes of 8-hydroxyquinoline. *Spectrosc. Lett.* 29, 995–1001. doi: 10.1080/00387019608007266

Conflict of Interest Statement: The authors declare that the research was conducted in the absence of any commercial or financial relationships that could be construed as a potential conflict of interest.

Copyright © 2016 Nixon and Ross. This is an open-access article distributed under the terms of the Creative Commons Attribution License (CC BY). The use, distribution or reproduction in other forums is permitted, provided the original author(s) or licensor are credited and that the original publication in this journal is cited, in accordance with accepted academic practice. No use, distribution or reproduction is permitted which does not comply with these terms.



Ferrioxamine Siderophores Detected amongst Iron Binding Ligands Produced during the Remineralization of Marine Particles

Imelda B. Velasquez¹, Enitan Ibisani¹, Elizabeth W. Maas^{2†}, Philip W. Boyd^{3,4}, Scott Nodder² and Sylvia G. Sander^{1,4*}

¹ Department of Chemistry, University of Otago, Dunedin, New Zealand, ² National Institute of Water and Atmosphere, Wellington, New Zealand, ³ Institute for Marine and Antarctic Studies, University of Tasmania, Hobart, Australia, ⁴ NIWA/University of Otago Research Centre for Oceanography, University of Otago, Dunedin, New Zealand

OPEN ACCESS

Edited by:

Claire Mahaffey,
University of Liverpool, UK

Reviewed by:

Martha Gledhill,
GEOMAR Helmholtz-Zentrum für
Ozeanforschung, Germany
Randelle M. Bundy,
Woods Hole Oceanographic
Institution, USA

*Correspondence:

Sylvia G. Sander
sylvia.sander@otago.ac.nz

† Present Address:

Elizabeth W. Maas,
Ministry for Primary Industries, Napier,
New Zealand

Specialty section:

This article was submitted to
Marine Biogeochemistry,
a section of the journal
Frontiers in Marine Science

Received: 07 May 2016

Accepted: 30 August 2016

Published: 22 September 2016

Citation:

Velasquez IB, Ibisani E, Maas EV,
Boyd PW, Nodder S and Sander SG
(2016) Ferrioxamine Siderophores
Detected amongst Iron Binding
Ligands Produced during the
Remineralization of Marine Particles.
Front. Mar. Sci. 3:172.
doi: 10.3389/fmars.2016.00172

The microbial degradation of marine particles is an important process in the remineralization of nutrients including iron. As part of the GEOTRACES process study (FeCycle II), we conducted incubation experiments with marine particles obtained from 30 to 100 m depth at two stations during austral spring in the subtropical waters east of the North Island of New Zealand. The particles were collected using *in-situ* pumps, and comprised mainly of suspended and slow sinking populations along with associated attached heterotrophic bacteria. In treatments with live bacteria, increasing concentrations of Fe binding ligands were observed with an average stability constant of $\log K_{\text{FeL}, \text{Fe}^{3+}} = 21.11 \pm 0.37$ for station 1 and 20.89 ± 0.25 for station 2. The ligand release rates varied between 2.54 and 11.8 $\text{pmol L}^{-1} \text{d}^{-1}$ (calculated for ambient seawater particle concentration) and were similar to those found in two Southern Ocean subsurface studies from ~ 110 m depths in subpolar and polar waters. Dissolved iron (DFe) was released at a rate between 0.33 and 2.09 $\text{pmol Fe L}^{-1} \text{d}^{-1}$ with a column integrated (30–100 m) flux of 107 and 58 $\text{nmol Fe m}^{-2} \text{day}^{-1}$ at station 1 and 2, respectively. Given a mixed layer DFe inventory of $\sim 48 \mu\text{mol m}^{-2}$ and $\sim 4 \mu\text{mol m}^{-2}$ at the time of sampling for station 1 and 2, this will therefore result in a DFe residence time of 1.2 and 0.18 years, assuming particle remineralization was the only source of iron in the mixed layer. The DFe release rates calculated were comparable to those found in the previously mentioned study of Southern Ocean water masses. Fe-binding ligand producing bacteria (CAS positive) abundance was found to increase throughout the duration of the experiment of 7–8 days. For the first time ferrioxamine type siderophores, including the well-known ferrioxamine B and G, have been quantified using chemical assays and LC-ESI-MS. Our subtropical study corroborates prior reports from the Southern Ocean of particle remineralization being an important source of DFe and ligands, and adds unprecedented detail by revealing that siderophores are probably an important component of the ligands released into subsurface waters during particle remineralisation.

Keywords: siderophores, voltammetry, dfb, particle remineralization, iron, particulate matter

INTRODUCTION

Iron is an essential metal required for many microbial enzymatic activities (Geider and La Roche, 1994). It plays a central role in controlling primary production over much of the world's ocean. Hence, many studies have focused on better understanding the biogeochemical cycle of iron in the ocean (Rue and Bruland, 1995, 1997; Behrenfeld et al., 1996; Boyd et al., 2000, 2005; Morel and Price, 2003; Moore et al., 2013). Previous studies revealed that over 99.9% of dissolved iron in the ocean is bound by iron-complexing ligands (Gledhill and van den Berg, 1994; Van den Berg, 1995; Tian et al., 2006; Sander et al., 2015). These iron-binding ligands are separated into operational classes based on trends in conditional stability constants— L_1 being the strongest Fe-binding ligand and L_2, L_3 etc. subsequently weaker ones (Rue and Bruland, 1995; Sander et al., 2011).

Many studies have investigated the production and sources of Fe-binding ligand classes (Gledhill and Buck, 2012). Siderophores and possibly other strong iron binding ligands with conditional stability constants similar to L_1 class ligands have been shown to be produced, and released, by heterotrophic bacteria and cyanobacteria in response to iron limitation (Reid et al., 1993; Wilhelm and Trick, 1994; Martinez et al., 2001; Gledhill et al., 2004; Mawji et al., 2008a) or in response to episodic Fe supply to take up Fe opportunistically (Adly et al., 2015). Ligands, although probably not siderophores, were also released or produced during micro and meso-zooplankton grazing on phytoplankton during an *in-situ* mesoscale iron enrichment experiments conducted in the western subarctic Pacific (Moore and Braucher, 2008) and our present FeCycle II study (Boyd et al., 2012). Other potential sources for iron binding ligand classes (L_1 and weaker ligands) include virus lysis (Poorvin et al., 2011), exopolysaccharides (Hassler et al., 2011), and humic substances (Laglera and van den Berg, 2009; Abualhaija and van den Berg, 2014; Mahmood et al., 2015).

Particulate iron (PFe) is often the dominant form of iron in the ocean (Frew et al., 2006; Lenes et al., 2009; Ellwood et al., 2014, 2015). Hunter and Boyd (2007) pinpointed the importance of understanding the particle dynamics of iron in an effort to better understand the origins of iron-complexing ligands. They proposed the so-called “ligand soup hypothesis,” which suggested that almost any particulate organic matter, after suitable mixing and timescale, will most likely generate iron-complexing ligands. Some potential sources of the “ligand soup” include the breakdown of sinking particles in biological material and residual terrestrial organic matter transported from the continental shelves (Hunter and Boyd, 2007). Aspects of the “ligand soup” hypothesis were confirmed in a series of experiments in Southern Ocean sub- and polar-waters in which incubation of suspended and slow-settling particles resulted in the release of both DFe and L_2 iron-binding ligands (Boyd et al., 2010).

The vertical distributions of iron-complexing ligands also provide insights as to the provenance of the ligand classes. Early papers already alluded to the possible linkage of the ligand distribution and microorganisms, due to a strong correlation between microbial abundance and ligand concentrations (Rue

and Bruland, 1995; Boye et al., 2001). Ibanmi et al. (2011) reported two ligand classes—termed sum of all ligand class (ΣL) and a strong ligand class (L_1). L_1 was restricted to the upper ocean (i.e., <200 m depth), whereas ΣL was observed throughout the water column down to 1000 m. These depth-dependent trends, showing the presence of different ligand classes in the upper stratum vs. throughout the water column were observed by researchers in the central Pacific Ocean although different terminologies were used to describe some of these observed ligand classes (Rue and Bruland, 1995, 1997; Buck et al., 2007; Bundy et al., 2014). As part of the GEOTRACES program, the entire ocean basins have been sampled and analyzed systematically for Fe-binding ligands. Results from some of these studies such as the one conducted in the North Atlantic Ocean (Buck et al., 2015) reported up to three ligand classes throughout the water column. Improved titration methodology and data evaluation is another reason for better ligand class classification and resolution (Wells et al., 2013; Pižeta et al., 2015).

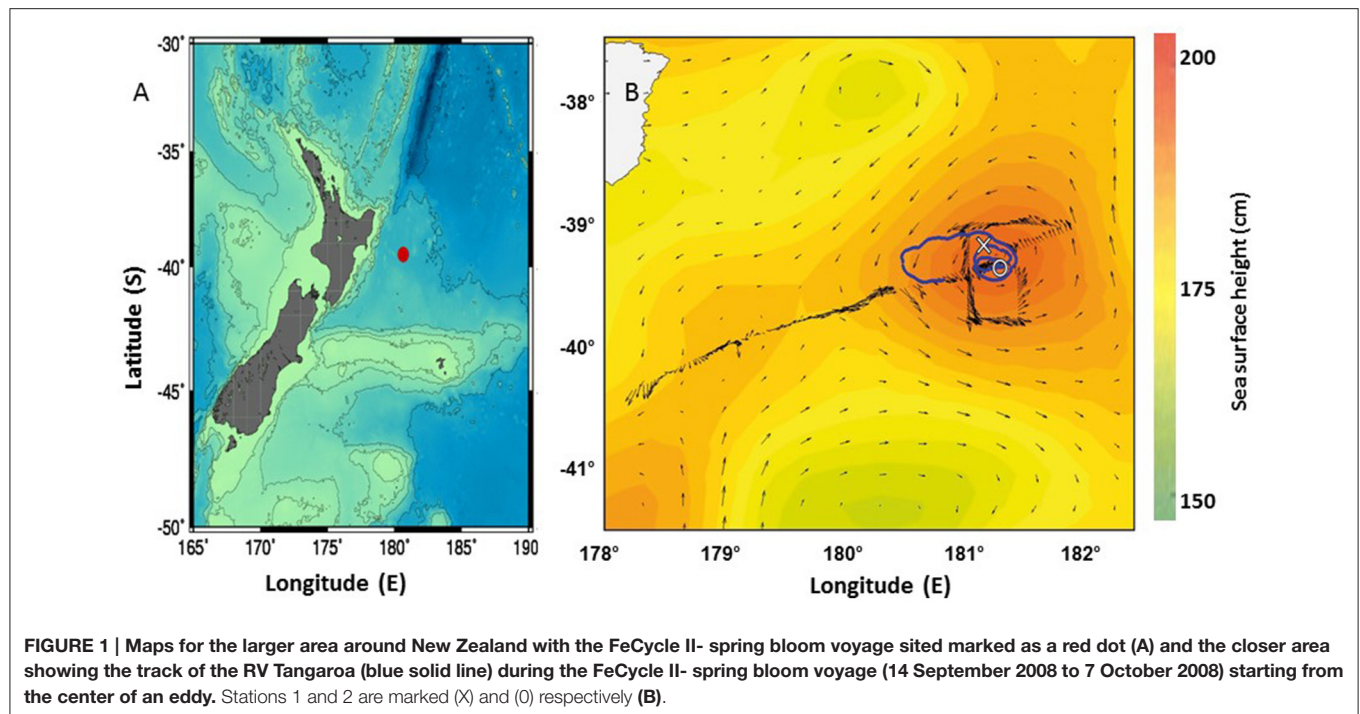
The evidence of joint iron and ligand release during a remineralization experiments was first published by Boyd et al. (2010), but no other parameters such as siderophore production, POC, nutrients or the presence of culturable heterotrophic and CAS active bacteria were measured in that pilot study. Therefore, we present the findings of a new framework of a remineralization experiment of marine particles performed during the FeCycle II GEOTRACES process study that targeted the spring bloom in subtropical waters east of the North Island of New Zealand. Special focus was drawn on the inter-relationship between POC, PFe, DFe stocks, and the inventory and chemical characterization of iron-complexing ligands during particle remineralization. The findings will help improve our conceptual understanding of the biogeochemical cycling of iron.

MATERIALS AND METHODS

Study Site

This study took place in high iron mesotrophic sub-tropical waters located off the east coast of the North Island of New Zealand as part of FeCycle II quasi-Lagrangian biogeochemical experiment (see Boyd et al., 2012; Weller et al., 2013 for further details). Two stations were visited during austral spring (September, 2008) on board the New Zealand research vessel *RV Tangaroa* to determine productivity and carbon export in New Zealand waters. The sampling location for FeCycle II was in open ocean waters (>2000 m bottom depth), ~200 km east of New Zealand. Station 1 at 39.21°S; 181.21°E (**Figure 1**) was sampled on the 20th September 2008, julian day 264 and corresponded to phase I of the study of an algal bloom. Station 2 at 39.40°S; 181.42°E (**Figure 1**) was sampled on the 27th September 2008, julian day 272, corresponding to phase II of FeCycle II (Boyd et al., 2012; Weller et al., 2013; LeClerc et al., 2014). Mixed layer depths for the entire cruise are given in Boyd et al. (2012) and Weller et al. (2013). For station 1, the mixed layer was ~78 m and for station 2 the mixed layer was <65 m.

All seawater samples were collected using a General Oceanics model 1018 autonomous intelligent rosette deployed on a Kevlar hydroline (Turner et al., 2004). All equipment



used throughout this work had been rigorously acid cleaned following the protocols recommended by (Sander et al., 2009) and experimental samples were stored in acid cleaned polyethylene bottles (Nalgene, Rochester, NY). Particles for the remineralization experiment as well as for PFe and POC analysis were taken by trace metal clean *in-situ* McLane pumps.

Remineralization Experiments

Samples collected at both sites were taken from 30 to 100 m to be able to calculate column integrated fluxes. Particles were collected by *in-situ* filtration. At station 1, 192 L (30 m depth) and 286 L (100 m) of seawater were filtered, whereas 195 L (30 m) and 196 L (100 m) of seawater were filtered at station 2. Seawater samples from each depth were filtered through a 5.0 μm acid washed polycarbonate filter with a diameter of 14 cm. This pore size was chosen in order to retain most particles and their associated attached bacteria while excluding free-living bacteria ($\sim 1 \mu\text{m}$). This pore size also allowed for better simplification of experimental outcomes and to ascribe any increases in DFe and L for ratio comparison particle attached bacteria. Using information from the Frew et al. (2006) study in subantarctic waters off New Zealand, we assumed that $\sim 70\%$ of all particles in the mixed layer are $> 5 \mu\text{m}$. The particles were re-suspended into 250 mL of 0.2 μm unfiltered seawater collected from depths and station corresponding to pump stations. Ten milliliters aliquots of concentrated particle suspension were then further diluted with unfiltered seawater to produce 18 incubation solutions of 250 mL. This resulted in concentration factors of 29 for station 1 at 30 m, 43 for station 1 at 100 m, and 30 for both depths at station 2.

All experiments were run in triplicate for each timepoint. Half of the incubation solutions (i.e., 9) were sterilized using

a domestic microwave adjusted to full power for 6 min prior to incubation (Boyd et al., 2010). Microwave sterilized samples from day 0 were filtered after cooling down to room temperature. Filter sterilized samples without particles (i.e., ambient seawater from 30 or 100m) were only analyzed at day 0, but not incubated because of previous results from the SAZ-Sense study had already shown that samples without particle enrichment did not produce significant amounts of ligands or DFe on a timescale of 8 days (Boyd et al., 2010). The first sets of experiments performed at station 1 were incubated close to ambient temperature of 14°C in the dark for 8 days using three samples per treatment (i.e., sterilized and unsterilized) per time point 0 (time-zero, immediately after particle resuspension), 4 and 8 days. However, due to logistical constraints the second experiment at station 2 was incubated for 7 days with time points at 0, 4, and 7 days.

All samples were packed in black bags before initiating the incubation experiments to avoid exposure to light and subsequent photochemical breakdown of ligands (Barbeau et al., 2001) and kept at 14°C, the ambient temperature at 30 and 100 m depth. At each time-point 3 samples of sterilized and unsterilized samples were filtered using a 0.2 μm acid washed polycarbonate filter membrane for DFe and iron-binding ligand analyses.

The remainder of the concentrated particle samples (i.e., 70 ml) from each experiment were re-suspended in 10 L of unfiltered seawater from the station and depth where the particles were taken using the *in-situ* pumps. The re-suspended samples were then incubated in the dark for 8 or 7 days at 14°C for molecular characterization of Fe-binding ligands (Velasquez et al., 2011).

Five additional surface samples (which were not incubated, see Supplementary Information Table S1) were taken throughout the cruise and pre-concentrated in a 300 mL column filled with

XAD-16 resin. These were extracted and analyzed parallel to the incubation experiment samples using chemical assays and LC-ESI-MS. The samples were taken for a separate study and results were not discussed in this paper. However, the results were used to verify absence/presence of ferrioxamine B and G and other masses with fragmentation pattern similar to known siderophores before the particle incubation experiments were done.

Particulate Carbon and Dissolved Nutrient Analysis

Particulate organic carbon (POC) measurements were done on parts of the same filter collected for the bioremineralization experiment as well as on full filters taken at 30 and 100 m using the McLane pumps. POC were measured at the National Institute of Water and Atmospheric Research (NIWA) laboratory in New Zealand. POC analyses were conducted on a Thermo-Finnigan Delta Plus Mass spectrometer using procedure MAM, 01-1090. Dissolved nutrients (N, P, Si) were analyzed on board ship by automated analysis (after Frew et al., 2001).

Bacterial Abundance and Culturable Bacteria

Bacteria abundances were determined by flow cytometry using a FACS Calibur instrument (Becton Dickinson) with CellQuest Vers. 3.3 software following the methods described in Lebaron et al. (1998). Samples were run on the high flow setting ($60 \mu\text{L min}^{-1}$) with a minimum of 10,000 counts per sample. The bacterial population was identified using a FL1 (green light, 530/30 BP filter, log scale) vs. SSC (Cell size, linear scale) scatter plot.

Samples for the determination of culturable bacteria were serially diluted in sterile phosphate buffer solution (PBS) and were spread plated in duplicate on Marine Agar (MA; Difco Laboratories) and Chrome azurol S (CAS) Agar plates. CAS plates were prepared as described by Schwyn and Neilands (1987). Both Marine Agar and CAS Agar plates were incubated at 15°C and were counted after 4 weeks for colony forming units.

Analysis of Iron-Complexing Ligands and Dissolved Iron

Iron-complexing ligands were determined by competing ligand equilibration-adsorptive cathodic stripping voltammetry (CLE-AdCSV) with 2-(2-Thiazolylazo)-p-cresol (TAC) as the competing ligand (Croot and Johansson, 2000). The voltammetric equipment consisted of a Metrohm VA 663 stand (Herisau, Switzerland) an IME 663 interface and a $\mu\text{Autolab}$ type III potentiostat (both Metrohm Autolab, Utrecht, The Netherlands). The working electrode was a hanging mercury drop electrode (HMDE) with a mercury drop size of $2 (0.4 \text{ mm}^2 \pm 10\%)$. The reference electrode was $\text{Ag}|\text{AgCl}|3 \text{ M KCl}$, and the counter electrode was a glassy carbon rod. All samples were contained in Teflon cells (Metrohm) during AdCSV analysis and stirred with the inbuilt all-PTFE Teflon stirring tip (1500 rpm) of the VA 663. The voltammetry system

was computer controlled using the GPES software (Version 4.9, 2001–2009).

All sample manipulations were performed in a Class 100 laminar airflow bench at room temperature. Milli-Q ultrapure water (MQ, $18 \text{ M}\Omega$) was used for the preparation of chemicals and rinsing throughout this study. Buffer solution of *N*-(2-hydroxyethyl)-piperazine-*N'*-2-propanesulfonic acid (EPPS, Sigma-Aldrich, St Louis, MO) was prepared in ammonium hydroxide (NH_4OH) to give a pH of 8.1. NH_4OH used for pH adjustments of the buffer was purified by passive vapor phase equilibration. A 10 mL Fe (III) stock solution was prepared from a standard solution of $1 \text{ g L}^{-1} \text{ FeCl}_3 \cdot 6\text{H}_2\text{O}$ (Sigma), and acidified to $\leq \text{pH } 2$ with quartz distilled HCl (q-HCl). A working iron standard solution ($0.4 \mu\text{M}$) was prepared daily from the stock $10 \mu\text{M}$ solution and acidified to $\leq \text{pH } 2$ with q-HCl. $5.5 \mu\text{M}$ stock solution of TAC (Aldrich) was prepared in quartz distilled methanol (q-MeOH) every 2–4 weeks. All chemicals were kept in the fridge.

For the Fe-ligand titration, subsamples (12 mL) of seawater were pipetted into a series of 14 Teflon bottles and buffered at pH 8.1 with $50 \mu\text{L}$ of EPPS buffer (1.0 M). Iron was added to twelve of the bottles, yielding concentrations from 0 to 6 nM. After 1 h equilibration, TAC was added to a final concentration of $3.5 \mu\text{M}$, and the sample was left to equilibrate for at least 8 h. The samples were measured by DP-AdCSV from the lowest to the highest concentration in the usual manner with parameters as described by Ibsanmi et al. (2011) without rinsing in between aliquots. Cell cups were rinsed with Milli-Q water between titrations to avoid carry-over. Specific Teflon bottles were always used for the same iron concentration added and they were only rinsed with either Milli-Q or the sample itself in between titrations to keep them in equilibrium. Two to three scans were usually obtained for each sample. The DFe in freshly thawed ligand samples were determined by UV digesting it for 6 h using a Photoreactor Model APQ 40 (Photochemical Reactors) with a 400-W medium-pressure Hg lamp. Samples that were not freshly thawed were acidified to pH 2 prior to UV digestion. The pH of the samples was brought back to pH 8.0 with isothermally distilled NH_4OH prior to analysis using the AdCSV protocols.

Ligand classifications were made according to the methods described by Ibsanmi et al. (2011). Briefly, L_1 is operationally defined as a strong ligand having $\log K_{\text{FeL1, Fe}^{3+}} \geq 22$ and $L_1 > \text{DFe}$, whereas ΣL is operationally defined as the sum of all iron-complexing ligands detectable under the chosen analytical window. Ligand parameters were calculated using ProMCC software (Omanović et al., 2015).

Ligand Characterization

Extraction of Siderophore-Type Compounds from XAD-16 Resin

Siderophore-like compounds were pre-concentrated by passing the filtered sample through an in-house prepared solid phase extraction (SPE) column containing 30 g pre-conditioned Amberlite XAD-16 resin (Sigma; Velasquez et al., 2011). The columns were loaded with organic compounds from the $0.2 \mu\text{m}$ filtered 10 L sample at the end of the incubation period. After loading the columns were washed with 500 mL MQ to remove

salt. The organic compounds were subsequently eluted with three bed volumes of 95% methanol (Merck, HPLC grade). The eluents were collected in q-HCl cleaned Teflon bottles and kept refrigerated for further processing.

Chemical Assays

Chemical assays were done to test for the presence of siderophore moieties in the methanolic extracts of the XAD-16 column. The chrome azurol S (CAS) test for general iron binding capability (Schwyn and Neilands, 1987), Arnow and Rioux tests for catecholates (Arnow, 1937; Rioux et al., 1983) and Csaky test for hydroxamate type compounds (Gillam et al., 1981) were applied.

C18-Solid Phase Extraction (SPE)

The methanolic XAD-16 extracts were dried using a SAVANT Speed Vac Plus SC210A and ~1.0 mg of sample was re-dissolved in 1.0 mL 5% acetonitrile (HPLC grade, Merck). The sample was passed through a 1.0 g SPE column (VARIAN Bond Elut C18-SPE). The sample was then eluted off sequentially with three bed-volumes of solutions with increasing methanol: water ratio (i.e., 10, 20, 30, and 70%). The different eluents were collected separately. The various methanol fractions were transferred to acid-cleaned Eppendorf tubes, and then evaporated until the volume of the sample remainder was reduced to <10 μ L, using the speed vac. The pre-concentrated samples were diluted with 50 μ L MQ and centrifuged for 3 min. The supernatant was injected into the HPLC.

HPLC Separation and Mass Spectrometry Determination

The HPLC and mass spectrometry analyses were performed on an analytical HPLC system (DIONEX Ultimate 3000 System) attached to a Quadrupole Time-of-Flight mass spectrometer QTOF-MS; micrOTOF-Q, Bruker Daltonics). Chromatographic separations were carried out using a reversed phase column (250 \times 4.6 mm, GraceSmart RP 18 5 μ , Grace Davison Discovery Sciences). Twenty microliters of sample was injected onto the column by means of an auto sampler. The HPLC separation was done in 52 min using a linear gradient of 6–90% acetonitrile:water with 0.1% formic acid. Two wavelengths (220 and 435 nm) were monitored to detect total hydrolysis products and ferric hydroxamate complexes, respectively.

The QTOF-MS used in this study utilized electrospray ionization (ESI) as its ion source and operated under positive mode. The scan range was set from 50 to 1000 m/z. The capillary voltage was 4500 V and the end plate offset was –500 V. The collision cell radio frequency (RF) was 90.0 voltage per pole (Vpp), the nebulizer pressure was set at 3.0 bar and the dry heater temperature was at 200°C. Throughout the analysis the dry gas flow rate was set at 7.0 L min⁻¹.

For the determination of the fragmentation pattern of the molecule, the instrument was optimized and set to MSMS Auto mode. Since the concentration of the siderophore-like compounds present in the sample were expected to be very low, the MSMS (second mass spectra obtained after fragmentation of the highest peak) absolute threshold was set to an intensity

of 500. To ensure that all masses of interest underwent MSMS analysis the machine was set to include chromatographic peaks with peak widths \geq 12 s. The setting takes into account fast rising chromatographic peaks which can include siderophore-like ions. A summation factor of 3 was used to increase the intensity of MSMS spectra. The data for both single MS and MSMS analyses were obtained and processed using Bruker Software.

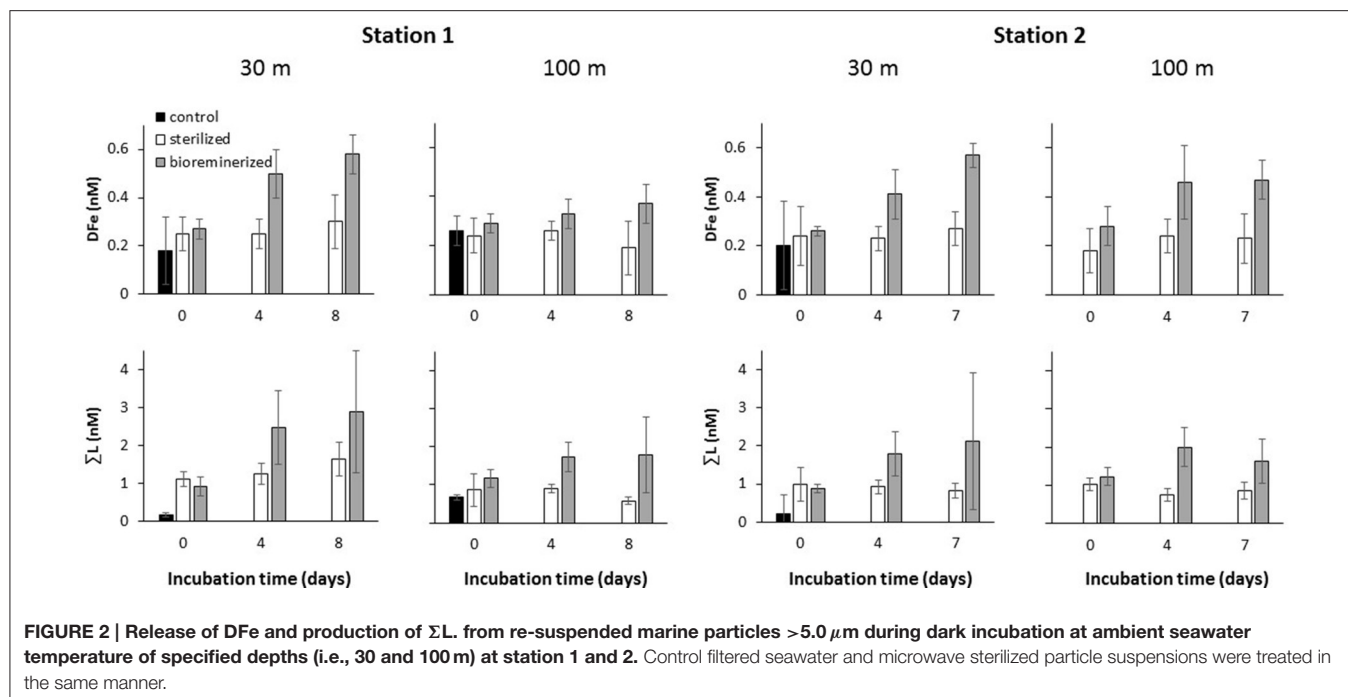
The mass spectrometer was calibrated using sodium formate calibrant. However, to ensure an accuracy of <10 ppm, desferrioxamine B (DFB) was also injected directly to the mass spectrometer for calibration. In this calibration, an accuracy of <2 ppm was generally obtained for the analysis. DFB was routinely used as a standard in the HPLC-MSMS analysis because it is commonly used as model siderophore. Other standards like mixed ferrioxamine, enterobactin, and aerobactin were interchangeably used as additional standards for the HPLC-MSMS analysis.

The natural Fe-siderophore complexes were identified using the natural Fe-isotopic ratio, which is a ratio of ⁵⁶Fe/⁵⁴Fe of 100/6.35 (De Hoffman and Stroobant, 1991). The criteria we looked for in details were: (1) ions that are bound to Fe should exhibit the Fe-isotopic pattern; (2) the ⁵⁴Fe isotope is confirmed if natural abundance is within the range of 1–7% and the mass accuracy is within <10 ppm (parts per million) and; (3) no molecular ion that is bound to Fe is present at the relevant retention time were observed in the blank. However, we are also reporting precursor ions that show the fragmentation pattern of ferrioxamines even in the absence of the Fe-complex.

RESULTS

D_{Fe} in microwave-sterilized particles treatments from both stations were not significantly different to the “no-particle” control treatment at the start of the experiment (**Figure 2** and **Table 1**). D_{Fe} in microwaved-sterilized samples collected from 100 m at station 2 were accidentally not analyzed. L₁ was detected in some of the sterilized samples but in low concentrations. Significant increases over 7 or 8 days in D_{Fe} and Σ L for the “live” particle samples were observed, while no L₁-ligands were detectable in any of the treatments from station 1 and 2 on day 8 or 7, respectively (**Table 1**). The total D_{Fe} and Σ L released or produced at both stations 1 and 2 were generally higher at 30 m depth as compared to the 100 m depth samples (**Table 2**). While D_{Fe} was released throughout all four incubations, Σ L release or production turned into removal or consumption after day 4 at station 2 for 100 m, which was the only sample taken from below the mixed layer.

The time-series of bacterial abundances in the samples with incubated particles is shown in **Figure 3**. For station 1, heterotrophic bacterial abundance was not significantly different on day 4 and 8. However, unfortunately no abundance data are available for day 0. At station 2, the 30 and 100 m samples both exhibited similar trends of peaking on day 4 and declining to close to initial abundances by day 7. Bacterial abundance did not change significantly over the duration of the treatment with sterilized particles. Bacterial abundance in the sterilized particles may represent dead or ghost cells counted by the flow



cytometer. In the bacterial agar plates, the responsive bacteria in the community showed the same trend for all stations and depths, i.e., an increase in culturable heterotopic bacteria, as determined on marine agar for the duration of the experiment. Likewise, the CAS active bacteria also exhibited significant increases in abundances between start and end of the experiment (see **Figure 4**).

Nutrient analyses were not done in replicates due to sample volume limitation. Since observed changes in nutrients throughout the experiments were quite small and no errors or outliers were determined, we are not showing data here. Nitrate in station 1 incubation experiment was 3 times higher at 30 m than at 100 m, but did not change with time. Ammonia clearly increased in the “live” samples at station 1 for both depths. Nutrients analyzed from samples of station 2 are even more variable throughout and no clear trends were observed. The POC concentration measured in the beginning of the experiment from sections of the ($5 \mu\text{m}$) *in-situ* filter were converted to ambient concentrations using the concentration factors for each station and depth. Ambient seawater POC samples were taken from the same filters as used by the *in-situ* pump at the same day and depth where particles were taken for the remineralization experiment. POC concentrations were 5.1 and $5.6 \mu\text{mol L}^{-1}$ at 30 m and 2.5 and $2.2 \mu\text{mol L}^{-1}$ at 100 m for stations 1 and 2 respectively. No significant changes of the above mentioned parameters were observed in the sterilized particle treatments.

Results of different chemical assays run on extracts from samples incubated with particles and from large volume ambient seawater were CAS assay positive, confirming the presence of Fe-binding ligands in incubations from both depths at each station (see **Table 3** and Supplementary Material Table S1). Similarly, hydroxamate moieties were found, using the Csaky assay, in

all treatments. At station 1, no catecholate type compounds were detected by the Rioux assay from the treatments at the both depths. However, concentrations around the detection limit of the method were found in treatments of both depths from station 2. The detection limit of Rioux assay was $0.16 \mu\text{M}$ in the methanolic extract, which translates to a concentration in the treatment of 1.4 nM . The results are summarized in **Table 3**.

Since the total amounts of dissolved organic material extracted from the particle remineralization experiments were very small, the intensities of the tandem MSMS analyses were relatively low but above the detection limit (45 nM based on DFB analyses with intensity of 10^2). From the 20% methanol extract, three siderophore-type compounds with m/z 585.31, 614.26 and 672.28 eluted off the C18-reverse phase column between 8 and 9 min (station 1, 30 m) while m/z 371.21 was observed at 11.3 min (station 1, 100 m). The natural Fe-isotopic pattern was observed in m/z 614.26 and 672.28 ($[\text{M}+\text{H}+\text{Fe}-3\text{H}]^+$). The tandem MSMS analysis of m/z 614.26 yielded low intensity fragments (see Supplementary Material Figures SI4–SI6). However, the mass differences were similar to those commonly observed in hydroxamate siderophores. The simulated molecular formula for m/z 614.26 was within 10 ppm accuracy compared to the known linear ferrioxamine B (DFB; **Figure 5A**). Likewise, MSMS of m/z 672.28 yielded very low intensity fragments but the simulated molecular formula has mass accuracy within 10 ppm and is comparable to the known linear hydroxamate siderophore, ferrioxamine G (DFG; **Figure 5B**). For quality assurance, ferrioxamine B and G in a mixed ferrioxamine standard were analyzed and found to co-elute at ~ 8.0 min (**Figure 5C**). The ion peaks m/z 585.31 and m/z 371.21 ($[\text{M}+\text{H}]^+$) did not exhibit the Fe-isotopic pattern but the MSMS fragments were equal to those of known

TABLE 1 | Iron speciation data showing the concentration of dissolved iron (DFe), sum of ligand (ΣL) and L_1 , in brackets, and their conditional stability constants with respect to Fe^{3+} ($LogK_{FeL1, Fe3+}$ and $LogK_{\Sigma L, Fe3+}$) observed during the remineralization experiments at 30 and 100 m of station 1 and 2.

ID (Depths)	Days	DFe (nM)	ΣL (nM) (L_1 (nM))	$LogK_{\Sigma L, Fe3+}$ ($LogK_{FeL1, Fe3+}$)
STATION 1				
Sterilized samples (30 m)	0	0.25 ± 0.07	1.12 ± 0.20 (0.25 ± 0.16)	21.19 ± 0.34 (22.71 ± 0.90)
	4	0.25 ± 0.06	1.25 ± 0.28	21.00 ± 0.32
	8	0.30 ± 0.11	1.65 ± 0.44	20.99 ± 0.32
Unsterilized samples (30 m)	0	0.27 ± 0.04	0.92 ± 0.26	20.92 ± 0.34
	4	0.50 ± 0.10	2.47 ± 0.97	20.94 ± 0.52
	8	0.58 ± 0.08	2.88 ± 1.60	21.29 ± 0.98
Sterilized samples (100 m)	0	0.24 ± 0.07	0.86 ± 0.43 (0.54 ± 0.10)	21.37 ± 0.42 (22.23 ± 0.38)
	4	0.26 ± 0.04	0.90 ± 0.12 (0.34 ± 0.06)	21.68 ± 0.30 (22.92 ± 0.90)
	8	0.19 ± 0.11	0.58 ± 0.10	21.81 ± 0.56
Unsterilized samples (100 m)	0	0.29 ± 0.04	1.17 ± 0.24	20.59 ± 0.26
	4	0.33 ± 0.06	1.73 ± 0.38	20.83 ± 0.24
	8	0.37 ± 0.08	1.79 ± 1.00	20.49 ± 0.40
STATION 2				
Sterilized samples (30 m)	0	0.24 ± 0.12	0.99 ± 0.45	21.23 ± 0.11
	4	0.23 ± 0.09	0.92 ± 0.18 (0.37 ± 0.06)	21.25 ± 0.45 (22.15 ± 0.60)
	7	0.27 ± 0.07	0.82 ± 0.20	20.71 ± 0.30
Unsterilized samples (30 m)	0	0.26 ± 0.02	0.88 ± 0.12	21.06 ± 0.22
	4	0.41 ± 0.10	1.80 ± 0.58	21.03 ± 0.36
	7	0.57 ± 0.05	2.13 ± 1.80	20.86 ± 0.74
Sterilized samples (100 m)	0	0.18 ± 0.09	1.02 ± 0.16	20.68 ± 0.18
	4	0.24 ± 0.07	0.74 ± 0.16 (0.35 ± 0.02)	21.05 ± 0.34 (22.33 ± 0.40)
	7	0.23 ± 0.10	0.86 ± 0.22	21.26 ± 0.30
Unsterilized samples (100 m)	0	0.28 ± 0.08	1.22 ± 0.24	20.77 ± 0.26
	4	0.46 ± 0.15	2.00 ± 0.52	20.81 ± 0.50
	7	0.47 ± 0.08	1.64 ± 0.58	20.35 ± 0.30

The definition of L_1 and ΣL are based on $Log K_{FeL1, Fe3+} > 22$; $Log K_{FeL1, Fe3+}$ represents all classes of ligands detectable within the analytical window.

a hydroxamate-type siderophores. However, these peaks may also be from non-siderophore compounds. The MSMS analysis of the m/z 371.21 precursor ion yielded very low intensity

TABLE 2 | ΣL production and DFe release rates from particle mineralization experiments.

I	II	III	IV	V	VI	VII	VIII	IX	X	XI	XII
Station I.D	Depths (m)	Incu- tion length	Concen- tration factor in incubation assuming 70% of particles are > 5 μm^a	Absolute ΣL production in incubation ($nmol L^{-1}$)	ΣL production rate converted to ambient seawater ($pmol L^{-1} d^{-1}$) (V/III/IV)	Absolute POC removal in incubation ($nmol L^{-1}$ day^{-1})	% POC remineralized to ΣL per day assuming L contains 25 C (e.g., DFB)	Absolute DFe release in incubation ($nmol L^{-1}$)	DFe release rate in seawater ($pmol L^{-1}$ d^{-1}) (IX/III/IV)	PFe in ambient seawater (nM) ^b	% PFe remineralized to DFe per day
1	30	8	20.7	1.96	11.8	6.50	0.094	0.31	1.87	5.38	0.035
	100	8	30.5	0.62	2.54	13.35	0.016	0.08	0.33	1.27	0.026
2	30	7	21.2	1.25	8.41	3.80	0.117	0.31	2.09	4.00	0.053
	100	7	21.6	0.42	2.78	2.21	0.068	0.19	1.26	1.29	0.097

^a(Frew et al., 2006).

^b(Ellwood et al., 2014).

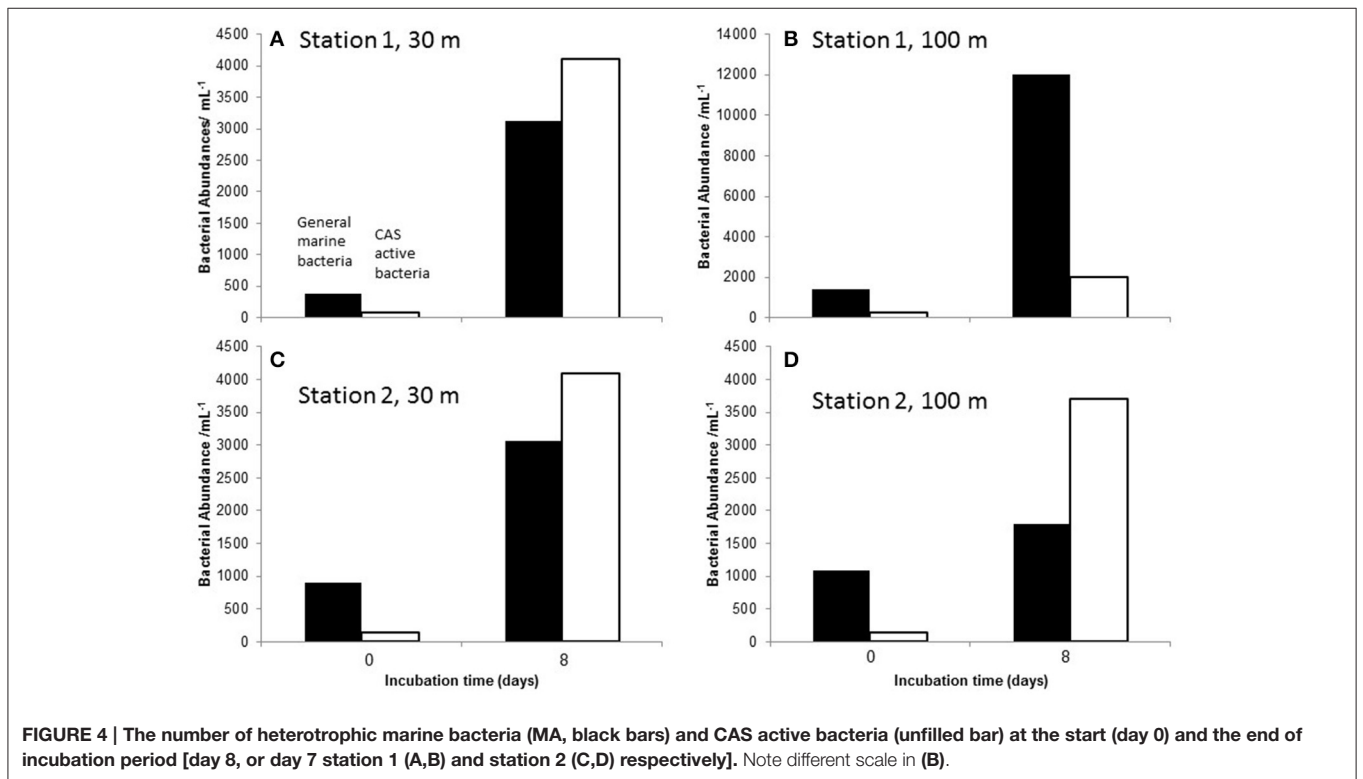
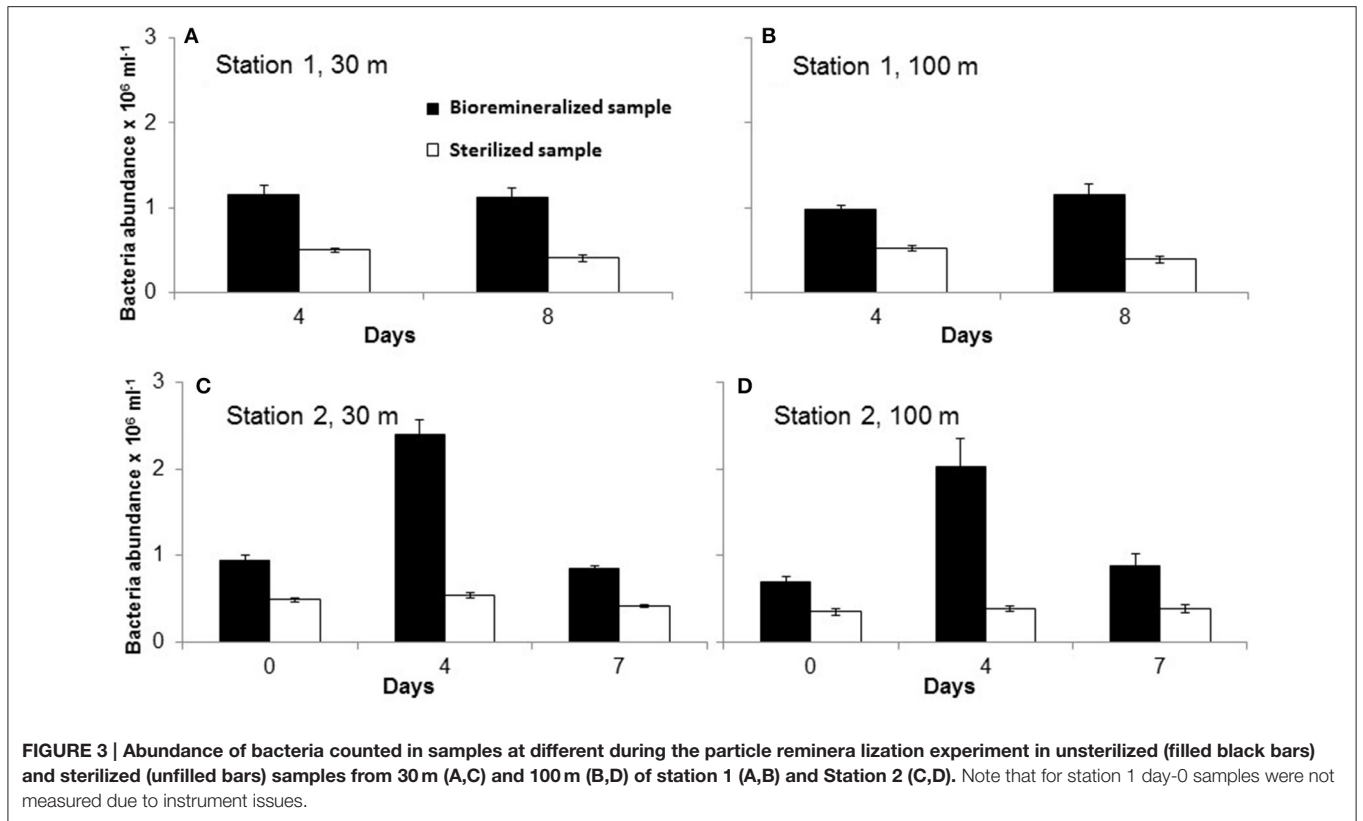
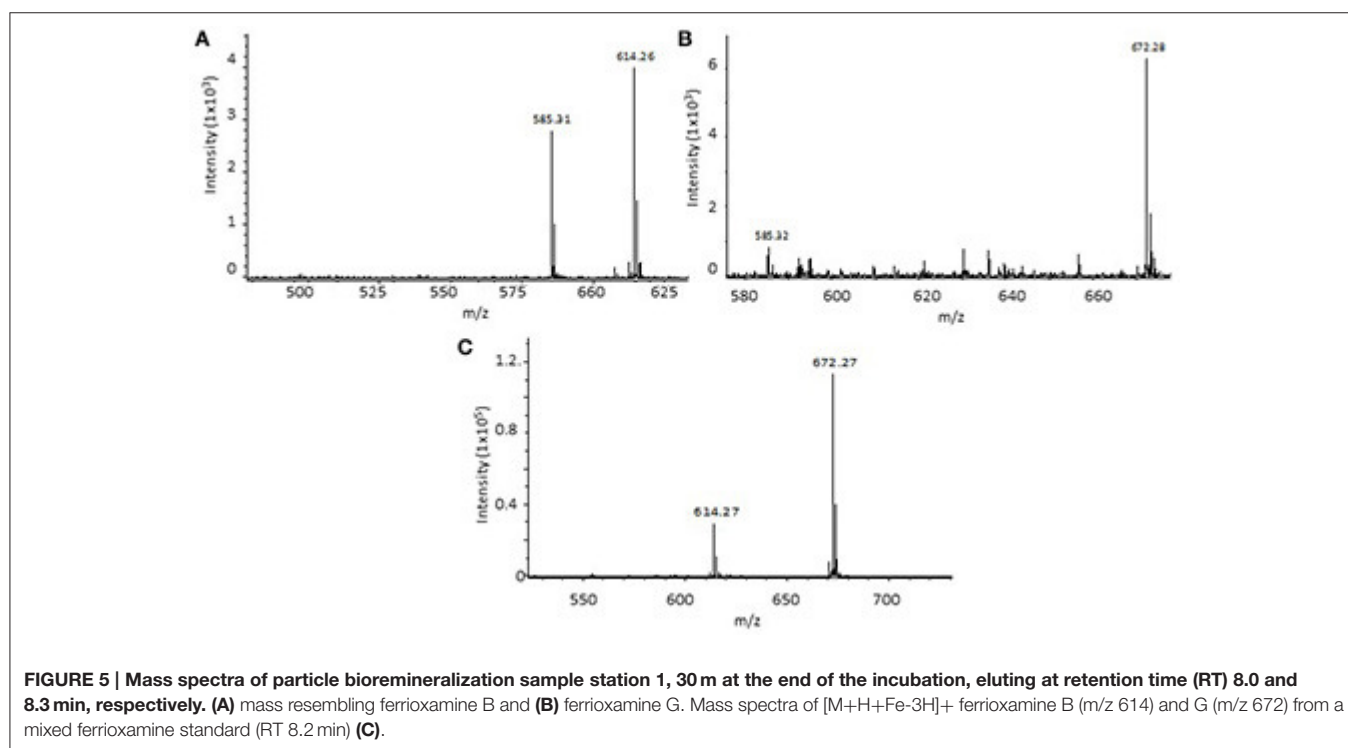


TABLE 3 | Summary of results from the characterization of siderophore type compounds extracted from incubation experiments of marine particles at the end of the treatment.

Sample ID	Assays			HPLC retention time (mi)	Precursor ion (<i>m/z</i>)	Comment
	CAS	Hydroxamate	Catecholates			
station 1 30 m	+	+	–	8.0	614.26	ferrioxamine B
				8.3	672.28	ferrioxamine G
				8.0	585.31	b
				11.3	371.21	b
100 m	+	+	–	11.3	371.23	b
station 2 30 m	+	+	+ ^a	11.3	371.23	b
				30.8	551.11	b
100 m	+	+	+ ^a	12.9	415.24	b
				12.9	437.23	b
				14.3	473.27	b
				14.3	495.24	b

^aAbsorbance very close to blank.

^bMolecular masses showing similar fragmentation patterns than ferrioxamine.



fragments and it was very difficult to evaluate fragment ions (see Supplementary Material Figure S17). However, high intensity Na adducts of the compound were observed ($[M+Na]$ *m/z* 393; $[M+2Na]$ *m/z* 415; $[M+3Na]$ *m/z* 437; $[M+4Na]$ *m/z* 459). The MS spectra of 30% SPE methanol fraction in 100 m sample of station 1 yielded *m/z* 371.23 and its Na adducts. The mass differences found in the MSMS of $[M+3Na]$ *m/z* 437 is also indicative of a hydroxamate-type siderophore (Feistner et al., 1993; Mawji et al., 2008b).

For the second incubation experiment (at station 2), the MS of the sample from day 7 of the 30 m treatment, likewise showed presence of *m/z* 371.21 (Table 3). An additional peak *m/z* 551.11 $[M+H]^+$ was observed together with its $[M+Na]^+$ *m/z* 573.09 at a retention time of 30.8 min. Mass differences of fragment ions indicated the presence of hydroxamate moieties, typical for ferrioxamine fragmentation (Feistner et al., 1993; Mawji et al., 2008b). The sample taken from day 7 of the 100 m treatment of station 2 yielded sodiated *m/z* 371.21 ($[M+2Na]$ *m/z* 415.24;

[M+3Na] m/z 437.23) and two ferri-siderophore-type ions ([M+H+Fe-3H]⁺) m/z 473.27 and m/z 495.24 (Table 3). The MSMS fragments of these two precursor ions suggests that the parent molecule may possibly be a ferrioxamine hydroxamate-type siderophore (Feistner et al., 1993; Mawji et al., 2008b). Further MS and MSMS spectra are given in the Supplementary Material.

DISCUSSION

Production of Iron-Complexing Ligands and Dissolved Iron

In this study, we demonstrate that samples with marine particles in the presence of live particle-attached culturable bacteria produce or release iron binding ligands and DFe, whereas treatments with sterilized particles did not. In a previous remineralization experiment during a Southern Ocean study (subpolar and polar waters, SAZ-Sense study), it was also shown that in filter-sterilized samples (<0.2 μm) neither the concentration of iron binding ligand, nor that of DFe increased significantly (Boyd et al., 2010). Unsurprisingly, it can be concluded that marine particles incubated in the dark were remineralized by attached bacteria (as the free-living bacteria were removed from the sea water, See Materials and Methods) and as a result Fe-binding ligands were produced at pM rates per day.

Table 2 shows calculations performed to estimate ligand production and DFe release rates in the concentrated particle suspension and converted to ambient seawater concentrations. The daily ligand production rate in seawater ranges from 2.54 $\text{pmol L}^{-1} \text{d}^{-1}$ (100 m depth) to 11.8 $\text{pmol L}^{-1} \text{d}^{-1}$ (30 m) for station 1, and rates for station 2 were slightly lower (see Table 2). Consideration of the estimated molecular size of Fe-binding ligands, in the order of 500–700 Da (e.g., DFB with 25 carbon atoms), means the ligand production rate can be converted into a DOC concentration and linked to a consumption of POC (see Table 2). For station 1, less POC was converted to L (0.094 and 0.016% for 30 and 100 m) than for station 2 where 0.117 and 0.068% of POC was converted to L per day.

The remineralization of PFe and the resulting release of DFe have also been calculated (Table 2). Since no PFe analysis was done directly in the incubations, the PFe concentrations from ambient seawater at the same depth one day after or before our sampling were used and extrapolated to our remineralization experiment. Errors associated with this extrapolation may be in the order of $\pm 10\%$, but orders of magnitude of the ratio of PFe being remineralized to DFe per day can still be ascertained of being between 0.026 and 0.097%.

In the present study, $\sim 2 \text{ pM L}^{-1} \text{d}^{-1}$ of ligands were released or produced at a depth of 100 m, and around $10 \text{ pM L}^{-1} \text{d}^{-1}$ at 30 m (see Table 2) in the subtropical waters East of New Zealand. In contrasting water masses (polar HNLC Southern Ocean, and a complex transition zone between subantarctic and subtropical waters), release rates were comparable in subsurface waters from $\sim 110 \text{ m}$ depth, i.e., 16.2 and $7.2 \text{ pM L}^{-1} \text{d}^{-1}$ (Boyd et al., 2010). These values were all calculated for ambient seawater

particle concentrations and display a surprising constancy across contrasting water masses.

Similarly, the DFe release rates were very comparable in all three water masses (subtropical, subantarctic, polar) ranging from $0.3 \text{ pmol L}^{-1} \text{day}^{-1}$ at 100 m in station 1 of the present study up to $3.6 \text{ pmol L}^{-1} \text{day}^{-1}$ at 111 m depth (subantarctic, Boyd et al., 2010). Interestingly PFe concentrations in the present study were one order of magnitude higher than in the water masses used in the Boyd et al. (2010) study. This discrepancy raises the question of which PFe pool will most likely be available for bacteria to be remineralized. In Boyd et al. (2010), it was postulated that detrital PFe, which contributes mostly to PFe export flux in the Southern Ocean waters (i.e., PFZ study site; Frew et al., 2006; Sarthou et al., 2008) would be the source of DFe during remineralization over a greater depth horizon, while algal PFe would probably be restricted mainly in the stratum within the mixed layer. This however cannot explain the release rates observed here as all but station 2, 100 m were within the mixed layer.

The column integrated DFe release calculated from values in Table 2 is $107 \text{ nmol m}^{-2} \text{day}^{-1}$ at station 1 and $58.1 \text{ nmol m}^{-2} \text{day}^{-1}$ at station 2 (for 30–100 m). These values compare well with results from the previous remineralization experiment (Boyd et al., 2010), i.e., $42 \text{ nmol m}^{-2} \text{day}^{-1}$ and $108 \text{ nmol m}^{-2} \text{day}^{-1}$ at the polar and subantarctic sites, respectively.

Given a mixed layer DFe inventory of $\sim 48 \text{ } \mu\text{mol m}^{-2}$ and $\sim 4 \text{ } \mu\text{mol m}^{-2}$ at the time of sampling for station 1 and 2 (Boyd et al., 2010), it would result in a DFe residence time of 1.2 and 0.18 years assuming that particle remineralization was the only source of iron to the mixed layer. These calculated residence times compares well with results from similar particle remineralization experiments in the PFZ and NSAZ of 0.4 and 0.2 year, respectively (Boyd et al., 2010) and those from a model simulation of the upper 103 m of a low-iron high-nutrient region, which were 1.4 year (Moore and Braucher, 2008). Our calculations are rough estimates for a body of water in the mixed layer right where we sampled. The lateral or vertical advection of DFe and any other biological process from biota $>5 \text{ } \mu\text{m}$ were not taken into account. The approximately one order of magnitude variability within 8 days in the same water mass demonstrates the dynamic of the process. Although it could be said that the residence times of iron binding ligands may be in the same order of magnitude we refrain from giving number here as the ligand concentration changed significantly throughout the bloom development and unfortunately we did not sample for a full ligand depth profile on day 254. Taking the ligand depth distribution from day 263 would make the residence time calculations meaningless.

The cell counts of both culturable bacteria types [i.e., heterotrophic bacterial community (MA) and Fe-binding ligand producing bacteria (CAS)] increased throughout all “live” particle treatment remineralization experiments (see Figure 4). The CAS assay is often used by microbiologist to test for siderophore production, however in general it detects any strong Fe-binding compound regardless of the function of the molecule. Thus, the increase in CAS active bacterial numbers may not necessarily prove that siderophore-producing bacteria

are present, but the increase in cell abundances at the end of the incubation provides evidence that Fe-binding ligand-producing bacteria are increasing in numbers in the suspension of particles (at greater than ambient concentrations) and these ligands may be siderophores. The failure to detect strong L_1 -type ligands in any of the treatments may mean that the concentration of siderophores produced is too low to be detected at the given DFe concentration or that the siderophores produced have stability constants $< \log K_{\text{FeL}_1, \text{Fe}^{3+}} = 22$ (Maldonado et al., 2005).

Although the bacterial community in the remineralization experiment was not characterized directly, such data was produced from ambient seawater and *in-situ* sediment trap incubations throughout the FeCycleII-Springbloom cruise. Results showed a very dynamic response of the community in this water mass throughout the bloom (LeClerc et al., 2014). They showed that the microbial community in the water column and particles collected in sediment traps (at 5 and 100 m depth) were very similar in their bacterial composition, and only bacterial abundances varied between the two different bloom phases and with depth. LeClerc et al. (2014) proposed the presence of a “core” microbial community in this locale. They also found that heterotrophic bacteria of the Roseobacter clade and some other bacteria rapidly colonized the particles from 5 to 100 m in high abundance. Roseobacter have been shown to produce siderophores (Poorvin et al., 2011) which may be a source of the ligands produced during our particle remineralization experiments.

The chemical characterization of Fe-binding ligands produced in the “live” particle treatments was done semi-quantitatively in methanolic extracts of the XAD-16. The CAS test is widely used due to its comprehensive, sensitive nature and can specifically detect Fe^{3+} binding ligands. In our study, CAS test gave positive results in all incubations at the end of the experiment. The negative results for the catecholate specific Arnow test may indicate either the absence of any catechol type of siderophore, or it could also mean that the catechol-functionality is sterically hindered. Samples from station 1 at 30 and 100 m, which were collected at the end (8 days) of the particle remineralization experiment were positive to Csaky (hydroxamate) and negative to both the catecholate sensitive Arnow and Rioux tests (Table 3). This suggests that the Fe-binding ligands produced during both incubations are likely hydroxamate-type siderophores. In particle remineralization incubations at station 2, two hydroxamate and a catechol type siderophores or a mixed type of siderophore may have been produced (Table 3).

The detected hydroxamate siderophores in the remineralization experiments only ranged from 9 to 24% of the $[\Sigma L]$. It may be an underestimate because the calculations were based on the concentration of hydroxamate compounds detected in the pre-concentrated XAD-16 methanol extracts and the extraction efficiency is $< 100\%$. It is not known what makes up the other 91–76% of Fe-binding ligands detected in our experiment, but exopolysaccharides, humic substances, porphyrins and others have also been shown to bind Fe at stability constants very similar to that detected in our experiments (Hutchins et al., 1999; Laglera and van den Berg, 2009; Hassler et al., 2011; Abualhaija and van den Berg, 2014).

We did not test for the presence of any of these compounds in this study.

Identification of Siderophores-Types by HPLC-MSMS

Molecular ions m/z 614.26 and m/z 672.28 were detected at the end of station 1's 30 m particle remineralization experiment. The mass spectrometry analysis suggests that these correspond to the well-known linear hydroxamate ferri-ferrioxamine B (DFB) $[\text{M}+\text{H}+\text{Fe}-3\text{H}]^+$ and ferri-ferrioxamine G (DFG) $[\text{M}+\text{H}+\text{Fe}-3\text{H}]^+$. The compounds were present at low intensity, however the Fe-isotopic pattern was very clear and the retention times fall within the elution time of the ferrioxamine B and G standards (Figures 5A–C). Feistner et al. (1993) reported that biosynthetic capabilities of an organism to produce siderophores can be flexible and considered the open chained ferrioxamines as biosynthetic intermediates of cyclic ferrioxamines (Feistner et al., 1993; Mawji et al., 2008b). But however, until to date, the presence of ferrioxamine B and G associated with the remineralization of marine particles had not been reported.

The ion m/z 585.31 did not exhibit the Fe-isotopic pattern, but, it was previously shown by (Feistner and Hsieh, 1995) that m/z 585 can be observed as a result of protonation at the N-terminal of the diaminopentane group, then followed by a charge-driven fragmentation in the N-terminal of the hydroxamate bond. The ion peak m/z 371.21 was found in station 1 at 30 and 100 m, and in station 2 at 30 m. Although it did not exhibit the Fe-isotopic pattern, the mass difference of its MSMS fragments were similar to those also obtained for the ferrioxamines (Feistner et al., 1993; Mawji et al., 2008b). In station 2 at the 100 m treatment, only the 2 and 3 Na adducts (m/z 415.24 and 437.23) of m/z 371.21 were obtained at the end of the experiment (7 days). The ion peak m/z 551.11 $[\text{M}+\text{H}]^+$ found in station 2 did not show the iron isotopic pattern (i.e., was not bound to Fe) in the 30 m sample, but the mass difference observed for the MSMS fragments were identical to those shown by Feistner et al. (1993) for ferrioxamines. Fe-bound ligands were observed for 100 m sample at station 2 which again showed fragmentation pattern of the hydroxamate ferrioxamine type siderophores. It is possible that the siderophores that we detected were photoproducts of siderophore molecules that were present in low levels. The Fe(III)-siderophore complex may have been truncated or undergone ligand oxidation due to photolysis leading to a lower binding strength (Barbeau et al., 2001). Molecular ions m/z 371, 551, 437, 415, 43, and 495 were also found in samples collected from ambient water which were not incubated (see Supplementary Material). No trace of m/z 585, 614, and 672 were observed in any extracts from the ambient samples.

It is clear that the siderophores found for both depths in each experiment are hydroxamates, but the known siderophores ferrioxamine B and G were only found in the incubation experiments of surface samples (30 m) from station 1. A shift in the dominant groups in the microbial community (LeClerc et al., 2014) will likely have an effect on the ligands present in the water and in the particulates. However, the information available from

our study is insufficient to clearly link the relationship between the microbes and the siderophore-type compounds that were identified.

CONCLUSION

In this study, two marine particle remineralization experiments were performed to investigate the production of ligands and the release of DFe in seawater at two depths at 30 and 100 m. Particulate samples were collected from the subtropical waters east of the North Island of New Zealand as part of the FeCycle II GEOTRACES process study. Significant ligand production was observed in treatments containing live particle attached heterotrophic bacteria. Hence, it can be concluded that some of the iron-complexing ligands measured in the ocean originated from the remineralization of particles.

Two main classes of ligands, namely strong (L_1) and sum of all ligands (ΣL), have been identified in our study. Open chained ferrioxamine B and G, as well as other unknown hydroxamate siderophores have been identified in samples from both particle remineralization experiments. Two other unidentified siderophore-types with their Na adducts were observed. The MSMS spectra of these compounds suggest that they are possibly hydroxamate types similar to ferrioxamines. The presence of siderophore-producing bacteria and results from other chemical assays suggest the mass spectrometric observations of siderophore production in the experimental treatments. The electrochemical analysis of L failed to detect L_1 from the samples, although siderophores were detected by MS. This finding questions whether siderophores present in the ocean are truly L_1 or their concentration and contribution into the ligand pool may be too small compared to other weaker organic

ligands produced during the remineralization and throughout in the open ocean.

AUTHOR CONTRIBUTIONS

IBV and SGS ran the experiment on board ship, PWB helped design the experiment. EWM measured bacterial data and helped their interpretation. EI performed voltammetric analysis, SN took particle samples and ran POC analysis. SGS, IBV, and EI wrote the manuscript which was commented by PWB and EWM.

FUNDING

EI and IBV received a University of Otago PhD scholarship. SGS and PWB were supported by Marsden grant UOO1117.

ACKNOWLEDGMENTS

Special thanks to the officers and crew members of *RV Tangaroa* during the FeCycle II study for making this work possible. We thank Michael Ellwood (PFe), Karen Thompson (nutrients and flow cytometry), and the trace metal clean sampling team onboard. We acknowledge financial support from the University of Otago, the National Institute of Water and Atmospheric Research (NIWA), and the Hanse-Wissenschaftskolleg Institute for Advanced Study, Delmenhorst, Germany.

SUPPLEMENTARY MATERIAL

The Supplementary Material for this article can be found online at: <http://journal.frontiersin.org/article/10.3389/fmars.2016.00172>

REFERENCES

- Abualhija, M. M., and van den Berg, C. M. G. (2014). Chemical speciation of iron in seawater using catalytic cathodic stripping voltammetry with ligand competition against salicylaldehyde. *Mar. Chem.* 164, 60–74. doi: 10.1016/j.marchem.2014.06.005
- Adly, C. L., Tremblay, J.-E., Powell, R. T., Armstrong, E., Peers, G., and Price, N. M. (2015). Response of heterotrophic bacteria in a mesoscale iron enrichment in the northeast subarctic Pacific Ocean. *Limnol. Oceanogr.* 60, 136–148. doi: 10.1002/lno.10013
- Arnou, L. E. (1937). Colorimetric determination of the components of 3,4-dihydroxyphenylalanine-tyrosine mixtures. *J. Biol. Chem.* 118, 531–537.
- Barbeau, K., Rue, E. L., Bruland, K. W., and Butler, A. (2001). Photochemical cycling of iron in the surface ocean mediated by microbial iron (III) -binding ligands. *Nature* 413, 409–413. doi: 10.1038/35096545
- Behrenfeld, M. J., Bale, A. J., Kolber, Z. S., Aiken, J., and Falkowski, P. G. (1996). Confirmation of iron limitation of phytoplankton photosynthesis in the equatorial Pacific Ocean. *Nature* 383, 508–511. doi: 10.1038/383508a0
- Boyd, P., Watson, A., Law, C., Abraham, E., Trull, T., Murdoch, R., et al. (2000). A mesoscale phytoplankton bloom in the polar Southern Ocean stimulated by iron fertilization. *Nature* 407, 695–702. doi: 10.1038/35037500
- Boyd, P. W., Iribarne, E., Sander, S. G., Hunter, K. A., and Jackson, G. A. (2010). Remineralization of upper ocean particles: implications for iron biogeochemistry. *Limnol. Oceanogr.* 55, 1271–1288. doi: 10.4319/lno.2010.55.3.1271
- Boyd, P. W., Law, C. S., Hutchins, D. A., Abraham, E. R., Croft, P. L., Ellwood, M., et al. (2005). FeCycle: attempting an iron biogeochemical budget from a mesoscale SF6 tracer experiment in unperturbed low iron waters. *Global Biogeochem. Cycles* 19:GB4S20. doi: 10.1029/2005GB002494
- Boyd, P. W., Strzpek, R., Chiswell, S., Chang, H., DeBruyn, J. M., Ellwood, M., et al. (2012). Microbial control of diatom bloom dynamics in the open ocean. *Geophys. Res. Lett.* 39:L18601. doi: 10.1029/2012GL053448
- Boye, M., van den Berg, C., de Jong, J., Leach, H., Croft, P. L., and de Baar, H. J. W. (2001). Organic complexation of iron in the Southern Ocean. *Deep Sea Res.* 48, 1477–1497. doi: 10.1016/S0967-0637(00)00099-6
- Buck, K. N., Lohan, M. C., Berger, C. J. M., and Bruland, K. W. (2007). Dissolved iron speciation in two distinct river plumes and an estuary: implications for riverine iron supply. *Limnol. Oceanogr.* 52, 843–855. doi: 10.4319/lno.2007.52.2.0843
- Buck, K. N., Sohst, B., and Sedwick, P. N. (2015). The organic complexation of dissolved iron along the U.S. GEOTRACES (GA03) North Atlantic Section. *Deep Sea Res. Part II* 116, 152–165. doi: 10.1016/j.dsr2.2014.11.016
- Bundy, R. M., Biller, D. V., Buck, K. N., Bruland, K. W., and Barbeau, K. A. (2014). Distinct pools of dissolved iron-binding ligands in the surface and benthic boundary layer of the California Current. *Limnol. Oceanogr.* 59, 769–787. doi: 10.4319/lno.2014.59.3.0769
- Croft, P. L., and Johansson, M. (2000). Determination of Iron Speciation by Cathodic Stripping Voltammetry in Seawater Using the Competing Ligand 2-(2-Thiazolylazo)-p-cresol (TAC). *Electroanalysis* 12, 565–576. doi: 10.1002/(SICI)1521-4109(200005)12:8<565::AID-ELAN565>3.0.CO;2-L

- De Hoffman, K., and Stroobant, V. (1991). Fast atom bombardment Tandem Mass spectrometric analysis of hydroxamate siderophores. *Biol. Mass Spectrom.* 20, 142–152. doi: 10.1002/bms.1200200308
- Ellwood, M. J., Hutchins, D. A., Lohan, M. C., Milne, A., Nasemann, P., Nodder, S. D., et al. (2015). Iron stable isotopes track pelagic iron cycling during a subtropical phytoplankton bloom. *Proc. Natl. Acad. Sci. U.S.A.* 112, E15–E20. doi: 10.1073/pnas.1421576112
- Ellwood, M. J., Nodder, S. D., King, A. L., Hutchins, D. A., Wilhelm, S. W., and Boyd, P. W. (2014). Pelagic iron cycling during the subtropical spring bloom, east of New Zealand. *Mar. Chem.* 160, 18–33. doi: 10.1016/j.marchem.2014.01.004
- Feistner, G. J., and Hsieh, L. L. (1995). On the collision-activated fragmentation of ferrioxamines: evidence for a succinimide-mediated mechanism. *J. Am. Soc. Mass Spectrom.* 6, 836–846. doi: 10.1016/1044-0305(95)00324-7
- Feistner, G. J., Stahl, D. C., and Gabrik, A. H. (1993). Ferrioxamine siderophores of *Erwinia Amylovora*. A capillary liquid chromatographic/Electrospray tandem mass spectrometric study. *J. Mass Spectrom.* 28, 163–175.
- Frew, R., Bowie, A., Croot, P., and Pickmere, S. (2001). Nutrient and trace metal geochemistry of an *in situ* iron-induced Southern Ocean bloom. *Deep Sea Res. Part II: Top. Stud. Oceanogr.* 48, 2467–2481. doi: 10.1016/S0967-0645(01)00004-2
- Frew, R. D., Hutchins, D. A., Nodder, S., Sanudo-Wilhelmy, S., Tovar-Sanchez, A., Leblanc, K., et al. (2006). Particulate iron dynamics during FeCycle in subantarctic waters southeast of New Zealand. *Global Biogeochem. Cycles* 20:GB1S93. doi: 10.1029/2005GB002558
- Geider, R. J., and La Roche, J. (1994). The role of iron in phytoplankton photosynthesis, and the potential for iron-limitation of primary productivity in the sea. *Photosyn. Res.* 39, 275–301. doi: 10.1007/BF00014588
- Gillam, A. H., Lewis, A. G., and Andersen, R. J. (1981). Quantitative determination of hydroxamic acids. *Anal. Chem.* 53, 841–844. doi: 10.1021/ac00229a023
- Gledhill, A., McCormack, P., Ussher, S., Achterberg, E., Mantoura, R. F. C., and Worsfold, P. J. (2004). Production of siderophore type chelates by mixed bacterioplankton populations in nutrient enriched seawater incubations. *Mar. Chem.* 88, 75–83. doi: 10.1016/j.marchem.2004.03.003
- Gledhill, M., and Buck, K. N. (2012). The organic complexation of iron in the marine environment: a review. *Front. Microbiol.* 3:69. doi: 10.3389/fmicb.2012.00069
- Gledhill, M., and van den Berg, C. M. G. (1994). Determination of complexation of iron(III) with natural organic complexing ligands in seawater using cathodic stripping voltammetry. *Mar. Chem.* 47, 41–54. doi: 10.1016/0304-4203(94)90012-4
- Hassler, C. S., Schoemann, V., Nichols, C. M., Butler, E. C. V., and Boyd, P. W. (2011). Saccharides enhance iron bioavailability to Southern Ocean phytoplankton. *Proc. Natl. Acad. Sci. U.S.A.* 108, 1076–1081. doi: 10.1073/pnas.1010963108
- Hunter, K. A., and Boyd, P. W. (2007). Iron-binding ligands and their role in the ocean biogeochemistry of iron. *Environ. Chem.* 4, 221–232. doi: 10.1071/EN07012
- Hutchins, D. A., Witter, A. E., Butler, A., and Luther, G. W. (1999). Competition among marine phytoplankton for different chelated iron species. *Nature (London)* 400, 858–861.
- Ibanmi, E., Sander, S. G., Boyd, P. W., Bowie, A. R., and Hunter, K. A. (2011). Vertical distributions of iron-(III) complexing ligands in the Southern Ocean. *Deep Sea Res. II: Top. Stud. Oceanogr.* 58, 2113–2125. doi: 10.1016/j.dsr.2.2011.05.028
- Laglera, L. M., and van den Berg, C. M. G. (2009). Evidence for geochemical control of iron by humic substances in seawater. *Limnol. Oceanogr.* 54, 610–619. doi: 10.4319/lo.2009.54.2.0610
- Lebaron, P., Ghiglione, J.-F., Fajon, C., Batailler, N., and Normand, P. (1998). Phenotypic and genetic diversity within a colony morphotype. *FEMS Microbiol. Lett.* 160, 137–143. doi: 10.1111/j.1574-6968.1998.tb12903.x
- LeClerc, G. R., DeBruyn, J. M., Maas, E. W., Boyd, P. W., and Wilhelm, S. W. (2014). Temporal changes in particle-associated microbial communities after interception by nonlethal sediment traps. *FEMS Microbiol. Ecol.* 87, 153–163. doi: 10.1111/1574-6941.12213
- Lenes, J. M., Walsh, J. J., Prospero, J. M., and Byrne, R. H. (2009). Response to “Aerosol iron deposition to the surface ocean - Modes of iron supply and biological responses” by PW Boyd, DS Mackie, and KA Hunter. *Mar. Chem.* 116, 56–57. doi: 10.1016/j.marchem.2009.07.006
- Mahmood, A., Abualhaja, M. M., van den Berg, C. M. G., and Sander, S. G. (2015). Organic speciation of dissolved iron in estuarine and coastal waters at multiple analytical windows. *Mar. Chem.* 177(Pt 5), 706–719. doi: 10.1016/j.marchem.2015.11.001
- Maldonado, M. T., Strzepek, R. F., Sander, S., and Boyd, P. W. (2005). Acquisition of iron bound to strong organic complexes-with different Fe binding groups and photochemical reactivities by plankton communities in Fe-limited subantarctic waters. *Global Biogeochem. Cycles* 19:GB4S23. doi: 10.1029/2005GB002481
- Martinez, J. S., Haygood, M. G., and Butler, A. (2001). Identification of a natural desferrioxamine siderophore produced by a marine bacterium. *Limnol. Oceanogr.* 46(Suppl. 7), 420–424. doi: 10.4319/lo.2001.46.2.0420
- Mawji, E., Gledhill, M., Milton, J. A., Tarran, G. A., Ussher, S., Thompson, A., et al. (2008a). Hydroxamate Siderophores: Occurrence and Importance in the Atlantic Ocean. *Environ. Sci. Technol.* 42, 8675–8680. doi: 10.1021/es801884r
- Mawji, E., Gledhill, M., Worsfold, P. J., and Achterberg, E. P. (2008b). Collision-induced dissociation of three groups of hydroxamate siderophores: ferrioxamines, ferrichromes and coprogens/fusigens. *Rapid Commun. Mass Spectrom.* 22, 2195–2202. doi: 10.1002/rcm.3604
- Moore, C. M., Mills, M. M., Arrigo, K. R., Berman-Frank, I., Bopp, L., Boyd, P. W., et al. (2013). Processes and patterns of oceanic nutrient limitation. *Nat. Geosci.* 6, 701–710. doi: 10.1038/ngeo1765
- Moore, J. K., and Braucher, O. (2008). Sedimentary and mineral dust sources of dissolved iron to the world ocean. *Biogeochemistry* 5, 631–656. doi: 10.5194/bg-5-631-2008
- Morel, F. M. M., and Price, I. G. (2003). The biogeochemical cycles of trace metals in the oceans. *Science* 300, 944–947. doi: 10.1126/science.1083545
- Omanović, D., Garnier, C., and Pižeta, I. (2015). ProMCC: an all-in-one tool for trace metal complexation studies. *Mar. Chem.* 173, 25–39. doi: 10.1016/j.marchem.2014.10.011
- Pižeta, I., Sander, S. G., Hudson, R. J. M., Omanović, D., Baars, O., Barbeau, K. A., et al. (2015). Interpretation of complexometric titration data: an intercomparison of methods for estimating models of trace metal complexation by natural organic ligands. *Mar. Chem.* 173, 3–24. doi: 10.1016/j.marchem.2015.03.006
- Poorvin, L., Sander, S. G., Velasquez, I., Ibanmi, E., LeClerc, G. R., and Wilhelm, S. W. (2011). A comparison of Fe bioavailability and binding of a catecholate siderophore with virus-mediated lysates from the marine bacterium *Vibrio alginolyticus* PWH3a. *J. Exp. Mar. Biol. Ecol.* 399, 43–47. doi: 10.1016/j.jembe.2011.01.016
- Reid, R. T., Live, D. H., Faulkner, D. J., and Butler, A. (1993). A siderophore from a marine bacterium with an exceptional ferric iron affinity constant. *Nature (London)* 366, 455–458. doi: 10.1038/366455a0
- Rioux, C., Jordan, D. C., and Rattray, J. B. M. (1983). Colorimetric determination of catechol siderophores in microbial cultures. *Anal. Biochem.* 133, 163–169. doi: 10.1016/0003-2697(83)90238-5
- Rue, E. L., and Bruland, K. W. (1995). Complexation of iron (III) by natural organic-ligands in the Central North Pacific as determined by a new competitive ligand equilibration adsorptive cathodic stripping voltammetric method. *Mar. Chem.* 50, 117–138. doi: 10.1016/0304-4203(95)00031-L
- Rue, E. L., and Bruland, K. W. (1997). The role of organic complexation on ambient iron chemistry in the Equatorial Pacific Ocean and the response of a mesoscale iron addition experiment. *Limnol. Oceanogr.* 42, 901–910. doi: 10.4319/lo.1997.42.5.0901
- Sander, S. G., Hunter, K. A., Harms, H., and Wells, M. (2011). Numerical approach to speciation and estimation of parameters used in modeling trace metal bioavailability. *Environ. Sci. Technol.* 45, 6388–6395. doi: 10.1021/es20113v
- Sander, S. G., Tian, F., Ibanmi, E. B., Currie, K. I., Hunter, K. A., and Frew, R. D. (2015). Spatial and seasonal variations of iron speciation in surface waters of the Subantarctic front and the Otago Continental Shelf. *Mar. Chem.* 173, 114–124. doi: 10.1016/j.marchem.2014.09.001
- Sander, S., Hunter, K., and Frew, R. (2009). “Sampling and measurement of trace metals in seawater,” in *Practical Guidelines for the Analysis of Seawater*, ed O. Wurl (Boca Raton, FL: CRC Press), 305–328.

- Sarthou, G., Vincent, D., Christaki, U., Obernoster, I., Timmermans, K. R., and Brussaard, C. P. D. (2008). The fate of biogenic iron during a phytoplankton bloom induced by natural fertilisation: impact of copepod grazing. *Deep Sea Res. II* 55, 734–752. doi: 10.1016/j.dsr2.2007.12.033
- Schwyn, B., and Neilands, J. B. (1987). Universal chemical assay for the detection and determination of siderophores. *Anal. Biochem.* 160, 47–56. doi: 10.1016/0003-2697(87)90612-9
- Tian, F., Frew, R., Strzepek, R., and Ellwood, M. (2006). “Iron organic complexation in the oligotrophic subtropical waters in the Tasman Sea,” in *Advances in Geoscience*, eds W.-H. Ip and Y.-T. Chen (Singapore: World Scientific Publishing Company), 75–89.
- Turner, S. M., Harvey, M. J., Law, C. S., Nightingale, P. D., and Liss, P. S. (2004). Iron-induced changes in oceanic sulfur biogeochemistry. *Geophys. Res. Lett.* 31:L14307. doi: 10.1029/2004GL020296
- Van den Berg, C. M. G. (1995). Evidence for organic complexation of iron in seawater. *Mar. Chem.* 50, 139–157. doi: 10.1016/0304-4203(95)00032-M
- Velasquez, I., Nunn, B. L., Ibsanmi, E., Goodlett, D. R., Hunter, K. A., and Sander, S. G. (2011). Detection of hydroxamate siderophores in coastal and Sub-Antarctic waters off the South Eastern Coast of New Zealand. *Mar. Chem.* 126, 97–107. doi: 10.1016/j.marchem.2011.04.003
- Weller, D. I., Law, C. S., Marriner, A., Nodder, S. D., Chang, F. H., Stephens, J. A., et al. (2013). Temporal variation of dissolved methane in a subtropical mesoscale eddy during a phytoplankton bloom in the southwest Pacific Ocean. *Prog. Oceanogr.* 116, 193–206. doi: 10.1016/j.pcean.2013.07.008
- Wells, M., Buck, K. N., and Sander, S. G. (2013). New approach to analysis of voltammetric ligand titration data improves understanding of metal speciation in natural waters. *Limnol. Oceanogr. Methods* 11, 450–465. doi: 10.4319/lom.2013.11.450
- Wilhelm, S. W., and Trick, C. G. (1994). Iron-limited growth of cyanobacteria; multiple siderophore production is a common response. *Limnol. Oceanogr.* 39, 1979–1984. doi: 10.4319/lo.1994.39.8.1979

Conflict of Interest Statement: The authors declare that the research was conducted in the absence of any commercial or financial relationships that could be construed as a potential conflict of interest.

Copyright © 2016 Velasquez, Ibsanmi, Maas, Boyd, Nodder and Sander. This is an open-access article distributed under the terms of the Creative Commons Attribution License (CC BY). The use, distribution or reproduction in other forums is permitted, provided the original author(s) or licensor are credited and that the original publication in this journal is cited, in accordance with accepted academic practice. No use, distribution or reproduction is permitted which does not comply with these terms.



Iron-Binding Ligands in the Southern California Current System: Mechanistic Studies

Randelle M. Bundy^{1*}, Mingshun Jiang², Melissa Carter¹ and Katherine A. Barbeau¹

¹ Geosciences Research Division, Scripps Institution of Oceanography, University of California, San Diego, San Diego, CA, USA, ² Harbor Branch Oceanographic Institute, Florida Atlantic University, Fort Pierce, FL, USA

The distributions of dissolved iron and organic iron-binding ligands were examined in water column profiles and deckboard incubation experiments in the southern California Current System (sCCS) along a transition from coastal to semi-oligotrophic waters. Analysis of the iron-binding ligand pool by competitive ligand exchange-adsorptive cathodic stripping voltammetry (CLE-ACSV) using multiple analytical windows (MAWs) revealed three classes of iron-binding ligands present throughout the water column (L_1 – L_3), whose distributions closely matched those of dissolved iron and nitrate. Despite significant biogeochemical gradients, ligand profiles were similar between stations, with surface minima in strong ligands (L_1 and L_2), and relatively constant concentrations of weaker ligands (L_3) down to 500 m. A phytoplankton grow-out incubation, initiated from an iron-limited water mass, showed dynamic temporal cycling of iron-binding ligands. A biological iron model was able to capture the patterns of the strong ligands in the grow-out incubation relatively well with only the microbial community as a biological source. An experiment focused on remineralization of particulate organic matter showed production of both strong and weak iron-binding ligands by the heterotrophic community, supporting a mechanism for *in-situ* production of both strong and weak iron-binding ligands in the subsurface water column. Photochemical experiments showed a variable influence of sunlight on the degradation of natural iron-binding ligands, providing some evidence to explain differences in surface ligand concentrations between stations. Patterns in ligand distributions between profiles and in the incubation experiments were primarily related to macronutrient concentrations, suggesting microbial remineralization processes might dominate on longer time-scales over short-term changes associated with photochemistry or phytoplankton growth.

Keywords: California Current Ecosystem, long term ecological research, iron limitation, dissolved iron-binding ligands, multiple analytical windows, electrochemistry

OPEN ACCESS

Edited by:

Maeve Carroll Lohan,
University of Southampton, UK

Reviewed by:

Christel Hassler,
University of Geneva, Switzerland
Julian Blasco,
Spanish National Research Council,
Spain

*Correspondence:

Randelle M. Bundy
rbundy@whoi.edu

Specialty section:

This article was submitted to
Marine Biogeochemistry,
a section of the journal
Frontiers in Marine Science

Received: 29 October 2015

Accepted: 29 February 2016

Published: 15 March 2016

Citation:

Bundy RM, Jiang M, Carter M and
Barbeau KA (2016) Iron-Binding
Ligands in the Southern California
Current System: Mechanistic Studies.
Front. Mar. Sci. 3:27.
doi: 10.3389/fmars.2016.00027

Abbreviations: CCS, California Current System; Chl *a*, chlorophyll *a*; CLE-ACSV, competitive ligand exchange-adsorptive cathodic stripping voltammetry; CSV, cathodic stripping voltammetry; CTD, conductivity, temperature, and depth sensor; dFe, dissolved Fe; DOC, dissolved organic carbon; DOM, dissolved organic matter; Fe, iron; FPE, fluorinated polyethylene; GF/F, glass fiber filter; HCl, hydrochloric acid; HMW, high molecular weight; HNLC, high nutrient low chlorophyll; HPLC, high performance liquid chromatography; LDPE, low density polyethylene; LTER, Long Term Ecological Research; L_x , an iron binding ligand class, where *x* denotes ligand class (1–4); MAWs, multiple analytical windows; MilliQ, purified water; POC, particulate organic carbon; PON, particulate organic nitrogen; S, salinity; S_{IN} , internal sensitivity; SA, salicylaldoxime; SAFe, Sampling and Analysis of iron (Fe); UV light, ultra-violet light.

INTRODUCTION

Dissolved iron (dFe) is an essential trace element for microbial growth in large areas of the ocean (Morel and Price, 2003). Phytoplankton growth in high nutrient low chlorophyll (HNLC) regions is especially susceptible to iron (Fe) limitation in surface waters (Martin et al., 1991). Some coastal eastern boundary upwelling regions such as the California Current System (CCS) can also have a range of Fe-limiting conditions, from the nearshore continental shelf to the transition zone extending 10–250 km offshore (Hutchins et al., 1998; King and Barbeau, 2007, 2011; Biller and Bruland, 2014). Iron (Fe) is necessary for primary production, but it is often scarce and almost always associated with a heterogeneous pool of organic ligands with varying reactivities (Rue and Bruland, 1995; van den Berg, 1995; Wu and Luther, 1995). Bacteria and phytoplankton must therefore use an assortment of cellular tools in order to access dFe from this diverse organic matter matrix (Granger and Price, 1999; Hutchins et al., 1999; Maldonado and Price, 1999), and determining the chemical nature of these unknown organic ligands is important for understanding the mechanisms of Fe-acquisition in the ocean.

Although dFe-binding ligands can be directly isolated from seawater (e.g., Mawji et al., 2008), dFe-binding organic ligands are most commonly detected using indirect electrochemical methods such as competitive ligand exchange-adsorptive cathodic stripping voltammetry (CLE-ACSV), which classifies ligands based on their concentrations and binding strengths (see review by Gledhill and Buck, 2012). The strengths of some of the strongest ligands identified in the ocean by electrochemical methods are nearly identical to model siderophores found in culture media. Likely, the dFe-binding ligands measured by electrochemistry could range from highly specific low molecular weight siderophore-type ligands to large macromolecules with only weak dFe-binding (Gledhill and Buck, 2012). The strongest dFe-binding ligands appear to be largely biologically produced, both as a strategy for combating Fe-limitation (Maldonado et al., 2002; Buck et al., 2010; Mawji et al., 2011) and for preventing Fe precipitation (Reid et al., 1993; Kondo et al., 2008). Cultured bacteria have been shown to produce siderophores (Amin et al., 2009; Vraspir and Butler, 2009), and CLE-ACSV measurements made in conjunction with high performance liquid chromatography (HPLC) methods have identified siderophores associated with natural bacteria assemblages (Gledhill et al., 2004; Mawji et al., 2011). Microbial communities may also be an *in-situ* source of weaker ligands to the subsurface water column during the remineralization of particulate organic matter (Boyd et al., 2010). It appears that bacteria may be a source of both strong and weak dFe-binding ligands in certain conditions, but it is less certain whether there are other biological processes affecting the distribution of dFe-binding ligands. Ligand maxima in the water column, for example, are often associated with the chlorophyll *a* maxima (Boye et al., 2001, 2005, 2006; Croot et al., 2004; Wagener et al., 2008; Ibisanni et al., 2011). However, it is still not clear from field studies what mechanisms may cause the elevated ligand concentrations at this depth in the water column.

In addition to biological changes to the ligand pool, photochemistry can also affect the concentration and strength of dFe-binding ligands. Laboratory studies have shown that some siderophores can be degraded by natural sunlight when bound to dFe, and their binding strength is subsequently decreased (Barbeau et al., 2001, 2003; Barbeau, 2006). This mechanism has been invoked to describe the minima in strong ligands often seen in surface waters (Gledhill and Buck, 2012). However, field studies to date have demonstrated mixed results with respect to photochemical degradation of natural dFe-binding ligands (Powell and Wilson-Finelli, 2003; Rijkenberg et al., 2006). Despite varied results in the field, modeling studies routinely invoke a photochemical sink of dFe-binding ligands in surface waters (Parekh et al., 2005; Fan, 2008; Tagliabue et al., 2009; Tagliabue and Volker, 2011; Jiang et al., 2013).

Although data suggests the presence of strong and weak dFe-binding ligands throughout the water column, the mechanisms linking ligand distributions to sources and sinks have not been well studied. This is despite the advent of large-scale projects such as GEOTRACES, which have vastly increased the number and spatial coverage of ligand measurements (Thuróczy et al., 2010, 2011a,b; Sander et al., 2014; Buck et al., 2015; Gerringa et al., 2015). Data in the Pacific is still forthcoming, but measurements from both Buck et al. (2015) and Gerringa et al. (2015) in the Atlantic, show the presence of strong dFe-binding ligands ($\log K_{FeL,Fe'}^{cond} > 12$) in the entire water column. Estimates from a meridional transect by Gerringa et al. (2015) suggest that these ligands are potentially long-lived relative to dFe (residence time of 779–1039 years), perhaps partly explaining their ubiquitous presence. These large datasets are critical not only for understanding ligand sources and sinks, but also for informing current biogeochemical modeling efforts, which are increasingly incorporating dFe-binding ligands (Archer and Johnson, 2000; Moore et al., 2004; Parekh et al., 2005; Fan, 2008; Moore and Braucher, 2008; Tagliabue et al., 2009; Tagliabue and Volker, 2011; Jiang et al., 2013; Boyd and Tagliabue, 2015).

Modeling studies have shown that incorporating dFe-binding ligand dynamics can have a large effect on the observed dFe concentrations (Tagliabue et al., 2014). Implementing ligand dynamics in biogeochemical models has so far been challenging however, because a spectrum of dFe-binding ligand strengths has been found to exist in seawater with a range of conditional stability constants ($\log K_{FeL,Fe'}^{cond}$) from 9.0 to 14.0 (Hunter and Boyd, 2007; Gledhill and Buck, 2012). Most studies to date have concentrated on measuring one particular ligand class in this spectrum, often denoted as strong “L₁” ligands or weaker “L₂” ligands. Based on recommendations from Gledhill and Buck (2012) some recent studies however, have focused on measuring several dFe-binding ligand classes in the same sample using CLE-ACSV with multiple analytical windows (MAWs; Bundy et al., 2014a,b; Sander et al., 2014; Mahmood et al., 2015) or displaying their data in terms of absolute rather than relative $\log K_{FeL,Fe'}^{cond}$ (Buck et al., 2015). These approaches have shed some light on the potential sources and sinks of both stronger and weaker ligands in the water column, but thus far MAW analysis has been restricted to the benthic boundary layer (Bundy et al., 2014a,b) and surface waters (Bundy et al.,

2014a,b; Sander et al., 2014; Mahmood et al., 2015). In Bundy et al. (2014a,b), a range of dFe-binding ligand strengths were detected and denoted as L₁–L₄. These ligand classes span the range of ligand strengths that have been observed in many other studies (Gledhill and Buck, 2012), but the processes associated with L₁–L₄ distributions in the subsurface water column are still uncertain. This study makes the first upper ocean profile measurements of dFe-binding organic ligands utilizing MAW CLE-ACSV, and seeks to link profile data with mechanistic deckboard dFe speciation studies carried out on the same cruise in the southern California Current region, also employing MAW CLE-ACSV.

METHODS

Sampling Region and Environmental Context

Samples for this study were collected as part of the California Current Ecosystem (CCE) Long-Term Ecological Research (LTER) program (<http://cce.lternet.edu/>) in the southern California Bight (Figure 1) on-board the R/V *Melville* in June–July 2011. This cruise was a CCE-LTER process cruise, which uses drifters in a Langrangian platform to follow distinct water masses (Landry et al., 2009; Krause et al., 2015). Each series of stations sampled within the same water mass were denoted as a “cycle” (Brzezinski et al., 2015; Krause et al., 2015). However, only one station from each cycle was sampled in this particular study, so sampling locations will simply be referred to as stations. Each station has been given the same number as the cycle to which it belongs (for example, station 1 was part of cycle 1) in order to compare to other studies from the same cruise (e.g., Brzezinski et al., 2015; Krause et al., 2015).

Sampling and Storage

All trace-metal clean samples were collected either using single Teflon-coated 12 L GO-Flo bottles (General Oceanics) mounted directly on non-metallic hydroline or 5 L X-Niskin bottles (Ocean Test Equipment) mounted on a powder-coated rosette deployed

on non-metallic hydroline (Cutter and Bruland, 2012) according to the methods described in Brzezinski et al. (2015). Filtered samples for dFe analysis were placed in 250 mL low-density polyethylene (LDPE) bottles, acidified to pH 1.8 (Optima HCl) and stored for at least 3 months until analysis in the lab. Samples collected for dFe-binding ligands were either run immediately (within 3 days) or stored frozen at -20°C until analysis. Results for fresh vs. frozen analyses of dFe-binding ligands have been shown to be indistinguishable in previous studies (Buck et al., 2012).

Filtered samples for silicate ($\text{Si}(\text{OH})_4$), phosphate (PO_4^{3-}), nitrate (nitrate+nitrite; denoted as NO_3^-), and chlorophyll *a* (chl *a*) were taken from the standard CTD rosette cast and on-board incubation experiments. Nutrient samples were collected in 40 ml polypropylene centrifuge tubes (Fisher Scientific) and frozen at -20°C before analysis. Chl *a* and phytoplankton pigment samples were placed in dark bottles and filtered onto glass fiber filters (GF/F filters, Fisher Scientific). Chl *a* samples were subsequently placed in acetone and analyzed on-board. Pigment samples were put in cryovials (Nalgene) and stored in liquid nitrogen until analysis in the lab. Microscopy samples for phytoplankton cell counts were collected in 50 mL glass vials and stored in 1% tetraborate buffered formalin until analysis.

Nutrients and Phytoplankton

Chl *a* samples from the depth-profiles and incubation experiments were run immediately on-board the ship, after being extracted for 24 h in acetone at -20°C . Chl *a* samples were analyzed using a Turner Designs 10-AU Fluorometer, fitted with a red-sensitive photomultiplier tube. Phytoplankton pigment samples were analyzed by HPLC according to Zapata et al. (2000). Macronutrients from the water column profiles and incubation experiments were analyzed by the Marine Science Institute Analytical Lab at the University of California Santa Barbara (<http://msi.ucsb.edu/services/analytical-lab>) using a Lachat QuickChem 8000. Samples for phytoplankton cell counts were first adjusted by volume to 60 mL before settling in a 50 mL Utermöhl settling chamber. They were then counted using a Zeiss phase-contrast inverted light microscope at 200x magnification (Utermöhl, 1958; UNESCO, 1981). Phytoplankton were classified by genera or the following broad categories: *Chaetoceros* spp., *Pseudo-nitzschia* spp., other diatoms ($>10\ \mu\text{m}$), dinoflagellates, flagellates ($<10\ \mu\text{m}$), and ciliates. The sample volume enumerated ranged from 5.6 to 1.1 mL (1/9 of slide) and detectable cell abundances were between 245 and 1227 cells L^{-1} , depending on the volume settled.

Dissolved Iron

The dFe was analyzed by flow injection analysis (FIA) after complete reduction of the dFe with sulfite according to King and Barbeau (2007, 2011). This method has been shown to yield accurate results with respect to SAFE (S1 and D2) and GEOTRACES (GS) consensus samples, and has a detection limit of $0.07\ \text{nmol L}^{-1}$ (three times the standard deviation of the blank, $n = 72$). Values obtained for S1 ($0.11 \pm 0.02\ \text{nmol L}^{-1}$, $n = 39$), D2 ($0.93 \pm 0.07\ \text{nmol L}^{-1}$, $n = 36$), and GS ($0.51 \pm 0.02\ \text{nmol L}^{-1}$, $n = 12$) compare well to the most recent

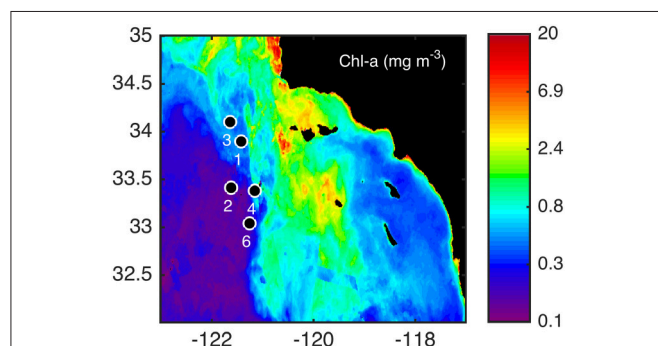


FIGURE 1 | Sampling locations for water column profiles and incubation experiments during the June/July 2011 cruise. Stations were sampled in the coastal (3, 4), frontal (1, 6), and oceanic (2) side of a distinct frontal feature (Brzezinski et al., 2015; Krause et al., 2015) shown over the averaged chlorophyll *a* (chl-*a*; mg m^{-3}) for the month of July in 2011.

consensus values (<http://es.ucsc.edu/~kbruland/GeotracesSaFe/kwbGeotracesSaFe.html>).

Dissolved Iron-Binding Ligands

The analysis of dFe-binding ligands was completed using (CLE-ACSV). This method has been used extensively for determining the concentration and binding strengths of dFe-binding ligands in seawater (see a recent review by Gledhill and Buck, 2012). Briefly, a natural sample is titrated with dFe in order to saturate the natural ligands. Then, a well-characterized electroactive ligand is added, in this case salicylaldoxime (SA). SA competes with the natural ligands for dFe, and the Fe(SA)_x complex is deposited on the mercury drop, and analyzed using adsorptive cathodic stripping voltammetry (ACSV) on a hanging mercury drop electrode (BioAnalytical Systems, Incorporated).

Titration were performed by first adding 50 μl of a 1.5 mol L^{-1} boric acid-ammonium buffer (sample pH = 8.2, NBS scale) to 10 mL aliquots of the sample. Next, 0–25 nmol L^{-1} dFe (range varied depending on the detection window) was added to 11 separate conditioned Teflon vials (Savillex) containing the sample and buffer. The buffer and dFe were left to equilibrate with the natural ligands in the sample for 2 h, before adding the appropriate concentration of SA depending on the detection window (17.7, 25.0, or 32.3 $\mu\text{mol L}^{-1}$ SA). The SA was equilibrated for 15 min before each aliquot was run separately using ACSV with a 150 s deposition time. All electrochemical parameters were the same as have been reported previously (Rue and Bruland, 1995; Buck et al., 2007), and all constants for SA were updated to the most recent calibration reported by Abualhaija and van den Berg (2014). Peak heights were determined using ECDSOFT and the sensitivity was optimized in ProMCC (Omanović et al., 2014). Results from selected samples at a single analytical window were also confirmed using BackCalc. Ligand concentrations and strengths were calculated both by traditional linearization techniques and using a unified multi-window approach (Hudson et al., 2003). The results between these two methods compared well when initial guesses from linearization techniques were used (Bundy et al., 2014a). However, a common sensitivity ratio (R_{AL}) has not yet been empirically determined for Fe MAW CLE-ACSV, because of a paucity of MAW data for Fe from a variety of lab groups and is an essential parameter in the unified multi-window approach (Mahmood et al., 2015). Since a rigorous intercomparison has yet to be completed for dFe-binding ligand titration data using new numerical methods, and an empirical R_{AL} has not yet been published, traditional linearization approaches were used in this study and are reported as the average between the concentration and strengths determined by a Ružić/van den Berg linearization (Mantoura and Riley, 1975) and Scatchard linearization (Scatchard, 1949). Although linearization approaches generally have higher error functions than numerical models of metal speciation when tested with artificial data (Pižeta et al., 2015), linear models still compare well with numerical speciation models when the sensitivity is optimized.

The concentration of the added ligand determines the detection window of the method, or the strength of the ligands

that can be detected. A higher detection window targets stronger ligands, while a lower window targets weaker ligands. For this study, three different concentrations of SA were used, or three detection windows, in order to examine several distinct ligand classes ($[\text{SA}] = 17.7, 25.0, \text{ and } 32.3 \mu\text{mol L}^{-1}$, $\alpha_{\text{Fe(SA)}_x} = 75, 115, \text{ and } 162$). One ligand class was detected at each analytical window, except the lowest detection window ($[\text{SA}] = 17.7 \mu\text{mol L}^{-1}$) where two ligand classes were detected. Each subsequent titration was performed with at least three points of overlap from the previous titration (in terms of the dFe additions), with the lowest analytical window having the highest dFe additions at the end of the titration. The strongest ligand class (L_1) was determined at the highest detection window (32.3 $\mu\text{mol L}^{-1}$ SA), the next ligand class (L_2) was detected at the middle detection window (25.0 $\mu\text{mol L}^{-1}$ SA) and the weakest ligand classes (L_3 and L_4) were detected at the lowest detection window (17.7 $\mu\text{mol L}^{-1}$ SA). The conditional stability constants defined for each ligand class was defined as $\log K_{\text{FeL}_1, \text{Fe}'}^{\text{cond}} \geq 12.0$ for L_1 , $\log K_{\text{FeL}_2, \text{Fe}'}^{\text{cond}} = 11.0$ – 12.0 for L_2 , $\log K_{\text{FeL}_3, \text{Fe}'}^{\text{cond}} = 10.0$ – 11.0 for L_3 , and $\log K_{\text{FeL}_4, \text{Fe}'}^{\text{cond}} \leq 10.0$ for L_4 (Bundy et al., 2014a,b).

Experimental Set-Up

Biological Incubation Experiments

Two experiments were conducted in this study to address biological sources of dFe-binding ligands in the CCS: one Fe addition phytoplankton grow-out experiment (experiment 1) and one remineralization experiment (experiment 2), which immediately followed the termination of the grow-out experiment. Both experiments were conducted at station 3 from water collected at 30 m in the subsurface chl *a* maximum (Figure 1). Whole seawater was collected and homogenized in a clean 50 L carboy before being aliquoted into acid-cleaned 4 L polycarbonate (PC) bottles. Experiments 1 and 2 contained a set of three unamended controls (Control A, B, and C) and three +Fe bottles (5 nmol L^{-1} FeCl_3 ; +Fe A, B, and C). All six bottles for experiments 1 and 2 were placed in on-deck flow-through incubators screened to 30% light levels, which were similar to *in-situ* light and temperature conditions. Bottles for experiment 2 were placed in 2 heavy-duty black garbage bags and also placed in the on-deck flow-through incubator. Experiment 1 was terminated after 6 days, and experiment 2 was terminated after 3 days. Experiment 2 was initiated using the phytoplankton biomass that had accumulated in the controls and +Fe treatments at the end of experiment 1, and were simply placed in the dark following the termination of the light portion of experiment 1 on day 6.

Samples for chl *a*, macronutrients [NO_3^- , PO_4^{3-} , and Si(OH)_4], phytoplankton pigments, phytoplankton cell counts, dFe, and dFe-binding ligands were taken from experiment 1. Experiment 2 was only sampled for dFe and dFe-binding ligands. Samples for chl *a* were taken every day from all six bottles in experiments 1, and macronutrients were sampled every 2 days from all six bottles. Pigment concentrations and phytoplankton cell counts were sampled on day 0 from the 50 L carboy (initial conditions) and day 6 (final conditions) in all controls and +Fe

bottles. The dFe and dFe-binding ligands were sampled every day in experiment 1, but only from one bottle of each treatment until day 6, when all bottles were sampled. For example, Control A and +Fe A bottles were sampled on days 1, 4, and 6, Control B and +Fe B were sampled on days 2, 5, and 6, and Control C and +Fe C were sampled on days 3 and 6. The dFe and ligands for experiment 2 were sampled on day 0, and then on day 3 (final conditions) from all treatments. A subset of the data from experiment 1 is also shown in Brzezinski et al. (2015).

Photochemical Experiments

Photochemical experiments were performed at stations 1, 2, and 6 at the depth of the chl *a* maximum (30, 70, and 20 m, respectively). Trace metal clean seawater was collected before sunrise and filtered in-line with a 0.2 μm Acropak-200 filter. Filtered seawater was homogenized in a clean carboy and dispensed into four conditioned quartz flasks with Teflon stoppers (Quartz Scientific). Two of the flasks were wrapped tightly in aluminum foil for the dark controls. All four flasks were placed in a shallow plastic tray coupled to the on-deck flow-through incubators and left in the natural sunlight for 12 h. Samples for dFe and dFe-binding ligands were taken randomly from one of the dark flasks for the initial time-point, and from each bottle (Dark A, B and Light A, B) at the end of the 12 h.

Modeling

A biological Fe model developed for the Southern Ocean (Jiang et al., 2013) was modified to test the experimental results of incubation experiment 1. The model resolves the classical food web and microbial loop, including three types of nutrients [NO_3^- , $\text{Si}(\text{OH})_4$, Fe] and two types of dFe-binding ligands (L_1 , L_2). The Fe cycle is simulated with five Fe species including dissolved inorganic Fe (Fe^3), dissolved Fe bound to the two stronger ligand classes ($\text{Fe}L_1$ and $\text{Fe}L_2$), and colloidal Fe and particulate Fe. The ligand dynamics include most of the key processes including bio-complexation, photo-degradation, thermal dissociation, L_1 ligand production by bacteria during Fe-stress conditions, and L_2 ligand production by the remineralization of particulate organic matter and via photochemical degradation of L_1 . No ligand production due to phytoplankton growth or zooplankton grazing is included (e.g., Barbeau et al., 1996; Sato et al., 2007), and there was no attempt to model the weakest ligand classes (L_3 and L_4). The model has been tested with data from shipboard grow-out incubation experiments and *in-situ* data during two cruises in the Antarctic Peninsula area, through zero-dimensional and one-dimensional experiments, respectively (Jiang et al., 2013). In this project, some of the model parameters were adjusted to the lower macronutrient conditions in the southern CCE (Table 1).

Statistical Analyses

A Pearson's correlation analysis was performed using the Statistics Toolbox in Matlab with all data from CTD profiles and the incubation experiment, including the dFe and ligand data. Missing values were replaced using a regression with depth for the profile data, or a regression with time for the incubation data

TABLE 1 | Ancillary measurements made in the water column as part of the CCE-LTER program for biological experiment 1 and used as initial parameters in the model.

Parameter	Measured value	Model initial value
PAR ($\mu\text{E m}^{-2} \text{ s}^{-1}$)	263.7	263.7
Temperature ($^{\circ}\text{C}$)	13.4	13.4
Chlorophyll (mg m^{-3})	0.93	0.99 ^a
Dissolved Fe (nmol L^{-1})	0.54 (5.54)	0.54 (3.54) ^b
Nitrate ($\mu\text{mol L}^{-1}$)	11.5	11.5
Silicate ($\mu\text{mol L}^{-1}$)	2.49	2.49
Particulate N ($\mu\text{mol L}^{-1}$)	1.015	1
DON ($\mu\text{mol L}^{-1}$)	8.8 ^c	10
Bacterial biomass ($\mu\text{mol L}^{-1}$)	0.27 ^d	0.27
L_1 (nmol L^{-1})	1.69	1.69
L_2 (nmol L^{-1})	0.86	0.86

^aThe model specifies the initial small phytoplankton and diatom biomass based on the measured chlorophyll using a C/N ratio of 6.625 and C/Chl ratio of 40:1.

^bModel initial Fe concentration for the plus Fe experiment was adjusted because the model was unable to reproduce the initial drop of about 2 nmol L^{-1} .

^cDON was converted from measured DOC ($58.4 \mu\text{mol L}^{-1}$) using a C/N ratio of 6.625.

^dBacteria biomass was converted from measured bacteria abundance ($1.07 \times 10^9 \text{ cells L}^{-1}$) using a biomass to cell ratio $20 \text{ mgC}/10^9 \text{ cells}$ (Lee and Fuhrman, 1987) and a Redfield C:N molar ratio of 6.625:1.

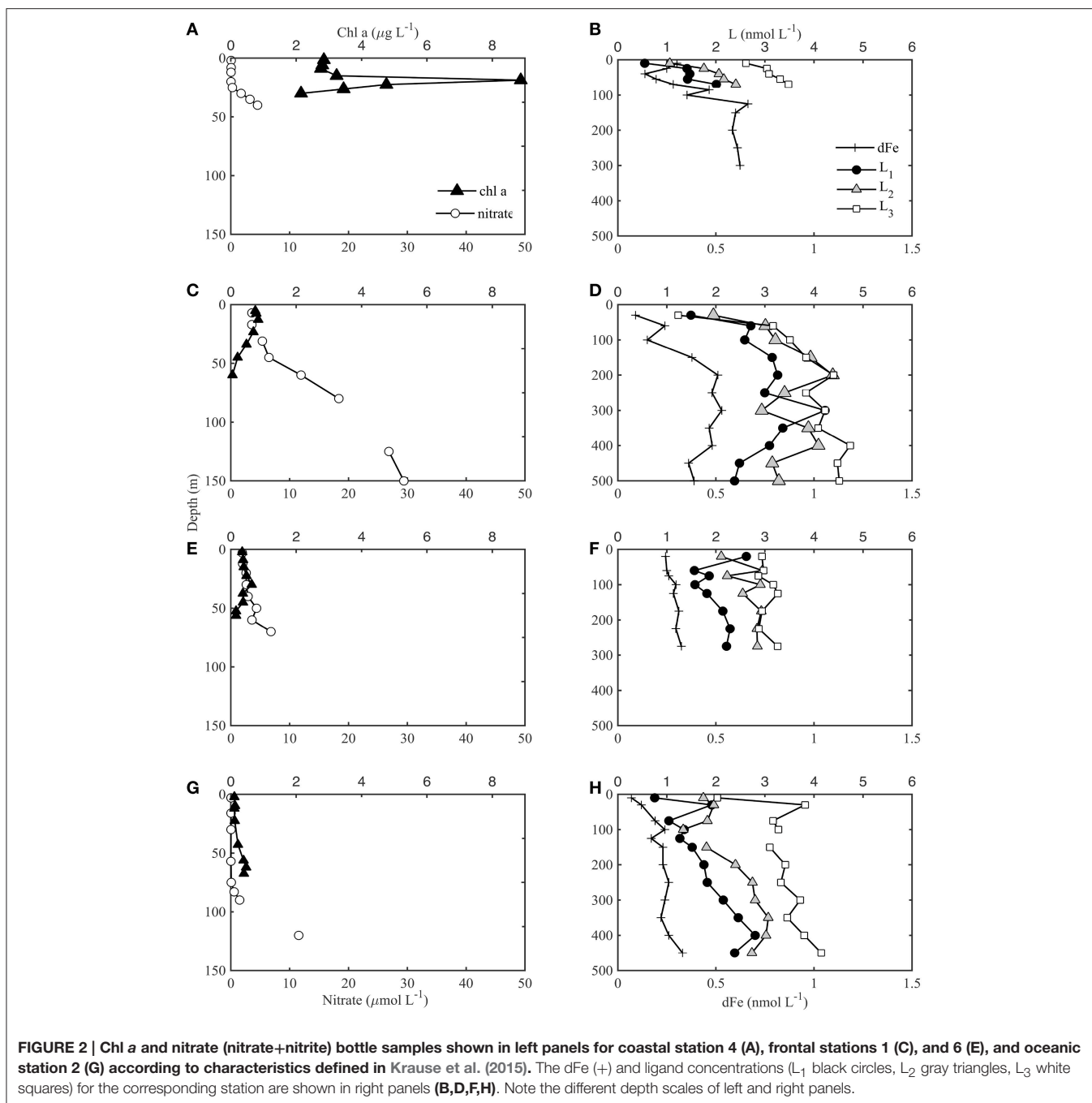
and all correlation coefficients are reported at the 95% confidence interval.

RESULTS

Water Column Profiles

Each station was loosely grouped as coastal, frontal or oceanic based on physical characteristics. CTD data was obtained for all stations (1–4 and 6, data not shown), and dFe and dFe-binding ligand depth profiles were collected for stations 1, 2, 4, and 6. Stations 3 and 4 were classified as coastal stations, stations 1 and 6 were frontal stations, and station 2 was considered oceanic, based on defined water mass characteristics in relation to a persistent frontal feature between cyclonic and anticyclonic eddies that was sampled in this region as part of the CCE-LTER program (Brzezinski et al., 2015; Krause et al., 2015). The depth and magnitude of the chl *a* maximum and nitracline corresponded well with these groupings, for the stations shown in Figure 2 where dFe and ligands were also sampled. Coastal station 4 (Figure 2A) was characterized by a relatively shallow biomass maximum (<50 m) and nitracline (<20 m). Very high chl *a* concentrations were observed at station 4 (up to $9 \mu\text{g L}^{-1}$), corresponding with almost complete drawdown of NO_3^- in surface waters. The frontal stations (Figures 2C,E) were hydrographically similar to the coastal stations but had a slightly deeper nitracline (40–50 m) and lower [chl *a*]. The oceanic station (station 2, Figure 2G) had a much deeper nitracline (> 50 m) and a deep chl *a* maximum relative to the coastal stations.

The [dFe] ranged from $<0.3 \text{ nmol L}^{-1}$ in surface waters to $\sim 0.8 \text{ nmol L}^{-1}$ at 500 m in the coastal station (Figure 2B). DFe in the southern CCS is characterized by low concentrations offshore and a deep ferricline, often deeper than 100 m (King and Barbeau, 2011). The dFe-binding ligands show a similar pattern



to dFe (Figure 2). The strongest ligands (L_1 , $\log K_{FeL_1, Fe'}^{cond} \geq 12.0$) were present throughout the water column down to 500 m (the deepest depth sampled). Most of the profiles showed a subsurface maxima in L_1 associated with the biomass maxima and then minima, before increasing slightly again at depths below 100 m. Although there were elevated L_1 concentrations at the chl *a* maxima, there were not higher ligand concentrations associated with the large bloom at station 4 (Figures 2A,B). Three of the four stations showed a minimum in L_1 in surface waters (Figures 2B,D,H), but frontal station 6 had elevated L_1 concentrations at the shallowest depth sampled (20 m,

Figure 2F). There is also some evidence at the base of the profiles that L_1 might begin to decline below 500 m, but it is difficult to determine without more sampling depths. For a detailed tabulation of all dFe and ligand profile data see the Supplementary Information (SI-1).

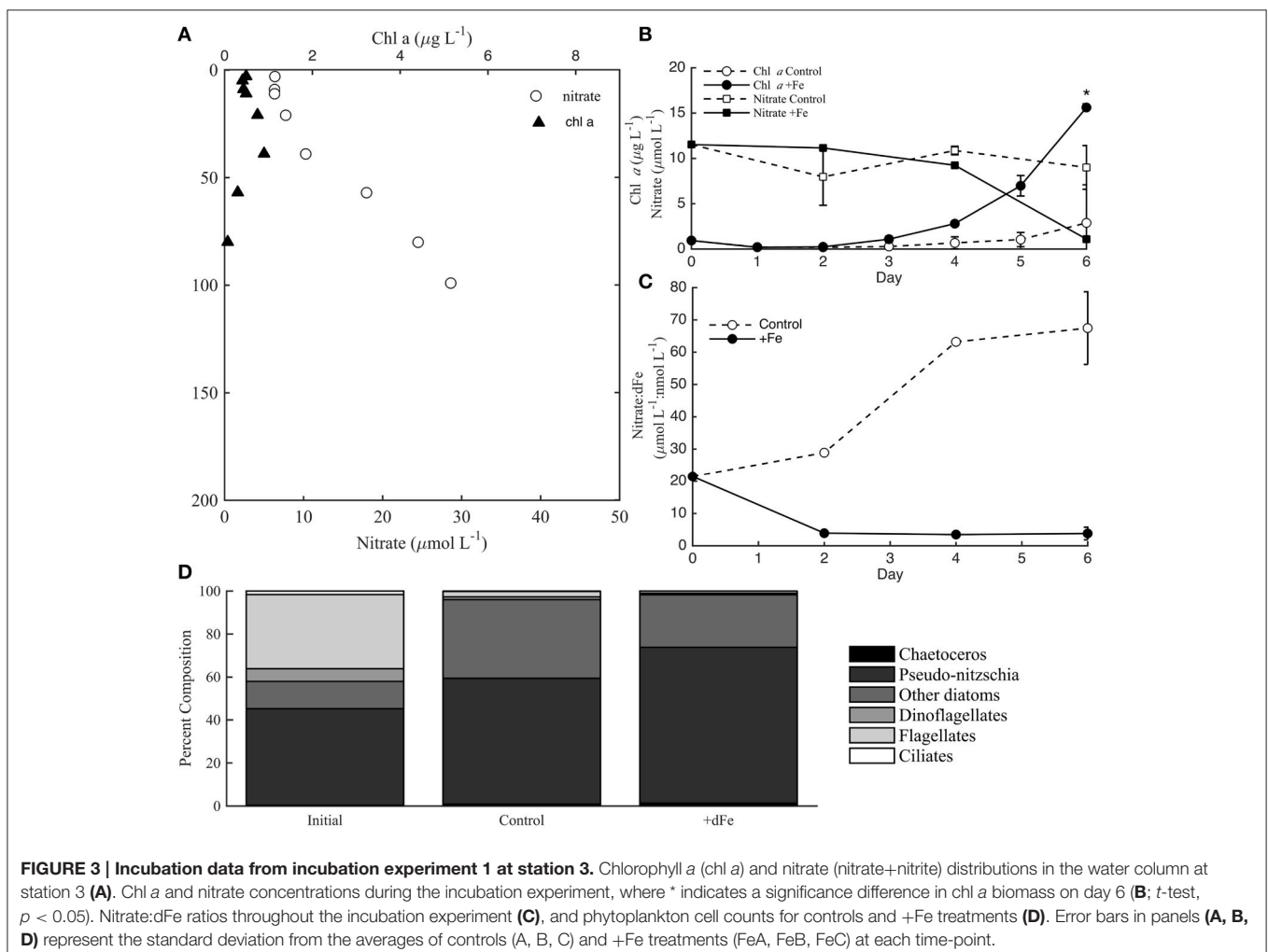
L_2 ligands ($\log K_{FeL_2, Fe'}^{cond} = 11.0-12.0$) were present in slightly higher concentrations than L_1 throughout most of the water column, but had a similar distribution with depth. There is also some evidence that L_2 began to decrease below 400 m at stations 1 and 2, but more sampling depths would be needed to confirm this pattern in deep waters. The L_2 concentration

was greatest at frontal station 1 (ranging from 1.5 to 4.2 nmol L⁻¹) compared to the other three stations where L₂ did not exceed 3 nmol L⁻¹. This matched the pattern in dFe and other ligand concentrations, perhaps due to enhanced mixing associated with the frontal zone at this station (Krause et al., 2015). L₃ was relatively distinct from the stronger ligands. [L₃] remained mostly constant throughout the water column, with a few exceptions in surface waters (Figures 2B,D,F,H). [L₃] was higher at the coastal station (station 4) and oceanic station (station 2) than in the frontal region. The highest concentrations of weaker ligands (L₃) in the upper 100 m were found in the oceanic station (stations 2), and the lowest concentrations of weaker ligands were in the frontal waters at stations 1 and 6. On average, this pattern was opposite for the stronger ligands. No L₄ ligands were detected in any of the profiles at any of the depths sampled. Pearson's correlation analysis for the profile data showed the strongest correlations between each of the ligand classes and nitrate (Supplementary Information SI-2), while relatively strong negative correlations were also observed with some of the variables that decrease with depth such as oxygen.

Biological Ligand Production Experiments

Incubation Experiment 1

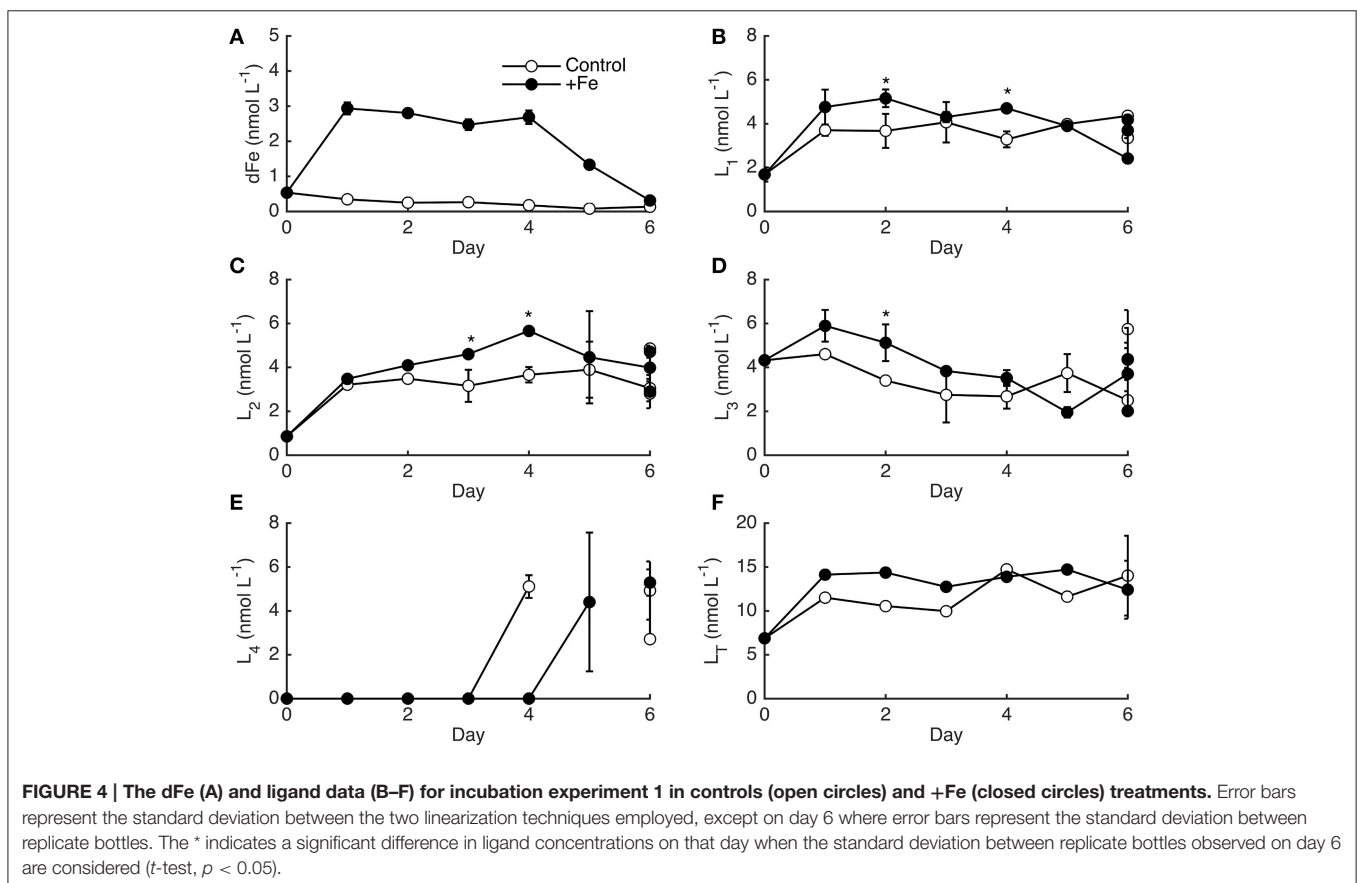
Experiment 1 was sampled at 30 m from an aged, upwelled water mass that had likely originated nearshore near Point Conception (Brzezinski et al., 2015; Krause et al., 2015). The initial conditions for the experiment had relatively elevated macronutrient concentrations (11.5 μmol L⁻¹ NO₃⁻; Figure 3A) and dFe (0.54 nmol L⁻¹). Thus, the phytoplankton community was likely not macronutrient limited. Little NO₃⁻ was drawn-down in controls, but significant macronutrient drawdown was observed by day 4 of the experiment in +Fe treatments (Figure 3B). The macronutrient drawdown was accompanied by a significant increase in chl *a* biomass in +Fe treatments compared to controls by day 6 (*t*-test, *p* < 0.05). Although the initial phytoplankton community was relatively diverse (Figure 3D), the increase in biomass by day 6 was almost entirely due to an increase in the abundance of diatoms, mostly *Pseudo-nitzschia* spp. (Figure 3D). The increase in diatoms was apparent both from cell counts (Figure 3D) and from elevated fucoxanthin pigment concentrations compared to initial conditions (Brzezinski et al., 2015). Although the total

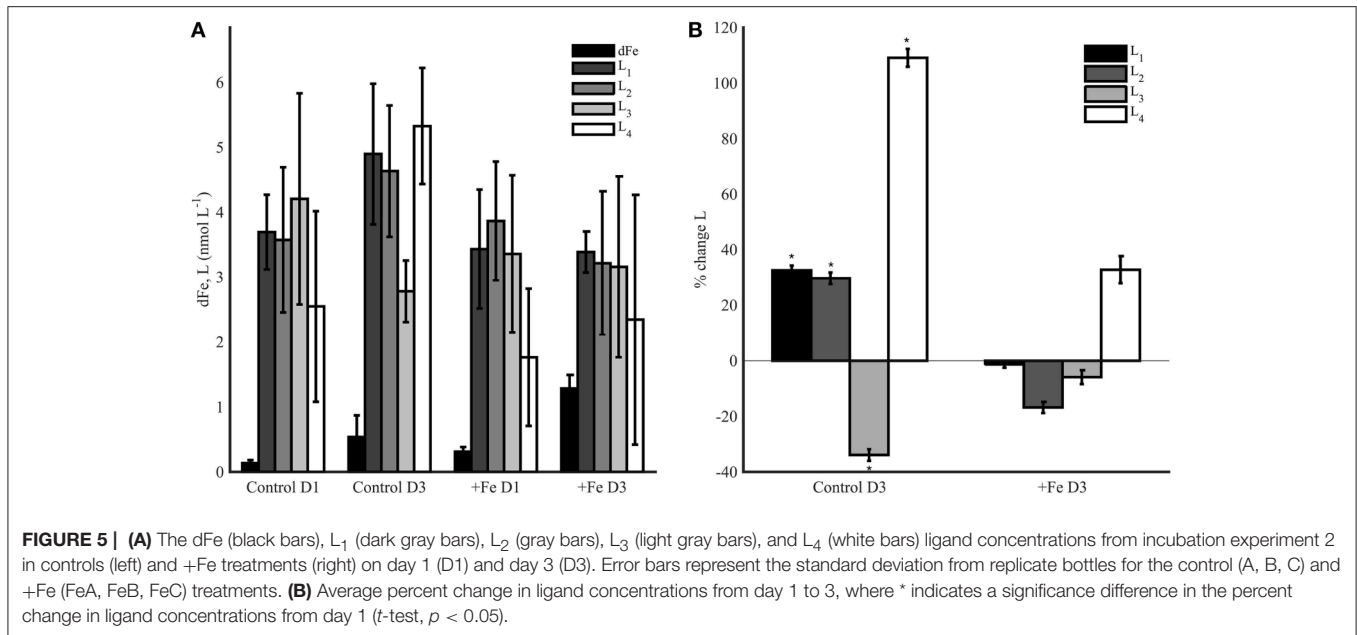


biomass was much higher in +Fe treatments, the phytoplankton community structure was very similar between the controls and +Fe treatments (Figure 3D). Even though the composition of the phytoplankton community was not significantly different between controls and +Fe treatments, the evolution of NO_3^- compared to dFe (NO_3^- : dFe; $\mu\text{mol L}^{-1}$: nmol L^{-1}) over the course of the experiment was drastically different in controls and +Fe bottles (Figure 3C). Previous work in this region has shown that NO_3^- : dFe ($\mu\text{mol L}^{-1}$: nmol L^{-1}) ratios greater than 12 are indicative of Fe-limitation of the diatom community (King and Barbeau, 2007). The initial water mass contained a NO_3^- : dFe ratio of 21.5, likely indicating that the diatom community was initially Fe-limited. However, the 5 nmol L^{-1} dFe addition in +Fe bottles appeared to alleviate this Fe-limitation based on the NO_3^- : dFe ratios observed over the course of the experiment (Figure 3C), and the increase in biomass by day 6 (Figure 3B).

Although the phytoplankton biomass response differed between controls and +Fe treatments, the temporal pattern of dFe-binding ligands was very similar (Figure 4), especially when considering the variability between bottle replicates on day 6. Most of the dFe was drawn-down in +Fe treatments after day 4 (Figure 4A), concomitant with the increase in phytoplankton biomass and decrease in NO_3^- . The dFe decreased slightly in controls, likely due to a combination of uptake and scavenging to the walls of the bottles. The strongest

ligands (L_1) increased in both controls and +Fe treatments from days 0 to 1, and then remained relatively constant for the remainder of the experiment, with slightly higher ligand concentrations on day 6 in two of the +Fe bottles (Figure 4B). L_2 ligands increased relatively consistently over the 6 days of the experiment (Figure 4C). The weaker ligands showed distinct temporal patterns compared to the stronger ligands, with L_3 slowly decreasing during the sampling period and L_4 ligands only appearing on days 4–6 (Figures 4D,E). Significant differences in ligand classes on each day of incubation experiment 1 were determined by accounting for the average percent standard deviation between replicate bottles that was observed on day 6 rather than from replicate titrations since only one bottle from each treatment was measured each day. The average percent standard deviation from replicate bottles (21% for L_1 , 27% for L_2 , 37% for L_3 , and 21% for L_4) was higher than the standard deviations observed between titrations (9% for L_1 , 12% for L_2 , 13% for L_3 , and 14% for L_4). The average ligand concentrations for each ligand class on day 6 were not statistically distinct in controls and +Fe treatments (*t*-test, $p > 0.05$), but certain days throughout the grow-out showed statistically significant differences in ligand concentrations (Figure 4). In general however, the overall temporal ligand patterns in controls and +Fe treatments were very similar between treatments.





Incubation Experiment 2

Experiment 2 was conducted in the dark for 3 days following the termination of experiment 1 on day 6. Control and +Fe bottles initially contained different amounts of phytoplankton biomass (Figure 3B), but relatively similar dFe and ligand concentrations (Figure 5A). The goal of this experiment was to assess microbial alteration of the ligand pool in response to distinct amounts of particulate biomass and Fe. Control bottles contained $0.14 \pm 0.05 \text{ nmol L}^{-1}$ dFe ($n = 3$) on day 1 of the experiment, and by day 3, $0.54 \pm 0.33 \text{ nmol L}^{-1}$ dFe had been remineralized ($n = 3$). In +Fe treatments the dFe increased from $0.31 \pm 0.07 \text{ nmol L}^{-1}$ ($n = 3$) on day 1 to $1.29 \pm 0.21 \text{ nmol L}^{-1}$ ($n = 3$) on day 3. In general, ligands increased more in the controls than in the +Fe treatments (Figure 5A), though there was high variability between replicate bottles. L₁ ligands increased by $32.6 \pm 1.7\%$ on average in controls ($n = 3$), but they decreased by $1.3 \pm 1.2\%$ in +Fe bottles ($n = 3$; Figure 5B). A similar pattern was seen for L₂ ligands, which increased by $29.7 \pm 2.1\%$ in control treatments, but decreased by $16.8 \pm 2.0\%$ in +Fe bottles ($n = 3$). L₃ ligands decreased in both treatments, but by a significantly higher percentage (*t*-test, $p < 0.05$) in controls ($33.9 \pm 2.1\%$) than in the +Fe case ($5.9 \pm 2.5\%$). The weakest ligands (L₄) showed the greatest change between days 1 and 3 in both treatments, but increased by a significantly (*t*-test, $p < 0.05$) greater percentage in controls ($109.1 \pm 3.2\%$) compared to +Fe bottles ($32.8 \pm 4.9\%$, $n = 3$). In general, the average concentration of total ligands (L₁+L₂+L₃+L₄) was higher in controls on day 3 than in +Fe bottles on day 3 (*t*-test, $p < 0.05$).

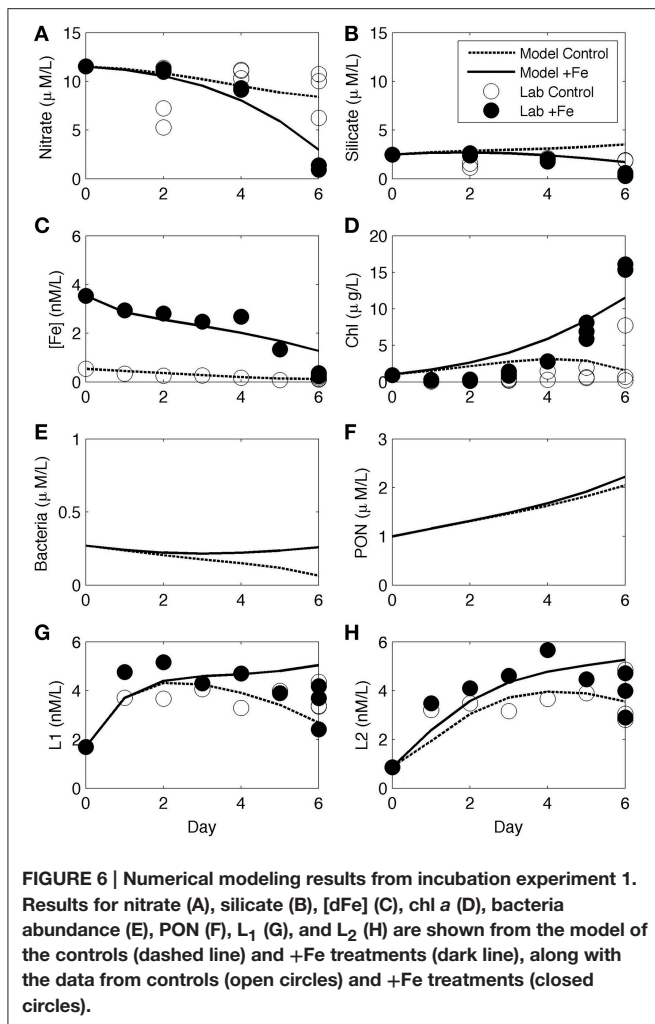
Modeling of Incubation Experiment 1

Numerical experiments were performed for incubation experiment 1 in order to investigate biological ligand sources and sinks based on non-measured parameters (e.g., bacterial

growth rate and abundance). As part of the CCE-LTER program, other ancillary data including some rate measurements were obtained at the same station and depth for experiment 1 (station 3) and were used as the initial values of key parameters in the model, with some adjustments (Table 1). Changes in nutrient concentrations over time both in control and +Fe treatments (Figures 6A–C) and the increase in chl *a* (Figure 6D) were all reasonably reproduced by the model. No measurements were made for bacterial abundance or organic matter concentrations during the course of experiment 1, but the model results show an increase in both bacteria and particulate organic nitrogen (PON) in +Fe treatments (Figures 6E,F). The temporal patterns in L₁ and L₂ were also described relatively well, with the exception of day 6, where the model shows greater separation between controls and +Fe bottles (Figures 6G, H). Initial ligand production in the model (days 0–2) is due to rapid ligand production in both treatments from residual Fe stress of the initial water mass (expressed as bacteria stress in the model), and constant photochemical degradation in both treatments. Lower rates of ligand production in later days of the incubation are because of higher ligand degradation rates (proportional to ligand concentrations) and lower bacteria biomass in the control case, as expressed in the model. The differences between treatments in the model become apparent between days 4 and 6, owing to larger differences in bacteria biomass and organic matter in +Fe treatments (Figures 6E,G) and ligand production from PON (e.g., Boyd et al., 2010).

Photochemical Experiments

Each photochemical experiment was completed using water collected from the chl *a* maximum at each station (30 m for station 1, 70 m for station 2, and 20 m for station 6). The first experiment at station 1 contained similar concentrations



of strong ligands in the initial condition and dark treatments, and slightly higher [L₂] were observed in the light treatment (Figure 7A), though the differences were not significant (*t*-test, $p > 0.05$). No weaker ligands (L₃) were observed in this experiment in the initial or final conditions. Experiments 2 and 3 from stations 2 and 6, respectively, showed different results (Figures 7B,C). Again, the dark bottles contained similar [dFe] and ligands as initial conditions in both experiments, but light treatments had lower concentrations of L₁ ligands and also contained L₃ ligands, which were absent initially and in the dark treatments (Figures 7B,C). The weakest ligands measured in this study (L₄ ligands) were not detected in any of the photochemical experiments.

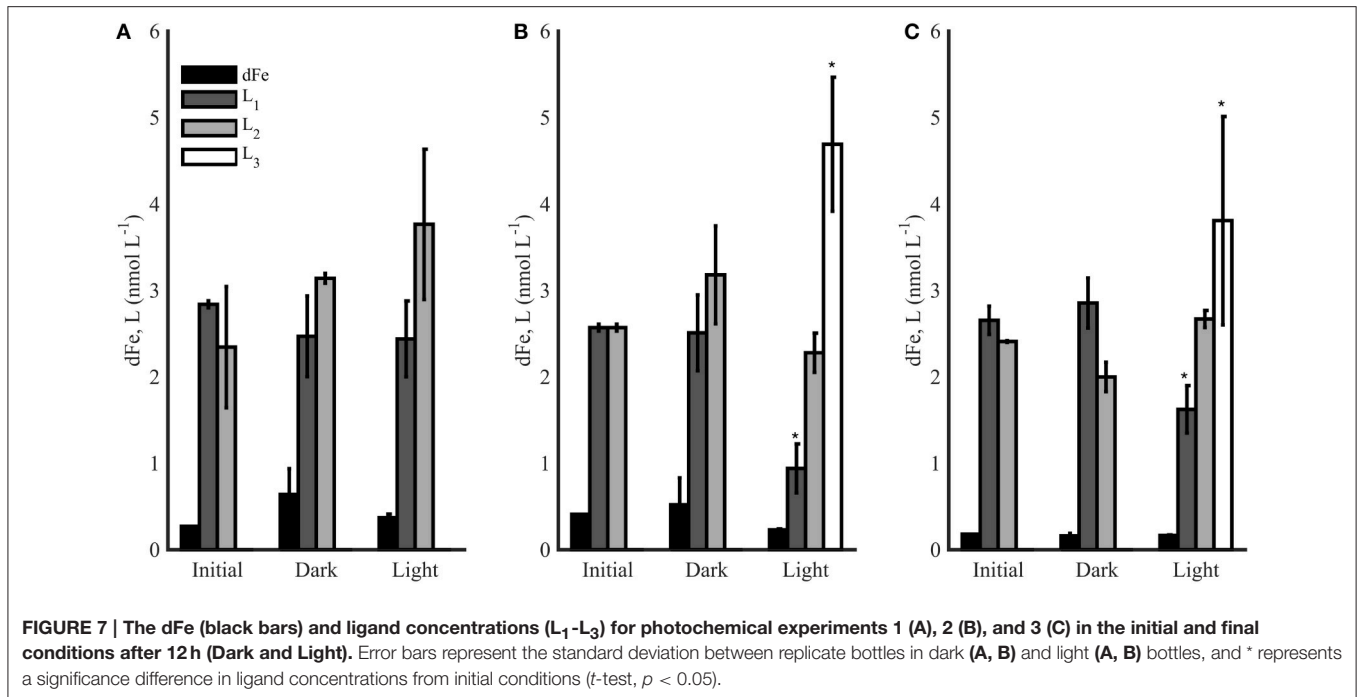
DISCUSSION

Distribution of Multiple Classes of Iron-Binding Ligands in the Southern California Current System

The dFe and ligand profiles in this study were similar to those measured in other oceanic regimes (see Gledhill and Buck, 2012),

with a minimum in ligands in surface waters and an increase with depth along with dFe and nitrate (Figure 2). Ligand profiles between stations were also similar, despite the differences in biogeochemical regimes sampled (Krause et al., 2015). Most of the profiles had a surface minimum in L₁ ligands (Figure 2), perhaps related to photochemical degradation, consistent with previous findings in surface waters (see Gledhill and Buck, 2012). This feature can be patchy however, since station 6 for example, had a maximum in L₁ at the shallowest depth sampled (20m, Figure 2F). The minimum in L₁ was also sometimes associated with elevated concentrations of L₃ in the profiles, though not at station 1. There appear to be other dynamics affecting [L₁] in the profiles as well, as a maximum in L₁ can be seen at stations 2 and 6 associated with, or near, the chl *a* maximum (Figure 2). Other studies have also observed a maximum in strong ligands associated with the biomass maximum (Rue and Bruland, 1995; van den Berg, 1995, 2006; Boye et al., 2001, 2005; Croot et al., 2004; Gerringa et al., 2006, 2008; Buck and Bruland, 2007; Wagener et al., 2008; Ibisanni et al., 2011). The mechanism leading to this feature is not entirely clear, but one field study done in the Canary Basin showed that 63% of the variance in ligands above, or coinciding with, the chl *a* maximum was explained by phytoplankton biomass and silicic acid concentrations (Gerringa et al., 2006). In this study, L₁ was defined as any ligands with a $\log K_{FeL_1, Fe'}^{cond} \geq 12.0$, and were present at all depths sampled (up to 500 m). In our previous work examining surface samples in the central and northern CCE we also found that L₁ declined in surface waters offshore (>200 km), perhaps due to degradation of the stronger ligand class, or a nearshore source, though only a few samples were measured offshore (Bundy et al., 2014b). Other studies have also noted a slight decline in ligand strength from coastal to offshore waters (Sander et al., 2014). All stations sampled in this region were within 200 km off the coast (Figure 1), and L₁ was present in surface waters of each station (Figure 2). Thus, it is still uncertain whether L₁ is restricted to within 200 km of the coast in this region. On a GEOTRACES zonal transect in the Atlantic however, recent work has shown L₁-type ligands (average $\log K_{FeL_1, Fe'}^{cond} = 12.38 \pm 0.22$, $n = 476$) throughout the entire water column, down to 6000 m (Buck et al., 2015). There is likely an *in-situ* source of strong ligands throughout the water column, or the residence time of strong ligands is longer than dFe (Gerringa et al., 2015).

L₂ distributions were very similar to the distributions of L₁ in the profiles (Figure 2). L₂ ligands, as defined in this study, are generally still considered “strong” in terms of previous work on dFe-binding ligands (Gledhill and Buck, 2012), and thus may be controlled by similar processes as L₁. Our other work in coastal regions has also demonstrated a strong coupling between these two ligand classes (Bundy et al., 2014a,b). From the bulk of previous studies measuring dFe-binding ligands, L₂ appears to be a relatively ubiquitous ligand class even in deeper waters (Gledhill and Buck, 2012). Buck et al. (2015) also measured an L₂ ligand class on the zonal Atlantic GEOTRACES transect ($\log K_{FeL_2, Fe'}^{cond} = 11.46 \pm 0.27$, $n = 450$) which was also present down to 6000 m along with L₁. Thus, similar processes may affect the cycling of L₁ and L₂ in the water column.



The distributions of the weaker ligands detected in the profiles (L₃) were somewhat distinct from the stronger ligands. L₃ concentrations were almost constant with depth at most stations, with a slight minimum in surface waters at station 1 (Figure 2). Evidence from our previous work has shown that L₃ ligands increase in surface samples in a transect from nearshore to offshore in the CCS (Bundy et al., 2014b), possibly due to degradation of L₁ and L₂. Elevated concentrations of L₃ in the profiles relative to stronger ligands support this preliminary hypothesis. The slight minimum in surface waters might be related to dissolved organic matter (DOC) uptake, if L₃ ligands comprise a portion of the labile organic matter pool utilized by bacteria. The hypothesis that microbial communities are responsible for altering the weaker ligand pool in the deep ocean (Hunter and Boyd, 2007; Boyd et al., 2010) is also supported by the results from the water column profiles, suggesting an *in-situ* source of weaker ligands in subsurface waters. Buck et al. (2015) also measured an L₃ ligand class ($\log K_{FeL_3, Fe}^{cond} = 10.84 \pm 0.14$, $n = 54$) detectable in subsurface waters, though less often than L₁ and L₂.

Iron-Binding Ligand Dynamics in Biological Incubation Studies

Two experiments were performed in this study in order to observe the temporal evolution of the ligand pool during phytoplankton growth (incubation experiment 1) and microbial remineralization of particles (incubation experiment 2). Each experiment revealed different possible mechanisms leading to alteration of the ligand pool over time. Incubation experiment 1 examined changes in dFe-binding ligands associated with an Fe-addition grow-out (Figure 4). Although there have been links between diatom growth and changes to the ligand pool

observed in previous incubation studies (Buck et al., 2010; King et al., 2012), incubation experiment 1 showed somewhat different results. Likely, some of these differences were related to the characteristics of the initial water mass. For example, experiment 1 was initiated under Fe-limiting conditions, as evidenced by the initial NO₃⁻:dFe (Figure 3C) and the eventual diatom response to Fe addition (Figure 3B). Experiment 1 also initially had elevated strong ligand concentrations, which continued to increase for the first few days of the experiment and then remained relatively constant after day 3 (Figure 4). It is possible that the high concentrations of strong ligands in experiment 1 remained elevated over time due to initial Fe-limitation of the planktonic community, in contrast to other incubation studies which were initiated in nutrient replete waters and evolved into Fe-limitation over the course of the incubation (Buck et al., 2010; King et al., 2012). This was corroborated by the modeling experiment, where the model could reasonably reproduce the initial increase in strong ligands from days 0 to 3 if the bacteria were Fe-stressed (Table 1). Another possibility is that these ligands continue to be produced, but are cycled over short timescales.

Overall, the difference in phytoplankton biomass in experiment 1 between controls and +Fe bottles was striking, yet the temporal ligand patterns were relatively similar. These results suggest that phytoplankton growth did not have a strong effect on the ligand concentrations observed. Bacteria were not directly sampled in incubation experiment 1 due to volume constraints, but the potential effect of nutrient limitation on bacteria growth was analyzed via modeling (Figure 6). Modeling results were able to depict the cycling of the stronger ligand pool (L₁ and L₂) reasonably well with only bacteria as the biological source of ligands (Figure 6). In this model, L₁ is

assumed to be solely from bacteria, while L_2 is assumed to be the product of PON degradation (Boyd et al., 2010) and photochemical degradation of L_1 . In the current case, we assumed the bacteria were at their maximum ligand productivity in both control and +Fe treatments due to the Fe-limited status of the initial water mass, so there was no difference in L_1 production between the two treatments. This was to explain the rapid L_1 increase in the first 2 days under both +Fe conditions (Fe replete) and controls (Fe deficient; **Figure 4**). With these assumptions, modeled L_1 and L_2 concentrations agree with the data reasonably well in both treatments. In the model, continual L_1 production occurs in controls due to Fe stress, and L_2 is primarily produced from photochemical degradation during days 0–2. During days 2–4, L_2 concentrations show more disparity between the two treatments, likely due to the combination of more L_1 and L_2 being produced in the +Fe treatment, due to higher bacterial abundance and more PON, respectively. Phytoplankton biomass began to increase in +Fe treatments after day 3, which translates into a larger increase in PON (**Figure 6F**) and more bacteria. It is this elevated PON and bacteria that lead to the difference in accumulated ligands, but the model yields larger differences in ligand concentrations on day 6 than was observed. It is possible that the model over-estimates bacteria biomass differences between treatments during the latter stages of the experiment, or other parameters not accounted for in the model are responsible for the trends observed. The average of all three triplicates of each treatment does not yield a significant difference between controls and +Fe bottles on day 6 (t -test, $p > 0.05$), and the differences between controls and +Fe bottles in terms of L_1 and L_2 distribution were minimal over the time course of the incubation, suggesting the evolution of Fe-stress in the treatments may not have been a major factor in ligand production. The model is able to replicate the observed ligand distributions relatively well by simply invoking two different biological mechanisms for strong ligand production—production of L_1 under Fe stress, and production of ligands associated with degradation of PON (L_2). Strong ligand production is generally understood to be an Fe acquisition strategy when Fe is scarce (Granger and Price, 1999). However, there is mounting evidence that bacteria also produce siderophores when macronutrients and/or Fe are replete (Gledhill et al., 2004; Mawji et al., 2011; Adly et al., 2015). Our results suggest that strong ligands can be modeled relatively well with only bacteria as a biological source of ligands under both Fe replete and Fe deficient conditions, though many other factors are likely to influence the temporal patterns observed.

We did not attempt to model the weaker ligands in incubation experiment 1, but several studies have shown a link between dFe-binding ligand production and diatom growth (Trick et al., 1983; Soria-Dengg et al., 2001; Gerringa et al., 2006; Rijkenberg et al., 2008; Buck et al., 2010; King et al., 2012). *Chaetoceros brevis* has been observed to alter the ligand pool in culture media (Rijkenberg et al., 2008; González et al., 2014), and was one of the dominant diatom species in experiment 1 (in both control and +Fe treatments). Other evidence from the field has shown that ligands are produced associated with large diatom blooms such as those observed during Ironex-II (Rue and Bruland, 1997)

and SEEDS II (Kondo et al., 2008). Phytoplankton have also been shown to release polysaccharides and other cellular material during growth (Watt, 1969; Mykkestad et al., 1989; Urbani et al., 2005), which may explain the increase in weaker ligands observed on days 4–6 in experiment 1 (**Figure 4D**). It is not entirely certain what compounds may comprise the weaker ligand pool in the marine environment, but the decrease in the L_3 ligand class over the duration of experiment 1 along with a slight increase at the termination of the experiment points to perhaps polysaccharides or some other form of relatively labile DOC (Ducklow et al., 1993). Polysaccharides would likely fall into the L_3 ligand category in this study (Hassler et al., 2011; Norman et al., 2015), and are readily consumed by most bacteria as a source of DOC (Zweifel et al., 1993; Arnosti et al., 1994). The L_4 ligand class was only detected on days 4–6 in experiment 1 (**Figure 4E**) and could be partially explained by the release of domoic acid by *Pseudo-nitzschia*, which are known to produce this compound during bloom formation (Rue and Bruland, 2001). Domoic acid has a $\log K_{FeL,Fe'}^{cond} = 8.6$, which falls into the L_4 class as defined in this study (Rue and Bruland, 2001). These ligands may have also been comprised of other degraded cellular material, such as viral lysis products (Poorvin et al., 2011), or other high molecular weight (HMW) compounds that have been shown to effectively bind dFe (Laglera and van den Berg, 2009; Abdulla et al., 2010). HMW compounds have also been identified in association with diatom growth in culture media containing *T. weiss* and *C. antiqua* (Fuse et al., 1993), suggesting other diatoms in experiment 1 may have contributed to the increase in the weaker ligand pool at the end of experiment 1 (Rijkenberg et al., 2008).

While diatoms were potentially responsible for changes in the ligand pool in incubation experiment 1, the production of dFe-binding ligands has also been associated with copepod grazing (Sato et al., 2007). Grazing could be one of the reasons for the initial increase in stronger ligands from day 0 to 1 (**Figures 4B,C**), though no copepods were evident in the incubation bottles. Grazing may also be an explanation for higher $[L_2]$ on days 3–5 in +Fe treatments in experiment 1 (**Figure 4C**), coinciding with elevated diatom growth on those days. However, due to similarities between controls and +Fe bottles in experiment 1, it is unlikely that phytoplankton grazing was a significant factor affecting ligand concentrations in that experiment. This hypothesis is corroborated by the modeling results for Experiment 1, which show there were potentially significant differences in grazing rates between controls and +Fe treatments during the later days of the experiments (data not shown). This implies there should be differences in ligand concentrations between treatments if zooplankton grazing was a significant source of ligands, but this was not observed.

The temporal pattern in ligands in incubation experiment 1 was likely the result of several processes, perhaps dominated by bacteria. The ability for the heterotrophic community to alter the ligand pool was explicitly tested in incubation experiment 2 (**Figure 5**). Microbial remineralization of organic particles has been examined previously by Boyd et al. (2010) in the Southern Ocean, who found that microbial breakdown of POC produced

dFe and L₂ ligands (Boyd et al., 2010). Our incubation study examined microbial remineralization of several ligand classes using MAWs, and found that almost all the ligand classes increased significantly over the incubation period in controls (days 1–3) and the overall ligand increase was greater in controls than +Fe treatments. It is possible the strong ligands produced during experiment 2 could be siderophores, especially in control treatments that contained very low [dFe] even after some had been remineralized (Figure 5). L₃ ligands demonstrated a different pattern than the other ligand classes in Experiment 2, since they decreased slightly from day 1 to 3, though the differences between the initial and final time points were not significant in either treatment (*t*-test, *p* > 0.05). Similar to experiment 1, it is possible that some form of labile DOC falls into the L₃ ligand category, which may have been consumed during this experiment. In contrast to L₃, L₄ clearly increased during experiment 2. This is consistent with other observations that have shown that HMW organic compounds, likely with weak dFe-binding, can increase due to DOC remineralization (Repeta et al., 2002).

Iron-Binding Ligand Dynamics in Photochemical Studies

Photochemical experiments from this region showed mixed results with respect to the effect of natural sunlight on the dFe-binding ligand pool (Figure 7). This is similar to other field efforts, where some studies have observed a decrease in the concentration of strong dFe-binding ligands upon exposure to natural sunlight (Powell and Wilson-Finelli, 2003) and others have seen no effect of UV light on ligands found in Dutch estuaries (Rijkenberg et al., 2006). Thus, it appears not all natural dFe-binding ligands are susceptible to photo-degradation, as has been shown with certain siderophores in laboratory studies (Barbeau et al., 2001, 2003; Barbeau, 2006). One reason for this difference in reactivity may be related to the size class, functional groups, or binding strength of the natural ligands present in the environment. Some of the natural dFe-binding ligands found by Powell and Wilson-Finelli (2003) had slightly elevated log $K_{FeL,Fe'}^{cond}$ compared to the Rijkenberg et al. (2006) study (log $K_{FeL,Fe'}^{cond} \sim 12$ compared to 10.1–11.0), and no degradation of the strong ligands was observed by Rijkenberg et al. (2006). L₁ ligands observed initially in photochemical experiment 1 were slightly weaker (log $K_{FeL,Fe'}^{cond} = 12.51 \pm 0.14$), though still stronger than in experiments 2 and 3 (13.70 ± 0.02 and 12.79 ± 0.15 , respectively; *t*-test, *p* < 0.05), though this difference is not striking. The differences in photochemical reactivity between experiments is most likely the result of distinctions in the initial water mass. It is notable that no L₃ ligands were detected initially in any of the photochemical experiments, despite the fact that L₃ ligands were detected in the water column at similar depths (Figure 2). We speculate that there was some scavenging of L₃ ligands onto the walls of the quartz flasks used in this study, since the initial samples were taken directly from the flasks after filling and we have noted this problem in other experiments with quartz (data not shown). This may be another reason for differences in field studies examining degradation of natural

ligands, if weaker ligands produced from photo-degradation are rapidly scavenged.

Another possible explanation for mixed findings in earlier publications may be related to analytical methods. This study employed MAW analysis, which enabled the detection of both the strongest and weakest dFe-binding ligands ($\alpha_{Fe(SA)_x} = 74 - 115$). Powell and Wilson-Finelli (2003) employed a low ($\alpha_{Fe(TAC)_2} = 55$) and high ($\alpha_{Fe(TAC)_2} = 300$) analytical window, while Rijkenberg et al. (2006) used only a high window ($\alpha_{Fe(TAC)_2} = 300$). It is possible that the competition strength in the Rijkenberg et al. (2006) study may have been too high to effectively detect some of the weaker dFe-binding ligands. These differences in analytical methods support the utility of using MAWs in the context of mechanistic ligand studies where more than one class of dFe-binding ligand may be detected.

Processes Affecting Iron-Binding Ligands in the Southern California Current System

To our knowledge, this is the first study to mechanistically link dFe-binding ligand profiles with deckboard incubation experiments on the same cruise, using MAW analysis of the ligand pool. Although only a few profiles were examined in this study, the stations were in biogeochemically distinct sampling regions and large hydrographic and biological gradients were also sampled vertically. Despite the relatively large gradients, the ligand profiles were very similar between stations. Coastal station 4, for example, had much higher [chl *a*] in the subsurface maximum, but did not show a difference in ligands at this depth compared to any other station (Figure 2). Similarly, incubation experiment 1 showed very little difference in the ligand pool between the Fe-limited vs. the Fe-replete phytoplankton community (Figure 4), despite the much higher biomass in +Fe bottles (Figure 3B). These findings suggest that large changes in phytoplankton biomass in surface waters may have little impact on the overall composition of the Fe-binding ligand pool on longer timescales.

MAW analysis helped to reveal the presence of three ligand classes at almost every sampling depth in the upper 500 m of the southern CCS, suggesting there are ubiquitous *in-situ* sources of each of these ligand classes, or they have a relatively long residence time. Although no other studies have used MAWs to measure dFe-binding ligand profiles, most recent studies agree that both strong and weak ligands are present throughout the water column (Buck et al., 2015; Gerringa et al., 2015). Experimental and statistical evidence from this study suggests a mechanism for the presence of both strong and weak ligands in surface and subsurface waters. The patterns in the ligand distributions between profiles were primarily correlated with nitrate distributions, which could point to microbial remineralization as a potentially dominant control on the ligand pool with depth over longer timescales (Gerringa et al., 2015). A field study also found a close link between ligand concentrations in surface waters, DOC and bacterial abundance (Wagener et al., 2008) and bacteria are known to be the dominant control on DOC in the ocean. Although some interesting features were also seen in the upper water column

that may be related to phytoplankton dynamics, these processes may occur on shorter timescales than microbial remineralization processes. Incubation experiment 2, which focused on the ability of the heterotrophic community to produce dFe-binding ligands from POC remineralization, showed that strong ligands can be produced during this process, in addition to the weaker ligands observed in Boyd et al. (2010). The results from incubation experiment 2 now provide a mechanism for *in-situ* strong ligand production in subsurface waters as well.

Although L₄ ligands appeared to be produced during both biological incubation experiments, none were detected in the profiles (Figure 2). It may be that these weaker dFe-ligand complexes are scavenged on longer timescales and were therefore not present in the station data, or that L₄ ligands have only a nearshore source such as the benthic boundary layer or coastal estuaries as seen in our previous work (Bundy et al., 2014a,b). L₄ ligands may only be present under certain conditions or on certain timescales in the oceanic water column. The biological incubation experiments performed in this study suggest that there are, however, *in-situ* sources for these very weak ligands in the oceanic environment.

Subsurface ligand concentrations could be largely controlled by the microbial community, but photochemical effects appear to impact near surface waters in this region as well. Evidence from photochemical experiments suggests that photochemical degradation of natural ligands can be variable, and may be restricted to the strongest or certain size classes of ligands. This may provide an explanation for regional differences between studies on photochemical effects (Powell and Wilson-Finelli, 2003; Rijkenberg et al., 2006) and the differences between stations

in this study (Figure 2). Additional explanations for the variable influence of photochemistry on the natural ligand pool will be important to constrain in future studies, as it appears to be a significant sink for L₁ in CCE surface waters.

AUTHOR CONTRIBUTIONS

RB and KB both contributed to the design of the experiments and the acquisition and interpretation of the ligand and nutrient data. MC analyzed, processed and interpreted the cell count data. MJ developed and tested the incubation experiment model. RB, MC, KB, and MJ critically revised the work for intellectual content and ensured the integrity of the reported data.

ACKNOWLEDGMENTS

We would like to thank the captain and crew of the *R/V Melville* and the CCE-LTER program. We would like to thank Teresa Fukuda for phytoplankton pigment measurements. We also thank Wendy Plante and Shane Hogle for help with sampling. RB, KB, and MC were supported by NSF OCE #10-2667 for the CCE-LTER program. MJ was funded by NSF ANT grant 0948378 and Harbor Branch Oceanographic Institute Foundation.

SUPPLEMENTARY MATERIAL

The Supplementary Material for this article can be found online at: <http://journal.frontiersin.org/article/10.3389/fmars.2016.00027>

REFERENCES

- Abdulla, H. A. N., Minor, E. C., Dias, R. F., and Hatcher, P. G. (2010). Changes in the compound classes of dissolved organic matter along an estuarine transect: a study using FTIR and C-13 NMR. *Geochim. Cosmochim. Acta* 74, 3815–3838. doi: 10.1016/j.gca.2010.04.006
- Abualhija, M. M., and van den Berg, C. M. (2014). Chemical speciation of iron in seawater using catalytic cathodic stripping voltammetry with ligand competition against salicylaldoxime. *Mar. Chem.* 164, 60–74. doi: 10.1016/j.marchem.2014.06.005
- Adly, C. L., Tremblay, J. E., Powell, R. T., Armstrong, E., Peers, G., and Price, N. M. (2015). Response of heterotrophic bacteria in a mesoscale iron enrichment in the northeast subarctic Pacific Ocean. *Limnol. Oceanogr.* 60, 136–148. doi: 10.1002/lno.10013
- Amin, S. A., Green, D. H., Küpper, F. C., and Carrano, C. J. (2009). Vibrioferrin, an unusual marine siderophore: iron binding, photochemistry, and biological implications. *Inorg. Chem.* 48, 11451–11458. doi: 10.1021/ic9016883
- Archer, D. E., and Johnson, K. (2000). A model of the iron cycle in the ocean. *Global Biogeochem. Cycles* 14, 269–279. doi: 10.1029/1999GB900053
- Arnosti, C., Repeta, D., and Blough, N. (1994). Rapid bacterial degradation of polysaccharides in anoxic marine systems. *Geochim. Cosmochim. Acta* 58, 2639–2652. doi: 10.1016/0016-7037(94)90134-1
- Barbeau, K. (2006). Photochemistry of organic iron(III) complexing ligands in oceanic systems. *Photochem. Photobiol.* 82, 1505–1516. doi: 10.1562/2006-06-16-IR-935
- Barbeau, K., Moffett, J. W., Caron, D. A., Croot, P. L., and Erdner, D. L. (1996). Role of protozoan grazing in relieving iron limitation of phytoplankton. *Nature* 380, 61–64. doi: 10.1038/380061a0
- Barbeau, K., Rue, E. L., Bruland, K. W., and Butler, A. (2001). Photochemical cycling of iron in the surface ocean mediated by microbial iron(III)-binding ligands. *Nature* 413, 409–413. doi: 10.1038/35096545
- Barbeau, K., Rue, E. L., Trick, C. G., Bruland, K. T., and Butler, A. (2003). Photochemical reactivity of siderophores produced by marine heterotrophic bacteria and cyanobacteria based on characteristic Fe(III) binding groups. *Limnol. Oceanogr.* 48, 1069–1078. doi: 10.4319/lno.2003.48.3.1069
- Billler, D. V., and Bruland, K. W. (2014). The central California Current transition zone: a broad region exhibiting evidence for iron limitation. *Prog. Oceanogr.* 120, 370–382. doi: 10.1016/j.pocean.2013.11.002
- Boyd, P. W., Ibsanmi, E., Sander, S. G., Hunter, K. A., and Jackson, G. A. (2010). Remineralization of upper ocean particles: Implications for iron biogeochemistry. *Limnol. Oceanogr.* 55, 1271–1288. doi: 10.4319/lno.2010.55.3.1271
- Boyd, P. W., and Tagliabue, A. (2015). Using the L* concept to explore controls on the relationship between paired ligand and dissolved iron concentrations in the ocean. *Mar. Chem.* 173, 52–66. doi: 10.1016/j.marchem.2014.12.003
- Boye, M., Aldrich, A., van den Berg, C. M., de Jong, J., Nirmaier, H., Veldhuis, M., et al. (2006). The chemical speciation of iron in the north-east Atlantic Ocean. *Deep-Sea Res. Part I-Oceanogr. Res. Papers* 53, 667–683. doi: 10.1016/j.dsr.2005.12.015
- Boye, M., Nishioka, J., Croot, P. L., Laan, P., Timmermans, K. R., and de Baar, H. J. (2005). Major deviations of iron complexation during 22 days of a mesoscale iron enrichment in the open Southern Ocean. *Mar. Chem.* 96, 257–271. doi: 10.1016/j.marchem.2005.02.002

- Boye, M., van den Berg, C. M., de Jong, J., Leach, H., Croot, P., and de Baar, H. J. (2001). Organic complexation of iron in the Southern Ocean. *Deep-Sea Res. Part I-Oceanogr. Res. Papers* 48, 1477–1497. doi: 10.1016/S0967-0637(00)00099-6
- Brzezinski, M. A., Krause, J. W., Bundy, R. M., Barbeau, K. A., Franks, P., Goericke, R., et al. (2015). Enhanced silica ballasting from iron stress sustains carbon export in a frontal zone within the California Current. *J. Geophys. Res.* 120, 4654–4669. doi: 10.1002/2015JC010829
- Buck, K. N., and Bruland, K. W. (2007). The physicochemical speciation of dissolved iron in the Bering Sea, Alaska. *Limnol. Oceanogr.* 52, 1800–1808. doi: 10.4319/lo.2007.52.5.1800
- Buck, K. N., Lohan, M. C., Berger, C. J. M., and Bruland, K. W. (2007). Dissolved iron speciation in two distinct river plumes and an estuary: Implications for riverine iron supply. *Limnol. Oceanogr.* 52, 843–855. doi: 10.4319/lo.2007.52.2.0843
- Buck, K. N., Moffett, J., Barbeau, K. A., Bundy, R. M., Kondo, Y., and Wu, J. (2012). The organic complexation of iron and copper: an intercomparison of competitive ligand exchange-adsorptive cathodic stripping voltammetry (CLE-ACSV) techniques. *Limnol. Oceanogr. Methods* 10, 496–515. doi: 10.3389/fmicb.2012.00069
- Buck, K. N., Selph, K. E., and Barbeau, K. A. (2010). Iron-binding ligand production and copper speciation in an incubation experiment of Antarctic Peninsula shelf waters from the Bransfield Strait, Southern Ocean. *Mar. Chem.* 122, 148–159. doi: 10.1016/j.marchem.2010.06.002
- Buck, K. N., Sohst, B., and Sedwick, P. N. (2015). The organic complexation of dissolved iron along the U.S. GEOTRACES North Atlantic transect. *Deep Sea Res. Part II- Top. Stud. Oceanogr.* 116, 152–165. doi: 10.1016/j.dsr2.2014.11.016
- Bundy, R. M., Abdulla, H. A., Hatcher, P., Biller, D. V., Buck, K. N., and Barbeau, K. A. (2014a). Iron-binding ligands and humic substances in the San Francisco Bay estuary and estuarine-influenced shelf regions of coastal California. *Mar. Chem.* 173, 183–194. doi: 10.1016/j.marchem.2014.11.005
- Bundy, R. M., Barbeau, K. A., Biller, D. V., Buck, K. N., and Bruland, K. W. (2014b). Distinct pools of dissolved iron-binding ligands in the surface and benthic boundary layer of the California Current. *Limnol. Oceanogr.* 59, 769–787. doi: 10.4319/lo.2014.59.3.0769
- Croot, P. L., Andersson, K., Ozturk, M., and Turner, D. R. (2004). The distribution and speciation of iron along 6 degrees E in the Southern Ocean. *Deep-Sea Res. Part II-Top. Stud. Oceanogr.* 51, 2857–2879. doi: 10.1016/j.dsr2.2003.10.012
- Cutter, G. A., and Bruland, K. W. (2012). Rapid and noncontaminating sampling system for trace elements in global ocean surveys. *Limnol. Oceanogr. Methods* 10, 425–436. doi: 10.4319/lo.2012.10.425
- Ducklow, H. W., Kirchman, D. L., Quinby, H. L., Carlson, C. A., and Dam, H. G. (1993). Stocks and dynamics of bacterioplankton carbon during the spring bloom in the eastern North-Atlantic ocean. *Deep-Sea Res. Part II-Top. Stud. Oceanogr.* 40, 245–263. doi: 10.1016/0967-0645(93)90016-G
- Fan, S. M. (2008). Photochemical and biochemical controls on reactive oxygen and iron speciation in the pelagic surface ocean. *Mar. Chem.* 109, 152–164. doi: 10.1016/j.marchem.2008.01.005
- Fuse, H., Takimura, O., Kamimura, K., and Yamaoka, Y. (1993). Marine algae excrete large molecular weight compounds keeping iron dissolved. *Biosci. Biotechnol. Biochem.* 57, 509–510. doi: 10.1271/bbb.57.509
- Gerringa, L. J. A., Blain, S., Laan, P., Sarthou, G., Veldhuis, M. J. W., Brussaard, C. P. D., et al. (2008). Fe-binding dissolved organic ligands near the Kerguelen Archipelago in the Southern Ocean (Indian sector). *Deep-Sea Res. Part II-Top. Stud. Oceanogr.* 55, 606–621. doi: 10.1016/j.dsr2.2007.12.007
- Gerringa, L. J. A., Rijkenberg, M. J. A., Schoemann, V., Laan, P., and de Baar, H. J. W. (2015). Organic complexation of iron in the West Atlantic Ocean. *Mar. Chem.* 177, 434–446. doi: 10.1016/j.marchem.2015.04.007
- Gerringa, L. J. A., Veldhuis, M. J. W., Timmermans, K. R., Sarthou, G., and de Baar, H. J. W. (2006). Co-variance of dissolved Fe-binding ligands with phytoplankton characteristics in the Canary Basin. *Mar. Chem.* 102, 276–290. doi: 10.1016/j.marchem.2006.05.004
- Gledhill, M., and Buck, K. N. (2012). The organic complexation of iron in the marine environment: a review. *Front. Microbiol.* 3:69. doi: 10.3389/fmicb.2012.00069
- Gledhill, M., McCormack, P., Ussher, S., Achterberg, E. P., Mantoura, R. F. C., and Worsfold, P. J. (2004). Production of siderophore type chelates by mixed bacterioplankton populations in nutrient enriched seawater incubations. *Mar. Chem.* 88, 75–83. doi: 10.1016/j.marchem.2004.03.003
- González, A. G., Santana-Casiano, J. M., González-Dávila, M., Pérez-Almeida, N., and Suárez de Tangil, M. (2014). Effect of *Dunaliella tertiolecta* organic exudates on the Fe(II) oxidation kinetics in seawater. *Environ. Sci. Technol.* 48, 7933–7941. doi: 10.1021/es5013092
- Granger, J., and Price, N. M. (1999). The importance of siderophores in iron nutrition of heterotrophic marine bacteria. *Limnol. Oceanogr.* 44, 541–555. doi: 10.4319/lo.1999.44.3.0541
- Hassler, C. S., Alasonati, E., Nichols, C. A. M., and Slaveykova, V. I. (2011). Exopolysaccharides produced by bacteria isolated from the pelagic Southern Ocean - Role in Fe binding, chemical reactivity, and bioavailability. *Mar. Chem.* 123, 88–98. doi: 10.1016/j.marchem.2010.10.003
- Hudson, R. J. M., Rue, E. L., and Bruland, K. W. (2003). Modeling complexometric titrations of natural water samples. *Environ. Sci. Technol.* 37, 1553–1562. doi: 10.1021/es025751a
- Hunter, K. A., and Boyd, P. W. (2007). Iron-binding ligands and their role in the ocean biogeochemistry of iron. *Environ. Chem.* 4, 221–232. doi: 10.1071/EN07012
- Hutchins, D. A., DiTullio, G. R., Zhang, Y., and Bruland, K. W. (1998). An iron limitation mosaic in the California upwelling regime. *Limnol. Oceanogr.* 43, 1037–1054. doi: 10.4319/lo.1998.43.6.1037
- Hutchins, D. A., Witter, A. E., Butler, A., and Luther, G. W. (1999). Competition among marine phytoplankton for different chelated iron species. *Nature* 400, 858–861. doi: 10.1038/23680
- Ibisami, E., Sander, S. G., Boyd, P. W., Bowie, A. R., and Hunter, K. A. (2011). Vertical distributions of iron-(III) complexing ligands in the Southern Ocean. *Deep Sea Res. Part II- Top. Stud. Oceanogr.* 58, 2113–2125. doi: 10.1016/j.dsr2.2011.05.028
- Jiang, M., Barbeau, K. A., Selph, K. E., Measures, C. I., Buck, K. N., Azam, F., et al. (2013). The role of organic ligands in iron cycling and primary productivity in the Antarctic Peninsula: a modeling study. *Deep Sea Res. Part II- Top. Stud. Oceanogr.* 90, 112–133. doi: 10.1016/j.dsr2.2013.01.029
- King, A. L., and Barbeau, K. (2007). Evidence for phytoplankton iron limitation in the southern California Current System. *Mar. Ecol. Prog. Ser.* 342, 91–103. doi: 10.3354/meps342091
- King, A. L., and Barbeau, K. A. (2011). Dissolved iron and macronutrient distributions in the southern California Current System. *J. Geophys. Res. Oceans* 116, 18. doi: 10.1029/2010JC006324
- King, A. L., Buck, K. N., and Barbeau, K. A. (2012). Quasi-Lagrangian drifter studies of iron speciation and cycling off Point Conception, California. *Mar. Chem.* 128, 1–12. doi: 10.1016/j.marchem.2011.11.001
- Kondo, Y., Takeda, S., Nishioka, J., Obata, H., Furuya, K., Johnson, W. K., et al. (2008). Organic iron(III) complexing ligands during an iron enrichment experiment in the western subarctic North Pacific. *Geophys. Res. Lett.* 35:L12601. doi: 10.1029/2008gl033354
- Krause, J., Brzezinski, M. A., Goericke, R., Landry, M. R., Ohman, M. D., Stukel, M. R., et al. (2015). Variability in diatom contributions to biomass, organic matter production and export across a frontal gradient in the California Current Ecosystem. *J. Geophys. Res. Oceans* 120, 1032–1047. doi: 10.1002/2014JC010472
- Laglera, L. M., and van den Berg, C. M. G. (2009). Evidence for geochemical control of iron by humic substances in seawater. *Limnol. Oceanogr.* 54, 610–619. doi: 10.4319/lo.2009.54.2.0610
- Landry, M. R., Ohman, M. D., Goericke, R., Stukel, M. R., and Tsyrlkevich, K. (2009). Lagrangian studies of phytoplankton growth and grazing relationships in a coastal upwelling ecosystem off Southern California. *Prog. Oceanogr.* 83, 208–216. doi: 10.1016/j.poc.2009.07.026
- Lee, S., and Fuhrman, J. A. (1987). Relationships between biovolume and biomass of naturally derived marine bacterioplankton. *Appl. Environ. Microbiol.* 53, 1298–1303.
- Mahmood, A., Abualhaja, M. M., van den Berg, C. M., and Sander, S. G. (2015). Organic speciation of dissolved iron in estuarine and coastal waters at multiple analytical windows. *Mar. Chem.* 177, 706–719. doi: 10.1016/j.marchem.2015.11.001
- Maldonado, M. T., Hughes, M. P., Rue, E. L., and Wells, M. L. (2002). The effect of Fe and Cu on growth and domoic acid production by *Pseudo-nitzschia*

- multiseries and *Pseudo-nitzschia australis*. *Limnol. Oceanogr.* 47, 515–526. doi: 10.4319/lo.2002.47.2.0515
- Maldonado, M. T., and Price, N. M. (1999). Utilization of iron bound to strong organic ligands by plankton communities in the subarctic Pacific Ocean. *Deep-Sea Res. Part II-Top. Stud. Oceanogr.* 46, 2447–2473. doi: 10.1016/S0967-0645(99)00071-5
- Mantoura, R. F. C., and Riley, J. P. (1975). Analytical concentration of humic substances from natural-waters. *Anal. Chim. Acta* 76, 97–106. doi: 10.1016/S0003-2670(01)81990-5
- Martin, J. H., Gordon, R. M., and Fitzwater, S. E. (1991). The case for iron. *Limnol. Oceanogr.* 36, 1793–1802. doi: 10.4319/lo.1991.36.8.1793
- Mawji, E., Gledhill, M., Milton, J. A., Tarran, G. A., Ussher, S., Thompson, A., et al. (2008). Hydroxamate Siderophores: Occurrence and Importance in the Atlantic Ocean. *Environ. Sci. Technol.* 42, 8675–8680. doi: 10.1021/es801884r
- Mawji, E., Gledhill, M., Milton, J. A., Zubkov, M. V., Thompson, A., Wolff, G. A., et al. (2011). Production of siderophore type chelates in Atlantic Ocean waters enriched with different carbon and nitrogen sources. *Mar. Chem.* 124, 90–99. doi: 10.1016/j.marchem.2010.12.005
- Moore, J. K., and Braucher, O. (2008). Sedimentary and mineral dust sources of dissolved iron to the world ocean. *Biogeosciences* 5, 631–656. doi: 10.5194/bg-5-631-2008
- Moore, J. K., Doney, S. C., and Lindsay, K. (2004). Upper ocean ecosystem dynamics and iron cycling in a global three-dimensional model. *Global Biogeochem. Cycles* 18:GB4028. doi: 10.1029/2004GB002220
- Morel, F. M. M., and Price, N. M. (2003). The biogeochemical cycles of trace metals in the oceans. *Science* 300, 944–947. doi: 10.1126/science.1083545
- Mykkestad, S., Holm-Hansen, O., Vårum, K. M., and Volcani, B. E. (1989). Rate of release of extracellular amino acids and carbohydrates from the marine diatom *Chaetoceros affinis*. *J. Plankton Res.* 11, 763–773. doi: 10.1093/plankt/11.4.763
- Norman, L., Worms, I. A. M., Angles, E., Bowie, A. R., Nichols, C. M., Pham, A. N., et al. (2015). The role of bacterial and algal exopolymeric substances in iron chemistry. *Mar. Chem.* 173, 148–161. doi: 10.1016/j.marchem.2015.03.015
- Omanović, D., Garnier, C., and Pižeta, I. (2014). ProMCC: an all-in-one tool for trace metal complexation studies. *Mar. Chem.* 173, 25–39. doi: 10.1016/j.marchem.2014.10.011
- Parekh, P., Follows, M. J., and Boyle, E. A. (2005). Decoupling of iron and phosphate in the global ocean. *Global Biogeochem. Cycles* 19:GB2020. doi: 10.1029/2004GB002280
- Pižeta, I., Sander, S. G., Hudson, R. J. M., Baars, O., Buck, K. N., Bundy, R. M., et al. (2015). Quantitative analysis of complexometric titration data: an intercomparison of methods for estimating models of metal complexation by mixtures of natural ligands. *Mar. Chem.* 173, 3–24. doi: 10.1016/j.marchem.2015.03.006
- Poorvin, L., Sander, S. G., Velasquez, I., Ibsanmi, E., Leclair, G. R., and Wilhelm, S. W. (2011). A comparison of Fe bioavailability and binding of a catecholate siderophore with virus-mediated lysates from the marine bacterium *Vibrio alginolyticus* PWH3a. *J. Exp. Mar. Biol. Ecol.* 399, 43–47. doi: 10.1016/j.jembe.2011.01.016
- Powell, R. T., and Wilson-Finelli, A. (2003). Photochemical degradation of organic iron complexing ligands in seawater. *Aquat. Sci.* 65, 367–374. doi: 10.1007/s00027-003-0679-0
- Reid, R. T., Live, D. H., Faulkner, D. J., and Butler, A. (1993). A siderophore from a marine bacterium with an exceptional ferric ion affinity constant. *Nature* 366, 455–458. doi: 10.1038/366455a0
- Repeta, D. J., Quan, T. M., Aluwihare, L. I., and Accardi, A. (2002). Chemical characterization of high molecular weight dissolved organic matter in fresh and marine waters. *Geochim. Cosmochim. Acta* 66, 955–962. doi: 10.1016/S0016-7037(01)00830-4
- Rijkenberg, M. J. A., Gerringa, L. J. A., Timmermans, K. R., Fischer, A. C., Kroon, K. J., Buma, A. G. J., et al. (2008). Enhancement of the reactive iron pool by marine diatoms. *Mar. Chem.* 109, 29–44. doi: 10.1016/j.marchem.2007.12.001
- Rijkenberg, M. J. A., Gerringa, L. J. A., Velzeboer, I., Timmermans, K. R., Buma, A. G. J., and de Baar, H. J. (2006). Iron-binding ligands in Dutch estuaries are not affected by UV induced photochemical degradation. *Mar. Chem.* 100, 11–23. doi: 10.1016/j.marchem.2005.10.005
- Rue, E. L., and Bruland, K. (2001). Domoic acid binds iron and copper: a possible role for the toxin produced by the marine diatom *Pseudo-nitzschia*. *Mar. Chem.* 76, 127–134. doi: 10.1016/S0304-4203(01)00053-6
- Rue, E. L., and Bruland, K. W. (1995). Complexation of iron(III) by natural organic-ligands in the central North Pacific as determined by a new competitive ligand equilibration adsorptive cathodic stripping voltammetric method. *Mar. Chem.* 50, 117–138. doi: 10.1016/0304-4203(95)00031-L
- Rue, E. L., and Bruland, K. W. (1997). The role of organic complexation on ambient iron chemistry in the equatorial Pacific Ocean and the response of a mesoscale iron addition experiment. *Limnol. Oceanogr.* 42, 901–910. doi: 10.4319/lo.1997.42.5.0901
- Sander, S. G., Tian, F., Ibsanmi, E. B., Currie, K. I., Hunter, K. A., and Frew, R. D. (2014). Spatial and seasonal variations of iron speciation in surface waters of the Subantarctic front and the Otago Continental Shelf. *Mar. Chem.* 173, 114–124. doi: 10.1016/j.marchem.2014.09.001
- Sato, M., Takeda, S., and Furuya, K. (2007). Iron regeneration and organic iron(III)-binding ligand production during *in situ* zooplankton grazing experiment. *Mar. Chem.* 106, 471–488. doi: 10.1016/j.marchem.2007.05.001
- Scatchard, G. (1949). The attractions of proteins for small molecules and ions. *Ann. N.Y. Acad. Sci.* 51, 660–672. doi: 10.1111/j.1749-6632.1949.tb27297.x
- Soria-Dengg, S., Reissbrodt, R., and Horstmann, U. (2001). Siderophores in marine, coastal waters and their relevance for iron uptake by phytoplankton: experiments with the diatom *Phaeodactylum tricoratum*. *Mar. Ecol. Prog. Ser.* 220, 73–82. doi: 10.3354/meps220073
- Tagliabue, A., Aumont, O., and Bopp, L. (2014). The impact of different external sources of iron on the global carbon cycle. *Geophys. Res. Lett.* 41, 920–926. doi: 10.1002/2013GL059059
- Tagliabue, A., Bopp, L., Aumont, O., and Arrigo, K. R. (2009). Influence of light and temperature on the marine iron cycle: From theoretical to global modeling. *Global Biogeochem. Cycles* 23:GB2017. doi: 10.1029/2008GB003214
- Tagliabue, A., and Volker, C. (2011). Towards accounting for dissolved iron speciation in global ocean models. *Biogeosciences* 8, 3025–3039. doi: 10.5194/bg-8-3025-2011
- Thuróczy, C. E., Gerringa, L. J. A., Klunder, M. B., Laan, P., and de Baar, H. J. W. (2011b). Observation of consistent trends in the organic complexation of dissolved iron in the Atlantic sector of the Southern Ocean. *Deep-Sea Res. Part II-Top. Stud. Oceanogr.* 58, 2695–2706. doi: 10.1016/j.dsr.2.2011.01.002
- Thuróczy, C. E., Gerringa, L. J. A., Klunder, M., Laan, P., Le Guitton, M., and de Baar, H. J. W. (2010). Speciation of Fe in the Eastern North Atlantic Ocean. *Deep-Sea Res. Part I-Oceanogr. Res. Papers* 57, 1444–1453. doi: 10.1016/j.dsr.2010.08.004
- Thuróczy, C. E., Gerringa, L. J. A., Klunder, M., Laan, P., Le Guitton, M., and de Baar, H. J. W. (2011a). Distinct trends in the speciation of iron between the shallow shelf seas and the deep basins of the Arctic Ocean. *J. Geophys. Res. Oceans* 116:C10009. doi: 10.1029/2010JC006835
- Trick, C., Andersen, R., Price, N., Gillam, A., and Harrison, P. (1983). Examination of hydroxamate-siderophore production by neritic eukaryotic marine phytoplankton. *Mar. Biol.* 75, 9–17. doi: 10.1007/BF00392625
- UNESCO (1981). Background papers and supporting data on the Practical Salinity Scale 1978. *UNESCO Technical Papers in Marine Science* 37.
- Urbani, R., Magaletti, E., Sist, P., and Cicero, A. M. (2005). Extracellular carbohydrates released by the marine diatoms *Cylindrotheca closterium*, *Thalassiosira pseudonana* and *Skeletonema costatum*: effect of P-depletion and growth status. *Sci. Total Environ.* 353, 300–306. doi: 10.1016/j.scitotenv.2005.09.026
- Utermöhl, H. (1958). Zur vervollkommnung der quantitativen Phytoplanktonmethodik. *Mitteilungen Internationale Vereinigung Theoretische Angewandte Limnologie* 9, 1–38.
- van den Berg, C. M. G. (1995). Evidence for organic complexation of iron in seawater. *Mar. Chem.* 50, 139–157. doi: 10.1016/0304-4203(95)00032-M
- van den Berg, C. M. G. (2006). Chemical speciation of iron in seawater by cathodic stripping voltammetry with dihydroxynaphthalene. *Anal. Chem.* 78, 156–163. doi: 10.1021/ac051441+
- Vraspir, J. M., and Butler, A. (2009). Chemistry of marine ligands and Siderophores. *Ann. Rev. Mar. Sci.* 1, 43–63. doi: 10.1146/annurev.marine.010908.163712

- Wagener, T., Pulido-Villena, E., and Guieu, C. (2008). Dust iron dissolution in seawater: results from a one-year time-series in the Mediterranean Sea. *Geophys. Res. Lett.* 35:L16601. doi: 10.1029/2008gl034581
- Watt, W. (1969). Extracellular release of organic matter from two freshwater diatoms. *Ann. Bot.* 33, 427–437.
- Wu, J. F., and Luther, G. W. (1995). Complexation of Fe(III) by natural organic-ligands in the northwest Atlantic-ocean by a competitive ligand equilibration method and a kinetic approach. *Mar. Chem.* 50, 159–177. doi: 10.1016/0304-4203(95)00033-N
- Zapata, M., Rodriguez, F., and Garrido, J. L. (2000). Separation of chlorophylls and carotenoids from marine phytoplankton: a new HPLC method using a reversed phase C-8 column and pyridine-containing mobile phases. *Mar. Ecol.-Prog. Ser.* 195, 29–45. doi: 10.3354/meps195029
- Zweifel, U. L., Norrman, B., and Hagstrom, A. (1993). Consumption of dissolved organic carbon by marine bacteria and demand for inorganic nutrients. *Mar. Ecol.-Prog. Ser.* 101, 23–23. doi: 10.3354/meps101023

Conflict of Interest Statement: The authors declare that the research was conducted in the absence of any commercial or financial relationships that could be construed as a potential conflict of interest.

Copyright © 2016 Bundy, Jiang, Carter and Barbeau. This is an open-access article distributed under the terms of the Creative Commons Attribution License (CC BY). The use, distribution or reproduction in other forums is permitted, provided the original author(s) or licensor are credited and that the original publication in this journal is cited, in accordance with accepted academic practice. No use, distribution or reproduction is permitted which does not comply with these terms.



First Evaluation of the Role of Salp Fecal Pellets on Iron Biogeochemistry

Damien J. E. Cabanes^{1*}, Louiza Norman², Juan Santos-Echeandía³, Morten H. Iversen^{4,5}, Scarlett Trimbom^{4,6}, Luis M. Laglera⁷ and Christel S. Hassler¹

¹ Department F.-A. Forel for environmental and aquatic sciences, Earth and Environmental Sciences, University of Geneva, Geneva, Switzerland, ² Department of Plant Sciences, University of Cambridge, Cambridge, UK, ³ CSIC Instituto de Investigaciones Marinas, Vigo, Spain, ⁴ Alfred Wegener Institute Helmholtz Centre for Polar and Marine Research, Bremerhaven, Germany, ⁵ MARUM, University of Bremen, Bremen, Germany, ⁶ Marine Botany, University of Bremen, Bremen, Germany, ⁷ FI-TRACE, Chemistry department, Universitat de les Illes Balears, Palma, Spain

OPEN ACCESS

Edited by:

Douglas Patrick Connelly,
National Oceanography Centre, UK

Reviewed by:

Katlin Louise Bowman,
University of California, Santa Cruz,
USA
Jeffrey Alistair Hawkes,
Uppsala University, Sweden

*Correspondence:

Damien J. E. Cabanes
Damien.Cabanes@unige.ch

Specialty section:

This article was submitted to
Marine Biogeochemistry,
a section of the journal
Frontiers in Marine Science

Received: 24 November 2016

Accepted: 21 December 2016

Published: 10 January 2017

Citation:

Cabanes DJE, Norman L,
Santos-Echeandía J, Iversen MH,
Trimbom S, Laglera LM and
Hassler CS (2017) First Evaluation of
the Role of Salp Fecal Pellets on Iron
Biogeochemistry.
Front. Mar. Sci. 3:289.
doi: 10.3389/fmars.2016.00289

Planktonic grazers such as salps may have a dominant role in iron (Fe) cycling in surface waters of the Southern Ocean (SO). Salps have high ingestion rates and egest large, fast sinking fecal pellets (FPs) that potentially contribute to the vertical flux of carbon. In this study, we determined the impact of FPs from *Salpa thompsoni*, the most abundant salp in the SO, on Fe biogeochemistry. During the Polarstern expedition ANT-XXVII/3, salps were sampled from a large diatom bloom area in the Atlantic sector of the SO. Extensive work on carbon export and salp FPs export at the sampling location had shown that salps were a minor component of zooplankton and were responsible for only a 0.2% consumption of the daily primary production. Furthermore, at 100 m, export efficiency of salp FPs was ~2–3 fold higher than that of the bulk of sinking particulate organic carbon (POC). After collection, salps were maintained in 200 μm screened seawater and their FPs were collected for further experiments. To investigate whether the FPs release Fe and/or Fe-binding ligands into the filtered seawater (FSW) under different experimental conditions, they were either incubated in the dark or under full sunlight at *in situ* temperatures for 24 h, or placed into the dark after a freeze/thaw treatment. We observed that none of the treatments caused release of dissolved Fe (dFe) or strong Fe ligands from the salp FPs. However, humic-substance like (HS-like) compounds, weak Fe ligands, were released at a rate of $8.2 \pm 4.7 \mu\text{g HS-like FP}^{-1} \text{ d}^{-1}$. Although the Fe content per salp FP was high at $0.33 \pm 0.02 \text{ nmol dFe FP}^{-1}$, the small contribution of salps to the zooplankton pool resulted in an estimated dFe export flux of $11.3 \text{ nmol Fe m}^{-2} \text{ d}^{-1}$ at 300 m. Since salp FPs showed an export efficiency at 100 m well above that shown by the bulk of sinking POC, our results suggest that in those areas of the SO where salps play a major role in the grazing of primary production, they could be actively contributing to the depletion of the dFe pool in surface water.

Keywords: *Salpa thompsoni*, fecal pellets, iron speciation, southern ocean, iron cycling, humic substances

INTRODUCTION

In the Southern Ocean (SO), known to be the largest high nutrient low chlorophyll (HNLC) oceanic region, iron (Fe) availability is paramount in controlling primary productivity with subsequent implications for atmospheric carbon dioxide concentrations (Martin et al., 1990; Blain et al., 2007; Hassler et al., 2012). Knowledge and study of the different potential Fe sources are thus proving to be of major importance. Depending on the region, Fe can enter the SO mixed layer *via* different “external” inputs such as seasonal sea-ice retreat, dust deposition, resuspension of coastal and shallow sediments (Duce and Tindale, 1991; Lannuzel et al., 2007; Moore and Braucher, 2008) and upwelling phenomena (de Jong et al., 2012). Nevertheless, it has been demonstrated that in the HNLC regions from the SO, recycled Fe can account up to 90% of the total Fe biological supply (Boyd et al., 2005, 2010; Tagliabue et al., 2014), emphasizing that Fe recycling is an essential process sustaining primary productivity.

Studies have shown that zooplankton grazing affects the recycling of trace metals (Hutchins and Bruland, 1994; Strzepek et al., 2005; Tovar-Sanchez et al., 2007), but the relative contribution of the different key SO grazers krill, salps and copepods with respect to Fe recycling vs. export is still virtually undefined (Sarhou et al., 2008). In the western subarctic Pacific, copepod grazing has been shown to be a major route for the release of regenerated Fe and organic Fe-binding ligands, key compounds for its reactivity and bioavailability (Sato et al., 2007). Krill have also been shown to have an important role in Fe recycling which might be essential to maintain primary production in the SO (Tovar-Sanchez et al., 2007). Nevertheless, despite an observed decline in krill stocks coupled with a coincident increase in salps (Atkinson et al., 2004; Alcaraz et al., 2014), the impact of salps on Fe recycling has yet to be assessed.

Compared to krill or copepods (Pakhomov et al., 2006; Ducklow et al., 2012), it has been suggested that salps strongly contribute to the vertical flux of biogenic carbon due to their production of large, fast sinking fecal pellets (FPs; Pakhomov et al., 2002). Sinking velocity is an important parameter since it will determine the residence time during which the FPs will be subjected in the mixed layer to physicochemical recycling processes such as photo-degradation, before being exported and undergoing further microbial decomposition and coprophagy (Turner, 2002; Rontani, 2008; Pisani et al., 2011; Giering et al., 2014). For instance, FPs sinking velocity produced by small salp aggregates (10–20 mm length) was estimated at around 200–400 m d⁻¹ and from larger aggregates (20–30 mm length) at around 700 m d⁻¹ (Phillips et al., 2009). However, those values can be highly variable depending on size, density, form, and nutritional content of the FPs. Extensive work during our cruise, spotlighted a high retention of the salp FPs in the upper 300 m at ~80% suggesting extensive recycling processes and thus, their relatively weak contribution to the carbon export (Iversen et al., 2016). This assumption is in contrast with the one from Pakhomov et al. (2002) and highlights that salp FPs are not always conduits for rapid export.

This study explores the interaction between salp FPs and Fe biogeochemistry. In order to quantify the impact of salp FPs to both Fe recycling and export, the release of dissolved Fe (dFe) and Fe-binding ligands from *Salpa thompsoni* FPs was studied during laboratory and on-board incubation experiments. These studies simulated the physicochemical conditions that freshly released FPs encounter during their residence in surface waters. FPs used in this study were produced by salps collected in a large diatom bloom within the SO, suggesting that FPs were packed with diatom cells and therefore, rich in nutrients, Fe, and ligands. In order to assess the impact of light on Fe chemistry, we exposed FPs to visible and UV light. Furthermore, we tested the impact of freezing in order to determine a potential release of Fe and/or Fe-binding ligands due to physical break-up of FPs. Additionally, we made direct measurements of Fe content within salp FPs as well as their Fe:C ratio. The latter measurements allowed to estimate the role of salp FPs for vertical Fe fluxes.

MATERIALS AND METHODS

Sample Collection

During the Antarctic expedition ANTXXVIII/3 on-board the *R.V. Polarstern* (January to March 2012; Wolf-Gladrow 2013), salps were sampled from the center of a stable diatom bloom at 51°12.38 S, 12°39.80 W. The chlorophyll-*a* concentrations within the diatom bloom reached up to 2 μg chlorophyll *a* L⁻¹ (Hoppe et al., 2015).

For experiments, salps were collected during the night at a sampling depth of 25 m using a bongo net with cod ends lined with plastic to minimize metal contamination. Seawater that was previously collected at a sampling depth of 25 m using a Teflon double diaphragm pump (Wilden A100 with Teflon fittings; Kelair Pumps Australia Pty Ltd) and polyethylene tubing was used to maintain the salps and rinse salps and FPs. The seawater, collected in using trace metal clean techniques, was then directly pumped into a shipboard laminar flow hood inside of a trace metal clean room container. The sampled seawater was either screened through a 200-μm plankton net (screened seawater, SSW) or 0.2-μm filter (filtered seawater, FSW) (Acropak 1000, PALL). The collected salps were gently rinsed three times with this FSW, placed in a 50 L tank filled with SSW and kept in the dark at the *in situ* seawater temperature (3°C). Every 6–8 h, approximately one third of the SSW was carefully replaced with fresh SSW. From the incubation tanks, FPs were collected with a clean plastic pipette followed by FSW rinse. The FPs were either placed in a 100 mL trace metal clean low density polyethylene (LDPE) bottle filled with FSW for the on-board experiments or stored at -80°C for laboratory experiments. The salp FPs were compact looking pellets packed with particles (described as “type 1” in Iversen et al., 2016).

On-Board Experiments

These experiments aimed to measure short-term effects of freezing and light exposure on dFe and Fe-binding ligands release from salp FPs. Indeed, particulate organic matter may undergo photochemical transformations in the upper surface water that may lead to a production of dissolved organic matter (Pisani et al.,

2011) likely to interact with Fe chemistry. In the same manner, freezing causes break-up of the particles within the FPs and will potentially result in release of dissolved organic compounds to the surrounding waters. Considering that salp FPs take about 4–24 h to travel the first 100 upper meters, all the incubations were performed over a period of 24 h (Iversen et al., 2016). The on-board experiments were done in FSW with and without FPs. Two 20 L carboys were filled with FSW and 40 FPs were added to one of them. For consistency, both carboys were rolled and shaken for 20 min in order to homogenize the FPs. The two homogenized seawater batches were then transferred into 4 L polycarbonate bottles that were exposed to three different experimental conditions. Two incubation bottles were (i) frozen at -20°C for 10 h followed by thawing in the dark at sea surface temperature (SST) for 24 h (“freezer”), (ii) incubated for 24 h in the dark (“dark”), or (iii) exposed for 24 h to natural visible sunlight at SST in an on-deck incubator with a “flow-through” seawater system (“VIS”). Finally, 2 L were sampled from each 20 L carboy into 2 L polycarbonate bottles for the analysis of initial parameters (“control”). Treatments “freezer” and “dark” were wrapped in several layers of black plastic to maintain dark conditions whilst treatment “VIS” was contained in clear plastic bags (double wrapped). At the end of the incubation period, unfiltered and filtered ($0.2\text{-}\mu\text{m}$, Nuclepore, Millipore) samples were collected from each incubation bottle for determination of Fe speciation, humic substance-like material (HS-like, weak Fe ligands), dFe and macronutrients. Samples for dFe and macronutrients were analyzed on-board whereas Fe speciation and HS-like samples were stored at -20°C until analysis at the University of Geneva.

We determined the amount Fe leaching from the FPs after a period of 48 h acidification at pH 2.0 (HCl, Ultrapur, Merck). Six FPs were placed in six 30 mL LDPE containers filled with 10 mL of filtered surface seawater (dFe = 0.15 nM) and kept at room temperature before analysis by voltammetry (Laglera et al., 2013) with internal calibration. FP suspensions were not filtered before analysis since voltammetry is not responsive to particulate Fe.

Laboratory Experiments

Laboratory experiments were performed in synthetic seawater [AQUIL media based on Price et al. (1989) using major salts only, pH = 8.13] to facilitate Fe binding ligands detection and to extend light exposure to ultraviolet light (“UV”). Four polytetrafluoroethylene-capped quartz sample tubes were filled with 10 mL of synthetic seawater and six FPs were added to two of them. One tube with FPs and one without FPs were placed under a sunlight simulator and exposed to UV and visible light (220–780 nm, 1940 $\mu\text{Einstein}$, ABET Technologies Sun 2000) for 30 min on ice prior to 24 h incubation in the dark at 4°C on an agitation plate (100 rpm; VWR STD 3500). The two other tubes were placed directly on the agitation plate without exposure to light (“dark”). After incubation, each sample was filtered on to a $0.2\text{-}\mu\text{m}$ polycarbonate filter for analysis of dFe, HS-like and Fe speciation. Samples for Fe speciation and HS-like were stored at -20°C and dFe samples were acidified [0.5% with quartz distilled hydrochloric acid (qHCl), VWR] and left at room temperature until analysis.

The total Fe content in FPs was determined after storing five FPs in a mixture of HCl/HNO₃ (pH = 1.52) for 2 months ($n = 2$) prior being analyzed by Inductively Coupled Plasma Mass Spectrometry (Agilent 7700). Aluminum (Al), nickel (Ni), copper (Cu), zinc (Zn), and molybdenum (Mo) were also quantified. Standard solutions for ICP (Sigma) were used for the calibrations and the blank averages in counts per second were 343 (^{27}Al), 18076 (^{56}Fe), 437 (^{64}Zn), 2848 (^{65}Cu), 120 (^{60}Ni), and 247 (^{98}Mo).

Analytical Techniques and Experimental Precautions

DFe, HS-like and Fe speciation analyses were performed using a $\mu\text{Autolab}$ potentiostat (Ecochemie, Netherlands) with a 663 Metrohm stand as in Norman et al. (2015) and Laglera et al. (2013). Fe speciation was measured by Competitive Ligand Exchange-Adsorptive Cathodic Stripping Voltammetry (CLE-AdCSV) as per Abualhaija and van den Berg (2014) in order to provide the concentration of Fe-binding ligands (L_T) and the conditional stability of their complexes with Fe ($K'_{\text{Fe}L}$). Analysis of SAFe (Sampling and Analysis of Fe) reference sample S ($0.101 \pm 0.005\text{ nM}$; $n = 3$), detection limit (0.05 nM) and side reaction coefficient for salicylaldehyde (SA) at a concentration of $5\text{ }\mu\text{M}$ ($\alpha_{\text{Fe}^3+\text{SA}} = 20.1$) were in accordance with the literature (Abualhaija and van den Berg, 2014; Mahmood et al., 2015). Peak heights and the chemical speciation parameters were calculated with ECDSOFT and proMCC software, respectively (Omanović et al., 2015). Titrations performed on AQUIL samples in the presence of 5 nM desferrioxamine B (DFB; **Figure 1C**) allowed us to validate our analytical method. Both L_T ($4.61 \pm 0.13\text{ nM}$; $n = 2$) and stability constant ($\log K'_{\text{Fe}L}$ of 12.25 ± 0.04) corresponded with reported values (Witter et al., 2000; Abualhaija and van den Berg, 2014). HS-like compounds were determined using the voltammetric method of Laglera et al. (2007) with standard addition on each sample of Suwannee River Fulvic Acid (SRFA, International Humic Substances Society, standard 1) for calibration. The limit of detection was $1.88\text{ }\mu\text{g SRFA.L}^{-1}$. DFe was measured onboard by catalytic cathodic voltammetry (Laglera et al., 2013) and a summary of data can be found in (Hoppe et al., 2015). Macronutrients (nitrate (NO_3^-), nitrite (NO_2^-), orthophosphate (PO_4^{3-}), and orthosilicate ($\text{Si}(\text{OH})_4$) were determined colorimetrically on-board using a Technicon TRAACS 800 autoanalyzer (details in Hoppe et al., 2015).

All plastic-ware was trace metal cleaned as per the GEOTRACES guidelines (Cutter et al., 2010) to avoid contamination. Experimental samples were sealed in triple bags during equilibration/incubation periods and all the manipulations were carried out in an ISO Class 5 laminar flow hood.

Salp FP Fluxes

Salp FP fluxes were collected with free-drifting sediment traps at 100 and 300 m and a detailed description is provided by Iversen et al. (2016). Salp FPs are very large and fairly easy to identify. They are very compact and much bigger than FPs from crustaceans like copepods, amphipods, and krill. They are further

surrounded by mucus membrane which differentiate salp pellets from physically formed aggregates such as marine snow. The sediment traps were surface attached to a buoy that provide GPS positions during the deployment. Additionally, the sediment trap had two surface floats for buoyancy as well as 12 small air-filled balls (used as wave-breakers). The trap deployments lasted ~24 h. The collection cylinders at the two depths contained a viscous gel that preserved the size, shape, and structure of the collected aggregates, including salp FPs (Iversen et al., 2016). We measured the x, y, and z dimensions of each salp FP in order to determine its volume and used a carbon to volume ratio to calculate carbon fluxes from salp FPs at 100 and 300 m. The carbon to volume ratio was determined from pellets produced during the pellet production incubation (Iversen et al., 2016).

Statistics

Statistical analysis was performed using Sigma Plot (Systat Software Inc.). Whether for the on-board or laboratory experiments, the various treatments (“freezer,” “dark,” and “VIS” for on-board incubations; “UV” and “dark” for laboratory experiments) did not have a significant impact on any parameter (one-way ANOVA, $p = 0.167$). A t -test was therefore performed to verify whether the FPs affected analytical parameters over all the treatments. Finally, the concentration differences related to the presence of FPs are presented as averages calculated over all the treatments.

RESULTS

Integrated numbers of salp individuals in the upper 250 m of the water column were between 19.8 and 54.4 individuals m^{-2} (Iversen et al., 2016). The daily egestion rate per *S. thompsoni*

individual and the carbon content from salp FPs measured at our sampling site were $0.33 \text{ FP ind}^{-1} \text{ h}^{-1}$ (resulting in a daily production of $310 \pm 126 \text{ FPs m}^{-2}$ for the upper 250 m) and $17.6 \pm 27 \mu\text{g C FP}^{-1}$, ($n = 33$), respectively (Iversen et al., 2016; **Table 1**). Those values are comparable to the average values reported from salp individuals and their respective FPs collected at the Western Antarctic Peninsula (WAP) of $0.25 \text{ FP ind}^{-1} \text{ h}^{-1}$ and $3.62 \mu\text{g C FP}^{-1}$, respectively (Phillips et al., 2009; Gleiber et al., 2012). According to calculated sinking rates, salp FPs take about 4–24 h to travel the 100 m upper meters (Iversen et al., 2016). Continuous sampling over 2 weeks using sediment traps at the location of the diatom bloom showed that carbon export by salp FPs products accounted in average for $1.6 \text{ mg C m}^{-2} \text{ d}^{-1}$ at 100 m and $0.6 \text{ mg C m}^{-2} \text{ d}^{-1}$ at 300 m (**Table 1**), indicating substantial recycling before 300 m depth (Iversen et al., 2016).

Fe and Other Trace Metals Content in Salp FPs

Results from the determination of leachable Fe from salp FPs and total trace-metals content are summarized in (**Table 2**). Our analysis revealed a total Fe concentration of $0.33 \pm 0.02 \text{ nmol Fe}$

TABLE 1 | Salp fecal pellets (FPs) properties from ANTXXVIII/3 expedition at the sampling site from Iversen et al. (2016).

FPs properties		
FPs production rate	($\text{FP ind}^{-1} \text{ h}^{-1}$)	0.33
FPs carbon content	($\mu\text{gC FP}^{-1}$)	17.6
FPs standing stock, upper 250 m	(FPs m^{-2})	310 ± 126
FPs carbon flux at 100 m	($\text{mgC m}^{-2} \text{ d}^{-1}$)	1.6
FPs carbon flux at 300 m	($\text{mgC m}^{-2} \text{ d}^{-1}$)	0.6

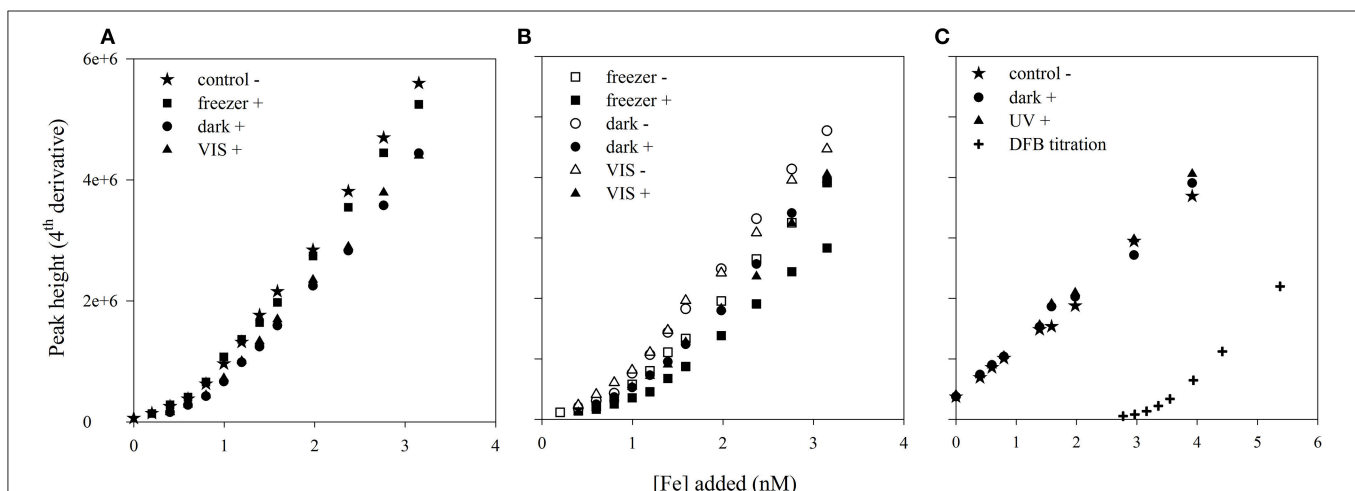


FIGURE 1 | Iron speciation titrations performed by CLE-AdCSV (Competitive Ligand Exchange-Adsorptive Cathodic Stripping Voltammetry) of $0.2 \mu\text{m}$ filtered seawater (FSW) (A) and unfiltered seawater (unFSW) (B) from on-board experiments, as well as on artificial seawater (AQUIL) from laboratory experiments (C). Presence or absence of salp fecal pellets (FPs) is indicated by “+” and “-”, respectively. Control curves correspond to the first sampling time, before the start of the incubation processes and “freezer” [freezing for 10 h followed by thawing in the dark at sea surface temperature (SST)], “dark” (24 h incubation in the dark, SST), “vis” (24 h incubation under natural sunlight, SST), and “UV” (30 min under UV and visible light followed by 24 h in the dark at 4°C) are the different treatments applied. Calibration titrations were performed in artificial seawater (AQUIL) in presence of 5 nM of the siderophore desferrioxamine B (DFB).

TABLE 2 | Amount of Fe leached after a period of 48 h at pH 2.0 and FPs trace metals content (iron [Fe], aluminum [Al], nickel [Ni], copper [Cu], zinc [Zn], and molybdenum [Mo]) after 2 months at pH 1.5.

Trace-metals content			Fe	Al	Ni	Cu	Zn	Mo
48 h	pH 2.0	$n = 6$	0.033 ± 0.04					
2 months	pH 1.5	$n = 2$	0.33 ± 0.02	1.45 ± 0.13	0.011 ± 0.001	0.025 ± 0.006	0.177 ± 0.002	0.003 ± 0.000

All the values are in nmol.FP^{-1} and n represent the number of replicates.

FP^{-1} ($n = 2$). Fe was in a very refractory form since only 10% was released following acidification to pH 2.0 for 48 h ($0.033 \pm 0.040 \text{ nmol.FP}^{-1}$, $n = 6$). Taking into account the total carbon content quantified in salp FPs collected during the same sampling period ($17.6 \pm 27 \mu\text{g C.FP}^{-1}$; Iversen et al., 2016), we estimated a Fe:C ratio of $225 \mu\text{mol Fe mol C}^{-1}$. Finally, ICP-MS analysis of other trace elements showed that aluminum was the most abundant element found in the FPs ($1.45 \pm 0.13 \text{ nmol.FP}^{-1}$) followed by Fe ($0.33 \pm 0.02 \text{ nmol.FP}^{-1}$), zinc ($0.177 \pm 0.002 \text{ nmol.FP}^{-1}$), copper ($0.025 \pm 0.006 \text{ nmol.FP}^{-1}$), nickel ($0.011 \pm 0.001 \text{ nmol.FP}^{-1}$), and molybdenum ($0.003 \pm 0.000 \text{ nmol.FP}^{-1}$).

On-Board Experiments

All measured parameters from the on-board incubation are summarized in the top part section of (Table 3). None of the experimental treatments (“freezer,” “dark,” and “VIS”) significantly increased PO_4^{3-} or NO_x ($\text{NO}_2^- + \text{NO}_3^-$) concentrations ($p = 0.49$ and 0.90 respectively, $n = 8$). In contrast, an increase in Si(OH)_4 concentrations ($p = 0.001$, $n = 8$) by $0.53 \pm 0.11 \mu\text{mol L}^{-1}$ was observed. No variation in dFe concentration was detected for any of the experimental treatments ($p = 0.26$, $n = 14$) despite a potential release of $0.66 \text{ nmol Fe L}^{-1}$ estimated from the salp FPs total Fe content. Results from Fe-binding ligand titrations indicated that FPs did not significantly affect L_T or $\log K'_{\text{FeL}}$ of the ligand class detected in filtered samples ($p = 0.14$ and 0.65 , $n = 8$; Figure 1A). Although for unfiltered samples, we observed a slight release of L_T from the FPs (between 0.07 and $0.22 \text{ nmol } L_T \text{ FP}^{-1}$; Figure 1B), this effect was, however, not statistically significant ($p = 0.088$ and $p = 0.46$, $n = 6$). HS-like concentrations increased significantly in the presence of FPs ($p = 0.031$, $n = 14$) by 16.43 ± 9.45 and $30.86 \pm 18.57 \mu\text{g L}^{-1}$ for filtered and unfiltered samples, respectively, corresponding to a release of 8.22 ± 4.72 and $15.43 \pm 9.28 \mu\text{g HS-like.FP}^{-1} \text{ d}^{-1}$ (since we had a concentration of two FPs per liter).

Laboratory Experiment

All measured parameters from the laboratory incubation are summarized in the bottom section of the (Table 3). For both treatments (“UV” and “dark”), the presence of FPs did not have any impact on the dFe concentrations ($p = 0.73$, $n = 4$). Similarly to the on-board experiments, we observed a release of humic substances ($p = 0.002$, $n = 4$) of $8.74 \pm 0.52 \mu\text{g L}^{-1}$ corresponding to a daily release of $0.78 \pm 0.05 \mu\text{g HS-like.FP}^{-1} \text{ d}^{-1}$. Based on the Fe organic complexation analyses, no

ligands were detected in any of the samples (both treatments, with and without FPs) since the titration curves were virtually linear (Figure 1C).

DISCUSSION

Salps were collected at the center of a stable diatom bloom covering an area of about 8000 km^2 between the Antarctic Polar Front and the Southern Antarctic Circumpolar Current Front (Strass et al., 2016). Compared to previous studies (Pakhomov et al., 2006; Phillips et al., 2009), low to medium abundances of salp were observed in the upper 250 m of the water column (19.8 to 54.4 ind m^{-2} ; Iversen et al., 2016). Particulate organic carbon per day produced as salp FPs was 3.3 mg C.m^{-2} , this is equivalent to salp ingesting and releasing daily only $\approx 0.2\%$ of the net primary production (NPP) estimated in the study area (1751 mg C m^{-2} , Hoppe et al., 2015). The total POC flux averaged over the 3 weeks of study at 100 m was 18% of the NPP, $317 \pm 175 \text{ mg C m}^{-2} \text{ d}^{-1}$. High POC transfer efficiencies were observed between 100 m and 300 m at $\sim 60\%$ (flux of $176 \pm 126 \text{ mg C m}^{-2} \text{ d}^{-1}$ at 300 m) mainly due to efficient sinking of diatoms (Roca Martí et al., 2016). Large fast sinking salp FPs are remarkably more efficiently exported below 100 m (about $\sim 50\%$ of the salp FP production is exported vs. $\sim 20\%$ POC). In their transit from 100 to 300 m, the transfer efficiencies are similar at $\sim 60\%$ (Figure 2).

Impact of Salp Fps on Macronutrient Concentrations

FPs are composed predominantly of organic compounds directly related to the material ingested (Madin, 1982; Manno et al., 2015). Therefore, the increasing dSi(OH)_4 concentrations observed in presence of FPs in our on-board experiments can be linked to the high ingestion rates of the salps at the time of sampling. Accordingly, dSi(OH)_4 concentrations were depleted in the collected FSW ($2.93 \mu\text{mol L}^{-1}$, Table 3). Our incubations showed that salp FPs released $265 \text{ nmol dSi(OH)}_4 \text{ FP}^{-1} \text{ d}^{-1}$. Using the daily salp FP production (Table 1) determined during the cruise, the integrated Si(OH)_4 release from salp FPs was $82.2 \mu\text{mol dSi(OH)}_4 \text{ m}^{-2} \text{ d}^{-1}$ in the upper 250 m (Table 4). Despite concentrations below $3 \mu\text{mol L}^{-1} \text{ dSi(OH)}_4$ in the upper 40 m, the Si(OH)_4 standing stock in the upper water column was stable with values ranging between ~ 600 and $700 \text{ mmol dSi(OH)}_4 \text{ m}^{-2}$ (Hoppe et al., 2015). Hence, the daily added dSi(OH)_4 concentrations from salp FPs were almost one

TABLE 3 | Concentrations of macronutrients (phosphate [PO₄³⁻], orthosilicate [Si(OH)₄], nitrate [NO_x = NO₃⁻ + NO₂⁻]), dissolved iron (dFe), humic-substances-like [HS-like], total ligand [L_T] as well as stability constant [log K'_{FeL}] data are given.

	FPS	PO ₄ ³⁻ μmol L ⁻¹	Si(OH) ₄ μmol L ⁻¹	NO _x	dFe nmol L ⁻¹	HS-like μg L ⁻¹	L _T nmol L ⁻¹	log K' _{FeL}
ON-BOARD EXPERIMENTS								
0.2 μm Filtrated Samples								
Control	-	1.25	2.93	20.00	0.22 ± 0.02	32.65 ± 0.88	0.99 ± 0.02	11.28 ± 0.02
	+	1.28	3.49	19.93	0.21 ± 0.01	47.66 ± 0.37	1.05 ± 0.03	11.26 ± 0.05
freezer	-	1.28 ± 0.02	3.15 ± 0.04	19.91 ± 0.01	0.25 ± 0.04	29.05 ± 0.93	0.95 ± 0.07	11.30 ± 0.11
	+	1.28 ± 0.01	3.68 ± 0.03	19.86 ± 0.06	0.17 ± 0.01	48.00 ± 1.01	1.01 ± 0.05	11.14 ± 0.05
dark	-	1.26 ± 0.01	3.09 ± 0.11	19.64 ± 0.04	0.19 ± 0.02	29.47 ± 0.24	0.98 ± 0.02	11.38 ± 0.03
	+	1.29 ± 0.00	3.77 ± 0.21	19.75 ± 0.07	0.15 ± 0.03	56.73 ± 1.65	0.98 ± 0.03	11.31 ± 0.04
VIS	-	2.03 ± 1.05	3.28 ± 0.36	19.66 ± 0.01	0.20 ± 0.10	12.76 ± 0.14	0.88 ± 0.04	11.23 ± 0.06
	+	1.72 ± 0.57	3.64 ± 0.04	19.61 ± 0.04	0.14 ± 0.01	17.27 ± 0.48	0.97 ± 0.03	11.37 ± 0.04
UNFILTERED SAMPLES								
freezer	-				0.22 ± 0.02	27.75 ± 0.25	1.16 ± 0.06	11.37 ± 0.07
	+				0.22 ± 0.00	71.79 ± 0.14	1.60 ± 0.07	11.23 ± 0.05
dark	-				0.16 ± 0.01	38.50 ± 0.31	1.08 ± 0.07	11.34 ± 0.10
	+				0.18 ± 0.02	77.41 ± 0.62	1.48 ± 0.04	11.15 ± 0.04
VIS	-				0.44 ± 0.29	13.54 ± 0.12	1.00 ± 0.05	11.20 ± 0.07
	+				0.36 ± 0.33	23.16 ± 0.09	1.14 ± 0.08	11.34 ± 0.1
LABORATORY EXPERIMENTS IN AQUIL								
Control	-				0.76 ± 0.04	3.23 ± 0.05	n.d.	n.d.
dark	-				0.70 ± 0.02	3.53 ± 0.09	n.d.	n.d.
	+				0.74 ± 0.02	11.75 ± 0.54	n.d.	n.d.
UV	-				0.73 ± 0.09	4.48 ± 0.09	n.d.	n.d.
	+				0.78 ± 0.01	13.73 ± 0.19	n.d.	n.d.

"n.d." denotes "not detected." Salp fecal pellets (FPs) presence or absence is indicated by + or - respectively. During the on-board experiments the following different treatments were applied: "freezer" [freezing for 10 h followed by thawing in the dark at sea surface temperature (SST)], "dark" (24 h incubation in the dark, SST) and "VIS" (24 h incubation under natural sunlight, SST). Samples from those treatments either remained unfiltered at the end of the incubations or were 0.2 μm filtered. During the laboratory experiments the following different treatments were applied: "dark" (24 h incubation in the dark at 4°C) and "UV" (30 min under UV and visible light followed by 24 h in the dark at 4°C). For both experiments (on-board and laboratory), control represents the subsampling done before to start incubation.

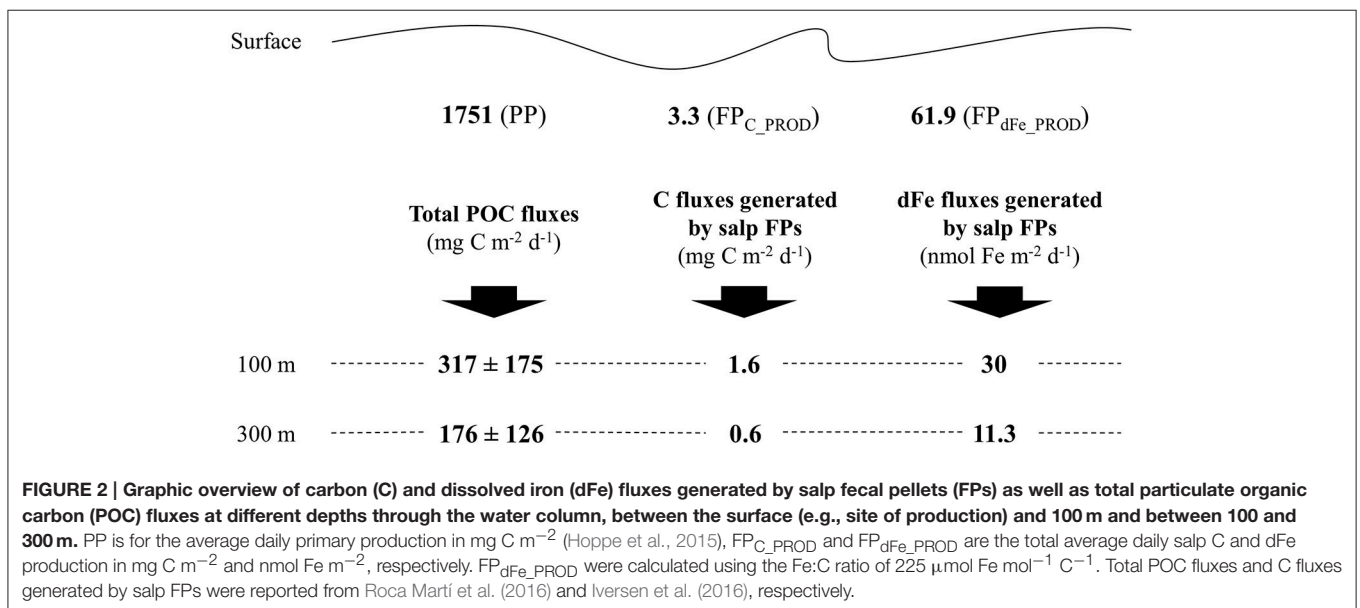


TABLE 4 | Estimated orthosilicate (Si(OH)₄), humic substances-like (HS-like), and dissolved iron (dFe) fluxes generated by salp FPs from on-board and laboratory experiments and Fe:C ratio.

Si(OH) ₄		
Release per FP	($\mu\text{mol FP}^{-1} \text{d}^{-1}$)	0.265 ^{af} ± 0.055
Flux, upper 250 m	($\mu\text{mol m}^{-2} \text{d}^{-1}$)	82.15 ^{af} ± 17.05
HS-LIKE		
Release per FP	($\mu\text{g FP}^{-1} \text{d}^{-1}$)	8.22 ^{af} ± 4.72
		15.43 ^{au} ± 9.28
		0.78 ^b ± 0.05
Flux, upper 250 m	($\text{mg m}^{-2} \text{d}^{-1}$)	2.55 ^{af} ± 1.46
		4.78 ^{au} ± 2.88
		0.24 ^b ± 0.02
DFE		
Fe release per salp (in FPs)	($\text{nmol ind}^{-1} \text{d}^{-1}$)	2.61 ^b
Standing stock, upper 250 m	(nmol m^{-2})	61.9 ^b
Flux at 300 m	($\text{nmol m}^{-2} \text{d}^{-1}$)	11 ^b
Fe:C ratio	($\mu\text{mol Fe mol C}^{-1}$)	225 ^b

^{af} On-board experiment, filtered samples.

^{au} On-board experiment, unfiltered samples.

^b Laboratory experiment.

order of magnitude below the standing stock, suggesting that the release observed of dSi(OH)₄ (corresponding to our three physico-chemical experimental treatments: “freezer,” “dark,” and “VIS”) would not have substantially contribute to the maintenance of the observed diatom bloom.

Impact of Salp Fps on DFe Concentrations

Satellite images showed that the diatom bloom maintained high chl *a* concentrations (> $\mu\text{g L}^{-1}$) for many weeks (weeks before and after our period of monitoring), implying sufficient Fe supply over all this period. DFe concentrations remained low at 0.1–0.2 in the upper 100 m during our 3 weeks sampling (Laglera et al., 2013; Hoppe et al., 2015). Due to the absence of major “external” Fe inputs at our sampling site, Fe recycling processes should have consequently played a major role in the maintaining of the diatom bloom. From our experimental results, the different treatments that we applied to the FPs did not lead to the release of dFe suggesting that salp FPs could have barely contributed to Fe recycling in the euphotic zone. However, we cannot discount biological processes such as zooplankton grazing on fecal products (coprophagy) and microbial degradation that were not evaluated in this work (Turner, 2002; Dagg et al., 2014; Morata and Seuthe, 2014). Acidification to pH 2.0, a treatment too mild to leach intracellular Fe from intact planktonic cells (Lannuzel et al., 2011), released only 10% of Fe associated with salp FPs (Table 2). In comparison, the same treatment was found to be strong enough to leach ~100% of the Fe in FPs egested by individuals of the SO copepod *Calanus simillimus* (Laglera et al., unpublished data). This difference might be explained by different ingestion procedures and gut passage efficiencies. Copepods crack and grind what they capture before ingestion, potentially allowing their FPs to be more easily degradable, contrary to the salp that are purely passive filterers (Kjørboe, 2011). In this sense, our results show that the Fe inside salp FPs is in extremely refractory form (possibly due to a low digestion efficiency), supporting the result that physico-chemical processes

did not alter our salp FPs content. Accordingly, the zooplankton group dominant in a determined area of the ocean can have an important effect on the percentage of Fe that is recycled in the euphotic zone.

The Fe:C ratio estimated in our salp FPs (225 $\mu\text{mol Fe mol C}^{-1}$; Table 4) is relatively high in comparison with the commonly observed Fe:C ratios in plankton of HNLC waters, which are in the order of 10–50 $\mu\text{mol Fe mol}^{-1} \text{C}^{-1}$ (Twining and Baines, 2013; Boyd et al., 2015). In the absence of other studies, it seems from our results that salps have neither significant Fe metabolic requirements nor do they accumulate Fe in their tissues. The enrichment of Fe in salp FPs determined during our experiments seems to demonstrate that most of the Fe ingested by the salps was packed into FPs, contrary to the copepods for whom half of ingested Fe was regenerated to dissolved forms (Schmidt et al., 1999) during the ingestion in a process denoted sloppy feeding. In the same way, using salp FP fluxes we determined an export at 100 and 300 m depth of ~30 $\text{nmol Fe m}^{-2} \text{d}^{-1}$ and ~11.3 $\text{nmol Fe m}^{-2} \text{d}^{-1}$ respectively (Table 4). In comparison to the total dFe stock in the upper 100 m at the sampling location (~10–15 $\mu\text{mol Fe m}^{-2}$; Laglera et al., 2013; Hoppe et al., 2015), our export flux represents only ~0.1% of this dFe standing stock, which is in agreement with low Fe exports estimated in previous works where salp FPs represent ~0.3% of the estimated total Fe used by phytoplankton across the SO (Boyd et al., 2012). Taking into account previous estimates of new Fe supplies resulting from island wake (vertical flux of 4 $\text{nmol Fe m}^{-2} \text{d}^{-1}$, Blain et al., 2007), atmospheric deposition (3.2–51.2 $\text{nmol Fe m}^{-2} \text{d}^{-1}$, Wagener et al., 2008), and seasonal sea-ice melt (<10–800 $\text{nmol Fe m}^{-2} \text{d}^{-1}$, Lancelot et al., 2009), our Fe sequestration flux (at 300 m) might significantly reduce new Fe supply in remote areas of limited inputs and high salp concentrations.

Regarding the other trace-metals, Fe was the most abundant essential element after Al, followed by Zn, Cu, Ni, and Mo, which is in accordance with the reported trace metal composition of marine phytoplankton (Twining and Baines, 2013). The high Al content determined in our salp FPs could be explained by the fact that the diatoms are able to take up significant amount of Al (both adsorption and incorporation into soft tissues) during bloom events (Moran and Moore, 1988; Ren et al., 2011) despite its recognized toxicity toward numerous organisms (Gillmore et al., 2016).

Impact of Salp Fps on Fe Organic Speciation

Fe-binding ligands are key compounds that control both Fe reactivity (Barbeau, 2006; Rijkenberg et al., 2006) and bioavailability to phytoplankton (Hassler et al., 2011a,b, 2015; Norman et al., 2014). In this study, we could not detect, after any treatment (“freezer,” “VIS,” “UV,” and “dark”), a release of ligands by salp FPs. Such an observation was not due to an absence of ligands in the pellets, but possibly to the reduction of the assimilation and digestion efficiency of the ingested food under blooming conditions referred to above (Von Harbou, 2009); i.e., salps could not break the hard frustule of a good percentage of the ingested diatoms.

Zooplankton grazing is known to be an important autochthonous source of colored and fluorescent organic

matter, including marine humic substances (Ortega-Retuerta et al., 2009; Nakayama et al., 2011). In fact, Fe-binding HS-like compounds were released in the presence of salp FPs and we could calculate an HS-like potential flux from FPs of 2.5 and 0.24 mg HS-like $\text{m}^{-2} \text{d}^{-1}$ for the field and laboratory work, respectively (Table 4). The difference could be explained by the fact that the field-work was carried out in SSW containing bacteria and viruses which could have enhanced the release of HS-like compounds. We therefore concluded that salp FPs could be a source of weak Fe-binding ligands with low $\log K'_{\text{Fe}^2\text{L}}$ likely below our analytical detection limit ($\alpha_{\text{Fe}^2\text{SA}} = 20.1$), explaining why we did not detect them by CLE-AdCSV. In line with this, previous work on humic substances showed that the $\log K'_{\text{Fe}^2\text{L}}$ values of their complexes with Fe were around 10.6 (Laglera and van den Berg, 2009), nearly 1 log unit below that of other major ligand groups. Hence, our results show that HS-like compounds contributed to the pool of photo-sensitive HS material likely to be autochthonously produced, such as exopolymeric substances or marine humic substances (Obnersterer and Herndl, 2000; Barbeau et al., 2003; Hassler et al., 2011a; Laglera et al., 2011). Unfortunately, to date, the nature of organic compounds contributing to the pool of HS material detected by CSV remains poorly characterized.

Environmental Implications

The SO plays a critical role in global ocean circulation (Lumpkin and Speer, 2007) and acts as a significant atmospheric CO_2 sink (Bopp et al., 2001; Sabine et al., 2004). As such, the ocean circulation dynamics of the SO globally affects biogeochemical cycles, biodiversity and climate regulation. The hypothesized increase in salp dominance in the SO due to a depletion of sea-ice (Atkinson et al., 2004) could enhance their annual contribution to carbon vertical flux. Compared to krill, salps consume more food more effectively (Perissinotto and Pakhomov, 1998), produce larger and denser FPs with high carbon content (Gleiber et al., 2012) and have higher sinking velocity (Phillips et al., 2009; Turner, 2015). Increasing abundances of salps over krill could imply important changes to the lower and higher trophic levels (Fraser and Hofmann, 2003) with strong implications for the biological pump activity and associated carbon sequestration.

Based on our incubation experimental settings, salps do not easily release strong Fe ligands as it is the case during grazing by other zooplankton groups such as copepods (Sato et al., 2007). However, the rapid release of weak Fe-binding ligands from salp FPs could affect Fe bioavailability by enhancing Fe solubility and accelerating Fe uptake (Hassler et al., 2011a,b). Therefore, Fe speciation in the presence of salps is difficult to predict as it will depend on food quality and egestion rate, both strongly dependent on the phytoplankton community and chlorophyll concentration present (Von Harbou, 2009).

Our study shows that salp FPs store high concentrations of Fe that are not released rapidly enough by physicochemical processes to enter the recycling loop before sinking below the euphotic zone. Differences in the decrease of organic carbon associated with the bulk of POC (which included particles such as single diatom cells, marine snow, and copepod and krill FPs) and with the salp FPs between the surface (e.g., site of production) and 100 m, indeed suggest that the export efficiencies of salp FPs

are 2.5-fold higher (Figure 2). Nevertheless, the organic carbon associated with FPs decrease by a factor of two as they settle down to 100 m, suggesting that biological recycling of FPs occur. In our case, relatively low salp numbers, compared to other reports from the Southern Ocean (Pakhomov et al., 2002; Atkinson et al., 2004; Phillips et al., 2009), allowed that Fe export was kept to a minimum, resulting in less Fe export that what would be exported in situation of high salp abundances. Under such conditions, with a carbon export in the form of salp FPs of about 20 mg C $\text{m}^{-2} \text{d}^{-1}$ at 300 m depth (Phillips et al., 2009), a Fe:C ratio of 225 $\mu\text{mol Fe mol C}^{-1}$ would generate an Fe export of $\approx 375 \text{ nmol Fe m}^{-2} \text{d}^{-1}$ which would deplete dFe stocks in HNLC areas during a period of a few days with consequences for phytoplankton Fe limitation.

More studies on biological remineralization processes associated with salp FPs are needed to estimate whether salp FPs contribute to Fe export. Due to changes in the dominance of zooplankton predicted across the SO and its potential impact for Fe biogeochemistry, comparative studies on the impact of grazing activities and FP degradation rates between salps, krill and copepods are urgently needed.

AUTHOR CONTRIBUTIONS

DC contributed to the experiments, chemical analyses, interpretation of data and redaction of the manuscript. LN contributed to the experiments, and redaction of the manuscript. JS contributed to the analyses. MI contributed to the interpretation of data as well as the manuscript. ST participated to the experiments and to manuscript. LL contributed to the analyses, interpretation of the data and the manuscript. CH contributed to the experimental design, interpretation of data as well to the manuscript.

FUNDING

DC was funded by the Swiss National Science Foundation (PP00P2_138955), LN by the UTS Chancellor Fellowship and CH by the Australian Research Council (Discovery Project DP1092892 and LIEF grand LE0989539) and the Swiss National Science Foundation (PP00P2_138955). LL and JS participation was funded by the MINECO of Spain (Grant CGL2010-11846-E) and the Government of the Balearic Islands (Grant AAEE083/09). ST was funded by the Deutsche Forschungsgemeinschaft (DFG) in the framework of the priority programme “Antarctic Research with comparative investigations in Arctic ice areas,” project TR 899/2 as well as the Helmholtz Impulse Fond (Helmholtz Young Investigators Group EcoTrace). MI was funded by the Helmholtz Association for the Helmholtz Young Investigator Group SeaPump.

ACKNOWLEDGMENTS

We would like to thank Captain and crew of the *RV. Polarstern*, as well as the scientific party, for their assistance and support during the ANT-XXVIII-3 voyage. We especially thank E. Pakhomov and B. Hunt for their assistance with the collection and maintenance of the salps and S. Ossebaar for the on-board macronutrient analysis.

REFERENCES

- Abualhija, M. M., and van den Berg, C. M. G. (2014). Chemical speciation of iron in seawater using catalytic cathodic stripping voltammetry with ligand competition against salicylaldehyde. *Mar. Chem.* 164, 60–74. doi: 10.1016/j.marchem.2014.06.005
- Alcaraz, M., Almeda, R., Duarte, C. M., Horstkotte, B., Lasternas, S., and Agustí, S. (2014). Changes in the C, N and P cycles by the predicted salps-krill shift in the Southern Ocean. *Front. Mar. Sci.* 1:45. doi: 10.3389/fmars.2014.00045
- Atkinson, A., Siegel, V., Pakhomov, E., and Rothery, P. (2004). Long-term decline in krill stock and increase in salps within the Southern Ocean. *Nature* 432, 100–103. doi: 10.1038/nature02996
- Barbeau, K. (2006). Photochemistry of organic iron(III) complexing ligands in oceanic systems. *Photochem. Photobiol.* 82, 1505–1516. doi: 10.1111/j.1751-1097.2006.tb09806.x
- Barbeau, K., Rue, E. L., Trick, C. G., Bruland, K. W., and Butler, A. (2003). Photochemical reactivity of siderophores produced by marine heterotrophic bacteria and cyanobacteria based on characteristic Fe(III) binding groups. *Limnol. Oceanogr.* 3, 1069–1078. doi: 10.4319/lo.2003.48.3.1069
- Blain, S., Queguiner, B., Armand, L., Belviso, S., Bombled, B., Bopp, L., et al. (2007). Effect of natural iron fertilization on carbon sequestration in the Southern Ocean. *Nature* 446, 1070–1074. doi: 10.1038/nature05700
- Bopp, L., Monfray, P., Aumont, O., Dufresne, J.-L., LeTreut, H., Madec, G., et al. (2001). Potential impact of climate change on marine export production. *Glob. Biogeochem. Cycles* 15, 81–99. doi: 10.1029/1999gb001256
- Boyd, P., Strzepek, R., Ellwood, M., Hutchins, D., Nodder, S., Twining, B., et al. (2015). Why are biotic iron pools uniform across high- and low-iron pelagic ecosystems? *Global Biogeochem. Cycles* 29, 1028–1043. doi: 10.1002/2014GB005014
- Boyd, P. W., Arrigo, K. R., Strzepek, R., and van Dijken, G. L. (2012). Mapping phytoplankton iron utilization: insights into southern ocean supply mechanisms. *J. Geophys. Res.* 117:C06009. doi: 10.1029/2011JC007726
- Boyd, P. W., Ibisani, E., Sander, S. G., Hunter, K. A., and Jackson, G. A. (2010). Remineralization of upper ocean particles: implications for iron biogeochemistry. *Limnol. Oceanogr.* 55, 1271–1288. doi: 10.4319/lo.2010.55.3.1271
- Boyd, P. W., Law, C. S., Hutchins, D. A., Abraham, E. R., Croot, P. L., Ellwood, M., et al. (2005). FeCycle: attempting an iron biogeochemical budget from a mesoscale SF6 tracer experiment in unperturbed low iron waters. *Global Biogeochem. Cycles* 19:GB4S20. doi: 10.1029/2005GB002494
- Cutter, G., Andersson, P., Codispoti, L., Croot, P., François, R., Lohan, M. C., et al. (2010). *Sampling and Sample-Handling Protocols for GEOTRACES Cruises*. Available online at: <http://www.geotraces.org/libraries/documents/Intercalibration/Cookbook.pdf>; <http://epic.awi.de/34484/1/Cookbook.pdf>
- Dagg, M. J., Jackson, G. A., and Checkley, D. M. (2014). The distribution and vertical flux of fecal pellets from large zooplankton in Monterey bay and coastal California. *Deep Sea Res.* 94(Pt I), 72–86. doi: 10.1016/j.dsr.2014.09.001
- de Jong, J., Schoemann, V., Lannuzel, D., Croot, P., deBaar, H., and Tison, J.-L. (2012). Natural iron fertilization of the Atlantic sector of the Southern Ocean by continental shelf sources of the Antarctic Peninsula. *J. Geophys. Res.* 117:G01029. doi: 10.1029/2011jg001679
- Duce, R. A., and Tindale, N. W. (1991). Atmospheric transport of iron and its deposition in the ocean. *Limnol. Oceanogr.* 36, 1715–1726. doi: 10.4319/lo.1991.36.8.1715
- Ducklow, H., Clarke, A., Dickhut, R., Doney, S. C., Geisz, H., Huang, K., et al. (2012). “The marine system of the western Antarctic Peninsula,” in *Antarctic Ecosystems: An Extreme Environment in a Changing World*, eds A. D. Rogers, N. M. Johnston, E. J. Murphy, A. Clarke (London: Blackwell), 121–159.
- Fraser, W. R., and Hofmann, E. E. (2003). A predator's perspective on causal links between climate change, physical forcing and ecosystem response. *Mar. Ecol. Prog. Ser.* 265, 1–15. doi: 10.3354/meps265001
- Giering, S. L. C., Sanders, R., Lampitt, R. S., Anderson, T. R., Tamburini, C., Boutrif, M., et al. (2014). Reconciliation of the carbon budget in the ocean's twilight zone. *Nature* 507, 480–483. doi: 10.1038/nature13123
- Gillmore, M. L., Golding, L. A., Angel, B. M., Adams, M. S., and Jolley, D. F. (2016). Toxicity of dissolved and precipitated aluminium to marine diatoms. *Aquat. Toxicol.* 174, 82–91. doi: 10.1016/j.aquatox.2016.02.004
- Gleiber, M. R., Steinberg, D. K., and Ducklow, H. W. (2012). Time series of vertical flux of zooplankton fecal pellets on the continental shelf of the western Antarctic Peninsula. *Mar. Ecol. Prog. Ser.* 471, 23–36. doi: 10.3354/meps10021
- Hassler, C. S., Alasonati, E., Mancuso Nichols, C. A., and Slaveykova, V. I. (2011a). Exopolysaccharides produced by bacteria isolated from the pelagic Southern Ocean—Role in Fe binding, chemical reactivity, and bioavailability. *Mar. Chem.* 123, 88–98. doi: 10.1016/j.marchem.2010.10.003
- Hassler, C. S., Norman, L., Mancuso Nichols, C. A., Clementson, L. A., Robinson, C., Schoemann, V., et al. (2015). Iron associated with exopolymeric substances is highly bioavailable to oceanic phytoplankton. *Mar. Chem.* 173, 136–147. doi: 10.1016/j.marchem.2014.10.002
- Hassler, C. S., Schoemann, V., Nichols, C. M., Butler, E. C., Boyd, P. W. (2012). “Iron bioavailability in the Southern Ocean” in *Oceanography and Marine Biology: An Annual Review*, Vol. 50, eds R. N. Gibson, R. J. A. Atkinson, J. D. M. Gordon, R. N. Hughes (Boca Raton, FL: CRC Press), 1–64.
- Hassler, C. S., Schoemann, V., Mancuso Nichols, C., Butler, E. C. V., and Boyd, P. W. (2011b). Saccharides enhance iron bioavailability to Southern Ocean phytoplankton. *Proc. Natl. Acad. Sci. U.S.A.* 108, 1076–1081. doi: 10.1073/pnas.1010963108
- Hoppe, C. J. M., Klaas, C., Ossebaar, S., Soppa, M. A., Cheah, W., Laglera, L. M., et al. (2015). Controls of primary production in two phytoplankton blooms in the Antarctic Circumpolar Current. *Deep Sea Res. Part II Top. Stud. Oceanogr.* doi: 10.1016/j.dsr2.2015.10.005. [Epub ahead of print].
- Hutchins, D. A., and Bruland, K. W. (1994). Grazer-mediated regeneration and assimilation of Fe, Zn and Mn from planktonic prey. *Mar. Ecol. Prog. Ser.* 110, 259–269. doi: 10.3354/meps110259
- Iversen, M. H., Pakhomov, E. A., Hunt, B. P. V., van der Jagt, H., Wolf-Gladrow, D., and Klaas, C. (2016). Sinkers or floaters? contribution from salp fecal pellets to the export flux during a large bloom event in the Southern Ocean. *Deep Sea Res. II*. [Epub ahead of print].
- Kjørboe, T. (2011). How zooplankton feed: mechanisms, traits and trade-offs. *Biol. Rev. Camb. Philos. Soc.* 86, 311–339. doi: 10.1111/j.1469-185X.2010.00148.x
- Laglera, L. M., Battaglia, G., and van den Berg, C. M. G. (2007). Determination of humic substances in natural waters by cathodic stripping voltammetry of their complexes with iron. *Anal. Chim. Acta* 599, 58–66. doi: 10.1016/j.aca.2007.07.059
- Laglera, L. M., Battaglia, G., and van den Berg, C. M. G. (2011). Effect of humic substances on the iron speciation in natural waters by CLE/CSV. *Mar. Chem.* 127, 134–143. doi: 10.1016/j.marchem.2011.09.003
- Laglera, L. M., Santos-Echeandía, J., Caprara, S., and Monticelli, D. (2013). Quantification of iron in seawater at the low picomolar range based on optimization of bromate/ammonia/dihydroxynaphthalene system by catalytic adsorptive cathodic stripping voltammetry. *Anal. Chem.* 85, 2486–2492. doi: 10.1021/ac303621q
- Laglera, L. M., and van den Berg, C. M. G. (2009). Evidence for geochemical control of iron by humic substances in seawater. *Limnol. Oceanogr.* 54, 610–619. doi: 10.4319/lo.2009.54.2.0610
- Lancelot, C., de Montety, A., Goosse, H., Becquevort, S., Schoemann, V., Pasquer, B., et al. (2009). Spatial distribution of the iron supply to phytoplankton in the Southern Ocean: a model study. *Biogeosciences* 6, 2861–2878. doi: 10.5194/bg-6-2861-2009
- Lannuzel, D., Bowie, A. R., Remenyi, T., Lam, P., Townsend, A., et al. (2011). Distributions of dissolved and particulate iron in the sub-Antarctic and Polar Frontal Southern Ocean (Australian sector). *Deep Sea Res. II* 58, 2094–2112. doi: 10.1016/j.dsr2.2011.05.027
- Lannuzel, D., Schoemann, V., de Jong, J., Tison, J.-L., and Chou, L. (2007). Distribution and biogeochemical behaviour of iron in the East Antarctic sea ice. *Mar. Chem.* 106, 18–32. doi: 10.1016/j.marchem.2006.06.010
- Lumpkin, R., and Speer, K. (2007). Global ocean meridional overturning. *J. Phys. Oceanogr.* 37, 2550–2562. doi: 10.1175/JPO3130.1
- Madin, L. P. (1982). Production, composition and sedimentation of salp fecal pellets in oceanic waters. *Mar. Biol.* 67, 39–45. doi: 10.1007/bf00397092
- Mahmood, A., Abualhija, M. M., van den Berg, C. M. G., and Sander, S. G. (2015). Organic speciation of dissolved iron in estuarine and coastal waters at multiple analytical windows. *Mar. Chem.* 177, 706–719. doi: 10.1016/j.marchem.2015.11.001
- Manno, C., Stowasser, G., Enderlein, P., Fielding, S., and Tarling, G. A. (2015). The contribution of zooplankton faecal pellets to deep-carbon

- transport in the Scotia Sea (Southern Ocean). *Biogeosciences* 12, 1955–1965. doi: 10.5194/bg-12-1955-2015
- Martin, J. H., Fitzwater, S. E., and Gordon, R. M. (1990). Iron deficiency limits phytoplankton growth in Antarctic waters. *Global Biogeochem. Cycles* 4, 5–12. doi: 10.1029/GB004i001p00005
- Moore, J. K., and Braucher, O. (2008). Sedimentary and mineral dust sources of dissolved iron to the world ocean. *Biogeosciences* 5, 631–656. doi: 10.5194/bg-5-631-2008
- Moran, S. B., and Moore, R. M. (1988). Evidence from mesocosm studies for biological removal of dissolved aluminium from sea water. *Nature* 335, 706–708. doi: 10.1038/335706a0
- Morata, N., and Seuthe, L. (2014). Importance of bacteria and protozooplankton for faecal pellet degradation. *Oceanologia* 56, 565–581. doi: 10.5697/oc.56-3.565
- Nakayama, Y., Fujita, S., Kuma, K., and Shimada, K. (2011). Iron and humic-type fluorescent dissolved organic matter in the Chukchi Sea and Canada Basin of the western Arctic Ocean. *J. Geophys. Res. Oceans* 116, C07031. doi: 10.1029/2010jc006779
- Norman, L., Cabanes, D. J. E., Blanco-Ameijeiras, S., Moisset, S. A. M., and Hassler, C. S. (2014). Iron biogeochemistry in aquatic systems: from source to bioavailability. *Chimia* 68, 764–771. doi: 10.2533/chimia.2014.764
- Norman, L., Worms, I. A. M., Angles, E., Bowie, A. R., Nichols, C. M., Ninh Pham, A., et al. (2015). The role of bacterial and algal exopolymeric substances in iron chemistry. *Mar. Chem.* 173, 148–161. doi: 10.1016/j.marchem.2015.03.015
- Obernosterer, I., and Herndl, G. J. (2000). Differences in the optical and biological reactivity of the humic and non-humic dissolved organic carbon component in two contrasting coastal marine environments. *Limnol. Oceanogr.* 45, 1120–1129. doi: 10.4319/lo.2000.45.5.1120
- Omanović, D., Garnier, C., and Pižeta, I. (2015). ProMCC: an all-in-one tool for trace metal complexation studies. *Mar. Chem.* 173, 25–39. doi: 10.1016/j.marchem.2014.10.011
- Ortega-Retuerta, E., Frazer, T. K., Duarte, C. M., Ruiz-Halpern, S., Tovar_Sanchez, A., Arrieta, J. M., et al. (2009). Biogeneration of chromophoric dissolved organic matter by bacteria and krill in the southern ocean. *Limnol. Oceanogr.* 54, 1941–1950. doi: 10.4319/lo.2009.54.6.1941
- Pakhomov, E. A., Dubischar, C. D., Strass, V., Brichta, M., and Bathmann, U. V. (2006). The tunicate *Salpa thompsoni* ecology in the Southern Ocean. I. Distribution, biomass, demography and feeding ecophysiology. *Mar. Biol.* 149, 609–623. doi: 10.1007/s00227-005-0225-9
- Pakhomov, E. A., Froneman, P. W., and Perissinotto, R. (2002). Salp/krill interactions in the Southern Ocean: spatial segregation and implications for the carbon flux. *Deep Sea Res. Part II Top. Stud. Oceanogr.* 49, 1881–1907. doi: 10.1016/S0967-0645(02)00017-6
- Perissinotto, R., and Pakhomov, E. A. (1998). The trophic role of the tunicate *Salpa thompsoni* in the Antarctic marine ecosystem. *J. Mar. Syst.* 17, 361–374. doi: 10.1016/S0924-7963(98)00049-9
- Phillips, B., Kremer, P., and Madin, L. (2009). Defecation by *Salpa thompsoni* and its contribution to vertical flux in the Southern Ocean. *Mar. Biol.* 156, 455–467. doi: 10.1007/s00227-008-1099-4
- Pisani, O., Yamashita, Y., and Jaffé, R. (2011). Photo-dissolution of flocculent, detrital material in aquatic environments: contributions to the dissolved organic matter pool. *Water Res.* 45, 3836–3844. doi: 10.1016/j.watres.2011.04.035
- Price, N. M., Harrison, G. I., Hering, J. G., Hudson, R. J., Nirel, P. M. V., and Palenik, B. (1989). Preparation and chemistry of the artificial algal culture medium aquil. *Biol. Oceanogr.* 6, 443–461.
- Ren, J.-L., Zhang, G.-L., Zhang, J., Shi, J.-H., Liu, S.-M., Li, F.-M., et al. (2011). Distribution of dissolved aluminium in the Southern Yellow Sea: influences of a dust storm and the spring bloom. *Mar. Chem.* 125, 69–81. doi: 10.1016/j.marchem.2011.02.004
- Rijkenberg, M. J. A., Gerringa, L. J. A., Carolus, V. E., Velzeboer, I., and de Baar, H. J. W. (2006). Enhancement and inhibition of iron photoreduction by individual ligands in open ocean seawater. *Geochim. Cosmochim. Acta* 70, 2790–2805. doi: 10.1016/j.gca.2006.03.004
- Roca Martí, M., Puigcorbó, V., Iversen, M. H., van der Loeff, M. R., Klaas, C., Cheah, W., et al. (2016). High particulate organic carbon export during the decline of a vast diatom bloom in the Atlantic sector of the Southern Ocean. *Deep Sea Res. II*. doi: 10.1016/j.dsr2.2015.12.007. [Epub ahead of print].
- Rontani, J.-F. (2008). “Photooxidative and autoxidative degradation of lipid components during the senescence of phototrophic organisms” in *Phytochemistry Research Progress*, ed T. Matsumoto (Hauptmann, NY: Nova Science Publishers), 115–144.
- Sabine, C. L., Feely, R. A., Gruber, N., Key, R. M., Lee, K., Bullister, J. L., et al. (2004). The oceanic sink for anthropogenic CO₂. *Science* 305, 367–371. doi: 10.1126/science.1097403
- Sarthou, G., Vincent, D., Christaki, U., Obernosterer, I., Timmermans, K. R., and Brussaard, C. P. D. (2008). The fate of biogenic iron during a phytoplankton bloom induced by natural fertilization: impact of copepod grazing. *Deep Sea Res. II* 55, 734–751. doi: 10.1016/j.dsr2.2007.12.033
- Sato, M., Takeda, S., and Furuya, K. (2007). Iron regeneration and organic iron(III)-binding ligand production during in situ zooplankton grazing experiment. *Mar. Chem.* 106, 471–488. doi: 10.1016/j.marchem.2007.05.001
- Schmidt, M. A., Zhang, Y. H., and Hutchins, D. A. (1999). Assimilation of Fe and carbon by marine copepods from Fe-limited and Fe-replete diatom prey. *J. Plankton Res.* 21, 1753–1764. doi: 10.1093/plankt/21.9.1753
- Strass, V. H., Leach, H., Prandke, H., Donnelly, M., Bracher, A. U., and Wolf-Gladrow, D. A. (2016). The physical environmental conditions for biogeochemical differences along the Antarctic Circumpolar Current in the Atlantic Sector during late austral summer 2012. *Deep Sea Res. II*. doi: 10.1016/j.dsr2.2016.05.018. [Epub ahead of print].
- Strzepek, R. F., Maldonado, M. T., Higgins, J. L., Hall, J., Safi, K., Wilhelm, S. W., et al. (2005). Spinning the “Ferrous Wheel”: the importance of the microbial community in an iron budget during the FeCycle experiment. *Global Biogeochem. Cycles* 19:GB4S26. doi: 10.1029/2005GB002490
- Tagliabue, A., Sallée, J.-B., Bowie, A. R., Lévy, M., Swart, S., and Boyd, P. W. (2014). Surface-water iron supplies in the Southern Ocean sustained by deep winter mixing. *Nat. Geosci.* 7, 314–320. doi: 10.1038/ngeo2101
- Tovar-Sanchez, A., Duarte, C. M., Hernandez-Leon, S., and Sanudo-Wilhelmy, S. A. (2007). Krill as a central node for iron cycling in the Southern Ocean. *Geophys. Res. Lett.* 34, L11601. doi: 10.1029/2006GL029096
- Turner, J. T. (2002). Zooplankton fecal pellets, marine snow and sinking phytoplankton blooms. *Aquat. Microb. Ecol.* 27, 57–102. doi: 10.3354/ame027057
- Turner, J. T. (2015). Zooplankton fecal pellets, marine snow, phytodetritus and the ocean’s biological pump. *Prog. Oceanogr.* 130, 205–248. doi: 10.1016/j.pocean.2014.08.005
- Twining, B. S., and Baines, S. B. (2013). The Trace Metal Composition of Marine Phytoplankton. *Annu. Rev. Mar. Sci.* 5, 191–215. doi: 10.1146/annurev-marine-121211-172322
- Von Harbou, L. (2009). *Trophodynamics of Salps in the Atlantic Southern Ocean*. Dissertation’s thesis, University of Bremen, Germany.
- Wagener, T., Guieu, C., Losno, R., Bonnet, S., and Mahowald, N. (2008). Revisiting atmospheric dust export to the Southern Hemisphere ocean: biogeochemical implications. *Global Biogeochem. Cycles* 22:GB2006. doi: 10.1029/2007GB002984
- Witter, A. E., Hutchins, D. A., Butler, A., and Luther, III G. W. (2000). Determination of conditional stability constants and kinetic constants for strong model Fe-binding ligands in seawater. *Mar. Chem.* 69, 1–17. doi: 10.1016/S0304-4203(99)00087-0

Conflict of Interest Statement: The authors declare that the research was conducted in the absence of any commercial or financial relationships that could be construed as a potential conflict of interest.

Copyright © 2017 Cabanes, Norman, Santos-Echeandía, Iversen, Trimborn, Laglera and Hassler. This is an open-access article distributed under the terms of the Creative Commons Attribution License (CC BY). The use, distribution or reproduction in other forums is permitted, provided the original author(s) or licensor are credited and that the original publication in this journal is cited, in accordance with accepted academic practice. No use, distribution or reproduction is permitted which does not comply with these terms.



Phytoplankton Virus Production Negatively Affected by Iron Limitation

Hans A. Slagter^{1*}, Loes J. A. Gerringa¹ and Corina P. D. Brussaard²

¹ Department of Ocean Systems, NIOZ Royal Institute for Sea Research, Utrecht University, Den Burg, Netherlands,

² Department of Marine Microbiology and Biogeochemistry, NIOZ Royal Institute for Sea Research, Utrecht University, Den Burg, Netherlands

Fe-limited monocultures of the ubiquitous algae *Micromonas pusilla* and *Phaeocystis globosa* were infected with their respective viruses (MpV and PgV) to ascertain the effect of Fe-limitation on phytoplankton host-virus dynamics. The effect of the viral shunt on Fe concentrations and bioavailability is starting to gain attention, since not only is Fe released through lysis, but also its solubility is increased by the simultaneous release of Fe-binding dissolved organic ligands. However, the effect of Fe-limitation on the process of viral lysis itself is poorly understood. In this study fine adjustment of a seawater-based culture medium including the use of ultra-clean trace metal conditions and protocols allowed for Fe-limited growth at nanomolar amounts as opposed to micromolar amounts typically employed in culturing. Viral lysates derived from Fe-limited and Fe-replete (for comparison) hosts were cross-inoculated in hosts of both Fe treatments, to judge the quality of the resulting lysate as well as the effect of Fe introduction after initial infection. For both phytoplankton host-virus systems, the virus burst size reduced strongly under Fe stress, i.e., on average $28 \pm 1\%$ of replete. Moreover, the MpV virus progeny showed highly reduced infectivity of $30 \pm 7\%$, whereas PgV infectivity was not affected. A small addition of Fe to Fe-limited cultures coming from the Fe-replete lysate counteracted the negative effect of Fe-limitation on phytoplankton virus production to some extent (but still half of replete), implying that the physiological history of the host at the moment of infection was an important underlying factor. These results indicate that Fe-limitation has the strong potential to reduce the loss of phytoplankton due to virus infection, thereby affecting the extent of Fe-cycling through the viral shunt. To what extent this affects the contribution of viral lysis-induced organic ligand release needs further study.

OPEN ACCESS

Edited by:

Sylvia Gertrud Sander,
University of Otago, New Zealand

Reviewed by:

Jessica Nicole Fitzsimmons,
Texas A&M University, USA
Aridane G. Gonzalez,
University of Western Brittany, France

*Correspondence:

Hans A. Slagter
hans.slagter@nioz.nl

Specialty section:

This article was submitted to
Marine Biogeochemistry,
a section of the journal
Frontiers in Marine Science

Received: 29 March 2016

Accepted: 16 August 2016

Published: 30 August 2016

Citation:

Slagter HA, Gerringa LJA and
Brussaard CPD (2016) Phytoplankton
Virus Production Negatively Affected
by Iron Limitation.
Front. Mar. Sci. 3:156.
doi: 10.3389/fmars.2016.00156

Keywords: algae, marine phytoplankton, marine viruses, iron, Fe speciation, Fe limitation

INTRODUCTION

Phytoplankton form the base of most marine pelagic food webs and are important in sequestering atmospheric carbon dioxide (CO₂) through photosynthesis. The production of phytoplankton is controlled by physicochemical variables (bottom-up) as well as by biological factors (top-down). Main bottom-up controls of phytoplankton are light and nutrient availability (Behrenfeld et al., 2006). The latter can be subdivided into major (nitrate, phosphate, and silicate) and micro-nutrients (e.g., iron; de Baar et al., 1990; Martin et al., 1990). Top-down factors, e.g., grazing and viral infection, influence the organic matter flux differently (Wilhelm and Suttle, 1999; Weitz and Wilhelm, 2012). While grazing transfers photosynthetically fixed carbon and organic nutrients up

the food chain (Calbet and Landry, 2004), viral lysis results in the release of the hosts' cellular content into the surrounding water (Gobler et al., 1997; Wilhelm and Suttle, 1999). Thereupon, the flow of nutrients through the microbial food web is stimulated by bacterial recycling of the dissolved and dead particulate matter (Brussaard et al., 2005; Suttle, 2005; Brussaard and Martínez, 2008). Virally-induced mortality of various different natural phytoplankton groups was found to be at least an equally important loss factor as microzooplankton grazing (Baudoux et al., 2007; Mojica et al., 2016).

In order to understand and predict changes in phytoplankton community composition, it is important to elucidate how bottom-up and top-down factors interact and affect phytoplankton population dynamics. Several studies using phytoplankton host-virus culture systems showed that major nutrient availability influences viral production (Maat and Brussaard, 2016 and see review by Mojica and Brussaard, 2014). For example, phosphorus (P) limitation of the virally infected phytoplankton host results in a prolonged latent period, i.e., the time between infection and the initial release of progeny viruses from the host cell, for the infecting viruses (Maat et al., 2014). Moreover, P-stress resulted in reduced viral burst size, i.e., the number of newly formed viruses released per lysed host cell (Bratbak et al., 1998; Maat et al., 2014). These studies proposed shortage of phosphorus as a viral production substrate as well as possible host energy deficiency as reasons for the lower and delayed viral particle yield. There is, however, virtually nothing known on the effect of micronutrient limitation on phytoplankton host-virus interactions.

Furthermore, as iron (Fe) solubility in seawater is low (Millero, 1998; Liu and Millero, 2002), marine phytoplankton depend on Fe-binding ligands to increase solubility and therefore bioavailability (Gledhill and van den Berg, 1994; Rue and Bruland, 1995). The redox state of Fe is an important factor in Fe bioavailability. The oxidized Fe(III) state is the more stable and thus prevalent state in marine conditions, while the reduced Fe(II) state is the more bioavailable (Breitbarth et al., 2010; Shaked and Lis, 2012). Release of reactive oxygen species during phytoplankton growth has been shown to contribute to bioavailability of Fe by facilitating reduction of Fe(III) (Kustka et al., 2005; Garg et al., 2007). Furthermore, organic exudates have been connected to lowered Fe(II) oxidation rates experimentally (González et al., 2014). Part of the Fe-binding ligand pool is thought to be of marine biological origin. Strong Fe-binding organic ligands called siderophores are purposefully produced by bacteria (Butler, 2005; Mawji et al., 2011). Humic acids and polysaccharide excretions are other recognized Fe chelators with a biological origin (Hassler et al., 2011; Laglera et al., 2011). The highest Fe-binding ligand concentrations generally correlate with biological activity (Rue and Bruland, 1995; Gerringa et al., 2006; Ibanmami et al., 2011). Viral lysis, releasing organic substances in seawater, may well be an important contributor to the ligand pool (Gobler et al., 1997; Poorvin et al., 2004, 2011). In these studies by Poorvin and others, it was found that bacterial and cyanobacterial lysates provided organically bound Fe in a form more bioavailable than supplied inorganic, ethylenediaminetetraacetic acid (EDTA) bound or desferrioxamine B (DFB) bound Fe. In comparison

to the studied bacteria's self-produced siderophores, lysates were also found to contain more bioavailable Fe.

Fe-limitation negatively affects phytoplankton physiology and growth (de Baar et al., 1990; Martin et al., 1990; Behrenfeld et al., 1996; Timmermans et al., 2001b). Besides energetic consequences of Fe-limitation in terms of the cell's ability to harvest light energy (Geider and La Roche, 1994), Fe is also found to be an essential micronutrient for DNA replication (Netz et al., 2012; Zhang, 2014). As parasites viruses are dependent on the metabolism of their host for the production of their progeny. We hypothesize that viral production depends on the degree of Fe-stress of the host. Viral lysis in turn affects the production of Fe-binding organic ligands and thus the solubility of the limiting Fe. Thus far, in terms of impact on Fe cycling, studies focussed solely on the release of Fe or Fe-binding organic ligands upon viral lysis and not on the virus growth cycle (Gobler et al., 1997; Poorvin et al., 2004, 2011). Here we examine virus production characteristics under Fe-limitation for two key ecologically relevant phytoplankton hosts: the nanoeukaryotic bloom-forming Prymnesiophyte *Phaeocystis globosa* and the picoeukaryotic Prasinophyte *Micromonas pusilla*. *Phaeocystis* is a globally occurring, bloom-forming genus (Vaulot et al., 1994), with *P. globosa* ecologically relevant in temperate marine waters (Schoemann et al., 2005). Viruses have been found to drive *P. globosa* bloom decline (Brussaard, 2004; Brussaard et al., 2005; Baudoux et al., 2006). *M. pusilla* is a common species that is distributed globally (Not et al., 2004, 2005; Vaulot et al., 2008). It has been speculated that viral control of this species is continuous (Cottrell and Suttle, 1995). As model species for diverse regions and ecological niches, these species were chosen in this study to offer a broad insight in the response to Fe-limitation of phytoplankton host-virus systems in world oceans subject to changing conditions. Limiting concentrations were of ecological relevance to represent a natural context.

METHODS

Materials Preparation

Cleaning of equipment and preparation of chemicals took place in a class 100 ultra-clean laboratory environment (Interflow). Culture handling and sampling were carried out in a 15°C climate chamber within the ultra-clean laboratory. When outside the ultra-clean environment, sample handling took place inside class 100 laminar flow hoods (Interflow). All rinsing and chemical dissolution and dilution was done using 18 MΩ deionized Milli-Q water (Merck Millipore), further referred to as MQ.

Prior to use, general labware of high- and low-density polyethylene (HDPE and LDPE, respectively) and fluorinated ethylene propylene (FEP) was cleaned thoroughly by pre-rinsing (5x) with MQ, followed by soaking in 6 M hydrochloric acid (HCl) for a minimum of 24 h, and a final thorough (5x) MQ rinsing. A sub-boiling quartz distillation apparatus (Savillex) was used to purify nitric acid (HNO₃) in triplicate, yielding Fe free quartz distilled (3QD) HNO₃. A 0.3 M 3QD-HNO₃ solution is used to fill stored bottles.

The polycarbonate (PC) culture flasks (50–500 mL, VWR) and bottles (1–2 L, Nalgene) were acid cleaned with 1 M HCl for a

minimum of 24 h, after which they were rinsed with MQ (5x). Finally, bottles were sterilized with a 10% volume of boiling MQ, i.e., the bottle with MQ was microwaved at 900 W to boiling point and left boiling for ~20 s. After vigorous shaking the hot MQ was poured out over the inverted lid. Culture vessels were then left to air-dry in a laminar flow bench for at least 2 h.

Culturing

Axenic cultures of the nanoeukaryotic Prymnesiophyte *P. globosa* G(A) (culture collection of the University of Groningen, the Netherlands) and the picoeukaryotic Prasinophyte *M. pusilla* LAC38 (Marine Research Center culture collection, Göteborg University, Sweden) were maintained under trace metal clean conditions.

A low Fe-containing medium (Low Trace: LT) based on natural seawater (DFe 0.2 nM, collected west of the Bay of Biscay, Atlantic Ocean after Rijkenberg et al., 2012) was designed without metal chelators such as EDTA. Chelators as EDTA are used as metal buffers in culture media, and are added in 10^{-6} – 10^{-3} M concentrations to ascertain that those transition metals added as micronutrients, e.g., Cu, Co, Fe, Mn, Mo, Ni, V, Zn, are kept in the dissolved phase through complexation by EDTA (Sunda and Huntsman, 1995). However, these high concentrations of artificial ligands completely overrule the natural chemistry of the metals, making the study of natural Fe binding organic ligands impossible (Gerringa et al., 2000). The medium was enriched with the macronutrients NaNO₃ (Sigma-Aldrich) and Na₂HPO₄ (Merck Millipore) to final concentrations of 128 and 8 μM, respectively. The following micronutrients were added: KBr (7.1 μM final concentration), NaF (3.0 μM), CaCl₂·2H₂O, (17.9 μM), SrCl₂·6H₂O (0.8 μM), MgCl₂·6H₂O (2.3 μM) and Na₂SeO₃ (10.0 nM). Vitamins H, B1, and B12 were added to final concentrations of 2.0, 296.0, and 0.4 nM, respectively. A combined Tris(hydroxymethyl) aminomethane (Tris) and HCl buffer was added to a 4.0 μM final concentration. Nutrient and buffer stock solutions were cleaned of trace metal contaminations by equilibration with MnO₂ after van den Berg and Kramer (1979). The MnO₂ was removed using a trace metal clean 47 mm diameter 0.2 μm pore size PC filter (Whatman) in a polysulfone (PSU) filter tower (Nalgene) with an electric vacuum pump (Merck Millipore). This cleaning process was performed twice. To maintain constant growth for multiple generations addition of additional trace metals proved essential. These trace metal additions were kept to a minimum in order to avoid influencing Fe speciation, e.g., interactions between Cu and Fe (González et al., 2016). *P. globosa* received an additional trace solution containing final concentrations of 2.0 nM ZnSO₄·7H₂O, 1.0 nM CoCl₂·6H₂O, 4.6 nM MnCl₂·4H₂O, and 0.6 nM Na₂MoO₄·2H₂O. *M. pusilla* showed poor physiological condition and growth using this trace solution. Because it was impossible to maintain as steady state under these conditions, a slightly different trace solution was used, containing final concentrations of 4.0 nM ZnSO₄·7H₂O, 5.0 nM CoCl₂·6H₂O, 1.0 nM CuSO₄·5H₂O, 1.0 nM NiSO₄·6H₂O, 1.0 nM Na₃VO₄, 1.0 nM K₂CrO₄, 9.1 nM MnCl₂·4H₂O, 4.1 nM Na₂MoO₄·2H₂O, and 1.0 nM H₂SeO₃. Fe was added from an acidified 3 μM FeCl stock solution made using a 1000 mg L⁻¹ ICP stock

(Fluka, Sigma-Aldrich). The Fe-limiting medium contained final concentrations of 1.0 and 3.0 nM Fe for *P. globosa* and *M. pusilla*, respectively. In comparison, the Fe-replete (control) medium contained 9.0 μM FeCl for both species.

Culture temperature was 15°C and irradiance was supplied at 90 μmol quanta m⁻² s⁻¹ under a 16:8 h light:dark cycle. Phytoplankton cultures were maintained semi-continuously to obtain and sustain constant and comparable physiology and growth, i.e., diluting the culture daily with new medium whereby the exact volume was determined by the maximum growth rate possible under Fe-limiting culture conditions without wash-out (Maat et al., 2014). The limiting Fe concentration determined the maximum cell abundance, which was determined before and after dilution using flow cytometry (Marie et al., 1999). At steady state, i.e., after at least 8 volume changes and consistent phytoplankton counts ($2.1 \pm 0.4 \times 10^6$ and $2.1 \pm 0.7 \times 10^6$ for *P. globosa* and *M. pusilla*, respectively), samples were collected for dissolved macronutrients (nitrogen and phosphorus) and Fe, as well as pigment composition. Nutrient samples (5 ml after washing of filter and tube) were 0.2 μm filtered (25 mm diameter Acrodisc, Pall) and frozen at -20°C until analysis. GF/C filtered (1.2 μm nominal pore size, 25 mm diameter, Whatman) algal pigment samples of 50 mL were frozen at -80°C until analysis.

Axenic viral lysate of the double-stranded DNA viruses PgV-07T (Baudoux and Brussaard, 2005) infecting *P. globosa* G(A) and MpV-08T (Martinez et al., 2014) infecting *M. pusilla* LAC38 were obtained by 10% v/v inoculation to exponentially growing phytoplankton host and checked for full lysis by flow cytometry (FCM). Fe-limited lysates of both phytoplankton viruses were initiated by 1% v/v inoculations with Fe-replete lysates, after which a minimum of 5 subsequent 10% v/v inoculations followed before use for the experiment. This way the Fe concentration in the Fe-limited lysate was similar to the Fe concentration in the Fe-limited host culture. The number of infective phytoplankton viruses was determined using the most probable number (MPN) endpoint dilution assay according to Suttle (1993). MPN data was analyzed using the University of British Columbia Computer Science department's Assay Analyser software program (Passmore et al., 2000).

Experimental Design

Steady state exponentially growing phytoplankton cultures were subdivided per treatment (Fe-limited and Fe-replete) in 6 replicate 500 mL culture flasks. Two days later the viral infection experiment started 3 h into the light period. For each treatment, 2 replicate cultures received viruses produced on Fe-limited host culture (VL), 2 replicates received viruses produced on Fe-replete host culture (VR), and 2 replicates did not receive viruses and served as non-infected controls (C). Fe-limited lysates were added not only to the respective Fe-limited host cultures, but also to the Fe-replete host in order to test for the reduced infectivity we observed under Fe-limitation (See Results). For this reason and to still guarantee a one-step infection cycle we aimed to add 20–25 viruses per algal cell for *P. globosa*. Given lower yields for *M. pusilla*, we endeavored to add at least 5–10 viruses per algal cell, while still maintaining a ~10% v/v addition. Similarly, Fe-replete lysate was also added to Fe-limited host cultures. This

caused a Fe-spike of about $0.9 \mu\text{M}$ (10% v/v of Fe-replete medium containing lysate), which allows testing whether a spike of Fe influences virus proliferation.

The moment viruses were added, cultures were maintained in batch. We examined the effect of frequent handling by taking along a control subculture per Fe-limited treatment that was only gently mixed once a day. Samples for phytoplankton and virus abundance as well as photosynthetic capacity (F_v/F_m) were taken every 4 h until full lysis of the cultures (48 h for *P. globosa* and 96 h for *M. pusilla*). Phytoplankton abundance and F_v/F_m were determined directly upon sampling, while viral abundance samples were fixed with glutaraldehyde (EM-grade, 0.5% final concentration), flash frozen in liquid nitrogen and stored at -80°C (Brussaard et al., 2010).

Analyses

High Performance Liquid Chromatography (HPLC) pigment analysis was performed on steady state phytoplankton samples after Zapata et al. (2000). Phytoplankton cells in fresh samples were discriminated and counted based on Chlorophyll-a red autofluorescence using a FACSCanto flow cytometer (Becton Dickinson) equipped with a 17 mW 633 nm HeNe red laser. Viral abundances were also determined by flow cytometry using a FACSCalibur flow cytometer (Becton Dickinson) equipped with a 15 mW 488 nm argon-ion blue laser triggered on green fluorescence, following the protocol by Brussaard et al. (2010). In short, samples were diluted 200–1000-fold using a 2 M Tris-HCl buffer at pH 8 and viruses were stained using the nucleic acid-specific fluorescent dye SYBR Green I (Molecular Probes[®], Life Technologies, Thermo Fisher). Raw data were analyzed using Cytowin (Vaulot, 1989; Version 4.31 available at <http://application.sb-roscoff.fr/Phyto/index.php>), whereby PgV and MpV were easily discriminated by plotting green nucleic acid-specific fluorescence vs. side scatter (Baudoux and Brussaard, 2005; Martínez et al., 2015).

The number of infective phytoplankton viruses was determined using the endpoint dilution assay according to Suttle (1993). In short, 10-fold dilution series were set up in 5 replicate tubes using a dilute Fe-replete phytoplankton culture at a density of $\sim 10^6$ cells mL^{-1} . A row of uninfected control tubes was added to each analysis. Cell lysis was regularly scored by eye and the final score after 14 days post-infection was used to calculate the number of infectious viruses. Dividing this number of infectious by the total number of PgV or MpV provided the % infectious viruses.

Photosynthetic capacity (F_v/F_m) measurements were performed using a Chlorophyll Fluorometer with a red emitter-detector unit (Water-PAM, Waltz). Samples were kept in the dark for 30 min at culturing temperature, after which chlorophyll autofluorescence was measured in duplicate in the dark adapted state (F_0) and after a saturation pulse of 2.5 s (F_m). F_v is defined as the difference between F_m and F_0 (Genty et al., 1989). Concentrations of dissolved inorganic macronutrients nitrate and orthophosphate were verified colorimetrically using a trAAcs 800 auto analyser (Murphy and Riley, 1962; Grasshoff, 1983), and were non-limiting at all times ($> 128 \mu\text{M}$ nitrate and $> 8 \mu\text{M}$ phosphate). Verification of the dissolved Fe concentration was

done using flow injection analysis after Klunder et al. (2011), the detection limit of this method was 0.01 nM.

RESULTS AND DISCUSSION

Steady State

Exponential growth rate (μ_{max}) for both Fe-limited and Fe-replete *P. globosa* and Fe-replete *M. pusilla* was $0.99 \pm 0.11 \text{ d}^{-1}$. *M. pusilla* showed, however, reduced growth under Fe-limitation ($0.63 \pm 0.07 \text{ d}^{-1}$). Initial difficulties encountered with consistent semi-continuous culturing of *M. pusilla* required us to increase the Fe concentration to 3 nM as compared to the 1 nM for *P. globosa*. Still, the lower steady state μ_{max} found for *M. pusilla* under Fe-limitation suggests a less efficient Fe-uptake or utilization of *M. pusilla* as compared to *P. globosa*. However, the photosynthetic capacity (F_v/F_m) of the Fe-limited *M. pusilla* remained high around 0.6. Thus, the smaller-sized *M. pusilla* requires more Fe to grow, albeit at a lower μ_{max} , while it is capable of retaining F_v/F_m at a value similar to Fe-replete conditions. Reduced F_v/F_m and growth rate under Fe-limitation has been reported for a small diatom species (Timmermans et al., 2001a); however, both variables were reduced for the same species and not one or the other as found in present study. Our result do not support the earlier reports that small phytoplankton (diatoms and cyanobacteria) are growing better under Fe-limitation than larger phytoplankton (Price et al., 1994; Timmermans et al., 2001b, 2004). Whether the differences are due to species-specific or phytoplankton group related responses is currently unclear.

The cellular Chlorophyll-a concentration at steady state was lower under Fe-limitation compared to the Fe-replete control cultures for both algal species (Tables 1, 2). For *M. pusilla* the reduction was larger, i.e., Chlorophyll-a concentration was only 40% of Fe-replete concentration, compared to 63% for *P. globosa*. In the Fe-limited *P. globosa* cultures, cellular Chlorophyll-c concentration was reduced (to a similar extent; Table 1), whereas for *M. pusilla* the Chlorophyll-b concentration also decreased compared to Fe-replete (Table 2). Furthermore, Fe-limitation led to a different distribution of light-harvesting xanthophylls in *P. globosa* (Table 1). Cellular 19'-hexafucoanthin concentration was found 5-fold higher in the Fe-limited cultures as compared to Fe-replete *P. globosa* ($4.8 \times 10^{-12} \text{ g cell}^{-1}$), while 19'-butanoyloxyfucoxanthin and fucoxanthin concentrations were 0 and 89% of Fe-replete, respectively. The photoprotective xanthophyll derivatives in Fe-limited *P. globosa* are increased relative to Chlorophyll-a, i.e., the diadinoxanthin concentration over Chlorophyll-a is 162% of Fe-replete (0.58 and $0.57 \times 10^{-11} \text{ g} \times \text{cell}^{-1}$, respectively) and the diatoxanthin concentration is 181% of Fe-replete (0.08 and $0.07 \times 10^{-11} \text{ g} \times \text{cell}^{-1}$, respectively). Fe-limited *M. pusilla* cultures (Table 2) had lower cellular Chlorophyll-b and light-harvesting xanthophyll concentrations. Relative to the Chlorophyll-a concentration, photoprotective xanthophyll derivatives antheraxanthin, zeaxanthin, and lutein were present in higher amounts. Only violaxanthin remains lower both in absolute and relative terms.

Overall, the pigment analysis shows that for both phytoplankton species the photosystem shifted toward a more

TABLE 1 | Steady state phytoplankton pigment composition in non-infected Fe-limited (first column) and Fe-replete (second column) *P. globosa* cultures.

Pigments	Treatment		Ratio
	Limited	Replete	
Chlorophyll a ^a	1.31	2.08	0.63
Chlorophyll c2 ^a	0.31	0.37	0.86
Chlorophyll c3 ^a	0.23	0.48	0.47
19'-hexafucoanthin ^b	0.48	0.09	5.16
19'-butanoyloxyfucoxanthin ^b	0.00	0.20	0.00
Fucoxanthin ^b	1.13	2.01	0.56
Diadinoxanthin ^c	0.58	0.57	1.02
Diatoxanthin ^c	0.08	0.07	1.07

Concentrations of pigments are expressed in 10^{-11} g cell⁻¹. The third column shows the ratio of Fe-limited over Fe-replete cultures, serving to indicate relative shifts in pigment composition. ^aChlorophylls, ^blight harvesting xanthophyll derivatives and ^cphotoprotective xanthophyll derivatives are grouped together.

TABLE 2 | Steady state phytoplankton pigment composition in non-infected Fe-limited (first column) and Fe-replete (second column) *M. pusilla* cultures.

Pigments	Treatment		Ratio
	Limited	Replete	
Chlorophyll a ^a	2.70	6.78	0.40
Chlorophyll b ^b	2.06	4.50	0.46
Neoxanthin ^b	0.44	0.88	0.50
Prasinolanthin ^b	0.71	1.52	0.47
Antheraxanthin ^c	0.27	0.12	2.33
Zeaxanthin ^c	0.17	0.10	1.75
Lutein ^c	0.13	0.29	0.44
Violaxanthin ^c	0.29	1.14	0.25

Concentrations of pigments are expressed in 10^{-11} g cell⁻¹. The third column shows the ratio of Fe-limited over Fe-replete cultures, serving to indicate relative shifts in pigment composition. ^aChlorophylls, ^blight harvesting xanthophyll derivatives and ^cphotoprotective xanthophyll derivatives are grouped together.

photoprotective character under Fe-limited conditions. The lower concentrations of chlorophyll and most light-harvesting xanthophylls furthermore indicated that the Fe-limited cells suffered a lower light-harvesting capacity. Fe is essential for all life and earlier studies showed that Fe-deficiency can lead to anemia in mammals, the dysfunction of Fe-dependent enzymes in yeast, the reduction of the amount of electron-transferring complexes and induction of chlorosis in plants, and a decrease in Fe-intensive light harvesting pigment synthesis and increased photoprotective pigments in phytoplankton (Geider et al., 1993; Mengel, 1994; van Leeuwe and Stefels, 2007; van de Poll et al., 2009; Zhang, 2014). In line with the fact that the Fe concentrations in the Fe-limited cultures were always below the limit of detection, these results confirm that both phytoplankton cultures were indeed Fe-limited, despite that *M. pusilla* showed healthy F_v/F_m . The more pronounced shift to photoprotective pigment production relative to light-harvesting Chlorophyll-a in *M. pusilla* compared to *P. globosa* is in agreement with the

strong decline in steady state *M. pusilla* cell abundance with Fe-limitation while F_v/F_m was unaffected. However, *M. pusilla* was unable to grow at 1 nM Fe while *P. globosa* grew well. Our results imply that *P. globosa* was more affected energetically by Fe-limitation, while *M. pusilla* suffered instead in overall cellular production.

Viral Infection Characteristics

Infection of both phytoplankton species resulted in one-step infection cycles with full lysis of the cultures whereas the non-infected controls grew or maintained constant cell number (Figures 1A,B, 2A,B). Cell growth in the non-infected Fe-replete cultures reflects the synchronized cell division during the dark period (Brussaard et al., 1999). In the Fe-limited cultures growth of *P. globosa* halted, which was due to stress from the frequent sampling, since the Fe-limited subcultures that were sampled only once a day did show some growth (data not shown). The F_v/F_m of the uninfected Fe-replete phytoplankton cultures remained constant (Figures 1C,D, 2C,D), whereby the small variations observed in the Fe-replete *P. globosa* cultures relate to the light:dark cycle (Figure 1D). The Fe-limited non-infected control cultures showed a decline in F_v/F_m over time as a result of the Fe deprivation, but to a lesser extent than the infected cultures.

When infected with the corresponding Fe-treatment virus (i.e., Fe-limited host with VL and Fe-replete host with VR), Fe-limitation resulted for the infected *P. globosa* in slightly delayed (about 4 h) and slower cell lysis than for the Fe-replete cultures (full lysis occurring about a day later; Figures 1A,B). F_v/F_m showed similar differences in temporal dynamics between the Fe-limited and Fe-replete infected cultures upon infection with these viruses (Figures 1C,D). At large, the infected *M. pusilla* cultures showed similar results (Figure 2). The alterations in host physiological condition in the Fe-limited cultures resulted for both phytoplankton species in slower release of virus progeny and reduced virus yield when infected with VL as compared to Fe-replete cultures (Figures 1E,F, 2E,F). The latent period, e.g., the time period to extracellular release of newly produced viruses, was however unaffected by Fe-limitation of the host. Experiments with the same strain of *M. pusilla* did show prolonged latent periods when under phosphorus (P) and nitrogen (N) limitation (Maat et al., 2014; Maat and Brussaard, 2016). These were suggested to be due to reduced substrate and host energy availability resulting from impaired photophysiology under major nutrient limitation. In our study Chlorophyll-a concentration was comparably reduced but F_v/F_m of Fe-limited steady state *M. pusilla* was not impaired. Then again, F_v/F_m of *P. globosa* cells prior to infection was reduced compared to Fe-replete, still not prolonging the latent period. We cannot be sure of the exact underlying mechanism from the here presented data, but the proliferation of DNA viruses is directly dependent on Fe due to the essential role Fe plays in the catalytic center of ribonucleotide reductase, produced early in infection to support dNTPs production needed for viral DNA synthesis (Romeo et al., 2001). As such, it can be speculated that not the time to produce a virus is affected but instead the number of viruses that can be produced before cell lysis occurs. The burst size of MpV and

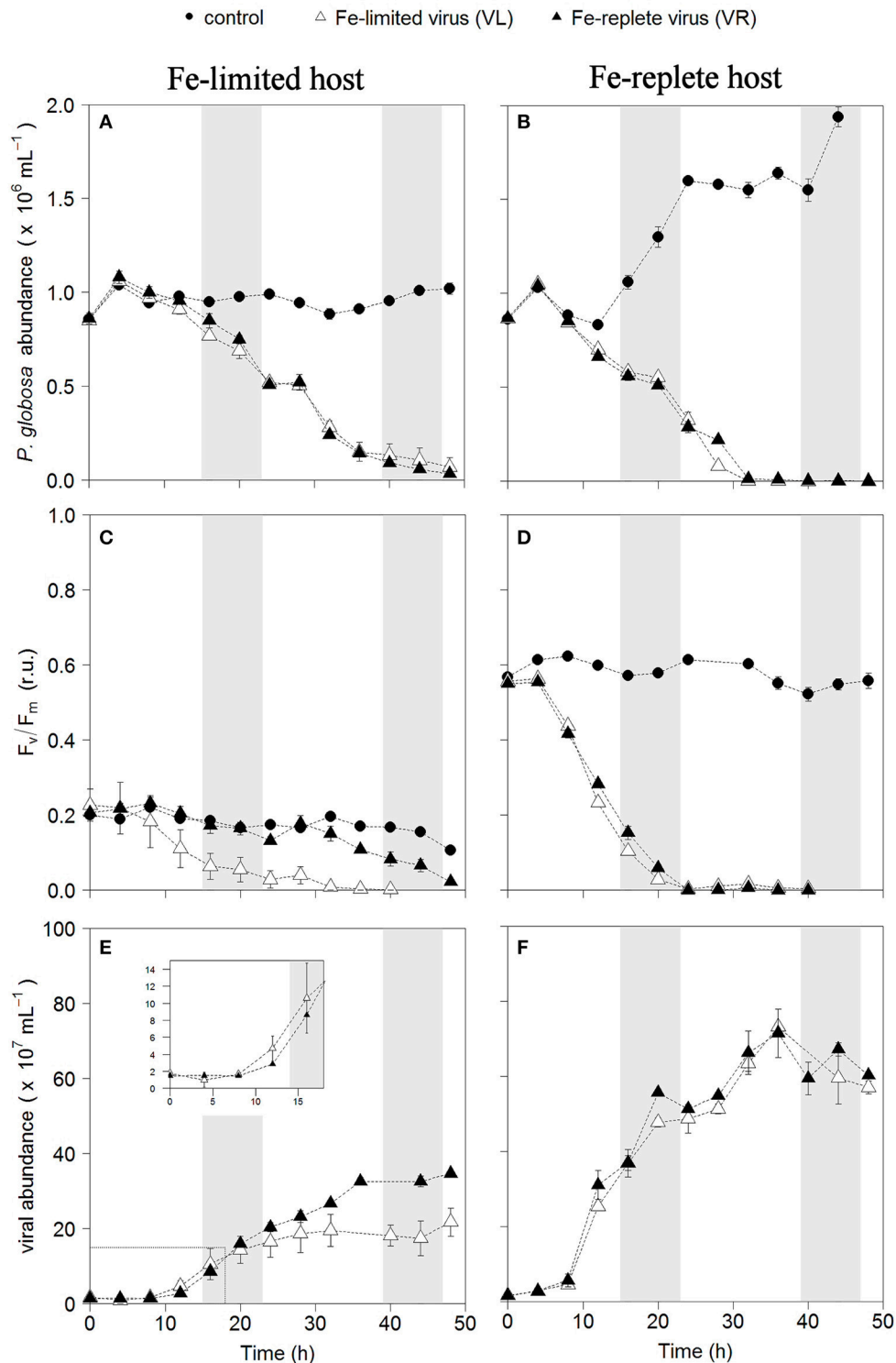


FIGURE 1 | Temporal dynamics of *P. globosa* viral infections: host cell abundance over time (h) in Fe-limited (A) and Fe-replete cultures (B); photosynthetic capacity (F_v/F_m) over time (h) of Fe-limited (C) and Fe-replete cultures (D); viral abundance in Fe-limited (E) and Fe-replete (F) cultures. Circles represent non-infected controls, black triangles represent infections with Fe-replete host derived viruses (VR) and white triangles represent infections with Fe-limited host derived viruses (VL). Error bars indicate deviation of replicates ($n = 2$); when not visible they fall within the symbols. Shaded areas indicate dark periods, explaining the slight declines in F_v/F_m for the Fe-replete non-infected host. Furthermore, the dark period illustrates the onset of the synchronized cell division. Inlay in (E) magnifies the first 20 h post-infection.

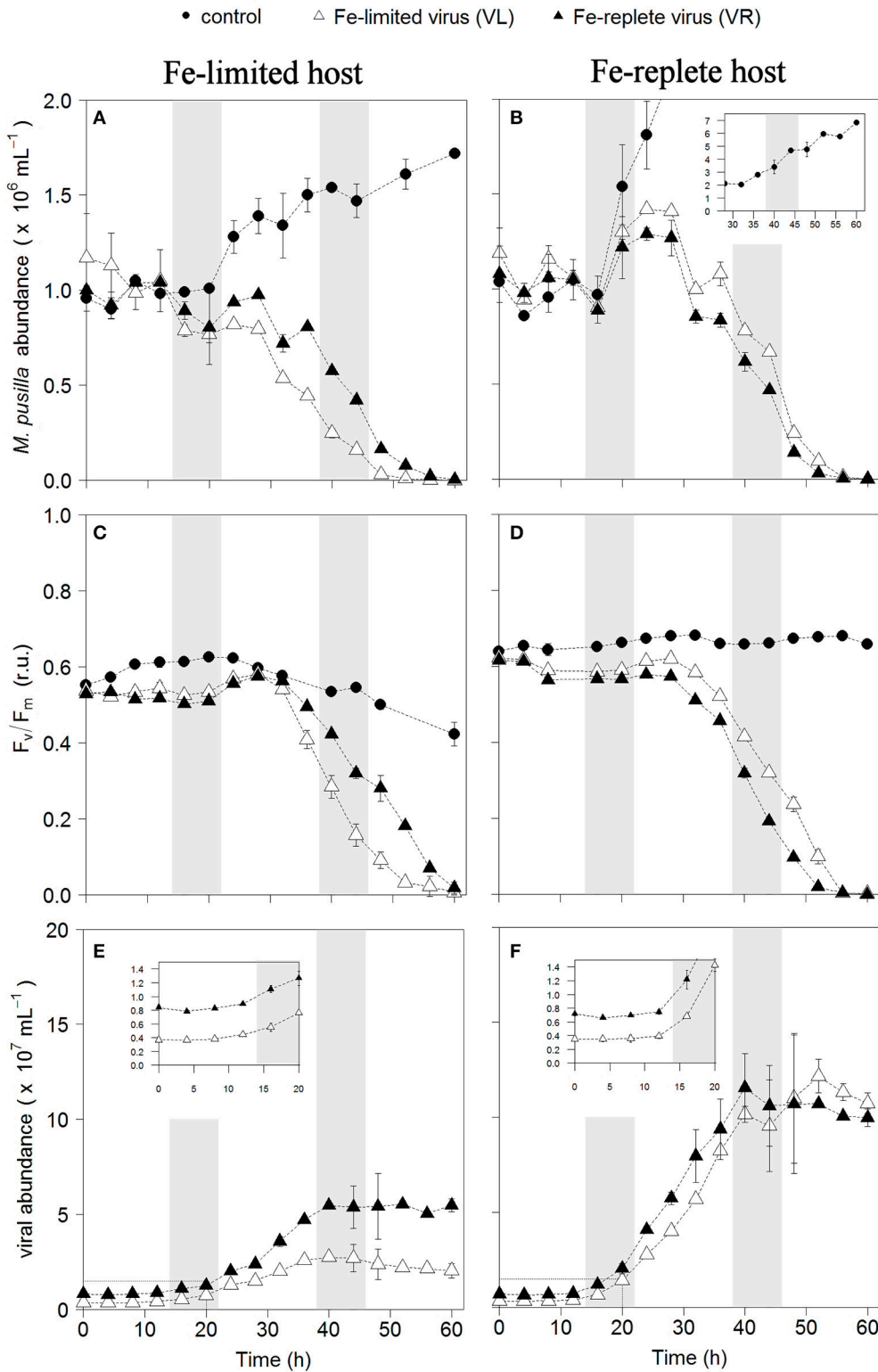


FIGURE 2 | Temporal dynamics of *M. pusilla* viral infections: host cell abundance over time (h) in Fe-limited (A) and Fe-replete cultures (B); photosynthetic capacity (F_v/F_m) over time (h) of Fe-limited (C) and Fe-replete cultures (D); viral abundance in Fe-limited (E) and Fe-replete (F) cultures. Circles represent non-infected controls, black triangles represent infections with Fe-replete host derived viruses (VR) and white triangles represent infections with
(Continued)

FIGURE 2 | Continued

Fe-limited host derived viruses (VL). Error bars indicate deviation of replicates ($n = 2$); when not visible these fall within the symbols. Shaded areas indicate dark periods, explaining the slight declines in F_v/F_m for the Fe-replete non-infected host. Furthermore, the dark period illustrates the onset of the synchronized cell division. Inlay in (B) shows off scale host control growth, inlays in (E,F) magnify the first 20 h post-infection.

PgV indeed decreased strongly under Fe-limitation, i.e., to 24 and 29% of the burst size produced under Fe-replete conditions (20 and 196 viruses lysed host cell⁻¹; **Table 3**). In comparison to *P. globosa*, the reduced growth rate of Fe-limited steady state *M. pusilla* did not significantly affect the extent of reduction in virus burst size. Nonetheless, *M. pusilla* required a higher cellular Fe concentration. This implies that Fe-limited *P. globosa*, able to grow at the lower Fe concentration, displays a more efficient virus proliferation (despite the low F_v/F_m at the start of infection).

Noteworthy, the higher Fe concentration needed to allow for sustainable growth of *M. pusilla* under Fe-limitation did not prevent the loss of infectivity of the virus progeny. Infectivity of the Fe-limited MpV lysate was reduced to $30 \pm 7\%$, while in contrast PgV did not show decreased infectivity for Fe-limited hosts. Our results signify that a stronger Fe-stress experienced by the Fe-limited *M. pusilla* (expressed in reduced growth rate) is more likely responsible for the production of impaired virus progeny than a changed photosynthetic capacity (F_v/F_m 0.2 for *P. globosa* compared to 0.6 for *M. pusilla*). The fact that total virus abundance, as measured after staining with a nucleic acid dye, was higher than the infective abundance indicates that (i) virus particles and (ii) viral nucleic acids were produced. Still, impaired capsid proteins or host receptors may explain a loss of infectivity. Alternatively, processes known to be Fe-intensive are DNA replication and repair (Netz et al., 2012; Zhang, 2014). Failure of DNA repair could indeed explain the result of reduced percentage infective viruses. Future research should not only focus on the causal aspects *per se* but also study what causes the dissimilarities in loss of infectivity between the algal viruses since different responses will directly regulate community composition. Furthermore, future studies should screen if and how other marine taxa and different viruses are affected by virus proliferation under Fe-limitation. For example, non-marine tailed bacteriophages have been found to contain iron ions in the tail proteins that can utilize the siderophore-bound iron receptors on the host cell membrane for attachment of the phage and subsequent infection of the bacterial host (Bartual et al., 2010). It is likely that similar interactions also exists for marine bacteriophages (Bonnain et al., 2016). Still open questions are whether such phages will obtain fewer iron ions in their tail under Fe-deprivation, and if this will negatively affect their infectivity. Furthermore, the recently proposed “Ferrojan Horse Hypothesis” by Bonnain et al. (2016) posits that introduction of phage-attached Fe may aid the host. More study is needed to test this theory and its potential interference with siderophore-specific uptake mechanisms and effect on Fe cycling.

For all Fe-replete cultures (i.e., high Fe concentration and consequently high F_v/F_m of around 0.6) and the Fe-limited *M. pusilla* the lysis dynamics and decline in F_v/F_m for the VR- and VL-infected cultures were largely comparable (**Figures 1D, 2D**). However, the Fe-treatment history of the virus (VL or

TABLE 3 | Burst sizes (number of virus progeny per lysed host cell) of PgV-07T and MpV-08T infecting Fe-replete and Fe-limited *P. globosa* (Pg) and *M. pusilla* (Mp), respectively.

Treatment	Burst size	% of replete
Pg replete + VR	671 ± 62	
Pg replete + VL	679 ± 5	
Pg limited + VL	196 ± 35	29 ± 0.2
Pg limited + VR	308 ± 4	46 ± 2.3
Mp replete + VR	84 ± 14	
Mp replete + VL	83 ± 6	
Mp limited + VL	20 ± 0	24 ± 5.2
Mp limited + VR	46 ± 2	54 ± 0.5

Viruses were derived from a Fe-replete host (VR) or a Fe-limited host (VL). Burst sizes for Fe-limited cultures are also expressed as a percentage of the corresponding infections in Fe-replete cultures.

VR) did matter in combination with Fe-limited *P. globosa* cells, i.e., infection with VR did delay the decline in F_v/F_m with more than a day (**Figure 1C**). Infection with a VR lysate is analogous to a relief in Fe-limitation at the time of infection. When the Fe-limited *P. globosa* cultures were infected with a VR lysate, they were effectively spiked with an Fe increase of ~10% relative to Fe-replete conditions (0.9 μM). The 100–300-fold increase of Fe with the addition of an Fe-replete lysate (0.9 μM vs. 1–3 nM) takes the culture Fe concentration well out of limitation ranges which are generally considered to be in nano- to picomolar ranges (de Baar et al., 1990; Martin et al., 1990; Brand, 1991). The concentration increase in our experiment is comparatively drastic to assure lifting of Fe-limitation to levels nearer normal replete cultures. This cross-inoculation provides insight in the potential effects of sudden introduction of Fe, e.g., with (seasonal) dust deposition or terrestrial runoff. The effect of this spike with Fe was apparently enough to prevent instant loss of photosynthetic capacity in the Fe-limited *P. globosa* cells. For both phytoplankton species, the improved physiological condition upon infection of Fe-limited host with VR virus resulted in enhanced viral production compared to Fe-limited infected with VL virus (by 1.6 and 2.3-fold for PgV and MpV, respectively; **Table 3**). The effect on burst size is thus stronger for the more Fe-sensitive *M. pusilla*, indicating that *M. pusilla* is more capable of mobilizing the Fe added for viral production. Utilization of the limiting macronutrient P when added post infection was also found to stimulate virus production of *M. pusilla* (Maat et al., 2016). Although, our results indicate that an infected host is capable of mobilizing the limiting Fe for viral production upon addition post infection, it did not lead to a complete recovery of virus production as compared to Fe-replete conditions (around 50% of the replete treatment; **Table 2**).

In conclusion, viral infection of both phytoplankton species is distinctly influenced by Fe-limitation. The differences in

sensitivity of the host to Fe-limitation subsequently affected the progeny virus growth properties. *Phaeocystis* and *Micromonas* occur in Fe-limited and Fe-replete conditions alike (Not et al., 2004, 2005; Schoemann et al., 2005). Viral lysis has been shown to be an important mortality term for *P. globosa* under natural conditions, and also *M. pusilla* is readily infected (Cottrell and Suttle, 1995; Brussaard, 2004; Brussaard et al., 2005; Baudoux et al., 2006; Martínez et al., 2015). Virus burst sizes became strongly reduced (on average by 70%) under Fe-limiting relative to Fe-replete conditions. Although, addition of Fe at the time of infection was utilized by the infected Fe-limited host to increase virus production, it was not to the level found under Fe-replete conditions. Thus, Fe-limitation irrevocably interfered with viral productivity. Additionally, Fe-limited *M. pusilla* demonstrated an evident effect on the quality of the viruses produced as only 30% were infective. The lowered virus infectivity and/or virus yield impair viral control of the specific host species under Fe-limitation. However, at the same time, reduced viral lysis may affect the productivity of remaining non-infected cells and of other phytoplankton species, because viral lysis is considered a driver of Fe cycling by releasing ligand-bound dissolved Fe-species back into the dissolved organic matter pool (Gobler et al., 1997; Poorvin et al., 2004, 2011). What relative contributions different ligands have, and in how far their release is facilitated or impaired by viral lysis requires further

study. Further experimental and *in-situ* study of phytoplankton host-virus dynamics under Fe-limitation is essential to elucidate the level of response specificity, but also the effects on the viral shunt in terms of nutrient cycling in general as well as Fe speciation.

AUTHOR CONTRIBUTIONS

LG, CB, and HS were responsible for the design of this research. HS, CB analyzed and interpreted data. HS, LG, and CB wrote the paper.

ACKNOWLEDGMENTS

We thank captain and crew of R.V. Pelagia and Micha Rijkenberg for their assistance in obtaining trace metal clean seawater stocks. We furthermore thank Josje Snoek for her assistance, Patrick Laan for dissolved Fe analysis, Swier Oosterhuis for pigment composition analysis, and Karel Bakker and Sharyn Ossebaar for nutrient analyses. We appreciate discussions with Douwe Maat, Klaas Timmermans and Willem van de Poll. This work was funded through a grant by the Netherlands Organization for Scientific Research (NWO) under contract number 822.01.018 to LG, and from the European Union Seventh Framework Programme (FP7/2007-2013) under grant agreement n 311975 (MaCuMBA) to CB.

REFERENCES

- Bartual, S. G., Otero, J. M., Garcia-Doval, C., Llamas-Saiz, A. L., Kahn, R., Fox, G. C., et al. (2010). Structure of the bacteriophage T4 long tail fiber receptor-binding tip. *Proc. Natl. Acad. Sci. U.S.A.* 107, 20287–20292. doi: 10.1073/pnas.1011218107
- Baudoux, A. C., and Brussaard, C. P. D. (2005). Characterization of different viruses infecting the marine harmful algal bloom species. *Phaeocystis globosa*. *Virology* 341, 80–90. doi: 10.1016/j.virol.2005.07.002
- Baudoux, A. C., Noordeloos, A. A. M., Veldhuis, M. J. W., and Brussaard, C. P. D. (2006). Virally induced mortality of *Phaeocystis globosa* during two spring blooms in temperate coastal waters. *Aquat. Microb. Ecol.* 44, 207–217. doi: 10.3354/ame044207
- Baudoux, A. C., Veldhuis, M. J. W., Witte, H. J., and Brussaard, C. P. D. (2007). Viruses as mortality agents of picophytoplankton in the deep chlorophyll maximum layer during IRONAGES III. *Limnol. Oceanogr.* 52, 2519–2529. doi: 10.4319/lo.2007.52.6.2519
- Behrenfeld, M. J., Bale, A. J., Kolber, Z. S., Aiken, J., and Falkowski, P. G. (1996). Confirmation of iron limitation of phytoplankton photosynthesis in the Equatorial Pacific Ocean. *Nature* 383, 508–511. doi: 10.1038/383508a0
- Behrenfeld, M. J., Worthington, K., Sherrell, R. M., Chavez, F. P., Strutton, P., McPhaden, M., et al. (2006). Controls on tropical Pacific Ocean productivity revealed through nutrient stress diagnostics. *Nature* 442, 1025–1028. doi: 10.1038/nature05083
- Bonnain, C., Breitbart, M., and Buck, K. N. (2016). The Ferrojan Horse Hypothesis: iron-virus interactions in the ocean. *Front. Mar. Sci.* 3:82. doi: 10.3389/fmars.2016.00082
- Brand, L. E. (1991). Minimum iron requirements of marine phytoplankton and the implications for the biogeochemical control of new production. *Limnol. Oceanogr.* 36, 1756–1771. doi: 10.4319/lo.1991.36.8.1756
- Bratbak, G., Jacobsen, A., Heldal, M., Nagasaki, K., and Thingstad, F. (1998). Virus production in *Phaeocystis pouchetii* and its relation to host cell growth and nutrition. *Aquat. Microb. Ecol.* 16, 1–9. doi: 10.3354/ame016001
- Breitbarth, E., Achterberg, E. P., Ardelan, M. V., Baker, A. R., Bucciarelli, E., Chever, F., et al. (2010). Iron biogeochemistry across marine systems—progress from the past decade. *Biogeosciences* 7, 1075–1097. doi: 10.5194/bg-7-1075-2010
- Brussaard, C. P. D. (2004). Viral control of phytoplankton populations - a review. *J. Eukaryot. Microbiol.* 51, 125–138. doi: 10.1111/j.1550-7408.2004.tb00537.x
- Brussaard, C. P. D., Mari, X., Van Bleijswijk, J. D. L., and Veldhuis, M. J. W. (2005). A mesocosm study of *Phaeocystis globosa* (Prymnesiophyceae) population dynamics: II. Significance for the microbial community. *Harmful Algae* 4, 875–893. doi: 10.1016/j.hal.2004.12.012
- Brussaard, C. P. D., and Martínez, J. M. (2008). Algal bloom viruses. *Plant Virus*. 2, 1–10. Available online at: <http://www.globalsciencebooks.info/Journals/PV.html>
- Brussaard, C. P. D., Payet, J. P., Winter, C., and Weinbauer, M. G. (2010). Quantification of aquatic viruses by flow cytometry. *Man. Aquat. Viral Ecol.* 11, 102–109. doi: 10.4319/mave.2010.978-0-9845591-0-7.102
- Brussaard, C. P. D., Thyrhaug, R., Marie, D., and Bratbak, G. (1999). Flow cytometric analyses of viral infection in two marine phytoplankton species, *Micromonas pusilla* (Prasinophyceae) and *Phaeocystis pouchetii* (Prymnesiophyceae). *J. Phycol.* 35, 941–948. doi: 10.1046/j.1529-8817.1999.3550941.x
- Butler, A. (2005). Marine siderophores and microbial iron mobilization. *Biometals* 18, 369–374. doi: 10.1007/s10534-005-3711-0
- Calbet, A., and Landry, M. R. (2004). Phytoplankton growth, microzooplankton grazing, and carbon cycling in marine systems. *Limnol. Oceanogr.* 49, 51–57. doi: 10.4319/lo.2004.49.1.0051
- Cottrell, M. T., and Suttle, C. A. (1995). Dynamics of lytic virus infecting the photosynthetic marine picoflagellate *Micromonas pusilla*. *Limnol. Oceanogr.* 40, 730–739. doi: 10.4319/lo.1995.40.4.0730
- de Baar, H. J. W., Buma, A. G. J., Nolting, R. F., Cadée, G. C., Jacques, G., and Treguer, P. J. (1990). On iron limitation of the southern ocean?: experimental observations in the Weddell and Scotia Seas. *Mar. Ecol. Prog. Ser.* 65, 105–122. doi: 10.3354/meps065105

- Garg, S., Rose, A. L., and Waite, T. D. (2007). Superoxide-mediated reduction of organically complexed iron(III): impact of pH and competing cations (Ca^{2+}). *Geochim. Cosmochim. Acta* 71, 5620–5634. doi: 10.1016/j.gca.2007.08.002
- Geider, R. J., and La Roche, J. (1994). The role of iron in phytoplankton photosynthesis, and the potential for iron-limitation of primary productivity in the sea. *Photosyn. Res.* 39, 275–301.
- Geider, R. J., La Roche, J., Greene, R. M., and Olaizola, M. (1993). Response of the photosynthetic apparatus of *Phaeodactylum tricoratum* (Bacillariophyceae) to nitrate, phosphate, or iron starvation. *J. Phycol.* 29, 755–766. doi: 10.1111/j.0022-3646.1993.00755.x
- Genty, B., Briantais, J. -M., and Baker, N. R. (1989). The relationship between the quantum yield of photosynthetic electron transport and quenching of chlorophyll fluorescence. *Biochim. Biophys. Acta* 990, 87–92. doi: 10.1016/S0304-4165(89)80016-9
- Gerringa, L. J. A., de Baar, H. J. W., and Timmermans, K. R. (2000). A comparison of iron limitation of phytoplankton in natural oceanic waters and laboratory media conditioned with EDTA. *Mar. Chem.* 68, 335–346. doi: 10.1016/S0304-4203(99)00092
- Gerringa, L. J. A., Veldhuis, M. J. W., Timmermans, K. R., Sarthou, G., and de Baar, H. J. W. (2006). Co-variance of dissolved Fe-binding ligands with phytoplankton characteristics in the canary basin. *Mar. Chem.* 102, 276–290. doi: 10.1016/j.marchem.2006.05.004
- Gledhill, M., and van den Berg, C. M. G. (1994). Determination of complexation of iron(III) with natural organic complexing ligands in seawater using cathodic stripping voltammetry. *Mar. Chem.* 47, 41–54. doi: 10.1016/0304-4203(94)90012-4
- Gobler, C. J., Hutchins, D. A., and Fisher, N. S. (1997). Release and bioavailability of C, N, P, Se, and Fe following viral lysis of a marine chrysophyte. *Limnol. Oceanogr.* 42, 1492–1504. doi: 10.4319/lo.1997.42.7.1492
- González, A. G., Pérez-Almeida, N., Santana-Casiano, J. M., Millero, F. J., and González-Dávila, M. (2016). Redox interactions of Fe and Cu in seawater. *Mar. Chem.* 179, 12–22. doi: 10.1016/j.marchem.2016.01.004
- González, A. G., Santana-Casiano, J. M., González-Dávila, M., Pérez-Almeida, N., and Suárez De Tangil, M. (2014). Effect of *Dunaliella tertiolecta* organic exudates on the Fe(II) oxidation kinetics in seawater. *Environ. Sci. Technol.* 48, 7933–7941. doi: 10.1021/es5013092
- Grasshoff, K. (1983). “Determination of nitrate.” in *Methods of Seawater Analysis*, eds K. Grasshoff, M. Erhardt, and K. Kremling (Weinheim: Verlag Chemie), 143–87.
- Hassler, C. S., Schoemann, V., Nichols, C. M., Butler, E. C. V., and Boyd, P. W. (2011). Saccharides enhance iron bioavailability to southern ocean phytoplankton. *Proc. Natl. Acad. Sci. U.S.A.* 108, 1076–1081. doi: 10.1073/pnas.1010963108
- Ibanmí, E., Sander, S. G., Boyd, P. W., Bowie, A. R., and Hunter, K. A. (2011). Vertical distributions of iron-(III) complexing ligands in the southern ocean. *Deep Sea Res. II* 58, 2113–2125. doi: 10.1016/j.dsr2.2011.05.028
- Klunder, M. B., Laan, P., Middag, R., De Baar, H. J. W., and van Ooijen, J. C. (2011). Dissolved iron in the southern ocean (Atlantic Sector). *Deep Sea Res. II* 58, 2678–2694. doi: 10.1016/j.dsr2.2010.10.042
- Kustka, A. B., Shaked, Y., Milligan, A. J., King, D. W., and Morel, F. M. M. (2005). Extracellular production of superoxide by marine diatoms: contrasting effects on iron redox chemistry and bioavailability. *Limnol. Oceanogr.* 50, 1172–1180. doi: 10.4319/lo.2005.50.4.1172
- Laglera, L. M., Battaglia, G., and van den Berg, C. M. G. (2011). Effect of humic substances on the iron speciation in natural waters by CLE/CSV. *Mar. Chem.* 127, 134–143. doi: 10.1016/j.marchem.2011.09.003
- Liu, X., and Millero, F. J. (2002). The Solubility of iron in seawater. *Mar. Chem.* 77, 43–54. doi: 10.1016/S0304-4203(01)00074-3
- Maat, D. S., and Brussaard, C. P. D. (2016). Both phosphorus and nitrogen limitation constrain viral proliferation in marine phytoplankton. *Aquat. Microb. Ecol.* 77, 87–97. doi: 10.3354/ame01791
- Maat, D. S., Crawford, K. J., Timmermans, K. R., and Brussaard, C. P. D. (2014). Elevated CO_2 and phosphate limitation favor *Micromonas pusilla* through stimulated growth and reduced viral impact. *Appl. Environ. Microbiol.* 80, 3119–3127. doi: 10.1128/AEM.03639-13
- Maat, D. S., Van Bleijswijk, J. D. L., Witte, H. J., and Brussaard, C. P. D. (2016). Virus production in phosphorus limited *Micromonas pusilla* stimulated by a supply of naturally low concentrations of different phosphorus sources, far into the lytic cycle. *FEMS Microbiol. Ecol.* 92:fw136. doi: 10.1093/femsec/fw136
- Marie, D., Partensky, F., Vaulot, D., and Brussaard, C. P. D. (1999). Enumeration of phytoplankton, bacteria, and viruses in marine samples. *Curr. Protoc. Cytom.* Chapter 11, Unit 11.11. doi: 10.1002/0471142956
- Martin, J. H., Fitzwater, S. E., and Gordon, R. M. (1990). Iron deficiency limits phytoplankton growth in antarctic waters. *Global Biogeochem. Cycles* 4, 5–12.
- Martínez, J. M., Boere, A., Gilg, I., van Lent, J. W. M., Witte, H. J., van Bleijswijk, J. D. L., et al. (2015). New lipid envelope-containing dsDNA virus isolates infecting *Micromonas pusilla* reveal a separate phylogenetic group. *Aquat. Microb. Ecol.* 74, 17–28. doi: 10.3354/ame01723
- Martínez, J. M., Swan, B. K., and Wilson, W. H. (2014). Marine viruses, a genetic reservoir revealed by targeted viromics. *ISME J.* 8, 1079–1088. doi: 10.1038/ismej.2013.214
- Mawji, E., Gledhill, M., Milton, J. A., Zubkov, M. V., Thompson, A., Wolff, G. A., et al. (2011). Production of siderophore type chelates in Atlantic Ocean Waters enriched with different carbon and nitrogen sources. *Mar. Chem.* 124, 90–99. doi: 10.1016/j.marchem.2010.12.005
- Mengel, K. (1994). Iron availability in plant tissues - iron chlorosis on calcareous soils. *Plant Soil* 165, 275–283. doi: 10.1007/BF00008070
- Millero, F. J. (1998). Solubility of Fe (III) in seawater. *Earth Planet. Sci. Lett.* 154, 323–329.
- Mojica, K. D. A., and Brussaard, C. P. D. (2014). Factors affecting virus dynamics and microbial host-virus interactions in marine environments. *FEMS Microbiol. Ecol.* 89, 495–515. doi: 10.1111/1574-6941.12343
- Mojica, K. D. A., Huisman, J., Wilhelm, S. W., and Brussaard, C. P. D. (2016). Latitudinal variation in virus-induced mortality of phytoplankton across the North Atlantic Ocean. *ISME J.* 10, 1–14. doi: 10.1038/ismej.2015.130
- Murphy, J., and Riley, J. P. (1962). A modified single solution method for the determination of phosphorous in natural waters. *Anal. Chim. Acta* 27, 31–36.
- Netz, D. J. A., Stith, C. M., Stümpfig, M., Köpf, G., Vogel, D., Genau, H. M., et al. (2012). Eukaryotic DNA polymerases require an iron-sulfur cluster for the formation of active complexes. *Nat. Chem. Biol.* 8, 125–132. doi: 10.1038/nchembio.721
- Not, F., Latasa, M., Marie, D., Cariou, T., Vaulot, D., and Simon, N. (2004). A Single Species, *Micromonas pusilla* (Prasinophyceae), dominates the eukaryotic picoplankton in the Western English Channel. *Appl. Environ. Microbiol.* 70, 4064–4072. doi: 10.1128/AEM.70.7.4064-4072.2004
- Not, F., Massana, R., Latasa, M., Marie, D., Colson, C., Eikrem, W., et al. (2005). Late summer community composition and abundance of photosynthetic picoeukaryotes in Norwegian and Barents Seas. *Limnol. Oceanogr.* 50, 1677–1686. doi: 10.4319/lo.2005.50.5.1677
- Passmore, R., Hsu, J., Liu, R. X., Tam, E., Cai, Y. W., Su Frasca, J., et al. (2000). *MPN Assay Analyzer*. Available online at: <http://www.ocgy.ubc.ca/~suttle/>
- Poorvin, L., Rinta-Kanto, J. M., Hutchins, D. A., and Wilhelm, S. W. (2004). Viral release of iron and its bioavailability to marine plankton. *Limnol. Oceanogr.* 49, 1734–1741. doi: 10.4319/lo.2004.49.5.1734
- Poorvin, L., Sander, S. G., Velasquez, I., Ibanmí, E., LeClerc, G. R., and Wilhelm, S. W. (2011). A comparison of Fe bioavailability and binding of a catecholate siderophore with virus-mediated lysates from the marine bacterium *Vibrio alginolyticus* PWH3a. *J. Exp. Mar. Biol. Ecol.* 399, 43–47. doi: 10.1016/j.jembe.2011.01.016
- Price, N. M., Ahner, B. A., and Morel, F. M. M. (1994). The Equatorial Pacific Ocean: grazer controlled phytoplankton populations in an iron-limited ecosystem. *Limnol. Oceanogr.* 39, 520–534.
- Rijkenberg, M. J. A., Steigenberger, S., Powell, C. F., van Haren, H., Patey, M. D., Baker, A. R., et al. (2012). Fluxes and distribution of dissolved iron in the Eastern (Sub-) Tropical North Atlantic Ocean. *Global Biogeochem. Cycles* 26, GB3004. doi: 10.1029/2011gb004264
- Romeo, A. M., Christen, L., Niles, E. G., and Kosman, D. J. (2001). Intracellular chelation of iron by bipyridyl inhibits DNA virus replication: ribonucleotide reductase maturation as a probe of intracellular iron pools. *J. Biol. Chem.* 276, 24301–24308. doi: 10.1074/jbc.M010806200
- Rue, E. L., and Bruland, K. W. (1995). Complexation of iron(III) by natural organic ligands in the central North Pacific as determined by a new competitive ligand equilibration/adsorptive cathodic stripping voltammetric method. *Mar. Chem.* 50, 117–138. doi: 10.1016/0304-4203(95)00031-L

- Schoemann, V., Becquevort, S., Stefels, J., Rousseau, V., and Lancelot, C. (2005). *Phaeocystis* blooms in the global ocean and their controlling mechanisms: a review. *J. Sea Res.* 53, 43–66. doi: 10.1016/j.seares.2004.01.008
- Shaked, Y., and Lis, H. (2012). Disassembling iron availability to phytoplankton. *Front. Microbiol.* 3:123. doi: 10.3389/fmicb.2012.00123
- Sunda, W. G., and Huntsman, S. A. (1995). Iron uptake and growth limitation in oceanic and coastal phytoplankton. *Mar. Chem.* 50, 189–206. doi: 10.1016/0304-4203(95)00035-P
- Suttle, C. A. (1993). "Enumeration and isolation of viruses," in *Handbook of Methods in Aquatic Microbial Ecology, 1st Edn.*, eds P. F. Kemp, B. F. Sherr, E. B. Sherr, and J. J. Cole (Boca Raton, FL: CRC Press), 121–134.
- Suttle, C. A. (2005). Viruses in the sea. *Nature* 437, 356–361. doi: 10.1038/nature04160
- Timmermans, K. R., Davey, M. S., van der Wagt, B., Snoek, J., Geider, R. J., Veldhuis, M. J. W., et al. (2001a). Co-Limitation by iron and light of *Chaetoceros brevis*, *C. dictyota* and *C. calcitrans* (Bacillariophyceae). *Mar. Ecol. Prog. Ser.* 217, 287–297. doi: 10.3354/meps217287
- Timmermans, K. R., Gerringa, L. J. A., de Baar, H. J. W., van der Wagt, B., Veldhuis, M. J. W., de Jong, J. T. M., et al. (2001b). Growth rates of large and small southern ocean diatoms in relation to availability of iron in natural seawater. *Limnol. Oceanogr.* 46, 260–266. doi: 10.4319/lo.2001.46.2.0260
- Timmermans, K. R., van der Wagt, B., and de Baar, H. J. W. (2004). Growth rates, half saturation constants, and silicate, nitrate, and phosphate depletion in relation to iron availability of four large open-ocean diatoms from the southern ocean. *Limnol. Oceanogr.* 49, 2141–2151. doi: 10.4319/lo.2004.49.6.2141
- van den Berg, C. M. G., and Kramer, J. R. (1979). Determination of complexing capacities of ligands in natural waters and conditional stability constants of the copper complexes by means of manganese dioxide. *Anal. Chim. Acta* 106, 113–120.
- van de Poll, W. H., Janknegt, P. J., van Leeuwe, M. A., Visser, R. J. W., and Buma, A. G. J. (2009). Excessive irradiance and antioxidant responses of an antarctic marine diatom exposed to iron limitation and to dynamic irradiance. *J. Photochem. Photobiol. B* 94, 32–37. doi: 10.1016/j.jphotobiol.2008.09.003
- van Leeuwe, M. A., and Stefels, J. (2007). "Photosynthetic responses in *Phaeocystis antarctica* towards varying light and iron conditions," in *Phaeocystis, Major Link in the Biogeochemical Cycling of Climate-Relevant Elements*, eds M. A. van Leeuwe, J. Stefels, S. Belviso, C. Lancelot, P. G. Verity, and W. W. C. Gieskes (Dordrecht: Springer), 61–70.
- Vaulot, D. (1989). *CYTOPC: Processing Software for Flow Cytometric Data*. signal and noise 2:8. Available online at: <http://application.sb-roscoff.fr/Phyto/index.php>
- Vaulot, D., Birrien, J.-L., Marie, D., Casotti, R., Veldhuis, M. J. W., Kraay, G. W., et al. (1994). Morphology, ploidy, pigment composition, and genome size of cultured strains of *Phaeocystis* (Prymnesiophyceae). *J. Phycol.* 30, 1022–1035.
- Vaulot, D., Eikrem, W., Viprey, M., and Moreau, H. (2008). The diversity of small eukaryotic phytoplankton (≤ 3 Mm) in marine ecosystems. *FEMS Microbiol. Rev.* 32, 795–820. doi: 10.1111/j.1574-6976.2008.00121.x
- Weitz, J. S., and Wilhelm, S. W. (2012). Ocean viruses and their effects on microbial communities and biogeochemical cycles. *F1000 Biol. Rep.* 8, 2–9. doi: 10.3410/B4-17
- Wilhelm, S. W., and Suttle, C. A. (1999). Viruses and nutrient cycles in the sea. *Bioscience* 49, 781. doi: 10.2307/1313569
- Zapata, M., Rodríguez, F., and Garrido, J. L. (2000). Separation of chlorophylls and carotenoids from marine phytoplankton: a new hplc method using a reversed phase C8 column and pyridine-containing mobile phases. *Mar. Ecol. Prog. Ser.* 195, 29–45. doi: 10.3354/meps195029
- Zhang, C. (2014). Essential functions of iron-requiring proteins in DNA replication, repair and cell cycle control. *Protein Cell* 5, 750–760. doi: 10.1007/s13238-014-0083-7

Conflict of Interest Statement: The authors declare that the research was conducted in the absence of any commercial or financial relationships that could be construed as a potential conflict of interest.

Copyright © 2016 Slagter, Gerringa and Brussaard. This is an open-access article distributed under the terms of the Creative Commons Attribution License (CC BY). The use, distribution or reproduction in other forums is permitted, provided the original author(s) or licensor are credited and that the original publication in this journal is cited, in accordance with accepted academic practice. No use, distribution or reproduction is permitted which does not comply with these terms.



The Ferrojan Horse Hypothesis: Iron-Virus Interactions in the Ocean

Chelsea Bonnain, Mya Breitbart and Kristen N. Buck*

College of Marine Science, University of South Florida, St. Petersburg, FL, USA

OPEN ACCESS

Edited by:

Toshi Nagata,
The University of Tokyo, Japan

Reviewed by:

Arvind Singh,
Physical Research Laboratory, India
Elvira Pulido-Villena,
Mediterranean Institute of
Oceanography, France
Dave Kirchman,
University of Delaware, USA

*Correspondence:

Kristen N. Buck
kristenbuck@usf.edu

Specialty section:

This article was submitted to
Marine Biogeochemistry,
a section of the journal
Frontiers in Marine Science

Received: 16 February 2016

Accepted: 17 May 2016

Published: 08 June 2016

Citation:

Bonnain C, Breitbart M and Buck KN
(2016) The Ferrojan Horse
Hypothesis: Iron-Virus Interactions in
the Ocean. *Front. Mar. Sci.* 3:82.
doi: 10.3389/fmars.2016.00082

Iron is an essential nutrient and the sub-nanomolar concentrations of iron in open ocean surface waters are often insufficient to support optimal biological activity. More than 99.9% of dissolved iron in these waters is bound to organic ligands, yet determining the identity of these ligands in seawater remains a major challenge. Among the potential dissolved organic ligands in the colloidal fraction captured between a 0.02 and a 0.2 μm filter persists an extremely abundant biological candidate: viruses, most of which are phages (viruses that infect bacteria). Recent work in non-marine model systems has revealed the presence of iron ions within the tails of diverse phages infecting *Escherichia coli*. Based on these findings and the presence of conserved protein motifs in marine phages, here we present several lines of evidence to support the hypothesis that phages are organic iron-binding ligands in the oceans. With average concentrations of 10^7 phages per milliliter surface seawater, we predict that phages could contain up to 0.7 pM iron, a value equivalent to as much as 70% of the colloidal fraction of organically complexed dissolved iron in the surface ocean. Additionally, the production and uptake of siderophores, a strategy that bacteria have developed for assimilating iron, renders cells vulnerable to phage infection due to the dual function of these cell surface receptors. Iron ions present in phage tails enable phages to exploit their bacterial host's iron-uptake mechanism via the "Ferrojan Horse Hypothesis" proposed herein, where the apparent gift of iron leads to cell lysis. Finally, if host iron stores are recycled during the assembly of progeny phages, as much as 14% of the cellular iron released into the water column upon lysis would already be incorporated into new phage tails. The potential role of phages as iron-binding ligands has significant implications for both oceanic trace metal biogeochemistry and marine phage-host interactions.

Keywords: iron, ligand, phage, marine, virus, siderophore, infection, bacteria

THE FERROJAN HORSE HYPOTHESIS

Iron is an essential micronutrient for microbial life. To thrive in the ocean, where iron concentrations are astonishingly low (Gordon et al., 1982), bacteria have evolved specialized iron-acquisition strategies, such as the production of siderophores (Neilands, 1957; Sandy and Butler, 2009). Siderophores are exceedingly strong organic iron-binding ligands produced by bacteria to outcompete other ligands for the binding and uptake of iron via a specific "trap door" receptor on the cell surface (Pawełek et al., 2006; Sandy and Butler, 2009; Vraspir and Butler, 2009; Hider and Kong, 2010). In non-marine systems, it has long been demonstrated that bacteriophages (phages; viruses that infect bacteria) take advantage of their bacterial hosts' vulnerabilities by utilizing the

siderophore-bound iron receptors on the bacterial cell surface membrane for infection, directly competing with siderophore-bound iron uptake (Neilands, 1979; Braun, 2009). These siderophore-bound iron receptors, collectively referred to as TonB-dependent receptors, are essential for bacterial iron acquisition (Luria and Delbruck, 1943; Braun et al., 1973; Hantke and Braun, 1975; Luckey et al., 1975; Braun and Endriss, 2007). Mutations in critical regions of these surface-exposed receptors are therefore selected against, providing an advantage to phages in the ongoing phage-host evolutionary arms race (Van Valen, 1973; Stern and Sorek, 2011; Samson et al., 2013).

A series of recent studies demonstrating the presence of iron ions in the tail proteins of several well-studied phages that infect enteric bacteria (Bartual et al., 2010; **Figure 1**) leads us to propose the “Ferrogan Horse Hypothesis” (*Ferrum* = Latin for iron; **Figure 2**). If marine phages, which are present at concentrations of ~10 million colloidal-sized (0.02–0.2 μm) particles per milliliter of surface seawater, contain similar amounts of iron, then a significant amount of the dissolved iron in the oceans could be complexed within phages. In this model, phages use the essential micronutrient iron in the manner of a Trojan horse: iron within the phage tail fibers is recognized by the host siderophore-bound iron receptor, enabling the phage to attach to the bacterial cell, puncture the cell membrane and inject its nucleic acid into the host for infection (**Figure 2**). Furthermore, we hypothesize that cellular iron stocks are recycled for incorporation into the tail fibers of new phage progeny during phage protein synthesis and assembly, which occurs inside the host cell prior to lysis (King, 1968; Chuprov-Netochin et al., 2010; Rohwer et al., 2014). Following cell lysis, host cell materials are remineralized via the viral shunt and new phages (containing a substantial fraction of the cellular iron) are released into the environment where they proceed to infect new hosts. Here we present the lines of evidence that support the plausibility for phages to act as organically complexed dissolved iron in the oceans and discuss the implications on oceanic biogeochemistry and phage-host interactions.

OCEANIC IRON BIOGEOCHEMISTRY

Bioavailable iron is scarce in open ocean surface waters due to its low solubility in oxic seawater at a pH of 8 and the vast distance from continental iron sources (Kuma et al., 1996; Johnson et al., 1997). This poses a challenge for marine microbes, since iron is essential for multiple biological functions, including the production of enzymes necessary for photosynthesis and respiration (Raven et al., 1999). As such, the iron quotas (Fe:C) for these cells are high relative to the requirements for any other trace metal (Bruland et al., 1991; Tortell et al., 1999; Morel and Price, 2003; Twining and Baines, 2013). In order to satisfy such a high iron requirement, marine bacteria have developed specialized mechanisms for iron acquisition. The synthesis and uptake of siderophores, which are high-affinity iron-chelating compounds, is a common strategy that bacteria use to secure iron from the marine environment

(Butler, 2005). The process of organic complexation protects dissolved iron from precipitation (Kuma et al., 1996), stabilizing the pool of bioavailable dissolved iron so that bacteria may then take up the entire complex via a siderophore-bound iron receptor (Sandy and Butler, 2009; Shaked and Lis, 2012). Furthermore, some bacteria have developed strategies to acquire the iron bound to siderophores produced by other bacteria, called “xenosiderophores” (Matzanke et al., 1997; Sandy and Butler, 2009; Cornelis, 2010; Gauglitz et al., 2014).

Iron bioavailability serves as a bottom-up control on primary productivity in much of the modern surface ocean, making characterization of iron speciation of vital importance to understanding the carbon cycle and global climate (e.g., Martin et al., 1989). The concentration of dissolved iron in seawater is largely regulated by organic complexation, with >99.9% of dissolved iron complexed by organic iron-binding ligands as measured by competitive ligand exchange-adsorptive cathodic stripping voltammetry (CLE-ACSV; Gledhill and van den Berg, 1994; Rue and Bruland, 1995). Most recently, applications of CLE-ACSV to basin-scale surveys of the Atlantic Ocean as part of the GEOTRACES program have reported widespread organic complexation, with iron-binding ligands present in excess of dissolved iron concentrations through most of the Atlantic water column (Buck et al., 2015; Gerringa et al., 2015).

Numerous studies have sought to identify the organic iron-binding ligands measured by CLE-ACSV throughout the oceans. The strongest known iron-binding ligands are siderophores, which are typically small, soluble molecules (<10 kDa or <0.02 μm), though some marine siderophores are colloidal in size (>0.02 μm but <0.2 μm) due to long fatty acid chains presumably used to tether the ligand to the bacterial cell that produced it (Martinez et al., 2003). Siderophores are the best-characterized strong iron-binding ligand class, yet the concentration of siderophores measured in the Atlantic Ocean is only 3–20 pM (Mawji et al., 2008)—though this is likely an underestimate due to the challenges of isolating siderophores from seawater (Vraspir and Butler, 2009; Gledhill and Buck, 2012). Iron-binding humic substances have been increasingly recognized as an important component of a weaker iron-binding ligand pool in the oceans, particularly in the deep sea and in coastal environments (Laglera et al., 2007, 2011; Laglera and van den Berg, 2009). Similar to humic substances, other weaker iron-binding ligands most likely also originate from the remineralization of organic matter in the oceans (Hunter and Boyd, 2007; Boyd and Ellwood, 2010; Boyd et al., 2010). These may include exopolymeric substances, transparent exopolymers, nanofibrils, and even the biotoxin domoic acid (**Figure 3**; Rue and Bruland, 2001; Mancuso Nichols et al., 2004; Stolpe and Hasselov, 2010; Hassler et al., 2011).

To date, few studies have combined size fractionation with iron-binding ligand measurements (Cullen et al., 2006; Thuroczy et al., 2010; Fitzsimmons et al., 2015). These studies have all measured the largest excess of strong iron-binding ligands within the soluble (<0.02 μm) size fraction, consistent with the traditional siderophore model. However, strong iron-binding

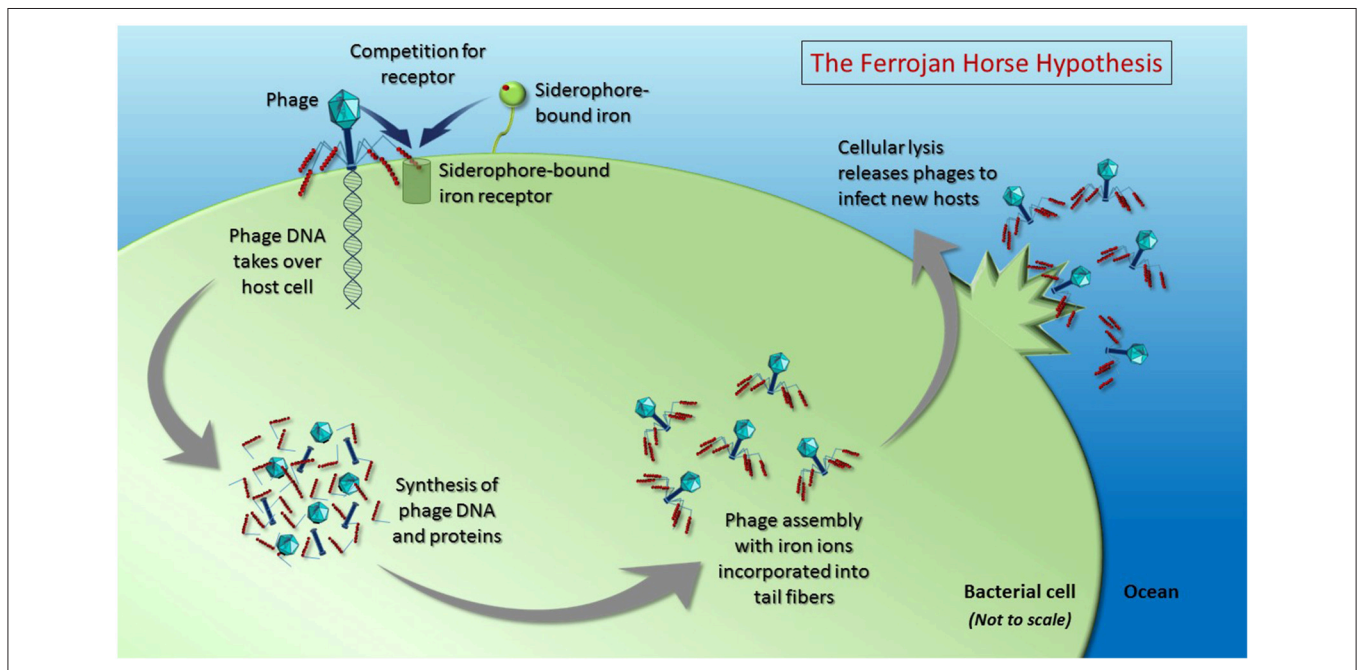
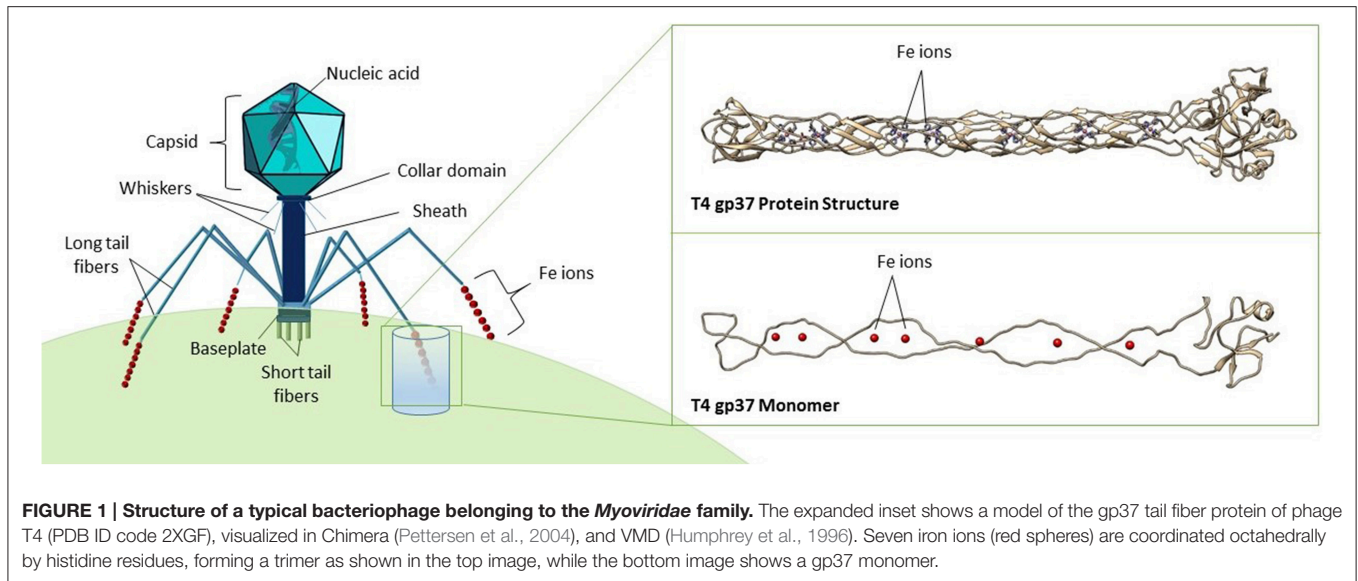


FIGURE 2 | The Ferrojan Horse Hypothesis depicts the use of iron ions (red spheres) within phage tail fibers to compete with siderophore-bound iron for access to the same receptor on the surface of the host cell. Once a phage docks on the cell surface, it can pierce the cell membrane and inject its nucleic acid, which takes over the host cell, instructing the cell to produce phage DNA and proteins. Cellular mechanisms are used to fold the proteins and assemble them into progeny phages, with iron from within the cell incorporated into the tail fibers. Upon cell lysis, new phages are released to infect hosts using the iron that has been pre-packaged within their tail fibers. This proposed recycling of cellular iron during phage production results in a depletion of the amount of iron available for remineralization upon lysis (i.e., via the viral shunt). Figure is not drawn to scale.

ligands were also detected within the colloidal fraction (0.02–0.2 μm), though at concentrations closer to that of dissolved iron with little to no excess ligands found in this size fraction (Cullen et al., 2006; Thuroczy et al., 2010; Fitzsimmons et al., 2015). Since measuring organic ligands that are already saturated with iron is particularly challenging by CLE-ACSV (e.g., Gledhill

and Buck, 2012), the persistence of colloidal iron in these studies was suggested to result from recent dust deposition of inorganic colloidal iron or an unknown but organically-stabilized colloidal iron complex. Size fractionation studies of dust dissolution from aerosols in the Atlantic Ocean have shown that iron in dust proceeds from particulate to colloidal to soluble size fractions

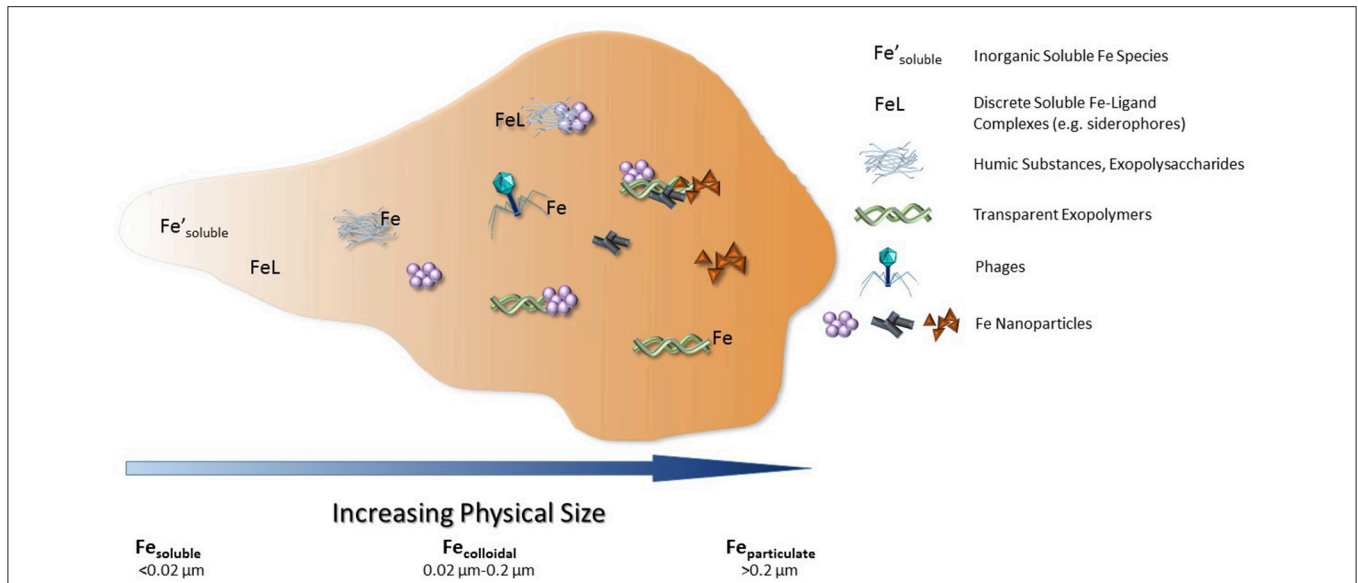


FIGURE 3 | Current dissolved iron-binding ligands identified within seawater, with the addition of phages within the colloidal size range. Figure modified from Gledhill and Buck (2012).

in the presence of strong organic iron-binding ligands like siderophores (Aguilar-Islas et al., 2010; Fishwick et al., 2014). In the absence of strong ligands, on the other hand, the iron remains in the colloidal size fraction, re-aggregates and is lost (Aguilar-Islas et al., 2010; Fishwick et al., 2014). The same may be expected of other particulate iron sources such as hydrothermal vents or shelf sediments, and the inorganic colloidal iron remains difficult to characterize. Recently, the ability of iron-oxidizing bacteria to produce iron oxides from hydrothermal vents has been proposed to contribute to the dissolved iron pool as a source of inorganic iron colloids (Emerson, 2016). While these studies highlight the complexity of iron speciation in seawater and the likelihood that inorganic iron colloids are an important dissolved iron species upon iron addition, the majority of the dissolved iron pool in the oceans is still thought to be organically complexed. Indeed, UV oxidation of seawater samples is commonly employed to release ligand-bound iron in seawater samples (Rue and Bruland, 1997; van den Berg, 2005; Biller and Bruland, 2012). Intriguingly, UV oxidation also reduces the infectivity of viruses and has been shown to destroy viral particles (Wilhelm et al., 1998); such treatment of phages in seawater would presumably also release any iron sequestered in phage tails.

The contribution of biologically sequestered iron to the organically complexed dissolved iron fraction has been largely ignored to date. The “biogenic” iron incorporated into the cells of phytoplankton and bacteria (typically $> 0.2 \mu\text{m}$ in diameter) can be a substantial portion of total (unfiltered) iron in the oceans, and when the fraction of dissolved iron is operationally defined as $< 0.45 \mu\text{m}$, many marine bacteria may contribute to the dissolved iron pool (Tortell et al., 1999). However, to our knowledge, no studies have explored the potential for viruses, the most abundant biological entities in the ocean, to contribute to the iron-binding

ligand pool in seawater, where they may account for a significant proportion of dissolved, and specifically colloidal ($0.02\text{--}0.2 \mu\text{m}$), organically complexed iron.

MARINE VIRUSES

With average concentrations of 10 million particles per milliliter, viruses (the majority of which are phages that infect bacteria) are the most abundant biological entities in the oceans (Wommack and Colwell, 2000; Breitbart, 2012). The impact of viruses on ocean biogeochemistry is often evoked purely through the act of host lysis (Fuhrman, 1999; Suttle, 2007), but very few studies have considered the chemical contributions of the viral particles themselves. Recent modeling work suggests that marine virus particles contain a significant amount of macronutrients (carbon, nitrogen, and phosphorus), and that the stoichiometric mismatch (i.e., the relative difference in elemental contents) between phages and their bacterial hosts has the potential to drive the differential release of nutrients upon cell lysis (Jover et al., 2014). However, no studies have considered the potential impact of trace elements within the structure of marine viral particles. If viruses contain or interact with trace metals such as iron, their small size and sheer abundance in the oceans would translate into a major influence for biogeochemical cycling of this vital micronutrient. Since phages dominate marine viral communities and the field of marine viral ecology is relatively young compared to the century of knowledge of phage biology (Rohwer and Segall, 2015; Salmond and Fineran, 2015), here we present the lines of evidence from non-marine model systems that suggest critical linkages may exist between phages and oceanic iron cycling.

EVIDENCE FROM NON-MARINE MODEL SYSTEMS

Iron within Phages Contributes to Colloidal Organically Complexed Dissolved Iron

Phage particles are composed of nucleic acids contained within a protein shell (capsid) with or without a proteinaceous tail, and occasionally surrounded by a lipid membrane (Figure 1; Hershey and Chase, 1952; Rohwer et al., 2014). A recent X-ray crystallography study demonstrated the presence of seven iron ions within the receptor-binding tip of each of the six long tail fibers (gp37) of phage T4, one of the most extensively studied *Escherichia coli* phages (Bartual et al., 2010). These iron ions, assumed to be Fe²⁺, are coordinated through paired histidine residues (HxH domains) in the phage's long tail fiber protein (Figure 1; Bartual et al., 2010). The octahedral coordination of iron ions by the paired histidine residues in phage tails suggests that the iron ions are a stable part of the phage particle which would contribute to the colloidal organically complexed iron pool (i.e., FeL). This is consistent with recent evidence that colloidal and particulate Fe(II) is more abundant in the oceans than previously considered and that the majority of this Fe(II) is associated with organic carbon (von der Heyden et al., 2014). The HxH domains (PFAM 03335; Figure 4) are present in the tail fibers of several model phages that infect *E. coli* such as T4 (family *Myoviridae*) and lambda (family *Siphoviridae*), where they are repeated a variable number of times (Finn et al., 2014). From the marine environment, we used BLAST similarity to T4 gp37 to identify HxH domains in putative tail fibers from several cyanophages infecting *Prochlorococcus* (phage P-SSM2) and *Synechococcus* (phages ACG2014f_1 and KBS-2A), as well as in an uncultured phage with an unknown host from the Mediterranean Sea (uvMED; Figure 4). The conservation of HxH motifs known to facilitate iron binding in the putative tail fibers of several marine phages suggests that these pathways documented in well-studied phages infecting *E. coli* may also occur within diverse phages in the oceans. Although the receptors for the vast majority of marine phages are yet unknown (Breitbart, 2012; Silva et al., 2016), if some marine phages also utilize siderophore-bound iron receptors for host infection, this mechanism would have major implications for our current understanding of marine phage-host interactions in the iron-limited surface ocean.

In addition to the tail fibers, conserved HxH domains within other phage structural proteins have also been shown to bind iron ions. For example, the baseplate assembly proteins of phages P2 and Φ92 (family *Myoviridae*), which form a membrane piercing spike, have recently been shown to contain iron ions coordinated octahedrally by paired histidine residues (Yamashita et al., 2011; Browning et al., 2012). Although the P2 and Φ92 proteins share conserved HxH motifs and the same function, the proteins that comprise the structure only share 19% amino acid identity. Since most phages with contractile tails (*Myoviridae*) utilize the same cell-puncturing mechanism (Leiman and Shneider, 2012), it is likely that distantly related *Myoviridae* may also contain iron-loaded tail spikes, even if these proteins cannot be identified

through sequence homology. In addition, the tail tip protein (gpL) of phage N15, a member of the *Siphoviridae* family of phages with non-contractile tails, binds an iron-sulfur cluster (Tam et al., 2013). While the function of this cluster remains unknown, it has been speculated to play a role in stabilizing the tail tip protein or in conformational changes that this protein undergoes during assembly or DNA injection (Tam et al., 2013), implying that the incorporation of metals into phage tails may broadly be utilized by diverse phages for strengthening and stabilizing host-piercing proteins.

In order to estimate the proportion of colloidal dissolved iron that could be bound within the tail fibers of oceanic phages, we calculated the number of iron atoms present in phage tail fibers based on knowledge from *E. coli* phage T4. According to Bartual et al. (2010), seven iron ions are coordinated within each of the six long tail fibers of phage T4 (Leiman et al., 2010), equaling 42 iron ions per phage. Using the average of 10⁷ viruses per milliliter of seawater (Wommack and Colwell, 2000; Breitbart, 2012; Parsons et al., 2012; Wommack et al., 2015) and assuming all viruses are tailed phages containing the same number of iron ions as T4, there are potentially a total of 4.2 × 10⁸ iron ions bound to phage tail fibers in a milliliter of seawater, accounting for up to 0.7 pM dissolved iron.

However, several caveats accompany these assumptions, which may significantly affect the relative impact of phages on dissolved iron concentrations. First, the presence of iron has not been demonstrated in any marine phage tails to date, so the numbers used here are based on well-studied model systems and the detection of conserved HxH motifs in marine phages. Since strong evolutionary relationships exist between marine and non-marine phages, with many phage proteins conserved across ecosystems, it is likely that successful infection strategies documented in non-marine model systems will also be present in the oceans (Rohwer et al., 2000; Sullivan et al., 2005). Second, the number of iron ions per phage tail fiber is likely to vary, as demonstrated by the variable number of HxH motifs seen in marine phage sequences (Figure 4). While our preliminary analyses have identified many HxH motifs among metagenomic sequences of uncultured marine viral communities (e.g., uvMED in Figure 4 and additional data not shown), the limited database of marine phage genomes and limited levels of sequence similarity between phage tail proteins despite their conserved function makes a complete analysis of the prevalence and abundance of conserved iron-binding motifs in phage tail fibers challenging. Third, marine viral communities are extremely diverse, containing viruses with a myriad of particle sizes and morphologies that infect hosts across all domains of life (Breitbart et al., 2007; Suttle, 2007; Rohwer and Thurber, 2009; Breitbart, 2012; Wommack et al., 2015). While tailed phages are consistently present in the oceans, the proportion of the viral community that they comprise can vary widely (Brum et al., 2013) and still requires further evaluation. A quantitative transmission electron microscopy study performed across the world's oceans demonstrated that tailed phages comprised between 8 and 49% of the total viral communities sampled (Brum et al., 2013). Repeating the above calculations using the lower bound of 8% tailed phages, phage

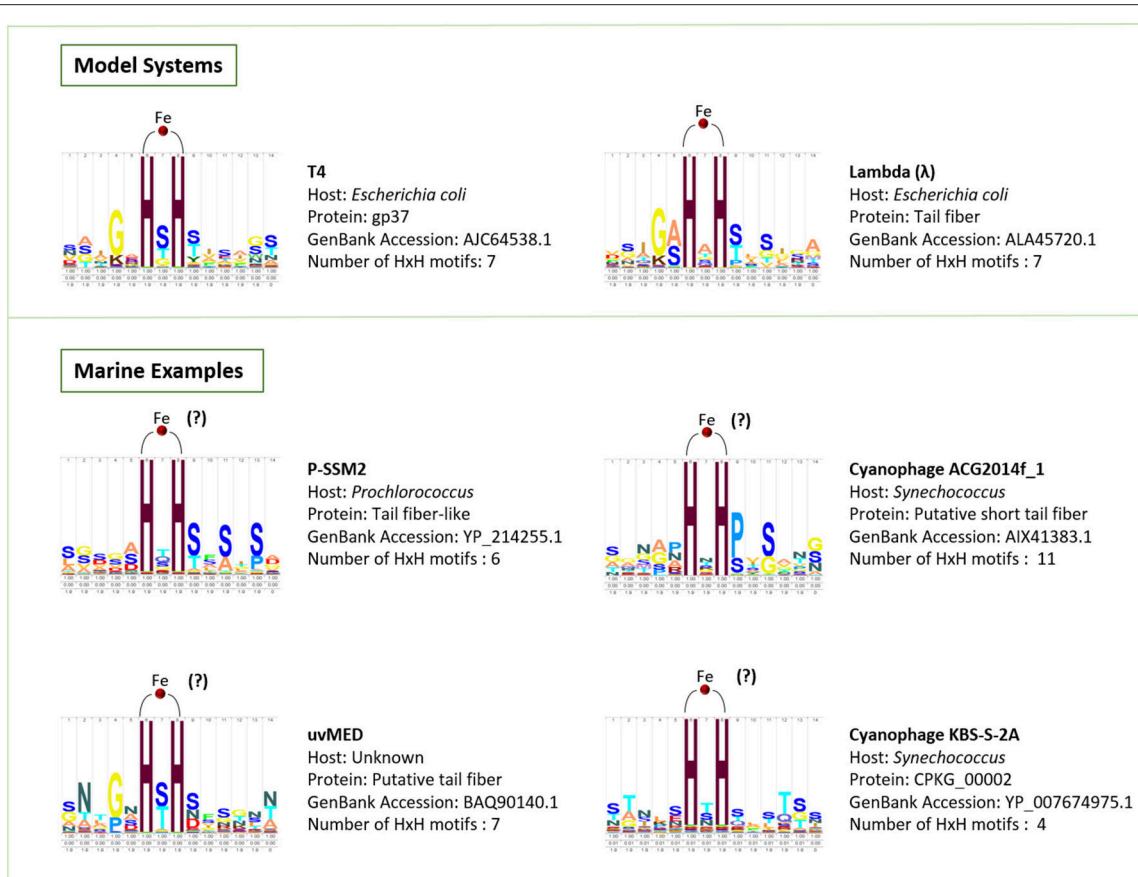


FIGURE 4 | HMM logos created using Skylign (Wheeler et al., 2014) for the HxH motifs that bind iron ions in the model phages T4 and lambda, as well as conserved HxH motifs identified here in the putative tail fiber proteins of marine phages, which we hypothesize play a role in binding iron.

tail fibers would account for 0.06 pM dissolved iron. In addition, phage tails may not be the only structural proteins that interact with iron. For example, Daughney et al. (2004) showed that iron could also adsorb to phage capsids, creating the possibility that non-tailed phages (and perhaps eukaryotic or archaeal viruses) could also play a role in iron cycling. Since these experiments used iron oxide concentrations far exceeding typical marine concentrations, future work is needed to explore the relevance of these studies to natural systems and test the ability of marine phage capsids to bind iron.

With average dissolved iron concentrations for open ocean surface waters of 0.01–0.2 nM (Johnson et al., 1997; Mawji et al., 2015) and the colloidal fraction accounting for 10–25% of the total dissolved iron at the surface (Nishioka et al., 2001; Bergquist et al., 2007; Fitzsimmons and Boyle, 2014), the proportion of iron bound to the tail fibers of phages in 1 ml of seawater could thus account for ~5.6–70% of the colloidal fraction of dissolved iron, depending on the proportion of tailed phages. When considering that siderophore-bound iron concentrations in the Atlantic Ocean may comprise 0.2–4.6% (likely an underestimate) of the soluble fraction of dissolved iron (Mawji et al., 2008), phages potentially constitute a similarly substantial proportion of ligand-bound iron within the colloidal fraction.

Phage Utilization of Outer Membrane Siderophore-Bound Iron Receptors

In 1943, Luria and Delbrück launched the field of bacterial genetics with their seminal work identifying mutants of *E. coli* strain B that were resistant to infection by a specific phage (Luria and Delbrück, 1943). Although not named in the original study, the phage used was T1 and one of the resistant mutants was designated *tonA*. It wasn't until 1973 that researchers were able to ascribe the phage resistance to a single monomeric protein, TonA (named for *T one* resistance), which was also shown to bind phage T5 and colicin M (Braun et al., 1973). The exciting discovery in 1975 that TonA was capable of transporting iron bound to the siderophore ferrichrome (Hantke and Braun, 1975; Luckey et al., 1975) later prompted a change in the protein's name from TonA to FhuA (named for ferric hydroxamate uptake; Kadner et al., 1980). It is now known that the outer membrane protein FhuA functions as a receptor for numerous phages (T1, T5, Φ 80, UC-1, H8; Lundrigan et al., 1983; Poon and Dhillon, 1987; Rabsch et al., 2007; Braun, 2009; Silva et al., 2016), as well as in the transport of ferrichrome, the peptide toxins colicin M, and microcin 25 (Braun et al., 1976), and the antibiotics albomycin and rifamycin CGP 4832 (which contain ferrichrome attached to an antimicrobial agent; Braun et al., 2001). Finally, the

broad host range phage H8 achieves infection via adsorption to a different siderophore-bound iron receptor, the outer membrane porin protein FepA, suggesting that utilizing TonB-dependent siderophore-bound iron receptors (including FhuA and FepA) is a highly effective infection strategy (Rabsch et al., 2007).

Iron is so critical for growth that bacteria must rely upon specialized systems for the uptake of siderophore-bound iron, even though these strategies render them vulnerable to phage infection (Neilands, 1979). This places bacterial host cells in a precarious position because mutations in critical regions of these surface-exposed receptors that could provide resistance against phage infection may compromise their ability to acquire the iron they need for growth (Rabsch et al., 2007), thus providing an advantage to phages in the ongoing phage-host evolutionary arms race (Van Valen, 1973; Stern and Sorek, 2011; Samson et al., 2013). Additionally, the dual function of these cell surface receptors in siderophore-bound iron uptake and phage infection creates competition for receptor binding. In early *in vitro* studies, several phages (T5, T1, Φ 80, UC-1) were shown to compete with ferrichrome for the FhuA receptor on the outer membrane of *E. coli* (Luckey et al., 1975; Wayne and Neilands, 1975; Hantke and Braun, 1978; Lundrigan et al., 1983; Bonhivers et al., 1996). Likewise, addition of iron bound to the siderophore enterobactin inhibits the binding of phage H8 to its receptor FepA (Rabsch et al., 2007).

Iron Incorporated into Phage Particles Prior to Host Lysis

Marine heterotrophic bacteria, which are highly abundant and contain significantly more iron per unit biomass than eukaryotic phytoplankton, have been estimated to account for up to half of the total iron in the marine environment (Tortell et al., 1996, 1999). While grazing of bacteria transfers cellular contents to higher trophic levels, phage infection plays an important role in regeneration of carbon, nutrients, and other elements through the viral shunt (Fuhrman, 1999; Wilhelm and Suttle, 1999). A growing body of literature has documented the critical roles of viral activity on iron cycling and bioavailability in the surface oceans (Gobler et al., 1997; Poorvin et al., 2004; Mioni et al., 2005). Experimental studies have demonstrated that organic iron-ligand complexes generated through phage lysis of infected bacterial cells are highly bioavailable and rapidly assimilated by heterotrophic bacteria (Poorvin et al., 2004; Mioni et al., 2005). In high nutrient, low chlorophyll (HNLC) systems, iron regeneration via phage lysis is critical for recycling organically complexed iron and speculated to regenerate enough dissolved iron to support some phytoplankton growth (Poorvin et al., 2004).

Although the source of the iron in phage tails has not yet been experimentally determined in any system, the fact that phage progeny fully assemble within the host cell prior to lysis, combined with the much higher iron concentrations inside bacterial cells compared to seawater, suggests that iron reserves in bacterial cells are the most likely source of the iron in phage tails (King, 1968; Tortell et al., 1999; Chuprov-Netochin et al., 2010; Rohwer et al., 2014). The incorporation of iron into phage tails

assembled within the bacterial cell has significant implications for understanding the biogeochemistry of dissolved organic matter and trace metals released as a result of bacterial host cell lysis. An average marine heterotrophic bacterial cell has an iron quota of 7.5 $\mu\text{mol Fe per mol C}$ (Tortell et al., 1996, 1999). Using an estimate of 20 fg C per cell (Ducklow, 2000), this translates to 7518 iron ions per heterotrophic bacterial cell. If marine phages contain similar amounts of iron in their tails as phage T4 (42 iron ions/phage; Bartual et al., 2010), and assuming an average burst size (number of progeny phages released through a lysis event) of 25 phages per infection (Wommack and Colwell, 2000; Parada et al., 2006), then $\sim 14\%$ of the bacterial iron previously assumed to be released into the water column as dissolved iron for remineralization would already be incorporated into new phage particles. The magnitude of this impact could vary widely as the calculations required several assumptions, including the iron quota of marine bacterial cells, which has been reported to range between 6.05 and 112 $\mu\text{mol Fe per mol C}$, depending on bioavailable iron concentrations (Brand, 1991; Tortell et al., 1996, 1999; Maldonado and Price, 1999; Boyd et al., 2010; Shire and Kustka, 2015), and the average burst size, which ranges from 10 to 500 for marine viruses (Wommack and Colwell, 2000; Parada et al., 2006). Nevertheless, if phage-bound iron originates from cellular iron reserves, this form of recycling and subsequent depletion of the iron available for remineralization upon lysis will be important to consider in modeling ocean biogeochemistry.

IMPLICATIONS AND FUTURE WORK

Here we have detailed several lines of evidence supporting the Ferrojan Horse Hypothesis. The three facets of this hypothesis are: (1) Phages constitute important iron-binding ligands in the marine environment, where they can account for a substantial portion of the colloidal fraction of organically complexed dissolved iron; (2) Marine phages compete with siderophore-bound iron for uptake receptors on the bacterial cell surface, effectively acting as a Trojan horse where the apparent gift of iron leads to cell lysis; (3) The iron incorporated into marine phage tails originates from bacterial cellular iron reserves, which reduces the amount of iron available for remineralization upon lysis. All the calculations described in this manuscript are based on knowledge from the structure of *E. coli* phage T4 as a model system (Bartual et al., 2010) and combined with average published values for viral abundance and dissolved iron concentrations within the surface oceans; therefore, a great deal of work still needs to be performed to validate this hypothesis and quantify its impact on ocean biogeochemistry and phage-host interactions. In addition, it is still unknown how strongly phages bind iron, or how this binding strength compares to known organic ligands such as siderophores within the marine environment. Yet if marine phages incorporate iron into their tail fibers as a mechanism to gain access to bacterial hosts through receptors developed for iron acquisition and uptake, as seen in the model system of *E. coli* and T4, this infection strategy could answer fundamental questions regarding marine

phage-host specificity and infection dynamics in the marine environment.

Notably, the competition for iron is not unique to the marine environment and the topics discussed here have broad implications for many ecosystems. For example, biomedical studies have demonstrated the importance of iron regulation within the human blood stream, with both pathogens and the human immune system manipulating iron as a tool for survival (Barasch and Mori, 2004; Drakesmith and Prentice, 2012; Barber and Elde, 2014). Analogous to the manner in which phages exploit bacterial siderophore-bound iron receptors, several mammalian viruses also utilize the cell-surface transferrin receptor for gaining entry to mammalian cells (Demogines et al., 2013). Additionally, although the mechanisms are largely unknown, recent phage therapy studies have demonstrated that the addition of iron-doped apatite nanoparticles to phages in solution enhances phage infection, resulting in an increase in the number of plaques forming on bacterial lawns by up to 128% (Andriolo et al., 2014). Given similarities in ionic strength and pH between seawater (Byrne and Breland, 1989) and blood (May et al., 1977), insights gained from human systems can aid in our understanding of the interactions between iron, bacteria, and viruses within the marine environment and vice versa.

Finally, although the Ferrojan Horse Hypothesis focuses on iron, the same concepts may be applicable to other essential nutrients found within the protein structure of phages, including metals like zinc and macronutrients like phosphorus. Zinc was found to be bound by histidines to one of the short tail fibers (gp12) of *E. coli* phage T4 in a manner similar to the iron ions in the T4 long tail fibers (Thomassen et al., 2003; Bartual et al., 2010). In addition, recent work by Jover et al. (2014) has estimated that viral particles can account for 0.01–24 nM of dissolved organic phosphorus in the oceans. Phages have a skewed C:N:P of ~20:7:1 (Jover et al., 2014), which is highly enriched in phosphorous and

nitrogen compared to the Redfield ratio of cellular life in the oceans, 106:16:1 (Redfield, 1958). This stoichiometric mismatch suggests that the chemical composition of phages should be further investigated to determine elements for which they can make disproportionately large contributions to marine chemistry.

Future research will test the Ferrojan Horse Hypothesis by documenting the ability of phages to act as iron-binding ligands within the oceans and exploring the role of iron exploitation in governing phage-host interactions. In the meantime, however, the linkages made in this manuscript clearly demonstrate the importance of considering the potential contributions of phages, as well as other biological entities, to the concentrations and biogeochemical cycling of dissolved trace metals and macronutrients in the ocean.

AUTHOR CONTRIBUTIONS

MB and KNB jointly conceived this hypothesis. CB took the lead in assembling evidence, compiling manuscript content, and creating graphics. All three authors contributed equally to writing the manuscript text and approved the manuscript for publication.

ACKNOWLEDGMENTS

The authors thank Dr. Leon Hardy at the University of South Florida Saint Petersburg for help visualizing the structure of phage T4 gp37 presented in **Figure 1** and Dr. Robert A. Edwards at San Diego State University for bioinformatics support. This work was supported by National Science Foundation grants from the Division of Integrative Organismal Systems (IOS-1456301) to MB and from the Division of Ocean Sciences (Chemical Oceanography, OCE-1446327) to KNB, as well as a donation from George H. Lorton. We thank three reviewers for their helpful contributions that improved this manuscript.

REFERENCES

- Aguilar-Islas, A. M., Wu, J., Rember, R., Johansen, A. M., and Shank, L. M. (2010). Dissolution of aerosol-derived iron in seawater: leach solution chemistry, aerosol type, and colloidal iron fraction. *Mar. Chem.* 120, 25–33. doi: 10.1016/j.marchem.2009.01.011
- Andriolo, J. M., Hensleigh, R. M., McConnell, C. A., Pedulla, M., Hailer, K., Kasinath, R., et al. (2014). Iron-doped apatite nanoparticles for improvement of phage therapy. *J. Vac. Sci. Technol. B* 32:06FD01. doi: 10.1116/1.4894460
- Barasch, J., and Mori, K. (2004). Cell biology - iron thievery. *Nature* 432, 811–813. doi: 10.1038/432811a
- Barber, M. F., and Elde, N. C. (2014). Escape from bacterial iron piracy through rapid evolution of transferrin. *Science* 346, 1362–1366. doi: 10.1126/science.1259329
- Bartual, S. G., Otero, J. M., Garcia-Doval, C., Llamas-Saiz, A. L., Kahn, R., Fox, G. C., et al. (2010). Structure of the bacteriophage T4 long tail fiber receptor-binding tip. *Proc. Natl. Acad. Sci. U.S.A.* 107, 20287–20292. doi: 10.1073/pnas.1011218107
- Bergquist, B. A., Wu, J., and Boyle, E. A. (2007). Variability in oceanic dissolved iron is dominated by the colloidal fraction. *Geochim. Cosmochim. Acta* 71, 2960–2974. doi: 10.1016/j.gca.2007.03.013
- Billler, D. V., and Bruland, K. W. (2012). Analysis of Mn, Fe, Co, Ni, Cu, Zn, Cd, and Pb in seawater using the Nobias-chelate PA1 resin and magnetic sector inductively coupled plasma mass spectrometry (ICP-MS). *Mar. Chem.* 130, 12–20. doi: 10.1016/j.marchem.2011.12.001
- Bonhivers, M., Ghazi, A., Boulanger, P., and Letellier, L. (1996). FhuA, a transporter of the *Escherichia coli* outer membrane, is converted into a channel upon binding of bacteriophage T5. *EMBO J.* 15, 1850–1856.
- Boyd, P. W., and Ellwood, M. J. (2010). The biogeochemical cycle of iron in the ocean. *Nat. Geosci.* 3, 675–682. doi: 10.1038/ngeo964
- Boyd, P. W., Ibsanmi, E., Sander, S. G., Hunter, K. A., and Jackson, G. A. (2010). Remineralization of upper ocean particles: implications for iron biogeochemistry. *Limnol. Oceanogr.* 55, 1271–1288. doi: 10.4319/lo.2010.55.3.1271
- Brand, L. E. (1991). Minimum iron requirements of marine-phytoplankton and the implications for the biogeochemical control of new production. *Limnol. Oceanogr.* 36, 1756–1771.
- Braun, V. (2009). FhuA (TonA), the career of a protein. *J. Bacteriol.* 191, 3431–3436. doi: 10.1128/JB.00106-09
- Braun, V., Bos, C., Braun, M., and Killmann, H. (2001). Outer membrane channels and active transporters for the uptake of antibiotics. *J. Infect. Dis.* 183, S12–S16. doi: 10.1086/318840
- Braun, V., and Endriss, F. (2007). Energy-coupled outer membrane transport proteins and regulatory proteins. *Biomol. Eng.* 20, 219–231. doi: 10.1007/s10534-006-9072-5

- Braun, V., Hancock, R. E. W., Hantke, K., and Hartmann, A. (1976). Functional organization of outer membrane of *Escherichia coli* - phage and colicin receptors as components of iron uptake systems. *J. Supramol. Struct.* 5, 37–58. doi: 10.1002/jss.400050105
- Braun, V., Schaller, K., and Wolff, H. (1973). Common receptor protein for phage T5 and colicin M in outer membrane of *Escherichia coli* B. *Biochim. Biophys. Acta* 323, 87–97. doi: 10.1016/0005-2736(73)90433-1
- Breitbart, M. (2012). Marine viruses: truth or dare. *Annu. Rev. Mar. Sci.* 4, 425–448. doi: 10.1146/annurev-marine-120709-142805
- Breitbart, M., Thompson, L. R., Suttle, C. A., and Sullivan, M. B. (2007). Exploring the vast diversity of marine viruses. *Oceanography* 20, 135–139. doi: 10.5670/oceanog.2007.58
- Browning, C., Shneider, M. M., Bowman, V. D., Schwarzer, D., and Leiman, P. G. (2012). Phage pierces the host cell membrane with the iron-loaded spike. *Structure* 20, 326–339. doi: 10.1016/j.str.2011.12.009
- Bruland, K. W., Donat, J. R., and Hutchins, D. A. (1991). Interactive influences of bioactive trace-metals on biological production in oceanic waters. *Limnol. Oceanogr.* 36, 1555–1577. doi: 10.4319/lo.1991.36.8.1555
- Brum, J. R., Schenck, R. O., and Sullivan, M. B. (2013). Global morphological analysis of marine viruses shows minimal regional variation and dominance of non-tailed viruses. *ISME J.* 7, 1738–1751. doi: 10.1038/ismej.2013.67
- Buck, K. N., Sohst, B., and Sedwick, P. N. (2015). The organic complexation of dissolved iron along the US GEOTRACES (GA03) North Atlantic Section. *Deep-Sea Res. Part II-Top. Stud. Oceanogr.* 116, 152–165. doi: 10.1016/j.dsr2.2014.11.016
- Butler, A. (2005). Marine siderophores and microbial iron mobilization. *Biometals* 18, 369–374. doi: 10.1007/s10534-005-3711-0
- Byrne, R. H., and Breland, J. A. (1989). High-precision multiwavelength pH determinations in seawater using cresol red. *Deep-Sea Res. Part A-Oceanogr. Res. Pap.* 36, 803–810. doi: 10.1016/0198-0149(89)90152-0
- Chuprov-Netochin, R. N., Faizullina, N. M., Sykilinda, N. N., Simakova, M. N., Mesyanzhinov, V. V., and Miroshnikov, K. A. (2010). The beta-helical domain of bacteriophage T4 controls the folding of the fragment of long tail fibers in a chimeric protein. *Russ. J. Bioorganic Chem.* 36, 172–178. doi: 10.1134/S1068162010020056
- Cornelis, P. (2010). Iron uptake and metabolism in pseudomonads. *Appl. Microbiol. Biotechnol.* 86, 1637–1645. doi: 10.1007/s00253-010-2550-2
- Cullen, J. T., Bergquist, B. A., and Moffett, J. W. (2006). Thermodynamic characterization of the partitioning of iron between soluble and colloidal species in the Atlantic Ocean. *Mar. Chem.* 98, 295–303. doi: 10.1016/j.marchem.2005.10.007
- Daughney, C. J., Chatellier, X., Chan, A., Kenward, P., Fortin, D., Suttle, C. A., et al. (2004). Adsorption and precipitation of iron from seawater on a marine bacteriophage (PWH3A-P1). *Mar. Chem.* 91, 101–115. doi: 10.1016/j.marchem.2004.06.003
- Demogines, A., Abraham, J., Choe, H., Farzan, M., and Sawyer, S. L. (2013). Dual host-virus arms races shape an essential housekeeping protein. *PLoS Biol.* 11:e1001571. doi: 10.1371/journal.pbio.1001571
- Drakesmith, H., and Prentice, A. M. (2012). Hepcidin and the iron-infection axis. *Science* 338, 768–772. doi: 10.1126/science.1224577
- Ducklow, H. (2000). “Bacterial production and biomass in the oceans,” in *Microbial Ecology of the Oceans*, ed D. L. Kirchman (New York, NY: Wiley-Liss Inc.), 85–120.
- Emerson, D. (2016). The irony of iron - biogenic iron oxides as an iron source to the ocean. *Front. Microbiol.* 6:1502. doi: 10.3389/fmicb.2015.01502
- Finn, R. D., Bateman, A., Clements, J., Coggill, P., Eberhardt, R. Y., Eddy, S. R., et al. (2014). Pfam: the protein families database. *Nucleic Acids Res.* 42, D222–D230. doi: 10.1093/nar/gkt1223
- Fishwick, M. P., Sedwick, P. N., Lohan, M. C., Worsfold, P. J., Buck, K. N., Church, T. M., et al. (2014). The impact of changing surface ocean conditions on the dissolution of aerosol iron. *Global Biogeochem. Cycles* 28, 1235–1250. doi: 10.1002/2014GB004921
- Fitzsimmons, J. N., and Boyle, E. A. (2014). Both soluble and colloidal iron phases control dissolved iron variability in the tropical North Atlantic Ocean. *Geochim. Cosmochim. Acta* 125, 539–550. doi: 10.1016/j.gca.2013.10.032
- Fitzsimmons, J. N., Bundy, R. M., Al-Subiai, S. N., Barbeau, K. A., and Boyle, E. A. (2015). The composition of dissolved iron in the dusty surface ocean: an exploration using size-fractionated iron-binding ligands. *Mar. Chem.* 173, 125–135. doi: 10.1016/j.marchem.2014.09.002
- Fuhrman, J. (1999). Marine viruses: biogeochemical and ecological effects. *Nature* 399, 541–548. doi: 10.1038/21119
- Gauglitz, J. M., Inishi, A., Ito, Y., and Butler, A. (2014). Microbial tailoring of acyl peptidic siderophores. *Biochemistry* 53, 2624–2631. doi: 10.1021/bi500266x
- Gerringa, L. J. A., Rijkenberg, M. J. A., Schoemann, V., Laan, P., and de Baar, H. J. W. (2015). Organic complexation of iron in the West Atlantic Ocean. *Mar. Chem.* 177, 434–446. doi: 10.1016/j.marchem.2015.04.007
- Gledhill, M., and Buck, K. N. (2012). The organic complexation of iron in the marine environment: a review. *Front. Microbiol.* 3:69. doi: 10.3389/fmicb.2012.00069
- Gledhill, M., and van den Berg, C. M. G. (1994). Determination of complexation of iron (III) with natural organic complexing ligands in seawater using cathodic stripping voltammetry. *Mar. Chem.* 47, 41–54. doi: 10.1016/0304-4203(94)90012-4
- Gobler, C. J., Hutchins, D. A., Fisher, N. S., Cosper, E. M., and Sañudo-Wilhelmy, S. A. (1997). Release and bioavailability of C, N, P, Se, and Fe following viral lysis of a marine chrysophyte. *Limnol. Oceanogr.* 42, 1492–1504. doi: 10.4319/lo.1997.42.7.1492
- Gordon, R. M., Martin, J. H., and Knauer, G. A. (1982). Iron in Northeast Pacific waters. *Nature* 299, 611–612. doi: 10.1038/299611a0
- Hantke, K., and Braun, V. (1975). Membrane receptor dependent iron transport in *Escherichia coli*. *FEBS Lett.* 49, 301–305. doi: 10.1016/0014-5793(75)80771-X
- Hantke, K., and Braun, V. (1978). Functional interaction of TonA-TonB receptor system in *Escherichia coli*. *J. Bacteriol.* 135, 190–197.
- Hassler, C. S., Alasonati, E., Nichols, C. A. M., and Slaveykova, V. I. (2011). Exopolysaccharides produced by bacteria isolated from the pelagic Southern Ocean - role in Fe binding, chemical reactivity, and bioavailability. *Mar. Chem.* 123, 88–98. doi: 10.1016/j.marchem.2010.10.003
- Hershey, A. D., and Chase, M. (1952). Independent functions of viral protein and nucleic acid in growth of bacteriophage. *J. Gen. Physiol.* 36, 39–56. doi: 10.1085/jgp.36.1.39
- Hider, R. C., and Kong, X. (2010). Chemistry and biology of siderophores. *Nat. Prod. Rep.* 27, 637–657. doi: 10.1039/b906679a
- Humphrey, W., Dalke, A., and Schulten, K. (1996). VMD: visual molecular dynamics. *J. Mol. Graphics* 14, 33–38. doi: 10.1016/0263-7855(96)00018-5
- Hunter, K. A., and Boyd, P. W. (2007). Iron-binding ligands and their role in the ocean biogeochemistry of iron. *Environ. Chem.* 4, 221–232. doi: 10.1071/EN07012
- Johnson, K. S., Gordon, R. M., and Coale, K. H. (1997). What controls dissolved iron concentrations in the world ocean? *Mar. Chem.* 57, 137–161.
- Jover, L. F., Effler, T. C., Buchan, A., Wilhelm, S. W., and Weitz, J. S. (2014). The elemental composition of virus particles: implications for marine biogeochemical cycles. *Nat. Rev. Microbiol.* 12, 519–528. doi: 10.1038/nrmicro3289
- Kadner, R. J., Heller, K., Coulton, J. W., and Braun, V. (1980). Genetic control of hydroxamate-mediated iron uptake in *Escherichia coli*. *J. Bacteriol.* 143, 256–264.
- King, J. (1968). Assembly of tail of bacteriophage T4. *J. Mol. Biol.* 32, 231–262. doi: 10.1016/0022-2836(68)90007-7
- Kuma, K., Nishioka, J., and Matsunaga, K. (1996). Controls on iron(III) hydroxide solubility in seawater: the influence of pH and natural organic chelators. *Limnol. Oceanogr.* 41, 396–407. doi: 10.4319/lo.1996.41.3.0396
- Laglera, L. M., Battaglia, G., and van den Berg, C. M. G. (2007). Determination of humic substances in natural waters by cathodic stripping voltammetry of their complexes with iron. *Anal. Chim. Acta* 599, 58–66. doi: 10.1016/j.aca.2007.07.059
- Laglera, L. M., Battaglia, G., and van den Berg, C. M. G. (2011). Effect of humic substances on the iron speciation in natural waters by CLE/CSV. *Mar. Chem.* 127, 134–143. doi: 10.1016/j.marchem.2011.09.003
- Laglera, L. M., and van den Berg, C. M. G. (2009). Evidence for geochemical control of iron by humic substances in seawater. *Limnol. Oceanogr.* 54, 610–619. doi: 10.4319/lo.2009.54.2.0610

- Leiman, P. G., Arisaka, F., van Raaij, M. J., Kostyuchenko, V. A., Aksyuk, A. A., Kanamaru, S., et al. (2010). Morphogenesis of the T4 tail and tail fibers. *Viol. J.* 7, 1–28. doi: 10.1186/1743-422X-7-355
- Leiman, P. G., and Shneider, M. M. (2012). Contractile tail machines of bacteriophages. *Viral Mol. Mach.* 726, 93–114. doi: 10.1007/978-1-4614-0980-9_5
- Luckey, M., Wayne, R., and Neilands, J. B. (1975). *In vitro* competition between ferrichrome and phage for outer membrane T5 receptor complex of *Escherichia coli*. *Biochem. Biophys. Res. Commun.* 64, 687–693. doi: 10.1016/0006-291X(75)90375-7
- Lundrigan, M. D., Lancaster, J. H., and Earhart, C. F. (1983). UC-1, a new bacteriophage that uses the TonA polypeptide as its receptor. *J. Virol.* 45, 700–707.
- Luria, S. E., and Delbruck, M. (1943). Mutations of bacteria from virus sensitivity to virus resistance. *Genetics* 28, 491–511.
- Maldonado, M. T., and Price, N. M. (1999). Utilization of iron bound to strong organic ligands by plankton communities in the subarctic Pacific Ocean. *Deep-Sea Res. Part II-Top. Stud. Oceanogr.* 46, 2447–2473. doi: 10.1016/S0967-0645(99)00071-5
- Mancuso Nichols, C. A., Garon, S., Bowman, J. P., Raguene, G., and Guezennec, J. (2004). Production of exopolysaccharides by Antarctic marine bacterial isolates. *J. Appl. Microbiol.* 96, 1057–1066. doi: 10.1111/j.1365-2672.2004.02216.x
- Martin, J. H., Gordon, R. M., Fitzwater, S., and Broenkow, W. W. (1989). VERTEX - Phytoplankton iron studies in the Gulf of Alaska. *Deep-Sea Res. Part A-Oceanogr. Res. Pap.* 36, 649–680. doi: 10.1016/0198-0149(89)90144-1
- Martinez, J. S., Carter-Franklin, J. N., Mann, E. L., Martin, J. D., Haygood, M. G., and Butler, A. (2003). Structure and membrane affinity of a suite of amphiphilic siderophores produced by a marine bacterium. *Proc. Natl. Acad. Sci. U.S.A.* 100, 3754–3759. doi: 10.1073/pnas.0637444100
- Matzanke, B. F., Bohnke, R., Mollmann, U., Reissbrodt, R., Schunemann, V., and Trautwein, A. X. (1997). Iron uptake and intracellular metal transfer in mycobacteria mediated by xenosiderophores. *Biomaterials* 10, 193–203. doi: 10.1023/A:1018351728081
- Mawji, E., Gledhill, M., Milton, J. A., Tarran, G. A., Ussher, S., Thompson, A., et al. (2008). Hydroxamate siderophores: occurrence and importance in the Atlantic Ocean. *Environ. Sci. Technol.* 42, 8675–8680. doi: 10.1021/es801884r
- Mawji, E., Schlitzer, R., Dodas, E. M., Abadie, C., Abouchami, W., Anderson, R. F., et al. (2015). The GEOTRACES intermediate data product 2014. *Mar. Chem.* 177, 1–8. doi: 10.1016/j.marchem.2015.04.005
- May, P. M., Linder, P. W., and Williams, D. R. (1977). Computer simulation of metal-ion equilibria in biofluids: models for the low-molecular-weight complex distribution of calcium(II), magnesium(II), manganese(II), iron(III), copper(II), zinc(II), and lead(II) ions in human blood plasma. *J. Chem. Soc. Dalton Trans.* 6, 588–595. doi: 10.1039/dt9770000588
- Mioni, C. E., Poorvin, L., and Wilhelm, S. W. (2005). Virus and siderophore-mediated transfer of available Fe between heterotrophic bacteria: characterization using an Fe-specific bioreporter. *Aquat. Microb. Ecol.* 41, 233–245. doi: 10.3354/ame041233
- Morel, F. M. M., and Price, N. M. (2003). The biogeochemical cycles of trace metals in the oceans. *Science* 300, 944–947. doi: 10.1126/science.1083545
- Neilands, J. B. (1957). Some aspects of microbial metabolism. *Bacteriol. Rev.* 21, 101–111.
- Neilands, J. B. (1979). Ionic function of bacteriophage receptors. *Trends Biochem. Sci.* 4, 115–118. doi: 10.1016/0968-0004(79)90396-7
- Nishioka, J., Takeda, S., Wong, C. S., and Johnson, W. K. (2001). Size-fractionated iron concentrations in the northeast Pacific Ocean: distribution of soluble and small colloidal iron. *Mar. Chem.* 74, 157–179. doi: 10.1016/S0304-4203(01)00013-5
- Parada, V., Herndl, G. J., and Weinbauer, M. G. (2006). Viral burst size of heterotrophic prokaryotes in aquatic systems. *J. Mar. Biol. Assoc. U.K.* 86, 613–621. doi: 10.1017/S002531540601352X
- Parsons, R. J., Breitbart, M., Lomas, M. W., and Carlson, C. A. (2012). Ocean time-series reveals recurring seasonal patterns of viroplankton dynamics in the northwestern Sargasso Sea. *ISME J.* 6, 273–284. doi: 10.1038/ismej.2011.101
- Pawelek, P. D., Croteau, N., Ng-Thow-Hing, C., Khursigara, C. M., Moiseeva, N., Allaire, M., et al. (2006). Structure of TonB in complex with PhuA, *E. coli* outer membrane receptor. *Science* 312, 1399–1402. doi: 10.1126/science.1128057
- Petersen, E. F., Goddard, T. D., Huang, C. C., Couch, G. S., Greenblatt, D. M., Meng, E. C., et al. (2004). UCSF chimera—a visualization system for exploratory research and analysis. *J. Comput. Chem.* 25, 1605–1612. doi: 10.1002/jcc.20084
- Poon, A. P. W., and Dhillon, T. S. (1987). The attachment sites of T5-host range temperate coliphages. *Virology* 158, 431–434. doi: 10.1016/0042-6822(87)90215-7
- Poorvin, L., Rinta-Kanto, J., Hutchins, D., and Wilhelm, S. (2004). Viral release of iron and its bioavailability to marine plankton. *Limnol. Oceanogr.* 49, 1734–1741. doi: 10.4319/lo.2004.49.5.1734
- Rabsch, W., Ma, L., Wiley, G., Najar, F. Z., Kaserer, W., Schuerch, D. W., et al. (2007). FepA- and TonB-dependent bacteriophage H8: receptor binding and genomic sequence. *J. Bacteriol.* 189, 5658–5674. doi: 10.1128/JB.00437-07
- Raven, J. A., Evans, M. C. W., and Korb, R. E. (1999). The role of trace metals in photosynthetic electron transport in O₂-evolving organisms. *Photosyn. Res.* 60, 111–149. doi: 10.1023/A:1006282714942
- Redfield, A. C. (1958). The biological control of chemical factors in the environment. *Am. Sci.* 46, 205–221.
- Rohwer, F., Segall, A., Steward, G., Seguritan, V., Breitbart, M., Wolven, F., et al. (2000). The complete genomic sequence of the marine phage Roseophage SIO1 shares homology with nonmarine phages. *Limnol. Oceanogr.* 45, 408–418. doi: 10.4319/lo.2000.45.2.0408
- Rohwer, F., and Segall, A. M. (2015). In retrospect: a century of phage lessons. *Nature* 528, 46–48. doi: 10.1038/528046a
- Rohwer, F., and Thurber, R. V. (2009). Viruses manipulate the marine environment. *Nature* 459, 207–212. doi: 10.1038/nature08060
- Rohwer, F., Youle, M., Maughan, H., and Hisakawa, N. (2014). *Life in Our Phage World: A Centennial Field Guide to the Earth's Most Diverse Inhabitants*. San Diego, CA: Wholon.
- Rue, E., and Bruland, K. (2001). Domoic acid binds iron and copper: a possible role for the toxin produced by the marine diatom *Pseudo-nitzschia*. *Mar. Chem.* 76, 127–134. doi: 10.1016/S0304-4203(01)00053-6
- Rue, E. L., and Bruland, K. W. (1995). Complexation of iron(III) by natural organic-ligands in the central north Pacific as determined by a new competitive ligand equilibration adsorptive cathodic stripping voltammetric method. *Mar. Chem.* 50, 117–138. doi: 10.1016/0304-4203(95)00031-L
- Rue, E. L., and Bruland, K. W. (1997). The role of organic complexation on ambient iron chemistry in the equatorial Pacific Ocean and the response of a mesoscale iron addition experiment. *Limnol. Oceanogr.* 42, 901–910. doi: 10.4319/lo.1997.42.5.0901
- Salmond, G. P. C., and Fineran, P. C. (2015). A century of the phage: past, present and future. *Nat. Rev. Microbiol.* 13, 777–786. doi: 10.1038/nrmicro3564
- Samson, J. E., Magadan, A. H., Sabri, M., and Moineau, S. (2013). Revenge of the phages: defeating bacterial defences. *Nat. Rev. Microbiol.* 11, 675–687. doi: 10.1038/nrmicro3096
- Sandy, M., and Butler, A. (2009). Microbial iron acquisition: marine and terrestrial siderophores. *Chem. Rev.* 109, 4580–4595. doi: 10.1021/cr9002787
- Shaked, Y., and Lis, H. (2012). Disassembling iron availability to phytoplankton. *Front. Microbiol.* 3:123. doi: 10.3389/fmicb.2012.00123
- Shire, D. M., and Kustka, A. B. (2015). Luxury uptake, iron storage and ferritin abundance in *Prochlorococcus marinus* (Synecococcales) strain MED4. *Phycologia* 54, 398–406. doi: 10.2216/14-109.1
- Silva, J. B., Storms, Z., and Sauvageau, D. (2016). Host receptors for bacteriophage adsorption. *FEMS Microbiol. Lett.* 363:fnw002. doi: 10.1093/femsle/fnw002
- Stern, A., and Sorek, R. (2011). The phage-host arms race: shaping the evolution of microbes. *Bioessays* 33, 43–51. doi: 10.1002/bies.201000071
- Stolpe, B., and Hasselov, M. (2010). Nanofibrils and other colloidal biopolymers binding trace elements in coastal seawater: significance for variations in element size distributions. *Limnol. Oceanogr.* 55, 187–202. doi: 10.4319/lo.2010.55.1.0187
- Sullivan, M. B., Coleman, M. L., Weigle, P., Rohwer, F., and Chisholm, S. W. (2005). Three *Prochlorococcus* cyanophage genomes: signature features and ecological interpretations. *PLoS Biol.* 3:e144. doi: 10.1371/journal.pbio.0030144
- Suttle, C. A. (2007). Marine viruses - major players in the global ecosystem. *Nat. Rev. Microbiol.* 5, 801–812. doi: 10.1038/nrmicro1750
- Tam, W., Pell, L. G., Bona, D., Tsai, A., Dai, X. X., Edwards, A. M., et al. (2013). Tail tip proteins related to bacteriophage lambda gpL coordinate an iron-sulfur cluster. *J. Mol. Biol.* 425, 2450–2462. doi: 10.1016/j.jmb.2013.03.032

- Thomassen, E., Gielen, G., Schutz, M., Schoehn, G., Abrahams, J. P., Miller, S., et al. (2003). The structure of the receptor-binding domain of the bacteriophage T4 short tail fibre reveals a knitted trimeric metal-binding fold. *J. Mol. Biol.* 331, 361–373. doi: 10.1016/S0022-2836(03)00755-1
- Thuroczy, C. E., Gerringa, L. J. A., Klunder, M. B., Middag, R., Laan, P., Timmermans, K. R., et al. (2010). Speciation of Fe in the Eastern North Atlantic Ocean. *Deep-Sea Res. Part I-Oceanogr. Res. Pap.* 57, 1444–1453. doi: 10.1016/j.dsr.2010.08.004
- Tortell, P. D., Maldonado, M. T., Granger, J., and Price, N. M. (1999). Marine bacteria and biogeochemical cycling of iron in the oceans. *FEMS Microbiol. Ecol.* 29, 1–11. doi: 10.1111/j.1574-6941.1999.tb00593.x
- Tortell, P. D., Maldonado, M. T., and Price, N. M. (1996). The role of heterotrophic bacteria in iron-limited ocean ecosystems. *Nature* 383, 330–332. doi: 10.1038/383330a0
- Twining, B. S., and Baines, S. B. (2013). The trace metal composition of marine phytoplankton. *Annu. Rev. Mar. Sci.* 5, 191–215. doi: 10.1146/annurev-marine-121211-172322
- van den Berg, C. M. G. (2005). Organic iron complexation is real, the theory is used incorrectly. *Comment on 'Measuring marine iron(III) complexes by CLE-AdSV'.* *Environ. Chem.* 2, 88–89. doi: 10.1071/EN05029
- Van Valen, L. (1973). A new evolutionary law. *Evol. Theor.* 1, 1–30.
- von der Heyden, B. P., Hauser, E. J., Mishra, B., Martinez, G. A., Bowie, A. R., Tylizszczak, T., et al. (2014). Ubiquitous presence of Fe(II) in aquatic colloids and its association with organic carbon. *Environ. Sci. Technol. Lett.* 1, 387–392. doi: 10.1021/ez500164v
- Vraspir, J. M., and Butler, A. (2009). Chemistry of marine ligands and siderophores. *Annu. Rev. Mar. Sci.* 1, 43–63. doi: 10.1146/annurev.marine.010908.163712
- Wayne, R., and Neilands, J. B. (1975). Evidence for common binding-sites for ferrichrome compounds and bacteriophage Phi-80 in cell-envelope of *Escherichia coli*. *J. Bacteriol.* 121, 497–503.
- Wheeler, T. J., Clements, J., and Finn, R. D. (2014). Skyline. *BMC Bioinform.* 15:7. doi: 10.1186/1471-2105-15-7
- Wilhelm, S. W., and Suttle, C. A. (1999). Viruses and nutrient cycles in the sea. *Bioscience* 49, 781–783. doi: 10.2307/1313569
- Wilhelm, S. W., Weinbauer, M. G., Suttle, C. A., and Jeffrey, W. H. (1998). The role of sunlight in the removal and repair of viruses in the sea. *Limnol. Oceanogr.* 43, 586–592. doi: 10.4319/lo.1998.43.4.0586
- Wommack, K. E., and Colwell, R. R. (2000). Virioplankton: viruses in aquatic ecosystems. *Microbiol. Mol. Biol. Rev.* 64, 69–114. doi: 10.1128/MMBR.64.1.69-114.2000
- Wommack, K. E., Nasko, D. J., Chopyk, J., and Sakowski, E. G. (2015). Counts and sequences, observations that continue to change our understanding of viruses in nature. *J. Microbiol.* 53, 181–192. doi: 10.1007/s12275-015-5068-6
- Yamashita, E., Nakagawa, A., Takahashi, J., Tsunoda, K.-I., Yamada, S., and Takeda, S. (2011). The host-binding domain of the P2 phage tail spike reveals a trimeric iron-binding structure. *Acta Crystallogr. Sect. F Struct. Biol. Cryst. Commun.* 67, 837–841. doi: 10.1107/s1744309111005999

Conflict of Interest Statement: The authors declare that the research was conducted in the absence of any commercial or financial relationships that could be construed as a potential conflict of interest.

Copyright © 2016 Bonnain, Breitbart and Buck. This is an open-access article distributed under the terms of the Creative Commons Attribution License (CC BY). The use, distribution or reproduction in other forums is permitted, provided the original author(s) or licensor are credited and that the original publication in this journal is cited, in accordance with accepted academic practice. No use, distribution or reproduction is permitted which does not comply with these terms.



Toward a Regional Classification to Provide a More Inclusive Examination of the Ocean Biogeochemistry of Iron-Binding Ligands

Christel S. Hassler^{1*}, Constant M. G. van den Berg² and Philip W. Boyd³

¹ Marine and Lake Biogeochemistry, Department F.-A. Forel, University of Geneva, Geneva, Switzerland, ² School of Environmental Sciences, University of Liverpool, Liverpool, UK, ³ Institute for Marine and Antarctic Studies, University of Tasmania, Hobart, TAS, Australia

OPEN ACCESS

Edited by:

Cecile Guieu,
Centre National de la Recherche
Scientifique, France

Reviewed by:

Arvind Singh,
Physical Research Laboratory, India
Loes Gerringa,
Royal Netherlands Institute for Sea
Research (NWO), Netherlands
Randelle M. Bundy,
Woods Hole Oceanographic
Institution, USA

*Correspondence:

Christel S. Hassler
christel.hassler@unige.ch

Specialty section:

This article was submitted to
Marine Biogeochemistry,
a section of the journal
Frontiers in Marine Science

Received: 23 September 2016

Accepted: 16 January 2017

Published: 01 February 2017

Citation:

Hassler CS, van den Berg CMG and
Boyd PW (2017) Toward a Regional
Classification to Provide a More
Inclusive Examination of the Ocean
Biogeochemistry of Iron-Binding
Ligands. *Front. Mar. Sci.* 4:19.
doi: 10.3389/fmars.2017.00019

Iron-binding ligands are paramount to understanding iron biogeochemistry and its potential to set the productivity and the magnitude of the biological pump in >30% of the ocean. However, the nature of these ligands is largely uncharacterized and little is known about their sources, sensitivity to photochemistry and biological transformation, or scavenging behavior. Despite many uncertainties, there is no doubt that ligands are produced by a wide range of biotic and abiotic processes, and that the bulk ligand pool encompasses a diverse range of molecules. Despite widespread recognition of the likelihood of a continuum of ligand classes making up the bulk ligand pool, studies to date largely focused on the dominant ligand. Thus, most studies have overlooked the need to assess where these targeted molecules fit across the spectrum of ligands that comprise the bulk ligand pool. Here we summarize present knowledge to critically assess the source(s), function(s), production pathways, and loss mechanisms of three important iron-binding organic ligand groups in order to assess their distinctive characteristics and how they link with observed ligand distributions. We considered that ligands are contained in broad groupings of exopolymer substances (EPS), humic substances (HS), and siderophores; using literature data for speciation modeling suggested that this adequately described the iron speciation reported in the ocean. We hypothesize that a holistic viewpoint of the multi-faceted controls on ligands dynamics is essential to begin to understand why some ligands can be expected to dominate in particular oceanic regions, depth strata, or exhibit seasonality and/or lateral gradients. We advocate that the development of a regional classification will enhance our understanding of the changing composition of the bulk ligand pool across the global ocean and to help address to what extent seasonality influences the makeup of this pool. This classification, based on selected functional ligand classes, can act as a bridge to use future ligand datasets to fill in the gaps in the continuum.

Keywords: iron, exopolymeric substances, humics, organic ligands, oceanic distribution

INTRODUCTION

In marine systems, more than 99.9% of dissolved Fe is associated with dissolved organic complexing ligands (Rue and Bruland, 1995; van den Berg, 1995) a component of the dissolved organic carbon (DOC) pool. Fe-binding organic ligands are essential for the functioning of the oceanic Fe cycle, enhancing the solubility of iron (Kuma et al., 1998; Schlosser et al., 2012) influencing its reactivity (i.e., defined here as chemical stability and accessibility to the biota), and hence availability to support phytoplankton growth (Maldonado et al., 2005; Hassler et al., 2011b, 2012). During the last three decades, research have revealed numerous and complex interactions between Fe chemistry and biology including inextricable linkages with ligands across the entire water column (Boyd and Ellwood, 2010; Gledhill and Buck, 2012). However, as highlighted by a recent Working Group funded by the Scientific Committee for Oceanic Research (SCOR, WG139, Organic ligands—a key control on trace metal biogeochemistry in the ocean, <http://neon.otago.ac.nz/research/scor/>), the composition and origin of Fe-binding organic ligands remain mostly unknown.

The use of proxies for iron binding ligands, such as bulk DOC concentrations, is an approach that was employed initially but was unable to predict Fe solubility and its global distribution (Völker and Tagliabue, 2015). Therefore, iron biogeochemical models are developing by considering organic ligands production and loss terms to reconcile model outputs with observations (Völker and Tagliabue, 2015). The identification of which fraction of the DOC pool (encompassing its sources production pathways, solubility, molecular weight, or other chemical characteristics) most influences Fe biogeochemistry is one of the major analytical obstacles in the field of marine biogeochemistry (Benner, 2011).

The conditional stability and the distribution of iron-binding organic ligands provide a means of demarcating different groups of ligands. Since 1994 (Gledhill and van den Berg, 1994), electrochemistry has been used to measure the concentration of Fe-binding ligands (L) and their conditional stability constants ($\log K_{Fe'L}$) both of which are important to define their impact on Fe biogeochemistry (Gledhill and Buck, 2012). Recent studies on iron chemical speciation have now revealed that the vertical zonation of organic ligands—with stronger ligands (L₁-type, $\log K_{Fe'L} \geq 12$ –13) observed in surface waters, when present, and weaker (L₂- to L₄-type, $\log K_{Fe'L}$ 10–12, and probably <10) throughout the water column—proposed by Hunter and Boyd (2007), was not consistent. Indeed, in the Atlantic Ocean, L₁ are reported throughout the water column (Buck et al., 2015; Gerringa et al., 2015, **Figure 1A**).

The concentration of Fe-binding ligands tends to be greater and shows most variability in surface waters, with peaks often found co-located with the subsurface chlorophyll maximum implying both a strong relationship with biological activity (Gledhill and Buck, 2012; Gerringa et al., 2015; Bundy et al., 2016) and rapid ligand turnover comparable to that reported for labile DOC (Hansell, 2013). Ligand turnover rates may potentially be derived from variability of organic ligand concentrations in depth profiles or seasonal studies, but in most cases, there are insufficient data to constrain turnover estimates. Recently, a 1000 year residence time was estimated for organic ligands in the North Atlantic Deep Water (NADW) (Gerringa et al., 2015), suggesting that ligands at depth are different from those in surface waters. Furthermore, this relatively large residence time means they can persist longer than dissolved iron (e.g., inorganic and organic iron chemical species below a 0.2–0.45 micron operational cut-off) and their longevity points to them

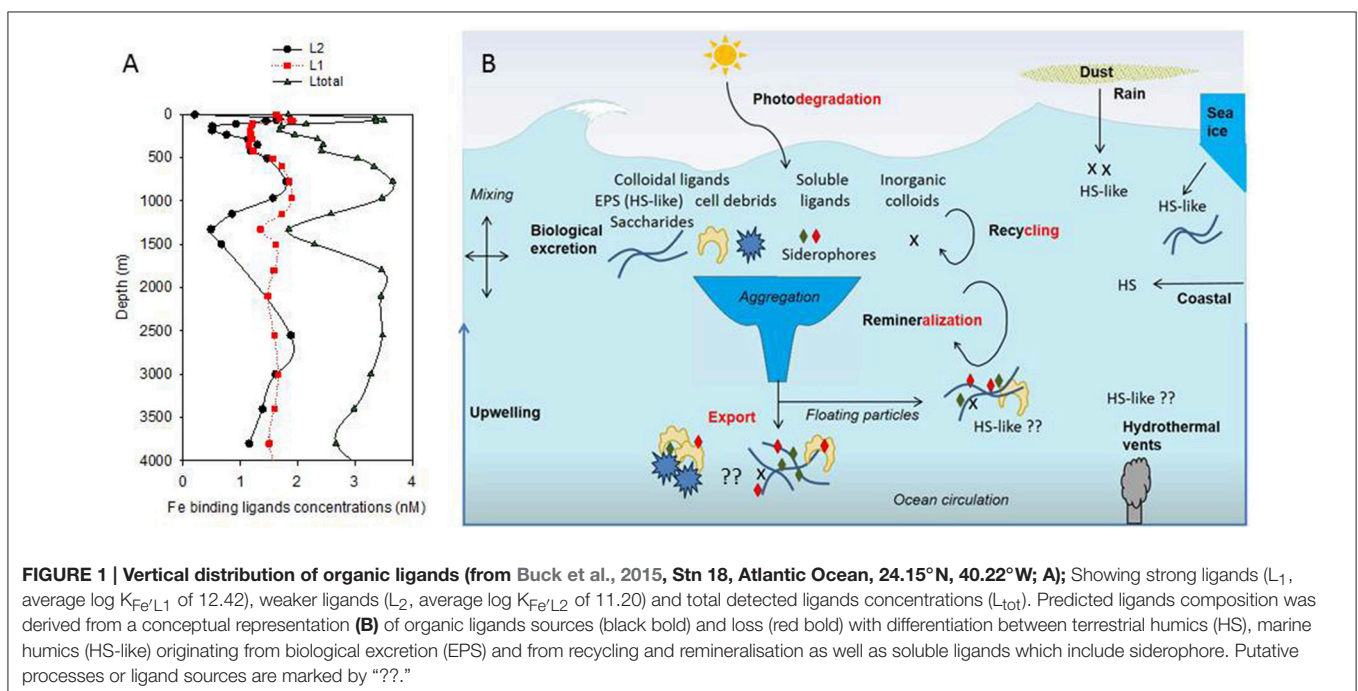


FIGURE 1 | Vertical distribution of organic ligands (from Buck et al., 2015, Stn 18, Atlantic Ocean, 24.15°N, 40.22°W; A); Showing strong ligands (L₁, average $\log K_{Fe'L_1}$ of 12.42), weaker ligands (L₂, average $\log K_{Fe'L_2}$ of 11.20) and total detected ligands concentrations (L_{tot}). Predicted ligands composition was derived from a conceptual representation (B) of organic ligands sources (black bold) and loss (red bold) with differentiation between terrestrial humics (HS), marine humics (HS-like) originating from biological excretion (EPS) and from recycling and remineralisation as well as soluble ligands which include siderophore. Putative processes or ligand sources are marked by "??"

being potentially reused, recycled, and/or refractory in nature and influence by ocean circulation. Based on our current understanding of external sources in addition to *in-situ* processes involved in ligand production (Table 1, Figure 1B; Gledhill and Buck, 2012), the case for different ligands is compelling. In the upper water column, a causal linkage can be made between organic ligands and the production of siderophores (which have conditional stability constants comparable to or considerably greater) than L_1 ligands (MacRellis et al., 2001), and bacterial/algal exudates associated with biological activity (Benner, 2011; Hassler et al., 2011a; Norman et al., 2015; Figure 1B). Phytoplankton can release several ligands including domoic acid, exopolymeric substances (EPS), and saccharides (Maldonado et al., 2002; Hassler et al., 2011b; Norman et al., 2015), thiols and phytochelatins (Leal et al., 1999; Dupont et al., 2004, 2006). This ligand distribution is superimposed on a background “profile” of ligands derived from the breakdown of biogenic particles (Boyd et al., 2010), particle-associated siderophores (likely at very low concentration) associated with particle-attached bacteria (Azam and Malfatti, 2007; Cordero et al., 2012), and other plant-derived organic matter. Generic cellular debris will ultimately be broken down by microbes (Letscher et al., 2011) to leave less labile dissolved organic matter such as humic material of marine origin (Figure 1B; Hansell, 2013). These humics would add to the pool of humic material from terrestrial origin entering the ocean (Moran et al., 2016). The ligands associated with particle breakdown tend to have lower conditional stability constants—more akin to L_2 – L_4 (Boyd et al., 2010; Bundy et al., 2015), and are observed throughout the water column (Gledhill and Buck, 2012; Hassler et al., 2012; Buck et al., 2015). Hence, three distinct groups of ligands stand out as potentially critical ones for iron biogeochemistry: siderophores, biological degradation/excretion products, and humics.

We focus here on distinctive characteristics (distribution, function, source, and distribution) of the three major ligand groups, in order to identify whether there are oceanic regions and/or strata in which particular organic ligands dominate. We then assess if this could be used to develop an ocean-wide classification and a holistic approach to understanding multi-faceted controls on ligands. To explore whether such a demarcation is possible, and its potential applications (such as driving targeted research on specific aspects of ligands), we distinguish and focus on organic ligands with different production and loss pathways, functions, and reactivity, likely to result in differences in their distribution across the ocean. The first group of ligand are humics substances, which are loosely-defined macromolecules. Here, we subdivided humics into several sub-groups based on their origins and production pathways, distinguishing terrestrial (HS) from marine humics (HS-like). Because of differing biological production pathways, fates, location, and stability of ligands in marine waters we further differentiate HS-like associated with refractory DOM and biological production of labile DOM as HS-like associated with remineralization and biological excretion, respectively (Table 1, Figure 1B). The second group of ligands, siderophores, are small molecules excreted by heterotrophic and cyano-bacteria in response to iron limitation. The third group of organic

ligands are biological degradation/excretion products at large (e.g., not restricted to bacterial origin and not necessarily specific to Fe limitation), comprising exopolymeric substances and polysaccharides as dominant compounds. Ultimately, our study explores the putative composition and variability of the bulk ligand pool (i.e., an extension to all ligand classes beyond the so called “ligand soup” of weaker ligands (typically assigned to L_2 – L_4 classes; Hunter and Boyd, 2007) in surface vs. subsurface waters, and from near-shore to offshore regions.

We hypothesize that the differences in the sources, turnover rate, production loss pathways can be used to differentiate marine regions where HS, EPS, and siderophores are expected to dominate Fe biogeochemistry. If it is so, we will discuss how the differences in iron binding conditional stability constants amongst these three groups of ligands is at present inconsistent with the concept of a continuum of organic ligands. We will then place this knowledge in a bigger picture to explore geographical and seasonal differences in the distribution of HS (and HS-like), EPS and siderophores, at regional scales including coastal, offshore, open ocean, and upwelling regions. Finally, we will explore biogeochemical consequences of the co-occurrence of these three groups of ligands by modeling Fe chemical speciation at three boundary conditions.

Such a generic approach aims to improve our conceptual understanding of how the multiple provenances of iron-binding ligands control biogeochemistry in different ocean regions, and whether they represent a continuum in iron-binding “potential.” This approach can provide a valuable platform for further research and a useful link to the global GEOTRACES survey (www.geotraces.org). We acknowledge that each of the ligand groups we are considering can be highly diverse (e.g., a wide range of siderophores, see Gledhill and Buck, 2012; Hassler et al., 2012 for reviews), and that techniques currently used for their analytical detection suggest an overlap between HS-like and HS, and HS-like and EPS (see Section Organic Ligands Distribution—Sources, Production, and Loss Pathways). Finally we acknowledge, that many more individual ligands, see (Boiteau and Repeta, 2015; Moran et al., 2016), and ligand classes remain to be characterized and identified as we move beyond these three nominal classes toward a continuum of ligands.

ORGANIC LIGANDS DISTRIBUTION—SOURCES, PRODUCTION, AND LOSS PATHWAYS

Evidence of the wide-ranging reactivity (i.e., labile, recalcitrant, refractory) of the DOC pool (Verdugo et al., 2004), combined with the current lack of detailed chemical resolution of DOC analytical techniques, have led to the suggestion that a continuum of Fe-binding organic ligands exists (Koopal et al., 2005). There is however a significant hysteresis in conditional stability constants between ligands associated with HS, breakdown products (HS-like from remineralization) and exuded material (EPS, HS-like from biological excretion), saccharides and siderophores, that enables demarcation between different groups of ligands (Table 1). These data suggest that there may

TABLE 1 | Summary of the different iron-binding organic ligands likely to be found in marine systems.

Sources	Origin	Type	Production zone	Log $K_{Fe/L}$
COASTAL				
	Terrestrial	HS (<i>humics and fulvics</i>)	Surface	11.1 <i>humics</i> ^a 10.6 <i>fulvics</i> ^a 10.2–12.0 <i>coastal</i> ^b 9.6–13.5 <i>estuary</i> ^{c,d}
ATMOSPHERIC DUST				
	Terrestrial	Inorganic colloids? ^e	Surface	11.65 ^f
	Biological?	HS-like ^{f,g} Saccharides ^f		
RAIN				
	Terrestrial?	HS-like?	Surface	11.1–12.8 ^h
	Biological?	Siderophore?		
HYDROTHERMAL VENTS				
	Terrestrial	HS-like (EPS)?	Deep	9.8–11.8 ^{i,j}
SEA-ICE AND ICEBERG				
	Biological	HS-like (EPS) Inorganic nano ⁿ	Surface	11.0–13.0 ^{k,l,m,n}
BIOLOGICAL EXCRETION/RELEASE				
<i>Unspecific</i>	Biological <i>most microorganisms</i>	HS-like (EPS) Saccharides (mono + poly) Porphyrins Ferritin Phytic acid Phaeophytin	Surface	<11.4–11.9 ^o 8.8 ^{p,mono} 12.0–12.4 ^{q,r} 11.7 ^q 10.8 ^s 12.2 ^q
<i>Specific</i>	Biological <i>bacteria, cyanobacteria</i> <i>Pseudonitzschia</i>	Siderophores Domoic acid	Surface	11.4–13.9 ^t 8.7 ^u
BIOLOGICAL TRANSFORMATION/REMINERALIZATION				
	Biological <i>bacteria</i>	HS-like Monosaccharides Porphyrine? EPS? Siderophores?	Deep	<12?
All			Surface	9.6–13.7 ^v
<i>In-situ measurements</i>			Deep	11–12 ^v

Source, origin, and conditional stability constant for iron-binding (log $K_{Fe/L}$) are shown in addition of putative type and production zone within the water column.

^aLaglera and van den Berg, 2009.

^bBatchelli et al., 2010.

^cGobler et al., 2002.

^dGerringa et al., 2007.

^eFitzsimmons et al., 2015.

^fHassler and Norman, unpublished data.

^gParis and Desboeufs, 2013.

^hCheize et al., 2012.

ⁱHawkes et al., 2013.

^jNichols et al., 2005.

^kBoye et al., 2001.

^lvan der Merwe et al., 2009.

^mLannuzel et al., 2015.

ⁿLin and Twining, 2012.

^oNorman et al., 2015.

^pCroot and Johansson, 2000.

^qWitter et al., 2000.

^rBruland et al., 2005.

^sMaldonado et al., 2005.

^tHassler et al., 2012.

^uRue and Bruland, 2001.

^vGledhill and Buck, 2012.

be a co-occurrence of extremely weak ligands (saccharides, L_3 and L_4), a group of ligands with very similar complex stability comprising HS, HS-like, EPS, and hemes (L_1 – L_3), whereas siderophores have $\log K_{Fe'L}$ values of ~ 12.2 and higher (L_1), i.e., indicative that there is not, presently, a continuum of conditional stability constants. More likely this trend results from a lack of resolution of the existing speciation methods ($\log K_{Fe'L}$ values ± 0.3 ; Gerringa et al., 2014), different outcomes across a range of speciation procedures (TAC vs. SA for instance), and the effect of not measuring speciation under equilibrium conditions. Moreover, inter-dependency between values for ligand concentration and $K_{Fe'L}$ may also contribute to an analytical bias, as an underestimation of the ligand concentration leads to overestimation of $K_{Fe'L}$ and vice versa (Hudson et al., 2003; Gerringa et al., 2014). An emerging combination of analytical approaches and evolving conceptual theories is beginning to advance this research field (e.g., Cordero et al., 2012; Boiteau and Repeta, 2015; Boyd and Tagliabue, 2015; Waska et al., 2016).

For most of the ocean the concentration of dissolved organic ligands exceeds that of dissolved iron (Gledhill and Buck, 2012; Boyd and Tagliabue, 2015) by around 1 nmol L^{-1} , suggesting a tight coupling between the iron and its complex pair. As different Fe sources are linked to distinctive ligands, such as sea-ice melt (Table 1), it is expected that the spatial variability of iron sources matches the variability of organic ligands, providing that *in-situ* recycling and biological activity are not dominating the pool of organic ligands (Figure 1B). Globally, the largest input of iron into the oceans was initially reported to come from atmospheric dust deposition (Duce and Tindale, 1991; Jickells et al., 2014) although this view has been subsequently challenged and overturned with hydrothermal and sedimentary sources being reported as more dominant, especially at high latitudes (Tagliabue et al., 2014; Resing et al., 2015). Other modes of iron supply include upwelling, coastal regions with large riverine and sedimentary inputs (Coale et al., 1996), and the cryosphere (Boyd et al., 2012). Unsurprisingly, iron-binding ligands were found in most of these iron sources (Figure 1B, Table 1): including sea-ice and icebergs (EPS, i.e., HS-like from bacterial excretion; van der Merwe et al., 2009), rainwater and dust (HS-like, saccharides), hydrothermal vents (HS and HS-like from bacterial excretion; Kleint et al., 2016), and refractory organic compounds that accumulate at depth (HS and HS-like from bacterial remineralization; Boyd et al., 2010; Heller et al., 2013; Medeiros et al., 2016). Therefore, regional and seasonal variations of the input of organic ligands within the euphotic zone are expected (see Section Toward a Map of Iron-Binding Ligand Distributions). External supply of iron and organic ligands may also result in additional ligand enrichment via the stimulation of *in-situ* biological production of organic ligands in surface waters (Wagener et al., 2008; Adly et al., 2015).

Indeed, the distribution of Fe-binding organic ligands in oceanic surface waters is consistent with multiple biological sources associated with biological Fe-stress, the recycling of organic carbon in surface waters (Gledhill and Buck, 2012) and its remineralization at depth (Boyd and Ellwood, 2010). Biologically produced Fe-binding organic ligands are (i) related

to alleviation of Fe stress [bacterially-produced siderophores (Rue and Bruland, 1995; Trick et al., 1995; Mawji et al., 2008; Velasquez et al., 2011), the toxin domoic acid produced by the diatom *Nitzschia* (Rue and Bruland, 2001; Maldonado et al., 2002)], (ii) retention of episodic iron input (Adly et al., 2015; Westrich et al., 2016), or (iii) ligands produced through biological recycling or basal biological activity such as hemes (Gledhill et al., 2013), ferritin (Castruita et al., 2008), polysaccharides (Ozturk et al., 2004; Hassler et al., 2011a), and EPS (Nichols et al., 2004; Hassler et al., 2011b; Norman et al., 2015). Interestingly, amongst most of these organic ligands, only EPS were reported to contribute to the pool of HS-like substances (Norman et al., 2015) which is not surprising given that EPS and HS are polyfunctional macromolecules.

Ligand loss terms could be associated with downward export fluxes mediated by biological production and chemical aggregation (Figure 1B). Export of organic carbon has been reported following large blooms (DiTullio et al., 2000), grazing activity (e.g., salps, Iversen et al., in review; Cabanes et al., in preparation) or along salinity gradients found in estuaries (Sholkovitz et al., 1978). It is currently unclear whether the transformation of organic compounds mediated by heterotrophic bacteria associated with the microbial carbon pump (e.g., accumulation of refractory DOM and remineralization) represents a loss or a production pathway for iron-binding organic ligands. The rapidly growing number of organic ligand measurements along with the basin-scale approach associated with GEOTRACES provide critical insights on the role of remineralization on the fate of ligands (e.g., Gerringa et al., 2015). Overall, remineralization is associated with a loss of organic ligands, since concentrations were found to decrease with depth and along the ocean circulation pathway, and furthermore a negative correlation was evident between ligands and apparent oxygen utilization in the NADW (Buck et al., 2015; Gerringa et al., 2015). Generally, the weaker ligands found at depth are thought to result from remineralization by heterotrophic bacteria (Hunter and Boyd, 2007; Boyd et al., 2010; Buck et al., 2015). The production of L_2 as well as L_1 ligands in remineralization experiments (Boyd et al., 2010; Bundy et al., 2016; Velasquez et al., 2016), clearly highlights a dynamic environment which is probably linked with bacterial colonization of sinking particles. Photochemistry is responsible for the production of weaker ligands and/or the degradation of iron binding ligands (e.g., Barbeau et al., 2001; Butler and Theisen, 2010; Gledhill and Buck, 2012), thus representing a loss pathway of strong ligands that can predominate in the upper few meters of surface waters (Figure 1) where they are likely to represent an important transient source of labile iron (Croot and Heller, 2012) to support phytoplankton growth.

Humics

The fluorescence properties of humics, identified by Parallel Factor Analysis (PARAFAC), have demonstrated that humic-like substances occur throughout the global ocean (Heller et al., 2013; Catala et al., 2016), accounting for 5–20% of the DOC in deep and coastal waters (Harvey et al., 1983). Based on their

specific signature (i.e., t-Peaks) riverine HS are found at depth in the North Atlantic and Pacific Oceans (up to 2000 and 5040 m, respectively; Medeiros et al., 2016). Based on their sources (riverine, run-off) high concentrations (mg/L) of the terrestrial HS is expected to occur in estuarine and coastal waters (Laglera and van den Berg, 2009; Krachler et al., 2015). An inverse ^{228}Ra modeling study (Kwon et al., 2014) has suggested that groundwater discharge is also an important source of HS whose signature is found throughout surface waters (i.e., 18 m depth) of the temperate Indian and North Atlantic Oceans. Other sources are sediments (Bordovsky, 1957), dust (Paris and Desboeufs, 2013, **Figure 2A**). To date, the characterization of organic ligands associated with hydrothermal vents, a terrestrial input, is in its infancy but will be highly relevant for upwelling regions (e.g., Sander and Koschinsky, 2011; Kleint et al., 2016); their potential contribution to any of the three groups of ligands considered is not yet known. In addition, rain contains humics but also malonic, citric, and oxalic acids that stabilize iron in solution (Willey et al., 2000) as well as iron binding ligands detected by electrochemistry (Cheize et al., 2012; **Table 1**).

It is now recognized that terrestrial DOC is exported to the ocean (Seidel et al., 2015), and is injected into oceanic deep waters via thermohaline circulation (Medeiros et al., 2016). At depth, HS is present at low concentrations but is stable (>24 ky; Lechtenfeld et al., 2014). Such high stability probably reflects low susceptibility to bacterial breakdown and infrequent photo-degradation occurring between ventilation cycles of deep water to the surface every ~ 1000 years (Primeau and Holzer, 2006). In the deep sea, the breakdown rate of this recalcitrant DOM is much slower and this pool reaches ^{14}C ages of 1000's of years (Jiao et al., 2010), which is consistent with the estimated 1000 year residence time of iron-binding organic ligands in the NADW (Gerringa et al., 2015). The distribution of fluorescent properties of dissolved organic matter, used as a proxy for humics (Coble, 2007), shows lower levels in surface waters, increasing at mid-depth, and becoming relatively constant in the deep waters (Yamashita et al., 2010; Heller et al., 2013; Catala et al., 2016). This distribution suggests that photo-degradation has the strongest impact on humics distribution whereas the processes of microbial degradation and particle adsorption are not reflected in the shape of vertical profiles. Knowledge of the iron-binding properties of HS and detection by ASV suggest that terrestrial HS makes up $\sim 18\%$ of the DOC pool in coastal and $\sim 4\%$ in deep ocean waters (Laglera and van den Berg, 2009; Bundy et al., 2014).

In open ocean surface waters, the fluorescence signature of humics appear to be best related to oxygen utilization and chlorophyll *a* concentrations as a result of *in-situ* production (Stolpe et al., 2014), hence a biologically-mediated distribution has been proposed (Yamashita et al., 2010; Tanaka et al., 2014; Catala et al., 2016). In this case, the peak in ligand concentrations associated with higher stocks of phytoplankton and bacteria could be associated with HS-like produced by biological excretion. Marine bacteria rapidly produce such material from labile compounds (Ogawa et al., 2001; Stolpe et al., 2014), thus acting as an *in-situ* source of marine HS-like material. Refractory DOM, (part of which would be HS-like substances)

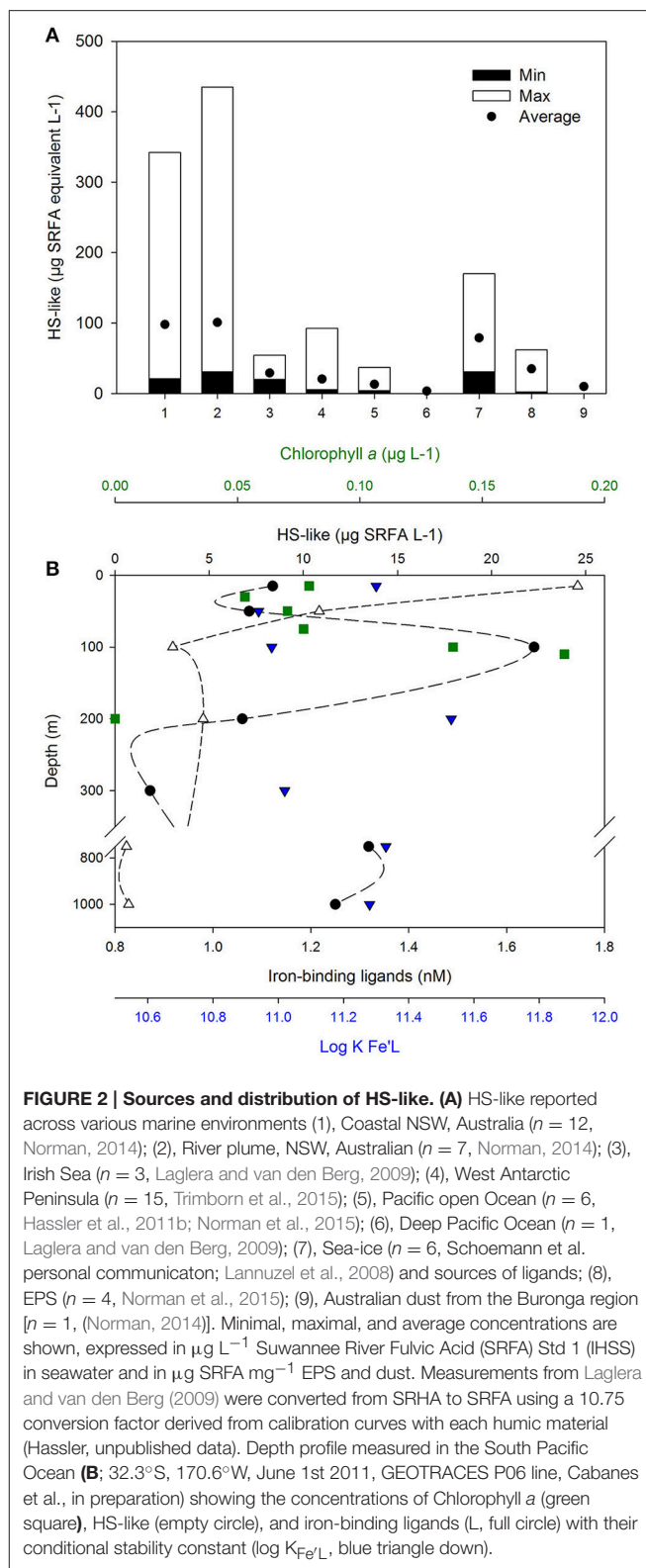


FIGURE 2 | Sources and distribution of HS-like. (A) HS-like reported across various marine environments (1), Coastal NSW, Australia ($n = 12$, Norman, 2014); (2), River plume, NSW, Australian ($n = 7$, Norman, 2014); (3), Irish Sea ($n = 3$, Laglera and van den Berg, 2009); (4), West Antarctic Peninsula ($n = 15$, Trimborn et al., 2015); (5), Pacific open Ocean ($n = 6$, Hassler et al., 2011b; Norman et al., 2015); (6), Deep Pacific Ocean ($n = 1$, Laglera and van den Berg, 2009); (7), Sea-ice ($n = 6$, Schoemann et al. personal communication; Lannuzel et al., 2008) and sources of ligands; (8), EPS ($n = 4$, Norman et al., 2015); (9), Australian dust from the Buronga region [$n = 1$, (Norman, 2014)]. Minimal, maximal, and average concentrations are shown, expressed in $\mu\text{g L}^{-1}$ Suwannee River Fulvic Acid (SRFA) Std 1 (IHSS) in seawater and in $\mu\text{g SRFA mg}^{-1}$ EPS and dust. Measurements from Laglera and van den Berg (2009) were converted from SRHA to SRFA using a 10.75 conversion factor derived from calibration curves with each humic material (Hassler, unpublished data). Depth profile measured in the South Pacific Ocean (**B**; 32.3°S , 170.6°W , June 1st 2011, GEOTRACES P06 line, Cabanes et al., in preparation) showing the concentrations of Chlorophyll *a* (green square), HS-like (empty circle), and iron-binding ligands (L, full circle) with their conditional stability constant ($\log K_{\text{FeL}}$, blue triangle down).

is also produced *in-situ* in the oceans and coastal seas as part of the remineralization of phytoplankton-derived organic matter (Burkhardt et al., 2014).

Humic signatures detected by electrochemistry (Laglera and van den Berg, 2009) were reported within HS, EPS and atmospheric dust, and are present in river plumes, coastal waters, sea-ice as well as in surface waters and at depth in the open ocean (Figure 2A; Laglera and van den Berg, 2009; Hassler et al., 2011b; Norman, 2014; Norman et al., 2015; Trimbom et al., 2015). This overlap in the detection of EPS, HS, and HS-like indicates a lack of resolution of the analytical techniques used (fluorescence, voltammetry) and therefore an inability to discriminate between the three compounds. Differences in fluorescent behavior of HS and HS-like substances (Heller et al., 2013; Stolpe et al., 2014) imply that there must be different reactivity, but identical responses to electrochemical detection suggests their speciation-reactivity is indistinguishable (Laglera and van den Berg, 2009). More studies are thus required to characterize whether HS-like have a structural or chemical signature in relation to their sources in order to further differentiate them. However, the observation that coastal studies have found correlations between HS-like and L₂ (Laglera and van den Berg, 2009; Abualhaija et al., 2015), but open ocean studies have variously found direct relationships between HS-like substances and L₂ Abualhaija et al., in review, and no relationship between the distribution of HS-like substances and L₂ (Cabanes et al., in preparation; Figure 2B) or Fe solubility (Heller et al., 2013), points toward regional differences in ligand distributions between coastal and open ocean.

Siderophores

Much of the corroborating evidence for the production of siderophores by bacteria and cyanobacteria came from early lab studies (e.g., Reid et al., 1993; Wilhelm and Trick, 1994) and measurements in the Atlantic and Southern Oceans (Mawji et al., 2008, 2011; Velasquez et al., 2011). The role of marine fungi which act in the decomposition and remineralization of organic matter is currently poorly documented. Many terrestrial fungi, including those in the rhizosphere, and marine fungi produce siderophores (Haselwandter, 1995; Baakza et al., 2004).

The molecular chemistry of siderophores is specifically designed to bind iron strongly (Vraspir and Butler, 2009) and these are expected to be amongst the strongest iron binding ligands. Enhanced production of siderophores should be linked to regional patterns in heterotrophic bacterial and cyanobacteria iron stress and its opportunistic alleviation (Kirchman et al., 2009; Adly et al., 2015; Westrich et al., 2016) using a wide range of iron acquisition strategies (Cordero et al., 2012; Moran et al., 2016). Most of the insights gained into siderophores distributions have relied upon the comparable conditional stability constants between them and the L₁ class of ligands, even though no direct links have been made to date between siderophores and the L₁ class (MacRellis et al., 2001). Time-series changes in L₁ ligand concentrations and shifts in heterotrophic bacterial activity (i.e., a rapid up-regulation of siderophore receptor expression) following a purposeful mesoscale iron enrichment in the NE Pacific provides further strong indirect evidence of such a linkage (Adly et al., 2015). Siderophores are likely not restricted to surface waters as heterotrophic bacteria are found throughout the water column (but at much lower abundances than in the surface ocean; Boyd et al., 1999) and sinking particles are heavily colonized by

bacteria (Ploug et al., 1999), some of which produce siderophores (Cordero et al., 2012; Figure 1B). Indeed, the production of siderophores and L₁ ligands were recently measured during a subsurface ocean remineralization experiment (Bundy et al., 2016; Velasquez et al., 2016).

It is to be noted that the presence of siderophores is not solely reported in low dissolved iron regions (Mawji et al., 2008). A transcriptomics study of the response of the cyanobacteria *Synechococcus* PCC7002 showed that the genes involved in the siderophores/iron uptake pathways (siderophores and receptors) were induced at inorganic iron concentrations typical of coastal areas (Blanco-Ameijeiras and Hassler, 2015), likely due to high biological iron requirements for growth. Moreover, strong iron-binding ligands were only reported following high iron addition in a study using *Alteromonas* sp. (Hogle et al., 2016). It is therefore reasonable to expect siderophores, at low concentrations, across most of the ocean (see Mawji et al., 2008; Boiteau et al., 2016a). Detection of individual siderophores in seawater is in its infancy but the combination of high-performance liquid chromatography with inductively-coupled plasma-mass spectrometry represents a promising method (Boiteau et al., 2013) which has recently been used to characterize the joint release/excretion of several siderophores in a *Synechococcus* lab culture (Boiteau and Repeta, 2015). Furthermore, low picomolar levels of individual siderophores, and lateral trends in their distribution were evident in both Californian waters and along the South Pacific GEOTRACES zonal section, suggesting distinct trends in the distribution of a range of siderophores (Boiteau et al., 2016a; Repeta et al., 2016). However, high concentrations of L₁ (~1 nmol L⁻¹) are often detected (e.g., Boyd and Tagliabue, 2015; Buck et al., 2015; Gerringa et al., 2015), clearly suggesting that not only siderophores contribute to this strong ligand pool.

Clearly, there must be loss terms for siderophores otherwise there would be a gradual build-up in their stocks. Photochemical breakdown of siderophores leading to the production of weaker ligands (Barbeau et al., 2001) or alteration of their complexing properties (Amin et al., 2009) is a leading candidate for siderophore loss in surface waters. However, there must be other highly influential loss processes such as grazing (surface and subsurface waters; Kraemer et al., 2006, 2015), as bacterial stocks are tightly controlled within the microbial food-web (which rapidly recycles iron; Strzepek et al., 2005). For example, the fate of siderophores within or on the surfaces of heterotrophic bacteria as they pass through the acidic (pH 3) micro zooplankton gut (Barbeau et al., 1996) is unknown. Viral lysis is also a major fate of heterotrophic bacteria (Boyd and Tagliabue, 2015), but again little is known about whether such processes alter the molecular chemistry of the siderophores. Finally, the fate of siderophores taken up by piracy strategy by other bacteria (Granger and Price, 1999; Cordero et al., 2012) is unclear, although the “public good” theory suggests an efficient recycling of siderophores.

Exopolymeric Substances and Saccharides

Interestingly, the most abundant components of dissolved organic matter are carbohydrates, with ~50% present as polysaccharides (Benner et al., 1992), which could be an

important component of the ligand soup. Vertical distributions of polysaccharides suggest that they are reactive in surface waters, rapidly consumed by microorganisms and part of the labile pool of DOC (Pakulski and Benner, 1994). As polysaccharides are a major constituent of EPS (see above), we thus assumed that EPS would follow a similar distributional pattern to that of polysaccharides (Figure 1A). The half-life of the EPS and polysaccharides is expected to be short (hours-years), their production rate high but their measured *in-situ* concentration is reported to be relatively “low” (e.g., nM EPS or μM carbon; Panagiotopoulos and Sempere, 2005; Norman et al., 2015). Indeed, neutral sugars within DOC have residence time shorter than 3 years (Repeta and Aluwihare, 2006). As for any short-lived reactive compounds, their importance might be under-estimated since they do not accumulate, but cycle, in the water column.

A large number of marine bacterio- and phyto-plankton release polysaccharides, either as EPS, or from intracellular storage products following cell lysis or grazing (e.g., Decho, 1990; Nichols et al., 2005, Figure 1B). Constituents of phytoplankton cells are expected to be present in surface waters, especially following the termination (i.e., cell senescence) and decline of phytoplankton blooms. Sources of actively excreted compounds such as EPS are mostly associated with biological activity in surface waters and sea-ice (Table 1). It is to be noted that *Alteromonas* sp., which synthesize strong iron binding ligands (L_1 typically assigned to siderophores, Hogle et al., 2016) also produce EPS able to strongly bind iron (Hassler et al., 2011a). Since EPS are produced for many functions (Decho, 1990; Hoagland et al., 1993; de Brouwer et al., 2005), they are likely to be present in relatively high concentrations (Hassler et al., 2011a; Norman et al., 2015). EPS are expected to be particularly abundant in waters characterized by high chlorophyll concentrations or on the base of sea-ice (Table 1). Carbohydrate exudation products tend to be linked to nutrient limitation and the stationary growth phase of cells (e.g., Mykkestad, 1977; Liu et al., 2001), such as at the decline of a phytoplankton bloom when cells continue to fix carbon photosynthetically but have insufficient nutrients available for macromolecular synthesis (e.g., Boyd et al., 2005). To date, a clear link between phytoplankton Fe limitation and the specific production of exopolymeric substances is missing but putative proteomic evidence has been presented (Nunn et al., 2013). However, EPS release is not restricted to surface waters; bacterial exopolymers were reported in the deep-ocean, including hydrothermal vents (e.g., Nichols et al., 2005), but their specific role(s) within Fe biogeochemistry remains unknown.

Saccharides and EPS iron-binding affinities usually assign them to the L_2 – L_4 ligand classes (Hassler et al., 2011b). However, recent data showed that EPS could contribute to the L_1 ligand pool (Norman et al., 2015), suggesting stronger binding stability constants for EPS (at the borderline of L_1 – L_2) than for pure saccharides (L_3 – L_4). Despite the nature of EPS remains unknown leading to unsolved mechanism(s) for iron binding, they are rich in polysaccharides pointing toward a role for carboxylic groups (Janse et al., 1996; Nichols et al., 2005). All EPS tested so far contributed to the pool of HS-like substances that are electrochemically detected (Hassler et al., 2011b; Norman et al.,

2015; Figure 2A). This suggests that they are a major contributor to the marine HS-like pool associated with biological excretion and hence mostly present in surface waters. Data suggest that EPS from phytoplankton are smaller in size and make a greater contribution toward organic ligands and HS-like substances than bacterial EPS (Norman et al., 2015); but differences in culture growth media and the EPS analytical protocol between studies prevent a definitive conclusion at present.

Considering that EPS could represent up to 1% the total DOC pool, their production rate could be as high as for labile DOC (0.15 – $0.25 \text{ Pg C yr}^{-1}$, Hansell, 2013; Norman et al., 2015). Based on the observation that 34% of bacterial EPS was carbon (Hassler et al., 2011a) and a median ligand contribution of $18 \mu\text{mol L g}^{-1}$ EPS (Hansell, 2013; Norman et al., 2015), the production rate of ligands from EPS of $2.4 \text{ nmol d}^{-1} \text{ L}^{-1}$, which is close to concentrations and production rates of ligands determined previously (Boyd et al., 2010; Gledhill and Buck, 2012; Völker and Tagliabue, 2015). This production rate suggests that EPS represent an important group of ligands accounting for most of iron binding ligands and $\sim 14\%$ HS-like substances in the Sub-Antarctic seasonal bloom occurring between Australia and New Zealand (Norman et al., 2015).

A Putative Role for Exopolymeric Substances in Size Distribution and Vertical Transfer of Iron-Binding Ligands

EPS are considered to play a central role in the vertical flux of matter between the surface and the deep ocean. Their solubility and their ability to clump together or with other organic macromolecules and form biogels (or TEP: Transparent Exopolymer Particles) over time enables them to contribute to the pool of dissolved organic matter (DOM) but also to that of particulate organic matter (POM) when aggregated. In the geomicrobiology literature there is also growing recognition of the role that gel production plays in retaining metals (Melton et al., 2014). Whereas, TEP is often associated with marine snow and particulate carbon export, this idea was challenged by the observation that TEP could be positively buoyant (c.f. seawater) (Azetsu-Scott and Passow, 2004; Laurenceau-Cornec et al., 2015). Therefore, EPS and TEP can also be associated with ascending organic material, colloids, and also with microorganisms (Azetsu-Scott and Passow, 2004). Recent studies have suggested that polysaccharides, EPS as well as viruses could represent a significant pool of colloidal iron binding ligands (Benner, 2011; Hassler et al., 2011a; Bonnain et al., 2016). Indeed, iron associated with the tails of phages might mimic Fe-siderophore complexes thus providing an efficient way to infect heterotrophic bacteria (Bonnain et al., 2016).

Because siderophores are small organic compounds (Butler and Theisen, 2010) able to solubilize colloidal Fe bearing minerals including oxyhydroxides (Kraemer et al., 2005), they are thus expected to be found in the soluble phase. However, soluble ligands show a lower conditional stability constant for iron binding than colloidal ligands (Boye et al., 2010), thus contradicting the hypothesis that siderophores are mainly present in the soluble phase. One possibility is that upon release the siderophores may become associated with organic colloids

(Buck et al., 2007). Similarly, hemes (<1000 Da) were measured in association with marine particles, possibly a result of their low solubility in seawater (Gledhill and Buck, 2012). EPS could hence potentially trap other important organic ligands or Fe oxides within the colloidal fraction (Stolpe and Hasselov, 2010; **Figure 1B**) but also in either sinking or ascending particles (Azetsu-Scott and Passow, 2004). This capacity of EPS to adsorb organic ligands and iron oxides takes the challenge of chemically characterizing natural Fe-binding ligands in the field a step further. Capture of biological molecules (e.g., the enzyme Rubisco) within the gel phase was reported and proposed as a stabilizing mechanism, by which remineralization is weakened resulting in a significant increase in their residence time up to decades (Orellana and Hansell, 2012).

IMPLICATIONS OF THE CO-EXISTENCE OF IRON-BINDING LIGANDS

In the presence of multiple Fe binding ligands, competition will take place for iron. Because siderophores are present at low pM levels whereas dissolved iron occurs at high pM levels, they tend to be saturated with iron even in presence of much higher concentrations of competing ligands that bind iron less strongly (e.g., L_2). This can be numerically verified using the following seawater composition based on relevant literature (**Figure 3A**): 0.1–1 nM dissolved Fe, 1.1 nM of ligands with a conditional $\log K'_{Fe'L} = 11.45$ and 10 pM siderophores with $\log K'_{Fe'L} = 12.5$ (these constants are based on Fe'). The concentration and stability constant for L_2 are the average values from a recent compilation of oceanic ligands (Caprara et al., 2016), whereas the siderophores concentration is representative of their concentrations in the ocean (e.g., Mawji et al., 2008, 2011; Repeta et al., 2016). The siderophore conditional stability constant was chosen to match that of desferrioxamine B a hydroxamate often used as a model siderophore (Maldonado et al., 2005; Hassler et al., 2013; Cabanes et al., in preparation). In spite of the relatively small difference in complex stability (10-fold) between the ligands species and the much more (100-fold) abundant background L_2 ligands, the 10 pM of siderophore is largely complexed with iron but, $\geq 98\%$ of the iron is associated with the L_2 ligands (**Figure 3A**). These calculations are based on the assumption of a steady-state of siderophore production, combined with a near-equilibrium in the complexation reactions, a scenario that most likely fails to reflect conditions in natural waters due to slow reaction kinetics (Hering and Morel, 1989).

It is anticipated that the concentration of siderophores is higher (perhaps tenfold) in the diffusion boundary layer of the bacterium producing them (Volker and Wolf-Gladrow, 1999) or in the surrounding particles colonized by heterotrophic bacteria (Cordero et al., 2012). In these specific locations, the amount of iron bound with siderophores could be proportionally greater than for the bulk seawater medium. Alternatively, there may be kinetic implications as the residence time within the diffusion layer is short (e.g., <0.1 s) for hydrophilic siderophores (Volker and Wolf-Gladrow, 1999) but could be longer for those equipped with a hydrophobic (lipophilic) tail. The kinetics of

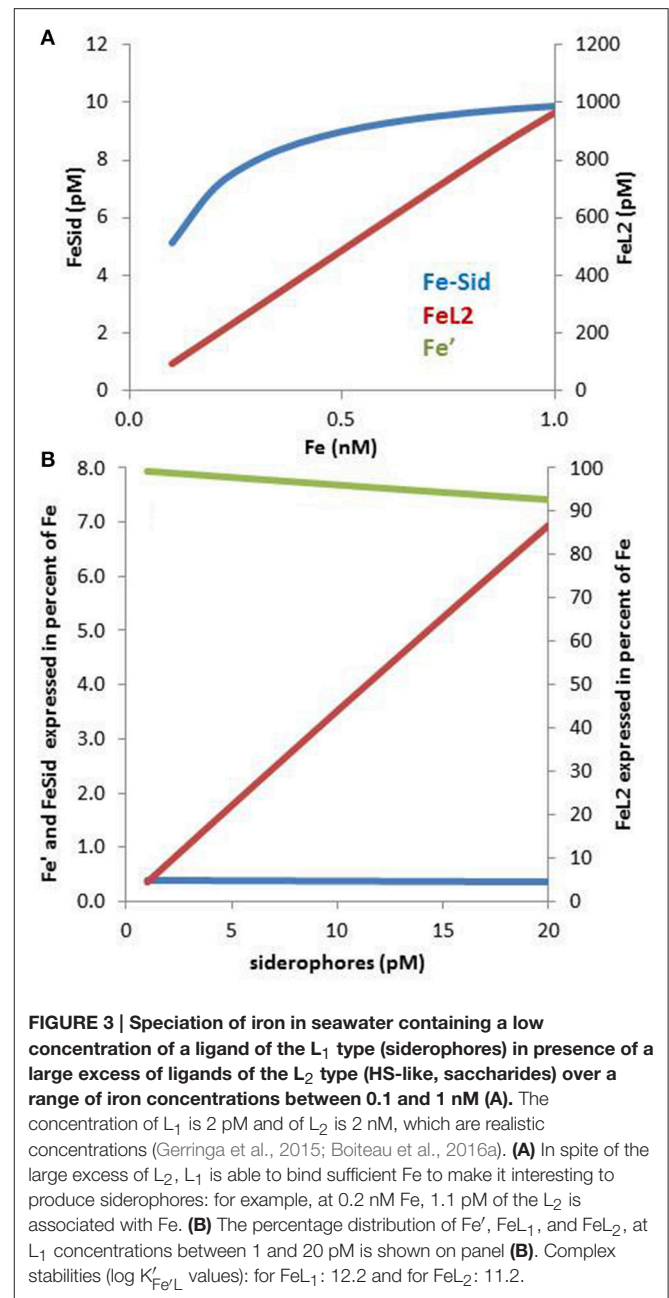


FIGURE 3 | Speciation of iron in seawater containing a low concentration of a ligand of the L_1 type (siderophores) in presence of a large excess of ligands of the L_2 type (HS-like, saccharides) over a range of iron concentrations between 0.1 and 1 nM (A). The concentration of L_1 is 2 pM and of L_2 is 2 nM, which are realistic concentrations (Gerringa et al., 2015; Boiteau et al., 2016a). (A) In spite of the large excess of L_2 , L_1 is able to bind sufficient Fe to make it interesting to produce siderophores: for example, at 0.2 nM Fe, 1.1 pM of the L_2 is associated with Fe. (B) The percentage distribution of Fe' , FeL_1 , and FeL_2 , at L_1 concentrations between 1 and 20 pM is shown on panel (B). Complex stabilities ($\log K'_{Fe'L}$ values): for FeL_1 : 12.2 and for FeL_2 : 11.2.

iron speciation between a recently released siderophore and iron (already complexed with background L_2 ligands in seawater) is probably controlled by the dissociation rate of organically bound iron, with a half-life of minutes [e.g., 9 min determined for Fe(III) bound with ligands in seawater; Abualhaija and van den Berg, 2014], which can be seen as relatively slow compared to phytoplankton Fe biological uptake rate (Hudson and Morel, 1990).

Only a few % of the FeL_2 species needs to dissociate to effectively saturate the siderophores in our numerical example. The observations of low concentrations (<10 pM) of siderophores (Boiteau et al., 2016a; Repeta et al., 2016) may be

due to energetic constraints associated with their production (Volker and Wolf-Gladrow, 1999) and the “public goods” theory, in which synergies and multiple uptake strategies take place amongst a consortium of heterotrophic bacteria (e.g., Cordero et al., 2012). The cost of siderophores production must be traded off against the benefit obtained from the ability to rapidly sequester iron that is supplied episodically such as by dust inputs (Boyd and Tagliabue, 2015; Westrich et al., 2016). Overall, these calculations (Figure 3A) point out that even a low concentration of siderophores is effective for bacterial uptake as they can use the bulk of Fe-L₂ complexes as a suitable exchangeable iron pool. On the other hand, the Fe-L₂ pool, representing more than 98% of the dissolved iron, is directly relevant for the overall iron solubility and residence time in surface water (Johnson et al., 1997). Moreover, if FeL₂ is highly bioavailable to phytoplankton, as suggested for EPS (Hassler et al., 2011b, 2014), this pool could potentially benefit phytoplankton growth (e.g., Hassler et al., 2011b). In this case, weak ligands would be important for iron phytoplankton nutrition, as reported for other metals such as Zn (Aristilde et al., 2012) and Cu (Walsh et al., 2015).

The relative contribution of ligands depends also on the “exchangeable” iron pool. This exchangeable pool is often referred to as the dissolved iron pool (Gledhill and Buck, 2012), a possibly misleading assumption as not all the dissolved iron might be exchangeable and as particulate iron can also react with organic ligands such as siderophores and HS (Kraemer et al., 2005; Paris and Desboeufs, 2013; Fishwick et al., 2014). It is also to be noted that the co-existence of multiple metals has implications for iron biogeochemistry as organic ligands may bind metals with different binding affinities, potentially leading to competition, representing a research direction mostly unexplored for *in-situ* oceanic ligands.

The conditional stability constant of desferrioxamine-B (DFB; Cheize et al., 2012; Abualhaija and van den Berg, 2014) in rain- and seawater is more than 5 orders of magnitude greater than that for other trace metals in simple electrolyte solutions [e.g., Al(III), Cu(II), Zn(II); Hernlem et al., 1996], suggesting that other metals cannot compete with binding of iron using similar siderophores. Copper and zinc complexation with HS-type ligands in seawater is strong (Yang and van den Berg, 2009), and copper and iron compete for L₂ type ligands in estuarine and coastal waters (Abualhaija et al., 2015). The conditional stability constants for marine organic ligands with nickel and cobalt are high (Martino et al., 2004; Ellwood et al., 2005; Bown et al., 2012; Baars and Croot, 2015) suggesting a possible competition with iron providing they bind with the same ligands. Indeed, Cu and Ni competition for binding to the same organic ligand has been recently observed (Boiteau et al., 2016b; this issue).

TOWARD A MAP OF IRON-BINDING LIGAND DISTRIBUTIONS

Several thousand organic compounds co-exist in seawater (e.g., Hertkorn et al., 2006). It is therefore unsurprising that numerous ligands are suspected to contribute to the overall electrochemical signature associated with L₁–L₄ (Table 1). The zonation of the

key sources, production and loss pathways for Fe-binding organic ligands (Table 1, Figure 1B) enables an initial geographical delineation of regions to be drawn, where different ligands might be expected to dominate the bulk ligand pool. Differences in the types of organic ligands (HS, EPS, and siderophores) can indeed be mapped onto oceanic regions from coastal to offshore (Figure 4). HS and EPS are expected to decrease with distance from the coast but EPS remain at a comparatively high baseline; siderophores are present at low concentrations and expected to increase with distance from the coast (see below). Such distribution can be refined to get an overview of their geographical distribution at a basin-scale. Key factors that will determine broad-scale ligand distributions include: location of major oceanographic features (such as High Nitrate Low Chlorophyll waters) or regions of high productivity and/or downward export flux; geographical location of land masses, and major rivers; the longevity of each ligand class (Table 2) and how this intersects with timescales of oceanic circulation to distribute ligands in the oceans’ interior. Smaller-scale regional characteristics, such as sea-ice dynamics, regions of dust supply, and phytoplankton seasonal bloom will be overlaid onto these broad-scale properties.

There is insufficient data for us to provide a robust quantitative estimate of the relative contribution of HS, EPS, and siderophores from the literature. We explore the implication of the co-existence of these three groups of ligands considering boundary conditions of their abundance in coastal, shelf, highly productive areas as well as open ocean (Figure 5). Using literature data and modeling projections, we have come up with preliminary estimates of the contribution of these ligand groups to the total ligand pool and iron chemistry (see Supplementary Material and Table S1 for details of the model parameterization). These projections enable us to provide the first estimates of the implication of the co-occurrence of these groups of

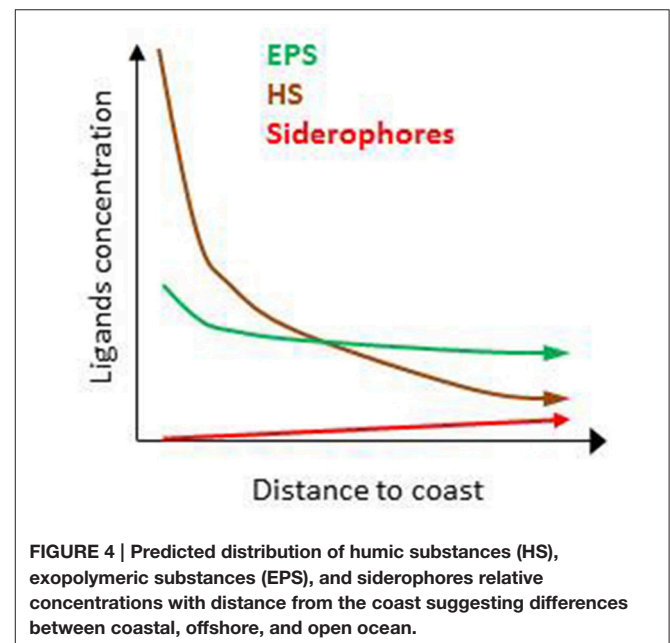


TABLE 2 | Expected regional and seasonal distribution of the different organic ligands in relation to their external and *in-situ* sources and production pathways.

Ligands sources	Low Chl <i>a</i>		High Chl <i>a</i>			Seasonality
	Fe-limited	Nutrient-limited	Coastal	Upwelling	Bloom	
EXTERNAL						
Coastal			++	++		SU
Atmospheric	+	++	+			
<i>dry</i>						SU
<i>wet</i>						SP-SU
Sea-ice	+	–	+			SP-SU
Hydrothermal	+			++		
IN-SITU						
Photochemical	++	++	+	+	+	SU
Biological						SP-SU
<i>Fe-stress</i>	++	–	±	±	±	
<i>Basal activity</i>	+	+	++	++	++	
<i>Recycling</i>	++	++	+	+	+	
<i>Remineralization</i>	+	+	++	++	++	

Large abundance, presence and absence of specific organic ligands are illustrated by the symbols ++, +, and –, respectively, whereas heterogeneity is shown by ±. Seasonality is associated with the season at which each sources is the most pronounced [spring (SP) and summer (SU)].

organic ligands in regions where specific ligands are expected to dominate.

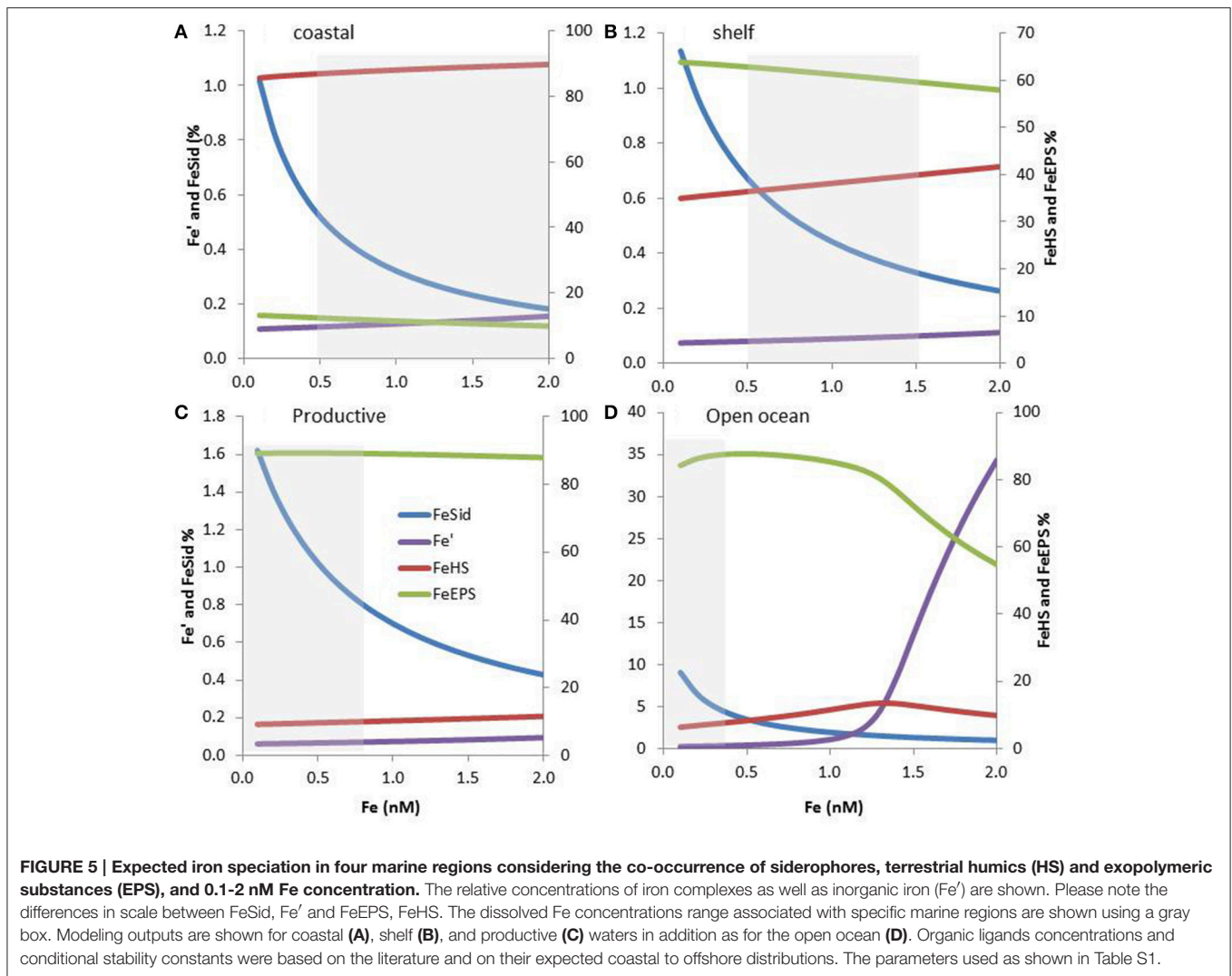
Broad Zonation of Ligand Distributions

Geographical Zonation of Organic Ligands

The terrestrial provenance of HS points to them being the dominant ligand type in coastal regions (Figure 4), with HS concentration decreasing with distance to the coast (due to dilution and mixing). Indeed, in our modeling projection, HS dominate the ligands pool in coastal water, representing up to 90% of the three groups of ligands considered here. With 85–90% of Fe bound to HS, HS dominate Fe biogeochemistry, hence representing an important group of L₂ ligands in coastal waters (Figure 5A). As we move out of the coast, HS decreases up to one order of magnitude in open ocean water, and there do not dominate Fe biogeochemistry (Figure 5D). Geographical land mass distributions and freshwater run-off patterns are thus key factors for the distribution of HS throughout the ocean. HS are expected to be a class of Fe-binding ligand that is present in significant amount both in surface coastal waters representing up to 18% of the DOC and ligands (Laglera and van den Berg, 2009; Bundy et al., 2014). Hence, HS will likely dominate the ligand pool in the Arctic which is close to riverine and sedimentary inputs. The Arctic is indeed a major source of DOC to the Atlantic Ocean (Benner et al., 2005). Terrestrial HS signatures based on ²²⁸Ra were also found for most of the Equatorial to temperate Indian Ocean (Kwon et al., 2014), where HS are expected to be significant contributors to the overall ligand pool. However, due to limited land mass, lower ²²⁸Ra signatures (Kwon et al., 2014) and thus lower input of HS is expected in the South Pacific and the Southern Ocean revealing large geographical demarcations between North and South hemispheres.

Oceanographic regionalization of organic ligands is also associated with the distribution of nutrients and chlorophyll *a* (Chl *a* as a proxy of biomass). In areas rich in nutrients and Chl *a*, usually observed in coastal, shelf and upwelling regions, organic ligands related to biological basal activity (EPS, saccharides, HS-like from excretion) could be a significant contributor to the group of organic ligands (see references herein, Figure 4). EPS can contribute to a significant amount of DOC, from ~1% up to 50% of DOC in extreme bloom situations (Orellana et al., 2003) and EPS could thus dominate the organic ligands pool in phytoplankton blooms. Given that more than 1000 cells/mL are reported across areas associated with low Chl *a* (e.g., gyres, northern Tasman Sea; Hassler et al., 2014), EPS are expected to be associated with a significant baseline signature in L₂ligands (Figure 4). In our numerical exercise, the decrease of HS from coastal to the shelf waters, makes that HS and EPS are equally contributing to the L₂ ligands pool, hence resulting in a complex situation where both EPS and HS contribute to FeL₂ complexes (Figure 5B). In productive regions, EPS could represent up to 80% of the ligands, resulting in 88–89% of the iron being bound to EPS, Fe biogeochemistry in these regions are thus dominated by EPS (Figure 5C).

In the open ocean, the distinction between Fe and macronutrient limitation (Table 2) differentiates between High Nutrient Low Chlorophyll (HNLC) and Low Nutrient Low Chlorophyll (LNLC) surface waters, respectively (Moore et al., 2013). Iron is an important primary or secondary limiting nutrient in most of these waters, which together represent more than 30% of the ocean (Boyd and Ellwood, 2010). In these regions, ligands excreted specifically in response to Fe stress such as siderophores are expected to be more abundant. Therefore, as recently observed in South Pacific waters (Boiteau et al., 2016a; Repeta et al., 2016), siderophore production is



expected to increase from inshore (Fe-replete) to offshore (often Fe-limited; **Figure 4**). Because siderophores are reported at low levels (pM; Mawji et al., 2008, 2011; Boiteau et al., 2016b) they never dominate the total organic ligand pool. However, in all numerical projections (**Figures 3, 5**), siderophores are saturated with iron, making them efficient for bacterial nutrition (see Section Implications of the Co-Existence of Iron-Binding Ligands). Because of EPS is present in significant amount in open ocean waters, they tend to dominate the L_2 ligand pool (**Figure 5D**).

Differences in organic ligand (HS-like) recycling in surface waters as well as remineralization at depth are expected between high and low Chl *a* regions, providing a geographical basis to identify differences between recycled and remineralized ligands. In oligotrophic regions, comprising most of the open ocean and high latitude regions (Moore et al., 2013), recycling of organic compounds, and nutrients is expected to be efficient despite the low biomass. Indeed, in HNLC regions such as the remote Southern Ocean, Fe recycling is efficient, providing up

to 90% of the Fe required to sustain phytoplankton growth (Hutchins et al., 1993; Strzepek et al., 2005; Sarthou et al., 2008; Poorvin et al., 2011). Alternatively, in high Chl *a* regions, which are mainly nutrient-replete, production rates of organic matter is high but recycling rates for organic matter and nutrients are often lower. The remineralization rates for DOC exported at depth from Hansell et al. (2012) provide an interesting framework to further reflect on potential global distribution of HS-like ligands associated with remineralization. Indeed, maximal remineralization rates were determined in the subtropical gyres and in the regions of deep-water formation in the North Hemisphere. On the other hand, in productive areas such as upwelling regions and in the Southern Ocean, remineralization rates were minimal.

Recent basin-scale studies in the Atlantic revealed a large-scale pattern for organic ligand concentrations and conditional stability constants (Buck et al., 2015; Gerringa et al., 2015) with greater concentrations of organic ligands at high latitudes. Weaker stability constants were reported in the Arctic whereas

the strongest ligands were reported in the Southern Ocean (Gerringa et al., 2015). The weaker conditional stability constants in the North could be attributed to large input of HS from the coast, contributing to L₂ and L₃ ligand classes, whereas in the South, strong ligands are likely due to widespread Fe limitation (siderophores) which prevail in the pelagic regions of the Southern Ocean (Tables 1, 2; e.g., Ibisami et al., 2011). From our zonation, differences in organic ligands at depth would also be expected from North to South with a dominance of HS and recently formed HS-like from sedimentary input and remineralization in the North, and HS-like from hydrothermal vents in the South. However, as stated earlier, we currently lack information about the specific chemical and structural signature of these organic compounds to refine their predicted zonation.

Vertical Zonation

Siderophore and EPS could contribute to the L₁ ligands detected in surface water, however the discrepancy between siderophore (pM) and L₁ concentrations (nM) suggest an important missing term, which is also the case for deep water (Figure 1A; Buck et al., 2015). Whether this discrepancy results from an analytical limitation to detect siderophores and/or whether other types of ligands are contributing remains unclear. In surface water, major constituents of the L₂ class are jointly attributed to external input (coastal, dust, rain, hydrothermal vents, and sea-ice) and biological activity related to (i) basal activity, (ii) iron limitation, and (iii) recycling (Table 1). The relative importance of the ligands constituting the L₁–L₄ pool clearly depends on location, season and regional characteristics (Table 2); but HS, augmented by *in-situ* produced HS-like, are expected to contribute to an important baseline of Fe binding ligands. Three major impasses lie ahead to further constrain the relative contribution of L₁ and L₂–L₄ ligands in surface waters: (i) a better delineation of basin-scale and seasonal distribution of L₁ ligands in surface waters, (ii) kinetic experiments needed for probing production rate and residence time of the different *in-situ* ligands, (iii) multiple analytical detection of ligands to better constrain the distribution, nature, and sources of strong but also weak ligands.

Ligand longevity or turnover is important to define in which depth strata specific ligands are observed (Figure 5A). Short-lived ligands are likely to be detected close to their sources of production and will not accumulate at depth. Given that siderophore concentrations do not increase with depth, they could be associated with short-lived compounds. However, at present, we cannot comment further on siderophore longevity as we know little on their loss terms and recycling rate, and their detection throughout the water column is limited due to their small concentration. Saccharides and EPS are expected to dominate in surface waters as extremely short-lived compounds with residence time of the order of hours. However, processes at depth associated with EPS aggregation, export, buoyant particles, and whether EPS remineralization results in HS-like substance could significantly affect such a view (see references herein). Long-lived compounds such as HS with a longevity exceeding the global overturning circulation will accumulate in deep waters (see reference herein).

In addition to longevity, remineralization is an important determinant of the distribution of organic ligands at depth (Figure 1B). Given that HS is part of the pool of recalcitrant DOC, their contribution to remineralization is expected to be minor as compared to HS-like (see references herein). Due to residence time >1 year and their presence within microgel, saccharides, EPS, and proteins are also expected in this subsurface pool (Repeta and Aluwihare, 2006; Orellana and Hansell, 2012). As stated earlier, siderophores are expected to occur but at extremely low concentrations, unlikely to be detected by complexometric titrations. We currently lack functional and structural delineation amongst HS, and the numerous sources of HS-like material, to further differentiate amongst these organic ligands. For example, due to the many sources of HS-like ligands and their limited characterization, it remains unclear whether EPS could be a good proxy for HS-like from biological activity, recycling and remineralization. Below 1000 m depth, both DOC and Fe-binding ligands decrease along the global circulation path across ocean basins (Gledhill and Buck, 2012; Hansell et al., 2012; Gerringa et al., 2015). This suggests that long-lived refractory Fe-binding ligands, such as HS and HS-like substances (as measured by chemical, functional, and structural studies; Laglera et al., 2007; Catala et al., 2015; Medeiros et al., 2016) are present in deep water in all ocean basins. In this case both HS and HS-like from remineralization, terrestrial inputs and possibly hydrothermal vents could be important contributors of the ligand soup at depth. In the deep ocean, the composition of the ligands soup is expected to be quite homogeneous and stable as compared to the surface waters.

Regional Geographical Zonation of Organic Ligands

Regional variation in organic ligands is expected in relation to specific distribution of their sources and seasonality that can in time be overlaid onto the broad zonation presented above (Figure 4). In large river plumes (such as the Amazon and Mississippi Rivers; e.g., Powell and Wilson-Finelli, 2003), HS would be expected to dominate the pool of organic ligands (Figure 5A). Moreover, the relative contribution of HS, from rivers, coast and upwelling regions, to the ligand “soup” is predicted to be seasonally influenced with changing strength in precipitation as well as variability in the intensity of boundary currents and upwelling (Bakun and Nelson, 1991).

Atmospheric dry and wet deposition can also carry significant amount of iron-binding organic ligands (Cheize et al., 2012; Paris and Desboeufs, 2013; Table 1). Based on patterns of global desert dust deposition into the ocean, organic ligands originating from atmospheric sources might be important in the subarctic Western Pacific, North and equatorial Atlantic (including the West African upwelling region), and North and equatorial Indian Oceans, as well as in the Mediterranean and Tasman Seas (Price and Morel, 1998; Jickells et al., 2005; Mahowald et al., 2005; Cropp et al., 2013; Guieu et al., 2014). Dust deposition is highly seasonal, peaking often in summer but overlaid with strong episodic deposition (e.g., Price and Morel, 1998; Jickells et al., 2005; Cropp et al., 2013). The extent of wet deposition of organic

ligands would be dependent on precipitation. For example, based on NASA's Tropical Rainfall Measuring Mission satellite (<https://pmm.nasa.gov/trmm>), precipitation has a consistent seasonality—for example heavy rain moves along the Equator in a seasonal pattern. Moreover, a significant amount of organic ligands is expected to be deposited at the time of monsoon (April–September) in the equatorial to temperate Indian and Pacific Oceans. Seasonal and geographical patterns of iron concentrations in rain suggests similar pattern in organic ligands with greater concentrations measured in spring and summer, as well as close to the coast (Willey et al., 2000). It is to be noted that the variability in the contribution and content of organic ligands associated with dry and wet deposition from differing sources (e.g., volcanic, desert, biomass burning, and anthropogenic) is mostly undocumented yet.

Sea-ice and icebergs can also be a significant source of organic ligands, but their influence is relevant only at high latitudes, in open ocean waters which are mostly iron-limited (Moore et al., 2013), but also close to the coast of Antarctica and the land masses associated with the Arctic region. At the time of Antarctic sea-ice melt, as the brine channels open, an important and rapid release of dissolved iron and organic ligands was observed (Lannuzel et al., 2007, 2015), suggesting a strong seasonal input (**Table 2**).

HS-like ligands from subsurface remineralization (Boyd et al., 2010; Heller et al., 2013; Medeiros et al., 2016) are expected to dominate in upwelling regions that are not under the major influence from hydrothermal inputs (e.g., Equator, Arabian Sea, Brazil Current, Peru, and Californian upwelling regions). Recently, studies have shown that hydrothermal vents can carry organic ligands and contribute to upwelled sources with significant (>10%) impact on downward particulate carbon export for most of the Southern Ocean below the Polar Front, north of New Zealand and south of 40°S in the Pacific Ocean (Resing et al., 2015), resulting in potential geographical differences amongst upwelled ligands. A better characterization of organic ligands from hydrothermal vents and their susceptibility to bacterial transformation would thus provide invaluable details for these areas.

Phytoplankton seasonal blooms usually occur in spring and autumn, episodes that will likely affect the composition of organic ligands. In bloom situations, biologically-produced ligands related to metabolic basal activity (e.g., EPS, saccharides; Orellana and Hansell, 2012) are likely to be dominant (**Figure 5C**). Indeed, under bloom situation the EPS from *Phaeocystis* could represent up to 50% of the *in-situ* DOC (Orellana et al., 2003). It is expected that, as the bloom evolves, either nutrient limitation will develop, resulting in the production of specific ligands (e.g., DA, siderophores), or grazing events will terminate the bloom resulting in the release of degradation products. Finally, frontal zones between major currents are usually associated with high Chl *a* variability compared to the surrounding waters (Belkin et al., 2009). Frontal regions are also reported to be important source regions for marine proteins such as Rubisco (Orellana and Hansell, 2012), suggesting that biologically-produced organic ligands might be important in frontal regions, a hypothesis that

could be readily tested as part of future GEOTRACES voyages that cross such transition zones.

OUTLOOK

Our understanding of organic ligands is currently too limited to draw a detailed map of their relative distribution, however, we have demonstrated that differences in the contribution of a range of organic ligands to the bulk ligand pool can be expected across oceanic regions from coastal to offshore and from surface to deep waters. These broad trends can be built upon by superimposing regional inputs, seasonal trends, and patterns in biomass and nutrient limitation (**Table 2**) onto them. In addition to these spatial patterns, a strong seasonality is expected for different ligand types, with greater organic ligand input from coastal, sea-ice, atmospheric, and biological sources in spring-summer whereas more HS-like ligands from remineralization are expected to reach surface waters in winter as vertical density gradients decrease. This combination of spatial and temporal gradients in different ligands supports our contention that a holistic viewpoint of the multi-faceted controls on ligands dynamics leading to a regional classification is essential to begin to understand why some ligands dominate in particular oceanic regions, depth strata, or exhibit seasonality and/or lateral gradients.

We advocate a number of approaches that will help to assign where this wide range of molecules fit across the spectrum of ligands that comprise the bulk ligand pool. For example, in order to track specific ligands and assess their distribution and residence time within the ocean, basin-scale studies simultaneously employing different techniques (such as liquid chromatography, mass spectroscopy, and electrochemistry) able to capture the diversity in composition and functions of organic ligands need to be complemented with isotopic and process studies testing specific analytical signatures related to sources. Such a trans-disciplinary approach will enable progress in resolving the nature of HS-like, as well as identifying what other components make up the rest of the strong L₁ ligand. Because many type of organic ligands and trace element co-occur in seawater their ability to compete need to be further investigated. Further work using the distribution of ligands sources as well as a combination of proxies for key processes is required to take this regional approach further and provide a global picture of the distribution of the significant iron-binding organic ligands. Additionally, processes studies are required to refine biological sources and turn-over rates of organic ligands. The regional classification of ligands proposed here should however, help to interpret datasets from on-going global surveys, design future experiments, and improve biogeochemical models.

AUTHOR CONTRIBUTIONS

All authors listed, have made substantial, direct and intellectual contribution to the work, and approved it for publication.

FUNDING

CH was funded by a SNF Professor Fellowship (PP00P2_138955). PB received support from an Australian Research Council Australian Laureate Fellowship project FL160100131 and Discovery Project DP130100679. Cv acknowledges general support from the University of Liverpool.

ACKNOWLEDGMENTS

Authors would like to thank Dr. Louiza Norman, Mr. Damien Cabanes, and Ms. Sonia Blanco-Almeijeiras for their

REFERENCES

- Abualhija, M. M., and van den Berg, C. M. G. (2014). Chemical speciation of iron in seawater using catalytic cathodic stripping voltammetry with ligand competition against salicylaldehyde. *Mar. Chem.* 164, 60–74. doi: 10.1016/j.marchem.2014.06.005
- Abualhija, M. M., Whitby, H., and van den Berg, C. M. G. (2015). Competition between copper and iron for humic ligands in estuarine waters. *Mar. Chem.* 172, 46–56. doi: 10.1016/j.marchem.2015.03.010
- Adly, C. L., Tremblay, J. E., Powell, R. T., Armstrong, E., Peers, G., and Price, N. M. (2015). Response of heterotrophic bacteria in a mesoscale iron enrichment in the northeast subarctic Pacific Ocean. *Limnol. Oceanogr.* 60, 136–148. doi: 10.1002/lno.10013
- Amin, S. A., Green, D. H., Kupper, F. C., and Carrano, C. J. (2009). Vibrio ferrin, an unusual marine siderophore: iron binding, photochemistry, and biological implications. *Inorg. Chem.* 48, 11451–11458. doi: 10.1021/ic9016883
- Aristilde, L., Xu, Y., and Morel, F. M. M. (2012). Weak organic ligands enhance zinc uptake in marine phytoplankton. *Environ. Sci. Technol.* 46, 5438–5445. doi: 10.1021/es300335u
- Azam, F., and Malfatti, F. (2007). Microbial structuring of marine ecosystems. *Nat. Rev. Microbiol.* 5, 782–791. doi: 10.1038/nrmicro1747
- Azetsu-Scott, K., and Passow, U. (2004). Ascending marine particles: significance of transparent exopolymer particles (TEP) in the upper ocean. *Limnol. Oceanogr.* 49, 741–748. doi: 10.4319/lo.2004.49.3.0741
- Baakza, A., Vala, A. K., Dave, B. P., and Dube, H. C. (2004). A comparative study of siderophore production by fungi from marine and terrestrial habitats. *J. Exp. Mar. Biol. Ecol.* 311, 1–9. doi: 10.1016/j.jembe.2003.12.028
- Baars, O., and Croot, P. L. (2015). Dissolved cobalt speciation and reactivity in the eastern tropical North Atlantic. *Mar. Chem.* 173, 310–319. doi: 10.1016/j.marchem.2014.10.006
- Bakun, A., and Nelson, C. S. (1991). The seasonal cycle of wind-stress curl in the subtropical easterly boundary current regions. *J. Phys. Oceanogr.* 21, 1815–1834. doi: 10.1175/1520-0485(1991)021<1815:TSCOWS>2.0.CO;2
- Barbeau, K., Moffett, J. W., Caron, D. A., Croot, P. L., and Erdner, D. L. (1996). Role of protozoan grazing in relieving iron limitation of phytoplankton. *Nature* 380, 61–64. doi: 10.1038/380061a0
- Barbeau, K., Rue, E. L., Bruland, K. W., and Butler, A. (2001). Photochemical cycling of iron in the surface ocean mediated by microbial iron(III)-binding ligands. *Nature* 413, 409–413. doi: 10.1038/35096545
- Batchelli, S., Muller, F. L. L., Chang, K. C., and Lee, C. L. (2010). Evidence for strong but dynamic iron-humic colloidal associations in humic-rich coastal waters. *Environ. Sci. Technol.* 44, 8485–8490. doi: 10.1021/es101081c
- Belkin, I. M., Cornillon, P. C., and Sherman, K. (2009). Fronts in large marine ecosystems. *Prog. Oceanogr.* 81, 223–236. doi: 10.1016/j.pocean.2009.04.015
- Benner, R. (2011). Loose ligands and available iron in the ocean. *Proc. Natl. Acad. Sci. U.S.A.* 108, 893–894. doi: 10.1073/pnas.1018163108
- Benner, R., Louchouart, P., and Amon, R. M. W. (2005). Terrigenous dissolved organic matter in the Arctic Ocean and its transport to surface and deep waters of the North Atlantic. *Global Biogeochem. Cycles* 19:11. doi: 10.1029/2004GB002398
- Benner, R., Pakulski, J. D., McCarthy, M., Hedges, J. I., and Hatcher, P. G. (1992). Bulk chemical characteristics of dissolved organic-matter in the ocean. *Science* 255, 1561–1564. doi: 10.1126/science.255.5051.1561
- Blanco-Ameijeiras, S., and Hassler, C. (2015). Iron limitation in the cyanobacteria *Synechococcus* SP.: from gene expression to physiological responses. *Eur. J. Phycol.* 50:92.
- Boiteau, R. M., Fitzsimmons, J. N., Repeta, D. J., and Boyle, E. A. (2013). Detection of iron ligands in seawater and marine cyanobacteria cultures by high-performance liquid chromatography-inductively coupled plasma-mass spectrometry. *Anal. Chem.* 85, 4357–4362. doi: 10.1021/ac3034568
- Boiteau, R. M., Mende, D. R., Hawco, N. J., McIlvin, M. R., Fitzsimmons, J. N., Saito, M. A., et al. (2016a). Siderophore-based microbial adaptations to iron scarcity across the eastern Pacific Ocean. *Proc. Nat. Acad. Sci. U.S.A.* 113, 14237–14242. doi: 10.1073/pnas.1608594113
- Boiteau, R. M., and Repeta, D. J. (2015). An extended siderophore suite from *Synechococcus* sp. PCC 7002 revealed by LC-ICPMS-ESIMS. *Metallomics* 7, 877–884. doi: 10.1039/C5MT00005J
- Boiteau, R. M., Mende, D. R., Hawco, N. J., McIlvin, M. R., Fitzsimmons, J. N., Saito, M. A., et al. (2016b). Structural characterization of nickel and copper binding ligands along the US GEOTRACES eastern Pacific zonal transect. *Front. Mar. Sci.* 3:243. doi: 10.3389/fmars.2016.00243
- Bonnain, C., Breitbart, M., and Buck, K. N. (2016). The ferrojan horse hypothesis: iron-virus interactions in the ocean. *Front. Mar. Sci.* 3:82. doi: 10.3389/fmars.2016.00082
- Bordovsky, O. K. (1957). Humic substances in the deposits of the western part of the Bering Sea. *Dokl. Akad. Nauk. SSSR* 113, 157–160.
- Bown, J., Boye, M., and Nelson, D. M. (2012). New insights on the role of organic speciation in the biogeochemical cycle of dissolved cobalt in the southeastern Atlantic and the Southern Ocean. *Biogeosciences* 9, 2719–2736. doi: 10.5194/bg-9-2719-2012
- Boyd, P. W., Arrigo, K. R., Strzepek, R., and van Dijken, G. L. (2012). Mapping phytoplankton iron utilization: insights into southern ocean supply mechanisms. *J. Geophys. Res. Oceans* 117. doi: 10.1029/2011JC007726
- Boyd, P. W., and Ellwood, M. J. (2010). The biogeochemical cycle of iron in the ocean. *Nat. Geosci.* 3, 675–682. doi: 10.1038/ngeo964
- Boyd, P. W., Goldblatt, R. H., and Harrison, P. J. (1999). Mesozooplankton grazing manipulations during *in vitro* iron enrichment studies in the NE subarctic Pacific. *Deep Sea Res. Part II Top. Stud. Oceanogr.* 46, 2645–2668. doi: 10.1016/S0967-0645(99)00079-X
- Boyd, P. W., Ibsanmi, E., Sander, S. G., Hunter, K. A., and Jackson, G. A. (2010). Remineralization of upper ocean particles: Implications for iron biogeochemistry. *Limnol. Oceanogr.* 55, 1271–1288. doi: 10.4319/lo.2010.55.3.1271
- Boyd, P. W., Law, C. S., Hutchins, D. A., Abraham, E. R., Croot, P. L., Ellwood, M., et al. (2005). FeCycle: attempting an iron biogeochemical budget from a mesoscale SF6 tracer experiment in unperturbed low iron waters. *Global Biogeochem. Cycles* 19:GB4S20. doi: 10.1029/2005GB002494
- Boyd, P. W., and Tagliabue, A. (2015). Using the L* concept to explore controls on the relationship between paired ligand and dissolved iron concentrations in the ocean. *Mar. Chem.* 173, 52–66. doi: 10.1016/j.marchem.2014.12.003

SUPPLEMENTARY MATERIAL

The Supplementary Material for this article can be found online at: <http://journal.frontiersin.org/article/10.3389/fmars.2017.00019/full#supplementary-material>

- Boye, M., Nishioka, J., Croot, P., Laan, P., Timmermans, K. R., Strass, V. H., et al. (2010). Significant portion of dissolved organic Fe complexes in fact is Fe colloids. *Mar. Chem.* 122, 20–27. doi: 10.1016/j.marchem.2010.09.001
- Boye, M., van den Berg, C. M. G., de Jong, J. T. M., Leach, H., Croot, P., and de Baar, H. J. W. (2001). Organic complexation of iron in the Southern Ocean. *Deep Sea Res. Part I Oceanogr. Res. Pap.* 48, 1477–1497. doi: 10.1016/S0967-0637(00)00099-6
- Bruland, K. W., Rue, E. L., Smith, G. J., and DiTullio, G. R. (2005). Iron, macronutrients and diatom blooms in the Peru upwelling regime: brown and blue waters of Peru. *Mar. Chem.* 93, 81–103. doi: 10.1016/j.marchem.2004.06.011
- Buck, K. N., Lohan, M. C., Berger, C. J. M., and Bruland, K. W. (2007). Dissolved iron speciation in two distinct river plumes and an estuary: implications for riverine iron supply. *Limnol. Oceanogr.* 52, 843–855. doi: 10.4319/lo.2007.52.2.0843
- Buck, K. N., Sohst, B., and Sedwick, P. N. (2015). The organic complexation of dissolved iron along the U.S. GEOTRACES (GA03) North Atlantic Section. *Deep Sea Res. Part II Top. Stud. Oceanogr.* 116, 152–165. doi: 10.1016/j.dsr2.2014.11.016
- Bundy, R. M., Abdulla, H. A. N., Hatcher, P. G., Biller, D. V., Buck, K. N., and Barbeau, K. A. (2015). Iron-binding ligands and humic substances in the San Francisco Bay estuary and estuarine-influenced shelf regions of coastal California. *Mar. Chem.* 173, 183–194. doi: 10.1016/j.marchem.2014.11.005
- Bundy, R. M., Biller, D. V., Buck, K. N., Bruland, K. W., and Barbeau, K. A. (2014). Distinct pools of dissolved iron-binding ligands in the surface and benthic boundary layer of the California Current. *Limnol. Oceanogr.* 59, 769–787. doi: 10.4319/lo.2014.59.3.0769
- Bundy, R. M., Jiang, M., Carter, M., and Barbeau, K. A. (2016). Iron-binding ligands in the Southern California current system: mechanistic studies. *Front. Mar. Sci.* 3:27. doi: 10.3389/fmars.2016.00027
- Burkhardt, B. G., Watkins-Brandt, K. S., Defforey, D., Paytan, A., and White, A. E. (2014). Remineralization of phytoplankton-derived organic matter by natural populations of heterotrophic bacteria. *Mar. Chem.* 163, 1–9. doi: 10.1016/j.marchem.2014.03.007
- Butler, A., and Theisen, R. M. (2010). Iron(III)-siderophore coordination chemistry: Reactivity of marine siderophores. *Coord. Chem. Rev.* 254, 288–296. doi: 10.1016/j.ccr.2009.09.010
- Caprara, S., Buck, K. N., Gerringa, L. J. A., Rijkenberg, M. J. A., and Monticelli, D. A. (2016). Compilation of iron speciation data for open oceanic waters. *Front. Mar. Sci.* 3:221. doi: 10.3389/fmars.2016.00221
- Castruita, M., Shaked, Y., Elmegreen, L. A., Stiefel, E. I., and Morel, F. M. M. (2008). Availability of iron from iron-storage proteins to marine phytoplankton. *Limnol. Oceanogr.* 53, 890–899. doi: 10.4319/lo.2008.53.3.0890
- Catala, T. S., Alvarez-Salgado, X. A., Otero, J., Iuculano, F., Companys, B., Horstkotte, B., et al. (2016). Drivers of fluorescent dissolved organic matter in the global epipelagic ocean. *Limnol. Oceanogr.* 61, 1101–1119. doi: 10.1002/lno.10281
- Catala, T. S., Reche, I., Fuentes-Lema, A., Romera-Castillo, C., Nieto-Cid, M., Ortega-Retuerta, E., et al. (2015). Turnover time of fluorescent dissolved organic matter in the dark global ocean. *Nat. Commun.* 6, 917–934. doi: 10.1038/ncomms6986
- Cheize, M., Sarthou, G., Croot, P. L., Bucciarelli, E., Baudoux, A.-C., and Baker, A. R. (2012). Iron organic speciation determination in rainwater using cathodic stripping voltammetry. *Anal. Chim. Acta* 736, 45–54. doi: 10.1016/j.aca.2012.05.011
- Coale, K. H., Fitzwater, S. E., Gordon, R. M., Johnson, K. S., and Barber, R. T. (1996). Control of community growth and export production by upwelled iron in the equatorial Pacific Ocean. *Nature* 379, 621–624. doi: 10.1038/379621a0
- Coble, P. G. (2007). Marine optical biogeochemistry: the chemistry of ocean color. *Chem. Rev.* 107, 402–418. doi: 10.1021/cr050350+
- Cordero, O. X., Ventouras, L. A., DeLong, E. F., and Polz, M. F. (2012). Public good dynamics drive evolution of iron acquisition strategies in natural bacterioplankton populations. *Proc. Natl. Acad. Sci. U.S.A.* 109, 20059–20064. doi: 10.1073/pnas.1213344109
- Croot, P. L., and Heller, M. I. (2012). The importance of kinetics and redox in the biogeochemical cycling of iron in the surface ocean. *Front. Microbiol.* 3:219. doi: 10.3389/fmicb.2012.00219
- Croot, P. L., and Johansson, M. (2000). Determination of iron speciation by cathodic stripping voltammetry in seawater using the competing ligand 2-(2-thiazolylazo)-p-cresol (TAC). *Electroanalysis* 12, 565–576. doi: 10.1002/(SICI)1521-4109(200005)12:8<565::AID-ELAN565>3.0.CO;2-L
- Cropp, R. A., Gabric, A. J., Levasseur, M., McTainsh, G. H., Bowie, A., Hassler, C. S., et al. (2013). The likelihood of observing dust-stimulated phytoplankton growth in waters proximal to the Australian continent. *J. Mar. Syst.* 117, 43–52. doi: 10.1016/j.jmarsys.2013.02.013
- de Brouwer, J. F. C., Wolfstein, K., Ruddy, G. K., Jones, T. E. R., and Stal, L. J. (2005). Biogenic stabilization of intertidal sediments: the importance of extracellular polymeric substances produced by benthic diatoms. *Microb. Ecol.* 49, 501–512. doi: 10.1007/s00248-004-0020-z
- Decho, A. W. (1990). Microbial exopolymer secretions in ocean environments - their role(s) in food webs and marine processes. *Oceanogr. Mar. Biol.* 28, 73–153.
- DiTullio, G. R., Grebmeier, J. M., Arrigo, K. R., Lizotte, M. P., Robinson, D. H., Leventer, A., et al. (2000). Rapid and early export of Phaeocystis antarctica blooms in the Ross Sea, Antarctica. *Nature* 404, 595–598. doi: 10.1038/35007061
- Duce, R. A., and Tindale, N. W. (1991). Atmospheric transport of iron and its deposition in the ocean. *Limnol. Oceanogr.* 36, 1715–1726. doi: 10.4319/lo.1991.36.8.1715
- Dupont, C. L., Moffett, J. W., Bidigare, R. R., and Ahner, B. A. (2006). Distributions of dissolved and particulate biogenic thiols in the subarctic Pacific Ocean. *Deep Sea Res. Part I Oceanogr. Res. Pap.* 53, 1961–1974. doi: 10.1016/j.dsr.2006.09.003
- Dupont, C. L., Nelson, R. K., Bashir, S., Moffett, J. W., and Ahner, B. A. (2004). Novel copper-binding and nitrogen-rich thiols produced and exuded by *Emiliania huxleyi*. *Limnol. Oceanogr.* 49, 1754–1762. doi: 10.4319/lo.2004.49.5.1754
- Ellwood, M. J., van den Berg, C. M. G., Boye, M., Veldhuis, M., de Jong, J. T. M., de Baar, H. J. W., et al. (2005). Organic complexation of cobalt across the Antarctic Polar Front in the Southern Ocean. *Mar. Freshw. Res.* 56, 1069–1075. doi: 10.1071/MF05097
- Fishwick, M. P., Sedwick, P. N., Lohan, M. C., Worsfold, P. J., Buck, K. N., Church, T. M., et al. (2014). The impact of changing surface ocean conditions on the dissolution of aerosol iron. *Global Biogeochem. Cycles* 28, 1235–1250. doi: 10.1002/2014GB004921
- Fitzsimmons, J. N., Bundy, R. M., Al-Subiai, S. N., Barbeau, K. A., and Boyle, E. A. (2015). The composition of dissolved iron in the dusty surface ocean: an exploration using size-fractionated iron-binding ligands. *Mar. Chem.* 173, 125–135. doi: 10.1016/j.marchem.2014.09.002
- Gerringa, L. J. A., Rijkenberg, M. J. A., Schoemann, V., Laan, P., and de Baar, H. J. W. (2015). Organic complexation of iron in the West Atlantic Ocean. *Mar. Chem.* 177, 434–446. doi: 10.1016/j.marchem.2015.04.007
- Gerringa, L. J. A., Rijkenberg, M. J. A., Thuroczy, C.-E., and Maas, L. R. M. (2014). A critical look at the calculation of the binding characteristics and concentration of iron complexing ligands in seawater with suggested improvements. *Environ. Chem.* 11, 114–136. doi: 10.1071/EN13072
- Gerringa, L. J. A., Rijkenberg, M. J. A., Wolterbeek, H. T., Verburg, T. G., Boye, M., and de Baar, H. J. W. (2007). Kinetic study reveals weak Fe-binding ligand, which affects the solubility of Fe in the Scheldt estuary. *Mar. Chem.* 103, 30–45. doi: 10.1016/j.marchem.2006.06.002
- Gledhill, M., Achterberg, E. P., Honey, D. J., Nielsdottir, M. C., and Rijkenberg, M. J. A. (2013). Distributions of particulate Heme b in the Atlantic and Southern Oceans—Implications for electron transport in phytoplankton. *Global Biogeochem. Cycles* 27, 1072–1082. doi: 10.1002/2013GB004639
- Gledhill, M., and Buck, K. N. (2012). The organic complexation of iron in the marine environment: a review. *Front. Microbiol.* 3:69. doi: 10.3389/fmicb.2012.00069
- Gledhill, M., and van den Berg, C. M. G. (1994). Determination of complexation of iron(III) with natural organic complexing ligands in seawater using cathodic stripping voltammetry. *Mar. Chem.* 47, 41–54. doi: 10.1016/0304-4203(94)90012-4
- Gobler, C. J., Donat, J. R., Consolvo, J. A., and Sañudo-Wilhelmy, S. A. (2002). Physicochemical speciation of iron during coastal algal blooms. *Mar. Chem.* 77, 71–89. doi: 10.1016/S0304-4203(01)00076-7

- Granger, J., and Price, N. M. (1999). The importance of siderophores in iron nutrition of heterotrophic marine bacteria. *Limnol. Oceanogr.* 44, 541–555. doi: 10.4319/lo.1999.44.3.0541
- Guiu, C., Ridame, C., Pulido-Villena, E., Bressac, M., Desboeufs, K., and Dulac, F. (2014). Impact of dust deposition on carbon budget: a tentative assessment from a mesocosm approach. *Biogeosciences* 11, 5621–5635. doi: 10.5194/bg-11-5621-2014
- Hansell, D. A. (2013). “Recalcitrant dissolved organic carbon fractions,” in *Annual Review of Marine Science*, Vol. 5, eds C. A. Carlson and S. J. Giovannoni (Palo Alto, CA: Annual Reviews), 421–445.
- Hansell, D. A., Carlson, C. A., and Schlitzer, R. (2012). Net removal of major marine dissolved organic carbon fractions in the subsurface ocean. *Global Biogeochem. Cycles* 26. doi: 10.1029/2011GB004069
- Harvey, G. R., Boran, D. A., Chesal, L. A., and Tokar, J. M. (1983). The structure of marine fulvic and humic acids. *Mar. Chem.* 12, 119–132. doi: 10.1016/0304-4203(83)90075-0
- Haselwandter, K. (1995). Mycorrhizal fungi - Siderophore production. *Crit. Rev. Biotechnol.* 15, 287–291. doi: 10.3109/07388559509147414
- Hassler, C. S., Alasonati, E., Nichols, C. A. M., and Slaveykova, V. I. (2011a). Exopolysaccharides produced by bacteria isolated from the pelagic Southern Ocean - Role in Fe binding, chemical reactivity, and bioavailability. *Mar. Chem.* 123, 88–98. doi: 10.1016/j.marchem.2010.10.003
- Hassler, C. S., Legiret, F. E., and Butler, E. C. V. (2013). Measurement of iron chemical speciation in seawater at 4°C: the use of competitive ligand exchange-adsorptive cathodic stripping voltammetry. *Mar. Chem.* 149, 63–73. doi: 10.1016/j.marchem.2012.12.007
- Hassler, C. S., Ridgway, K. R., Bowie, A. R., Butler, E. C. V., Clementson, L. A., Doblin, M. A., et al. (2014). Primary productivity induced by iron and nitrogen in the Tasman Sea: an overview of the PINTS expedition. *Mar. Freshw. Res.* 65, 517–537. doi: 10.1071/MF13137
- Hassler, C. S., Schoemann, V., Boye, M., Tagliabue, A., Rozmarynowycz, M., and McKay, R. M. L. (2012). “Iron bioavailability in the southern ocean,” in *Oceanography and Marine Biology: An Annual Review*, Vol. 50, eds R. N. Gibson, R. J. A. Atkinson, J. D. M. Gordon, and R. N. Hughes (Palo Alto, CA: Annual Reviews), 1–63.
- Hassler, C. S., Schoemann, V., Nichols, C. M., Butler, E. C. V., and Boyd, P. W. (2011b). Saccharides enhance iron bioavailability to Southern Ocean phytoplankton. *Proc. Natl. Acad. Sci. U.S.A.* 108, 1076–1081. doi: 10.1073/pnas.1010963108
- Hawkes, J. A., Gledhill, M., Connelly, D. P., and Achterberg, E. P. (2013). Characterisation of iron binding ligands in seawater by reverse titration. *Anal. Chim. Acta* 766, 53–60. doi: 10.1016/j.aca.2012.12.048
- Heller, M. I., Gaiero, D. M., and Croot, P. L. (2013). Basin scale survey of marine humic fluorescence in the Atlantic: Relationship to iron solubility and H₂O₂. *Global Biogeochem. Cycles* 27, 88–100. doi: 10.1029/2012GB004427
- Hering, J. G., and Morel, F. M. M. (1989). Slow coordination reactions in seawater. *Geochim. Cosmochim. Acta* 53, 611–618. doi: 10.1016/0016-7037(89)90004-5
- Hernlem, B. J., Vane, L. M., and Sayles, G. D. (1996). Stability constants for complexes of the siderophore desferrioxamine B with selected heavy metal cations. *Inorgan. Chim. Acta* 244, 179–184. doi: 10.1016/0020-1693(95)04780-8
- Hertkorn, N., Benner, R., Frommberger, M., Schmitt-Kopplin, P., Witt, M., Kaiser, K., et al. (2006). Characterization of a major refractory component of marine dissolved organic matter. *Geochim. Cosmochim. Acta* 70, 2990–3010. doi: 10.1016/j.gca.2006.03.021
- Hoagland, K. D., Rosowski, J. R., Gretz, M. R., and Roemer, S. C. (1993). Diatom extracellular polymeric substances - function, fine-structure, chemistry, and physiology. *J. Phycol.* 29, 537–566. doi: 10.1111/j.0022-3646.1993.00537.x
- Hogle, S. L., Bundy, R. M., Blanton, J. M., Allen, E. E., and Barbeau, K. A. (2016). Copiotrophic marine bacteria are associated with strong iron-binding ligand production during phytoplankton blooms. *Limnol. Oceanogr. Lett.* 1, 36–43. doi: 10.1002/lo.10026
- Hudson, R. J. M., and Morel, F. M. M. (1990). Iron transport in marine phytoplankton: kinetics of cellular and medium coordination reactions. *Limnol. Oceanogr.* 35, 1002–1020. doi: 10.4319/lo.1990.35.5.1002
- Hudson, R. J. M., Rue, E. L., and Bruland, K. W. (2003). Modeling complexometric titrations of natural water samples. *Environ. Sci. Technol.* 37, 1553. doi: 10.1021/es025751a
- Hunter, K. A., and Boyd, P. W. (2007). Iron-binding ligands and their role in the ocean biogeochemistry of iron. *Environ. Chem.* 4, 221–232. doi: 10.1071/EN07012
- Hutchins, D. A., DiTullio, G. R., and Bruland, K. W. (1993). Iron and regenerated production: evidence for biological iron recycling in two marine environments. *Limnol. Oceanogr.* 38, 1242–1255. doi: 10.4319/lo.1993.38.6.1242
- Ibisanmi, E., Sander, S. G., Boyd, P. W., Bowie, A. R., and Hunter, K. A. (2011). Vertical distributions of iron-(III) complexing ligands in the Southern Ocean. *Deep Sea Res. Part II Top. Stud. Oceanogr.* 58, 2113–2125. doi: 10.1016/j.dsr2.2011.05.028
- Janse, I., van Rijssel, M., Gottschal, J. C., Lancelot, C., and Gieskes, W. W. C. (1996). Carbohydrates in the North Sea during spring blooms of Phaeocystis: a specific fingerprint. *Aquat. Microbiol. Ecol.* 10, 97–103. doi: 10.3354/ame010097
- Jiao, N., Herndl, G. J., Hansell, D. A., Benner, R., Kattner, G., Wilhelm, S. W., et al. (2010). Microbial production of recalcitrant dissolved organic matter: long-term carbon storage in the global ocean. *Nat. Rev. Microbiol.* 8, 593–599. doi: 10.1038/nrmicro2386
- Jickells, T., Boyd, P. W., and Hunter, K. A. (2014). “Biogeochemical Impacts of Dust on the Global Carbon Cycle,” in *Mineral Dust – A Key Player in the Earth System*, eds P. Knippertz and J.-B. W. Stuut (Heidelberg: Springer), 359–384.
- Jickells, T. D., An, Z. S., Andersen, K. K., Baker, A. R., Bergametti, G., Brooks, N., et al. (2005). Global iron connections between desert dust, ocean biogeochemistry, and climate. *Science* 308, 67–71. doi: 10.1126/science.1105959
- Johnson, K. S., Gordon, R. M., and Coale, K. H. (1997). What controls dissolved iron concentrations in the world ocean? *Mar. Chem.* 57, 137–161. doi: 10.1016/S0304-4203(97)00043-1
- Kirchman, D. L., Moran, X. A. G., and Ducklow, H. (2009). Microbial growth in the polar oceans - role of temperature and potential impact of climate change. *Nat. Rev. Microbiol.* 7, 451–459. doi: 10.1038/nrmicro2115
- Kleint, C., Hawkes, J. A., Sander, S. G., and Koschinsky, A. (2016). Voltammetric investigation of hydrothermal iron speciation. *Front. Mar. Sci.* 3:75. doi: 10.3389/fmars.2016.00075
- Koopal, L. K., Saito, T., Pinheiro, J. P., and van Riemsdijk, W. H. (2005). Ion binding to natural organic matter: general considerations and the NICA–Donnan model. *Colloids Surf. A Physicochem. Eng. Asp.* 265, 40–54. doi: 10.1016/j.colsurfa.2004.11.050
- Krachler, R., Krachler, R. F., Wallner, G., Hann, S., Laux, M., Cervantes Recalde, M. F., et al. (2015). River-derived humic substances as iron chelators in seawater. *Mar. Chem.* 174, 85–93. doi: 10.1016/j.marchem.2015.05.009
- Kraemer, S. M., Butler, A., Borer, P., and Cervini-Silva, J. (2005). “Siderophores and the dissolution of iron-bearing minerals in marine systems,” in *Molecular Geomicrobiology*, eds J. E. Banfield, J. CerviniSilva, and K. H. Nealson (Palo Alto, CA: Mineralogical Society of America), 53–84.
- Kraemer, S. M., Crowley, D. E., and Kretzschmar, R. (2006). Geochemical aspects of phytosiderophore-promoted iron acquisition by plants. *Adv. Agron.* 91, 1–46. doi: 10.1016/S0065-2113(06)91001-3
- Kraemer, S. M., Duckworth, O. W., Harrington, J. M., and Schenkeveld, W. D. C. (2015). Metallophores and trace metal biogeochemistry. *Aquat. Geochem.* 21, 159–195. doi: 10.1007/s10498-014-9246-7
- Kuma, K., Katsumoto, A., Kawakami, H., Takatori, F., and Matsunaga, K. (1998). Spatial variability of Fe(III) hydroxide solubility in the water column of the northern North Pacific Ocean. *Deep Sea Res. Part I Oceanogr. Res. Pap.* 45, 91–113. doi: 10.1016/S0967-0637(97)00067-8
- Kwon, E. Y., Kim, G., Primeau, F., Moore, W. S., Cho, H. M., DeVries, T., et al. (2014). Global estimate of submarine groundwater discharge based on an observationally constrained radium isotope model. *Geophys. Res. Lett.* 41, 8438–8444. doi: 10.1002/2014GL061574
- Laglera, L. M., Battaglia, G., and van den Berg, C. M. G. (2007). Determination of humic substances in natural waters by cathodic stripping voltammetry of their complexes with iron. *Anal. Chim. Acta* 599, 58–66. doi: 10.1016/j.aca.2007.07.059
- Laglera, L. M., and van den Berg, C. M. G. (2009). Evidence for geochemical control of iron by humic substances in seawater. *Limnol. Oceanogr.* 54, 610–619. doi: 10.4319/lo.2009.54.2.0610
- Lannuzel, D., Grotti, M., Abelloschi, M. L., and van der Merwe, P. (2015). Organic ligands control the concentrations of dissolved iron in Antarctic sea ice. *Mar. Chem.* 174, 120–130. doi: 10.1016/j.marchem.2015.05.005

- Lannuzel, D., Schoemann, V., de Jong, J., Chou, L., Delille, B., Becquevort, S., et al. (2008). Iron study during a time series in the western Weddell pack ice. *Mar. Chem.* 108, 85–95. doi: 10.1016/j.marchem.2007.10.006
- Lannuzel, D., Schoemann, V., de Jong, J., Tison, J. L., and Chou, L. (2007). Distribution and biogeochemical behaviour of iron in the East Antarctic sea ice. *Mar. Chem.* 106, 18–32. doi: 10.1016/j.marchem.2006.06.010
- Laurenceau-Cornec, E. C., Trull, T. W., Davies, D. M., De La Rocha, C. L., and Blain, S. (2015). Phytoplankton morphology controls on marine snow sinking velocity. *Mar. Ecol. Prog. Ser.* 520, 35–56. doi: 10.3354/meps11116
- Leal, M. F. C., Vasconcelos, M. T. S. D., and van den Berg, C. M. G. (1999). Copper-induced release of complexing ligands similar to thiols by *Emiliania huxleyi* in seawater cultures. *Limnol. Oceanogr.* 44, 1750–1762. doi: 10.4319/lo.1999.44.7.1750
- Lechtenfeld, O. J., Kattner, G., Flerus, R., McCallister, S. L., Schmitt-Kopplin, P., and Koch, B. P. (2014). Molecular transformation and degradation of refractory dissolved organic matter in the Atlantic and Southern Ocean. *Geochim. Cosmochim. Acta* 126, 321–337. doi: 10.1016/j.gca.2013.11.009
- Letscher, R. T., Hansell, D. A., and Kadko, D. (2011). Rapid removal of terrigenous dissolved organic carbon over the Eurasian shelves of the Arctic Ocean. *Mar. Chem.* 123, 78–87. doi: 10.1016/j.marchem.2010.10.002
- Lin, H., and Twining, B. S. (2012). Chemical speciation of iron in Antarctic waters surrounding free-drifting icebergs. *Mar. Chem.* 128, 81–91. doi: 10.1016/j.marchem.2011.10.005
- Liu, H. B., Laws, E. A., Villareal, T. A., and Buskey, E. J. (2001). Nutrient-limited growth of *Aureoumbra lagunensis* (Pelagophyceae), with implications for its capability to outgrow other phytoplankton species in phosphate-limited environments. *J. Phycol.* 37, 500–508. doi: 10.1046/j.1529-8817.2001.037004500.x
- MacRellis, H. M., Trick, C. G., Rue, E. L., Smith, G., and Bruland, K. W. (2001). Collection and detection of natural iron-binding ligands from seawater. *Mar. Chem.* 76, 175–187. doi: 10.1016/S0304-4203(01)00061-5
- Mahowald, N. M., Baker, A. R., Bergametti, G., Brooks, N., Duce, R. A., Jickells, T. D., et al. (2005). Atmospheric global dust cycle and iron inputs to the ocean. *Global Biogeochem. Cycles* 19. doi: 10.1029/2004GB002402
- Maldonado, M. T., Hughes, M. P., Rue, E. L., and Wells, M. L. (2002). The effect of Fe and Cu on growth and domoic acid production by *Pseudo-nitzschia* multiseriales and *Pseudo-nitzschia* australis. *Limnol. Oceanogr.* 47, 515–526. doi: 10.4319/lo.2002.47.2.0515
- Maldonado, M. T., Strzpek, R. F., Sander, S., and Boyd, P. W. (2005). Acquisition of iron bound to strong organic complexes, with different Fe binding groups and photochemical reactivities, by plankton communities in Fe-limited subantarctic waters. *Global Biogeochem. Cycles* 19. doi: 10.1029/2005GB002481
- Martino, M., Turner, A., and Nimmo, M. (2004). Distribution, speciation and particle-water interactions of nickel in the Mersey Estuary, UK. *Mar. Chem.* 88, 161–177. doi: 10.1016/j.marchem.2004.03.007
- Mawji, E., Gledhill, M., Milton, J. A., Tarran, G. A., Ussher, S., Thompson, A., et al. (2008). Hydroxamate siderophores: occurrence and importance in the Atlantic Ocean. *Environ. Sci. Technol.* 42, 8675–8680. doi: 10.1021/es801884r
- Mawji, E., Gledhill, M., Milton, J. A., Zubkov, M. V., Thompson, A., Wolff, G. A., et al. (2011). Production of siderophore type chelates in Atlantic Ocean waters enriched with different carbon and nitrogen sources. *Mar. Chem.* 124, 90–99. doi: 10.1016/j.marchem.2010.12.005
- Medeiros, P. M., Seidel, M., and Niggemann, J. (2016). A novel molecular approach for tracing terrigenous dissolved organic matter into the deep ocean. *Glob. Biogeochem. Cycles* 30, 689–699. doi: 10.1002/2015GB005320
- Melton, E. D., Swanner, E. D., Behrens, S., Schmidt, C., and Kappler, A. (2014). The interplay of microbially mediated and abiotic reactions in the biogeochemical Fe cycle. *Nat. Rev. Microbiol.* 12, 797–808. doi: 10.1038/nrmicro3347
- Moore, J. K., Lindsay, K., Doney, S. C., Long, M. C., and Misumi, K. (2013). Marine ecosystem dynamics and biogeochemical cycling in the community earth system model [cesm1(bgc)]: comparison of the 1990s with the 2090s under the RCP4.5 and RCP8.5 Scenarios. *J. Clim.* 26, 9291–9312. doi: 10.1175/JCLI-D-12-00566.1
- Moran, M. A., Kujawinski, E. B., Stubbins, A., Fatland, R., Aluwihare, L. I., Buchan, A., et al. (2016). Deciphering ocean carbon in a changing world. *Proc. Natl. Acad. Sci. U.S.A.* 113, 3143–3151. doi: 10.1073/pnas.1514645113
- Mykledstad, S. (1977). Production of carbohydrates by marine planktonic diatoms. 2. Influence of N-P ratio in growth medium on assimilation ratio, growth-rate, and production of cellular and extracellular carbohydrates by *Chaetoceros-Affinis* var *Willei* (Gran) Hustedt and *Skeletonema-costatum* (Grev) Cleve. *J. Exp. Mar. Biol. Ecol.* 29, 161–179. doi: 10.1016/0022-0981(77)90046-6
- Nichols, C. A. M., Garon, S., Bowman, J. P., Raguene, G., and Guezennec, J. (2004). Production of exopolysaccharides by Antarctic marine bacterial isolates. *J. Appl. Microbiol.* 96, 1057–1066. doi: 10.1111/j.1365-2672.2004.02216.x
- Nichols, C. A. M., Guezennec, J., and Bowman, J. P. (2005). Bacterial exopolysaccharides from extreme marine environments with special consideration of the southern ocean, sea ice, and deep-sea hydrothermal vents: a review. *Mar. Biotechnol.* 7, 253–271. doi: 10.1007/s10126-004-5118-2
- Norman, L. (2014). *The Role of Natural Organic Ligands in Transformations of Iron Chemistry in Seawater and Their Effect on the Bioavailability or Iron to Marine Phytoplankton*. Ph.D. thesis, School of the Environment, University of Technology, Sydney.
- Norman, L., Worms, I. A. M., Angles, E., Bowie, A. R., Nichols, C. M., Ninh Pham, A., et al. (2015). The role of bacterial and algal exopolymeric substances in iron chemistry. *Mar. Chem.* 173, 148–161. doi: 10.1016/j.marchem.2015.03.015
- Nunn, B. L., Faux, J. F., Hippmann, A. A., Maldonado, M. T., Harvey, H. R., Goodlett, D. R., et al. (2013). Diatom proteomics reveals unique acclimation strategies to mitigate Fe limitation. *PLoS ONE* 8:e75653. doi: 10.1371/journal.pone.0075653
- Ogawa, H., Amagai, Y., Koike, I., Kaiser, K., and Benner, R. (2001). Production of refractory dissolved organic matter by bacteria. *Science* 292, 917–920. doi: 10.1126/science.1057627
- Orellana, M. V., and Hansell, D. A. (2012). Ribulose-1,5-bisphosphate carboxylase/oxygenase (RuBisCO): A long-lived protein in the deep ocean. *Limnol. Oceanogr.* 57, 826–834. doi: 10.4319/lo.2012.57.3.0826
- Orellana, M. V., Lessard, E. J., Dycus, E., Chin, W. C., Foy, M. S., and Verdugo, P. (2003). Tracing the source and fate of biopolymers in seawater: application of an immunological technique. *Mar. Chem.* 83, 89–99. doi: 10.1016/S0304-4203(03)00098-7
- Ozturk, M., Croot, P. L., Bertilsson, S., Abrahamsson, K., Karlson, B., David, R., et al. (2004). Iron enrichment and photoreduction of iron under UV and PAR in the presence of hydroxycarboxylic acid: implications for phytoplankton growth in the Southern Ocean. *Deep Sea Res. Part II Top. Stud. Oceanogr.* 51, 2841–2856. doi: 10.1016/j.dsr2.2000.10.001
- Pakulski, J. D., and Benner, R. (1994). Abundance and distribution of carbohydrates in the ocean. *Limnol. Oceanogr.* 39, 930–940. doi: 10.4319/lo.1994.39.4.0930
- Panagiotopoulos, C., and Sempere, R. (2005). Analytical methods for the determination of sugars in marine samples: a historical perspective and future directions. *Limnol. Oceanogr. Methods* 3, 419–454. doi: 10.4319/om.2005.3.419
- Paris, R., and Desboeufs, K. V. (2013). Effect of atmospheric organic complexation on iron-bearing dust solubility. *Atmos. Chem. Phys.* 13, 4895–4905. doi: 10.5194/acp-13-4895-2013
- Ploug, H., Grossart, H. P., Azam, F., and Jorgensen, B. B. (1999). Photosynthesis, respiration, and carbon turnover in sinking marine snow from surface waters of Southern California Bight: implications for the carbon cycle in the ocean. *Mar. Ecol. Prog. Ser.* 179, 1–11. doi: 10.3354/meps179001
- Poorvin, L., Sander, S. G., Velasquez, I., Ibanem, E., LeClerc, G. R., and Wilhelm, S. W. (2011). A comparison of Fe bioavailability and binding of a catecholate siderophore with virus-mediated lysates from the marine bacterium *Vibrio alginolyticus* PWH3a. *J. Exp. Mar. Biol. Ecol.* 399, 43–47. doi: 10.1016/j.jembe.2011.01.016
- Powell, R. T., and Wilson-Finelli, A. (2003). Importance of organic Fe complexing ligands in the Mississippi River plume. *Estuar. Coast. Shelf Sci.* 58, 757. doi: 10.1016/S0272-7714(03)00182-3
- Price, N. M., and Morel, F. M. M. (1998). “Biological cycling of iron in the ocean,” in *Metal Ions in Biological Systems*, eds A. Sigel and H. Sigel (New York, NY: Marcel Dekker) 1–36.
- Primeau, F. W., and Holzer, M. (2006). The ocean’s memory of the atmosphere: residence-time and ventilation-rate distributions of water masses. *J. Phys. Oceanogr.* 36, 1439–1456. doi: 10.1175/JPO2919.1
- Reid, R. T., Live, D. G., Faulkner, D. J., and Butler, A. (1993). A siderophore from a marine bacterium with an exceptional ferric iron affinity constant. *Nature* 366, 455–458. doi: 10.1038/366455a0

- Repeta, D. J., and Aluwihare, L. I. (2006). Radiocarbon analysis of neutral sugars in high-molecular-weight dissolved organic carbon: implications for organic carbon cycling. *Limnol. Oceanogr.* 51, 1045–1053. doi: 10.4319/lo.2006.51.2.1045
- Repeta, D., Boiteau, R. M., Mende, D. R., and DeLong, E. F. (2016). “Microbes Adapt to Iron Scarcity through Siderophore Production across the Eastern Tropical Pacific,” in *Ocean Science Meeting, AGU/ASLO/TOS* (New Orleans, LA).
- Resing, J. A., Sedwick, P. N., German, C. R., Jenkins, W. J., Moffett, J. W., Sohst, B. M., et al. (2015). Basin-scale transport of hydrothermal dissolved metals across the South Pacific Ocean. *Nature* 523, 200–U140. doi: 10.1038/nature14577
- Rue, E., and Bruland, K. (2001). Domoic acid binds iron and copper: a possible role for the toxin produced by the marine diatom *Pseudo-nitzschia*. *Mar. Chem.* 76, 127–134. doi: 10.1016/S0304-4203(01)00053-6
- Rue, E. L., and Bruland, K. W. (1995). Complexation of iron(III) by natural organic-ligands in the central north pacific as determined by a new competitive ligand equilibration adsorptive cathodic stripping voltammetric method. *Mar. Chem.* 50, 117–138. doi: 10.1016/0304-4203(95)00031-L
- Sander, S. G., and Koschinsky, A. (2011). Metal flux from hydrothermal vents increased by organic complexation. *Nat. Geosci.* 4, 1–6. doi: 10.1038/ngeo1088
- Sarthou, G., Vincent, D., Christaki, U., Obernosterer, I., Timmermans, K. R., and Brussaard, C. P. D. (2008). The fate of biogenic iron during a phytoplankton bloom induced by natural fertilisation: Impact of copepod grazing. *Deep Sea Res. Part II Top. Stud. Oceanogr.* 55, 734–751. doi: 10.1016/j.dsr2.2007.12.033
- Schlosser, C., De La Rocha, C. L., Streu, P., and Croot, P. L. (2012). Solubility of iron in the Southern Ocean. *Limnol. Oceanogr.* 57, 684–697. doi: 10.4319/lo.2012.57.3.0684
- Seidel, M., Yager, P. L., Ward, N. D., Carpenter, E. J., Gomes, H. R., Krusche, A. V., et al. (2015). Molecular-level changes of dissolved organic matter along the Amazon River-to-ocean continuum. *Mar. Chem.* 177, 218–231. doi: 10.1016/j.marchem.2015.06.019
- Sholkovitz, E. R., Boyle, E. A., and Price, N. B. (1978). Removal of dissolved humic acids and iron during estuarine mixing. *Earth Planet. Sci. Lett.* 40, 130–136. doi: 10.1016/0012-821X(78)90082-1
- Stolpe, B., and Hasselov, M. (2010). Nanofibrils and other colloidal biopolymers binding trace elements in coastal seawater: significance for variations in element size distributions. *Limnol. Oceanogr.* 55, 187–202. doi: 10.4319/lo.2010.55.1.0187
- Stolpe, B., Zhou, Z. Z., Guo, L. D., and Shiller, A. M. (2014). Colloidal size distribution of humic- and protein-like fluorescent organic matter in the northern Gulf of Mexico. *Mar. Chem.* 164, 25–37. doi: 10.1016/j.marchem.2014.05.007
- Strzepek, R. F., Maldonado, M. T., Higgins, J. L., Hall, J., Safi, K., Wilhelm, S. W., et al. (2005). Spinning the “Ferrous Wheel”: The importance of the microbial community in an iron budget during the FeCycle experiment. *Global Biogeochem. Cycles* 19. doi: 10.1029/2005GB002490
- Tagliabue, A., Williams, R. G., Rogan, N., Achterberg, E. P., and Boyd, P. W. (2014). A ventilation-based framework to explain the regeneration-scavenging balance of iron in the ocean. *Geophys. Res. Lett.* 41, 7227–7236. doi: 10.1002/2014GL061066
- Tanaka, K., Kuma, K., Hamasaki, K., and Yamashita, Y. (2014). Accumulation of humic-like fluorescent dissolved organic matter in the Japan Sea. *Sci. Rep.* 4. doi: 10.1038/srep05292
- Trick, C. G., Wilhelm, S. W., and Brown, C. M. (1995). Alterations in cell pigmentation, protein expression, and photosynthetic capacity of the cyanobacterium *Oscillatoria tenuis* grown under low iron conditions. *Can. J. Microbiol.* 41, 1117–1123. doi: 10.1139/m95-155
- Trimborn, S., Hoppe, C. J. M., Taylor, B. B., Bracher, A., and Hassler, C. (2015). Physiological characteristics of open ocean and coastal phytoplankton communities of Western Antarctic Peninsula and Drake Passage waters. *Deep Sea Res. Part I Oceanogr. Res. Pap.* 98, 115–124. doi: 10.1016/j.dsr.2014.12.010
- van den Berg, C. M. G. (1995). Evidence for organic complexation of iron in seawater. *Mar. Chem.* 50, 139–157. doi: 10.1016/0304-4203(95)00032-M
- van der Merwe, P., Lannuzel, D., Nichols, C. A. M., Meiners, K., Heil, P., Norman, L., et al. (2009). Biogeochemical observations during the winter-spring transition in East Antarctic sea ice: evidence of iron and exopolysaccharide controls. *Mar. Chem.* 115, 163–175. doi: 10.1016/j.marchem.2009.08.001
- Velasquez, I., Ibsanmi, E., Maas, E. W., Boyd, P. W., Nodder, S., and Sander, S. G. (2016). Ferrioxamine siderophores detected amongst iron binding ligands produced during the remineralization of marine particles. *Front. Mar. Sci.* 3:172. doi: 10.3389/fmars.2016.00172
- Velasquez, I., Nunn, B. L., Ibsanmi, E., Goodlett, D. R., Hunter, K. A., and Sander, S. G. (2011). Detection of hydroxamate siderophores in coastal and Sub-Antarctic waters off the South Eastern Coast of New Zealand. *Mar. Chem.* 126, 97–107. doi: 10.1016/j.marchem.2011.04.003
- Verdugo, P., Alldredge, A. L., Azam, F., Kirchman, D. L., Passow, U., and Santschi, P. H. (2004). The oceanic gel phase: a bridge in the DOM-POM continuum. *Mar. Chem.* 92, 67–85. doi: 10.1016/j.marchem.2004.06.017
- Völker, C., and Tagliabue, A. (2015). Modeling organic iron-binding ligands in a three-dimensional biogeochemical ocean model. *Mar. Chem.* 173, 67–77. doi: 10.1016/j.marchem.2014.11.008
- Volker, C., and Wolf-Gladrow, D. A. (1999). Physical limits on iron uptake mediated by siderophores or surface reductases. *Mar. Chem.* 65, 227–244. doi: 10.1016/S0304-4203(99)00004-3
- Vraspir, J. M., and Butler, A. (2009). Chemistry of marine ligands and siderophores. *Ann. Rev. Mar. Sci.* 1, 43–63. doi: 10.1146/annurev.marine.010908.163712
- Wagener, T., Guieu, C., Losno, R., Bonnet, S., and Mahowald, N. (2008). Revisiting atmospheric dust export to the Southern Hemisphere ocean: biogeochemical implications. *Global Biogeochem. Cycles* 22. doi: 10.1029/2007gb002984
- Walsh, M. J., Goodnow, S. D., Vezeau, G. E., Richter, L. V., and Ahner, B. A. (2015). Cysteine enhances bioavailability of copper to marine phytoplankton. *Environ. Sci. Technol.* 49, 12145–12152. doi: 10.1021/acs.est.5b02112
- Waska, H., Dittmar, T., and Koschinsky, A. (2016). Fe- and Cu-complex formation with artificial ligands investigated by ultra-high resolution Fourier-transform ion cyclotron resonance mass spectrometry (FT-ICR-MS): implications for natural metal-organic complex studies. *Front. Mar. Sci.* 3:119. doi: 10.3389/fmars.2016.00119
- Westrich, J. R., Ebling, A. M., Landing, W. M., Joyner, J. L., Kemp, K. M., Griffin, D. W., et al. (2016). Saharan dust nutrients promote *Vibrio* bloom formation in marine surface waters. *Proc. Natl. Acad. Sci. U.S.A.* 113, 5964–5969. doi: 10.1073/pnas.1518080113
- Wilhelm, S. W., and Trick, C. G. (1994). Iron-limited growth of cyanobacteria - multiple siderophore production is a common response. *Limnol. Oceanogr.* 39, 1979–1984. doi: 10.4319/lo.1994.39.8.1979
- Wiley, J. D., Kieber, R. J., Eymann, M. S., and Avery, G. B. (2000). Rainwater dissolved organic carbon: concentrations and global flux. *Global Biogeochem. Cycles* 14, 139–148. doi: 10.1029/1999GB900036
- Witter, A. E., Hutchins, D. A., Butler, A., and Luther, G. W. (2000). Determination of conditional stability constants and kinetic constants for strong model Fe-binding ligands in seawater. *Mar. Chem.* 69, 1–17. doi: 10.1016/S0304-4203(99)00087-0
- Yamashita, Y., Cory, R. M., Nishioka, J., Kuma, K., Tanoue, E., and Jaffe, R. (2010). Fluorescence characteristics of dissolved organic matter in the deep waters of the Okhotsk Sea and the northwestern North Pacific Ocean. *Deep Sea Res. Part II Top. Stud. Oceanogr.* 57, 1478–1485. doi: 10.1016/j.dsr2.2010.02.016
- Yang, R., and van den Berg, C. M. (2009). Metal complexation by humic substances in seawater. *Environ. Sci. Technol.* 43, 7192–7197. doi: 10.1021/es900173w

Conflict of Interest Statement: The authors declare that the research was conducted in the absence of any commercial or financial relationships that could be construed as a potential conflict of interest.

Copyright © 2017 Hassler, van den Berg and Boyd. This is an open-access article distributed under the terms of the Creative Commons Attribution License (CC BY). The use, distribution or reproduction in other forums is permitted, provided the original author(s) or licensor are credited and that the original publication in this journal is cited, in accordance with accepted academic practice. No use, distribution or reproduction is permitted which does not comply with these terms.



A Compilation of Iron Speciation Data for Open Oceanic Waters

Salvatore Caprara^{1,2}, Kristen N. Buck², Loes J. A. Gerringa³, Micha J. A. Rijkenberg³ and Damiano Monticelli^{1*}

¹ Dipartimento di Scienza e Alta Tecnologia, Università degli Studi dell'Insubria, Como, Italy, ² College of Marine Science, University of South Florida, St. Petersburg, FL, USA, ³ Department of Ocean Systems, Royal Netherlands Institute for Sea Research, Utrecht University, Texel, Netherlands

Keywords: iron, speciation, organic ligand, seawater, dataset, metal titration

INTRODUCTION

Iron has been demonstrated to play a major role in limiting primary productivity in large areas of the ocean since the first formulation of the iron hypothesis (Martin, 1990). Efforts and papers devoted to this complex and multidisciplinary research topic (Jickells et al., 2005) saw an exponential increase over the last 25 years (Boyd and Ellwood, 2010). As a consequence, the latest available count (Tagliabue et al., 2016) tells us that the concentration of iron has been determined in around 20,000 oceanic water samples up to 2014. After the noteworthy achievement of reliable iron concentration profiles, the interest of the scientific community moved on to try and understand the fast dynamic of this metal in oceanic waters. However, one of the main factors that determine the concentration of Fe in the oceans is its complexation to organic Fe-binding ligands: this is the reason why Fe speciation measurement made its way in the topic early (Gledhill and van den Berg, 1994; Rue and Bruland, 1995): research aims at establishing the role played by ligands in iron solubility, bioavailability and, as a whole, in its biogeochemical cycle (Hiemstra and van Riemsdijk, 2006; Hunter and Boyd, 2007; Boyd and Ellwood, 2010; Gledhill and Buck, 2012; Boyd and Tagliabue, 2015; Völker and Tagliabue, 2015). A higher iron solubility has since long been connected to the presence of strong binding ligands (Johnson et al., 1997; Liu and Millero, 2002): whether this implies a higher productivity, i.e., an increase in the bioavailable fraction, is still a matter of investigation and strongly depends on the nature of the ligands (Chen and Wang, 2008; Boyd and Ellwood, 2010; Gledhill and Buck, 2012; Shaked and Lis, 2012). An attempt to directly model the dynamics of iron binding ligands in oceanic waters has been recently presented (Völker and Tagliabue, 2015).

The possibility to understand and correctly account for the biogeochemistry of iron in the oceans relies on the quality of the data. Robust analytical methods are clearly needed in speciation studies: the best performances in term of detection capabilities, selectivity, matrix tolerance and clean techniques are mandatory to achieve reliable results. In particular, competitive ligand equilibration coupled to adsorptive cathodic stripping voltammetry (CLE-AdCSV) has been invariantly used to characterize iron complexing species, i.e., the concentration of the ligand and the conditional stability constant for the formation of the iron-ligand complex (structural characterization is outside the aim of this data report: the interested reader is referred to recent papers on this topic Gledhill and Buck, 2012; Boiteau et al., 2013). Four different artificial ligands have been used for the CLE-AdCSV procedure: 1-nitroso-2-naphthol, NN (Gledhill and van den Berg, 1994); salicylaldoxime, SA, originally developed in 1995 (Rue and Bruland, 1995) and revised in 2014 (Abualhaja and van den Berg, 2014); 2-(2-thiazolylazo)-p-cresol, TAC (Croot and Johansson, 2000) and dihydroxynaphthalene, DHN (van den Berg, 2006). The importance of a correct analysis of the resulting CLE-CSV titration data and the assessment of its errors is the final critical step in this procedure (Monticelli et al., 2010; Laglera et al., 2013; Gerringa et al., 2014; Pižeta et al., 2015).

OPEN ACCESS

Edited by:

Antonio Tovar-Sanchez,
Spanish National Research Council,
Spain

Reviewed by:

Francisco Delgadillo-Hinojosa,
Universidad Autónoma de Baja
California, Mexico
Juan Santos,
Instituto Español de Oceanografía,
Spain

*Correspondence:

Damiano Monticelli
damiano.monticelli@uninsubria.it

Specialty section:

This article was submitted to
Marine Biogeochemistry,
a section of the journal
Frontiers in Marine Science

Received: 29 July 2016

Accepted: 25 October 2016

Published: 14 November 2016

Citation:

Caprara S, Buck KN, Gerringa LJA,
Rijkenberg MJA and Monticelli D
(2016) A Compilation of Iron
Speciation Data for Open Oceanic
Waters. *Front. Mar. Sci.* 3:221.
doi: 10.3389/fmars.2016.00221

The present data report aims at making published data on ligand concentration in open oceanic waters available to the scientific community to foster the understanding of the role played by natural ligand in iron biogeochemical cycle. As per the nature of the data report paper, only a preliminary discussion of the data is presented in the form of possible uses of the dataset.

DESCRIPTION OF THE DATASET

The dataset “Iron speciation dataset.xlsx” can be found following this permanent link <https://figshare.com/s/6572ca173695f4a03738>. Data were collected from published papers: pre-2012 papers were obtained from a recent review on the subject (Gledhill and Buck, 2012), whereas literature searches were employed for post-2012 research articles. The dataset covers the 1994–2015 timespan (papers published in 2016 are not included). Source papers are reported in **Table 1** together with the investigated region, the filter cutoff employed, the nature of the added ligand and the data treatment.

The dataset includes observations for open oceanic waters only, i.e., off-shelf sampling locations. Open ocean data were selected and in-shelf, costal, estuarine and closed basin data (Mediterranean Sea, Black Sea, etc.) were excluded. Data obtained during fertilization experiments were also excluded: only off-patch or pre-fertilization data were included from those studies. Analogously, data from waters sampled in areas close to hydrothermal vents or thawing ice were not included. The idea is to create a consistent dataset, trying and collecting a tentatively homogeneous set of data. Most of the data were directly available as electronic datasets, whereas a few, mainly the oldest ones, had to be digitized from figures.

The iron speciation dataset includes around 1732 iron speciation data, organized by chronological order. In particular, we reported for each data point (whenever available): the reference in the form author-year, the sampling date, depth, and location (as decimal degrees), dissolved iron concentration (DFe, nM), the logarithm of the side coefficient for the formation of the iron-added ligand complex ($\log \alpha_{Fe'AL}$), ligand concentration (nM) and the logarithm of the conditional stability constant for the formation of the iron-ligand complex ($\log K_{FeL,Fe'}^{cond}$). The latter are reported as both $K_{FeL,Fe^{3+}}^{cond}$ and $K_{FeL,Fe'}^{cond}$: to normalize data, $K_{FeL,Fe^{3+}}^{cond}$ were transformed to $K_{FeL,Fe'}^{cond}$ using a factor of 10^{10} for the inorganic alpha, $\alpha_{Fe'}$ (Hudson et al., 1992). The green filled cells in the dataset signal that $K_{FeL,Fe^{3+}}^{cond}$ was originally reported in those papers, and was converted to $K_{FeL,Fe'}^{cond}$ here. When more than one ligand class was determined, their concentrations and conditional stability constants are reported in additional columns. We follow the common practice to use the simplified expression “ligand concentration” and use the nanomolar concentration unit, although we should properly indicate binding sites and use the nanoequivalent of nM iron as the unity of measurement. The employed filter cutoff for each study is reported in **Table 1**: in case ligands were determined in more than one size fraction, the additional data are reported

in the second sheet of the dataset named “Size Fractionated,” together with the filter cutoff employed.

DATA PRESENTATION AND DISCUSSION

The dataset is intended to provide marine scientists and the broader community with the published data for iron ligand characteristics. In the following sections, we present different cuts through the data showing different possible uses of the dataset. A detailed discussion of the data is nevertheless outside the aim of the present data report: only general trends (or their absence) will be presented.

A first evidence from the dataset is the strongly uneven distribution of the data: 1185 out of 1732 data are from Atlantic Ocean waters, 232 from the Pacific, 214 from the Indian Ocean and the remaining ones from Polar regions, 51 from the Arctic (N of the Arctic Circle) and 50 from the Southern Ocean (south of 60° S). Accordingly, any discussion of this dataset is necessarily biased and reflects the features of the basins where the samples were collected.

Checking for consistency in the procedure or for the presence of bias is a possible way to extract information from the data. **Figure 1A** shows the measured side reaction coefficient $\alpha_{Fe'L}$ (defined as the product of the conditional stability constant $K_{FeL,Fe'}^{cond}$ and the free ligand concentration $[L']$, $\alpha_{Fe'L} = K_{FeL,Fe'}^{cond} \cdot [L']$) as a function of the side reaction coefficient $\alpha_{Fe'AL}$, the alpha coefficient for the complexation of iron by the added ligand as obtained from the relevant papers ($[L']$ was calculated from the data by standard thermodynamic calculations van den Berg and Donat, 1992). The lowest and the two highest $\alpha_{Fe'AL}$ employed show very good agreement between the experimental data and their expected detection windows defined as the range 0.1–10 $\alpha_{Fe'AL}$ (van den Berg et al., 1990). The four central competition strengths with $1.86 < \log \alpha_{Fe'AL} < 2.5$ show most of their data outside the traditionally suggested upper limit for the detection window. This apparent discrepancy should be discussed in light of different factors: (1) the definition of the detection window as the range 0.1–10 $\alpha_{Fe'AL}$ is an approximate estimation defining the optimal range for the CLE methods: several studies demonstrated that a three orders of magnitude window is a more realistic estimate (Apte et al., 1988); (2) the choice of the method to treat/transform the data obtained from the titrations impacts the results, distinctively when more than one ligand class is calculated (Laglera et al., 2013; Pižeta et al., 2015) and may alter the traditionally agreed idea about the position and width of the detection window. This point is anyhow worth of future investigation. Conversely, figures lower than the expected lowest limit of the detection window may be easily explained by the saturation of the natural ligands at ambient iron concentrations.

A further interesting point is the possibility that the difference in the data is due to the authors employing different analytical procedures, including different data treatment. The lack of standardization and validation protocols in this field, caused by the absence of reference material and the shortage of routine interlaboratory exercises, makes this risk sensible (see also the Conclusion section). Analysis of variance (ANOVA) conducted

TABLE 1 | Data sources for the iron speciation database listed in chronological order.

Region	AL	AL conc (μM)	log alpha $_{Fe/AL}$	Fraction (pore size, μm)	Data treatment	References
Atlantic Ocean	NN	1; 5	1.9; 2.5	0.45	van den Berg Ružić	Gledhill and van den Berg, 1994
Central N Pacific	SA	27.5	1.86	0.2	van den Berg Ružić	Rue and Bruland, 1995
Pacific Southern Ocean	NN	1	1.9	0.45	non-linear Gerringa	Nolting et al., 1998
NW Atlantic	NN	20	3.04	0.2	van den Berg Ružić and non-linear Gerringa	Witter and Luther, 1998
NE Indian	NN	20	3.04	0.4	van den Berg Ružić	Witter et al., 2000
Atlantic Southern Ocean	NN	5	2.5	0.2	van den Berg Ružić	Boye et al., 2001
S and Equatorial Atlantic	SA	30	1.94	0.22	Non-linear Gerringa	Powell and Donat, 2001
NE Atlantic	NN	5	2.5	0.2	van den Berg Ružić	Boye et al., 2003
Atlantic Southern Ocean	TAC	10	2.4	0.4	Non-linear Gerringa	Croot et al., 2004
	NN	5; 10; 20	2.4; 3.4; 4.3	0.4		
Atlantic Southern Ocean	TAC	10	2.4	0.2	van den Berg Ružić	Boye et al., 2005
NE Atlantic	NN	5	2.5	0.2	van den Berg Ružić	Boye et al., 2006
Atlantic Ocean	TAC	10.6	2.45	0.2	Non-linear Gerringa	Cullen et al., 2006
NE Atlantic	TAC	10	2.4	0.2	Non-linear Gerringa	Gerringa et al., 2006
Pacific Southern Ocean	TAC	10	2.4	0.2	Non-linear Gerringa	Tian et al., 2006
Pacific Ocean	DHN	0.5; 1	2.22; 2.56	0.1	van den Berg Ružić	van den Berg, 2006
Tropical North Pacific	TAC	10	2.4	0.4	van den Berg Ružić	Hopkinson and Barbeau, 2007
Sulu Sea (Tropical N Pacific)	TAC	10	2.4	0.22	van den Berg Ružić	Kondo et al., 2007
Indian Southern Ocean	TAC	10	2.4	0.2	Non-linear Gerringa	Gerringa et al., 2008
Tropical N Atlantic	TAC	10	2.4	0.2	Non-linear Gerringa	Rijkenberg et al., 2008
Antarctic polar Front	TAC	10	2.4	0.2	van den Berg Ružić	Boye et al., 2010
NE Atlantic	TAC	10	2.4	0.2	Non-linear Gerringa	Thuróczy et al., 2010
Indian Southern Ocean	TAC	10	2.4	0.4	Non-linear Gerringa	Ibisanmi et al., 2011
N Atlantic	TAC	10	2.4	0.2	Non-linear Gerringa	Mohamed et al., 2011
Arctic Ocean	TAC	10	2.4	0.2	Non-linear Gerringa	Thuróczy et al., 2011a
Atlantic Southern Ocean	TAC	10	2.4	0.2	Non-linear Gerringa	Thuróczy et al., 2011b
Central Pacific	TAC	10	2.4	0.22	Non-linear Gerringa	Kondo et al., 2012
Atlantic Southern Ocean	TAC	10	2.4	0.2	Non-linear Gerringa	Schlosser et al., 2012
Atlantic Southern Ocean	TAC	10	2.4	0.2	Non-linear Gerringa	Thuróczy et al., 2012
N Atlantic	SA	27.5	1.86	0.2	van den Berg Ružić and Scatchard	Buck et al., 2015
Atlantic Ocean	SA	25; 32.5	1.78; 2.00	0.2	van den Berg Ružić and Scatchard	Fitzsimmons et al., 2015a
Pacific Ocean	SA	25	1.77	0.4	van den Berg Ružić and Scatchard	Fitzsimmons et al., 2015b
W Atlantic	TAC	10	2.4	0.2	Non-linear Gerringa	Gerringa et al., 2015

AL, artificial ligand; DHN, dihydroxynaphthalene; NN, 1-nitroso-2-naphthol; TAC, 2-(2-thiazolylazo)-p-cresol. Reference for data treatment methods: van den Berg (1982), Ružić (1982) and Scatchard (1949), non-linear Gerringa et al. (1995) reviewed in 2014 Gerringa et al. (2014).

separately on the ligand concentration (C_L) and $\log K_{FeL,Fe}^{cond}$ data, revealed that the null hypothesis of equal values obtained by the authors should be rejected ($\log K_{FeL,Fe}^{cond}$: $n = 1618$, $F = 43$, $p < 0.05$; C_L : $n = 1725$, $F = 71$, $p < 0.05$). These results are not clearly conclusive about any presence of bias among the authors or the analytical procedures, as different samples were analyzed by authors, although some of the oldest, pre-2000 data seem to show lower $\log K_{FeL,Fe}^{cond}$ and higher C_L . Application to a more homogeneous subset of data, e.g., different procedures for the same basin, could result in more definite inferences.

The relationship between iron and ligand concentrations is presented in **Figure 1B**. Beside the presence of some outliers, the linear correlation is significant ($n = 1727$, $r = 0.445$, $p < 0.01$): the intercept (0.87 ± 0.033) and the slope (0.92 ± 0.044) point to an average excess of 0.9 nM ligand with respect to total iron concentration, irrespective of total Fe as evidenced by the almost 1:1 increase of ligand with iron concentration. This linear model does not imply any cause/effect relationship between the two parameters and it is intended to be descriptive rather than predictive.

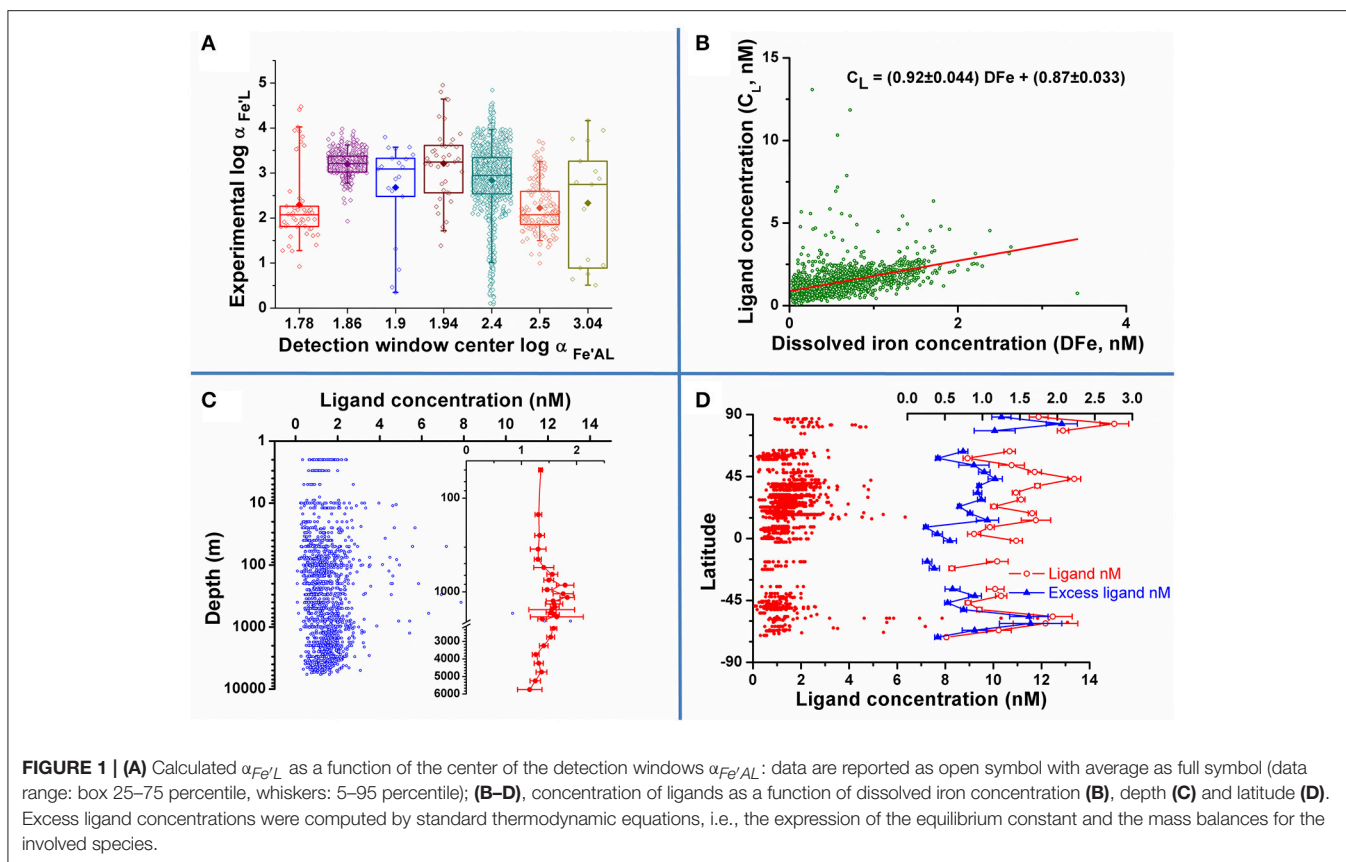


Figure 1C depicts the concentration of ligands for oceanic waters as a function of depth (note the log scale on the y-axis used to show possible trends in the upper part of the water column). No clear global trend emerges from open ocean data reported in the literature. The averaged data (see inset) shows a very uniform value down to a depth of 500 m, an enrichment in mid depth waters (<500 m to around 2000 m), possibly due to the remineralization of organic matter at these depths, and a decrease thereafter down to values similar to the ones determined in the upper part of the water column. This trend is anyhow hardly significant standing the variability in the data evidenced by their standard deviation (error bars in the graph represents the standard deviation of the mean): any strong depth trend on the global scale seems to be absent, although a higher variability of ligand concentrations in mid depth waters emerges.

As a final example of possible global trends, data for ligand concentrations on the entire water column as a function of sampling latitude are reported in **Figure 1D** (data averaged on a 5 degree base in the right section of the figure). Notwithstanding the high variability in the data, northern hemisphere waters are on average richer in ligands than the Austral ones, as already observed for Atlantic water samples (Gerringa et al., 2015). More detailed, northern hemisphere waters seem to show alternating minima and maxima in ligand concentrations: a minimum right North of the Equator (0–10 degrees), an enriched area extending up to mid latitudes (10–50 degrees), another minimum around 60° and again higher concentrations in the Arctic Ocean. A

similar trend is observed for the excess ligand concentrations. Depleted and enriched areas are also present in the Austral hemisphere waters, although the limited number of data calls for caution in stating any trend.

CONCLUSIONS

The collection of published data on iron ligand concentrations is a first mandatory step in understanding the role played by iron ligands in the biogeochemical oceanic cycle of this element. The overall picture emerging from the data is the ubiquitous presence of ligands in open oceanic waters, with an average ~0.9 nM excess with respect to dissolved iron concentration. Depth profiles show little to no tendency on a global averaged scale, whereas latitudinal trends are clearly visible, with northern hemisphere waters enriched in iron ligands (samples from the Atlantic Ocean mainly). As far as the Atlantic is concerned, ligands contributed to the Arctic by tributary rivers have been recently put forward as an explanation for this latitudinal trend (Gerringa et al., 2015).

Several points should be addressed before an exhaustive and reliable picture of the topic may be achieved and data used for the understanding of the iron cycle or its modeling. The first issue is that available data are strongly biased: around 70% of the samples were collected in the Atlantic Ocean and any conclusion is accordingly strongly biased by the provenance

of the samples. Accordingly, representative sampling of world oceanic waters is the major gap to be filled: the GEOTRACES program (www.geotraces.org) is expected to contribute much to this aim. A second class of fundamental issues is related to the analytical procedures, their validation and reliability. Analytical procedures are cumbersome at the moment, requiring large volume of samples (120–150 mL) and 3–5 h of analysis time. Recent advancement in methods for total iron determination including reduction in sample size and analysis time (Caprara et al., 2015) may strongly contribute in the definition of higher performance speciation procedures, although at the moment the method was only validated for dissolved iron determination and not for the CLE-CSV procedure. Standing the difficulties in validating the employed analytical methods as standard reference materials are not available, calibration of the procedures may be achieved by intercomparison exercises, i.e., analyzing real or simulated samples distributed among participating laboratories. Data treatment should be included in this calibration procedure because of its value in achieving reliable results (Hudson et al., 2003; Laglera et al., 2013; Gerringa et al., 2014; Laglera and Filella, 2015; Pižeta et al., 2015). This process would ensure that results obtained by different laboratories are traceable to a common set of interlaboratory samples. Unfortunately, this procedure is not common practice at present, although

intercalibration cruises have been organized (Buck et al., 2012) and results of a GEOTRACES cross-over station for ligands is submitted together with this paper (Buck et al., unpublished). A further related issue is the correlation between sampling areas and authors: any bias among the procedures used by different authors is at risk of resulting in erroneous evaluations of spatial trends.

AUTHOR CONTRIBUTIONS

All the authors contributed to this study. SC: Built the database; KB, LG, and MR: Contributed to the writing and correction of the manuscript; DM: Devised the data report, did the bibliographic research and drafted the manuscript. All the five authors reviewed the final version of the manuscript and contributed to the discussion of the data.

FUNDING

DM acknowledges Università degli Studi dell'Insubria, project FAR2015 KB was supported by a U.S. National Science Foundation award, OCE-1441969 LG and MR acknowledge the Dutch funding agency ZKO (project number 839.08.410) of the National Science Foundation NWO for funding.

REFERENCES

- Abualhija, M. M., and van den Berg, C. M. G. (2014). Chemical speciation of iron in seawater using catalytic cathodic stripping voltammetry with ligand competition against salicylaldehyde. *Mar. Chem.* 164, 60–74. doi: 10.1016/j.marchem.2014.06.005
- Apte, S. C., Gardner, M. J., and Ravenscroft, J. E. (1988). An evaluation of voltammetric titration procedures for the determination of trace metal complexation in natural waters by use of computers simulation. *Anal. Chim. Acta* 212, 1–21. doi: 10.1016/S0003-2670(00)84124-0
- Boiteau, R. M., Fitzsimmons, J. N., Repeta, D. J., and Boyle, E. A. (2013). Detection of iron ligands in Seawater and Marine Cyanobacteria cultures by high-performance liquid chromatography–inductively coupled plasma-mass spectrometry. *Anal. Chem.* 85, 4357–4362. doi: 10.1021/ac3034568
- Boyd, P. W., and Ellwood, M. J. (2010). The biogeochemical cycle of iron in the ocean. *Nat. Geosci.* 3, 675–682. doi: 10.1038/ngeo964
- Boyd, P. W., and Tagliabue, A. (2015). Using the L^* concept to explore controls on the relationship between paired ligand and dissolved iron concentrations in the ocean. *Mar. Chem.* 173, 52–66. doi: 10.1016/j.marchem.2014.12.003
- Boye, M., Aldrich, A., van den Berg, C. M. G., de Jong, J. T. M., Nirmaier, H., Veldhuis, M., et al. (2006). The chemical speciation of iron in the north-east Atlantic Ocean. *Deep-Sea Res. I Oceanogr. Res. Pap.* 53, 667–683. doi: 10.1016/j.dsr.2005.12.015
- Boye, M. B., Aldrich, A. P., van den Berg, C. M. G., de Jong, J. T. M., Veldhuis, M. J. W., and de Baar, H. J. W. (2003). Horizontal gradient of the chemical speciation of iron in surface waters of N.E. Atlantic Ocean. *Mar. Chem.* 80, 129–143. doi: 10.1016/S0304-4203(02)00102-0
- Boye, M., Nishioka, J., Croot, P., Laan, P., Timmermans, K. R., Strass, V. H., et al. (2010). Significant portion of dissolved organic Fe complexes in fact is Fe colloids. *Mar. Chem.* 122, 20–27. doi: 10.1016/j.marchem.2010.09.001
- Boye, M., Nishioka, J., Croot, P. L., Laan, P., Timmermans, K. R., and de Baar, H. J. W. (2005). Major deviations of iron complexation during 22 days of a mesoscale iron enrichment in the open Southern Ocean. *Mar. Chem.* 96, 257–271. doi: 10.1016/j.marchem.2005.02.002
- Boye, M., van den Berg, C. M. G., de Jong, J. T. M., Leach, H., Croot, P., and de Baar, H. J. W. (2001). Organic complexation of iron in the Southern Ocean. *Deep-Sea Res. I Oceanogr. Res. Pap.* 48, 1477–1497. doi: 10.1016/S0967-0637(00)00099-6
- Buck, K. N., Moffett, J., Barbeau, K. A., Bundy, R. M., Kondo, Y., and Wu, J. (2012). The organic complexation of iron and copper: An intercomparison of competitive ligand exchange-adsorptive cathodic stripping voltammetry (CLE-ACSV) techniques. *Limnol. Oceanogr.* 10, 496–515. doi: 10.4319/lom.2012.10.496
- Buck, K. N., Sohst, B., and Sedwick, P. N. (2015). The organic complexation of dissolved iron along the U.S. GEOTRACES (GA03) North Atlantic Section. *Deep-Sea Res. Part II: Top. Stud. Oceanogr.* 116, 152–165. doi: 10.1016/j.dsr2.2014.11.016
- Caprara, S., Laglera, L. M., and Monticelli, D. (2015). Ultrasensitive and Fast Voltammetric Determination of Iron in Seawater by Atmospheric Oxygen Catalysis in 500 μ l Samples. *Anal. Chem.* 87, 6357–6363. doi: 10.1021/acs.analchem.5b01239
- Chen, M., and Wang, W.-X. (2008). Accelerated uptake by phytoplankton of iron bound to humic acids. *Aquat. Biol.* 3:155–166. doi: 10.3354/ab00064
- Croot, P. L., Andersson, K., Öztürk, M., and Turner, D. R. (2004). The distribution and speciation of iron along 6°E in the Southern Ocean. *Deep-Sea Res. II* 51, 2857–2879. doi: 10.1016/j.dsr2.2003.10.012
- Croot, P. L., and Johansson, M. (2000). Determination of iron speciation by cathodic stripping voltammetry in seawater using the competing ligand 2-(2-thiazolylazo)-p-cresol (TAC). *Electroanalysis* 12, 565–576. doi: 10.1002/(SICI)1521-4109(200005)12:8<565::AID-ELAN565>3.0.CO;2-L
- Cullen, J. T., Bergquist, B. A., and Moffett, J. W. (2006). Thermodynamic characterization of the partitioning of iron between soluble and colloidal species in the Atlantic Ocean. *Mar. Chem.* 98, 295–303. doi: 10.1016/j.marchem.2005.10.007
- Fitzsimmons, J. N., Bundy, R. M., Al-Subiai, S. N., Barbeau, K. A., and Boyle, E. A. (2015a). The composition of dissolved iron in the dusty surface ocean: an exploration using size-fractionated iron-binding ligands. *Mar. Chem.* 173, 125–135. doi: 10.1016/j.marchem.2014.09.002

- Fitzsimmons, J. N., Hayes, C. T., Al-Subia, S. N., Zhang, R., Morton, P. L., Weisend, R. E., et al. (2015b). Daily to decadal variability of size-fractionated iron and iron-binding ligands at the Hawaii Ocean Time-series Station ALOHA. *Geochim. Cosmochim. Acta* 171, 303–324. doi: 10.1016/j.gca.2015.08.012
- Gerringa, L. J. A., Blain, S., Laan, P., Sarthou, G., Veldhuis, M. J. W., Brussaard, C. P. D., et al. (2008). Fe-binding dissolved organic ligands near the Kerguelen Archipelago in the Southern Ocean (Indian sector). *Deep-Sea Res. Part II: Top. Stud. Oceanogr.* 55, 606–621. doi: 10.1016/j.dsr2.2007.12.007
- Gerringa, L. J. A., Rijkenberg, M. J. A., Schoemann, V., Laan, P., and de Baar, H. J. W. (2015). Organic complexation of iron in the West Atlantic Ocean. *Mar. Chem.* 177, 434–446. doi: 10.1016/j.marchem.2015.04.007
- Gerringa, L. J. A., Rijkenberg, M. J. A., Thuróczy, C. E., and Maas, L. R. M. (2014). A critical look at the calculation of the binding characteristics and concentration of iron complexing ligands in seawater with suggested improvements. *Environ. Chem.* 11, 114–136. doi: 10.1071/EN13072
- Gerringa, L. J. A., Veldhuis, M. J. W., Timmermans, K. R., Sarthou, G., and de Baar, H. J. W. (2006). Co-variance of dissolved Fe-binding ligands with phytoplankton characteristics in the Canary Basin. *Mar. Chem.* 102, 276–290. doi: 10.1016/j.marchem.2006.05.004
- Gerringa, L. J., Herman, P. M., and Poortvliet, T. C. (1995). Comparison of the linear Van den Berg/Ruzic transformation and a non-linear fit of the Langmuir isotherm applied to Cu speciation data in the estuarine environment. *Mar. Chem.* 48, 131–142. doi: 10.1016/0304-4203(94)00041-B
- Gledhill, M., and Buck, K. N. (2012). The organic complexation of iron in the marine environment: a review. *Front. Microbiol.* 3:69. doi: 10.3389/fmicb.2012.00069
- Gledhill, M., and van den Berg, C. M. G. (1994). Determination of complexation of iron(III) with natural organic complexing ligands in seawater using cathodic stripping voltammetry. *Mar. Chem.* 47, 41–54. doi: 10.1016/0304-4203(94)90012-4
- Hiemstra, T., and van Riemsdijk, W. H. (2006). Biogeochemical speciation of Fe in ocean water. *Mar. Chem.* 102, 181–197. doi: 10.1016/j.marchem.2006.03.008
- Hopkinson, B. M., and Barbeau, K. A. (2007). Organic and redox speciation of iron in the eastern tropical North Pacific suboxic zone. *Mar. Chem.* 106, 2–17. doi: 10.1016/j.marchem.2006.02.008
- Hudson, R. J. M., Covault, D. M., and Morel, F. M. M. (1992). Investigations of iron coordination and redox reactions in seawater using 59Fe radiometry and ion-pair solvent extraction of amphiphilic iron complexes. *Mar. Chem.* 38, 209–235. doi: 10.1016/0304-4203(92)90035-9
- Hudson, R. J. M., Rue, E. L., and Bruland, K. W. (2003). Modeling complexometric titrations of natural water samples. *Environ. Sci. Technol.* 37, 1553–1562. doi: 10.1021/es025751a
- Hunter, K. A., and Boyd, P. W. (2007). Iron-binding ligands and their role in the ocean biogeochemistry of iron. *Environ. Chem.* 4, 221–232. doi: 10.1071/EN07012
- Ibanm, E., Sander, S. G., Boyd, P. W., Bowie, A. R., and Hunter, K. A. (2011). Vertical distributions of iron-(III) complexing ligands in the Southern Ocean. *Deep-Sea Res. II Top. Stud. Oceanogr.* 58, 2113–2125. doi: 10.1016/j.dsr2.2011.05.028
- Jickells, T. D., An, Z. S., Andersen, K. K., Baker, A. R., Bergametti, C., Brooks, N., et al. (2005). Global iron connections between desert dust, ocean biogeochemistry, and climate. *Science* 308, 67–71. doi: 10.1126/science.1105959
- Johnson, K. S., Michael Gordon, R., and Coale, K. H. (1997). What controls dissolved iron concentrations in the world ocean? *Mar. Chem.* 57, 137–161.
- Kondo, Y., Takeda, S., and Furuya, K. (2007). Distribution and speciation of dissolved iron in the Sulu Sea and its adjacent waters. *Deep-Sea Res. II Top. Stud. Oceanogr.* 54, 60–80. doi: 10.1016/j.dsr2.2006.08.019
- Kondo, Y., Takeda, S., and Furuya, K. (2012). Distinct trends in dissolved Fe speciation between shallow and deep waters in the Pacific Ocean. *Mar. Chem.* 134–135, 18–28. doi: 10.1016/j.marchem.2012.03.002
- Laglera, L. M., Downes, J., and Santos-Echeandia, J. (2013). Comparison and combined use of linear and non-linear fitting for the estimation of complexing parameters from metal titrations of estuarine samples by CLE/AdCSV. *Mar. Chem.* 155, 102–112. doi: 10.1016/j.marchem.2013.06.005
- Laglera, L. M., and Filella, M. (2015). The relevance of ligand exchange kinetics in the measurement of iron speciation by CLE-AdCSV in seawater. *Mar. Chem.* 173, 100–113. doi: 10.1016/j.marchem.2014.09.005
- Liu, X. W., and Millero, F. J. (2002). The solubility of iron in seawater. *Mar. Chem.* 77, 43–54. doi: 10.1016/S0304-4203(01)00074-3
- Martin, J. H. (1990). Glacial-interglacial CO₂ change: the iron hypothesis. *Paleoceanography* 5, 1–13. doi: 10.1029/PA005i001p00001
- Mohamed, K. N., Steigenberger, S., Nielsdottir, M. C., Gledhill, M., and Achterberg, E. P. (2011). Dissolved iron(III) speciation in the high latitude North Atlantic Ocean. *Deep-Sea Res. I Oceanogr. Res. Pap.* 58, 1049–1059. doi: 10.1016/j.dsr.2011.08.011
- Monticelli, D., Dossi, C., and Castelletti, A. (2010). Assessment of accuracy and precision in speciation analysis by competitive ligand equilibration-cathodic stripping voltammetry (CLE-CSV) and application to Antarctic samples. *Anal. Chim. Acta* 675, 116–124. doi: 10.1016/j.aca.2010.07.009
- Nolting, R. F., Gerringa, L. J. A., Swagerman, M. J. W., Timmermans, K. R., and De Baar, H. J. W. (1998). Fe (III) speciation in the high nutrient, low chlorophyll Pacific region of the Southern Ocean. *Mar. Chem.* 62, 335–352. doi: 10.1016/S0304-4203(98)00046-2
- Pižeta, I., Sander, S. G., Hudson, R. J. M., Omanović, D., Baars, O., Barbeau, K. A., et al. (2015). Interpretation of complexometric titration data: An intercomparison of methods for estimating models of trace metal complexation by natural organic ligands. *Mar. Chem.* 173, 3–24. doi: 10.1016/j.marchem.2015.03.006
- Powell, R. T., and Donat, J. R. (2001). Organic complexation and speciation of iron in the South and equatorial Atlantic. *Deep Sea Res. Part II Top. Stud. Oceanogr.* 48, 2877–2893. doi: 10.1016/S0967-0645(01)00022-4
- Rijkenberg, M. J. A., Powell, C. F., Dall'Osto, M., Nielsdottir, M. C., Patey, M. D., Hill, P. G., et al. (2008). Changes in iron speciation following a Saharan dust event in the tropical North Atlantic Ocean. *Mar. Chem.* 110, 56–67. doi: 10.1016/j.marchem.2008.02.006
- Rue, E. L., and Bruland, K. W. (1995). Complexation of iron(III) by natural organic ligands in the Central North Pacific as determined by a new competitive ligand equilibration adsorptive cathodic stripping voltammetric method. *Mar. Chem.* 50, 117–138. doi: 10.1016/0304-4203(95)00031-L
- Ruzić, I. (1982). Theoretical aspects of the direct titration of natural waters and its information yield for trace metal speciation. *Anal. Chim. Acta* 140, 99–113. doi: 10.1016/S0003-2670(01)95456-X
- Scatchard, G. (1949). The attractions of proteins for small molecules and ions. *Ann. N. Y. Acad. Sci.* 51, 660–672. doi: 10.1111/j.1749-6632.1949.tb27297.x
- Schlosser, C., de la Rocha, C. L., Streu, P., and Croot, P. L. (2012). Solubility of iron in the Southern Ocean. *Limnol. Oceanogr.* 57, 684–697. doi: 10.4319/lo.2012.57.3.0684
- Shaked, Y., and Lis, H. (2012). Disassembling iron availability to phytoplankton. *Front. Microbiol.* 3:123. doi: 10.3389/fmicb.2012.00123
- Tagliabue, A., Aumont, O., DeAth, R., Dunne, J. P., Dutkiewicz, S., Galbraith, E., et al. (2016). How well do global ocean biogeochemistry models simulate dissolved iron distributions? *Glob. Biogeochem. Cycles* 30, 149–174. doi: 10.1002/2015GB005289
- Thuróczy, C. E., Alderkamp, A. C., Laan, P., Gerringa, L. J. A., Mills, M. M., Van Dijken, G. L., et al. (2012). Key role of organic complexation of iron in sustaining phytoplankton blooms in the Pine Island and Amundsen Polynyas (Southern Ocean). *Deep-Sea Res. Part II Top. Stud. Oceanogr.* 71–76, 49–60. doi: 10.1016/j.dsr2.2012.03.009
- Thuróczy, C. E., Gerringa, L. J. A., Klunder, M. B., Laan, P., and de Baar, H. J. W. (2011b). Observation of consistent trends in the organic complexation of dissolved iron in the Atlantic sector of the Southern Ocean. *Deep Sea Res. Part II Top. Stud. Oceanogr.* 58, 2695–2706. doi: 10.1016/j.dsr2.2011.01.002
- Thuróczy, C. E., Gerringa, L. J. A., Klunder, M. B., Middag, R., Laan, P., Timmermans, K. R., et al. (2010). Speciation of Fe in the Eastern North Atlantic Ocean. *Deep-Sea Res. I Oceanogr. Res. Pap.* 57, 1444–1453. doi: 10.1016/j.dsr.2010.08.004
- Thuróczy, C. E., Gerringa, L. J. A., Klunder, M., Laan, P., Le Guitton, M., and De Baar, H. J. W. (2011a). Distinct trends in the speciation of iron between the shallow shelf seas and the deep basins of the Arctic Ocean. *J. Geophys. Res.* 116:C10009. doi: 10.1029/2010JC006835
- Tian, F., Frew, R. D., Sander, S., Hunter, K. A., and Ellwood, M. J. (2006). Organic iron(III) speciation in surface transects across a frontal zone: The Chatham Rise, New Zealand. *Mar. Freshw. Res.* 57, 533–544. doi: 10.1071/MF05209

- van den Berg, C. M. G. (1982). Determination of copper complexation with natural organic ligands in seawater by equilibration with MnO₂. *Theory Mar. Chem.* 11, 307–322. doi: 10.1016/0304-4203(82)90028-7
- van den Berg, C. M. G. (2006). Chemical speciation of iron in seawater by cathodic stripping voltammetry with dihydroxynaphthalene. *Anal. Chem.* 78, 156–163. doi: 10.1021/ac051441+
- van den Berg, C. M. G., and Donat, J. R. (1992). Determination and data evaluation of copper complexation by organic ligands in sea water using cathodic stripping voltammetry at varying detection windows. *Anal. Chim. Acta* 257, 281–291. doi: 10.1016/0003-2670(92)85181-5
- van den Berg, C. M. G., Nimmo, M., Daly, P., and Turner, D. R. (1990). Effects of the detection window on the determination of organic copper speciation in estuarine waters. *Anal. Chim. Acta* 232, 149–159. doi: 10.1016/S0003-2670(00)81231-3
- Völker, C., and Tagliabue, A. (2015). Modeling organic iron-binding ligands in a three-dimensional biogeochemical ocean model. *Mar. Chem.* 173, 67–77. doi: 10.1016/j.marchem.2014.11.008
- Witter, A. E., Lewis, B. L., and Luther III, G. W. (2000). Iron speciation in the Arabian Sea. *Deep-Sea Res. Part II Top. Stud. Oceanogr.* 47, 1517–1539. doi: 10.1016/S0967-0645(99)00152-6
- Witter, A. E., and Luther, G. W. III. (1998). Variation in Fe-organic complexation with depth in the Northwestern Atlantic Ocean as determined using a kinetic approach. *Mar. Chem.* 62, 241–258. doi: 10.1016/S0304-4203(98)00044-9

Conflict of Interest Statement: The authors declare that the research was conducted in the absence of any commercial or financial relationships that could be construed as a potential conflict of interest.

Copyright © 2016 Caprara, Buck, Gerringa, Rijkenberg and Monticelli. This is an open-access article distributed under the terms of the Creative Commons Attribution License (CC BY). The use, distribution or reproduction in other forums is permitted, provided the original author(s) or licensor are credited and that the original publication in this journal is cited, in accordance with accepted academic practice. No use, distribution or reproduction is permitted which does not comply with these terms.



Structural Characterization of Natural Nickel and Copper Binding Ligands along the US GEOTRACES Eastern Pacific Zonal Transect

Rene M. Boiteau^{1,2}, Claire P. Till^{3,4}, Angel Ruacho⁵, Randelle M. Bundy¹, Nicholas J. Hawco^{1,2}, Amy M. McKenna⁶, Katherine A. Barbeau⁵, Kenneth W. Bruland³, Mak A. Saito¹ and Daniel J. Repeta^{1*}

¹ Department of Marine Chemistry and Geochemistry, Woods Hole Oceanographic Institution, Woods Hole, MA, USA, ² Department of Earth, Atmospheric, and Planetary Sciences, Massachusetts Institute of Technology, Cambridge, MA, USA, ³ Ocean Sciences Department, University of California, Santa Cruz, CA, USA, ⁴ Chemistry Department, Humboldt State University, Arcata, CA, USA, ⁵ Scripps Institution of Oceanography, University of California, San Diego, La Jolla, CA, USA, ⁶ National High Magnetic Field Laboratory, Florida State University, Tallahassee, FL, USA

OPEN ACCESS

Edited by:

Christel Hassler,
University of Geneva, Switzerland

Reviewed by:

Peter Croot,
National University of Ireland, Galway,
Ireland

Hannelore Waska,
University of Oldenburg, Germany

*Correspondence:

Daniel J. Repeta
drepeta@whoi.edu

Specialty section:

This article was submitted to
Marine Biogeochemistry,
a section of the journal
Frontiers in Marine Science

Received: 01 August 2016

Accepted: 08 November 2016

Published: 30 November 2016

Citation:

Boiteau RM, Till CP, Ruacho A, Bundy RM, Hawco NJ, McKenna AM, Barbeau KA, Bruland KW, Saito MA and Repeta DJ (2016) Structural Characterization of Natural Nickel and Copper Binding Ligands along the US GEOTRACES Eastern Pacific Zonal Transect. *Front. Mar. Sci.* 3:243. doi: 10.3389/fmars.2016.00243

Organic ligands form strong complexes with many trace elements in seawater. Various metals can compete for the same ligand chelation sites, and the final speciation of bound metals is determined by relative binding affinities, concentrations of binding sites, uncomplexed metal concentrations, and association/dissociation kinetics. Different ligands have a wide range of metal affinities and specificities. However, the chemical composition of these ligands in the marine environment remains poorly constrained, which has hindered progress in modeling marine metal speciation. In this study, we detected and characterized natural ligands that bind copper (Cu) and nickel (Ni) in the eastern South Pacific Ocean with liquid chromatography tandem inductively coupled plasma mass spectrometry (LC-ICPMS), and high-resolution electrospray ionization mass spectrometry (ESIMS). Dissolved Cu, Ni, and ligand concentrations were highest near the coast. Chromatographically unresolved polar compounds dominated ligands isolated near the coast by solid phase extraction. Offshore, metal and ligand concentrations decreased, but several new ligands appeared. One major ligand was detected that bound both Cu²⁺ and Ni²⁺. Based on accurate mass and fragmentation measurements, this compound has a molecular formula of [C₂₀H₂₁N₄O₈S₂+M]⁺ (M = metal isotope) and contains several azole-like metal binding groups. Additional lipophilic Ni complexes were also present only in oligotrophic waters, with masses of 649, 698, and 712 m/z (corresponding to the ⁵⁸Ni metal complex). Molecular formulae of [C₃₂H₅₄N₃O₆S₂Ni]⁺ and [C₃₃H₅₆N₃O₆S₂Ni]⁺ were determined for two of these compounds. Addition of Cu and Ni to the samples also revealed the presence of additional compounds that can bind both Ni and Cu. Although these specific compounds represent a small fraction of the total dissolved Cu and Ni pool, they highlight the compositional diversity and spatial heterogeneity of marine Ni and Cu ligands, as well as variability in the extent to which different metals in the same environment compete for ligand binding.

Keywords: copper, nickel, marine ligands, metal competition, GEOTRACES, Eastern Pacific

INTRODUCTION

Strong organic ligands affect the solubility and reactivity of Cu and Ni in marine environments and impact the bioavailability of these essential micronutrient metals (Vraspir and Butler, 2009). Studies of Cu speciation using electrochemical methods show that more than 99% of dissolved Cu is complexed by strong organic ligands in the surface ocean (Coale and Bruland, 1988, 1990; Moffett et al., 1990; Donat and van den Berg, 1992; Campos and van den Berg, 1994; Moffett, 1995; Buck and Bruland, 2005; Jacquot et al., 2013; Thompson et al., 2014; Jacquot and Moffett, 2015). In comparison, a smaller fraction (30–50%) of dissolved Ni is complexed by strong organic ligands (van den Berg and Nimmo, 1987; Nimmo and van Den Berg, 1989; Zhang et al., 1990; Donat et al., 1994; Achterberg and Van Den Berg, 1997; Saito and Moffett, 2004; Saito et al., 2005). Although these electrochemical studies do not provide direct information on the chemical composition of ligands, they do suggest that structurally diverse ligands with distinct sources and binding strengths are present throughout the ocean (e.g., Buck and Bruland, 2005; Bundy et al., 2013).

Marine organisms are capable of producing a wide variety of Cu and Ni chelators that could potentially contribute to the natural ligand pool. Some Ni and Cu chelators such as glutathione, phytochelatin, and metallothioneins are produced to chelate metals as a detoxification mechanism (Ahner et al., 1994, 1997, 2002; Dupont et al., 2004; Freeman et al., 2004; Wei and Ahner, 2005; Devez et al., 2009). Other chelators such as methanobactins and staphylopinins are produced to facilitate Cu or Ni acquisition (Kim et al., 2004; El Ghazouani et al., 2012; Ghssein et al., 2016). Ni is a constituent of some metabolite cofactors such as the tetrapyrrole F430, the prosthetic group of the enzyme involved in the final step of methanogenesis (Allen et al., 2014), while other pyrrole and azole-based modified peptides are known to have a strong affinity for Ni and Cu, although their physiological roles are unknown (Michael et al., 1993; Bertram and Pattenden, 2007; Comba et al., 2014). Although not directly produced by microbes, marine humic compounds, structurally heterogeneous refractory degradation products of organic matter decay, may also complex Cu and Ni (Baker and Khalili, 2003; Yang and Van den Berg, 2009; Whitby and Van den Berg, 2014; Abualhaija et al., 2015).

The chemical composition of Cu and Ni ligands determines their metal binding stability constants and turnover rates. In general, there is competition between the two metals for ligand binding sites, with Cu^{2+} usually forming more stable organic complexes compared to Ni^{2+} , following the Irving Williams series (Irving and Williams, 1953). Since ligand concentrations are nearly always in excess of Cu concentrations, Cu tends to saturate stronger ligands, leaving weaker ligands free to coordinate Ni (and other cations). Thus, the speciation of metals depends on the relative binding strengths of co-occurring ligands for Cu and Ni. The rate at which these ligands approach equilibrium (i.e., kinetics of metal association and dissociation) also depends on ligand structure, as do the

rates at which the ligands are produced and degraded in the environment.

Ligands also affect metal redox chemistry. The +II oxidation state of inorganic Cu and Ni are thermodynamically favored in oxic seawater (Turner et al., 1981). However, Cu can be reduced to the +I oxidation state by biological and photochemical processes (Moffett and Zika, 1983; Wuttig et al., 2013). Organic ligands possessing hard base electron donors such as nitrogen and oxygen can stabilize the +II oxidation state, while ligands with sulfur binding groups such as phytochelatin or methanobactin can stabilize the +I state, and can even catalyze Cu^{2+} reduction (Michael et al., 1993; Walsh and Ahner, 2013).

Structural characterization of organic ligands in seawater has remained challenging. Ligands occur at very low concentrations within a highly complex mixture of organic matter. Since high salinity matrices are unsuitable for most mass spectral techniques, solid phase extraction is typically used to remove salts and concentrate ligands. Solid phase extraction resins are available with a range of surface chemistries that can be selected to retain different fractions of the organic ligand pool (Waska et al., 2015). Liquid chromatography coupled to inductively coupled plasma mass spectrometry (LC-ICPMS) provides a means to detect and quantify metal ligand complexes directly, and to investigate compositional changes between samples (Mounicou et al., 2009; Boiteau et al., 2013). However, LC-ICPMS does not provide information on the chemical identity of ligands. Chromatographic separation combined with electrospray ionization mass spectral characterization (ESIMS) provides molecular weights for metal-containing compounds based on peak coherence between chromatographic features that match the isotopic fine structure of metals such as Fe, Cu and Ni (Mounicou et al., 2009; Baars et al., 2014, 2015; Boiteau and Repeta, 2015). Finally, high mass accuracy Fourier transform ion cyclotron resonance mass spectrometry (FT-ICRMS) can achieve resolving power and mass accuracy sufficient to assign elemental formulas to metal containing compounds (McKenna et al., 2014; Waska et al., 2015).

In this study, we combined these techniques to provide robust molecular formula assignments to several of the major nickel and copper binding compounds in the Eastern Pacific. This region exhibits strong surface gradients in metal concentrations and biological activity. The surface waters in the eastern upwelling region off Ecuador and Peru are some of the most productive in the world, fueled by the supply of nutrients and metals from deep waters (Pennington et al., 2006). In the western offshore region, metal concentrations are very low and can influence microbial community composition (Moore et al., 2013). We detected Ni and Cu ligands derived from seawater extracts using LC-ICPMS. We then used LC-ESIMS and metal isotope pattern detection algorithms to characterize metal binding compounds by molecular weight and mass fragmentation spectra, and determined molecular formulae through ESI FT-ICRMS. Finally, we investigated the effect of metal additions on the competition of metals for binding these compounds.

METHODS

Materials and Reagents

Samples were collected and processed using protocols to minimize trace metal contamination (Boiteau et al., in press). All solutions were prepared using trace metal clean reagents and high purity water (18.2 M Ω cm, qH₂O). LCMS grade methanol (MeOH; Optima, Fisher Scientific) used for chromatography was further purified by sub-boiling-point distillation in a Polytetrafluoroethylene (PTFE) still to reduce metal contamination. PTFE solid phase extraction (SPE) column hardware and vials were cleaned overnight with 0.1% detergent (Citranox), rinsed with qH₂O, soaked in 1 N HCl (trace metal grade, Fisher Scientific) for 1–2 days before a final qH₂O rinse. PTFE tubing and polyethersulfone capsule filters (0.2 μ m Millipore) used to process seawater were flushed overnight with 1% HCl and rinsed with qH₂O. Low-density polyethylene sample bottles for trace metal concentration measurements were cleaned in accordance with GEOTRACES sampling protocols (<http://www.geotraces.org>), stored in dilute (~0.1 N) HNO₃, and rinsed three times with filtered sample before filling. Boric acid buffer (1.5 M) for electrochemical measurements of Cu binding ligands was prepared in 0.4 N aqueous NH₄OH (Optima, Fisher Scientific). A 4 mM stock of salicylaldoxime (SA; > 98%) was prepared in methanol (Optima LCMS, Fisher Scientific) and was replaced every 6 months or as needed. Copper standards (100 nM to 10 μ M) were diluted from an atomic adsorption standard (1000 ppm, Spex CertiPrep) into pH 2 qH₂O (acidified with Optima grade HCl). For electrochemical Ni measurements, a 0.5 M EPPS buffer [N-(2-hydroxyethyl)piperazine-N-(3-propanesulfonic acid)] and a 1.5 M sodium nitrite solution were each prepared in qH₂O and percolated through cleaned Chelex-100 resin (Biorad) before use. Dimethylglyoxime (DMG) was recrystallized as described by Saito and Moffett (2001) and added to Optima MeOH (Fisher Scientific) for a final concentration of 0.1 M. The Ni stock solution was diluted from an AA standard (CertiPrep; 1 mg L⁻¹) to a final concentration of 1 μ M. Ferrioxamine E and cyanocobalamin standards were purchased from Sigma Aldrich (St. Louis, Mo, USA).

Sampling

Samples were collected during the GEOTRACES Eastern Pacific Zonal Transect cruise (October–December, 2013) from Manta, Ecuador to Papeete, Tahiti (GP16; **Figure 1A**). Seawater was collected from 3 m depth with a trace metal clean PTFE tow-fish pump system while steaming between stations (Bruland et al., 2005). Discrete samples for voltammetry and metal concentration measurements were filtered through a 0.2 μ m capsule filter (Polyethersulfone, Pall acropak). Metal concentration samples were acidified at sea with the equivalent of 4 mL of 6 M quartz-distilled HCl per liter of seawater (resulting in a pH of 1.7–1.8). Samples for ligand titrations were stored at –20°C until analysis, in acid-clean fluorinated polyethylene bottles. To collect samples for trace metal ligand characterization by chromatography mass spectrometry, seawater was pumped from an under way tow-fish sampling system at a flow rate of 250 mL/min through a 0.2 μ m polyethersulfone capsule filter

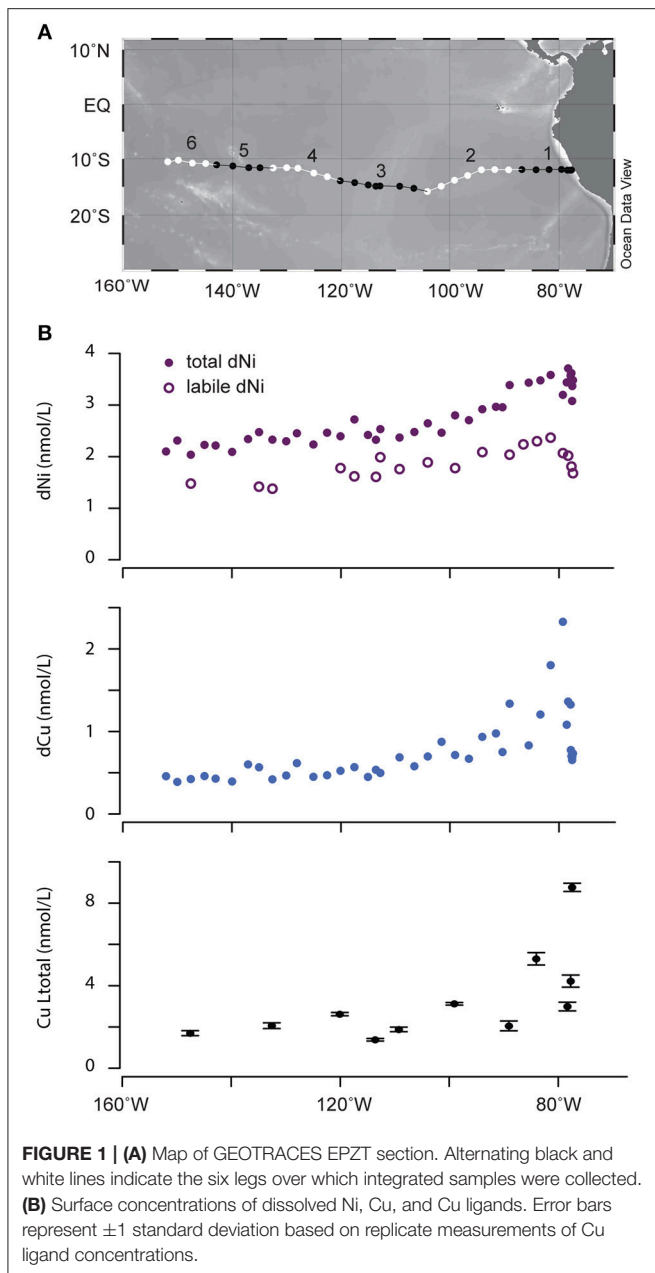
followed by a custom PTFE extraction column (2 cm \times 6.5 cm) packed with 20 g polystyrene divinylbenzene resin beads (ENV, Agilent Bondesil). After 600–800 L of water was passed through a column (representing a sampling interval of 1000–2000 km collected over 4–13 days), the column was frozen onboard and replaced with a fresh column for the next sample. Six samples were collected in total (**Figure 1A**). A sampling blank, collected by pumping only 200 mL of seawater through a column, was processed and analyzed along with the six samples. No Cu or Ni ligands were detected by LCMS in the sampling blank. Before sample collection, the extraction columns were activated by washing with three column volumes of MeOH followed by three column volumes of pH2 qH₂O (acidified with HCl), before a final rinse with qH₂O. Samples were stored at –20°C. Prior to analysis, columns were thawed, rinsed with 500 mL of qH₂O to remove salts, and the organic compounds were eluted with 250 mL of MeOH. Methanol extracts were concentrated by rotary evaporation in an acid cleaned quartz flask and diluted to a final volume of 6 mL with qH₂O. An aliquot of the sample was spiked with 1 μ M cyanocobalamin (Sigma Aldrich) as an internal standard.

Cu Ligand Electrochemical Titrations

Characterization of organic Cu binding ligands across the EPZT section was carried out via competitive ligand exchange adsorptive cathodic stripping voltammetry (CLE-ACSV). CLE-ACSV is an electrochemical method that employs the competition for Cu between a well-characterized ligand [here salicylaldoxime (SA)] and the natural seawater ligands to determine the thermodynamic stabilities of the natural ligands (Campos and van den Berg, 1994). Frozen samples were thawed in a refrigerator and vigorously shaken prior to analysis. The sample was then aliquoted (10 mL) into pre-conditioned PTFE vials and buffered with 1.5 M boric acid-ammonia to pH 8.2. The vials were spiked with increasing concentrations of Cu ranging from 0 to 25 nM, to saturate the natural ligands. The buffer and Cu were left to equilibrate with the natural ligands for 2 h after which the competing ligand, SA, was added at a concentration of 5 μ M and left to equilibrate for 15 min. Eleven-point titrations were carried out in duplicate on a controlled growth mercury electrode (Bioanalytical Systems Incorporated) with electrochemical parameters as used previously (Buck and Bruland, 2005; Bundy et al., 2013), and the peaks detected represent SA-labile Cu complexes established during our equilibration period. Due to the short 15 min equilibration time, it is possible that the apparent natural ligand binding strength (logK) is overestimated compared to results from methods that use a longer equilibration time. Peaks generated from titrations were extracted using the ECDSOFT software package and processed with ProMCC (Omanović et al., 2014) utilizing a single ligand model.

Electrochemical Determination of Labile Ni

Labile Ni was measured using cathodic stripping voltammetry with an Eco-Chemie μ Autolab-III analyzer connected to a Metrohm 663 VA Stand with a hanging mercury drop electrode. Sample aliquots (8.5 mL) were placed in cleaned and conditioned



PE vials, recrystallized DMG was added to a final concentration of $200 \mu\text{M}$, and allowed to equilibrate overnight in the dark. Just prior to analysis, $100 \mu\text{L}$ EPPS buffer was added to each sample. Samples were then purged with ultra high purity N_2 and conditioned at -0.6 V for 60 s while stirring. This was followed by a 10 s equilibration step and then a linear sweep from -0.6 V to -1.4 V with a 10 V s^{-1} scan rate. Labile Ni concentrations were determined using triplicate measurements of the initial concentrations followed by 4 standard additions of 1.0, 2.0, 3.0, and 4.0 nM Ni. Labile Ni concentrations were defined as the proportion of total dissolved Ni that was bound to DMG after the 12 h equilibration period, which likely represents weakly bound organic Ni compounds and free Ni^{2+} . The remaining fraction

of non-labile Ni represents strong organic Ni compounds with thermodynamic conditional stability constants ($\log K$) ranging from 18.45 to 18.68 given the analytical window used in this study (van den Berg and Nimmo, 1987).

Trace Metal Concentration Measurements

Dissolved Cu and Ni were analyzed using previously described methods (Biller and Bruland, 2012; Parker et al., 2016). Briefly, metals of interest were preconcentrated by extraction from buffered seawater (pH 6.0) onto 2 cm columns of Nobias PA1 chelating resin, and eluted with 1N quartz-distilled HNO_3 . The eluent was analyzed on an Element XR Inductively Coupled Plasma Mass Spectrometer (Thermo Scientific) in counting mode. Cu and Ni were both analyzed in medium resolution and have recoveries $>96\%$. Samples were UV irradiated prior to preconcentration.

LC-ICPMS-ESIMS Characterization

Organic ligand samples from solid phase extraction were separated by high pressure liquid chromatography (HPLC, Agilent bioinert 1260 series) using a C8 column (Hamilton, $2.1 \times 100 \text{ mm}$, $3 \mu\text{m}$ particle size) and polyetheretherketone (PEEK) tubing and connectors. Compounds were separated over a gradient from 10% MeOH in H_2O to 90% MeOH over 50 min followed by isocratic elution at 90% MeOH using 5 mM aqueous ammonium formate as a buffer, and a flow rate of 0.2 mL/min. The flow of the LC column was coupled directly to either ICPMS or ESIMS, using a PEEK post column splitter to reduce the flow to $50 \mu\text{L}/\text{min}$.

ICPMS parameters were modified from Boiteau et al. (2013). The ICPMS was fitted with a perfluoroalkoxy micronebulizer (PFA-ST, Elemental Scientific), a cyclonic spray chamber cooled to 0°C , and platinum sample and skimmer cones. To prevent organic deposition onto the cones, oxygen gas was introduced at a rate of 25 mL/min. Measurements were made in kinetic energy discrimination mode using 4.2 mL/min He as a collision gas. ^{59}Co , ^{58}Ni , ^{60}Ni , ^{63}Cu , and ^{65}Cu were monitored with an integration time of 0.05 s each. Concentrations of Ni and Cu ligands detected by LC-ICPMS were calculated by integrating peak areas for the ^{60}Ni and ^{63}Cu signals between 5 and 60 min, and converting this area to concentration based on a six point calibration curve of an Fe-ferrioxamine E standard solution (retention time = 19.8 min), with signal sensitivities intercalibrated between metals using ratios obtained by analyzing a 10 ppb Fe, Cu, and Ni solution in 5% nitric acid (Optima, Fisher Scientific).

To determine the mass of the Ni and Cu ligands, the flow from the LC was coupled to an Orbitrap Fusion mass spectrometer (Thermo Scientific) fitted with a heated electrospray ionization (ESI) source. ESI parameters were set to a capillary voltage of 3500 V, sheath, auxiliary and sweep gas flow rates of 12, 6, and 2 (arbitrary units), and ion transfer tube and vaporizer temperatures of 300 and 75°C . MS scans were collected in high resolution (450 K) positive ionization mode. Ions were trapped using a quadrupole isolation window of 1 m/z and were then fragmented using a high energy collision induced dissociation energy of 35%. LC-ESIMS data was converted to mzXML file

format with the proteowizard msConvert toolkit (Chambers et al., 2012). Retention times between the LC-ICPMS and LC-ESIMS data were aligned by applying a constant time offset to match the retention time of the cyanocobalamin $[M + H]^{2+}$ peak ($m/z = 678$) with the corresponding LC-ICPMS ^{59}Co peak. An isotope pattern search algorithm was used to detect the masses of ions containing Cu and Ni by identifying m/z and intensity features from each scan that fit the mass differences and natural abundance ratios of ^{63}Cu and ^{65}Cu or ^{58}Ni and ^{60}Ni within a mass tolerance of 0.003 m/z and a ratio tolerance of 20%, and then align with the retention time of the LC-ICPMS peaks within 0.1 min. LC-ESIMS data is available as a MassIVE dataset (<https://massive.ucsd.edu>, accession MSV000080173).

FT-ICR MS Analysis

Organic extract samples were diluted 1:1 in HPLC grade methanol (JT Baker Chemical Co., Centre Valley, PA) with 2% formic acid (by volume) for FT-ICRMS analysis. Sample solutions were analyzed with a custom-built FT-ICR mass spectrometer (Kaiser et al., 2011a) equipped with a 9.4 T horizontal 220 mm bore diameter superconducting solenoid magnet (Oxford Instruments, Abingdon, U.K.) operated at room temperature, and a modular ICR data station (Predator) (Blakney et al., 2011) facilitated instrument control, data acquisition, and data analysis. Solutions were infused via a microelectrospray source (Emmett et al., 1998) (50 μm i.d. fused silica emitter) at 500 nL/min by a syringe pump. Positive ions generated at atmospheric pressure enter the skimmer region (~ 2 Torr) through a heated metal capillary (7 A), pass through the first radio frequency (rf)-only quadrupole, and are accumulated (3–5 s) in an octopole equipped with tilted wire extraction electrodes for improved ion extraction and transmission (Wilcox et al., 2002). Helium gas introduced during accumulation collisionally cools ions prior to transfer through two rf-only quadrupoles (total length 127 cm) (2.0 MHz and 255 V_{p-p} amplitude) into a 7-segment open cylindrical ICR cell (Kaiser et al., 2011b) based on the Tolmachev configuration (Tolmachev et al., 2011). For each sample, quadrupole mass filtering within a defined m/z range (~ 5 –30 Da) that corresponded to compounds A–D was applied prior to external ion accumulation in order to improve resolving power and ICR dynamic range (McKenna et al., 2013). Broadband frequency (chirp) excitation (700–70 kHz at a sweep rate of 50 Hz/ μs and amplitude of 350 V_{p-p}) accelerated the ions to a cyclotron orbital radius detected by differential current induced between opposed 120° detection electrodes inside the ICR cell. Fifty individual transients of 6.8 s duration were averaged, apodized with a single-sided Hanning weight function, and zero-filled once prior to fast Fourier transformation. Due to increased complexity at higher m/z , broadband phase correction (Xian et al., 2010, 2012) was applied to each mass spectrum to increase resolution of isobaric species. Absorption-mode spectral resolving power is higher by a factor of up to 2 than magnitude-mode resolving power. The achieved mass spectral resolving power ($m/\Delta m_{50\%}$, in which $\Delta m_{50\%}$ is the mass spectral peak width at half maximum peak height) was $\sim 2,000,000$ – $2,500,000$ in mass isolated segments at m/z 500.

ICR frequencies were converted to ion masses based on the quadrupolar trapping potential approximation (Shi et al., 2000). Each m/z spectrum was internally calibrated with respect to an abundant homologous alkylation series whose members differ in mass by integer multiples of 14.01565 Da (mass of a CH_2 unit) and further iterated based on the “walking” calibration equation (Savory et al., 2011). Calibration for quadrupole mass isolated segments typically relied on 30–60 calibration points with sub-ppm mass error (10–70 ppb) root-mean-square error achieved for all peaks with signal magnitude greater than six times the baseline noise.

LC-ICPMS Metal Exchange Experiment

To investigate metal binding competition among Ni and Cu ligands, splits of the sample extract were spiked with 1 mM citrate stock solutions containing (a) no metal, (b) 100 μM Cu, (c) 100 μM Ni, or (d) 100 μM Cu + 100 μM Ni. Citrate was used as a buffer (pH 6.4) and weak stabilizing ligand to keep the metals soluble. Metal stock solutions were prepared from 1000 ppm metal reference standard solutions in 2% nitric acid (Fisher scientific) diluted in qH_2O containing 1 mM trisodium citrate dihydrate (Fisher bioreagents). Ninety microliters of sample extract was mixed with 10 μL of the metal stock solution and incubated at room temperature in the dark for 12 h prior to analysis. Samples were analyzed by LC-ICPMS as described above, but using a different chromatography system (UltiMate 3000, Dionex).

RESULTS

Distributions of Cu, Ni, and Electrochemically Detected Cu and Ni Ligands in the Eastern Tropical South Pacific Ocean

Concentrations of dissolved Cu and Ni and metal binding ligands were measured across surface waters in the eastern tropical South Pacific Ocean (Table 1). Higher concentrations of both metals were observed near the coast, likely reflecting inputs from aerosols and from upwelling of subsurface waters that are rich in diagenetically remobilized metals released from coastal sediments (Jacquot et al., 2013; Baker et al., 2016). Moving offshore, Cu and Ni levels decreased until both metals reached relatively stable values west of 100°W (0.4 and 2 nM for Cu and Ni, respectively). For Cu, total ligand concentrations measured by CLE-ACSV consistently exceeded dissolved Cu concentrations across the section by a factor of 1.6–12 (Table 1). Cu ligand concentrations followed the same general trend as dissolved Cu, with higher concentrations near the coast. Ligand binding strength generally decreased moving offshore. These results suggest that the concentration of free (uncomplexed) dissolved Cu is $<< 1\%$ throughout the surface of the eastern tropical South Pacific Ocean. In contrast, uncomplexed or weakly complexed dissolved Ni (measured as electrochemically labile dissolved Ni, Figure 1B) concentrations ranged between 48 and 78% of total dissolved Ni. The trend of decreasing concentration offshore was also observed for labile Ni, with a

TABLE 1 | Concentration of dissolved Ni, Cu, and Cu ligands in surface waters of the Eastern Pacific.

Longitude (°W)	Ni (nmol/kg)	Cu (nmol/kg)	labile Ni (nM)	±	Ltotal (nM)	±	logK	±
77.4	3.47	0.73	1.67	0.023	8.77	0.20	13.95	0.01
77.6	3.36	0.69						
77.6	3.07	0.65						
77.7	3.61	0.70	1.80	0.032	4.23	0.29	13.87	0.28
77.8	3.59	0.77						
77.9	3.56	1.32						
78.3	3.70	1.36	2.01	0.048	3.00	0.21	13.49	0.12
78.6	3.43	1.07						
79.3	3.19	2.32	2.06	0.084				
81.5	3.57	1.80	2.36	0.071				
83.4	3.47	1.20						
84.0			2.29	0.068	5.31	0.30	13.47	0.21
85.6	3.43	0.83						
86.5			2.23	0.025				
89.1	3.38	1.33	2.03	0.001	2.06	0.24	13.00	0.16
90.4	2.95	0.74						
91.5	2.96	0.97						
94.1	2.91	0.93	2.08	0.026				
96.5	2.70	0.66						
99.0	2.79	0.71	1.77	0.004	3.13	0.06	12.55	0.14
101.5	2.45	0.87						
104.1	2.64	0.69	1.88	0.008				
106.5	2.47	0.57						
109.2	2.36	0.68	1.75	0.019	1.89	0.11	13.37	0.09
112.8	2.52	0.49	1.98	0.013				
113.6	2.32	0.53	1.60	0.036	1.39	0.06	12.83	0.04
115.1	2.41	0.44						
117.5	2.71	0.56	1.61	0.025				
120.1	2.39	0.52	1.77	0.121	2.63	0.08	12.99	0.11
122.5	2.45	0.46						
125.1	2.22	0.44						
128.1	2.44	0.61						
130.0	2.29	0.46						
132.6	2.32	0.41	1.37	0.162	2.07	0.14	13.05	0.09
135.0	2.47	0.56	1.41	0.029				
137.0	2.33	0.59						
140.0	2.08	0.39						
143.0	2.21	0.42						
145.0	2.22	0.45						
147.5	2.03	0.42	1.47	0.010	1.71	0.12	12.72	0.05
150.0	2.30	0.38						
152.1	2.09	0.45						

Concentration of strong ligands (Ltotal) and conditional stability constant ± standard deviation.

lower percentage of labile Ni in coastal stations (Stations 1–6; 57% average labile Ni) compared to the other stations in the transect (Stations 7–34; 68% average labile Ni). If the difference between total dissolved Ni and labile Ni represents the strong organic Ni-binding ligand concentrations, then Ni ligands ranged from 1 to 2 nM at Stations 1–6 and <1 nM in the remaining stations.

LCMS Ligand Characterization

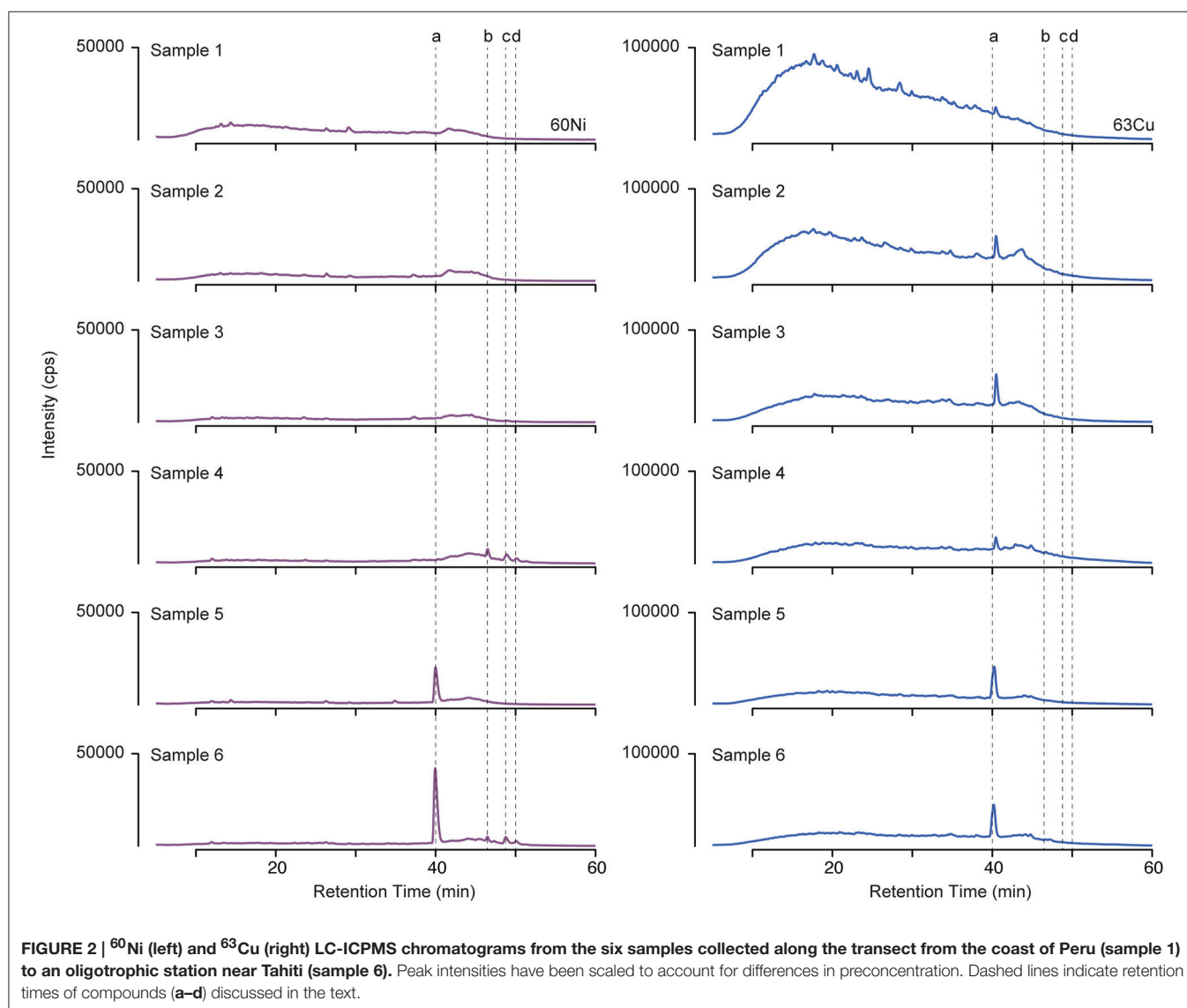
Organic ligands complexed to Cu and Ni were isolated by solid phase extraction from surface seawater across six sections of the GEOTRACES cruise (**Figure 1A**). Ligands were separated by liquid chromatography, and the Ni and Cu associated with them was detected by ICPMS. Metal containing compounds appear in the resulting chromatograms as peaks in signal intensity

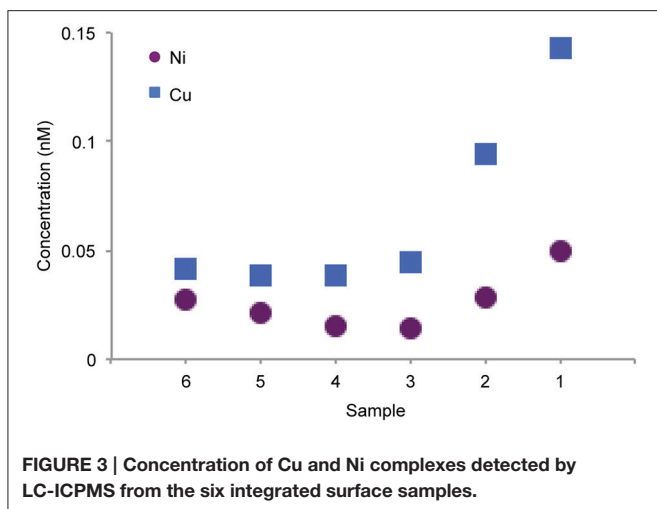
(Figure 2). This method only detects the metal-complexed portion of the ligand pool, and peak intensity reflects the amount of metal associated with the complex. Retention time provides a measure of the polarity of a compound, with more polar compounds eluting earlier in the chromatogram.

For both Cu and Ni, the highest ligand concentrations were detected by LC-ICPMS in the coastal region (Figure 3, sample 1), in agreement with electrochemical measurements of total Cu ligands. It should be noted that the LC-ICPMS and electrochemical methods employed here are not directly comparable in terms of which components of the ligand pool they target. Nonetheless, the agreement between the methods in terms of broad ligand distribution patterns is interesting. In the coastal sample, nearly all Cu and Ni eluted in a broad, unresolved feature appearing between 10 and 30 min. Small amounts of chromatographically resolved ligands appear as numerous sharp peaks atop the broad unresolved feature. These data suggests a very complex assemblage of structurally diverse ligands for

both Cu and Ni. Moving offshore, ligands slowly decreased in concentration, but a larger fraction of the total ligand appeared as distinct compounds. Overall, the LCMS method used in this study captured 6–20% of the dissolved Cu and only 1–2% of total dissolved Ni across the transect, consistent with the findings of other studies that used similar solid phase extraction methods (Waska et al., 2015). The remaining metal is presumably either (1) unchelated or bound to very polar organic chelates that are not retained by SPE, (2) bound to nonpolar chelates that are strongly retained by SPE and do not elute with methanol, or (3) bound weakly such that they dissociate from the organic chelate during the extraction process.

Several discrete Ni and Cu compounds were resolved and identified from the organic extracts (Figure 4). In samples 5 and 6, we characterized a compound eluting at 39.8 min that binds both Ni (m/z 567.015) and Cu (m/z 572.009; Table 2, compound a). A low intensity co-eluting peak with mass 511 m/z was also observed that matches the apo (metal free) form of the complex





containing 2H^+ in lieu of the metal ion, and suggests that Ni and Cu were in the $2+$ oxidation state. MS^2 fragmentation spectra of the Ni and Cu forms of compound **a** revealed similar fragments and neutral losses (Figure 5). Some additional major fragments were observed in the Cu complex fragmentation spectra (263.981, 393.997, and 527.440 m/z) but were absent from the Ni spectrum. These fragments could be derived from an isobaric interfering ion (571.410 m/z) that co-eluted with the 572.009 m/z ion and fell within the quadrupole mass isolation window (red values, Figure 5). The apo, Ni, and Cu forms of this compound were not detected in the ESIMS spectra of samples 1–4.

Another major compound that bound only Cu eluted as a sharp peak at 40.2 min in the LC-ICPMS chromatograms of samples 1–4 (Figure 2). This peak increased in abundance in samples 2 and 3 and then decreased in samples collected farther offshore. Unfortunately, no ESIMS ion pair matching the Cu isotope pattern could be identified in these samples at this retention time, potentially due to matrix suppression effects, poor ionization of the compound, or a compound mass that was outside of the instrument's analytical range.

Finally, three compounds that only appeared in the Ni chromatogram were detected at 46.4, 48.6, and 49.9 min in samples 4 and 6 (Figure 4, compounds **b–d**). The ^{58}Ni monoisotopic mass of these compounds was determined to be 649.148, 698.280, and 712.295 m/z . The MS^2 spectra of compound **b** (m/z 649.148) exhibited three major neutral losses: 77.978 (likely $\text{CH}_2\text{O}_2\text{S}$), 243.130, and 301.117 m/z . However, a coeluting isobaric ion (m/z 648.539) fell within the quadrupole isolation window, and it is possible that some of the fragments are derived from this interfering ion. Compound **d** is structurally related to compound **c** based on their similar MS^2 fragmentation patterns (Figure 5), differing only by the presence of an additional CH_2 . The masses of the apo forms of compounds **b–d** (calculated by substituting 2H^+ for Ni^{2+}) were not observed in the LC-ESIMS spectra.

To facilitate molecular formula assignments, we used FT-ICRMS to obtain sub-ppm mass measurement accuracy within the mass ranges of compounds **a–d**. Accurate masses were

obtained for compounds **a** and **c**, while compounds **b** and **d** were below detection. The achieved ultrahigh resolving power of the FT-ICRMS shown in Figure 6 ($m/\Delta m_{50\%} = 2,400,000$ at m/z 569) was sufficient to resolve ^{34}S isotopologues of compound **a** that remained unresolved at lower resolving power (LC-ESIMS). Molecular formula predictions for compounds **a** and **c** were first generated based on MS^2 fragmentation data with the assistance of CSI-FingerID, which combines MS^2 fragmentation tree computation and machine learning (Dührkop et al., 2015). To create a list of metal free fragment masses as an input to CSI-FingerID, we subtracted the mass of the metal from metal containing fragments that were identified based on their isotopic signature. We compared the top scoring molecular formula predictions to all molecular formulas containing C, H, N, O, P, and S within 2ppm of the exact mass determined by FT-ICRMS. $[\text{C}_{20}\text{H}_{21}\text{N}_4\text{O}_8\text{S}_2+\text{M}]^+$ (where M refers to a Ni or Cu isotopologue) and $[\text{C}_{32}\text{H}_{54}\text{N}_3\text{O}_6\text{S}_2\text{Ni}]^+$ were the only molecular formulae that were consistent with both the MS^2 and accurate mass results for compounds **a** and **c** respectively. Compound **d** was then assigned a formula of $[\text{C}_{33}\text{H}_{56}\text{N}_3\text{O}_6\text{S}_2\text{Ni}]^+$ based on its structural similarity to compound **c**. Searches for the molecular formulae of the apo forms of compounds **a**, **c**, and **d** in the Pubchem database did not yield any matches that are consistent with the MS^2 fragmentation patterns, suggesting that they are novel compounds. Obtaining full structures for these compounds requires additional characterization.

Cu and Ni Addition Experiment

LC-ICPMS enables direct detection of the metals that are associated with each ligand, and could potentially be used to monitor the exchange of ligand bound metal. As a preliminary investigation of metal competition and exchange using LC-ICPMS, an aliquot of sample 6 was spiked with a large excess of Cu, Ni, and a combination of both metals, then allowed to equilibrate for 12–15 h prior to analysis by LC-ICPMS to monitor Cu and Ni. This treatment saturates uncomplexed ligands and drives metal exchange by changing the relative availability of Cu vs. Ni for ligand binding.

When Cu was added to the sample, there was a large increase in signal intensity in the LC-ICPMS chromatogram of Cu peaks relative to the unamended sample (Figure 7). Three additional chromatographic peaks with very high intensities appeared at 38.9, 39.7, and 43.0 min. This experiment demonstrates that there was a significant portion of uncomplexed ligand in the organic extract that became saturated with the addition of excess Cu. These results are consistent with electrochemical data that indicated free (uncomplexed) Cu ligands were at least 5x more abundant than Cu (Figure 1). The addition of Ni did not significantly affect the distribution of Cu containing compounds. The Cu baseline was slightly elevated in the Ni addition treatment, likely due to residual Cu carryover adsorbed to the walls of the injector flow-path or column from the preceding Cu addition analysis.

Nickel addition did, however, cause new peaks to appear in the Ni ICPMS chromatogram at 37.1, and 38.5 min (Figure 7). Yet these peaks were absent when both Ni and Cu were added, indicating that Ni was outcompeted by Cu for binding to these

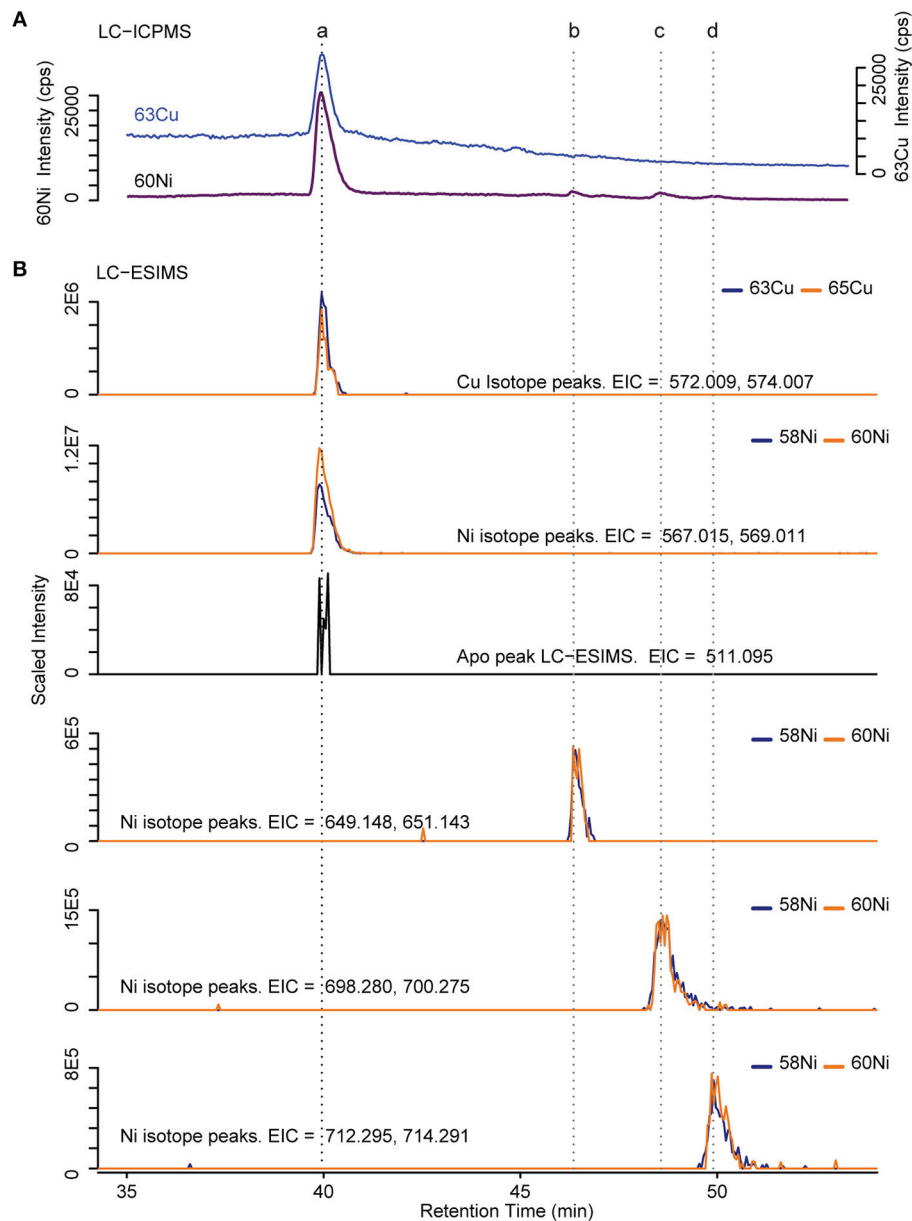
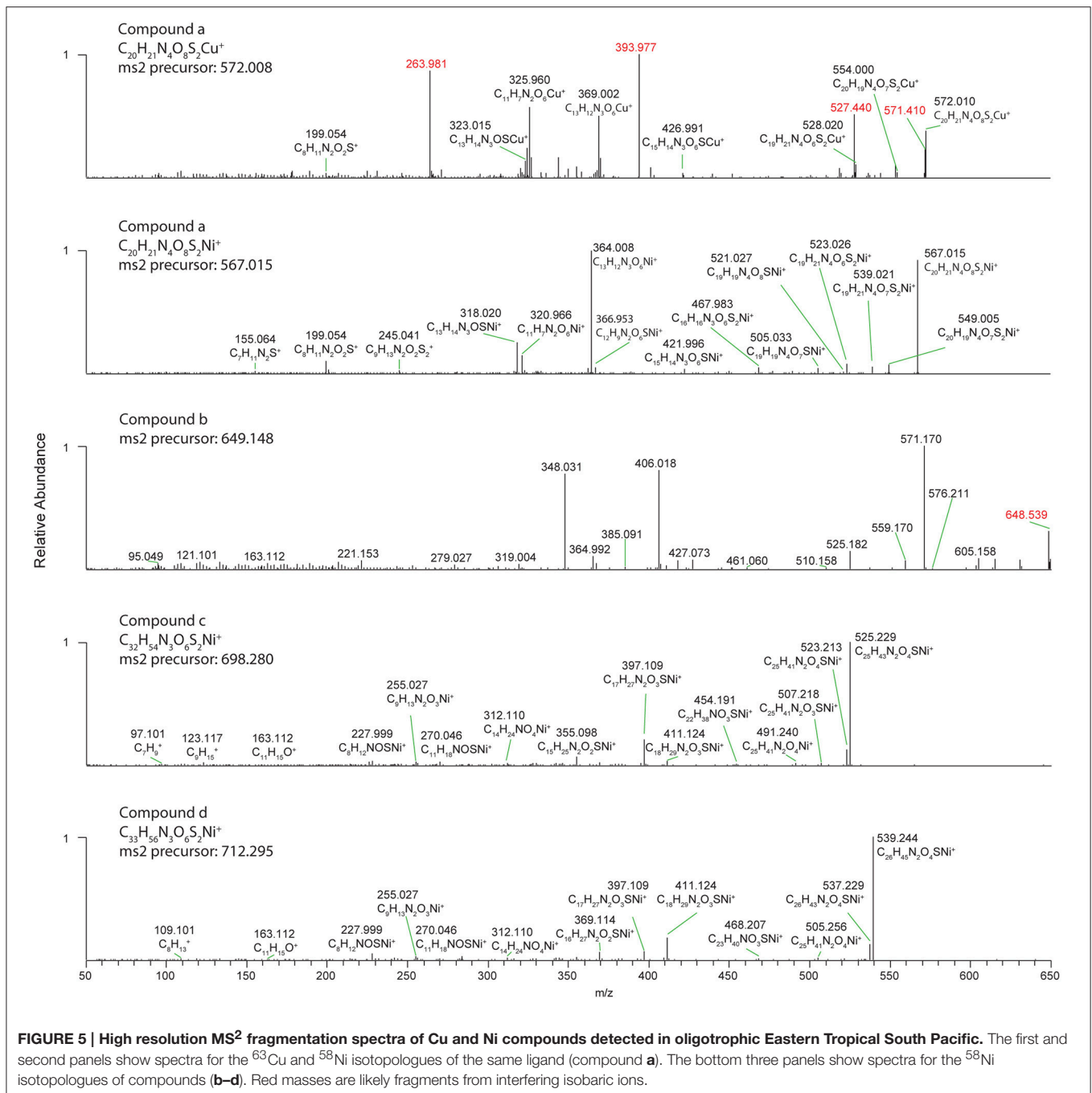


FIGURE 4 | Determination of Cu and Ni compound mass. (A) ICPMS chromatogram of ^{63}Cu and ^{60}Ni . Dashed lines indicate retention times of identified compounds **(B)** Extracted ion chromatograms (EIC) from positive mode ESIMS. Blue and orange lines correspond to the light and heavy metal isotopologues respectively. The intensity of the heavy isotopologue has been scaled by the natural abundance ratio of $^{58}\text{Ni}/^{60}\text{Ni}$ or $^{63}\text{Cu}/^{65}\text{Cu}$ (multiplied by 2.6 or 2.2 respectively) so that the isotopologues overlap.

TABLE 2 | Ni and Cu compounds detected across the GEOTRACES EPZT transect.

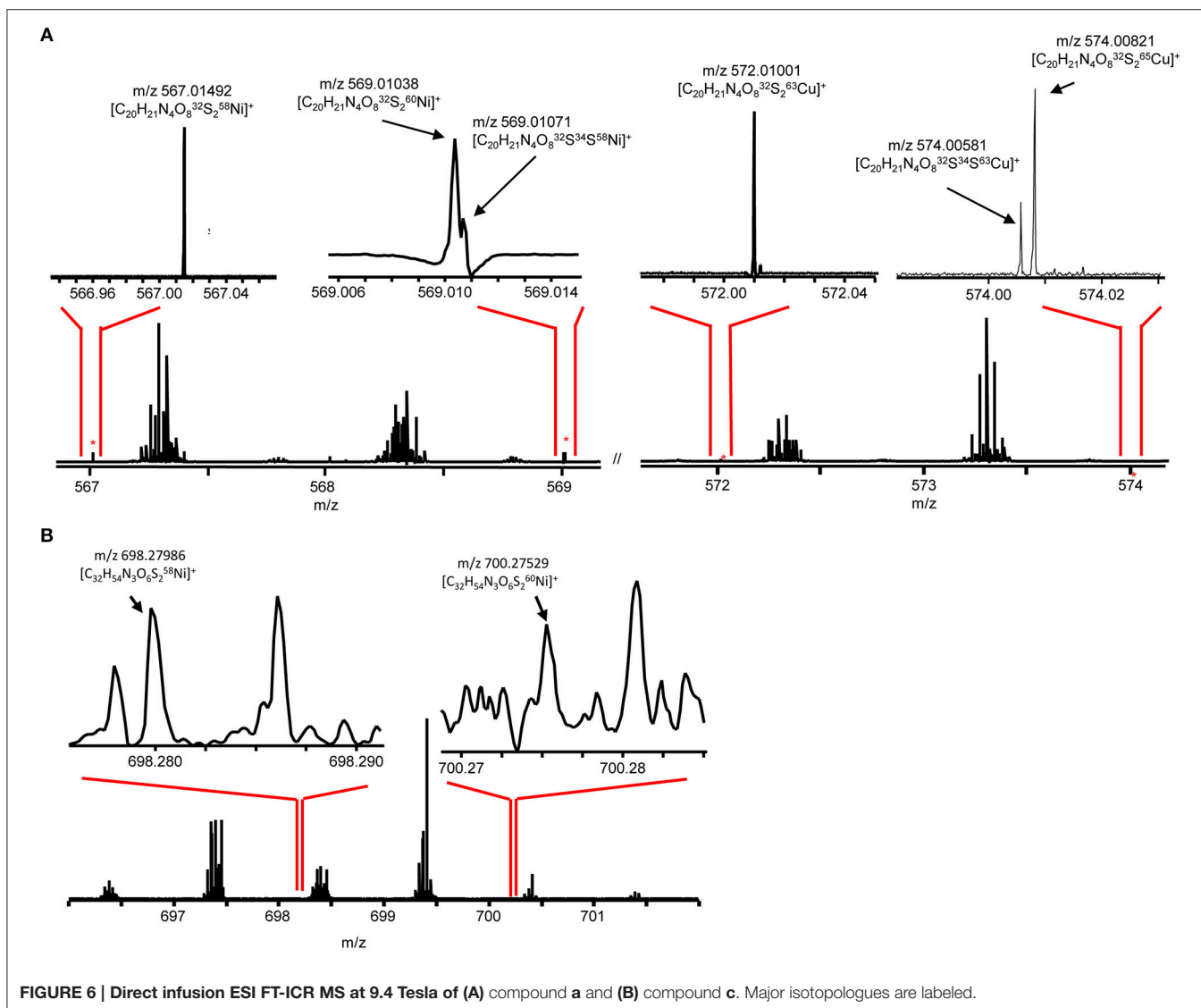
Compound	Retention time (min)	Molecular formula	Apo Form m/z	^{58}Ni Form m/z	^{60}Ni Form m/z	^{63}Cu Form m/z	^{65}Cu Form m/z
a	39.8	$[\text{C}_{20}\text{H}_{21}\text{N}_4\text{O}_3\text{S}_2 + \text{M}]^+$	511.095	567.015	569.011	572.009	574.007
b	46.4			649.148	651.143		
c	48.6	$[\text{C}_{32}\text{H}_{54}\text{N}_3\text{O}_6\text{S}_2 + \text{M}]^+$		698.28	700.275		
d	49.9	$[\text{C}_{33}\text{H}_{56}\text{N}_3\text{O}_6\text{S}_2 + \text{M}]^+$		712.295	714.291		



ligands. The major uncomplexed Cu binding ligands at 38.9, 39.7, and 43.0 min did not appear in the Ni chromatogram after Ni addition. These three Cu binding ligands did not outcompete the added citrate for Ni binding, suggesting very weak Ni binding for these compounds and better selectivity for Cu. The metal addition treatments did not affect the intensity of the Ni or Cu peaks detected for compound a (39.8 min), showing that this compound was saturated with metal in the original sample and has slow metal exchange kinetics.

DISCUSSION

These results provide a first glimpse of the distribution and chemical diversity of natural dissolved Cu and Ni complexes in the Eastern Pacific Ocean. The LC-ICPMS methods detected a fraction of the total dissolved metal (6–20% for Cu and 1–2% for Ni). LC-ICPMS only detects ligands if they are complexed to metals. It is important to note that despite efforts to minimize sample treatment, some changes in metal speciation are possible during extraction, since the final extract has a

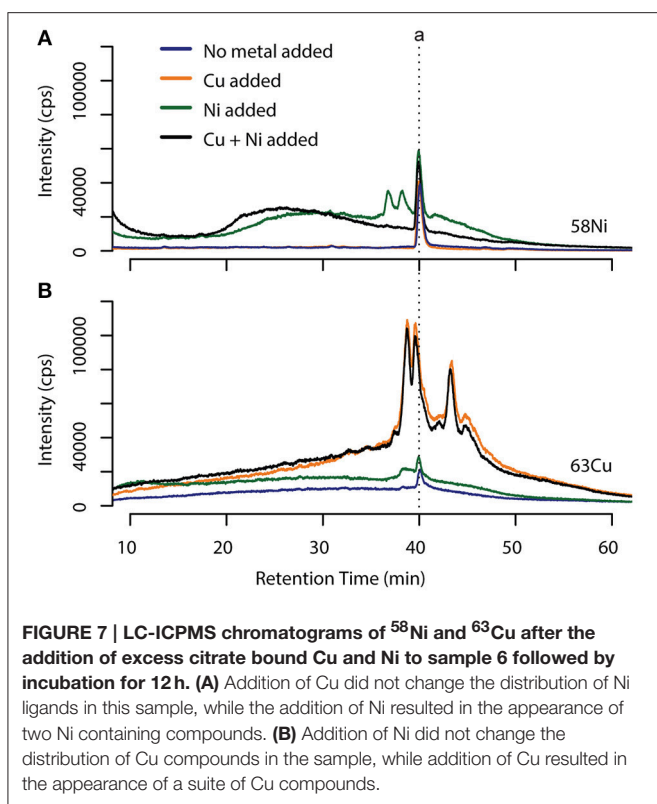


higher concentration of organic matter, a slightly lower pH (between 6 and 8), and much lower salt concentration than natural seawater. These differences can alter the kinetics of metal exchange compared to natural marine conditions but are unlikely to change the relative metal affinities of different ligands. Therefore, we believe the complexes observed in the LC-ICPMS chromatograms in **Figure 2** probably represent strong ligands that bind these metals under native conditions.

Inshore Heterogeneous Ligands Detected by LC-ICPMS

The fraction of total dissolved Cu and Ni ligands in seawater detected by LC-ICPMS is particularly high inshore, between 80 and 90°W. In this region, ligands were predominantly polar, structurally heterogeneous compounds that eluted between 10 and 30 min (**Figure 2**). The LC-ICPMS chromatograms are qualitatively similar to chromatograms of coastal seawater

organic extracts monitored by atomic fluorescence detection to investigate metal-organic speciation. These studies concluded that marine metal binding ligands are a complex mixture of many different compounds with a wide range of polarities (Mackey, 1983a; Mackey and O'Sullivan, 1990). One potential source of these heterogeneous polar ligands is the organic matter upwelled from low oxygen subsurface water. Continental shelf sediments have been suggested as a major source of Cu ligands (Skrabal et al., 1997, 2000; Bundy et al., 2013) including humic materials that form as organic matter decays after burial (Whitby and Van den Berg, 2014; Abualhaija et al., 2015). Humic materials likely contribute to the broad, chromatographically unresolved baseline eluting between 10 and 30 min. In addition, there are small, discrete chromatographic peaks superimposed on the unresolved baseline suggesting that well defined compounds of biological origin are likely present as well. This is consistent with previous studies that observed strong Cu ligands in highly productive regions (Coale and Bruland, 1988, 1990; Moffett et al., 1990;



Moffett, 1995). Unfortunately we were unable to detect Cu or Ni isotopologues at these retention times using LC-ESIMS due to interferences and ion suppression from the extremely complex matrix of coeluting compounds.

Structural Characterization of Defined Cu and Ni Ligands

In contrast to the broad suite of polar compounds found in the coastal upwelling sample, the well-defined Cu and Ni binding compounds **a–d** were only observed in the low-metal oligotrophic surface waters between 120 and 160°W. Based on the molecular formula assignments of the parent and fragment ions observed by ESIMS, these compounds are novel multi-dentate metal chelators. Compound **a** [$C_{20}H_{21}N_4O_8S_2+M$]⁺ was particularly abundant, accounting for 4–5% of the Cu and 5–8% of Ni detected by LC-ICPMS in samples 5 and 6. The overall compound has 12 degrees of unsaturation, including rings plus double bonds. One domain of this molecule is represented by the ions [$C_{11}H_7N_2O_6+M$]⁺. The large number of heteroatoms and degrees of unsaturation in this fragment imply the presence of heavily conjugated cyclic azole-like functional groups. The nitrogen atoms of such groups serve as the electron donor of many strong Cu and Ni chelators including cyclic peptides and porphyrins. The remaining half of the molecule is represented by [$C_9H_{13}N_2O_2S_2$]⁺. The sulfur atoms appear to be associated with thiols, as indicated by an observed neutral loss of CH₂S and the fragment C₆H₁₀NS₂⁺. Furthermore, the loss of CO₂ between the fragments of

C₇H₁₁N₂S⁺ and C₈H₁₁N₂O₂S⁺ imply the presence of a labile carboxylic acid. This second half of the compound appears to have lower metal affinity, since the representative fragments were not observed in association with Ni or Cu. However, a fragment that retains one of the azole-like nitrogen groups [$C_{13}H_{14}N_3OS+M$]⁺ does bind the metal, further implicating nitrogen as a key metal binding moiety. The closest structural analogs to compound **a** among well-studied biological Cu and Ni chelators may be other multi-dentate ligands that possess aromatic nitrogen based ligands, such as porphyrins or cyclic azole-based peptides.

Compounds **c** and **d** are larger molecules with 7 degrees of unsaturation. As with compound **a**, multiple N and O electron donors appear to be more important for metal binding than S, as indicated by the fact that one or both sulfurs are missing from all of the fragments that retain Ni, such as C₂₅H₄₁N₂O₄Ni⁺ and C₁₄H₂₄NO₄Ni⁺. In these molecules, sulfur is associated with domains represented by the major neutral loss of C₇H₁₁NOS and fragments C₈H₁₂NOSNi⁺ and C₁₁H₁₈NOSNi⁺. These compounds also possess a hydrocarbon domain represented by the fragment C₁₁H₁₅O⁺ that contribute to the hydrophobicity of these compounds and the late retention times.

These ligands provide insight into structural elements that are likely shared by other marine ligands with similar chemical properties (e.g., binding affinity, redox potential, bioavailability) and biological roles. However, fewer structures of marine Cu and Ni ligands are known compared to other ligand classes such as siderophores (Vraspir and Butler, 2009). While extracellular Cu binding ligands have been detected from a wide variety of ecologically abundant marine phytoplankton and bacterial taxa (Moffett and Brand, 1996; Croot et al., 1999, 2000; Gordon et al., 2000; Wiramanaden et al., 2008), few of these ligands have been structurally characterized. The combined LCMS approach we used here is well suited for rapid screening of laboratory pure cultures for Ni and Cu ligands, and offers the potential to expand the catalog of characterized ligands and their biological sources.

The appearance of compounds **a–d** in the western part of the transect suggest that they may be involved in metabolic processes that are unique to the oligotrophic ocean. One possibility is that these compounds are used to regulate intracellular free metal concentrations. As microbes concentrate iron, cobalt, and other scarce metals from the environment via transporters with imperfect specificity, they also concentrate more abundant metals including Cu and Ni (Waldron et al., 2007; Waldron and Robinson, 2009). Specialized chelators may be needed to prevent Cu or Ni from occupying binding sites in proteins that are meant for other metals. Alternatively, these Ni and Cu complexes may be cofactors used in metabolic processes that only occur in oligotrophic waters, perhaps as a substitution for scarce metals. Such cofactors are often tetrapyrroles such as the Ni cofactor F430 used by methane oxidizing archaea (Allen et al., 2014). These intracellular metal compounds could be released into the dissolved ligand pool by cell lysis (Ahner et al., 1997; Dupont et al., 2004; Wei and Ahner, 2005). Another possibility is that these compounds are released by microbes in order to

enhance metal uptake. Such strategies may provide an advantage to microbes that inhabit the oligotrophic Eastern tropical Pacific ocean where free Cu could potentially be in short supply (Jacquot et al., 2013).

Additional metal complexes were also observed for which masses could not be detected by LC-ESIMS due to ion suppression from coeluting compounds. Improving the separation of these metal bound compounds from the organic background using multiple dimensions of chromatography may resolve this issue. Furthermore, the saturation of free ligands with added Ni and Cu gave rise to intense chromatographic peaks. Future work will focus on the LC-ESIMS characterization of these compounds, which likely correspond to weaker ligands in the samples. Some of these appear to have affinity for Cu but not Ni while others bind Ni as well, and these diverse metal binding behaviors may reflect different electron donating functional domains.

Other methods of extracting organic compounds from seawater may offer additional analytical windows for ligand characterization. The solid phase extraction method used in this study was selected due to the low organic background of the ENV resin and stability across a wide range of pH values. Other hydrophobic resins or other elution solvents may recover a different fraction of the total dissolved metal and ligands (Mills et al., 1982; Mackey, 1983b; Waska et al., 2015). In addition, other extraction approaches such as immobilized metal affinity chromatography have been used to extract weak or uncomplexed metal ligands from seawater (Ross et al., 2003). The composition of the ligands retained by these other extraction methods remains poorly constrained, but the LC-ICPMS-ESIMS approaches described here can be adapted to survey the composition of these extracts.

Slow Dissociation Kinetics of Compound a

The presence of both Ni and Cu complexes of compound **a** raises questions about the dynamics of Ni and Cu competition for metal binding sites. Two factors are important—the binding affinity of the chelator to different metals as the system approaches equilibrium, and the kinetics of metal exchange. Although Cu²⁺ ligand complexes are typically more stable than Ni²⁺ complexes in aqueous solutions (Irving and Williams, 1953), compound **a** did not release any bound Ni²⁺ after the addition of excess Cu²⁺ in our experiments. This suggests that the dissociation kinetics of compound **a** with Ni are much slower than the 12 h equilibration time used in this study. For such compounds, the metal that they bind in the ocean may reflect metal association rates rather than equilibrium binding constants. The kinetics of metal association depend on free metal ion concentrations and the loss rate of water from the inner coordination sphere of those metals (Hering and Morel, 1989, 1990). In this case of Ni and Cu competition, the significantly slower water loss rate of Ni compared to Cu may be offset by the higher free metal ion concentration of Ni (inferred from high labile Ni measurements), since over 99% of Cu is complexed by strong organic ligands throughout the transect, while <50% of dissolved Ni is strongly complexed. Alternatively, the metal

speciation of these compounds may reflect the intracellular environment where metal-ligand complexes can form, likely in the presence of very low intracellular metal abundances (Rae et al., 1999), and subsequent slow dissociation kinetics as these metal-ligand complexes are released. Slow dissociation kinetics may be common for strong ligands of other metals as well. Nickel can impact the solubility and bioavailability of scarce micronutrient Co by competing for the same ligand sites, and the result of this competition may well be controlled by kinetics rather than thermodynamics (Saito and Moffett, 2001). Furthermore, strong iron binding ligands such as siderophores can have lifetimes of several months before dissociation (Witter et al., 2000), although the compounds themselves are likely taken up or degraded on shorter timescales similar to other peptidic compounds. These examples of slow dissociation kinetics are an important consideration for experiments and models of metal speciation, particularly for strong ligands that are capable of binding multiple metals.

CONCLUSIONS

In this study, we used a mass spectrometry based approach to detect and characterize Cu and Ni ligands in the US GEOTRACES section across the eastern tropical South Pacific Ocean. Using both mass spectrometric and electrochemical approaches, we found that the concentrations of Cu and Ni ligands are highest in the coastal upwelling region of the section, where ligands occur as a very complex mixture of chromatographically unresolved compounds. Ligand concentrations were lower in offshore oligotrophic surface waters, where structurally well-defined ligands become relatively more important. The partial structural characterization of these compounds reveals that these are multi-dentate ligands with hard base electron donors that bind metals in the 2+ oxidation state. Discovering the biological source of these ligands is the key to understanding their distinct distributions across the surface ocean as well as their role in biogeochemical metal cycles. The analyses presented here are well suited for the compound specific discovery and investigation of other metal chelators. As we learn more about the compounds that bind these metals in the ocean, structural similarities will continue to emerge and facilitate future identifications. This information will help generate specific molecular targets and model compounds that can be tracked through the environment and provide greater insight into mechanisms of metal cycling and connections with microbial ecology.

AUTHOR CONTRIBUTIONS

RMBO and DR designed the study, NH collected the samples, RMBO, and AM determined ligand composition, CT measured metal concentrations. AR measured Cu ligand concentrations and binding strengths, RMBU measured labile nickel concentrations, AM performed FTICRMS analyses, RMBO, NH, RMBU, KAB, MS, and DR analyzed the field data,

RMBO and DR wrote the manuscript with contributions from all authors.

ACKNOWLEDGMENTS

We would like to thank chief scientists James Moffett and Chris German, as well as Alan Shiller, Cheryl Zurbrick, and Geoffrey Smith for assistance with sample collection, and the scientists and crew of the R/V *Thomas G. Thompson*. Support was provided by the National Science Foundation

(NSF) program in Chemical Oceanography (OCE-1356747, OCE-1233261, OCE-1233733, OCE-1233502, and OCE-1237034), the NSF Science and Technology Center for Microbial Oceanography Research and Education (C-MORE; DBI-0424599), the Gordon and Betty Moore Foundation (#3298 and 3934), and the Simons Foundation (#329108, DR). A portion of this work was performed at the National High Magnetic Field Laboratory, which is supported by NSF Division of Materials Research through DMR-11-57490, and the State of Florida.

REFERENCES

- Abualhija, M. M., Whitby, H., and van den Berg, C. M. G. (2015). Competition between copper and iron for humic ligands in estuarine waters. *Mar. Chem.* 172, 46–56. doi: 10.1016/j.marchem.2015.03.010
- Achterberg, E. P., and Van Den Berg, C. M. G. (1997). Chemical speciation of chromium and nickel in the western Mediterranean. *Deep Sea Res. Part II Top. Stud. Oceanogr.* 44, 693–720. doi: 10.1016/S0967-0645(96)00086-0
- Ahner, B. A., Morel, F. M. M., and Moffett, J. W. (1997). Trace metal control of phytochelatin production in coastal waters. *Limnol. Oceanogr.* 42, 601–608. doi: 10.4319/lo.1997.42.3.0601
- Ahner, B. A., Price, N. M., and Morel, F. M. (1994). Phytochelatin production by marine phytoplankton at low free metal ion concentrations: laboratory studies and field data from Massachusetts Bay. *Proc. Natl. Acad. Sci. U.S.A.* 91, 8433–8436. doi: 10.1073/pnas.91.18.8433
- Ahner, B. A., Wei, L., Oleson, J. R., and Ogura, N. (2002). Glutathione and other low molecular weight thiols in marine phytoplankton under metal stress. *Mar. Ecol. Prog. Ser.* 232, 93–103. doi: 10.3354/meps232093
- Allen, K. D., Wegener, G., and White, R. H. (2014). Discovery of multiple modified F430 coenzymes in methanogens and anaerobic methanotrophic archaea suggests possible new roles for F430 in nature. *Appl. Environ. Microbiol.* 80, 6403–6412. doi: 10.1128/AEM.02202-14
- Baars, O., Morel, F. M. M., and Perlman, D. H. (2014). ChelomEx: isotope-assisted discovery of metal chelates in complex media using high-resolution LC-MS. *Anal. Chem.* 86, 11298–11305. doi: 10.1021/ac503000e
- Baars, O., Zhang, X., Morel, F. M. M., and Seyedsayamdost, M. R. (2015). The siderophore metabolome of *Azotobacter vinelandii*. *Appl. Environ. Microbiol.* 82, 27–39. doi: 10.1128/AEM.03160-15
- Baker, A. R., Thomas, M., Bange, H. W., and Plasencia Sanchez, E. (2016). Soluble trace metals in aerosols over the tropical south-east Pacific offshore of Peru. *Biogeosciences* 13, 817–825. doi: 10.5194/bg-13-817-2016
- Baker, H., and Khalili, F. (2003). Comparative study of binding strengths and thermodynamic aspects of Cu(II) and Ni(II) with humic acid by Schubert's ion-exchange method. *Anal. Chim. Acta* 497, 235–248. doi: 10.1016/j.aca.2003.08.036
- Bertram, A., and Pattenden, G. (2007). Marine metabolites: metal binding and metal complexes ofazole-based cyclic peptides of marine origin. *Nat. Prod. Rep.* 24, 18–30. doi: 10.1039/b612600f
- Biller, D. V., and Bruland, K. W. (2012). Analysis of Mn, Fe, Co, Ni, Cu, Zn, Cd, and Pb in seawater using the Nobias-chelate PA1 resin and magnetic sector inductively coupled plasma mass spectrometry (ICP-MS). *Mar. Chem.* 130–131, 12–20. doi: 10.1016/j.marchem.2011.12.001
- Blakney, G. T., Hendrickson, C. L., and Marshall, A. G. (2011). Predator data station: a fast data acquisition system for advanced FT-ICR MS experiments. *Int. J. Mass Spectrom.* 306, 246–252. doi: 10.1016/j.ijms.2011.03.009
- Boiteau, R. M., Fitzsimmons, J. N., Repeta, D. J., and Boyle, E. A. (2013). Detection of iron ligands in seawater and marine cyanobacteria cultures by high-performance liquid chromatography-inductively coupled plasma-mass spectrometry. *Anal. Chem.* 85, 4357–4362. doi: 10.1021/ac3034568
- Boiteau, R. M., Hawco, N. J., Mende, D. R., McIlvin, M. R., Fitzsimmons, J. N., Sedwick, P. N., et al. (in press). Siderophore-based microbial adaptations to iron scarcity across the eastern Pacific Ocean. *PNAS*.
- Boiteau, R. M., and Repeta, D. J. (2015). An extended siderophore suite from *Synechococcus* sp. PCC 7002 revealed by LC-ICPMS-ESIMS. *Metallomics* 7, 877–884. doi: 10.1039/C5MT00005J
- Bruland, K. W., Rue, E. L., Smith, G. J., and DiTullio, G. R. (2005). Iron, macronutrients and diatom blooms in the Peru upwelling regime: brown and blue waters of Peru. *Mar. Chem.* 93, 81–103. doi: 10.1016/j.marchem.2004.06.011
- Buck, K. N., and Bruland, K. W. (2005). Copper speciation in San Francisco Bay: a novel approach using multiple analytical windows. *Mar. Chem.* 96, 185–198. doi: 10.1016/j.marchem.2005.01.001
- Bundy, R. M., Barbeau, K. A., and Buck, K. N. (2013). Sources of strong copper-binding ligands in Antarctic Peninsula surface waters. *Deep. Res. Part II Top. Stud. Oceanogr.* 90, 134–146. doi: 10.1016/j.dsr2.2012.07.023
- Campos, M. L. A. M., and van den Berg, C. M. G. (1994). Determination of copper complexation in sea water by cathodic stripping voltammetry and ligand competition with salicylaldehyde. *Anal. Chim. Acta* 284, 481–496. doi: 10.1016/0003-2670(94)85055-0
- Chambers, M. C., Maclean, B., Burke, R., Amodei, D., Ruderman, D. L., Neumann, S., et al. (2012). A cross-platform toolkit for mass spectrometry and proteomics. *Nat. Biotechnol.* 30, 918–920. doi: 10.1038/nbt.2377
- Coale, K. H., and Bruland, K. W. (1988). Copper complexation in the Northeast Pacific. *Limnol. Oceanogr.* 33, 1084–1101. doi: 10.4319/lo.1988.33.5.1084
- Coale, K. H., and Bruland, K. W. (1990). Spatial and temporal variability in copper complexation in the North Pacific. *Deep Sea Res. Part A Oceanogr. Res. Pap.* 37, 317–336. doi: 10.1016/0198-0149(90)90130-N
- Comba, P., Dovalil, N., Gahan, L. R., Hanson, G. R., and Westphal, M. (2014). Cyclic peptide marine metabolites and CuII. *Dalt. Trans.* 43, 1935–1956. doi: 10.1039/C3DT52664J
- Croot, P. L., Moffett, J. W., and Brand, L. E. (2000). Production of extracellular Cu complexing ligands by eucaryotic phytoplankton in response to Cu stress. *Limnol. Oceanogr.* 45, 619–627. doi: 10.4319/lo.2000.45.3.0619
- Croot, P. L., Moffett, J. W., and Luther, G. W. (1999). Polarographic determination of half-wave potentials for copper-organic complexes in seawater. *Mar. Chem.* 67, 219–232. doi: 10.1016/S0304-4203(99)00054-7
- Devez, A., Achterberg, E., and Gledhill, M. (2009). Metal ion-binding properties of phytochelatin and related ligands. *Met. Ions Life Sci.* 5, 441–481. doi: 10.1039/9781847559531-00441
- Donat, J. R., Lao, K. A., and Bruland, K. W. (1994). Speciation of dissolved copper and nickel in South San Francisco Bay: a multi-method approach. *Anal. Chim. Acta* 284, 547–571. doi: 10.1016/0003-2670(94)85061-5
- Donat, J. R., and van den Berg, C. M. G. (1992). A new cathodic stripping voltammetric method for determining organic copper complexation in seawater. *Mar. Chem.* 38, 69–90. doi: 10.1016/0304-4203(92)90068-L
- Dührkop, K., Shen, H., Meusel, M., Rousu, J., and Böcker, S. (2015). Searching molecular structure databases with tandem mass spectra using CSI:FingerID. *Proc. Natl. Acad. Sci. U.S.A.* 112, 12580–12585. doi: 10.1073/pnas.1509788112
- Dupont, C. L., Nelson, R. K., Bashir, S., Moffett, J. W., and Ahner, B. A. (2004). Novel copper-binding and nitrogen-rich thiols produced and exuded by *Emiliania huxleyi*. *Limnol. Oceanogr.* 49, 1754–1762. doi: 10.4319/lo.2004.49.5.1754
- El Ghazouani, A., Baslé, A., Gray, J., Graham, D. W., Firkbank, S. J., and Dennison, C. (2012). Variations in methanobactin structure influences copper utilization

- by methane-oxidizing bacteria. *Proc. Natl. Acad. Sci. U.S.A.* 109, 8400–8404. doi: 10.1073/pnas.1112921109
- Emmett, M. R., White, F. M., Hendrickson, C. L., Shi, S. D., and Marshall, A. G. (1998). Application of micro-electrospray liquid chromatography techniques to FT-ICR MS to enable high-sensitivity biological analysis. *J. Am. Soc. Mass Spectrom.* 9, 333–340. doi: 10.1016/S1044-0305(97)00287-0
- Freeman, J. L., Persans, M. W., Nieman, K., Albrecht, C., Peer, W., Pickering, I. J., et al. (2004). Increased glutathione biosynthesis plays a role in nickel tolerance in *thlaspi* nickel hyperaccumulators. *Plant Cell* 16, 2176–2191. doi: 10.1105/tpc.104.023036
- Ghssein, G., Brutesco, C., Ouerdane, L., Fojcik, C., Izaute, A., Wang, S., et al. (2016). Biosynthesis of a broad-spectrum nicotianamine-like metallophore in *Staphylococcus aureus*. *Science* 352, 1105–1109. doi: 10.1126/science.aaf1018
- Gordon, A. S., Donat, J. R., Kango, R. A., Dyer, B. J., and Stuart, L. M. (2000). Dissolved copper-complexing ligands in cultures of marine bacteria and estuarine water. *Mar. Chem.* 70, 149–160. doi: 10.1016/S0304-4203(00)00019-0
- Hering, J. G., and Morel, F. M. M. (1989). Slow coordination reactions in seawater. *Geochim. Cosmochim. Acta* 53, 611–618. doi: 10.1016/0016-7037(89)90004-5
- Hering, J., and Morel, F. (1990). Kinetics of trace metal complexation: ligand-exchange reactions. *Environ. Sci. Technol.* 25, 242–252. doi: 10.1021/es00072a014
- Irving, H., and Williams, R. (1953). The stability of transition-metal complexes. *J. Chem. Soc.* 3, 3192–3210. doi: 10.1039/jr9530003192
- Jacquot, J. E., Kondo, Y., Knapp, A. N., and Moffett, J. W. (2013). The speciation of copper across active gradients in nitrogen-cycle processes in the eastern tropical South Pacific. *Limnol. Oceanogr.* 58, 1387–1394. doi: 10.4319/lo.2013.58.4.1387
- Jacquot, J. E., and Moffett, J. W. (2015). Copper distribution and speciation across the International GEOTRACES Section GA03. *Deep. Res. Part II Top. Stud. Oceanogr.* 116, 187–207. doi: 10.1016/j.dsr2.2014.11.013
- Kaiser, N. K., Quinn, J. P., Blakney, G. T., Hendrickson, C. L., and Marshall, A. G. (2011a). A novel 9.4 tesla FTICR mass spectrometer with improved sensitivity, mass resolution, and mass range. *J. Am. Soc. Mass Spectrom.* 22, 1343–1351. doi: 10.1007/s13361-011-0141-9
- Kaiser, N. K., Savory, J. J., McKenna, A. M., Quinn, J. P., Hendrickson, C. L., and Marshall, A. G. (2011b). Electrically compensated fourier transform ion cyclotron resonance cell for complex mixture mass analysis. *Anal. Chem.* 83, 6907–6910. doi: 10.1021/ac201546d
- Kim, H. J., Graham, D. W., DiSpirito, A. A., and Alterman, M. A. (2004). Methanobactin, a copper-acquisition compound from methane-oxidizing bacteria. *Science* 305, 16–19. doi: 10.1126/science.1098322
- Mackey, D. J. (1983a). Metal-organic complexes in seawater - An investigation of naturally occurring complexes of Cu, Zn, Fe, Mg, Ni, Cr, Mn and Cd using high-performance liquid chromatography with atomic fluorescence detection. *Mar. Chem.* 13, 169–180. doi: 10.1016/0304-4203(83)90012-9
- Mackey, D. J. (1983b). The strong complexing capacity of seawater - an investigation of south-eastern Australian coastal waters. *Mar. Chem.* 14, 73–87. doi: 10.1016/0304-4203(83)90071-3
- Mackey, D. J., and O'Sullivan, J. E. (1990). Metal - organic interactions in sea water: an ecosystem experiment. *Anal. Chim. Acta* 232, 161–170.
- McKenna, A. M., Marshall, A. G., and Rodgers, R. P. (2013). Heavy petroleum composition. 4. Asphaltene compositional space. *Energy Fuels* 27, 1257–1267. doi: 10.1021/ef301747d
- McKenna, A. M., Williams, J. T., Putman, J. C., Aeppli, C., Reddy, C. M., Valentine, D. L., et al. (2014). Unprecedented ultrahigh resolution FT-ICR mass spectrometry and parts-per-billion mass accuracy enable direct characterization of nickel and vanadyl porphyrins in petroleum from natural seeps. *Energy Fuels* 28, 2454–2464. doi: 10.1021/ef5002452
- Michael, J. P., Pattenden, G., and Michael, B. J. P. (1993). Marine metabolites and metal ion chelation: the facts and the fantasies. *Angew. Chemie Int. Ed.* 32, 1–130. doi: 10.1002/anie.199300013
- Mills, G. L., Hanson, A. K., and Quinn, J. G. (1982). Chemical studies of copper-organic complexes isolated from estuarine waters using C18 Reverse-phase liquid chromatography. *Mar. Chem.* 11, 355–377. doi: 10.1016/0304-4203(82)90031-7
- Moffett, J. W. (1995). Temporal and spatial variability of copper complexation by strong chelators in the Sargasso Sea. *Deep. Res. Part I* 42, 1273–1295. doi: 10.1016/0967-0637(95)00060-J
- Moffett, J. W., and Brand, L. E. (1996). Production of strong, extracellular Cu chelators by marine cyanobacteria in response to Cu stress. *Limnol. Oceanogr.* 41, 388–395. doi: 10.4319/lo.1996.41.3.0388
- Moffett, J. W., and Zika, R. G. (1983). Oxidation kinetics of Cu(I) in seawater: implications for its existence in the marine environment. *Mar. Chem.* 13, 239–251. doi: 10.1016/0304-4203(83)90017-8
- Moffett, J. W., Zika, R. G., and Brand, L. E. (1990). Distribution and potential sources and sinks of copper chelators in the Sargasso Sea. *Deep Sea Res. Part A, Oceanogr. Res. Pap.* 37, 27–36. doi: 10.1016/0198-0149(90)90027-S
- Moore, C. M., Mills, M. M., Arrigo, K. R., Berman-Frank, I., Bopp, L., Boyd, P. W., et al. (2013). Processes and patterns of oceanic nutrient limitation. *Nat. Geosci.* 6, 701–710. doi: 10.1038/ngeo1765
- Mounicou, S., Szpunar, J., and Lobinski, R. (2009). Metallomics: the concept and methodology. *Chem. Soc. Rev.* 38, 1119–1138. doi: 10.1039/b713633c
- Nimmo, M., and van Den Berg, C. M. G. (1989). The chemical speciation of dissolved nickel, copper, vanadium, and iron in liverpool bay, Irish Sea. *Estuar. Coast. Shelf Sci.* 29, 57–74. doi: 10.1016/0272-7714(89)90073-5
- Omanović, D., Garnier, C., and Pižeta, I. (2014). ProMCC: an all-in-one tool for trace metal complexation studies. *Mar. Chem.* 173, 25–39. doi: 10.1016/j.marchem.2014.10.011
- Parker, C. E., Brown, M. T., and Bruland, K. W. (2016). Scandium in the open ocean: a comparison with other group 3 trivalent metals. *Geophys. Res. Lett.* 43, 2758–2764. doi: 10.1002/2016gl067827
- Pennington, J. T., Mahoney, K. L., Kuwahara, V. S., Kolber, D. D., Calienes, R., and Chavez, F. P. (2006). Primary production in the eastern tropical Pacific: a review. *Prog. Oceanogr.* 69, 285–317. doi: 10.1016/j.pcean.2006.03.012
- Rae, T. D., Schmidt, P. J., Pufahl, R. A., Culotta, V. C., and O'halloran, T. V. (1999). Undetectable intracellular free copper: the requirement of a copper chaperone for superoxide dismutase. *Science* 284, 805–808. doi: 10.1126/science.284.5415.805
- Ross, A. R., Ikononou, M. G., and Orians, K. J. (2003). Characterization of copper-complexing ligands in seawater using immobilized copper(II)-ion affinity chromatography and electro-spray ionization mass spectrometry. *Mar. Chem.* 83, 47–58. doi: 10.1016/S0304-4203(03)00095-1
- Saito, M. A., and Moffett, J. W. (2001). Complexation of cobalt by natural organic ligands in the Sargasso Sea as determined by a new high-sensitivity electrochemical cobalt speciation method suitable for open ocean work. *Mar. Chem.* 75, 49–68. doi: 10.1016/S0304-4203(01)00025-1
- Saito, M. A., and Moffett, J. W. (2004). Cobalt and nickel in the Peru upwelling region: a major flux of labile cobalt utilized as a micronutrient. *Glob. Biogeochem. Cycles* 18, 1–14. doi: 10.1029/2003GB002216
- Saito, M. A., Rocap, G., and Moffett, J. W. (2005). Production of cobalt binding ligands in a *Synechococcus* feature at the Costa Rica upwelling dome. *Limnol. Oceanogr.* 50, 279–290. doi: 10.4319/lo.2005.50.1.0279
- Savory, J. J., Kaiser, N. K., McKenna, A. M., Xian, F., Blakney, G. T., Rodgers, R. P., et al. (2011). Parts-per-billion fourier transform ion cyclotron resonance mass measurement accuracy with a “Walking” calibration equation. *Anal. Chem.* 83, 1732–1736. doi: 10.1021/ac102943z
- Shi, S. D. H., Drader, J. J., Freitas, M. A., Hendrickson, C. L., and Marshall, A. G. (2000). Comparison and interconversion of the two most common frequency-to-mass calibration functions for Fourier transform ion cyclotron resonance mass spectrometry. *Int. J. Mass Spectrom.* 195–196, 591–598. doi: 10.1016/S1387-3806(99)00226-2
- Skrabal, S. A., Donat, J. R., and Burdige, D. J. (1997). Fluxes of copper-complexing ligands from estuarine sediments. *Limnol. Oceanogr.* 42, 992–996. doi: 10.4319/lo.1997.42.5.0992
- Skrabal, S. A., Donat, J. R., and Burdige, D. J. (2000). Pore water distributions of dissolved copper and copper-complexing ligands in estuarine and coastal marine sediments. *Geochim. Cosmochim. Acta* 64, 1843–1857. doi: 10.1016/S0016-7037(99)00387-7
- Thompson, C. M., Ellwood, M. J., and Sander, S. G. (2014). Dissolved copper speciation in the Tasman Sea, SW Pacific Ocean. *Mar. Chem.* 164, 84–94. doi: 10.1016/j.marchem.2014.06.003
- Tolmachev, A. V., Robinson, E. W., Wu, S., Smith, R. D., and Paša-Toli, L. (2011). Trapping radial electric field optimization in compensated FTICR cells. *J. Am. Soc. Mass Spectrom.* 22, 1334–1342. doi: 10.1007/s13361-011-0167-z
- Turner, D., Whitfield, M., and Dickson, A. (1981). The equilibrium speciation of dissolved components in freshwater and sea water at 25°C and 1 atm pressure.

- Geochim. Cosmochim. Acta* 45, 855–881. doi: 10.1016/0016-7037(81)90115-0
- van den Berg, C. M. G., and Nimmo, M. (1987). Determination of interactions of nickel with dissolved organic material in seawater using cathodic stripping voltammetry. *Sci. Total Environ.* 60, 185–195. doi: 10.1016/0048-9697(87)90415-3
- Vraspir, J. M., and Butler, A. (2009). Chemistry of marine ligands and siderophores. *Ann. Rev. Mar. Sci.* 1, 43–63. doi: 10.1146/annurev.marine.010908.163712
- Waldron, K. J., and Robinson, N. J. (2009). How do bacterial cells ensure that metalloproteins get the correct metal? *Nat. Rev. Microbiol.* 7, 25–35. doi: 10.1038/nrmicro2057
- Waldron, K. J., Tottey, S., Yanagisawa, S., Dennison, C., and Robinson, N. J. (2007). A periplasmic iron-binding protein contributes toward inward copper supply. *J. Biol. Chem.* 282, 3837–3846. doi: 10.1074/jbc.M609916200
- Walsh, M. J., and Ahner, B. A. (2013). Determination of stability constants of Cu(I), Cd(II) and Zn(II) complexes with thiols using fluorescent probes. *J. Inorg. Biochem.* 128, 112–123. doi: 10.1016/j.jinorgbio.2013.07.012
- Waska, H., Koschinsky, A., Ruiz Chanco, M. J., and Dittmar, T. (2015). Investigating the potential of solid-phase extraction and Fourier-transform ion cyclotron resonance mass spectrometry (FT-ICR-MS) for the isolation and identification of dissolved metal–organic complexes from natural waters. *Mar. Chem.* 173, 78–92. doi: 10.1016/j.marchem.2014.10.001
- Wei, L., and Ahner, B. A. (2005). Sources and sinks of dissolved phytochelatin in natural seawater. *Limnol. Oceanogr.* 50, 13–22. doi: 10.4319/lo.2005.50.1.0013
- Whitby, H., and Van den Berg, C. M. G. (2014). Evidence for copper-binding humic substances in seawater. *Mar. Chem.* 173, 282–290. doi: 10.1016/j.marchem.2014.09.011
- Wilcox, B. E., Hendrickson, C. L., and Marshall, A. G. (2002). Improved ion extraction from a linear octopole ion trap: SIMION analysis and experimental demonstration. *J. Am. Soc. Mass Spectrom.* 13, 1304–1312. doi: 10.1016/S1044-0305(02)00622-0
- Wiramanaden, C. I. E., Cullen, J. T., Ross, A. R. S., and Orians, K. J. (2008). Cyanobacterial copper-binding ligands isolated from artificial seawater cultures. *Mar. Chem.* 110, 28–41. doi: 10.1016/j.marchem.2008.02.003
- Witter, A. E., Hutchins, D. A., Butler, A., and Luther, G. W. III. (2000). Determination of conditional stability constants and kinetic constants for strong model Fe-binding ligands in seawater. *Mar. Chem.* 69, 1–17. doi: 10.1016/S0304-4203(99)00087-0
- Wuttig, K., Heller, M. I., and Croot, P. L. (2013). Pathways of superoxide (O₂⁻) decay in the Eastern Tropical North Atlantic. *Environ. Sci. Technol.* 47, 10249–10256. doi: 10.1021/es401658t
- Xian, F., Corilo, Y. E., Hendrickson, C. L., and Marshall, A. G. (2012). Baseline correction of absorption-mode Fourier transform ion cyclotron resonance mass spectra. *Int. J. Mass Spectrom.* 325–327, 67–72. doi: 10.1016/j.ijms.2012.06.007
- Xian, F., Hendrickson, C. L., Blakney, G. T., Beu, S. C., and Marshall, A. G. (2010). Automated broadband phase correction of fourier transform ion cyclotron resonance mass spectra. *Anal. Chem.* 82, 8807–8812. doi: 10.1021/ac101091w
- Yang, R., and Van den Berg, C. M. G. (2009). Metal complexation by humic substances in seawater. *Environ. Sci. Technol.* 43, 7192–7197. doi: 10.1021/es900173w
- Zhang, H., van den Berg, C. M. G., and Wollast, R. (1990). The determination of interactions of cobalt (II) with organic compounds in seawater using cathodic stripping voltammetry. *Mar. Chem.* 28, 285–300. doi: 10.1016/0304-4203(90)90049-1

Conflict of Interest Statement: The authors declare that the research was conducted in the absence of any commercial or financial relationships that could be construed as a potential conflict of interest.

Copyright © 2016 Boiteau, Till, Ruacho, Bundy, Hawco, McKenna, Barbeau, Bruland, Saito and Repeta. This is an open-access article distributed under the terms of the Creative Commons Attribution License (CC BY). The use, distribution or reproduction in other forums is permitted, provided the original author(s) or licensor are credited and that the original publication in this journal is cited, in accordance with accepted academic practice. No use, distribution or reproduction is permitted which does not comply with these terms.



Using ^{67}Cu to Study the Biogeochemical Cycling of Copper in the Northeast Subarctic Pacific Ocean

David M. Semeniuk^{1*}, Randelle M. Bundy^{2†}, Anna M. Posacka¹, Marie Robert³, Katherine A. Barbeau² and Maria T. Maldonado¹

OPEN ACCESS

Edited by:

Sylvia Gertrud Sander,
University of Otago, New Zealand

Reviewed by:

Benjamin Twining,
Bigelow Laboratory for Ocean
Sciences, USA
Cédric Garnier,
Université de Toulon, France

*Correspondence:

David M. Semeniuk
david.semeniuk@gmail.com

†Present Address:

David M. Semeniuk,
Institute of Geological Sciences and
Oeschger Center for Climate Change
Research, University of Bern, Bern,
Switzerland;
Randelle M. Bundy,
Marine Chemistry and Geochemistry,
Woods Hole Oceanographic
Institution, Woods Hole, MA, USA

Specialty section:

This article was submitted to
Marine Biogeochemistry,
a section of the journal
Frontiers in Marine Science

Received: 28 January 2016

Accepted: 06 May 2016

Published: 03 June 2016

Citation:

Semeniuk DM, Bundy RM,
Posacka AM, Robert M, Barbeau KA
and Maldonado MT (2016) Using
 ^{67}Cu to Study the Biogeochemical
Cycling of Copper in the Northeast
Subarctic Pacific Ocean.
Front. Mar. Sci. 3:78.
doi: 10.3389/fmars.2016.00078

¹ Department of Earth, Ocean, and Atmospheric Sciences, University of British Columbia, Vancouver, BC, Canada, ² Scripps Institution of Oceanography, University of California San Diego, La Jolla, CA, USA, ³ Institute of Ocean Sciences, Fisheries and Oceans Canada, Sidney, BC, Canada

Microbial copper (Cu) nutrition and dissolved Cu speciation were surveyed along Line P, a coastal to open ocean transect that extends from the coast of British Columbia, Canada, to the high-nutrient-low-chlorophyll (HNLC) zone of the northeast subarctic Pacific Ocean. Steady-state size fractionated Cu uptake rates and Cu:C assimilation ratios were determined at *in situ* Cu concentrations and speciation using a ^{67}Cu tracer method. The cellular Cu:C ratios that we measured ($\sim 30 \mu\text{mol Cu mol C}^{-1}$) are similar to recent estimates using synchrotron x-ray fluorescence (SXRF), suggesting that the ^{67}Cu method can determine *in situ* metabolic Cu demands. We examined how environmental changes along the Line P transect influenced Cu metabolism in the sub-microplankton community. Cellular Cu:C assimilation ratios and uptake rates were compared with net primary productivity, bacterial abundance and productivity, total dissolved Cu, Cu speciation, and a suite of other chemical and biological parameters. Total dissolved Cu concentrations ($[\text{Cu}]_d$) were within a narrow range (1.5–2.8 nM), and Cu was bound to a ~ 5 -fold excess of strong ligands with conditional stability constants ($K_{\text{CuL,Cu}^{2+}}^{\text{cond}}$) of $\sim 10^{14}$. Free Cu^{2+} concentrations were low (pCu 14.4–15.1), and total and size fractionated net primary productivity (NPP_V ; $\mu\text{g C L}^{-1} \text{d}^{-1}$) were negatively correlated with inorganic Cu concentrations ($[\text{Cu}']$). We suggest this is due to greater Cu' drawdown by faster growing phytoplankton populations. Using the relationship between $[\text{Cu}']$ drawdown and NPP_V , we calculated a regional photosynthetic Cu:C drawdown export ratio between 1.5 and $15 \mu\text{mol Cu mol C}^{-1}$, and a mixed layer residence time (2.5–8 years) that is similar to other independent estimates (2–12 years). Total particulate Cu uptake rates were between 22 and 125 times faster than estimates of Cu export; this is possibly mediated by rapid cellular Cu uptake and efflux by phytoplankton and bacteria or the effects of grazers and bacterial remineralization on dissolved Cu. These results provide a more detailed understanding of the interactions between Cu speciation and microorganisms in seawater, and suggest that marine phytoplankton modify Cu speciation in the open ocean.

Keywords: iron, copper, uptake, trace metal, ligand, northeast subarctic Pacific Ocean, Line P

INTRODUCTION

While it is well established that iron (Fe) availability limits primary productivity in up to 40% of the global surface oceans (Moore et al., 2004; Boyd et al., 2007), other trace elements may exert influence over phytoplankton community composition and growth. Copper (Cu) is unique because it is a required micronutrient (e.g., Palenik and Morel, 1991; Chadd et al., 1996; Maldonado et al., 2006; Peers and Price, 2006), but it can also be toxic to marine phytoplankton at relatively low concentrations (Sunda and Huntsman, 1983; Brand et al., 1986; Moffett et al., 1997; Mann et al., 2002; Levy et al., 2007). Indeed, limited field evidence suggests that Cu may be causing toxicity to coastal phytoplankton communities (Moffett et al., 1997; Jordi et al., 2012). Despite the potential nutritional and toxic effects of Cu in marine phytoplankton, little is known about how Cu is influencing planktonic rate processes in unpolluted, open ocean environments.

Both the concentration and speciation of a metal will determine whether it is limiting or toxic to marine phytoplankton (Hudson, 1998; Sunda, 2012). Copper is bound to a suite of strong and weak organic ligands in seawater, resulting in >99.9% of the dissolved Cu being complexed, and free Cu^{2+} concentrations of $10^{-13.5}$ to $10^{-16.3}$ M (van den Berg, 1984; Coale and Bruland, 1988; Moffett and Dupont, 2007; Buck et al., 2010; Bundy et al., 2013; Jacquot et al., 2013; Thompson et al., 2014; Heller and Croot, 2015; Jacquot and Moffett, 2015). Free Cu^{2+} makes up ~4% of the total inorganic Cu (Cu') pool, with the remainder dominated by CuCO_3 and CuOH^- (Turner et al., 1981). Early physiological work proposed that Cu' , but not organically complexed Cu, was the substrate for transporters in marine phytoplankton when $[\text{Cu}']$ was high (Sunda and Guillard, 1976; Anderson and Morel, 1978; Sunda and Huntsman, 1995). The total dissolved Cu concentration in the surface ocean (0.2–3 nM) is similar to $[\text{Cu}']$ that causes toxicity in many phytoplankton species (>0.1 nM; Brand et al., 1986). Thus, it was proposed that the Cu-binding ligands found in seawater are produced by Cu-sensitive prokaryotes to complex Cu' , thereby detoxifying it (Moffett and Brand, 1996; Moffett et al., 1997; Croot et al., 2000; Gordon et al., 2000; Mann et al., 2002; Wiramanaden et al., 2008). However, some organically complexed Cu appears to be bioavailable to eukaryotic marine phytoplankton (Hudson, 1998; Quigg et al., 2006; Guo et al., 2010; Semeniuk et al., 2015; Walsh et al., 2015). Thus, organic ligands may play a variety of roles in mediating Cu availability to different marine plankton groups.

The buffering of low $[\text{Cu}']$ by strong organic ligands may have negative effects on eukaryotic marine phytoplankton growth. Indeed, some Fe-limited phytoplankton have higher metabolic dependencies on Cu (Peers et al., 2005; Annett et al., 2008; Semeniuk et al., 2009; Guo et al., 2012; Biswas et al., 2013). This may be due to upregulation of the Cu-containing photosynthetic electron shuttle plastocyanin and the multiple-Cu containing oxidase component of a high affinity Fe transport system in diatoms (Maldonado et al., 2006; Peers and Price, 2006; Kustka et al., 2007). Recent surveys of Cu speciation in surface waters (e.g., Moffett and Dupont, 2007; Buck et al., 2010; Bundy et al.,

2013; Jacquot et al., 2013; Thompson et al., 2014; Jacquot and Moffett, 2015) have reported $[\text{Cu}']$ low enough ($<10^{-14}$ M) to co-limit the growth of Fe-limited phytoplankton communities (Peers et al., 2005; Annett et al., 2008; Guo et al., 2012). Only a handful of large volume incubation process studies have examined the influence of Cu on Fe-limited phytoplankton, and conflicting evidence for and against Fe-Cu co-limitation has emerged (Coale, 1991; Peers et al., 2005; Wells et al., 2005; Kustka et al., 2015; Semeniuk et al., 2016). Additional work evaluating *in situ* metal bioavailability and the link between metabolic Cu and Fe requirements of natural phytoplankton assemblages is warranted.

There has been a recent surge of metal speciation data in seawater in concert with the international GEOTRACES program. However, few studies have examined how *in situ* trace metal speciation influences either metal bioavailability to marine phytoplankton and bacteria, or planktonic rate processes in surface oceans. Few tools are available to examine *in situ* cellular metal concentrations and accumulation rates, and each has unique advantages and disadvantages. Measurements of total bulk particulate metals provide precise particulate metal concentration data, but these include unknown lithogenic contributions that must be corrected (reviewed by Lam et al., 2015). Metal quotas of single cells have been reported using synchrotron X-ray fluorescence, but this method is resource and technically intensive and is currently undertaken by only one group (e.g., Twining et al., 2003). Commercially available radioisotopes and enriched stable isotopes can be used to track cellular metal assimilation (e.g., Maldonado and Price, 1999; Dupont et al., 2010; Cox et al., 2014). Although small isotope additions are made, they are often higher than *in situ* concentrations in order to overcome instrumental detection limits. Thus, what controls *in situ* rates of trace metal uptake by plankton inhabiting oceanic waters remains largely unknown.

Using the carrier free short-lived gamma emitting radioisotope ^{67}Cu ($t_{1/2} = 2.58$ days), we made the first measurements of Cu assimilation in natural phytoplankton assemblages without significantly altering *in situ* Cu chemistry (Semeniuk et al., 2009, 2015). This is enabled by the relatively high concentration of dissolved Cu in surface seawater compared to other trace mineral nutrients (e.g., iron, <0.1 nM), and the high specific activity of ^{67}Cu . In the present study, we expand on our early work by measuring Cu assimilation at many stations and depths, which allows us to assess how well the ^{67}Cu tracer assays compare with previous laboratory and field studies. We use the tracer to determine how prokaryotic and eukaryotic Cu assimilation co-varies with Cu concentration, speciation, and a suite of biological and chemical parameters along Line P, a coastal-open ocean transect that extends from the British Columbia coast to the low-Fe surface waters in the northeast subarctic Pacific Ocean. In addition to contributing measurements of total dissolved Cu and Cu speciation for surface waters in this region, this dataset provides an opportunity to examine possible relationships between Cu chemistry and planktonic rate processes across high and low Fe-containing surface waters across a large geographical region.

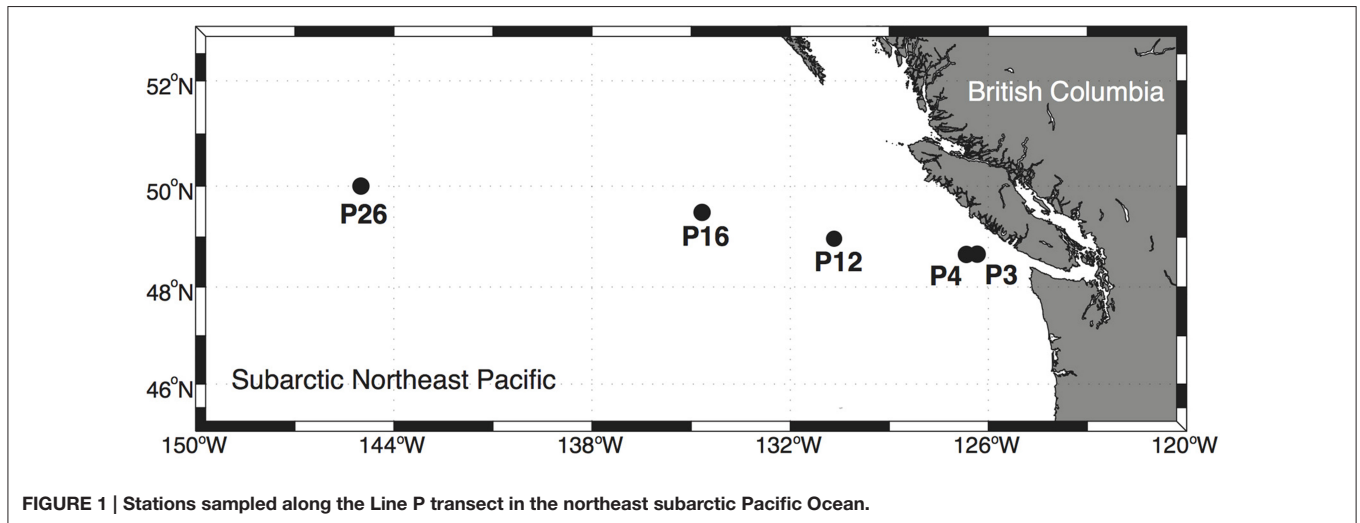


FIGURE 1 | Stations sampled along the Line P transect in the northeast subarctic Pacific Ocean.

MATERIALS AND METHODS

Plastic Cleaning

All plastics were rigorously cleaned in Class 100 conditions before the cruise. The polycarbonate bottles used for the Cu uptake assays, Cu:C assimilation ratios, and primary productivity measurements were cleaned for 1 week each with 3% Extran, 6 M HCl, and 1 M HNO₃ and were rinsed thoroughly with ultra-pure water (18 MΩ cm resistivity; Millipore) between each cleaning step. Sample bottles for dissolved metals (250 mL low-density polyethylene; LDPE) and Cu ligands (500 mL LDPE) were cleaned according to GEOTRACES protocols (Cutter et al., 2010).

Experimental Design and Execution

Net primary productivity, phytoplankton biomass, total dissolved Cu concentrations, Cu speciation, Cu:C assimilation ratios, Cu uptake rates, and a suite of other variables were surveyed at multiple depths along the Line P transect (Tables 1–3; Figure 1). The depths sampled were in the mixed layer and subsurface chlorophyll maximum at each station, with light intensities spanning an order of magnitude (Table 2; Figure 2). The depths and stations sampled represent waters that may be influenced by coastal processes (P3), macronutrient limited coastal (P4) and oceanic (P12) waters, as well as Fe-limited oceanic waters (P16 and P26) (Boyd and Harrison, 1999; Whitney and Freeland, 1999; Peña and Varela, 2007). The diverse light and nutrient regimes in surface waters along Line P provide a range of physical and chemical variation that may influence Cu nutrition in marine phytoplankton and bacteria.

Water Collection and Station Parameterization along Line P

Between August 17 and 26, 2011, surface waters were sampled on board the C.C.G.S. John P. Tully (Cruise, 2011-27) at five stations along the Line P transect (Figure 1). Low nitrate concentrations at stations P3, P4, and P12, and high nitrate concentrations at

P16 and P26 confirmed that the first three stations were nitrate-limited, while the latter two stations were likely in the HNLC region (Table 2). A few hours before dawn on each sampling day, water was pumped from between 7 and 40 m depth using a trace metal clean (TMC) Teflon[®] diaphragm pump and Teflon[®] lined tubing attached to a Kevlar[®] wire (Johnson et al., 2005). Water was pumped directly into a Class 100 laminar flow hood where it was sampled. Around noon on each sampling day, profile data were collected at each station as previously described (Semeniuk et al., 2016).

Samples collected for Cu uptake rates, Cu:C assimilation ratios, and net primary productivity were immediately placed in on-deck incubators supplied with water continuously pumped from 5 m depth until radiotracer additions could be made (<3 h). The sampled depths were inside and below the mixed layer, and spanned a range of light intensities from 3 to 39% of I₀ (Table 2). The *in situ* light intensities for each depth were maintained (± 4%) using neutral density screening.

Biological and Chemical Sampling and Analysis

Samples for total and size fractionated chl *a* concentrations, macronutrient concentrations, maximum variable fluorescence yield (F_v/F_m; using fluorescence induction/relaxation; FIRE Satlantic), and total bacterial abundance (determined by flow cytometry; Becton-Dickinson FACSCalibur) were collected and analyzed as previously described (Semeniuk et al., 2016). Cyanobacteria and picoeukaryotes were sampled and enumerated by flow cytometry according to Taylor et al. (2013).

Dissolved Cu Concentrations and Speciation

Total dissolved Cu ([Cu]_d) samples were collected and analyzed by flow injection analysis and chemiluminescence using UV-oxidized samples (as described by Semeniuk et al., 2016). Dissolved Cu speciation samples were collected using the same procedure as for total dissolved Cu samples,

but the sample bottles were not acidified, and instead they were immediately frozen and stored at -20°C until further analysis. The Cu speciation measurements—conditional stability constant ($\log K_{\text{CuL},\text{Cu}^{2+}}^{\text{cond}}$), ligand concentration, and free Cu^{2+} concentration—were determined via competitive ligand exchange-adsorptive cathodic stripping voltammetry. Due to restrictions on sample volume, a single analytical window was employed in triplicate using $5\ \mu\text{M}$ of the competing ligand, salicylaldehyde (SA), which represents an average of strong and some weaker Cu-binding ligands (L). This moderate analytical window was chosen in order to detect both strong and weaker Cu-binding ligands to ensure an accurate determination of Cu^{2+} . This window however, may have missed much of the weaker ligand pool (e.g., Heller and Croot, 2015), but weaker ligands are expected to have a small effect on the Cu^{2+} concentrations in the open ocean and in general, Cu^{2+} is relatively insensitive to the analytical window employed (Bruland et al., 2000), especially in the low $[\text{Cu}]_d$ of unpolluted environments (where $[\text{L}] > [\text{Cu}]$). Moreover, more recent analysis of samples collected along Line P using multiple analytical windows revealed relatively low weak ligand concentrations ($1\text{--}5\ \text{nM}$; $\log K_{\text{CuL},\text{Cu}^{2+}}^{\text{cond}} < 11$) (Bundy, unpub.). The titrations performed here were completed using 12 titration points and up to $40\ \text{nM}$ added Cu in order to fully titrate the ligands within the detection window. A detailed description of the theory and methodology is provided in Bundy et al. (2013) and Semeniuk et al. (2015).

Cu Uptake Rates, Cu:C Assimilation Ratios, and Net Primary Productivity

Copper uptake rates and Cu:C assimilation ratios were measured using the gamma emitting radioisotope ^{67}Cu (half-life = 62 h; provided by TRIUMF, Vancouver BC) and $\text{H}^{14}\text{CO}_3^-$ (Perkin Elmer). The $37\ \text{MBq}$ ^{67}Cu “mother” stock was kept in $0.005\ \text{M}$ HCl, and diluted at least 2500-fold in the $250\ \text{mL}$ assay bottles to prevent significant pH changes. Approximately $10\ \text{mL}$ of seawater from each assay bottle were filtered through acid-cleaned $0.22\ \mu\text{m}$ porosity Acrodisc filters (Pall) using an acid-cleaned rubberless syringe. The filtrate was collected in a TMC $15\ \text{mL}$ falcon tube. Approximately $5\ \text{kBq}$ of ^{67}Cu from the primary stock was added to $10\ \text{mL}$ filtrate, and allowed to complex with the excess strong Cu ligands for at least 2 h before being added to the assay bottles. The Cu concentration was not measured in the ^{67}Cu mother stock that we took to sea. However, the background Cu contamination in isotope stocks received by our laboratory is routinely monitored via quadrupole ICP-MS, and the Cu concentration of the mother stock is always $< 50\ \text{nM}$. At most, $100\ \mu\text{L}$ of the ^{67}Cu mother stock (pre-equilibrated with $10\ \text{mL}$ of filtered seawater) was added to $250\ \text{mL}$ of collected seawater, resulting in at most a $0.02\ \text{nM}$ Cu addition. This corresponds to a maximum possible increase in dissolved Cu of 1.4% in our assays. Given that the excess of Cu ligands along the transect were between 6.3 and $17.4\ \text{nM}$, there would have been sufficient excess Cu ligands to complex the $0.02\ \text{nM}$ ^{67}Cu addition. Since the ^{67}Cu tracer would have been completely complexed by the excess *in situ* Cu ligands, and the total dissolved

Cu concentration changed negligibly, the Cu uptake rates and Cu:C assimilation ratios are likely representative of *in situ* values.

A 2 h reaction time is commonly used for titrating Cu ligands with CuSO_4 for speciation analysis by electrochemical techniques (Moffett and Dupont, 2007; Buck et al., 2010; Bundy et al., 2013; Jacquot et al., 2013; Jacquot and Moffett, 2015), and so there should have been adequate time for the excess strong ligands to complex the tracer in our assays. However, we can also estimate whether the excess concentration of Cu-binding ligands present along Line P would have complexed the added ^{67}Cu tracer in that time. The forward reaction rate for complexation of trace metals by organic ligands is described as $k_f = K_{\text{OS}}k_{-w}$, where K_{OS} is the stability constant for formation of the outer electron-sphere (M^{-1}), and k_{-w} is the rate constant for loss of the first water molecule from the inner metal hydration sphere (s^{-1} ; Morel et al., 1991; Hudson, 1998). The K_{OS} value can vary between 0.3 and $8\ \text{M}^{-1}$ in seawater, depending on the charges of the reacting metal and ligand species (Morel et al., 1991), and so would have a negligible effect on the overall rate constant. Instead, metal chelation is often rate-limited by loss of the first water molecule from the outer hydration sphere (Hudson, 1998). The water loss rate constant for Cu^{2+} ($\sim 10^9\ \text{s}^{-1}$; Hudson, 1998) is high, and so complex formation would be very rapid. In support of this, the forward reaction rate constant measured for Cu^{2+} complexation by unprotonated ethylenediamine tetraacetic acid (EDTA^{4-}) in $0.1\ \text{M}$ NaCl is also very fast ($\sim 2 \times 10^9\ \text{M}^{-1}\ \text{s}^{-1}$; Hering and Morel, 1988). In seawater, the high concentration of Ca^{2+} competes with Cu^{2+} for chelation, reducing both the strength of the Cu-ligand complex and k_f (Hering and Morel, 1988). The k_f decreases as dissociation of the Ca^{2+} -ligand complex, and not k_{-w} , becomes the rate limiting step. This is particularly important for weaker metal-binding ligands that are primarily complexed to Ca^{2+} in seawater. For example, the stability constant for Cu^{2+} EDTA decreases from 17.9 to ~ 10.5 in seawater (Coale and Bruland, 1988; Zamzow et al., 1998; Croot et al., 1999). Similarly, the forward reaction half-life for complexation of Cu^{2+} by EDTA decreases from nearly instantaneous to 2 h in seawater (Hering and Morel, 1988).

Using multiple analytical windows, both strong and weak Cu-binding ligands have recently been detected in seawater (Buck et al., 2010; Bundy et al., 2013; Heller and Croot, 2015). While we are unaware of kinetic data for Cu complexation by strong model organic ligands in seawater, forward reaction rates for Fe complexation by strong organic ligands (0.1 to $2 \times 10^6\ \text{M}^{-1}\ \text{s}^{-1}$) are similar to k_{-w} ($8 \times 10^6\ \text{s}^{-1}$) (Hudson et al., 1992; Witter et al., 2000). This is likely due to a much smaller proportion of the stronger ligand pool being complexed to Ca^{2+} . Assuming the same applies for complexation of inorganic Cu by the *in situ* strong organic ligands, then the ^{67}Cu tracer addition would have been complexed immediately by the *in situ* strong ligands. However, if the *in situ* weak ligands behave like EDTA—a relatively weak ligand compared to the strong *in situ* ligands—then complexation of the ^{67}Cu by them would have been relatively slow and incomplete in our 2 h equilibration time. There is little experimental data for Cu complexation kinetics by natural organic matter in seawater, particularly for open ocean

waters. Coale and Bruland (1988) reported that Cu complexation by the strong ligand pool occurred within 5 min at an open ocean station in the North Pacific. However, forward kinetic rate constants have been determined for Cu binding by dissolved organic matter in the Krka estuary (Croatia), and equilibration times were slow (>2 h) (Louis et al., 2009). Given the similarity between our study site and that for Coale and Bruland (1988), we suggest the ^{67}Cu tracer was rapidly complexed by strong Cu-ligand pool, but it may not have been at equilibrium with the weak Cu-ligand pool. Although the concentration of weak Cu-binding ligands is low along Line P (1–5 nM; Bundy unpub.), their role in mediating Cu bioavailability remains unknown. Further work investigating Cu-ligand reaction kinetics of strong and weak *in situ* ligands would greatly assist future speciation and tracer research.

Previous work along Line P has demonstrated that short-term uptake rates are significantly faster than long-term net uptake rates due to either cellular efflux or remineralization of particulate Cu by micrograzers (Semeniuk et al., 2009, 2015). Thus, both short-term (2 h incubation) and long-term (24 h incubation) uptake rates were measured. Two hours before dawn on each sampling day, 250 mL of seawater were sampled from either the cubitainers or the Teflon pumping system into TMC 250 mL polycarbonate bottles. Sampling occurred inside a Class 100 laminar flow hood. A 10 mL sub-sample was taken from each assay bottle for the ^{67}Cu and *in situ* ligand pre-complexation step (see above), and the bottles were immediately placed inside the on-deck incubators at the appropriate light levels. Once the ^{67}Cu tracer complexation was complete, the 250 mL assay bottles were retrieved, and the 10 mL ^{67}Cu tracer was added. For the 24 h Cu:C assimilation ratio assays, 185 kBq of $\text{H}^{14}\text{CO}_3^-$ were also added to each 250 mL bottle. The bottle lids were sealed with parafilm, and the bottles were immediately returned to the on-deck incubators. Duplicate bottles were prepared for both Cu uptake rate and Cu:C assimilation ratio assays.

After the specified incubation time, the assay bottles were retrieved from the incubators, and a 1 mL “initial” subsample was taken from each bottle in order to determine the total activity of ^{14}C and/or ^{67}Cu added to each bottle. To each $\text{H}^{14}\text{CO}_3^-$ initial sample, 500 μL of 6 M NaOH was added to prevent off gassing of $^{14}\text{CO}_2$. The volume of each bottle was recorded, and the seawater was gently vacuum-filtered onto a series of 47 mm diameter 5, 1, and 0.22 μm polycarbonate filters (AMD) separated by nylon drain discs (Millipore). Just before the filters went dry, 20 mL of 1 mM diethylene triamine pentaacetic acid (DTPA) in seawater adjusted to pH 8 were added to the filters to remove any surface-associated tracer (Crook et al., 2003). The filters were completely immersed in the 1 mM DTPA wash for 10 min, the wash was then drained, and 20 mL of filtered seawater (FSW) was applied to rinse away loosely associated tracer. The filters were vacuumed dry to prevent transfer of filtered cells between the filters and drain discs. Each filter was carefully folded and placed inside a 7 mL borosilicate scintillation vial. To each scintillation vial, 1 mL of FSW was added, and the vials were vortexed for 30 s to remove filter-bound cells. Filters collected from the 24 h Cu:C assimilation ratio assays were immediately acidified with 100 μL of 6 M HCl

to degas inorganic ^{14}C for 24 h before 1 mL of FSW was added. The activity of ^{67}Cu in each vial was determined using a sea-going gamma counter (Semeniuk et al., 2009). Background ^{67}Cu counts were performed on analysis days and subtracted from the sample counts. After ^{67}Cu counting, sample vials containing ^{14}C were filled with 50% ScintiSafe scintillation cocktail (Fisher) and archived until further analysis in the laboratory once the ^{67}Cu had decayed. Once the ^{67}Cu had decayed (>8 half-lives), the activity of ^{14}C was determined with a Beckman LS65005514 scintillation counter with an internal ^{14}C quench curve.

Filter blanks and kill controls were performed in triplicate at P26 (10 m depth) in order to account for abiotic adsorption of ^{67}Cu to the polycarbonate filters and particles that was not removed by the DTPA wash. For filter blanks, the 0.22 μm filtered seawater was spiked for 2 min with pre-complexed ^{67}Cu , the seawater was filtered, and the filters were processed as in the Cu uptake assays. Glutaraldehyde (2% final concentration) was added to another set of triplicate bottles filled with unfiltered seawater, and the cells were fixed for 2 h before pre-complexed ^{67}Cu was added. The killed bottles were incubated for 2 h alongside the short-term Cu uptake rates, and similarly processed. The average activity for the filter blanks + kill controls (~20% of the total filter activity on average; 15% from the filter, and 5% from the cells) was subtracted from the assay filters for all stations and depths.

The specific activity of ^{67}Cu (disintegrations per minute; DPM per mol) in the assays conducted along the transect was calculated by dividing the activity measured in 1 mL of unfiltered sample (DPM per mL) by the total dissolved Cu concentration measured in UV-digested samples (mol per mL; see above). The specific activity of ^{14}C was calculated in the same way, but we assumed a dissolved inorganic carbon concentration of 2.1 mM. The total amount of Cu and/or C on each polycarbonate filter was determined by dividing the activity on each filter (DPM per filter) by the specific activity of the isotope (DPM per mol).

Volumetric Cu uptake rates (ρCu_V ; mol Cu $\text{L}^{-1} \text{h}^{-1}$) were determined by dividing mol of Cu on each filter by the sample volume filtered and the incubation time. In order to calculate carbon-normalized Cu uptake rates, we estimated particulate organic carbon concentrations in each size fraction using previously published conversion factors. For the 0.22–1 μm size fraction, total bacterial abundance was converted to organic carbon using 20 fg C bacterium $^{-1}$ (Lee and Fuhrman, 1987). For the 1–5 μm and >5 μm size fractions, [chl *a*] was converted to organic carbon using 50 g C g chl *a* $^{-1}$ (Booth et al., 1993). Total ρCu_B was determined by the sum of volumetric Cu uptake rates divided by total particulate carbon concentrations derived from the total bacterial abundance and total particulate [chl *a*].

Cu:C assimilation ratios ($\mu\text{mol Cu mol C}^{-1}$) measured over 24 h were calculated for each size fraction by dividing the Cu uptake rate by the C uptake rate measured for each size fraction. Total particulate Cu:C assimilation ratios were calculated by dividing the sum of size-fractionated particulate Cu by sum of size-fractionated particulate C. The Cu:C assimilation ratios for the 0.22–1 μm size fraction include both photosynthetic and non-photosynthetic bacteria. Non-photosynthetic bacteria

will acquire Cu without fixing ^{14}C , and will then result in an overestimate of the Cu:C assimilation ratios for the smallest size fraction of phytoplankton.

The Cu:C assimilation ratios presented herein are not equivalent to steady-state Cu quotas measured in previous laboratory studies (Annett et al., 2008; Guo et al., 2012). Previous laboratory studies acclimated phytoplankton to 24 h light. In contrast, our field Cu:C assimilation ratio assays were performed for 24 h under a day-night cycle. During the night hours, Cu uptake may have taken place while fixation of ^{14}C stopped and respiration of previously fixed ^{14}C likely occurred. Freshly fixed organic carbon can be quickly metabolized after a few hours (Halsey et al., 2011). Thus, the Cu:C assimilation ratios measured in phytoplankton communities sampled along Line P may be higher than those determined in laboratory studies.

Net primary productivity (NPP) along the transect was determined using $\text{H}^{14}\text{CO}_3^-$. Just before dawn on each sampling day, four 60 mL TMC polycarbonate bottles were rinsed and filled with sample water and spiked with 185 kBq of $\text{H}^{14}\text{CO}_3^-$. A 0.5 mL subsample was taken from each bottle in order to determine the total activity of ^{14}C added, and 0.5 mL of 6 M NaOH was added to prevent degassing of $^{14}\text{CO}_2$. One bottle was immediately wrapped in aluminum foil and placed in an opaque black plastic bag as a “dark” bottle to account for non-photosynthetic carbon fixation and non-specific ^{14}C binding. Bottles were incubated at *in situ* light and temperature for 24 h in the on-deck incubators. After the incubation, the volume of each bottle was recorded and the contents were gently filtered onto 25 mm GFF filters. The filters were then placed into 7 mL scintillation vials, and 100 μL of 6 M HCl was added to degas inorganic ^{14}C for 24 h. The filters were then immersed in scintillation cocktail and archived until they could be analyzed in the laboratory.

RESULTS

Depth Profiles along Line P

Mixed layer seawater density was highest at P26 (24.50 kg m^{-3}), decreased along the transect toward P4 (23.54 kg m^{-3}), and increased slightly at P3 (23.70 kg m^{-3}) (Figure 2). Mixed layer depths ranged two-fold (15–31 m), and were deepest farthest offshore (P16 and P26) (Table 1). Light attenuation was greatest at P3 (light attenuation coefficient, $k_D = 0.211 \text{ m}^{-1}$), and so the euphotic zone depth (Z_{eu}) was shallowest at this station (22 m) (Tables 1, 2). At stations P4 through P26, light attenuation (light attenuation coefficient, $k_D = 0.093\text{--}0.096$) and the euphotic depths (48–49 m) were similar (Tables 1, 2).

Mixed layer nitrate concentrations were below detection (0.2 μM ; Barwell-Clarke and Whitney, 1996) at P3, P4, and P12 (Table 2 and Figure 2). However, they were elevated at P16 (5.20 μM) and P26 (11.2 μM), which is characteristic of HNLC waters. Phosphate and silicic acid concentrations were not limiting across the transect. At P3, a broad fluorescence peak was present from 5 to 30 m depth (Figure 2). Dissolved oxygen (DO) was elevated in the mixed layer at this station (293–298 μM), showed a large decrease between 12 and 17 m (280 μM), and increased again below the thermocline (300 μM) (Figure 2). Subsurface chlorophyll maxima (SCM) were most

pronounced below the thermocline at P4 (~45 m) and P12 (~35 m), and corresponded with increased nitrate concentrations, increased DO, and low light levels (<5% of the incident irradiation; I_0) (Figure 2). Smaller SCM were present at P16 and P26 and corresponded to subsurface DO maxima. The discrete depths sampled across the transect corresponded to a range of irradiances between 3 and 39% of I_0 (Table 2).

Copper Concentrations and Speciation

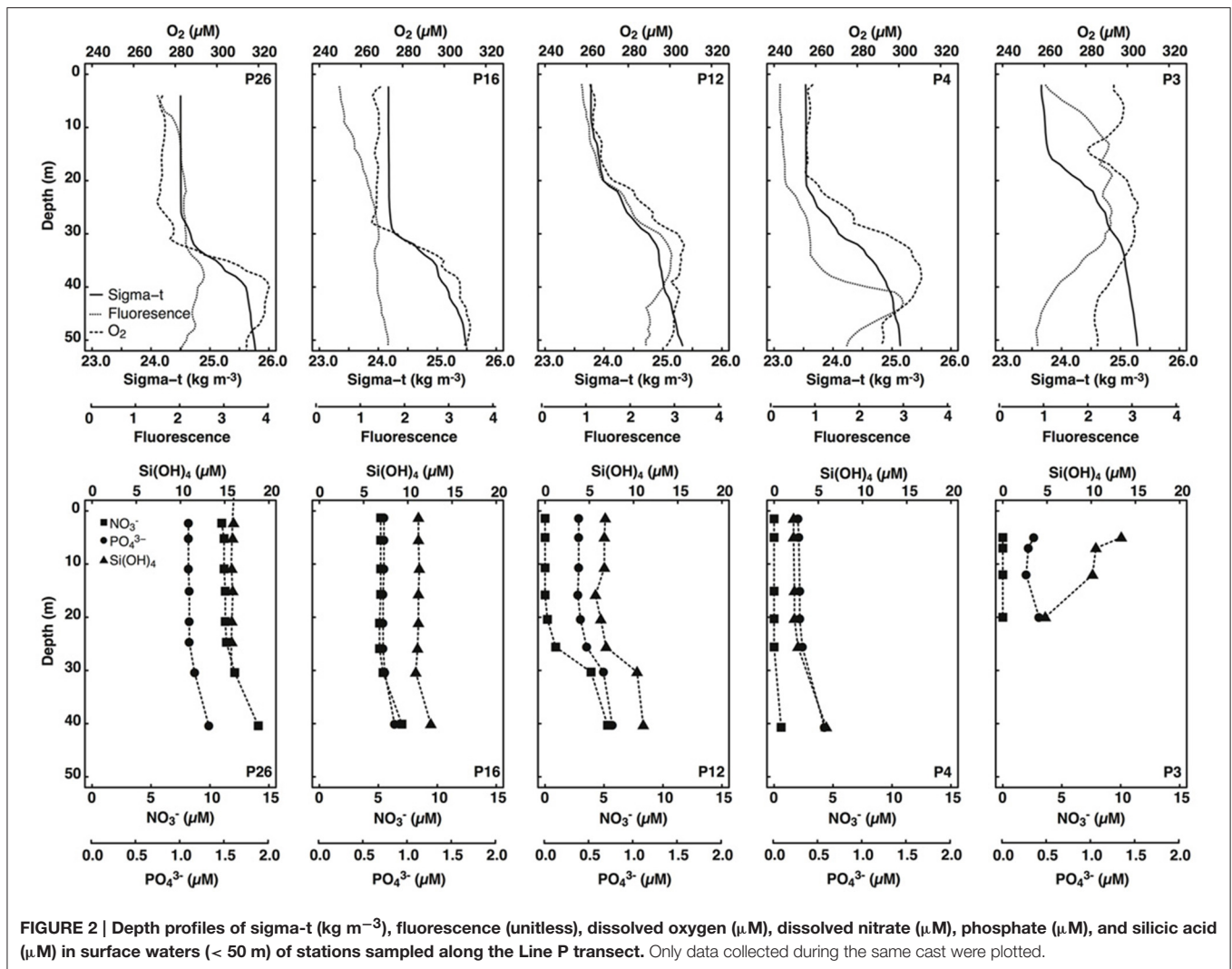
Total dissolved Cu concentrations ranged between 1.5 and 2.8 nM along the transect (Table 3). Dissolved Cu was highest near the coast at P3 (2.4–2.8 nM). Mixed layer $[\text{Cu}]_d$ decreased along the transect toward P20 (1.7 nM), and increased at P26 (2.1 nM). Dissolved ligand concentrations were highest at P3 (14.7 and 17.4 nM at 7 and 12 m depth, respectively). Ligands were between three and seven-fold in excess of $[\text{Cu}]_d$, and with high $\log K_{\text{CuL}, \text{Cu}^{2+}}^{\text{cond}}$ (13.7–14.5). The average $[\text{L}]:[\text{Cu}]_d$ ratio was 4.8 ± 1.2 ($n = 12$) (Table 3). The $[\text{L}]:[\text{Cu}]_d$ ratios at P3 were generally higher at both depths (6.1–6.2) compared to the remaining 10 depths sampled along the transect (4.6 ± 1.1 ; $n = 10$) (Table 3). Ligand concentrations were positively correlated with $[\text{Cu}]_d$ (slope = 5.9; $r^2 = 0.44$, $p = 0.0184$).

The excess strong [L] resulted in inorganic Cu concentrations ($[\text{Cu}']$) between 19 and 94 fM and coincident pCu values ($-\log[\text{Cu}^{2+}]$) ranging between 15.1 and 14.4 along the transect (Table 3). At each station, $[\text{Cu}']$ tended to be lowest at the shallowest depth and increase with depth. Notably, the lowest $[\text{Cu}']$ measured along the transect corresponded with the highest NPP_V at P26 (10 m depth). The $[\text{Cu}]_d$, [L], and $[\text{Cu}']$ at the shallowest depth sampled at each station were compared with surface salinities along the transect sampled at 5 m depth (Figure 3). $[\text{Cu}]_d$ and [L] were highest at the lowest salinities near the coast, and decreased offshore to P16, and increased again at P26. $[\text{Cu}']$ was more variable, and did not show an obvious trend with salinity.

Biomass and Productivity

Total [chl *a*] varied more than 20-fold along Line P varied between 0.04 and 0.96 $\mu\text{g chl } a \text{ L}^{-1}$, with highest concentrations at P3, and lowest in the mixed layer at P4 (Table 4). The 0.22–1, 1–5, and >5 μm size fractions made up 7 ± 8 , 48 ± 15 , and $45 \pm 12\%$ of the total [chl *a*] across the transect, respectively (Table 5). The 0.22–1 μm size fraction made up <10% of the total [chl *a*] at all sampling depths except for 12 m at P3 (31%). Cyanobacteria and picoeukaryote abundance varied between 0.77–200 $\times 10^6$ cells L^{-1} , and 0.55–16.3 $\times 10^6$ cells L^{-1} , respectively (Table 4). They were most abundant at P3 and tended to be more prevalent at deeper depths at all stations (e.g., P4, P12, and P16). The maximum fluorescence yield (F_v/F_m) was highest near the coast (0.23–0.64), lowest at P16 (0.19–0.29), and decreased toward the HNLC waters (Table 4).

NPP_V ranged between 11 and 110 $\mu\text{g C L}^{-1} \text{ d}^{-1}$. It was highest in the mixed layer at P26 (110 $\mu\text{g C L}^{-1} \text{ d}^{-1}$), and co-occurred with a higher F_v/F_m (0.29) compared to the mixed layer at P16 (41 $\mu\text{g C L}^{-1} \text{ d}^{-1}$; $F_v/F_m = 0.19$) (Table 4). These rates are within the range previously reported for the upper 40 m along Line P in the summer (10–100 $\mu\text{g C L}^{-1} \text{ d}^{-1}$) (Boyd and Harrison, 1999).



NPP_B ranged between 74 and $583 \mu\text{g C } \mu\text{g chl } a^{-1} \text{ d}^{-1}$, with the fastest rate ($583 \mu\text{g C } \mu\text{g chl } a^{-1} \text{ d}^{-1}$) in the mixed layer at P4.

Total bacterial abundance between stations P4 and P26 varied between 0.82 and $3.66 \times 10^9 \text{ cells L}^{-1}$, and was an order of magnitude higher at P3 (32.0 – $32.2 \times 10^9 \text{ cells L}^{-1}$) (Table 4). Volumetric and cell-normalized rates of bacterial productivity varied between 0.98 and $4.78 \mu\text{g C L}^{-1} \text{ d}^{-1}$, and 0.41 and $4.85 \text{ fg C cell}^{-1} \text{ d}^{-1}$, respectively. Both volumetric and carbon-normalized rates of bacterial productivity were fastest at P16 and P26. Bacterial abundance and productivity were within the range previously reported for summer months along Line P (0.80 – $1.35 \times 10^9 \text{ cells L}^{-1}$ and 2 – $6 \mu\text{g C L}^{-1} \text{ d}^{-1}$, respectively) (Sherry et al., 1999).

Correlations of Cu Assimilation, Biomass, Productivity, and Cu Speciation

The concomitant sampling of total dissolved Cu, Cu speciation, and various measures of biological biomass and productivity allow us to determine how Cu might influence microorganisms along Line P. There were a number of statistically significant

TABLE 1 | Locations, sampling dates, seafloor depths, mixed layer depths, and k_D of the stations sampled along Line P in August, 2011.

Station	Latitude (N)	Longitude (W)	Sampling date	Seafloor depth (m)	MLD (m)	k_D (m^{-1})
P3	48°37.50'	126°20.02'	Aug 17, 2011	815	15	0.211
P4	48°39.00'	126°40.00'	Aug 18, 2011	1320	23	0.093
P12	48°58.91'	130°39.91'	Aug 21, 2011	3230	15	0.093
P16	49°17.00'	134°40.00'	Aug 22–23, 2011	3620	31	0.093
P26	49°59.95'	144°59.99'	Aug 26, 2011	4225	29	0.096

correlations along the transect (for p -values, see Table 6). Total NPP_V , as well as 1 – $5 \mu\text{m}$ and $>5 \mu\text{m}$ NPP_V (from the size-fractionated Cu:C assimilation ratio assays) were negatively correlated with $[\text{Cu}']$ ($r^2 = -0.63$ to -0.86) and positively correlated with $\log K_{\text{CuL,Cu}^{2+}}^{\text{cond}}$ ($r^2 = 0.63$ – 0.74) (Figures 4A,C). These correlations are stronger than those between NPP_V and nitrate ($r^2 = 0.54$), phosphate ($r^2 = 0.56$), or silicic acid ($r^2 =$

TABLE 2 | Light intensities, euphotic zone depth (Z_{eu}), and macronutrient concentrations (μM) at each sampling depth along Line P.

Station	Z_{eu} (m)	Sampling depth (m)	% Surface irradiance (I_0) ^a (%)	% I_0 of incubation ^b (%)	$[\text{NO}_3^-]$	$[\text{PO}_4^{3-}]$	$[\text{Si}(\text{OH})_4]$
P3	22	7	22	26	BDL ^c	0.29	10.53
		12	10	11	BDL	0.27	10.15
P4	49	10	39	42	BDL	0.29	2.25
		20	16	18	BDL	0.29	2.30
		40	3	5	0.60	0.57	5.90
P12	49	10	39	42	BDL	0.38	6.70
		20	16	18	0.20	0.40	6.30
		40	3	5	5.30	0.76	11.10
P16	49	10	39	42	5.20	0.73	11.30
		37	3	5	7.00	0.85	12.60
P26	48	10	38	42	11.20	1.09	15.80
		35	4	5	13.10	1.24	ND ^d

Depths in bold are below the mixed layer.

^a% Surface irradiance measured at each sampling depth.

^b% Surface irradiance experienced by the Cu uptake and primary productivity incubations.

^cBDL: below detection limit; detection limits for NO_3^- , PO_4^{3-} , and $\text{Si}(\text{OH})_4$ were 0.2, 0.02, and 0.5 μM , respectively (Barwell-Clarke and Whitney, 1996).

^dND: not determined.

0.54) (Table 6). There were no significant correlations between NPP_B and either $[\text{Cu}']$ or $\log K_{\text{CuL}, \text{Cu}^{2+}}^{\text{cond}}$, with or without the inclusion of the P4 outlier sampled at 10 m (Figures 4B,D). Total chl *a*, as well as $>5 \mu\text{m}$ chl *a*, were not strongly correlated with NPP_V ($r^2 = 0.41$ and 0.51 , respectively; Table 6), while chl *a* in the $1-5 \mu\text{m}$ size fraction was not correlated with NPP_V ($p > 0.05$). This indicates that the correlations between $[\text{Cu}']$, $\log K_{\text{CuL}, \text{Cu}^{2+}}^{\text{cond}}$, and NPP_V may not have been solely driven by changes in biomass. Ligand concentrations were positively correlated with total particulate $[\text{chl } a]$ ($r^2 = 0.39$), $>5 \mu\text{m}$ $[\text{chl } a]$ ($r^2 = 0.46$), and bacterial abundance ($r^2 = 0.65$; Table 6).

Cu:C Assimilation Ratios

The Cu:C assimilation ratios ranged between 0.4 and $80 \mu\text{mol Cu mol C}^{-1}$ across the transect (Table 5). The average Cu:C assimilation ratios were similar across the transect for all size fractions (28 ± 20 , 27 ± 16 , 30 ± 21 , and 27 ± 11 for the $0.22-1 \mu\text{m}$, $1-5 \mu\text{m}$, $>5 \mu\text{m}$, and total particulate size fractions, respectively). The Cu:C assimilation ratios were not correlated with $[\text{Cu}]_d$, $[\text{Cu}']$, $[\text{L}]$, or $\log K_{\text{CuL}, \text{Cu}^{2+}}^{\text{cond}}$.

Cu Uptake Rates

Total particulate $\rho\text{Cu}_{\text{ST}, \text{C}}$ varied ~ 9 -fold, and ranged between 1.1 ± 0.1 and $10 \pm 1 \mu\text{mol Cu mol C}^{-1} \text{h}^{-1}$. Size-fractionated $\rho\text{Cu}_{\text{ST}, \text{C}}$ were more variable, and varied up to 130-fold across the size fractions (ranging from $0.7 \pm 0.1-94 \pm 13 \mu\text{mol Cu mol C}^{-1} \text{h}^{-1}$). Average $\rho\text{Cu}_{\text{ST}, \text{C}}$ were similar for the $1-5 \mu\text{m}$ ($17 \pm 24 \mu\text{mol Cu mol C}^{-1} \text{h}^{-1}$) and $>5 \mu\text{m}$ ($14 \pm 16 \mu\text{mol Cu mol C}^{-1} \text{h}^{-1}$) size fractions, and were slowest for the $0.22-1 \mu\text{m}$ size fraction ($1.6 \pm 0.8 \mu\text{mol Cu mol C}^{-1} \text{h}^{-1}$). Average $\rho\text{Cu}_{\text{ST}, \text{V}}$ along the transect were similar for all size fractions ($\sim 5 \text{ pmol Cu L}^{-1} \text{h}^{-1}$) (Table 5).

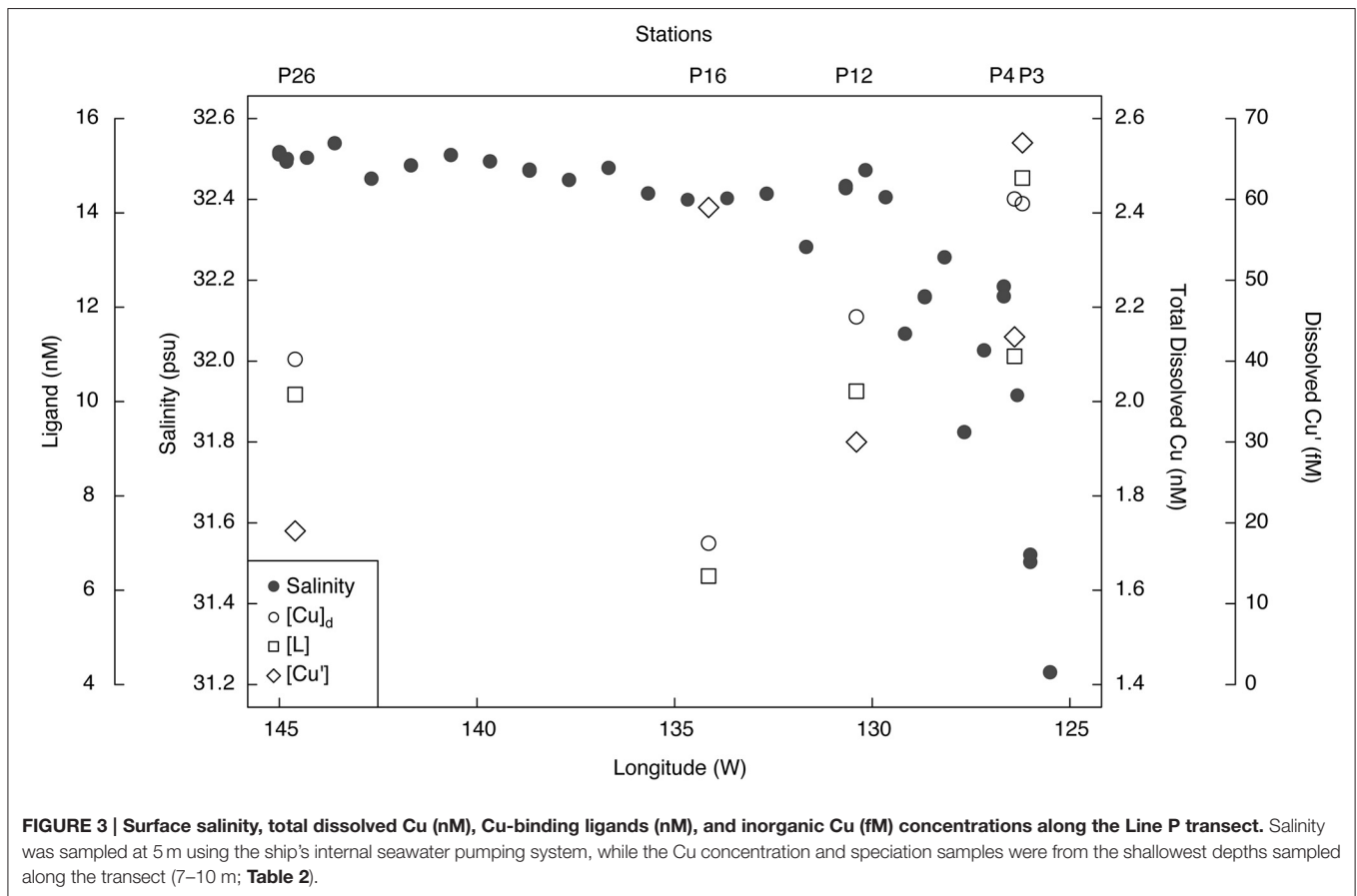
Total particulate long-term volumetric uptake rates ($\rho\text{Cu}_{\text{LT}, \text{V}}$) varied 3.8-fold, and ranged between 33 ± 10 and $125 \pm 40 \text{ pmol Cu L}^{-1} \text{d}^{-1}$. Similar to $\rho\text{Cu}_{\text{ST}, \text{V}}$, average $\rho\text{Cu}_{\text{LT}, \text{V}}$ were similar

TABLE 3 | Total dissolved Cu, ligand concentrations, conditional stability constants, inorganic Cu concentration, and the dissolved $[\text{L}]:[\text{Cu}]_d$ ratio at each sampling depth along Line P.

Station	Sampling depth (m)	$[\text{L}]$ (nM)	$\log K_{\text{CuL}, \text{Cu}^{2+}}^{\text{cond}}$	$[\text{Cu}]_d$ (nM)	ρCu ($-\log[\text{Cu}^{2+}]$)	$[\text{Cu}']$ (fM)	$[\text{L}]:[\text{Cu}]_d$
P3	7	14.7	13.9	2.4	14.6	66.7	6.1
	12	17.4	13.7	2.8	14.4	94.0	6.2
P4	10	11.0	14.2	2.4	14.8	44.1	4.5
	20	10.4	13.8	1.5	14.6	65.9	7.1
	40	7.6	14.2	1.8	14.7	46.0	4.2
P12	10	10.2	14.3	2.2	14.9	30.4	4.7
	20	8.8	14.3	2.2	14.7	43.6	4.0
	40	11.0	14.0	1.9	14.7	53.0	5.7
P16	10	6.3	14.2	1.7	14.6	58.8	3.7
	37	7.8	14.0	1.9	14.6	60.0	4.0
P26	10	10.2	14.5	2.1	15.1	18.7	4.9
	35	7.0	14.5	2.2	14.9	33.1	3.1

Depths in bold are below the mixed layer.

for the $0.22-1 \mu\text{m}$ ($23 \pm 17 \text{ pmol Cu L}^{-1} \text{d}^{-1}$), $1-5 \mu\text{m}$ ($31 \pm 13 \text{ pmol Cu L}^{-1} \text{d}^{-1}$), and $>5 \mu\text{m}$ ($33 \pm 17 \text{ pmol Cu L}^{-1} \text{d}^{-1}$) size fractions, and varied 187-fold among the size fractions (0.3 ± 0.1 to $125 \pm 20 \text{ pmol Cu L}^{-1} \text{d}^{-1}$). Unlike $\rho\text{Cu}_{\text{ST}, \text{V}}$ the $\rho\text{Cu}_{\text{LT}, \text{V}}$ for the $0.22-1 \mu\text{m}$ size fraction were not slower than the other size fractions. Variation of carbon-normalized Cu uptake rates ($\rho\text{Cu}_{\text{LT}, \text{C}}$) in the total (five-fold), $1-5 \mu\text{m}$ (16-fold), and $>5 \mu\text{m}$ (21-fold) size fractions was similar to variation in $\rho\text{Cu}_{\text{ST}, \text{C}}$. However, $\rho\text{Cu}_{\text{LT}, \text{C}}$ in the $0.22-1 \mu\text{m}$ size fraction was more variable (155-fold) than $\rho\text{Cu}_{\text{ST}, \text{C}}$ (five-fold). While there were no significant correlations between $\rho\text{Cu}_{\text{LT}, \text{C}}$ and any measure of Cu speciation along the transect for the eukaryotic size fractions,



$\rho\text{Cu}_{\text{LT,C}}$ in the 0.22–1 μm size fraction was positively correlated with $\log K_{\text{CuL,Cu}^{2+}}^{\text{cond}}$ ($r^2 = 0.64$, $p = 0.0055$) (**Table 6**).

Short-term Cu uptake rates are in excess of long-term uptake rates due to either cellular efflux or remineralization by micrograzers (Semeniuk et al., 2015). The ratio of short-term:long-term uptake ratios (ST:LT) was calculated by first converting the hourly short-term rates ($\text{pmol Cu L}^{-1} \text{h}^{-1}$) into daily rates ($\text{pmol Cu L}^{-1} \text{d}^{-1}$). Average $\rho\text{Cu}_{\text{ST,V}}$ for all size fractions was ~ 11 -times faster than $\rho\text{Cu}_{\text{LT,V}}$, and the total ST:LT ratios ranged between 2.7 and 11.2 across the transect (**Table 5**). The ST:LT ratios were more variable for the 0.22–1 μm size fraction (1.8–187) than the 1–5 or $>5 \mu\text{m}$ size fractions (1.9–10.5). The two highest ST:LT values in the 0.22–1 μm size fraction (52 and 187) were outliers at P16. Without these outliers, the average ST:LT ratios for all size fractions were consistently lower at P26 (2.7 ± 1.0) and P16 (3.3 ± 1.1 ; without the two outliers) than P4 (6.9 ± 9.2) or P12 (6.5 ± 2.0).

DISCUSSION

Distribution of Total Dissolved Cu in Line P Surface Waters

We present some of the first measurements of dissolved Cu in the northeast subarctic Pacific Ocean. Total dissolved Cu

varied 1.9-fold across the transect (1.5–2.8 nM). These values are similar to surface water $[\text{Cu}]_{\text{d}}$ previously measured along Line P (1.2–3.5 nM; Martin et al., 1989; Semeniuk et al., 2009), in the North Pacific (0.6–3.5 nmol kg^{-1}) (Boyle et al., 1977; Coale and Bruland, 1988), northwest subarctic Pacific and Bering Sea (1.2–2 nM) (Moffett and Dupont, 2007), and in Washington coastal waters south of the Line P transect (1.86–5.25 nmol kg^{-1}) (Jones and Murray, 1984).

Dissolved Cu was highest in less saline waters near the coast (salinity = 31.5–32) and decreased offshore. The elevated $[\text{Cu}]_{\text{d}}$ at P3 (7 and 12 m depth) and at 10 m depth at P4 may be due to their closer proximity to terrestrial and shelf sources of Cu. Upwelling begins at these stations by March, due to Ekman pumping as the California and Alaska currents bifurcate along the British Columbia coast (Thomson, 1981; Foreman et al., 2011). Intermediate waters (250–500 m) off the coast of Washington are enriched in Cu (2–3 nM) relative to surface waters (Jones and Murray, 1984). Upwelling of these waters could account for the observed enrichment of $[\text{Cu}]_{\text{d}}$ at P3 and P4.

Surface water $[\text{Cu}]_{\text{d}}$ at P26 (2.1–2.2 nM) was higher than previously measured at this station (1.44–1.54 nmol kg^{-1}) (Martin et al., 1989). Total dissolved Cu at P26 was also higher than $[\text{Cu}]_{\text{d}}$ at P16 (1.7–1.9 nM). Dissolved Fe in the mixed layer was also significantly higher at P26 (0.13–0.21 nM) relative

TABLE 4 | Biomass and rate parameters measured at each sampling depth along Line P.

Station	Depth (m)	Chl <i>a</i> ($\mu\text{g L}^{-1}$)	F_v/F_m	Bacteria ^a (10^9 cells L^{-1})	Cyanobacteria (10^6 cells L^{-1})	Picoeukaryotes (10^6 cells L^{-1})	NPP_V ($\mu\text{g C L}^{-1} \text{d}^{-1}$)	NPP_B ($\mu\text{g C } \mu\text{g chl } a^{-1} \text{d}^{-1}$)	BP_V ($\mu\text{g C L}^{-1} \text{d}^{-1}$)	BP_B ($\text{fg C cell}^{-1} \text{d}^{-1}$)
P3	7	0.898	ND ^b	32.0	200	16.3	ND	ND	ND	ND
	12	0.958	ND	32.2	177	13.0	ND	ND	ND	ND
P4	10	0.044	0.64	1.08	1.73	0.55	25.2	583	1.88	1.74
	20	0.138	0.51	1.08	1.42	1.61	10.8	74	1.52	1.41
	40	0.549	0.23	2.11	38	5.08	46.8	85	3.96	1.87
P12	10	0.428	0.38	2.30	0.82	3.10	45.6	108	3.04	1.32
	20	0.202	0.29	3.66	1.23	3.86	40.8	202	1.49	0.41
	40	0.127	0.24	2.06	ND	ND	32.4	253	0.98	0.48
P16	10	0.262	0.19	1.25	0.77	2.63	40.8	157	2.33	1.86
	37	0.241	0.29	0.99	4.70	4.82	34.8	143	4.78	4.85
P26	10	0.418	0.29	1.10	4.79	7.97	110.4	264	1.97	1.80
	35	0.440	0.24	0.82	2.45	11.7	75.6	173	4.67	5.73

Depths in bold are below the mixed layer. Volumetric (NPP_V) and chl *a*-normalized (NPP_B) net primary productivity was measured over 24 h. Volumetric (BP_V) and cell-normalized (BP_B) bacterial productivity was measured over 3–4 h.

^aTotal bacterial abundance (heterotrophic and autotrophic bacteria).

^bND: not determined.

to P16 (0.03–0.07 nM) (Cullen, unpub. data). Recent dissolved lead (Pb) isotope data along Line P indicate that the source of dissolved Pb in the upper 75 m at P26 is from Asian dust sources (McAlister, 2015). At stations P4 through P20, North American dust sources were the dominant sources of metals to surface waters (McAlister, 2015). Thus, the higher Fe and Cu concentrations at P26 compared to P16 could be due to atmospheric dust deposition from Asia. It is also possible that transport of coastal waters via mesoscale eddies (Johnson et al., 2005) or isopycnal transport from continental margins (Lam et al., 2006) carried Cu and Fe to the P26 mixed layer. However, satellite altimetry anomalies demonstrate that there was not an eddy at P26 during the time of sampling (Figure 5). Though it is difficult to distinguish between atmospheric and isopycnal transport of Cu to P26 with our data, sporadic atmospheric dust deposition events have been previously linked to primary productivity increases at P26 (Bishop et al., 2002; Hamme et al., 2010). Interestingly, [chl *a*], F_v/F_m (a physiological indicator for Fe-limitation), picoeukaryote abundance, and NPP_V were also elevated at P26 compared to P16. These data suggest that a recent atmospheric dust deposition event may have occurred at P26 shortly before our arrival.

Cu Speciation in Surface Waters along Line P

Strong Cu binding ligands were present across the transect at all sampling depths, and were always in excess of the total dissolved Cu concentrations, resulting in sparingly low inorganic Cu concentrations. Compared to previous studies (Buck et al., 2010; Bundy et al., 2013), a single analytical window was employed (5 μM SA) along with higher Cu additions, in order to detect a wider range of ligands. This method was used to achieve the most accurate estimate of Cu^{2+} while using a single titration window. The ligand concentration range (6.3–17.4 nM) and strength

($\log K_{\text{CuL}, \text{Cu}^{2+}}^{\text{cond}} = 13.7\text{--}14.5$) represent both stronger and weaker ligands. Thus, the concentrations reported here are higher than those reported for just the strong ligand class by other groups, using a different analytical window (2–4 nM; e.g., Jacquot et al., 2013). Although this study used a different analytical window than a study in a similar region (Moffett and Dupont, 2007), the calculations of Cu^{2+} were very similar. This is likely because Cu^{2+} determinations have been found to be largely independent of analytical window, within a relatively wide range (Bruland et al., 2000). The ligand strengths ($\log K_{\text{CuL}, \text{Cu}^{2+}}^{\text{cond}}$) are similar to those previously reported for the northwest Pacific Ocean and Bering Sea (13.5–14; Moffett and Dupont, 2007), the Southern Ocean (14–16.4; Buck et al., 2010; Bundy et al., 2013), the eastern tropical south Pacific Ocean (13.5–14.5; Jacquot et al., 2013), and the north Atlantic Ocean (12.9–14.2; Jacquot and Moffett, 2015).

Although the provenance and structure of the strong Cu-binding ligands in the open ocean is unknown, there are a number of possible sources and candidate compounds. *Synechococcus* and the heterotrophic bacterium *Vibrio alginolyticus* produce strong Cu-binding ligands ($\log K_{\text{CuL}, \text{Cu}^{2+}}^{\text{cond}} = 13$) when experiencing Cu-toxicity (Moffett and Brand, 1996; Gordon et al., 2000). The concentration of these ligands is normally in excess (0–50%) of the total dissolved Cu in the growth medium. The significant positive correlation between total bacterial cell densities and [L] ($r^2 = 0.65$, $p = 0.0016$) suggests that prokaryotes may be a source of strong Cu ligands along Line P. Since [L] was not correlated with cyanobacteria abundance, heterotrophic bacteria may produce the majority of these strong Cu binding ligands.

Similar to $[\text{Cu}]_d$, [L] was highest near the fresher coastal surface waters and decreased toward the open ocean. The higher [L]: $[\text{Cu}]_d$ ratio at P3 compared to the average ratio across the transect suggests that there may be an additional source of strong Cu binding ligands along the shelf. Ligands in marine sediment

TABLE 5 | Size-fractionated Cu:C assimilation ratios (24 h), short-term Cu uptake rates (2 h), long-term Cu uptake rates (24 h), and the short-term:long-term uptake rate ratio for each sampling depth along Line P in August 2011.

Station	Depth (m)	Size (μm)	Chl a ($\mu\text{g L}^{-1}$)	Cu:C assimilation ratio ($\mu\text{mol Cu mol C}^{-1}$)	$\rho\text{Cu}_{\text{ST,V}}$ ($\text{pmol Cu L}^{-1} \text{h}^{-1}$)	$\rho\text{Cu}_{\text{ST,C}}$ ($\mu\text{mol Cu mol C}^{-1} \text{h}^{-1}$)	$\rho\text{Cu}_{\text{LT,V}}$ ($\text{pmol Cu L}^{-1} \text{d}^{-1}$)	$\rho\text{Cu}_{\text{LT,C}}$ ($\mu\text{mol Cu mol C}^{-1} \text{d}^{-1}$)	ST:LT ratio
P3	7	0.22–1	0.08		7.7 ± 1.2	0.7 ± 0.1			
		1–5	0.48		3.3 ± 0.8	5.3 ± 1.2			
		>5	0.33		4.1 ± 0.1	1.9 ± 0.02			
		Total	0.90		15 ± 1.5	1.1 ± 0.1			
	12	0.22–1	0.30		12 ± 0.9	1.1 ± 0.1			
		1–5	0.15		6.7 ± 0.6	3.4 ± 0.3			
>5		0.51		6.5 ± 0.3	4.7 ± 0.2				
	Total	0.96		25 ± 1.7	1.8 ± 0.1				
P4	10	0.22–1	0.004	69 ± 23	6.3 ± 0.9	3.5 ± 0.5	23 ± 1	13 ± 0.1	6.6
		1–5	0.02	53 ± 6	7.8 ± 1.1	94 ± 13	36 ± 13	433 ± 32	5.2
		>5	0.02	36 ± 5	5.2 ± 0.7	62 ± 8	40 ± 0.3	472 ± 4	3.2
		Total	0.044	46 ± 5	19 ± 3	10 ± 1	98 ± 4	50 ± 2	4.7
	20	0.22–1	0.01	38 ± 0.4	4.3 ± 0.6	2.4 ± 0.3	5 ± 2	3 ± 1	21.3
		1–5	0.09	58 ± 10	6.6 ± 0.8	18 ± 2	15 ± 0.4	40 ± 1	10.5
		>5	0.04	28 ± 0.4	4.4 ± 0.4	26 ± 2	13 ± 2	78 ± 15	8.1
		Total	0.14	39 ± 3	15 ± 2	6.5 ± 0.7	33 ± 5	14 ± 2	11.2
	40	0.22–1	0.04	43 ± 4	5.6 ± 0.8	1.6 ± 0.2	41 ± 6	12 ± 2	3.3
		1–5	0.30	28 ± 2	6.1 ± 0.1	4.9 ± 10.1	38 ± 2	31 ± 2	3.8
		>5	0.21	26 ± 4	3.5 ± 0.04	4.0 ± 0.1	39 ± 1	45 ± 1	2.1
		Total	0.55	31 ± 1	15 ± 1	2.7 ± 0.2	119 ± 9	21 ± 2	3.1
P12	10	0.22–1	0.01	27 ± 4	8.4 ± 0.9	2.2 ± 0.2	30 ± 2	8 ± 0.4	6.8
		1–5	0.16	15 ± 3	8.1 ± 1.9	12 ± 3	18 ± 2	28 ± 3	10.5
		>5	0.26	15 ± 1	5.7 ± 0.5	5.3 ± 0.5	22 ± 1	21 ± 1	6.2
		Total	0.43	19 ± 2	22 ± 3	4.0 ± 0.6	70 ± 4	13 ± 1	7.6
	20	0.22–1	0.003	35 ± 4	6.4 ± 1.4	1.1 ± 0.2	47 ± 3	8 ± 1	3.3
		1–5	0.07	22 ± 1	6.3 ± 0.5	22 ± 2	25 ± 2	85 ± 7	6.1
		>5	0.13	18 ± 2	5.0 ± 0.2	9.2 ± 0.3	16 ± 1	30 ± 2	7.4
		Total	0.20	26 ± 1	18 ± 2	2.5 ± 0.3	87 ± 6	13 ± 1	4.9
	40	0.22–1	0.003	22 ± 1	3.6 ± 1.5	1.1 ± 0.4	17 ± 2	5 ± 0.4	5.2
		1–5	0.07	12 ± 1	4.8 ± 0.2	16 ± 1	14 ± 1	49 ± 4	8.0
		>5	0.05	14 ± 2	2.7 ± 0.2	13 ± 1	11 ± 1	52 ± 4	5.9
		Total	0.13	16 ± 0.3	11 ± 2	2.8 ± 0.4	42 ± 3	11 ± 1	6.4
P16	10	0.22–1	0.01	0.4 ± 0.1	2.5 ± 0.02	1.2 ± 0.01	0.3 ± 0.1	0.3 ± 0.1	187.4
		1–5	0.14	18 ± 1	6.1 ± 0.9	10 ± 2	30 ± 2	51 ± 4	4.9
		>5	0.11	51 ± 5	5.8 ± 0.7	13 ± 2	51 ± 6	112 ± 14	2.7
		Total	0.26	24 ± 2	14 ± 1	4.6 ± 0.1	81 ± 9	26 ± 3	4.3
	37	0.22–1	0.01	2 ± 1	2.8 ± 0.03	1.7 ± 0.02	1.1 ± 0.3	0.8 ± 0.2	52.4
		1–5	0.16	31 ± 9	4.3 ± 0.5	6.5 ± 0.7	38 ± 1	56 ± 2	2.8
>5		0.08	80 ± 23	4.9 ± 0.4	15 ± 1	61 ± 24	183 ± 71	1.9	
	Total	0.24	34 ± 4	12 ± 0.04	4.6 ± 0.02	100 ± 25	38 ± 10	2.9	

(Continued)

TABLE 5 | Continued

Station	Depth (m)	Size (μm)	Chl <i>a</i> ($\mu\text{g L}^{-1}$)	Cu:C assimilation ratio ($\mu\text{mol Cu mol C}^{-1}$)	$\rho\text{Cu}_{\text{ST,V}}$ ($\text{pmol Cu L}^{-1} \text{h}^{-1}$)	$\rho\text{Cu}_{\text{ST,C}}$ ($\mu\text{mol Cu mol C}^{-1} \text{h}^{-1}$)	$\rho\text{Cu}_{\text{LT,V}}$ ($\text{pmol Cu L}^{-1} \text{d}^{-1}$)	$\rho\text{Cu}_{\text{LT,C}}$ ($\mu\text{mol Cu mol C}^{-1} \text{d}^{-1}$)	ST:LT ratio
P26	10	0.22–1	0.02	18 ± 5	2.4 ± 0.02	1.3 ± 0.01	31 ± 4	17 ± 2	1.8
		1–5	0.16	12 ± 6	4.2 ± 0.1	6.4 ± 0.1	46 ± 3	69 ± 4	2.2
		>5	0.24	14 ± 6	5.9 ± 0.03	5.9 ± 0.03	34 ± 6	34 ± 6	4.2
		Total	0.42	14 ± 5	12 ± 0.01	3.6 ± 0.01	111 ± 4	32 ± 1	2.7
35	10	0.22–1	0.02	23 ± 5	2.5 ± 0.1	1.8 ± 0.1	33 ± 4	24 ± 3	1.8
		1–5	0.27	17 ± 3	5.4 ± 0.4	4.8 ± 0.3	50 ± 12	44 ± 11	2.6
		>5	0.15	22 ± 5	7.8 ± 0.6	13 ± 1	43 ± 4	69 ± 7	4.4
		Total	0.44	20 ± 4	15.7 ± 0.9	5.0 ± 0.3	125 ± 20	40 ± 6	3.0

Cu:C assimilation ratios were determined using ^{67}Cu and ^{14}C . Carbon-normalized uptake rates were measured using ^{67}Cu , and dividing by particulate C concentrations derived from bacterial abundance and chl *a* concentrations (see Section Materials and Methods for details). The ST:LT ratios were calculated by converting the hourly short-term Cu uptake rates to daily dates, and then dividing by the long-term Cu uptake rates. Errors represent half the range for two replicate measurements, and values in bold are for the total particulate size fraction.

porewaters, though weaker than in surface waters, can exceed 100 nM concentrations and can diffuse into the overlying bottom water (Skrabal et al., 2000; Shank et al., 2004). As intermediate waters pass over the shelf sediments during upwelling, they may become enriched in weaker Cu binding ligands. The lowest $\log K_{\text{CuL,Cu}^{2+}}^{\text{cond}}$ measured along the transect were for P3 (12 m depth), and suggests that shelf waters might be a source of weaker Cu ligands in this region. Humic substances bind Cu ($\log K_{\text{CuL,Cu}^{2+}}^{\text{cond}} = 12$; Whitby and van den Berg, 2015) and may be a portion of the ligand pool in coastal stations. Humic substances are electrochemically active, and their peaks were observed in the coastal stations (data not shown). Inorganic Cu concentrations varied five-fold (19–94 fM) with a corresponding pCu range of 15.1–14.5. While the $[\text{Cu}']$ values are lower than previous measurements in the North Pacific (0.8–2.4 pM; Coale and Bruland, 1988), this is likely due to the lower analytical detection window and different electrochemical method (ASV compared to CSV in this study) used by Coale and Bruland (Bruland et al., 2000; Buck et al., 2012).

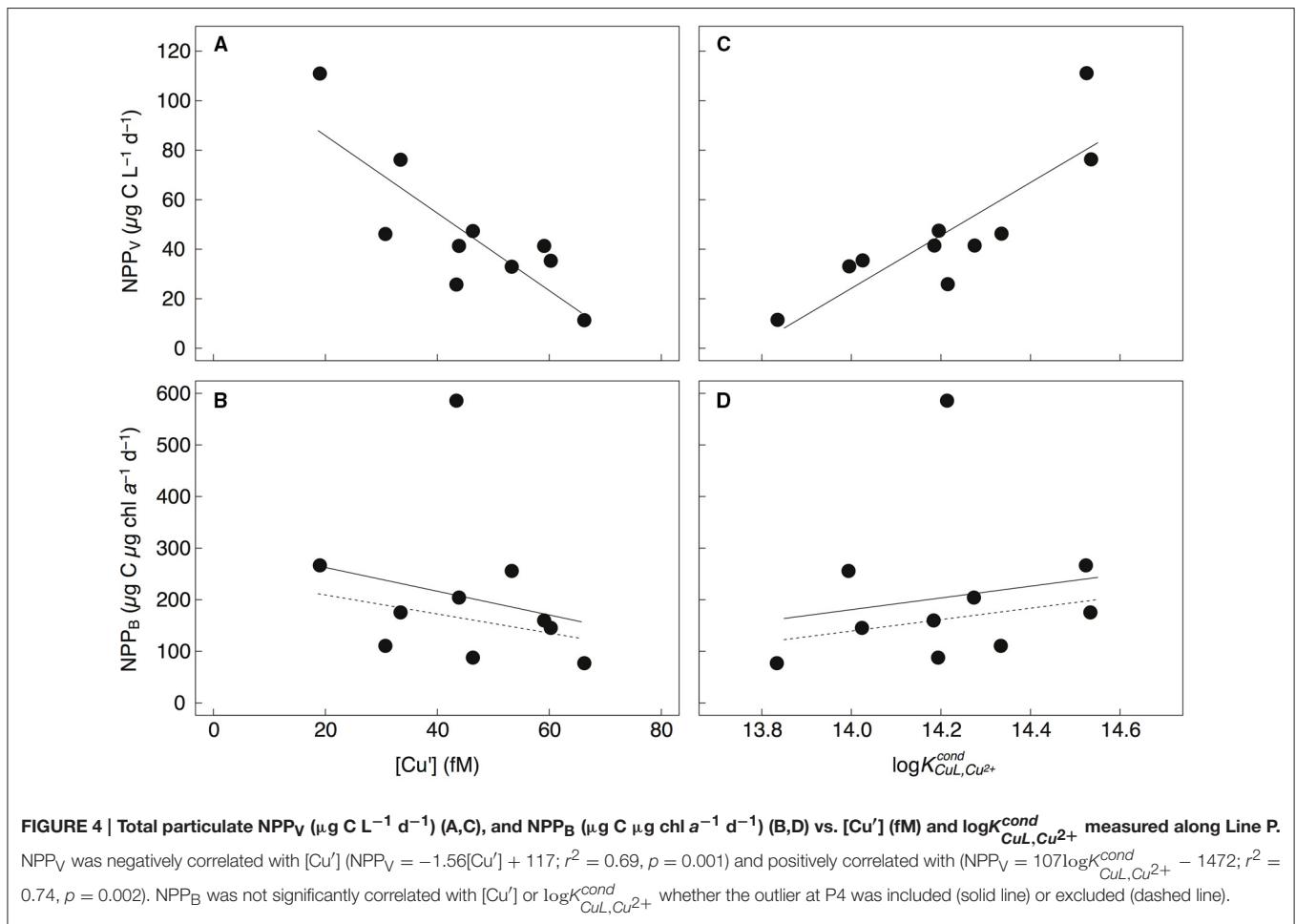
Surface water $[\text{Cu}']$ tended to be lower at shallower depths across the transect, and may imply biological utilization of Cu' and export of particulate Cu below the mixed layer. The negative correlations between NPP_V and $[\text{Cu}']$ for all sampling depths and stations for the 1–5 μm , >5 μm , and total particulate size fractions (Figure 4; Table 6) support this. We did not observe a similar correlation between chl *a*-normalized NPP (NPP_B) and $[\text{Cu}']$. However, the C:chl *a* ratio of autotrophs can vary more than six-fold at P26 (Booth et al., 1993; Peña and Varela, 2007), and by more than 10-fold between laboratory strains (MacIntyre et al., 2002). This variability likely precluded any significant correlation between NPP_V $[\text{Cu}']$. Given laboratory and field evidence for Cu' uptake by phytoplankton (Sunda and Guillard, 1976; Sunda and Huntsman, 1995; Semeniuk et al., 2015; Walsh et al., 2015), we propose that Cu' drawdown by the phytoplankton communities along the transect is the most likely explanation for this trend.

TABLE 6 | Statistically significant Pearson correlations of biomass, productivity, Cu uptake, and chemical parameters measured along Line P in August 2011.

Size fraction	Variable 1	Variable 2	r^2	p-value
Total	[Chl <i>a</i>]	NPP_V	0.41	0.0460
	[Chl <i>a</i>]	[L]	0.39	0.0301
	[Chl <i>a</i>]	[Picocukaryote]	0.76	0.0005
	[Chl <i>a</i>]	[Total Bacteria]	0.63	0.0021
	NPP_V	$[\text{Cu}']$	0.69	0.0010
	NPP_V	$\log K_{\text{CuL,Cu}^{2+}}^{\text{cond}}$	0.74	0.0018
	NPP_V	$[\text{NO}_3^-]$	0.54	0.0027
	NPP_V	$[\text{PO}_4^{3-}]$	0.56	0.0123
	NPP_V	$[\text{Si}(\text{OH})_4]$	0.54	0.0155
>5 μm	F_V/F_m	[L]	0.43	0.0383
	[Chl <i>a</i>]	NPP_V	0.51	0.0195
		[L]	0.46	0.0154
		$[\text{Cu}]_d$	0.42	0.0226
		NPP_V^*	$[\text{Cu}']$	0.86
NPP_V^*		$\log K_{\text{CuL,Cu}^{2+}}^{\text{cond}}$	0.69	0.0029
1–5 μm	NPP_V^*	$[\text{Cu}']$	0.63	0.0062
	NPP_V^*	$\log K_{\text{CuL,Cu}^{2+}}^{\text{cond}}$	0.63	0.0063
	NPP_V^*	$[\text{NO}_3^-]$	0.69	0.0028
	NPP_V^*	$[\text{PO}_4^{3-}]$	0.70	0.0026
	NPP_V^*	$[\text{Si}(\text{OH})_4]$	0.61	0.0127
0.22–1 μm	[Total Bacteria]	[L]	0.65	0.0016
	[Total Bacteria]	$[\text{Cu}]_d$	0.42	0.0216
	BP_V	[L]	0.43	0.0417
	$r\text{Cu}_{\text{LT,C}}$	$\log K_{\text{CuL,Cu}^{2+}}^{\text{cond}}$	0.64	0.0055

Correlations with $r^2 > 0.6$ are in bold, while those in italics have negative slopes.

^{14}C fixation data collected for each size fraction during the Cu:C assimilation ratio assays was used to calculate volumetric net primary productivity rates for the 1–5 μm and >5 μm size fractions (data not shown).

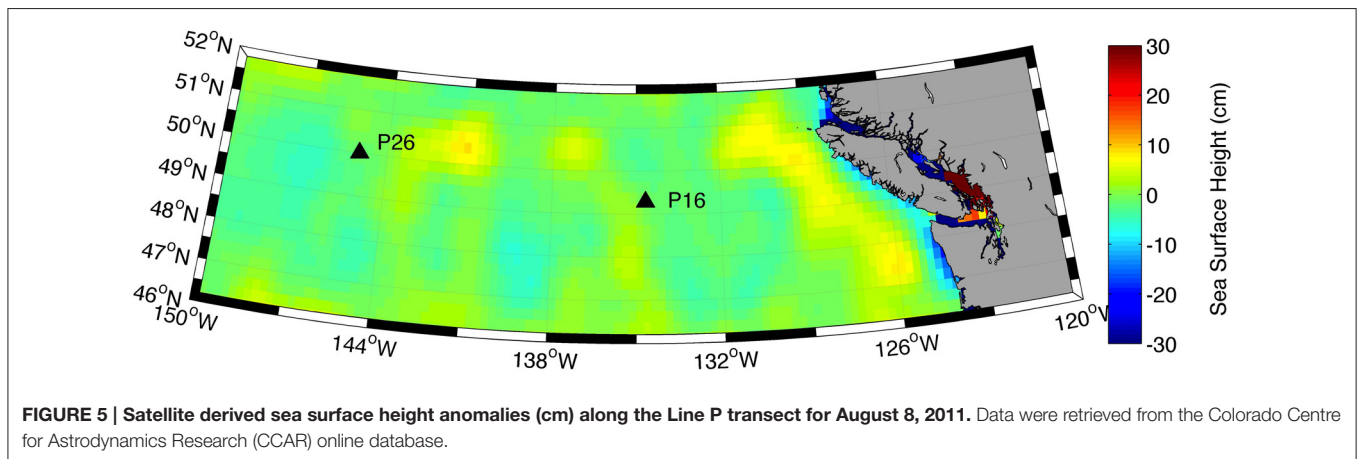


Assessing the ^{67}Cu Tracer Technique to Measure Cellular Cu Accumulation

Few direct measurements of cellular Cu quotas—defined as the intracellular ratio of Cu normalized to organic C (e.g., Sunda and Huntsman, 1995)—have been made in marine phytoplankton (Table 7). Similar to standard 24 h oceanographic incubation assays (e.g., H_2^{18}O , $^{15}\text{NO}_3^-$ incubations) the Cu:C assimilation ratios presented here and in our previous study (Semeniuk et al., 2009) assume that the phytoplankton physiology is minimally perturbed over the course of the 24 h assay. Thus, while the accumulation of cellular ^{67}Cu and ^{14}C may vary diurnally, the ratio of the incorporation of each tracer after 24 h will represent a pseudo-steady state Cu:C assimilation ratio, as long as the added tracers are at equilibrium (see Section Cu Uptake Rates, Cu:C Assimilation Ratios, and Net Primary Productivity). Assuming similar environmental conditions, our ratios should be comparable to other field and laboratory estimates of Cu:C quotas of phytoplankton isolates and mixed assemblages.

The Cu:C assimilation ratios ($\sim 30 \mu\text{mol Cu mol C}^{-1}$) across the transect were ~ 10 -times higher ($1\text{--}4 \mu\text{mol Cu mol C}^{-1}$) than during our previous investigation (Semeniuk et al., 2009). There were two major differences between the experimental setup in this study and our previous study. First, in our previous

study, the ^{67}Cu tracer was allowed to equilibrate with the *in situ* ligands for 30 min, while we chose a 2 h equilibration time here. Stronger Cu-binding ligands will have a faster forward reaction rate constant than weaker ligands due to competition with calcium (see Section Cu Uptake Rates, Cu:C Assimilation Ratios, and Net Primary Productivity). Thus, we could expect the ^{67}Cu tracer to be rapidly bound to the strong ligand pool first, and more of the ^{67}Cu tracer would equilibrate with the weaker ligand pool with a longer equilibration time. Since Cu bound to weaker organic ligands is more bioavailable than Cu bound to stronger ligands (Semeniuk et al., 2015; Walsh et al., 2015), the different equilibration times used in the two studies could have changed the relative bioavailability of the ^{67}Cu tracer. Second, in our previous study, water was collected in the mid to late afternoon, spiked with ^{67}Cu and ^{14}C , and allowed to incubate for 24 h. In the present study, we spiked the water with the isotopes just before dawn. Thus, cells spent a greater proportion in the light near the start of the incubation than in our previous study. A greater amount of fixed ^{14}C would have been available for respiration during the night than in our previous study. Freshly fixed organic ^{14}C can be respired within hours after initially fixed (Halsey et al., 2011), and so this would result in higher Cu:C assimilation ratios as observed in the present study. Both methodological



differences may have caused the higher Cu:C assimilation ratios here. Average particulate Cu uptake rates were ~ 5 -times faster than in our previous study, while the average total NPP_V ($\sim 45 \mu\text{g C L}^{-1} \text{d}^{-1}$) were half as fast ($\sim 85 \mu\text{g C L}^{-1} \text{d}^{-1}$; calculated using data reported in **Table 4** by Semeniuk et al., 2009). Thus, the tracer equilibration time appears to play a more important role, and future work should compare the effect of ^{67}Cu equilibration times with the *in situ* ligands on the measured Cu:C assimilation ratios.

The size fractionated Cu:C assimilation ratios reported here ($0.4\text{--}80.2 \mu\text{mol Cu mol C}^{-1}$) are within the range of Cu quotas reported in previous laboratory studies ($0.04\text{--}156 \mu\text{mol Cu mol C}^{-1}$) (**Table 7**). In addition, independent measurements of cellular Cu quotas in natural phytoplankton communities compare well with our Cu:C ratios ($4\text{--}70 \mu\text{mol Cu mol C}^{-1}$) (Twining et al., 2015). Average cellular Cu:C ratios were higher in autotrophic flagellates and picoeukaryotes ($\sim 30 \mu\text{mol Cu mol C}^{-1}$) than in diatoms ($\sim 4 \mu\text{mol Cu mol C}^{-1}$). Although we did not determine the phytoplankton species composition along the transect, diatoms rarely make up more than 25% of the total [chl *a*] along Line P during the year (Steiner et al., 2012), and would make up a small portion of the particulate Cu:C. These data suggest that the Cu:C ratios determined here using ^{67}Cu and ^{14}C approximate *in situ* values. Further work comparing ^{67}Cu and SXRF methods on the same samples would greatly benefit the veracity of both methods.

Geochemical estimates of the Cu:C ratios of exported material can be derived from the slope of $[\text{Cu}]_d$ and $[\text{PO}_4^{3-}]$ measured across the nutricline ($\Delta[\text{Cu}]_d:\Delta[\text{PO}_4^{3-}]$) in different ocean basins (assuming a C:P ratio of 106). The range of these ratios ($0.98\text{--}24 \mu\text{mol Cu mol C}^{-1}$; **Table 7**) is within our observations and those reported by Twining et al. (2015). However, the average Cu:C ratio ($\sim 5 \mu\text{mol Cu mol C}^{-1}$) determined using $\Delta[\text{Cu}]_d:\Delta[\text{PO}_4^{3-}]$ is smaller than the average size fractionated Cu:C ratios reported here and for single cells reported by Twining et al. (2015). Interestingly, the Cu:C ratios of single diatom cells in the North Atlantic ($\sim 4 \mu\text{mol Cu mol C}^{-1}$; Twining et al., 2015) is similar to Cu:C ratios determined using $\Delta[\text{Cu}]_d:\Delta[\text{PO}_4^{3-}]$. The $\Delta[\text{Cu}]_d:\Delta[\text{PO}_4^{3-}]$ method only

takes into account Cu and C remineralized from exported material (e.g., diatoms), and not organic material remineralized in shallow waters (e.g., flagellates). Thus, diatoms may be primarily responsible for removing Cu from the mixed layer. In support of this, Löscher (1999) observed a positive correlation between dissolved silicic acid and total $[\text{Cu}]_d$ in the Southern Ocean.

Only two studies have reported steady-state Cu uptake rates in phytoplankton grown in similar $[\text{Cu}']$ (Annett et al., 2008; Guo et al., 2012). We calculated cell-specific Cu uptake rates along the transect using the $1\text{--}5 \mu\text{m}$ size fraction $\rho\text{Cu}_{\text{LT,V}}$ and picoeukaryote abundance, and compared them to steady state Cu uptake rates measured in laboratory studies. The average cell-normalized Cu uptake rates across the transect was $14 \pm 19 \text{amol Cu cell}^{-1} \text{d}^{-1}$, and ranged between 4 and $65 \text{amol Cu cell}^{-1} \text{d}^{-1}$. Removing the anomalously high value at P4 (10 m), the average uptake rate decreases to $7 \pm 2 \text{amol Cu cell}^{-1} \text{d}^{-1}$. The average steady-state net cellular Cu uptake rates measured for nine phytoplankton species with cell diameters between 1 and $5 \mu\text{m}$ was $1 \pm 0.8 \text{amol Cu cell}^{-1} \text{d}^{-1}$, with a range of $0.03\text{--}3.5 \text{amol Cu cell}^{-1} \text{d}^{-1}$ (Annett et al., 2008; Guo et al., 2012). Thus, the estimates of cellular Cu uptake rates across the transect are slightly faster than would be predicted using laboratory data. The difference between the laboratory and field estimates could be due to phytoplankton community composition structure and experimental designs (e.g., steady state conditions and 24 h light in the lab; diurnal cycles and varying light in the field). More recent estimates of short-term cellular Cu uptake rates at P26 ($\sim 8 \text{amol Cu cell}^{-1} \text{d}^{-1}$; Semeniuk et al., 2015) are within the range reported here.

Environmental Controls of Biogenic Cu along Line P

Some phytoplankton have higher Cu demands during Fe limitation (Peers et al., 2005; Wells et al., 2005; Maldonado et al., 2006; Annett et al., 2008; Guo et al., 2012; Biswas et al., 2013). Oceanic phytoplankton strains have higher basal metabolic Cu requirements compared to coastal strains, and may reflect an increased reliance on Cu in waters with chronically low Fe (Peers and Price, 2006; Annett et al., 2008).

TABLE 7 | Particulate Cu:C ratios in natural phytoplankton communities and laboratory strains grown under Cu-limiting and toxic conditions.

Study Type	Cu:C ratio ($\mu\text{mol Cu mol C}^{-1}$)	Method of Cu:C ratio determination	Study
Laboratory	0.56–150	^{14}C and GFAAS ^a	Sunda and Huntsman, 1995
	1.07–156	CHN Analyzer and GFAAS ^b	Chang and Reinfelder, 2000
	0.40–9.01	HR-ICP-MS ^c	Ho et al., 2003
	0.32–6.32	^{14}C and ^{67}Cu ^d	Annett et al., 2008
	0.04–6.20	^{14}C and ^{67}Cu ^d	Guo et al., 2012
Field	4.6–5.1	GFAAS ^e	Sunda and Huntsman, 1995
	2.8–6.4	Nutricline $\Delta[\text{Cu}]_d:\Delta[\text{PO}_4^{3-}]^f$	Sunda and Huntsman, 1995
	0.98–23.6	Nutricline $\Delta[\text{Cu}]_d:\Delta[\text{PO}_4^{3-}]^f$	Annett et al., 2008
	1.35–4.21	^{14}C and ^{67}Cu ^g	Semeniuk et al., 2009
	4–70	SXRF ^h and Microscopy	Twining et al., 2015
	12–80	^{14}C and ^{67}Cu ^g	This study ^h

^aCells were filtered and rinsed with Gulf Stream seawater before undergoing acid-digestion. Particulate Cu and C concentrations were determined by graphite furnace atomic adsorption spectroscopy (GFAAS) and standard $\text{H}^{14}\text{CO}_3^-$ incubations, respectively.

^bCells were filtered and rinsed with experimental media. Particulate Cu and C concentrations were determined by graphite furnace atomic adsorption spectroscopy (GFAAS) and standard CHN analysis, respectively.

^cCells were filtered and rinsed with chelexed synthetic ocean water before undergoing acid-digestion. Cellular Cu and P were measured using a HR-ICP-MS, and Cu:C ratios were calculated assuming a particulate C:P ratio of 106.

^dCells were incubated with ^{67}Cu and $\text{H}^{14}\text{CO}_3^-$ under steady state conditions and continuous light for 24 h before harvested by filtration and washed with a 1 mM DTPA wash.

^eParticulate Cu and P reported by Martin et al. (1976) and Collier and Edmonds (1983) were converted to Cu:C using a particulate C:P ratio of 106.

^fCalculated from the linear slope of $[\text{PO}_4^{3-}]$ vs. $[\text{Cu}]_d$ in the nutricline, and assuming a particulate C:P ratio of 106.

^hCellular Cu concentrations were determined for single cells using Synchrotron X-Ray Fluorescence (SXRF), and cellular C was calculated from cell volume and carbon concentration conversion factors.

^gSurface water samples were incubated at in situ light and temperature with ^{67}Cu and $\text{H}^{14}\text{CO}_3^-$ for 24 h before harvested by filtration and washed with a 1 mM DTPA wash.

^hData for the 0.22–1 μm size fraction were omitted due to the presence of heterotrophic bacteria in this fraction.

In previous work, Fe uptake and Cu assimilation rates were positively correlated for large (>20 μm) phytoplankton along the Line P transect, indicating that Fe and Cu metabolisms may be linked in large cells (Semeniuk et al., 2009). Indeed, a recent incubation study at station P26 confirmed that large (>5 μm), Fe-limited phytoplankton increase Fe uptake using their high-affinity Fe transport systems when provided with 1 nM CuSO_4 (Semeniuk et al., 2016), suggesting that Fe limitation may increase Cu demand along Line P, an HNLC region.

The somewhat elevated Fe concentrations measured at P26, possibly caused by an Fe-input event (see Section Distribution of Total Dissolved Cu in Line P Surface Waters), provide an

opportunity to test whether natural Fe-enrichment can influence the Cu physiology of marine phytoplankton. Compared to P26 where the community was clearly Fe-limited, the Cu:C assimilation ratios and $\rho\text{Cu}_{\text{LT,C}}$ were consistently higher at P16 for both 1–5 μm and >5 μm size fractions. Furthermore, the differences between Cu:C assimilation ratios and $\rho\text{Cu}_{\text{LT,C}}$ measured at P16 and P26 were greater for the >5 μm (62–73%) than the 1–5 μm (0–47%) size fraction. These data indicate that there may be an interaction between Fe and Cu metabolism in indigenous phytoplankton communities, and that larger phytoplankton in HNLC regions may have a greater dependence on Cu availability.

Previous laboratory studies have hypothesized that Cu' concentrations determine Cu bioavailability to marine phytoplankton (Sunda and Guillard, 1976; Anderson and Morel, 1978; Sunda and Huntsman, 1995). Thus, we hypothesized that Cu:C assimilation ratios and Cu uptake rates might correlate with $[\text{Cu}]_d$ and/or $[\text{Cu}']$. There were no correlations between $\rho\text{Cu}_{\text{ST,C}}$, $\rho\text{Cu}_{\text{LT,C}}$, and Cu:C assimilation ratios with $[\text{Cu}']$ for the 1–5 μm or >5 μm size fractions across the transect, and so $[\text{Cu}']$ likely does not determine Cu uptake rates or cellular quotas in natural marine phytoplankton communities. Laboratory studies of isolated marine phytoplankton strains have demonstrated that organically complexed Cu is bioavailable (Hudson, 1998; Quigg et al., 2006; Annett et al., 2008; Guo et al., 2010; Walsh et al., 2015). *In situ* Cu ligand complexes were also bioavailable to marine phytoplankton surveyed at P26 in 2008 (Semeniuk et al., 2015). Despite this, Cu uptake rates or Cu:C assimilation ratios were not correlated with $[\text{Cu}]_d$. Since phytoplankton Cu quotas and steady-state Cu uptake rates can vary by an order of magnitude among taxa grown in identical Cu concentrations (Ho et al., 2003; Annett et al., 2008; Guo et al., 2012), phytoplankton species composition, Fe availability, or some other unknown factor, may primarily determine particulate biogenic Cu concentrations in surface waters.

Dissolved-Particulate Cu Cycling and Cu Residence Times

Similar to our previous studies of Cu uptake rates at P26 (Semeniuk et al., 2009, 2015), short-term Cu uptake rates were faster than long-term uptake rates for all size classes along the Line P transect. Our previous work at station P26 demonstrated that particulate Cu concentrations plateaued within 4–8 h of adding the ^{67}Cu tracer, and decreased up to 65% between 8 and 12 h later (Semeniuk et al., 2015). We hypothesized that cellular efflux or remineralization by micrograzers may account for this. Thus, Cu cycling between dissolved and particulate phases in surface waters may be rapid compared to the export of particulate Cu from surface waters.

Assuming that the relationship between total particulate NPP_V and $[\text{Cu}']$ is due to biological utilization across the transect, we can calculate the net Cu:C drawdown ratio in surface waters along Line P using this slope (1.56 $\mu\text{g C fmol Cu}^{-1} \text{d}^{-1}$; Figure 4), and a range of phytoplankton specific growth rates reported for this region (0.2–1 d^{-1} ; Booth, 1988). The calculated range, 1.5–7.7 $\mu\text{mol Cu mol C}^{-1}$, assumes that only Cu' is being

incorporated into or onto particles. Recent estimates suggest that between 0 and 90% of the Cu being acquired by indigenous marine phytoplankton is organically complexed (Semeniuk et al., 2015). If 50% of the dissolved Cu removed from surface waters was organically complexed, then the net Cu:C drawdown ratio would increase to 3–15 $\mu\text{mol Cu mol C}^{-1}$. Timothy et al. (2013) reports that 2–3 $\text{mmol C m}^{-2} \text{d}^{-1}$ is exported to 200 m depth at P26 during the late summer. This depth is below the permanent halocline at ~ 150 m along the transect, which limits the winter mixed layer depth (Gargett, 1991). Using a middle value for the net Cu:C drawdown ratio ($\sim 10 \mu\text{mol Cu mol C}^{-1}$), we estimate a Cu export to 200 m of 20–30 $\text{nmol Cu m}^{-2} \text{d}^{-1}$. Integrated over a 20 m summer mixed layer depth, this corresponds to an estimated net loss of Cu from the mixed layer of 1–1.5 $\text{pmol Cu L}^{-1} \text{d}^{-1}$. Given the total dissolved surface Cu concentrations across Line P varied by ~ 2 -fold (1.46–2.79 nM), we estimate the residence time for Cu in the mixed layer (mixed layer $[\text{Cu}]_{\text{diss}} \div$ estimated net loss) along Line P between 2.5 and 8 years. This is similar to other independent surface layer residence time estimates in the tropical Atlantic Ocean (3–12 years; Helmers and Schrems, 1995) and the North Pacific Ocean (~ 9 years; Takano et al., 2014). The surface residence time is much longer than other bioactive metals, such as Fe (6–150 days; Bergquist and Boyle, 2006; Ellwood et al., 2014), or Co (~ 100 days; Saito and Moffett, 2002), and reflects the higher total dissolved Cu concentrations in surface waters (0.2–3 nM) compared to other bioactive metals (0.01–0.2 nM).

The total particulate uptake rates measured using ^{67}Cu (33–125 $\text{pmol Cu L}^{-1} \text{d}^{-1}$) are 22–125 times faster than our estimates of Cu export (1–1.5 $\text{pmol Cu L}^{-1} \text{d}^{-1}$). Assuming that the source and loss terms in the surface mixed layer are at steady state, this indicates that a Cu atom in the surface ocean would exchange between dissolved and particulate phases 22–125 times before being exported. Copper enters phytoplankton through either a high- or low-affinity Cu transport system

(Guo et al., 2010, 2015). The HACuTS can be down- or up-regulated, while the low-affinity transport system (LACuTS) seems to be constitutively expressed (Guo et al., 2010). The LACuTS is likely a non-specific divalent metal transporter (e.g., NRAMPs, ZIP) (Sunda and Huntsman, 1983; Guo et al., 2015). Thus, if intracellular Cu increases above the cell's metabolic demand due to non-specific uptake, it will have to be effluxed or detoxified intracellularly. Copper efflux is a common mechanism in bacteria to prevent intracellular metal toxicity (Silver, 1996), and ATP-powered heavy metal resistance pumps have been identified in numerous α -, β -, and γ -proteobacteria (Ridge et al., 2008). Copper efflux has also been documented in marine prokaryotic and eukaryotic phytoplankton (Foster, 1977; Hall et al., 1979; Croot et al., 2003; Quigg et al., 2006; Semeniuk et al., 2015; Walsh et al., 2015), suggesting that Cu efflux might be a common physiological mechanism of Cu homeostasis in marine microorganisms. In addition, micrograzing and bacterial remineralization might mediate fast exchange of Cu between the dissolved and the particulate pools, as recently shown for Ni and Zn (Twining et al., 2014). Therefore, fast biological Cu uptake and efflux, as well as efficient micrograzing and bacterial remineralization of Cu in surface waters might have significant impacts on the cycling of Cu in the sea.

AUTHOR CONTRIBUTIONS

The experimental design was carried out by DS and MM. Sample collection and analysis were performed by DS, AP, RB, and MR. All authors contributed to data interpretation, and the manuscript was primarily written by DS.

FUNDING

DS, AP, and MM were funded by a Natural Sciences and Engineering Council of Canada Discovery grant.

REFERENCES

- Anderson, D. M., and Morel, F. M. M. (1978). Copper sensitivity of *Gonyaulax tamarensis*. *Limnol. Oceanogr.* 23, 283–295. doi: 10.4319/lo.1978.23.2.0283
- Annett, A. L., Lapi, S., Ruth, T. J., and Maldonado, M. T. (2008). The effects of Cu and Fe availability on the growth and Cu:C ratios of marine diatoms. *Limnol. Oceanogr.* 53, 2451–2461. doi: 10.4319/lo.2008.53.6.2451
- Barwell-Clarke, J., and Whitney, F. A. (1996). *Institute of Ocean Sciences Nutrient Methods and Analysis*, Vol. 182. Canadian Technical Report of Hydrography and Ocean Sciences, Institute of Ocean Sciences.
- Bergquist, B. A., and Boyle, E. A. (2006). Dissolved iron in the tropical and subtropical Atlantic Ocean. *Glob. Biogeochem. Cycle* 20, GB1015. doi: 10.1029/2005GB002505
- Bishop, J. K. B., Davis, R. E., and Sherman, J. T. (2002). Robotic observations of dust storm enhancement of carbon biomass in the North Pacific. *Science* 298, 817–821. doi: 10.1126/science.1074961
- Biswas, H., Bandyopadhyay, D., and Waite, A. (2013). Copper addition helps alleviate iron stress in a coastal diatom: response of *Chaetoceros gracilis* from the Bay of Bengal to experimental Cu and Fe addition. *Mar. Chem.* 157, 224–232. doi: 10.1016/j.marchem.2013.10.006
- Booth, B. C. (1988). Size classes and major taxonomic groups of phytoplankton at two locations in the subarctic Pacific Ocean in May and August, 1984. *Mar. Bio.* 97, 275–286. doi: 10.1007/BF00391313
- Booth, B. C., Lewin, J., and Postel, J. R. (1993). Temporal variation in the structure of autotrophic and heterotrophic communities in the subarctic Pacific. *Prog. Oceanogr.* 32, 57–99. doi: 10.1016/0079-6611(93)90009-3
- Boyd, P. W., and Harrison, P. J. (1999). Phytoplankton dynamics in the NE subarctic Pacific. *Deep Sea. Res. II* 46, 2405–2432. doi: 10.1016/S0967-0645(99)00069-7
- Boyd, P. W., Jickells, T., Law, C. S., Blain, S., Boyle, E. A., Buesseler, K. O., et al. (2007). Mesoscale iron enrichment experiments 1993–2005: synthesis and future directions. *Science* 315, 612–617. doi: 10.1126/science.1131669
- Boyle, E. A., Sclater, F. R., and Edmond, J. M. (1977). The distribution of dissolved copper in the Pacific. *Earth Planet. Sci. Lett.* 37, 38–54. doi: 10.1016/0012-821X(77)90144-3
- Brand, L. E., Sunda, W. G., and Guillard, R. R. L. (1986). Reduction of marine phytoplankton reproduction rates by copper and cadmium. *J. Exp. Mar. Biol. Ecol.* 96, 225–250. doi: 10.1016/0022-0981(86)90205-4
- Bruland, K. W., Rue, E. L., Donat, J. R., Skrabal, S. A., and Moffett, J. W. (2000). Intercomparison of voltammetric techniques to determine the chemical speciation of dissolved copper in a coastal seawater sample. *Anal. Chim. Acta* 405, 99–113. doi: 10.1016/S0003-2670(99)00675-3
- Buck, K. N., Moffet, J., Barbeau, K. A., Bundy, R. M., Kondo, Y., and Wu, J. (2012). The organic complexation of iron and copper: an intercomparison of competitive ligand exchange–adsorptive cathodic stripping voltammetry (CLE-ACSV) techniques. *Limnol. Oceanogr. Methods* 10, 496–515. doi: 10.4319/lom.2012.10.496

- Buck, K. N., Selph, K. E., and Barbeau, K. A. (2010). Iron-binding ligand production and copper speciation in an incubation experiment of Antarctic Peninsula shelf waters from the Bransfield Strait, Southern Ocean. *Mar. Chem.* 122, 148–159. doi: 10.1016/j.marchem.2010.06.002
- Bundy, R. M., Barbeau, K. A., and Buck, K. N. (2013). Sources of strong copper-binding ligands in Antarctic Peninsula surface waters. *Deep Sea Res. II* 90, 134–146. doi: 10.1016/j.dsr2.2012.07.023
- Chadd, H. E., Newman, J., Mann, N. H., and Carr, N. G. (1996). Identification of iron superoxide dismutase and a copper/zinc superoxide dismutase enzyme activity within the marine cyanobacterium *Synechococcus* sp. WH (7803). *FEMS Microbiol. Lett.* 138, 161–165. doi: 10.1111/j.1574-6968.1996.tb08150.x
- Chang, S. L., and Reinfelder, J. R. (2000). Bioaccumulation, subcellular distribution, and trophic transfer of copper in a coastal marine diatom. *Environ. Sci. Technol.* 34, 4931–4935. doi: 10.1021/es001213r
- Coale, K. H. (1991). Effects of iron, manganese, copper, and zinc enrichments on productivity and biomass in the Subarctic Pacific. *Limnol. Oceanogr.* 36, 1851–1864. doi: 10.4319/lo.1991.36.8.1851
- Coale, K. H., and Bruland, K. W. (1988). Copper complexation in the Northeast Pacific. *Limnol. Oceanogr.* 33, 1084–1101. doi: 10.4319/lo.1988.33.5.1084
- Collier, R. W., and Edmonds, J. M. (1983). “Plankton compositions and trace element fluxes from the surface ocean,” in *Trace Metals in Sea Water*, eds C. S. Wong, E. Boyle, K. W. Bruland, J. D. Burton, and E. D. Goldberg (New York, NY: Springer), 789–809.
- Cox, A. D., Noble, A. E., and Saito, M. A. (2014). Cadmium enriched stable isotope uptake and addition experiments with natural phytoplankton assemblages in the Costa Rica Upwelling Dome. *Mar. Chem.* 166, 70–81. doi: 10.1016/j.marchem.2014.09.009
- Croot, P. L., Karlson, B., van Elteren, J. T., and Kroon, J. J. (2003). Uptake and efflux of ⁶⁴Cu by the marine cyanobacterium *Synechococcus* (WH7803). *Limnol. Oceanogr.* 48, 179–188. doi: 10.4319/lo.2003.48.1.0179
- Croot, P. L., Moffet, J. W., and Brand, L. E. (2000). Production of extracellular Cu complexing ligands by eucaryotic phytoplankton in response to Cu stress. *Limnol. Oceanogr.* 45, 619–627. doi: 10.4319/lo.2000.45.3.0619
- Croot, P. L., Moffett, J. W., and Luther, G. W. (1999). Polarographic determination of half-wave potentials for copper-organic complexes in seawater. *Mar. Chem.* 67, 219–232. doi: 10.1016/S0304-4203(99)00054-7
- Cutter, G., Andersson, P., Codispoti, L., Croot, P., Francois, R., Lohan, M., et al. (2010). *Sampling and Sample-Handling Protocols for GEOTRACES Cruises*.
- Dupont, C. L., Buck, K. N., Palenik, B., and Barbeau, K. (2010). Nickel utilization in phytoplankton assemblages from contrasting oceanic regimes. *Deep Sea Res. I* 57, 553–566. doi: 10.1016/j.dsr.2009.12.014
- Ellwood, M. J., Nodder, S. D., King, A., Hutchins, D. A., Wilhelm, S. W., and Boyd, P. W. (2014). Pelagic iron cycling during the subtropical spring bloom, east of New Zealand. *Mar. Chem.* 160, 18–33. doi: 10.1016/j.marchem.2014.01.004
- Foreman, M. G. G., Pal, B., and Merryfield, W. J. (2011). Trends in upwelling and downwelling winds along the British Columbia shelf. *J. Geophys. Res.* 116, C10023. doi: 10.1029/2011JC006995
- Foster, P. L. (1977). Copper exclusion as a mechanism of heavy metal tolerance in a green alga. *Nature* 269, 322–323. doi: 10.1038/269322a0
- Gargett, A. E. (1991). Physical processes and the maintenance of nutrient-rich euphotic zones. *Limnol. Oceanogr.* 36, 1527–1545. doi: 10.4319/lo.1991.36.8.1527
- Gordon, A. S., Donat, J. R., Kango, R. A., Dyer, B. J., and Stuart, L. M. (2000). Dissolved copper-complexing ligands in cultures of marine bacteria and estuarine water. *Mar. Chem.* 70, 149–160. doi: 10.1016/S0304-4203(00)00019-0
- Guo, J., Annett, A. L., Taylor, R. L., Lapi, S., Ruth, T. J., and Maldonado, M. T. (2010). Copper uptake kinetics of coastal and oceanic diatoms. *J. Phycol.* 46, 1218–1228. doi: 10.1111/j.1529-8817.2010.00911.x
- Guo, J., Green, B. R., and Maldonado, M. T. (2015). Sequence analysis and gene expression of potential components of copper transport and homeostasis in *Thalassiosira pseudonana*. *Protist* 166, 58–77. doi: 10.1016/j.protis.2014.11.006
- Guo, J., Lapi, S., Ruth, T. J., and Maldonado, M. T. (2012). The effects of iron and copper availability on the copper stoichiometry of marine phytoplankton. *J. Phycol.* 48, 312–325. doi: 10.1111/j.1529-8817.2012.01133.x
- Hall, A., Fielding, A. H., and Butler, M. (1979). Mechanisms of copper tolerance in the marine fouling alga *Ectocarpus siliculosus* – evidence for an exclusion mechanism. *Mar. Biol.* 54, 195–199. doi: 10.1007/BF00395780
- Halsey, K. J., Milligan, A. J., and Behrenfeld, M. J. (2011). Linking time-dependent carbon-fixation efficiencies in *Dunaliella tertiolecta* (chlorophyceae) to underlying metabolic pathways. *J. Phycol.* 47, 66–76. doi: 10.1111/j.1529-8817.2010.00945.x
- Hamme, R. C., Webley, P. W., Crawford, W. R., Whitney, F. A., DeGrandpre, M. D., Emerson, S. R., et al. (2010). Volcanic ash fuels anomalous plankton bloom in subarctic northeast Pacific. *Geophys. Res. Lett.* 37, L19604. doi: 10.1029/2010GL044629
- Heller, M. I., and Croot, P. L. (2015). Copper speciation and distribution in the Atlantic sector of the Southern Ocean. *Mar. Chem.* 173, 253–268. doi: 10.1016/j.marchem.2014.09.017
- Helmers, E., and Schrems, O. (1995). Wet deposition of metals to the tropical north and south Atlantic Ocean. *Atmos. Environ.* 29, 2475–2484. doi: 10.1016/1352-2310(95)00159-V
- Hering, J. G., and Morel, F. M. M. (1988). Kinetics of trace metal complexation: role of alkaline-earth metals. *Environ. Sci. Technol.* 22, 1469–1478. doi: 10.1021/es00177a014
- Ho, T. Y., Quigg, A., Finkel, Z. V., Milligan, A. J., Wyman, K., Falkowski, P. G., et al. (2003). The elemental composition of some marine phytoplankton. *J. Phycol.* 39, 1145–1159. doi: 10.1111/j.0022-3646.2003.03-090.x
- Hudson, R. J. M. (1998). Which aqueous species control the rates of trace metal uptake by aquatic biota? Observations and predictions of non-equilibrium effects. *Sci. Total Environ.* 219, 95–115. doi: 10.1016/S0048-9697(98)00230-7
- Hudson, R. J., Covault, D. T., and Morel, F. M. M. (1992). Investigations of iron coordination and redox reactions in seawater using ⁵⁹Fe radiometry and ion-pair solvent extraction of amphiphilic iron complexes. *Mar. Chem.* 38, 209–235. doi: 10.1016/0304-4203(92)90035-9
- Jacquot, J. E., and Moffett, J. W. (2015). Copper distribution and speciation across the international GEOTRACES Section GA03. *Mar. Chem.* 116, 187–207. doi: 10.1016/j.dsr.2.2014.11.013
- Jacquot, J. E., Kondo, Y., Knapp, A. N., and Moffett, J. W. (2013). The speciation of copper across active gradients in nitrogen-cycle processes in the eastern tropical South Pacific. *Limnol. Oceanogr.* 58, 1387–1394. doi: 10.4319/lo.2013.58.4.1387
- Johnson, W. K., Miller, L. A., Sutherland, N. E., and Wong, C. S. (2005). Iron transport by mesoscale Haida eddies in the Gulf of Alaska. *Deep Sea Res. II* 52, 933–953. doi: 10.1016/j.dsr.2.2004.08.017
- Jones, C. J., and Murray, J. W. (1984). Nickel, cadmium, and copper in the northeast Pacific off the coast of Washington. *Limnol. Oceanogr.* 29, 711–720. doi: 10.4319/lo.1984.29.4.0711
- Jordi, A., Basterretxea, G., Tovar-Sanchez, A., Alastuey, A., and Querol, X. (2012). Copper aerosols inhibit phytoplankton growth in the Mediterranean Sea. *Proc. Nat. Acad. Sci. U.S.A.* 109, 21246–21249. doi: 10.1073/pnas.1207567110
- Kustka, A. B., Allen, A. E., and Morel, F. M. M. (2007). Sequence analysis and transcriptional regulation of iron acquisition genes in two marine diatoms. *J. Phycol.* 43, 715–729. doi: 10.1111/j.1529-8817.2007.00359.x
- Kustka, A. B., Jones, B. M., Hatta, M., Field, M. P., and Milligan, A. J. (2015). The influence of iron and siderophores on eukaryotic phytoplankton growth rates and community composition in the Ross Sea. *Mar. Chem.* 173, 195–207. doi: 10.1016/j.marchem.2014.12.002
- Lam, P. J., Bishop, J. K. B., Henning, C. C., Marcus, M. A., Waychunas, G. A., and Fung, I. Y. (2006). Wintertime phytoplankton bloom in the subarctic Pacific supported by continental margin iron. *Global Biogeochem. Cycle* 20, Gb1006. doi: 10.1029/2005GB002557
- Lam, P. J., Twining, B. S., Jeandel, C., Roychoudhury, A., Resing, J. A., Santschi, P. H., et al. (2015). Methods for analyzing the concentration and speciation of major and trace elements in marine particles. *Progr. Oceanogr.* 133, 32–42. doi: 10.1016/j.pocean.2015.01.005
- Lee, S., and Fuhrman, J. A. (1987). Relationships between biovolume and biomass of naturally derived marine bacterioplankton. *App. Environ. Microb.* 53, 1298–1303.
- Levy, J. L., Stauber, J. L., and Jolley, D. F. (2007). Sensitivity of marine microalgae to copper: the effect of biotic factors on copper adsorption and toxicity. *Sci. Total Environ.* 387, 141–154. doi: 10.1016/j.scitotenv.2007.07.016
- Löscher, B. M. (1999). Relationships among Ni, Cu, Zn, and major nutrients in the Southern Ocean. *Mar. Chem.* 67, 67–102. doi: 10.1016/S0304-4203(99)00050-X
- Louis, Y., Garnier, C., Lenoble, V., Omanović, D., Mounier, S., and Pižeta, I. (2009). Characterisation and modelling of marine dissolved organic matter

- interactions with major and trace cations. *Mar. Environ. Res.* 67, 100–107. doi: 10.1016/j.marenvres.2008.12.002
- MacIntyre, H. L., Kana, T. M., Anning, T., and Geider, R. J. (2002). Photoacclimation of photosynthesis irradiance response curves and photosynthetic pigments to microalgae and cyanobacteria. *J. Phycol.* 38, 17–38. doi: 10.1046/j.1529-8817.2002.00094.x
- Maldonado, M. T., Allen, A. E., Chong, J. S., Lin, K., Leus, D., Karpenko, N., et al. (2006). Copper-dependent iron transport in coastal and oceanic diatoms. *Limnol. Oceanogr.* 51, 1729–1743. doi: 10.4319/lo.2006.51.4.1729
- Maldonado, M. T., and Price, N. M. (1999). Utilization of iron bound to strong organic ligands by plankton communities in the subarctic Pacific Ocean. *Deep Sea Res. II* 46, 2447–2473. doi: 10.1016/S0967-0645(99)00071-5
- Mann, E. L., Ahlgren, N., Moffett, J. W., and Chrisolm, S. W. (2002). Copper toxicity and cyanobacterial ecology in the Sargasso Sea. *Limnol. Oceanogr.* 47, 976–988. doi: 10.4319/lo.2002.47.4.0976
- Martin, J. H., Bruland, K. W., and Broenkow, W. W. (1976). “Cadmium transport in the California Current,” in *Marine Pollutant Transfer*, eds H. J. Windom and R. A. Duce (Toronto, ON: Lexington Books, D. C. Health and Co.), 159–184.
- Martin, J. H., Gordon, R. M., Fitzwater, S., and Broenkow, W. W. (1989). Vertex: phytoplankton/iron studies in the Gulf of Alaska. *Deep Sea Res.* 36, 649–680. doi: 10.1016/0198-0149(89)90144-1
- McAlister, J. (2015). *Biogeochemistry of Dissolved Gallium and Lead Isotopes in the Northeast Pacific and Western Arctic Oceans*. Doctoral dissertation. Available online at: <https://circle.ubc.ca>
- Moffett, J. W., and Brand, L. E. (1996). Production of strong, extracellular Cu chelators by marine cyanobacteria in response to Cu stress. *Limnol. Oceanogr.* 41, 388–395. doi: 10.4319/lo.1996.41.3.0388
- Moffett, J. W., and Dupont, C. (2007). Cu complexation by organic ligands in the sub-arctic NW Pacific and Bering Sea. *Deep Sea Res. I* 54, 586–595. doi: 10.1016/j.dsr.2006.12.013
- Moffett, J. W., Brand, L. E., Croot, P. L., and Barbeau, K. A. (1997). Cu speciation and cyanobacterial distribution in harbors subject to anthropogenic Cu inputs. *Limnol. Oceanogr.* 42, 789–799. doi: 10.4319/lo.1997.42.5.0789
- Moore, J. K., Doney, S. C., and Lindsay, K. (2004). Upper ocean ecosystem dynamics and iron cycling in a global three-dimensional model. *Global Biogeochem. Cycle* 18, GB4028. doi: 10.1029/2004GB002220
- Morel, F. M. M., Hudson, R. J. M., and Price, N. M. (1991). Limitation of productivity by trace metals in the sea. *Limnol. Oceanogr.* 36, 1742–1755. doi: 10.4319/lo.1991.36.8.1742
- Palenik, B., and Morel, F. M. M. (1991). Amine oxidases of marine phytoplankton. *Appl. Environ. Microbiol.* 57, 2440–2443.
- Peers, G., and Price, N. M. (2006). Copper-containing plastocyanin used for electron transport by an oceanic diatom. *Nature* 441, 341–344. doi: 10.1038/nature04630
- Peers, G., Quesnel, S. A., and Price, N. M. (2005). Copper requirements for iron acquisition and growth of coastal and oceanic diatoms. *Limnol. Oceanogr.* 50, 1149–1158. doi: 10.4319/lo.2005.50.4.1149
- Peña, M. A., and Varela, D. E. (2007). Seasonal and interannual variability in phytoplankton and nutrient dynamics along Line P in the NE subarctic Pacific. *Prog. Oceanogr.* 75, 200–222. doi: 10.1016/j.pocean.2007.08.009
- Quigg, A., Reinfelder, J. R., and Fisher, N. S. (2006). Copper uptake kinetics in diverse marine phytoplankton. *Limnol. Oceanogr.* 51, 893–899. doi: 10.4319/lo.2006.51.2.0893
- Ridge, P. G., Zhang, Y., and Gladyshev, V. N. (2008). Comparative genomic analyses of copper transporters and cuproproteomes reveal evolutionary dynamics of copper utilization and its link to oxygen. *PLoS ONE* 3:e1378. doi: 10.1371/journal.pone.0001378
- Saito, M. A., and Moffett, J. W. (2002). Temporal and spatial variability of cobalt in the Atlantic Ocean. *Geochim. Cosmochim. Acta* 66, 1943–1953. doi: 10.1016/S0016-7037(02)00829-3
- Semeniuk, D. M., Bundy, R. M., Payne, C. D., Barbeau, K. A., and Maldonado, M. T. (2015). Acquisition of organically complexed copper by marine phytoplankton and bacteria in the northeast subarctic Pacific Ocean. *Mar. Chem.* 173, 222–233. doi: 10.1016/j.marchem.2015.01.005
- Semeniuk, D. M., Cullen, J. T., Johnson, W. K., Gagnon, K., Ruth, T. J., and Maldonado, M. T. (2009). Plankton copper requirements and uptake in the subarctic Northeast Pacific Ocean. *Deep Sea Res. I* 56, 1130–1142. doi: 10.1016/j.dsr.2009.03.003
- Semeniuk, D. M., Taylor, R. L., Bundy, R. M., Johnson, W. K., Cullen, J. T., Robert, M., et al. (2016). Iron–copper interactions in iron-limited phytoplankton in the northeast subarctic Pacific Ocean. *Limnol. Oceanogr.* 61, 279–297. doi: 10.1002/lno.10210
- Shank, G. C., Skrabal, S. A., Whitehead, R. F., and Kieber, R. J. (2004). Fluxes of strong Cu-complexing ligands from sediments of an organic-rich estuary. *Est. Coast. Sci.* 60, 349–358. doi: 10.1016/j.ecss.2004.01.010
- Sherry, N. D., Boyd, P. W., Sugimoto, K., and Harrison, P. J. (1999). Seasonal and spatial patterns of heterotrophic bacterial production, respiration, and biomass in the subarctic NE Pacific. *Deep Sea Res. II* 46, 2557–2578. doi: 10.1016/S0967-0645(99)00076-4
- Silver, S. (1996). Bacterial resistances to toxic metal ions - a review. *Gene* 179, 9–19. doi: 10.1016/S0378-1119(96)00323-X
- Skrabal, S. A., Donat, J. R., and Burdige, D. J. (2000). Pore water distributions of dissolved copper and copper-complexing ligands in estuarine and coastal marine sediments. *Geochim. Cosmochim. Acta* 64, 1843–1857. doi: 10.1016/S0016-7037(99)00387-7
- Steiner, N. S., Robert, M., Arychuk, M., Levasseur, M. L., Merzouk, A., Peña, M. A., et al. (2012). Evaluating DMS measurements and model results in the Northeast subarctic Pacific from 1996–(2010). *Biogeochemistry* 110, 269–285. doi: 10.1007/s10533-011-9669-9
- Sunda, W. G. (2012). Feedback interactions between trace metal nutrients and phytoplankton in the ocean. *Front. Microbiol.* 3:204. doi: 10.3389/fmicb.2012.00204
- Sunda, W. G., and Guillard, R. R. L. (1976). Relationship between cupric ion activity and toxicity of copper to phytoplankton. *Mar. Res.* 34, 511–529.
- Sunda, W. G., and Huntsman, S. A. (1983). Effect of competitive interactions between manganese and copper on cellular manganese and growth in estuarine and oceanic species of the diatom *Thalassiosira*. *Limnol. Oceanogr.* 28, 924–934. doi: 10.4319/lo.1983.28.5.0924
- Sunda, W. G., and Huntsman, S. A. (1995). Regulation of copper concentration in the oceanic nutricline by phytoplankton uptake and regeneration cycles. *Limnol. Oceanogr.* 40, 132–137. doi: 10.4319/lo.1995.40.1.0132
- Takano, S., Tanimizu, M., Hirata, T., and Sohrin, Y. (2014). Isotopic constraints on biogeochemical cycling of copper in the ocean. *Nat. Commun.* 5:5663. doi: 10.1038/ncomms6663
- Taylor, R. L., Semeniuk, D. M., Payne, C. D., Zhou, J., Tremblay, J.-É., Cullen, J. T., et al. (2013). Colimitation by light, nitrate, and iron in the Beaufort Sea in late summer. *J. Geophys. Res. Oceans* 118, 1–17. doi: 10.1002/jgrc.20244
- Thompson, C. M., Ellwood, M. J., and Sander, S. G. (2014). Dissolved copper speciation in the Tasman Sea, SW Pacific Ocean. *Mar. Chem.* 164, 84–94. doi: 10.1016/j.marchem.2014.06.003
- Thomson, R. E. (1981). Oceanography of the British Columbia coast. *Can. Spec. Publ. Fish. Aquat. Sci.* 56, 291.
- Timothy, D. A., Wong, C. S., Barwell-Clarke, J. E., Page, J. S., White, L. A., and Macdonald, R. W. (2013). Climatology of sediment flux and composition in the subarctic Northeast Pacific Ocean with biogeochemical implications. *Prog. Oceanogr.* 116, 95–129. doi: 10.1016/j.pocean.2013.06.017
- Turner, D. R., Whitfield, M., and Dickson, A. G. (1981). The equilibrium speciation of dissolved components in freshwater and seawater at 25°C and 1 atm pressure. *Geochim. Cosmochim. Acta* 45, 855–881. doi: 10.1016/0016-7037(81)90115-0
- Twining, B. S., Baines, S. B., Fisher, N. S., Maser, J., Vogt, S., Jacobsen, C., et al. (2003). Quantifying trace elements in individual aquatic protist cells with a synchrotron X-ray fluorescence microprobe. *Anal. Chem.* 75, 3806–3816. doi: 10.1021/ac034227z
- Twining, B. S., Nodder, S. D., King, A. L., Hutchins, D. A., LeClerc, G. R., DeBruyn, J. M., et al. (2014). Differential remineralization of major and trace elements in sinking diatoms. *Limnol. Oceanogr.* 59, 689–704. doi: 10.4319/lo.2014.59.3.0689
- Twining, B. S., Rauschenberg, S., Morton, P. L., and Vogt, S. (2015). Metal contents of phytoplankton and labile particulate material in the North Atlantic Ocean. *Prog. Oceanogr.* 137, 261–283. doi: 10.1016/j.pocean.2015.07.001
- van den Berg, D. M. G. (1984). Determination of the complexing capacity and conditional stability constants of complexed of copper(II) with natural organic ligands in seawater by cathodic stripping voltammetry of copper-catechol complex ons. *Mar. Chem.* 15, 1–18. doi: 10.1016/0304-4203(84)90035-5

- Walsh, M. J., Goodnow, S. D., Vezeau, G. E., Richter, L. V., and Ahner, B. A. (2015). Cysteine enhances bioavailability of copper to marine phytoplankton. *Environ. Sci. Technol.* 49, 12145–12152. doi: 10.1021/acs.est.5b02112
- Wells, M. L., Trick, C. G., Cochlan, W. P., Hughes, M. P., and Trainer, V. L. (2005). Domoic acid: the synergy of iron, copper, and the toxicity of diatoms. *Limnol. Oceanogr.* 50, 1908–1917. doi: 10.4319/lo.2005.50.6.1908
- Whitby, H., and van den Berg, C. M. G. (2015). Evidence for copper-binding humic substances in seawater. *Mar. Chem.* 173, 282–290. doi: 10.1016/j.marchem.2014.09.011
- Whitney, F. A., and Freeland, H. J. (1999). Variability in upper-ocean water properties in the NE Pacific Ocean. *Deep Sea Res. II* 46, 2351–2370. doi: 10.1016/S0967-0645(99)00067-3
- Wiramanaden, C. I. E., Cullen, J. T., Ross, A. R. S., and Orians, K. J. (2008). Cyanobacterial copper-binding ligands isolated from artificial seawater cultures. *Mar. Chem.* 110, 28–41. doi: 10.1016/j.marchem.2008.02.003
- Witter, A. E., Hutchins, D. A., Butler, A., and Luther, G. W. (2000). Determination of conditional stability constants and kinetic constants for strong model Fe-binding ligands in seawater. *Mar. Chem.* 69, 1–17. doi: 10.1016/S0304-4203(99)00087-0
- Zamzow, H., Coale, K. H., Johnson, K. S., and Sakamoto, C. M. (1998). Determination of copper complexation in seawater using flow injection analysis with chemiluminescence detection. *Anal. Chim. Acta* 377, 133–144. doi: 10.1016/S0003-2670(98)00618-7

Conflict of Interest Statement: The authors declare that the research was conducted in the absence of any commercial or financial relationships that could be construed as a potential conflict of interest.

Copyright © 2016 Semeniuk, Bundy, Posacka, Robert, Barbeau and Maldonado. This is an open-access article distributed under the terms of the Creative Commons Attribution License (CC BY). The use, distribution or reproduction in other forums is permitted, provided the original author(s) or licensor are credited and that the original publication in this journal is cited, in accordance with accepted academic practice. No use, distribution or reproduction is permitted which does not comply with these terms.



Chemical Speciation of Copper in a Salt Marsh Estuary and Bioavailability to Thaumarchaeota

Hannah Whitby^{1*}, James T. Hollibaugh² and Constant M. G. van den Berg³

¹ Laboratoire des Sciences de l'Environnement Marin (LEMAR), Technopole Brest Iroise, Plouzané, France, ² Department of Marine Sciences, University of Georgia, Athens, Georgia, ³ Department of Earth, Ocean and Ecological Sciences, University of Liverpool, Liverpool, United Kingdom

OPEN ACCESS

Edited by:

Kristen Nicolle Buck,
University of South Florida, United States

Reviewed by:

Jochen Nuester,
Bigelow Laboratory for Ocean Sciences, United States
Mar Nieto-Cid,
Consejo Superior de Investigaciones Científicas (CSIC), Spain
Katherine Barbeau,
University of California, San Diego, United States

*Correspondence:

Hannah Whitby
hannah.whitby@live.co.uk

Specialty section:

This article was submitted to Marine Biogeochemistry, a section of the journal *Frontiers in Marine Science*

Received: 30 January 2017

Accepted: 22 May 2017

Published: 13 June 2017

Citation:

Whitby H, Hollibaugh JT and van den Berg CMG (2017) Chemical Speciation of Copper in a Salt Marsh Estuary and Bioavailability to Thaumarchaeota. *Front. Mar. Sci.* 4:178. doi: 10.3389/fmars.2017.00178

The concentrations of dissolved copper (Cu_d), copper-binding ligands, thiourea-type thiols, and humic substances (HS_{Cu}) were measured in estuarine waters adjacent to Sapelo Island, Georgia, USA, on a monthly basis from April to December 2014. Here we present the seasonal cycle of copper speciation within the estuary and compare it to the development of an annually occurring bloom of Ammonia Oxidizing Archaea (AOA), which require copper for many enzymes. Two types of complexing ligands (L_1 and L_2) were found to dominate with mean complex stabilities ($\log K'_{\text{CuL}}$) of 14.5 and 12.8. Strong complexation resulted in lowering the concentration of free cupric ion (Cu^{2+}) to femtomolar (fM) levels throughout the study and to sub-fM levels during the summer months. A Thaumarchaeota bloom during this period suggests that this organism manages to grow at very low Cu^{2+} concentrations. Correlation of the concentration of the L_1 ligand class with a thiourea-type thiol and the L_2 ligand class with HS_{Cu} provide an interesting dimension to the identity of the ligand classes. Due to the stronger complex stability, 82–99% of the copper was bound to L_1 . Thiourea-type thiols typically form Cu(I) species, which would suggest that up to ~90% copper could be present as Cu(I) in this region. In view of the very low concentration of free copper ($\text{pCu} > 15$ at the onset and during the bloom) and a reputedly high requirement for copper, it is likely that the Thaumarchaeota are able to access thiol-bound copper directly.

Keywords: copper speciation, cathodic stripping voltammetry, humic substances, thiols, thiourea, organic ligands, thaumarchaeota, ammonia-oxidizing archaea

INTRODUCTION

Free Cu^{2+} is well-known for its toxicity to marine microorganisms (Anderson and Morel, 1978; Sunda and Guillard, 1976). The toxicity threshold varies between species with pM concentrations found to affect cyanobacteria (Brand et al., 1986), well below typical ambient concentrations of dissolved Cu. The speciation of dissolved copper in seawater is usually dominated by organic ligands (Moffett and Dupont, 2007), forming relatively stable complexes with around 99% of the dissolved Cu. The oxidation state of organic copper is generally implied to be Cu(II) at natural pH (Leal and van den Berg, 1998) as inorganic copper(I) is unstable in seawater in spite of stabilization by chloride complexation (Nelson and Mantoura, 1984) and is oxidized to copper(II) in a matter of minutes by dissolved oxygen (Sharma and Millero, 1988). Nevertheless around 10% of the dissolved copper in ocean surface waters has been shown to be Cu(I) (Moffett and Zika, 1988) and potentially up to 80% Cu(I) in estuarine waters (Buerge-Weirich and Sulzberger, 2004). Concentrations of copper

complexing organic ligands in seawater and their complex stability constants ($\log K'_{\text{Cu}^{2+L}}$ value, based on Cu^{2+} and L' and abbreviated here to $\log K'_{\text{CuL}}$) are typically measured by titrations with copper, using cathodic stripping voltammetry (CSV) and competitive ligand equilibration (CLE-CSV; van den Berg, 1984; Donat et al., 1994). Ocean and coastal waters contain ligands with a large range of complex stabilities, that have for now been subdivided into at least two distinct ligand classes (L_1 and L_2), with $\log K'_{\text{CuL1}} = 13\text{--}16$ and $\log K'_{\text{CuL2}} = 10\text{--}13$ (Moffett et al., 1990; Laglera and van den Berg, 2003; Buck and Bruland, 2005; Bundy et al., 2013; Muller and Batchelli, 2013).

Complexed copper is considered less bioavailable and thus less toxic than free Cu^{2+} (Donat et al., 1994; Moffett et al., 2012; Oldham et al., 2014). Several marine microorganisms have been shown to release copper-binding ligands, such as thiols or phytochelatins, in response to copper (Rijstenbil et al., 1998; Leal et al., 1999; Gordon et al., 2000; Dupont and Ahner, 2005), and are therefore a source of thiols in the water. Thiols are organo-sulfur compounds containing the—SH functional group important for metal detoxification in cell metabolism, forming part of a variety of biogenic sulfur species in the marine environment (Radford-Knoery and Cutter, 1994; Tang et al., 2000). Typical thiols include glutathione (GSH), cysteine and their dimers (e.g., oxidized glutathione, GSSG), as well as larger GSH-cysteine chains (phytochelatins) and mercapto compounds. Reduced sulfur substances (RSS) describe a wider group, which also contains dimethyl sulfide (DMS), thioureas, and thioamides (Laglera and Tovar-Sanchez, 2012). Although, thioureas and thioamides may not technically be considered thiols due to favoring the thione form, we will include them in the discussion of thiols within this paper. Thiols have been shown to occur in estuarine (Dryden et al., 2007), coastal (Tang et al., 2000), and open ocean waters (Le Gall and van den Berg, 1998; Dupont et al., 2006; Swarr et al., 2016), suggesting that they could play a major role in the ocean biogeochemistry of copper. As well as cell exudates, sources of thiols include pore waters (Zhang et al., 2004) and sewage effluents (Dryden et al., 2007). RSS typically form Cu(I) complexes (Leal and van den Berg, 1998; Konigsberger et al., 2015) although Cu(II)-thiolates have been generated artificially (Kitajima et al., 1990). Different thiols bind copper with a range of $\log K'_{\text{CuL}}$ values, typically $\log K'_{\text{CuL}} = 12\text{--}14$ (Laglera and van den Berg, 2003) in salinities from estuarine to seawater. Unidentified thiols from hydrothermal vents have been measured with $\log K'_{\text{CuL}}$ values of 12.5–13.5 (Sander et al., 2007) and other natural ligands, suspected to be unidentified thiol compounds, have been measured with $\log K'_{\text{CuL}}$ values of 14–16 (Laglera and van den Berg, 2003).

Humic substances are another source of copper-binding ligands with a complex stability of $\log K'_{\text{CuL}} = 12\text{--}13.5$ (Kogut and Voelker, 2001; Whitby and van den Berg, 2015). Humic substances occur in abundance in estuarine and coastal waters (Muller and Batchelli, 2013), accounting for up to 40–60% of DOM (McKnight and Aiken, 1998), with around 4–20% of DOM as humic acid and the majority as fulvics and non-humic material (Sholkovitz, 1976). Humics form 5–25% of dissolved organic carbon (DOC) in the surface ocean (Benner, 2002). The fraction of terrestrial humics which survives estuarine mixing is

important for transporting dissolved trace metals, such as copper and iron, to coastal and open ocean waters (Laglera et al., 2011; Misumi et al., 2013; Bundy et al., 2015).

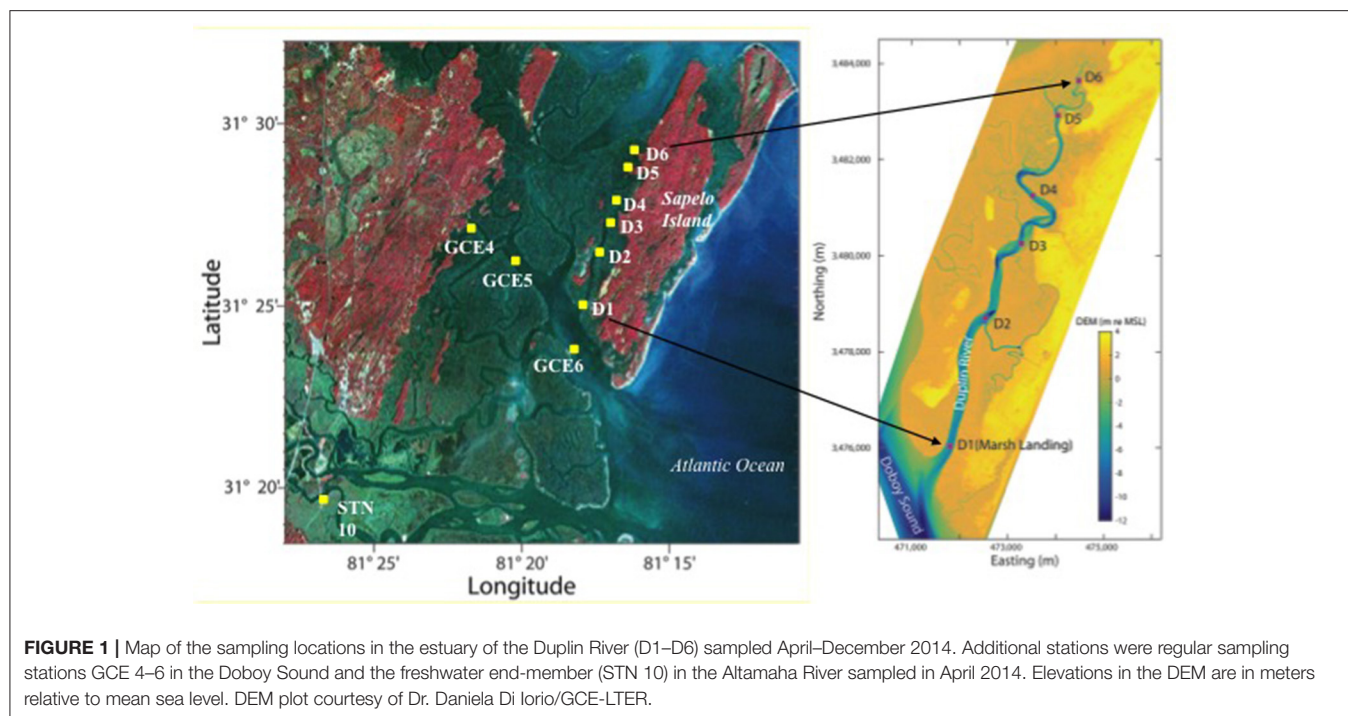
Although, potentially toxic, copper is important in many cellular processes, such as in iron uptake (Peers et al., 2005; Maldonado et al., 2006), even substituting for iron in biochemical pathways of iron-limited *Thalassiosira oceanica* (Peers and Price, 2006). Ionic copper [as Cu(I) or Cu(II)] is required in enzymatic pathways related to oxidation-reduction reactions such as polyphenol (Arnon, 1949) and ammonia oxidation. Genomes of ammonia-oxidizing archaea (AOA) contain many Cu-dependent metalloenzymes (Amin et al., 2013) with inferred high copper requirements. They differ in this regard from ammonia oxidizing bacteria (AOB), which use Fe-dependent metalloenzymes for many of the same functions. AOA are one of several organisms demonstrated in culture studies to be limited by the availability of copper (Amin et al., 2013), along with methane oxidizing archaea (Glass and Orphan, 2012) and some phytoplankton (Annett et al., 2008; Guo et al., 2010; Walsh et al., 2015). AOA are significant contributors to nitrification and thus to the global nitrogen cycle (Francis et al., 2005; Beman et al., 2010) contributing significantly to nitrous oxide (N_2O) fluxes (Santoro and Casciotti, 2011). They are the dominant ammonia oxidizers in the pelagic ocean, accounting for up to 40% of total picoplankton cells in the mesopelagic ocean (Karner et al., 2001) and Antarctic winter populations (Church et al., 2003). Thaumarchaea are responsible for a major fraction of carbon fixation below the euphotic zone (Herndl et al., 2005; Ingalls et al., 2006) and in Antarctic coastal waters during winter (Tolar et al., 2016b).

The main objective of this study was to assess Cu speciation, the ligand identity and possible impact on phytoplankton and AOA growth in estuarine waters. Waters adjacent to Sapelo Island, Georgia, were selected for this study, as they are the location of a regular bloom of Thaumarchaeota, a phylum of the Archaea, which bloom annually from July to September in this region (Hollibaugh et al., 2014).

METHODS

Sample Collection

Surface samples were collected monthly from April to December 2014 from 6 stations along the Duplin River, D1–D6 from the RV Salty Dawg, except November, which was not sampled. Additional samples from the Doboy Sound (GCE 4, 5, 6) and the major freshwater end-member of the marsh complex (the Altamaha River, STN 10) were collected at the beginning of the study, in April 2014 (Figure 1). Samples were collected directly into sample bottles (acid-soaked, 2,000 mL amber HDPE, rinsed three times with sample) from a depth of ~20 cm below the surface by reaching overboard and filling the bottle with the mouth pointed upstream while the vessel motored slowly forward. The samples were filtered on the same day as collection through 47 mm diameter, 0.22 μm filters (Millipore, GVWP) held in a Nalgene polycarbonate filtering apparatus, which had been soaked in 0.1 M HCl and rinsed with sample 3 times before use. The filtrate was poured into acid soaked and filtrate-rinsed



bottles (500 or 1,000 mL fluorinated polyethylene, FLPE) that were frozen at -80°C immediately after filling to be shipped by courier from GA to the UK for analysis. Once reaching the UK they were stored at -20°C . Upon thawing, samples were swirled gently before use, stored in the dark at 4°C and analyzed within 3 days of defrosting.

The filters were removed from the filter rig using plastic forceps and placed into Whirl-Pak bags with 1 mL of lysis buffer, then frozen and stored at -80°C until DNA extraction. Additional samples for DNA analysis were collected weekly from a dock at Marsh Landing (31.4179° , -81.2962° ; adjacent to Station 1) for another project. Although, efforts were made to collect samples at low tide, there is some variation in the tidal stage at the time of sampling. Samples from July and August were collected during the ebb just before low tide; June, October, and December samples were collected at the lowest point in the tide; samples from April and May were collected at the very beginning of the flood tide and September samples were collected midway through the flood tide.

Equipment and Reagents

The measurements of dissolved copper and complexing ligands were performed by voltammetry as described previously by Whitby and van den Berg (2015). The voltammetric measurements were carried out using a μ -Autolab III potentiostat (Ecochemie, Netherlands) connected to a 663 VA stand (Metrohm) with a hanging mercury drop electrode (HMDE). The set-up included an Ag/AgCl reference electrode with a 3 M KCl salt bridge and a glassy carbon counter electrode, and solutions were stirred with a rotating polytetrafluoroethylene (PTFE) rod. We use a glassy carbon counter electrode as

platinum counter electrodes are likely to release platinum ions into solutions (van den Berg et al., 1988). The software was modified to discard 2, instead of the usual 4, drops of mercury between scans to minimize mercury usage. Voltammetric scans used the differential-pulse mode for CSV and the square-wave mode for anodic stripping voltammetry (ASV). The deposition time was between 10 and 30 s for CSV and up to 2.5 min for ASV. Quartz (silica) and PTFE voltammetric cells were cleaned using 0.1 M HCl (trace metal grade) and rinsed with deionized water followed by UV-digested sample before determination. The UV-digestion apparatus contained a high-pressure, 125-W mercury-vapor lamp (van den Berg, 2014), either positioned horizontally above a sample aliquot or surrounded by four 30-mL quartz sample tubes with PTFE caps. The stock borate/ammonia pH buffer (1 M boric acid/0.3 M ammonia) used in all CSV measurements was UV-digested to remove organic matter and contaminating metals were removed by leaving overnight with $100\ \mu\text{M}$ manganese dioxide (MnO_2) (van den Berg, 1982) followed by filtration ($0.2\ \mu\text{m}$).

Total Dissolved Copper

Seawater was UV-irradiated (UVSW) in a conditioned quartz voltammetric cell for 45 min and left to cool. The dissolved copper was determined either by CSV in the presence of $20\ \mu\text{M}$ salicylaldehyde (SA) and 0.01 M borate/ammonia pH buffer ($\text{pH}_{\text{NBS}} 8.15$) (Campos and van den berg, 1994), or by ASV at pH 2 (June, September, and December samples), or both for inter-comparison. For CSV measurements, the sample was UV-irradiated in the voltammetric cell at the original sample pH, and measured at a deposition potential of $-0.15\ \text{V}$, a deposition time of 30 s, and a 1-s potential jump to $-1.2\ \text{V}$ to desorb any

residual organic matter prior to the scan. For ASV measurements, the sample was UV-irradiated and measured at pH 2, using a deposition potential of -0.9 V for 120 or 300 s, followed by 10 s at -1.4 V. Measurements using ASV were found to agree with CSV measurements within the standard deviation of 3 repeat measurements, and additional comparisons on NASS-6 reference material (National Research Council Canada) using ASV were within 5% of the certified value.

Complexing Capacity Titrations

The concentration of copper complexing ligands in each sample was determined by CLE-CSV with ligand competition against SA (Campos and van den berg, 1994). Samples were diluted to 50% for the titrations, to reduce organic interference and lower the concentration range of copper additions, similar to previous studies on estuarine waters (Abualhaija et al., 2015). Dilution was with UV digested sample or, when sample was limited, a mixture of MQ with UV digested Atlantic seawater, combined so as to equal the salinity of the sample being titrated. The starting concentration of Cu in each titration was therefore equal to, or lower than, the concentration of the sample and was accounted for within the calculation. The ligand concentrations were corrected to account for dilution, but the $\log K'_{CuL}$ values were not affected since the salinity was maintained.

For each titration, 80 mL of sample and 80 mL UVSW were transferred to a 250-mL Teflon bottle (Nalgene), and 0.01 M borate buffer and 20 μ M SA added. Aliquots of 10 mL seawater, mixed with buffer and SA, were pipetted into 14 25-mL polystyrene (Sterilin) vials with polyethylene lids. The vials were conditioned with UVSW followed by conditioning with diluted sample before initial use. They were rinsed with MQ between different samples but not between titrations of the same sample to minimize de-conditioning. Copper was added to each vial in steps of progressively increasing concentration, typically from 0 to 200 nM. The usual increments were 0, 5, 10, 15, 20, 25, 30, 40, 50, 75, 100, 125, 150, 200 nM Cu. These were then left to equilibrate overnight prior to analysis. The addition of SA in excess prior to the addition of Cu(II) minimized the risk of oxidizing natural thiols by the Cu(II) added during titrations as it kept the concentration of Cu^{2+} low (Moingt et al., 2010). Similarly, we kept samples in the dark when not in use and equilibrated titrations overnight to minimize exposure to light and reduce the risk of photooxidation (Laglera and van den Berg, 2006). The labile copper concentration (i.e., that which bound with the added SA) in each cell was then determined by CLE-CSV using a 15 s deposition time. The deposition potential was -0.15 V, followed by a 9 s quiescence period at 0 V from where the scan was initiated. No potential jumps were made for the measurement of labile copper. Two fresh copper additions were made at the end of each titration (usually two additions of 50 nM copper) and measured immediately to calibrate the sensitivity of the titration curve, but these were not used in data fitting.

Humic Substances and Thiols

Copper-binding humic substances (HS_{Cu}) were determined by CSV at a deposition potential of $+0.05$ V, after saturation with copper (50–100 nM) in the presence of borate buffer (pH_{NBS}

8.15) (Whitby and van den Berg, 2015), with a deposition time of between 10 and 30 s depending on the concentration. Reference humic acid used for calibrations was Suwannee River humic acid [SRHA, International Humic Substances Society (IHSS) Standard II 2S101H], which was dissolved in MQ water to a concentration of 0.1 g L⁻¹ and stored in the dark at 4°C when not in use. Samples were diluted 90% with UVSW to minimize interference by organic matter and to remain within the linear range (2 mg/L HS in the presence of 50 nM Cu with a 15 s deposition time). A 1-s potential jump from 0 to -0.2 V and back (without stirring) was used to remove possible iodide interference, and scans were initiated from 0 V. A background subtraction was performed on each scan, consisting of the subtraction of a 1-s scan, which provides a flat baseline for more accurate measurement of the HS_{Cu} peak and accounts for any diffusion-current from excess inorganic copper. Concentrations of HS_{Cu} calibrated on the scale of mg HA L⁻¹ were converted to the nM scale by multiplying with the binding capacity of 18 nmole Cu mg⁻¹ HS_{Cu} (Whitby and van den Berg, 2015). The humic standard was used without purification since HS_{Cu} measurements were performed in the presence of excess copper.

Stock thiourea (TU) and thioacetamide (TA) (both reagent grade, Fluka) standard solutions were prepared by dissolution in MQ to a concentration of 0.1 M and kept in the dark at 4°C, with dilutions prepared to 10⁻⁵ M for thiol measurements. Thiol measurements were modified from existing methods (Laglera and van den Berg, 2003; Laglera and Tovar-Sanchez, 2012) and were made in the presence of borate buffer. The deposition time was between 10 and 30 s depending on the concentration. Measurements were performed without addition of Cu or SA, with a deposition potential of $+0.05$ V, and a 1-s potential jump to -0.2 V to eliminate iodide interference as in HS_{Cu} measurements; although the background subtraction described by Laglera and Tovar-Sanchez (2012) was not employed. Under these conditions we found that thiourea and thioacetamide had the same sensitivity and produced the same thiol concentration in samples, as opposed to differing sensitivities observed when using a deposition potential of -0.1 V (used in earlier work on thiols; Laglera and van den Berg, 2003). Thiol analyses were performed without sample dilution.

Detection Window

At the competing ligand concentration of 20 μ M SA, the detection window is centered at an α -coefficient ($\log \alpha_{CuSA}$) of 5.6, strong enough to compete with ligands occurring at 10's of nM with complex stability ($\log K'_{CuL}$) of 12–15. We attempted to use a lower detection window to detect weaker ligands (by using 1 and 2 μ M SA, $\log \alpha_{CuSA} \sim 4$), but titrations were not successful due to interference from the HS_{Cu} peak at around the same potential as the Cu-SA peak (at around -0.2 V), even with sample dilution. Data were interpreted using the van den Berg/Ruzic linearization procedure (Campos and van den berg, 1994) within ProMCC software (Omanovic et al., 2015). $\log K'_{CuL}$ values are provided on the basis of Cu^{2+} and L':

$$K'_{CuL} = [CuL]/([Cu^{2+}][L'])$$

where $[L']$ is the concentration of L not complexed by Cu. $[L']$ is affected by side-reactions with major cations and H^+ , and the K' values are therefore conditional on the experimental salinity and pH.

Thaumarchaea Quantification

Thaumarchaea abundance was determined by quantitative PCR. Microbial biomass was collected by filtration through 0.22 μm pore size, 47 mm diameter Durapore filters, and frozen at -80°C until processed. Samples of the filtrate were frozen at -80°C for nutrient analysis. Lysozyme, proteinase K, and sodium dodecyl sulfate (SDS) were used to extract deoxyribonucleic acid (DNA) from the filters; the extract was then purified with phenol:chloroform and concentrated by precipitation with ethanol as described previously (Bano and Hollibaugh, 2002). Marine group I Archaea (Thaumarchaeota) 16S rRNA (*rrs*) and Archaea ammonia monooxygenase subunit A (*amoA*) genes were quantified using primers ARCHGI334F/ARCHGI554R/TM519AR (Suzuki et al., 2000) and Arch-amoA-for/Arch-amoA-rev (Wuchter et al., 2006), respectively, and protocols described previously (Kalanetra et al., 2009; Tolar et al., 2013) with an iCycler iQTM Real-Time qPCR detection system (BioRad).

Data Archiving

Copper speciation data collected during this study are archived in the GCE-LTER (<http://gce-lter.marisci.uga.edu>) data repository under catalog number CHM-OTH-1702, and water quality and qPCR data under catalog number MIC-GCED-1702. Additional data from the study site are available from GCE-LTER (Stations ML, "Marsh Landing"; and GCE10, "Hunt Camp") and from the Sapelo Island National Estuarine Research Reserve at <http://cdmo.baruch.sc.edu/get/export.cfm>.

RESULTS

Hydrography

The Duplin River (31.4167° , -81.2974°) is a tidal creek within the Sapelo Island National Estuarine Research Reserve. It separates Sapelo Island from the salt marshes bordering the mainland, but is not a true river. The tidal influence is predominantly from the south-western side where the Duplin River meets Doboy Sound (Figure 1). The Duplin River drains an extensive area of salt marsh through a network of smaller channels. It is also influenced by freshwater inputs from rivers and groundwater from Sapelo Island as well as water draining from the salt marsh at low tides ($>2\text{ m}$ mean amplitude). The area is thus a complex network with multiple end-member mixing. Surface water salinity along the Duplin (stations D1–D6) ranged from 13 to 30 during the period studied, with salinity generally lowest in the April samples and highest in September (Supplementary Figure 1A). As well as variation in tide level between sampling months, April experienced the heaviest monthly rainfall, with a major event occurring on the day of sampling (NOAA, 2015). Surface water temperature increased steadily from April to August, with highest surface water

temperatures of $\sim 30.4^\circ\text{C}$, decreasing to $\sim 14^\circ\text{C}$ in December (Supplementary Figure 1B).

Dissolved Copper

The broad salinity range encountered during the study resulted in a wide range of Cu_d concentrations, since at salinities below 20 the flocculation of Cu_d and humic substances increases with increasing salinity, although this is followed by little removal above salinity 20 (Sholkovitz, 1976). Cu_d generally decreased with increasing salinity: from a mean along the Duplin River (stations D1–D6) of 25 nM in April (wide range of Cu_d : 7.1–65 nM across salinity 13–17) to a mean of 4.5 nM in October (Cu_d range: 2.9–6.1 nM, at higher salinities of 27–28; Supplementary Figure 2). Increased rainfall, particularly during a major storm event in April, could have played a role in the higher concentrations encountered in April, as intense rainfall events at low tide can cause increased erosion leading to elevated trace metal concentrations (Moskalski et al., 2013; Guan et al., 2015). Cu_d was relatively constant with a mean of 6.1 nM between July and September (Cu_d range 3.6–9.6 nM, salinity range 21–30), decreasing in October and increasing by December.

Identifying CSV Peaks

Preliminary CSV measurements of samples from the Duplin River estuary showed the presence of a voltammetric peak at $\sim -0.5\text{ V}$ (Supplementary Figure 3), corresponding with the peak potential for sulfide and certain thiols (Al-Farawati and van den Berg, 1997; Laglera and van den Berg, 2003; Laglera and Tovar-Sanchez, 2012). Stability of this peak over multiple repeat scans indicated that it was not sulfide (Al-Farawati and van den Berg, 1997). We compared cysteine, thiourea, thioacetamide, methanethiol, allylthiourea, and both oxidized and reduced forms of glutathione to the natural peak to determine which would be most suitable as a model thiol compound. We found that thiourea and thioacetamide behaved most similarly to the natural thiol peak in terms of peak shape, position and appearance, and standard additions increased the size of the natural peak, supporting other work on coastal waters where thiourea and thioacetamide were also found to be the best candidates (Al-Farawati and van den Berg, 2001; Laglera and van den Berg, 2003). The voltammetric peak measured for this type of species is that of mercury-bound sulfide (Hg-thiol), and is not due to the reduction of copper stabilized as a copper-bound thiol as for glutathione (Le Gall and van den Berg, 1993) or cysteine (van den Berg et al., 1988), which occur at more positive potentials and have a broader peak appearance. Measurements of the natural thiols were therefore made without any addition of Cu(II), eliminating the risk of thiol oxidation by added Cu(II) (Moingt et al., 2010).

The optimum deposition potential for the natural thiol peak was found to be $+0.05\text{ V}$. At this potential the sensitivity of the analysis for thiourea was found to be the same as that for thioacetamide, with standard additions of either compound giving the same concentration (on the molar scale) compared to differences noted at lower (negative) deposition potentials. The signals from various thiols are known to coalesce into one signal at deposition potentials between $+0.02$ and $+0.07\text{ V}$ (Laglera

and Tovar-Sanchez, 2012). Since differences in the sensitivity of thioacetamide and thiourea occur at lower potentials (Laglera and Tovar-Sanchez, 2012), we tested the effect of lowering the deposition potential on the response of thiourea, thioacetamide, and the natural thiol in our samples. Lowering the deposition potential from +0.05 V to -0.1 V caused only a minor decrease (4%) in the sensitivity of the natural thiol but the sensitivity for the thioacetamide dropped by 80%, and the thiourea became undetectable. The difference in the sensitivity behavior of the different model thiols at the electrode compared to the natural thiol peak suggests that the natural thiol may be more similar chemically to thioacetamide than thiourea, but is not identical to either of these, although surface-active materials in the sample (such as HS_{Cu}) may affect this analysis. Since both thiourea and thioacetamide gave the same response with standard additions at +0.05 V, this deposition potential was chosen. Despite the deposition potential demonstrating that the natural peak was more similar to thioacetamide rather than to thiourea, thiourea was selected as the standard in order to be comparable to other work, since measurements reported in thiourea (TU) equivalents are generally more common. Since at +0.05 V the same concentration was measured whether using standard additions of thiourea or thioacetamide, the choice of standard had no effect on our measurements of thiol concentrations.

Copper-Binding Ligands

Two ligand classes were detected at all stations across all months, with $\log K'_{\text{CuL}}$ values differing by more than a unit between the distinct classes. The ligand concentrations in Duplin River waters ranged from 16 to 51 nM for L_1 (72 nM in the Altamaha river end-member) and 30 to 112 nM for L_2 (163 nM in the end-member) (Figures 2A,B). The ligand concentrations were inversely related with increasing salinity during individual sampling events (Figures 2A,B) with the seasonal effects imposing scatter on plots of the combined data. The overall variation we observed was therefore a combination of salinity and seasonal effects.

The mean $\log K'_{\text{CuL1}}$ across the study was 14.5 ± 0.3 , with $\log K'_{\text{CuL1}}$ ranging from 14.0 to 15.2 and varying by a combination of salinity and seasonal effects (Figures 3A,B). The mean value for $\log K'_{\text{CuL2}}$ was 12.8 ± 0.4 with $\log K'_{\text{CuL2}}$ ranging from 12.1 to 13.4 (Figures 3A,B). Fitting the $\log K'_{\text{CuL}}$ values as function of salinity to a simple model based on Mg-ion competition:

$$\log K'_{\text{CuL}}(\text{Sal}) = \log K'_{\text{CuL}}(\text{Sal} = 0) - \log \alpha_{\text{MgL}};$$

shows that a decrease in the complex stability with increasing salinity (Figure 3B) can be explained by competition with major cations. Here the complex stability for any given salinity [$K'_{\text{CuL}}(\text{Sal})$] was calculated from that at zero salinity by subtracting a side-reaction coefficient for Mg^{2+} ($\log \alpha_{\text{MgL}}$), computed using non-linear data fitting (Figure 3B). Because the concentration of Mg^{2+} is 5 times greater than that of Ca^{2+} , we assumed that Mg^{2+} would be the dominant competing cation, but the competition could also include Ca^{2+} or a combination of the two. Increases in $\log K'_{\text{CuL1}}$ and $\log K'_{\text{CuL2}}$ during August–December in the higher salinity (25–30) range (Figure 3B) are not consistent

with expectations from the model: the sampling bias toward higher salinity in these months (Supplementary Figure 1) should have given lower $\log K'_{\text{CuL}}$ values. The high values we found suggest that different ligands with stronger binding constants were dominant during this period.

Composition of the Ligand Classes

Since thiols and humic substances are likely candidates for copper-binding ligands, their concentrations were compared to those of the individual ligand classes (L_1 and L_2) and their sum, as obtained from titrations. The sum of the concentrations of thiourea-type thiol and humic substances correlated very well with the sum of L_1 and L_2 (L_T) across the seasonal cycle (Figure 4A) with a slope of 0.89 ± 0.08 , $\rho = 0.82$ (where ρ is Spearman's rank correlation coefficient), suggesting they represent the key complexing agents. The concentration of the thiourea-type thiol correlated well with the concentration of L_1 throughout the study (Figure 4B), with a slope of 1.11 ± 0.13 , $\rho = 0.85$, suggesting L_1 is primarily a thiourea-type thiol. The concentration of HS_{Cu} correlated well with L_2 (Figure 4C), with a slope of 0.85 ± 0.08 , $\rho = 0.70$, suggesting that HS_{Cu} is a good model for L_2 in these waters. For all three correlations, $p < 0.0001$, $n = 41$.

Titration of Mixtures of Model Ligands

Mixtures of thiols and humic substances added to UVSW were titrated with copper to evaluate whether we could reproduce titration results from samples using model ligands. Thiourea and SRHA were added to a UV-digested sample of salinity 18.5 (May D5) to a concentration of 10 nM and 1 mg L^{-1} , respectively [equivalent to 18 nanomole $(\text{mg HA})^{-1}$ Cu-binding capacity; Whitby and van den Berg, 2015). Ligand titrations of the mixture showed the presence of two copper binding ligands: $L_1 = 10.9 \pm 0.6$ nM and $L_2 = 19.1 \pm 0.4$, in good agreement with the added concentrations of thiourea and humic acid. The data fit for the model ligand titration is shown in Supplementary Figure 5. The stability constant obtained for L_2 in the model ligand titration, $\log K'_{\text{CuL2}} = 12.3 \pm 0.4$, agreed well with $\log K'_{\text{CuL}}$ expected for humics in seawater, and is also similar to that for the L_2 -ligands within the samples. The stability constant for L_1 from the model ligand titration, $\log K'_{\text{CuL1}} = 14.9 \pm 0.4$, was also similar to $\log K'_{\text{CuL1}}$ of the samples.

Titrations of higher concentrations of thiols (30 nM thiourea) and humic-type ligands (3.5 mg L^{-1} SRHA) were found to cause the plots of reactive copper vs. added copper to level off at Cu levels >40 nM. This behavior implies electrode saturation by Cu-SA at an unexpectedly low copper level, suggesting a surfactant effect on the electrode of the naturally occurring humic substances or thiol species causing electrode saturation. The same behavior was observed in titrations of UVSW with a higher concentration (50 nM) of thioacetamide (without humic substances). Interestingly, this phenomenon in the synthetic ligand mixtures replicated that seen in titrations of actual samples before dilution to 50%, suggesting that it may be a common problem in titrations of estuarine waters containing high concentrations of thiol-type ligands and humics.

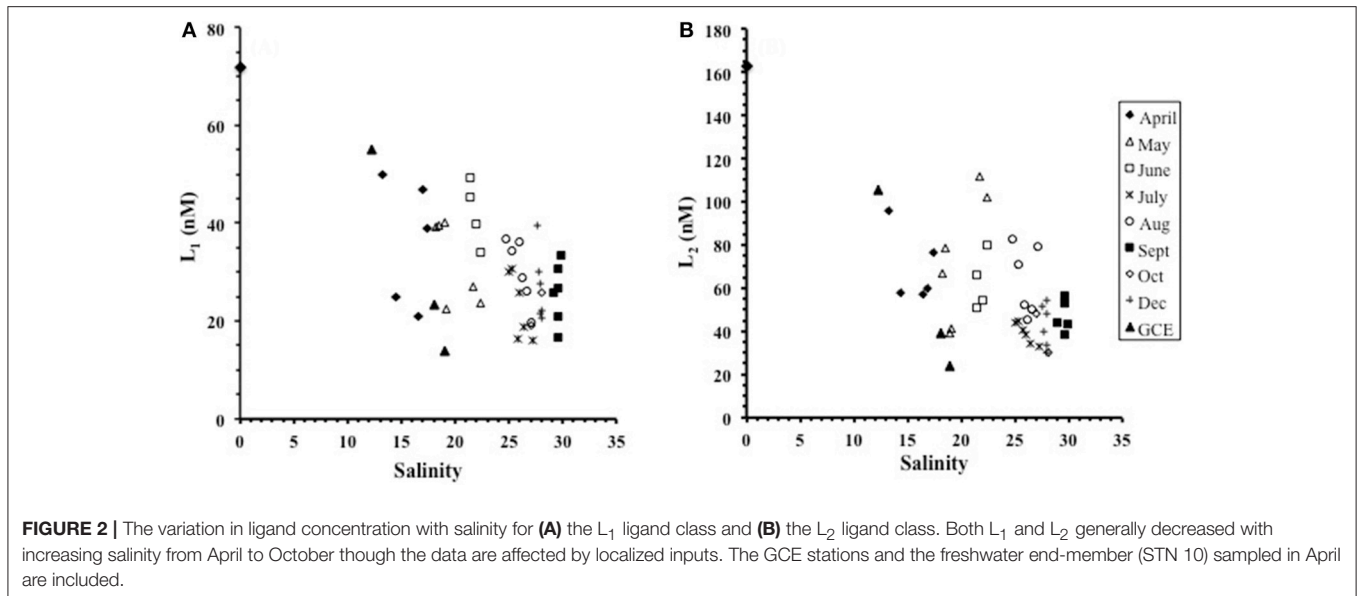


FIGURE 2 | The variation in ligand concentration with salinity for (A) the L₁ ligand class and (B) the L₂ ligand class. Both L₁ and L₂ generally decreased with increasing salinity from April to October though the data are affected by localized inputs. The GCE stations and the freshwater end-member (STN 10) sampled in April are included.

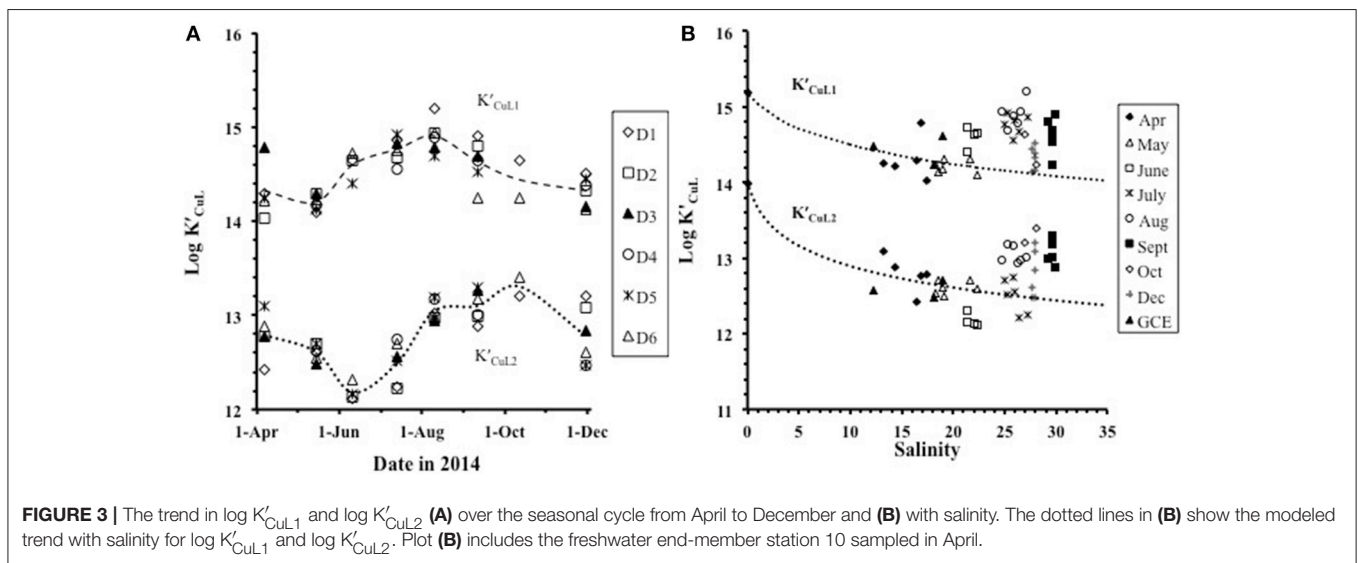


FIGURE 3 | The trend in log K'_{CuL1} and log K'_{CuL2} (A) over the seasonal cycle from April to December and (B) with salinity. The dotted lines in (B) show the modeled trend with salinity for log K'_{CuL1} and log K'_{CuL2}. Plot (B) includes the freshwater end-member station 10 sampled in April.

Thaumarchaeota

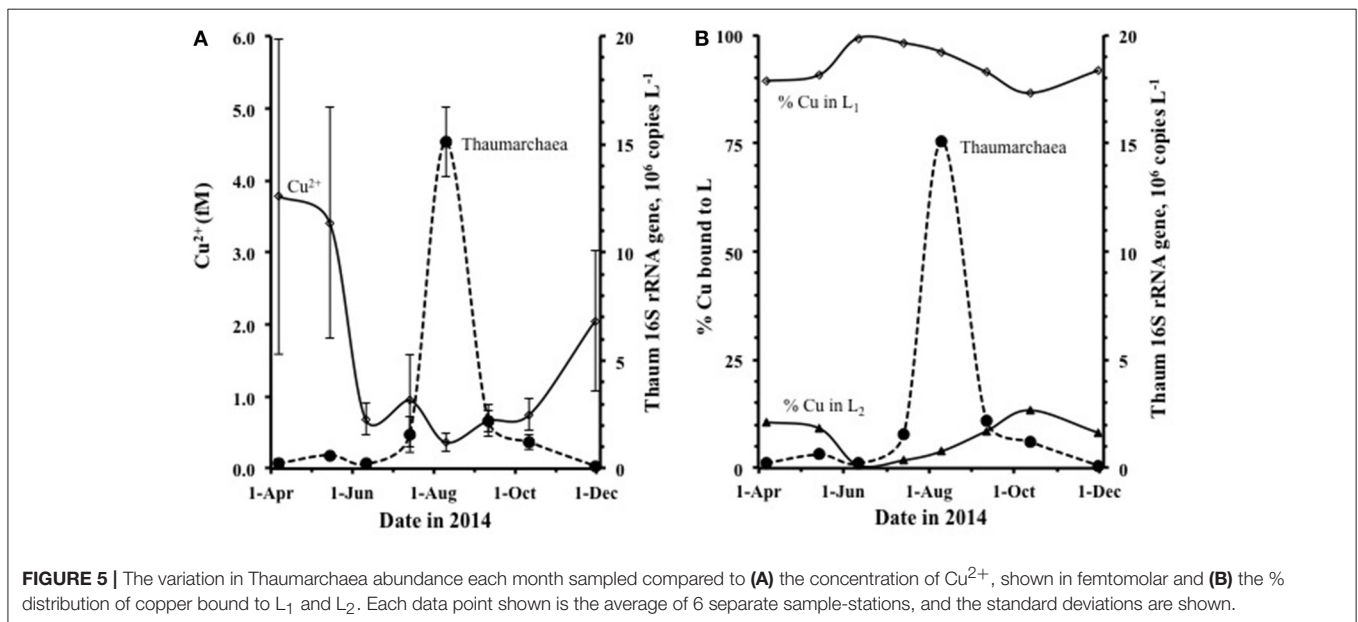
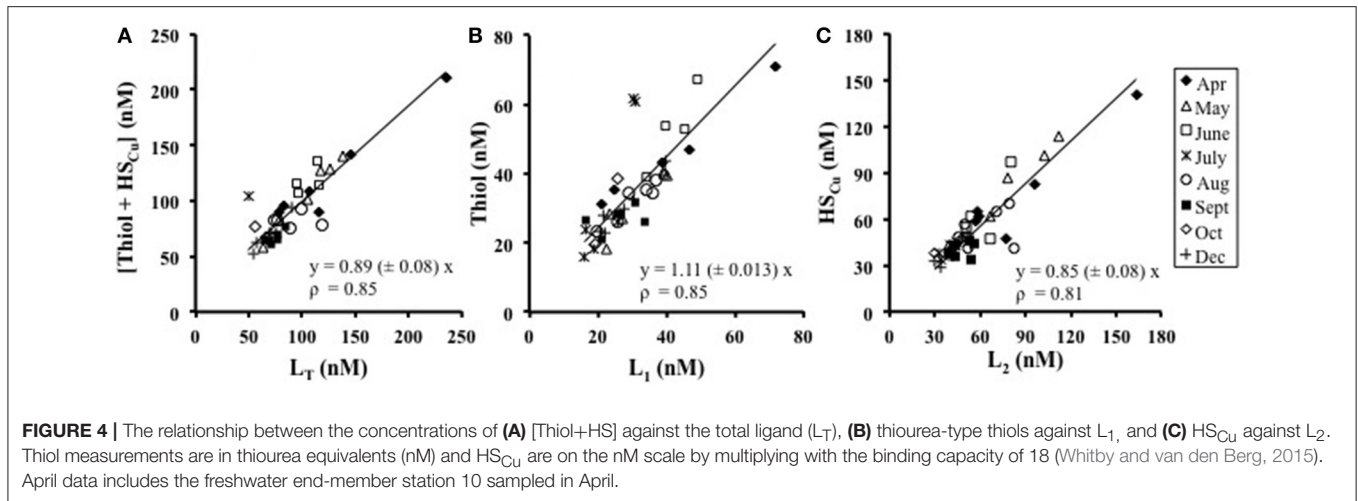
The abundance of Thaumarchaeota was low and stable through the spring and early summer, then increased dramatically from July, with peak abundance in August at all 6 stations (Figures 5A,B), dissipating by September. The pattern seen in average monthly data (gene copies L⁻¹) from 6 stations along the Duplin River (taken simultaneously with samples used for metal speciation) is consistent with data from weekly samples taken at the mouth of the Duplin River (Marsh Landing, shown in Supplementary Figure 6) and is therefore not an artifact of our sampling regime. Comparison of the time course of Thaumarchaeota abundance to that of [Cu²⁺] (Figure 5) shows that the Thaumarchaeota abundance started to increase when [Cu²⁺] decreased, with the bloom occurring during the period of lowest of Cu²⁺ concentration (Figure 5A). Calculation of the distribution of copper between L₁ and L₂ showed little

variation during the study (Figure 5B) with 90–99% of the copper always bound with L₁, suggesting that the concentration of free inorganic copper was the only variable during this period of possible relevance to the bloom of Thaumarchaeota.

DISCUSSION

Seasonality in the Data

The salinity in our samples showed a systematic seasonal increase from April to September (Supplementary Figure 1A). Salinity ranged from 13 to 18 in April to 23–27 in August, and 27–31 in subsequent months. The ligand concentrations ranged from 16 to 51 nM (L₁) and 30 to 112 nM (L₂) over the study. High concentrations of both L₁ and L₂ in the low-salinity, riverine, end-member (STN 10) demonstrate a contribution of the freshwater source to the relationship between ligand



concentration and salinity (Figure 2), with the effect of local freshwater inputs superimposed on this broader scale pattern. The composition of Duplin River water cannot be modeled by conservative mixing between fresh and seawater, as variation in the strength and location of freshwater inputs violates the assumptions of a 2-member mixing model (Smith and Hollibaugh, 1993). Localized inputs on the Duplin River cause major deviations in the salinity plots and, since sampling was conducted over several months, it is not possible to derive a single theoretical dilution line.

Despite the complexity of the system, L_1 was generally conservative with salinity except in September and October. In June and September L_1 demonstrated large variability between stations of similar salinity, ranging from 34 to 49 nM at Sal 21 to 22, and 16.6 to 33.6 nM at Sal 29.6 to 29.9. These large differences between stations of almost identical salinity indicate

that local processes, such as contributions from pore waters or from temporally varying processes linked to biological activity, affected conditions at individual stations. This suggests that as well as a freshwater source, L_1 is both produced and utilized along the estuary and, as a result, local concentrations may vary seasonally. This is consistent with the identification of L_1 as a thiol-type species, since sediment and pore waters are likely sources of thiols (Kiene et al., 1990; Zhang et al., 2004), which have been shown to diffuse out of sediments in similar shallow water marshes (Chapman et al., 2009).

Comparison of the data (Figure 4C) showed HS_{Cu} to correspond with L_2 (slope 0.85 ± 0.08). Most of the humic material along the estuary likely originates from terrestrial material delivered to the study area by the Altamaha River, although marine-derived humics may also be present from exchange with coastal waters. The concentration of both L_2

and HS_{Cu} decreased with increasing salinity in April, October, and December (Supplementary Figure 4), consistent with a dominant terrestrial origin of these humic-type ligands and similar to that found in other estuaries such as that of the Mersey Estuary (Supplementary Figure 4). Between May and September, concentrations of L_2 and HS_{Cu} either remained constant or increased with increasing salinity >25 . This suggests a mid-estuarine source of L_2 and HS_{Cu} , which could be from increased fluxes of sedimentary organic carbon into the estuary, potentially partly linked to higher bioturbation by fiddler crabs and other invertebrates during summer. Published records show DOC concentrations range from around 3.0 to 9.0 mg/L along the estuary and are not conservative with salinity (Hodson, 2005; Medeiros et al., 2017). Like L_2 , the concentration of humic substances was generally highest in spring and generally constant from September to December, with elevated concentrations relative to salinity in August.

Potential Issues of the Detection Window and Freezing Temperature

A high detection window was necessary in order to resolve strong ligands in this work because the HS_{Cu} peak interfered with the peak for CuSA at lower SA concentrations despite sample dilution. The high detection window may have impacted the detection of weaker ligands if these are out-competed by the added ligand (SA). At the detection window used here (20 μM SA, $\alpha_{\text{CuSA}} = 10^{5.6}$) competing ligands are required to bind copper with $\alpha_{\text{CuL}} \gg 10^{3.6}$ to have an effect of $\gg 1\%$, and preferably nearer 10^4 to take variability of the data into account. The L_1 -type ligands had values for $\log K'_{\text{CuL1}} > 14$, which means values for $\alpha_{\text{CuL1}} > 10^6$ at the 10 nM level, and the L_1 species were easily detectable. The L_2 type ligands had values for $\log K'_{\text{CuL2}} > 12.1$, giving values for $\alpha_{\text{CuL2}} > 10^{4.1}$, sufficiently strong for detection at the 10 nM level. The actual concentrations of L_2 were well above the 10 nM level (Supplementary Table 1), and values for $\log K'_{\text{CuL2}}$ averaged 12.2–13.0, therefore L_2 was also readily detected at this high detection window. However, putative (L_3) ligands with significantly lower complex stabilities ($\log K'_{\text{CuL3}} < 11$) would have caused relatively minor competition against the SA unless at levels of $\text{L}_3 > 10^{-7}$ M, therefore these were not detected in this work.

A secondary methodological issue is that samples were frozen at -80°C immediately after filling to be shipped by courier from GA to the UK for analysis. Once reaching the UK they were stored at -20°C . It has been shown that open ocean samples stored at -80°C can provide different results in comparison to samples that were not frozen or that were stored at -20°C (Buck et al., 2012) and this must be considered in relation to the ligand data presented here. Buck et al. (2012) found that samples from the chlorophyll *a* maximum frozen at -80°C underestimated [L] compared to unfrozen samples, but found the same $\log \text{Cu}^{2+}$ (14.56 and 14.51, respectively). They also reported that [L] was overestimated and $\log K'_{\text{CuL1}}$ was underestimated if deep-water (3,000 m) samples were frozen, although again this resulted in similar $\log \text{Cu}^{2+}$ values (e.g., 13.1, 12.5, and 12.7 for unfrozen, frozen at -20°C and at -80°C , respectively).

Since the composition of DOC from estuarine waters is likely more similar to productive surface waters than to old, deep water, we would therefore most likely be underestimating the ligand concentration and overestimating $\log K'_{\text{CuL}}$, resulting in an overestimation (or no change) in our estimate of Cu^{2+} concentrations.

Complex Stabilities and Possible Competition Effects

The two ligand classes were distinguished on the basis of an average difference in complex stability ($\log K'_{\text{CuL}}$) of 1.7 log units, with $\log K'_{\text{CuL1}}$ ranging from 14 to 15.2 (mean 14.5) and $\log K'_{\text{CuL2}}$ ranging from 12.1 to 14 (mean 12.8). The large ranges for the complex stabilities suggest that either there are more ligands within each group (e.g., substituted thiols and reduced sulfur compounds or different compounds within the humic species), that data are affected by competing reactions, or both. Competition is an aspect that has not been considered experimentally in this work. This competition could be a result of different metal ions binding the same ligand, thus lowering the apparent complex stability. Several metals, like iron, copper, cobalt, and aluminum are known to bind humic substances in seawater and will therefore compete (Yang and van den Berg, 2009; Abualhaija et al., 2015; Whitby and van den Berg, 2015). It is not yet known whether this affects the apparent complex stability significantly. Studies on SRHA standards have demonstrated that the degree of competition between copper and calcium for binding sites in humic substances is weaker than expected (Averett et al., 1994), potentially due to the larger ionic radius of calcium, or because calcium binds more strongly to functional groups containing oxygen, whereas copper forms stronger complexes with sulfur and nitrogen (Nieboer and Richardson, 1980).

Variation in the complex stability could also be due to a seasonal change in the composition of the components contributing to each ligand class; for example, humic material with higher $\log K'_{\text{CuL2}}$ may be more common later in the year. Similarly, the composition of the compounds contributing to the thiol peak may change, either through variation in the type of compounds released biologically across the season or by modification of the chemical structure of the compounds over time. For example, thiols can be microbially transformed from one type to another: glutathione can be transformed into mercaptoacetate and mercaptoethanol via cysteine and 3-mercaptopyruvate (Kiene et al., 1990). Although, voltammetry can distinguish between some similar thiols (such as glutathione and cysteine) it lacks resolution to conclusively distinguish between other similar compounds (e.g., thiourea and thioacetamide) unless the deposition potential is varied in detail (Laglera et al., 2014). The natural thiols detected here could therefore be a mixture of thiols with similar peaks varying seasonally, and/or include degradation products of localized algal blooms, and include different sulfur species. Furthermore, a small contribution from a low concentration of a very strong ligand such as a chalkophore (Kim et al., 2004) would not be identified but could exaggerate the apparent value for \log

K'_{CuL1} . Chalkophores are high affinity, copper-complexing agents secreted by specific bacteria forming very strong Cu(I) complexes (Hakemian et al., 2005; El Ghazouani et al., 2012). Chalkophores may be an important ligand in copper complexation, but very little is currently known about the predominance and significance of chalkophores in the marine environment. Models suggest they can outcompete complexation by fulvic-type material (Kraemer et al., 2015). As with any speciation method, CLE-CSV can only detect a certain fraction of the entire pool of ligands, limited by the detection window (Wells et al., 2013; Monticelli and Caprara, 2015), which can span 2–3 orders of magnitude in α_{CuL} (Apte et al., 1988). This, and the fact that ligands with similar $\log K'_{CuL}$ are difficult to resolve within a detection window, mean that unresolved species lead to weighted averages of all ligands within that window (Miller and Bruland, 1997). Therefore, the presence of a very strong ligand at low concentration could exaggerate the values for $\log K'_{CuL1}$ even if L_1 was mostly comprised of a slightly weaker ligand. This may explain the higher than expected $\log K'_{CuL1}$ value for the thiol.

Composition of the Ligand Classes

A study on the Elizabeth River in Virginia measured six different thiol compounds with concentrations varying seasonally (Dryden et al., 2007). They did not test for thiourea or thioacetamide, but found that mercaptosuccinic acid and 2-mercaptoethanol (which we did not test) correlated with the ligand concentration. It is possible that mercaptosuccinic acid could be contributing to the thiol peak observed in our samples, but not 2-mercaptoethanol as its peak potential is more positive and similar to that of cysteine (Casassas et al., 1985). The thiol concentration in the Elizabeth River, particularly mercaptosuccinic acid, was also found to be highest in June similar to our findings, as well as being high in October.

Previous studies in estuarine waters have suggested that thiols likely contribute to the weaker L_2 ligand class, which binds 3–23% of copper (Laglera and van den Berg, 2003) with lower $\log K'_{CuL}$ values than those observed here (Luther et al., 1991; Walsh and Ahner, 2013). Our results show the concentration of the natural thiol best correlates with that of the L_1 ligand class with a high $\log K'_{CuL1}$, although as discussed this may be the weighted average of thiols plus other very strong ligands present at low concentration. Another study of copper complexation in organic-rich estuarine waters also detected two similar ligand classes with $\log K'_{CuL}$ values of $\log K'_{CuL1}$ of 14.9–15.9 (present at a concentration of <4 nM) and $\log K'_{CuL2}$ of 11.8–12.7, at concentrations of 50–170 nM (Muller and Batchelli, 2013). Muller and Batchelli (2013) concluded that humic substances made up the stronger ligand class (as opposed to L_2 as we suggest) based on the riverine source and estuarine mixing behavior of their L_1 ligand class. The L_1 and L_2 ligand classes in our study were of similar concentration to one another and a reasonable correlation (though weaker) can also be drawn between L_1 with humic substances and L_2 with the thiol concentration. However, Suwannee River humics (SRHA) have a $\log K'_{CuL} = 12$ (Whitby and van den Berg, 2015), too low to account for L_1 , and SRHA is likely a good candidate for the humics since the Altamaha and Suwannee rivers are geographically close, drain similar terrestrial environments and

are chemically similar (Annett et al., 2008). Furthermore, the results of the model ligand titration suggest that within a mixture of humic acid and a thiourea-type thiol, the concentration of thiourea corresponds to L_1 and humics to L_2 providing further support for our interpretation of the composition of the ligand classes in the samples.

The correlation of the thiourea-type thiol and HS_{Cu} with L_1 and L_2 , respectively, suggests that on average thiols could make up ~40% and humics around 60% of the total available copper ligands (L_T) measured at this detection window in the estuarine waters around Sapelo Island, potentially in addition to low concentrations of very strong ligands incorporated into L_1 or much weaker ligands not detected. The percentage distribution of strong and weaker ligands is similar to that found in the Mersey Estuary where humics were around 69% of total available copper-binding ligands (Abualhaija et al., 2015), whereas thiols have previously been found to account for ~15% of the total ligand in the Elizabeth River (Dryden et al., 2007).

Although, both ligand classes were in excess of copper with the bulk of the ligand pool composed of L_2 , calculation of the speciation of copper over L_1 and L_2 showed that the distribution of copper was 82–99% associated with L_1 (as CuL_1). CuL_1 generally decreased with increasing salinity across the period studied, whereas the resulting percentage bound to L_2 (CuL_2) generally increased with increasing salinity, noticeably increasing during the course of the Thaumarchaeota bloom. Due to the presence of the strong L_1 -ligands, the free cupric ion concentration was also extremely low throughout the study. Concentrations of Cu^{2+} ranged from 0.9 to 7.5 fM and generally increased with increasing salinity, despite Cu_d decreasing with increasing salinity. The concentration of Cu^{2+} in the Duplin River decreased from a mean of 3.8 ± 2.2 fM in April (range 2.6–7.5 fM) to a minimum of 0.4 ± 0.1 fM in August (range 0.2–0.5 fM) during the peak of the Thaumarchaeota bloom (Supplementary Figures 6A,B).

Previous measurements suggest that thiols bind copper as a Cu(I) species (Leal and van den Berg, 1998; Konigsberger et al., 2015; Barman et al., 2016). From our assumption based on the correlation between thiourea-type thiols and L_1 , an important deduction from this work is that most of the copper in these coastal waters would appear to occur in the reduced form of Cu(I). Copper is thought to occur predominantly as Cu(II) in natural waters containing dissolved oxygen, with around 10% of inorganic copper in surface seawater as Cu(I) due to its stabilization as a chloride species and photochemical effects (Nelson and Mantoura, 1984; Jones et al., 1985; Moffett and Zika, 1988). Our data may suggest that this Cu(I) fraction is much greater, and may in fact dominate the copper chemistry in our samples in the form of a Cu(I)-thiol species. This is consistent with findings along the Scheldt Estuary, where the fraction of $Cu(I)/Cu_{tot}$ ranged from 5 to 80%, depending on a combination of salinity (chloride stabilization) and thiol complexation (Buerge-Weirich and Sulzberger, 2004). The tendency for thiol species and Cu(I) to occur in these waters is further enhanced at low concentrations of dissolved oxygen during the summer, which happens regularly at the Marsh Landing site (Hollibaugh et al., 2014) (data from

Sapelo Island National Estuarine Research Reserve archived at <http://cdmo.baruch.sc.edu/get/export.cfm>). It should be noted, however, that recent work using a fluorometric method and direct titration of thiols with Cu(I) (Walsh and Ahner, 2013) has indicated that some Cu(I)-thiol complexes may be considerably weaker than previously suggested by electrochemical techniques (e.g., Leal and van den Berg, 1998), and therefore not stable in natural seawater systems. Further work is necessary to determine the actual significance of Cu(I) organic complexes in oceanic and estuarine regimes.

Implications for Thaumarchaeota

A major finding of our study is that the Thaumarchaeota in the Duplin River were found to grow and even thrive (ammonia oxidation rates $>100 \text{ nmol L}^{-1} \text{ d}^{-1}$, Tolar et al., 2016a,c) at extremely low Cu^{2+} concentrations, sub- 10^{-15} M , well below Cu^{2+} concentrations thought to be limiting ($[\text{Cu}^{2+}] < 10^{-12.7} \text{ M}$; (Amin et al., 2013)). During this study there was no obvious limitation of ammonia oxidation as a result of the low Cu^{2+} concentrations, in contrast to previous reports for Cu^{2+} concentrations $>6 \times 10^{-15} \text{ M}$ in the presence of strong copper-binding ligands (Jacquot et al., 2014). Work with the Thaumarchaeote *Nitrosopumilus maritimus* strain SCM1 has suggested possible copper limitation when $[\text{Cu}^{2+}] < 0.2 \text{ pM}$ (Amin et al., 2013), whereas our work demonstrates that closely related ($>99\%$ 16S rRNA similarity) Thaumarchaeota apparently grow well at 1/1,000th this concentration of Cu^{2+} . These comparisons suggest that there is either large variability in the copper requirements between different strains, which seems unlikely given the fundamental roles played by Cu-containing metalloenzymes in AOA (Walker et al., 2010), or that some forms of complexed copper are available to Thaumarchaeota. Although Cu^{2+} was extremely low, the concentration of Cu_d was much higher than Cu^{2+} , with mean Cu_d 6.7 nM in August. During the bloom, up to 99% of copper was bound to the strongest L_1 ligand, with $\log K'_{\text{CuL}_1}$ as high as 15.2, suggesting that its dissociation is kinetically slow. It is therefore likely that Thaumarchaeota are indifferent to the low Cu^{2+} concentration and are able to access the strongly complexed copper directly.

One explanation for the difference observed in natural samples compared to laboratory experiments may be the use of artificial ligands such as EDTA to induce Cu^{2+} limitation. Thaumarchaeota may not be able to access EDTA-bound Cu(II), however it is plausible that they have mechanisms for obtaining naturally complexed copper [such as thiol-bound Cu(I)]. Coastal and oceanic phytoplankton species have been demonstrated to access Cu bound within strong organic complexes (Guo et al., 2010) and some open ocean phytoplankton can acquire copper complexed with natural and artificial ligands with $\log K'_{\text{CuL}}$ up to 15.8 (Semeniuk et al., 2015). A study on San Francisco Bay found copper to be 99% complexed, at $\log K'_{\text{CuL}} = 12.1$, and suggested that this complexation was dominated by the presence of anthropogenic EDTA in those waters (Bedsworth and Sedlak, 1999). Microcosm experiments on a diatom bloom within those samples revealed that this complexed Cu was largely unavailable to the species studied (Beck et al., 2002) despite the relatively low $\log K'_{\text{CuL}}$ values. Furthermore, diatoms and coccolithophores

demonstrate reduced growth rates when cultured in the presence of EDTA (Muggli and Harrison, 1996), and Amin et al. (2013) report that EDTA concentrations of 11–100 $\mu\text{mol L}^{-1}$ proved lethal to *N. maritimus*.

Cu uptake has been shown to be controlled by the oxidation state of the metal and by the metal:ligand ratio, rather than by the concentration of inorganic species of Cu in solution (Semeniuk et al., 2009). The speciation of Cu will affect its availability to microorganisms depending on whether uptake is as Cu(I) or Cu(II), as the uptake may involve a change in oxidation state with associated reaction rates. It is unclear whether Thaumarchaeota are acquiring the thiol-bound copper [as Cu(I)], or the humic-bound copper [as Cu(II)]. Although, in terms of availability it should be easier to access the more weakly bound, L_2 -complexed copper, we hypothesize that the Thaumarchaeota are accessing the more strongly bound, L_1 -complexed copper, thought to be thiols, as this is the more abundant fraction. This is consistent with uptake studies showing that addition of Cu(I) ligands enhanced Cu uptake in presence of organically bound Cu(II), suggesting that the mechanism for Cu(II) uptake may even rely on the enzymatic reduction of Cu(II) to Cu(I) (Semeniuk et al., 2015). Cu(II) is reduced to Cu(I) within 2–40 min by Cu(I) binding thiols like glutathione and cysteine (Leal and van den Berg, 1998). Cu-limitation has been demonstrated to increase rates of cell surface reduction of Cu(II) to Cu(I) in *Emiliania huxleyi* (Walsh et al., 2015). They demonstrated that cysteine can increase the bioavailability of copper to copper-limited cells through the reductive release of Cu(I) from Cu(II) ligands such as EDTA. This mechanism may be relevant in Duplin River waters where free copper is very low but L_1 -bound copper, thought to be thiol-bound and potentially amounting to up to 99% of the dissolved copper, is relatively abundant.

The mechanism for copper uptake by Thaumarchaeota is not fully understood. The bloom starts when the free Cu' is already very low (Figure 5A), indicating that the availability of inorganic Cu' , whether as Cu(I) or as Cu(II), is not important. We hypothesize that the copper arrives at the cell as a Cu(I)-thiol species, where there is a direct exchange of copper to Cu-binding groups on the cell wall, allowing active transport of the copper into the cell through a high affinity transporter, as described for *E. huxleyi* (Walsh et al., 2015). We suspect that the low Cu^{2+} is not driven directly by the Thaumarchaeota through production of L_1 , but rather that L_1 is released independently, likely by other microorganisms in the water column or from the sediment and pore waters. Other work has demonstrated that the Thaumarchaeote *N. maritimus* SCM1 did not release strong Cu-binding ligands when under low copper stress (Amin et al., 2013) and the concentration of L_1 does not correlate with the onset of the bloom.

Possible Sources of the Ligands

The concentrations of both L_1 and L_2 were high in the freshwater end-member suggesting a terrestrial or freshwater source for both ligand classes, but both also displayed addition and removal processes along the estuary. Other species that bloom in the area include numerous bacteria (Fallon et al., 1986; Gifford et al., 2011, 2013), diatoms (Williams, 1964; Pomeroy et al.,

1981), green algae and euglenoids as well as dinoflagellates (Berman, 1983). The dinoflagellate *Amphidinium carterae*, more common in coastal regions, has been found to produce very strong ligands (Croot et al., 2000) and dinoflagellates, specifically *Kryptoperidinium* sp., have been documented to bloom in August in the Duplin River (Berman, 1983). A study on the seasonal cycle of copper speciation within a fjord in Sweden also found stronger ligands in the summer months ($\log K'_{\text{CuL}}$ 12.9–14.2) causing a pCu of 11.7–13.8 (Croot, 2003). The L_1 ligands measured in the fjord were thought to be related to the seasonal cycle of *Synechococcus* blooming in the area at this time, and which are known to produce L_1 ligands (Moffett et al., 1990; Moffett, 1995). *Synechococcus* are the second most abundant bacterioplankton fraction in waters offshore of the Duplin River in summer (Lu et al., 2015). As well as water column sources for ligands, likely sources of thiols are benthic microbes and sulfur-containing amino acids within the sediment (Kiene et al., 1990; Chapman et al., 2009), whilst the humics in this type of environment are likely products of relatively recent degradation of local plant matter (Averett et al., 1994) such as fungal breakdown of lignocellulose (Newell, 2001; Buchan et al., 2003). *Spartina alterniflora* and many of the higher plants in the marsh also release dimethylsulfoniopropionate (DMSP) (Bacic et al., 1998; Kiehn and Morris, 2010), which can add be an additional source of thiols.

CONCLUSION

Our study indicates that thiols and humic substances are the dominant ligands for copper within the Duplin River estuary, and waters around Sapelo Island. The evidence suggests that around 90% of Cu_d is complexed to strong L_1 ligands, thought to be a thiourea-type thiol based on the correlation with the concentration of L_1 . Although, this work contributes to our understanding of the identity of the ligand classes, combining this work with additional ligand characterization methods would better identify the nature of the thiols and other compounds dominating Cu complexation in these waters. The good agreement between L_T and [thiols + HS_{Cu}], as well as the success of the model ligand titration in distinguishing between model compounds as two separate classes, is consistent with previous studies suggesting that thiols and HS_{Cu} are the dominant ligand types responsible for controlling copper speciation in estuarine environments and can induce very low

REFERENCES

- Abualhaija, M. M., Whitby, H., and van den Berg, C. M. G. (2015). Competition between copper and iron for humic ligands in estuarine waters. *Mar. Chem.* 172, 46–56. doi: 10.1016/j.marchem.2015.03.010
- Al-Farawati, R., and van den Berg, C. M. G. (1997). The determination of sulfide in seawater by flow-analysis with voltammetric detection. *Mar. Chem.* 57, 277–286. doi: 10.1016/S0304-4203(97)0014-5
- Al-Farawati, R., and van den Berg, C. M. G. (2001). Thiols in coastal waters of the western North Sea and English Channel. *Environ. Sci. Technol.* 35, 1902–1911. doi: 10.1021/es000073i

concentrations of Cu^{2+} . However, low concentrations of a very strong ligand could be contributing to the high $\log K'_{\text{CuL}_1}$ values we found and influencing the Cu^{2+} concentration. It is likely that low-oxygen sulfur-containing muds are a source of the thiols and further investigation into this process would add to our understanding of this complex system.

A key finding of this study is that Thaumarchaeota that bloom regularly at the study site do not appear to be limited by low inorganic copper availability and are capable of growth and activity at free Cu^{2+} concentrations of 0.4×10^{-15} M (pCu 15.4), previously thought to be limiting. It is likely that, since Thaumarchaeota appear to have a high copper requirement, they have developed pathways for obtaining copper from strongly bound species. Based on our data, we hypothesize that the Thaumarchaeota are utilizing complexed copper, possibly as thiol-bound Cu(I). Future studies could focus on Cu availability to natural populations of Thaumarchaeota in a laboratory setting, using natural ligands to induce limitation rather than artificial compounds such as EDTA.

AUTHOR CONTRIBUTIONS

HW collected samples, prepared all of the data and graphs, and wrote the paper for publication. JH collected samples, provided information, and co-wrote the paper. CvdB supervised and co-wrote the paper.

ACKNOWLEDGMENTS

HW was supported by a scholarship of the Natural Environmental Research Council (NE/K500975/1). JH thanks NSF OCE 13-35838 for funding this research. We thank Meredith Ross and Qian Liu for their work generating the Thaumarchaea abundance data. We also thank Jacob Shalack, the skipper of the RV Salty Dawg, supported by NSF OCE 12-37140, for his assistance in sample collection. This is publication 1048 from the University of Georgia Marine Institute. CvdB is grateful for on-going support from the University of Liverpool.

SUPPLEMENTARY MATERIAL

The Supplementary Material for this article can be found online at: <http://journal.frontiersin.org/article/10.3389/fmars.2017.00178/full#supplementary-material>

- Amin, S. A., Moffett, J. W., Martens-Habbena, W., Jacquot, J. E., Han, Y., Devol, A., et al. (2013). Copper requirements of the ammonia-oxidizing archaeon *Nitrosopumilus maritimus* SCM1 and implications for nitrification in the marine environment. *Limnol. Oceanogr.* 58, 2037–2045. doi: 10.4319/lo.2013.58.6.2037
- Anderson, D. M., and Morel, F. M. M. (1978). Copper sensitivity of *Gonyaulax tamerensis*. *Limnol. Oceanogr.* 23, 283–295. doi: 10.4319/lo.1978.23.2.0283
- Annett, A. L., Lapi, S., Ruth, T. J., and Maldonado, M. T. (2008). The effects of Cu and Fe availability on the growth and Cu: C ratios of marine diatoms. *Limnol. Oceanogr.* 53, 2451–2461. doi: 10.4319/lo.2008.53.6.2451
- Apte, S. C., Gardner, M. J., and Ravenscroft, J. E. (1988). An evaluation of voltammetric titration procedures for the determination of trace-metal

- complexation in natural-waters by use of computer-simulation. *Anal. Chim. Acta* 212, 1–21. doi: 10.1016/S0003-2670(00)84124-0
- Arnon, D. I. (1949). Copper enzymes in isolated chloroplasts. Polyphenoloxidase in *Beta vulgaris*. *Plant Physiol.* 24, 1–15. doi: 10.1104/pp.24.1.1
- Averett, R. C., Leenheer, J. A., McKnight, D. M., and Thorn, K. A. (1994). *Humic Substances in the Suwannee River, Georgia: Interactions, Properties, and Proposed Structures*. U.S. Geological Water-Supply Paper 2373, U.S. Geological Survey.
- Bacic, M. K., Newell, S. Y., and Yoch, D. C. (1998). Release of dimethylsulfide from dimethylsulfoniopropionate by plant-associated salt marsh fungi. *Appl. Environ. Microbiol.* 64, 1484–1489.
- Bano, N., and Hollibaugh, J. T. (2002). Phylogenetic composition of bacterioplankton assemblages from the Arctic Ocean. *Appl. Environ. Microbiol.* 68, 505–518. doi: 10.1128/AEM.68.2.505-518.2002
- Barman, M. K., Sinha, A. K., and Nembenna, S. (2016). An efficient and recyclable thiourea-supported copper(I) chloride catalyst for azide-alkyne cycloaddition reactions. *Green Chem.* 18, 2534–2541. doi: 10.1039/C5GC02545A
- Beck, N. G., Bruland, K. W., and Rue, E. L. (2002). Short-term biogeochemical influence of a diatom bloom on the nutrient and trace metal concentrations in South San Francisco bay microcosm experiments. *Estuaries* 25, 1063–1076. doi: 10.1007/BF02692204
- Bedsworth, W. W., and Sedlak, D. L. (1999). Sources and environmental fate of strongly complexed nickel in estuarine waters: the role of ethylenediaminetetraacetate. *Environ. Sci. Technol.* 33, 926–931. doi: 10.1021/es9809556
- Beman, J. M., Sachdeva, R., and Fuhrman, J. A. (2010). Population ecology of nitrifying Archaea and Bacteria in the Southern California Bight. *Environ. Microbiol.* 12, 1282–1292. doi: 10.1111/j.1462-2920.2010.02172.x
- Benner, R. (2002). *Chemical Composition and Reactivity*. San Diego, CA: Elsevier.
- Berman, T. (1983). Phosphorus uptake by microplankton in estuarine and coastal shelf waters near Sapelo Island, Georgia, USA. *Estuaries* 6, 160–166. doi: 10.2307/1351706
- Brand, L. E., Sunda, W. G., and Guillard, R. R. L. (1986). Reduction of marine-phytoplankton reproduction rates by copper and Cadmium. *J. Exp. Mar. Biol. Ecol.* 96, 225–250. doi: 10.1016/0022-0981(86)90205-4
- Buchan, A., Newell, S. Y., Butler, M., Biers, E. J., Hollibaugh, J. T., and Moran, M. A. (2003). Dynamics of bacterial and fungal communities on decaying salt marsh grass. *Appl. Environ. Microbiol.* 69, 6676–6687. doi: 10.1128/AEM.69.11.6676-6687.2003
- Buck, K. N., and Bruland, K. W. (2005). Copper speciation in San Francisco Bay: a novel approach using multiple analytical windows. *Mar. Chem.* 96, 185. doi: 10.1016/j.marchem.2005.01.001
- Buck, K. N., Moffett, J., Barbeau, K. A., Bundy, R. M., Kondo, Y., and Wu, J. F. (2012). The organic complexation of iron and copper: an intercomparison of competitive ligand exchange-adsorptive cathodic stripping voltammetry (CLE-ACSV) techniques. *Limnol. Oceanogr. Methods* 10, 496–515. doi: 10.4319/lom.2012.10.496
- Buerge-Weirich, D., and Sulzberger, B. (2004). Formation of Cu(I) in estuarine and marine waters: application of a new solid-phase extraction method to measure Cu(I). *Environ. Sci. Technol.* 38, 1843–1848. doi: 10.1021/es034845x
- Bundy, R. M., Abdulla, H. A. N., Hatcher, P. G., Biller, D. V., Buck, K. N., and Barbeau, K. A. (2015). Iron-binding ligands and humic substances in the San Francisco Bay estuary and estuarine-influenced shelf regions of coastal California. *Mar. Chem.* 173, 183–194. doi: 10.1016/j.marchem.2014.11.005
- Bundy, R. M., Barbeau, K. A., and Buck, K. N. (2013). Sources of strong copper-binding ligands in Antarctic Peninsula surface waters. *Deep Sea Res. Part II Top. Stud. Oceanogr.* 90, 134–146. doi: 10.1016/j.dsr2.2012.07.023
- Campos, M., and van den berg, C. M. G. (1994). Determination of copper complexation in sea-water by cathodic stripping voltammetry and ligand competition with salicylaldehyde. *Anal. Chim. Acta* 284, 481–496. doi: 10.1016/0003-2670(94)85055-0
- Casassas, E., Arino, C., and Esteban, M. (1985). Cathodic stripping voltammetry of 2-mercaptoethanol. *Anal. Chim. Acta* 176, 113–119. doi: 10.1016/S0003-2670(00)81638-4
- Chapman, C. S., Capodaglio, G., Turetta, C., and van den Berg, C. M. G. (2009). Benthic fluxes of copper, complexing ligands and thiol compounds in shallow lagoon waters. *Mar. Environ. Res.* 67, 17–24. doi: 10.1016/j.marenvres.2008.07.010
- Church, M. J., Delong, E. F., Ducklow, H. W., Karner, M. B., Preston, C. M., and Karl, D. M. (2003). Abundance and distribution of planktonic Archaea and Bacteria in the waters west of the Antarctic Peninsula. *Limnol. Oceanogr.* 48, 1893–1902. doi: 10.4319/lo.2003.48.5.1893
- Croot, P. L. (2003). Seasonal cycle of copper speciation in Gullmar Fjord, Sweden. *Limnol. Oceanogr.* 48, 764–776. doi: 10.4319/lo.2003.48.2.0764
- Croot, P. L., Moffett, J. W., and Brand, L. E. (2000). Production of extracellular Cu complexing ligands by eucaryotic phytoplankton in response to Cu stress. *Limnol. Oceanogr.* 45, 619–627. doi: 10.4319/lo.2000.45.3.0619
- Donat, J. R., Lao, K. A., and Bruland, K. W. (1994). Speciation of dissolved copper and nickel in South San-Francisco Bay - a multimethod approach. *Anal. Chim. Acta* 284, 547–571. doi: 10.1016/0003-2670(94)85061-5
- Dryden, C. L., Gordon, A. S., and Donat, J. R. (2007). Seasonal survey of copper-complexing ligands and thiol compounds in a heavily utilized, urban estuary: Elizabeth River, Virginia. *Mar. Chem.* 103, 276–288. doi: 10.1016/j.marchem.2006.09.003
- Dupont, C. L., and Ahner, B. A. (2005). Effects of copper, cadmium, and zinc on the production and exudation of thiols by *Emiliania huxleyi*. *Limnol. Oceanogr.* 50, 508–515. doi: 10.4319/lo.2005.50.2.0508
- Dupont, C. L., Moffett, J. W., Bidigare, R. R., and Ahner, B. A. (2006). Distributions of dissolved and particulate biogenic thiols in the subtropical Pacific Ocean. *Deep Sea Res. Part I Oceanogr. Res. Pap.* 53, 1961–1974. doi: 10.1016/j.dsr.2006.09.003
- El Ghazouani, A., Basle, A., Gray, J., Graham, D. W., Firbank, S. J., and Dennison, C. (2012). Variations in methanobactin structure influences copper utilization by methane-oxidizing bacteria. *Proc. Natl. Acad. Sci. U.S.A.* 109, 8400–8404. doi: 10.1073/pnas.1112921109
- Fallon, R. D., Newell, S. Y., Sherr, B. F., and Sherr, E. B. (1986). Factors affecting bacterial biomass and growth in the Duplin River estuary and coastal Atlantic Ocean. *Ifremer Actes de Colloques* 3, 137–145.
- Francis, C. A., Roberts, K. J., Beman, J. M., Santoro, A. E., and Oakley, B. B. (2005). Ubiquity and diversity of ammonia-oxidizing archaea in water columns and sediments of the ocean. *Proc. Natl. Acad. Sci. U.S.A.* 102, 14683–14688. doi: 10.1073/pnas.0506625102
- Gifford, S. M., Sharma, S., Booth, M., and Moran, M. A. (2013). Expression patterns reveal niche diversification in a marine microbial assemblage. *ISME J.* 7, 281–298. doi: 10.1038/ismej.2012.96
- Gifford, S. M., Sharma, S., Rinta-Kanto, J. M., and Moran, M. A. (2011). Quantitative analysis of a deeply sequenced marine microbial metatranscriptome. *ISME J.* 5, 461–472. doi: 10.1038/ismej.2010.141
- Glass, J. B., and Orphan, V. J. (2012). Trace metal requirements for microbial enzymes involved in the production and consumption of methane and nitrous oxide. *Front. Microbiol.* 3:61. doi: 10.3389/fmicb.2012.00061
- Gordon, A. S., Donat, J. R., Kango, R. A., Dyer, B. J., and Stuart, L. M. (2000). Dissolved copper-complexing ligands in cultures of marine bacteria and estuarine water. *Mar. Chem.* 70, 149–160. doi: 10.1016/S0304-4203(00)00019-0
- Guan, J., Yan, B., Zhu, H., Wang, L., Lu, D., and Cheng, L. (2015). Flux characteristics of total dissolved iron and its species during extreme rainfall event in the midstream of the Heilongjiang river. *J. Environ. Sci.* 30, 74–80. doi: 10.1016/j.jes.2014.10.009
- Guo, J., Annett, A. L., Taylor, R. L., Lapi, S., Ruth, T. J., and Maldonado, M. T. (2010). Copper-uptake kinetics of coastal and oceanic diatoms. *J. Phycol.* 46, 1218–1228. doi: 10.1111/j.1529-8817.2010.00911.x
- Hakemian, A. S., Tinberg, C. E., Kondapalli, K. C., Telser, J., Hoffman, B. M., Stemmler, T. L., et al. (2005). The copper chelator methanobactin from *Methylosinus trichosporium* OB3b binds copper(I). *J. Am. Chem. Soc.* 127, 17142–17143. doi: 10.1021/ja0558140
- Herndl, G. J., Reinthaler, T., Teira, E., van Aken, H., Veth, C., Pernthaler, A., et al. (2005). Contribution of Archaea to total prokaryotic production in the deep Atlantic Ocean. *Appl. Environ. Microbiol.* 71, 2303–2309. doi: 10.1128/AEM.71.5.2303-2309.2005
- Hodson, R. E. (2005). *December 2003 Surface Water Dissolved Organic Carbon Concentrations at Ten Georgia Coastal Ecosystems LTER Sampling Sites*. Georgia Coastal Ecosystems LTER Data Catalog.
- Hollibaugh, J. T., Gifford, S. M., Moran, M. A., Ross, M. J., Sharma, S., and Tolar, B. E. (2014). Seasonal variation in the metatranscriptomes of a Thaumarchaeota population from SE USA coastal waters. *ISME J.* 8, 685–698. doi: 10.1038/ismej.2013.171

- Ingalls, A. E., Shah, S. R., Hansman, R. L., Aluwihare, L. I., Santos, G. M., Druffel, E. R. M., et al. (2006). Quantifying archaeal community autotrophy in the mesopelagic ocean using natural radiocarbon. *Proc. Natl. Acad. Sci. U.S.A.* 103, 6442–6447. doi: 10.1073/pnas.0510157103
- Jacquot, J. E., Horak, R. E. A., Amin, S. A., Devol, A. H., Ingalls, A. E., Armbrust, E. V., et al. (2014). Assessment of the potential for copper limitation of ammonia oxidation by Archaea in a dynamic estuary. *Mar. Chem.* 162, 37–49. doi: 10.1016/j.marchem.2014.02.002
- Jones, G. J., Waite, T. D., and Smith, J. D. (1985). Light-dependent reduction of copper(II) and its effect on cell-mediated, thiol-dependent superoxide production. *Biochem. Biophys. Res. Commun.* 128, 1031–1036. doi: 10.1016/0006-291X(85)90151-2
- Kalanetra, K. M., Bano, N., and Hollibaugh, J. T. (2009). Ammonia-oxidizing Archaea in the Arctic Ocean and Antarctic coastal waters. *Environ. Microbiol.* 11, 2434–2445. doi: 10.1111/j.1462-2920.2009.01974.x
- Karner, M. B., Delong, E. F., and Karl, D. M. (2001). Archaeal dominance in the mesopelagic zone of the Pacific Ocean. *Nature* 409, 507–510. doi: 10.1038/35054051
- Kiehn, W. M., and Morris, J. T. (2010). Variability in dimethylsulfoniopropionate (DMSP) concentrations in *Spartina alterniflora* and the effect on *Littoraria irrorata*. *Mar. Ecol. Prog. Ser.* 406, 47–55. doi: 10.3354/meps08548
- Kiene, R. P., Malloy, K. D., and Taylor, B. F. (1990). Sulfur-containing amino-acids as precursors of thiols in anoxic coastal sediments. *Appl. Environ. Microbiol.* 56, 156–161.
- Kim, H. J., Graham, D. W., Dispirito, A. A., Alterman, M. A., Galeva, N., Larive, C. K., et al. (2004). Methanobactin, a copper-acquisition compound from methane-oxidizing bacteria. *Science* 305, 1612–1615. doi: 10.1126/science.1098322
- Kitajima, N., Fujisawa, K., and Morooka, Y. (1990). Formation and characterization of a mononuclear (acylperoxo)copper(II) complex. *Inorg. Chem.* 29, 357–358. doi: 10.1021/ic00328a001
- Kogut, M. B., and Voelker, B. M. (2001). Strong copper-binding behavior of terrestrial humic substances in seawater. *Environ. Sci. Technol.* 35, 1149–1156. doi: 10.1021/es0014584
- Konigsberger, L. C., Konigsberger, E., Hefter, G., and May, P. M. (2015). Formation constants of copper(I) complexes with cysteine, penicillamine and glutathione: implications for copper speciation in the human eye. *Dalton Trans.* 44, 20413–20425. doi: 10.1039/C5DT02129D
- Kraemer, S. M., Duckworth, O. W., Harrington, J. M., and Schenkeveld, W. D. C. (2015). Metallophores and trace metal biogeochemistry. *Aquat. Geochem.* 21, 159–195. doi: 10.1007/s10498-014-9246-7
- Laglera, L. M., Battaglia, G., and van den Berg, C. M. G. (2011). Effect of humic substances on the iron speciation in natural waters by CLE/CSV. *Mar. Chem.* 127, 134–143. doi: 10.1016/j.marchem.2011.09.003
- Laglera, L. M., Downes, J., Tovar-Sanchez, A., and Monticelli, D. (2014). Cathodic pseudopolarography: a new tool for the identification and quantification of cysteine, cystine and other low molecular weight thiols in seawater. *Anal. Chim. Acta* 836, 24–33. doi: 10.1016/j.aca.2014.05.026
- Laglera, L. M., and Tovar-Sanchez, A. (2012). Direct recognition and quantification by voltammetry of thiol/thioamide mixes in seawater. *Talanta* 89, 496–504. doi: 10.1016/j.talanta.2011.12.075
- Laglera, L. M., and van den Berg, C. M. G. (2003). Copper complexation by thiol compounds in estuarine waters. *Mar. Chem.* 82, 71–89. doi: 10.1016/S0304-4203(03)00053-7
- Laglera, L. M., and van den Berg, C. M. G. (2006). Photochemical oxidation of thiols and copper complexing ligands in estuarine waters. *Mar. Chem.* 101, 130–140. doi: 10.1016/j.marchem.2006.01.006
- Leal, M. F. C., and van den Berg, C. M. G. (1998). Evidence for strong copper(I) complexation by organic ligands in seawater. *Aquat. Geochem.* 4, 49–75. doi: 10.1023/A:1009653002399
- Leal, M. F. C., Vasconcelos, M., and van den Berg, C. M. G. (1999). Copper-induced release of complexing ligands similar to thiols by *Emiliania huxleyi* in seawater cultures. *Limnol. Oceanogr.* 44, 1750–1762. doi: 10.4319/lo.1999.44.7.1750
- Le Gall, A.-C., and van den Berg, C. M. G. (1993). Cathodic stripping voltammetry of glutathione in natural waters. *Analyst* 118, 1411–1415. doi: 10.1039/an931801411
- Le Gall, A.-C., and van den Berg, C. M. G. (1998). Folic acid and glutathione in the water column of the North East Atlantic. *Deep Sea Res. Part I Oceanogr. Res. Pap.* 45, 1903–1918. doi: 10.1016/S0967-0637(98)00042-9
- Lu, X. X., Sun, S. L., Zhang, Y. Q., Hollibaugh, J. T., and Mou, X. Z. (2015). Temporal and vertical distributions of bacterioplankton at the Gray's Reef National Marine Sanctuary. *Appl. Environ. Microbiol.* 81, 910–917. doi: 10.1128/AEM.02802-14
- Luther, G. W., Church, T. M., and Powell, D. (1991). Sulfur speciation and sulfide oxidation in the water column of the black sea. *Deep Sea Res. Part A Oceanogr. Res. Pap.* 38, S1121–S1137.
- Maldonado, M. T., Allen, A. E., Chong, J. S., Lin, K., Leus, D., Karpenko, N., et al. (2006). Copper-dependent iron transport in coastal and oceanic diatoms. *Limnol. Oceanogr.* 51, 1729–1743. doi: 10.4319/lo.2006.51.4.1729
- McKnight, D. M., and Aiken, G. R. (1998). "Sources and age of aquatic humus," in *Aquatic Humic Substances: Ecology and Biogeochemistry*, eds D. Hessen and L. Tranvik (Berlin: Springer-Verlag), 9–39.
- Medeiros, P. M., Babcock-Adams, L., Seidel, M., Castelao, R. M., Di Lorio, D., Hollibaugh, J. T., et al. (2017). Export of terrigenous dissolved organic matter across a broad continental shelf. *Limnol. Oceanogr.* doi: 10.1002/lno.10528. [Epub ahead of print].
- Miller, L. A., and Bruland, K. W. (1997). Competitive equilibration techniques for determining transition metal speciation in natural waters: Evaluation using model data. *Anal. Chim. Acta* 343, 161–181. doi: 10.1016/S0003-2670(96)00565-X
- Misumi, K., Lindsay, K., Moore, J. K., Doney, S. C., Tsumune, D., and Yoshida, Y. (2013). Humic substances may control dissolved iron distributions in the global ocean: Implications from numerical simulations. *Global Biogeochem. Cycles* 27, 450–462. doi: 10.1002/gbc.20039
- Moffett, J. W. (1995). Temporal and spatial variability of copper complexation by strong chelators in the sargasso-sea. *Deep Sea Res. Part I Oceanogr. Res. Pap.* 42, 1273–1295. doi: 10.1016/0967-0637(95)00060-J
- Moffett, J. W., and Dupont, C. (2007). Cu complexation by organic ligands in the sub-arctic NW Pacific and Bering Sea. *Deep Sea Res. Part I Oceanogr. Res. Pap.* 54, 586–595. doi: 10.1016/j.dsr.2006.12.013
- Moffett, J. W., Tuit, C. B., and Ward, B. B. (2012). Chelator-induced inhibition of copper metalloenzymes in denitrifying bacteria. *Limnol. Oceanogr.* 57, 272–280. doi: 10.4319/lo.2012.57.1.0272
- Moffett, J. W., and Zika, R. G. (1988). Measurement of copper(I) in surface waters of the sub-tropical Atlantic and Gulf of Mexico. *Geochim. Cosmochim. Acta* 52, 1849–1857. doi: 10.1016/0016-7037(88)90008-7
- Moffett, J. W., Zika, R. G., and Brand, L. E. (1990). Distribution and potential sources and sinks of copper chelators in the Sargasso Sea. *Deep Sea Res. Part A Oceanogr. Res. Pap.* 37, 27–36. doi: 10.1016/0198-0149(90)90027-S
- Moingt, M., Bressac, M., Belanger, D., and Amyot, M. (2010). Role of ultraviolet radiation, mercury and copper on the stability of dissolved glutathione in natural and artificial freshwater and saltwater. *Chemosphere* 80, 1314–1320. doi: 10.1016/j.chemosphere.2010.06.041
- Monticelli, D., and Caprara, S. (2015). Voltammetric tools for trace element speciation in fresh waters: methodologies, outcomes and future perspectives. *Environ. Chem.* 12, 683–705. doi: 10.1071/EN14233
- Moskalski, S. M., Torres, R., Bizimis, M., Goni, M., Bergamaschi, B., and Fleck, J. (2013). Low-tide rainfall effects on metal content of suspended sediment in the Sacramento-San Joaquin Delta. *Cont. Shelf Res.* 56, 39–55. doi: 10.1016/j.csr.2013.02.001
- Muggli, D. L., and Harrison, P. J. (1996). EDTA suppresses the growth of oceanic phytoplankton from the Northeast Subarctic Pacific. *J. Exp. Mar. Biol. Ecol.* 205, 221–227. doi: 10.1016/S0022-0981(96)02611-1
- Muller, F. L. L., and Batchelli, S. (2013). Copper binding by terrestrial versus marine organic ligands in the coastal plume of River Thurso, North Scotland. *Estuar. Coast. Shelf Sci.* 133, 137–146. doi: 10.1016/j.ecss.2013.08.024
- NOAA (2015). *Old Tower, Sapelo Island, Doboy Sound, GA (US) Stationid: 8675622. Tides and Currents, NOAA.gov.* Available online at: <http://www.tidesandcurrents.noaa.gov/noaatidepredictions/viewDailyPredictions.jsp?bmon=12&bday=15&byear=2015&timelength=daily&timeZone=2&dataUnits=0&datum=MLLW&timeUnits=2&interval=highlow&format=Submit&Stationid=8675622>
- Nelson, A., and Mantoura, R. F. C. (1984). Voltammetry of copper species in estuarine waters. Part I. Electrochemistry of copper species in chloride media. *J. Electroanal. Chem.* 164, 237–252. doi: 10.1016/S0022-0728(84)80209-0

- Newell, S. Y. (2001). Multiyear patterns of fungal biomass dynamics and productivity within naturally decaying smooth cordgrass shoots. *Limnol. Oceanogr.* 46, 573–583. doi: 10.4319/lo.2001.46.3.0573
- Nieboer, E., and Richardson, D. H. S. (1980). The replacement of the non-descript term heavy-metals by a biologically and chemically significant classification of metal-ions. *Environ. Poll. B Chem. Phys.* 1, 3–26. doi: 10.1016/0143-148X(80)90017-8
- Oldham, V. E., Swenson, M. M., and Buck, K. N. (2014). Spatial variability of total dissolved copper and copper speciation in the inshore waters of Bermuda. *Mar. Pollut. Bull.* 79, 314–320. doi: 10.1016/j.marpolbul.2013.12.016
- Omanovic, D., Gamier, C., and Pizeta, I. (2015). ProMCC: an all-in-one tool for trace metal complexation studies. *Mar. Chem.* 173, 25–39. doi: 10.1016/j.marchem.2014.10.011
- Peers, G., and Price, N. M. (2006). Copper-containing plastocyanin used for electron transport by an oceanic diatom. *Nature* 441, 341–344. doi: 10.1038/nature04630
- Peers, G., Quesnel, S. A., and Price, N. M. (2005). Copper requirements for iron acquisition and growth of coastal and oceanic diatoms. *Limnol. Oceanogr.* 50, 1149–1158. doi: 10.4319/lo.2005.50.4.1149
- Pomeroy, L. R., Wiegert, R. G., and Wiebe, W. J. (1981). *The Ecology of a Salt Marsh*. New York, NY: Springer-Verlag New York Inc.
- Radford-Knoery, J., and Cutter, G. A. (1994). Biogeochemistry of dissolved hydrogen sulfide species and carbonyl sulfide in the western North Atlantic Ocean. *Geochim. Cosmochim. Acta* 58, 5421–5431. doi: 10.1016/0016-7037(94)90239-9
- Rijstenbil, J. W., Haritonidis, S., Malea, P., Seferlis, M., and Wijnholds, J. A. (1998). Thiol pools and glutathione redox ratios as possible indicators of copper toxicity in the green macroalgae *Enteromorpha* spp. from the scheldt estuary (SW Netherlands, Belgium) and Thermaikos Gulf (Greece, N Aegean Sea). *Hydrobiologia* 385, 171–181. doi: 10.1023/A:1003502428466
- Sander, S. G., Koschinsky, A., Massoth, G., Stott, M., and Hunter, K. A. (2007). Organic complexation of copper in deep-sea hydrothermal vent systems. *Environ. Chem.* 4, 81–89. doi: 10.1071/EN06086
- Santoro, A. E., and Casciotti, K. L. (2011). Enrichment and characterization of ammonia-oxidizing archaea from the open ocean: phylogeny, physiology and stable isotope fractionation. *ISME J.* 5, 1796–1808. doi: 10.1038/ismej.2011.58
- Semeniuk, D. M., Bundy, R. M., Payne, C. D., Barbeau, K. A., and Maldonado, M. T. (2015). Acquisition of organically complexed copper by marine phytoplankton and bacteria in the northeast subarctic Pacific Ocean. *Mar. Chem.* 173, 222–233. doi: 10.1016/j.marchem.2015.01.005
- Semeniuk, D. M., Cullen, J. T., Johnson, W. K., Gagnon, K., Ruth, T. J., and Maldonado, M. T. (2009). Plankton copper requirements and uptake in the subarctic Northeast Pacific Ocean. *Deep Sea Res. Part I Oceanogr. Res. Pap.* 56, 1130–1142. doi: 10.1016/j.dsr.2009.03.003
- Sharma, V. K., and Millero, F. J. (1988). Effect of ionic interactions on the rates of oxidation of Cu(I) with O₂ in natural waters. *Mar. Chem.* 25, 141–161. doi: 10.1016/0304-4203(88)90061-8
- Sholkovitz, E. R. (1976). Flocculation of dissolved organic and inorganic matter during mixing of river water and seawater. *Geochim. Cosmochim. Acta* 40, 831–845. doi: 10.1016/0016-7037(76)90035-1
- Smith, S. V., and Hollibaugh, J. T. (1993). Coastal metabolism and the oceanic organic-carbon balance. *Rev. Geophys.* 31, 75–89. doi: 10.1029/92RG02584
- Sunda, W. G., and Guillard, R. R. L. (1976). Relationship between cupric ion activity and toxicity of copper to phytoplankton. *J. Mar. Res.* 34, 511–529.
- Suzuki, M. T., Taylor, L. T., and Delong, E. F. (2000). Quantitative analysis of small-subunit rRNA genes in mixed microbial populations via 5'-nuclease assays. *Appl. Environ. Microbiol.* 66, 4605–4614. doi: 10.1128/AEM.66.11.4605-4614.2000
- Swarr, G. J., Kading, T., Lamborg, C. H., Hammerschmidt, C. R., and Bowman, K. L. (2016). Dissolved low-molecular weight thiol concentrations from the U.S. GEOTRACES North Atlantic Ocean zonal transect. *Deep Sea Res. Part I Oceanogr. Res. Pap.* 116, 77–87. doi: 10.1016/j.dsr.2016.06.003
- Tang, D. G., Hung, C. C., Warnken, K. W., and Santschi, P. H. (2000). The distribution of biogenic thiols in surface waters of Galveston Bay. *Limnol. Oceanogr.* 45, 1289–1297. doi: 10.4319/lo.2000.45.6.1289
- Tolar, B. B., King, G. M., and Hollibaugh, J. T. (2013). An analysis of thaumarchaeota populations from the northern gulf of Mexico. *Front. Microbiol.* 4:72. doi: 10.3389/fmicb.2013.00072
- Tolar, B. B., Powers, L. C., Miller, W. L., Wallsgrove, N. J., Popp, B. N., and Hollibaugh, J. T. (2016a). Ammonia oxidation in the ocean can be inhibited by nanomolar concentrations of hydrogen peroxide. *Front. Mar. Sci.* 3:237. doi: 10.3389/fmars.2016.00237
- Tolar, B. B., Ross, M. J., Wallsgrove, N. J., Liu, Q., Aluwihare, L. I., Popp, B. N., et al. (2016b). Contribution of ammonia oxidation to chemoautotrophy in Antarctic coastal waters. *ISME J.* 10, 2605–2619. doi: 10.1038/ismej.2016.61
- Tolar, B. B., Wallsgrove, N. J., Popp, B. N., and Hollibaugh, J. T. (2016c). Oxidation of urea-derived nitrogen by Thaumarchaeota-dominated marine nitrifying communities. *Environ. Microbiol.* doi: 10.1111/1462-2920.13457. [Epub ahead of print].
- van den Berg, C. M. (2014). *UV Digestion Apparatus*. Available online at: http://pcwww.liv.ac.uk/~sn35/Site/UV_digestion_apparatus.html/journalabbrev 2014
- van den Berg, C. M. G. (1982). Determination of copper complexation with natural organic ligands in seawater by equilibration with MnO₂ II. Experimental procedures and application to surface seawater. *Mar. Chem.* 11, 323–342. doi: 10.1016/0304-4203(82)90029-9
- van den Berg, C. M. G. (1984). Determination of the complexing capacity and conditional stability constants of complexes of copper(II) with natural organic ligands in seawater by cathodic stripping voltammetry of copper-catechol complex ions. *Mar. Chem.* 15, 1–18. doi: 10.1016/0304-4203(84)90035-5
- van den Berg, C. M. G., Househam, B. C., and Riley, J. P. (1988). Determination of cystine and cysteine in seawater using cathodic stripping voltammetry in the presence of Cu(II). *J. Electroanal. Chem.* 239, 137–148. doi: 10.1016/0022-0728(88)80275-4
- Walker, C. B., De La Torre, J. R., Klotz, M. G., Urakawa, H., Pinel, N., Arp, D. J., et al. (2010). *Nitrosopumilus maritimus* genome reveals unique mechanisms for nitrification and autotrophy in globally distributed marine crenarchaea. *Proc. Natl. Acad. Sci. U.S.A.* 107, 8818–8823. doi: 10.1073/pnas.0913531107
- Walsh, M. J., and Ahner, B. A. (2013). Determination of stability constants of Cu(I), Cd(II) & Zn(II) complexes with thiols using fluorescent probes. *J. Inorg. Biochem.* 128, 112–123. doi: 10.1016/j.jinorgbio.2013.07.012
- Walsh, M. J., Goodnow, S. D., Vezeau, G. E., Richter, L. V., and Ahner, B. A. (2015). Cysteine enhances bioavailability of copper to marine phytoplankton. *Environ. Sci. Technol.* 49, 12145–12152. doi: 10.1021/acs.est.5b02112
- Wells, M., Buck, K. N., and Sander, S. G. (2013). New approach to analysis of voltammetric ligand titration data improves understanding of metal speciation in natural waters. *Limnol. Oceanogr. Methods* 11, 450–465. doi: 10.4319/lom.2013.11.450
- Whitby, H., and van den Berg, C. M. G. (2015). Evidence for copper-binding humic substances in seawater. *Mar. Chem.* 173, 282–290. doi: 10.1016/j.marchem.2014.09.011
- Williams, R. B. (1964). Division rates of salt-marsh diatoms in relation to salinity + cell-size. *Ecology* 45, 877–880. doi: 10.2307/1934940
- Wuchter, C., Abbas, B., Coolen, M. J. L., Herfort, L., VAN Bleijswijk, J., Timmers, P., et al. (2006). Archaeal nitrification in the ocean. *Proc. Natl. Acad. Sci. U.S.A.* 103, 12317–12322. doi: 10.1073/pnas.0600756103
- Yang, R., and van den Berg, C. M. (2009). Metal complexation by humic substances in seawater. *Environ. Sci. Technol.* 43, 7192–7197. doi: 10.1021/es900173w
- Zhang, J. Z., Wang, F. Y., House, J. D., and Page, B. (2004). Thiols in wetland interstitial waters and their role in mercury and methylmercury speciation. *Limnol. Oceanogr.* 49, 2276–2286. doi: 10.4319/lo.2004.49.6.2276

Conflict of Interest Statement: The authors declare that the research was conducted in the absence of any commercial or financial relationships that could be construed as a potential conflict of interest.

Copyright © 2017 Whitby, Hollibaugh and van den Berg. This is an open-access article distributed under the terms of the Creative Commons Attribution License (CC BY). The use, distribution or reproduction in other forums is permitted, provided the original author(s) or licensor are credited and that the original publication in this journal is cited, in accordance with accepted academic practice. No use, distribution or reproduction is permitted which does not comply with these terms.



Distribution and Speciation of Dissolved Iron in Jiaozhou Bay (Yellow Sea, China)

Han Su¹, Rujun Yang^{1*}, Ivanka Pižeta², Dario Omanović², Shirong Wang¹ and Yan Li¹

¹ College of Chemistry and Chemical Engineering, Ocean University of China, Qingdao, China, ² Division for Marine and Environmental Research, Ruđer Bošković Institute, Zagreb, Croatia

OPEN ACCESS

Edited by:

Antonio Tovar-Sanchez,
Consejo Superior de Investigaciones
Científicas, Spain

Reviewed by:

Loes Gerringa,
NIOZ-Royal Netherlands Institute for
Sea Research, Netherlands
Constant Marius G. Van Den Berg,
University of Liverpool, UK

*Correspondence:

Rujun Yang
yangrj@ouc.edu.cn

Specialty section:

This article was submitted to
Marine Biogeochemistry,
a section of the journal
Frontiers in Marine Science

Received: 31 January 2016

Accepted: 03 June 2016

Published: 17 June 2016

Citation:

Su H, Yang R, Pižeta I, Omanović D,
Wang S and Li Y (2016) Distribution
and Speciation of Dissolved Iron in
Jiaozhou Bay (Yellow Sea, China).
Front. Mar. Sci. 3:99.
doi: 10.3389/fmars.2016.00099

The distribution of total dissolved iron (DFe) and its chemical speciation were studied in vertical profiles of the shallow and semi-closed Jiaozhou Bay (JZB, China) during two contrasting periods: summer (July 19th, 2011) and spring (May 10th, 2012). Samples collected from the surface, middle and bottom layers were analyzed by competitive ligand exchange-adsorptive cathodic stripping voltammetry (CLE-aCSV). The mean DFe concentration during the summer period (median 18.8 nM; average 20.7 nM) was higher than in the spring period (median 12.4 nM; average 16.9 nM), whereas the spatio-temporal variation in spring was larger than in summer. The DFe-values showed distinct regional and seasonal differences, ranging from 5.6 to 107 nM in spring period and 13.4 to 43.4 nM in summer period. In spring, the highest DFe-values were observed in the eastern coastal region, especially near an industrial area (up to 107 nM), whereas the DFe distribution in summer was relatively even. Due to a tide influence, the vertical variations in the DFe and L_t in both seasons were not significant. On average, the L_t concentration (one class of ligand was estimated in all samples), was higher in spring (35.2 ± 23.4 nM) than in summer (31.1 ± 10.3 nM). A statistically significant correlation was found between L_t and DFe concentrations, it was higher for the summer period than for the spring period. The conditional stability constants (logK') of organic complexes with iron were weaker in spring (11.7 ± 0.3) than in summer (12.3 ± 0.3). The concentrations of L_t were higher in comparison to DFe in all samples: the average [L_t]/[DFe] ratio in the spring and summer samples was 2.4 and 1.5, respectively. Speciation calculations showed that the DFe in the JZB existed predominantly (over 99.99%) in the form of strong organic complexes in both seasons.

Keywords: dissolved iron, organic ligand, horizontal and vertical distribution, speciation, coastal water, the Jiaozhou Bay (JZB)

INTRODUCTION

Iron (Fe) is an essential trace element in marine environments and plays an important role in the biochemistry and physiology of phytoplankton (Martin and Fitzwater, 1988; Sunda et al., 1991). The world's surface HNLC (high nutrient low chlorophyll) oceans area has influenced phytoplankton growth due to low concentration of iron (Coale, 2004). In the 1990's, Martin hypothesized that the low concentration of iron in oceans across the globe limited the absorption

of CO₂ from the atmosphere and subsequently had an important influence on the global climate (Martin, 1990). After that, iron fertilizing experiments were arranged in the HNLC area (Boyd et al., 2007; Buesseler et al., 2008). The results indicated that in the HNLC area, the addition of iron increased the growth of marine phytoplankton and also influenced local CO₂ absorption and nutrient consumption (biogeochemical cycles of carbon, Boyd et al., 2007).

It has been shown that not only low concentrations, but also low bio-availability of dissolved iron may limit the growth of marine organisms (Morel et al., 1991; Sunda et al., 1991; Poorvin et al., 2004). Since ~99.9% of the dissolved iron (DFe) is complexed by strong organic ligands (Rue and Bruland, 1995; van den Berg, 1995), not all is equally bioavailable. It is known that ligand-complexed iron is available and taken up by organisms, for example eukaryotic phytoplankton assimilating porphyrin-complexed iron and prokaryotes uptaking siderophore-complexed iron (Hutchins et al., 1999). On the other hand, Fe-binding organic ligands (L_t) buffer DFe concentrations by preventing the formation of insoluble oxy-hydroxides (Rue and Bruland, 1995; Wu and Luther, 1995; Kuma et al., 1996; Mawji et al., 2008), because Fe-organic complexes have higher stability constants than inorganic ones (Hudson and Morel, 1993; Nagai et al., 2007). Therefore, the character of L_t plays an important role in the biogeochemical cycles of iron in global open oceans (Buck et al., 2007).

The concentrations of L_t vary widely in marine environment: for open oceans, L_t concentration is low, e.g., 0.44 nM was observed in Indian Sector of the Southern Ocean (Gerringa et al., 2008), 17.6 nM was observed in the Atlantic Sector of the Southern Ocean (Croot and Johansson, 2000), and range from 0.09 to 0.77 nM in Central N Pacific (Rue and Bruland, 1995). In coastal waters, the L_t is higher than in the open ocean, whereas the highest concentrations of L_t were observed in the estuary areas and river plumes [e.g., 526 nM in the Scheldt Estuary; 4.3–64.1 nM in the Mississippi River plume (Powell and Wilson-Finelli, 2003; Gerringa et al., 2007)]. In the coastal area of the East China Sea, the L_t ranged from 5.2 to 132 nM (Su et al., 2015).

The most accepted method for determination of concentrations of L_t and the conditional stability constants (logK') of metal-organic ligands in marine samples is competitive ligand exchange-adsorptive cathodic stripping voltammetry (CLE-aCSV; Gledhill and van den Berg, 1994; van den Berg, 1995). It is based on titration of the samples with a metal of interest in which competitive ligand is added. One to two ligand classes were usually determined. The speciation analysis results (concentration of accessible organic ligands, L_t, and conditional stability constant, logK') depend not only on the quality of the experimental titration data, but also on the applied mathematical treatment (Pižeta et al., 2015). In recent studies only one class of ligands was estimated in Liverpool Bay (Abualhajja et al., 2015; Sander et al., 2015) and the Otago Continental Shelf (Sander et al., 2015). However, two classes of organic ligands were often reported in seawater samples, a stronger ligand (L₁; logK'₁) and weaker (L₂) ligand (logK'₂; Rue and Bruland, 1995; Cullen et al., 2006; Buck et al., 2007). The values of logK' were close to the

values obtained by model ligands with organic matter such as siderophores produced by bacteria (Hider and Kong, 2010), porphyrins derived from pigments (Witter et al., 2000), and degradation products from marine and terrestrial organisms, among other humic substances (HS; Laglera and van den Berg, 2009). While interpreting results from CLE-aCSV one should further bear in mind that ligand—DFe coordination could be different from 1:1 ratio, and that not all DFe in a given sample is in an exchangeable form with respect to the added competitive ligand, having as a consequence a possible overestimation of L_t and higher logK' (Cullen et al., 2006; Thuróczy et al., 2010; Gledhill and Buck, 2012).

The coastal zone is influenced by iron input from river waters, which may be transported a long distance (Powell and Wilson-Finelli, 2003; Su et al., 2015). Rainwater is also a significant source of iron in surface waters (Kieber et al., 2001), especially through rivers collecting drainage water and entering into coastal waters. A factor that may speed-up the depletion of DFe is algal bloom. Marine phytoplankton cells when of high density, would uptake bioavailable iron and decrease the DFe concentration (Boye et al., 2001, 2003). Appearance of anoxia (due to red tide) in bottom water and sediments may cause the release of iron from sediments into surrounding waters (Sundby et al., 1986; Zhu et al., 2012). In coastal areas where monsoons blow, they transport dust and may be another factor that influence the distribution of DFe and L_t, which may lead to seasonal variation in the DFe and L_t, such as Funka Bay (Japan, Tsunogai and Uematsu, 1978) and Arabian Sea (Siefert et al., 1999). In recent years, as the economy has developed, anthropogenic sources such as industrial wastewater, sewage, agriculture irrigation, and other activities influence more and more the biogeochemical cycling of the DFe and L_t in coastal areas.

Due to the limited water exchange, semi-closed bays like Jiaozhou Bay (JZB) are vulnerable marine ecosystems, sensitive to any kind of change or pollution, and could be used to evaluate the contribution of natural and anthropogenic sources on DFe and L_t concentrations on the system itself (Kremling et al., 1997; Öztürk et al., 2003; Nagai et al., 2007).

JZB water body with a surface area of 390 km² is connected with the Yellow Sea through a narrow mouth that starts in Tuandao and ends in Xuejiadao with a width of merely 3.1 km (Li et al., 2014; **Figure 1**). The JZB is surrounded by a highly industrialized and populated area, the biggest being Qingdao city, having a total population of ~8.7 million inhabitants. The eastern coastal JZB is an industrial and residential area, while the western coastal area is mainly an agriculture and aquaculture district. JZB has an average water depth of ~7 m, shallow in the northwest and deep in the southeast (**Figure 1**; Chen et al., 2009). The average tidal range of JZB is 2.7 m, with a maximum of 6.9 m, inducing strong turbulent mixing (Deng et al., 2010). The amount of river water entering the JZB varies seasonally, more than 10 rivers dry up in the winter and spring seasons but carry a large quantity of anthropogenic contaminants into this area in the rainy summer season (Ma et al., 2014). According to the report on Marine Environmental Quality of Qingdao (2014), red tides happen every year in spring and in summer (Bulletin of Marine Environmental

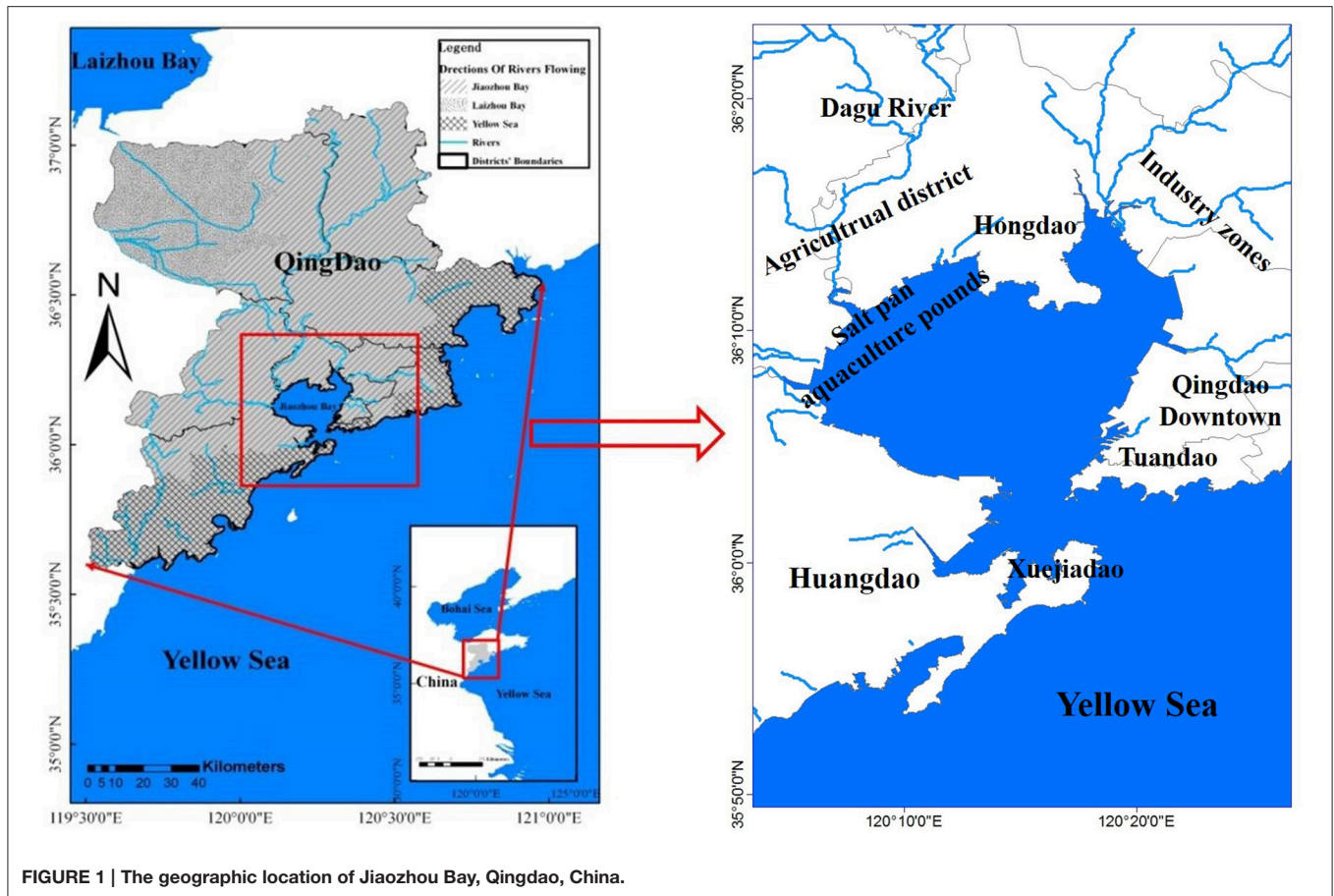


FIGURE 1 | The geographic location of Jiaozhou Bay, Qingdao, China.

Status of China for the year of 2011 and 2012¹; Liu et al., 2005).

The purpose of this work is to provide an insight into the distribution and speciation of dissolved iron (DFe) and its organic ligands (L_t) in relation to anthropo-biogeochemical changes of the water in the JZB, caused by anthropogenic inputs through the rivers inflow or naturally driven disturbances as a consequence of tide, rain, or increased biological activity.

SAMPLING AND ANALYTICAL PROCEDURES

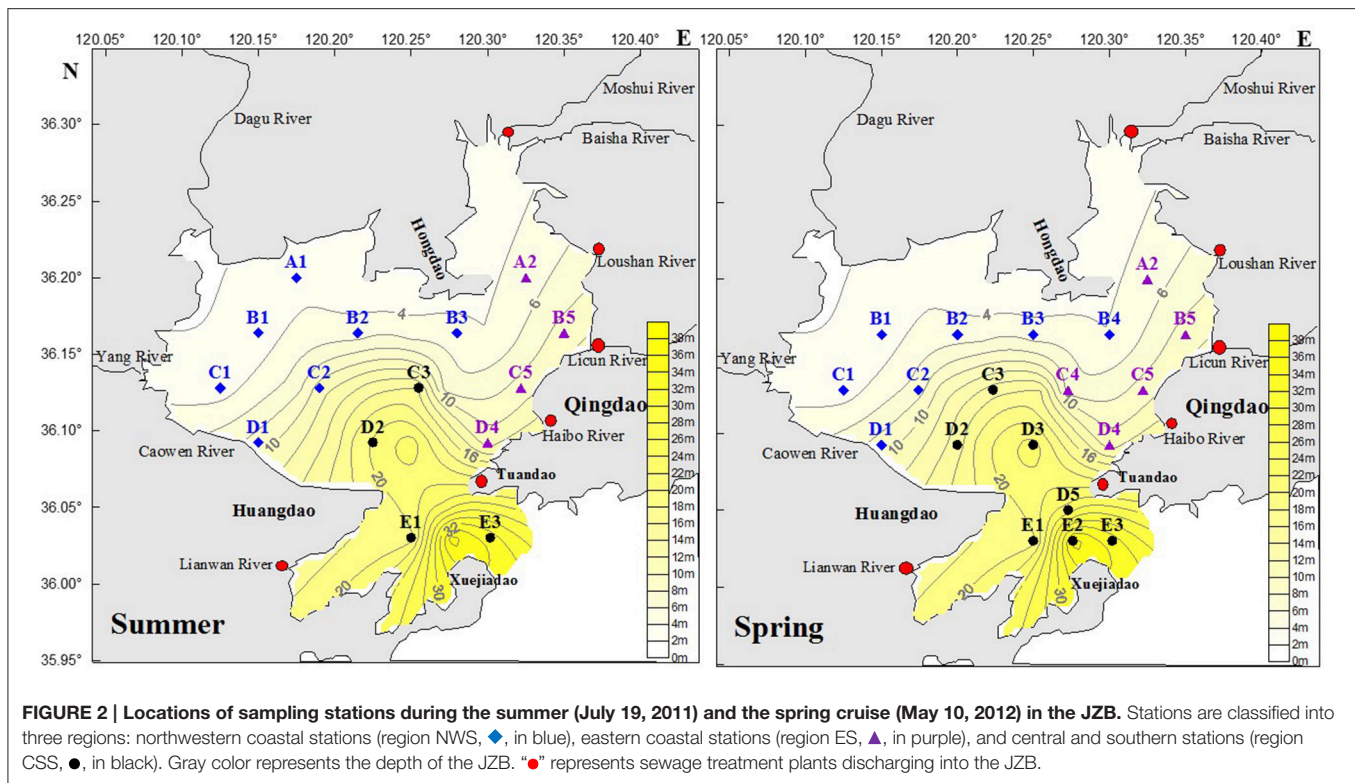
Samples Collection

Samples were collected during two cruises on a wooden boat in the JZB in summer (July 19, 2011) and spring (May 10, 2012). The sampling stations were located between 120.12–120.35°E and 35.03–36.20°N. The seawater samples were collected from five sections, which were identified as A, B, C, D and E, from each position at three depths (Figure 2; note slight differences in positions and number of sampling stations between summer and spring).

¹<http://www.coi.gov.cn/gongbao/huanjing/>.

Based on the relative distance to the bay mouth and the different influence from industry and agriculture, the sample stations were classified into three groups:

1. The northwest coastal stations (NWS) having shallow water (~4 m depth, Figure 2) and weaker water exchange with the Yellow Sea than other areas of the JZB (Lü et al., 2010). In the NWS area, there are salt pans and aquaculture ponds, such as shrimps and shellfish ponds (Guo et al., 2012; Ma et al., 2014; Figure 1). The northern and western coastal districts of JZB are mainly agricultural (Liu et al., 2014).
2. The eastern coastal stations (ES) were near downtown and were deeper than the western and northern JZB stations (Figure 2). The eastern coastal area of JZB is industrial with high population density. Different industries are located in this area, including electroplating, metal processing, rubber manufacturing, petrochemistry, machinery manufacturing, etc. (Deng et al., 2010). The rivers (Moshui, Baisha, Loushan, Licun, and Haibo Rivers) in the ES region have become the sewage channels for Qingdao city (Figure 2).
3. The central and southern stations (CSS) have the strongest water exchange and tidal influence, along with big topographic relief, slope and submarine depression (Figure 2). A narrow channel near the mouth of the



bay is seriously impacted by strong tidal currents (Ding, 1992).

Samples were collected with metal-clean modified Teflon-coated PVC Go-Flo bottles (UPVC/PTFE, 140 × 670 mm, Tianjin, National Ocean Technology Center, China) with a plastic rope. After recovery, the samples were immediately subsampled into 1 L low-density polyethylene bottles (LDPE, Nalgene, USA), and were then pressure-filtered through an acid-cleaned 0.4 μm-pore polycarbonate filter (47 mm × 0.4 μm, Millipore, Ireland). The filtered seawater samples for DFe analysis were collected into three clean 30 ml LDPE bottles (Nalgene, USA), immediately acidified to pH < 2 using HCl (Suprapur, Merck, Germany), and stored for more than 3 months before measurements, then analyzed for DFe concentration. Other filtered seawater samples were collected in a clean 250 mL LDPE bottles and frozen for subsequent analysis of Fe speciation. All of these procedures were performed in a class-100 clean laminar flow bench.

Bottle Washing and Reagents

The sample bottles were washed several times with 10% (v/v) HCl (Guaranteed reagent, Sinopharm, China) and rinsed thoroughly with a Milli-Q water, as described in details by Su et al. (2015). All reagents were made in Milli-Q water (18.2 MΩ, Millipore, USA). The hydrochloric acid (HCl, mass fraction 30%) was ultra-pure grade (Merck, 1.00318.1000, Germany). Ammonium hydroxide was prepared with a vapor-phase transfer from reagent-grade concentrated NH₄OH into ultra-high purity H₂O. A stock standard solution of 1000.0 mg/L Fe(NO₃)₃ (chromatographically pure, Merck, Germany) was prepared and diluted to 100, 10, and 1 μM (in pH = 2)

to obtain working solutions. The competitive ligand used was 2,3-dihydroxynaphthalene (DHN; chromatographically pure, Merck, Germany), and a stock standard solution of 0.1 M DHN was prepared and diluted to 100 μM. BrO₃⁻ (0.4 M; BHD, UK)/POPSO (0.1 M; chromatographically pure, Merck, Germany) as a buffer solution was purified using 100 μM MnO₂ (van den Berg, 2006).

Determination of Total Dissolved Iron and Organic Fe-Binding Ligands

The total dissolved iron in acidified seawater samples and organic Fe-binding ligands in thawed samples were determined by CLE-aCSV method and a 797 VA computrace instrument (Metrohm, Switzerland). Detailed information on the determination of DFe and L_t (i.e., electrochemical parameters and the process of determination) were provided elsewhere (van den Berg, 2006; Su et al., 2015). In short, voltammetric parameters were as follows: method differential pulse voltammetry, deposition potential -0.2 V, deposition time 60 s, pulse amplitude 0.05 V, pulse time 0.02 s, scan rate 90 mV/s, initial potential 0.0 V, final potential -1.2 V.

For determination of DFe concentration, 40 μL of 0.01 M DHN and 0.5 mL of BrO₃⁻/POPSO was added to a 10 ml of sample to adjust the pH to 8.0–8.1. DFe concentration was determined for every sample in triplicate (from three bottles/subsamples). We added a higher concentration of DHN (40 μM) for the determination of DFe than for the determination of L_t and logK (1.5 μM). For determination of L_t and its iron binding conditional stability constant (logK_{FeL}[′]), every seawater sample was pipetted into a series of 13 Teflon tubes (Nalgene,

USA) and titrated with at least 10 Fe additions (the range of iron additions: 0, 0.5, 1.0, 2.0, 3.0, 4.0, 6.0, 10.0, 15.0, 20.0, 30.0, 40.0, 50.0, and 70.0 nM) in order to fully saturate all ligand sites. After 30 min equilibration of samples with iron additions, DHN was added to the final concentration of 1.5 μ M. These samples were further equilibrated for 12–17 h. Before measurement, Teflon tubes were well-conditioned using an iron solution of the same concentration. Subsequently, equilibrated samples were transferred to a measurement cell, from low to high iron addition aliquots, and measured at pH 8.0–8.1.

The side reaction coefficient (α_{FeDHN}) for 1.5 μ M of DHN was calculated by:

$$\alpha_{FeDHN} = K_{FeDHN}^{cond} \times [DHN'] = 10^{8.51} \times 1.5 \times 10^{-6} = 485.4$$

For this method $[DHN'] = [DHN]_T$, since $[DHN'] \gg [DFe]$.

The results of each titration set (signal height vs. added Fe concentration) were treated by ProMCC software (Omanović et al., 2015). Sensitivity (S) was adopted from the last five points of titration data. Langmuir/Gerringa non-linear fitting was applied assuming one- and two-ligand models. The one-ligand model was adopted in all cases.

Inorganic Fe (Fe') of the samples was related to the initial iron reduction peak current, i_{p0} :

$$[Fe'] = i_{p0} / (S \times \alpha_{FeDHN}) \quad (a)$$

The other way of estimating inorganic Fe, with obtained results from titration experiment, i.e., L_t and $\log K'$ relies on Equation (9) from Omanović et al. (2015):

$$[Fe'] = \frac{-\alpha + \sqrt{\alpha^2 + \frac{4[DFe]}{K'}}}{2} \quad (b)$$

where $\alpha = (-[DFe] + [L_t] + 1/K')$.

The two approaches will be checked and compared. Estimations that take into account parameters of iron complexation with organic ligands (b) should be more reliable, as they are calculated from more data points. From the other side, propagation of errors that is inherent to complex calculations makes the simpler expression (a) also valuable.

The percentage of complexed DFe (%FeL) was calculated from:

$$\%FeL = \frac{[DFe] - [Fe']}{[DFe]} \times 100\%$$

Temperature, Salinity, and Nutrients Measurements

The surface water temperature was measured *in-situ* at the sampling sites by a digital thermometer with a long probe. The salinity of surface water was measured by a salinometer (SYA2-2, China; calibrated by standard seawater provided by National Center of Ocean Standards and Metrology, Tianjin, China) in for that specified subsamples after coming back to the laboratory. Nutrients levels (total dissolved nitrogen and phosphorus) were

measured in the laboratory using spectrophotometry (Grasshoff et al., 1983) after the water was passed through an acid-clean 0.4 μ m-pore filter.

RESULTS

Results of all measured and calculated parameters: dissolved iron, calculated and estimated iron-organic ligands parameters, inorganic iron, percentage of organically bound iron as well as temperature, salinity, total dissolved nitrogen, and phosphorus, for both contrasting summer and spring periods, are summarized in **Tables 1, 2**.

Distribution of Dissolved Iron in the JZB

The contour plots of spatial distributions of DFe concentrations in surface, middle, and bottom seawater layers in the JZB in summer period are shown in **Figures 3A–C**. The spatial distributions in all three layers exhibited a weak horizontal gradient, progressively decreasing from the CSS region ([DFe] ranged from 13.4 to 43.4 nM, median 19.8 nM, average \pm SD 23.7 \pm 9.7 nM) to the ES region ([DFe] ranged from 14.8 to 29.8 nM, median 18.7 nM, average \pm SD 19.5 \pm 4.6 nM), and NWS ([DFe] ranged from 13.5 to 32.1 nM, median 17.2 nM, average \pm SD 19.2 \pm 4.9 nM). Although not significant, the vertical profiles of average DFe concentration in all regions showed a decrease with depth.

The spatial distributions of DFe concentrations in the surface, middle and bottom seawater layers during the spring period are shown in **Figures 3D–F**. A strong horizontal decrease in DFe from the eastern to the western and central side of the bay is obvious. The highest variability in [DFe] (from 5.6 to 107 nM; median 9.8 nM, average \pm SD 24.1 \pm 28.3 nM) was observed in the ES region. In the NWS region, [DFe] ranged from 8.3 to 31.4 nM (median 13.5 nM, average \pm SD 13.6 \pm 5.8 nM) and in the CSS region, [DFe] ranged from 8.1 to 26.8 nM (median 14.1 nM, average \pm SD 14.5 \pm 5.5 nM). Similar to the summer period, DFe concentrations decreased with depth in all three layers.

Distribution of Iron Organic Ligands in the JZB

In all samples from the spring and summer periods only one class of Fe-binding ligand was estimated (further in the text denoted as total ligand concentration, $[L_t]$; **Figure 4**).

The spatial distributions of $[L_t]$ in the surface, middle and bottom samples for the summer campaign are shown in **Figures 4A–C**. On average, L_t concentrations were about 50% higher than [DFe], with a statistically significant correlation with ([DFe]; $R^2 = 0.54$, $n = 46$, $p < 0.001$; **Figure 5**). While vertical profiles of $[L_t]$ showed an evident decrease with depth (surface layer: 37.1 \pm 10.0 nM; middle layer: 30.4 \pm 9.7 nM, bottom layer: 26.3 \pm 9.7 nM), the horizontal variation between regions was minor (ES region: 32.0 \pm 9.3 nM; NWS region: 31.4 \pm 11.0 nM; CSS region: 29.9 \pm 10.8 nM). The relatively narrow range of $\log K'$ obtained in all summer samples (12.3 \pm 0.4; $n = 46$) revealed an absence of any horizontal or vertical gradients, pointing on the similarity in organic ligand complexation characteristics

TABLE 1 | Dissolved iron DFe (average from three determinations \pm standard deviation); iron ligand characteristics L_t , $\log K'$ (\pm 95% confidence interval determined through fitting to Langmuir/Gerringa model) and $[L_t]/[DFe]$; inorganic iron (Fe^+ , pM, both calculated by expression a and b) and the percentage of complexed DFe (%FeL, calculated by expression a) at all stations in spring and summer.

ID	Dep (m)	[DFe] (nM)	$[L_t]$ (nM)	$\log K'$	$[L_t]/[DFe]$	[Fe ⁺] (pM)		%FeL	Dep (m)	[DFe] (nM)	$[L_t]$ (nM)	$\log K'$	$[L_t]/[DFe]$	[Fe ⁺] (pM)		%FeL
						(a)	(b)							(a)	(b)	
NWS	0	27.3 \pm 2.6	54.3 \pm 3.0	12.6 \pm 0.2	2	0.19	99.999	0.25	-	-	-	-	-	-	-	-
	3	16.0 \pm 1.2	22.1 \pm 0.3	11.8 \pm 0.1	1.4	1.33	99.992	4.15	-	-	-	-	-	-	-	-
B1	0	20.6 \pm 2.1	30.5 \pm 0.6	12.2 \pm 0.1	1.5	1.4	99.993	1.31	0	10.2 \pm 0.8	17.3 \pm 0.5	11.7 \pm 0.1	1.7	0.88	99.991	2.86
	2	25.7 \pm 1.5	44.3 \pm 1.7	12.2 \pm 0.2	1.7	0.79	99.997	0.87	2	7.6 \pm 0.5	14.0 \pm 1.6	11.6 \pm 0.1	1.8	0.9	99.988	2.98
B2	0	32.1 \pm 3.2	52.6 \pm 0.6	12.9 \pm 0.4	1.6	0.17	99.999	0.2	0	9.2 \pm 1.9	22.4 \pm 1.4	12.7 \pm 0.3	2.4	0.43	99.995	0.14
	2	14.5 \pm 1.3	20.3 \pm 1.7	11.6 \pm 0.1	1.4	1.08	99.993	6.27	2	9.0 \pm 1.1	26.1 \pm 0.6	11.6 \pm 0.1	2.9	0.88	99.99	1.32
B3	0	14.1 \pm 1.7	35.6 \pm 0.6	12.2 \pm 0.2	2.5	0.3	99.998	0.41	0	17.5 \pm 1.4	48.1 \pm 1.4	11.8 \pm 0.1	2.7	0.8	99.995	0.91
	2	15.9 \pm 1.4	19.8 \pm 0.5	11.7 \pm 0.1	1.2	1.48	99.991	8.11	2	17.3 \pm 0.7	50.3 \pm 0.9	11.6 \pm 0.1	2.9	1.21	99.993	1.32
B4	0	21.4 \pm 2.0	26.0 \pm 0.4	12.4 \pm 0.3	1.2	0.21	99.999	1.85	4	15.2 \pm 0.85	22.7 \pm 0.7	11.8 \pm 0.2	1.5	1.08	99.993	3.21
	0	-	-	-	-	-	-	-	0	12.0 \pm 0.6	54.9 \pm 3.8	10.9 \pm 0.1	4.6	0.92	99.992	3.52
C1	0	16.3 \pm 2.1	27.9 \pm 0.9	12.6 \pm 0.2	1.7	0.22	99.999	0.35	0	14.8 \pm 2.3	39.5 \pm 1.9	11.5 \pm 0.1	2.7	1.09	99.993	1.89
	1	14.0 \pm 0.9	24.5 \pm 0.4	12.6 \pm 0.1	1.7	0.27	99.998	0.33	-	-	-	-	-	-	-	-
C2	0	20.6 \pm 1.4	47.8 \pm 2.7	12.3 \pm 0.1	2.3	0.34	99.998	0.38	0	14.6 \pm 1.7	30.4 \pm 1.6	11.3 \pm 0.1	2.1	0.86	99.994	4.63
	5	21.4 \pm 1.6	33.7 \pm 1.3	12.7 \pm 0.2	1.6	0.23	99.999	0.35	3	14.4 \pm 0.4	34.6 \pm 3.2	11.2 \pm 0.1	2.4	0.78	99.995	4.5
D1	0	16.9 \pm 1.0	24.2 \pm 0.5	12.3 \pm 0.2	1.4	1.42	99.992	1.16	0	31.4 \pm 3.7	53.4 \pm 0.8	12.1 \pm 0.2	1.7	0.84	99.997	1.13
	5	23.5 \pm 1.3	30.2 \pm 0.9	12.2 \pm 0.1	1.3	1.81	99.992	2.21	5	9.5 \pm 1.7	25.8 \pm 1.1	11.5 \pm 0.1	2.7	1.16	99.988	1.84
ES	0	16.3 \pm 0.7	24.8 \pm 1.5	12.5 \pm 0.2	1.5	0.48	99.997	0.61	0	9.8 \pm 2.0	21.8 \pm 0.6	11.6 \pm 0.1	2.2	1.25	99.987	2.05
	2	17.2 \pm 1.6	28.2 \pm 1.8	12.1 \pm 0.1	1.6	0.96	99.994	1.24	2	8.9 \pm 2.1	27.4 \pm 1.0	11.9 \pm 0.2	3.1	0.5	99.994	0.61
B5	0	18.6 \pm 1.5	43.3 \pm 1.8	12.4 \pm 0.2	2.3	0.29	99.998	0.3	0	107 \pm 2.9	144 \pm 3.5	12.2 \pm 0.2	1.3	2.25	99.998	1.82

(Continued)

TABLE 1 | Continued

ID	Dep (m)	[DFe] (nM)	[L _t] (nM)	logK'	[L _t]/[DFe]	[Fe'] (pM)	%FeL (a)	[Fe'] (b) (pM)	Dep (m)	[DFe] (nM)	[L _t] (nM)	logK'	[L _t]/[DFe]	[Fe'] (a) (pM)	%FeL (a)	[Fe'] (b) (pM)	[Fe'] (b) (pM)
C4	5	20.8 ± 1.4	42.4 ± 2.4	12.3 ± 0.2	2	0.8	99.996	0.48	5	58.9 ± 3.2	104 ± 1.5	11.7 ± 0.1	1.8	2.71	99.995	2.61	
	8	21.1 ± 1.0	41.4 ± 2.4	12.3 ± 0.3	2	0.36	99.998	0.52	8	55.5 ± 4.3	109 ± 3.2	11.8 ± 0.1	2	1.41	99.997	1.64	
	-	-	-	-	-	-	-	-	0	9.1 ± 1.5	38.5 ± 1.0	11.3 ± 0.1	4.2	1.2	99.997	1.55	
C5	0	26.4 ± 2.0	41.9 ± 2.3	12.3 ± 0.2	1.6	0.58	99.998	0.85	0	22.3 ± 2.3	40.6 ± 1.2	12.1 ± 0.2	1.8	0.53	99.998	0.97	
	5	19.4 ± 2.3	34.3 ± 0.9	12.0 ± 0.1	1.8	1.23	99.994	1.3	5	6.9 ± 1.5	27.2 ± 0.8	11.6 ± 0.1	4	0.52	99.992	0.85	
	8	18.9 ± 1.8	28.5 ± 0.4	12.1 ± 0.1	1.5	1.13	99.994	1.56	8	9.4 ± 1.1	45.5 ± 1.5	11.5 ± 0.1	4.9	0.52	99.994	0.82	
D4	0	29.8 ± 2.5	38.0 ± 1.0	12.6 ± 0.3	1.3	0.89	99.997	0.91	0	22.6 ± 1.4	34.3 ± 0.6	11.7 ± 0.1	1.5	2.51	99.989	3.85	
	5	14.8 ± 1.0	21.6 ± 2.4	12.2 ± 0.2	1.5	0.78	99.995	1.37	3	12.4 ± 2.0	27.1 ± 0.6	11.7 ± 0.1	2.2	1.31	99.989	1.68	
	10	14.8 ± 3.0	17.4 ± 0.7	12.3 ± 0.1	1.2	0.97	99.993	2.85	8	14.6 ± 0.4	40.4 ± 0.6	12.3 ± 0.2	2.8	0.43	99.997	0.28	
C3	0	21.0 ± 1.4	35.2 ± 1.3	13.1 ± 0.3	1.7	1.15	99.995	0.12	0	12.2 ± 1.1	35.1 ± 2.0	10.9 ± 0.1	2.9	1.19	99.99	6.7	
	10	17.3 ± 0.8	22.3 ± 1.1	12.3 ± 0.2	1.3	1.25	99.993	1.73	7	10.4 ± 1.1	31.2 ± 1.9	11.5 ± 0.1	3	0.97	99.991	1.58	
	15	15.5 ± 0.7	17.7 ± 1.3	12.2 ± 0.1	1.1	1.07	99.993	4.44	14	8.1 ± 0.8	22.5 ± 0.3	11.5 ± 0.1	2.8	0.78	99.99	1.78	
D2	0	25.8 ± 2.0	34.1 ± 1.3	12.7 ± 0.1	1.3	0.85	99.997	0.62	0	11.1 ± 1.7	34.4 ± 0.8	11.8 ± 0.1	3.1	0.66	99.994	0.75	
	10	13.4 ± 0.9	14.9 ± 0.6	12.1 ± 0.2	1.1	1	99.992	7.06	7	10.4 ± 1.2	24.5 ± 1.5	11.6 ± 0.1	2.3	0.94	99.991	1.85	
	-	-	-	-	-	-	-	-	14	26.8 ± 2.4	30.6 ± 2.7	11.6 ± 0.1	1.1	2.86	99.989	17.62	
D3	-	-	-	-	-	-	-	-	0	19.5 ± 2.1	32.0 ± 2.5	12.1 ± 0.3	1.6	0.94	99.995	1.24	
	-	-	-	-	-	-	-	-	10	21.6 ± 1.2	33.8 ± 0.7	12.0 ± 0.1	1.6	1.08	99.995	1.77	
	-	-	-	-	-	-	-	-	20	17.0 ± 1.4	22.2 ± 0.2	11.9 ± 0.1	1.3	1.92	99.999	4.11	
D5	-	-	-	-	-	-	-	-	0	9.8 ± 1.5	24.8 ± 1.0	11.6 ± 0.1	2.5	1.15	99.988	1.64	
	-	-	-	-	-	-	-	-	10	8.6 ± 1.8	38.1 ± 3.0	11.5 ± 0.1	4.4	0.69	99.992	0.92	
	-	-	-	-	-	-	-	-	20	8.2 ± 1.5	19.3 ± 1.3	11.7 ± 0.1	2.3	0.88	99.989	1.47	
E1	0	19.2 ± 0.9	23.4 ± 2.2	12.9 ± 0.3	1.2	0.57	99.997	0.58	0	9.8 ± 0.3	12.3 ± 2.5	11.2 ± 0.1	1.3	0.95	99.99	24.43	
	5	19.9 ± 1.5	24.8 ± 5.6	12.8 ± 0.3	1.2	0.49	99.998	0.64	10	14.1 ± 1.0	28.6 ± 1.1	12.1 ± 0.2	2	0.5	99.996	0.77	
	10	17.2 ± 1.9	21.1 ± 3.5	12.1 ± 0.3	1.2	1.09	99.994	3.5	15	15.4 ± 0.8	42.6 ± 1.0	11.7 ± 0.1	2.8	0.88	99.994	1.13	
E2	-	-	-	-	-	-	-	-	0	22.6 ± 2.1	36.4 ± 1.4	12.1 ± 0.1	1.6	1.08	99.995	1.3	
	-	-	-	-	-	-	-	-	15	15.2 ± 1.7	23.1 ± 1.0	11.5 ± 0.1	1.5	1.39	99.991	6.08	
	-	-	-	-	-	-	-	-	30	23.4 ± 1.2	25.0 ± 0.8	11.8 ± 0.1	1.1	1.61	99.993	22.83	
E3	0	40.4 ± 1.0	42.6 ± 0.3	12.9 ± 0.1	1.1	3.08	99.992	2.31	0	11.3 ± 1.7	15.8 ± 0.6	11.9 ± 0.1	1.4	1.23	99.989	3.16	

(Continued)

TABLE 1 | Continued

ID	Dep (m)	[DFe] (nM)	[L _t] (nM)	logK'	[L _t]/[DFe]		[Fe']		%FeL	Dep (m)	[DFe] (nM)	[L _t] (nM)	logK'	[L _t]/[DFe]		[Fe']		%FeL	[Fe'] (pM)
					(a)	(b)	(a)	(b)						(a)	(b)	(a)	(b)		
	5	19.8 ± 2.3	28.5 ± 1.6	12.3 ± 0.1	1.4	1.55	99.992	1.14	15	14.2 ± 1.8	29.1 ± 2.5	12.0 ± 0.1	2.1	0.89	99.994	0.95			
	10	43.4 ± 3.0	49.0 ± 1.4	12.1 ± 0.1	1.1	3.42	99.992	6.15	30	14.9 ± 1.7	20.8 ± 3.3	11.9 ± 0.1	1.4	1.63	99.989	3.18			
	15	23.5 ± 1.2	33.1 ± 2.5	12.0 ± 0.2	1.4	1.59	99.993	2.45											
	20	18.2 ± 0.8	23.9 ± 3.9	11.9 ± 0.2	1.3	1.23	99.993	4.02											
	25	38.0 ± 2.0	47.4 ± 0.4	12.5 ± 0.1	1.2	1.18	99.997	1.28											
NWS	Average ± SD	19.2 ± 4.9	31.4 ± 11.0	12.2 ± 0.4	1.6 ± 0.4	0.9 ± 0.6	99.995	2.0 ± 2.1		13.6 ± 5.8	32.0 ± 13.7	11.6 ± 0.4	2.4 ± 0.8	0.9 ± 0.2	99.993	2.6 ± 1.5			
	Median	17.2	29.1	12.2	1.5	0.95	99.994	1.4		13.5	27.5	11.6	2.4	0.88	99.993	2.86			
ES	Average ± SD	19.5 ± 4.6	32.0 ± 9.3	12.3 ± 0.2	1.6 ± 0.3	0.8 ± 0.3	99.996	1.1 ± 0.7		24.1 ± 28.3	49.3 ± 37.8	11.8 ± 0.3	2.8 ± 1.1	1.1 ± 0.8	99.993	1.5 ± 0.9			
	Median	18.7	31.4	12.3	1.6	0.84	99.995	1.08		9.8	35.2	11.7	2.6	0.61	99.994	1.55			
CSS	Average ± SD	23.7 ± 9.7	29.9 ± 10.8	12.4 ± 0.4	1.3 ± 0.2	1.4 ± 0.8	99.994	2.6 ± 2.2		14.5 ± 5.5	27.7 ± 7.7	11.7 ± 0.3	2.1 ± 0.9	1.2 ± 0.5	99.992	5.0 ± 7.2			
	Median	19.8	26.7	12.3	1.2	1.16	99.993	2.02		14.1	28.6	11.7	2	0.97	99.991	1.77			

toward Fe in the JZB (Table 1). A fairly uniform distribution of DFe organic fraction (>99.99% of FeL) was observed (Table 1). However, a distinctly different [L_t]/[DFe] ratio was obtained for the CSS region (1.3 ± 0.2) compared to the ES (1.6 ± 0.3) and NWS (1.6 ± 0.4) regions (Table 1). Calculations showed slight variations of inorganic Fe concentrations by region (in average [Fe'] = 1.0 ± 0.7 pM (expression a, n = 46) and 1.9 ± 1.9 pM (expression b, n = 46) in the whole JZB; Table 1). Comparisons of two approaches of inorganic Fe estimation showed good correlation of both estimation in the ES region, while for the NWS and CSS regions, expression b gave higher estimations. The high estimations of inorganic Fe mainly coincident with lower stability constants.

The spatial distributions of [L_t] in the surface, middle and bottom samples for the spring campaign are shown in Figures 4D–F. The [L_t] exceeded the [DFe] for all samples and showed a statistically significant correlation with [DFe] (R² = 0.784, n = 53, p < 0.0001; Figure 5). Similar to summer vertical profiles, the average [L_t] decreased with depth (surface layer: 38.7 ± 28.1 nM; middle layer: 35.4 ± 19.4 nM; bottom layer: 31.4 ± 21.8 nM). Contrary to a uniform horizontal distribution evidenced in summer, in the spring period there were evident differences in L_t between regions (ES: 49.3 ± 37.8 nM; NWS: 32.0 ± 13.7 nM; CSS: 27.7 ± 7.7 nM). On average, lower conditional stability constants (logK') in the spring period were obtained than in summer period (11.7 ± 0.3; n = 53) with no significant differences between the regions (Table 1). However, [L_t]/[DFe] ratios in spring were evidently higher than in summer, with a clear difference between regions: ES: 2.8 ± 1.1; NWS: 2.4 ± 0.8; CSS: 2.1 ± 0.8. Similar to summer, organically complexed iron fraction accounted for more than 99.99% of DFe. The calculated concentration of inorganic Fe—in average [Fe'] = 1.1 ± 0.5 pM (expression a, n = 53) and 3.2 ± 4.8 pM [expression b, n = 53] did not differ much from the summer period (Table 1). Similar to summer period, two estimates of inorganic Fe correlate well for the ES region, while even more extreme values were calculated with expression b especially in the CSS region, where at some locations inorganic Fe was estimated to more than 20 pM. These samples were characterized by low stability constants.

Results from Physical and Chemical Parameters Measurements

The main physico-chemical parameters (temperature and salinity) were measured *in-situ*, at the surface (Table 2).

Total dissolved nitrogen (TDN) and phosphorus (TDP) concentrations were determined in all surface samples as well (Table 2).

DISCUSSION

Chemical and Physical Parameters and Factors That Influence the Behavior of Iron in the JZB

Salinity of the JZB was influenced by factors such as the tide, freshwater, and salt pans. The tide increases salinity of the JZB, because the Yellow Sea water of higher salinity mixes

TABLE 2 | Temperature (T, °C) and salinity (S), total dissolved nitrogen (TDN, μM) and total dissolved phosphorus (TDP, μM) at the surface layer of each sampling station in summer and spring in the JZB.

Region	Site	Summer period				Spring period			
		T (°C)	S	[TDN] (μM)	[TDP] (μM)	T (°C)	S	[TDN] (μM)	[TDP] (μM)
NWS	A1	24.6	32.1	–	–	–	–	–	–
	B1	24.5	31.6	72.1	0.64	17.2	30.6	52.2	–
	B2	24.2	31.3	84.8	0.98	17.2	30.6	49.5	0.47
	B3	24.4	29.9	92.3	1.07	17.1	30.9	59.6	0.57
	B4	–	–	–	–	17.9	30.5	72.2	1.16
	C1	25.0	31.8	82.1	0.58	17.1	31.4	54.1	0.35
	C2	23.5	30.2	52.0	0.76	15.5	30.9	66.5	0.70
	D1	24.5	29.8	–	–	16.4	30.8	–	0.3
	A2	22.4	30.2	90.1	1.32	18.3	30.8	72.3	1.43
	B5	23.4	29.8	–	–	17.0	30.3	91.2	1.80
	C4	–	–	–	–	15.3	32.2	49.1	0.65
	C5	23.1	30.4	87.1	0.91	16.0	31.0	48.1	0.75
	D4	22.6	31.6	–	0.84	14.3	31.3	41.2	0.42
	CSS	C3	22.9	31.7	–	–	14.4	31.6	52.3
D2		22.8	32.3	68.2	0.71	14.2	31.1	–	–
D3		–	–	–	–	14.4	31.3	36.8	0.36
D5		–	–	–	–	14.6	31.1	39.8	0.39
E1		22.7	30.7	57.5	0.56	13.4	31.2	30.8	0.34
E2		–	–	–	–	13.5	31.5	34.0	–
E3		23.1	30.8	52.2	0.69	14.0	31.1	34.2	0.27
NWS	Avg.	24.4	31.0	76.7	0.81	16.9	30.8	59.0	0.59
ES	Avg.	22.9	30.5	88.6	1.02	16.2	31.1	60.4	1.01
CSS	Avg.	22.9	31.4	59.3	0.65	14.1	31.3	38.0	0.34

Dep (m) represented the depth of sampling. Here, “–” refers to the parameter “not determined” in these analyses.

with freshwater that rivers bring into the bay. Although in the west-northern bay, there are many salt pans, which would increase salinity of the JZB due to their flooding (Figure 1), the continuous freshwater mixing with high salinity water at estuaries results in no big variations of salinity that we measured in our study in any of the three regions (Table 2).

Total dissolved nitrogen (TDN) and phosphorus (TDP) concentrations in the ES region were higher than in the other two regions (Table 2). Industrial wastewater and sewage had the biggest impact on nutrients in the JZB. The ratio of TDN to TDP in spring and summer (87:1 and 88:1, respectively) was much higher than the Redfield ratio (15:1, Redfield, 1958); the TDP may be the main limiting factor of phytoplankton growth in the JZB (Guo et al., 2012), and consequently may influence the distribution of DFe.

Monsoons can disturb surface water and increase dissolved iron deposition from the atmosphere to a surface water (Lin and Twining, 2012), thereby increasing the DFe concentrations of the semi-closed JZB. Due to the proximity to land, a large amount of atmospheric inputs might have contributed to high

iron concentrations (Baker et al., 2003). During a monsoon, the influence of atmospheric inputs may be greater than at other times. In our results, the DFe concentrations of surface water in spring were higher than in the middle and bottom water, while this phenomenon was not observed in summer. This might be due to the prevailing northwest monsoon in Qingdao (Tan et al., 2012), especially from March to May when we collected spring seawater samples (Figure 3).

Due to the narrow entrance of the JZB, tidal movement induces strong turbulent mixing and nearly homogeneous vertical profiles of temperature and salinity (Ding, 1992) at the bay mouth. This has caused no distinct vertical differentiation of DFe-values, except at station E1 (Figure 3 and Table 1).

DFe of the whole inner bay is not likely to be influenced by sediment resuspension because of bedrock and minimal sediment of the seafloor (Chen et al., 2012a). The river and silt input from rivers would directly increase the DFe concentrations under the tidal movement. Higher river runoff in summer may increase the DFe concentrations more than in spring (Figures 3, 6, see Section Sources and Removal of DFe).

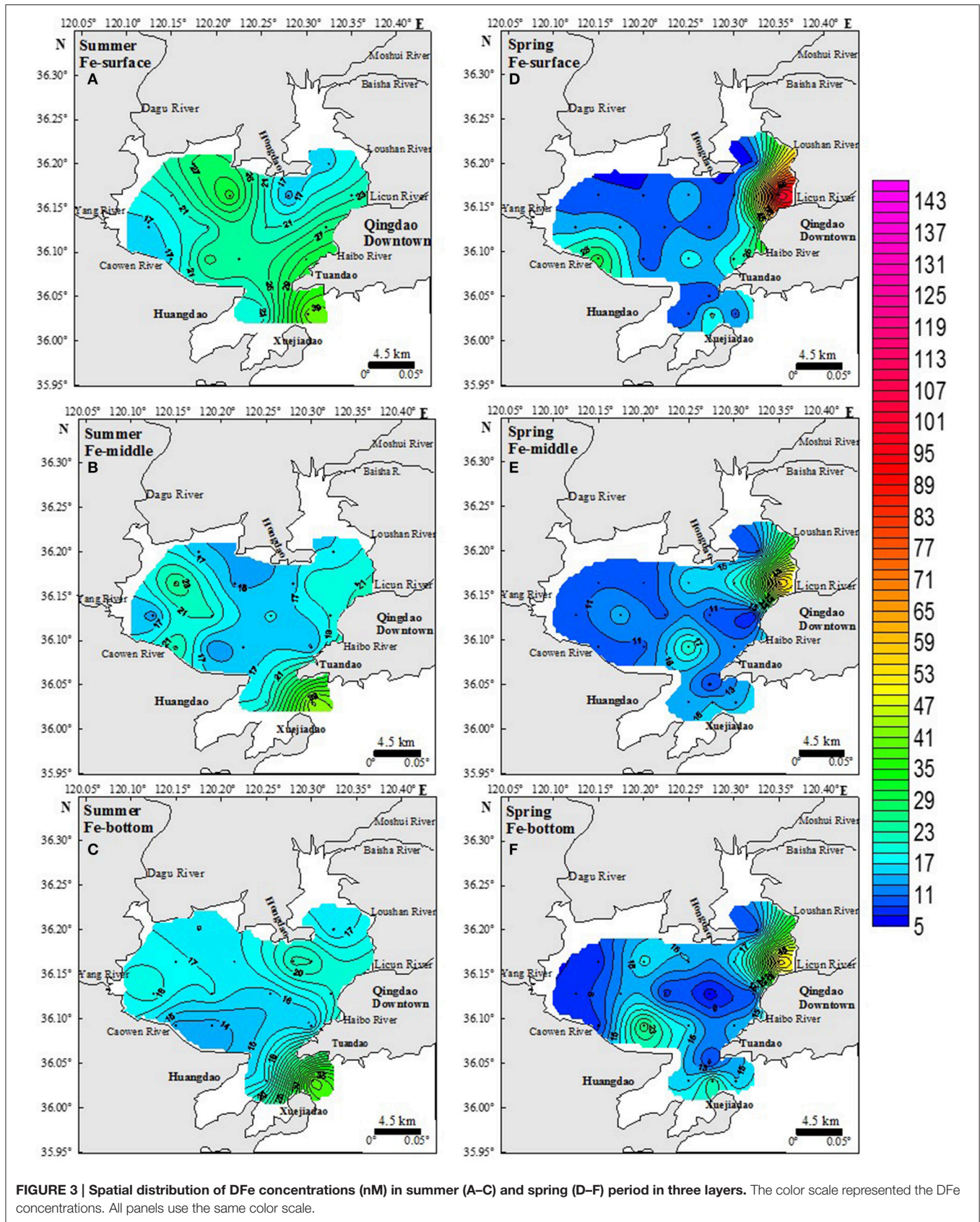


FIGURE 3 | Spatial distribution of DFe concentrations (nM) in summer (A–C) and spring (D–F) period in three layers. The color scale represented the DFe concentrations. All panels use the same color scale.

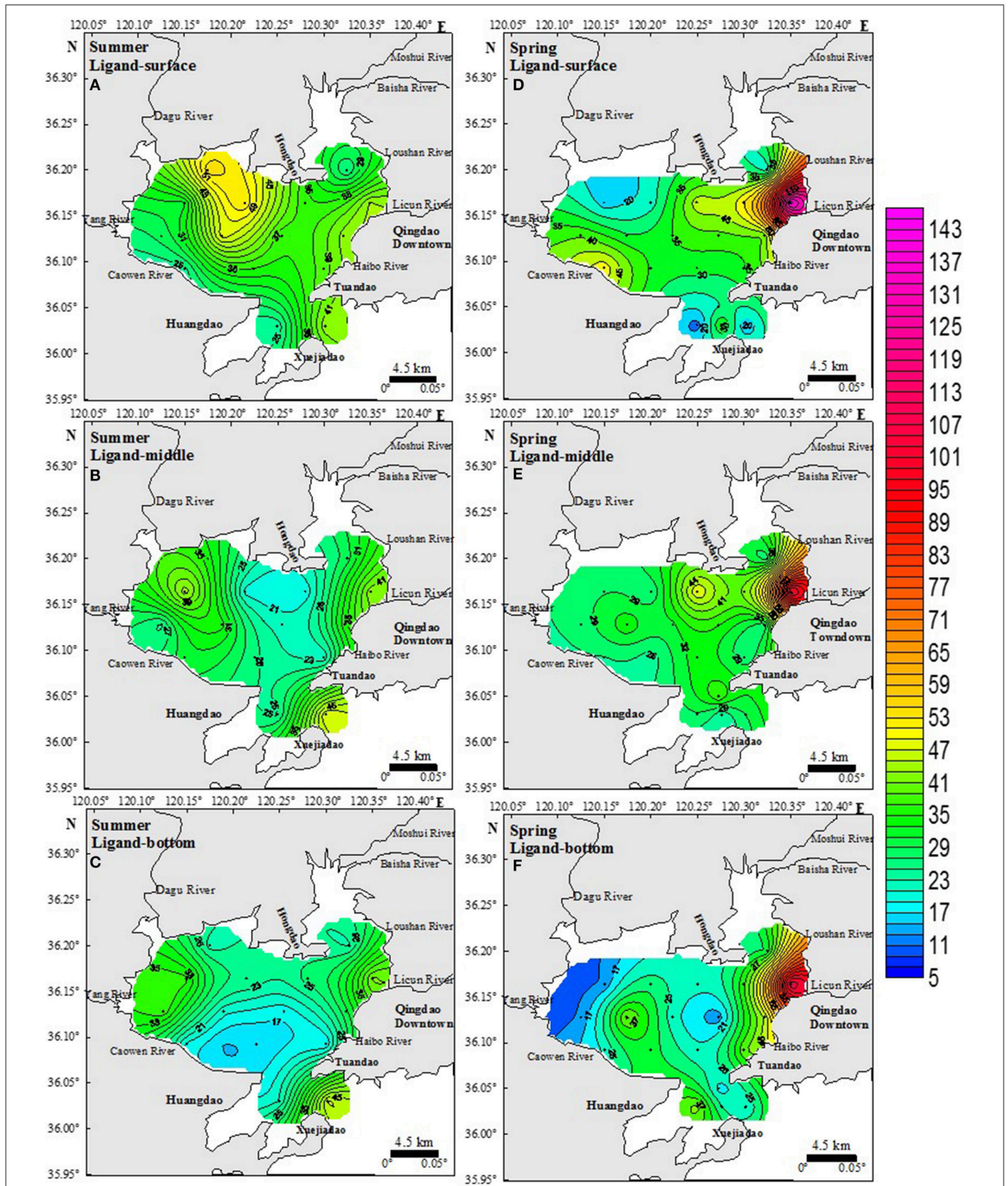


FIGURE 4 | Spatial distribution of ligand concentrations (nM) in summer (left side) and spring periods (right side) in surface (A,D), middle (B,E), and bottom (C,F) seawater layers. The color scale represented the L_1 concentrations. All panels use the same color scale as the color scale of DFe concentration in Figure 3.

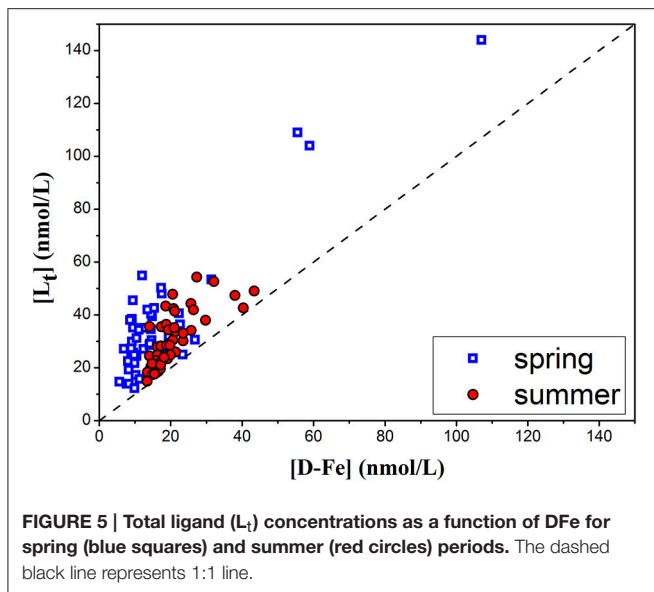


FIGURE 5 | Total ligand (L_t) concentrations as a function of DFe for spring (blue squares) and summer (red circles) periods. The dashed black line represents 1:1 line.

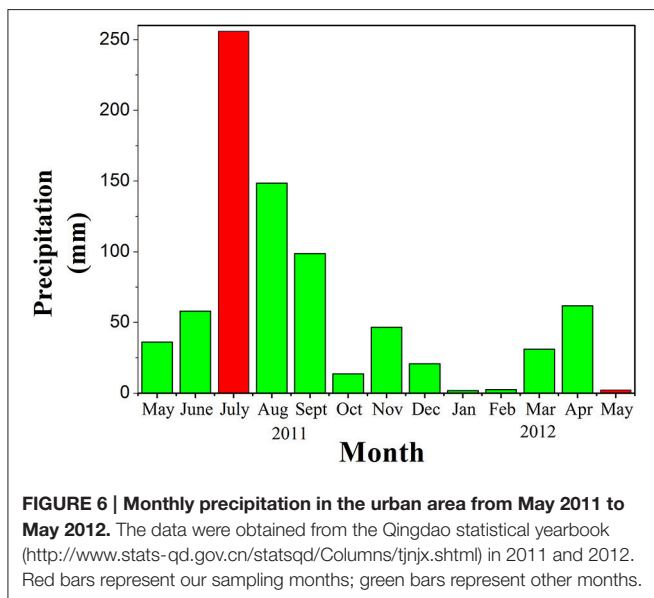


FIGURE 6 | Monthly precipitation in the urban area from May 2011 to May 2012. The data were obtained from the Qingdao statistical yearbook (<http://www.stats-qd.gov.cn/statsqd/Columns/tjnjx.shtml>) in 2011 and 2012. Red bars represent our sampling months; green bars represent other months.

Figure 7 shows the residual current in the JZB after building the cross-bay bridge (completed on June, 2011). The tidal current in the JZB is classified as a regular semidiurnal tidal current (Li et al., 2014). As seen in **Figure 7**, many circulations of residual current were observed in the inner JZB, and more residual currents appeared in summer than in spring (He et al., 2013). This may result in better vertical and horizontal uniformity of [DFe] in summer, compared to spring. The residual current in the eastern JZB hindered the diffusion of pollutants to the middle and western JZB (**Figure 7**); therefore, the DFe-values in the eastern JZB were higher than in the middle and the western JZB (Li et al., 2014). In addition, because of residual currents north of Huangdao, DFe may be partly enriched and its diffusion hindered into the rest of the JZB (**Figure 7**); hence, high DFe concentrations were observed there in spring

and in summer. Being influenced by tide, residual circulation and wind, hydrodynamic force of the JZB is complex and may significantly influence the migration and diffusion of DFe (**Figure 7**).

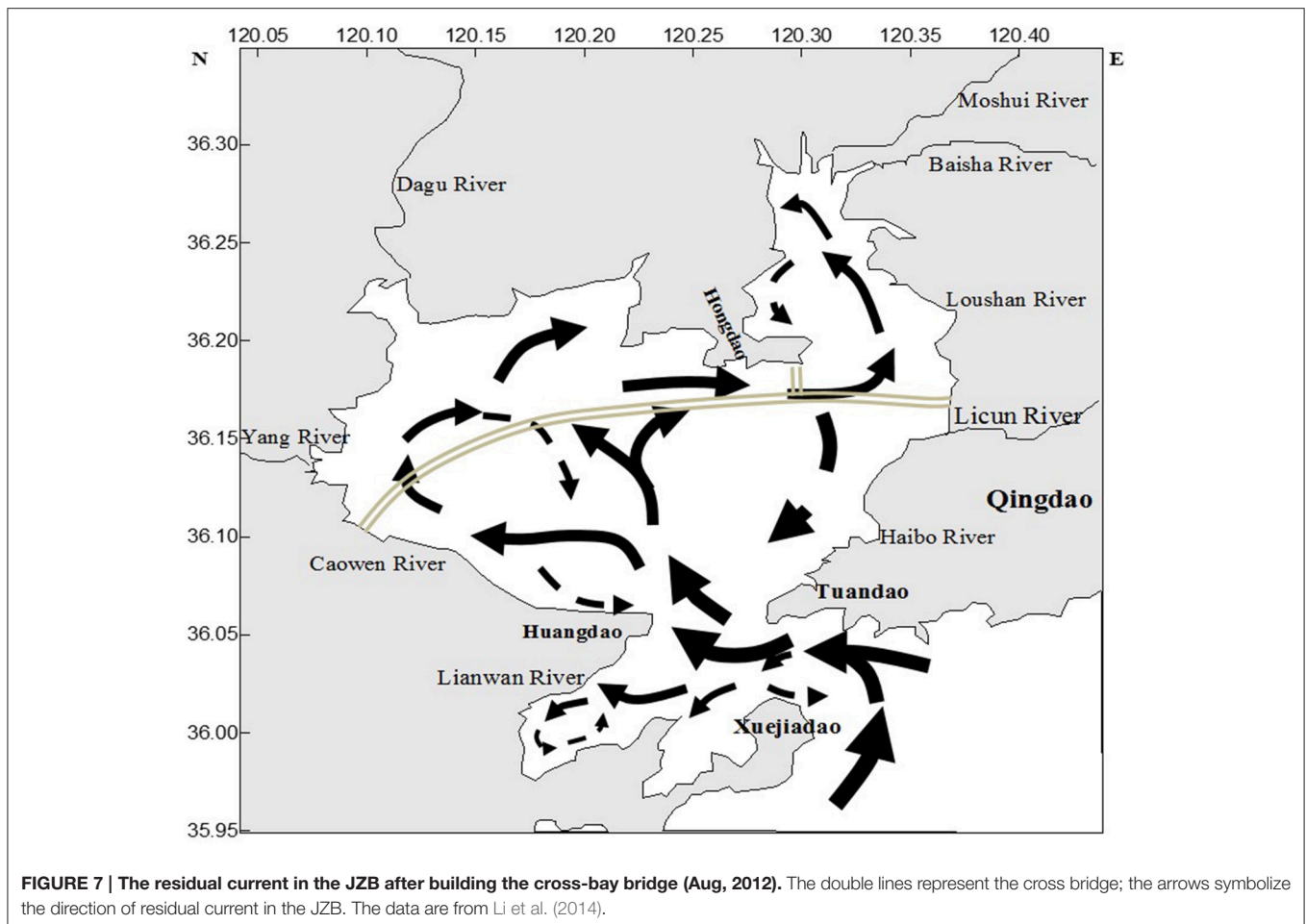
The water exchange capacity (WEC) of the JZB is an apparent phenomenon from residual currents and have significant spatial differences (Liu et al., 2004). According to Lü et al. (2010)'s study about WEC, two regions were observed to have the weakest WEC, the west-southwestern part and the most northeastern part of the JZB, which has water residence time longer than 80 days due to a weak WEC (Lü et al., 2010). Therefore, the DFe of these two regions (the northwest of the Huangdao Island and at the Caowen River estuary) could be accumulate to high concentrations in spring and in summer (**Figure 3**).

The Iron Biogeochemical Cycle in JZB Sources and Removal of DFe

The highest DFe concentrations were measured at Licun River estuary in the eastern area of the JZB, especially in spring (**Figure 3**). Spring is a dry season in Qingdao area (**Figure 6**). Most of the rivers that are located in the eastern part of the bay (Licun, Haibo, and Loushan Rivers (He et al., 2013) are highly polluted with industrial wastewater and domestic sewage that contain DFe. The sewage treatment plants along the eastern side of the JZB (**Figure 2**), release $\sim 1.14 \times 10^6$ t/d of waste water into the JZB (Qingdao Bureau of Statistics, 2014). The western part of the JZB is an agricultural area, with lower wastewater discharge containing DFe, especially in spring (**Figure 3**).

Summer season is the wet season in Qingdao area. The annual rain fall mainly occurs in July. As a result, the river input to the JZB is higher than in spring, especially in the western area of the JZB. In the ES, however, the concentration of DFe in rain water (75 nM, unpublished data) was lower than in waste water. So comparing to spring, the DFe concentration decreased at Licun River estuary due to the dilution of rivers entering into the bay with rain water. However, in the western bay (NWS region), rivers in summer carry higher flux of fresh water into the JZB than that in spring, especially the Dagou ($\sim 177\%$ of all annual river runoff to the JZB, Sheng et al., 2014), but also Yang and Caowen Rivers (**Figure 6**, Sheng et al., 2014). Fresh water in rivers has high DFe concentration (Wang and Liu, 2003; Stolpe et al., 2010) and would increase DFe in the seawater. Our results showed that the DFe concentration in the NWS region in summer was much higher than that in spring (**Figure 3**), indicating that rivers that flow through agricultural regions are sources of DFe in the NWS region. It seems to be a net effect of source and removal of DFe (will be discussed later), but generally indicating lower influence from agricultural impacts than from industrial ones on the DFe concentration in the JZB.

Rainfall not only increased the discharge of rivers, but also directly increased the DFe concentration in the JZB seawater. In general, the DFe concentrations in summer were much higher than those in spring, which may be caused by the input of rainwater (**Table 1**, **Figure 6**). Our summer campaign (July 19, 2011) was conducted just after the highest rainfall event of that



year (July 2–4, 2011), which induced a strong disturbance and mixing among different regions (Figure 6, Qingdao statistical yearbook in 2011 and 2012²). Additionally, strong rain causing flood events, brought terrigenous sewage/water through rivers entering into the bay, which caused an increase of the DFe concentration. In the central bay, which was less influenced by the input of wastewater than the ES and NWS region, higher DFe concentration of surface water in summer than in spring was detected (Figure 3). This was the influence of direct input of rainwater. High DFe concentrations of the JZB water cannot easily drain out from the bay and exchange with Yellow Sea, causing a long residence time of DFe (Figure 7).

Removal of DFe from the JZB is particularly noticed at the entrance of the bay, where from summer to spring there was a significant decrease in dissolved iron concentration (Figure 3), indicating that water exchange with the Yellow sea occurred. However, especially in the coastal areas of the bay, the removal of DFe is ascribed to consumption by the biota which is eventually, by degradation and sinking, eliminated from the water column. Seasonal differences of temperature and nutrients concentration corroborate this hypothesis. It is known that a growth of

phytoplankton and bacteria requires the uptake of available Fe from the seawater (Brand et al., 1983; Hutchins et al., 1999). According to Wang (2013) in his study of phytoplankton in the JZB, phytoplankton cell abundance and chlorophyll *a* in spring were higher than in summer (Wang, 2013). Sufficient nutrients in the NWS region supported the growth of phytoplankton and as a result, the uptake of the DFe causing lowering of DFe, which was noticed on the plumes of these two rivers. During spring blooms (February) in the JZB, the DFe concentrations decreased significantly (Schoemann et al., 1998). Our results with the DFe concentrations in the NWS region in summer being higher than that in spring (Figure 3 and Table 1) corroborated Wang's study. The amount of phytoplankton in spring was larger than in summer (Wang, 2013), and these phytoplankton and zooplankton metabolites apparently have taken up available iron and decreased the DFe concentrations. Consequently, DFe in the NWS region decreased more than in the ES region, and in the NWS region it was higher in summer than in spring (Figure 3 and Table 1). Furthermore, suspended particles in seawater adsorb Fe attached to particulate organic functional groups (de Baar and de Jong, 2001), and so decrease the concentration of DFe [in the JZB, the organic suspended particles (OSP) make up more than a half of suspended particles, especially in the south

²Statistical Bureau of Qingdao. Available online at: <http://www.stats-qd.gov.cn> (in Chinese).

of the JZB due to the port of Qingdao near station D4 (Bi et al., 2007)]. Due to the impact of tide, some OSP would be swept out by the seawater, and the DFe would be released again, resulting in high DFe concentrations of the CSS region in summer (Figure 3).

Iron-complexing Organic Ligands

An excess of organic ligands over DFe concentrations was observed in both spring and summer periods, which indicated that DFe in the JZB existed mostly in the form of strong organic complexes (Table 1) that play a governing role in maintaining iron in dissolved state. This observation is expected and is consistent with previous CLE-aCSV studies, such as in the open ocean surface waters and coastal waters (Rue and Bruland, 1995; Boye et al., 2001, 2003; Powell and Wilson-Finelli, 2003; Buck and Bruland, 2007; Buck et al., 2007).

In spring, the highest $[L_t]$ was observed near the estuary of the Licun River in the ES region and was ascribed to constant riverine inputs from industry and domestic wastewater associated with the slow water exchange (dilution factor) in the ES region (Figure 4). These wastewaters contained high concentrations of dissolved organic matter (DOM), polychlorinated biphenyl, protein-like and humic-like component, etc. (Guo et al., 2011; Lu et al., 2014), which might be a part of L_t . Furthermore, the L_t concentrations in this region (Industrial region) in spring were higher than that in the NWS region (agricultural region; Figure 4). It directs us toward the conclusion that L_t has a more industrial source than an agricultural source.

Our results also show that the L_t concentration of the NWS region in summer was much higher than in spring (Figure 4 and Table 1). This was because the rainfall brought a large amount of organic pesticide and humic substances (HS) from the farmland into the Dagu and Yang Rivers in the NWS region. Hexachlorocyclohexane soprocide (HCH, Yang et al., 2011) and dichloro diphenyl trichloroethane (DDT, Peng et al., 2014) contamination were reported in this area. These organic pesticides may complex with DFe and become one kind of ligand because of carboxylic, hydroxyl and phenolic functional groups (Nuzzo et al., 2013). According to the study of HS in the JZB, Dagu River was an important source of HS in the JZB (Ji et al., 2006). Laglera and van den Berg's study has given some evidence that L_t was partly composed of humic substances (HS; Laglera et al., 2007; Laglera and van den Berg, 2009), as well as studies of Jones and Bundy (Jones et al., 2011; Bundy et al., 2014). Also, HS derived terrestrial inputs have been found in coastal as well as in deep waters, contributing to the pool of Fe-binding ligands (Laglera and van den Berg, 2009; Bundy et al., 2014). During irrigating of farmlands and heavy rainfall, soil is carried into river water and then into the whole JZB. It matches with the hypothesis that river water entering into NWS region was a source of L_t . Therefore, in the NWS, irrigating activities in combination with rain impact L_t concentrations.

On the other hand, the seasonal variation of L_t in the CSS region was smaller than that of the ES region (spring > summer, Figure 4). However, the CSS region, being in the middle of the bay, was less influenced by terrestrial sources than the ES and the NWS regions.

In the combination with the influence by the industry and agriculture, regular annual phytoplankton blooms and protozoan grazing in the JZB would increase %FeL, like lipophilic endogenous cellular exudates such as dissolved free and combined amino acids (Nagata and Kirchman, 1991; Öztürk et al., 2002). From May (spring campaign) to July (summer campaign) phytoplankton blooms in the JZB may be mainly limited by phosphate (PO_4-P ; Guo et al., 2012). In spring, the highest total dissolved phosphorus concentrations (TDP) were observed at stations A2 and B5 in the ES region (Table 2), which was impacted by terrestrial input. The TDP in these areas increased the growth of phytoplankton (Chen et al., 2012b; Guo et al., 2012). It is to be presumed that iron organic ligands and their excess were produced during degradation of dead cells and released during grazing, thus these ligands would stabilize high DFe concentration (Gerringa et al., 2006). The L_t is related to the TDP-values which matches with the highest DFe-values observed in that region (Figures 3, 4). The NWS region (where nutrients were used up after the spring bloom) and the CSS region (with a few terrestrial sources and strong WEC) were characterized with limited phytoplankton growth in spring, which was indicated by low L_t concentrations and also low DFe-values (Table 1 and Guo et al., 2012).

The $\log K'$ -values in the spring samples were weaker than in the summer ones (Table 1). Though it isn't clearly known what forms weak ligands, previous studies have implied that they may be a combination of degraded cellular material from seawater (Hunter and Boyd, 2007), like polysaccharides (Hassler et al., 2011), thiols, and heme (Hopkinson et al., 2008).

Iron Speciation and Bioavailability

Iron limitations on phytoplankton growth may occur even though the DFe-value is abundant (Nagai et al., 2007). The JZB is eutrophic and has had outbreaks of red tides every year since 1997. Diatoms, such as *Skeletonemacostatum*, are the dominant species in the JZB, whereas cyanobacteria such as *Synechococcus* spp. were low (average 4.7%) among the total biomass of phytoplankton in the JZB (Wu et al., 2005; Zhao et al., 2005). These phenomena may be influenced by low available iron in the JZB. Although high iron concentrations were observed in the JZB, almost all of DFe was complexed by organic ligands (Table 1). On average, higher conditional stability constants in summer than in spring remind us on possible formation of colloidal inert iron (Gledhill and Buck, 2012).

Variation of DFe and L_t in the Two Contrasting Periods

Variations of DFe between summer and spring period were observed (Figures 3–5). The average concentrations of DFe in summer were higher than in spring. The reasons that account for this difference were direct wet deposition from rain water as well as the increased river input from larger amounts of rainfall in summer. The rainfalls in summer and spring were 256 and 2.2 mm, respectively (Figure 6). In summer, direct rain input and the reaction of drainage from land to rivers and their estuaries increased nutrients in the JZB, as well as dissolved iron, also shown by other authors (Wang, 2013). However, less

variations of L_t were observed between two sampling periods than that of DFe. The possible reason for this might be mainly dissolved iron coming from rain fall in summer that increased total iron concentrations in the JZB, but also iron consumed by phytoplankton in the spring period that decreased its dissolved fraction. These results can be corroborated by the increased ratio of $[L_t]$ to $[DFe]$ from summer to spring. The average ratio of $[L_t]$ to $[DFe]$ of the NWS, ES, and CSS in spring were higher than that in summer (Table 1). According to Willey's study (Willey et al., 2000) inorganic Fe species were found to dominate in rainwater at pH from 4.0 to 5.0 [free Fe(II) ion, Fe(III)-oxalate and $Fe(OH)_2^+$].

There are two main mechanisms governing concentration of DFe, one is the input of industrial and rain wastewater, the other is the uptake by organisms. In general, the seasonal variations of DFe were higher than that of L_t (Figures 3, 4; Table 1).

CONCLUSION

The studied distribution of DFe, its organic ligands and inorganic Fe during two contrasting spring and summer periods in surface, middle and bottom layers of the JZB indicated that DFe of the NWS, ES and CSS regions was mostly influenced by agriculture, industrial, and domestic wastewater, and tides, respectively. The influence from industrial and domestic wastewater was much stronger than the influence from agriculture. The riverine and rainfall contribution to input of iron into the shallow JZB regularly, season-dependent, increases the DFe concentrations. Iron-complexing organic ligands were represented by one class of ligands with seasonal dependent stability constants, stronger in summer period. They greatly exceeded the DFe concentration,

so they played a governing role in maintaining iron in the water column in both contrasting periods. The L_t is related to TDP-values, while $[L_t]/[DFe]$ ratio seems to be affected by rain season in summer and by biomass production in spring.

Additional data collection and analyses are envisaged in order to corroborate the main processes governing iron distribution and speciation proposed in this study.

AUTHOR CONTRIBUTIONS

RY designed experiments; RY, SW and YL collected samples; RY, HS, SW and YL carried out experiments; RY, HS and SW analyzed experimental results; RY, HS, IP and DO analyzed data and developed analysis tools; RY, HS, IP and DO wrote the manuscript.

ACKNOWLEDGMENTS

This work was financially supported by the National Science Foundation of China (all awarded to RY, 41140037, 41276069), the Young Scientist Award Science Foundation of Shandong, China (awarded to RY, BS2010HZ026), the Open Science Funding of the Key Lab of The First Institute of Oceanography, SOA (awarded to RY, MESE-2011-03), and the visiting scholar funding of the Key Laboratory of Physical Oceanography of Ministry of Education, China (awarded to Chunlei Fan). We acknowledge bilateral Chinese-Croatian project "Determination of trace metal speciation in coastal waters: toward developing new criteria for water quality control and risk assessment" (PI RY and IP), that enabled our collaboration. This work is also supported by the Croatian Science Foundation under the project number IP-2014-09-7530-MEBTRACE (PI DO).

REFERENCES

- Abualhaija, M. M., Whitby, H., and van den Berg, C. M. G. (2015). Competition between copper and iron for humic ligands in estuarine waters. *Mar. Chem.* 172, 46–56. doi: 10.1016/j.marchem.2015.03.010
- Baker, A. R., Kelly, S. D., Biswas, K. F., Witt, M., and Jickells, T. D. (2003). Atmospheric deposition of nutrients to the Atlantic Ocean. *Geophys. Res. Lett.* 30, 2296–2299. doi: 10.1029/2003gl018518
- Bi, L., Bai, J., Zhao, Z., Li, Y., and Yun, Z. (2007). Characteristics of suspended particles in summer in Jiaozhou Bay. *Mar. Environ. Sci.* 26, 518–522.
- Boyd, P. W., Jickells, T., Law, S., Blain, S., Boyle, E. A., Buesseler, K. O., et al. (2007). Mesoscale iron enrichment experiments 1993–2005: synthesis and future directions. *Science* 315, 612–617. doi: 10.1126/science.1131669
- Boye, M., Aldrich, A. P., van den Berg, C. M. G., de Jong, J. T. M., Veldhuis, M., and Baar, H. J. W. (2003). Horizontal gradient of the chemical speciation of iron in surface waters of the northeast Atlantic Ocean. *Mar. Chem.* 80, 129–143. doi: 10.1016/S0304-4203(02)00102-0
- Boye, M., van den Berg, C. M. G., de Jong, J. T. M., Leach, H., Croot, P., and Baar, H. J. M. (2001). Organic complexation of iron in the Southern Ocean. *Deep Sea Res. I* 48, 1477–1497. doi: 10.1016/S0967-0637(00)00099-6
- Brand, L. E., Sunda, W. G., and Guillard, R. R. L. (1983). Limitation of marine phytoplankton reproductive rates by zinc, manganese, and iron. *Limnol. Oceanogr.* 28, 1182–1198. doi: 10.4319/lo.1983.28.6.1182
- Buck, K. N., and Bruland, K. W. (2007). The physicochemical speciation of dissolved iron in the Bering Sea, Alaska. *Limnol. Oceanogr.* 52, 1800–1808. doi: 10.4319/lo.2007.52.5.1800
- Buck, K. N., Lohan, M. C., Berger, C. J. M., and Bruland, K. W. (2007). Dissolved iron speciation in two distinct river plumes and an estuary: implications for riverine iron supply. *Limnol. Oceanogr.* 52, 843–855. doi: 10.4319/lo.2007.52.2.0843
- Buesseler, K. O., Doney, S. C., Karl, D. M., Boyd, P. W., Caldeira, K., Chai, F., et al. (2008). Environment: ocean iron fertilization—moving forward in a sea of uncertainty. *Science* 319, 162. doi: 10.1126/science.1154305
- Bundy, R. M., Biller, D. V., Buck, K. N., Bruland, K. W., and Barbeau, K. A. (2014). Distinct pools of dissolved iron-binding ligands in the surface and benthic boundary layer of the California current. *Limnol. Oceanogr.* 59, 769–787. doi: 10.4319/lo.2014.59.3.0769
- Chen, B., Zhang, Y., Liu, J., and Kong, X. (2012a). Tidal current dynamic characteristic and its relation with suspended sediment concentration in Jiaozhou Bay. *Adv. Mar. Sci.* 30, 24–35 (in Chinese with English abstract).
- Chen, C., Yang, G., Gao, X., Yu, J., and Wu, G. (2012b). Nutrients distributional characteristics and eutrophication in the sea-surface microlayer and subsurface water in the Jiaozhou Bay. *Acta Sci. Circum.* 32, 1856–1865 (in Chinese).
- Chen, H., Hua, F., Liu, N., and Sun, X. (2009). Study on variability of coastline and water depth of Jiaozhou Bay in recent years. *Adv. Mar. Sci.* 27, 149–154 (in Chinese with English abstract).
- Coale, K. H. (2004). Southern ocean iron enrichment experiment: carbon cycling in high- and low-Si waters. *Science* 304, 408–414. doi: 10.1126/science.1089778
- Croot, P. L., and Johansson, M. (2000). Determination of iron speciation by cathodic stripping voltammetry in seawater using the competing ligand 2-(2-Thiazolylazo)-p-cresol (TAC). *Electroanalysis* 12, 565–576. doi: 10.1002/(SICI)1521-4109(200005)12:8<565::AID-ELAN565>3.0.CO;2-L

- Cullen, J. T., Bergquist, B. A., and Moffett, J. W. (2006). Thermodynamic characterization of the partitioning of iron between soluble and colloidal species in the Atlantic Ocean. *Mar. Chem.* 98, 295–303. doi: 10.1016/j.marchem.2005.10.007
- de Baar, H. J., and de Jong, J. T. (2001). “Distributions, sources and sinks of iron in seawater,” in *IUPAC Series on Analytical and Physical Chemistry of Environmental Systems, Vol. 7*, eds D. R. Turner and K. A. Hunter (West Sussex: John Wiley & Sons Ltd), 123–254.
- Deng, B., Zhang, J., Zhang, G., and Zhou, J. (2010). Enhanced anthropogenic heavy metal dispersal from tidal disturbance in the Jiaozhou Bay, North China. *Environ. Monit. Assess.* 161, 349–358. doi: 10.1007/s10661-009-0751-x
- Ding, W. L. (1992). “Tides and tidal currents,” in *Ecology and Living Resources of Jiaozhou Bay*, ed R.Y. Liu (Beijing: Science Press), 30–56 (in Chinese).
- Gerringa, L. J. A., Blain, S., Laan, P., Sarthou, G., Veldhuis, M. J. W., Brussaard, C. P. D., et al. (2008). Fe-binding dissolved organic ligands near the Kerguelen Archipelago in the Southern Ocean (Indian sector). *Deep Sea Res. II Top. Stud. Oceanogr.* 55, 606–621. doi: 10.1016/j.dsr2.2007.12.007
- Gerringa, L. J. A., Rijkenberg, M. J. A., Wolterbeek, H. T., Verburg, T. G., Boye, M., and de Baar, H. J. W. (2007). Kinetic study reveals weak Fe-binding ligand, which affects the solubility of Fe in the Scheldt estuary. *Mar. Chem.* 103, 30–45. doi: 10.1016/j.marchem.2006.06.002
- Gerringa, L. J. A., Veldhuis, M. J. W., Timmermans, K. R., Sarthou, G., and de Baar, H. J. W. (2006). Co-variance of dissolved Fe-binding ligands with phytoplankton characteristics in the Canary Basin. *Mar. Chem.* 102, 276–290. doi: 10.1016/j.marchem.2006.05.004
- Gledhill, M., and Buck, K. N. (2012). The organic complexation of iron in the marine environment: a review. *Front. Microbiol.* 3:69. doi: 10.3389/fmicb.2012.00069
- Gledhill, M., and van den Berg, C. M. G. (1994). Determination of complexation of iron(III) with natural organic complexing ligands in seawater using cathodic stripping voltammetry. *Mar. Chem.* 47, 41–54. doi: 10.1016/0304-4203(94)90012-4
- Grasshoff, K., Kremling, K., and Ehrhardt, M. (1983). *Methods of Seawater Analysis*. New York, NY: John Wiley & Sons.
- Guo, F., Zhao, J., Chen, J. F., Chen, B. J., Liu, C. X., and Zhang, Y. (2012). Nitrogen and phosphorus pollution in shellfish culture area of Jiaozhou Bay. *Prog. Fishery Sci.* 33, 116–122 (in Chinese with English abstract).
- Guo, J., Yin, Y., Zheng, L., Yu, W., Zhao, H., and Yang, D. (2011). The distribution and risk assessment of polychlorinated biphenyl in surface sediments in estuaries of Jiaozhou Bay, China. *J. Agro Environ. Sci.* 30, 965–972 (in Chinese).
- Hassler, C. S., Alasonati, E., Mancuso Nichols, C. A., and Slaveykova, V. I. (2011). Exopolysaccharides produced by bacteria isolated from the pelagic Southern Ocean—Role in Fe binding, chemical reactivity, and bioavailability. *Mar. Chem.* 123, 88–98. doi: 10.1016/j.marchem.2010.10.003
- He, S., Li, G., and Shi, J. (2013). Distribution of heavy metals in surficial sediments of Jiaozhou Bay and its influencing factors. *Mar. Geol. Front.* 29, 41–48 (in Chinese with English abstract). doi: 10.16028/j.1009-2722.2013.04.005
- Hider, R. C., and Kong, X. (2010). Chemistry and biology of siderophores. *Nat. Prod. Rep.* 27, 637–657. doi: 10.1039/b906679a
- Hopkinson, B. M., Roe, K. L., and Barbeau, K. A. (2008). Heme uptake by *Microscilla marina* and evidence for heme uptake systems in the genomes of diverse marine bacteria. *Appl. Environ. Microbiol.* 74, 6263–6270. doi: 10.1128/AEM.00964-08
- Hudson, R. J., and Morel, F. M. (1993). Trace metal transport by marine microorganisms, implications of metal coordination kinetics. *Deep Sea Res. I Oceanogr. Res. Pap.* 40, 129–150. doi: 10.1016/0967-0637(93)90057-A
- Hunter, K. A., and Boyd, P. W. (2007). Iron-binding ligands and their role in the ocean biogeochemistry of iron. *Environ. Chem.* 4, 221–232. doi: 10.1071/EN07012
- Hutchins, D. A., Witter, A. E., Butler, A., and Luther, G. W. (1999). Competition among marine phytoplankton for different chelated iron species. *Nature* 400, 858–861. doi: 10.1038/23680
- Ji, N. Y., Zhao, W. H., Wang, J. T., and Miao, H. (2006). Change of Humic-like fluorescence characteristics of dissolved organic matter from Dagou River to Jiaozhou Bay. *Environ. Sci.* 27, 1073–1077 (in Chinese with English abstract).
- Jones, M. E., Beckler, J. S., and Taillefer, M. (2011). The flux of soluble organic-iron (III) complexes from sediments represents a source of stable iron (III) to estuarine waters and to the continental shelf. *Limnol. Oceanogr.* 56, 1811–1823. doi: 10.4319/lo.2011.56.5.1811
- Kieber, R. J., Williams, K., Willey, J. D., Skrabal, S., and Avery, G. B. (2001). Iron speciation in coastal rainwater, concentration and deposition to seawater. *Mar. Chem.* 73, 83–95. doi: 10.1016/S0304-4203(00)00097-9
- Kremling, K., Tokos, J. J. S., Brugmann, L., and Hansen, H. P. (1997). Variability of dissolved and particulate trace metals in the Kiel and Mecklenburg bights of the Baltic Sea, 1990–1992. *Mar. Pollut. Bull.* 37, 15–27. doi: 10.1016/s0025-326x(96)00060-4
- Kuma, K., Nishioka, J., and Matsunaga, K. (1996). Controls on iron (III) hydroxide solubility in seawater: the influence of pH and natural organic chelators. *Limnol. Oceanogr.* 41, 396–407. doi: 10.4319/lo.1996.41.3.0396
- Laglera, L. M., Battaglia, G., and van den Berg, C. M. G. (2007). Determination of humic substances in natural waters by cathodic stripping voltammetry of their complexes with iron. *Anal. Chim. Acta* 599, 58–66. doi: 10.1016/j.aca.2007.07.059
- Laglera, L. M., and van den Berg, C. M. G. (2009). Evidence for geochemical control of iron by humic substances in seawater. *Limnol. Oceanogr.* 54, 610–619. doi: 10.4319/lo.2009.54.2.0610
- Li, P., Li, G., Qiao, L., Chen, X., Shi, J., Gao, F., et al. (2014). Modeling the tidal dynamic changes induced by the bridge in Jiaozhou Bay, Qingdao, China. *Continental Shelf Res.* 84, 43–53. doi: 10.1016/j.csr.2014.05.006
- Lin, H., and Twining, B. S. (2012). Chemical speciation of iron in Antarctic waters surrounding free-drifting icebergs. *Mar. Chem.* 128–129, 81–91. doi: 10.1016/j.marchem.2011.10.005
- Liu, J., Guo, Z. R., Yuan, X. J., Zhang, B., and Ma, Z. Y. (2014). Temporal and spatial variation of nutrients in the rivers around Jiaozhou Bay and its fluxes into the sea. *Environ. Chem.* 33, 262–268 (in Chinese with English abstract). doi: 10.7524/j.issn.0254-6108.2014.02.014
- Liu, S. M., Zhang, J., Chen, H. T., and Zhang, G. S. (2005). Factors influencing nutrient dynamics in the eutrophic Jiaozhou Bay, North China. *Prog. Oceanogr.* 66, 66–85. doi: 10.1016/j.pocean.2005.03.009
- Liu, Z., Wei, H., Liu, G., and Zhang, J. (2004). Simulation of water exchange in Jiaozhou Bay by average residence time approach. *Estuar. Coast Shelf Sci.* 61, 25–35. doi: 10.1016/j.ecss.2004.04.009
- Lu, J., Sun, S., Zhang, G., and Zhao, Z. (2014). Temporal and spatial variation of fluorescence characteristics of dissolved organic matters during summer of 2011 in Jiaozhou Bay. *Mar. Sci.* 38, 1–6 (in Chinese with English abstract). doi: 10.11759/hyxx20130325001
- Lü, X. G., Zhao, C., Xia, C. S., and Qiao, F. L. (2010). Numerical study of water exchange in the Jiaozhou Bay and the tidal residual currents near the bay mouth. *Acta Oceanol. Sin.* (in Chinese), 2, 20–30 (in Chinese with English abstract).
- Ma, L., Yang, X., Qi, Y., Liu, Y., and Zhang, J. (2014). Oceanic area change and contributing factor of Jiaozhou Bay. *Sci. Geogr. Sin.* 3, 365–369 (in Chinese with English abstract).
- Marine Environmental Quality of Qingdao (2014). Available online at: <http://ocean.qingdao.gov.cn/n12479801/n32205288/160125182106067781.html>
- Martin, J. H. (1990). Glacial-interglacial CO₂ change, the iron hypothesis. *Paleoceanography* 5, 1–13. doi: 10.1029/PA005i001p00001
- Martin, J. H., and Fitzwater, S. E. (1988). Iron deficiency limits phytoplankton growth in the north-east Pacific subarctic. *Nature* 331, 341–343. doi: 10.1038/331341a0
- Mawji, E., Gledhill, M., Milton, J. A., Tarran, G. A., Ussher, S., Thompson, A., et al. (2008). Hydroxamate siderophores: occurrence and importance in the Atlantic Ocean. *Environ. Sci. Technol.* 42, 8675–8680. doi: 10.1021/es801884r
- Öztürk, M., Bizsel, N., and Steinnes, E. (2003). Iron speciation in eutrophic and oligotrophic Mediterranean coastal waters; impact of phytoplankton and protozoan blooms on iron distribution. *Mar. Chem.* 81, 19–36. doi: 10.1016/S0304-4203(02)00137-8
- Morel, F. M., Hudson, R. J., and Price, N. M. (1991). Limitation of productivity by trace metals in the sea. *Limnol. Oceanogr.* 36, 1742–1755. doi: 10.4319/lo.1991.36.8.1742
- Öztürk, M., Steinnes, E., and Sakshaug, E. (2002). Iron Speciation in the Trondheim Fjord from the perspective of iron limitation for phytoplankton. *Estuar. Coast Shelf Sci.* 55, 197–212. doi: 10.1006/ecss.2001.0897

- Nagai, T., Imai, A., Matsushige, K., Yokoi, K., and Fukushima, T. (2007). Dissolved iron and its speciation in a shallow eutrophic lake and its inflowing rivers. *Water Res.* 41, 775–784. doi: 10.1016/j.watres.2006.10.038
- Nagata, T., and Kirchman, D. L. (1991). Release of dissolved free and combined amino acids by bacterivorous marine flagellates. *Limnol. Oceanogr.* 36, 433–443. doi: 10.4319/lo.1991.36.3.0433
- Nuzzo, A., Sánchez, A., Fontaine, B., and Piccolo, A. (2013). Conformational changes of dissolved humic and fulvic superstructures with progressive iron complexation. *J. Geochem. Explor.* 129, 1–5. doi: 10.1016/j.gexplo.2013.01.010
- Omanović, D., Garnier, C., and Pižeta, I. (2015). ProMCC: an all-in-one tool for trace metal complexation studies. *Mar. Chem.* 173, 25–39. doi: 10.1016/j.marchem.2014.10.011
- Peng, J., Song, J., Li, C., and Yu, L. (2014). Risk assesment of ingesting polyunsaturated fatty acids and organochlorine pesticide residues in five seaweeds from Jiaozhou Bay. *Oceanol. Limnol. Sin.* 45, 80–87 (in Chinese).
- Pižeta, I., Sander, S., Hudson, R., Omanović, D., Baars, O., Barbeau, K., et al. (2015). Interpretation of complexometric titration data: an intercomparison of methods for estimating models of trace metal complexation by natural organic ligands. *Mar. Chem.* 173, 3–24. doi: 10.1016/j.marchem.2015.03.006
- Poorvin, L., Rinta-Kanto, J. M., and Hutchins, D. A. (2004). Viral release of iron and its bioavailability to marine plankton. *Limnol. Oceanogr.* 49, 1734–1741. doi: 10.4319/lo.2004.49.5.1734
- Powell, R. T., and Wilson-Finelli, A. (2003). Importance of organic Fe complexing ligands in the Mississippi River plume. *Estuar. Coast Shelf Sci.* 58, 757–763. doi: 10.1016/S0272-7714(03)00182-3
- Qingdao Bureau of Statistics (2014). *Qingdao Statistical Yearbook-2013[M]*. Beijing: China Statistics Press.
- Redfield, A. C. (1958). The biological control of chemical factors in the environment. *Am. Sci.* 46, 230A, 205–221.
- Rue, E. L., and Bruland, K. W. (1995). Complexation of iron(III) by natural organic ligands in the Central North Pacific as determined by a new competitive ligand equilibration/adsorptive cathodic stripping voltammetric method. *Mar. Chem.* 50, 117–138. doi: 10.1016/0304-4203(95)00031-L
- Sander, S. G., Tian, F., Ibisani, E. B., Currie, K. I., Hunter, K. A., and Frew, R. D. (2015). Spatial and seasonal variations of iron speciation in surface waters of the Subantarctic front and the Otago Continental Shelf. *Mar. Chem.* 173, 114–124. doi: 10.1016/j.marchem.2014.09.001
- Schoemann, V., de Baar, H. J. W., de Jong, J. T. M., and Lancelot, C. (1998). Effects of phytoplankton blooms on the cycling of manganese and iron in coastal waters. *Limnol. Oceanogr.* 43, 1427–1441. doi: 10.4319/lo.1998.43.7.1427
- Sheng, M., Cui, J., Shi, Q., Li, L., and Deng, Y. (2014). Analysis of sediment discharge characteristics of Rivers in Jiaozhou Bay, Qingdao City. *J. China Hydrol.* 34, 92–96 (in Chinese with English abstract).
- Siefert, R. L., Johansen, A. M., and Hoffmann, M. R. (1999). Chemical characterization of ambient aerosol collected during the southwest monsoon and intermonsoon seasons over the Arabian Sea, Labile-Fe (II) and other trace metals. *J. Geophys. Res.* 104, 3511–3526. doi: 10.1029/1998JD100067
- Stolpe, B., Guo, L., Shiller, A. M., and Hasselöv, M. (2010). Size and composition of colloidal organic matter and trace elements in the Mississippi River, Pearl River and the northern Gulf of Mexico, as characterized by flow field-flow fractionation. *Mar. Chem.* 118, 119–128. doi: 10.1016/j.marchem.2009.11.007
- Su, H., Yang, R., Zhang, A., and Li, Y. (2015). Dissolved iron distribution and organic complexation in the coastal waters of the East China Sea. *Mar. Chem.* 173, 208–221. doi: 10.1016/j.marchem.2015.03.007
- Sunda, W. G., Swift, D. G., and Huntsman, S. A. (1991). Low iron requirement for growth in oceanic phytoplankton. *Nature* 351, 55–57. doi: 10.1038/351055a0
- Sundby, B., Anderson, L. G., Hall, P. O. J., Iverfeldt, A., van der Loeff, M. M. R., and Westerlund, S. F. G. (1986). The effect of oxygen on release and uptake of cobalt, manganese, iron and phosphate at the sediment-water interface. *Geochim. Cosmochim. Acta* 50, 1281–1288. doi: 10.1016/0016-7037(86)90411-4
- Tan, S., Shi, G., and Wang, H. (2012). Long-range transport of spring dust storms in Inner Mongolia and impact on the China seas. *Atmos. Environ.* 46, 299–308. doi: 10.1016/j.atmosenv.2011.09.058
- Thuróczy, C., Gerringa, L., Klunder, M. B., Middag, R., Laan, P., Timmermans, K. R., et al. (2010). Speciation of Fe in the Eastern North Atlantic Ocean. *Deep Sea Res. Part I Oceanogr. Res. Pap.* 57, 1444–1453. doi: 10.1016/j.dsr.2010.08.004
- Tsunogai, S., and Uematsu, M. (1978). Particulate manganese, iron and aluminum in coastal water, Funka Bay, Japan. *Geochem. J.* 12, 39–46. doi: 10.2343/geochemj.12.39
- van den Berg, C. M. (1995). Evidence for organic complexation of iron in seawater. *Mar. Chem.* 50, 139–157. doi: 10.1016/0304-4203(95)00032-M
- van den Berg, C. M. G. (2006). Chemical speciation of iron in seawater by cathodic stripping voltammetry with dihydroxynaphthalene. *Anal. Chem.* 78, 156–163. doi: 10.1021/ac051441+
- Wang, W. (2013). *The Influence of Typhoon-Induced Precipitation on the Supplementary of Biogenic Elements, the Abundance and Structure of Phytoplankton in Jiaozhou Bay*. Thesis 93, Ocean University of China (in Chinese and English abstract).
- Wang, Z., and Liu, C. (2003). Distribution and partition behavior of heavy metals between dissolved and acid-soluble fractions along a salinity gradient in the Changjiang Estuary, eastern China. *Chem. Geol.* 202, 383–396. doi: 10.1016/j.chemgeo.2002.05.001
- Wiley, J. D., Kieber, R. J., Williams, K. H., Crozier, J. S., Skrabal, S. A., and Avery, G. B. (2000). Temporal variability of iron speciation in coastal rainwater. *J. Atmos. Chem.* 37, 185–205. doi: 10.1023/A:1006421624865
- Witter, A. E., Hutchins, D. A., Butler, A., and Luther, G. W. III. (2000). Determination of conditional stability constants and kinetic constants for strong model Fe-binding ligands in seawater. *Mar. Chem.* 69, 1–17. doi: 10.1016/S0304-4203(99)00087-0
- Wu, J., and Luther, G. W. III. (1995). Complexation of Fe (III) by natural organic ligands in the Northwest Atlantic Ocean by a competitive ligand equilibration method and a kinetic approach. *Mar. Chem.* 50, 159–177. doi: 10.1016/0304-4203(95)00033-N
- Wu, Y. L., Sun, S., and Zhang, Y. S. (2005). Long-term change of environment and its influence on phytoplankton community structure in Jiaozhou Bay. *Oceanol. Limnol. Sin.* 36, 487–498 (in Chinese with English abstract).
- Yang, D., Ding, Z., Zheng, L., Bu, Z., and Shi, Q. (2011). Homogeneity of HCH distribution in the Jiaozhou Bay waters. *Coast. Eng.* 30, 66–74 (in Chinese with English abstract).
- Zhao, S. J., Xiao, T., Li, H. B., and Xu, J. H. (2005). Distribution of *Synechococcus* spp. in Jiaozhou Bay. *Oceanol. Limnol. Sin.* 36, 534–540 (in Chinese with English abstract).
- Zhu, M., Hao, X., Shi, X., Yang, G., and Li, T. (2012). Speciation and spatial distribution of solid-phase iron in surface sediments of the East China Sea continental shelf. *Appl. Geochem.* 27, 892–905. doi: 10.1016/j.apgeochem.2012.01.004

Conflict of Interest Statement: The authors declare that the research was conducted in the absence of any commercial or financial relationships that could be construed as a potential conflict of interest.

Copyright © 2016 Su, Yang, Pižeta, Omanović, Wang and Li. This is an open-access article distributed under the terms of the Creative Commons Attribution License (CC BY). The use, distribution or reproduction in other forums is permitted, provided the original author(s) or licensor are credited and that the original publication in this journal is cited, in accordance with accepted academic practice. No use, distribution or reproduction is permitted which does not comply with these terms.



Fe-Binding Dissolved Organic Ligands in the Oxidic and Suboxic Waters of the Black Sea

Loes J. A. Gerringa^{1*}, Micha J. A. Rijkenberg¹, Johann Bown¹, Andrew R. Margolin², Patrick Laan¹ and Hein J. W. de Baar^{1,3}

¹ Department of Ocean Systems, NIOZ Royal Netherlands Institute for Sea Research, Utrecht University, Texel, Netherlands,

² Rosenstiel School of Marine and Atmospheric Science, University of Miami, Miami, FL, USA, ³ Department Ocean Ecosystems, University of Groningen, Groningen, Netherlands

OPEN ACCESS

Edited by:

Sylvia Gertrud Sander,
University of Otago, New Zealand

Reviewed by:

Randelle M. Bundy,
Woods Hole Oceanographic
Institution, USA
Luis Miguel Laglera,
Universidad Islas Baleares, Spain

*Correspondence:

Loes J. A. Gerringa
loes.gerringa@nioz.nl

Specialty section:

This article was submitted to
Marine Biogeochemistry,
a section of the journal
Frontiers in Marine Science

Received: 13 January 2016

Accepted: 17 May 2016

Published: 31 May 2016

Citation:

Gerringa LJA, Rijkenberg MJA,
Bown J, Margolin AR, Laan P and
de Baar HJW (2016) Fe-Binding
Dissolved Organic Ligands in the Oxidic
and Suboxic Waters of the Black Sea.
Front. Mar. Sci. 3:84.
doi: 10.3389/fmars.2016.00084

In the oxygen-rich layer of the Black Sea, above the permanent halocline, the Fe and nitrate concentrations are low where fluorescence is relatively high, indicating uptake by phytoplankton. In this study we used ligand exchange adsorptive cathodic stripping voltammetry (CLE-aCSV), using 2-(2-Thiazolylazo)-p-cresol (TAC) as measuring ligand, to investigate the role of Fe-binding dissolved organic ligands in keeping Fe in the dissolved phase and potentially biologically available. The conditional stability constant, $\log K'$, was between 21 and 22 in most samples, which is on average lower than in ocean water. The Fe-binding dissolved organic ligand concentrations varied between 0.35 and 4.81 nEq of M Fe, which was higher than the dissolved concentration of Fe (DFe) as found in most samples. At two stations ligands were saturated in the surface. At one station ligands were saturated near the oxycline, where ligand concentrations seemed to increase, indicating that they play a role in keeping Fe in the dissolved phase across the redox gradient. At the fluorescence maximum (between 40 and 50 m), the dissolved organic ligand binding capacity ($\alpha\text{FeL} = K'[\text{L}']$) of Fe was at its highest while the concentration DFe was at its lowest. Here, we find a statistically significant, positive relationship between fluorescence and the logarithm of αFeL , along with fluorescence and the ratio of the total ligand concentration over DFe. These relationships are best explained by phytoplankton utilizing Fe from Fe-binding organic ligands, resulting in an increase in free Fe-binding ligands.

Keywords: GEOTRACES, Black Sea, Fe speciation, Fe-binding dissolved organic ligands, iron

INTRODUCTION

The Black Sea is the largest permanently anoxic basin on Earth. It is vertically stratified, caused by dense Mediterranean seawater that sinks as it enters the basin via the Bosphorus, flowing below the less dense surface waters that are strongly influenced by river input. A consequence of the strong vertical stratification is a permanent halocline between 50 and 120 m that separates the underlying anoxic layer, containing high sulfide concentrations, from the overlying oxygenated surface layer (OL); between them is a suboxic zone (Sorokin, 2002a,b; Pakhomova et al., 2014; Margolin et al., 2016). The vertical diffusive flux of oxygen from the OL to the underlying suboxic zone is insufficient to meet the oxygen consumption demands for the degradation of sinking organic

material. The suboxic zone, or redoxcline, is characterized by steep gradients of physicochemical properties with large consequences for microbial, physical and chemical processes. These processes in turn affect the solubility of Fe, which varies strongly along this redoxcline (Lewis and Landing, 1991; Dellwig et al., 2010), and other redoxcline environments (Dyrssen and Kremling, 1990; Van Cappellen and Wang, 1996; Taylor et al., 2001; Dellwig et al., 2010). As oxygen decreases in concentration, Fe(III) is reduced to Fe(II), increasing its solubility. In the anoxic water below the redoxcline, the solubility of Fe(II) decreases as sulfide concentrations increase, resulting in Fe precipitation (Lewis and Landing, 1991).

In the OL, the concentration of dissolved Fe (DFe) depends on external sources like dust and rivers, and on internal processes such as the dissolution of Fe-containing particles, and the presence of Fe-binding dissolved organic ligands (Rue and Bruland, 1995; Liu and Millero, 2002; Rijkenberg et al., 2006a,b; 2008; Wagener et al., 2008; Croot and Heller, 2012; Gledhill and Buck, 2012). Fe-binding dissolved organic ligands form a tiny part (<0.1%), of the dissolved organic carbon (DOC) pool, and are not well defined (Gledhill and Buck, 2012; and references herein). They can consist of highly specific Fe-binding siderophores, humic substances or polysaccharides, existing in either the truly dissolved (<0.02 μm) or colloidal (>0.02 and <0.2 μm) phases (Bergquist et al., 2007; Thuróczy et al., 2010, 2011; Hassler et al., 2015). Siderophores are produced by bacteria as a response to Fe stress (Macrellis et al., 2001; Gledhill et al., 2004; Martinez and Butler, 2007; Mawji et al., 2011), whereas humic substances are expected to exist mostly in coastal areas and near rivers and estuaries (Laglera and van den Berg, 2009; Batchelli et al., 2010). Fe-binding dissolved organic ligands can also be produced during zooplankton grazing (Sato et al., 2007; Sarthou et al., 2008).

DOC concentrations in the OL range from $\sim 125 \mu\text{M}$ near the OL-suboxic zone boundary to $>180 \mu\text{M}$ at the surface (Ducklow et al., 2007; Margolin et al., 2016), compared to $\sim 75 \mu\text{M}$ at the ocean surface (Hansell et al., 2009). In the OL below the euphotic zone, aerobic mineralization of organic matter regenerates inorganic nutrients and metals, such as Fe (Boyd et al., 2010), and probably also Fe-binding dissolved organic ligands (Witter et al., 2000; Gerringa et al., 2006; Gledhill and Buck, 2012). DOC is introduced into the Black Sea from two major sources: one is rivers enriched with terrigenous DOC with concentrations of $\sim 300 \mu\text{M}$ (Cauwet et al., 2002; Saliot et al., 2002); the second is the Sea of Marmara, bringing moderate concentrations ($\sim 70 \mu\text{M}$) via the Bosphorus Strait (Polat and Tuğrul, 1995; Margolin et al., 2016). Thus, there is a relatively high content of humic substances compared to the oceans, which might have consequences for the concentrations and characteristics of the Fe-binding dissolved organic ligands in the Black Sea.

As far as we know, Fe-binding dissolved organic ligands have not yet been studied in the Black Sea, although Lewis and Landing (1991) recognized that colloidal and organically-complexed Fe species of humic origin accounted for 10–30% of the DFe in the OL. We expect that the organic complexation of Fe is an important factor in its chemistry and its biological availability.

Humic substances may form an important part of the dissolved organic ligand pool. It is likely that the Fe-binding dissolved organic ligands and its interaction with the Fe redox chemistry influence its fluxes through the redoxcline (Maldonado et al., 2001; Shaked et al., 2005; Rijkenberg et al., 2006a, 2008; Nishioka et al., 2009; Fujii et al., 2010; Croot and Heller, 2012; Shaked and Lis, 2012; Kustka et al., 2015). To investigate the role of organic Fe-binding complexation in the Fe chemistry of the Black Sea, we sampled the upper 85 m across the basin during the Dutch GEOTRACES GA04-N cruise (64PE373) in 2013 for the voltammetric determination of Fe-binding dissolved organic ligands.

METHODS

Sampling

Approximately 900 mL samples were taken from the ultra-clean CTD and filtered through a 0.2 μm filter using N_2 overpressure in a clean-air laboratory unit (Rijkenberg et al., 2015). For the analyses of the ligand characteristics, six bottles in the upper 85 m of the Black Sea (at depths 10, 25, 40, 55, 70, and 85 m) were sampled at 6 stations (stations 2, 3, 4, 5, 6, and 11) with a few samples taken at stations 1 (40 m) and 12 (10 and 35 m) (Figure 1). More samples were taken for DFe, DOC and nitrate, however, DOC was not sampled at station 1 (shown in Figures 2, 3).

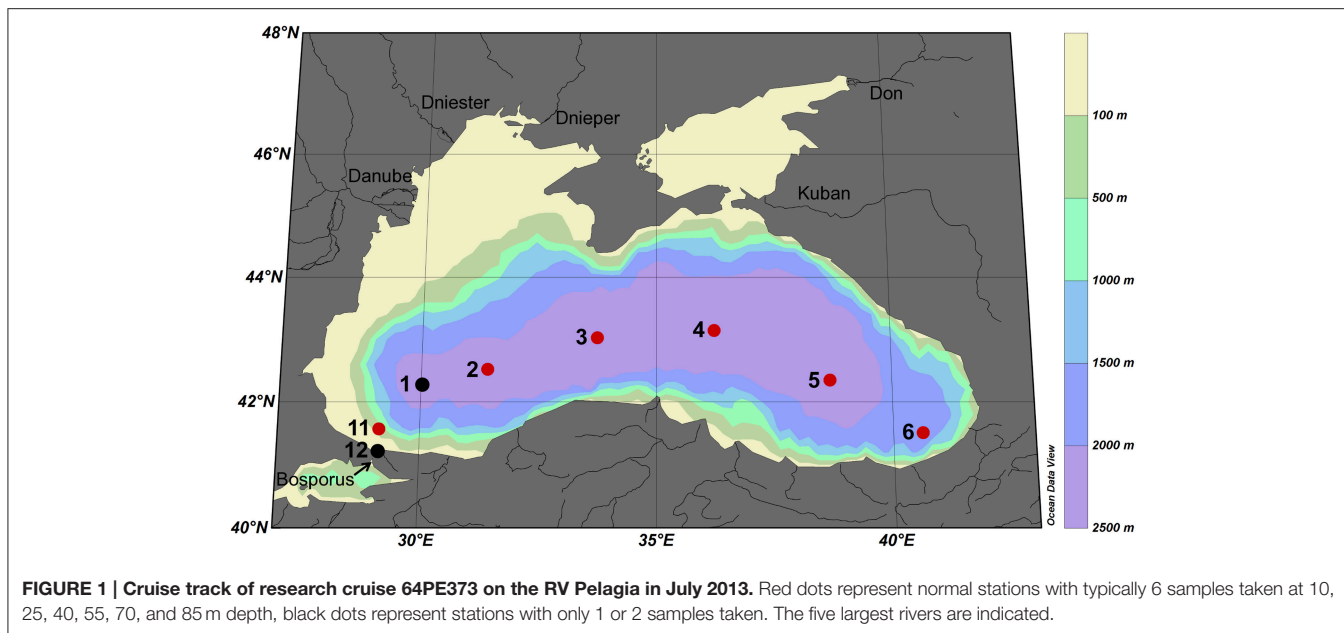
Samples were kept at 4°C in the dark. Fe-binding dissolved organic ligand characteristics were analyzed on board no more than 2 days after sampling. Immediately before the start of the analysis of the ligand characteristics, separate samples were taken from the un-acidified samples. These samples were acidified to pH 1.8 and measured according to the description in Section Flow Injection Analysis of DFe. Separate samples were not taken at station 11.

DOC data is from Margolin et al. (2016). Density and oxygen data were obtained from the CTD consisting of a SBE9plus underwater unit, a SBE11plusV2 deck unit, a SBE3plus thermometer, a SBE4 conductivity sensor, and a SBE43 dissolved oxygen sensor. The CTD oxygen sensor data were calibrated against discrete samples measured on board by Winkler titration (Reinthal et al., 2006). The salinity data calculated from the CTD temperature and conductivity was calibrated against salinity measured in discrete samples analyzed on board with a Guildline 8400B Autosol using OSIL standard water batch P155. Fluorescence was measured as the beam attenuation at 660 nm using a Chelsea Aquatracka MKIII fluorometer. The fluorometer signal was calibrated against Chlorophyll *a* and is expressed as $\mu\text{g Chl}a \text{ dm}^{-3}$.

Analyses

Organic Speciation of Fe

Competing Ligand Exchange—adsorptive Cathodic Stripping Voltammetry (CLE-aCSV) was performed using two setups consisting of a $\mu\text{Autolab}$ potentiationstat (Metrohm Autolab B.V., formerly Ecochemie, the Netherlands), a 663 VA stand with a Hg drop electrode (Metrohm) and a 778 sample processor with ancillary pumps and Dosimats (Metrohm), all controlled using



a laptop running Nova 1.9 (Metrohm Autolab B.V.). The VA stands were mounted on elastic-suspended wooden platforms in aluminum frames developed at the NIOZ to minimize motion-induced noise, while electrical noise and backup power was provided by Fortress 750 UPS systems for spike suppression and noise filtering (Best Power). Sample manipulations were performed in laminar flow cabinets.

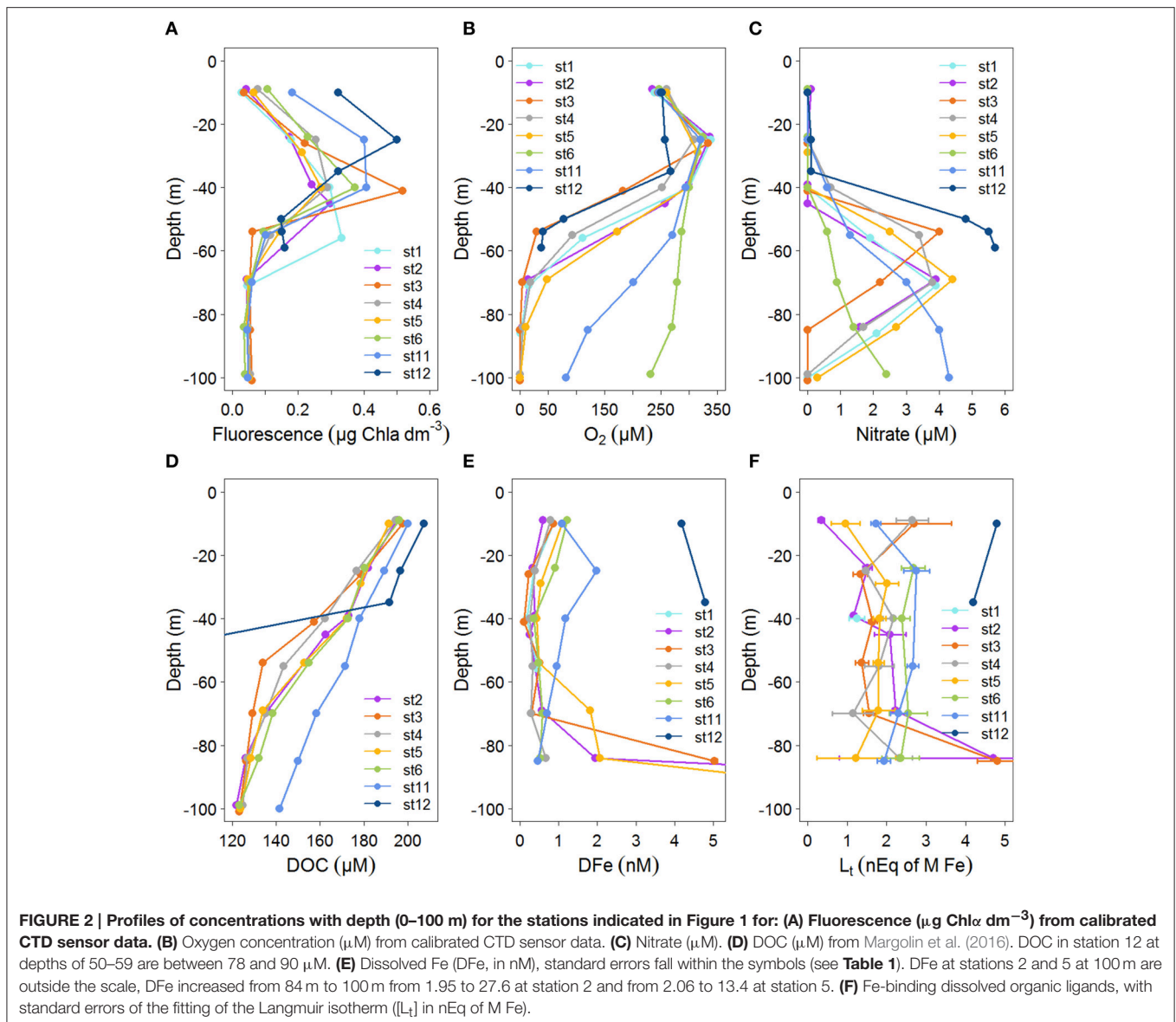
Organic complexation of Fe was determined by CLE- aCSV using 2-(2-Thiazolylazo)-p-cresol (TAC) as a measuring ligand (Croot and Johanson, 2000). The binding characteristics of Fe-binding dissolved organic ligands, the ligand concentration $[L_t]$ (in nano-equivalents of molar Fe, nEq of M Fe) and the conditional binding strength K' (M^{-1}), commonly expressed as $\log K'$ were determined. The measuring ligand TAC with a final concentration of $10 \mu M$ was used, and the complex $(TAC)_2-Fe$ was measured after equilibration (> 6 h). A borate-ammonia buffer was used to maintain pH in the samples during voltammetric scans. The buffer was adjusted to keep the pH at 8.05 in a titration subsample consisting of seawater, buffer and Fe standard additions. Buffers were prepared at NIOZ, where they were cleaned of trace metal contaminations using equilibration with MnO_2 particles after van den Berg and Kramer (1979). The increments of Fe concentrations used in the titration subsamples were 0 (2x), 0.2, 0.4, 0.6, 0.8, 1.0, 1.2, 1.5, 2, 2.5, 3, 4, 6, and 8 nM. Using a non-linear regression of the Langmuir isotherm, the ligand concentration $[L_t]$ and the binding strength K' (given as $\log K'$ in **Table 1A** and text) were estimated. By including the sensitivity, the conversion of the recorded signal (nA) into a concentration (nM), as an unknown parameter in the non-linear regression, we allow for the possibility that the visually linear part of the titration curve is still affected by unsaturated natural ligands (Gerringa et al., 2014). The increments of Fe concentrations listed above were too low for the 10 m sample at station 3, since there $[L']$ was 4.6 nEq of M Fe. The estimation of

$[L_t]$ was not statistically robust, as shown by the large standard error (SE) (**Table 1**) (Laglera et al., 2013; Gerringa et al., 2014). To fully saturate samples, Fe additions were extended to a concentration of 12 nM in the 10, 55, and 70 m samples at station 11, while they were further extended to 20 nM in the 20 and 85 m samples, along with the 10 m sample at station 5.

Using $[L_t]$ and K' , the concentrations of Fe bound to a natural Fe-binding ligand $[FeL]$, the inorganic Fe $[Fe']$ and the natural unbound ligand $[L']$ were calculated using the assumption of chemical equilibrium and the mass balance $DFe = [Fe^{3+}](1+10^{10.1}+K'[L'])$ and $[L_t] = [FeL]+[L']$, respectively by repeated calculations using Newton's algorithm (Press et al., 1986). The parameters from Liu and Millero (2002) were used and an inorganic side reaction coefficient of $10^{10.1}$ was obtained, close to the value of 10^{10} determined by Hudson et al. (1992). For DFe in this calculation, the concentrations used were estimated in the separate samples taken from the un-acidified bottles (see above), except for those taken at station 11. Here, DFe concentrations that were determined in samples that were acidified immediately after collection were used. DFe obtained from the subsamples at station 1–6, were 16% lower than DFe obtained in immediately acidified samples (unpublished data), due to wall adsorption in the un-acidified sample bottles. This agrees well with Gerringa et al. (2014), who reported that DFe concentrations in samples taken from un-acidified samples from the Western Atlantic Ocean were 13% lower than in immediately acidified samples.

The ligand characteristics were calculated with two models, one assuming the presence of one ligand class and the other assuming the presence of two ligand classes (**Table 1A**). The two ligand model converged successfully only at a few samples.

The side reaction coefficient of the ligands (αFeL , given as $\log(\alpha FeL)$) was also calculated as the product of K' and $[L']$. In samples where two ligand classes could be discriminated,



two values of αFeL were calculated: αFeL with the data from the one ligand model and the other with the data from the two ligand model (K'_1 and $[L'_1]$ and K'_2 and $[L'_2]$; Table 1A). αFeL reflects the capacity of the dissolved organic ligands to bind with Fe, which can be seen as its ability to compete for Fe with other ligands and with adsorption sites on particles. Since the K' at station 12 is unknown, αFeL cannot be calculated. αFeL is a better parameter to characterize the Fe-binding dissolved organic ligands than the K' and $[L']$ separately because the Langmuir equation does not treat K' and $[L']$ independently from each other. If an analytical error forces an underestimation of one, the other one is automatically overestimated (Hudson et al., 2003). Moreover, $[L']$ is, in contrast to $[L_t]$, independent of DFe (Thuróczy et al., 2010).

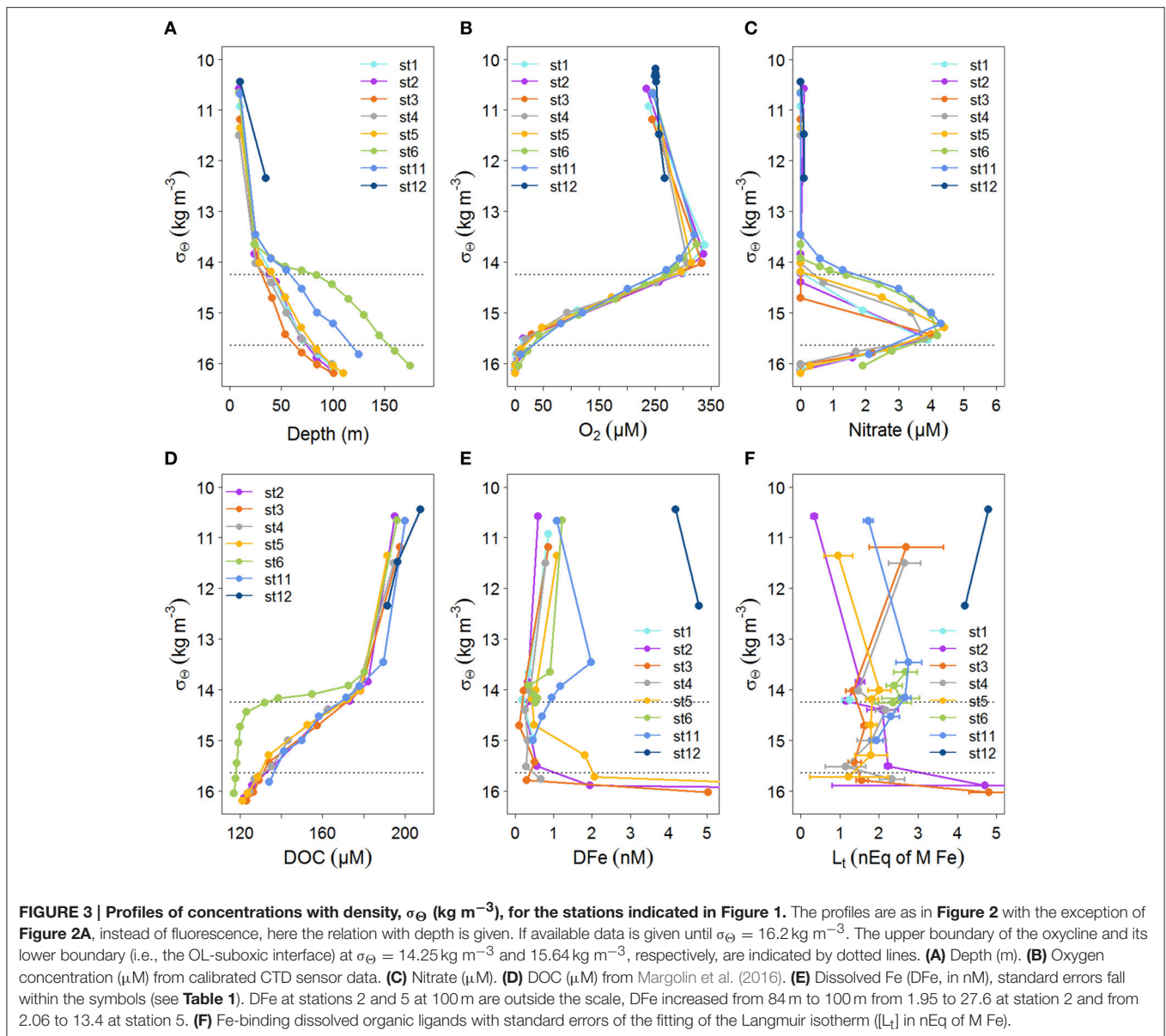
The ratio $[L_t]/\text{DFe}$ (Table 1B) indicates the saturation of the ligands that are saturated with Fe if the ratio ≤ 1 and

unsaturated when >1 (Thuróczy et al., 2010), while ignoring other competing metals (Gerringa et al., 2014; Laglera and Filella, 2015).

Flow Injection Analysis of DFe

The DFe concentrations required for data interpretation were measured at sea using an automated Flow Injection Analysis (FIA) (Klunder et al., 2011) taken from the bottles sampled for Fe complexation.

Filtered (0.2 μm , Sartorius Sartobran 300) and acidified (pH 1.8, 2 ml/L 12M Baseline grade Seastar HCl) seawater was concentrated on a column containing iminodiacetic acid (IDA). IDA only binds with transition metals and not the interfering salts. The column was then washed with ultrapure water, and eluted with 0.4 M HCl (Suprapur, Merck). After mixing with 0.6 mM luminol (Aldrich), 0.6 M hydrogen peroxide (Suprapur,



Merck) and 0.96 M ammonium (Suprapur, Merck) the reaction pH was ~ 10 . The resulting oxidation of luminol with peroxide was catalyzed by Fe to produce a blue light that was detected with a photon counter. The Fe concentration was calculated using a standard calibration line, where a known amount of Fe was added to seawater containing low concentrations of Fe. Using this calibration line, a number of counts per nM Fe were obtained. Samples were analyzed in triplicate and average DFe concentrations and SEs are given (Table 1). On average, the SE was 1.5%, generally being $<3\%$ in samples with DFe concentrations higher than 0.1 nM. The average blank was determined to be at 0.033 nM, defined as the intercept of a low Fe sample loaded for 5, 10, and 20 s and was measured daily. The limit of detection of 0.019 nM was defined as 3 times the SE of the mean of the daily measured blanks (loaded for 10 s). To better understand the day-to-day variations, a

duplicate sample was measured again at least 24 h later than the first measurement. The differences between these measurements were on the order of 1–20%, while the largest differences were measured in samples with low DFe concentrations. To correct for this day-to-day variation, a lab standard (sample acidified for more than 6 months) was measured daily. The consistency of the FIA system over the course of the day was verified using a drift standard. For the long-term consistency and absolute accuracy, certified SAFe and GEOTRACES reference material (Johnson et al., 2007) were measured on a regular basis.

Nutrients

Nitrate was determined on board colorimetrically (Grasshoff et al., 1983) on a Bran en Luebbe trAAcs 800 Autoanalyzer. The detection limit was 0.011 μM .

TABLE 1A | Dissolved Fe (DFe) in nM with standard error of the analysis, the ligand characteristics [L_t] (in nEq of M Fe) and logK' (M⁻¹) with standard error of the fitting of the Langmuir isotherm (Gerringa et al., 2014).

Station	Depth	DFe	SE	logK'	SEu	SEd	logK' ₁	SEu	SEd	logK ₂	SEu	SEd	[L _t]	SE	[L _{t1}]	SE	[L _{t2}]	SE
1	40	0.17	0.004	22.03	0.32	0.18							1.25	0.19				
2	9	0.56	0.000	22.19	NA	0.37							0.35	0.08				
	24	0.28	0.001	22.21	0.16	0.12							1.51	0.12				
	39	0.11	0.004	22.02	0.10	0.08							1.17	0.07				
	45	0.15	0.005	21.48	0.15	0.11							2.09	0.40				
	69	0.50	0.006	22.01	0.07	0.06							2.23	0.09				
	84	1.81	0.007	20.74	0.32	0.18							4.71	3.91				
3	10	0.77	0.005	20.83	0.13	0.10							5.02	2.35				
	26	0.13	0.038	21.93	0.25	0.16							1.34	0.18				
	41	0.06	0.002	22.53	0.31	0.18							1.65	0.11				
	41	0.06	0.002				22.77	NA	0.52	21.25	NA	0.51			0.71	2.10	1.25	1.83
	54	0.29	0.029	21.66	0.13	0.10							1.38	0.17				
	54	0.29	0.029				22.07	0.40	0.21	21.31	NA	0.68			0.81	0.58	3.05	13.74
	70	0.26	0.008	21.94	0.15	0.11							1.57	0.15				
	85	4.76	0.078	21.26	0.08	0.07							4.81	0.51				
4	9	0.92	0.016	21.28	0.09	0.07							2.65	0.41				
	25	0.37	0.010	21.95	0.06	0.06							1.48	0.06				
	40	0.36	0.007	21.65	0.12	0.10							2.16	0.26				
	40	0.36	0.007				24.38	NA	0.54	21.02	0.23	0.15			0.41	0.09	2.75	0.87
	55	0.57	0.006	21.40	0.17	0.12							1.81	0.37				
	70	0.25	0.002	21.33	0.49	0.23							1.15	0.52				
	84	0.62	0.009	21.44	0.10	0.08							2.33	0.32				
5	10	1.05	0.018	21.20	0.59	0.24							0.96	0.36				
	29	0.49	0.001	21.54	0.13	0.10							2.01	0.29				
	40	0.29	0.006	21.92	0.13	0.10							1.82	0.16				
	54	0.50	0.008	21.86	0.11	0.08							1.80	0.14				
	69	0.40	0.005	21.46	0.19	0.13							1.80	0.41				
	84	0.40	0.004	21.09	1.11	0.28							1.23	1.00				
6	24	0.81	0.009	21.50	0.09	0.07							2.68	0.30				
	40	0.30	0.008	21.62	0.08	0.06							2.39	0.20				
	40	0.30	0.008				23.78	NA	0.44	20.90	0.15	0.11			0.32	0.09	2.83	0.60
	70	0.65	0.005	21.24	0.11	0.09							2.55	0.48				
	84	0.53	0.004	21.40	0.15	0.11							2.36	0.48				
11	10	1.09	0.009	22.02	0.17	0.12							1.73	0.13				
	25	1.98	0.011	21.69	0.25	0.16							2.76	0.32				
	55	0.96	0.020	21.91	0.10	0.08							2.67	0.15				
	70	0.70	0.015	21.77	0.14	0.11							2.31	0.21				
	85	0.46	0.006	21.84	0.13	0.10							1.94	0.17				
	85	0.46	0.006				23.01	NA	0.71	21.18	NA	0.35			0.61	0.74	2.41	0.77
12	10	4.18	0.030	NA	NA	NA							4.80	NA				
	35	4.79	0.028	NA	NA	NA							4.20	NA				

All samples have been fitted to a 1 ligand and a 2 ligand model. Where 2 ligands could be distinguished the results of both models are shown in two separate lines.

TABLE 1B | The sum of ligands (1 or the sum of 2 ligands concentrations, the ratio between $[L_t]$, or the sum of both ligands, and D_{Fe} , $\log(\alpha_{FeL})$, (for one or for two ligands), $[Fe']$ and $[L']$ (both in M), for one or for two ligand classes, $[L'_1]$ and $[L'_2]$, were calculated from the first three variables in Table 1A (see Methods).

Station	Depth	Sum $[L_t]$	$[L_t]/D_{Fe}$	$[Fe']$	$[L']$	$[L'_1]$	$[L'_2]$	$\log(\alpha_{FeL})$
1	40	1.25	7.16	1.90E-13	1.06E-09			13.06
2	9	0.35	0.62	2.12E-10	1.32E-12			10.32
	24	1.51	5.34	1.79E-13	1.24E-09			13.30
	39	1.17	10.95	1.21E-13	1.06E-09			13.05
	45	2.09	14.05	3.19E-13	1.95E-09			12.77
	69	2.23	4.43	3.58E-13	1.72E-09			13.25
	84	4.71	2.61	1.41E-11	2.92E-09			12.21
3	10	5.02	6.56	3.34E-12	4.30E-09			12.46
	26	1.34	10.41	1.57E-13	1.22E-09			13.01
	41	1.65	26.01	1.47E-14	1.60E-09			13.73
	41	1.96	30.93	1.96E-14		6.50E-10	1.25E-09	13.61
	54	1.38	4.72	7.34E-13	1.09E-09			12.70
	54	3.86	13.24	2.70E-13		6.50E-10	2.92E-09	13.13
	70	1.57	5.97	2.90E-13	1.32E-09			13.06
	85	4.81	1.01	1.55E-10	2.06E-10			11.57
4	9	2.65	2.88	3.50E-12	1.74E-09			12.52
	25	1.48	4.00	4.68E-13	1.11E-09			13.00
	40	2.16	6.04	5.59E-13	1.78E-09			12.91
	40	3.16	8.82	3.11E-14		5.91E-11	2.74E-09	14.16
	55	1.81	3.18	2.28E-12	1.24E-09			12.49
	70	1.15	4.51	1.66E-12	8.98E-10			12.28
	84	2.33	3.77	1.64E-12	1.70E-09			12.67
5	10	0.96	0.91	1.41E-10	5.13E-11			10.91
	29	2.01	4.12	1.16E-12	1.53E-09			12.72
	40	1.82	6.34	2.83E-13	1.52E-09			13.11
	54	1.80	3.59	6.69E-13	1.31E-09			12.97
	69	1.80	4.53	1.23E-12	1.42E-09			12.61
	84	1.23	3.03	4.93E-12	8.23E-10			12.01
6	24	2.68	3.29	1.73E-12	1.85E-09			12.77
	40	2.39	8.05	4.28E-13	2.08E-09			12.94
	40	3.15	10.62	1.26E-13		4.55E-11	2.81E-09	13.47
	70	2.55	3.90	2.49E-12	1.90E-09			12.52
	84	2.36	4.42	1.46E-12	1.81E-09			12.66
11	10	1.73	1.59	2.04E-12	6.44E-10			12.83
	25	2.76	1.39	6.45E-12	7.88E-10			12.59
	55	2.67	2.79	8.63E-13	1.70E-09			13.14
	70	2.31	3.29	9.32E-13	1.60E-09			12.98
	85	1.94	4.17	5.71E-13	1.49E-09			13.01
	85	3.02	6.50	2.32E-13		2.12E-10	2.34E-09	13.40
12	10	4.80	NA	NA				NA
	35	4.20	NA	NA				NA

RESULTS

Hydrography

The density structure of the Black Sea waters (as σ_θ in kg m^{-3}) is controlled by salinity resulting from the mixing between Mediterranean Sea and river waters. Temperature is less important for maintaining the basin's density structure. At the surface, temperature varies seasonally, resulting in a temperature minimum at ~ 50 m referred to as the cold intermediate layer (CIL). The CIL's maximum temperature boundaries are 8°C isotherms, with its core at $\sigma_\theta \approx 14.6 \text{ kg m}^{-3}$ (Konovalov and Murray, 2001; Margolin et al., 2016). Between the upper boundary of the CIL (i.e., lower boundary of the euphotic zone) and the OL-suboxic interface is the oxycline (Margolin et al., 2016), that ranged from $\sigma_\theta = 14.25\text{--}15.64 \text{ kg/m}^3$ (Figures 3A–F), at slightly lower densities than those found by Konovalov et al. (2001). The onset of sulfide began at $\sigma_\theta = 16.2 \text{ kg m}^{-3}$, again, at a slightly lower density than previously found (Konovalov and Murray, 2001). This was always below 85 m and thus, none of our samples contained sulfide.

Samples were taken at the same depths at each station, however, oxygen concentrations between stations were not consistent with respect to depth, while they were consistent with respect to σ_θ (compare Figures 2B, 3B). Below ~ 50 m at the eastern and western boundaries of the Black Sea (i.e., at stations 6 and 11), oxygen was high and nitrate was low (Figures 2B,C), corresponding to deepening of the OL and suboxic zone (Figures 2B, 3A). High DOC and low DFe were also observed below 50 m at station 11 (Figures 2D,E). This is likely due to the general circulation (Kempe et al., 1990; Buesseler et al., 1994; Yemenicioglu et al., 2006). The wind-driven, counter clockwise (cyclonic) Rim Current flows along the coasts over the shelves and exchanges water between them and the central basin (Oguz et al., 1998; Oguz, 2002; Zhou et al., 2014).

The boundaries of the OL and suboxic zone followed the contours of the σ_θ isopycnal surfaces across the basin, which was also reflected in other parameters, like DOC, nitrate, DFe (Figures 2B–D, 3B–D), salinity and sulfide (Margolin et al., 2016). In the upper 10 m, salinity ranged from a maximum of ~ 18.36 in the central basin to 17.17 and 17.87 at the western and eastern boundaries, respectively, with the lowest salinity near the Bosphorus at station 12 (Margolin et al., 2016). Salinity generally increased sharply to a depth of 85 m, reflected in σ_θ (Figure 3A), and gradually increased with depth below 85 m (Margolin et al., 2016).

Biogeochemistry

At the surface (~ 10 m), oxygen concentrations were $\sim 240 \mu\text{M}$ at all stations, increasing to a maximum of $320\text{--}340 \mu\text{M}$ at a depth of ~ 25 m, with the exception of station 12 near the Bosphorus (Figures 1, 2B). Below ~ 40 m, concentrations decreased with depth at all stations, reaching $100 \mu\text{M}$ at ~ 95 m at the western boundary (station 11), ~ 50 m in the central basin (stations 3 and 4) and ~ 135 m on the eastern boundary (station 6) (Figures 1, 2B). The onset of anoxia (and the redoxcline) was also shallowest in the central basin (e.g., ~ 80 m

at stations 3 and 4) and was deeper at the basin's western and eastern boundaries (e.g., 111 and 185 m, respectively; Figures 1, 2B).

At stations 2–6 DOC decreased from $>180 \mu\text{M}$ near the surface to $125\text{--}130 \mu\text{M}$ at 85 m (Figure 2D). In the upper 55 m at station 3, DOC decreased more sharply with depth than at all other stations. DOC decreased most gradually with depth at station 11 (Figure 2B). Generally, DOC profiles were similar at stations 2–6 with respect to depth (Figure 2D), while they were unique with respect to σ_θ at station 6, having lower concentrations at $\sigma_\theta > 14 \text{ kg m}^{-3}$ (Figure 3D). At station 11, the depth profile of DOC deviates from other stations below ~ 50 m, being $\sim 20 \mu\text{M}$ higher than other stations at these depths (Figure 2D). However, DOC at station 11 does not deviate from other stations when related to density (Figure 3D).

Nitrate is low ($<0.2 \mu\text{M}$) at all stations in the upper ~ 40 m, increasing to a water-column maximum of $3.9\text{--}5.7 \mu\text{M}$ between ~ 50 m (at stations 3 and 12) and 150 m (station 6) (Figure 2C, deep data shown in Figure 3C). This nitrate maximum approximately marks the OL-suboxic interface (Murray et al., 1995). Below this maximum in the underlying redoxcline, nitrate is removed by denitrification (Margolin et al., 2016).

The fluorescence depth distribution is generally determined by nutrient availability from below (see also Figures 2A,C), and light from above. During our study, the fluorescence maximum was between 40 and 60 m at stations 1–6 and between 20 and 30 m at stations 11 and 12 (Figures 2, 4A).

DFe and Fe-Binding Dissolved Organic Ligands

DFe concentrations generally ranged from 0 to ~ 2 nM in the upper 85 m at stations 1–11, with one sample at station 3 having a concentration of 4.67 nM at 85 m (Figure 2E). DFe was also high at the two depths sampled near the Bosphorus at station 12 (4.18 nM at 10 m and 4.80 nM at ~ 37 m) (Figure 2E). Concentrations near the surface at stations 2–6 ranged from 0.56 nM (at station 2) to 1.08 nM (at station 6) and decreased with depth in the upper 40 m reaching concentrations ranging between 0.06 nM (at station 3) and 0.36 nM (at station 5) at ~ 40 m. The concentration of DFe at station 11 was also ~ 1 nM (1.09 nM) near the surface, similar to stations 2–6. However, only at station 11 did concentrations first increase to 1.98 nM at 25 m followed by a decrease to concentrations of ~ 1 nM at 40 m. Between 40 and 85 m, concentrations increased slightly with depth at stations 2, 4, and 6 and increased considerably at stations 3 and 5. The high DFe concentrations coincided with samples taken from below the oxycline (Figure 3E). At station 11, concentrations gradually decreased to 0.46 at 85 m.

Between 40 and 85 m, concentrations tended to increase slightly with depth at stations 1, 4, and 6 and increased considerably at stations 3 and 5. The high DFe concentrations coincided with samples taken from below the oxycline (Figure 3E). At station 11, concentrations gradually decreased to 0.46 at 85 m.

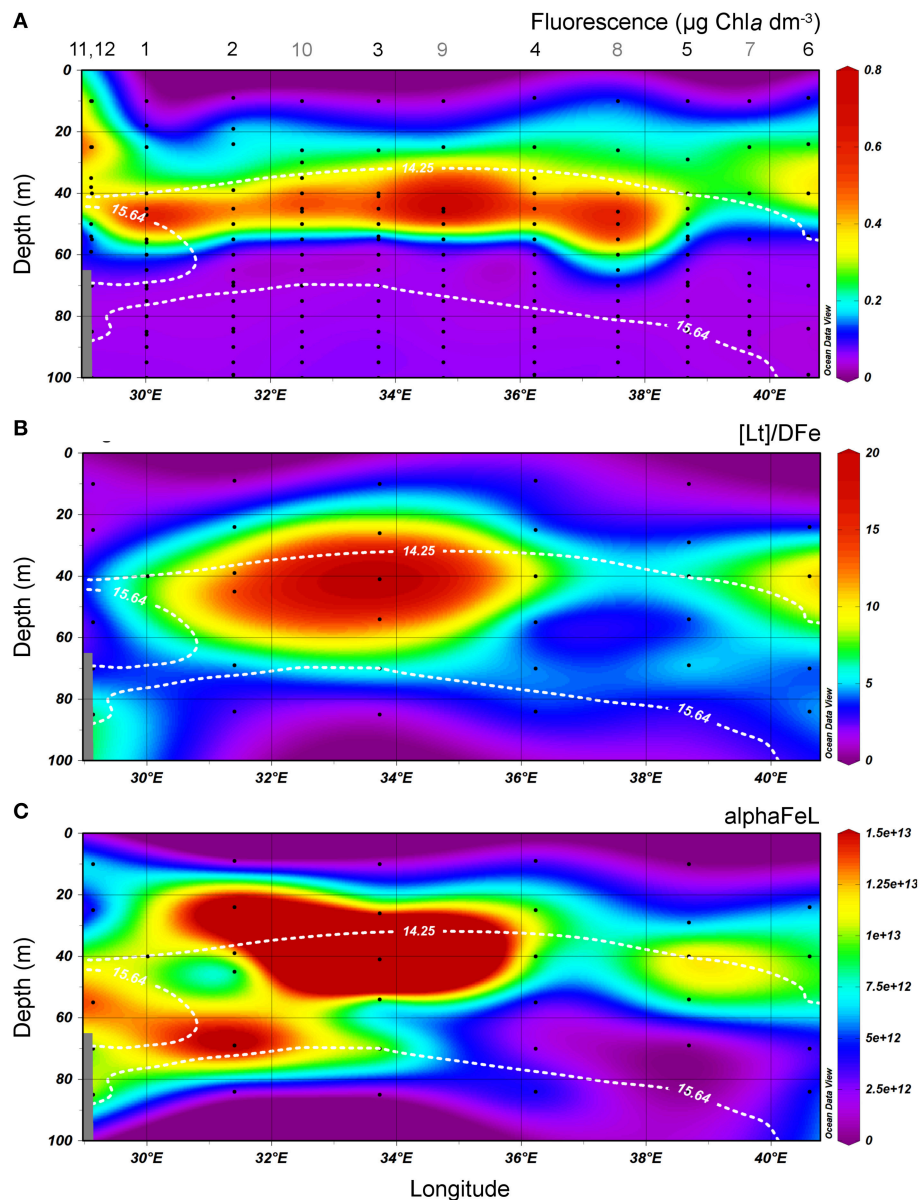


FIGURE 4 | Transects of the cruise track of the upper 100 m from East to West. The upper boundary of the oxycline and its lower boundary (i.e., the OL-suboxic interface) at $\sigma_{\theta} = 14.25 \text{ kg m}^{-3}$ and 15.64 kg m^{-3} , respectively, are indicated by white dotted lines. **(A)** Fluorescence ($\mu\text{g Chla dm}^{-3}$) from calibrated CTD sensor data. **(B)** the ratio $[L_t]/DFe$. **(C)** αFeL . **(B,C)** are both dimensionless. All data points are shown. Stations numbers are indicated above transect A. Note that more stations (indicated with gray numbers) were sampled for fluorescence. In samples where two ligands could be discriminated, the data of the two ligand model was used to calculate $[L_t]/DFe$ and αFeL , $[L_t]$ being the sum of both ligands.

$[L_t]$ varied between 0.35 and 4.81 nEq of M Fe, with the highest concentration ranges found in the samples collected near the surface and at 85 m (**Figure 2F**). At station 12 near the Bosphorus, high $[L_t]$ of ~ 5 nEq of M Fe was found near the surface, while ~ 4 nEq of M Fe was found at ~ 37 m. At stations 1–6 and 11, concentrations generally ranged from ~ 1 to ~ 3 nEq of M Fe, with exceptions near the surface and at 85 m (**Figure 2F**). Near the surface at stations 2, 5, and 11, $[L_t]$ were low (station 2 had the lowest $[L_t]$) and increased to a depth of 25 m, whereas at stations 3 and 4 in the center of the basin, $[L_t]$ were elevated

near the surface (~ 3 nEq of M Fe), decreasing to ~ 1 nEq at 25 m. $[L_t]$ ranged from 1 to 2.8 nEq of M Fe between ~ 25 and 70 m. At stations 2 and 3, $[L_t]$ increased sharply from concentrations of ~ 1 – 2 nEq of M Fe at ~ 70 to concentrations of ~ 5 nEq of M Fe at 85 m. At station 4, $[L_t]$ increased slightly from ~ 70 to 85 m, and **Figure 3F** shows that the increase at this depth range at stations 2–4 occurred below the oxycline. At stations 6 and 11, the deepest samples were taken above the redoxcline.

The values of $\log K'$ were between 20.74 and 22.55 for all samples, but most of them were between 21 and 22 (25 of 34

samples) (Table 1A). Low $\log K'$ values (<21) were found at stations 2 and 3 at 85 m and at 10 m, respectively. These low values are probably the result of an underestimation since the Langmuir equation does not treat K' and $[L']$ independently from each other, as described in the Method section. If an analytical error underestimates one, the other is automatically overestimated (Hudson et al., 2003). The samples with $\log K' < 21$ had a relatively high $[L_t]$ with large standard errors. High $\log K'$ values (>22) were observed at stations 1 (10 m), 2 (4 of 6 depths) and the 40 m sample at station 3 (Table 1A).

In three samples (10 m samples at stations 2 and 5 and 85 m sample at station 3), the ligands were saturated resulting in a low ratio $[L_t]/D_{Fe}$ (between 0.6 and 1). In all other samples $[L_t]/D_{Fe}$ was between 1.5 and 26, with highest values typically at 40–54 m depth (Table 1B).

When the more complex two ligand model was applied, two ligand classes could be discriminated in 5 samples: station 3 at 40 and 54 m, station 4 at 40 m, station 6 at 40 m and station 11 at 85 m (Table 1A). The $\log K'$ of the stronger ligand varied between 22.07 and 24.38, while the $\log K'$ of the weaker ligand was between 20.9 and 21.31 (Table 1A). Only up to a few data points could be used for the calculation of the stronger ligand (2 or 3), giving results with large standard errors (Gerringa et al., 2014). $[L_t]$ of the stronger ligand varied between 0.32 and 0.81, and $[L_t]$ of the weaker varied between 1.25 and 3.05 nEq of M Fe.

DISCUSSION

Possibility of Interferences by Variations in Ionic Strength and Redox Potential

The low salinity of the OL in the Black Sea (17.17–20.71) would favor higher $\log K'$ values, since ions have higher activities at lower ionic strength. To calculate the ligand characteristics we used a binding constant between our measuring ligand TAC and Fe of $\log \beta_{Fe(TAC)_2} = 22.4$, as estimated by Croot and Johanson (2000). They applied their method with the estimated $\log \beta_{Fe(TAC)_2} = 22.4$ for $S = 24$ – 34 , whereas Gerringa et al. (2007) concluded that $\beta_{Fe(TAC)_2}$ did not change much until salinities as low as $S = 10$, making it an acceptable calculation for the Black Sea. A recently unpublished calibration of TAC at different salinities in melted sea ice samples by Gerringa, confirmed that the conditional binding strength $\beta_{Fe(TAC)_2}$ did not change between $S = 36$ and $S = 10$. Although the salinity did not influence $\beta_{Fe(TAC)_2}$ it might influence the binding of Fe with the naturally occurring ligands. The method of Gledhill and van den Berg (1994) using the measuring ligand 1-nitroso-2-naphthol (NN), predicted a difference of 0.3 in $\log \beta_{Fe(NN)_3}$ between $S = 17.17$ and $S = 34$. Buck et al. (2007) used salicylaldoxime (SA) as their measuring ligand, and the conditional binding strength of $\log \beta_{Fe(SA)_2}$ shifted by 0.11. Abualhaija and van den Berg (2014) introduced a different method using the same measuring ligand SA. Using this new SA method, Abualhaija et al. (2015) calibrated the constants of the two SA complexes, FeSA and FeSA₂, against salinity. They found a shift in $\log K'_{FeSA}$ of 0.06 over the above S range and a shift in $\log \beta_{Fe(SA)_2}$ of 0.4. These calibrations of

conditional binding constants of the measuring ligands NN and SA give an indication of the effect of salinity on conditional stability constants of naturally occurring ligands. The differences are not large, however, our results obtained at the relative low salinities of the OL in the Black Sea may not be comparable with results obtained at higher salinity.

Samples were not kept at the ambient redox conditions prior to analysis, however, there wasn't a noticeable offset between D_{Fe} in our samples and those measured in samples that were immediately acidified. Even in the samples with ligands that were (nearly) saturated with Fe, including the only sample taken below the oxycline (from 85 m at station 3), Fe did not precipitate in the sample bottles prior to analysis. Thus, correct determinations of D_{Fe} were obtained. Apparently even after changing the redox conditions, the ligands kept Fe in the dissolved phase.

The Ligand Characteristics $\log K'$ and $[L_t]$ Compared to Literature Values

Compared to the Fe ligand characteristics measured in other marine environments, the $\log K'$ of 21–22 obtained here is relatively low, while a $[L_t]$ of 1–2.8 nEq of M Fe is similar to values found by others in a diverse range of oceans and seas (Rue and Bruland, 1995; Cullen et al., 2006; Gledhill and Buck, 2012; Gerringa et al., 2015). Data obtained with the same method and equipment in the Western Atlantic resulted in a higher $\log K'$ of 22.49 (standard error from mean, $SE = 0.55$, $N = 246$) and comparable average $[L_t] = 1.25$ ($SE = 0.51$, $N = 246$) (Gerringa et al., 2015). Kondo et al. (2007, 2012) used the same measuring ligand, but with another buffer, EPPS. They measured high $\log K'$ values at high salinities in the coastal Sulu Sea ($\log K' = 22.3$ – 24.1 , $pH = 8$ in Kondo et al., 2007) as well as in the open Pacific (78% of the $\log K'$ values were >22 , $pH = 8.1$ in Kondo et al., 2012). In the present study in the Black Sea the $\log K'$ is relatively low, although lower conditional stability constants have been reported before (Rue and Bruland, 1995; Cullen et al., 2006).

The Black Sea has a large river input, according to Margolin et al. (2016), the contribution of river water in the OL is ~50% resulting in DOC concentrations being 2.5 times higher than in the open ocean (Ducklow et al., 2007). Jones et al. (2011) showed that organic complexation is essential for the transport of Fe from the sediment and out of the estuaries. Most likely humics contribute to a large extend to the Fe-binding organic ligand pool leaving the estuaries. These humics have a relatively low $\log K'$ according to Laglera and van den Berg (2009). They measured, using DHN as measuring ligand at $pH = 8$, the $\log K'$ of fulvic and humic acids and of samples rich in humics to be between 20.6 and 21.1. These low $\log K'$ values of humics forms an explanation of the relatively low $\log K'$ that we found. Results from the literature on $\log K'$ in coastal surface waters with low salinities and potentially large river influence agree well with our results, having also found lower values [20.3–22.1 in Gledhill et al. (1998), using NN as measuring ligand and $pH = 6.9$; 20.8–21 in Croot and Johanson (2000) using the same measuring ligand TAC and $pH = 8.05$ as in the present study; 20.1–21.4 in Rijkenberg et al. (2006b) using the same measuring ligand TAC and $pH = 8.05$, as in the present study; 20.3–21.5

in Buck and Bruland (2007) using SA as measuring ligand and $pH = 8.2$]. However, Buck et al. (2007), using the same method as Buck and Bruland (2007), measured higher $\log K'$ values of 21.9–23 in estuarine waters with salinities between 1.4 and 33.9. Mahmood et al. (2015) and Abualhaija et al. (2015) (both using SA at $pH = 8.1$) did not find a relationship between salinity and $\log K'$ in the Mersey estuary but $[L_t]$ did decrease with salinity. Thus, although most coastal research resulted in relatively low $\log K'$ values, probably due to the large input of terrigenous DOC from rivers, not all studies come to the same conclusion. Bundy et al. (2015) distinguished strong and weak ligand groups in estuarine samples. They suggested that both ligand groups consisted of humic materials and that these large molecules have different binding sites. Whether these sites are available to bind Fe depend on environmental conditions. This is an interesting view that might form the explanation for the absence of a discrete relationship between salinity and properties of the dissolved Fe binding ligands. In the Black Sea we might attribute the low the $\log K'$ values to the nature of DOM, but we do not find a relationship between $[L_t]$ and DOC in the Black Sea, as Wagener et al. (2008) found during a time series in the Mediterranean Sea.

Sources and Sinks of Fe and Fe-Binding Dissolved Organic Ligands

At stations 1–6, DFe was slightly elevated at the surface and high near the redoxcline. In the upper 50 m of stations 11 and 12 near the Bosphorus (excluding the surface sample at station 11), DFe was higher than in the rest of the basin. Rivers are the most probable sources of DFe for these coastal stations compared to the basin interior. At station 6, DFe is higher in the upper 40 m than at stations 1–5 and 11. According to the findings of Margolin et al. (2016), the highest percentages of freshwater were found near the surface, which penetrated deeper at station 6 than at other stations. This higher percentage of freshwater at station 6 explains why the σ_θ , oxygen and nitrate depth profiles at stations 1–5 are more similar to station 11 than station 6. This may also explain the higher DFe in the upper 40 m at station 6, when compared to stations 1–5. However, the depth profiles of DOC and $[L_t]$ at station 6 are comparable to those at stations 2–5 (Figures 2D,F), while the DOC vs. density profile is unique (Figure 3). When comparing DOC, between stations 6 and 11, and to a lesser extent DFe, it is surprising that their distributions with respect to density are so different since both stations are located near the boundaries of the basin (Figures 1, 3D,E) and both are affected by the Rim Current. One possibility could be that processes that remove DOC are influenced more strongly or are controlled by depth rather than density. Another possible explanation for this difference is that station 6 was sampled on the eastern boundary of the Batumi eddy, which is an anti-cyclonic (clockwise), semi-permanent eddy located to the east of the Rim Current's eastern boundary (Oguz et al., 1993, 1998; Margolin et al., 2016). It is possible that the Batumi eddy is responsible for the unique DOC distribution at station 6. Influences from rivers or other anthropogenic sources are predominantly in the northwestern part of the Black Sea and are not expected to play a large role at station 6 (Borysova et al., 2005).

The anoxic water in the deep basin is known to be a source of Fe from below (Spencer and Brewer, 1971; Dyrssen and Kremling, 1990; Lewis and Landing, 1991; Tankéré et al., 2001; Yemenicioglu et al., 2006), shown here by the elevated concentrations below the oxycline (Figure 3E).

In the OL at stations 3 and 4, the Fe-binding dissolved organic ligands are higher near the surface than below, which is not observed in the other stations (Figure 2F). Apparently there is either a source of ligands in the center of the basin or greater degradation of organic ligands at the sides of the basin. Rivers as sources are expected to be more important along the coasts and especially in the north-west, where the largest rivers enter the Black Sea (Figure 1). The effect of lateral transport of organic ligands from the shelf is expected to be less in the central stations 3 and 4. Another probable explanation for a heterogeneous distribution of organic ligands might be the hydrography of the Black Sea, through the existence of the cyclonic and anticyclonic gyres and eddies (Oguz et al., 1993, 1998).

$[L_t]$ tend to be elevated in the suboxic zone below the oxycline (Figure 3F), while no $[L_t]$ data is available in the underlying anoxic layer. The ligands are either formed in suboxic conditions or concentrated at the redoxcline, however, with the data obtained here we cannot distinguish between these possible processes. Witter et al. (2000) found an increase in $[L_t]$ in the oxygen minimum zone of the Arabian Sea and attributed this to biological degradation, suggesting that these ligands are breakdown products. They did not find a relationship between $\log K'$ and the oxygen concentration. The pH influences metal speciation and it decreases with decreasing oxygen. At some of our sampled depths alkalinity and dissolved inorganic carbon (DIC) were measured, which enabled the calculation of pH. Error was estimated according to Dickson and Riley (1978) (unpublished results N. M. Clargo). In the top 10 m the pH varied between 8.15 and 8.39 (± 0.0244). At station 6 the pH remained round 8.22–8.23 (± 0.0244) between 10 and 85 m. At station 5 however, the pH decreased to 7.91 (± 0.0244) at 55 m ($\sigma_\theta = 14.65 \text{ kg/m}^3$). Hiscock and Millero (2006) found similar values, the pH was 8.3 in the upper 40 m of the Black Sea and decreased to 7.7 and 7.4 in the oxycline ($\sigma_\theta = 14.25\text{--}15.64 \text{ kg/m}^3$). According to Gledhill et al. (2015) a decrease in pH from 8.3 to 6.8 results in a decrease in organic complexation and an even larger decrease in inorganic complexation. The simultaneous decrease results in a decrease in organic complexation when expressed to $[\text{Fe}^{3+}]$ but in an increase when compared to $[\text{Fe}']$. This might explain the high $\log K'$ values measured in the suboxic zone of the tropical North Pacific by Hopkinson and Barbeau (2007). They attributed these relatively strong ligands either to chemical processes at low oxygen concentrations that stabilized labile Fe compounds or to production by *Prochlorococcus* population present in this suboxic zone. However, like we did in the Black Sea, they measured complexation at the constant pH of 8.05, and thus no information about the actual in situ changes in organic complexation could be obtained.

Complex redox cycling, such as the oxidation of reduced Fe(II) as it diffuses upwards, and the reduction of sinking Fe(III)(hydr)oxides occur near the redoxcline (Spencer and Brewer, 1971; Sorokin, 2002b; Yemenicioglu et al., 2006; Dellwig

et al., 2010). $[L_t]$ near the redoxcline will have consequences for the redox processes of Fe, since organic ligands are known to influence the oxidation and reduction of Fe (Santana-Casiano et al., 2000; Rijkenberg et al., 2006a; González et al., 2012) (in fact, this effect is used by CLE-aCSV, which change the half-wave potential of metals like Fe by complexing it to for example TAC). Increasing and decreasing oxidation rates of Fe(II) in seawater depend on the nature of the organic matter added (Santana-Casiano et al., 2000, 2010; Rijkenberg et al., 2006a; González et al., 2012). Since $[L_t]$ tends to be saturated near the redoxcline, the net effect of these reactions likely keeps DFe in the OL and suboxic zone, decreasing the flux to the anoxic layer and retarding particle formation.

The Availability of Organically Complexed DFe

The ratio $[L_t]/DFe$ had a maximum where ligands were relatively under saturated, corresponding to high fluorescence (Figures 2A, 4A,B). This ratio decreased due to increasing DFe concentrations above and below the fluorescence maximum (Table 1B, Figures 2A, 4A,B). In general, the $\log(\alpha FeL)$ (i.e., the capacity of the dissolved organic ligands to bind with Fe) ranged from 12 to 14.16, with the two highest values (13.13 to 14.16) coinciding with the five samples in which two ligand classes were discriminated (Table 1B, Figure 4C). There were three samples outside of this range with low $\log(\alpha FeL)$ values (10.31, 10.91, and 11.57) and low $[L_t]/DFe$ ratios indicating ligands that were saturated with Fe (i.e., the 10 m samples at stations 2 and 5 and the 85 m sample at station 3). At the fluorescence maximum (40–50 m in Figures 2A, 4A), the $[L_t]/DFe$ ratio and $\log(\alpha FeL)$ tended to have their highest values (Figures 4B,C), and DFe its lowest. We found a significant correlation between $\log(\alpha FeL)$ and fluorescence and between $[L_t]/DFe$ and fluorescence (Table 2). $[L_t]/DFe$ and $\log(\alpha FeL)$ of station 11 appear to be heavily influenced by elevated DFe from the shelves. αFeL is close to zero when ligands are saturated with Fe. Removing station 11 and the samples where the ligands were saturated with Fe (10 m at station 2 and 5 and 85 m at station 3) from the data does indeed result in a better relationship between fluorescence with $\log(\alpha FeL)$ and with $[L_t]/DFe$ (Table 2, Figure 5). According to our relationships only part of the Fe binding organic ligand properties can be explained by fluorescence. This means that other sources contribute to the Fe binding ligand pool. Humics from the shelves and rivers can be laterally transported as also found by others in estuaries (Laglera and van den Berg, 2009; Batchelli et al., 2010; Jones et al., 2011; Laglera et al., 2011; Abualhaija et al., 2015; Bundy et al., 2015; Mahmood et al., 2015). Arthur et al. (1994) suggested that >25% of the organic carbon in sediments was of terrestrial origin, whereas in 1996 Coble could really detect humic-like components in the Black Sea samples (Coble, 1996). Margolin et al. (2016) concluded that in our recent samples, >50% of DOC likely has a terrigenous source. Although humics are expected to be important, we cannot exclude the contribution of siderophores from bacterio-plankton (Macrellis et al., 2001; Gledhill et al., 2004; Martinez and Butler, 2007; Mawji et al., 2011)

and zooplankton grazing (Sato et al., 2007; Sarthou et al., 2008) as source of ligands in the Black Sea.

The increasing $\log(\alpha FeL)$ results from an increase in $[L']$. $[L']$ can increase due to an increase in $[L_t]$, an accumulation of ligands by for example microbial production (Rue and Bruland, 1995; Gerringa et al., 2006; Tian et al., 2006; Buck and Bruland, 2007) or a lateral supply (Laglera and van den Berg, 2009; Batchelli et al., 2010; Jones et al., 2011; Laglera et al., 2011; Abualhaija et al., 2015; Bundy et al., 2015; Mahmood et al., 2015). Alternatively, $[L']$ can increase due to the biological utilization of Fe from organic Fe-complexes (decreasing $[FeL]$ at a constant $[L_t]$). Here we define biological utilization of Fe as the transfer of Fe from the ligand pool to the cells without defining if the Fe is internalized or is adsorbed or bound to the outside of the cell. However, Twining et al. (2015) found that externally scavenged Fe was not a significant Fe fraction of life phytoplankton cells. Anyway, the consequence of the biological utilization of Fe is that $[L']$ increases because Fe is removed from the organic ligands. In the Black Sea, the suggested biological utilization of Fe from the natural dissolved organic ligands resulted in low $[Fe']$ (inorganic Fe not bound by dissolved organic ligands, Table 1B).

Fe complexed by natural dissolved organic ligands is biologically available, as observed by Maldonado et al. (2001, 2005) in the Southern Ocean and sub-Antarctic waters. Maldonado et al. (2005) and Shaked et al. (2005) showed that Fe was taken up from strong Fe binding organic ligands by bacteria and phytoplankton including diatoms. Photochemistry of the Fe-complexes appeared to play a role, although according to Maldonado et al. (2005) the photolability of the ligands was not the determining factor. Shaked et al. (2005) introduced a new uptake model in which extracellular reduction at the cell wall was a necessary step in the uptake process. The reductive step theory has the advantage that it is non-specific for both the type of micro-organisms and the organic Fe-species (Shaked and Lis, 2012). However, other uptake processes exist, see references in Shaked and Lis (2012). The low $[Fe']$ and high $[L']$ that we find indicates that most ligands were not destroyed during biological utilization leaving the ligands intact for further complexation of Fe.

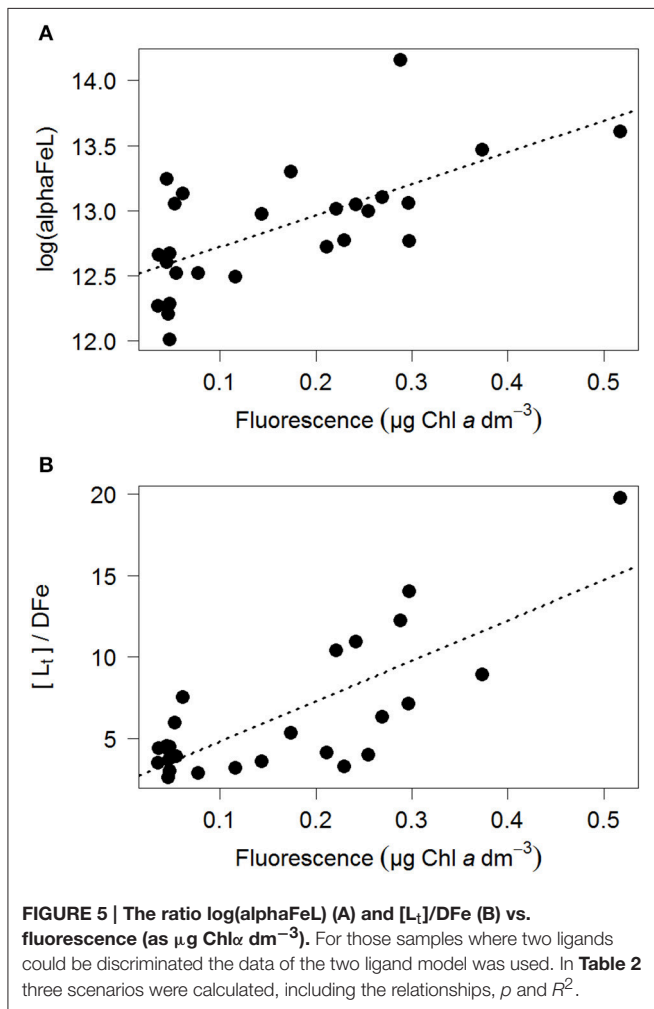
Acknowledging the existence of two ligand classes in five samples improves the correlation between fluorescence with $\log(\alpha FeL)$ and with $[L_t]/DFe$ even more (Figure 5, Table 2). Four out of the five samples in which two ligand classes were distinguished occurred in the fluorescence maximum. Also here it is tempting to conclude that phytoplankton produced the relative strong ligand class, as was concluded by a.o. Rue and Bruland (1995). However, another explanation might be that Fe has been utilized by phytoplankton, not only from the relatively weak Fe-binding organic ligands, but also from the relatively strong Fe-binding organic ligands. When the relatively strong Fe-binding organic ligands are unsaturated, these can be titrated with Fe during the analysis and thus can be distinguished (Gerringa et al., 2014).

Although a relationship between $[L_t]$ and the fluorescence maximum has been observed before (Gerringa et al., 2006), this is not the case for αFeL . The reason that this relationship

TABLE 2 | The relationships between $\log(\alpha\text{FeL})$ and $[\text{L}_t]/\text{DFe}$ (both dimensionless) with fluorescence (as $\mu\text{g Chl } a \text{ dm}^{-3}$).

Y	X	Samples	N	One ligand model			Two ligand model		
				R^2	p	Equation	R^2	p	Equation
Logalpha	Fluorescence	All	34	0.19	<0.01	$Y = 2.4X + 12.3$	0.20	<0.01	$Y = 2.7X + 12.3$
		-st11	29	0.28	<0.001	$Y = 3.1X + 12.1$	0.31	<0.001	$Y = 3.5X + 12.1$
		-st11 - 3	26	0.43	<0.001	$Y = 2.0X + 12.5$	0.41	<0.001	$Y = 2.4X + 12.2$
$[\text{L}_t]/\text{DFe}$	Fluorescence	All	34	0.35	<0.001	$Y = 23.8X + 2.1$	0.39	<0.001	$Y = 20.7X + 2.2$
		-st11	29	0.53	<0.001	$Y = 30.4X + 1.5$	0.35	<0.001	$Y = 19.1X + 2.7$
		-st11 - 3	26	0.49	<0.001	$Y = 28.5X + 2.1$	0.59	<0.001	$Y = 24.8X + 2.3$

Three scenarios were calculated for A: all samples, B: all samples minus station 11, C: all samples minus station 11 and three samples with saturated ligands. Relationships are given for: Left: data using only the 1 ligand model. Right: data using the results of the two ligand model for samples where this model could be applied successfully.



is shown so clearly here might be due to the Black Sea's inland setting and local DFe sources. DFe concentrations are relatively high especially near the redoxcline, and relatively low DFe exists at 40 m depth where the maximum fluorescence was recorded (**Figures 2A,E**). This contrast over a relatively shallow depth range may highlight the relationship between fluorescence with $\log(\alpha\text{FeL})$ and with $[\text{L}_t]/\text{DFe}$.

CONCLUSIONS

Compared with ligand characteristics from open ocean environments the $\log K'$ of 21–22 measured in the OL of the Black Sea is relatively low. This is probably due to the more coastal sources of DOC (i.e., terrigenous origin), and is likely not because of the Black Sea's lower salinity. $[\text{L}_t]$ of 1–2.8 nEq of M Fe is similar to the average values found in other seas and oceans.

Sampling at different redox environments where different redox processes occur, did not affect the $\log K'$ within the detection window of our method (Apte et al., 1988; Sander et al., 2011; Gerringa et al., 2014; Laglera and Filella, 2015; Pižeta et al., 2015). In the suboxic zone DFe was higher due to an increase in solubility. Also $[\text{L}_t]$ increased in the suboxic zone and the ligands here were saturated with Fe. Ligands were also saturated with Fe near the Bosphorus and at 2 stations in the surface. Everywhere else it was the presence of unsaturated dissolved organic ligands that determined the solubility of Fe. This means that in the OL, the solubility and chemical availability of DFe is largely controlled by the dissolved organic ligands.

A significant relationship existed between the alpha coefficient of the dissolved organic ligands and fluorescence, and also between the ratio $[\text{L}_t]/\text{DFe}$ and fluorescence. These relationships are best explained by Fe bound by dissolved organic ligands being utilized by phytoplankton.

An interesting observation was that $[\text{L}_t]$ increased near the suboxic zone at most stations. Transport of Fe over the oxic–anoxic boundary depends strongly on redox processes and the solubility of Fe. Organic complexation of Fe, affecting Fe solubility and redox processes, can therefore play an important role in the vertical transport of Fe in the Black Sea (Santana-Casiano et al., 2010; González et al., 2012).

AUTHOR CONTRIBUTIONS

MR, LG, and HD were responsible for the design of this research. LG, JB, PL, and AM analyzed data. LG and MR did data interpretation. The first draft of the manuscript was made by LG and MR. All other co-authors contributed considerably to

make the second and third drafts. All authors agreed on the final version of this manuscript.

ACKNOWLEDGMENTS

We thank Captain Pieter Kuijt and his crew of RV Pelagia for their hospitality and help during cruise 64PE373. We further thank everybody involved at Royal NIOZ who made this expedition possible. Jan van Ooijen measured nitrate.

REFERENCES

- Abualhaija, M. M., and van den Berg, C. M. G. (2014). Chemical speciation of iron in seawater using catalytic cathodic stripping voltammetry with ligand competition against salicylaldehyde. *Mar. Chem.* 164, 60–74. doi: 10.1016/j.marchem.2014.06.005
- Abualhaija, M. M., Whitby, H., and van den Berg, C. M. (2015). Competition between copper and iron for humic ligands in estuarine waters. *Mar. Chem.* 172, 46–56. doi: 10.1016/j.marchem.2015.03.010
- Apte, S. C., Gardner, M. J., and Ravenscroft, J. E. (1988). An evaluation of voltammetric titration procedures for the determination of trace metal complexation in natural waters by use of computer simulation. *Anal. Chim. Acta* 212, 1–21. doi: 10.1016/S0003-2670(00)84124-0
- Arthur, M. A., Dean, W. E., Neff, E. D., Hay, B. J., King, J., and Jones, G. (1994). Varve calibrated records of carbonate and organic carbon accumulation over the last 20000 years in the Black Sea. *Glob. Biogeochem. Cycl.* 8, 195–217. doi: 10.1029/94GB00297
- Batchelli, S., Muller, F. L. L., Chang, K. C., and Lee, C. L. (2010). Evidence for strong but dynamic iron-humic colloidal associations in humic-rich coastal waters. *Environ. Sci. Technol.* 44, 8485–8490. doi: 10.1021/es101081c
- Bergquist, B. A., Wu, J., and Boyle, E. A. (2007). Variability in oceanic dissolved iron is dominated by the colloidal fraction. *Geochim. Cosmochim. Acta* 71, 2960–2974. doi: 10.1016/j.gca.2007.03.013
- Borysova, O., Kondakov, A., Paleari, S., Rautalahti-Miettinen, E., Stolberg, F., and Daler, D. (2005). *Eutrophication in the Black Sea Region; Impact Assessment and Causal Chain Analysis*. Kalmar: University of Kalmar.
- Boyd, P. W., Ibanmami, E., Sander, S. G., Hunter, K. A., and Jackson, G. A. (2010). Remineralization of upper ocean particles: implications for iron biogeochemistry. *Limnol. Oceanogr.* 55, 1271–1288. doi: 10.4319/lo.2010.55.3.1271
- Buck, K. N., and Bruland, K. W. (2007). The physicochemical speciation of dissolved iron in the Bering Sea, Alaska. *Limnol. Oceanogr.* 52, 1800–1808. doi: 10.4319/lo.2007.52.5.1800
- Buck, K. N., Lohan, M. C., Berger, C. J. M., and Bruland, K. W. (2007). Dissolved iron speciation in two distinct river plumes and an estuary: implications for riverine iron supply. *Limnol. Oceanogr.* 52, 843–855. doi: 10.4319/lo.2007.52.2.0843
- Buesseler, K. O., Livingston, H. D., Ivanov, L., and Romanov, A. (1994). Stability of the oxic-anoxic interface in the Black Sea. *DSR* 41, 283–296. doi: 10.1016/0967-0637(94)90004-3
- Bundy, R. M., Abdulla, H. A., Hatcher, P. G., Biller, D. V., Buck, K. N., and Barbeau, K. A. (2015). Iron-binding ligands and humic substances in the San Francisco Bay estuary and estuarine-influenced shelf regions of coastal California. *Mar. Chem.* 173, 183–194. doi: 10.1016/j.marchem.2014.11.005
- Cauwet, G., Deliat, G., Krastev, A., Shtereva, G., Becquevort, S., Lancelot, C., et al. (2002). Seasonal DOC accumulation in the Black Sea: a regional explanation for a general mechanism. *Mar. Chem.* 79, 193–205. doi: 10.1016/S0304-4203(02)00064-6
- Coble, P. G. (1996). Characterization of marine and terrestrial DOM in seawater using excitation-emission matrix spectroscopy. *Mar. Chem.* 51, 325–346. doi: 10.1016/0304-4203(95)00062-3
- Croot, P. L., and Johanson, M. (2000). Determination of iron speciation by cathodic stripping voltammetry in seawater using the competing ligand 2-(2-Thiazolylazo)-p-cresol (TAC). *Electroanalysis* 12, 565–576. doi: 10.1002/(SICI)1521-4109(200005)12:8<565::AID-ELAN565>3.0.CO;2-L
- Sharyn Ossebaar measured hydrogen sulfide. Nikki Clargo and Lesley Salt measured oxygen for Sven Ober and Hendrik van Aken to calibrate the oxygen sensors. We thank Nikki Clargo for calculating pH values for us on a very short notice. We acknowledge the Dutch funding agency (project number: 822.01.015) of the national science foundation NWO for funding of this work as part of GEOTRACES. The data were collected within the GEOTRACES programme and can be requested at the British Ocean Data Centre (<http://www.bodc.ac.uk>).
- Croot, P. L., and Heller, M. I. (2012). The importance of kinetics and redox in the biogeochemical cycling of iron in the surface ocean. *Front. Microbiol.* 3:219. doi: 10.3389/fmicb.2012.00219
- Cullen, J. T., Bergquist, B. A., and Moffett, J. W. (2006). Thermodynamic characterization of the partitioning of iron between soluble and colloidal species in the Atlantic Ocean. *Mar. Chem.* 98, 295–303. doi: 10.1016/j.marchem.2005.10.007
- Dellwig, O., Leipe, T., März, C., Glockzin, M., Pollehne, F., Schnetger, B., et al. (2010). A new particulate Mn–Fe–P-shuttle at the redoxcline of anoxic basins. *Geochim. Cosmochim. Acta* 74, 7100–7115. doi: 10.1016/j.gca.2010.09.017
- Dickson, A. G., and Riley, J. P. (1978). The effect of analytical error on the evaluation of the components of the aquatic carbon dioxide system. *Mar. Chem.* 6, 77–85. doi: 10.1016/0304-4203(78)90008-7
- Ducklow, H. W., Hansell, D. A., and Morgan, J. A. (2007). Dissolved organic carbon and nitrogen in the Western Black Sea. *Mar. Chem.* 105, 140–150. doi: 10.1016/j.marchem.2007.01.015
- Dyrssen, D., and Kremling, K. (1990). Increasing hydrogen sulfide concentration and trace metal behavior in the anoxic Baltic waters. *Mar. Chem.* 30, 193–204. doi: 10.1016/0304-4203(90)90070-S
- Fujii, M., Rose, A. L., Omura, T., and Waite, T. D. (2010). Effect of Fe(II) and Fe(III) transformation kinetics on iron acquisition by a toxic strain of *Microcystis aeruginosa*. *Environ. Sci. Technol.* 44, 1980–1986. doi: 10.1021/es901315a
- Gerringa, L. J. A., Veldhuis, M. J. W., Timmermans, K. R., Sarthou, G., and de Baar, H. J. W. (2006). Co-variance of dissolved Fe-binding ligands with biological observations in the Canary Basin. *Mar. Chem.* 102, 276–290. doi: 10.1016/j.marchem.2006.05.004
- Gerringa, L. J. A., Rijkenberg, M. J. A., Wolterbeek, H. T., Verburg, T., Boye, M., and de Baar, H. J. W. (2007). Kinetic study reveals weak Fe-binding ligand, which affects the solubility of Fe in the Scheldt estuary. *Mar. Chem.* 103, 30–45. doi: 10.1016/j.marchem.2006.06.002
- Gerringa, L. J. A., Rijkenberg, M. J. A., Thuróczy, C.-E., and Maas, L. R. M. (2014). A critical look at the calculation of the binding characteristics and concentration of iron complexing ligands in seawater with suggested improvements. *Environ. Chem.* 11, 114–136. doi: 10.1071/EN13072
- Gerringa, L. J. A., Rijkenberg, M. J. A., Schoemann, V., Laan, P., and de Baar, H. J. W. (2015). Organic complexation of iron in the West Atlantic Ocean. *Mar. Chem.* 177, 434–446. doi: 10.1016/j.marchem.2015.04.007
- Gledhill, M., and van den Berg, C. M. G. (1994). Determination of complexation of iron (III) with natural organic complexing ligands in seawater using cathodic stripping voltammetry. *Mar. Chem.* 47, 41–54. doi: 10.1016/0304-4203(94)90012-4
- Gledhill, M., van den Berg, C. M. G., Nolting, R. F., and Timmermans, K. R. (1998). Variability in the speciation of iron in the northern North Sea. *Mar. Chem.* 59, 283–300. doi: 10.1016/S0304-4203(97)00097-2
- Gledhill, M., McCormack, P., Ussher, S., Achterberg, E. P., Mantoura, R. F. C., and Worsfold, P. J. (2004). Production of siderophore type chelate by mixed bacterioplankton populations in nutrient enriched seawater incubations. *Mar. Chem.* 88, 75–83. doi: 10.1016/j.marchem.2004.03.003
- Gledhill, M., and Buck, K. N. (2012). The organic complexation of iron in the marine environment: a review. *Front. Microbiol.* 3:69. doi: 10.3389/fmicb.2012.00069
- Gledhill, M., Achterberg, E. P., Li, K., Mohamed, K. N., and Rijkenberg, M. J. (2015). Influence of ocean acidification on the complexation of iron and

- copper by organic ligands in estuarine waters. *Mar. Chem.* 177, 421–433. doi: 10.1016/j.marchem.2015.03.016
- González, A. G., Santana-Casiano, J. M., González-Dávila, M., and Pérez, N. (2012). Effect of organic exudates of *Phaeodactylum tricornutum* on the Fe(II) oxidation rate constant. *Cienc. Mar.* 38, 245–261. doi: 10.7773/cm.v38i1B.1808
- Grasshoff, K., Ehrhard, M., and Kremling, K. (1983). *Methods of Seawater analysis*. Weinheim: Verlag Chemie GmbH. 419.
- Hansell, D. A., Carlson, C. A., Repeta, D. J., and Schlizter, R. (2009). Dissolved organic matter in the ocean: a controversy stimulates new insights. *Oceanography* 22, 202–211. doi: 10.5670/oceanog.2009.109
- Hassler, C. S., Norman, L., Mancuso, N. C. A., Clementson, L. A., Robinson, C., Schoemann, V., et al. (2015). Iron associated with exopolymeric substances is highly bioavailable to oceanic phytoplankton. *Mar. Chem.* 173, 136–147. doi: 10.1016/j.marchem.2014.10.002
- Hiscock, W. T., and Millero, F. J. (2006). Alkalinity of the anoxic waters in the Western Black Sea. *DSR II* 53, 1787–1801. doi: 10.1016/j.dsr.2.2006.05.020
- Hopkinson, B. M., and Barbeau, K. A. (2007). Organic and redox speciation of iron in the eastern tropical North Pacific suboxic zone. *Mar. Chem.* 106, 2–17. doi: 10.1016/j.marchem.2006.02.008
- Hudson, R. J. M., Covault, D. T., and Morel, F. M. M. (1992). Investigations of iron coordination and redox reactions in seawater using ⁵⁹Fe radiometry and ion-pair solvent extraction of amphiphilic iron complexes. *Mar. Chem.* 38, 209–235. doi: 10.1016/0304-4203(92)90035-9
- Hudson, R. J. M., Rue, E. L., and Bruland, K. W. (2003). Modeling complexometric titrations of natural water samples. *Environ. Sci. Technol.* 37, 1553. doi: 10.1021/es025751a
- Johnson, K. S., Boyle, E., Bruland, K., Measures, C., Moffett, J., Aquilarislas, A., et al. (2007). Developing standards for dissolved iron in seawater. *Eos Trans.* 88, 131. doi: 10.1029/2007EO110003
- Jones, M. E., Beckler, J. S., and Taillefert, M. (2011). The flux of soluble organic-iron (III) complexes from sediments represents a source of stable iron (III) to estuarine waters and to the continental shelf. *Limnol. Oceanogr.* 56, 1811–1823. doi: 10.4319/lo.2011.56.5.1811
- Kempe, S., Liebezett, G., and Diercks, A.-R. (1990). Water balance in the Black Sea. *Nature* 346, 419. doi: 10.1038/346419a0
- Klunder, M. B., Laan, P., Middag, R., De Baar, H. J. W., and van Ooijen, J. C. (2011). Dissolved iron in the Southern Ocean (Atlantic sector). *DSR II* 58, 2678–2694. doi: 10.1016/j.dsr.2.2010.10.042
- Kondo, Y., Takeda, S., and Furuya, K. (2007). Distribution and speciation of dissolved iron in the Sulu Sea and its adjacent waters. *DSR II* 54, 60–80. doi: 10.1016/j.dsr.2.2006.08.019
- Kondo, Y., Takeda, S., and Furuya, K. (2012). Distinct trends in dissolved Fe speciation between shallow and deep waters. *Mar. Chem.* 134–135, 18–28. doi: 10.1016/j.marchem.2012.03.002
- Konovalov, S. K., and Murray, J. W. (2001). Variations in the chemistry of the Black Sea on a time scale of decades (1960–1995). *J. Mar. Syst.* 31, 217–243. doi: 10.1016/S0924-7963(01)00054-9
- Konovalov, S. K., Ivanov, L. I., and Samodurov, A. S. (2001). Fluxes and budget of sulphide and ammonia in the Black Sea anoxic layer. *J. Mar. Syst.* 31, 203–216. doi: 10.1016/S0924-7963(01)00053-7
- Kustka, A. B., Jones, B. M., Hatta, M., Field, M. P., and Milligan, A. J. (2015). The influence of iron and siderophores on eukaryotic phytoplankton growth rates and community composition in the Ross Sea. *Mar. Chem.* 173, 195–207. doi: 10.1016/j.marchem.2014.12.002
- Laglera, L. M., Battaglia, G., and van den Berg, C. M. G. (2011). Effect of humic substances on the iron speciation in natural waters by CLE/CSV. *Mar. Chem.* 127, 134–143. doi: 10.1016/j.marchem.2011.09.003
- Laglera, L. M., Downes, J., and Santos-Echeandía, J. (2013). Comparison and combined use of linear and non-linear fitting for the estimation of complexing parameters from metal titrations of estuarine samples by CLE/AdCSV. *Mar. Chem.* 155, 102–112. doi: 10.1016/j.marchem.2013.06.005
- Laglera, L. M., and Filella, M. (2015). The relevance of ligand exchange kinetics in the measurement of iron speciation by CLE–AdCSV in seawater. *Mar. Chem.* 173, 100–113. doi: 10.1016/j.marchem.2014.09.005
- Laglera, L. M., and van den Berg, C. M. G. (2009). Evidence for geochemical control of iron by humic substances in seawater. *Limnol. Oceanogr.* 54, 610–619. doi: 10.4319/lo.2009.54.2.0610
- Lewis, B. L., and Landing, W. M. (1991). The biogeochemistry of manganese and iron in the Black Sea. *DSR* 38 (Suppl. 2), S773–S803. doi: 10.1016/S0198-0149(10)80009-3
- Liu, X., and Millero, F. J. (2002). The solubility of iron in seawater. *Mar. Chem.* 77, 43–54. doi: 10.1016/S0304-4203(01)00074-3
- Macrellis, H. M., Trick, C. G., Rue, E. L., Smith, G., and Bruland, K. (2001). Collection and detection of natural iron-binding ligands from seawater. *Mar. Chem.* 76, 175–187. doi: 10.1016/S0304-4203(01)00061-5
- Mahmood, A., Abualhija, M. M., van den Berg, C. M., and Sander, S. G. (2015). Organic speciation of dissolved iron in estuarine and coastal waters at multiple analytical windows. *Mar. Chem.* 177, 706–719. doi: 10.1016/j.marchem.2015.11.001
- Margolin, A. R., Gerringa, L. J. A., Hansell, D. A., and Rijkenberg, M. J. A. (2016). Net removal of dissolved organic carbon in the anoxic waters of the Black Sea. *Mar. Chem.* 183, 13–24. doi: 10.1016/j.marchem.2016.05.003
- Martinez, J. S., and Butler, A. (2007). Marine amphiphilic siderophores: marinobactin structure, uptake, and microbial partitioning. *J. Inorg. Biochem.* 101, 1692–1698. doi: 10.1016/j.jinorgbio.2007.07.007
- Maldonado, M. T., Boyd, P. W., Strzepek, R., LaRoche, J. L., Waite, A., Croot, P. L., et al. (2001). Phytoplankton physiological responses to changing iron chemistry during a mesoscale Southern Ocean iron enrichment. *Limnol. Oceanogr.* 46, 1802–1808. doi: 10.4319/lo.2001.46.7.1802
- Maldonado, M. T., Strzepek, R. F., Sander, S., and Boyd, P. W. (2005). Acquisition of iron bound to strong organic complexes, with different Fe binding groups and photochemical reactivities, by plankton communities in Fe-limited subantarctic waters. *Glob. Biogeochem. Cycles* 19, GB4S23. doi: 10.1029/2005gb002481
- Mawji, E., Gledhill, M., Milton, J., Zubkov, M., Thompson, A., Wolff, G., et al. (2011). Production of siderophore type chelates in Atlantic Ocean waters enriched with different carbon and nitrogen sources. *Mar. Chem.* 124, 90–99. doi: 10.1016/j.marchem.2010.12.005
- Murray, J. W., Codispoti, L. A., and Friederich, G. E. (1995). “Oxidation–reduction environments: the suboxic zone in the Black Sea,” in *Aquatic Chemistry: Interfacial and Interspecies Processes*, Vol. 224, eds C. P. Huang, C. R. O’Melia, and J. J. Morgan (Washington, DC: American Chemical Society, The Black Sea Ecology and Oceanography), 157–176. doi: 10.1021/ba-1995-0244.ch007
- Nishioka, J., Takeda, S., Kondo, Y., Obata, H., Doi, T., Tsumune, D., et al. (2009). Changes in iron concentrations and bio-availability during an open-ocean mesoscale iron enrichment in the western subarctic Pacific, SEEDS II. *DSR II* 56, 2796–2809. doi: 10.1016/j.dsr.2.2009.06.006
- Oguz, T., Latun, V. S., Latif, M. A., Vladimirov, V. V., Sur, H. I., Markov, A. A., et al. (1993). Circulation in the surface and intermediate layers of the Black Sea. *DSR I* 40, 1597–1612. doi: 10.1016/0967-0637(93)90018-x
- Oguz, T., Ivanov, L. I., and Besiktepe, S. (1998). “Circulation and hydrographic characteristics of the Black Sea during July 1992,” in *Ecosystem Modeling As a Management Tool for the Black Sea*. NATO Science Series, Vol. 2, eds L. I. Ivanov and T. Oguz (Dordrecht: Kluwer Academic Publishers), 69–91.
- Oguz, T. (2002). Role of physical processes controlling oxycline and suboxic layer structures in the Black Sea. *Glob. Biogeochem. Cycles* 16, 3–13–13. doi: 10.1029/2001gb001465
- Pakhomova, S., Vinogradova, E., Yakushev, E., Zatsepina, A., Shtereva, G., Chasovnikov, V., et al. (2014). Interannual variability of the Black Sea Proper oxygen and nutrients regime: the role of climatic and anthropogenic forcing. *Est. Coast. Shelf Sci.* 140, 134–145. doi: 10.1016/j.ecss.2013.10.006
- Pižeta, I., Sander, S. G., Hudson, R. J. M., Baars, O., Barbeau, K. A., Buck, K. N., et al. (2015). Quantitative analysis of complexometric titration data: an intercomparison of methods for estimating models of metal complexation by mixtures of natural ligands. *Mar. Chem.* 173, 3–24. doi: 10.1016/j.marchem.2015.03.006
- Polat, S. C., and Tuğrul, S. (1995). Nutrient and organic carbon exchanges between the Black and Marmara Seas through the Bosphorus Strait. *Cont. Shelf Res.* 15, 1115–1132. doi: 10.1016/0278-4343(94)00064-T
- Press, W. H., Flannery, B. P., Teukolsky, S. A., and Vetterling, W. T. (1986). “Root finding and nonlinear sets of equations,” in *Numerical Recipes*, eds W. H. Press, S. A. Teukolsky, W. T. Vetterling, and B. P. Flannery (Cambridge: Cambridge University Press), 347–393.
- Reinthal, T., Bakker, K., Manuels, R., van Ooijen, J., and Herndl, G. J. (2006). Fully automated spectrophotometric approach to determine oxygen

- concentrations in seawater via continuous-flow analysis. *Limnol. Oceanogr. Methods* 4, 358–366. doi: 10.4319/lo.m.2006.4.358
- Rue, E. L., and Bruland, K. W. (1995). Complexation of iron(III) by natural organic ligands in the Central North Pacific as determined by a new competitive ligand equilibration/adsorptive cathodic stripping voltammetric method. *Mar. Chem.* 50, 117–138. doi: 10.1016/0304-4203(95)00031-L
- Rijkenberg, M. J. A., de Baar, H. J. W., Bakker, K., Gerringa, L. J. A., Keijzer, E., Laan, M., et al. (2015). “PRISTINE”, a new high volume sampler for ultraclean sampling of trace metals and isotopes. *Mar. Chem.* 177, 501–509. doi: 10.1016/j.marchem.2015.07.001
- Rijkenberg, M. J. A., Gerringa, L. J. A., Carolus, V. E., Velzeboer, I., and de Baar, H. J. W. (2006a). Enhancement and inhibition of iron photoreduction by individual ligands in open ocean seawater. *Geochim. Cosmochim. Acta* 70, 2790–2805. doi: 10.1016/j.gca.2006.03.004
- Rijkenberg, M. J. A., Gerringa, L. J. A., Velzeboer, I., Timmermans, K. R., Buma, A. G. J., and de Baar, H. J. W. (2006b). Iron-binding ligands in Dutch estuaries are not affected by UV induced photochemical degradation. *Mar. Chem.* 100, 11–23. doi: 10.1016/j.marchem.2005.10.005
- Rijkenberg, M. J. A., Gerringa, L. J. A., Timmermans, K. R., Fischer, A. C., Kroon, K. J., Buma, A. G. J., et al. (2008). Enhancement of the reactive iron pool by marine diatoms. *Mar. Chem.* 109, 29–44. doi: 10.1016/j.marchem.2007.12.001
- Saliot, A., Parrish, C. C., Sadouni, N., Bouloubassi, I., Fillaux, J., and Cauwet, G. (2002). Transport and fate of Danube Delta terrestrial organic matter in the Northwest Black Sea mixing zone. *Mar. Chem.* 79, 243–259. doi: 10.1016/S0304-4203(02)00067-1
- Sander, S. G., Hunter, K. A., Harms, H., and Wells, M. (2011). Numerical approach to speciation and estimation of parameters used in modeling trace metal bioavailability. *Environm. Sci. Technol.* 45, 6388–6395. doi: 10.1021/es200113v
- Santana-Casiano, J. M., González-Dávila, M., Rodríguez, M. J., and Millero, F. J. (2000). The effect of organic compounds on the oxidation kinetics of Fe(II). *Mar. Chem.* 70, 211–222. doi: 10.1016/S0304-4203(00)00027-X
- Santana-Casiano, J. M., Gonzalez-Davila, M., Gonzalez, A. G., and Millero, F. J. (2010). Fe(III) reduction in the presence of catechol in seawater. *Aquat. Geochem.* 16, 467–482. doi: 10.1007/s10498-009-9088-x
- Sarthou, G., Vincent, D., Christaki, U., Obernosterer, I., Timmermans, K. R., and Brussaard, C. (2008). The fate of biogenic iron during a phytoplankton bloom induced by natural fertilisation: impact of copepod grazing. *DSR II*, 55, 734–751. doi: 10.1016/j.dsr2.2007.12.033
- Sato, M., Takeda, S., and Furuya, K. (2007). Iron regeneration and organic iron(III)-binding ligand production during in situ zooplankton grazing experiment. *Mar. Chem.* 106, 471–488. doi: 10.1016/j.marchem.2007.05.001
- Shaked, Y., and Lis, H. (2012). Disassembling iron availability to phytoplankton. *Front. Microbiol.* 3:123. doi: 10.3389/fmicb.2012.00123
- Shaked, Y., Kustka, A. B., and Morel, F. M. M. (2005). A general kinetic model for iron acquisition by eukaryotic phytoplankton. *Limnol. Oceanogr.* 50, 872–882. doi: 10.4319/lo.2005.50.3.0872
- Sorokin, Y. I. (2002a). “Hydrochemistry,” in *The Black Sea: Ecology and Oceanography*, ed K. Martens (Leiden: Backhuys Publishers), 181–236.
- Sorokin, Y. I. (2002b). “Biogeochemistry of sulphur and redox processes,” in *The Black Sea: Ecology and Oceanography*, ed K. Martens (Leiden: Backhuys Publishers), 237–285.
- Spencer, D. W., and Brewer, P. G. (1971). Vertical advection diffusion and redox potentials as controls on the distribution of manganese and other trace metals dissolved in waters of the Black Sea. *J. Geophys. Res.* 76, 5877–5892. doi: 10.1029/JC076i024p05877
- Tankéré, S. P. C., Muller, F. L. L., Burton, J. D., Statham, P. J., Guieu, C., and Martin, J. M. (2001). Trace metal distributions in shelf waters of the north-western Black Sea. *Cont. Res.* 21, 1501–1532. doi: 10.1016/S0278-4343(01)00013-9
- Taylor, G. T., Iabichella, M., Ho, T.-Y., Scranton, M. I., Thunell, R. C., Muller-Karger, F., et al. (2001). Chemoautotrophy in the redox transition zone of the Cariaco Basin: a significant midwater source of organic carbon production. *Limnol. Oceanogr.* 46, 148–163. doi: 10.4319/lo.2001.46.1.0148
- Thuróczy, C.-E., Gerringa, L. J. A., Klunder, M. B., Middag, R., Laan, P., Timmermans, K. R., et al. (2010). Speciation of Fe in the Eastern North Atlantic Ocean. *DSR I* 57, 1444–1453. doi: 10.1016/j.dsr.2010.08.004
- Thuróczy, C.-E., Gerringa, L. J. A., Klunder, M., Laan, P., Le Guitton, M., and de Baar, H. J. W. (2011). Distinct trends in the speciation of iron between the shelf seas and the deep basins of the Arctic Ocean. *J. Geophys. Res.* 116:C10009. doi: 10.1029/2010JC006835
- Tian, F., Frew, R. D., Sander, S., Hunter, K. A., and Ellwood, M. J. (2006). Organic iron(III) speciation in surface transects across a frontal zone: the Chatham Rise, New Zealand. *Mar. Freshw. Res.* 57, 533–544. doi: 10.1071/MF05209
- Twining, B. S., Rauschenberg, S., Morton, P. L., and Vogt, S. (2015). Metal contents of phytoplankton and labile particulate material in the North Atlantic Ocean. *Prog. Oceanogr.* 137, 261–283. doi: 10.1016/j.pocan.2015.07.001
- Van Cappellen, P., and Wang, Y. (1996). Cycling of iron and manganese in surface sediments: a general theory for the coupled transport and reaction of carbon, oxygen, nitrogen, sulfur, iron, and manganese. *Am. J. Sci.* 296, 197–243. doi: 10.2475/ajs.296.3.197
- van den Berg, C. M. G., and Kramer, J. R. (1979). Determination of complexing capacities of ligands in natural waters and conditional stability constants of the cooper complexes by means of manganese dioxide. *Anal. Chim. Acta* 106, 113–120. doi: 10.1016/S0003-2670(01)83711-9
- Wagener, T., Pulido-Villena, E., and Guieu, C. (2008). Dust iron dissolution in seawater: results from a one-year time-series in the Mediterranean Sea. *Geophys. Res. Lett.* 35:L16601. doi: 10.1029/2008GL034581
- Witter, A. E., Lewis, B. L., and Luther, G. W. (2000). Iron speciation in the Arabian Sea. *DSR II* 47, 1517–1539. doi: 10.1016/S0967-0645(99)00152-6
- Yemenicoglu, S., Erdogan, S., and Tuğrul, S. (2006). Distribution of dissolved forms of iron and manganese in the Black Sea. *DSR II* 53, 1842–1855. doi: 10.1016/j.dsr2.2006.03.014
- Zhou, F., Shapiro, G., and Wobus, F. (2014). Cross-shelf exchange in the northwestern Black Sea. *J. Geophys. Res.* 119, 2143–2164. doi: 10.1002/2013JC009484

Conflict of Interest Statement: The authors declare that the research was conducted in the absence of any commercial or financial relationships that could be construed as a potential conflict of interest.

Copyright © 2016 Gerringa, Rijkenberg, Bown, Margolin, Laan and de Baar. This is an open-access article distributed under the terms of the Creative Commons Attribution License (CC BY). The use, distribution or reproduction in other forums is permitted, provided the original author(s) or licensor are credited and that the original publication in this journal is cited, in accordance with accepted academic practice. No use, distribution or reproduction is permitted which does not comply with these terms.



Voltammetric Investigation of Hydrothermal Iron Speciation

Charlotte Kleint^{1*}, Jeffrey A. Hawkes², Sylvia G. Sander³ and Andrea Koschinsky¹

¹ Department of Physics & Earth Sciences, School of Engineering and Science, Jacobs University Bremen, Bremen, Germany, ² Analytical Chemistry, Department of Chemistry – BMC, Uppsala University, Uppsala, Sweden, ³ Marine and Freshwater Chemistry, NIWA/University of Otago Research Centre for Oceanography, Department of Chemistry, University of Otago, Dunedin, New Zealand

OPEN ACCESS

Edited by:

Frank Wenzhöfer,
Alfred-Wegener-Institute Helmholtz
Center for Polar and Marine Research,
Germany

Reviewed by:

Brandy Marie Toner,
University of Minnesota–Twin Cities,
USA
Marta Plavsic,
Rudjer Boskovic Institute, Croatia

*Correspondence:

Charlotte Kleint
c.kleint@jacobs-university.de

Specialty section:

This article was submitted to
Marine Biogeochemistry,
a section of the journal
Frontiers in Marine Science

Received: 10 February 2016

Accepted: 29 April 2016

Published: 13 May 2016

Citation:

Kleint C, Hawkes JA, Sander SG and
Koschinsky A (2016) Voltammetric
Investigation of Hydrothermal Iron
Speciation. *Front. Mar. Sci.* 3:75.
doi: 10.3389/fmars.2016.00075

Hydrothermal vent fluids are highly enriched in iron (Fe) compared to ambient seawater, and organic ligands may play a role in facilitating the transport of some hydrothermal Fe into the open ocean. This is important since Fe is a limiting micronutrient for primary production in large parts of the world's surface ocean. We have investigated the concentration and speciation of Fe in several vent fluid and plume samples from the Nifonea vent field, Coriolis Troughs, New Hebrides Island Arc, South Pacific Ocean using competitive ligand exchange–adsorptive cathodic stripping voltammetry (CLE–AdCSV) with salicylaldoxime (SA) as the artificial ligand. Our results for total dissolved Fe (dFe) in the buoyant hydrothermal plume samples showed concentrations up to 3.86 μM dFe with only a small fraction between 1.1 and 11.8% being chemically labile. Iron binding ligand concentrations ([L]) were found in μM level with strong conditional stability constants up to $\log K_{\text{FeL}, \text{Fe}^{3+}}$ of 22.9. Within the non-buoyant hydrothermal plume above the Nifonea vent field, up to 84.7% of the available Fe is chemically labile and [L] concentrations up to 97 nM were measured. [L] was consistently in excess of Fe_{lab} , indicating that all available Fe is being complexed, which in combination with high Fe_{lab} values in the non-buoyant plume, signifies that a high fraction of hydrothermal dFe is potentially being transported away from the plume into the surrounding waters, contributing to the global oceanic Fe budget.

Keywords: iron, CLE-AdCSV, hydrothermal vents, organic complexation, Vanuatu, New Hebrides Island Arc, Nifonea vent field

INTRODUCTION

Iron (Fe) is an essential micronutrient for all marine organisms. Although Fe is the fourth most abundant element in the earth's crust (Hans Wedepohl, 1995), dissolved Fe (dFe, $<2 \mu\text{M}$) concentrations are low in the world's oceans, typically $<1 \text{ nM}$ in the deep ocean and even lower ($<0.2 \text{ nM}$) in surface waters, due to microbial uptake and the low solubility of $\text{Fe}(\text{OH})_3$ in seawater (Johnson et al., 1997; Maldonado and Price, 2001; Liu and Millero, 2002). Iron exists in two oxidation states in seawater: the bioavailable and relatively soluble Fe(II), occurring naturally in chemically reducing conditions such as hydrothermal vent fluids, and Fe(III), which is the dominant form in oxidized seawater (Landing and Westerlund, 1988). Since the bioavailable and soluble Fe(II) is rapidly oxidized to thermodynamically stable and insoluble Fe(III) in oxic waters, microorganisms have adapted to natural Fe limitation by producing metal chelating organic molecules. These organic ligands, for example siderophores, are able to protect Fe(III) from

precipitation and may be reduced by microorganisms to bioavailable Fe(II) complexes (Kraemer, 2004; Gledhill and Buck, 2012). Recent studies by Gledhill et al. (2015) and Stockdale et al. (2016) showed that a large portion of DOM also binds Fe(III), which may be an additional and more general passive, not biologically active, control on Fe concentrations in the oceans.

Until recently, atmospheric dust inputs and fluxes from the continental margins were believed to be the major Fe sources for the surface ocean (Moore et al., 2004). However, hydrothermal vents, which host fluid Fe concentrations up to seven orders of magnitude greater than the typical deep ocean, have recently been shown to play an important role in the deep ocean Fe budget (Bennett et al., 2008; Saito et al., 2013; German et al., 2015; Hatta et al., 2015; Resing et al., 2015), and this has implications for surface ocean dFe concentrations (Tagliabue et al., 2010). Due to their high acidity and fluid temperatures above 400°C, metals such as Fe are leached out of the host rock as the fluid circulates through the basaltic crust. Most of this dissolved Fe is directly precipitated around the vent outlets as Fe-sulfides or is oxidized to Fe oxyhydroxides upon mixing with oxic seawater (German et al., 1991; Rudnicki and Elderfield, 1993), and a substantial portion of these mineral phases may exist in the operationally defined “dissolved” fraction as colloids or nanoparticles (Yücel et al., 2011; Hawkes et al., 2013a, 2014; Gartman et al., 2014). These nanoparticles might be transported away from vents in the dissolved fraction, making an important contribution to the global oceanic Fe budget. A second mechanism by which hydrothermal Fe may be stabilized after venting into the ocean is via chelation with organic ligands, stabilizing Fe(III) in the dissolved phase, which can then be transported away from the vent site (Bennett et al., 2008; Toner et al., 2009; Sander and Koschinsky, 2011; Hawkes et al., 2013a). Iron that is available for natural organic ligands is the part of total Fe that is not precipitated or stabilized by inorganic compounds, called labile Fe. In this study, we are assuming that labile Fe is organically bound only and not inorganic colloids, which would then be non-labile. Hydrothermally derived dFe is transported over thousands of kilometers away from its source into the open ocean (Fitzsimmons et al., 2014; Resing et al., 2015). The relative importance of the inorganic vs. organic stabilization may have important consequences in the long-term stability and bioavailability of the hydrothermal Fe, and the relative contribution of these stabilization mechanisms remains highly uncertain. In surface and oxic deep waters, organic complexation dominates the speciation of Fe, since most (>98%) dissolved species are bound to strong organic ligands increasing Fe solubility and therefore also the total dissolved Fe concentration in the world’s oceans (Gledhill and van den Berg, 1994; Rue and Bruland, 1995; Wu and Luther, 1995; Boyd et al., 2010), whereas inorganic colloids are often important at redox boundaries such as in hydrothermal plumes and oxidized sediment pore waters (Homoky et al., 2009; Hawkes et al., 2014). Studying the sources, sinks as well as the chemical speciation of hydrothermal Fe is therefore a crucial step in order to understand the bioavailability and cycling of Fe in our oceans.

The hydrothermal island arc system at the Coriolis Troughs, near the islands of Vanuatu and east of New Caledonia

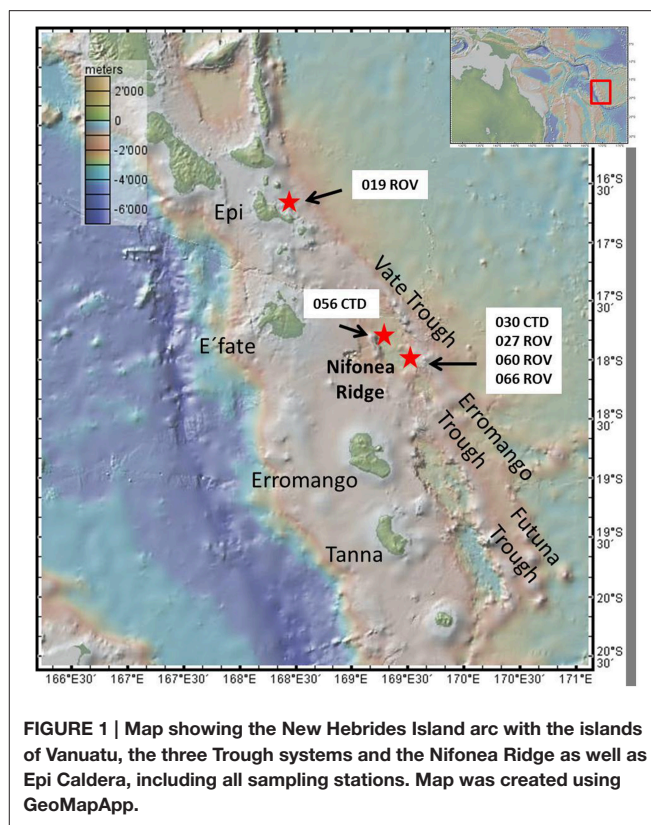


FIGURE 1 | Map showing the New Hebrides Island arc with the islands of Vanuatu, the three Trough systems and the Nifonea Ridge as well as Epi Caldera, including all sampling stations. Map was created using GeoMapApp.

has not previously been studied with respect to organic Fe complexation. Studying the role of island arc systems with respect to hydrothermal metal contribution to the water column is important, since these vents make up ~9% of global hydrothermal flux (Baker et al., 2008), are often rich in trace metals (de Ronde et al., 2011; Leybourne et al., 2012), and often occur at shallower water depths compared to Mid Oceanic Ridge (MOR) systems—potentially having a more direct impact on surface water chemistry (Hawkes et al., 2014). To broaden the knowledge and understanding on global hydrothermal dFe speciation and distribution, we determined the total and chemically labile iron concentrations (dFe, Fe_{lab}) together with corresponding Fe ligand concentrations ([L]) and their iron-binding strengths ($\log K_{FeL, Fe^{3+}}$) at the hydrothermal vent fields in the Coriolis Troughs, New Hebrides Island Arc.

MATERIALS AND METHODS

Samples

All hydrothermal fluid samples were collected within the Coriolis Troughs in the year 2013 during research cruise SO 229. The Coriolis Troughs lie east of the Erromango and Tana islands, and are situated in the Vanuatu backarc basin east of the southern New Hebrides island arc. The system is composed of three major depressions orientated NNW-SSE, the Vate Trough in the North, the Erromango Trough in the middle, and the Futuna Trough in the South (Figure 1). Since 1969, the troughs themselves have been intensively studied, however only little is known about the

TABLE 1 | Overview on hydrothermal samples taken for Fe speciation.

Sample ID	Type of sample	Samplingdevice	Location	Water depth (m)	H ₂ S (μM)	pH	Eh
30 CTD 1500	non-buoyant Plume	CTD	18°7,76' S 169°31,03' E	1500	n.d.	n.d.	n.d.
30 CTD 1550	non-buoyant Plume	CTD	18°7,76' S 169°31,03' E	1550	n.d.	n.d.	n.d.
30 CTD 1600	non-buoyant Plume	CTD	18°7,76' S 169°31,03' E	1600	n.d.	n.d.	n.d.
30 CTD 1650	non-buoyant Plume	CTD	18°7,76' S 169°31,03' E	1650	n.d.	n.d.	n.d.
30 CTD 1700	non-buoyant Plume	CTD	18°7,76' S 169°31,03' E	1700	n.d.	n.d.	n.d.
56 CTD 1600	BG water sample	CTD	18°2,00' S 169°21,98' E	1600	n.d.	n.d.	n.d.
19 ROV 06	Diffuse vent, vent outlet	KIPS	16°41,28' S 168°24,50' E	<400	n.d.	n.d.	n.d.
27 ROV 11	Clear Smoker, buoyant plume	Niskin	18°7,80' S 169°30,75' E	1860	20	7.2	-233
27 ROV 14	Black smoker, vent outlet	KIPS	18°7,78' S 169°31,06' E	1860	6200	3.3	-267
27 ROV 15	Black smoker, buoyant plume	Niskin	18°7,78' S 169°31,06' E	1860	n.d.	7.4	-161
27 ROV 16	Black smoker, buoyant plume	Niskin	18°7,78' S 169°31,06' E	1860	n.d.	7.3	-7
60 ROV 01	Clear Smoker, vent outlet	KIPS	18°7,68' S 169°31,17' E	1873	7800	4.7	-214
60 ROV 02	Clear Smoker, buoyant plume	Niskin	18°7,68' S 169°31,17' E	1873	200	6.4	-258
60 ROV 07	Black Smoker, buoyant plume	Niskin	18°7,72' S 169°31,11' E	1873	100	6.9	-286
66 ROV 05	Black Smoker, buoyant plume	Niskin	18°7,78' S 169°31,10' E	1862	300	6.0	n.d.

pH and Eh were measured on-board using a WTW® multimeter. H₂S was also determined on-board using a WinLab® photometer. All three parameters were measured immediately after sample recovery. Samples 27 ROV 14 (vent outlet), 15 and 16 (in buoyant plume) were taken at the same vent as well as samples 60 ROV 01 (vent outlet) and 02 (in buoyant plume). KIPS samples are always pure fluids taken in the vent outlet, while Niskin samples represent diluted fluids taken in the buoyant plume above the vents. The CTD plume is a non-buoyant plume. BG, background sample taken in an area with no hydrothermal venting in 1600 m water depth; n.d., not determined.

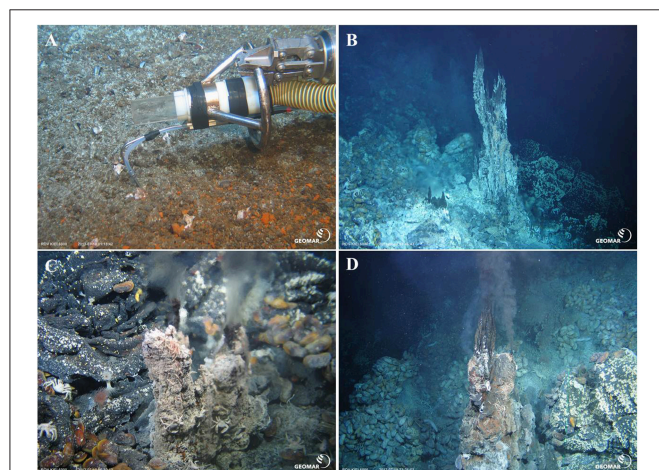


FIGURE 2 | (A) Diffuse, low temperature hydrothermal venting at Epi Caldera (19 ROV 06). **(B)** Black smoker, at Nifonea ridge (27 ROV 14, 15, and 16). **(C)** Clear, high temperature (348°C) vent at Nifonea ridge (60 ROV 01 and 02). **(D)** Black smoker (170°C) at Nifonea ridge (66 ROV 05). (Pictures taken by ROV KIEL 6000, GEOMAR Kiel, Germany). Panel **(A)** also shows the use of the KIPS system with the titanium nozzle and parallel high-temperature sensor.

hydrothermal system within the troughs (Greene and Exon, 1988; Price et al., 1993; Iizasa et al., 1998; Nasemann, 2015; Schmidt et al. under review). During a research cruise in 2001, McConachy et al. (2005) discovered a new large hydrothermal vent field, the “Nifonea vent field” in the central Vate Trough, east of Nifonea Ridge.

Except for sample 19 ROV 06 (taken at the Epi Caldera) all other hydrothermal fluid samples were taken within the Nifonea vent field. Additional to several black smokers and

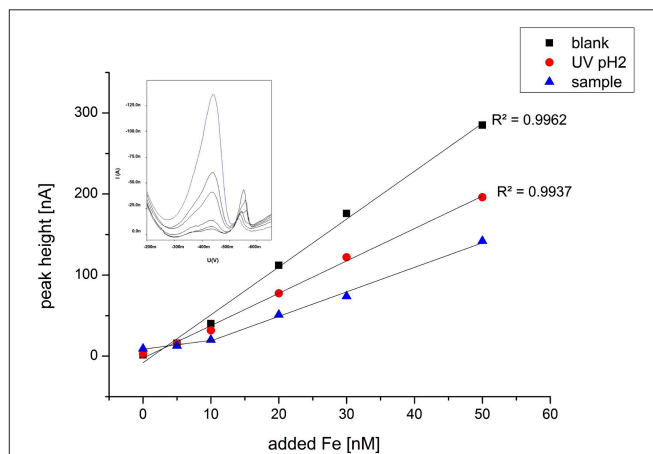


FIGURE 3 | Typical titration curve exemplarily chosen for sample 27 ROV 11 with Fe standard additions at pH 8.15 and 100 μM SA for the reagent blank, a UV digested sample at pH 2 and the regular sample. The sample without any Fe addition was equilibrated overnight. The voltammogram shows the standard additions of Fe to sample 27 ROV 11.

diffuse vent fields; a non-buoyant hydrothermal plume was detected above the Nifonea vent field by turbidity anomalies in the water column and was sampled using the on-board conductivity-temperature-depth (CTD) rosette water sampler at five different water depths. **Figure 2** shows four different sampled vent sites; diffuse venting at Epi Caldera and two black smokers as well as one high-temperature clear vent fluid in the Nifonea vent field. For the direct sampling of hydrothermal fluids from the high-temperature vents, the fully remotely controlled flow-through system KIPS (Kiel Pumping System, KIPS-4; Garbeschönberg et al., 2006) entirely made of polytetrafluoroethylene

(PTFE) and high-purity titanium was deployed on the ROV *KIEL 6000*. Samples were collected via a titanium nozzle, which was connected to four PTFE sampling bottles, one liter each. Parallel to the nozzle is an on-line high-temperature sensor monitoring the temperature at the point of sampling, which helps in detecting the most focused vent outlets. Within the Nifonea vent field, maximum temperatures of 368°C were measured at single black smoker vent outlets (Haase, 2013; Schmidt et al. under review). **Figure 2A** shows the sampling titanium nozzle with the high-temperature sensor attached to it, while sampling a diffuse hydrothermal vent field at the Epi Caldera. Before filling the sampling tube and sample bottles, both were rinsed with the hydrothermal fluid for several minutes. This KIPS sampling technique is fully remotely controlled on board the research vessel and therefore allows a detailed fluid sampling in defined areas. In addition to the KIPS system, three metal-free, acid cleaned Niskin bottles were deployed at the front porch of the ROV to sample the mixing zones of pure fluid and seawater, the buoyant plume.

In total, one non-buoyant hydrothermal plume (five samples) and nine different hydrothermal fluid samples have been taken for dFe, Fe_{lab}, and [L] analysis (**Table 1**).

Methods

Most Fe measurements were performed by voltammetric analysis using a 757 VA Computrace (Metrohm) at Jacobs University Bremen, Germany. The three-electrode configuration included a hanging mercury drop electrode (HMDE) as the working electrode, a double junction Ag/AgCl/3 M KCl reference electrode, and a glassy carbon counter electrode. Since most fluid samples taken by the ROV *KIEL 6000* were believed to have dFe concentrations in μM range, all ROV samples were additionally analyzed using a Spectro Ciros Vision ICP-OES at Jacobs University Bremen.

On board SO 229, samples were filtered (0.2 μM) and acidified (suprapure HCl, pH 2) if used for metal determination or frozen directly after filtration if used for speciation. Samples were stored in acid-cleaned LDPE or HDPE fluorinated bottles. At shore, a 10 ppm Fe stock solution was prepared in suprapure 0.1 M HCl (using the 1000 ppm Fe single element standard, Joint Ventures). Iron standard solutions for voltammetric analysis (10 and 1 μM) were prepared daily by diluting the 10 ppm Fe stock solution with ultrapure deionized water (DI, 18.2 M Ω /cm). An aqueous stock solution of 0.1 M salicylaldehyde (SA) from Sigma-Aldrich was prepared in suprapure 0.1 M HCl and stored at 4°C. SA standard solutions (10 and 1 mM) were regularly prepared from the 0.1 M SA stock solution. A borate buffer was mixed out of 1 M boric acid and 0.35 M suprapure ammonia. To remove trace metals, this solution was passed over a chelating ion exchange resin (chelex 100, BioRad) before use.

Total dissolved Fe (dFe) was determined in 10 mL of the acidified sample, with the addition of an artificial ligand (SA; final concentration 25 μM ; Rue and Bruland, 1995; Buck and Bruland, 2007; Buck et al., 2007; Abualhaija and van den Berg, 2014). After the SA addition, the sample was allowed to stand for about 2 h, before the pH was adjusted to ~ 8.15 using suprapure NH₃ and the borate buffer (10 mM

final concentration). DFe concentrations in each sample were then determined by adsorptive cathodic stripping voltammetry (AdCSV), which detects the electrochemically-active complex FeSA using standard addition method. All sample and titration vials were conditioned typically three times prior to each measurement.

Voltammetric parameters were modified from Abualhaija and van den Berg (2014). This includes purging of the sample with compressed air (instead of N₂) at 1 bar, deposition at -0.05 V with an initial deposition time of 120 s (this was later adjusted to shorter times due to high Fe concentrations) and a cathodic scan from -0.05 to -0.8 V using the differential pulse (DP) mode. Every measurement was repeated three times for quality control and reproducibility. Additionally, the seawater reference material for trace metals NASS-6 from the National Research Council Canada was measured along the samples for dFe as quality control. The analytical error for NASS-6 was within the range of $\pm 5\%$ of the reference value.

For labile Fe (Fe_{lab}) measurements, the sample was thawed at 4°C overnight. Ten milliliters of the sample were pipetted into an already conditioned PTFE titration vessel and equilibrated overnight at $\sim \text{pH } 8.15$ (borate buffer, 10 mM final concentration) and 100 μM SA. Due to high dFe concentrations, ROV samples were first diluted with ultrapure deionized water in the same salinity as the sample. The next day, regular Fe standard additions were made with 10 min equilibration time after each addition, using the same voltammetric parameters as for dFe. The chemically labile Fe that we are measuring is the fraction of iron in the sample as FeSA complex. This means that it dissociated from its previous complex with natural ligands to be available to our artificial ligand SA under these conditions, i.e., it is labile. Curvature in the standard addition data points suggested that, despite the high SA concentration of 100 μM , there was still competition between some natural ligands and SA at low Fe additions (**Figure 3**). To estimate concentration and binding strength of possible Fe-complexing ligands we made five additions of Fe. Plotting this data in ProMCC, using the complete complexation-fitting model, one-ligand model, resulted in reasonable Fe binding ligand concentrations (Omanović et al., 2015).

To validate this data, a regular titration with 12 Fe additions equilibrated overnight was prepared for two of the non-buoyant plume samples (30 CTD 1500 and 30 CTD 1650). Twelve aliquots (10 ml each) of each sample were separated in 15 ml PTFE vials. The borate buffer (final concentration 10 mM), as well as increasing Fe concentrations at approximately logarithmic steps are given to each sample, ranging from 0 to 300 nM, depending on the expected ligand concentration. After 2 h of equilibration, the artificial ligand SA was added at a concentration of 25 μM . All 12 sample aliquots were allowed to equilibrate overnight and subsequently analyzed the next day, using the same parameters as for the dFe (**Table 2**). Since results of the standard addition titration and the regular titration were very similar, we decided to show and work with the results of the standard addition method in this study.

As a second method proof, we also measured a pH 2 UV digested sample and a reagent blank (used for dilution) using

TABLE 2 | Comparison of [L] and $\log K_{FeL,Fe^{3+}}$ data obtained with a standard addition titration and a regular classic titration with 12 separate Fe additions and overnight equilibration.

Sample ID	[L] std add (μM)	$\log K_{FeL,Fe^{3+}}$ std add	[L] regular (μM)	$\log K_{FeL,Fe^{3+}}$ regular
30 CTD 1500	0.013 \pm 0.002	21.3 \pm 0.21	0.015 \pm 0.002	21.1 \pm 0.32
30 CTD 1650	0.097 \pm 0.008	19.7 \pm 0.06	0.095 \pm 0.001	22.4 \pm 0.07

Data fitting was done in ProMCC, using the one ligand–complete complexation-fitting model.

TABLE 3 | Iron speciation data for hydrothermal plume and fluid samples taken on SO 229.

Sample ID	Type of sample	dFe (μM)	dMn (nM)	[L] (μM) using dFe	$\log K_{FeL,Fe^{3+}}$	Fe_{lab} (nM)	Proportional Fe_{lab} (%)	$E_{[L]}$ (nM)	Proportional $E_{[L]}$ (%)
30 CTD 1500	Plume	0.010	n.d.	0.013 \pm 0.002	21.4 \pm 0.21	3.11	32.4	3.47	26.6
30 CTD 1550	Plume	0.028	n.d.	0.036 \pm 0.005	21.6 \pm 0.37	6.81	24.9	9.24	25.7
30 CTD 1600	Plume	0.014	n.d.	n.d.	n.d.	n.d.	n.d.	n.d.	n.d.
30 CTD 1650	Plume	0.030	n.d.	0.097 \pm 0.008	19.7 \pm 0.06	25.50	84.7	67.3	69.4
30 CTD 1700	Plume	0.010	n.d.	n.d.	n.d.	5.93	59.2	n.d.	n.d.
56 CTD 1600	BG water sample	0.007	0.14	0.013 \pm 0.001	20.8 \pm 0.52	0.74	10.5	5.71	43.9
19 ROV 06	Diffuse vent	0.46	2.6	0.55 \pm 0.01	22.9 \pm 0.09	5	1.1	91	16.5
27 ROV 11	Clear smoker	0.82	0.2	1.08 \pm 0.03	22.2 \pm 0.07	32	4.0	260	24.1
27 ROV 14	Black smoker	379	229	n.d.	n.d.	n.d.	n.d.	n.d.	n.d.
27 ROV 15	Black smoker	1.68	0.8	2.08 \pm 0.09	21.9 \pm 0.11	143	8.5	400	19.2
27 ROV 16	Black smoker	3.86	1.7	3.89 \pm 0.04	22.1 \pm 0.06	457	11.8	30	0.8
60 ROV 01	Clear smoker	67	164	n.d.	n.d.	n.d.	n.d.	n.d.	n.d.
60 ROV 02	Clear smoker	0.86	1.7	0.98 \pm 0.04	22.1 \pm 0.13	61	7.1	116	11.8
60 ROV 07	Black smoker	0.54	2.4	0.58 \pm 0.01	22.3 \pm 0.06	33	6.0	41	7.1
66 ROV 05	Black smoker	111	60	n.d.	n.d.	n.d.	n.d.	n.d.	n.d.

Data fitting was done in ProMCC, using the complete complexation-fitting model. Additional to dMn, dFe, [L] and Fe_{lab} concentrations we calculated proportional Fe_{lab} values, excess ligand ($E_{[L]}$) concentrations and proportional $E_{[L]}$ values for hydrothermal plume and fluid samples taken on SO 229. $\log K_{FeL,Fe^{3+}}$ shows the stability constant of the metal ligand complex. BG, background sample taken in an area with no hydrothermal venting in 1600 m water depth; n.d., not determined.

the same procedure and voltammetric parameters as for the regular samples. These results did not show the curvature in the beginning at low Fe additions, confirming that the curvature is not a methodological artifact but truly sample related (Figure 3).

RESULTS

Total Dissolved Fe and Labile Fe Concentrations

Our non-buoyant plume samples had dFe concentrations between 10 and 30 nM, compared to a background concentration of 7 nM (Table 3). These concentrations represent an approximate dilution of vent fluids of \sim 38,000. Samples 30 CTD 1500 (10 nM Fe) and 30 CTD 1700 (10 nM Fe) taken directly above and beneath the plume show only little enriched dFe concentrations compared to the background seawater sample. The three samples taken within the plume core are enriched compared to regular seawater and follow the turbidity signal of the CTD water sampler (Figure 4), which can be used as a tracer for hydrothermal plumes. The highest peak in turbidity also shows the highest dFe concentration for the hydrothermal plume. These observations agree with a recent study on the same plume (Nasemann, 2015).

For the vent fluids taken at the seafloor, our samples had dFe concentrations in a much wider range; between 0.46 μM for sample 19 ROV 06 taken from a diffuse vent up to 379 μM for black smoker sample 27 ROV 14 taken directly in the vent outlet. It can be observed that both KIPS samples 27 ROV 14 and 60 ROV 01 that are also characterized by highest H_2S and lowest pH values of all samples, show higher dFe concentrations than the samples taken with Niskin bottles above the same vents, which in general would represent more diluted fluids. However, one sample, 66 ROV 05, taken \sim 1 m above the vent outlet had an unusually high dFe concentration (111 μM) although taken with a Niskin bottle and not the KIPS system. Sample 19 ROV 06, also collected using KIPS had a dFe concentration of 0.46 μM , much lower than all other KIPS samples, which can be explained by the fact that this site is a diffuse vent field, as opposed to a high temperature clear or black smoker as all other fluid samples. Additionally, clear smoker samples 27 ROV 11, 60 ROV 01, and 60 ROV 02 had lower dFe concentrations than comparable samples taken at black smokers.

The proportion of chemically labile Fe (Fe_{lab}) in dFe increased during development of the buoyant hydrothermal plume from values between 1 and 11.8% near the vent mouth to values between 25 and 85% in the non-buoyant plume. The term “labile Fe” is defined as the dFe which is bound to SA after

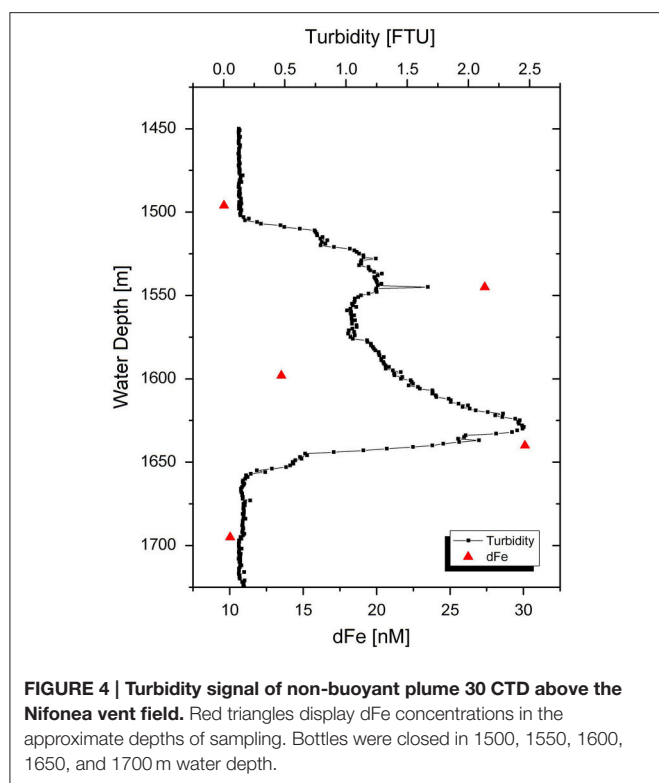


FIGURE 4 | Turbidity signal of non-buoyant plume 30 CTD above the Nifonea vent field. Red triangles display dFe concentrations in the approximate depths of sampling. Bottles were closed in 1500, 1550, 1600, 1650, and 1700 m water depth.

equilibration with $100\ \mu\text{M}$ SA overnight at room temperature ($\alpha_{\text{FeSA}} = 3.39 \times 10^{12}$, $\alpha_{\text{FeSA}2} = 1.58 \times 10^{12}$). This is quite a high overall side reaction coefficient for out-competing natural ligands, but high dFe and [L] concentrations required a higher than normal SA concentration. The fact that a curvature was still found (Figure 3) in the standard addition curve indicated some ligand exchange, thus validating the SA concentration used. After overnight equilibration, we made five standard additions with 10 min equilibration time after each addition and used the data to estimate the Fe binding strength of the competing ligands. Due to the observed curvature, the determined Fe_{lab} concentrations should be considered minimum estimates (Table 3). In general, a strong linear correlation can be observed between dFe and Fe_{lab} for all fluid samples as shown in Figure 5.

Iron Binding Ligand Concentrations

Concentrations for Fe binding ligands [L] within the non-buoyant hydrothermal plume ranged between 13 and $97\ \text{nM}$, with stability constants ($\log K_{\text{FeL}, \text{Fe}^{3+}}$) varying from 19.7 to 21.6. Generally, the “plume core” samples had higher ligand concentrations than the ones beneath and above the inner plume. Sample 30 CTD 1500 taken above the plume had a very similar [L] concentration as the background seawater sample. As already shown for dFe and Fe_{lab} , a strong correlation can be observed when plotting dFe against [L] (Figure 6). Since all ROV samples plot slightly above the 1:1 diagonal, we can assume that all available Fe is being complexed. The CTD samples seem to plot on the diagonal. Fe_{lab} and [L] show a correlation of $R^2 = 0.972$ (Figure 7).

Iron binding ligand data for the samples collected in the buoyant plume very close to the high temperature vents had concentrations ranging from 0.55 up to $3.89\ \mu\text{M}$ or from 0.10 up to $3.03\ \mu\text{M}$ depending on the initial Fe concentration used for calculations (dFe or Fe_{lab} , respectively), while more diluted fluids had higher [L] concentrations (Table 4). Stability constants for the buoyant plume samples ranged from $\log K_{\text{FeL}, \text{Fe}^{3+}} 21.9$ up to 22.9 or from $\log K_{\text{FeL}, \text{Fe}^{3+}} 19.7$ up to 21.9, again, depending on the initial Fe concentration used for calculation (dFe or Fe_{lab} , respectively). The general trend shows that the higher the dFe concentration, the higher the [L] concentration. When calculating the excess ligand ($E_{[\text{L}]}$) concentrations and proportional $E_{[\text{L}]}$ for all samples, an opposite trend to the Fe_{lab} values can be found in buoyant plume samples (Table 3). The most diluted buoyant plume sample 27 ROV 16 had the highest proportional Fe_{lab} values but lowest $E_{[\text{L}]}$; a trend which is not continued in the non-buoyant plume samples, where Fe_{lab} values rather seem to mimic $E_{[\text{L}]}$ values.

DISCUSSION

In this study, we adapted the traditional titration method (Rue and Bruland, 1995) due to problems arising from the high Fe concentrations and inorganic matrix of the hydrothermal samples. Our original goal was simply to assess the concentration of labile Fe in each sample (Hawkes et al., 2013b), but curvature in the standard additions allowed us to estimate some strong Fe binding ligand characteristics. Despite a short 10-minute equilibration time after each Fe addition and a high concentration of SA ($100\ \mu\text{M}$), some Fe in the samples was complexed by natural ligands. The classic titration worked satisfactorily for the non-buoyant hydrothermal plume samples, which we carried out for two exemplarily chosen samples to compare results of both methods (Table 2). The two methods gave similar results for [L], but on one occasion quite different results for the conditional binding strength, $\log K$. This may be due to the equilibration time, which may favor certain types of ligand according to the coordination mechanism. Regardless, both methods were able to extract some labile Fe from natural complexes.

A second consideration was whether to use the total dissolvable Fe concentration (dFe) in the calculation of the ligand characteristics or to use the labile Fe concentration (e.g., Hawkes et al., 2013b). If some dFe is present as inorganic colloids which we suppose here do not participate in the equilibrium, the ligand concentration and strength would be overestimated by using dFe in the calculations. However, if some ligand complexes which do participate are too strong in the detection window employed, these factors will be underestimated. We calculated the ligand parameters using both iron concentrations for all ROV samples, which had relatively low Fe_{lab} values with a maximum of 11.8%, giving us a minimum and maximum estimate for [L], which vary greatly, particularly in $\log K$ (Table 4). The results gathered from the use of dFe are probably unrealistic, as it is generally accepted that a significant portion of hydrothermal dFe is inorganically bound in mineral matrices (Yücel et al.,

TABLE 4 | Comparison of the different calculated ligand characteristics [L] and $\log K_{FeL,Fe^{3+}}$ for all ROV samples using dFe or Fe_{lab} as initial iron concentrations.

Sample ID	dFe (μM)	Fe_{lab} (μM)	[L] (μM) using dFe	$\log K_{FeL,Fe^{3+}}$	[L] (μM) using Fe_{lab}	$\log K_{FeL,Fe^{3+}}$
19 ROV 06	0.46	0.005	0.55 ± 0.01	22.9 ± 0.09	0.11 ± 0.05	21.9 ± 1.48
27 ROV 11	0.82	0.032	1.08 ± 0.03	22.2 ± 0.07	0.42 ± 0.18	21.0 ± 0.42
27 ROV 14	379	n.d.	n.d.	n.d.	n.d.	n.d.
27 ROV 15	1.68	0.143	2.08 ± 0.09	21.9 ± 0.11	1.54 ± 1.37	20.1 ± 0.65
27 ROV 16	3.86	0.457	3.89 ± 0.04	22.1 ± 0.06	3.03 ± 1.82	19.7 ± 0.39
60 ROV 01	67	n.d.	n.d.	n.d.	n.d.	n.d.
60 ROV 02	0.86	0.061	0.98 ± 0.04	22.1 ± 0.13	0.23 ± 0.10	21.0 ± 0.63
60 ROV 07	0.54	0.033	0.58 ± 0.01	22.3 ± 0.06	0.10 ± 0.05	20.8 ± 0.62
66 ROV 05	111	n.d.	n.d.	n.d.	n.d.	n.d.

2011; Hawkes et al., 2013a, 2014; Gartman et al., 2014). We also know that our determined value of Fe_{lab} is an underestimation, due to the curvature in the standard additions, but these ligand parameters are probably a more realistic estimation of the Fe speciation in the plume. The high ligand concentration and fairly low binding coefficient are in line with previous results gathered by reverse titration (Hawkes et al., 2013b), and may result from complexation of Fe with less specific binding groups on DOM than in surface waters (Gledhill et al., 2015; Stockdale et al., 2016).

Fe Speciation within the Buoyant and Non-buoyant Hydrothermal Plume

A speciation study for five single layers of the 30 CTD non-buoyant hydrothermal plume above the Nifonea vent field showed highly elevated dFe and [L] concentrations compared to the surrounding seawater, especially in the plume center. Consistently present excess ligand concentrations between 25 and 69% indicate that all available Fe (Fe_{lab}) is being complexed and stabilized. A recent study by Nasemann (2015) showed that dFe concentrations mimic those of particulate Fe, indicating nearly equal amounts of dissolved and particulate Fe in the non-buoyant plume. These findings are also reflected by the turbidity signal. However, they found that particulate Fe concentration decreased above plume depths (>1500 m), dFe continued to be elevated above the plume, which may indicate incomplete particle formation at the upper end of the plume, or stabilization of the dissolved species. Our findings that dFe and [L] concentration increase toward the plume core are in good agreement with the findings of Bennett et al. (2008) and also support the theory that these high dFe and [L] concentrations are not coming from the mixing with open ocean water or the true vent fluid but rather from diffuse venting adjacent to the high temperature vents.

All plume samples as well as the background seawater sample were taken with the research vessel's own CTD water sampler, which was not an official trace metal clean CTD and might explain the relatively high dFe background concentrations of 7 nM, which would then also apply for the non-hydrothermal plume samples. However, plume samples are still enriched in dFe compared to the background sample.

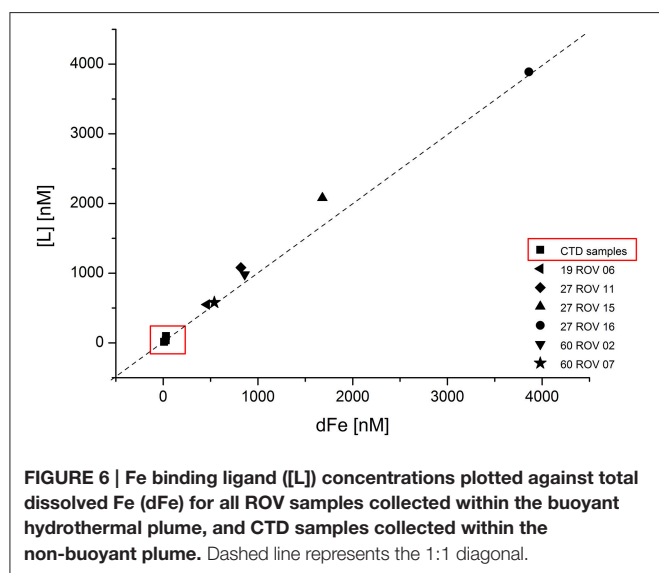
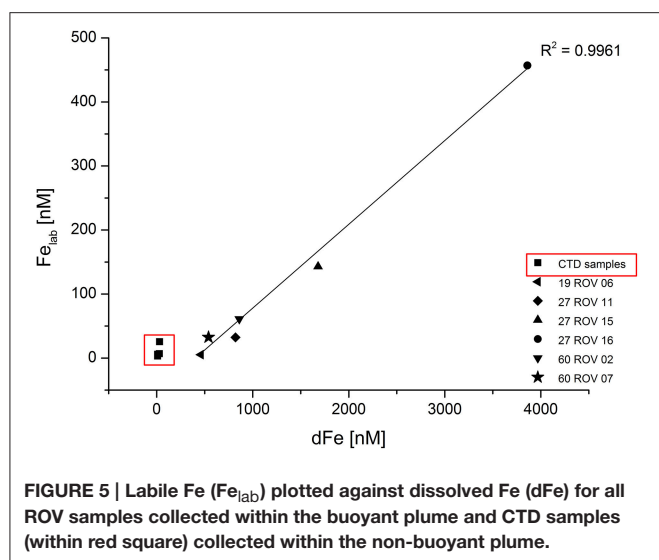
Calculating [L] with dFe as initial Fe concentration, the buoyant plume shows [L] concentrations being consistently in

excess compared to dFe concentrations (Table 4). However, this might be specific to the Nifonea hydrothermal vent field with its many high temperature vents, such as 27 ROV, where dFe and [L] concentrations in μM range were measured in the fluids on the seafloor. Using Fe_{lab} values for calculations, [L] concentrations are higher than Fe_{lab} but consistently lower than dFe, which is in agreement with previous studies (Bennett et al., 2008; Hawkes et al., 2013a; e.g., Buck et al., 2015).

The ratio of Fe_{lab} :dFe was characteristically higher in the samples taken from black smoker chimneys than those taken at diffuse venting sites or clear smokers, suggesting that sub-surface processes removed labile Fe or preferentially led to non-labile forms of Fe, such as sulfide nanoparticles and oxidized colloids. In the buoyant hydrothermal plume, the proportion of labile Fe increased as the plume was diluted, indicating either that Fe species became more labile over the timescale of plume formation sampled (~hours), or that non-labile forms of dFe were preferentially removed. The latter explanation is more likely, as colloidal oxy-hydroxide particles are likely to gradually aggregate into species larger than the “dissolved” cutoff (>0.2 μm ; Honeyman and Santschi, 1989; Hawkes et al., 2014).

The Source and Nature of Fe Ligand Complexes

Iron binding ligand concentrations around the vent outlets were distributed very heterogeneously varying from 0.55 up to 3.89 μM or 0.10 up to 3.03 μM , depending on the initial Fe concentration used for calculation; however, seem to be highly related to the corresponding dFe or Fe_{lab} concentration (Figures 6, 7). The fact that elevated dFe and Fe_{lab} concentrations in the buoyant plume also led to higher [L] concentrations, gives reason for the assumption that these ligands have their source close to these vent outlets. When calculating the proportion of labile Fe, it can be observed that for the buoyant plume, only between 1.1 and 11.8% are actually chemically labile, while Fe_{lab} increases with plume dilution. Interesting are samples 27 ROV 14, 15, and 16, which are all from the same vent, with 27 ROV 16 being a more diluted fluid than 27 ROV 15, while 27 ROV 14 represents the actual high temperature vent fluid. While 27 ROV 14 shows dFe concentrations up to 379 μM , a lot of dFe is probably lost as particulate or colloidal



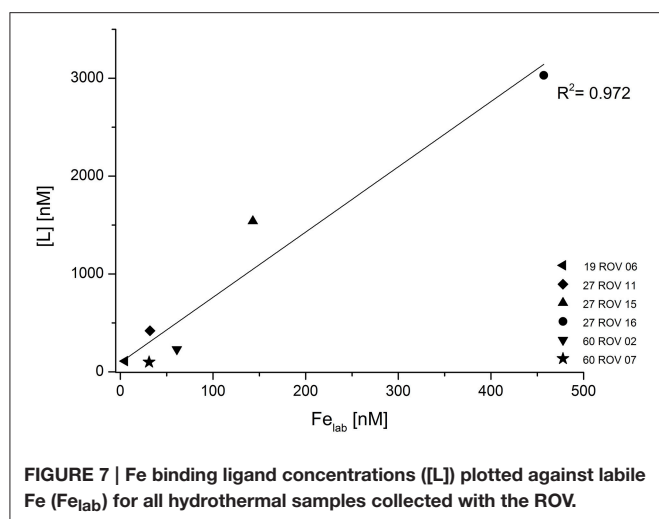
Fe sulfides or oxyhydroxides directly after seawater mixing as shown in sample 27 ROV 15 (1.68 μM dFe). The even higher diluted fluid 27 ROV 16, shows higher Fe_{lab} and higher [L] concentrations than 27 ROV 15, indicating that the ligand source could be present within the plume, as bacteria, which actively produce organic ligands or organo-sulfur compounds (Toner et al., 2009), or adjacent to the vent site in areas of diffuse fluid flow (Bennett et al., 2008). The diffuse vent sample 19 ROV 06, taken with the KIPS system, shows lowest dFe and lowest [L] concentrations and at the same time also the lowest value of Fe_{lab} :dFe, with only 1.1%, which we would rather expect from a pure hydrothermal fluid sample (Yücel et al., 2011). Additionally, pure hydrothermal fluids, sampled directly out of the vent outlet, have low concentrations of complex organic matter, so we would not expect to find organic ligands in these samples (Hawkes et al., 2015; McCollom et al., 2015). However, an important fraction (up to 11.8%) of dFe in the early buoyant plume was chemically

labile and in equilibrium with high concentrations of natural chelating ligands, as indicated by their competition for added Fe during titration (Figure 3). UV digestion at pH 2 followed by pH neutralization and measurement showed a decrease in dFe and Fe_{lab} and an increase in sensitivity. This may indicate a loss of Fe to inorganic particles after destruction of organic molecules, and a loss of organic competition for added Fe, respectively (Figure 3).

The close relationship between [L] and dFe concentrations in the buoyant plume (Figure 6) suggests either that the ligands have a similar source as the Fe (Bennett et al., 2008) or that the observed voltammetric behavior of dFe is an inherent feature of Fe in organic rich seawater (Hawkes et al., 2013a, 2015), due to the diverse functionality of the organic mixture (Gledhill et al., 2015; Stockdale et al., 2016) and the gradual and possibly weak aggregation of oxy-hydroxide and other colloidal Fe phases (Honeyman and Santschi, 1989; Mackey and Zirino, 1994). This strong correlation between dFe and [L] was already observed in previous studies (Buck and Bruland, 2007; Buck et al., 2007; Lannuzel et al., 2015). Regardless of their source or identification, these organic ligands seem to control the solubility and therefore also the bioavailability of dFe (Buck et al., 2007). Buck and Bruland (2007) also suggested that dFe might be required for the production of these ligands. All of these previous studies focused on different water types including estuarine waters, river plumes, surface waters, and Antarctic sea ice. To our knowledge, no other studies have yet been reported on dFe, Fe_{lab} , and [L] in hydrothermal buoyant plume samples and since our samples show a very strong correlation of dFe and [L] (Figure 6), these results confirm previous outcomes and imply that also in hydrothermal plumes, [L] might control the concentration of dFe. The additional good correlation between Fe_{lab} and [L] (Figure 7) gives reason for the suggestion that [L] might also control Fe_{lab} in these environments or vice versa.

Highest stability constant and thereby the highest binding strength of the [L] complex was measured in sample 19 ROV 06 ($\log K_{FeL,Fe^{3+}} = 22.9$ or 21.9, using dFe or Fe_{lab} for calculation, respectively), a diffuse vent fluid, however sampled with KIPS and thereby a quite pure fluid. All other ROV samples analyzed for [L] and $\log K$ are sampled within the buoyant plume and had values between $\log K_{FeL,Fe^{3+}} = 19.7$ and $\log K_{FeL,Fe^{3+}} = 22.3$, signifying for strong ligands (Gledhill and Buck, 2012). Stability constants for the non-buoyant hydrothermal plume, calculated using dFe as initial iron concentration were lower with values between $\log K_{FeL,Fe^{3+}} = 19.7$ and $\log K_{FeL,Fe^{3+}} = 21.6$. Since we used the standard addition method to determine [L] and $\log K$ -values, we only had five data points available, which leads to greater uncertainty and possibly an overestimation of the $\log K$ -value. However, since there is no other comparable data published for high temperature vent fluids, our data might serve as a first approach, leaving room for further method development and more data analysis.

During the analysis we used SA as an artificial ligand for all samples and purged with air. In this case a possible reverse titration is not a good option as the FeSA peak would decrease with increasing SA concentration (Abualhaija and van den Berg,



2014). To validate our data, a reverse titration using 1-nitroso-2-naphthol (NN) as an artificial ligand as demonstrated by Hawkes et al. (2013b) would be a reasonable next step.

Distribution of Fe from Hydrothermal Vents

Our speciation results suggest that nearly all of the hydrothermally derived dFe in the buoyant plumes is strongly complexed or part of nano-particles and colloids, and not chemically labile in the time scale of 1 day during plume dispersal. In the true vent fluids, most of the Fe will occur as Fe(II), however, only meters away from where the fluid gets mixed with oxic seawater, Fe(III) will be the dominant oxidation state (Sander and Koschinsky, 2011). Our oxidation half-life calculations of Fe ($t_{1/2} = 1.1$ h; calculated using equations by Millero et al., 1987; Statham et al., 2005) confirmed that Fe should be in the Fe(III) form in all the non-buoyant and most of the buoyant plume samples. Since these fluids are very high in sulfide and the oxidation half-life is very short, a high fraction of Fe is most likely bound as pyrite nanoparticles and Fe oxy-hydroxide colloids, rather than by organic stabilizing ligands (Luther et al., 2001; Yücel et al., 2011; Hawkes et al., 2013a). In high temperature vents, it has been shown that about 5–25% of hydrothermally derived dFe is released into the deep ocean in the form of nano particulate pyrite, while these nanoparticles can behave like dissolved metals, by not settling and thereby being transported away from the vent source into the plume or even further (Yücel et al., 2011; Gartman et al., 2014), contributing significantly to the global oceanic dFe budget, which could also be the case for the vents in the Nifonea vent field. However, since we did not analyze for pyrite or other nano-particulate Fe-species, we can only say that results from our study show evidence for $<0.2 \mu\text{m}$ particles containing Fe. In addition to these inorganic stabilization mechanisms, we also found that the proportion of organic Fe binding ligands participating in Fe speciation is higher in the non-buoyant plume than in the buoyant plume, as indicated by high Fe_{lab} (up to 84.7% in the non-buoyant plume) and [L], providing a large fraction of dFe which may be transported over a longer distance as [L]

complexes. Since the fraction of Fe_{lab} increased with plume dilution, a process removing the colloids or transferring them into the labile phase must occur in the transition zone between the early buoyant plume and the non-buoyant plume. Our results conform well to the growing body of literature which suggests that iron binding ligands are intricately linked with transport of Fe from hydrothermal vent fields (Bennett et al., 2008; Sander and Koschinsky, 2011; Resing et al., 2015). In terms of the various modeling scenarios presented in Resing et al. (2015), we found little evidence to suggest that the hydrothermal flux of organic ligands was significantly greater than that of dFe, and rather support the theory that only a portion of dFe transport from hydrothermal vent fields is in the form of organic complexes, with the rest present as non-chemically labile nano-particles and colloids.

CONCLUSION

Here, we report for the first time apparent Fe-binding organic ligand concentrations in μM range for a high temperature hydrothermal vent field. Iron binding ligand concentrations were found in excess compared to labile Fe concentrations for all samples in the buoyant and non-buoyant plume of the high temperature vents. [L] is highly dependent on dFe, which suggests that at least some of the organic Fe stabilizing ligands might originate near the hydrothermal vents where most of the dFe is being released. For the buoyant hydrothermal plumes, however, most of the dFe is present as nano- and colloidal mineral phases, and is not chemically labile. The fact that more diluted buoyant plume samples had a higher proportion of Fe_{lab} and [L] concentrations provides support for the theory that the ligands are most likely supplied from areas of diffuse flow adjacent to the high temperature vent sites (Bennett et al., 2008).

Our results suggest that also the Nifonea vent field is releasing dissolved and stabilized Fe into the ocean, which might exist in the water column for a long time span. Since the Nifonea vent field plume was detected between 1500 and 1700 m water depth, it is unlikely that dFe supplied by this system reaches the photic zone (<200 m), as the studied area is not located within an upwelling region. However, in shallower island arc settings as the Lesser Antilles Island Arc, hydrothermal discharge often occurs as diffuse venting in very shallow water depths (~ 10 m) rather than as direct emanating fluids, which, looking at our results in this study, suggests that hydrothermal Fe may have a more direct impact on the surface water chemistry. Other settings, such as the Kermadec Arc, hosting several high temperature hydrothermal vents in different water depths from 1600 to only 200 m (de Ronde et al., 2007), would also be very interesting to study with respect to Fe speciation and long term stabilized dFe transport into the deep-ocean and especially surface waters.

AUTHOR CONTRIBUTIONS

First author CK was solely responsible for collection and analysis of all hydrothermal samples mentioned in this study. Interpretation of the data was mainly

performed by CK and JH with discussions with SS and AK. All authors contributed to the final version of this manuscript.

ACKNOWLEDGMENTS

We gratefully acknowledge the BMBF (German Federal Ministry of Education and Research) for funding the project 03G 0229. Thanks are due to Captain D. Korte, the officers and the crew

of the RV SONNE as well the ROV KIEL 6000 crew (GEOMAR Kiel) for their excellent co-operation and effort during the cruise. We also like to thank Dr. D. Garbe-Schönberg for fluid sampling with the KIPS system during SO 229. We acknowledge C. van den Berg and P. Nasemann for helpful discussions. CK's Ph.D. project is funded by MARUM, University Bremen through the Excellence Cluster "The Ocean in the Earth System" (GB4). We are thankful to the two reviewers for their insightful comments.

REFERENCES

- Abualhaja, M. M., and van den Berg, C. M. G. (2014). Chemical speciation of iron in seawater using catalytic cathodic stripping voltammetry with ligand competition against salicylaldehyde. *Mar. Chem.* 164, 60–74. doi: 10.1016/j.marchem.2014.06.005
- Baker, E. T., Embley, R. W., Walker, S. L., Resing, J. A., Lupton, J. E., Nakamura, K., et al. (2008). Hydrothermal activity and volcano distribution along the Mariana arc. *J. Geophys. Res.* 113, B08S09. doi: 10.1029/2007JB005423
- Bennett, S. A., Achterberg, E. P., Connelly, D. P., Statham, P. J., Fones, G. R., and German, C. R. (2008). The distribution and stabilisation of dissolved Fe in deep-sea hydrothermal plumes. *Earth Planet. Sci. Lett.* 270, 157–167. doi: 10.1016/j.epsl.2008.01.048
- Boyd, P. W., Mackie, D. S., and Hunter, K. A. (2010). Aerosol iron deposition to the surface ocean—Modes of iron supply and biological responses. *Mar. Chem.* 120, 128–143. doi: 10.1016/j.marchem.2009.01.008
- Buck, K. N., and Bruland, K. W. (2007). The physicochemical speciation of dissolved iron in the Bering Sea, Alaska. *Limnol. Oceanogr.* 52, 1800–1808. doi: 10.4319/lo.2007.52.5.1800
- Buck, K. N., Lohan, M. C., Berger, C. J. M., and Bruland, K. W. (2007). Dissolved iron speciation in two distinct river plumes and an estuary: Implications for riverine iron supply. *Limnol. Oceanogr.* 52, 843–855. doi: 10.4319/lo.2007.52.2.0843
- Buck, K. N., Sohst, B., and Sedwick, P. N. (2015). The organic complexation of dissolved iron along the U.S. GEOTRACES (GA03) North Atlantic Section. *Deep Sea Res. II Top. Stud. Oceanogr.* 116, 152–165. doi: 10.1016/j.dsr2.2014.11.016
- de Ronde, C. E. J., Baker, E. T., Massoth, G. J., Lupton, J. E., Wright, I. C., Sparks, R. J., et al. (2007). Submarine hydrothermal activity along the mid-Kermadec Arc, New Zealand: large-scale effects on venting. *Geochem. Geophys. Geosys.* 8. doi: 10.1029/2006gc001495
- de Ronde, C. E. J., Massoth, G. J., Butterfield, D. A., Christenson, B. W., Ishibashi, J., Ditchburn, R. G., et al. (2011). Submarine hydrothermal activity and gold-rich mineralization at Brothers Volcano, Kermadec Arc, New Zealand. *Miner. Depos.* 46, 541–584. doi: 10.1007/s00126-011-0345-8
- Fitzsimmons, J. N., Boyle, E. A., and Jenkins, W. J. (2014). Distal transport of dissolved hydrothermal iron in the deep South Pacific Ocean. *Proc. Natl. Acad. Sci. U.S.A.* 111, 16654–16661. doi: 10.1073/pnas.1418778111
- Garbe-Schönberg, D., Koschinsky, A., Ratmeyer, V., Jähmlich, H., and Westernstroeer, U. (2006). KIPS—a new multiport valve-based all-teflon fluid sampling system for ROVs. *Geophys. Res. Abstr.* 8, 07032.
- Gartman, A., Findlay, A. J., and Luther, G. W. (2014). Nanoparticulate pyrite and other nanoparticles are a widespread component of hydrothermal vent black smoker emissions. *Chem. Geol.* 366, 32–41. doi: 10.1016/j.chemgeo.2013.12.013
- German, C. R., Fleer, A. P., Bacon, M. P., and Edmond, J. M. (1991). Hydrothermal scavenging at the Mid-Atlantic Ridge: radionuclide distributions. *Earth Planet. Sci. Lett.* 105, 170–181. doi: 10.1016/0012-821X(91)90128-5
- German, C. R., Legendre, L. L., Sander, S. G., Niquil, N., Luther, G. W., Bharati, L., et al. (2015). Hydrothermal Fe cycling and deep ocean organic carbon scavenging: model-based evidence for significant POC supply to seafloor sediments. *Earth Planet. Sci. Lett.* 419, 143–153. doi: 10.1016/j.epsl.2015.03.012
- Gledhill, M., Achterberg, E. P., Li, K., Mohamed, K. N., and Rijkenberg, M. J. A. (2015). Influence of ocean acidification on the complexation of iron and copper by organic ligands in estuarine waters. *Mar. Chem.* 177, 421–433. doi: 10.1016/j.marchem.2015.03.016
- Gledhill, M., and Buck, K. N. (2012). The organic complexation of iron in the marine environment: a review. *Front. Microbiol.* 3:69. doi: 10.3389/fmicb.2012.00069
- Gledhill, M., and van den Berg, C. M. G. (1994). Determination of complexation of iron(III) with natural organic complexing ligands in seawater using cathodic stripping voltammetry. *Mar. Chem.* 47, 41–54. doi: 10.1016/0304-4203(94)90012-4
- Greene, H. G., and Exon, N. F. (1988). Acoustic stratigraphy and hydrothermal activity within Epi Submarine Caldera, Vanuatu, New Hebrides Arc. *Geo-Marine Lett.* 8, 121–129. doi: 10.1007/BF02326088
- Haase, K. M. (2013). *Shipboard Scientists, 2013. Volcanism, Hydrothermal Activity and Vent Biology in the Coriolis Troughs*. New Hebrides Island Arc. RV Sonne SO-229 Cruise Report.
- Hans Wedepohl, K. (1995). The composition of the continental crust. *Geochim. Cosmochim. Acta* 59, 1217–1232. doi: 10.1016/0016-7037(95)00038-2
- Hatta, M., Measures, C. I., Wu, J., Roshan, S., Fitzsimmons, J. N., Sedwick, P., et al. (2015). An overview of dissolved Fe and Mn distributions during the 2010–2011 U.S. GEOTRACES north Atlantic cruises: GEOTRACES GA03. *Deep Sea Res. II Top. Stud. Oceanogr.* 116, 117–129. doi: 10.1016/j.dsr2.2014.07.005
- Hawkes, J. A., Connelly, D. P., Gledhill, M., and Achterberg, E. P. (2013a). The stabilisation and transportation of dissolved iron from high temperature hydrothermal vent systems. *Earth Planet. Sci. Lett.* 375, 280–290. doi: 10.1016/j.epsl.2013.05.047
- Hawkes, J. A., Connelly, D. P., Rijkenberg, M. J. A., and Achterberg, E. P. (2014). The importance of shallow hydrothermal island arc systems in ocean biogeochemistry. *Geophys. Res. Lett.* 41, 942–947. doi: 10.1002/2013GL058817
- Hawkes, J. A., Gledhill, M., Connelly, D. P., and Achterberg, E. P. (2013b). Characterisation of iron binding ligands in seawater by reverse titration. *Anal. Chim. Acta* 766, 53–60. doi: 10.1016/j.aca.2012.12.048
- Hawkes, J. A., Rossel, P. E., Stubbins, A., Butterfield, D., Connelly, D. P., Achterberg, E. P., et al. (2015). Efficient removal of recalcitrant deep-ocean dissolved organic matter during hydrothermal circulation. *Nat. Geosci.* 8, 856–860. doi: 10.1038/ngeo2543
- Homoky, W. B., Severmann, S., Mills, R. A., Statham, P. J., and Fones, G. R. (2009). Pore-fluid Fe isotopes reflect the extent of benthic Fe redox recycling: evidence from continental shelf and deep-sea sediments. *Geology* 37, 751–754. doi: 10.1130/G25731A.1
- Honeyman, B. D., and Santschi, P. H. (1989). A Brownian-pumping model for oceanic trace metal scavenging: evidence from Th isotopes. *J. Mar. Res.* 47, 951–992. doi: 10.1357/002224089785076091
- Iizasa, K., Kawasaki, K., Maeda, K., Matsumoto, T., Saito, N., and Hirai, K. (1998). Hydrothermal sulfide-bearing Fe-Si oxyhydroxide deposits from the Coriolis Troughs, Vanuatu backarc, southwestern Pacific. *Mar. Geol.* 145, 1–21. doi: 10.1016/S0025-3227(97)00112-6
- Johnson, K. S., Gordon, R. M., and Coale, K. H. (1997). What controls dissolved iron concentrations in the world ocean? *Mar. Chem.* 57, 137–161. doi: 10.1016/S0304-4203(97)00043-1
- Kraemer, S. M. (2004). Iron oxide dissolution and solubility in the presence of siderophores. *Aquat. Sci. Res.* 66, 3–18. doi: 10.1007/s00027-003-0690-5
- Landing, W. M., and Westerlund, S. (1988). The solution chemistry of iron(II) in Framvaren Fjord. *Mar. Chem.* 23, 329–343. doi: 10.1016/0304-4203(88)90102-8

- Lannuzel, D., Grotti, M., Abelloschi, M. L., and van der Merwe, P. (2015). Organic ligands control the concentrations of dissolved iron in Antarctic sea ice. *Mar. Chem.* 174, 120–130. doi: 10.1016/j.marchem.2015.05.005
- Leybourne, M. I., de Ronde, C. E. J., Wysoczanski, R. J., Walker, S. L., Timm, C., Gibson, H. L., et al. (2012). Geology, hydrothermal activity, and sea-floor massive sulfide mineralization at the rumble ii west mafic caldera. *Econ. Geol.* 107, 1649–1668. doi: 10.2113/econgeo.107.8.1649
- Liu, X., and Millero, F. J. (2002). The solubility of iron in seawater. *Mar. Chem.* 77, 43–54. doi: 10.1016/S0304-4203(01)00074-3
- Luther, G. W., Rozan, T. F., Taillefert, M., Nuzzio, D. B., Di Meo, C., Shank, T. M., et al. (2001). Chemical speciation drives hydrothermal vent ecology. *Nature* 410, 813–816. doi: 10.1038/35071069
- Mackey, D. J., and Zirino, A. (1994). Comments on trace metal speciation in seawater or do “onions” grow in the sea? *Anal. Chim. Acta* 284, 635–647. doi: 10.1016/0003-2670(94)85068-2
- Maldonado, M. T., and Price, N. M. (2001). Reduction and transport of organically bound iron by *Thalassiosira Oceanica* (Bacillariophyceae). *J. Phycol.* 37, 298–310. doi: 10.1046/j.1529-8817.2001.037002298.x
- McCollom, T. M., Seewald, J. S., and German, C. R. (2015). Investigation of extractable organic compounds in deep-sea hydrothermal vent fluids along the Mid-Atlantic Ridge. *Geochim. Cosmochim. Acta* 156, 122–144. doi: 10.1016/j.gca.2015.02.022
- McConachy, T. F., Arculus, R. J., Yeats, C. J., Binns, R. A., Barriga, F. J. A. S., McInnes, B. I. A., et al. (2005). New hydrothermal activity and alkaline volcanism in the backarc Coriolis Troughs, Vanuatu. *Geology* 33, 61. doi: 10.1130/G20870.1
- Millero, F. J., Sotolongo, S., and Izaguirre, M. (1987). The oxidation kinetics of Fe(II) in seawater. *Geochim. Cosmochim. Acta* 51, 793–801. doi: 10.1016/0016-7037(87)90093-7
- Moore, J. K., Doney, S. C., and Lindsay, K. (2004). Upper ocean ecosystem dynamics and iron cycling in a global three-dimensional model. *Global Biogeochem. Cycles* 18. doi: 10.1029/2004GB002220
- Nasemann, P. (2015). *Characterization of Hydrothermal Sources of Iron in the Oceans Constraints from Iron Stable Isotopes*. Dunedin: University of Otago.
- Omanović, D., Garnier, C., and Pižeta, I. (2015). ProMCC: an all-in-one tool for trace metal complexation studies. *Mar. Chem.* 173, 25–39. doi: 10.1016/j.marchem.2014.10.011
- Price, R. C., Maillat, P., and Johnson, D. P. (1993). Interpretation of GLORIA sidescan sonar imagery for the coriolis troughs of the new hebrides backarc. *Geo Marine Lett.* 13, 71–81. doi: 10.1007/BF011204548
- Resing, J. A., Sedwick, P. N., German, C. R., Jenkins, W. J., Moffett, J. W., Sohst, B. M., et al. (2015). Basin-scale transport of hydrothermal dissolved metals across the South Pacific Ocean. *Nature* 523, 200–203. doi: 10.1038/nature14577
- Rudnicki, M. D., and Elderfield, H. (1993). A chemical model of the buoyant and neutrally buoyant plume above the TAG vent field, 26 degrees N, Mid-Atlantic Ridge. *Geochim. Cosmochim. Acta* 57, 2939–2957. doi: 10.1016/0016-7037(93)90285-5
- Rue, E. L., and Bruland, K. W. (1995). Complexation of iron(III) by natural organic ligands in the Central North Pacific as determined by a new competitive ligand equilibration/adsorptive cathodic stripping voltammetric method. *Mar. Chem.* 50, 117–138. doi: 10.1016/0304-4203(95)00031-L
- Saito, M. A., Noble, A. E., Tagliabue, A., Goepfert, T. J., Lamborg, C. H., and Jenkins, W. J. (2013). Slow-spreading submarine ridges in the South Atlantic as a significant oceanic iron source. *Nat. Geosci.* 6, 775–779. doi: 10.1038/ngeo1893
- Sander, S. G., and Koschinsky, A. (2011). Metal flux from hydrothermal vents increased by organic complexation. *Nat. Geosci.* 4, 145–150. doi: 10.1038/ngeo1088
- Satham, P. J., German, C. R., and Connelly, D. P. (2005). Iron (II) distribution and oxidation kinetics in hydrothermal plumes at the Kairei and Edmond vent sites, Indian Ocean. *Earth Planet. Sci. Lett.* 236, 588–596. doi: 10.1016/j.epsl.2005.03.008
- Stockdale, A., Tipping, E., Lofts, S., and Mortimer, R. J. G. (2016). The effect of ocean acidification on organic and inorganic speciation of trace metals. *Environ. Sci. Technol.* 50, 1906–1913. doi: 10.1021/acs.est.5b05624
- Tagliabue, A., Bopp, L., Dutay, J.-C., Bowie, A. R., Chever, F., Jean-Baptiste, P., et al. (2010). Hydrothermal contribution to the oceanic dissolved iron inventory. *Nat. Geosci.* 3, 252–256. doi: 10.1038/ngeo818
- Toner, B. M., Fakra, S. C., Manganini, S. J., Santelli, C. M., Marcus, M. A., Moffett, J. W., et al. (2009). Preservation of iron(II) by carbon-rich matrices in a hydrothermal plume. *Nat. Geosci.* 2, 197–201. doi: 10.1038/ngeo433
- Wu, J., and Luther, G. W. (1995). Complexation of Fe(III) by natural organic ligands in the Northwest Atlantic Ocean by a competitive ligand equilibration method and a kinetic approach. *Mar. Chem.* 50, 159–177. doi: 10.1016/0304-4203(95)00033-N
- Yücel, M., Gartman, A., Chan, C. S., and Luther, G. W. (2011). Hydrothermal vents as a kinetically stable source of iron-sulphide-bearing nanoparticles to the ocean. *Nat. Geosci.* 4, 367–371. doi: 10.1038/ngeo1148

Conflict of Interest Statement: The authors declare that the research was conducted in the absence of any commercial or financial relationships that could be construed as a potential conflict of interest.

Copyright © 2016 Kleint, Hawkes, Sander and Koschinsky. This is an open-access article distributed under the terms of the Creative Commons Attribution License (CC BY). The use, distribution or reproduction in other forums is permitted, provided the original author(s) or licensor are credited and that the original publication in this journal is cited, in accordance with accepted academic practice. No use, distribution or reproduction is permitted which does not comply with these terms.



Dissolved Zn and its speciation in the northeastern Indian Ocean and the Andaman Sea

Taejin Kim *, Hajime Obata and Toshitaka Gamo

Department of Chemical Oceanography, Atmosphere and Ocean Research Institute, The University of Tokyo, Kashiwa, Japan

OPEN ACCESS

Edited by:

Maeve Carroll Lohan,
University of Plymouth, UK

Reviewed by:

Antonio Cobelo-Garcia,
Instituto de Investigaciones
Marinas - Consejo Superior de
Investigaciones Cientificas, Spain
Marta Plavsic,
Ruder Bošković Institute, Croatia

*Correspondence:

Taejin Kim,
Department of Chemical
Oceanography, Atmosphere and
Ocean Research Institute, The
University of Tokyo, 5-1-5
Kashiwanoha, Kashiwa,
Chiba 277-8564, Japan
tjkim@aori.u-tokyo.ac.jp

Specialty section:

This article was submitted to
Marine Biogeochemistry,
a section of the journal
Frontiers in Marine Science

Received: 05 June 2015

Accepted: 07 August 2015

Published: 25 August 2015

Citation:

Kim T, Obata H and Gamo T (2015)
Dissolved Zn and its speciation in the
northeastern Indian Ocean and the
Andaman Sea. *Front. Mar. Sci.* 2:60.
doi: 10.3389/fmars.2015.00060

Total dissolved Zn and Zn speciation were investigated by cathodic stripping voltammetry (CSV) in the northeastern Indian Ocean and the Andaman Sea. Vertical distributions of total dissolved Zn concentration (C_{Zn}) in the northeastern Indian Ocean and the Andaman Sea reflect that the deep water from the Andaman Sea was rapidly replaced by incoming waters from the northeastern Indian Ocean across the sills and was homogenized by vertical mixing. In the Andaman Sea, C_{Zn} at the near surface, <50 m in depth, ranged from 0.33 to 1.14 nM at the southernmost station, which is an order of magnitude higher than those at the northernmost station, 0.03–0.22 nM, where is in close proximity to the estuaries of the Irrawaddy and Salween rivers. However, the Si concentration in the near surface water, 16.3 μ M, was highest at the northernmost station of the Andaman Sea. In the northeastern Indian Ocean, only one sample was applied to estimate total ligand concentrations (C_L) and conditional stability constants ($K'_{ZnL,Zn^{2+}}$) for organic complexation of Zn. The C_L and $K'_{ZnL,Zn^{2+}}$ in the northeastern Indian Ocean were 0.5 nM and 10.0, whereas those of the Andaman Sea were 0.4–0.9 nM and 9.6–11.4, respectively. We observed no clear relationship between chlorophyll a (Chl a) and C_L in the Andaman Sea. Various sources of Zn complexing ligands might be derived in the Andaman Sea, not only from bacteria and phytoplankton, but also from the Irrawaddy–Salween rivers.

Keywords: trace metal, zinc, speciation, ligand, Indian Ocean, Andaman Sea

Introduction

Zn is used in numerous enzyme systems involved with a variety of metabolic processes (Vallee and Auld, 1990). In the ocean, total dissolved Zn concentration (C_{Zn}) has a nutrient-like vertical profile with a particularly strong correlation with silicate (Bruland, 1980). However, a previous study showed that biogenic opal has low Zn content, which suggests that Zn is not directly involved with Si uptake and that the amount of Zn incorporated into opal represents only 1–3% of the total amount taken up by diatoms (Ellwood and Hunter, 2000). Thamatrakoln and Hildebrand (2008) also suggested that Zn is not involved in silicon uptake or in silicon transporter proteins. A recent study has shown that scavenging of dissolved Zn onto sinking particles could be a reason of deeper Zn regeneration, generating depth profiles similar to that of silicate (John and Conway, 2014). Low Zn concentrations could limit CO_2 uptake and, ultimately, the growth rate in some cells through reduced production of the enzyme carbonic anhydrase (CA; Price and Morel, 1990; Morel et al., 1994; Lane and Morel, 2000). Low rates of phosphate uptake from dissolved organic P in

oligotrophic waters have been linked to the limitation of available Zn in seawater via its central role in the enzyme alkaline phosphatase (Shaked et al., 2006). At high concentrations, Zn could be toxic to phytoplankton and bacteria (Sunda and Huntsman, 1996, 1998; Chen et al., 2008). Moreover, low Zn concentrations in surface seawater could limit growth of some kinds of phytoplankton (Brand et al., 1983; Sunda and Huntsman, 1998, 2000), although Zn limitation has not been observed in field studies (Coale et al., 2003; Crawford et al., 2003; Lohan et al., 2005; Jakuba et al., 2012).

In most surface waters, natural organic ligands strongly bind Zn and dominate the speciation of the total Zn pool. Organic complexation reduces the fractions of free-metal ions (Zn^{2+}) to levels as low as 1 pM (Bruland et al., 1991; Ellwood and van den Berg, 2000). Culture experiments have shown that Zn^{2+} concentration of <1 pM limits the growth of some phytoplankton species (Brand et al., 1983; Sunda and Huntsman, 1992, 1995). Therefore, the study of Zn speciation is important for understanding the oceanic biogeochemical cycling of Zn. In the open oceans, studies of Zn complexation in surface water of the North Pacific and North Atlantic reveal that >95% of Zn is complexed to organic ligands (Bruland, 1989; Donat and Bruland, 1990; Ellwood and van den Berg, 2000; Jakuba et al., 2012), whereas Zn predominated as inorganic Zn in both surface and deep waters of the Southern Ocean (Baars and Croot, 2011). In marginal seas, few studies indicated relatively high total ligand concentrations (C_L) and relatively low conditional stability constants ($K'_{ZnL,Zn^{2+}}$) in the surface waters of the Black Sea (Muller et al., 2001), Bering Sea (Jakuba et al., 2012), Sea of Okhotsk, and Sea of Japan (East Sea) (Kim et al., 2015b) compared with those in open oceans. The main sources of Zn complexing ligands could be humic substances (Campbell et al., 2002), phytoplankton and bacteria-excreted organic substances (Bruland, 1989), and pore waters from estuarine marine sediments (Skrabal et al., 2006). However, more Zn speciation studies are needed to determine distributions and sources of Zn ligands.

The northeastern Indian Ocean, including the Bay of Bengal and the Andaman Sea (Figure 1), is characterized by surface current systems with strong monsoon seasonality (Shankar et al., 2002), and the biogeochemical cycles in the basins are significantly influenced by fluvial dissolved substances and suspended sediment loads (Milliman and Meade, 1983; Robinson et al., 2007). The Ganges and Brahmaputra rivers carry a large amount of terrestrial debris, $\sim 2 \times 10^{12}$ kg/yr, into the northern part of the Bay of Bengal, which corresponds to $\sim 10\%$ of the world's fluvial discharge (Milliman and Meade, 1983). In the Bay of Bengal, this high accumulation of sediment has created a broad submarine alluvial Bengal Fan and has affected the topography of the entire sea bottom.

This study presents the distributions of C_{Zn} and Zn speciation in the northeastern Indian Ocean and the Andaman Sea by using competitive ligand equilibration-adsorptive cathodic stripping voltammetry (CSV) to characterize organic Zn complexing ligands and their influence on the chemical speciation of Zn.

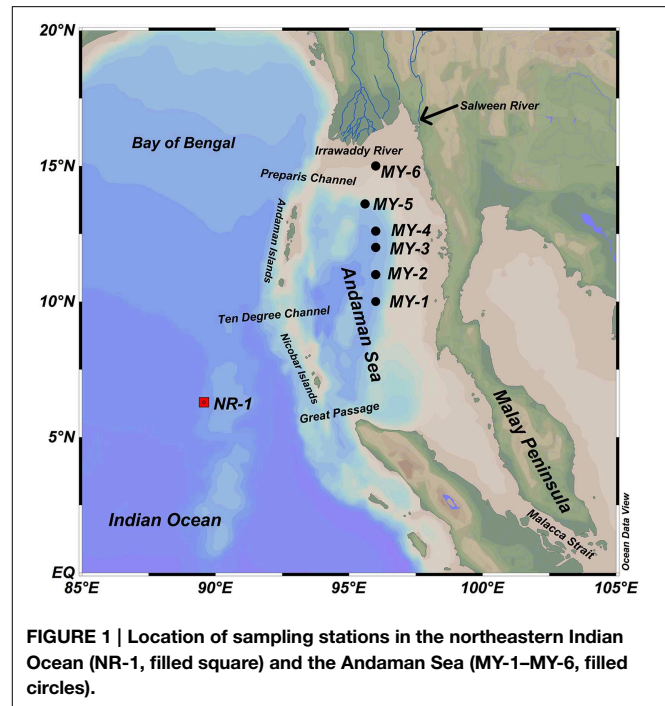


FIGURE 1 | Location of sampling stations in the northeastern Indian Ocean (NR-1, filled square) and the Andaman Sea (MY-1–MY-6, filled circles).

Materials and Methods

Sample Collection and Storage

Seawater samples were collected in the northeastern Indian Ocean (NR-1) and the Andaman Sea (MY-1–MY-6) during R/V *Hakuho-maru* research cruise KH-13-4 in July and August, 2013. Locations of the sampling stations are indicated in Figure 1.

The Andaman Sea is a marginal sea of the Indian Ocean that extends between the Malay Peninsula on the east and the Andaman and Nicobar islands on the west. The Andaman Sea forms the far eastern part of the northern Indian Ocean and is separated from the western Bay of Bengal by the Andaman–Nicobar island chain. In the northern region, a the submarine delta created by outflow of the Irrawaddy and Salween rivers is connected to the eastern shallow shelves along the Malay Peninsula and the Malacca Strait (Robinson et al., 2007). From the shelves, the sea bottom drops off sharply into a large central basin and two smaller basins deeper than 2000 m extending along the north–south island arc. The maximum depth is 4180 m at the south end of the central basin. The sill depths of the channels across the Andaman–Nicobar Ridge are shallower than 1800 m. Therefore, the deep water below this depth of the Andaman Sea Basin is isolated from the Bay of Bengal, and its maximum water temperature remains approximately 2°C down to the bottom (Sarma and Narvekar, 2001). Previous studies reported the vertical profiles of dissolved rare earth elements (Nozaki and Alibo, 2003), ^{230}Th (Okubo et al., 2004) and Al, in addition to In and Ce (Obata et al., 2004). C_{Zn} and its speciation in the Andaman Sea, however, have not been reported thus far.

The sampling methods have been detailed in previous research (Kim et al., 2015a). Briefly, seawater samples were

collected by using acid-cleaned Teflon-coated X-type Niskin samplers. The O-rings inside the Niskin samplers and the spigots were replaced with Viton and Teflon parts, respectively. X-type Niskin bottles were cleaned by using a 1% alkaline surfactant (Extran MA01), 0.1 M HCl (Special Grade, Wako Pure Chemical Industries) and Millipore Milli-Q water. The acid-cleaned Teflon-coated X-type Niskin bottles were then deployed on a conductivity–temperature–depth carousel multi-sampling system (SBE-911plus and SBE-32 water sampler, Sea Bird Electronics, Inc.), on which a Zn sacrificial anode was replaced with an Al anode to avoid the possibility of Zn contamination from the frame. For sub-sampling, the Niskin-X bottles were detached from the carousel frame and were carefully moved into a clean space filled with HEPA-filtered air in the onboard laboratory of the research vessel. Seawater samples were filtered by using an acid-cleaned 0.2- μ m, Acropak capsule filter (PALL Co.) directly connected to the Niskin-X Teflon spigot. The filtered samples were stored in acid-cleaned 500-mL low-density polyethylene bottles (Nalgene Co., Ltd) after being rinsed at least four times with filtered seawater. The samples were then acidified to achieve a pH < 1.8 by using ultrapure HCl (Tamapure AA-100, Tama chemicals) and were placed in storage for later measurement of C_{Zn} . The filtered samples for Zn speciation analysis were frozen immediately after collection until just before analysis.

Total Dissolved Zn Analysis

CSV was used to determine the C_{Zn} in the seawater (van den Berg, 1985; Donat and Bruland, 1990; Ellwood and van den Berg, 2000; Lohan et al., 2002; Kim et al., 2015a). In this study, the 757 VA Computrace (Metrohm) voltammetric system was used. The reference electrode was Ag/saturated AgCl, 3 M KCl. The counter electrode was composed of glassy carbon, and the working electrode was a hanging mercury drop electrode. To decompose interfering dissolved organic matter and metal complexing organic ligands, which occur naturally in seawater (van den Berg, 1985), an ultraviolet (UV) irradiation system was used (Kim et al., 2015a). In this study, seawater samples were UV-irradiated over 40 min to ensure the full breakdown of naturally occurring dissolved organic matter by using a high-pressure mercury vapor UV lamp (450 Watts, UM-453B-A, USHIO). The sample solution was kept cold with ice to prevent water evaporation during the UV-irradiation.

Following UV-irradiation, 10 mL of the seawater sample was added to a Teflon cell with 100 μ M ammonium 1-pyrrolidinedithiocarbamate (APDC) and 2 mM buffer solution piperazine-1,4-bis (2-ethanesulfonic acid) (PIPES). The pH values of the samples were adjusted to 7.0 by adding ultrapure aqueous ammonia (Tamapure AA-100, Tama chemicals). In the Teflon cell, Zn was complexed with APDC (Zn-PDC) and absorbed onto the hanging mercury drop electrode. The reduction current peak of Zn^{2+} in the adsorbed Zn-PDC complexes was found to be approximately -1.1 V. Voltammetric conditions included differential pulse mode, 4 min 99.9995% N_2 gas purge, 60–300 s deposition time at -0.3 V, 8 s equilibration time, and a negative scan from -0.75 to -1.2 V with a 0.05 V pulse amplitude, 0.02 s pulse time, 0.0047 V voltage step, 0.2 s step

time, and 0.024 V/s sweep rate. The potential of the electrode was scanned in the negative direction. The concentrations of Zn in the seawater were calibrated by using a standard addition method (Lohan et al., 2002). The procedural blank value was obtained from Zn-removed seawater, which was passed through a chelating resin column (NOBIAS CHELATE-PA1, Hitachi High-Tec) (Kim et al., 2015a). This Zn-removed seawater was UV-digested. The deposition time for the Zn-removed seawater was 360 s. The resulting procedural blank value was calculated to be 71 ± 8 pM ($n = 7$). This blank value was used to calculate the C_{Zn} , which were subtracted from the measured values. The detection limit, calculated as three times the standard deviation of measurements of the blank values for purified seawater, was 26 pM. To assess the accuracy of the entire analytical procedure, Zn concentrations in SAFe samples S (SAFe Intercalibration North Pacific 2004, surface seawater) and D2 (SAFe Intercalibration North Pacific 2004; 1000 m) (Johnson et al., 2007) were determined and compared. The results of this intercalibration were 0.063 ± 0.002 nmol/kg for S and 7.37 ± 0.13 nmol/kg for D2, which are in good agreement with the reported consensus values of $S = 0.069 \pm 0.010$ nmol/kg and $D2 = 7.43 \pm 0.25$ nmol/kg (<http://www.geotraces.org/science/intercalibration/322-standards-and-reference-materials>).

Zn Speciation Theory

Zn speciation was determined through titration by using competitive ligand equilibrium/adsorptive CSV (van den Berg, 1985; Donat and Bruland, 1990), which uses a competitive equilibrium between Zn-complexing ligands naturally present in the sample and a competing ligand (APDC). A titration curve is produced by adding increasing concentrations of Zn. Once the natural ligands are saturated with Zn, the reduction peak current will be increased proportionally to the added Zn concentration (Figure 2). The C_{Zn} of a sample can be defined as

$$C_{Zn} = [Zn'] + [ZnL] + [ZnPDC], \quad (1)$$

where $[Zn']$ is the concentration of inorganic Zn, $[ZnPDC]$ is the concentration of Zn complexed with APDC, and $[ZnL]$ is the concentration of Zn complexed by natural ligands. By using a simple one-ligand model, the complexation of Zn in seawater by natural ligands can be defined as

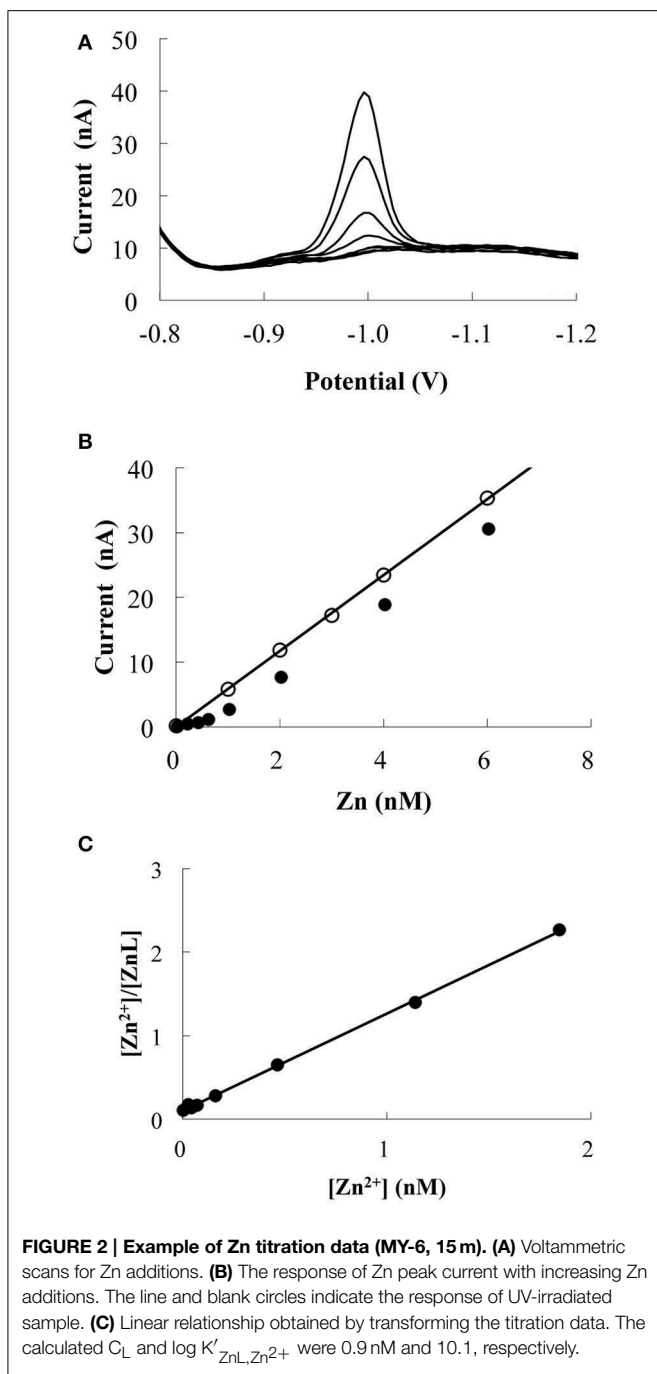
$$K'_{ZnL,Zn^{2+}} = \frac{[ZnL]}{[Zn^{2+}][L]}, \quad (2)$$

where $K'_{ZnL,Zn^{2+}}$ is the conditional stability constant of the Zn complex with respect to Zn^{2+} in seawater, and $[L]$ is the concentration of the free ligand.

The C_L of a sample can be defined as

$$C_L = [ZnL] + [L']. \quad (3)$$

Substitution for $[L']$ in Equation (2) using Equation (3) and rearranging terms gives the van den Berg/Ružić linearization



(Ružić, 1982; van den Berg, 1982). The equation for the resulting line is

$$\frac{[Zn^{2+}]}{[ZnL]} = \frac{[Zn^{2+}]}{C_L} + \frac{1}{(K'_{ZnL,Zn^{2+}} \times C_L)}. \quad (4)$$

When values of $[Zn^{2+}]/[ZnL]$ are plotted against corresponding values of $[Zn^{2+}]$, a linear relationship is obtained with a slope equal to $1/C_L$ and with the intercept yielding $1/(K'_{ZnL,Zn^{2+}} \times C_L)$.

The observed reduction peak current (i_p) is related to the concentration of Zn^{2+} by the equation

$$[Zn^{2+}] = \frac{i_p}{S \times \alpha'}, \quad (5)$$

where S is the sensitivity, which is calibrated by standard additions to UV-irradiated seawater (UVSW), and α' is the overall side reaction coefficient for Zn:

$$\alpha' = \alpha_{Zn} + \alpha_{ZnPDC}, \quad (6)$$

where α_{Zn} is the inorganic side reaction coefficient for Zn. A value of 2.2 (Turner et al., 1981; Donat and Bruland, 1990; Jakuba et al., 2008, 2012) was used in this study. α_{ZnPDC} , the side reaction coefficient for Zn with PDC, is fixed by the concentration of PDC added to the sample. α_{ZnPDC} can be calculated as

$$\alpha_{ZnPDC} = K'_{ZnPDC} [APDC'], \quad (7)$$

where K'_{ZnPDC} is a conditional stability constant, and $[APDC']$ is the concentration of APDC not complexed by Zn^{2+} . Because this $[APDC']$ is much greater than that of Zn, the total APDC concentration ($[APDC']_T$) can be selected for calculations. A K'_{ZnPDC} value of $10^{4.4}$ was used for seawaters of pH 8.2 with borate buffer (Ellwood and van den Berg, 2000). $[ZnL]$ can be calculated as

$$[ZnL] = C_{Zn} - \left(\frac{i_p}{S}\right), \quad (8)$$

where (i_p/S) is equal to labile Zn (Zn_{labile}) concentration ($= [Zn'] + [ZnPDC]$). Combining Equations (5) and (8), $[Zn^{2+}]/[ZnL]$ can be calculated as

$$\frac{[Zn^{2+}]}{[ZnL]} = \frac{i_p}{\alpha' \times ((S \times C_{Zn}) - i_p)}. \quad (9)$$

Finally, once C_L and $K'_{ZnL,Zn^{2+}}$ have been determined, the concentration of Zn^{2+} can be calculated by the following quadratic equation (Ellwood and van den Berg, 2000):

$$[Zn^{2+}]^2 \cdot \alpha_{Zn} \cdot K'_{ZnL,Zn^{2+}} + [Zn^{2+}] (K'_{ZnL,Zn^{2+}} \cdot C_L - K'_{ZnL,Zn^{2+}} \cdot C_{Zn} + \alpha_{Zn}) - C_{Zn} = 0 \quad (10)$$

Experimental

Acid-cleaned Teflon vials were used for Zn titration. To minimize the effects of adsorption onto the vial walls, the Teflon vials were rinsed twice with 10 mL of the sample. After rinsing, 10 mL of the seawater sample and 4 mM of borate buffer were added to each Teflon vial; the borate buffer was added to achieve a pH of 8.2. Each vial was then spiked with Zn concentrations of 0.2–6.0 nM and was allowed to equilibrate. After 2 h, 25 μ M of APDC was added to each vial. The APDC was allowed to equilibrate for 12 h (Ellwood and van den Berg, 2000; Lohan et al., 2005). At this APDC concentration, the detection window of the method is approximately from $K'_{ZnL,Zn^{2+}} = 10^7$ to 10^{12} for a

C_L of 1 nM. The first two vials were not spiked with Zn and were used as replicates for the starting point of the titration. The voltammetric conditions were differential pulse mode, 4 min N_2 gas purge, 180 s deposition time at -0.6 V, 8 s equilibration time, and a negative scan from -0.75 to -1.2 V with a 0.05 V pulse amplitude, 0.02 s pulse time, 0.0047 V voltage step, 0.2 s step time, and 0.024 V/s sweep rate. One example of the titration is shown in **Figure 2**.

Zn speciation data obtained by using linear fit were compared with those obtained by non-linear fitting (Gerringa et al., 1995). When non-linear fitting was applied to the Zn titration data from this study, there was generally good agreement with the C_L and $\log K'_{ZnL,Zn^{2+}}$ calculated by the linear method, with differences of ~ 0.2 nM and ~ 0.2 , respectively. Thus, both linear and non-linear models generally produced consistent results for Zn speciation with the competitive ligand equilibrium/adsorptive CSV method.

Chl *a*, Silicate, and Salinity Determination

Chlorophyll *a* (Chl *a*) was measured by using the following fluorometric method. For the analysis of Chl *a*, 290 mL seawater samples were immediately filtered through 25 mm Whatman GF/F glass fiber filters maintaining vacuum levels of 0.02 MPa or less. The filters were placed in polypropylene vials and were extracted in 6.0 mL N, N-dimethylformamide. The samples were allowed to be extracted for 1–2 days in a freezer at -20°C . After removal from the cold environment, the extracted samples were placed in a 13 mm glass cuvette and measured on a Turner Designs 10-AU field fluorometer with a chlorophyll optical kit for the non-acidification method (Welschmeyer, 1994). The concentrations of Chl *a* in the sample ($\mu\text{g/L}$) were calculated from the reading by using calibration and scaling factors.

Silicate concentrations were determined by using an auto analyzer SWAAT (BLTEC Japan). β -molybdosilicic acid is formed by the reaction of silicate with molybdate at pH levels of 1–1.8. The β -molybdosilicic acid is reduced by Sn(II) to form molybdenum blue with an absorbance maximum at 630 nm. Data were corrected by using seawater reference nutrient material (KANSO).

Practical salinity was measured by using an Autosol laboratory salinometer (Model 8400B, Guildline Instruments Ltd., Canada). The sampling bottles for practical salinity tests were prepared according to Joint Global Ocean Flux Study protocol. The Autosol was standardized by using International Association for the Physical Sciences of the Oceans standard seawater.

Results

Hydrography

Table 1 shows the data obtained in this study. The surface salinities at <50 m in the Andaman Sea (MY-1–MY-6), 28.624–33.864, were relatively lower than those of in the northeastern Indian Ocean (NR-1, 34.226–34.228). Additionally, the surface salinities in the Andaman Sea were gradually increased from north to south (**Table 1**). **Figure 3** shows the vertical profiles of salinity, potential temperature, and dissolved O_2 in both the

northeastern Indian Ocean (NR-1) and the Andaman Sea (MY-1 and MY-3). The deep water of the northeastern Indian Ocean is most simply characterized as a tongue of circumpolar water extending north from the south (Wyrтки, 1971). In the Southern Ocean, the original circumpolar deep water has relatively high salinity and O_2 due to the presence of North Atlantic Deep Water. Although dissolved O_2 is consumed by respiration during the northward transport of the deep water, the salinity in circumpolar deep water of the northeastern Indian Ocean (NR-1) and the Andaman Sea (MY-1 and MY-3), remains high as indicated by the maximum salinity of >35.000 at 275–596 m (**Figure 3A**).

The potential temperature in both the northeastern Indian Ocean and the Andaman Sea are comparable to a depth of 1000 m (**Figure 3B**), although the deep waters below 1500 m of the Andaman Sea are consistently warmer than those of the northeastern Indian Ocean. Below 1500 m, the potential temperatures in the Andaman Sea are relatively uniform (4.99 – 5.32°C), where as those of northeastern Indian Ocean were decreased from 4.55 to 1.80°C (**Figure 3B**).

Dissolved O_2 decreases sharply from the surface to a minimum of <20 $\mu\text{mol/L}$ at 298–396 m for NR-1, 198–249 m for MY-1, and 239 m for MY-3. In deep layers, dissolved O_2 concentrations increase toward the bottom. The high dissolved O_2 concentration near the bottom at station NR-1 suggests that the bottom and the deep waters are fed from the south. The sharp decrease in dissolved O_2 from the surface with increasing depth is attributed to high productivity, and the shallow depths of the O_2 minimum and the salinity maximum are indicative of the upwelling regime of the northeastern Indian Ocean, which is consistent with the general circulation pattern (Schmitz, 1995). The profiles of dissolved O_2 in the northeastern Indian Ocean and the Andaman Sea are separated below 1000 m, which is consistent with those of potential temperature. The deep water of the Andaman Sea has uniform concentrations for dissolved O_2 , whereas it increases with depth in the northeastern Indian Ocean (**Figure 3C**). The O_2 profile indicates that the deep water of the Andaman Sea is highly similar to that of the inflowing water from northeastern Indian Ocean in the Bay of Bengal, suggesting that the deep Andaman Sea water is replaced rapidly before detectable dissolved O_2 consumption occurs in its deep water (Okubo et al., 2004).

Total Dissolved Zn and Silicate Concentrations

In this study, the vertical distributions of C_{Zn} were nutrient type (**Figure 4A**), which is similar to previous studies in the North Pacific (Bruland et al., 1978, 1979, 1994; Bruland, 1980; Lohan et al., 2002; Cutter and Bruland, 2012; Kim et al., 2015a), South Atlantic (Wyatt et al., 2014), southern Indian Ocean (Gosnell et al., 2012), and Southern Ocean (Crook et al., 2011). The Si concentrations were strongly correlated with C_{Zn} (**Figure 4B**). Vertical profiles in the northeastern Indian Ocean (NR-1) and the Andaman Sea (MY-1 and MY-3) also showed similar features such that both C_{Zn} and Si were separated below 1500 m.

In the Andaman Sea, C_{Zn} in near the surface water (<50 m) ranged from 0.33 nM to 1.14 nM at the southernmost station (MY-1), which was an order of magnitude higher than those of the northernmost station (MY-6, 0.03 – 0.22 nM) (**Table 1**). On

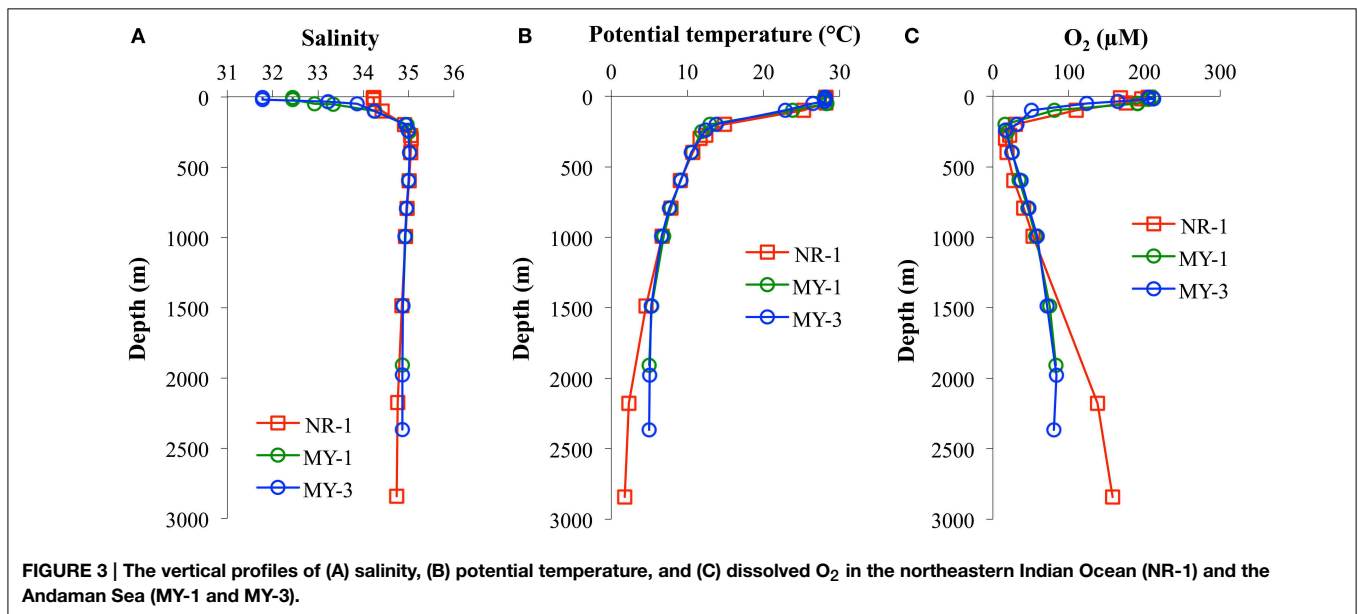
TABLE 1 | Seawater analysis results and associated hydrographic data obtained in this study.

Station	Depth m	Potential temperature °C	Salinity PSU	O ₂ μmol/L	Si μL	C _{Zn} nM	Chl <i>a</i> μg/L	C _L nM	Log K' _{ZnL,Zn²⁺}	Zn ²⁺ nM	Zn _{labile} nM
NR-1 (6°29'N,89°57'E)	5	28.18	34.226	205.4	1.5	0.75	0.6				
	10	28.18	34.226	168.2	1.4	1.03	0.6				
	17	28.19	34.226	196.3	1.4	0.26	0.6	0.5	10.0	0.047	
	19	28.19	34.226	204.5	1.6	0.94	0.7				
	49	28.19	34.228	175.9	1.5	0.92	0.6				0.25
	100	25.22	34.414	110.1	10.0	0.74	0.2				0.17
	199	14.87	34.913	29.6	29.8	2.00					1.00
	274	12.41	35.043	22.4	31.6	3.14					1.22
	298	11.65	35.055	16.8	33.9	2.14					1.36
	396	10.71	35.049	18.9	37.8	2.36					0.91
	596	9.07	35.008	27.4	57.5	2.54					1.00
	794	7.85	34.969	40.8	73.4	4.14					1.87
	993	6.72	34.933	52.8	83.6	3.54					1.41
	1486	4.55	34.852		107.3	4.83					2.11
2176	2.30	34.757	137.9	130.0	8.61					3.53	
2842	1.80	34.736	158.2	135.2	8.43					3.27	
MY-1 (10°00'N,96°00'E)	5	27.98	32.185	211.0	2.5	0.69	0.4	0.9	10.4	0.063	
	20	28.00	32.201	205.2	2.4	1.14	0.4				
	50	28.28	32.664	191.3	2.9	0.33	0.6				
	53	28.35	32.818	191.1	2.9	0.35	0.5	0.7	10.9	0.011	
	100	23.80	34.293	81.0	13.9	0.54	0.1	0.8	11.4	0.008	
	198	12.94	34.964	16.1	35.7	1.98					0.52
	249	11.87	35.010	19.4	35.5	1.41					0.48
	397	10.59	35.025	25.9	43.9	2.06					1.22
	595	9.17	35.002	34.6	56.9	2.77					
	793	7.77	34.960	46.4	72.6	3.84					2.54
	992	6.86	34.928	56.4	74.5	3.67					2.16
1486	5.32	34.876	75.2	101.8	4.28					3.14	
1907	5.00	34.864	83.0	101.4	4.48					1.62	
MY-2 (11°00'N,96°00'E)	5	28.10	32.411	213.6	2.6	0.13	0.3	0.5	10.7	0.007	
MY-3 (12°00'N,96°00'E)	5	28.09	31.777	205.7	4.1	0.22	0.2	0.4	10.3	0.039	
	20	28.11	31.865	212.0	4.2	0.52	0.3				
	35	28.03	33.292	164.6	5.9	0.31	0.8	0.8	9.8	0.061	
	50	26.48	33.864	124.0	8.9	0.57	0.5				
	100	22.88	34.360	50.7	17.9	1.45					0.34
	199	13.79	34.947	31.6	32.9	1.71					0.64
	239	12.45	34.989	16.4		1.77					0.62
	398	10.53	35.026	25.1	44.2	2.33					1.45
	596	9.12	34.998	37.3	54.9	2.64					
	794	7.62	34.954	47.4	76.8	2.79					1.01
	992	6.64	34.921	58.5	88.2	3.72					1.35
	1486	5.25	34.872	71.8	104.2	4.31					1.42
	1978	5.01	34.862	83.9	104.8	4.31					1.48
	2367	4.99	34.861	80.5	107.5	4.69					1.59
MY-4 (12°36'N,96°00'E)	5	28.00	30.443	212.1	3.9	0.39	0.8				
MY-5 (13°36'N,95°36'E)	5	27.78	28.771	224.1	4.3	0.23	1.2	0.6	10.0	0.036	
	20	28.24	31.474	202.6	3.9	0.14	0.5				

(Continued)

TABLE 1 | Continued

Station	Depth m	Potential temperature °C	Salinity PSU	O ₂ μmol/L	Si μL	C _{Zn} nM	Chl <i>a</i> μg/L	C _L nM	Log K' _{ZnL,Zn²⁺}	Zn ²⁺ nM	Zn _{labile} nM
	45	28.63		176.0		0.14		0.4	10.4	0.013	
	50	28.13	33.393	122.0	5.8	0.10	0.1	0.5	10.2	0.011	
	74	26.37	33.782	129.2	9.6	0.43	0.2	0.7	10.2	0.052	
	101	24.05	34.053	76.5	15.6	0.97	0.2				0.43
	122	20.48	34.702	7.2	22.7	1.28					0.67
	149	14.34	34.878	21.4	34.3	1.91	0.1				
	194	13.24	34.702	7.3	38.0	1.80					1.27
MY-6 (15°00'N,96°00'E)	5	27.88	28.624	221.6	16.3	0.12	2.6	0.7	9.6	0.023	
	10	27.94	29.443	216.7	11.1	0.11	2.5				
	15	30.81	30.771	200.4	5.4	0.03	2.2	0.9	10.1	0.002	
	20	31.05	30.977	197.2	5.4	0.07	1.9	0.6	9.7	0.013	
	31	31.53	31.553	183.2	6.2	0.07	1.0	0.7	10.2	0.006	
	40	32.40	32.293	150.8	8.1	0.22	0.2				
	51	32.65	32.625	126.5	10.3	0.20	0.1	0.5	10.4	0.019	
	59	33.08	33.086	106.8	10.9	0.21	0.1	0.5	10.2	0.030	



the contrary, the highest Si concentration in the near surface water, 16.3 μM, was at the northernmost station of the Andaman Sea (MY-6), which is close to the estuaries of the Irrawaddy–Salween rivers.

Labile Zn Concentrations

The Zn titrations of most samples in the northeastern Indian Ocean (NR-1, $n = 12$) and the Andaman Sea (MY-1, $n = 7$ and MY-3, $n = 9$) showed a linear increase with added Zn²⁺, indicating that all of the natural ligands in the sample were already saturated with Zn. To understand Zn speciation in the saturated samples, we show the vertical profiles of Zn_{labile} (Table 1, Figure 4C). By using CSV under the same conditions as those of titration (pH 8.2, addition of 25 μM APDC, 12 h

equilibration time), Zn_{labile} was determined in natural samples without adding Zn and with no UV-irradiation. In this study, Zn_{labile} would include not only Zn²⁺ and inorganic Zn, but also the part of Zn weakly complexed with organic ligands. The Zn_{labile} concentrations in NR-1 ranged from 0.17 to 3.53 nM (49–2842 m), whereas those in the Andaman Sea ranged from 0.48 to 3.14 nM (MY-1, 198–1907 m) and 0.34 to 1.59 nM (MY-3, 100–2367 m; Table 1, Figure 4C).

Total Ligand Concentrations and Conditional Stability Constants

In this study, C_L and log K'_{ZnL,Zn²⁺} were obtained from only one sample at 17 m in the northeastern Indian Ocean and 16 samples between 5 and 74 m in the Andaman Sea (Table 1). In the

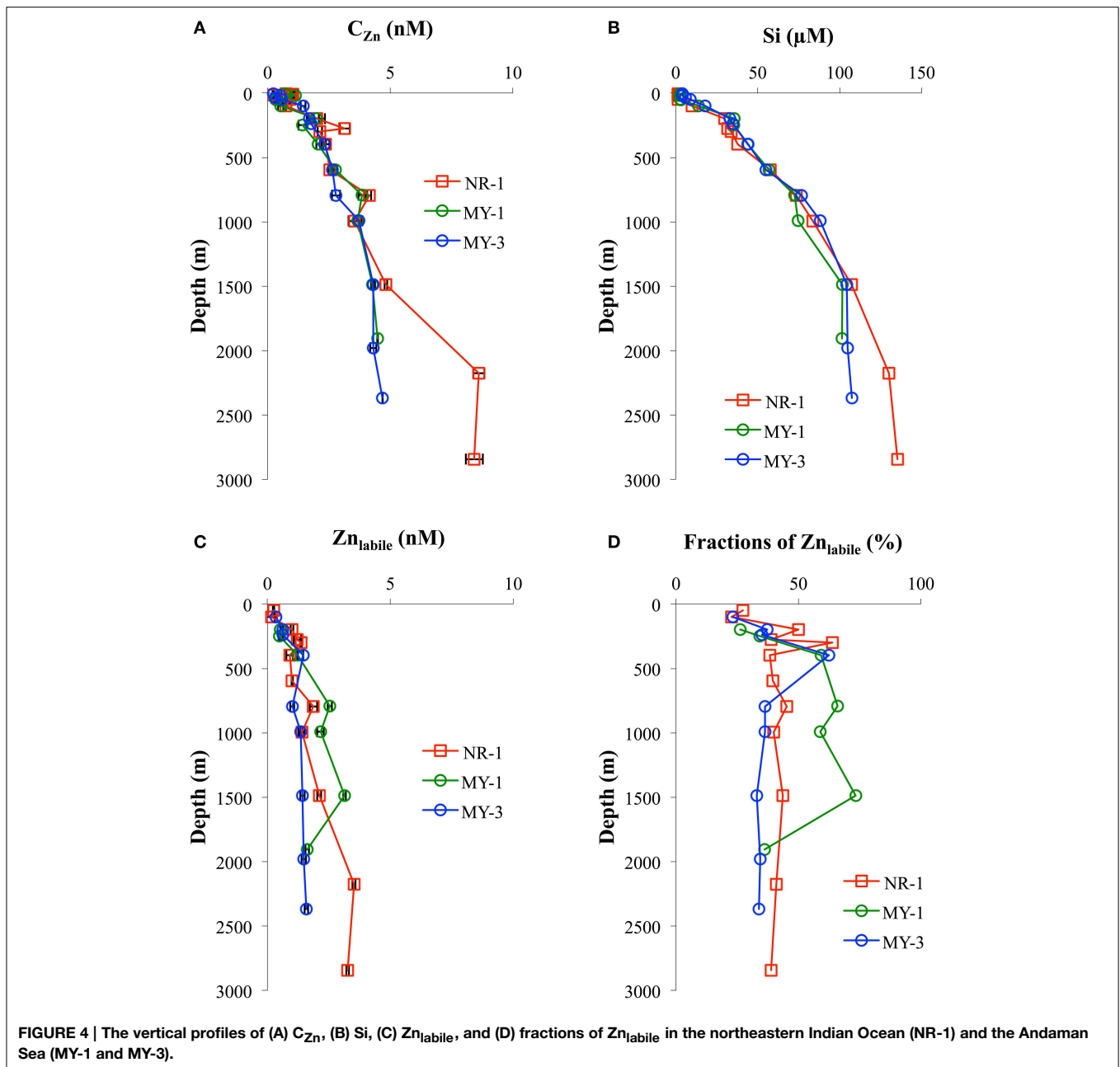


FIGURE 4 | The vertical profiles of (A) C_{Zn} , (B) Si, (C) Zn_{labile} , and (D) fractions of Zn_{labile} in the northeastern Indian Ocean (NR-1) and the Andaman Sea (MY-1 and MY-3).

northeastern Indian Ocean (NR-1), the Zn titration for most of the samples showed a linear increase with added Zn^{2+} , indicating that the natural ligands in the sample were already almost saturated with Zn. Thus, only one estimate of $\log K'_{ZnL, Zn^{2+}}$ could be obtained from the titration data for NR-1.

The C_L and $\log K'_{ZnL, Zn^{2+}}$ in the northeastern Indian Ocean (NR-1, 17 m) were 0.5 nM and 10.0, whereas those of the Andaman Sea (MY-1–MY-6) were 0.4–0.9 nM and 9.6–11.4 (Table 1), respectively. In the Andaman Sea, the highest C_L , 0.9 nM, was observed at both MY-1 and MY-6 (Table 1). The resultant free Zn^{2+} concentrations in the northeastern Indian Ocean and the Andaman Sea were 0.047 nM and 0.002–0.066 nM, respectively (Table 1).

Discussion

Total Dissolved Zn

In the northeastern Indian Ocean (NR-1), the average of the C_{Zn} within the upper 200 m was 0.94 ± 0.53 nM ($n = 7$), which is in good agreement with 0.96 ± 0.59 nM ($n = 29$) reported in a recent study in the northern Indian Ocean (Vu and Sohrin, 2013), but lower than 2.25 ± 1.18 nM ($n = 26$) reported for the northwestern Indian Ocean (Saager et al., 1992). From the surface to 1500 m in depth, the vertical distributions of C_{Zn} in the northeastern Indian Ocean (NR-1) and the Andaman Sea (MY-1 and MY-3) showed almost identical concentrations. Below 1500 m, the C_{Zn} in the northeastern

Indian Ocean increased almost twice, from 4.83 to 8.61 nM, whereas the concentrations remained nearly constant with depth in the Andaman Sea, from 4.28 to 4.69 nM (Figure 4A). The deep water of the Andaman Sea is separated from that of the Bay of Bengal by the Andaman–Nicobar Ridge. Because the Prepara Channel is shallower than 250 m, deep water can be exchanged mainly through the 10 Degree Channel, with a maximum sill depth of approximately 800 m, and the Great Passage, with a maximum depth of approximately 1800 m (Nozaki and Alibo, 2003). Okubo et al. (2004) used the scavenging–mixing model with vertical distribution of ^{230}Th to estimate that the residence time in deep water (<1250 m) is 6 years, suggesting that the deep water appears to be rapidly replaced by the incoming waters from the northeastern Indian Ocean across the sills and is then homogenized by vertical mixing.

At the surface distributions, very low C_{Zn} , <0.3 nM, was observed at <50 m depth at northern stations (MY-5 and MY-6), where the salinities were also low (28.624–33.393) (Table 1). This indicates that the river water from the Irrawaddy–Salween rivers affects C_{Zn} in the northern area of the Andaman Sea.

Figure 5 shows the C_{Zn} and Si concentrations as function of salinity. C_{Zn} showed a trend of very low concentrations in the low salinity zone, <34, in the northern Andaman Sea. During the sampling period, the southwest monsoon from June to November caused the outflows of freshwater from Irrawaddy–Salween rivers to increase more than one order of magnitude compared with results of the northeastern monsoon in winter (Robinson et al., 2007). This freshwater outflow is the third-largest contributor of sediment load after the Amazon and Ganges–Brahmaputra rivers (Robinson et al., 2007). The high level of sediment load from the Irrawaddy–Salween rivers may be related to the lower C_{Zn} .

Flocculation of humic acids may lead to removal of trace metals; however, the C_{Zn} will be less affected because Zn appears to exist predominantly in inorganic forms in river water, primarily with chloride (Hart and Davies, 1981; Kuwabara et al., 1989). Sediment resuspension also could affect the removal of trace metals. For example, pore water infusion is a major source of Fe to the water column in high turbidity zones. Once released into the water column, dissolved Fe is rapidly oxidized and precipitated (Zwolsman, 1994). The *in situ* formation of Fe (oxy) hydroxides, which are effective scavengers of dissolved Zn (Johnson, 1986), will lead to the removal of dissolved Zn in a low salinity, high turbidity area.

This study determined that the low concentrations of C_{Zn} in northern stations (MY-5 and MY-6) are also correlated with high Chl *a* contents. In MY-6, the northernmost station, the highest Chl *a* content was obtained (2.6 $\mu\text{g/L}$, 5 m). This value is significantly higher than those in the northeastern Indian Ocean as well as those at southern station of the Andaman Sea (Table 1). This result may indicate removal of C_{Zn} in the northern Andaman Sea by biological uptake. The involvement of trace metals in biological cycles is a well-known process in the open ocean (Bruland et al., 1991); similar processes have also been reported in estuaries (Kuwabara et al., 1989; Shiller and Boyle, 1991; Zwolsman et al., 1997).

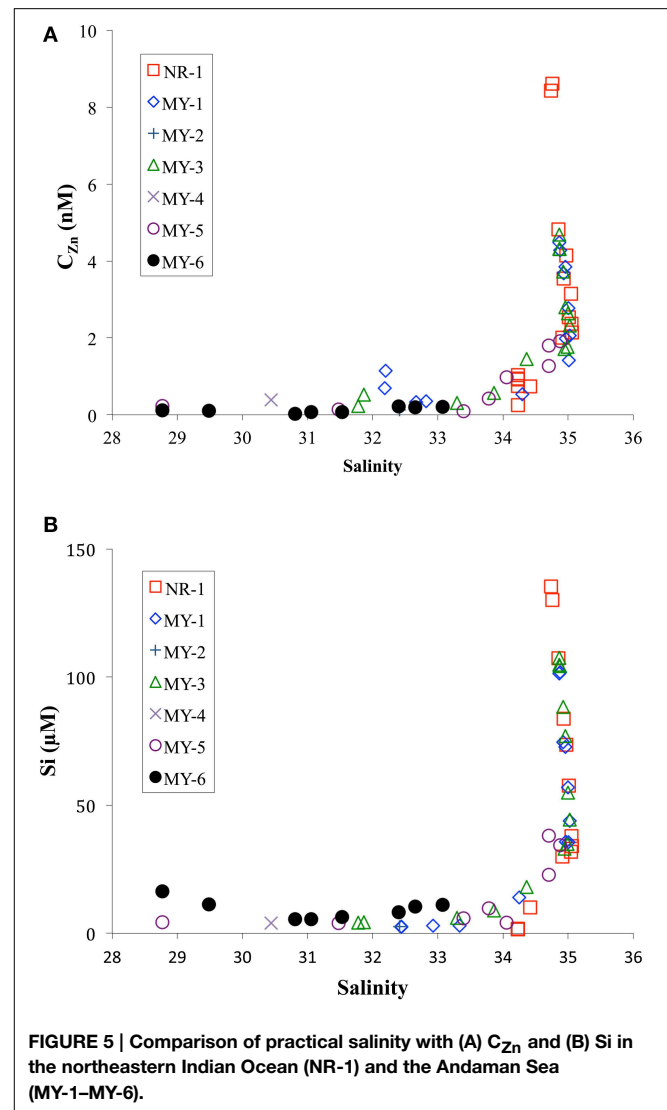


FIGURE 5 | Comparison of practical salinity with (A) C_{Zn} and (B) Si in the northeastern Indian Ocean (NR-1) and the Andaman Sea (MY-1–MY-6).

At the southern stations (MY-1, MY-2, and MY-3) of the Andaman Sea, the C_{Zn} at <50 m showed a similar range, 0.13–1.14 nM, compared with those of the northeastern Indian Ocean (NR-1), 0.26–1.03 nM. During the summer, the Summer Monsoon Current flows eastward as a continuous current from the western Arabian Sea to the northeastern Indian Ocean (Shankar et al., 2002). Therefore, the Summer Monsoon Current, by intruding into the Andaman Sea, may influence the surface Zn concentrations in both the northeastern Indian Ocean and the Andaman Sea.

Relationship between Total Dissolved Zn and Silicate

In this study, the C_{Zn} profiles were similar to those of silicates (Figures 4A,B). Similar to that with the C_{Zn} , the Si concentrations were different below 1500 m between the northeastern Indian Ocean (NR-1) and the Andaman Sea (MY-1 and MY-3) (Figure 4B).

In contrast to the C_{Zn} , the Si concentrations in shallow water of the Andaman Sea <50 m at MY-5 (4.3–5.8 μM) and MY-6 (5.4–16.3 μM) were relatively higher at than those in the northeastern Indian Ocean (NR-1, 1.4–1.6 μM), and at southern stations (MY-1, 2.4–2.9 μM) (Table 1). This result indicates that the Si concentrations in MY-5 and MY-6 are influenced by the Irrawaddy–Salween rivers. Figure 6 shows the relationship between C_{Zn} and Si concentrations obtained in this study. In the Andaman Sea, the slope value was relatively lower (0.043 ± 0.001) than that of northeastern Indian Ocean (0.052 ± 0.004) (Figure 6).

In the northeastern Indian Ocean (NR-1), the C_{Zn} strongly correlated with Si ($R^2 = 0.913$; Figure 6). The obtained slope value in the northeastern Indian Ocean, 0.052 ± 0.004 , was in a good agreement with that reported in a previous study of the southwestern Indian Ocean (0.049) (Morley et al., 1993).

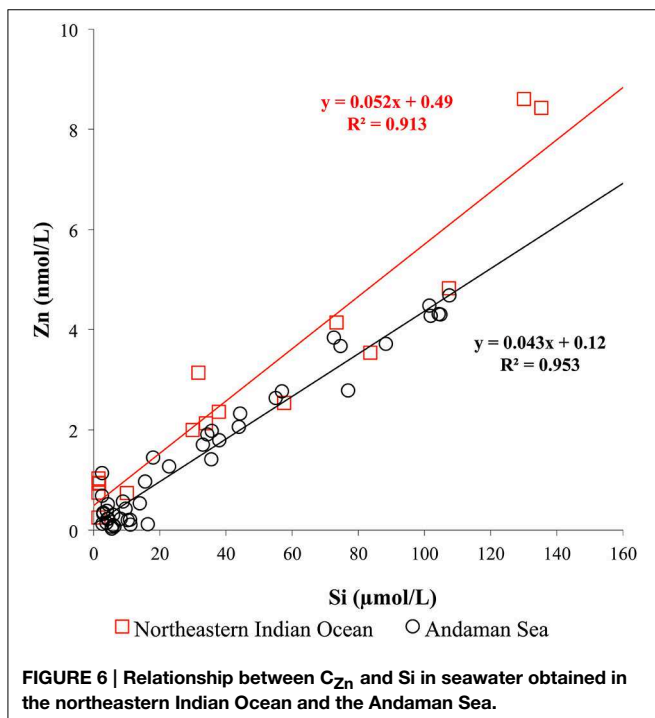


FIGURE 6 | Relationship between C_{Zn} and Si in seawater obtained in the northeastern Indian Ocean and the Andaman Sea.

However, it is slightly lower than the values of 0.062 reported in previous studies in the northwestern Indian Ocean (Saager et al., 1992), 0.059 in the southern Indian Ocean (Gosnell et al., 2012) and 0.064 in the northern and southern Indian Ocean (Vu and Sohrin, 2013). The results of this study indicate that Zn is relatively depleted than Si in the northeastern Indian Ocean.

The lower slope value of the Andaman Sea, 0.043 ± 0.001 , is attributed to the relatively high Si concentrations and lower C_{Zn} in its surface layers (Figure 6). As previously mentioned, high levels of sediment load from the Irrawaddy–Salween rivers could affect removal of dissolved Zn by precipitation in a low salinity, high turbidity area. Moreover, high Chl *a* contents were obtained at this area, suggesting that phytoplankton uptake also could be a reason for the low C_{Zn} .

If we subtract the Zn:Si data of deep water >1500 m in the northeastern Indian Ocean (NR-1), the slope value is calculated as 0.038 ± 0.004 , which is almost identical to that of the Andaman Sea (0.043 ± 0.001). This similarity of slope values also supports that both northeastern Indian Ocean and Andaman Sea could communicate at depths above 1500 m.

Zn Complexation in the Andaman Sea

The C_L in the Andaman Sea ranged from 0.4 to 0.9 nM, which is lower than those in the other marginal seas (Table 2). Previous studies showed higher C_L in the Black Sea (7.8–16.6 nM) (Muller et al., 2001); the Bering Sea (3.6 nM) (Jakuba et al., 2012); the Sea of Okhotsk (2.6 nM); and the Sea of Japan (East Sea) (1.3 nM) (Kim et al., 2015b). Only one C_L value in the northeastern Indian Ocean (NR-1) was calculated as 0.5 nM and is relatively lower than those of the Andaman Sea, which might suggest some specific ligand sources in the Andaman Sea. The C_L generally showed positive correlation with the C_{Zn} in this study (Figure 7). In contrast, the C_L was poorly correlated to the C_{Zn} in MY-6, the northernmost station in the Andaman Sea.

The $\log K'_{ZnL,Zn^{2+}}$ of natural organic ligands in the Andaman Sea ranged from 9.6 to 11.5, which is higher than that reported in previous studies of the marginal seas (Table 2). The $\log K'_{ZnL,Zn^{2+}}$ value in the northeastern Indian Ocean was 10.0, which is comparable to that in previous studies in which the Zn ligand was determined by using CSV in the open oceans such as the western subtropical North Pacific (9.5–10.8); the western

TABLE 2 | Zn complexation data from other relevant seawater studies.

Region	Sample	C_L (nmol/L)	$\log K'_{ZnL,Zn^{2+}}$	Method	References
OPEN OCEAN					
Northeastern Indian Ocean	17 m	0.5	10.0	CSV	This study
MARGINAL SEA					
Andaman Sea	5–100 m	0.4–0.9	9.6–11.4	CSV	This study
Sea of Okhotsk	20 m	2.6	9.5	CSV	Kim et al., 2015b
Sea of Japan (East Sea)	20 m	1.3	9.2	CSV	Kim et al., 2015b
Bering Sea	20 m	3.6	9.6	ASV	Jakuba et al., 2012
Black Sea	10 m	7.8–16.6	9.7–10.7	ASV	Muller et al., 2001

The values of $\log K'_{ZnL,Zn^{2+}}$ for ASV method are calculated by the equation ($K'_{ZnL,Zn^{2+}} = K'_{ZnL,Zn^{2+}} \times \alpha_{Zn^{2+}}$).

subarctic North Pacific (9.7–10.2) (Kim et al., 2015b); the eastern subarctic North Pacific (10.5) (Lohan et al., 2005); the South Pacific (10.6) (Ellwood, 2004); and the North Atlantic (10.0–10.5) (Ellwood and van den Berg, 2000).

In the northeastern Indian Ocean (NR-1), as previously mentioned, the Zn titration for most samples showed linear increase with added Zn^{2+} . Therefore, only one estimate of C_L (0.5 nM) and $\log K'_{ZnL,Zn^{2+}}$ (10.0) could be obtained from the titration data for NR-1. The detection window in this study is from $K'_{ZnL,Zn^{2+}} = 10^7$ to 10^{12} for a C_L of 1 nM. Although the detection window covers the range of $K'_{ZnL,Zn^{2+}}$ values reported in previous studies ($10^{7.5}$ – $10^{11.3}$) (van den Berg, 1985; Donat and Bruland, 1990; Ellwood and van den Berg, 2000; Ellwood, 2004; Lohan et al., 2005; Jakuba et al., 2008), strong Zn complexing ligands with $K'_{ZnL,Zn^{2+}}$ values $>10^{12}$ might not be detected if any.

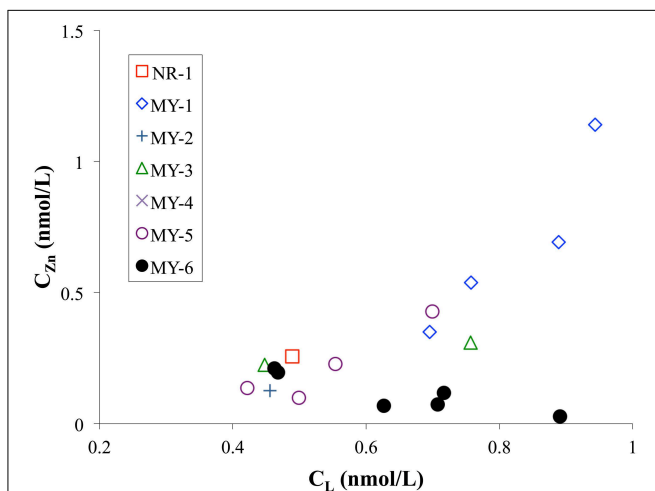


FIGURE 7 | Comparison of C_L and C_{Zn} in the northeastern Indian Ocean (NR-1) and the Andaman Sea (MY-1–MY-6).

To determine the Zn speciation in Zn-saturated waters, we also examined the vertical profiles of Zn_{labile} (Figure 4C). At NR-1, the fractions of Zn_{labile} to the C_{Zn} ranged from 39 to 45% at >500 m, whereas those of MY-1 and MY-3 at >500 m ranged from 36 to 73% and 33 to 36%, respectively (Figure 4D). Because we determined the Zn_{labile} in the samples without acidification, some of the Zn in the seawater may have been adsorbed onto the walls of the storage bottles and the voltammetric cells. Recent research has shown that the fraction of UV-irradiated seawater without acidification (C_{UVSW}) to C_{Zn} ranged from 85 to 94% and has indicated that the differences between C_{Zn} and C_{UVSW} were caused partially by adsorption to the walls of bottles and cells (Kim et al., 2015b). Even if the adsorption is considered, non-labile fractions of Zn still exist through the water columns of the northeastern Indian Ocean and the Andaman Sea. The non-labile fractions of Zn likely include inert Zn-organic complexes at specific conditions, as suggested in a previous study (Baars and Croot, 2011). At >500 m, the fractions of Zn_{labile} between NR-1 (39–45%) and MY-3 (33–36%), showed similar trends as that of C_{Zn} , which differed below 1500 m (Figures 4C,D). On the contrary, relatively high fractions of Zn_{labile} , 59–73%, existed between 794 and 1486 m at MY-1 (Figures 4C,D), although the bottom sample showed a similar fraction range (36%) with that of NR-1 and MY-3. Such high fractions of Zn_{labile} at MY-1, 793–1486 m, were likely affected by the continental slope, where is in very close to MY-1 (Figure 1). There might be some specific removal mechanisms for the Zn complexing ligand at those depths.

Possible Sources of Zn Complexing Ligands

The origin of Zn complexing ligands is still under debate, in which humic substances (Campbell et al., 2002), substances from pore waters via estuarine marine sediments (Skrabal et al., 2006), phytoplankton, and bacteria-excreted organic substances (Bruland, 1989) are thought to act as the ligands. In the open ocean, earlier study by Bruland (1989) mentioned that Zn complexing ligands were possibly derived from bacteria

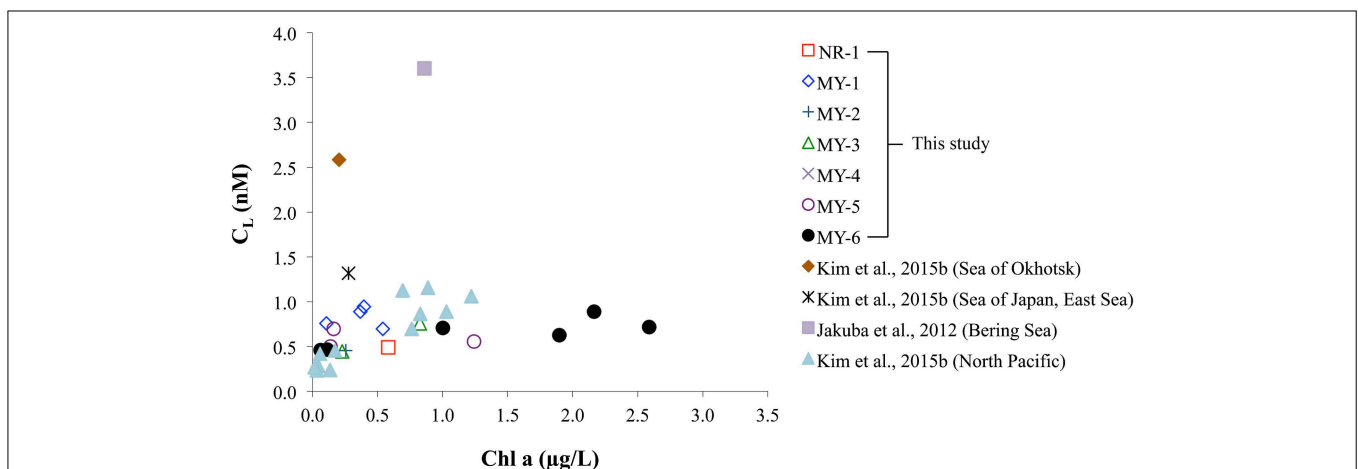


FIGURE 8 | Comparison of Chl a and C_L obtained in this study and data from previous studies in the Sea of Okhotsk, Sea of Japan (East Sea), North Pacific (Kim et al., 2015b), and Bering Sea (Jakuba et al., 2012), respectively.

and phytoplankton in the central subtropical North Pacific. In high productivity regions, Zn complexing ligands might also be derived from phytoplankton and bacteria. If organic substances excreted by phytoplankton and bacteria are the main source of Zn complexing ligands, a relationship between Zn ligands and Chl *a* is expected.

The relationship between Chl *a* and the C_L obtained in this study was compared with those of previous studies (Figure 8). In the Andaman Sea (from MY-1 to MY-6), the relationship between Chl *a* and C_L differed from that of other marginal seas, in which low Chl *a* and high C_L can be observed. Previous studies in the marginal seas mentioned that Zn complexing ligands could be derived from the bacterial breakdown of particulate organic matter in the Black Sea (Muller et al., 2001) and phytoplankton in the Bering Sea (Jakuba et al., 2012). However, we could not observe a clear relationship between Chl *a* and C_L in the Andaman Sea, even though the C_L was slightly increased with an increase in Chl *a* contents at the northernmost station (MY-6; Figure 8). This result suggests that different sources of Zn complexing ligands might be dominant in the Andaman Sea. A previous study in the Sea of Okhotsk indicated that humic substances from fresh water might be a source of Zn complexed ligands in the Sea of Okhotsk, where the low salinities in shallower waters are influenced by the fluvial discharge from the Amur River (Kim et al., 2015b). The surface waters of the Andaman Sea are also influenced by the Irrawaddy–Salween rivers, which suggests that humic substances could be a source of Zn complexing ligands. However, relatively high $\log K'_{ZnL,Zn^{2+}}$ values, 9.6–11.4, have been obtained in the Andaman Sea compared with those of the Sea of Okhotsk (9.5) (Table 2), indicating that Zn is strongly complexed with organic ligands in the Andaman Sea. A previous study showed that terrestrial humic substances are not strong chelators for Zn, whereas strong ligands for Cu exist in estuarine environments, which suggests that the largest fraction of complexing ligands found in estuarine water columns is derived from sedimentary diagenetic processes (Skrabal et al., 2006). Because the Irrawaddy–Salween rivers are the third-largest contributor of sediment load influenced (Robinson et al., 2007), this high level of sediment load might be related with Zn complexing ligands, which are likely to be complex and heterogeneous. Based on the first C_{Zn} and its speciation data obtained in the northeastern Indian Ocean and

the Andaman Sea, further research is needed to clarify the sources of Zn complexing ligands in these regions.

Conclusions

Our results show that a strong influence of fluvial discharge from the Irrawaddy–Salween rivers might affect the surface distribution of C_{Zn} and its speciation. In the northern Andaman Sea, where high levels of sediment particles are transported and Chl *a* contents are high, relatively lower C_{Zn} than those of the southern Andaman Sea might suggest the removal of C_{Zn} by inorganic coprecipitation and biological uptake in this area. The vertical distributions of C_{Zn} in the northeastern Indian Ocean (NR-1) and the Andaman Sea (MY-1 and MY-3) were almost similar from the surface to a depth of 1500 m. Below that depth, the C_{Zn} differed, indicating that the deep water in the Andaman Sea was rapidly replaced by the incoming water from the northeastern Indian Ocean across the sills and was then homogenized by vertical mixing.

In the northeastern Indian Ocean, although only one estimate of C_L and $K'_{ZnL,Zn^{2+}}$ could be obtained, probable C_L are lower than those of the Andaman Sea. In the Andaman Sea, we could not observe a clear relationship between Chl *a* and C_L , although latter C_L increased slightly with an increase in Chl *a* content at the northernmost station (MY-6). This result may suggest that sources of Zn complexing ligands other than bacteria and phytoplankton might be dominant in the Andaman Sea, which is largely influenced by the Irrawaddy–Salween rivers.

Acknowledgments

This study was supported by Grants-in-Aid for Scientific Research (A) (Nos. 19253006 and 23253001) and Grants-in-Aid for Scientific Research (B) (No. 24310006) from Monokasho (the Ministry of Education, Culture, Sports, Science and Technology: MEXT). We are grateful to Rie Sato for the nutrient analysis. We would also like to thank all the crews and participants of cruises on the R/V *Hakuho-maru* and Dr. Hodaka Kawahata (The University of Tokyo) and Dr. Mayuri Inoue (Okayama University) for their assistance on the research cruise. We thank to the two reviewers for their useful comments that helped to improve the manuscript.

References

- Baars, O., and Croot, P. L. (2011). The speciation of dissolved zinc in the Atlantic sector of the Southern Ocean. *Deep Sea Res. II* 58, 2720–2732. doi: 10.1016/j.dsr2.2011.02.003
- Brand, L. E., Sunda, W. G., and Guillard, R. R. (1983). Limitation of marine phytoplankton reproductive rates by zinc, manganese, and iron. *Limnol. Oceanogr.* 28, 1182–1198. doi: 10.4319/lo.1983.28.6.1182
- Bruland, K. W. (1980). Oceanographic distributions of cadmium, zinc, nickel, and copper in the North Pacific. *Earth Planet. Sci. Lett.* 47, 176–198. doi: 10.1016/0012-821X(80)90035-7
- Bruland, K. W. (1989). Complexation of zinc by natural organic ligands in the central North Pacific. *Limnol. Oceanogr.* 34, 269–285. doi: 10.4319/lo.1989.34.2.0269
- Bruland, K. W., Donat, J. R., and Hutchins, D. A. (1991). Interactive influences of bioactive trace metals on biological production in oceanic waters. *Limnol. Oceanogr.* 36, 1555–1577. doi: 10.4319/lo.1991.36.8.1555
- Bruland, K. W., Franks, R. P., Knauer, G. A., and Martin, J. H. (1979). Sampling and analytical methods for the determination of copper, cadmium, zinc, and nickel at the nanogram per liter level in sea water. *Anal. Chim. Acta* 105, 233–245. doi: 10.1016/S0003-2670(01)83754-5
- Bruland, K. W., Knauer, G. A., and Martin, J. H. (1978). Zinc in north-east Pacific water. *Nature* 271, 741–743. doi: 10.1038/271741a0
- Bruland, K. W., Orians, K. J., and Cowen, J. P. (1994). Reactive trace metals in the stratified central North Pacific. *Geochim. Cosmochim. Acta* 58, 3171–3182. doi: 10.1016/0016-7037(94)90044-2
- Campbell, P. G. C., Errécalde, O., Fortin, C., Hiriart-Baer, V. P., and Vigneault, B. (2002). Metal bioavailability to phytoplankton—applicability of the biotic

- ligand model. *Comp. Biochem. Physiol. C Toxicol. Pharmacol.* 133, 189–206. doi: 10.1016/s1532-0456(02)00104-7
- Chen, D., Qian, P.-Y., and Wang, W.-X. (2008). Biokinetics of cadmium and zinc in a marine bacterium: influences of metal interaction and pre-exposure. *Environ. Toxicol. Chem.* 27, 1794–1801. doi: 10.1897/07-565.1
- Coale, K. H., Wang, X., Tanner, S. J., and Johnson, K. S. (2003). Phytoplankton growth and biological response to iron and zinc addition in the Ross Sea and Antarctic Circumpolar Current along 170°W. *Deep Sea Res. II* 50, 635–653. doi: 10.1016/S0967-0645(02)00588-X
- Crawford, D. W., Lipsen, M. S., Purdie, D. A., Lohan, M. C., Statham, P. J., Whitney, F. A., et al. (2003). Influence of zinc and iron enrichments on phytoplankton growth in the northeastern subarctic Pacific. *Limnol. Oceanogr.* 48, 1583–1600. doi: 10.4319/lo.2003.48.4.1583
- Croot, P. L., Baars, O., and Streu, P. (2011). The distribution of dissolved zinc in the Atlantic sector of the Southern Ocean. *Deep Sea Res. II* 58, 2707–2719. doi: 10.1016/j.dsr2.2010.10.041
- Cutter, G. A., and Bruland, K. W. (2012). Rapid and noncontaminating sampling system for trace elements in global ocean surveys. *Limnol. Oceanogr. Methods* 10, 425–436. doi: 10.4319/lom.2012.10.425
- Donat, J. R., and Bruland, K. W. (1990). A comparison of two voltammetric techniques for determining zinc speciation in Northeast Pacific Ocean waters. *Mar. Chem.* 28, 301–323. doi: 10.1016/0304-4203(90)90050-M
- Ellwood, M. J. (2004). Zinc and cadmium speciation in subantarctic waters east of New Zealand. *Mar. Chem.* 87, 37–58. doi: 10.1016/j.marchem.2004.01.005
- Ellwood, M. J., and Hunter, K. A. (2000). The incorporation of zinc and iron into the frustule of the marine diatom *Thalassiosira pseudonana*. *Limnol. Oceanogr.* 45, 1517–1524. doi: 10.4319/lo.2000.45.7.1517
- Ellwood, M. J., and van den Berg, C. M. G. (2000). Zinc speciation in the Northeastern Atlantic Ocean. *Mar. Chem.* 68, 295–306. doi: 10.1016/S0304-4203(99)00085-7
- Gerringa, L. J. A., Herman, P. M. J., and Poortvliet, T. C. W. (1995). Comparison of the linear Van den Berg/Ruziĉ transformation and a non-linear fit of the Langmuir isotherm applied to Cu speciation data in the estuarine environment. *Mar. Chem.* 48, 131–142. doi: 10.1016/0304-4203(94)00041-B
- Gosnell, K. J., Landing, W. M., and Milne, A. (2012). Fluorometric detection of total dissolved zinc in the southern Indian Ocean. *Mar. Chem.* 132–133, 68–76. doi: 10.1016/j.marchem.2012.01.004
- Hart, B. T., and Davies, S. H. R. (1981). Trace metal speciation in the freshwater and estuarine regions of the Yarra River, Victoria. *Estuar. Coast. Shelf Sci.* 12, 353–374. doi: 10.1016/S0302-3524(81)80001-1
- Jakuba, R. W., Moffett, J. W., and Saito, M. A. (2008). Use of a modified, high-sensitivity, anodic stripping voltammetry method for determination of zinc speciation in the North Atlantic Ocean. *Anal. Chim. Acta* 614, 143–152. doi: 10.1016/j.aca.2008.03.006
- Jakuba, R. W., Saito, M. A., Moffett, J. W., and Xu, Y. (2012). Dissolved zinc in the subarctic North Pacific and Bering Sea: its distribution, speciation, and importance to primary producers. *Global Biogeochem. Cycles* 26, GB2015. doi: 10.1029/2010GB004004
- John, S. G., and Conway, T. M. (2014). A role for scavenging in the marine biogeochemical cycling of zinc and zinc isotopes. *Earth Planet. Sci. Lett.* 394, 159–167. doi: 10.1016/j.epsl.2014.02.053
- Johnson, C. A. (1986). The regulation of trace element concentrations in river and estuarine waters contaminated with acid mine drainage: the adsorption of Cu and Zn on amorphous Fe oxyhydroxides. *Geochim. Cosmochim. Acta* 50, 2433–2438. doi: 10.1016/0016-7037(86)90026-8
- Johnson, K. S., Boyle, E., Bruland, K. W., Coale, K., Measures, C., Moffett, J., et al. (2007). Developing standards for dissolved iron in seawater. *Eos Trans. AGU* 88, 131–132. doi: 10.1029/2007EO110003
- Kim, T., Obata, H., Gamo, T., and Nishioka, J. (2015a). Sampling and onboard analytical methods for determining subnanomolar concentrations of zinc in seawater. *Limnol. Oceanogr. Methods* 13, 30–39. doi: 10.1002/lom3.10004
- Kim, T., Obata, H., Kondo, Y., Ogawa, H., and Gamo, T. (2015b). Distribution and speciation of dissolved zinc in the western North Pacific and its adjacent seas. *Mar. Chem.* 173, 330–341. doi: 10.1016/j.marchem.2014.10.016
- Kuwabara, J. S., Chang, C. C. Y., Cloern, J. E., Fries, T. L., Davis, J. A., and Luoma, S. N. (1989). Trace metal associations in the water column of South San Francisco Bay, California. *Estuar. Coast. Shelf Sci.* 28, 307–325. doi: 10.1016/0272-7714(89)90020-6
- Lane, T. W., and Morel, F. M. (2000). Regulation of carbonic anhydrase expression by zinc, cobalt, and carbon dioxide in the marine diatom *Thalassiosira weissflogii*. *Plant Physiol.* 123, 345–352. doi: 10.1104/pp.123.1.345
- Lohan, M. C., Crawford, D. W., and Purdie, D. A. (2005). Iron and zinc enrichments in the northeastern subarctic Pacific: ligand production and zinc availability in response to phytoplankton growth. *Limnol. Oceanogr.* 50, 1427–1437. doi: 10.4319/lo.2005.50.5.1427
- Lohan, M. C., Statham, P. J., and Crawford, D. W. (2002). Total dissolved zinc in the upper water column of the subarctic North East Pacific. *Deep Sea Res. II* 49, 5793–5808. doi: 10.1016/S0967-0645(02)00215-1
- Milliman, J. D., and Meade, R. H. (1983). World-wide delivery of river sediment to the oceans. *J. Geol.* 91, 1–21. doi: 10.1086/628741
- Morel, F. M. M., Reinfelder, J. R., Roberts, S. B., Chamberlain, C. P., Lee, J. G., and Yee, D. (1994). Zinc and carbon co-limitation of marine phytoplankton. *Nature* 369, 740–742. doi: 10.1038/369740a0
- Morley, N. H., Statham, P. J., and Burton, J. D. (1993). Dissolved trace metals in the southwestern Indian Ocean. *Deep Sea Res. I* 40, 1043–1062. doi: 10.1016/0967-0637(93)90089-L
- Muller, F. L. L., Gulin, S. B., and Kalvøy, Å. (2001). Chemical speciation of copper and zinc in surface waters of the western Black Sea. *Mar. Chem.* 76, 233–251. doi: 10.1016/S0304-4203(01)00060-3
- Nozaki, Y., and Alibo, D. S. (2003). Importance of vertical geochemical processes in controlling the oceanic profiles of dissolved rare earth elements in the northeastern Indian Ocean. *Earth Planet. Sci. Lett.* 205, 155–172. doi: 10.1016/S0012-821X(02)01027-0
- Obata, H., Nozaki, Y., Alibo, D. S., and Yamamoto, Y. (2004). Dissolved Al, In, and Ce in the eastern Indian Ocean and the Southeast Asian Seas in comparison with the radionuclides ²¹⁰Pb and ²¹⁰Po. *Geochim. Cosmochim. Acta* 68, 1035–1048. doi: 10.1016/j.gca.2003.07.021
- Okubo, A., Obata, H., Nozaki, Y., Yamamoto, Y., and Minami, H. (2004). ²³⁰Th in the Andaman Sea: rapid deep-sea renewal. *Geophys. Res. Lett.* 31, L22306. doi: 10.1029/2004GL020226
- Price, N. M., and Morel, F. M. M. (1990). Cadmium and cobalt substitution for zinc in a marine diatom. *Nature* 344, 658–660. doi: 10.1038/344658a0
- Robinson, R. A. J., Bird, M. I., Oo, N. W., Hoey, T. B., Aye, M. M., Higgitt, D. L., et al. (2007). The Irrawaddy River Sediment Flux to the Indian Ocean: the original nineteenth-century data revisited. *J. Geol.* 115, 629–640. doi: 10.1086/521607
- Ruziĉ, I. (1982). Theoretical aspects of the direct titration of natural waters and its information yield for trace metal speciation. *Anal. Chim. Acta* 140, 99–113. doi: 10.1016/S0003-2670(01)95456-X
- Saager, P. M., de Baar, H. J. W., and Howland, R. J. (1992). Cd, Zn, Ni and Cu in the Indian Ocean. *Deep Sea Res. A* 39, 9–35. doi: 10.1016/0198-0149(92)90017-N
- Sarma, V. V. S. S., and Narvekar, P. V. (2001). A study on inorganic carbon components in the Andaman Sea during the post monsoon season. *Oceanol. Acta* 24, 125–134. doi: 10.1016/S0399-1784(00)01133-6
- Schmitz, W. J. (1995). On the interbasin-scale thermohaline circulation. *Rev. Geophys.* 33, 151–173. doi: 10.1029/95RG00879
- Shaked, Y., Xu, Y., Leblanc, K., and Morel, F. M. M. (2006). Zinc availability and alkaline phosphatase activity in *Emiliania huxleyi*: implications for Zn-P co-limitation in the ocean. *Limnol. Oceanogr.* 51, 299–309. doi: 10.4319/lo.2006.51.1.0299
- Shankar, D., Vinayachandran, P. N., and Unnikrishnan, A. S. (2002). The monsoon currents in the north Indian Ocean. *Prog. Oceanogr.* 52, 63–120. doi: 10.1016/S0079-6611(02)00024-1
- Shiller, A. M., and Boyle, E. (1991). Trace elements in the Mississippi River Delta outflow region: behavior at high discharge. *Geochim. Cosmochim. Acta* 55, 3241–3251. doi: 10.1016/0016-7037(91)90486-O
- Skrabal, S. A., Lieseke, K. L., and Kieber, R. J. (2006). Dissolved zinc and zinc-complexing ligands in an organic-rich estuary: benthic fluxes and comparison with copper speciation. *Mar. Chem.* 100, 108–123. doi: 10.1016/j.marchem.2005.12.004
- Sunda, W. G., and Huntsman, S. A. (1992). Feedback interactions between zinc and phytoplankton in seawater. *Limnol. Oceanogr.* 37, 25–40. doi: 10.4319/lo.1992.37.1.0025
- Sunda, W. G., and Huntsman, S. A. (1995). Cobalt and zinc interreplacement in marine phytoplankton: biological and geochemical implications. *Limnol. Oceanogr.* 40, 1404–1417. doi: 10.4319/lo.1995.40.8.1404

- Sunda, W. G., and Huntsman, S. A. (1996). Antagonisms between cadmium and zinc toxicity and manganese limitation in a coastal diatom. *Limnol. Oceanogr.* 41, 373–387. doi: 10.4319/lo.1996.41.3.0373
- Sunda, W. G., and Huntsman, S. A. (1998). Interactions among Cu^{2+} , Zn^{2+} , and Mn^{2+} in controlling cellular Mn, Zn, and growth rate in the coastal alga *Chlamydomonas*. *Limnol. Oceanogr.* 43, 1055–1064. doi: 10.4319/lo.1998.43.6.1055
- Sunda, W. G., and Huntsman, S. A. (2000). Effect of Zn, Mn, and Fe on Cd accumulation in phytoplankton: implications for oceanic Cd cycling. *Limnol. Oceanogr.* 45, 1501–1516. doi: 10.4319/lo.2000.45.7.1501
- Thamatrakoln, K., and Hildebrand, M. (2008). Silicon uptake in diatoms revisited: a model for saturable and nonsaturable uptake kinetics and the role of silicon transporters. *Plant Physiol.* 146, 1397–1407. doi: 10.1104/pp.107.107094
- Turner, D. R., Whitfield, M., and Dickson, A. G. (1981). The equilibrium speciation of dissolved components in freshwater and sea water at 25°C and 1 atm pressure. *Geochim. Cosmochim. Acta* 45, 855–881. doi: 10.1016/0016-7037(81)90115-0
- Vallee, B. L., and Auld, D. S. (1990). Zinc coordination, function, and structure of zinc enzymes and other proteins. *Biochemistry* 29, 5647–5659. doi: 10.1021/bi00476a001
- van den Berg, C. M. G. (1982). Determination of copper complexation with natural organic ligands in seawater by equilibration with MnO_2 I. Theory. *Mar. Chem.* 11, 307–322. doi: 10.1016/0304-4203(82)90028-7
- van den Berg, C. M. G. (1985). Determination of the zinc complexing capacity in seawater by cathodic stripping voltammetry of zinc—APDC complex ions. *Mar. Chem.* 16, 121–130. doi: 10.1016/0304-4203(85)90017-9
- Vu, H. T. D., and Sohrin, Y. (2013). Diverse stoichiometry of dissolved trace metals in the Indian Ocean. *Sci. Rep.* 3:1745. doi: 10.1038/srep01745
- Welschmeyer, N. A. (1994). Fluorometric analysis of chlorophyll *a* in the presence of chlorophyll *b* and pheopigments. *Limnol. Oceanogr.* 39, 1985–1992. doi: 10.4319/lo.1994.39.8.1985
- Wyatt, N. J., Milne, A., Woodward, E. M. S., Rees, A. P., Browning, T. J., Bouman, H. A., et al. (2014). Biogeochemical cycling of dissolved zinc along the GEOTRACES South Atlantic transect GA10 at 40°S. *Global Biogeochem. Cycles* 28, 44–56. doi: 10.1002/2013GB004637
- Wyrtki, K. (1971). *Oceanographic Atlas of the International Indian Ocean Expedition*. Washington, DC: National Science Foundation.
- Zwolsman, J. J. G. (1994). Seasonal variability and biogeochemistry of phosphorus in the scheldt estuary, South-west Netherlands. *Estuar. Coast. Shelf Sci.* 39, 227–248. doi: 10.1006/ecss.1994.1061
- Zwolsman, J. J. G., Van Eck, B. T. M., and Van Der Weijden, C. H. (1997). Geochemistry of dissolved trace metals (cadmium, copper, zinc) in the Scheldt estuary, southwestern Netherlands: impact of seasonal variability. *Geochim. Cosmochim. Acta* 61, 1635–1652. doi: 10.1016/S0016-7037(97)00029-X

Conflict of Interest Statement: The authors declare that the research was conducted in the absence of any commercial or financial relationships that could be construed as a potential conflict of interest.

Copyright © 2015 Kim, Obata and Gamo. This is an open-access article distributed under the terms of the Creative Commons Attribution License (CC BY). The use, distribution or reproduction in other forums is permitted, provided the original author(s) or licensor are credited and that the original publication in this journal is cited, in accordance with accepted academic practice. No use, distribution or reproduction is permitted which does not comply with these terms.



Influence of Ocean Acidification on the Organic Complexation of Iron and Copper in Northwest European Shelf Seas; a Combined Observational and Model Study

Lizeth Avendaño¹, Martha Gledhill^{1,2*}, Eric P. Achterberg^{1,2}, Victoire M. C. Rérolle¹ and Christian Schlosser^{1,2}

¹ Ocean and Earth Science, National Oceanography Centre, University of Southampton, Southampton, UK, ² GEOMAR Helmholtz Centre for Ocean Research Kiel, Kiel, Germany

OPEN ACCESS

Edited by:

Sylvia Gertrud Sander,
University of Otago, New Zealand

Reviewed by:

David Turner,
University of Gothenburg, Sweden
Mona Wells,
Xi'an Jiaotong-Liverpool University,
China

*Correspondence:

Martha Gledhill
mgledhill@geomar.de

Specialty section:

This article was submitted to
Marine Biogeochemistry,
a section of the journal
Frontiers in Marine Science

Received: 12 November 2015

Accepted: 14 April 2016

Published: 29 April 2016

Citation:

Avendaño L, Gledhill M,
Achterberg EP, Rérolle VMC and
Schlosser C (2016) Influence of Ocean
Acidification on the Organic
Complexation of Iron and Copper in
Northwest European Shelf Seas; a
Combined Observational and Model
Study. *Front. Mar. Sci.* 3:58.
doi: 10.3389/fmars.2016.00058

The pH of aqueous solutions is known to impact the chemical speciation of trace metals. In this study we conducted titrations of coastal seawaters with iron and copper at pH 7.91, 7.37, and 6.99 (expressed on the total pH scale). Changes in the concentration of iron and copper that complexed with the added ligands 1-nitroso-2-naphthol and salicylaldehyde respectively were determined by adsorptive cathodic stripping voltammetry—competitive ligand equilibrium (AdCSV-CLE). Interpretation of the results, assuming complexation by a low concentration of discrete ligands, showed that conditional stability constants for iron complexes increased relative to inorganic iron complexation as pH decreased by approximately 1 log unit per pH unit, whilst those for copper did not change. No trend was observed for concentrations of iron and copper complexing ligands over the pH range examined. We also interpreted our titration data by describing chemical binding and polyelectrolytic effects using non-ideal competitive adsorption in Donnan-like gels (NICA-Donnan model) in a proof of concept study. The NICA-Donnan approach allows for the development of a set of model parameters that are independent of ionic strength and pH, and thus calculation of metal speciation can be undertaken at ambient sample pH or the pH of a future, more acidic ocean. There is currently a lack of basic NICA-Donnan parameters applicable to marine dissolved organic matter (DOM) so we assumed that the measured marine dissolved organic carbon could be characterized as terrestrial fulvic acids. Generic NICA-Donnan parameters were applied within the framework of the software program visual MINTEQ and the metal—added ligand concentrations [MeAL] calculated for the AdCSV-CLE conditions. For copper, calculated [MeAL] using the NICA-Donnan model for DOM were consistent with measured [MeAL], but for iron an inert fraction with kinetically inhibited dissolution was required in addition to the NICA-Donnan model in order to approximate the trends observed in measured [MeAL]. We calculated iron and copper speciation in Northwest European shelf water samples at ambient alkalinity and projected increased $p\text{CO}_2$ concentrations as a demonstration of the potential of the approach.

Keywords: trace metals, speciation, pH, iron solubility, NICA-Donnan, CLE-AdCSV

INTRODUCTION

The increase in atmospheric CO₂ concentrations over the past two centuries has led to an enhanced CO₂ uptake by the oceans (Feely et al., 2004). This uptake has lowered the surface ocean pH (Caldeira and Wickett, 2003), and changed the balance of the carbonate species (Doney, 2006), leading to a decrease in the carbonate ion concentration (CO₃²⁻) and an increase in aqueous CO₂ and bicarbonate concentrations (Zeebe and Wolf-Gladrow, 2001; Orr et al., 2005). The increase in atmospheric partial pressure of CO₂ (*p*CO₂) from preindustrial (~280 μatm) to current levels (~400 μatm) has already caused a reduction of ca. 0.1 pH units (Caldeira and Wickett, 2003; Feely et al., 2004). If anthropogenic CO₂ emissions and ocean CO₂ uptake continues along current trends, a decrease in pH of about 0.3–0.5 units by the year 2100 in the surface oceans is possible (Brewer, 1997; Zeebe and Wolf-Gladrow, 2001; Feely et al., 2004; Orr et al., 2005; Doney, 2006). Carbonate ion concentrations are expected to drop by half over this century, making it more difficult for marine calcifying organisms to form biogenic calcium carbonate (CaCO₃), and to maintain their external skeletons (Orr et al., 2005). These changes in ocean chemistry could have strong impacts on marine ecosystems, even under future scenarios in which most of the remaining fossil fuel derived CO₂ is not released (Kleypas et al., 1999; Riebesell et al., 2000; Caldeira and Wickett, 2003; Langdon et al., 2003).

Changes in ocean pH and carbonate chemistry could also have significant impacts on the chemical speciation of essential trace elements in seawater (Millero et al., 2009; Shi et al., 2010; Gledhill et al., 2015). In the surface ocean, trace metals that have a significant biological role for oceanic phytoplankton are manganese, iron, cobalt, copper, zinc, and cadmium (Morel and Price, 2003). Iron is an essential micronutrient involved in fundamental cellular processes, including respiration, photosynthesis, nitrogen uptake and nitrogen fixation (Geider and La Roche, 1994; Raven et al., 1999; Hogle et al., 2014). Iron controls productivity, species composition and trophic structure of microbial communities in large regions of the ocean (Sunda and Huntsman, 1995a; Johnson et al., 1997; Hunter and Boyd, 2007). Iron concentrations in oceanic waters are very low due to its low solubility and effective removal from the surface ocean by phytoplankton (Liu and Millero, 2002). Organic complexation is thought to maintain dissolved iron concentrations above its inorganic solubility (Liu and Millero, 2002), whilst potentially reducing the concentrations of the soluble, bioavailable inorganic species (Shaked and Lis, 2012). It has been demonstrated that iron deficiency limits phytoplankton growth in High Nitrate Low Chlorophyll (HNLC) waters such as the equatorial and subarctic Pacific, Southern Ocean, and coastal upwelling regions (Martin and Fitzwater, 1988; Boye et al., 2005; Boyd et al., 2007). Furthermore, in nutrient poor, low latitude waters iron helps to regulate nitrogen fixation (Moore et al., 2009). As a consequence, iron strongly influences oceanic CO₂ drawdown in these regions (De Baar et al., 2008). A decrease in seawater pH from 8.1 to 7.4, which would correspond to an increase in *p*CO₂ to approximately 1800 μatm, will increase the solubility of Fe(III) by about 40%, which could have a large impact on biogeochemical

cycles (Morel and Price, 2003; Millero et al., 2009). A decrease in pH has also been suggested to result in higher iron availability to phytoplankton, as a result of enhanced proton competition for the available iron-binding ligand places (Raven et al., 2005; Millero et al., 2009). A recent estuarine study suggested that concentrations of inorganic, bioavailable iron would increase 3 fold with a pH reduction from 8.18 to 7.41 (Gledhill et al., 2015), but that concentrations of dissolved organic carbon (DOC) could play an overriding role in determining iron speciation. The acid-base chemistry of the DOC binding sites is thus likely to be of key importance to any changes in iron speciation under future climate change scenarios (Shi et al., 2010).

Copper is an essential micronutrient for marine phytoplankton. It is involved in iron uptake (Peers et al., 2005), and in the ocean's nitrogen cycle (Jacquot et al., 2013). Limitation of phytoplankton growth has also been observed in laboratory phytoplankton strains at free copper ion concentrations of less than 10⁻¹⁵ M (Sunda and Huntsman, 1995b; Annett et al., 2008; Guo et al., 2012). Cu(II) is also toxic and free copper (II) ion concentrations as low as 10⁻¹² M have been shown to reduce growth in marine phytoplankton (Brand et al., 1986) resulting in a relatively narrow optimal growth range. Complexation of copper by organic ligands can decrease its toxicity by decreasing the free cupric ion concentration (Moffett and Brand, 1996; Moffett et al., 1997; Croot et al., 2000). A pH decrease may reduce copper binding by both organic ligands and carbonate, therefore making copper more bioavailable and consequently toxic to marine phytoplankton. It has been predicted that the increase for the free form of copper (Cu²⁺) under a scenario where pH is reduced to 7.5, will be as high as 30% (Millero et al., 2009) whilst Gledhill et al. (2015) found that Cu²⁺ concentrations could increase in estuaries by an order of magnitude under a similar scenario of pH reduction to 7.4, if DOC concentrations remained the same. Such increases could thus result in a higher potential for copper toxicity in coastal and estuarine ecosystems.

There are only a few studies that have considered the effect of ocean acidification on the speciation and/or bioavailability of trace metals to marine organisms (Turner et al., 1981; Byrne et al., 1988; Byrne, 2002; Millero et al., 2009; Shi et al., 2010; Gledhill et al., 2015). Here we extend our recent investigations (Gledhill et al., 2015) into the impact of decreasing pH on the complexation of iron and copper at reduced pH to waters of the Northwest European shelf seas. The aim of this study was to experimentally determine changes in the speciation of iron and copper that might result from an increase in *p*CO₂ and a consequent decrease in surface ocean pH. We therefore carried out competitive ligand equilibrium (CLE) titrations using adsorptive cathodic stripping voltammetry as a detection method (AdCSV) on 20 samples collected from Northwest European shelf seas at pH 7.91, 7.37, and 6.99 (expressed on the total pH scale). We used salicylaldoxime (H₂SA) as the competing ligand for copper, and 1-nitroso-2-naphthol (HNN) as the competing ligand for iron. Competitive ligand equilibrium titrations are generally interpreted as analogous to adsorption isotherms (Ruzic, 1982; Gerringa et al., 1995). Adsorption isotherms can be interpreted using a number of different models (Foo and Hameed, 2010). In this study we used two different methods that have previously

been applied to marine waters to interpret our data (Gerringa et al., 1995; Hiemstra and Van Riemsdijk, 2006). Firstly we treated the natural metal complexing ligands (L_i) as discrete ligands and utilized the Langmuir isotherm to obtain conditional stability constants ($K_{MeL,Me}^{cond}$) and ligand concentrations $[L_i]$ for each sample (Gerringa et al., 1995, 2014). Secondly we used the NICA-Donnan model, which considers dissolved organic matter (DOM) to be heterogeneous and non-ideal, and subject to multicomponent competition and electrostatic interactions (Koopal et al., 2005) and thus we considered DOM to contain a continuous distribution of binding sites analogous to complex organic compounds like fulvic acids (Laglera et al., 2007; Laglera and Van Den Berg, 2009; Batchelli et al., 2010; Hassler et al., 2011; Whitby and Van Den Berg, 2015). For the NICA-Donnan approach we compared calculated and measured concentrations of metal-added ligand complexes, given the determined DOC concentrations (Gledhill et al., 2015). The utility of the NICA-Donnan approach was then demonstrated through calculation of the speciation of iron and copper in our coastal water samples at the natural pH and total alkalinity of the samples observed during the cruise (Ribas-Ribas et al., 2014) and at 280, 900 and 1900 μatm $p\text{CO}_2$ (approximately $2 \times$ and $5 \times$ 2014 values), assuming total alkalinity and DOC remain unchanged.

MATERIALS AND METHODS

Sample Collection

Seawater samples were collected in Northwest European shelf seas (Figure 1, Table S1) during the RRS *Discovery* 366 cruise in June and July 2011. Surface seawater (ca. 2–3 m deep) was collected daily from a towed fish and was filtered in-line inside a clean container through a 0.2 μm pore size filter capsule (Sartobran P-300, Sartorius). The seawater was stored in 250 ml low density polyethylene bottles (250 mL LDPE; Nalgene) for the subsequent determination of iron and copper speciation. Bottles were pre-cleaned according to a standard protocol described by Achterberg et al. (2001) and just prior to sampling were rinsed thoroughly with deionised water (MilliQ, Millipore; >18.2 m Ω cm) and then with seawater. Samples for copper-binding ligand analysis were stored at 4°C for subsequent analysis on board the ship (within 1 day). Samples for the determination of iron speciation were frozen immediately after collection (-20°C) and analyzed in a clean laboratory at the National Oceanography Centre, Southampton. Samples for the determination of total dissolved trace metals were collected using 60 ml LDPE bottles (Nalgene), acidified to pH 1.8 (0.011 M final concentration) using ultraclean HCl (Romil UpA grade) and stored at room temperature.

Determination of pH and Dissolved Organic Carbon

The pH of the original seawater sample was determined on the total pH scale (pH_{total}) using an automated pH system (Rérolle et al., 2012) connected to the ship's underway water supply, which collected water at a depth of ~ 5 m. pH was determined using spectrophotometry with Thymol Blue as the pH indicator (Clayton and Byrne, 1993; Rérolle et al., 2012). The

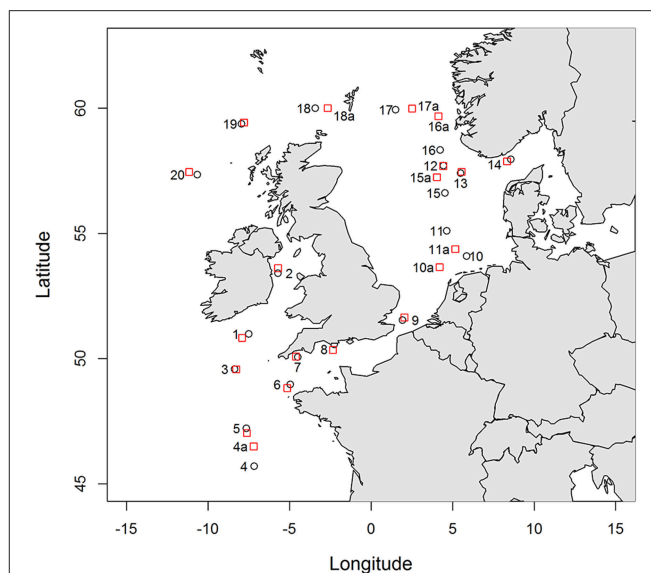


FIGURE 1 | Locations sampled from the CTD cast (red squares) and from the underway sampling system (black circles). Where stations are not directly adjacent, underway samples are labeled with the station number and the letter a.

spectrophotometric method had a precision of 1 mpH units and measured pH values were within 0.004 pH units of certified Tris pH buffer (Scripps Institute of Oceanography, University of San Diego).

The pH of buffer solutions used during titrations was determined on the IUPAC scale (pH_{NBS}). Although, the IUPAC scale is not optimal for seawater, stability constants describing metal complexation are determined on this scale and so it was considered appropriate for this study. pH was determined on titration aliquots immediately post analysis using a Metrohm pH meter. For comparative purposes, buffered seawater (in the absence of any added ligands) was also measured with the spectrophotometric technique (Rérolle et al., 2012), and respective values obtained on the total pH scale (pH_{total}), which were: 6.99 ± 0.01 for pH_{NBS} 7.2, 7.37 ± 0.005 for pH_{NBS} 7.6, and 7.91 ± 0.005 for pH_{NBS} 8.05. pH_{NBS} was thus 0.21 ± 0.03 pH units higher than pH_{total} at 20°C (Gledhill et al., 2015).

Dissolved organic carbon was determined on samples collected from the stainless steel CTD rosette (Macgilchrist et al., 2014). For our study we used results from the sample collected from CTD stations positioned closest to our underway sample obtained at a depth between 2 and 9 m. Samples were filtered through precombusted (450°C , 4 h) glass fiber filters (0.7 μm nominal cutoff; MF300, Fisher Scientific) into precombusted glass ampoules and immediately acidified to pH 2 with 5 M HCl. The ampoules were flame sealed, stored at room temperature and analyzed on shore by high temperature catalytic combustion (Badr et al., 2003). We obtained a value of $41.8 \pm 0.9 \mu\text{M C}$ ($n = 15$) for acidified deep seawater reference material provided by D. Hansell (University of Miami) against a certified concentration range of 41–43 $\mu\text{M C}$.

Determination of Total Dissolved Iron and Copper Concentrations

Total dissolved metal concentrations were determined by inductively coupled plasma—mass spectrometry (ICP-MS) on acidified ($\text{pH}_{\text{NBS}} 1.8$) samples after a salt removal and off-line pre-concentration/matrix removal step using a Toyopearl AF-650M chelating column (Milne et al., 2010). Briefly, 12 ml of the acidified sample in an acid cleaned 30 ml FEP bottle (Nalgene) was spiked with a multi-element standard of isotopes (containing the stable isotopes ^{65}Cu , and ^{57}Fe) with known enrichments over their natural abundance. The spiked samples were left for overnight equilibration. Subsequently, the samples were buffered to $\text{pH } 6.4 \pm 0.2$ using 2 M ammonium acetate, prepared with ultrapure acetic acid and ammonia (Fisher Optima).

The buffered sample was then pumped over the preconcentration column, at 2 ml min^{-1} . The column was rinsed with 1 ml de-ionized water to remove salts, and subsequently the metals were eluted for 30 s using 1 ml of 1M distilled HNO_3 (Savilex). The eluent was collected into acid cleaned autosampler polypropylene vials (OmniVials; 4 ml) and capped.

The extracted samples were analyzed using a high resolution-ICP-MS (Element XR, Thermofisher). The sample was introduced via a $100 \mu\text{l}$ Teflon nebuliser connected to a PFA spray chamber. Measurements for iron, and copper were performed in medium resolution mode ($R = 4000$). The detection limit was determined to be 0.033 and $0.054 \text{ nmol L}^{-1}$ for iron and copper, respectively, and blank values were typically 0.06 nmol L^{-1} for iron and 0.02 nmol L^{-1} for copper. Values determined for the SAFe surface reference sample were within the consensus range ($0.09 \pm 0.03 \text{ nmol L}^{-1}$ for iron, and $0.55 \pm 0.06 \text{ nmol L}^{-1}$ for copper).

Determination of Iron and Copper Speciation Via Competitive Ligand Exchange with Detection by Adsorptive Cathodic Stripping Voltammetry (CLE)

Determination of the iron and copper speciation in seawater was performed via measurement of the quantity of each metal (Me) that is available to complex with an added ligand (AL) using CLE-AdCSV, with 1-nitroso-2-naphthol (HNN) for iron (Yokoi and Van Den Berg, 1992; Gledhill and Van Den Berg, 1994; Van Den Berg, 1995), and salicylaldehyde (H_2SA) for copper (Campos and van den Berg, 1994) as the competing ligands.

The electrochemical system consisted of a potentiostat ($\mu\text{Autolab Ecochemie}$, Netherlands) with a static mercury drop electrode (Metrohm, 663 VA stand), a KCl reference electrode (Ag/AgCl in 3M KCl saturated with AgCl) and a counter electrode of glassy carbon. Two systems were used in parallel on board ship for the analysis of copper speciation, and one system in the laboratory for the analysis of iron speciation.

All chemicals were prepared in a clean electrochemistry laboratory under a Class 100 laminar flow bench at room temperature (20°C). A stock solution of 0.01 M HNN (Sigma) was prepared in methanol (Fisher, HPLC grade). A stock solution

of 0.01 M H_2SA (Sigma) was prepared in 0.1 M HCl (Romil, SpA grade). Standard Fe(III) and Cu(II) solutions of 10^{-6} M for additions were prepared using a 1000 mg/L ICP-MS stock solution (Fisher Scientific), and were acidified to $\text{pH } 2$ using HCl (Romil, SpA grade).

Stock solutions of 1 M N-2-hydroxyethylpiperazine-N'-ethanesulphonic acid (HEPES; Fisher Aristar grade) pH buffer were prepared in 0.35 , 0.6 , and 0.9 M ammonia (Romil, SpA grade) in order to provide a pH of 7.2 , 7.6 , and 8.05 upon 100-fold dilution with sea water. HEPES was cleaned prior to use by the addition of HNN with subsequent removal of HNN and $\text{Fe}(\text{NN})_3$ using a previously activated C_{18} SepPak column (Whatman).

For the ship-board determination of copper speciation, the pH was adjusted in three individual 250 ml LDPE bottles to 8.05 , 7.6 , and 7.2 through addition of pH adjusted 1 M HEPES buffers (0.01 M final concentration) immediately after collection, and with a 0.01 M solution of the competing ligand H_2SA ($10 \mu\text{M}$ final concentration). The samples were subsequently equilibrated for a minimum period of 1 h at room temperature ($\sim 20^\circ\text{C}$). An aliquot of 15 ml of the sample solution was then pipetted into 30 ml polystyrene cups. A copper (II) standard solution was spiked to give an added concentration range between 0 and 30 nM in 14 steps. The copper and ligands in the sample aliquots were allowed to equilibrate overnight ($>12 \text{ h}$) at room temperature.

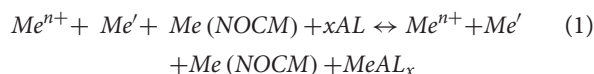
The concentration of $\text{Cu}(\text{HSA})_2$ in the samples was determined using the following procedure: (i) removal of oxygen from the samples for 5 min with nitrogen gas (oxygen free grade), after which 5 fresh Hg drops were formed, (ii) a deposition potential of -0.1 V was applied for 60 s whilst the solution was stirred to facilitate the adsorption of the $\text{Cu}(\text{HSA})_2$ to the Hg drop, and (iii) at the end of the adsorption period, the stirrer was stopped and the potential was scanned from -0.1 to -0.4 V using the square wave method at a frequency of 100 Hz . The stripping current (peak height) from the reduction of the adsorbed $\text{Cu}(\text{HSA})_2$ complex was recorded. The pH on each of the titration steps was checked after each measurement and found to agree with the pH prior to measurement.

Iron speciation was determined in a clean laboratory under a Class 100 laminar flow bench, in Southampton. The frozen samples for the iron speciation measurements were thawed prior to analysis to reach room temperature, and then buffered using the same procedure as for the copper samples. In the case of the iron titrations, an added ligand concentration of $1 \mu\text{M}$ NN was used, with the exception of the $\text{pH } 8.05$ experiment ($2 \mu\text{M}$ NN). Added iron concentrations ranged between 0 and 8 nM in 14 steps, pipetted into 30 ml polytetrafluoroethylene (PTFE) vessels. Samples were left to equilibrate for 16 h (overnight).

The concentration of $\text{Fe}(\text{NN})_3$ was determined after de-aeration of the sample with nitrogen gas (5 min). A deposition potential at -0.1 V was used with a deposition time of 3 min; the scanning mode was sample-DC from -0.15 V to -0.65 V at a scan rate of 50 mV s^{-1} , the reduction peak of iron appeared at approximately -0.45 V .

Data Treatment Applied to Competitive Ligand Exchange Titrations

Addition of a competing or added ligand to natural seawater results in the establishment of a new equilibrium between the free metal (Me^{n+}), inorganic metal complexes (Me'), natural organic complexing material (NOCM) and the AL.



The approach assumes that the concentration of the competing AL species is in excess of the binding sites in the NOCM, and works optimally when the binding sites in NOCM are in excess of the metal concentration in the sample. Addition to the sample of further free metal (Me^{n+}) in increasing increments, accompanied by determination of the concentration of $MeAL_x$ and calculation of Me' and Me^{n+} using known equilibrium constants allows for the estimation of the concentration of $Me(NOCM)$ at each titration point in the experiment. Modeling the relative changes in all four components of the equilibrium allows for the relative concentration and strength of the NOCM binding sites to be established. In this study we used two approaches to model changes in metal speciation during the titration: (1) the single window discrete ligand approach and (2) the NICA-Donnan model. The first approach allowed us to obtain conditional stability constants $K_{MeL_i}^{cond}$ and the maximum concentration of metal that could bind to NOCM in each sample at the three pH levels at which the samples were analyzed. The second approach was used to calculate the speciation of iron and copper independent of pH, pCO_2 , and DOC concentrations and thus allowed for examination of the impact of future increases in pCO_2 to be investigated in North West European shelf sea waters.

Results of CLE-AdCSV are highly dependent on the method used to define the sensitivity of the electrochemical response (Pizeta et al., 2015). In this study we used the internal method, which calculates $MeAL_x$ concentrations from the slope of the saturated part of the titration curve, normally the last three to five titration points. Average slopes observed at the three different pHs in this study are given in **Table 1**. Although slopes were variable between samples, we observed no systematic difference in slope with DOC (results not shown) for either iron or copper. Copper titrations were performed at sea on two separate instruments made up of the same components. A large difference in slope (ca. 2.3 \times) was observed between the two instruments employed for copper titrations.

The Single Detection Window Discrete Ligand Approach

In the single detection window discrete ligand approach (hereafter referred to simply as the discrete ligand approach), NOCM is considered to consist of classes of discrete ligands (L_i) which vary in strength. The strongest ligand class is termed L_1 and progressively weaker ligands L_2 , L_3 etc. Importantly in this approach, the stoichiometry between Me and L_i is assumed to be 1:1 (Pizeta et al., 2015). This approach has been used extensively for describing metal complexation in marine systems and considerable effort has been directed toward determining

TABLE 1 | Average slopes observed for the last three titration points at different titration pHs.

pH _{NBS}	Slope (nA nmol ⁻¹)	
	FeNN ₃	ΣCu(HSA) _x
8.0	0.83 ± 0.09	2.1 ± 0.5; 4.5 ± 0.2
7.6	0.95 ± 0.61	1.9 ± 0.6; 4.8 ± 0.6
7.2	0.84 ± 0.22	2.1 ± 0.8; 4.9 ± 0.7

Slopes are given separately for the two instruments used for copper titrations.

different ligand classes (e.g., Sander et al., 2011) in the hope of properly representing the full range of metal complexes likely to be present in the marine environment. In our study we undertook titrations at different pH for each sample, applying one added ligand concentration for each metal. The theoretical considerations for the determination of natural ligand binding characteristics assuming discrete ligands has been described in detail for iron and HNN by Gledhill and Van Den Berg (1994); Van Den Berg (1995), and in the case of Cu with H₂SA by Campos and van den Berg (1994). The overall mass balance, conditional stability constants for $MeAL_x$ and the sensitivity of the voltammetric response are used to determine concentrations of Me' and MeL_i for each titration point. Values for Me' and MeL_i are then used to calculate the conditional stability $K_{MeL_i}^{cond}$ and ligand concentration [L_i] of the metal ligand complex using the equation

$$[MeL_i] = \frac{K_{MeL_i}^{cond} [L_i] [Me']}{(1 + K_{MeL_i}^{cond} [Me'])} \quad (2)$$

where $K_{MeL_i}^{cond}$ is the conditional stability constant for metal complexation with the natural ligand (L_i). Equation (1) is equivalent to the Langmuir isotherm and $K_{MeL_i}^{cond}$ and [L_i] were calculated using non-linear regression (Gerringa et al., 1995) and a script in the computer program R (Gerringa et al., 2014). The coefficients and constants used in the discrete ligand approach in this study are listed in **Table 2**. Although the discrete ligand approach has been extensively used to describe metal complexation in the marine environment, a limitation of this approach is that the conditional stability constants and ligand concentrations are, by definition, conditional and thus specific to the ionic strength, pH and temperature of the sample at the time it was analyzed.

Modeling Iron and Copper Complexation by Dissolved Organic Matter with the Non-Ideal Competitive Adsorption-Donnan Approach

The NICA-Donnan approach is one of a suite of modeling approaches (Dudal and Gérard, 2004; Tipping, 2005; Stockdale et al., 2015; Tipping et al., 2015) that attempts to represent the complexity of metal complexation with DOM in a way which is independent of pH, ionic strength and the presence of competing cations. In the NICA-Donnan model, DOM is considered to behave like humic or fulvic acids (Kinniburgh et al., 1996; Koopal et al., 2005). The NICA-Donnan model accounts for both the

TABLE 2 | Conditional stability constants for added ligands and inorganic side reaction coefficients for iron and copper used in this study.

pHNBS	$\log K_{Fe(NN)_3, Fe3+}^{cond}$	$\log K_{CuHSA, Cu2+}^{cond}$	$\log \beta_{Cu(HSA)_2, Cu2+}^{cond}$	$\log \alpha_{Fe'}$	$\log \alpha_{Cu'}$
8.0	29.3	8.4	14.0	9.8	0.89
7.6	29.3	8.0	13.2	8.8	0.27
7.2	29.2	7.7	12.4	8.1	-0.09

chemical (NICA) and electrostatic (Donnan) affinity of binding sites. In the NICA component, the overall equation used to obtain the fraction of total number of binding sites ($\theta_{i,max}$) occupied by the *i*th component (e.g., proton, iron, copper) at concentration C_i is

$$\theta_{i,max} = \frac{(K_i \cdot C_i)^{n_i}}{\sum_i (K_i \cdot C_i)^{n_i}} \cdot \frac{\{\sum_i (K_i \cdot C_i)^{n_i}\}^p}{1 + \{\sum_i (K_i \cdot C_i)^{n_i}\}^p} \quad (3)$$

where the NICA constant (K_i) describes the mean binding affinity for the *i*th component, n_i is the non-ideality constant, and p is width of the binding site distribution (Koopal et al., 2005). The overall density of binding sites ($Q_{max,T}$) is assumed to be equivalent to the density of proton binding sites ($Q_{maxH,T}$). Proton affinities (K_H) are considered to occur in a continuous Sips bimodal affinity distribution that is thought to encompass two groups of binding sites—a low proton affinity (acidic) group and a high proton affinity (basic) group of sites (Koopal et al., 2005). The following normalization condition is thus used to give thermodynamic consistency to the NICA isotherm and calculate of the amount ($Q_{i,max}$) of component *i*, bound by DOM, where n_H is the non-ideality constant for the binding of protons

$$Q_{i,max} = Q_{max,T} \theta_{i,max} \left(\frac{n_i}{n_H} \right) \quad (4)$$

Substituting Equation (3) in Equation (4) the following general expression describing the binding of metal, Me (Cu or Fe) by marine DOM (Milne et al., 2003)

$$Q_{Me} = Q_{max1,T} \frac{n_{Me,1}}{n_{H1}} \cdot \frac{(K_{Me,1} \cdot C_{Me})^{n_{Me,1}}}{(K_{H,1} \cdot C_H)^{n_{H,1}} + (K_{Me,1} \cdot C_{Me})^{n_{Me,1}}} \cdot \frac{\{(K_{H,1} \cdot C_H)^{n_{H,1}} + (K_{Me,1} \cdot C_{Me})^{n_{Me,1}}\}^{p1}}{1 + \{(K_{H,1} \cdot C_H)^{n_{H,1}} + (K_{Me,1} \cdot C_{Me})^{n_{Me,1}}\}^{p1}} + Q_{max2,T} \frac{n_{Me,2}}{n_{H2}} \cdot \frac{(K_{Me,2} \cdot C_{Me})^{n_{Me,2}}}{(K_{H,2} \cdot C_H)^{n_{H,2}} + (K_{Me,2} \cdot C_{Me})^{n_{Me,2}}} \cdot \frac{\{(K_{H,2} \cdot C_H)^{n_{H,2}} + (K_{Me,2} \cdot C_{Me})^{n_{Me,2}}\}^{p2}}{1 + \{(K_{H,2} \cdot C_H)^{n_{H,2}} + (K_{Me,2} \cdot C_{Me})^{n_{Me,2}}\}^{p2}} \quad (5)$$

where $Q_{max1,T}$, $Q_{max2,T}$ refer to the total number of type 1 and type 2 proton binding sites respectively.

The NICA approach is combined with the Donnan model in order to account for electrostatic interactions that occur in gel like substances. The Donnan model relates the molecular charge

σ of a natural organic molecule to its Donnan volume V_D and electrostatic potential ψ .

$$\sigma = V_D \sum_i z_i C_{0,i} e^{-\frac{z_i F \psi}{RT}} \quad (6)$$

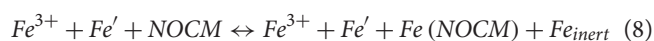
where z_i is the valence of the *i*th component, $C_{0,i}$ is the concentration of *i*th component in solution, F is the Faraday constant, R the gas constant and T the absolute temperature (K). The Donnan volume is related to ionic strength through the empirical formula (Benedetti et al., 1996)

$$\log V_D = 0.57 (1 - \log I) - 1 \quad (7)$$

The combined NICA-Donnan model was applied to our dataset using the computer program visual MINTEQ v 3.0 (vMINTEQ; Gustafsson, 2012). vMINTEQ incorporates the NICA-Donnan model into a calculation of the speciation of inorganic and simple organic molecules (such as ethylenediaminetetraacetic acid, EDTA) or ions at thermodynamic equilibrium. vMINTEQ uses stability constants from the NIST database (Martell and Smith, 2004) for inorganic and simple organic complexes. The salinity of each sample was used to derive the molality of the major ions Na^+ , K^+ , Ca^{2+} , Mg^{2+} , Sr^{2+} , Cl^- , SO_4^{2-} , Br^- , BO_3^{3+} , and F^- for a temperature of 20°C and a density of 1025 kg m^{-3} . The inorganic/simple organic part of the algorithm has not been optimized for modeling at ionic strengths as high as seawater. We used the extended Davies equation to correct for ionic interactions, but many components lack the Debye-Hückel constants required to properly extend the calculations into the ionic strength range of seawater. Comparison of calculated speciation for the carbonate system (Gledhill et al., 2015) with that produced by CO₂SYS, a speciation model specifically designed for seawater (Pierrot et al., 2006), resulted in underestimation of $[CO_3^{2-}]$, a factor which is likely related to the ionic strength algorithm employed in vMINTEQ (Gledhill et al., 2015). Here, as in our previous study, we therefore forced the total $[CO_3^{2-}]$ concentration to agree with the total $[CO_3^{2-}]$ concentration produced by CO₂SYS by multiplying total inorganic carbon (T_c) by 1.2 in order to compensate for the underestimation of total $[CO_3^{2-}]$ and improve the calculation of inorganic copper species across our pH range. Forcing $[CO_3^{2-}]$ concentrations resulted in $82.0 \pm 0.4\%$ and $68.2 \pm 0.8\%$ ($n = 20$) of inorganic copper being present as carbonate species in our samples at pH 8.1 and 7.6 respectively, which is of similar magnitude to that calculated by Millero et al. (2009).

For the NICA-Donnan model, we considered DOC in our samples to consist entirely of fulvic acids. We applied the

generic parameters for total binding sites $Q_{maxH,T}$, binding site distribution (p), the NICA constant (K) and non-ideality constant (n_H) for type 1 (acidic) and 2 (basic) sites to describe FA proton binding, and NICA constants and non-ideality constants for complexation of FA by the major competing ions calcium, magnesium and strontium. The generic parameter set for the NICA-Donnan model has been derived from pH or metal titration experiments on soil and freshwater fulvic fractions (Milne et al., 2003). The Donnan equation, which accounts for the effects of ionic strength, has been established using a relatively limited dataset (Benedetti et al., 1996), albeit one that extends up to an ionic strength of 1. Similar characterization of marine DOM has yet to be undertaken and is challenging because of the difficulties of isolating and preconcentrating sufficient DOM to carry out such experiments. For NICA-Donnan modeling of iron and copper complexation with fulvic acid, we first used two parameter sets based on more recent studies (see **Table 3**) in marine waters. The presence of an inert iron fraction (Gledhill and Buck, 2012) was accounted for by first calculating iron solubility in our samples using the sample DOC concentration, the relevant NICA-Donnan parameters and ferrihydrite precipitation with the solubility constant derived by Liu and Millero (1999) at the pH of the original seawater sample (i.e., not the pH of the titration). An additional equation was added in order to consider the presence of an inert fraction at saturated concentrations of Fe' that did not react with NN within the timescale of our titration



Once Fe_{inert} was calculated and subtracted from the dFe concentration, then the equilibrium between NN and Fe^{3+} , Fe' , and $Fe(NOCM)$ was calculated with vMINTEQ. Salicylaldoxime and HNN were added as ligands to vMINTEQ. Protonation constants for the added ligands were taken from the NIST critical stability constant database (**Table 3**; Martell and Smith, 2004). Stability constants for vMINTEQ for complexation of copper with HSA^- , and iron with NN^- were empirically derived from titrations of added ligands with EDTA and, for SA, from titrations in UV-irradiated seawater varying the H_2SA concentration (Gledhill et al., 2015). The derived stability constants are conditional to the ionic strength and major ion composition of seawater and valid for the pH range used in our study. Concentrations of $MeAL_x$ were calculated in vMINTEQ at the pH and $[CO_3^{2-}]$ concentrations of the experimental titration pH. Calculated concentrations of $MeAL_x$ were compared to measured concentrations of $MeAL_x$ in order to empirically minimize the root mean squared error. We then used the best parameter set to calculate iron and copper speciation in our samples at the observed pH_{NBS} and $1.2 \times T_c$ calculated by CO_2SYS from measured total alkalinity and pCO_2 values of 280, 400, 900, and 1900 μatm . Calculations were carried out at 20°C as this was the temperature at which titrations were performed and there is little information with respect to how NICA-Donnan complexation in seawater will change with temperature.

The updated thermodynamic database, components database, and the NICA-Donnan databases used in this study are provided

as Data sheet 1 in Supplementary Material. Because of the limitations resulting from the mechanism used to correct for ionic strength and the lack of knowledge with respect to the complexation properties of marine DOC, these databases should be used with caution and the results presented here should thus be regarded in the context of “proof of concept,” rather than a fully accurate interpretation of iron and copper speciation in these waters. Nevertheless, useful information can be obtained from applying this approach to marine systems with respect to the general behavior of complex DOM over the pH range of our study.

RESULTS

Salinity, Sea Surface Temperature (SST°C) and Surface pH

The hydrography of the cruise has been discussed in more detail by Poulton et al. (2014). Salinity varied between 31.3 and 35.8 at the 20 sampling stations, except in the Skagerrak area where a salinity of 27.4 was observed (**Figure 2A**). Sea surface temperature (SST) varied between 11.2 and 17.1°C, with the lowest value observed at station 2 in the Irish Sea and the highest at station 14 in the Skagerrak area.

The concentrations of DOC ranged between 61 and 145 $\mu mol L^{-1}$ (**Figure 2B**), with the maximum value observed at station 14 in the Skagerrak area. The high DOC concentration observed in the surface waters (<5 m) at this station was associated with a surface extrusion of high temperature, low salinity waters that originated from the Baltic Sea or the coastal waters of Sweden. Similar high DOC values (>100 $\mu mol L^{-1}$) were also observed at <5 m in the adjacent two CTD stations (Macgilchrist et al., 2014).

Surface seawater pH_{Total} at the 20 sampling stations varied from 8.04 to 8.23 (**Figure 2C**), with the highest values observed at station 18 in the northern North Sea and station 19 in the Atlantic sector of the cruise, which had some of the lowest temperature values observed during the cruise, and featured enhanced chlorophyll concentrations (up to 1.6 $\mu g L^{-1}$ Poulton et al., 2014). Lowest pH values were observed at station 8 in the English Channel and at the southern North Sea stations (10, 11, 15).

Total dissolved iron (dFe) concentrations varied between 0.5 and 5.4 nM (**Figure 3A**), with an average of 2.2 ± 1.5 nM except in the southern North Sea (station 10) and the Skagerrak area (station 14), where dFe concentrations were high (21.0 and 10.6 nM, respectively). Total dissolved copper (dCu) concentrations varied between 0.4 and 5.1 nM (**Figure 3B**), with an average of 2.3 ± 1.3 nM.

Organic and Copper Binding Ligand Characteristics in the Northwest European Shelf Seas – the Effect of Acidification

The enhanced concentrations of dFe and dCu typically observed in the shelf sea waters resulted in natural ligand pools that were close to saturation, if not saturated, for many of our titrations. As such fitting the discrete ligand model was problematic for many of our samples as was also reported for deep ocean

TABLE 3 | Constants used for NICA-Donnan modeling.

	Iron		Copper		Added ligand
	FA1	FA2	FA1	FA2	
A ^a	log K = 3.6, n = 0.3	log K = 11.2, n = 0.15	log K = 0.26, n = 0.63	log K = 7.26, n = 0.36	Fe(NN) ₃ , log K = 32.5, pK _{aHNN} = 7.9 ^c
B ^b	log K = 2.8, n = 0.36	log K = 8.3, n = 0.23	log K = 0.26, n = 0.63	log K = 8.26, n = 0.36	Cu(HSA) ⁺ , log K = 18 ^c Cu(HSA) ₂ , log K = 41.1
C	log K = 3.6, n = 0.26	log K = 8.3, n = 0.23	log K = 0.26, n = 0.63	log K = 5.26, n = 0.53	pK _{aHSA} = 12.1 ^c pK _{aH2SA} = 21.29 ^c pK _{aH3SA} = 22.7 ^c

^a Gledhill et al., 2015.

^b Hiemstra and Van Riemsdijk, 2006.

^c Martell and Smith, 2004.

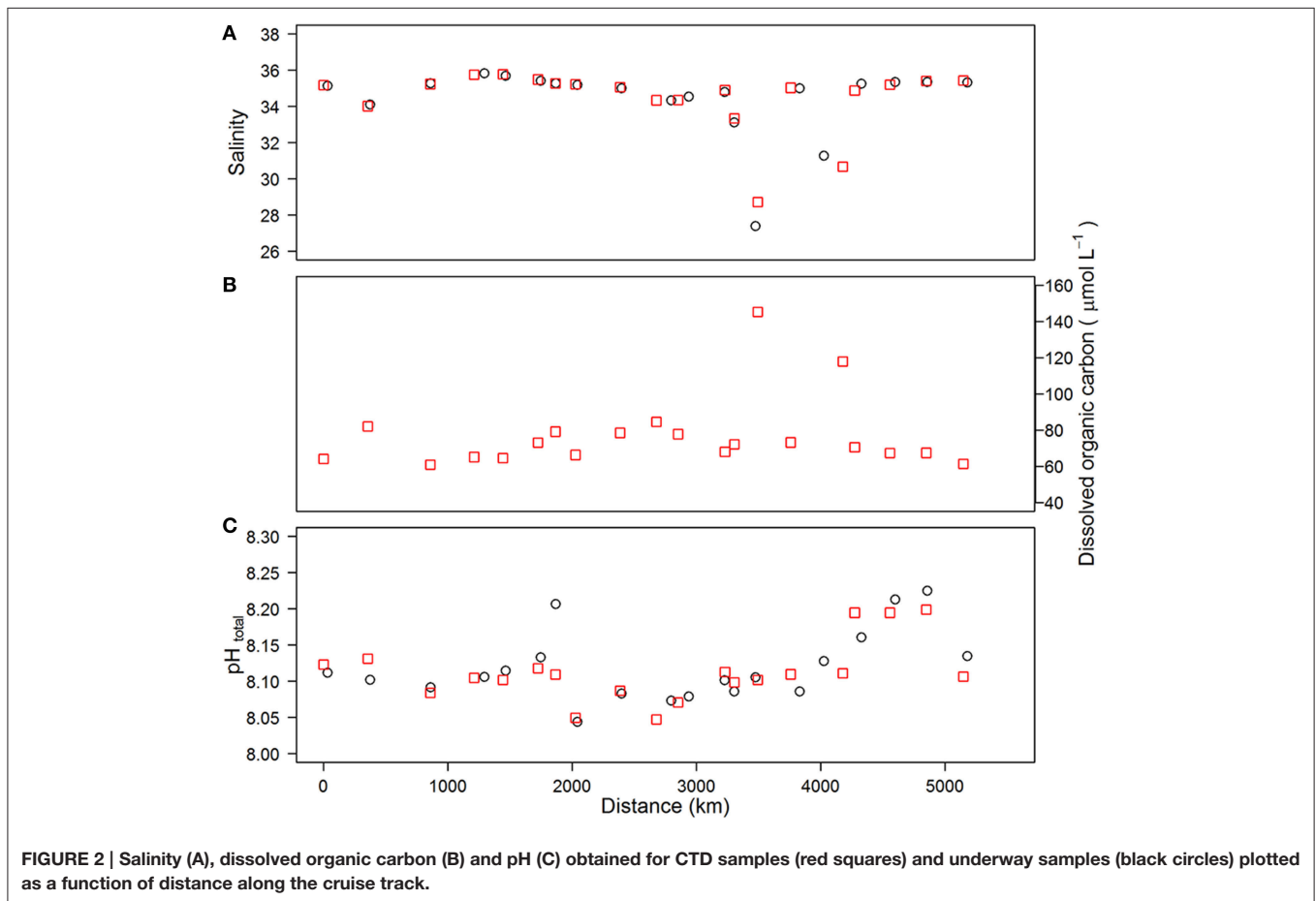
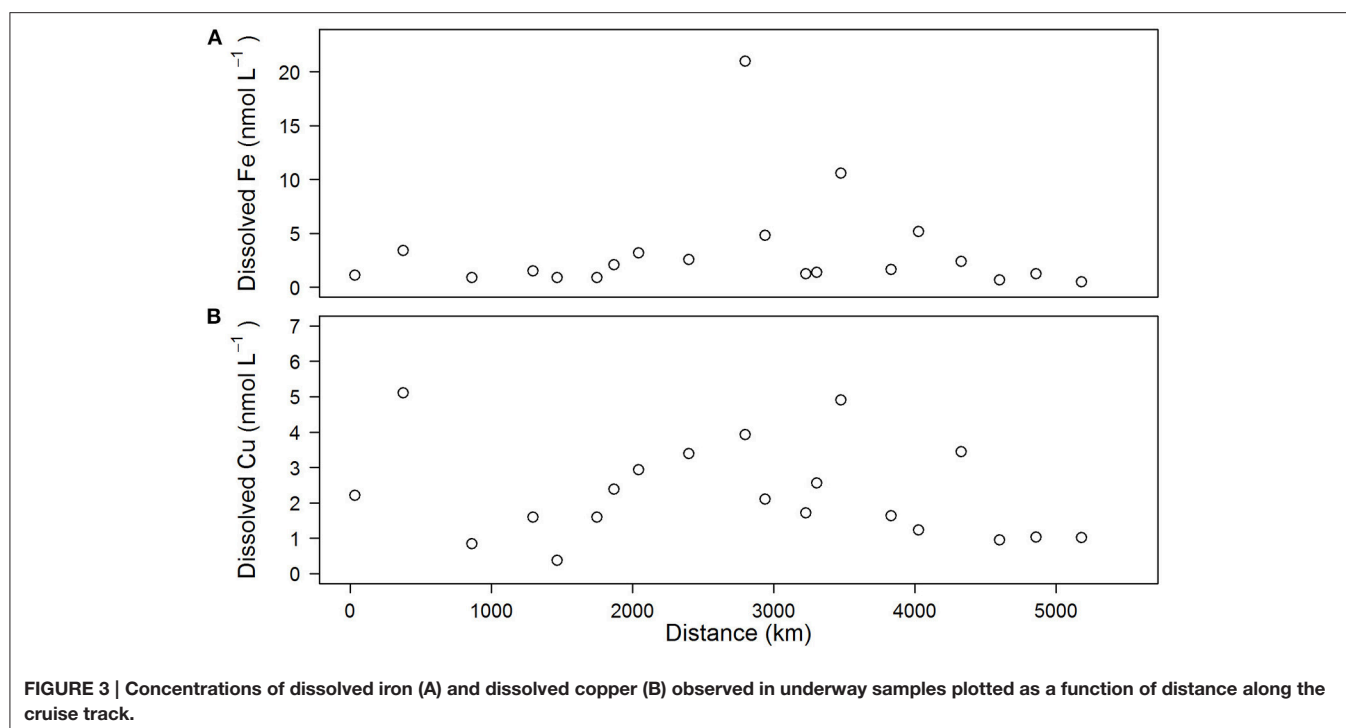


FIGURE 2 | Salinity (A), dissolved organic carbon (B) and pH (C) obtained for CTD samples (red squares) and underway samples (black circles) plotted as a function of distance along the cruise track.

hydrothermal samples (Hawkes et al., 2013). Results are only presented for titrations that produced a significant fit for $\log K_{MeL_i, Me}^{cond}$ and $L_{i, Me}$ at the 90% confidence level (i.e., $p < 0.1$). Thus, 13 out of 30 titrations were successfully fitted to the discrete ligand model for iron, whilst 16 out of 30 fits were successful for copper. In order to examine the potential cause for the fit failing, we assessed the impact of random error on a simulated titration similar to that observed for station 1. We randomly generated 2, 5, and 10% error on each titration point for 10

simulated titrations and then analyzed the resultant simulated titrations with the non-linear discrete ligand model. Our analysis, indicated that a random error of as little as 2% on each titration point would result in poor fits ($p > 0.1$) for the discrete ligand model in two out of five simulations using our metal addition regime, a random error of 5% resulted in $p > 0.1$ for 60% of the fits and a random error of 10% resulted in complete failure (i.e., no successful fits) of the discrete model approach.



Iron and Copper Binding Ligands [$L_{i,Fe}$], [$L_{i,Cu}$] and Stability Constants

Metal binding ligand concentrations [$L_{i,Me}$] determined using our detection windows in the surface waters of the Northwest European shelf seas for the range of pH_{NBS} 8.05–7.2 are given in Table S2 and shown in **Figure 4**. Iron binding ligand concentrations [$L_{i,Fe}$] at pH_{NBS} 8.05 averaged of 4.7 ± 2.0 nM ($n = 7$). At pH_{NBS} 7.6, [$L_{i,Fe}$] averaged 4.0 ± 0.8 nM ($n = 2$), and at pH 7.2, [$L_{i,Fe}$] averaged 2.6 ± 0.8 nM ($n = 3$), excluding station 10, where a value of 22.6 nM was observed. There was no apparent trend of [$L_{i,Fe}$] with pH.

Copper-binding ligand concentrations [$L_{i,Cu}$] at pH_{NBS} 8.05 averaged 3.4 ± 1.3 nM ($n = 3$). At pH 7.6, [$L_{i,Cu}$] averaged 6.0 ± 3.3 nM ($n = 7$), and at pH_{NBS} 7.2, [$L_{i,Cu}$] averaged 6.0 ± 3.6 nM ($n = 6$). As in the case of iron, there was no trend in [$L_{i,Cu}$] with the decline of pH_{NBS} from 8.05 to 7.2 (**Figure 4B**). Results for $\log K_{FeL_i,Fe'}^{cond}$ obtained in this study are shown in **Figure 4C**, Table S2. $\log K_{FeL_i,Fe'}^{cond}$ increased with decreasing pH, from approximately 11.2 at pH_{NBS} 8.05, to 11.7 at pH_{NBS} 7.6 and 13.1 at pH_{NBS} 7.2. In contrast $\log K_{CuL_i,Cu'}^{cond}$ did not show a trend with a decrease in pH (**Figure 4D**, Table S2).

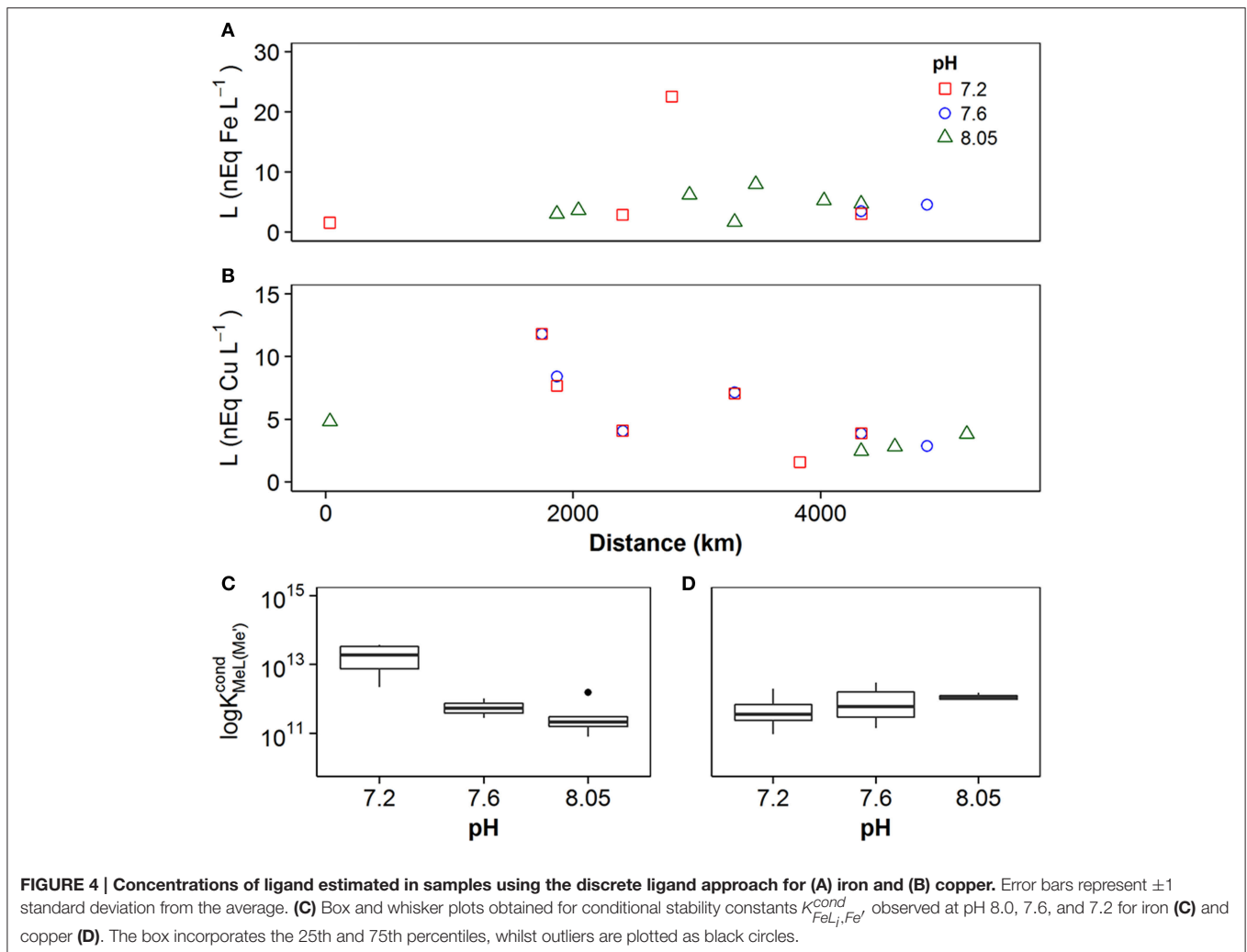
NICA-Donnan Modeling of Iron and Copper Complexation

Selection of NICA-Donnan parameters

The addition of HNN and H_2SA to vMINTEQ allowed the concentrations of $FeNN_3$ and $\Sigma Cu(HSA)_x$ to be calculated as a function of NICA-Donnan binding by DOC. Our study region covered a wide range of dissolved iron concentrations, with particularly elevated concentrations in the North Sea, as also

observed previously (Gledhill et al., 1998). At such high iron concentrations, it is likely that some of the iron measured as dissolved iron, would be present in an inert, potentially colloidal fraction (Gledhill and Buck, 2012; Hawkes et al., 2013; Von Der Heyden and Roychoudhury, 2015). **Figure 5** shows the impact of accounting for the presence of an inert phase that is in selective disequilibrium with HNN, for three titrations on samples 3, 10, and 14, which were determined to have very different dFe concentrations (0.9, 21, and 10.6 respectively). Our titration data showed that measured $FeNN_3$ did not depend greatly on the concentration of dFe originally present in the sample, as illustrated in **Figure 5A**. These results suggest that only a fraction of the iron was actually in equilibrium with HNN (Gledhill and Buck, 2012). Calculating [$FeNN_3$] concentrations with the assumption that all dFe was in equilibrium with HNN, results in increased $FeNN_3$ when dFe concentrations are higher as observed in **Figure 5B**. However, when an inert fraction is calculated according to Equation (8), prior to calculating the equilibrium between the added ligand, Fe^{3+} , Fe' , and $Fe(NOCM)$ then we obtained a pattern more representative of our observations (**Figure 5C**). We used insoluble ferrihydrite as our inert fraction in this study, as increasing the strength of complexation parameters describing NOCM in an attempt to create an “inert” Fe fraction bound to NOCM resulted in a similar trend to **Figure 5B**, albeit with lower calculated $FeNN_3$ concentrations. Our observations could thus only be described by incorporation of a solid phase with kinetically inhibited dissolution into our model.

Plots of calculated $MeAL_x$ vs measured $MeAL_x$ produced after incorporation of an inert iron fraction using three different parameter sets are shown in **Figure 6**. We adopted an empirical



approach to model optimization, as this was a proof of concept study. Root mean squared errors obtained from comparison of measured vs. calculated data at each pH are presented in **Table 4**. For iron, parameters derived for our previous estuarine study (A) and by Hiemstra and Van Riemsdijk (2006) (B) resulted in an overestimation of $FeNN_3$ at lower pH values, although those derived by Hiemstra and Van Riemsdijk (2006) resulted in an improved fit as observed from lower RMSE (**Table 4**). Increasing the apparent strength of the more acidic fraction (FA1) by both reducing the non-ideality factor for FA1 to 0.26 and increasing the NICA constant to 3.6 improved the fit at lower pH (**Figure 6C**, **Table 4**). It should be noted here that we assumed the inert iron fraction was also inert to the change in temperature as it is commonly assumed that there is no impact on titration data from freezing (Buck et al., 2012). We assumed the inert fraction was also inert to the change in pH on the timescale of our titrations ($< \text{day}$) as incorporating ferrihydrite precipitation at the pH of the titration resulted in an increased RMSE for iron at pH 7.6 and pH 7.8 (results not shown) and thus a pH trend inconsistent with observed results. For

copper, parameters derived for our estuarine study (A) resulted in a better approximation of $\Sigma Cu(HSA)_x$ with no pH bias in RMSE, although $\Sigma Cu(HSA)_x$ was consistently underestimated (**Figure 6**). Set A was, however, an improvement on the generic parameters (Milne et al., 2003; Set B, **Table 3**) and a further decrease in $\log K_{FA2(Cu)}$ and n_{FA2Cu} resulted in an improved fit of the calculated to the measured $\Sigma Cu(HSA)_x$ concentrations (**Figure 6C**).

In order to understand the potential impact of the different NICA-Donnan model parameters on conditional stability constants and ligand concentrations, we applied the discrete model approach to the simulated titration datasets. Results from the calculation of stability constants and ligand concentrations from the simulated titrations are shown in **Figure 7**. We compared $[L_{i,Me}]$ determined from our titrations ($L_{measured}$) with the apparent $[L_{i,Me}]$ determined from the simulated titrations ($L_{NICA-Donnan}$) (**Figures 7A,B**), and we plotted the average of the conditional stability constants for each pH and for the three different model parameter sets in **Figures 7C,D**. For iron, $\log K_{FeLi,Fe'}^{cond}$ and $L_{i,Fe}$ obtained from simulated data agreed quite

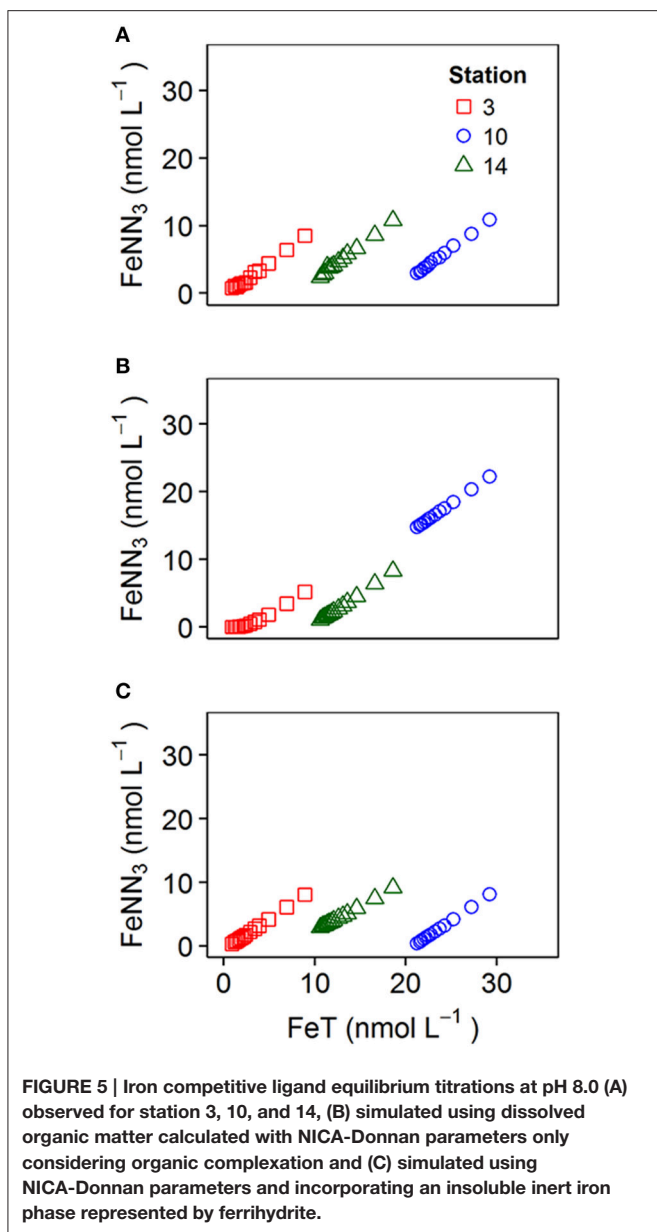


FIGURE 5 | Iron competitive ligand equilibrium titrations at pH 8.0 (A) observed for station 3, 10, and 14, (B) simulated using dissolved organic matter calculated with NICA-Donnan parameters only considering organic complexation and (C) simulated using NICA-Donnan parameters and incorporating an insoluble inert iron phase represented by ferrihydrite.

well with that obtained from the real titrations. Correlation coefficients between $L_{NICA-Donnan}$ and $L_{measured}$ were > 0.95 for all three parameter sets for iron. For copper, $\log K_{CuLi,Cu'}^{cond}$ obtained for the simulated titrations were within the range of those obtained for real samples (Figure 7D), but ligand concentrations did not agree well for any of the applied parameter sets (Figure 7B).

Application of the NICA-Donnan Model to the Prediction of the Impact of Increasing pCO_2 on Iron and Copper Complexation

Increasing pCO_2 from 280 to 400, 900, and 1900 μatm resulted in decreases in pH of 0.13, 0.45, and 0.75 pH units respectively, while the concentration of carbonate ions decreased to 78, 42, and

TABLE 4 | RMSE (nmol L⁻¹) obtained on comparison of measured $MeAL_x$ concentrations with calculated $MeAL_x$ concentrations obtained using vMINTeq.

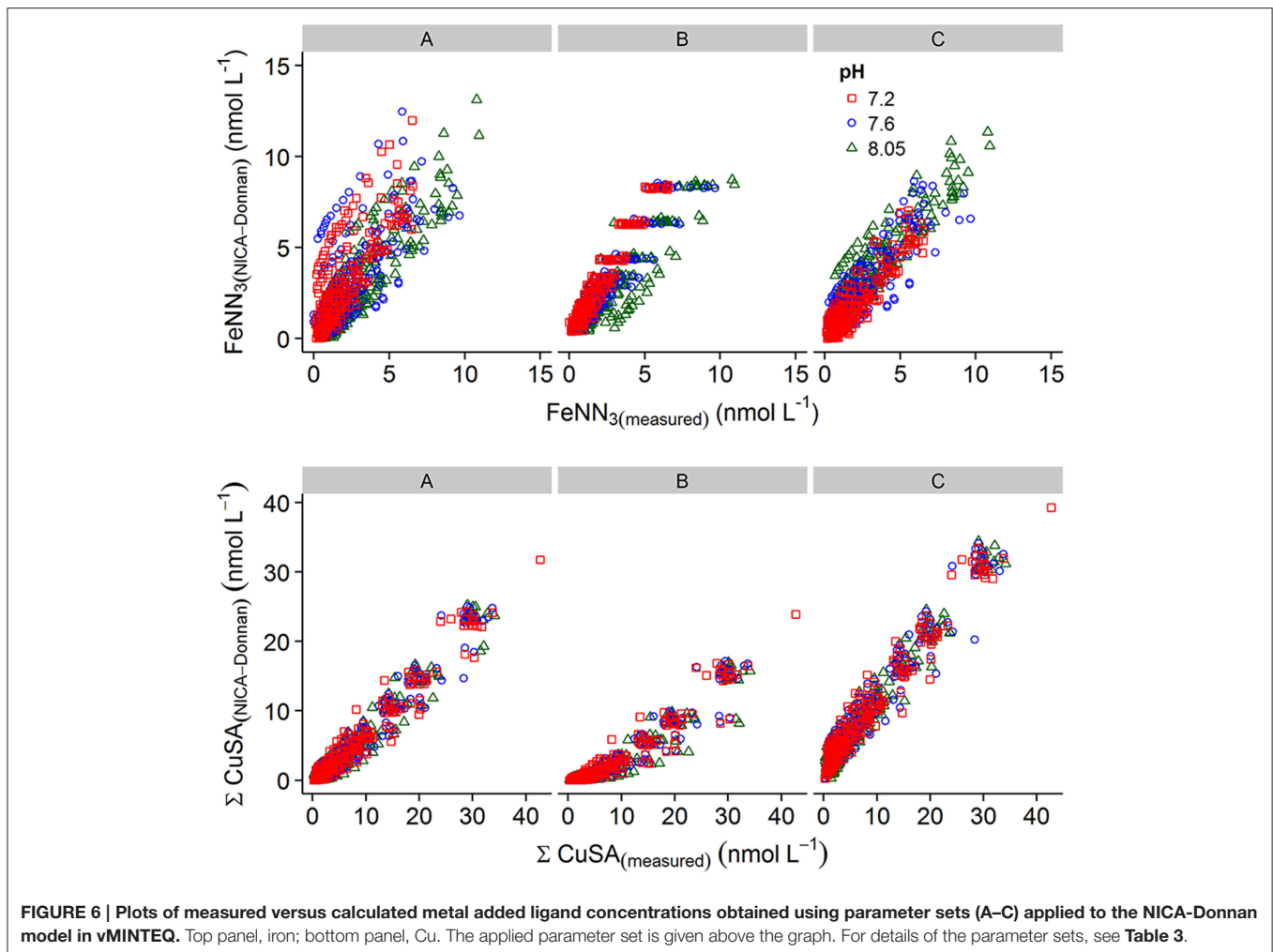
Parameter Set	pH	Iron	Copper
A	8.05	1.2	3.88
	7.6	1.9	3.55
	7.2	1.8	3.55
B	8.05	0.9	7.2
	7.6	1.0	6.8
	7.2	1.2	6.7
C	8.05	1.1	2.1
	7.6	1.0	2.4
	7.2	0.7	2.4

22% of preindustrial levels respectively. The projected changes in these inorganic major ions would thus be expected to have an impact on both iron and copper speciation. Results obtained from calculation of the speciation of iron and copper in our shelf sea samples at decreased pH and CO_3^{2-} ion concentrations are presented in Figures 8, 9. Figure 8 shows the proportion of metal bound to fulvic acid analogs (“Bound”), the inert fraction (“Inert”—for iron only) and present as simple inorganic ion pairs or as the free metal (“Inorganic”), while Figure 9 shows the changes in inorganic iron (pFe') and free Cu^{2+} (pCu^{2+}) in more detail. Iron was present mainly in the bound fraction, with the inert fraction becoming important at iron concentrations greater than ca. 4–5 nM, (depending on the concentration of DOC) at $pCO_2 < 400 \mu atm$. When modeled as inorganic ferric hydroxides, the inert fraction was reduced by increases in pCO_2 , so that at pCO_2 levels of 1900 μatm , bound iron reached concentrations as high as ca. 10.9 nM at Station 10. In this study, we observed that the concentration of the biologically available inorganic iron decreased (i.e., pFe' increased since it is the negative log of the inorganic iron concentration, Figure 9A) with increasing pCO_2 . However, this trend was reversed when iron concentrations were high enough to result in the formation of an inert fraction (i.e., when the solubility of Fe' was exceeded, and ferrihydrite was formed).

Copper was predominantly present bound to DOM (71–95%, Figure 8). Free Cu^{2+} concentrations were calculated to vary between ca. 10^{-12} and 10^{-10} nM, with increasing pCO_2 resulting in increased free Cu^{2+} concentrations (Figure 9B), as reported previously (Gledhill et al., 2015).

DISCUSSION

In this study we have undertaken the most comprehensive investigation to date into changes in the speciation of the trace metals iron and copper that result from changes in pH. We interpreted measurements of metal speciation using CLE-AdCSV with the discrete ligand approach and a NICA-Donnan modeling approach. We applied two data interpretation approaches in this study, but there are further approaches that have been applied to trace metal complexation in the marine environment including



those described in Pizeta et al. (2015), WHAM VII (Stockdale et al., 2011, 2015) and the Stockholm Humic Model (Gustafsson, 2001; Ndungu, 2012). In our discussion, we will first examine the changes in $\log K_{MeLi,Me'}^{cond}$ and $L_{i,Me}$ concentrations with pH obtained with the discrete ligand approach. We then assess the potential of the NICA-Donnan model as an alternative method for the interpretation of CLE titrations. Finally, we illustrate the potential utility of the NICA-Donnan approach through an investigation of the potential effects of an increase in pCO_2 on the iron and copper speciation in our shelf sea samples.

The Single Detection Window Discrete Ligand Approach

The discrete ligand approach allowed us to identify an increase in conditional stabilities for iron natural ligand complexes of the order of 1.9 log units with a decrease in pH from 8.05 to 7.2 (Figure 4), similar to that observed previously by Gledhill et al. (2015) who observed an increase of 2 log units with a decrease in pH from 8.3 to 6.8. This increase in $\log K_{FeLi,Fe'}^{cond}$ with a decrease in pH provides further evidence for the dependence

of iron binding on the pH of seawater and suggests that in a more acidic ocean, ligand strengths are likely to increase relative to the strength of inorganic complexation, largely as a result of decreases in the concentration of hydroxide ions. Although the relative trend with pH was similar to previous observations, conditional stabilities for iron detected in this study were slightly stronger than those observed in the previous estuarine study, especially at lower pH. This could relate to real changes in binding site characteristics as DOM is transported offshore and aged. On the other hand, the experimental results on which the estuarine model was based were acknowledged to be less reliable below pH 8 as the detection window was not optimal (Gledhill et al., 2015). In this study, we adjusted the concentration of the added ligand HNN (from $2 \mu\text{mol L}^{-1}$ used in Gledhill et al. (2015) to $1 \mu\text{mol L}^{-1}$ in this study) in order to lower our detection window and thereby improve the reliability of estimates obtained with the discrete ligand approach at lower pH. The increase in the conditional stabilities observed at low pH could thus be related to a reduction in systematic errors associated with fitting the discrete ligand model resulting from improved detection window selection. Nevertheless, it was a notable feature of our study that

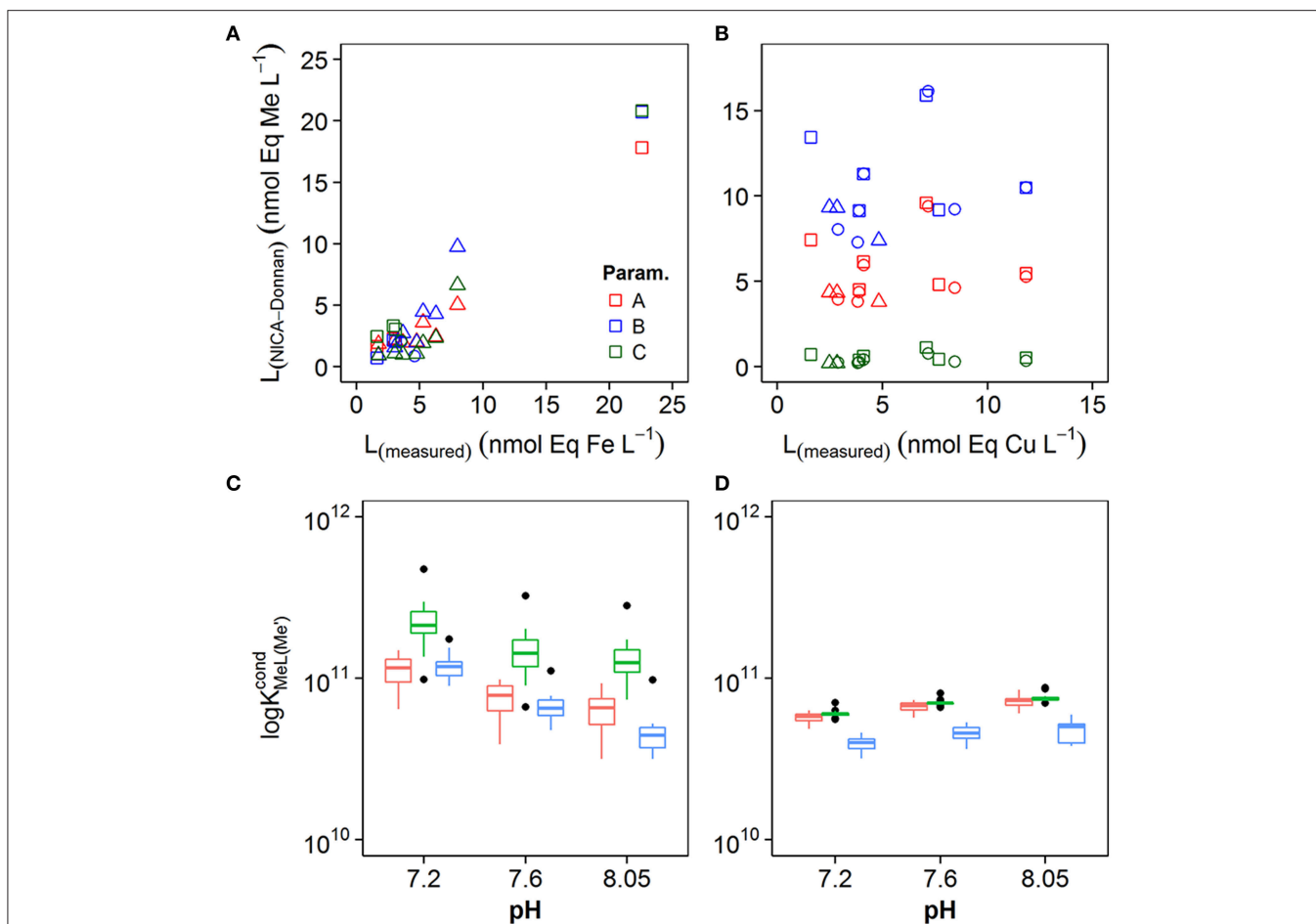


FIGURE 7 | Comparison of ligand concentrations estimated from measured $MeAL_x$ ($L_{(measured)}$) with ligand concentrations estimated from calculated $MeAL_x$ ($L_{(NICA-Donnan)}$) for (A) iron and (B) copper. (C) Box and whisker plots obtained for conditional stability constants $K_{FeL_i, Fe'}^{cond}$ from calculated $MeAL_x$ concentrations at pH 8.0, 7.6, and 7.2 for iron (C) and copper (D). The box incorporates the 25th and 75th percentiles, whilst outliers are plotted as black diamonds. The parameter sets used to obtain $MeAL_x$ are represented by the different colors (see legend).

the non-linear fit used for the discrete ligand approach was not significant at the 90% confidence level for many of our CLE-AdCSV titrations. A simple randomized error experiment on a simulated titration suggested that incurring a random error of 5% on each titration point would result in successful fit for only 4 out of 10 titrations. (i.e., if the titration was repeated on the same sample 10 times, only 4 of the resultant datasets would predict $\log K_{FeL_i, Fe'}^{cond}$ or $L_{i, Fe}$ with >90% confidence), which is close to the number of titrations that returned $\log K_{FeL_i, Fe'}^{cond}$ and $L_{i, Fe}$ for our dataset. We chose HNN as the added ligand because it is possible to determine iron over a relatively wide pH range, however undoubtedly the level of random error incurred during our titrations was exacerbated by the use of an added ligand with relatively low sensitivity (ca. 0.8 nA nmol⁻¹), which resulted in low peak heights, even for concentrations of iron present in samples in this shelf sea study.

In the case of copper, no trend in $\log K_{CuL_i, Cu'}^{cond}$ was detected with decreasing pH (Figure 4). This is in contrast to the previous estuarine study where a decrease of 0.7 units from pH 8.0 to

7.2 was observed. Similarly, we did not observe any changes in $L_{i, Cu}$ with a decrease in pH, unlike the small decrease observed in Gledhill et al. (2015). Although, the number of titrations that returned $\log K_{CuL_i, Cu'}^{cond}$ and $L_{i, Cu}$ for our copper dataset was higher than those for iron, the use of a high detection window (10 μM SA) affected our ability to detect any significant changes in ligand stabilities outside our selected window. A high detection window also likely affected our ability to obtain good titration fits for all our samples. $L_{i, Cu}$ increased with dissolved copper concentrations and samples with the highest observed $L_{i, Cu}$ were situated very close to the UK coastline (Station 7 and 8, Figure 1, Table S1).

The NICA-Donnan Approach

The addition of the added ligands to the thermodynamic database in vMINTeq allowed us to calculate the concentrations of $MeAL_x$ and thus directly compare them to those determined by CLE-AdCSV. This approach thus represents an alternative for interpreting CLE experiments. The approach is more robust, in

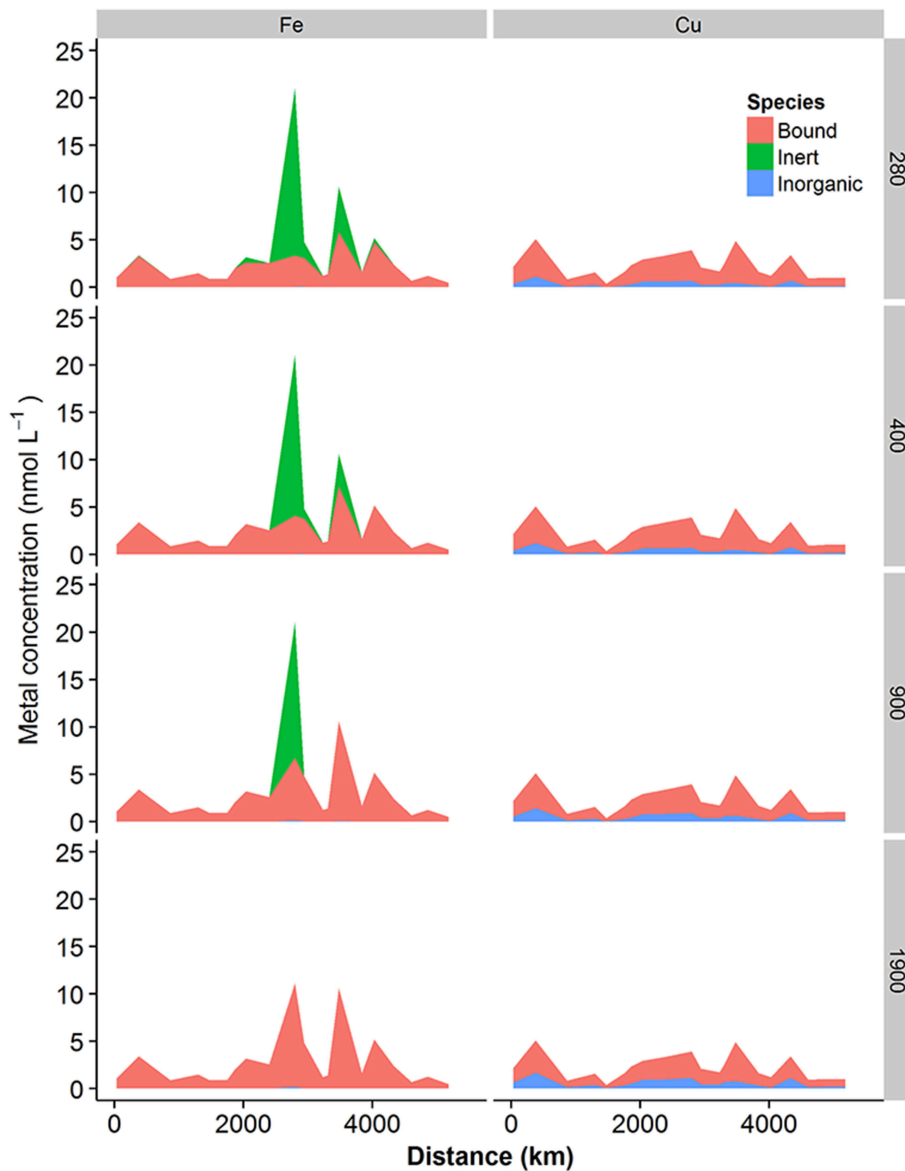


FIGURE 8 | Concentrations of metal complexed with DOM (bound), inert (ferrihydrate, iron only) or labile inorganic complexes (OH^- , CO_3^{2-} , etc) calculated for increasing concentrations of atmospheric CO_2 . Iron speciation is presented in the left column and copper speciation in the right column. $p\text{CO}_2$ Applied to the model is indicated to the right of the figure.

that the complete dataset could be used to optimize the model parameters. Furthermore, the software could be used to account for inert components as well as binding with DOM to give a more complete picture of metal speciation. The approach thereby overcomes some of the bias introduced by a single detection window approach (Gledhill and Buck, 2012; Pizeta et al., 2015). Our approach in this study was empirical, and further rigor could be achieved with a statistically sound optimization of the results, once basic parameters such as the number and acidity of marine DOM binding sites were known with greater certainty (e.g., Weber et al., 2006). We found that incorporation of an inert phase was required in order to calculate $\text{Fe}(\text{NN})_3$

concentrations to within an order of magnitude of measured $\text{Fe}(\text{NN})_3$ concentrations in samples with high dissolved iron (Figure 5). We examined the addition of a “strong organic fraction” as an inert phase, but this resulted in an overall reduction in calculated $\text{Fe}(\text{NN})_3$ concentration when binding sites were under saturated, followed by large increases in $\text{Fe}(\text{NN})_3$ when binding sites were saturated. This pattern of behavior did not fit the measured $\text{Fe}(\text{NN})_3$ concentrations, which were low for titration points with zero added iron even for stations 10 and 14 where initial $d\text{Fe}$ concentrations were 21.0 and 10.6 nM, respectively. We therefore assumed an inert phase for iron with kinetically inhibited dissolution and which was thus

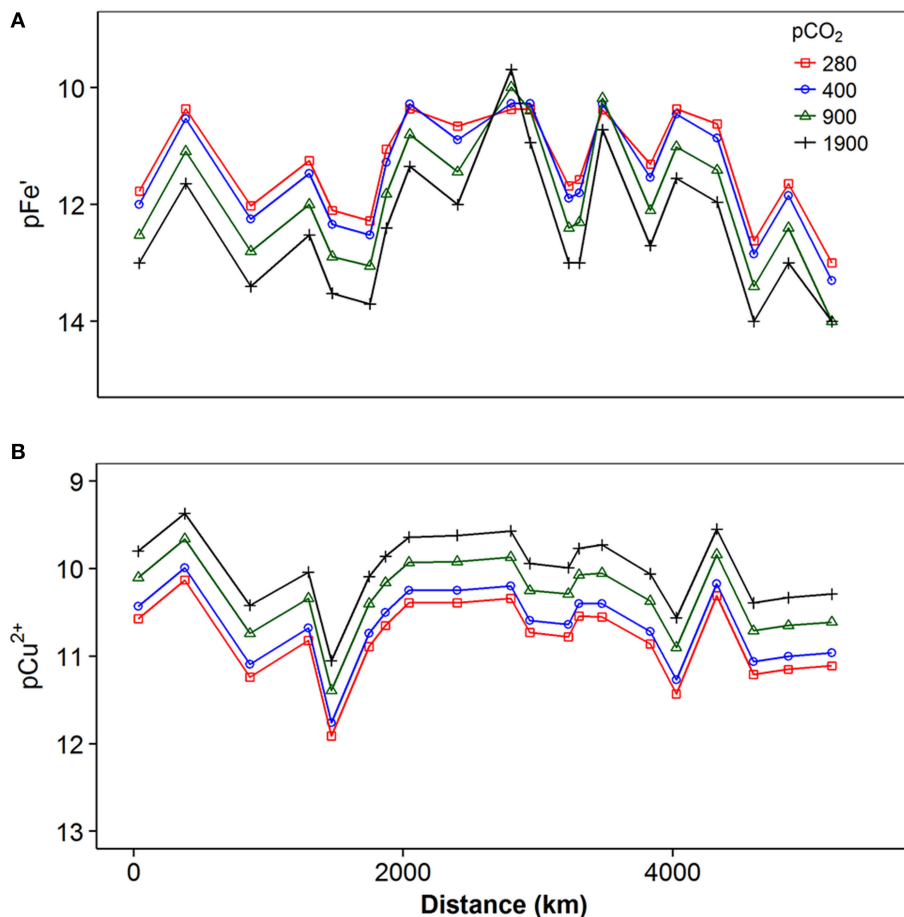


FIGURE 9 | Concentration of (A) inorganic iron expressed as pFe' ($-\log[Fe']$) and (B) free copper expressed as pCu^{2+} ($-\log[Cu^{2+}]$) calculated for different pCO_2 levels from preindustrial (280 μatm) to approximately five times current values (1900 μatm).

represented through incorporation of ferrihydrite as a possible solid. Inclusion of such an inert phase would be consistent with previous studies showing that natural colloidal iron phases are unavailable for biological uptake over timescales of days (Kuma and Matsunaga, 1995; Chen and Wang, 2001). Although, observed $Fe(NN)_3$ concentrations were better represented using ferrihydrite, this approach is likely an oversimplification of the true situation. Initial calculation of $Fe(NN)_3$ allowed the inert phase to equilibrate to the titration pH. These initial calculations resulted in increased RMSE at lower pH (results not shown), and suggested that the inert fraction did not respond as iron oxyhydroxides would, if allowed to reach equilibrium. This lack of apparent response of the inert phase to changing pH could result from either inappropriate description of the inert phase (i.e., it is not ferrihydrite) or inappropriate experimental design (e.g., insufficient equilibration time) or both. As the inert phase did not react with our added metal, pH or our added ligand (at the applied detection window) it was difficult to infer any further information with respect to its solubility or nature from the experiments undertaken in this study. Other studies have shown that increasing the added ligand concentration can result

in the determination of higher $Fe(NN)_3$ concentrations (Hawkes et al., 2013), suggesting that NN may react with this fraction of iron at higher detection windows. It is therefore possible that the inert phase might more closely approximate a colloidal fraction of mixed organic and inorganic composition, rather than one consisting of ferrihydrite. Nevertheless, in the absence of studies that more explicitly address the chemical character of this inert phase and its solubility, we continued to use ferrihydrite as a first approximation of the inert phase.

Having settled upon our analog for the inert iron phase, further work allowed for the reduction of the RMSE between measured and calculated concentrations of $Fe(NN)_3$. The parameters derived in our estuarine study were found to be too strong in this respect, while those derived by Hiemstra and Van Riemsdijk (2006) too weak at low pH. We achieved our lowest RMSE with a parameter set closely resembling that of Hiemstra and Van Riemsdijk (2006), but with slightly stronger complexation at lower pH.

For copper, we did not require an inert phase in order to describe our measured $\Sigma Cu(HSA)_2$ concentrations, consistent with current knowledge of copper solubility in seawater.

However, the $\Sigma\text{Cu}(\text{HSA})_2$ calculated for our measured data from the internal slope obtained during the CLE-AdCSV measurements were very close to the total dissolved copper concentration. Clearly an H_2SA concentration of $10\ \mu\text{mol L}^{-1}$ was sufficient to outcompete most of the natural binding sites present in the samples. Although, this was unfortunate, and explains the difficulties observed when applying the discrete ligand approach (poor significance of the fits) it did place an upper constraint on the strength of the binding sites in these shelf sea waters.

We applied the discrete ligand approach to the calculated concentrations of MeAL_x in an effort to compare the two methods. Stability constants and ligand concentrations were in good agreement with those determined from measured MeAL_x for iron, suggesting that our NICA-Donnan parameters could reproduce the observed trends in iron complexation. However, for copper, although stability constants were similar, the variability observed in $L_{i,\text{Cu}}(\text{measured})$ was not observed in apparent $L_{i,\text{Cu}}(\text{NICA-Donnan})$. As mentioned in Section The Discrete Ligand Approach above, a trend of increasing concentrations of $L_{i,\text{Cu}}(\text{NICA-Donnan})$ with increasing dissolved Cu concentrations was observed, with highest concentrations at stations 7 and 8. Stations 7 and 8 were situated in close proximity to the UK coast and also returned low conditional stability constants ($\log K_{\text{CuL}_i,\text{Cu}'}^{\text{cond}} = 11.0 - 11.4$) when compared to other samples in the shelf waters (Table S2). Thus, it could be that the DOM in this region of the study area had a more “terrestrial” character. In support of this, parameter sets A and B which were derived for estuarine and terrestrial DOM respectively (Milne et al., 2003; Gledhill et al., 2015) also resulted in higher ligand concentrations when applying the discrete ligand approach to calculated MeAL_x concentrations (Figure 7). Alternatively, it is also possible that the application of the discrete ligand approach to the measurements on samples 7 and 8 resulted in an incorrect “local minima” in the fitting routine that underestimated $\log K_{\text{CuL}_i,\text{Cu}'}^{\text{cond}}$ and overestimated $L_{i,\text{Cu}}(\text{measured})$. This potential issue was not restricted to the Gerringa et al. (2014) routine applied here, as the same results were obtained for other available routines (e.g., ProMCC, results not shown; Pizeta et al., 2015). Such results highlight the care that needs to be applied when assessing data produced by the discrete ligand approach, especially when applying only one, potentially non-optimal detection window. In this respect, we found the NICA-Donnan approach a more robust method for interpreting CLE-AdCSV titrations.

The overall reduction in RMSE observed for parameter set C suggested that these parameters better described the whole dataset than either Set A or B. It should be stressed however, that these parameters were empirically derived and thus do not represent a true optimization of the NICA-Donnan model for marine NOCM. Set C parameters resulted in RMSEs for MeAL_x concentrations of the same order as the measured MeAL_x concentrations determined at the lowest point of the titration curve (i.e., when no metal had been added). The final parameters selected to describe our coastal dataset were weaker than that derived for our estuarine study for both iron and copper and it is interesting to note that this trend was

observed for both metals. This could relate to a real change in binding characteristics as DOM is transported from the estuarine environment to shelf sea waters. Further, knowledge of the basic binding site characteristics of marine DOM from different environments could also potentially shed light on such changes (Muller and Bleie, 2008; Louis et al., 2009). However, it is also possible that application of the NICA-Donnan model to the interpretation of metal complexation in seawater would benefit from a changed experimental design. In particular, it would be useful to determine binding characteristics at different detection windows as well as at varying pH. This study therefore supports recent work that suggests there is likely to be much to gain from employing a combination of titration techniques (Pizeta et al., 2015) with varied detection windows.

Potential Effect of Changes in pCO_2 on Iron and Copper Speciation in Coastal Waters

The increased iron binding strength of the acidic type binding sites in the NICA-Donnan parameter set developed in this study resulted in a reverse of the trend observed previously for estuarine waters (Gledhill et al., 2015). In our shelf sea waters Fe' concentrations decreased with increasing pCO_2 because binding with NOCM was stronger than ion pair interactions with hydroxides. As the NICA-Donnan parameterization of marine DOM is still in its infancy, this result must be treated with some caution. However, when both estuarine and shelf sea water studies are considered together, they do suggest that small changes in the strengths of binding sites on marine DOM can bring quite dramatic reversals in iron speciation trends with pH. Iron binding with DOM thus appears to be finely balanced at natural seawater pH. The trend for decreasing Fe' was reversed when Fe' concentrations reached saturation and ferrihydrite precipitated (e.g., stations 10 and 14), so that at high iron concentrations, Fe' concentrations increased with increasing pCO_2 because the increased solubility of ferrihydrite at lower pH had a larger overall effect on Fe' concentrations than the decrease resulting from complexation by DOM. This could result in similar potential effect on dFe as that observed by Breitbarth et al. (2010). However, this increase in Fe' resulted from the use of ferrihydrite as the analog for the inert iron fraction, which as mentioned in Section The NICA-Donnan Approach, may not be entirely representative. Our results for copper were generally consistent with those observed in the previous estuarine study, even though a small refinement of the parameters defining copper binding to DOM was necessary. Thus, increased pCO_2 generally results in increased pCu^{2+} as a result of decreased CO_3^{2-} ion concentrations.

Carbonate ion concentration, pH, DOC and the concentrations of iron and copper varied significantly over the course of our cruise track. In addition, temperature, salinity and dissolved oxygen concentrations (Poulton et al., 2014) also varied. All of these parameters will affect metal speciation and it is beyond the scope of the present study to address the influence of the latter variables. Nevertheless, interpretation of metal speciation measurements using the NICA-Donnan or other NOCM models such as WHAM or the Stockholm Humic

model (Ndungu, 2012; Stockdale et al., 2015) could allow for the development of a more comprehensive understanding of the interactive influence of all of these parameters on metal speciation and thus greater understanding of the link between productivity and metal biogeochemistry. For example, the highest pH values were observed in the Atlantic and Northern North Sea sectors of the cruise, but these high pH values did not clearly influence concentrations of $p\text{Fe}'$ or $p\text{Cu}^{2+}$ because the variability in dissolved iron and copper concentrations had an overriding impact on the distribution of the metal species.

Nevertheless, increased $p\text{CO}_2$ resulted in changes in pH and $[\text{CO}_3^{2-}]$ which were ca. 4x times greater in magnitude than the changes observed over the cruise track. When DOM binding sites were unsaturated, this resulted in an order of magnitude decrease in $p\text{Fe}'$ and an order of magnitude increase in $p\text{Cu}^{2+}$. This compared to a change in calculated $p\text{Fe}'$ of 3 orders of magnitude and in calculated $p\text{Cu}^{2+}$ of approximately 2 orders of magnitude over the course of our cruise track, for a $p\text{CO}_2$ of 400 μatm . Thus, as suggested previously (Gledhill et al., 2015), the natural variability in $p\text{Fe}'$ and $p\text{Cu}^{2+}$ resulting from changes in DOC and metal concentration observed in shelf sea waters is higher than the change likely to result from increasing atmospheric $p\text{CO}_2$. Nevertheless, our results suggest that increased $p\text{CO}_2$ imposes a consistent chronic change in iron and copper speciation that has the potential to result in further added stress to marine microbial communities. Thus, further decreases in $p\text{Fe}'$ is likely to have a biological effect when dissolved iron concentrations are low. Should open ocean iron complexation be similarly dependent on pH, microbial communities in HNLC waters will experience lower $p\text{Fe}'$ in the future than is currently the case. Likewise increases in $p\text{Cu}^{2+}$ will have the greatest impact when dissolved copper concentrations are high and microbial communities in contaminated coastal regions will potentially experience further increases in the toxic $p\text{Cu}^{2+}$ species as atmospheric CO_2 concentrations rise.

REFERENCES

- Achterberg, E. P., Holland, T. W., Bowie, A. R., Fauzi, R., Mantoura, C., and Worsfold, P. J. (2001). Determination of iron in seawater. *Anal. Chim. Acta* 442, 1–14. doi: 10.1016/S0003-2670(01)01091-1
- Annett, A. L., Lapi, S., Ruth, T. J., and Maldonado, M. T. (2008). The effects of Cu and Fe availability on the growth and Cu : C ratios of marine diatoms. *Limnol. Oceanogr.* 53, 2451–2461. doi: 10.4319/lo.2008.53.6.2451
- Badr, E. S. A., Achterberg, E. P., Tappin, A. D., Hill, S. J., and Braungardt, C. B. (2003). Determination of dissolved organic nitrogen in natural waters using high-temperature catalytic oxidation. *Trends Anal. Chem.* 22, 819–827. doi: 10.1016/S0165-9936(03)01202-0
- Batchelli, S., Muller, F. L. L., Chang, K. C., and Lee, C. L. (2010). Evidence for strong but dynamic iron-humic colloidal associations in humic-rich coastal waters. *Environ. Sci. Technol.* 44, 8485–8490. doi: 10.1021/es101081c
- Benedetti, M. F., Van Riemsdijk, W. H., Koopal, L. K., Kinniburgh, D. G., Goody, D. C., and Milne, C. J. (1996). Metal ion binding by natural organic matter: from the model to the field. *Geochim. Cosmochim. Acta* 60, 2503–2513. doi: 10.1016/0016-7037(96)00113-5
- Boyd, P. W., Jickells, T., Law, C. S., Blain, S., Boyle, E. A., Buesseler, K. O., et al. (2007). Mesoscale iron enrichment experiments 1993–2005: synthesis and future directions. *Science* 315, 612–617. doi: 10.1126/science.1131669

AUTHOR CONTRIBUTIONS

LA carried out the CLE-AdCSV titrations, interpreted the data and wrote the manuscript, MG modeled the results, interpreted the data and also wrote the manuscript, EA designed the study, interpreted the data and contributed to the manuscript, VR measured pH, interpreted the data and contributed to the manuscript, CS measured trace metals, interpreted the data and contributed to the manuscript.

ACKNOWLEDGMENTS

The authors gratefully acknowledge the reviewers for their constructive comments on the manuscript. The authors would like to thank the crew and scientists of the RRS *Discovery* for their assistance during the cruise, P. Lodeiro for his advice on the NICA-Donnan model and R.J.A. Rijkenberg for his help with the discrete ligand fitting routine in R. LA was funded through a CONACYT (Consejo Nacional de Ciencia y Tecnología) scholarship from the Mexican Government (Award number 179623). This work is a contribution to the UK Ocean Acidification Research Programme (UKOA), which was jointly funded by the Department for Environment, Food and Rural Affairs (DEFRA), the Natural Environment Research Council (NERC) and the Department for Energy and Climate Change (DECC) under grant agreement no. NE/H017348/1. Additional funding for modeling was provided by GEOMAR - Helmholtz Centre for Ocean Research.

SUPPLEMENTARY MATERIAL

The Supplementary Material for this article can be found online at: <http://journal.frontiersin.org/article/10.3389/fmars.2016.00058>

- Boye, M., Nishioka, J., Croot, P. L., Laan, P., Timmermans, K. R., and De Baar, H. J. W. (2005). Major deviations of iron complexation during 22 days of a mesoscale iron enrichment in the open Southern Ocean. *Mar. Chem.* 96, 257–271. doi: 10.1016/j.marchem.2005.02.002
- Brand, L. E., Sunda, W. G., and Guillard, R. R. L. (1986). Reduction of marine-phytoplankton reproduction rates by copper and cadmium. *J. Exp. Mar. Biol. Ecol.* 96, 225–250. doi: 10.1016/0022-0981(86)90205-4
- Breitbarth, E., Bellerby, R. G., Neill, C., Ardelan, M. V., Meyerhofer, M., Zollner, E., et al. (2010). Ocean acidification affects iron speciation during a coastal seawater mesocosm experiment. *Biogeosciences* 7, 1065–1073. doi: 10.5194/bg-7-1065-2010
- Brewer, P. G. (1997). Ocean chemistry of the fossil fuel CO_2 signal: the haline signal of “business as usual”. *Geophys. Res. Lett.* 24, 1367–1369. doi: 10.1029/97GL01179
- Buck, K. N., Moffett, J., Barbeau, K. A., Bundy, R. M., Kondo, Y., and Wu, J. (2012). The organic complexation of iron and copper: an intercomparison of competitive ligand exchange-adsorptive cathodic stripping voltammetry (CLE-ACSV) techniques. *Limnol. Oceanogr. Methods* 10, 496–515. doi: 10.4319/lom.2012.10.496
- Byrne, R. H. (2002). Inorganic speciation of dissolved elements in seawater: the influence of pH on concentration ratios. *Geochem. Trans.* 3, 11–16. doi: 10.1186/1467-4866-3-11

- Byrne, R. H., Kump, L. R., and Cantrell, K. J. (1988). The influence of temperature and pH on trace-metal speciation in seawater. *Mar. Chem.* 25, 163–181. doi: 10.1016/0304-4203(88)90062-X
- Caldeira, K., and Wickett, M. E. (2003). Anthropogenic carbon and ocean pH. *Nature* 425, 365–365. doi: 10.1038/425365a
- Campos, M. L. A. M., and van den Berg, C. M. G. (1994). Determination of copper complexation in sea water by cathodic stripping voltammetry and ligand competition with salicylaldehyde. *Anal. Chim. Acta* 284, 481–496. doi: 10.1016/0003-2670(94)85055-0
- Chen, M., and Wang, W. X. (2001). Bioavailability of natural colloid-bound iron to marine plankton: influences of colloidal size and aging. *Limnol. Oceanogr.* 46, 1956–1967. doi: 10.4319/lo.2001.46.8.1956
- Clayton, T. D., and Byrne, R. H. (1993). Spectrophotometric seawater pH measurements - total hydrogen-ion concentration scale calibration of m-cresol purple and at-sea results. *Deep Sea Res. I Oceanogr. Res. Papers* 40, 2115–2129. doi: 10.1016/0967-0637(93)90048-8
- Croot, P. L., Moffett, J. W., and Brand, L. E. (2000). Production of extracellular Cu complexing ligands by eucaryotic phytoplankton in response to Cu stress. *Limnol. Oceanogr.* 45, 619–627. doi: 10.4319/lo.2000.45.3.619
- De Baar, H. J. W., Gerringa, L. J. A., Laan, P., and Timmermans, K. R. (2008). Efficiency of carbon removal per added iron in ocean iron fertilization. *Marine Ecol. Progr. Ser.* 364, 269–282. doi: 10.3354/meps07548
- Doney, S. C. (2006). The dangers of ocean acidification. *Sci. Am.* 294, 58–65. doi: 10.1038/scientificamerican0306-58
- Dudal, Y., and Gérard, F. (2004). Accounting for natural organic matter in aqueous chemical equilibrium models: a review of the theories and applications. *Earth Sci. Rev.* 66, 199–216. doi: 10.1016/j.earscirev.2004.01.002
- Feely, R. A., Sabine, C. L., Lee, K., Berelson, W., Kleypas, J., Fabry, V. J., et al. (2004). Impact of anthropogenic CO₂ on the CaCO₃ system in the oceans. *Science* 305, 362–366. doi: 10.1126/science.1097329
- Foo, K. Y., and Hameed, B. H. (2010). Insights into the modeling of adsorption isotherm systems. *Chem. Eng. J.* 156, 2–10. doi: 10.1016/j.cej.2009.09.013
- Geider, R. J., and La Roche, J. (1994). The role of iron in phytoplankton photosynthesis, and the potential for iron-limitation of primary productivity in the sea. *Photosyn. Res.* 39, 275–301. doi: 10.1007/BF00014588
- Gerringa, L. J. A., Herman, P. M. J., and Poortvliet, T. C. W. (1995). Comparison of the linear van den Berg/Ruzic transformation and a non-linear fit of the Langmuir isotherm applied to Cu speciation data in the estuarine environment. *Mar. Chem.* 48, 131–142. doi: 10.1016/0304-4203(94)00041-B
- Gerringa, L. J. A., Rijkenberg, M. J. A., Thuróczy, C.-E., and Maas, L. R. M. (2014). A critical look at the calculation of the binding characteristics and concentration of iron complexing ligands in seawater with suggested improvements. *Environ. Chem.* 11, 114–136. doi: 10.1071/EN13072
- Gledhill, M., Achterberg, E. P., Li, K., Mohamed, K. N., and Rijkenberg, M. J. A. (2015). Influence of ocean acidification on the complexation of iron and copper by organic ligands in estuarine waters. *Mar. Chem.* 177, 421–433. doi: 10.1016/j.marchem.2015.03.016
- Gledhill, M., and Buck, K. N. (2012). The organic complexation of iron in the marine environment: a review. *Front. Microbiol.* 3:69. doi: 10.3389/fmicb.2012.00069
- Gledhill, M., and Van Den Berg, C. M. G. (1994). Determination of complexation of iron (III) with natural organic complexing ligands in sea water using cathodic stripping voltammetry. *Mar. Chem.* 47, 41–54. doi: 10.1016/0304-4203(94)90012-4
- Gledhill, M., Van Den Berg, C. M. G., Nolting, R. F., and Timmermans, K. R. (1998). Variability in the speciation of iron in the northern North Sea. *Mar. Chem.* 59, 283–300. doi: 10.1016/S0304-4203(97)00097-2
- Guo, J., Lapi, S., Ruth, T. J., and Maldonado, M. T. (2012). The effects of iron and copper availability on the copper stoichiometry of marine phytoplankton. *J. Phycol.* 48, 312–325. doi: 10.1111/j.1529-8817.2012.01133.x
- Gustafsson, J. P. (2001). Modeling the acid-base properties and metal complexation of humic substances with the Stockholm Humic Model. *J. Colloid Interface Sci.* 244, 102–112. doi: 10.1006/jcis.2001.7871
- Gustafsson, J. P. (2012). Visual MINTEQ Version 3.0. Stockholm: KTH, Department of Land and Water Resources Engineering.
- Hassler, C. S., Alasonati, E., Nichols, C., a., M., and Slaveykova, V. I. (2011). Exopolysaccharides produced by bacteria isolated from the pelagic Southern Ocean - Role in Fe binding, chemical reactivity, and bioavailability. *Mar. Chem.* 123, 88–98. doi: 10.1016/j.marchem.2010.10.003
- Hawkes, J. A., Gledhill, M., Connelly, D. P., and Achterberg, E. P. (2013). Characterisation of iron binding ligands in seawater by reverse titration. *Anal. Chim. Acta* 766, 53–60. doi: 10.1016/j.aca.2012.12.048
- Hiemstra, T., and Van Riemsdijk, W. H. (2006). Biogeochemical speciation of Fe in ocean water. *Mar. Chem.* 102, 181–197. doi: 10.1016/j.marchem.2006.03.008
- Hogle, S. L., Barbeau, K. A., and Gledhill, M. (2014). Heme in the marine environment: from cells to the iron cycle. *Metallomics* 6, 1107–1120. doi: 10.1039/c4mt00031e
- Hunter, K. A., and Boyd, P. W. (2007). Iron-binding ligands and their role in the ocean biogeochemistry of iron. *Environ. Chem.* 4, 221–232. doi: 10.1071/EN07012
- Jacquot, J. E., Kondo, Y., Knapp, A. N., and Moffett, J. W. (2013). The speciation of copper across active gradients in nitrogen-cycle processes in the eastern tropical South Pacific. *Limnol. Oceanogr.* 58, 1387–1394. doi: 10.4319/lo.2013.58.4.1387
- Johnson, K. S., Gordon, R. M., and Coale, K. H. (1997). What controls dissolved iron concentrations in the world ocean? *Mar. Chem.* 57, 137–161.
- Kinniburgh, D. G., Milne, C. J., Benedetti, M. F., Pinheiro, J. P., Filius, J., Koopal, L. K., et al. (1996). Metal ion binding by humic acid: application of the NICA-Donnan model. *Environ. Sci. Technol.* 30, 1687–1698. doi: 10.1021/es950695h
- Kleypas, J. A., Buddemeier, R. W., Archer, D., Gattuso, J. P., Langdon, C., and Opdyke, B. N. (1999). Geochemical consequences of increased atmospheric carbon dioxide on coral reefs. *Science* 284, 118–120. doi: 10.1126/science.284.5411.118
- Koopal, L. K., Saito, T., Pinheiro, J. P., and Van Riemsdijk, W. H. (2005). Ion binding to natural organic matter: general considerations and the NICA-Donnan model. *Colloids Surfaces A Physic. Eng. Aspects* 265, 40–54. doi: 10.1016/j.colsurfa.2004.11.050
- Kuma, K., and Matsunaga, K. (1995). Availability of colloidal ferric oxides to coastal marine phytoplankton. *Mar. Biol.* 122, 1–11. doi: 10.1007/BF00349272
- Laglera, L. M., Battaglia, G., and Van Den Berg, C. M. G. (2007). Determination of humic substances in natural waters by cathodic stripping voltammetry of their complexes with iron. *Anal. Chim. Acta* 599, 58–66. doi: 10.1016/j.aca.2007.07.059
- Laglera, L. M., and Van Den Berg, C. M. G. (2009). Evidence for geochemical control of iron by humic substances in seawater. *Limnol. Oceanogr.* 54, 610–619. doi: 10.4319/lo.2009.54.2.0610
- Langdon, C., Broecker, W. S., Hammond, D. E., Glenn, E., Fitzsimmons, K., Nelson, S. G., et al. (2003). Effect of elevated CO₂ on the community metabolism of an experimental coral reef. *Global Biogeochem. Cycles* 17:1011. doi: 10.1029/2002GB001941
- Liu, X., and Millero, F. J. (1999). The solubility of iron hydroxide in sodium chloride solutions. *Geochim. Cosmochim. Acta* 63, 3487–3497. doi: 10.1016/S0016-7037(99)00270-7
- Liu, X. W., and Millero, F. J. (2002). The solubility of iron in seawater. *Mar. Chem.* 77, 43–54. doi: 10.1016/S0304-4203(01)00074-3
- Louis, Y., Garnier, C., Lenoble, V., Omanovic, D., Mounier, S., and Pižeta, I. (2009). Characterisation and modeling of marine dissolved organic matter interactions with major and trace cations. *Mar. Environ. Res.* 67, 100–107. doi: 10.1016/j.marenvres.2008.12.002
- Macgilchrist, G. A., Shi, T., Tyrrell, T., Richier, S., Moore, C. M., Dumousseaud, C., et al. (2014). Effect of enhanced pCO₂ levels on the production of dissolved organic carbon and transparent exopolymer particles in short-term bioassay experiments. *Biogeosciences* 11, 3695–3706. doi: 10.5194/bg-11-3695-2014
- Martell, A. E., and Smith, R. M. (2004). *Critically Selected Stability Constants of Metal Complexes*. Gaithersburg, MD: NIST Standard Reference Data.
- Martin, J. H., and Fitzwater, S. E. (1988). Iron-deficiency limits phytoplankton growth in the Northeast Pacific Subarctic. *Nature* 331, 341–343. doi: 10.1038/331341a0
- Millero, F. J., Woosley, R., Ditrolio, B., and Waters, J. (2009). Effect of ocean acidification on the speciation of metals in seawater. *Oceanography* 22, 72–85. doi: 10.5670/oceanog.2009.98
- Milne, A., Landing, W., Bizimis, M., and Morton, P. (2010). Determination of Mn, Fe, Co, Ni, Cu, Zn, Cd and Pb in seawater using high resolution magnetic sector inductively coupled mass spectrometry (HR-ICP-MS). *Anal. Chim. Acta* 665, 200–207. doi: 10.1016/j.aca.2010.03.027

- Milne, C. J., Kinniburgh, D. G., Van Riemsdijk, W. H., and Tipping, E. (2003). Generic NICA-Donnan model parameters for metal-ion binding by humic substances. *Environ. Sci. Technol.* 37, 958–971. doi: 10.1021/es0258879
- Moffett, J. W., and Brand, L. E. (1996). Production of strong extracellular Cu chelators by marine cyanobacteria in response to Cu stress. *Limnol. Oceanogr.* 41, 388–395. doi: 10.4319/lo.1996.41.3.0388
- Moffett, J. W., Brand, L. E., Croot, P. L., and Barbeau, K. A. (1997). Cu speciation and cyanobacterial distribution in harbors subject to anthropogenic Cu inputs. *Limnol. Oceanogr.* 42, 789–799. doi: 10.4319/lo.1997.42.5.0789
- Moore, C. M., Mills, M. M., Achterberg, E. P., Geider, R. J., Laroche, J., Lucas, M. I., et al. (2009). Large-scale distribution of Atlantic nitrogen fixation controlled by iron availability. *Nat. Geosci.* 2, 867–871. doi: 10.1038/ngeo667
- Morel, F. M. M., and Price, N. M. (2003). The biogeochemical cycles of trace metals in the oceans. *Science* 300, 944–947. doi: 10.1126/science.1083545
- Muller, F. L. L., and Bleie, B. (2008). Estimating the organic acid contribution to coastal seawater alkalinity by potentiometric titrations in a closed cell. *Anal. Chim. Acta* 619, 183–191. doi: 10.1016/j.aca.2008.05.018
- Ndungu, K. (2012). Model predictions of copper speciation in coastal water compared to measurements by analytical voltammetry. *Environ. Sci. Technol.* 46, 7644–7652. doi: 10.1021/es301017x
- Orr, J. C., Fabry, V. J., Aumont, O., Bopp, L., Doney, S. C., Feely, R. A., et al. (2005). Anthropogenic ocean acidification over the twenty-first century and its impact on calcifying organisms. *Nature* 437, 681–686. doi: 10.1038/nature04095
- Peers, G., Quesnel, S. A., and Price, N. M. (2005). Copper requirements for iron acquisition and growth of coastal and oceanic diatoms. *Limnol. Oceanogr.* 50, 1149–1158. doi: 10.4319/lo.2005.50.4.1149
- Pierrot, D., Lewis, E., and Wallace, D. W. R. (2006). *MS Excel Program Developed for CO₂ System Calculations. ORNL/CDIAC-105a*. Oak Ridge: Carbon Dioxide Information Analysis Center, Oak Ridge National Laboratory, U.S. Department of Energy. doi: 10.3334/CDIAC/otg.CO2SYS_XLS_CDIAC105a
- Pizeta, I., Sander, S. G., Hudson, R. J. M., Omanovic, D., Baars, O., Barbeau, K. A., et al. (2015). Interpretation of complexometric titration data: an intercomparison of methods for estimating models of trace metal complexation by natural organic ligands. *Mar. Chem.* 173, 3–24. doi: 10.1016/j.marchem.2015.03.006
- Poulton, A. J., Stinchcombe, M. C., Achterberg, E. P., Bakker, D. C. E., Dumoussaud, C., Lawson, H. E., et al. (2014). Coccolithophores on the north-west European shelf: calcification rates and environmental controls. *Biogeosciences* 11, 3919–3940. doi: 10.5194/bg-11-3919-2014
- Raven, J. A., Caldeira, K., Elderfield, H., Houegh-Guldberg, O., Liss, P. S., Riebesell, U., et al. (2005). *Ocean Acidification due to Increasing Atmospheric Carbon Dioxide*. London: The Royal Society.
- Raven, J. A., Evans, M. C. W., and Korb, R. E. (1999). The role of trace metals in photosynthetic electron transport in O₂-evolving organisms. *Photosyn. Res.* 60, 111–149. doi: 10.1023/A:1006282714942
- Rérolle, V. M. C., Floquet, C. F. A., Mowlem, M. C., Bellerby, R. R. G. J., Connelly, D. P., and Achterberg, E. P. (2012). Seawater-pH measurements for ocean-acidification observations. *Trac Trends Anal. Chem.* 40, 146–157. doi: 10.1016/j.trac.2012.07.016
- Ribas-Ribas, M., Rérolle, V. M. C., Bakker, D. C. E., Kitidis, V., Lee, G. A., Brown, I., et al. (2014). Intercomparison of carbonate chemistry measurements on a cruise in northwestern European shelf seas. *Biogeosciences* 11, 4339–4355. doi: 10.5194/bg-11-4339-2014
- Riebesell, U., Zondervan, I., Rost, B., Tortell, P. D., Zeebe, R. E., and Morel, F. M. M. (2000). Reduced calcification of marine plankton in response to increased atmospheric CO₂. *Nature* 407, 364–367. doi: 10.1038/35030078
- Ruzic, I. (1982). Theoretical aspects of the direct titration of natural-waters and its information yield for trace-metal speciation. *Anal. Chim. Acta* 140, 99–113. doi: 10.1016/S0003-2670(01)95456-X
- Sander, S. G., Hunter, K. A., Harms, H., and Wells, M. (2011). Numerical approach to speciation and estimation of parameters used in modeling trace metal bioavailability. *Environ. Sci. Technol.* 45, 6388–6395. doi: 10.1021/es200113v
- Shaked, Y., and Lis, H. (2012). Disassembling iron availability to phytoplankton. *Front. Microbiol.* 3:123. doi: 10.3389/fmicb.2012.00123
- Shi, D. L., Xu, Y., Hopkinson, B. M., and Morel, F. M. M. (2010). Effect of Ocean Acidification on Iron Availability to Marine Phytoplankton. *Science* 327, 676–679. doi: 10.1126/science.1183517
- Stockdale, A., Tipping, E., Hamilton-Taylor, J., and Lofts, S. (2011). Trace metals in the open oceans: speciation modeling based on humic-type ligands. *Environ. Chem.* 8, 304–319. doi: 10.1071/EN11004
- Stockdale, A., Tipping, E., and Lofts, S. (2015). Dissolved trace metal speciation in estuarine and coastal waters: comparison of WHAM/Model VII predictions with analytical results. *Environ. Toxicol. Chem.* 34, 53–63. doi: 10.1002/etc.2789
- Sunda, W. G., and Huntsman, S. A. (1995a). Iron uptake and growth limitation in oceanic and coastal phytoplankton. *Mar. Chem.* 50, 189–206.
- Sunda, W. G., and Huntsman, S. A. (1995b). Regulation of copper concentration in the oceanic nutricline by phytoplankton uptake and regeneration cycles. *Limnol. Oceanogr.* 40, 132–137.
- Tipping, E. (2005). *Cation Binding by Humic Substances*. Cambridge: Cambridge University Press.
- Tipping, E., Lofts, S., and Stockdale, A. (2015). Metal speciation from stream to open ocean: modeling v. measurement. *Environ. Chem.* doi: 10.1071/en15111
- Turner, D. R., Whitfield, M., and Dickson, A. G. (1981). The equilibrium speciation of dissolved components in fresh-water and seawater at 25 degrees C and 1 atm pressure. *Geochim. Cosmochim. Acta* 45, 855–881. doi: 10.1016/0016-7037(81)90115-0
- Van Den Berg, C. M. G. (1995). Evidence for organic complexation of iron in seawater. *Mar. Chem.* 50, 139–157. doi: 10.1016/0304-4203(95)00032-M
- Von Der Heyden, B. P., and Roychoudhury, A. N. (2015). A review of colloidal iron partitioning and distribution in the open ocean. *Mar. Chem.* 177, 9–19. doi: 10.1016/j.marchem.2015.05.010
- Weber, C. L., Vanbriesen, J. M., and Small, M. S. (2006). A stochastic regression approach to analyzing thermodynamic uncertainty in chemical speciation modeling. *Environ. Sci. Technol.* 40, 3872–3878. doi: 10.1021/es0523035
- Whitby, H., and Van Den Berg, C. M. G. (2015). Evidence for copper-binding humic substances in seawater. *Mar. Chem.* 173, 282–290. doi: 10.1016/j.marchem.2014.09.011
- Yokoi, K., and Van Den Berg, C. M. G. (1992). The determination of iron in seawater using catalytic cathodic stripping voltammetry. *Electroanalysis* 4, 65–69. doi: 10.1002/elan.1140040113
- Zeebe, R. E., and Wolf-Gladrow, D. A. (2001). *CO₂ in Seawater: Equilibrium, Kinetics, Isotopes*. Amsterdam; New York, NY: Elsevier.

Conflict of Interest Statement: The authors declare that the research was conducted in the absence of any commercial or financial relationships that could be construed as a potential conflict of interest.

Copyright © 2016 Avendaño, Gledhill, Achterberg, Rérolle and Schlosser. This is an open-access article distributed under the terms of the Creative Commons Attribution License (CC BY). The use, distribution or reproduction in other forums is permitted, provided the original author(s) or licensor are credited and that the original publication in this journal is cited, in accordance with accepted academic practice. No use, distribution or reproduction is permitted which does not comply with these terms.



Toward a Quality-Controlled and Accessible Pitzer Model for Seawater and Related Systems

David R. Turner^{1*}, Eric P. Achterberg², Chen-Tung A. Chen³, Simon L. Clegg⁴, Vanessa Hatje⁵, Maria T. Maldonado⁶, Sylvia G. Sander⁷, Constant M. G. van den Berg⁸ and Mona Wells⁹

¹ Department of Marine Sciences, University of Gothenburg, Gothenburg, Sweden, ² GEOMAR Helmholtz Centre for Ocean Research, Kiel, Germany, ³ Department of Oceanography, National Sun Yat-sen University, Kaohsiung, Taiwan, ⁴ School of Environmental Sciences, University of East Anglia, Norwich, UK, ⁵ Centro Interdisciplinar de Energia e Ambiente, Instituto de Química, Universidade Federal da Bahia, Salvador, Brazil, ⁶ Department of Earth Ocean and Atmospheric Sciences, University of British Columbia, Vancouver, BC, Canada, ⁷ Department of Chemistry, NIWA/University of Otago Research Centre for Oceanography, Dunedin, New Zealand, ⁸ Earth and Ocean and Ecological Sciences, University of Liverpool, Liverpool, UK, ⁹ Department of Environmental Science, Xi'an Jiaotong-Liverpool University, Suzhou, China

We elaborate the need for a quality-controlled chemical speciation model for seawater and related natural waters, work which forms the major focus of SCOR Working Group 145. Model development is based on Pitzer equations for the seawater electrolyte and trace components. These equations can be used to calculate activities of dissolved ions and molecules and, in combination with thermodynamic equilibrium constants, chemical speciation. The major tasks to be addressed are ensuring internal consistency of the Pitzer model parameters (expressing the interactions between pairs and triplets of species, which ultimately determines the calculated activities), assessing uncertainties, and identifying important data gaps that should be addressed by new measurements. It is recognized that natural organic matter plays an important role in many aquatic ecosystems, and options for including this material in a Pitzer-based model are discussed. The process of model development begins with the core components which include the seawater electrolyte and the weak acids controlling pH. This core model can then be expanded by incorporating additional chemical components, changing the standard seawater composition and/or broadening the range of temperature and pressure, without compromising its validity. Seven important areas of application are identified: open ocean acidification; micronutrient biogeochemistry and geochemical tracers; micronutrient behavior in laboratory studies; water quality in coastal and estuarine waters; cycling of nutrients and trace metals in pore waters; chemical equilibria in hydrothermal systems; brines and salt lakes.

Keywords: chemical speciation, seawater, modeling, equilibria, pH, trace metals, biogeochemical cycles

1. INTRODUCTION

Ocean composition is changing at an unprecedented rate as a result of anthropogenic pressures, with important implications for the health of the oceans and for economic activities. In a recent survey of global ocean research priorities, ocean acidification and the effects of cumulative stressors were identified as two of the top three areas of concern (Rudd, 2014). Understanding

OPEN ACCESS

Edited by:

Marta Álvarez,
Instituto Español de Oceanografía,
Spain

Reviewed by:

Marta Plavsic,
Rudjer Boskovic Institute, Croatia
Wei-Dong Zhai,
Shandong University, China

***Correspondence:**

David R. Turner
david.turner@marine.gu.se

Specialty section:

This article was submitted to
Marine Biogeochemistry,
a section of the journal
Frontiers in Marine Science

Received: 31 May 2016

Accepted: 26 July 2016

Published: 16 September 2016

Citation:

Turner DR, Achterberg EP, Chen C-TA, Clegg SL, Hatje V, Maldonado MT, Sander SG, van den Berg CMG and Wells M (2016) Toward a Quality-Controlled and Accessible Pitzer Model for Seawater and Related Systems. *Front. Mar. Sci.* 3:139. doi: 10.3389/fmars.2016.00139

the impacts of ocean acidification on areas of human concern, such as fisheries, is a matter of great urgency. Knowledge of chemical speciation, which describes the distribution of the elements between different chemical forms, is essential to understand how changes in ocean chemistry affect bioavailability of different elements (Tessier and Turner, 1995). For example, the speciation of both carbonate and (micronutrient) trace metals are complex functions of natural water composition, pH, temperature, and pressure. Changes in ocean chemistry may be small on an annual basis, but are modulated on short time and space scales by physical parameters, such as salinity, temperature, and irradiance, as well as variations in upwelling and ocean currents. Therefore, these chemical changes need to be measured accurately and consistently across the globe to monitor and understand contemporary processes. In addition, chemical changes need to be modeled accurately to evaluate future scenarios and remediation strategies. These requirements are linked by the need to understand chemical speciation—for example that of carbonate and trace metal micronutrients—both in natural waters and in the reference materials and solutions used for analytical method verification and instrument calibration.

Recognizing the importance of chemical speciation modeling, SCOR, the Scientific Committee on Ocean Research of the International Council for Science, created Working Group 145 tasked with establishing a reference seawater chemical speciation model that is user-friendly, and freely available to the marine science community. This paper, which constitutes the first report from the Working Group, describes the approach that will be used and identifies different applications to be supported by this chemical speciation model. These span a variety of aquatic environments, and include measurement, calibration and laboratory studies. Each application has its own requirements for the chemical species to be included, and the physical conditions (temperature and pressure) to be covered. To this end, we have proposed a set of core components that are essential for all marine science applications, followed by the specific requirements for each application. This approach is summarized in **Figure 1**, where in addition to the core components, seven different groups of application have been identified. The major tasks for the Working Group include: ensuring self-consistency of the chemical speciation model and traceability of its parameters to thermodynamic measurements, establishing quantitatively the uncertainties in the calculated speciation, and identifying important data gaps to be addressed by new measurements.

2. THEORY

2.1. Pitzer Equations

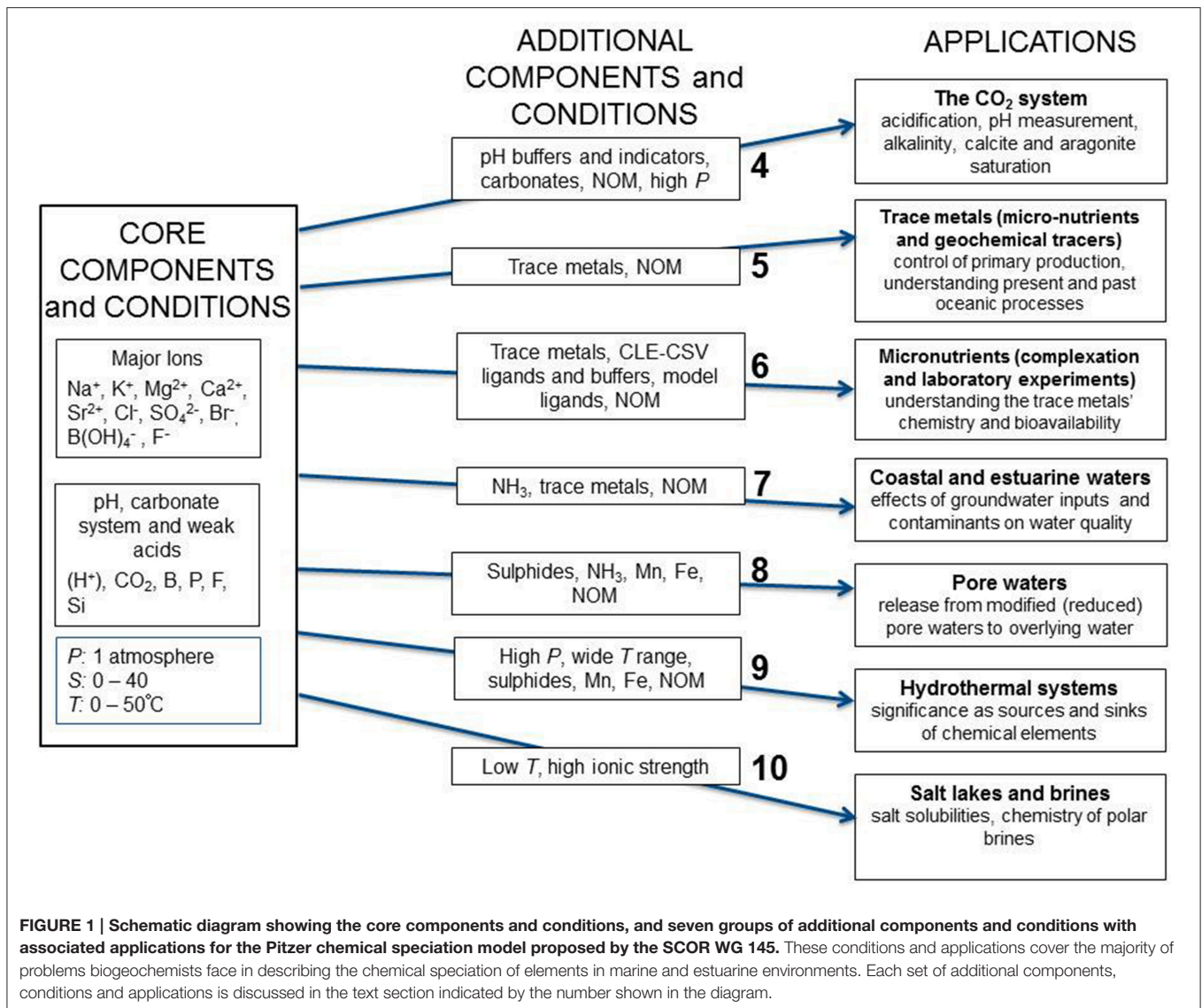
The form in which a trace element or other component of seawater is present, and its tendency to react, depends on its *activity* (Clegg and Whitfield, 1991). This is the product of its concentration (usually mol per kg seawater), and an activity coefficient (γ) which is a complex function of temperature, pressure, and salinity (or, more generally, solution composition). Many of the important reactions in seawater involve acid-base equilibria, which introduces pH as a further variable.

The Pitzer model (Pitzer, 1991) is a set of equations to calculate activity coefficients (and hence all forms of chemical equilibria) in aqueous solutions as functions of composition and concentration, temperature, and pressure. The equations for water and solute activities, and thermal and volumetric properties, are derived from a single expression for the excess Gibbs energy of the solutions. The equations contain sets of parameters (which are functions of temperature and pressure) of two kinds: “pure” solution parameters whose values are determined by fitting to data for solutions containing single electrolytes (e.g., NaCl, MgSO₄); and “mixture” parameters whose values are determined from measurements containing, typically, two different electrolytes with a common ion. (e.g., NaCl and Na₂SO₄).

The data needed to build a model of a complex mixture, such as seawater, include: solvent and solute activities, apparent molar enthalpies and heat capacities (yielding the variation of the model parameters with temperature), apparent molar volumes and compressibilities (the variation of the parameters with pressure), salt solubilities, liquid/liquid phase partitioning, equilibrium partial pressures of volatile solutes, and others. The model is described in detail by Pitzer (1991), and its application to the chemistry of natural waters by Clegg and Whitfield (1991). For any solution, the major effort in constructing a Pitzer model is the determination of the parameter values; a process that often includes the resolution of differences between inconsistent sets of data, and obtaining approximate values of parameters for which there are no data.

The principal Pitzer chemical speciation model of seawater is that of Millero and co-workers at the University of Miami (Millero and Roy, 1997; Millero and Pierrot, 1998; Waters and Millero, 2013). Using many of the same data sources, Clegg and Whitfield (1995) also developed a seawater model, including the protonation of dissolved ammonia. The model of Millero and co-workers is applicable primarily to major ions in seawater (from 0 to 50°C, and 0 to >40 salinity) containing the species H⁺, Na⁺, K⁺, Mg²⁺, Ca²⁺, Sr²⁺, Cl⁻, Br⁻, OH⁻, HCO₃⁻, B(OH)₄⁻, HSO₄⁻, SO₄²⁻, CO₃²⁻, CO₂, B(OH)₃, and H₂O. The use of the model to calculate pH, and some of the problems concerning pH scales that still need to be addressed, are discussed by Waters and Millero (2013). There is, as yet, no comprehensive evaluation of the uncertainties in model-calculated speciation arising from uncertainties in the thermodynamic measurements upon which they are based. The data for trace metal activities and complexation in seawater—which are important for understanding their behavior and fate—are best described as patchy, and the effects of pressure on activities are only well characterized for aqueous solutions of some of the major seawater electrolytes (e.g., NaCl). This limits the accuracy of calculations of chemical speciation in the subsurface ocean.

The parameters that comprise the Pitzer models developed for seawater are drawn from many sources, include data up to a century old, and are often not optimized for solutions of seawater but rather for modeling brines, e.g., Harvie et al. (1984). To our knowledge, the number of new studies yielding the activities and other data needed to improve the model has been in decline



for many years, though the need to quantitatively understand ocean biogeochemistry, especially carbonate chemistry, has increased significantly. Furthermore, there is no comprehensive evaluation relating the capabilities of speciation models, and the measurements upon which they are based, to current and future needs in chemical oceanography as exemplified in current programs, such as the international GEOTRACES Program (Henderson et al., 2007).

The matrix of Pitzer parameters for major ions in seawater—of the composition noted above but excluding Sr²⁺ and boric acid—is considerable: 36 sets of cation-anion interactions, and potentially 210 ternary or “mixture” parameters that express the interactions between two dissimilar ions of one charge type, and one of the opposite charge type. Some of these can be neglected if all the interacting species are at very low concentration. Nevertheless, the large numbers of interactions and the fact that they can vary with both temperature and pressure emphasizes the

need to (1) assess the completeness and reliability of the model, (2) validate its basis in measured thermodynamic properties (including analyses to relate the uncertainties in the output quantities of the model to those of the fundamental data—for each interaction—upon which it is based); and (3) establish the sets of measurements still needed to adequately characterize the behavior of seawater, estuarine and other natural waters encountered worldwide. The treatment of uncertainties could adopt the methods applied to the IAPWS 1995 equation of state for water (Feistel et al., 2016).

When Pitzer equations are used to calculate activity coefficients, the stability constants used for the chemical equilibria are *thermodynamic constants* K , which are functions of temperature and pressure only. However, many practical applications make use of *stoichiometric constants* K^* (sometimes also called conditional constants), which are expressed in terms of concentrations and are thus functions of temperature,

pressure and solution composition. This dependence on solution composition—via the activity coefficients γ —limits the practical value of stoichiometric constants. Taking the dissociation of HF as an example, and using square brackets to represent concentrations:

$$K^* = [H^+][F^-]/[HF] = K \cdot (\gamma_{HF}/\gamma_{H^+} \gamma_{F^-}) \quad (1)$$

Values of the stoichiometric constant K^* measured in normal seawater can be used only for solutions of seawater composition and for the salinity, or salinities, for which K^* has been determined. Any variations from seawater composition—such as might be found in enclosed seas, pore waters, and some estuaries—will lead to changes in the values of the three activity coefficients in the equation above and therefore a change in K^* .

Models based on the Pitzer equations are used to calculate chemical speciation at equilibrium, although there is of course no guarantee that a particular system is at equilibrium. In marine environments, the different redox couples that are present are, in general, not in equilibrium with each other. The Pitzer equations can be used to examine this phenomenon by calculating the equilibrium speciation in the two oxidation states of a redox couple: combining measured total concentrations and the standard potential for the couple allows the degree of disequilibrium to be established. Such calculations can also be used to establish the relative oxidizing or reducing power of different redox couples at *in situ* conditions. A knowledge of the equilibrium speciation may also contribute to the analysis of rate processes in places where complexation of a metal ion affects the rate of oxidation (Santana-Casiano et al., 2005).

2.2. Natural Organic Matter (NOM)

The Pitzer equations are applicable to reactions involving relatively simple chemical species whose chemical composition and structure are well defined. Natural organic matter (NOM) in natural waters, including seawater, falls outside this definition since it is a polydisperse material comprising a mixture of many different molecular structures (Koch et al., 2005). Modeling of NOM in seawater is currently restricted to its complexation of trace metals; the available information is derived from competitive ligand exchange cathodic stripping voltammetry (CLE-CSV) titrations (section 6.1), which are summarized as the “concentrations” and “stability constants” of one or more ligand classes. This operational summary cannot be applied in conditions that depart from those used in the titration, although in many cases a broad agreement between different studies has been observed. An alternative strategy worthy of investigation is the use of modeling approaches for freshwater NOM, following extensive laboratory studies of extracted material. Three modeling approaches have been developed: the Windermere Humic Acid Model (WHAM) (Tipping et al., 2011); the Stockholm Humic Model (SHM) (Gustafsson, 2001); and the NICA-Donnan model (Koopal et al., 2005). All three approaches explicitly recognize the polydisperse nature of NOM, and also explicitly treat the development of charge due to ionization and complexation reactions. The model codes developed for these approaches in fresh waters use simple extended Debye-Hückel equations for the calculation of activity coefficients. These

equations are not adequate for use in seawater. However, the WHAM formulation has recently been combined with a Pitzer model (Ulfsbo et al., 2015), providing the basis to test this approach for NOM modeling in seawater.

3. CORE COMPONENTS AND CONDITIONS

3.1. The Seawater Electrolyte

The basis of any speciation model that aims to predict activity coefficients accurately is the background electrolyte that determines the physicochemical properties of seawater, and the chemical environment experienced by trace species. On a molar concentration basis, seven chemical elements account for 99.9% of the dissolved species in seawater. Models of the seawater electrolyte normally include the 11 elements whose concentrations exceed $1 \mu\text{mol kg}^{-1}$ and constitute a constant or near-constant proportion of salinity. These are, in order of descending concentration, chlorine (Cl), sodium (Na), magnesium (Mg), sulfur (S), calcium (Ca), potassium (K), (inorganic) carbon (C), bromine (Br), boron (B), strontium (Sr), and fluorine (F).

The definition of the core speciation model also includes the ranges of the three master variables temperature, salinity, and pressure. A temperature range of 0–50°C and a salinity range of 0–50 correspond to the ranges of many speciation models, although the most complete data collection is usually at 25°C. Information on pressure dependence is often limited, so the core speciation model that the Working Group will consider is initially for 1 atmosphere pressure.

3.2. pH

The practical scales used by chemical oceanographers to measure pH are summarized by Waters and Millero (2013). The complexities of these scales, and the difficulty of defining pH, arise because neither the concentration nor the activity of H^+ can be measured directly and independently of other quantities (Dickson, 1984). On the *total* scale, the H^+ associated with SO_4^{2-} (as HSO_4^-) is included in the pH, so that:

$$\begin{aligned} \text{pH}_T &= -\log_{10} ([H^+] + [HSO_4^-]) \\ &= -\log_{10} \{ [H^+] (1 + [SO_4^{2-}]/K_{HSO_4}^*) \} \quad (2) \end{aligned}$$

The *seawater* pH scale also includes the H^+ bound to F^- (as HF), so that,

$$\begin{aligned} \text{pH}_{SWS} &= -\log_{10} ([H^+] + [HSO_4^-] + [HF]) \\ &= -\log_{10} \{ [H^+] (1 + [SO_4^{2-}]/K_{HSO_4}^* + [F^-]/K_{HF}^*) \} \quad (3) \end{aligned}$$

In the above equations the stoichiometric dissociation constants $K_{HSO_4}^*$ (for reaction $HSO_4^- \leftrightarrow H^+ + SO_4^{2-}$) and K_{HF}^* ($HF \leftrightarrow H^+ + F^-$) vary with temperature, pressure, and salinity. More generally, they vary with chemical composition which affects pH in natural waters whose composition differs from that of normal seawater.

The total and seawater pH scales have been adopted for the following practical reason: the artificial seawater solutions used for the characterization of pH buffers and pH indicators must contain a relatively high concentration of sulfate in order to

match the major ionic composition of natural seawater. However, glass and hydrogen pH electrodes respond only to the free H^+ in solution, while analytical hydrogen ion concentrations obtained from measurements on these scales include both H^+ and HSO_4^- . This difference is significant: $-\log_{10}[H^+]$ and pH_T at salinity 35 and $25^\circ C$ differ by 0.128 pH units, while the difference between pH_T and pH_{SWS} is only 0.005 units. The accuracy with which the free H^+ concentration can be determined from pH_T and pH_{SWS} is currently limited by the accuracy with which $K^*_{HSO_4}$ is known (Waters and Millero, 2013). Waters and Millero recommend further work to resolve discrepancies between measured and modeled activity coefficients in seawater-like solutions containing sulfate.

Figure 2 shows concentrations of the principal species controlling pH in a salinity 35 seawater at $25^\circ C$, calculated using an ion-interaction speciation model (Clegg and Whitfield, 1995). It is clear, from the relatively high concentrations of carbonate and borate, that seawater pH is largely controlled by equilibria involving these species.

3.3. Weak Acids

The chemical species in the model include the weak acids that are involved in defining the pH and alkalinity of seawater. These are clearly illustrated in the open-ended definition of total alkalinity A_T (Dickson, 1981):

$$A_T = [HCO_3^-] + 2[CO_3^{2-}] + [B(OH)_4^-] + [OH^-] + [HPO_4^{2-}] + 2[PO_4^{3-}] + [SiO(OH)_3^-] + [NH_3] + \dots - [H^+] - [HSO_4^-] - [HF] - [H_3PO_4] - \dots \quad (4)$$

The core chemical species in the model have been selected based on a significant contribution ($>1 \mu\text{mol kg}^{-1}$) to A_T in the open ocean. This includes all the species in Equation (4), with the exception of the weak base ammonia.

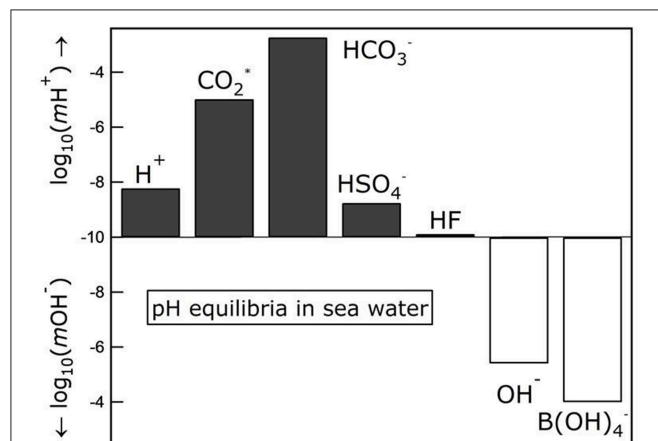


FIGURE 2 | Concentrations of the principal species controlling pH in salinity 35 seawater at $25^\circ C$, calculated using an ion-interaction speciation model (Clegg and Whitfield, 1995). CO_2^* refers to the sum of dissolved CO_2 and H_2CO_3 .

4. THE CO_2 SYSTEM

4.1. Limitations of Current Calculation Programs

A number of software packages are freely available for carrying out calculations on the CO_2 system, and are based on stoichiometric constants parameterized as a function of salinity, temperature, and pressure (Orr et al., 2015). However, the use of salinity as a master variable carries the drawback that these calculations are not applicable to waters of different compositions. This is a particular problem at lower salinities where major ion composition of the seawater/freshwater mixture does not correspond simply to diluted seawater. Compared with seawater, river waters generally have high Mg, Ca, and borate concentrations relative to Na, Cl, and SO_4 . Furthermore, river waters are typically high in organic ligands of various molecular sizes. This material can contribute to alkalinity, as noted above, and its decomposition in estuaries can cause substantial changes in the CO_2 system (Cai, 2011; Chen et al., 2013; Yang et al., 2013).

The interpretation of measured alkalinity, and its use in calculations of CO_2 equilibria in natural waters, requires identification of all the relevant weak acids (i.e., those that contribute more than ca. $1 \mu\text{mol kg}^{-1}$ to the alkalinity), and their degrees of dissociation at the temperature, salinity, and pressure of interest. This presents an analytical challenge in many estuarine and brackish waters where natural organic matter can make a significant contribution to alkalinity (Hernandez-Ayon et al., 2007; Kulinski et al., 2014). Complete modeling of the CO_2 system in such waters will also require a treatment of the acid-base chemistry of this material. Overall, there is a great deal to be gained by integrating calculations of the carbon dioxide system, and pH, into a Pitzer model of chemical speciation.

4.2. Calcium Carbonate Solubility

An aspect of ocean acidification that has received a great deal of attention is the concomitant increase in the solubility of calcium carbonate, and its consequences for calcifying marine organisms. A large number of experiments have been carried out exposing different calcifying (and non-calcifying) marine organisms to reduced pH. These experiments show a range of results, and that, at least in the short term, not all calcifying organisms are negatively affected (Dupont and Poertner, 2013). It is, however, clear that oceanic pH is falling and that organisms that precipitate the more soluble forms of calcium carbonate will be greatly affected. Corals, for example, precipitate aragonite, which is the most soluble pure form of calcium carbonate, although high magnesium calcites can have even higher solubilities (Haese et al., 2014). Projections show that aragonite will become undersaturated in large parts of the ocean during the next century. As for the CO_2 system equilibria in solution, the solubility products of calcite and aragonite are currently available as functions of salinity, temperature, and pressure (Millero, 2007). Incorporation of these equilibria into a Pitzer framework would enable improved calculations of the solubility products of calcite and aragonite in waters whose composition differs from standard seawater.

4.3. Buffers for pH Measurement

The recognition of ocean acidification as “the other CO₂ problem” has highlighted the need for precise and accurate pH measurements in seawater. Two methods are currently recognized as meeting these requirements: glass electrodes calibrated in artificial seawater buffers; and indicator spectrophotometry (Dickson et al., 2007), also calibrated against buffer solutions. The most widely used buffer for this purpose is “tris” (2-amino-2-hydroxymethyl-1,3-propanediol), although alternative buffers, such as 2-aminopyridine, morpholine (tetrahydro-1,4-isoxazine) and bis (2-amino-2-methyl-1,3-propanediol) can be used when the pH departs significantly from the normal seawater range (Dickson, 1993). The pH values assigned to these buffers are available as functions of salinity and temperature, and have been derived by least-squares fitting pH values determined from a large number of potentiometric measurements in cells without liquid junctions (DelValls and Dickson, 1998). As yet, these measurements cover a limited salinity range (20–40). An alternative approach to fitting the buffer pH values to semi-empirical functions of salinity and temperature, is to derive Pitzer parameters for the interactions of these two buffers with the components of seawater. This would then allow these important pH buffers to be incorporated into the planned unified model of seawater, and also facilitate the treatment of low salinity buffer solutions.

4.4. Sulphonephthalein Indicators

Indicator spectrophotometry has gained wide acceptance as the method of choice for measurements of seawater pH. These measurements require the stoichiometric stability constant of the indicator dye at the salinity and temperature of the measurement. This is currently achieved by laboratory measurements of these constants under a range of conditions, followed by least squares fitting of the data to semi-empirical functions of salinity and temperature (Liu et al., 2011). As with the pH buffers, an alternative approach to fitting the indicator pH values to semi-empirical functions of salinity and temperature is to derive Pitzer parameters for the interactions of the relevant indicators with the components of seawater. This would allow these indicators to be incorporated into the planned unified seawater model. The most important indicators are m-cresol purple, phenol red and thymol blue, which are used for pH measurements; and also bromocresol green and bromocresol purple which are used for the determination of alkalinity by the single point method.

5. TRACE METALS: MICRONUTRIENTS AND GEOCHEMICAL TRACERS

The key role of trace metals in ocean science has been recognized in the development of the GEOTRACES programme (Henderson et al., 2007), which is coordinating a global survey of trace elements and isotopes in the ocean. GEOTRACES focuses on the behavior of trace metals as micronutrients and as tracers for ocean processes; this division of roles is not exclusive: some trace metals, such as Cd and Mn, fall into both categories.

5.1. Micronutrients

It is now recognized that the bioavailability of iron is a key factor in determining primary production and/or phytoplankton community structure in large areas of the ocean (Turner and Hunter, 2001). The thermodynamically stable oxidation state in oxic waters, Fe(III), is poorly soluble with a solubility of the order of 10⁻¹¹ mol L⁻¹ in seawater in the absence of organic ligands (Liu and Millero, 2002). However, strong organic complexation can maintain significantly higher concentrations. While organic complexation by (as yet) not fully characterized ligands dominates the speciation of Fe(III), there is continuing interest in defining the inorganic complexation and solubility as essential supporting information. There is also considerable interest in Fe(II), both as a component of anoxic waters, and as metastable Fe(II) produced by photochemical reduction in surface waters. The speciation of this metastable Fe(II) and its effects on Fe oxidation rates are key factors determining the bioavailability of Fe in sunlit surface waters.

While much attention has been focused on Fe in recent years, several other metals are essential for biological processes. A recent review gives the generalized ranking of trace metal content in phytoplankton as Fe ≈ Zn > Mn ≈ Ni ≈ Cu >> Co ≈ Cd (Twining and Baines, 2013). While all these metals act as micronutrients, some can also have toxic effects at elevated concentrations (Cd, Ni, Cu, Zn, see also section 7.2). Four of these metals (Fe, Zn, Cu, and Cd) are obligatory core parameters on GEOTRACES cruise sections, which are providing extensive new information on these metals, both in terms of dissolved (<0.2 μm) concentrations and CLE-CSV titration data (see section 6.1). Chemical speciation modeling will provide an excellent tool to help extract full value from these unique global datasets.

5.2. Tracers of Ocean Processes

Manganese is present as insoluble MnO₂ at equilibrium in oxic seawater. However, relatively slow oxidation rates result in dissolved Mn concentrations at the nM level. This slow oxidation has led to the use of Mn as a tracer for releases from anoxic environments, where Mn is present as dissolved Mn(II), and from hydrothermal systems where significant amounts of reduced Mn are released into the surrounding waters (German et al., 1999). The speciation of dissolved Mn has been considered to be dominated by weakly complexed Mn(II), but recent work indicates that Mn(III) may also be present at significant concentrations (Luther et al., 2015).

In surface waters, Al has been used as a tracer for dust input, which is a major source of Fe to the ocean. The strong correlation between dissolved Al and silicic acid has prompted suggestions of biological control of Al distributions (van Hulten et al., 2014). However, for example in the Mediterranean Sea, the correlation between Al and Si could be explained purely by vertical transport of biogenic particles (Rolison et al., 2015).

The lanthanides series are a powerful set of tracers because of their coherent and predictable behavior. Lanthanides have been used in many studies to investigate redox conditions (Liu et al., 1988; Sholkovitz and Schneider, 1991), particulate exchange and scavenging processes (Andersson et al., 2008),

water mass transport (Scher and Martin, 2004; Haley et al., 2008) and identification of benthic sources of pore fluid (Abbott et al., 2015). More recently, the lanthanides' widespread use in high-technology processes and products is increasing their environmental occurrence. For example, lanthanides are now being used as tracers of wastewater-derived contaminants in the marine environment (Hatje et al., 2014, 2016).

The close relationship between the depth profiles of Cd and phosphate concentrations makes Cd an attractive candidate as a proxy for phosphate concentrations in palaeoceanography, although the relationship shows significant variation (de Baar et al., 1994).

6. MICRONUTRIENTS: COMPLEXATION AND LABORATORY EXPERIMENTS

6.1. CLE-CSV Titrations

The most widely used method for characterizing the organic complexation of trace metals in seawater is currently Competitive Ligand Exchange (CLE), although direct electrochemical measurements by Anodic Stripping Voltammetry (ASV) are also used, e.g., Sinoir et al. (2016). CLE involves the addition of a competing ligand which has two properties: it forms a complex that competes for trace metals with the natural unknown ligands present in the sample; and it forms a complex with the target trace metal that adsorbs on a mercury electrode and can thus be detected by Cathodic Stripping Voltammetry (CSV). The methods of fitting the CLE/CSV and ASV titration data accurately have been improved significantly in recent times (Pizeta et al., 2015). However, to enable accurate CLE characterization of the complexation of the trace metal with unknown ligands, it is essential to quantify the complexation of the metal by the added competing ligand, as well as competition reactions with other metals.

For CLE measurements, the most commonly used added ligands are SA (salicylaldoxime), which complexes with Cu and Fe (Campos and van den Berg, 1994; Buck et al., 2007; Abualhaija and van den Berg, 2014); NN (1-nitroso-2-naphthol), which complexes with Fe (Aldrich and van den Berg, 1998); APDC (aminopyrrolidinedithiocarbamate), which complexes with Zn (van den Berg, 1985); and DHN (dihydroxynaphthalene), which complexes with Fe (van den Berg, 2006). Other relevant ligands are TAC [2-(2-thiazolylazo)-p-cresol], which has been used as competing ligand for the determination of Fe organic complexation in seawater (Croot and Johansson, 2000; Sander et al., 2015); and DMG (dimethylglyoxime), which has been used for determinations of Co and Ni complexation (van den Berg et al., 1991; Ellwood and van den Berg, 2001).

In addition to modeling the chemistry of the added ligands, attention needs to be paid to the buffers added to control pH in the CSV measurements. Optimal buffers are those near the natural pH of the water. While the carbonate system acts as the major pH buffer in seawater, sample deaeration undertaken during the CSV analysis disrupts this function, so that an additional buffer is needed. As well as buffering close to the natural pH of seawater, the added buffer must have only weak interactions with the trace metals being

studied, so that it does not act as an additional competing ligand. The two buffers that are most commonly used are EPPS [4-(2-hydroxyethyl)-1-piperazinepropanesulphonic acid] and HEPES [4-(2-hydroxyethyl) piperazine-1-ethanesulphonic acid], however phosphate buffer is becoming more popular as it can be cleaned very efficiently to remove any traces of organic ligands and trace metals. A quantitative understanding of these buffers' chemistry in seawater would allow the buffering effect to be calculated more accurately, thus providing a better definition of the chemical conditions of the complexation titrations.

6.2. Model Ligands for Laboratory Experiments

Model organic chelators are used in culture media to ensure that the inorganic trace metal concentrations stay constant during culturing. Furthermore, the use of these chelators, in conjunction with chemical equilibrium modeling, allows the researcher to manipulate the inorganic concentration of a given trace metal while maintaining the inorganic concentrations of the remaining bioactive trace elements unchanged. This design is especially suitable for controlled physiological studies investigating the response of phytoplankton to limiting or toxic trace metal concentrations. The most common general model chelator in culture studies is EDTA (ethylenediaminetetraacetic acid; Price et al., 1988; Sunda et al., 2005). However, the chelator of choice may vary depending on the research question. For example, if Cu is the metal of interest, one might use DTPA (diethylene triamine pentaacetic acid) instead of EDTA, given that DTPA is a stronger chelator of Cu than EDTA.

Limiting growth in cultures by manipulation of a specific trace metal is often challenging, and requires the use of well-chosen metal chelators. For example, siderophores, such as DFB (desferrioxamine B), and DFE (desferrioxamine E), are often used to significantly reduce the concentrations of inorganic Fe in the culture media, and thus induce Fe limitation in phytoplankton with extremely low Fe requirements (Strzepek et al., 2011). Similarly, Cu specific chelators, such as Cyclam (1,4,8,11-tetraazacyclotetradecane) and Cyclen (1,4,7,10-tetraazacyclododecane) are frequently used to induce Cu limitation in phytoplankton cultures (Semeniuk, 2014). In addition, these organic ligands are frequently used in uptake experiments (Semeniuk et al., 2015), as they are believed to mimic naturally occurring strong organic ligands of Fe and Cu in seawater. Naturally occurring thiols, such as glutathione, cysteine and thiourea are known to strongly bind Cu and other chalcophilic metals (Laglera and van den Berg, 2003). Chemical modeling that includes these organic chelators will greatly enhance our understanding of the chemical speciation of the trace metals in laboratory growth and uptake media, as well as *in situ* oceanic conditions.

7. COASTAL AND ESTUARINE SYSTEMS

7.1. Estuaries and Groundwater Discharge

Estuaries are where the river water meets seawater, and where the mixture interacts with the land, oceans, atmosphere, sediments, and biota. The freshwater end members are typically richer in major nutrients (nitrate, nitrite, ammonia,

phosphate, and silicate) compared with ocean waters, hence biological productivities are generally high in estuaries. River waters subject to anthropogenic influence frequently have high concentrations of micronutrients and toxic elements (Liu et al., 2010), while permafrost degradation affects the chemistry of Arctic rivers and coastal seas through the mobilization of organic matter (Semiletov et al., 2016). Furthermore, submarine groundwaters with unique chemical compositions discharge into many estuaries and coastal waters (Zhang and Mandal, 2012). In the case of eutrophication, the pH and dissolved oxygen concentration are both lowered following organic matter breakdown, with consequences for acid-base and redox reactions. Moreover, when riparian tidal freshwater lands and oligohaline marshes are inundated by seawater, competition by major cations, such as Mg and Ca can result in the release of trace metals from particulate matter (Wang et al., 2012; Zhang and Mandal, 2012).

7.2. Contaminant Discharge

The United Nations Environmental Programme (UNEP, 2013) has highlighted the phenomenon of “global chemical intensification”: in many parts of the world, the anthropogenic inputs of metals to the ocean are estimated to be far greater than non-anthropogenic inputs, and the way in which this affects global biogeochemical cycles and ecosystem diversity is as yet poorly understood. Islam and Tanaka (2004) and Davies (1978) noted that the 10 most significant contaminant elements in marine waters are, in order of decreasing toxicity Hg, Cd, Ag, Ni, Se, Pb, Cu, Cr, As, and Zn. Four of these (Cd, Ni, Cu, and Zn) are classified as key micronutrients (Twining and Baines, 2013), and Se and Cr can in addition act as micronutrients.

Specific examples of contaminant discharge include runoff from metal mines, their associated mine tailings, and also naturally occurring acid rock drainage springs. The metals that are commonly found at elevated concentrations (micromolar to millimolar) in mine runoff include Fe, Cu, Zn (Brown et al., 2005; Braungardt et al., 2007), and depending on the ore formations, may also include Cd, Ni, Ag, Au, As. High acidity (pH < 1) is associated with the oxidation of iron pyrites and the subsequent formation of sulfuric acid. High acidity also mobilizes metals and prevents their removal by precipitation and scavenging.

Industrial discharges are also potential sources of inorganic contaminants, including those from metallurgical industry (metals), fertilizer industry (N, P), and desalination plants (metals). Furthermore, domestic waste water treatment operations discharge inorganic contaminants into receiving waters, and the growth of aquaculture in coastal zones is associated with increasing pollution by inorganic compounds.

8. PORE WATERS

Pore waters are aqueous solutions that occupy the pore spaces between particles in sediments and can often be considered in equilibrium with the sediments. Diagenetic reactions within sediments and at the sediment-pore water interface control, among others, the recycling of nutrients, carbon, trace elements and contaminants, the dissolution of carbonates, the flux of

organic matter to benthic communities and the burial of several elements (see for example Berner, 1980; Klinkhammer, 1980; Klinkhammer et al., 1982). Pore water studies have provided a link between water column transport processes and sedimentary accumulation by showing evidence for the release of metals associated with the degradation of organic matter (Sholkovitz et al., 1989).

Chemical changes across redox interfaces in marine systems can have a profound impact on metal solubility and bioavailability. At these oxic-anoxic interfaces, changes in oxidation state, as well as complexation with reduced sulfur species and formation of insoluble sulfides, are common. In coastal areas, redox interfaces are found in anoxic sediments, in anoxic basins and fjords, as well as in sewage outfalls. In the open ocean, oxic-anoxic interfaces are less common, but changes in trace metal solubility and speciation are often observed in oxygen minimum zones. Thus, water columns with oxic-anoxic interfaces have an impact on the cycling of trace metals in the global ocean.

Knowledge of biogeochemical processes in marine sediments and benthic fluxes of pore water is essential for understanding the global carbon cycle and climate (Berner, 1980; Siegenthaler and Sarmiento, 1993; Ridgwell and Hargreaves, 2007). Moreover, pore water is a key exposure route for metal contaminants to organisms associated with the sediments, in particular infauna (Chapman et al., 2002). Knowledge of metal speciation in pore waters is necessary for the development of predictions of bioavailability and for reliable risk assessment strategies. This knowledge could be incorporated in biotic ligand models to derive better-founded quality criteria for marine environments.

8.1. Sulfides

The need to model chemistry in anoxic pore waters, and to understand the chemical processes occurring at the oxic/anoxic boundary, focuses attention on redox reactions, and on the chemistry of reduced oxidation states. The most abundant of these are NH₃, Fe(II), Mn(II), and sulfide. The most challenging of these species for chemical modeling is sulfide. In the last 2 decades, metal sulfide speciation in aquatic systems has become of great interest, due to the discovery of nanomolar levels of sulfide in oxic seawater (Luther and Tsamakis, 1989). Sulfides become stable in oxic conditions by forming complexes with trace elements, especially with Hg, Cu (Dyrssen, 1988; Luther and Tsamakis, 1989); and Pb (Bura-Nakic et al., 2007). These metal (M)—sulfide species in oxic waters include simple MHS⁺ (or M(HS)₂)⁰ complexes, but also higher-order unprotonated clusters (multinuclear oligomers) with high stability constants (Rozaan et al., 2000). In the case of Cu and Zn, the resulting metal-sulfide species are resistant to oxidation in oxic waters and include a mixture of dissolved metal-sulfide complexes and active metal-sulfide nanoparticles (Rozaan et al., 1999; Sukola et al., 2005).

9. HYDROTHERMAL SYSTEMS

Hydrothermal venting occurs in two forms: as hot (up to 450°C), or diffuse venting (5–100°C). Hot vents are mainly found close to mid ocean ridges, subduction zones, and arcs;

whilst diffuse venting also occurs off axis and in areas with mild tectonic activity. Recently, it has been argued that seafloor venting may provide a significant source of the bio-essential Fe, Cu, and Zn, as well as other metals, due to their stabilization with organic ligands and nanoparticulate sulfides (Sander and Koschinsky, 2011; Yucel et al., 2011; Nishioka et al., 2013). These results place new constraints on submarine metal vent fluxes worldwide, including an indication that the majority of Fe supplied to hydrothermal plumes should come from entrainment of diffuse flow (German et al., 2015). Submarine hydrothermal venting has recently been suggested to have the potential to impact ocean biogeochemistry at the global scale (Tagliabue et al., 2010; Sander and Koschinsky, 2011; Wu et al., 2011; Fitzsimmons et al., 2014). This is the case because processes active in hydrothermal plumes are so vigorous that the residence time of seawater cycling through hydrothermal plumes is comparable to the residence time of deep-water mixing by thermohaline circulation.

9.1. High Temperature Venting (> 100°C)

Since hot hydrothermal vents expel fluid at temperatures between 100 and 450°C, depending on vent activity and depth, these fluids are highly reactive and far from thermodynamic equilibrium with the surrounding seawater. Besides their high temperature, they exhibit extreme pH values (<3 or >9), are highly reduced and may have a very different ionic composition to that of standard seawater. In fact, the fluid composition is defined by the underlying bedrock, pressure and temperature, and may reflect phase separation. Once the venting fluids encounter cold oxygenated seawater, precipitation reactions occur instantly, resulting in the commonly seen black (or white) smokers. While the chemical signature of hot hydrothermal vents can be followed in the hydrothermal plume over thousands of kilometers, the temperature will only be >300°C for seconds or millimeters after discharge. Most chemical reactions with the seawater will occur at temperatures between 4 and 300°C. Taking samples that are representative of *in-situ* conditions is almost impossible as samples will undergo spontaneous degassing upon the release of pressure, and cooling. Thus, to fully understand the reactions and processes occurring at depth in the presence of high temperature and pressure, it is essential to model the speciation of the fluid at *in situ* conditions.

9.2. Low Temperature Venting (<100°C)

Shallow vents are of great importance for the supply of micro- and macronutrients to the photic zone. In contrast to hot vents, the majority of shallow vents are characterized by diffuse venting, making them an interesting field of research and a natural laboratory to link speciation with biological uptake and toxicity (Klevenz et al., 2012; Kleint et al., 2015). For the vast majority of chemical tracers enriched in vent fluids, net fluxes to the oceans are modified as these tracers are incorporated into Fe-rich polymetallic sulfide and oxyhydroxide particles that sink to the seafloor at or close to mid ocean ridges (Mottl and McConachy, 1990; German et al., 1991; Kadko, 1993). Since

diffuse vent fluids have undergone modification in the sub-seafloor and are composed of more than 90% seawater, they have had time to partially equilibrate with ambient seawater. However, often they are still exposed to reducing conditions. The mixing zone for diffuse venting is in the order of meters. Beyond that mixing zone, minor ions still undergo reactions that need to be modeled to understand the chemistry and biological uptake in the vicinity of these diffuse vents.

10. SALT LAKES AND BRINES

Brines, i.e., natural waters with substantially higher ionic strengths than seawater, are formed in two ways: during ice formation in polar waters where salt rejection increases the salt content of the remaining water; and during evaporation in salt lakes.

10.1. Polar Brines

Polar regions are subject to intensive research activities, as they are particularly sensitive to rising temperatures and increasing atmospheric CO₂ concentrations, whilst at the same time playing a key role in global biogeochemical cycles and climate. Ocean acidification adds another stressor to these rapidly changing ecosystems (Orr et al., 2005). Polar regions experience extremes in primary productivity. In the Southern Ocean, low productivity is common in extensive regions with low iron supply, while high productivity is observed in regions with substantial iron supply from sediments (South Georgia) or ice melt (Nielsdottir et al., 2012). Whereas, iron supply over a large part of the Arctic is considered sufficient to sustain primary productivity (Klunder et al., 2012), the macro-nutrient concentrations may become exhausted following ice retreat. The freezing of sea ice results in brines with high salinity (100 or more), with freezing points well below that of normal seawater (ca. -1.8°C). These are conditions that are not included in chemical speciation models for seawater. In particular, the carbonate system in the polar oceans is not adequately described at sub-zero temperatures and salinities >50. In order to improve our mechanistic understanding of the dynamics of polar carbonate chemistry, and to allow quantification of CO₂ fluxes across the atmosphere-ice-seawater interfaces, Pitzer based chemical speciation models covering these conditions will be valuable.

10.2. Salt Lakes

Salt lakes are systems with very high ionic strength, the record being held by Don Juan Pond (Antarctica), which contains 3.72 mol kg⁻¹ CaCl₂ and 0.5 mol kg⁻¹ NaCl (Marion, 1997). The major focus in modeling of salt lakes and brines is the accurate prediction of precipitation equilibria as a function of temperature and composition (e.g., Harvie et al., 1984; Vanèina et al., 1986, 1997; Greenberg and Møller, 1989), with two major areas of application. The first is in understanding the evolution of past environments. An example is the modeling of evaporite sequences (layers of different salts accumulated over time) to infer the temperatures, concentrations, and compositions in the water body at the time of deposition. This type of work can be used to link the evolution of the water body

to long term climate variations. The second area concerns the modeling of future scenarios. Interest here is focused on water bodies that are saturated, or close to saturation, by one or more salts in response to changes in inflow/outflow and evaporation. Such changes can be due to human activities. The Dead Sea, for example, is decreasing in volume, resulting in salt precipitation.

11. CONCLUDING REMARKS

This paper outlines the programme of work for the development of a quality-controlled chemical speciation model for seawater and related systems, including descriptions of the different applications that can benefit from the model. Ensuring accessibility by the marine science community will be addressed in a future publication. SCOR Working Group 145 welcomes

comments on the proposed programme of work. Comments can be sent to the corresponding author.

AUTHOR CONTRIBUTIONS

DT developed the overall structure of the paper. All authors contributed sections of text to this paper, and approved the submitted version.

FUNDING

This work was partially supported by Award #1243377 from the U.S. National Science Foundation to the Scientific Committee on Oceanic Research (SCOR), and is a contribution from SCOR Working Group 145. SGS received funding from MBIE contract C01X1005.

REFERENCES

- Abbott, A. N., Haley, B. A., McManus, J., and Reimers, C. E. (2015). The sedimentary flux of dissolved rare earth elements to the ocean. *Geochim. Cosmochim. Acta* 154, 186–200. doi: 10.1016/j.gca.2015.01.010
- Abualhaija, M. M., and van den Berg, C. M. G. (2014). Chemical speciation of iron in seawater using catalytic cathodic stripping voltammetry with ligand competition against salicylaldehyde. *Mar. Chem.* 164, 60–74. doi: 10.1016/j.marchem.2014.06.005
- Aldrich, A. P., and van den Berg, C. M. G. (1998). Determination of iron and its redox speciation in seawater using catalytic cathodic stripping voltammetry. *Electroanalysis* 10, 369–373. doi: 10.1002/(sici)1521-4109(199805)10:6<369::aid-elanc369>3.3.co;2-n
- Andersson, P. S., Porcelli, D., Frank, M., Bjork, G., Dahlqvist, R., and Gustafsson, O. (2008). Neodymium isotopes in seawater from the Barents Sea and Fram Strait Arctic-Atlantic gateways. *Geochim. Cosmochim. Acta* 72, 2854–2867. doi: 10.1016/j.gca.2008.04.008
- Berner, R. A. (1980). *Early Diagenesis, a Theoretical Approach*. Princeton, NJ: Princeton University Press.
- Braungardt, C. B., Achterberg, E. P., Gledhill, M., Nimmo, M., Elbaz-Poulichet, F., Cruzado, A., et al. (2007). Chemical speciation of dissolved Cu, Ni, and Co in a contaminated estuary in southwest Spain and its influence on plankton communities. *Environ. Sci. Technol.* 41, 4214–4220. doi: 10.1021/es063042h
- Brown, J., Sander, S., Craw, D., and Hunter, K. (2005). Measurement of labile metals in acid rock drainage springs, New Zealand: field application of anodic stripping voltammetry. *Appl. Geochem.* 20, 1533–1545. doi: 10.1016/j.apgeochem.2005.04.014
- Buck, K. N., Lohan, M. C., Berger, C. J. M., and Bruland, K. W. (2007). Dissolved iron speciation in two distinct river plumes and an estuary: implications for riverine iron supply. *Limnol. Oceanogr.* 52, 843–855. doi: 10.4319/lo.2007.52.2.0843
- Bura-Nakic, E., Krznaric, D., Jurasin, D., Helz, G. R., and Ciglenecki, I. (2007). Voltammetric characterization of metal sulfide particles and nanoparticles in model solutions and natural waters. *Anal. Chim. Acta* 594, 44–51. doi: 10.1016/j.aca.2007.04.065
- Cai, W. J. (2011). Estuarine and coastal ocean carbon paradox: CO₂ sinks or sites of terrestrial carbon incineration? *Ann. Rev. Mar. Sci.* 3, 123–145. doi: 10.1146/annurev-marine-120709-142723
- Campos, M. L. A. M., and van den Berg, C. M. G. (1994). Determination of copper complexation in sea-water by cathodic stripping voltammetry and ligand competition with salicylaldehyde. *Anal. Chim. Acta* 284, 481–496.
- Chapman, P. M., Wang, F., Germano, J. D., and Batley, G. (2002). Pore water testing and analysis: the good, the bad, and the ugly. *Mar. Pollut. Bull.* 44, 359–366. doi: 10.1016/s0025-326x(01)00243-0
- Chen, C. T. A., Huang, T. H., Chen, Y. C., Bai, Y., He, X., and Kang, Y. (2013). Air-sea exchanges of CO₂ in the world's coastal seas. *Biogeosciences* 10, 6509–6544. doi: 10.5194/bg-10-6509-2013
- Clegg, S. L., and Whitfield, M. (1995). A chemical model of seawater including dissolved ammonia and the stoichiometric dissociation constant of ammonia in estuarine water and seawater from –2°C to 40°C. *Geochim. Cosmochim. Acta* 59, 2403–2421. doi: 10.1016/0016-7037(95)00135-2
- Clegg, S., and Whitfield, M. (1991). “Activity coefficients in natural waters,” in *Activity Coefficients in Electrolyte Solutions, 2nd Edn.*, ed K. S. Pitzer (Boca Raton, FL: CRC Press), 279–434.
- Croot, P. L., and Johansson, M. (2000). Determination of iron speciation by cathodic stripping voltammetry in seawater using the competing ligand 2-(2-thiazolylazo)-p-cresol (TAC). *Electroanalysis* 12, 565–576. doi: 10.1002/(sici)1521-4109(200005)12:8<565::aid-elanc565>3.3.co;2-c
- Davies, A. G. (1978). Pollution studies with marine plankton; Part II. Heavy metals. *Adv. Mar. Biol.* 15, 381–508.
- de Baar, H. J. W., Saager, P. M., Nolting, R. F., and Vandermeer, J. (1994). Cadmium versus phosphate in the world ocean. *Mar. Chem.* 46, 261–281. doi: 10.1016/0304-4203(94)90082-5
- DelValls, T. A., and Dickson, A. G. (1998). The pH of buffers based on 2-amino-2-hydroxymethyl-1,3-propanediol (tris) in synthetic sea water. *Deep Sea Res.* 45, 1541–1554. doi: 10.1016/s0967-0637(98)00019-3
- Dickson, A. G. (1981). An exact definition of total alkalinity and a procedure for the estimation of alkalinity and total inorganic carbon from titration data. *Deep Sea Res.* 28A, 609–623.
- Dickson, A. G. (1984). pH scales and proton transfer reactions in saline media such as seawater. *Geochim. Cosmochim. Acta* 48, 2299–2308.
- Dickson, A. G. (1993). pH buffers for sea-water media based on the total hydrogen-ion concentration scale. *Deep Sea Res.* 40, 107–118. doi: 10.1016/0967-0637(93)90055-8
- Dickson, A., Sabine, C., and Christian, J. (eds.). (2007). *Guide to Best Practices for Ocean CO₂ Measurements*. Sidney, BC: PICES Special Publication 3.
- Dupont, S., and Poertner, H. O. (2013). A snapshot of ocean acidification research. *Mar. Biol.* 160, 1765–1771. doi: 10.1007/s00227-013-2282-9
- Dyrssen, D. (1988). Sulfide complexation in surface water. *Mar. Chem.* 24, 143–153.
- Ellwood, M. J., and van den Berg, C. M. G. (2001). Determination of organic complexation of cobalt in seawater by cathodic stripping voltammetry. *Mar. Chem.* 75, 33–47. doi: 10.1016/s0304-4203(01)00024-x
- Feistel, R., Lovell-Smith, J. W., Saunders, P., and Seitz, S. (2016). Uncertainty of empirical correlation equations. *Metrologia* 53, 1079–1090. doi: 10.1088/0026-1394/53/4/1079
- Fitzsimmons, J. N., Boyle, E. A., and Jenkins, W. J. (2014). Distal transport of dissolved hydrothermal iron in the deep South Pacific Ocean. *Proc. Natl. Acad. Sci. U.S.A.* 111, 16654–16661. doi: 10.1073/pnas.1418778111

- German, C. R., Campbell, A. C., and Edmond, J. M. (1991). Hydrothermal scavenging at the mid-atlantic ridge - modification of trace-element dissolved fluxes. *Earth Planet. Sci. Lett.* 107, 101–114. doi: 10.1016/0012-821x(91)90047-1
- German, C. R., Legendre, L. L., Sander, S. G., Niquil, N., Luther, G. W. III, Bharati, L., et al. (2015). Hydrothermal Fe cycling and deep ocean organic carbon scavenging: model-based evidence for significant POC supply to seafloor sediments. *Earth Planet. Sci. Lett.* 419, 143–153. doi: 10.1016/j.epsl.2015.03.012
- German, C. R., Rudnicki, M. D., and Klinkhammer, G. P. (1999). A segment-scale survey of the Broken Spur hydrothermal plume. *Deep Sea Res.* 46, 701–714. doi: 10.1016/s0967-0637(98)00078-8
- Greenberg, J. P., and Möller, N. (1989). The prediction of mineral solubilities in natural waters - a chemical equilibrium model for the Na-K-Ca-Cl-SO₄-H₂O system to high concentration from 0°C to 250°C. *Geochim. Cosmochim. Acta* 53, 2503–2518. doi: 10.1016/0016-7037(89)90124-5
- Gustafsson, J. P. (2001). Modeling the acid-base properties and metal complexation of humic substances with the stockholm humic model. *J. Colloid Interface Sci.* 244, 102–112. doi: 10.1006/jcis.2001.7871
- Haese, R. R., Smith, J., Weber, R., and Trafford, J. (2014). High-Magnesium calcite dissolution in tropical continental shelf sediments controlled by ocean acidification. *Environ. Sci. Technol.* 48, 8522–8528. doi: 10.1021/es501564q
- Haley, B. A., Frank, M., Spielhagen, R. F., and Eisenhauer, A. (2008). Influence of brine formation on Arctic Ocean circulation over the past 15 million years. *Nat. Geosci.* 1, 68–72. doi: 10.1038/ngeo.2007.5
- Harvie, C. E., Möller, N., and Weare, J. H. (1984). Prediction of mineral solubilities in natural waters: the Na-K-Mg-Ca-H-Cl-SO₄-OH-HCO₃-CO₃-H₂O system to high ionic strength at 25°C. *Geochim. Cosmochim. Acta* 48, 723–751.
- Hatje, V., Bruland, K. W., and Flegal, A. R. (2014). Determination of rare earth elements after pre-concentration using NOBIAS-chelate PA-1 (R) resin: method development and application in the San Francisco Bay plume. *Mar. Chem.* 160, 34–41. doi: 10.1016/j.marchem.2014.01.006
- Hatje, V., Bruland, K. W., and Flegal, A. R. (2016). Increases in anthropogenic gadolinium anomalies and rare earth element concentrations in San Francisco Bay over a 20 year record. *Environ. Sci. Technol.* 50, 4159–4168. doi: 10.1021/acs.est.5b04322
- Henderson, G. M., Anderson, R. F., Adkins, J., Andersson, P., Boyle, E. A., Cutter, G., et al. (2007). GEOTRACES - An international study of the global marine biogeochemical cycles of trace elements and their isotopes. *Chem. Erde* 67, 85–131. doi: 10.1016/j.chemer.2007.02.001
- Hernandez-Ayon, J. M., Zirino, A., Dickson, A. G., Camiro-Vargas, T., and Valenzuela-Espinoza, E. (2007). Estimating the contribution of organic bases from microalgae to the titration alkalinity in coastal seawaters. *Limnol. Oceanogr.* 5, 225–232. doi: 10.4319/lom.2007.5.225
- Kadko, D. (1993). Excess Po-210 and nutrient recycling within the California coastal transition zone. *J. Geophys. Res.* 98, 857–864. doi: 10.1029/92jc01932
- Kleint, C., Kuzmanovski, S., Powell, Z., Buehring, S. I., Sander, S. G., and Koschinsky, A. (2015). Organic Cu-complexation at the shallow marine hydrothermal vent fields off the coast of Milos (Greece), Dominica (Lesser Antilles) and the Bay of Plenty (New Zealand). *Mar. Chem.* 173, 244–252. doi: 10.1016/j.marchem.2014.10.012
- Klevenz, V., Sander, S. G., Perner, M., and Koschinsky, A. (2012). Amelioration of free copper by hydrothermal vent microbes as a response to high copper concentrations. *Chem. Ecol.* 28, 405–420. doi: 10.1080/02757540.2012.666531
- Klinkhammer, G., Heggie, D. T., and Graham, D. W. (1982). Metal diagenesis in oxic marine-sediments. *Earth Planet. Sci. Lett.* 61, 211–219. doi: 10.1016/0012-821x(82)90054-1
- Klinkhammer, G. P. (1980). Early diagenesis in sediments from the eastern Equatorial Pacific. 2. Pore water metal results. *Earth Planet. Sci. Lett.* 49, 81–101. doi: 10.1016/0012-821x(80)90151-x
- Klunder, M. B., Bauch, D., Laan, P., de Baar, H. J. W., van Heuven, S., and Ober, S. (2012). Dissolved iron in the Arctic shelf seas and surface waters of the central Arctic Ocean: impact of Arctic river water and ice-melt. *J. Geophys. Res.* 117:C01027. doi: 10.1029/2011jc007133
- Koch, B. P., Witt, M. R., Engbrodt, R., Dittmar, T., and Kattner, G. (2005). Molecular formulae of marine and terrigenous dissolved organic matter detected by electrospray ionization Fourier transform ion cyclotron resonance mass spectrometry. *Geochim. Cosmochim. Acta* 69, 3299–3308. doi: 10.1016/j.gca.2005.02.027
- Koopal, L. K., Saito, T., Pinheiro, J. P., and van Riemsdijk, W. H. (2005). Ion binding to natural organic matter: general considerations and the NICA-Donnan model. *Colloids Surf. A* 265, 40–54. doi: 10.1016/j.colsurfa.2004.11.050
- Kulinski, K., Schneider, B., Hammer, K., Machulik, U., and Schulz-Bull, D. (2014). The influence of dissolved organic matter on the acid-base system of the Baltic Sea. *J. Mar. Syst.* 132, 106–115. doi: 10.1016/j.jmarsys.2014.01.011
- Laglera, L. M., and van den Berg, C. M. G. (2003). Copper complexation by thiol compounds in estuarine waters. *Mar. Chem.* 82, 71–89. doi: 10.1016/s0304-4203(03)00053-7
- Liu, K.-K., Atkinson, L., Quinones, R., and Talaue-McManus, L. (eds.). (2010). *Carbon and Nutrient Fluxes in Continental Margins: A Global Synthesis*. Berlin: Springer-Verlag.
- Liu, X., Patsavas, M. C., and Byrne, R. H. (2011). Purification and characterization of meta-cresol purple for spectrophotometric seawater pH measurements. *Environ. Sci. Technol.* 45, 4862–4868. doi: 10.1021/es200665d
- Liu, X. W., and Millero, F. J. (2002). The solubility of iron in seawater. *Mar. Chem.* 77, 43–54. doi: 10.1016/s0304-4203(01)00074-3
- Liu, Y. G., Miah, M. R. U., and Schmitt, R. A. (1988). Cerium - a chemical tracer for paleo-oceanic redox conditions. *Geochim. Cosmochim. Acta* 52, 1361–1371. doi: 10.1016/0016-7037(88)90207-4
- Luther, G. W. III, Madison, A. S., Mucci, A., Sundby, B., and Oldham, V. E. (2015). A kinetic approach to assess the strengths of ligands bound to soluble Mn(III). *Mar. Chem.* 173, 93–99. doi: 10.1016/j.marchem.2014.09.006
- Luther, G. W., and Tsamakis, E. (1989). Concentration and form of dissolved sulfide in the oxic water column of the ocean. *Mar. Chem.* 27, 165–177. doi: 10.1016/0304-4203(89)90046-7
- Marion, G. M. (1997). A theoretical evaluation of mineral stability in Don Juan Pond, Wright Valley, Victoria Land. *Antarct. Sci.* 9, 92–99.
- Millero, F. J. (2007). The marine inorganic carbon cycle. *Chem. Rev.* 107, 308–341. doi: 10.1021/cr0503557
- Millero, F. J., and Pierrot, D. (1998). A chemical equilibrium model for natural waters. *Aquat. Geochem.* 4, 153–199. doi: 10.1023/a:1009656023546
- Millero, F. J., and Roy, R. N. (1997). A chemical equilibrium model for the carbonate system in natural waters. *Croatia Chemica Acta* 70, 1–38.
- Mottl, M. J., and McConachy, T. F. (1990). Chemical processes in buoyant hydrothermal plumes on the East Pacific Rise near 21°N. *Geochim. Cosmochim. Acta* 54, 1911–1927. doi: 10.1016/0016-7037(90)90261-i
- Nielsdottir, M. C., Bibby, T. S., Moore, C. M., Hinz, D. J., Sanders, R., Whitehouse, M., et al. (2012). Seasonal and spatial dynamics of iron availability in the Scotia Sea. *Mar. Chem.* 130, 62–72. doi: 10.1016/j.marchem.2011.12.004
- Nishioka, J., Obata, H., and Tsumune, D. (2013). Evidence of an extensive spread of hydrothermal dissolved iron in the Indian Ocean. *Earth Planet. Sci. Lett.* 361, 26–33. doi: 10.1016/j.epsl.2012.11.040
- Orr, J. C., Epitalon, J. M., and Gattuso, J. P. (2015). Comparison of ten packages that compute ocean carbonate chemistry. *Biogeosciences* 12, 1483–1510. doi: 10.5194/bg-12-1483-2015
- Orr, J. C., Fabry, V. J., Aumont, O., Bopp, L., Doney, S. C., Feely, R. A., et al. (2005). Anthropogenic ocean acidification over the twenty-first century and its impact on calcifying organisms. *Nature* 437, 681–686. doi: 10.1038/nature04095
- Pitzer, K. S. (ed.). (1991). *Activity Coefficients in Electrolyte Solutions*. Boca Raton, FL: CRC Press.
- Pizeta, I., Sander, S. G., Hudson, R. J. M., Omanovic, D., Baars, O., Barbeau, K. A., et al. (2015). Interpretation of complexometric titration data: an intercomparison of methods for estimating models of trace metal complexation by natural organic ligands. *Mar. Chem.* 173, 3–24. doi: 10.1016/j.marchem.2015.03.006
- Price, N. M., Harrison, G. I., Hering, J. G., Robert, J. M. H., Nirel, P. M. V., Palenik, B., et al. (1988). Preparation and chemistry of the artificial algal culture medium aquil. *Biol. Oceanogr.* 6, 443–461.
- Ridgwell, A., and Hargreaves, J. C. (2007). Regulation of atmospheric CO₂ by deep-sea sediments in an Earth system model. *Global Biogeochem. Cycles* 21:GB2008. doi: 10.1029/2006gb002764
- Rolison, J. M., Middag, R., Stirling, C. H., Rijkenberg, M. J. A., and de Baar, H. J. W. (2015). Zonal distribution of dissolved aluminium in the Mediterranean Sea. *Mar. Chem.* 177, 87–100. doi: 10.1016/j.marchem.2015.05.001
- Rozan, T. F., Benoit, G., and Luther, G. W. (1999). Measuring metal sulfide complexes in oxic river waters with square wave voltammetry. *Environ. Sci. Technol.* 33, 3021–3026. doi: 10.1021/es981206r

- Rozan, T. F., Lassman, M. E., Ridge, D. P., and Luther, G. W. (2000). Evidence for iron, copper and zinc complexation as multinuclear sulphide clusters in oxic rivers. *Nature* 406, 879–882. doi: 10.1038/35022561
- Rudd, M. A. (2014). Scientists' perspectives on global ocean research priorities. *Front. Mar. Sci.* 1:36. doi: 10.3389/fmars.2014.00036
- Sander, S. G., and Koschinsky, A. (2011). Metal flux from hydrothermal vents increased by organic complexation. *Nat. Geosci.* 4, 145–150. doi: 10.1038/ngeo1088
- Sander, S. G., Tian, F., Ibsanmi, E. B., Currie, K. I., Hunter, K. A., and Frew, R. D. (2015). Spatial and seasonal variations of iron speciation in surface waters of the Subantarctic front and the Otago Continental Shelf. *Mar. Chem.* 173, 114–124. doi: 10.1016/j.marchem.2014.09.001
- Santana-Casiano, J. M., González-Dávila, M., and Millero, F. J. (2005). Oxidation of nanomolar levels of Fe(II) with oxygen in natural waters. *Environ. Sci. Technol.* 39, 2073–2079. doi: 10.1021/es049748y
- Scher, H. D., and Martin, E. E. (2004). Circulation in the Southern Ocean during the Paleogene inferred from neodymium isotopes. *Earth Planet. Sci. Lett.* 228, 391–405. doi: 10.1016/j.epsl.2004.10.016
- Semeniuk, D. M. (2014). *Copper Nutrition and Transport Mechanisms in Plankton Communities in the Northeast Pacific Ocean*. Ph.D. University of British Columbia.
- Semeniuk, D. M., Bundy, R. M., Payne, C. D., Barbeau, K. A., and Maldonado, M. T. (2015). Acquisition of organically complexed copper by marine phytoplankton and bacteria in the northeast subarctic Pacific Ocean. *Mar. Chem.* 173, 222–233. doi: 10.1016/j.marchem.2015.01.005
- Semiletov, I., Pipko, I., Gustafsson, O., Anderson, L. G., Sergienko, V., Pugach, S., et al. (2016). Acidification of East Siberian Arctic Shelf waters through addition of freshwater and terrestrial carbon. *Nat. Geosci.* 9, 361–365. doi: 10.1038/ngeo2695
- Shahidul Islam, M., and Tanaka, M. (2004). Impacts of pollution on coastal and marine ecosystems including coastal and marine fisheries and approach for management: a review and synthesis. *Mar. Pollut. Bull.* 48, 624–649. doi: 10.1016/j.marpolbul.2003.12.004
- Sholkovitz, E. R., Piepgras, D. J., and Jacobsen, S. B. (1989). The pore water chemistry of rare-earth elements in Buzzards Bay sediments. *Geochim. Cosmochim. Acta* 53, 2847–2856. doi: 10.1016/0016-7037(89)90162-2
- Sholkovitz, E. R., and Schneider, D. L. (1991). Cerium redox cycles and rare-earth elements in the Sargasso Sea. *Geochim. Cosmochim. Acta* 55, 2737–2743. doi: 10.1016/0016-7037(91)90440-g
- Siegenthaler, U., and Sarmiento, J. L. (1993). Atmospheric carbon dioxide and the ocean. *Nature* 365, 119–125.
- Sinoir, M., Ellwood, M. J., Butler, E. C. V., Bowie, A. R., Mongin, M., and Hassler, C. S. (2016). Zinc cycling in the Tasman Sea: Distribution, speciation and relation to phytoplankton community. *Mar. Chem.* 182, 25–37. doi: 10.1016/j.marchem.2016.03.006
- Strzepek, R. F., Maldonado, M. T., Hunter, K. A., Frew, R. D., and Boyd, P. W. (2011). Adaptive strategies by Southern Ocean phytoplankton to lessen iron limitation: uptake of organically complexed iron and reduced cellular iron requirements. *Limnol. Oceanogr.* 56, 1983–2002. doi: 10.4319/lo.2011.56.6.1983
- Sukola, K., Wang, F. Y., and Tessier, A. (2005). Metal-sulfide species in oxic waters. *Anal. Chim. Acta* 528, 183–195. doi: 10.1016/j.aca.2004.10.009
- Sunda, W., Price, N. M., and Morel, F. M. M. (2005). "Trace metal ion buffers and their use in culture studies," in *Algal Culturing Techniques*, ed R. Anderson (Burlington, NC: Academic Press), 35–65.
- Tagliabue, A., Bopp, L., Dutay, J. C., Bowie, A. R., Chever, F., Jean-Baptiste, P., et al. (2010). Hydrothermal contribution to the oceanic dissolved iron inventory. *Nat. Geosci.* 3, 252–256. doi: 10.1038/ngeo818
- Tessier, A., and Turner, D. R. (eds.) (1995). *Metal Speciation and Bioavailability in Aquatic Systems*. Chichester: John Wiley.
- Tipping, E., Lofts, S., and Sonke, J. (2011). Humic ion-binding model VII: a revised parameterisation of cation-binding by humic substances. *Environ. Chem.* 8, 225–235. doi: 10.1071/EN11016
- Turner, D. R., and Hunter, K. A. (eds.) (2001). *The Biogeochemistry of Iron in Seawater*. Chichester: John Wiley.
- Twining, B. S., and Baines, S. B. (2013). "The trace metal composition of marine phytoplankton," in *Annual Review of Marine Science*, Vol. 5, eds C. A. Carlson and S. J. Giovannoni (Palo Alto, CA: Annual Reviews), 191–215.
- Ulfso, A., Kuliński, K., Anderson, L. G., and Turner, D. R. (2015). Modelling organic alkalinity in the Baltic Sea using a Humic-Pitzer approach. *Mar. Chem.* 168, 18–26. doi: 10.1016/j.marchem.2014.10.013
- UNEP (2013). *Global Chemicals Outlook: Towards Sound Management of Chemicals*. Nairobi: United Nations Environment Programme.
- Vaněina, V., Kester, D. R., and Bilinski, H. (1997). Application of the Pitzer model to solar salt brine chemistry. *Croatica Chemica Acta* 70, 55–69.
- Vaněina, V., Plavšić, M., Bilinski, H., Branica, M., and Millero, F. J. (1986). Preparation and solubility of northpore from brine and its adsorption properties for Cu(II) and Cd(II) in seawater. *Geochim. Cosmochim. Acta* 50, 1329–1336. doi: 10.1016/0016-7037(86)90309-1
- van den Berg, C. M. G. (1985). Determination of the zinc complexing capacity in seawater by cathodic stripping voltammetry of zinc-APDC complex ions. *Mar. Chem.* 16, 121–130.
- van den Berg, C. M. G. (2006). Chemical speciation of iron in seawater by cathodic stripping voltammetry with dihydroxynaphthalene. *Anal. Chem.* 78, 156–163. doi: 10.1021/ac051441+
- van den Berg, C. M. G., Khan, S. H., Daly, P. J., Riley, J. P., and Turner, D. R. (1991). An electrochemical study of Ni, Sb, Se, Sn, U and V in the estuary of the Tamar. *Estuarine Coast. Shelf Sci.* 33, 309–322.
- van Hulst, M. M. P., Sterl, A., Middag, R., de Baar, H. J. W., Gehlen, M., Dutay, J. C., et al. (2014). On the effects of circulation, sediment resuspension and biological incorporation by diatoms in an ocean model of aluminium. *Biogeosciences* 11, 3757–3779. doi: 10.5194/bg-11-3757-2014
- Wang, D., Lin, W., Yang, X., Zhai, W., Dai, M., and Chen, C. T. A. (2012). Occurrences of dissolved trace metals (Cu, Cd, and Mn) in the Pearl River Estuary (China), a large river-groundwater-estuary system. *Cont. Shelf Res.* 50, 54–63. doi: 10.1016/j.csr.2012.10.009
- Waters, J. F., and Millero, F. J. (2013). The free proton concentration scale for seawater pH. *Mar. Chem.* 149, 8–22. doi: 10.1016/j.marchem.2012.11.003
- Wu, J., Wells, M. L., and Rember, R. (2011). Dissolved iron anomaly in the deep tropical-subtropical Pacific: evidence for long-range transport of hydrothermal iron. *Geochim. Cosmochim. Acta* 75, 460–468. doi: 10.1016/j.gca.2010.10.024
- Yang, L., Hong, H., Chen, C. T. A., Guo, W., and Huang, T. H. (2013). Chromophoric dissolved organic matter in the estuaries of populated and mountainous Taiwan. *Mar. Chem.* 157, 12–23. doi: 10.1016/j.marchem.2013.07.002
- Yucel, M., Gartman, A., Chan, C. S., and Luther, G. W. III (2011). Hydrothermal vents as a kinetically stable source of iron-sulphide-bearing nanoparticles to the ocean. *Nat. Geosci.* 4, 367–371. doi: 10.1038/ngeo1148
- Zhang, J., and Mandal, A. K. (2012). Linkages between submarine groundwater systems and the environment. *Curr. Opin. Environ. Sustain.* 4, 219–226. doi: 10.1016/j.cosust.2012.03.006

Conflict of Interest Statement: The authors declare that the research was conducted in the absence of any commercial or financial relationships that could be construed as a potential conflict of interest.

Copyright © 2016 Turner, Achterberg, Chen, Clegg, Hatje, Maldonado, Sander, van den Berg and Wells. This is an open-access article distributed under the terms of the Creative Commons Attribution License (CC BY). The use, distribution or reproduction in other forums is permitted, provided the original author(s) or licensor are credited and that the original publication in this journal is cited, in accordance with accepted academic practice. No use, distribution or reproduction is permitted which does not comply with these terms.

Advantages of publishing in Frontiers



OPEN ACCESS
Articles are free to read,
for greatest visibility



COLLABORATIVE PEER-REVIEW
Designed to be rigorous
– yet also collaborative,
fair and constructive



FAST PUBLICATION
Average 85 days from
submission to publication
(across all journals)



COPYRIGHT TO AUTHORS
No limit to article
distribution and re-use



TRANSPARENT
Editors and reviewers
acknowledged by name
on published articles



SUPPORT
By our Swiss-based
editorial team



IMPACT METRICS
Advanced metrics
track your article's impact



GLOBAL SPREAD
5'100'000+ monthly
article views
and downloads



LOOP RESEARCH NETWORK
Our network
increases readership
for your article

Frontiers

EPFL Innovation Park, Building I • 1015 Lausanne • Switzerland
Tel +41 21 510 17 00 • Fax +41 21 510 17 01 • info@frontiersin.org
www.frontiersin.org

Find us on

